

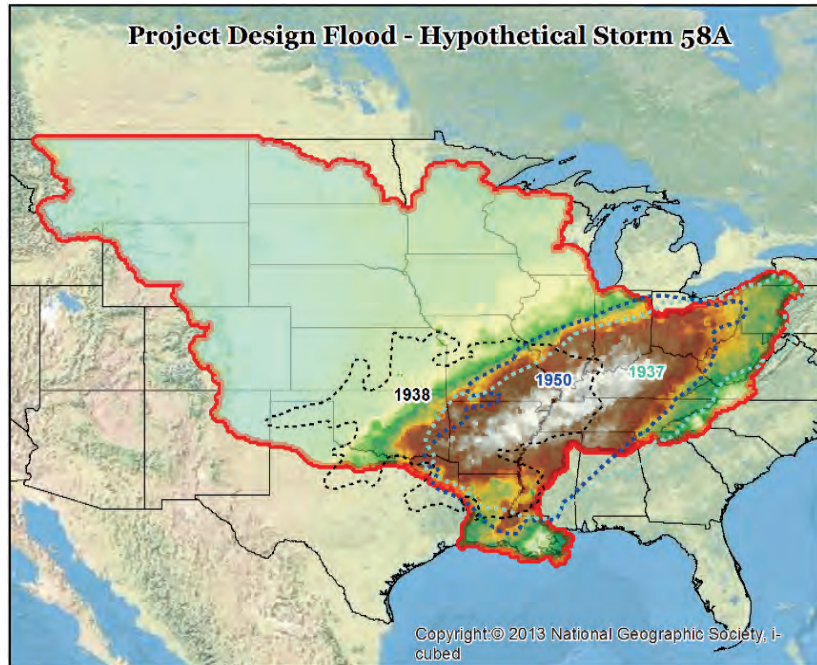


US Army Corps of Engineers®



Mississippi River and Tributaries Flowline Assessment Hydrology Report

MRG&P Report No. 24; Volume 2 • December 2018



MRG&P

Mississippi River
Geomorphology &
Potamology Program



Mississippi River and Tributaries Flowline Assessment Hydrology Report

Roger A. Gaines and Sarah E. Girdner

*U.S. Army Engineer District, Memphis
167 N. Main St. Room B-202
Memphis, TN 38103*

Bill J. Frederick

*U.S. Army Corps of Engineers, Mississippi Valley Division
1400 Walnut Street
Vicksburg, MS 39180*

Report 2 of a series

Approved for public release; distribution is unlimited.

Prepared for U.S. Army Corps of Engineers, Mississippi Valley Division
Mississippi River Geomorphology & Potamology Program
1400 Walnut Street
Vicksburg, MS 39180

Under Project No. 449963, "Mississippi River and Tributaries Flowline Assessment"

Abstract

Periodically, a historical flood of record inundates the Lower Mississippi River and tributaries, which calls into question the adequacy of the Project Design Flood (PDF). The most recent of these, the 2011 flood, was a result of precipitation that was approximately 60% of the PDF rainfall, yet measured discharges were within 78% to 91% of PDF flows. Thus, the 2011 flood was the impetus for the re-evaluation of the 1955 hydrology that derives the PDF. This assessment replicates the 1955 hydrology with current technological advancements, re-generates that hydrology with a new methodology, and assesses extreme flood events that occurred after 1955. Individual storm event precipitation and temperature point data inputs were pieced together from different archives and converted to raster grids to generate a spatially continuous storm event over the entire Mississippi River Basin for Hypothetical (HYPO) 52A, 56, 58A, and 63. HYPO 58A remains the PDF storm for the Mississippi River and Tributaries project.

DISCLAIMER: The contents of this report are not to be used for advertising, publication, or promotional purposes. Citation of trade names does not constitute an official endorsement or approval of the use of such commercial products. All product names and trademarks cited are the property of their respective owners. The findings of this report are not to be construed as an official Department of the Army position unless so designated by other authorized documents.

DESTROY THIS REPORT WHEN NO LONGER NEEDED. DO NOT RETURN IT TO THE ORIGINATOR.

Contents

Abstract.....	ii
Figures and Tables.....	vi
Preface	xxxiii
Unit Conversion Factors.....	xxxiv
1 Introduction	1
1.1 Objective	1
1.2 Background.....	3
1.2.1 Statement of Problem.....	3
1.2.2 Limitations.....	4
1.2.3 1955 Study for the Mississippi River and Tributaries (MR&T) Project Design Flood (PDF).....	5
1.3 Approach	38
2 Current Flowline Assessment (2016).....	39
2.1 General criteria	41
2.2 Analysis framework.....	42
2.2.1 Unsteady hydrodynamic model (HEC-RAS).....	42
2.2.2 Hydrologic model linkages.....	44
2.3 Procedural approach	49
2.4 Hydrologic model	53
2.4.1 Basic CHPS-FEWS model.....	54
2.4.2 Primary NWS hydrologic operations.....	57
2.4.3 Running NWS CHPS for the Flowline project.....	58
2.4.4 NWS RFCs in the Flowline assessment area	60
2.4.5 CHPS precipitation and temperature forcings import process.....	64
2.4.6 Other required RFC forcings.....	65
2.4.7 Data exchange	66
2.4.8 RFC flowline modeling procedure	67
2.4.9 Storm simulations.....	81
2.4.10 TVA Flowline modeling procedure	83
2.5 Land use considerations.....	88
2.6 Infiltration and base flow considerations.....	90
2.7 HYPO storm combinations	92
2.7.1 Storm sequencing.....	93
2.7.2 Evaluation of new HYPO storm sequence	109
2.8 Storm development	110
2.8.1 Precipitation	113
2.8.2 Temperature data	119
2.8.3 Interpolation schemes	124
2.8.4 Quality assurance	129

2.8.5	<i>An overview of digitized precipitation events</i>	137
2.9	Storm transpositioning.....	144
2.9.1	<i>HEC-MetVue enhancements</i>	144
2.9.2	<i>Post-processing</i>	145
2.9.3	<i>Data source and specifications</i>	145
2.9.4	<i>Data processing</i>	146
2.9.5	<i>Spatial analysis of results</i>	146
2.9.6	<i>Quantitative analysis: Volume conservation</i>	151
2.9.7	<i>Quality assurance: Volume conservation</i>	156
2.10	Reservoir regulation effects	159
2.10.1	<i>Reservoir Selection</i>	160
2.10.2	<i>Reservoir routing</i>	168
2.10.3	<i>Reductions from standard reservoir operations</i>	183
2.11	Alternative regulation effects	186
2.12	Synopsis of methodology differences, 2016 versus 1955.....	197
2.12.1	<i>Climatic inputs</i>	198
2.12.2	<i>Hydrologic modeling</i>	199
2.13	Paleoflood considerations	200
2.14	Climate change considerations.....	201
2.14.1	<i>Regional documentation on climate change</i>	201
2.14.2	<i>Discharge as a surrogate for precipitation</i>	205
2.14.3	<i>NDT and CHAT</i>	205
2.14.4	<i>Watershed vulnerability assessment (VA) tool</i>	228
2.14.5	<i>Climate-change summary</i>	238
3	Results	239
3.1	Comparison of peak flows for HYPO storms	239
3.1.1	<i>Hydrograph shape and volume</i>	241
3.1.2	<i>Hydrograph timing</i>	244
3.2	HEC-RAS inflow boundary discharge hydrographs	247
3.3	Peak flows for the Lower Ohio and Mississippi Rivers	254
4	Summary	269
	References	271
	Appendix A: Agency Correspondence —National Weather Service Scope of Work	274
	Appendix B: HYPO 58A	283
	Appendix C: HYPO 52A	349
	Appendix D: HYPO 56	381
	Appendix E: HYPO 63	450
	Appendix F: Decision Documents	521

Appendix G: Historic and HYPO Storm Meteorology	544
Appendix H: Mississippi River 2011 Post Flood Assessment: Task 1 – Adequacy of MR&T Project Design Flood	659
Appendix I: Reservoir Maps	660
Appendix J: Hydrograph Tabulations	681
Appendix K: Precipitation Tabulations	682
Report Documentation Page	

Figures and Tables

Figures

Figure 1-1. Seasonal distribution of flow as a percentage between the Mississippi and Ohio Rivers (Chester and Metropolis, IL, respectively).....	8
Figure 1-2. Seasonal distribution of flow as a percentage between the Missouri and Mississippi Rivers (Hermann, MO, and Grafton, IL, respectively).....	9
Figure 1-3. Seasonal distribution of flow as a percentage between the Arkansas and White Rivers and the Mississippi River (Pine Bluff, AR; Clarendon, AR; and Arkansas City/Greenville, respectively).....	10
Figure 1-4. Watershed map from 1955 analysis of the MR&T PDF.....	13
Figure 1-5. HYPO 52A, 56, 58A, and 63 sequence from Memorandum Report No. 1 (MRC 1955, Appendix J).....	21
Figure 1-6. Infiltration indices, rainfall-excess curves, and base flows from the 1955 Study (MRC 1955).....	23
Figure 1-7. Plot of regulation effects from Cairo to Memphis reach of Mississippi River.....	28
Figure 1-8. E, N, and D reservoirs listed in Memorandum Report No. 1 (MRC 1955).....	30
Figure 2-1. Mississippi River Basin with HEC-RAS extent shown.*	42
Figure 2-2. HEC-RAS model extent and inflow boundary locations.....	43
Figure 2-3. Hydrologic sub-basins providing local inputs to HEC-RAS model.....	44
Figure 2-4. Mississippi River Basin showing NWS RFC sub-basins.....	45
Figure 2-5. HEC-RAS Model schematization for 1955 hydrologic inputs.....	47
Figure 2-6. HEC-RAS Model schematization for 2016 hydrologic inputs.....	48
Figure 2-7. Team alignment and general roles for simulation of historic events.....	52
Figure 2-8. General team process to generate regulated results for HYPO storm modeling.....	52
Figure 2-9. CHPS schematic.....	55
Figure 2-10. FEWS concept for managing inputs, modeling, and outputs.....	56
Figure 2-11. FEWS management of model input and output.....	56
Figure 2-12. Forecast model initial state considerations.....	59
Figure 2-13. Map of the NWS RFCs and TVA hydrologic service areas participating in the Flowline assessment.....	60
Figure 2-14. Display of precipitation dataset imported into CHPS. The RFCs used the same import configuration so that a single set of ESRI ASCII grid parameters could be used.....	64
Figure 2-15. Plot showing the difference between RFC simulated regulated outflows at Pickwick Dam on the Lower Tennessee River vs. the hand-adjusted regulation performed by TVA using RiverWare.....	70
Figure 2-16. TVA reservoir system modeled in RiverWare.....	87
Figure 2-17. Land use comparison within Mississippi River Basin.....	89

Figure 2-18. HYPO 58A flow chart representation of meteorological combination (above dashed line) and computation approach used for Memorandum Report No. 1 (MRC 1955).	94
Figure 2-19. HYPO 52A flow chart representation of meteorological combination (above dashed line) and computation approach used for Memorandum Report No. 1 (MRC 1955).	95
Figure 2-20. HYPO 56 flow chart representation of meteorological combination (above dashed line) and computation approach used for Memorandum Report No. 1 (MRC 1955).	95
Figure 2-21. HYPO 63 flow chart representation of meteorological combination (above dashed line) and computation approach used for Memorandum Report No. 1 (MRC 1955).	96
Figure 2-22. Map showing different regions of precipitation for the HYPO 58A CM sequence.	97
Figure 2-23. Map showing different regions of precipitation for the HYPO 52A CM sequence.	98
Figure 2-24. Map showing different regions of precipitation for the HYPO 56 CM sequence.	99
Figure 2-25. Map showing different regions of precipitation for the HYPO 63 CM sequence.	100
Figure 2-26. Map showing the spatial representation of precipitation for HYPO 52A, 56, 58A, 63, and 11-73 SS.	102
Figure 2-27. HYPO 58A SS.	102
Figure 2-28. Smithland unregulated discharge hydrograph, HYPO 58A.	105
Figure 2-29. Smithland regulated discharge hydrograph, HYPO 58A-R.	105
Figure 2-30. Chester unregulated discharge hydrographs, HYPO 58A.	106
Figure 2-31. Chester regulated discharge hydrographs, HYPO 58A.	106
Figure 2-32. Clarendon unregulated discharge hydrographs, HYPO 58A.	107
Figure 2-33. Clarendon regulated discharge hydrographs, HYPO 58A.	107
Figure 2-34. Shreveport unregulated discharge hydrographs, HYPO 58A.	108
Figure 2-35. Shreveport regulated discharge hydrographs, HYPO 58A.	108
Figure 2-36. HYPO 11-73 SS.	109
Figure 2-37. Published map of 1950 cumulative storm isohyets.	112
Figure 2-38. Interpolated map of 1950 cumulative storm isohyets.	112
Figure 2-39. HYPO 58A – 6–24 January 1937 (a) (top left) storm coverage over the Mississippi River Basin; (b) (bottom left) isohyetal for unadjusted January 1937 storm; (c) (top right) comparison of mass rainfall curves for original point precipitation data versus the processed/interpolated precipitation data for the unadjusted storm; and (d) (bottom right) comparison of 1955 precipitation, 2016 precipitation, and 2016 post-processed precipitation at select locations.	115
Figure 2-40. HYPO 58A – 3-16 January 1950 (a) (top left) storm coverage over the Mississippi River Basin; (b) (bottom left) isohyetal for storm; (c) (top right) comparison of mass rainfall curves for original point precipitation data versus the processed/ interpolated precipitation data; and (d) (bottom right) comparison of	

1955 precipitation, 2016 precipitation, and 2016 post-processed precipitation at select locations.....	116
Figure 2-41. HYPO 58A – 14–18 February 1938 (a) (top left) storm coverage over the Mississippi River Basin; (b) (bottom left) isohyetal for storm with and without transposition; (c) (top right) comparison of mass rainfall curves for original point precipitation data versus the processed/interpolated precipitation data for the storm with and without transposition; and (d) (bottom right) comparison of 1955 precipitation, 2016 precipitation, 2016 post-processed precipitation, and 2016 transposed precipitation at select locations.....	117
Figure 2-42. HYPO 58A (a) (top left) storm sequencing with warm-up and cool down periods; (b) (bottom left) warm-up precipitation coverage over the Mississippi River Basin; (c) (top right) 1937, 1950, and 1938 combined storm coverage over the Mississippi River Basin; and (d) (bottom right) cool down precipitation coverage over the Mississippi River Basin.	118
Figure 2-43. Sample map of temperatures from HYPO 58A: USACE dataset developed from NOAA Archives for 1937 period.	121
Figure 2-44. Sample map of temperatures from HYPO 58A: NCRFC historical average temperatures.....	122
Figure 2-45. NCRFC computed flows for Mississippi River at Chester, IL, using two different temperature inputs; HYPO 58A unregulated flow.....	124
Figure 2-46. Depth-area curves for 1955 and 2016 individual storms composing HYPO 58A.....	132
Figure 2-47. Depth-area curves for 1955 and 2016 total HYPO 58A event.....	133
Figure 2-48. Depth-area curve for 1955 and 2015 individual storm events composing HYPO 58A over Drainage Basin 1.	133
Figure 2-49. Depth-area curve for 1955 and 2015 individual storm events composing HYPO 58A over Drainage Basin 2.	134
Figure 2-50. Depth-area curve for 1955 and 2015 individual storm events composing HYPO 58A over Drainage Basin 3.	134
Figure 2-51. Depth-area curve for 1955 and 2015 individual storm events composing HYPO 58A over Drainage Basin 4.	135
Figure 2-52. Depth-area curve for 1955 and 2015 individual storm events composing HYPO 58A over Drainage Basin 5.	135
Figure 2-53. Depth-area Curve for 1955 and 2015 individual storm events composing HYPO 58A over Drainage Basin 6.	136
Figure 2-54. Depth-area curve for 1955 and 2015 individual storm events composing HYPO 58A over Drainage Basin 7.....	136
Figure 2-55. Example of 6-hour isohyets map from 1937 storm event from HMR 34.....	138
Figure 2-56. Storm total precipitation from the January 6–24 precipitation event from MRPFs (MRC 1955).....	141
Figure 2-57. Simulated hydrograph for HYPO 58A from MRPFs (MRC 1955).	142
Figure 2-58. Original precipitation grid, 15 February 1938 at 0000 GMT.	147
Figure 2-59. Transposed precipitation grid, 15 February 1938 at 0000 GMT.	148
Figure 2-60. Original precipitation grid, 15 February 1938 at 0600 GMT.	148

Figure 2-61. Transposed precipitation grid, 15 February 1938 at 0600 GMT.....	149
Figure 2-62. Grid map of original grid, 09 May 1943 at 0600 GMT.....	150
Figure 2-63. Grid map of transformed grid, 09 May 1943 at 0600 GMT.	150
Figure 2-64. Grid map of transformed grid, 09 May 1943 at 0600 GMT, trimmed to the original watershed boundaries and grid extents.	151
Figure 2-65. Summary of percent volume difference between the transformed and original grids for the 1943 event.....	155
Figure 2-66. 2016 reservoirs modeled in current analysis.*	167
Figure 2-67. Kentucky and Barkley LMRFC and TVA routing results.....	180
Figure 2-68. Regulation flow reductions for HYPO 58A, 52A, 56, and 63 in the 1955 and 2016 hydrology studies.	185
Figure 2-69. Flow Diagram developed from 1955 Study showing 240 kcfs flow from Middle Mississippi River at Cairo, IL.....	186
Figure 2-70. HYPO 58A Hydrographs for Ohio River at Metropolis, IL: Unregulated, Regulated, and Modified Kentucky and Barkley reservoir releases.	189
Figure 2-71. Plot of Mod 1 Kentucky and Barkley Reservoir operations for HYPO 58A-R.....	191
Figure 2-72. Mod 1 regulation outflows compared to the base regulation outflows.	192
Figure 2-73. Plot of Mod 2 Kentucky and Barkley Reservoir operations for HYPO 58A-R.....	192
Figure 2-74. Mod 2 regulation outflows compared to the base regulation outflows.	193
Figure 2-75. Plot of Mod 3 Kentucky and Barkley Reservoir operations for HYPO 58A-R.....	194
Figure 2-76. Mod 3 regulation outflows compared to the base regulation outflows.	194
Figure 2-77. Plot of Mod 4 Kentucky and Barkley Reservoir operations; HYPO 58A-R.....	195
Figure 2-78. Mod 4 regulation outflows compared to the base regulation outflows.	195
Figure 2-79. Plot of Mod 5 Kentucky and Barkley Reservoir operations for HYPO 58A-R.....	196
Figure 2-80. HUC-4 drainage basins and gage locations selected for climate change analysis.	207
Figure 2-81. USGS Gage 3611500, Ohio River at Metropolis, IL, nonstationarity detection.....	208
Figure 2-82. USGS Gage 3611500, Ohio River at Metropolis, IL, stationarity trend analysis.....	209
Figure 2-83. USGS Gage 6934500, Missouri River at Hermann, MO, nonstationarity detection.....	210
Figure 2-84. USGS Gage 6934500, Missouri River at Hermann, MO, stationarity trend analysis.....	211

Figure 2-85. USGS Gage 7022000, Mississippi River at Thebes, IL, nonstationarity detection.....	212
Figure 2-86. USGS Gage 7022000, Mississippi River at Thebes, IL, stationarity trend analysis.....	213
Figure 2-87. USGS Gage 7289000, Mississippi River at Vicksburg, MS, nonstationarity detection.....	214
Figure 2-88. USGS Gage 7289000, Mississippi River at Vicksburg, MS, stationarity trend analysis.	215
Figure 2-89. USGS Gage 7374000, Mississippi River at Baton Rouge, LA, nonstationarity detection.....	216
Figure 2-90. USGS Gage 7374000, Mississippi River at Baton Rouge, LA, stationarity trend analysis.	217
Figure 2-91. Range of annual maximum monthly flow for 1111-Lower Arkansas River Basin.	218
Figure 2-92. Annual maximum monthly flow for 1111-Lower Arkansas River Basin. Trendline Equation: $Q = -25.8837 * (\text{Water Year}) + 104718$, $p = 0.04$	219
Figure 2-93. Range of annual maximum monthly flow for 1101-Upper White River Basin.....	219
Figure 2-94. Annual maximum monthly flow for 1101-Upper White River Basin. Trendline Equation: $Q = 13.1126 * (\text{Water Year}) + 53765.7$, $p = 0.44$	220
Figure 2-95. Range of annual maximum monthly flow for 0701-Mississippi River Headwaters.	220
Figure 2-96. Annual maximum monthly flow for 0701-Mississippi River Headwaters. Trendline Equation: $Q = 5.00965 * (\text{Water Year}) + 5041.06$, $p = 0.16$	221
Figure 2-97. Range of annual maximum monthly flow for 0809-Lower Mississippi River Basin.	221
Figure 2-98. Annual maximum monthly flow for 0809-Lower Mississippi River Basin. Trendline Equation: $Q = 2.35076 * (\text{Water Year}) + 32968$, $p = 0.76$	222
Figure 2-99. Range of annual maximum monthly flow for 1030-Lower Missouri River Basin.	222
Figure 2-100. Annual maximum monthly flow for 1030-Lower Missouri River Basin. Trendline Equation: $Q = 37.2536 * (\text{Water Year}) + -52125.6$, $p < 0.0001$	223
Figure 2-101. Range of annual maximum monthly flow for 0604-Lower Tennessee River Basin.....	223
Figure 2-102. Annual maximum monthly flow for 0604-Lower Tennessee River Basin. Trendline Equation: $Q = 14.876 * (\text{Water Year}) + 13754.2$, $p = 0.07$	224
Figure 2-103. Range of annual maximum monthly flow for 0513-Cumberland River Basin.	224
Figure 2-104 Annual maximum monthly flow for 0513-Cumberland River Basin. Trendline Equation: $Q = 47.6113 * (\text{Water Year}) + -52125.6$, $p = 0.002$	225
Figure 2-105. Range of annual maximum monthly flow for 0514-Lower Ohio River Basin.....	225
Figure 2-106. Annual maximum monthly flow for 0514-Lower Ohio River Basin. Trendline Equation: $Q = 47.9137 * (\text{Water Year}) + -45758.8$, $p < 0.0001$	226

Figure 2-107. Range of annual maximum monthly flow for 1114-Red Sulfur.....	226
Figure 2-108. Annual maximum monthly flow for 1114-Red Sulfur. Trendline Equation: $Q = - 6.0463 * (\text{Water Year}) + 204856$, $p = 0.003$	227
Figure 2-109. MVD business line vulnerability assessment for the wet scenario 2085 epoch.	230
Figure 2-110. MVD business line vulnerability assessment for the dry scenario 2085 epoch.	231
Figure 2-111. Summary of projected climate trends and impacts on USACE business lines for Region 05 – Ohio (USACE 2015a).	232
Figure 2-112. Summary of projected climate trends and impacts on USACE business lines for Region 06 – Tennessee (USACE 2015b).	233
Figure 2-113. Summary of projected climate trends and impacts on USACE business lines for Region 07 – Upper Mississippi (USACE 2015c).	234
Figure 2-114. Summary of projected climate trends and impacts on USACE business lines for Region 08 – Lower Mississippi (USACE 2015d).	235
Figure 2-115. Summary of projected climate trends and impacts on USACE business lines for Region 10 – Missouri River (USACE 2015e).	236
Figure 2-116. Summary of projected climate trends and impacts on USACE business lines for Region 11 – Arkansas, White, and Red Rivers (USACE 2015f).	237
Figure 3-1. HYPO storm event comparison for HYPO 52A, 56, 58A, and 63 plus the 2016 HYPO 11-73 storm for Cairo, IL, for the combined confluence flows.	241
Figure 3-2. Comparing peak flows near the Mississippi/Ohio River confluence.	244
Figure 3-3. HYPO 58A hydrographs: Missouri River at Hermann, MO.	248
Figure 3-4. HYPO 58A hydrographs: Mississippi River at St. Louis, MO.	248
Figure 3-5. HYPO 58A hydrographs: Mississippi River at Chester, IL.	249
Figure 3-6. HYPO 58A hydrographs: Big Muddy River at Murphysboro, IL.	249
Figure 3-7. HYPO 58A hydrographs: Cumberland River at Barkley Dam.	250
Figure 3-8. HYPO 58A hydrographs: Tennessee River at Kentucky Dam.	250
Figure 3-9. HYPO 58A hydrographs: Ohio River at Smithland, IL.	251
Figure 3-10. HYPO 58A hydrographs: Arkansas River at Pine Bluff, AR.	251
Figure 3-11. HYPO 58A hydrographs: Red River at Shreveport, LA.	252
Figure 3-12. HYPO 58A hydrographs: Ouachita River at Monroe, LA.	252
Figure 3-13. HYPO 58A hydrographs: Red River at Alexandria, LA.	253
Figure 3-14. HYPO 58A hydrographs: Fulton, LA.	253
Figure 3-15. Alexandria, LA, HYPO 58A 1955 unregulated flow compared to 2016 unregulated flow generated by the RFC.	255
Figure 3-16. Alton, IL, HYPO 58A 1955 unregulated flow compared to 2016 unregulated flow generated by the RFC.	256
Figure 3-17. Hermann, MO, HYPO 58A 1955 unregulated flow compared to 2016 unregulated flow generated by the RFC.	256
Figure 3-18. Little Rock, AR, HYPO 58A 1955 unregulated flow compared to 2016 unregulated flow generated by the RFC.	257

Figure 3-19. St. Louis, MO, HYPO 58A 1955 unregulated and regulated flow compared to 2016 unregulated and regulated flow generated by the RFC.....	257
Figure 3-20. Arkansas City, AR, HYPO 58A 1955 and 2016 regulated and unregulated flow compared to the 2016 regulated historic HEC-RAS results.*	258
Figure 3-21. Cairo, IL, HYPO 58A 1955 and 2016 regulated and unregulated flow compared to the 2016 regulated historic HEC-RAS results.	259
Figure 3-22. Clarendon, AR, HYPO 58A 1955 and 2016 regulated and unregulated flow compared to the 2016 regulated historic HEC-RAS results.*	259
Figure 3-23. Metropolis, IL, HYPO 58A 1955 and 2016 regulated and unregulated flow compared to the 2016 regulated historic HEC-RAS results.	260
Figure 3-24. Latitude of Red River Landing, LA, HYPO 58A 1955 and 2016 regulated and unregulated flow compared to the 2016 regulated historic HEC-RAS results.*	260
Figure 3-25. HYPO 58A HEC-RAS hydrograph: Ohio River at Cairo, IL.....	261
Figure 3-26. HYPO 58A HEC-RAS hydrograph: Combined Ohio and Mississippi River flow near Cairo, IL.	261
Figure 3-27. HYPO 58A HEC-RAS hydrograph: Mississippi River at Hickman, KY.	262
Figure 3-28. HYPO 58A HEC-RAS hydrograph: Mississippi River at Memphis, TN.	262
Figure 3-29. HYPO 58A HEC-RAS hydrograph: Mississippi River at Helena, AR.	263
Figure 3-30. HYPO 58A HEC-RAS hydrograph: Mississippi River at Arkansas City, AR.....	263
Figure 3-31. HYPO 58A HEC-RAS hydrograph: Mississippi River at Greenville, MS.....	264
Figure 3-32. HYPO 58A HEC-RAS hydrograph: Mississippi River at Lake Providence, LA.	264
Figure 3-33. HYPO 58A HEC-RAS hydrograph: Mississippi River at Vicksburg, MS.....	265
Figure 3-34. HYPO 58A HEC-RAS hydrograph: Mississippi River at Natchez, MS.	265
Figure 3-35. HYPO 58A HEC-RAS hydrograph: Mississippi River at Red River Landing, LA.....	266
Figure 3-36. HYPO 58A HEC-RAS hydrograph: Mississippi River at Baton Rouge, LA.	266
Figure 3-37. HYPO 58A HEC-RAS hydrograph: Mississippi River at Donaldsonville, LA.	267
Figure 3-38. HYPO 58A HEC-RAS hydrograph: Mississippi River at Carrollton, LA.	267
Figure 3-39. HYPO 58A HEC-RAS hydrograph: Mississippi River at Empire, LA.....	268
Figure 3-40. HYPO 58A HEC-RAS hydrograph: Mississippi River at Venice, LA.....	268
Figure B-1. HYPO 58A local input at Acme, LA.	283
Figure B-2. HYPO 58A local input at Arkansas City, AR.....	284
Figure B-3. HYPO 58A local input at Arlington, TN.	284
Figure B-4. HYPO 58A local input at Barbre Landing, LA.....	285
Figure B-5. HYPO 58A local input at Baton Rouge, LA.....	285
Figure B-6. HYPO 58A local input at Belzoni, MS.....	286
Figure B-7. HYPO 58A local input at Bogota, TN.....	286

Figure B-8. HYPO 58A local input at Bolivar, TN.....	287
Figure B-9. HYPO 58A local input at Brunswick, TN.....	287
Figure B-10. HYPO 58A local input at Cairo, IL.....	288
Figure B-11. HYPO 58A local input at Cape Girardeau, MO.....	288
Figure B-12. HYPO 58A local input at Chester, MO.....	289
Figure B-13. HYPO 58A local input at Clarendon, AR.....	289
Figure B-14. HYPO 58A local input at Clayton, MS.....	290
Figure B-15. HYPO 58A local input at Columbia Lock and Dam, LA.....	290
Figure B-16. HYPO 58A local input at Des Arc, AR.....	291
Figure B-17. HYPO 58A local input at Dyersburg, TN.....	291
Figure B-18. HYPO 58A local input at Georgetown, AR.....	292
Figure B-19. HYPO 58A local input at Germantown, TN.....	292
Figure B-20. HYPO 58A local input at Greenwood, MS.....	293
Figure B-21. HYPO 58A local input at Greer's Ferry Dam, AR.....	293
Figure B-22. HYPO 58A local input at Grenada Dam, MS.....	294
Figure B-23. HYPO 58A local input at Halls, TN.....	294
Figure B-24. HYPO 58A local input at Helena, AR.....	295
Figure B-25. HYPO 58A local input at Jonesville, MS.....	295
Figure B-26. HYPO 58A local input at Kenton, TN.....	296
Figure B-27. HYPO 58A local input at Kentucky Dam, KY.....	296
Figure B-28. HYPO 58A local input at Madison, AR.....	297
Figure B-29. HYPO 58A local input at Memphis, TN.....	297
Figure B-30. HYPO 58A local input at Murphysboro, IL.....	298
Figure B-31. HYPO 58A local input at Natchez, MS.....	298
Figure B-32. HYPO 58A local input at New Madrid, MO.....	299
Figure B-33. HYPO 58A local input at Newport, AR.....	299
Figure B-34. HYPO 58A local input at Obion, TN.....	300
Figure B-35. HYPO 58A local input at Obion, TN, at the Mississippi River confluence.....	300
Figure B-36. HYPO 58A local input at Owl City, TN.....	301
Figure B-37. HYPO 58A local input at Paducah, KY.....	301
Figure B-38. HYPO 58A local input at Parkin, AR.....	302
Figure B-39. HYPO 58A local input at Patterson, AR.....	302
Figure B-40. HYPO 58A local input at Pendleton, AR.....	303
Figure B-41. HYPO 58A local input at Rochelle, LA.....	303
Figure B-42. HYPO 58A local input at Rosetta, MS.....	304
Figure B-43. HYPO 58A local input at Simmesport, LA.....	304
Figure B-44. HYPO 58A local input at Smithland Lock and Dam, IL.....	305
Figure B-45. HYPO 58A local input at Vicksburg, MS.....	305
Figure B-46. HYPO 58A local input at Whitehall, LA.....	306

Figure B-47. HYPO 58A local input at Wichliffe, KY.	306
Figure B-48. HYPO 58A local input at Willows, MS.	307
Figure B-49. HYPO 58A local input at Woodville, MS.....	307
Figure B-50. HYPO 58A local input at Yazoo City, MS.	308
Figure B-51. HYPO 58A routed through Clinton Dam - ~3 days from Hermann, MO.....	309
Figure B-52. HYPO 58A routed through Glen Elder Dam - ~8 days from Hermann, MO.....	310
Figure B-53. HYPO 58A routed through Hillsdale Dam - ~3-4 days from Hermann, MO.....	310
Figure B-54. HYPO 58A routed through Kanopolis Dam - ~9 days from Hermann, MO.....	311
Figure B-55. HYPO 58A routed through Melvern Dam - ~4 days from Hermann, MO.....	311
Figure B-56. HYPO 58A routed through Milford Dam - ~6 days from Hermann, MO.....	312
Figure B-57. HYPO 58A routed through Perry Dam - ~4 days from Hermann, MO.	312
Figure B-58. HYPO 58A routed through Pomme De Terre Dam - ~3 days from Hermann, MO.....	313
Figure B-59. HYPO 58A routed through Pomona Dam - ~4 days from Hermann, MO.....	313
Figure B-60. HYPO 58A routed through Rathbun Dam - ~4 days from Hermann, MO.....	314
Figure B-61. HYPO 58A routed through Smithville Dam - ~3 days from Hermann, MO.....	314
Figure B-62. HYPO 58A routed through Stockton Dam - ~3-4 days from Hermann, MO.....	315
Figure B-63. HYPO 58A routed through Truman Dam - ~2-3 days from Hermann, MO.....	315
Figure B-64. HYPO 58A routed through Tuttle Creek Dam - ~5 days from Hermann, MO.....	316
Figure B-65. HYPO 58A routed through Wilson Dam - ~9 days from Hermann, MO.....	316
Figure B-66. HYPO 58A routed through Big Bend Dam - 11+ days from Hermann, MO.....	317
Figure B-67. HYPO 58A routed through Fort Peck Dam - 11+ days from Hermann, MO.....	318
Figure B-68. HYPO 58A routed through Fort Randall Dam - 11+ days from Hermann, MO.....	318
Figure B-69. HYPO 58A routed through Garrison Dam - 11+ days from Hermann, MO.....	319
Figure B-70. HYPO 58A routed through Gavins Point Dam - 11+ days from Hermann, MO.....	319
Figure B-71. HYPO 58A routed through Oahe Dam - 11+ days from Hermann, MO.	320

Figure B-72. HYPO 58A routed through Coralville Dam.....	321
Figure B-73. HYPO 58A routed through Red Rock Dam.....	321
Figure B-74. HYPO 58A routed through Saylorville Dam.	322
Figure B-75. HYPO 58A routed through Arkabutla Dam - ~13 days from Vicksburg, MS.	323
Figure B-76. HYPO 58A routed through Bayou Bodcau Dam - ~6 days from Alexandria, LA.	324
Figure B-77. HYPO 58A routed through Blakely Mountain Dam - ~20+ days from the Mississippi River.....	324
Figure B-78. HYPO 58A routed through Degray Dam - ~20+ days from the Mississippi River.	325
Figure B-79. HYPO 58A routed through Enid Dam - ~12 days from Vicksburg, MS.	325
Figure B-80. HYPO 58A routed through Grenada Dam - ~8 days from Vicksburg, MS.	326
Figure B-81. HYPO 58A routed through Caddo Dam - ~6 days from Alexandria, LA.	326
Figure B-82. HYPO 58A routed through Narrows Dam - ~20+ days from the Mississippi River.	327
Figure B-83. HYPO 58A routed through Sardis Dam - ~12 days from Vicksburg, MS.	327
Figure B-84. HYPO 58A routed through Wallace Lake Dam - ~5 days from Alexandria, LA.	328
Figure B-85. HYPO 58A routed through Barren River Lake - ~11 days from Cairo, IL.....	329
Figure B-86. HYPO 58A routed through Cagles Mill Lake - ~13 days from Cairo, IL.....	329
Figure B-87. HYPO 58A routed through CM Harden Lake - ~14 days from Cairo, IL.....	330
Figure B-88. HYPO 58A routed through Green River Lake - ~13 days from Cairo, IL.....	330
Figure B-89. HYPO 58A routed through J. E. Roush Lake - ~16+ days from Cairo, IL.....	331
Figure B-90. HYPO 58A routed through Mississinewa Lake - ~15 days from Cairo, IL.....	331
Figure B-91. HYPO 58A routed through Monroe Lake - ~12 days from Cairo, IL.	332
Figure B-92. HYPO 58A routed through Nolin River Lake - ~10 days from Cairo, IL.....	332
Figure B-93. HYPO 58A routed through Patoka Lake - ~10 days from Cairo, IL.	333
Figure B-94. HYPO 58A routed through Rough River Lake - ~9 days from Cairo, IL.	333
Figure B-95. HYPO 58A routed through Salamonie Lake ~15 days from Cairo, IL.	334
Figure B-96. HYPO 58A routed through Barkley Dam - ~2 days from Cairo, IL.	335
Figure B-97. HYPO 58A routed through Center Hill Dam - ~7 days from Cairo, IL.....	335
Figure B-98. HYPO 58A routed through Cheatham Dam - ~5 days from Cairo, IL.....	336
Figure B-99. HYPO 58A routed through Cordell Hull Dam - ~7 days from Cairo, IL.	336
Figure B-100. HYPO 58A routed through Dale Hollow Dam - ~8 days from Cairo, IL.....	337

Figure B-101. HYPO 58A routed through Great Falls - ~7 days from Cairo, IL.	337
Figure B-102. HYPO 58A routed through J. Percy Priest Dam - ~6 days from Cairo, IL.....	338
Figure B-103. HYPO 58A routed through Kentucky Dam - ~1 days from Cairo, IL.	338
Figure B-104. HYPO 58A routed through Old Hickory Dam - ~6 days from Cairo, IL.....	339
Figure B-105. HYPO 58A routed through Wolf Creek Dam - ~8 days from Cairo, IL.....	339
Figure B-106. HYPO 58A routed through Fort Gibson Dam - ~4 days from Pine Bluff, AR.....	340
Figure B-107. HYPO 58A routed through Hugo Dam - ~13 days from Alexandria, LA.	341
Figure B-108. HYPO 58A routed through Keystone Lake - ~5 days from Pine Bluff, AR.....	341
Figure B-109. HYPO 58A routed through Lake Texoma - ~14 days from Alexandria, LA.	342
Figure B-110. HYPO 58A routed through Oologah Lake - ~6 days from Pine Bluff, AR.....	342
Figure B-111. HYPO 58A routed through Skiatook Lake - ~6 days from Pine Bluff, AR.....	343
Figure B-112. HYPO 58A routed through Tenkiller Lake - ~3 days from Pine Bluff, AR.....	343
Figure B-113. HYPO 58A routed through Heyburn Dam - ~3 days from Pine Bluff, AR.....	344
Figure B-114. HYPO 58A routed through Bull Shoals Dam - ~7 days from Clarendon, AR.	345
Figure B-115. HYPO 58A routed through Greers Ferry Dam - ~4 days from Clarendon, AR.	345
Figure B-116. HYPO 58A routed through Norfolk Dam - ~7 days from Clarendon, AR.....	346
Figure B-117. HYPO 58A routed through Carlyle Lake Dam - ~2 days from Chester, IL.....	347
Figure B-118. HYPO 58A routed through Lake Shelbyville Dam - ~5 days from Chester, IL.....	347
Figure B-119. HYPO 58A routed through Mark Twain Lake - ~2 days from Hermann, MO.....	348
Figure B-120. HYPO 58A routed through Wappapello Lake - ~18 days from the confluence of the Saint Francis and Mississippi Rivers.	348
Figure C-5. Depth-area curves for 1955 and 2016 individual storms comprising HYPO 52A.....	356
Figure C-6. Depth-area curves for 1955 and 2016 total HYPO 52A event.....	356
Figure C-7. Depth-area curve for 1955 and 2015 individual storm events comprising HYPO 52A over Drainage Basin 1.	357
Figure C-8. Depth-area curve for 1955 and 2015 individual storm events comprising HYPO 52A over Drainage Basin 2.	357

Figure C-9. Depth-area curve for 1955 and 2015 individual storm events comprising HYPO 52A over Drainage Basin 3.....	358
Figure C-10. Depth-area curve for 1955 and 2015 individual storm events comprising HYPO 52A over Drainage Basin 4.....	358
Figure C-11. Depth-Area Curve for 1955 and 2015 individual storm events comprising HYPO 52A over Drainage Basin 5.....	359
Figure C-12. Depth-area curve for 1955 and 2015 individual storm events comprising HYPO 52A over Drainage Basin 7.....	359
Figure C-13. HYPO 52A hydrographs: Missouri River at Hermann, MO.....	362
Figure C-14. HYPO 52A hydrographs: Mississippi River at Alton, IL.....	363
Figure C-15. HYPO 52A hydrographs: Mississippi River at St. Louis, MO.....	363
Figure C-16. HYPO 52A hydrographs: Mississippi River at Chester, IL.....	364
Figure C-17. HYPO 52A hydrographs: Big Muddy River at Murphysboro, IL.....	364
Figure C-18. HYPO 52A hydrographs: Cumberland River at Barkley Dam.....	365
Figure C-19. HYPO 52A hydrographs: Tennessee River at Kentucky Dam.....	365
Figure C-20. HYPO 52A hydrographs: Ohio River at Smithland, IL.....	366
Figure C-21. HYPO 52A hydrographs: Arkansas River at Pine Bluff, AR.....	366
Figure C-22. HYPO 52A hydrographs: Shreveport, LA.....	367
Figure C-23. HYPO 52A hydrographs: Monroe, LA.....	367
Figure C-24. HYPO 52A hydrographs: Alexandria, LA.....	368
Figure C-25. HYPO 52A hydrographs: Fulton, LA.....	368
Figure C-26. Alexandria, LA, HYPO 52A 1955 unregulated flow compared to 2016 unregulated flow generated by the RFC.....	370
Figure C-27. Alton, IL, HYPO 52A 1955 unregulated flow compared to 2016 unregulated flow generated by the RFC.....	371
Figure C-28. Hermann, MO, HYPO 52A 1955 unregulated flow compared to 2016 unregulated flow generated by the RFC.....	371
Figure C-29. Little Rock, AR, HYPO 52A 1955 unregulated flow compared to 2016 unregulated flow generated by the RFC.....	372
Figure C-30. Arkansas City, AR, HYPO 52A 1955 unregulated flow compared to 2016 unregulated flow generated by the RFC.....	372
Figure C-31. Cairo, IL, HYPO 52A 1955 unregulated flow compared to 2016 unregulated flow generated by the RFC.....	373
Figure C-32. Clarendon, AR, HYPO 52A 1955 unregulated flow compared to 2016 unregulated flow generated by the RFC.....	373
Figure C-33. Metropolis, IL, HYPO 52A 1955 unregulated flow compared to 2016 unregulated flow generated by the RFC.....	374
Figure C-34. St. Louis, MO, HYPO 52A 1955 unregulated flow compared to 2016 unregulated flow generated by the RFC.....	374
Figure C-35. Red River Landing, LA, HYPO 52A 1955 unregulated flow compared to 2016 unregulated flow generated by the RFC.....	375
Figure C-36. Barkley Dam HYPO 52A inflow compared to outflow.....	376
Figure C-37. Center Hill Dam HYPO 52A inflow compared to outflow.....	376

Figure C-38. Cheatham Hill Dam HYPO 52A inflow compared to outflow.	377
Figure C-39 . Cordell Hull Dam HYPO 52A inflow compared to outflow.	377
Figure C-40. Dale Hollow Dam HYPO 52A inflow compared to outflow.	378
Figure C-41. Great Falls HYPO 52A inflow compared to outflow.	378
Figure C-42. J. Percy Priest Dam HYPO 52A inflow compared to outflow.	379
Figure C-43. Kentucky Dam HYPO 52A inflow compared to outflow.	379
Figure C-44. Old Hickory Dam HYPO 52A inflow compared to outflow.	380
Figure C-45. Wolf Creek Dam HYPO 52A inflow compared to outflow.	380
Figure D-1. HYPO 56 – 13–26 March 1913 (a) (top left) storm coverage over the Mississippi River Basin; (b) (bottom left) isohyetal for unadjusted March 1913 storm; (c) (top right) comparison of mass rainfall curves for original point precipitation data versus the processed/interpolated precipitation data for the unadjusted storm; and (d) (bottom right) comparison of 1955 precipitation, 2016 precipitation, and 2016 post-processed precipitation at select locations.	382
Figure D-2. HYPO 56 – 12–16 April 1927 (a) (top left) storm coverage over the Mississippi River Basin; (b) (bottom left) isohyetal for unadjusted April 1927 storm; (c) (top right) comparison of mass rainfall curves for original point precipitation data versus the processed/interpolated precipitation data for the unadjusted storm; and (d) (bottom right) comparison of 1955 precipitation, 2016 precipitation, and 2016 post-processed precipitation at select location.	383
Figure D-3. Corrected 12–16 April 1927 (a) (top left) storm coverage over the Mississippi River Basin; (b) (bottom left) isohyetal for unadjusted April 1927 storm; (c) (top right) comparison of mass rainfall curves for original point precipitation data versus the processed/interpolated precipitation data for the unadjusted storm; and (d) (bottom right) comparison of 1955 precipitation, 2016 precipitation, and 2016 post-processed precipitation at select location.	384
Figure D-4. HYPO 56 (a) (top left) storm sequencing with warm-up and recession periods; (b) (bottom left) warm-up precipitation coverage over the Mississippi River Basin; (c) (top right) 1927 and 1913 combined storm coverage over the Mississippi River Basin; and (d) (bottom right) recession precipitation coverage over the Mississippi River Basin.	385
Figure D-5. Depth-area curves for 1955 and 2016 individual storms comprising HYPO 56.	387
Figure D-6. Depth-area curves for 1955 and 2016 total HYPO 56 event.	387
Figure D-7. Depth-area curve for 1955 and 2015 individual storm events comprising HYPO 56 over Drainage Basin 1.	388
Figure D-8. Depth-area curve for 1955 and 2015 individual storm events comprising HYPO 56 over Drainage Basin 2.	388
Figure D-9. Depth-area curve for 1955 and 2015 individual storm events comprising HYPO 56 over Drainage Basin 3.	389
Figure D-10. Depth-area curve for 1955 and 2015 individual storm events comprising HYPO 56 over Drainage Basin 4.	389
Figure D-11. Depth-area curve for 1955 and 2015 individual storm events comprising HYPO 56 over Drainage Basin 5.	390
Figure D-12. Depth-area curve for 1955 and 2015 individual storm events comprising HYPO 56 over Drainage Basin 6.	390

Figure D-13. Depth-area curve for 1955 and 2015 individual storm events comprising HYPO 56 over Drainage Basin 7.....	391
Figure D-14. HYPO 56 hydrographs: Missouri River at Hermann, MO.....	393
Figure D-15. HYPO 56 hydrographs: Mississippi River at Alton, IL.....	394
Figure D-16. HYPO 56 hydrographs: Mississippi River at St. Louis, MO.....	394
Figure D-17. HYPO 56 hydrographs: Mississippi River at Chester, IL.....	395
Figure D-18. HYPO 56 hydrographs: Big Muddy River at Murphysboro, IL.....	395
Figure D-19. HYPO 56 hydrographs: Cumberland River at Barkley Dam.....	396
Figure D-20. HYPO 56 hydrographs: Tennessee River at Kentucky Dam.....	396
Figure D-21. HYPO 56 hydrographs: Ohio River at Smithland, IL.....	397
Figure D-22. HYPO 56 hydrographs: Arkansas River at Pine Bluff, AR.....	397
Figure D-23. HYPO 56 hydrographs: Shreveport, LA.....	398
Figure D-24. HYPO 56 hydrographs: Monroe, LA.....	398
Figure D-25. HYPO 56 hydrographs: Alexandria, LA.....	399
Figure D-26. HYPO 56 hydrographs: Fulton, LA.....	399
Figure D-26. Alexandria, LA, HYPO 56 1955 unregulated flow compared to 2016 unregulated flow generated by the RFC.....	401
Figure D-27. Alton, IL, HYPO 56 1955 unregulated flow compared to 2016 unregulated flow generated by the RFC.....	402
Figure D-28. Hermann, MO, HYPO 56 1955 unregulated flow compared to 2016 unregulated flow generated by the RFC.....	402
Figure D-29. Little Rock, AR, HYPO 56 1955 unregulated flow compared to 2016 unregulated flow generated by the RFC.....	403
Figure D-30. St. Louis, MO, HYPO 56 1955 unregulated flow compared to 2016 unregulated flow generated by the RFC.....	403
Figure D-31. Arkansas City, AR, HYPO 56 1955 unregulated flow compared to 2016 unregulated flow generated by the RFC.....	404
Figure D-32. Cairo, IL, HYPO 56 1955 unregulated flow compared to 2016 unregulated flow generated by the RFC.....	404
Figure D-33. Clarendon, AR, HYPO 56 1955 unregulated flow compared to 2016 unregulated flow generated by the RFC.....	405
Figure D-34. Metropolis, IL, HYPO 56 1955 unregulated flow compared to 2016 unregulated flow generated by the RFC.....	405
Figure D-35. Latitude of Red River Landing, LA, HYPO 56 1955 unregulated flow compared to 2016 unregulated flow generated by the RFC.....	406
Figure D-36. HYPO 56 HEC-RAS hydrograph: Ohio River at Cairo, IL.....	407
Figure D-37. HYPO 56 HEC-RAS hydrograph: Combined Ohio and Mississippi River flow near Cairo, IL.....	407
Figure D-38. HYPO 56 HEC-RAS hydrograph: Mississippi River at Hickman, KY.....	408
Figure D-39. HYPO 56 HEC-RAS hydrograph: Mississippi River at Memphis, TN.....	408
Figure D-40. HYPO 56 HEC-RAS hydrograph: Mississippi River at Helena, AR.....	409

Figure D-41. HYPO 56 HEC-RAS hydrograph: Mississippi River at Arkansas City, AR.*	409
Figure D-42. HYPO 56 HEC-RAS hydrograph: Mississippi River at Greenville, MS.	410
Figure D-43. HYPO 56 HEC-RAS hydrograph: Mississippi River at Lake Providence, LA.*	410
Figure D-44. HYPO 56 HEC-RAS hydrograph: Mississippi River at Vicksburg, MS.....	411
Figure D-45. HYPO 56 HEC-RAS hydrograph: Mississippi River at Natchez, MS.	411
Figure D-46. HYPO 56 HEC-RAS hydrograph: Mississippi River at Red River Landing, LA.....	412
Figure D-47. HYPO 56 HEC-RAS hydrograph: Mississippi River at Baton Rouge, LA.	412
Figure D-48. HYPO 56 HEC-RAS hydrograph: Mississippi River at Donaldsonville, LA.	413
Figure D-49. HYPO 56 HEC-RAS hydrograph: Mississippi River at Carrollton, LA.	413
Figure D-50. HYPO 56 HEC-RAS hydrograph: Mississippi River at Empire, LA.....	414
Figure D-51. HYPO 56 HEC-RAS hydrograph: Mississippi River at Venice, LA.....	414
Figure D-52. Barren River Lake HYPO 56 inflow compared to outflow.	415
Figure D-53. Cagles Mill Lake HYPO 56 inflow compared to outflow.	416
Figure D-54. CM Harden Lake HYPO 56 inflow compared to outflow.	416
Figure D-55. Green River Lake HYPO 56 inflow compared to outflow.	417
Figure D-56. Je Roush Lake HYPO 56 inflow compared to outflow.....	417
Figure D-57. Mississinewa Lake HYPO 56 inflow compared to outflow.	418
Figure D-58. Monroe Lake HYPO 56 inflow compared to outflow.	418
Figure D-59. Nolin River Lake HYPO 56 inflow compared to outflow.	419
Figure D-60. Patoka Lake HYPO 56 inflow compared to outflow.....	419
Figure D-61. Rough River HYPO 56 inflow compared to outflow.	420
Figure D-62. Salamonie Lake HYPO 56 inflow compared to outflow.	420
Figure D-63. Barkley Dam HYPO 56 inflow compared to outflow.....	421
Figure D-64. Center Hill Dam HYPO 56 inflow compared to outflow.....	421
Figure D-65. Cheatham Hill Dam HYPO 56 inflow compared to outflow.	422
Figure D-66. Cordell Hull Dam HYPO 56 inflow compared to outflow.....	422
Figure D-67. Dale Hollow Dam HYPO 56 inflow compared to outflow.....	423
Figure D-68. Great Falls HYPO 56 inflow compared to outflow.	423
Figure D-69. J. Percy Priest Dam HYPO 56 inflow compared to outflow.	424
Figure D-70. Kentucky Dam HYPO 56 inflow compared to outflow.....	424
Figure D-71. Old Hickory Dam HYPO 56 inflow compared to outflow.	425
Figure D-72. Wolf Creek Dam HYPO 56 inflow compared to outflow.....	425
Figure D-73. Arkabutla Dam HYPO 56 inflow compared to outflow.	426
Figure D-74. Sardis Dam HYPO 56 inflow compared to outflow.	426
Figure D-75. Enid Dam HYPO 56 inflow compared to outflow.....	427
Figure D-76. Grenada Dam HYPO 56 inflow compared to outflow.....	427

Figure D-77. Bayou Bodcau Dam HYPO 56 inflow compared to outflow.	428
Figure D-78. Caddo Dam HYPO 56 inflow compared to outflow.	428
Figure D-79. Wallace Lake dam HYPO 56 inflow compared to outflow.	429
Figure D-80. Narrows Dam HYPO 56 inflow compared to outflow.	429
Figure D-81. Degray Dam HYPO 56 inflow compared to outflow.....	430
Figure D-82. Blakely Mountain Dam HYPO 56 inflow compared to outflow.....	430
Figure D-83. Coralville Dam HYPO 56 inflow compared to outflow.....	431
Figure D-84. Saylorville Dam HYPO 56 inflow compared to outflow.	431
Figure D-85. Carlyle Lake Dam HYPO 56 inflow compared to outflow.....	432
Figure D-86. Lake Shelbyville Dam HYPO 56 inflow compared to outflow.	432
Figure D-87. Mark Twain Lake HYPO 56 inflow compared to outflow.....	433
Figure D-88. Wappapello Lake Dam HYPO 56 inflow compared to outflow.....	433
Figure D-89. Big Bend DAM HYPO 56 inflow compared to outflow.	434
Figure D-90. Fort Peck Dam HYPO 56 inflow compared to outflow.	434
Figure D-91. Fort Randall Dam HYPO 56 inflow compared to outflow.....	435
Figure D-92. Garrison Dam HYPO 56 inflow compared to outflow.....	435
Figure D-93. Gavin's Point Dam HYPO 56 inflow compared to outflow.	436
Figure D-94. Oahe Dam HYPO 56 inflow compared to outflow.	436
Figure D-95. Clinton Dam HYPO 56 inflow compared to outflow.....	437
Figure D-96. Glen Elder Dam HYPO 56 inflow compared to outflow.....	437
Figure D-97. Hillsdale Dam HYPO 56 inflow compared to outflow.....	438
Figure D-98. Kanopolis Dam HYPO 56 inflow compared to outflow.	438
Figure D-99. Melvern Dam HYPO 56 inflow compared to outflow.....	439
Figure D-100. Milford Dam HYPO 56 inflow compared to outflow.	439
Figure D-101. Perry Dam HYPO 56 inflow compared to outflow.....	440
Figure D-102. Pomme De Terre Dam HYPO 56 inflow compared to outflow.....	440
Figure D-103. Pomona Dam HYPO 56 inflow compared to outflow.	441
Figure D-104. Rathbun Dam HYPO 56 inflow compared to outflow.	441
Figure D-105. Smithville Dam HYPO 56 inflow compared to outflow.	442
Figure D-106. Stockton Dam HYPO 56 inflow compared to outflow.	442
Figure D-107. Truman Dam HYPO 56 inflow compared to outflow.....	443
Figure D-108. Tuttle Creek Dam HYPO 56 inflow compared to outflow.....	443
Figure D-109. Wilson Dam HYPO 56 inflow compared to outflow.....	444
Figure D-110. Bull Shoals Dam HYPO 56 inflow compared to outflow.	444
Figure D-111. Greer's Ferry Dam HYPO 56 inflow compared to outflow.	445
Figure D-112. Norfolk Dam HYPO 56 inflow compared to outflow.	445
Figure D-113. Fort Gibson Dam HYPO 56 inflow compared to outflow.	446
Figure D-114. Hugo Dam HYPO 56 inflow compared to outflow.	446
Figure D-115. Keystone Lake HYPO 56 inflow compared to outflow.	447

Figure D-116. Lake Texoma HYPO 56 inflow compared to outflow.	447
Figure D-117. Oologah Lake HYPO 56 inflow compared to outflow.....	448
Figure D-118. Skiatook Lake HYPO 56 inflow compared to outflow.	448
Figure D-119. Tenkiller Lake HYPO 56 inflow compared to outflow.....	449
Figure D-120. Wister Lake HYPO 56 inflow compared to outflow.	449
Figure E-1. HYPO 63 – 12–16 April 1927 (a) (top left) storm coverage over the Mississippi River Basin; (b) (bottom left) isohyetal for unadjusted April 1927 storm; (c) (top right) comparison of mass rainfall curves for original point precipitation data versus the processed/interpolated precipitation data for the unadjusted storm; and (d) (bottom right) comparison of 1955 precipitation, 2016 precipitation, and 2016 post-processed precipitation at select location.	451
Figure E-2. Corrected 12–16 April 1927 (a) (top left) storm coverage over the Mississippi River Basin; (b) (bottom left) isohyetal for unadjusted April 1927 storm; (c) (top right) comparison of mass rainfall curves for original point precipitation data versus the processed/interpolated precipitation data for the unadjusted storm; and (d) (bottom right) comparison of 1955 precipitation, 2016 precipitation, and 2016 post-processed precipitation at select location.	452
Figure E-3. HYPO 63 – 15–20 May 1943 (a) (top left) storm coverage over the Mississippi River Basin; (b) (bottom left) isohyetal for storm; (c) (top right) comparison of mass rainfall curves for original point precipitation data versus the processed/ interpolated precipitation data; and (d) (bottom right) comparison of 1955 precipitation, 2016 precipitation, and 2016 processed precipitation.	453
Figure E-4. HYPO 63 – 7–12 May 1943 (a) (top left) storm coverage over the Mississippi River Basin; (b) (bottom left) isohyetal for storm; (c) (top right) comparison of mass rainfall curves for original point precipitation data versus the processed/ interpolated precipitation data; and (d) (bottom right) comparison of 1955 precipitation, 2016 precipitation, and 2016 processed precipitation.	454
Figure E-5. HYPO 63 (a) (top left) storm sequencing with warm-up and recession periods; (b) (bottom left) warm-up precipitation coverage over the Mississippi River Basin; (c) (top right) 1943 AND 1927 combined storm coverage over the Mississippi River Basin; and (d) (bottom right) recession precipitation coverage over the Mississippi River Basin.	455
Figure E-6. Depth-area curves for 1955 and 2016 individual storms comprising HYPO 63.	457
Figure E-7. Depth-area curves for 1955 and 2016 total HYPO 63 event.	458
Figure E-8. Depth-area curve for 1955 and 2015 individual storm events comprising HYPO 63 over Drainage Basin 1.	458
Figure E-9. Depth-area curve for 1955 and 2015 individual storm events comprising HYPO 63 over Drainage Basin 2.	459
Figure E-10. Depth-area curve for 1955 and 2015 individual storm events comprising HYPO 63 over Drainage Basin 3.	459
Figure E-11. Depth-area curve for 1955 and 2015 individual storm events comprising HYPO 63 over Drainage Basin 4.	460
Figure E-12. Depth-area curve for 1955 and 2015 individual storm events comprising HYPO 63 over Drainage Basin 5.	460

Figure E-13. Depth-area curve for 1955 and 2015 individual storm events comprising HYPO 63 over Drainage Basin 6.	461
Figure E-14. Depth-area curve for 1955 and 2015 individual storm events comprising HYPO 63 over Drainage Basin 7.	461
Figure E-15. HYPO 63 hydrographs: Missouri River at Hermann, MO.	464
Figure E-16. HYPO 63 hydrographs: Mississippi River at Alton, IL.	465
Figure E-17. HYPO 63 hydrographs: Mississippi River at St. Louis, MO.	465
Figure E-18. HYPO 63 hydrographs: Mississippi River at Chester, IL.	466
Figure E-19. HYPO 63 hydrographs: Big Muddy River at Murphysboro, IL.	466
Figure E-20. HYPO 63 hydrographs: Cumberland River at Barkley Dam.	467
Figure E-21. HYPO 63 hydrographs: Tennessee River at Kentucky Dam.	467
Figure E-22. HYPO 63 hydrographs: Ohio River at Smithland, IL.	468
Figure E-23. HYPO 63 hydrographs: Arkansas River at Pine Bluff, AR.	468
Figure E-24. HYPO 63 hydrographs: Shreveport, LA.	469
Figure E-25. HYPO 63 hydrographs: Monroe, LA.	469
Figure E-26. HYPO 63 hydrographs: Alexandria, LA.	470
Figure E-27. HYPO 63 hydrographs: Fulton, LA.	470
Figure E-28. Alexandria, LA, HYPO 63 1955 unregulated flow compared to 2016 unregulated flow generated by the RFC.	472
Figure E-29. Alton, IL, HYPO 63 1955 unregulated flow compared to 2016 unregulated flow generated by the RFC.	473
Figure E-30. Hermann, MO, HYPO 63 1955 unregulated flow compared to 2016 unregulated flow generated by the RFC.	473
Figure E-31. Little Rock, AK, HYPO 63 1955 unregulated flow compared to 2016 unregulated flow generated by the RFC.	474
Figure E-32. Arkansas City, AR, HYPO 63 1955 unregulated flow compared to 2016 unregulated flow generated by the RFC.	474
Figure E-33. Cairo, IL, HYPO 63 1955 unregulated flow compared to 2016 unregulated flow generated by the RFC.	475
Figure E-34. Clarendon, AR, HYPO 63 1955 unregulated flow compared to 2016 unregulated flow generated by the RFC.	475
Figure E-35. Metropolis, IL, HYPO 63 1955 unregulated flow compared to 2016 unregulated flow generated by the RFC.	476
Figure E-36. St. Louis, MO, HYPO 63 1955 unregulated flow compared to 2016 unregulated flow generated by the RFC.	476
Figure E-37. Red River Landing, LA, HYPO 63 1955 unregulated flow compared to 2016 unregulated flow generated by the RFC.	477
Figure E-38. HYPO 63 HEC-RAS hydrograph: Ohio River at Cairo, IL.	478
Figure E-39. HYPO 63 HEC-RAS hydrograph: Combined Ohio and Mississippi River flow near Cairo, IL.	478
Figure E-40. HYPO 63 HEC-RAS hydrograph: Mississippi River at Hickman, KY.	479
Figure E-41. HYPO 63 HEC-RAS hydrograph: Mississippi River at Memphis, TN.	479

Figure E-42. HYPO 63 HEC-RAS hydrograph: Mississippi River at Helena, AR.....	480
Figure E-43. HYPO 63 HEC-RAS hydrograph: Mississippi River at Arkansas City, AR.....	480
Figure E-44. HYPO 63 HEC-RAS hydrograph: Mississippi River at Greenville, MS.....	481
Figure E-45. HYPO 63 HEC-RAS hydrograph: Mississippi River at Lake Providence, LA.	481
Figure E-46. HYPO 63 HEC-RAS hydrograph: Mississippi River at Vicksburg, MS.	482
Figure E-47. HYPO 63 HEC-RAS hydrograph: Mississippi River at Natchez, MS.....	482
Figure E-48. HYPO 63 HEC-RAS hydrograph: Mississippi River at Red River Landing, LA.....	483
Figure E-49. HYPO 63 HEC-RAS hydrograph: Mississippi River at Baton Rouge, LA.	483
Figure E-50. HYPO 63 HEC-RAS hydrograph: Mississippi River at Donaldsonville, LA.	484
Figure E-51. HYPO 63 HEC-RAS hydrograph: Mississippi River at Carrollton, LA.	484
Figure E-52. HYPO 63 HEC-RAS hydrograph: Mississippi River at Empire, LA.	485
Figure E-53. HYPO 63 HEC-RAS hydrograph: Mississippi River at Venice, LA.	485
Figure E-54. Barren River Lake HYPO 63 inflow compared to outflow.....	486
Figure E-55. Cagles Mill Lake HYPO 63 inflow compared to outflow.	487
Figure E-56. CM Harden Lake HYPO 63 inflow compared to outflow.	487
Figure E-57. Green River Lake HYPO 63 inflow compared to outflow.	488
Figure E-58. J. E. Roush Lake HYPO 63 inflow compared to outflow.	488
Figure E-59. Mississnewa Lake HYPO 63 inflow compared to outflow.....	489
Figure E-60. Monroe Lake HYPO 63 inflow compared to outflow.....	489
Figure E-61. Nolin River Lake HYPO 63 inflow compared to outflow.....	490
Figure E-62. Patoka Lake HYPO 63 inflow compared to outflow.	490
Figure E-63. Rough River Lake HYPO 63 inflow compared to outflow.	491
Figure E-64. Salamonie Lake HYPO 63 inflow compared to outflow.....	491
Figure E-65. Barkley Dam HYPO 63 inflow compared to outflow.	492
Figure E-66. Center Hill Dam HYPO 63 inflow compared to outflow.	492
Figure E-67. Cheatham Dam HYPO 63 inflow compared to outflow.	493
Figure E-68. Cordell Hull Dam HYPO 63 inflow compared to outflow.	493
Figure E-69. Dale Hollow Dam HYPO 63 inflow compared to outflow.....	494
Figure E-70. Great Falls HYPO 63 inflow compared to outflow.....	494
Figure E-71. Barkley Dam HYPO 63 inflow compared to outflow.....	495
Figure E-72. J. Percy Priest Dam HYPO 63 inflow compared to outflow.	495
Figure E-73. Kentucky Dam HYPO 63 inflow compared to outflow.....	496
Figure E-74. Old Hickory Dam HYPO 63 inflow compared to outflow.....	496
Figure E-75. Wolf Creek Dam HYPO 63 inflow compared to outflow.	497
Figure E-76. Arkabutla Dam HYPO 63 inflow compared to outflow.....	497
Figure E-77. Bayou Bodcau Dam HYPO 63 inflow compared to outflow.....	498

Figure E-78. Blakely Mountain Dam HYPO 63 inflow compared to outflow.	498
Figure E-79. Caddo Dam HYPO 63 inflow compared to outflow.	499
Figure E-80. Degray Dam HYPO 63 inflow compared to outflow.	499
Figure E-81. Enid Dam HYPO 63 inflow compared to outflow.	500
Figure E-82. Grenada Dam HYPO 63 inflow compared to outflow.	500
Figure E-83. Narrows Dam HYPO 63 inflow compared to outflow.	501
Figure E-84. Sardis Dam HYPO 63 inflow compared to outflow.	501
Figure E-85. Wallace Lake Dam HYPO 63 inflow compared to outflow.	502
Figure E-86. Carlyle Lake Dam HYPO 63 inflow compared to outflow.	502
Figure E-87. Lake Shelbyville Dam HYPO 63 inflow compared to outflow.	503
Figure E-88. Mark Twain Lake HYPO 63 inflow compared to outflow.	503
Figure E-89. Wappapello Lake Dam HYPO 63 inflow compared to outflow.	504
Figure E-90. Big Bend Dam HYPO 63 inflow compared to outflow.	504
Figure E-91. Fort Peck Dam HYPO 63 inflow compared to outflow.	505
Figure E-92. Fort Randall Dam HYPO 63 inflow compared to outflow.	505
Figure E-93. Garrison Dam HYPO 63 inflow compared to outflow.	506
Figure E-94. Gavin’s Point Dam HYPO 63 inflow compared to outflow.	506
Figure E-95. Oahe Dam HYPO 63 inflow compared to outflow.	507
Figure E-96. Clinton Dam HYPO 63 inflow compared to outflow.	507
Figure E-97. Glen Elder Dam HYPO 63 inflow compared to outflow.	508
Figure E-98. Hillsdale Dam HYPO 63 inflow compared to outflow.	508
Figure E-99. Kanopolis Dam HYPO 63 inflow compared to outflow.	509
Figure E-100. Melvern Dam HYPO 63 inflow compared to outflow.	509
Figure E-101. Milford Dam HYPO 63 inflow compared to outflow.	510
Figure E-102. Perry Dam HYPO 63 inflow compared to outflow.	510
Figure E-103. Pomme De Terre Dam HYPO 63 inflow compared to outflow.	511
Figure E-104. Pomona Dam HYPO 63 inflow compared to outflow.	511
Figure E-105. Rathbun Dam HYPO 63 inflow compared to outflow.	512
Figure E-106. Smithville Dam HYPO 63 inflow compared to outflow.	512
Figure E-107. Stockton Dam HYPO 63 inflow compared to outflow.	513
Figure E-108. Truman Dam HYPO 63 inflow compared to outflow.	513
Figure E-109. Tuttle Creek Dam HYPO 63 inflow compared to outflow.	514
Figure E-110. Wilson Dam HYPO 63 inflow compared to outflow.	514
Figure E-111. Bull Shoals Dam HYPO 63 inflow compared to outflow.	515
Figure E-112. Greer’s Ferry Dam HYPO 63 inflow compared to outflow.	515
Figure E-113. Norfolk Dam HYPO 63 inflow compared to outflow.	516
Figure E-114. Fort Gibson Dam HYPO 63 inflow compared to outflow.	516
Figure E-115. Hugo Dam HYPO 63 inflow compared to outflow.	517
Figure E-116. Keystone Lake HYPO 63 inflow compared to outflow.	517

Figure E-117. Lake Texoma HYPO 63 inflow compared to outflow.	518
Figure E-118. Oologah Lake HYPO 63 inflow compared to outflow.	518
Figure E-119. Skiatook Lake HYPO 63 inflow compared to outflow.....	519
Figure E-120. Tenkiller Lake HYPO 63 inflow compared to outflow.	519
Figure E-121. Wister Lake HYPO 63 inflow compared to outflow.....	520
Figure F-1. Flow difference due to NWS and TVA Pickwick outflow calculations.	524
Figure F-2. Diagram of HYPO 58A storm sequences.	527
Figure F-3. Historic hydrograph example.....	532
Figure F-4. Script output hydrograph example.	533
Figure F-5. River profile example plot.	536
Figure F-6. Example levee profile plot.....	537
Figure F-7. Example levee profile plot.	538
Figure F-8. Flow diagram representing 1955 PDF discharges (also used for Refined 1973 Flowline).....	541
Figure F-9. Plotted discharge hydrographs from MRC archive 1955 tabulations.....	542
Figure G-10. Comparison of 1955 and 2016 hydrographs for HYPO 58A.	543
Figure G-1. Comparison of generated storm total precipitation with observational data for the 23–27 March 1913 storm event.	552
Figure G-2. Comparison of generated storm total precipitation with observational data for the 12–16 April 1927 storm event.	553
Figure G-3. Comparison of generated storm total precipitation with observational data for the 28–30 June 1928 storm event.	554
Figure G-4. Comparison of generated storm total precipitation with observational data for the 17–25 January 1937 storm event.....	555
Figure G-5. Comparison of generated storm total precipitation with observational data for the 14–19 February 1938 storm event.....	556
Figure G-6. Comparison of generated storm total precipitation with observational data for the 8–10 May 1943 storm event.	557
Figure G-7. Comparison of generated storm total precipitation with observational data for the 16–19 May 1943 storm event.....	558
Figure G-8. Comparison of generated storm total precipitation with observational data for the 3–7 January 1950 storm event.....	559
Figure G-9. 21–24 March 1913 Daily Weather Maps.....	568
Figure G-10. 25–28 March 1913 Daily Weather Maps.....	568
Figure G-11. 12–hour isohyets maps for 24–25 March 1913 storm event.....	569
Figure G-12. 10–13 April 1927 Daily Weather Maps.	573
Figure G-13. 14–17 April 1927 Daily Weather Maps.	573
Figure G-14. 12–hour isohyets maps for 12–16 April 1927 storm event (12-14 April).....	574
Figure 3.3 12-hour isohyets maps for 12–16 April 1927 storm event (14-16 April).....	574
Figure G-16. 27–30 June 1928 Daily Weather Maps.	578

Figure G-17. 12-hour isohyets maps for the June 28–July 1 storm event.....	578
Figure G-18. 6–9 January 1937 Daily Weather Maps.....	582
Figure G-19. 10–13 January 1937 Daily Weather Maps.....	583
Figure G-20. 14–17 January 1937 Daily Weather Maps.....	583
Figure G-21. 18–21 January 1937 Daily Weather Maps.....	584
Figure G-22. 22–25 January 1937 Daily Weather Maps.....	584
Figure G-23. 6-hour isohyets for the 17–25 January 1937 storm event (17-18 January).....	585
Figure G-24. 6-hour isohyets maps for 17–25 January 1937 storm event (17-20 January).....	586
Figure G-25. 6-hour isohyets maps for 17–25 January 1937 storm event (22-24 January).....	587
Figure G-26. 6-hour isohyets maps for 17–25 January 1937 storm event (24-25 January).....	588
Figure G-27. Atmospheric soundings at Murfreesboro, TN, on 17, 20, and 24 January 1937.....	589
Figure G-28. 13–16 February 1938 Daily Weather Maps.....	593
Figure G-29. 17–20 1938 Daily Weather Maps.....	593
Figure G-30. 6-hour isohyets maps for the 14–19 February 1938 storm event (14-15 February).....	594
Figure G-31. 6-hour isohyets maps for 14–19 February 1938 storm event (15-16 February).....	594
Figure G-32. 6-hour isohyets maps for 14–19 February 1938 storm event (16-17 February).....	595
Figure G-33. 6-hour isohyets maps for 14–19 February 1938 storm event (17-18 February).....	595
Figure G-34. 6-hour isohyets maps for 14–19 February 1938 storm event (18-19 February).....	596
Figure G-35. 100–500 mb thickness chart for 14 February 1938.....	596
Figure G-36. 5-8 May 1943 Daily Weather Maps.....	600
Figure G-37. 9–12 May 1943 Daily Weather Maps.....	600
Figure G-38. 6-hour isohyets maps for the 8–10 May 1943 storm event (8-9 May).....	601
Figure G-39. 6-hour isohyets maps for 8–10 May 1943 storm event (9-10 May).....	601
Figure G-40. 6-hour isohyets maps for 8–10 May 1943 storm event (10 May).....	602
Figure G-41. 13–16 May 1943 Daily Weather Maps.....	607
Figure G-42. 17–20 May 1943 Daily Weather Maps.....	607
Figure G-43. 6-hour isohyets maps for the 16–19 May 1943 storm event (16-17 May).....	608
Figure G-44. 6-hour isohyets maps for 16–19 May 1943 storm event (18-19 May).....	608
Figure G-45. 27–30 March 1945 Daily Weather Maps.....	612

Figure G-46. 31 March–3 April 1945 Daily Weather Maps.	612
Figure G-47. Total Precipitation for the 3–16 January 1950 storm.	616
Figure G-48. 2–5 January 1950 Daily Weather Maps.	617
Figure G-49. 6–9 January 1950 Daily Weather Maps.	617
Figure G-50. 10–13 January 1950 Daily Weather Maps.	618
Figure G-51. 14–17 January 1950 Daily Weather Maps.	618
Figure G-52. 6-hour isohyets for the 3–7 January 1950 storm (3 January).	619
Figure G-53. 6-hour isohyets maps for 3–7 January 1950 storm event (4 January).	619
Figure G-54. 6-hour isohyets maps for 3–7 January 1950 storm event (5 January).	620
Figure G-55. 6-hour isohyets maps for 3–7 January 1950 storm event (6 January).	620
Figure G-56. Example temperature (°C) shapefile for 6 January 1950, 12 UTC for the Mississippi River Basin.	622
Figure G-57. 15–18 April 1973 Daily Weather Maps.	626
Figure G-58. 19–22 April 1973 Daily Weather Maps.	626
Figure G-59. 23–26 April 1973 Daily Weather Maps.	627
Figure G-60. 19–22 March 1975 Daily Weather Maps.	630
Figure G-61. 23–26 March 1975 Daily Weather Maps.	630
Figure G-62. 27–30 March 1975 Daily Weather Maps.	631
Figure G-63. 28 June–1 July 1993 Daily Weather Maps.	637
Figure G-64. 2–5 July 1993 Daily Weather Maps.	638
Figure G-65. 27 February–2 March 1997 Daily Weather Maps.	640
Figure G-66. 3–6 March 1997 Daily Weather Maps.	640
Figure G-67. 7–10 March 1997 Daily Weather Maps.	641
Figure G-68. Summer/fall 2010 (top left), winter 2010/2011 (top right), spring 2011 (bottom left), and annual (Jun 2010/May 2011) precipitation rankings by U.S. climate division.	643
Figure G-69. 19–22 April 2011 Daily Weather Maps.	648
Figure G-70. 23–26 April 2011 Daily Weather Maps.	648
Figure G-71. 27–30 April 2011 Daily Weather Maps.	649
Figure G-72. 1–4 May 2011 Daily Weather Maps.	649
Figure G-73. 1950 Precipitation gage locations contained in USACE dataset.	651
Figure G-74. 1950 Precipitation observer locations in NWS dataset.	652
Figure G-75. Sample of USACE 1950 precipitation data.	654
Figure G-76. Sample of daily NWS observer and USACE 1950 precipitation data.	655
Figure G-77. Illustration of calculating daily values from 6-hourly data and effect on comparison to NWS COOP values.	656
Figure G-78. Sample of final spreadsheet showing precipitation data validation for 1950 event.	657

Figure I-1. Reservoir locations, Alabama and Mississippi.....	661
Figure I-2. Reservoir locations, Arkansas and Louisiana.....	662
Figure I-3. Reservoir Locations, Colorado.....	663
Figure I-4. Reservoir locations, Tennessee and Georgia.....	664
Figure I-5. Reservoir locations, Iowa.....	665
Figure I-6. Reservoir locations, Illinois.....	666
Figure I-7. Reservoir locations, Kansas.....	667
Figure I-8. Reservoir locations, Kentucky.....	668
Figure I-9. Reservoir locations, Minnesota.....	669
Figure I-10. Reservoir locations, Missouri.....	670
Figure I-11. Reservoir locations, North Dakota and South Dakota.....	671
Figure I-12. Reservoir locations, Nebraska.....	672
Figure I-13. Reservoir locations, Ohio.....	673
Figure I-14. Reservoir locations, Oklahoma and Texas.....	674
Figure I-15. Reservoir locations, Pennsylvania.....	675
Figure I-16. Reservoir locations, West Virginia and Virginia.....	676
Figure I-17. Reservoir locations, Wyoming.....	677
Figure I-18. Reservoir locations, Indiana.....	678
Figure I-19. Reservoir locations, Montana.....	679
Figure I-20. Reservoir locations, Wisconsin.....	680

Tables

Table 1-1. List of reports included in the overall project.....	2
Table 1-2. PDFs for Lower Mississippi River from 1858 to 2016.....	11
Table 1-3. Major storms selected for the 1955 Study (MRC 1955).....	14
Table 1-4. Storm transpositions applied in the 1955 Study.....	15
Table 1-5. Peak flow order of magnitudes in relation to the 13 floods selected in the 1955 report.....	17
Table 1-6. Modifications to 1950 routing tables (Memorandum Report No. 1 [MRC 1955]).....	25
Table 1-7. Operation of flood control features (Memorandum Report No. 1 [MRC 1955]).....	25
Table 1-8. Puls routing method for seven reaches (Memorandum Report No. 1 [MRC 1955]).....	26
Table 1-9. Reservoir groups for 1955 Study (Memorandum Report No. 1 [MRC 1955]).*	27
Table 1-10. Group EN reservoir data by basin (from Table G-1 Memorandum Report No. 1 [MRC 1955]).....	28
Table 1-11. Group E, N, and D reservoirs from Memorandum Report Number 1 (MRC 1955).*	31

Table 1-12. Summary of peak flows from Table H-2 (Memorandum Report No. 1 [MRC 1955]).	34
Table 1-13. Reservoir group EN reductions by HYPO storm.	36
Table 2-1. LMRFC reservoir models.	70
Table 2-2. Regulation within OHRFC.	75
Table 2-3. Coordination between OHRFC and Nashville District, USACE.	77
Table 2-4. TVA reservoirs.	85
Table 2-5. Land use within the Mississippi River Basin obtained from the U.S. Department of Agriculture.	89
Table 2-6. Infiltration coefficients from 1955 Study.*	90
Table 2-7. SS and CM peak flow results compared to historic peak flow values.	103
Table 2-8. Percent differences from the historic 58A peak flow values.	104
Table 2-9. HYPO 11-73 results compared to 1955 HYPO storm results.	110
Table 2-10. Temperature effects on computed peak unregulated flows at select locations for HYPO 58A.	122
Table 2-11. Comparison of incremental values from the legend in Figure 2-56 to observational data (inches).	139
Table 2-12. Absolute maximum of the percent difference of cell counts between each transposed grid and the original grid (1938).*	153
Table 2-13. Absolute maximum of the percent difference of volume between each transposed grid and the original grid (1938).*	154
Table 2-14. Volume percent difference summary statistics for 1943 event transposition.*	156
Table 2-15. Summary of total precipitation volume conservation.*	157
Table 2-16. Python scripts developed to transpose storms.	158
Table 2-17. Reservoirs modeled to determine regulated outflows for HYPO storms.	161
Table 2-18. Reservoirs and impoundment dates for ABRFC and MBRFC.*	169
Table 2-19. Vicksburg reservoir maximum release rates by season.	172
Table 2-20. Daily flow values to use for Wright-Patman releases during HYPO storms.	175
Table 2-21. Daily flow values to use for Lake O' the Pines releases during HYPO storms.	176
Table 2-22. Little Rock District reservoir minimum, maximum, and routine flood control releases.	178
Table 2-23. Peak flows from HEC-RAS simulation for TVA and NWS regulation methods for Tennessee River, HYPO 58A.	181
Table 2-24. MVS reservoir release guidance.	182
Table 2-25. Reservoir peak flow reductions in percent for four HYPO storms.	184
Table 2-26. Tabulated peak discharges for Ohio River at Metropolis, IL, with changes from the base regulated model result.	189
Table 2-27. Observed climate trends within the six major basins in the Mississippi River Basin as summarized in USACE (2015a-f).	203

Table 2-28. Projected climate trends within the six major basins in the Mississippi River Basin as summarized in USACE (2015a-f).....	204
Table 2-29. Stationarity analysis on selected gage locations that impact the Lower Mississippi River.	217
Table 2-30. HUC 4 basins from USACE Climate Change Web Analysis Tool with calculated significance, <i>p</i>	227
Table 3-1. HYPO peak unregulated flow comparisons at select locations.....	240
Table 3-2. Hydrograph volume and shape comparisons for HYPO 58A.	243
Table 3-3. Comparing peak flows near the Mississippi/Ohio River confluence.....	245
Table 3-4. Tabulated flows from 1955 routing calculations.....	247
Table 3-5. Comparison of peak flow values for HYPO 58A.....	254
Table B-1. Reductions in peak flows from regulation for HYPO 58A.	308
Table C-1. Hydrograph volume and shape comparisons for HYPO 52A.....	361
Table C-2. Comparison of peak flow values for HYPO 52A.....	369
Table D-1. Hydrograph volume and shape comparisons for HYPO 56.	392
Table D-2. Comparison of peak flow values for HYPO 56.....	400
Table E-1. Hydrograph volume and shape comparisons for HYPO 63.....	463
Table E-2. Comparison of peak flow values for HYPO 63.	471
Table F-1. ESC membership.	521
Table F-2. Decision Documents for ESC approval.	522
Table F-3. Peak flows from HEC-RAS simulation for different regulation methods for Tennessee River, HYPO 58A.	525
Table F-4. Current key locations identified.....	534
Table F-5. Example deficiency table.*	538
Table G-1. Maximum precipitation amounts at specific locations (1930–2011).....	545
Table G-2. Runoff from Mississippi River Basin (1930–2011) (sfd = square feet per day).....	545
Table G-3. HYPO Storms and historic events used to assemble them.....	546
Table G-4. Historic storm events used to build HYPO storm sequences.....	547
Table G-5. Storm transpositions used to build HYPO storm sequences.	547
Table G-6. Selected storms for analysis in producing and verifying HYPO flood scenarios.	561
Table G-7. Significant flood crest stages and dates at Cairo, IL.....	563
Table G-8. Storms and summary information.....	564
Table G-9. Top 20 recorded rainfall gauges (inches) for the 23–27 March 1913 precipitation event.....	567
Table G-10. Top 20 recorded rainfall gauges (inches) for the 12–16 April 1927 precipitation event.....	572
Table G-11. Top 20 recorded rainfall gauges (inches) for the June 28 – July 1 precipitation event.....	577
Table G-12. Top 20 recorded rainfall gauges (inches) for the 5 January – 25 January 1937 precipitation event.....	581

Table G-13. Top 20 recorded rainfall gauges (inches) for the 14–19 February 1938 precipitation event.	592
Table G-14. Top 20 recorded rainfall gauges (inches) for the 8–10 May 1943 precipitation event.	599
Table G-15. Top 20 recorded rainfall gauges (inches) for the 12–20 May 1943 precipitation event.	606
Table G-16. Top 20 recorded rainfall gauges (inches) for the 28 March–2 April 1945 precipitation event.	611
Table G-17. Top 20 recorded rainfall gauges (inches) for the 3–16 January 1950 precipitation event.	616
Table G-18. Additional historic events for building new HYPO storm sequences.	623
Table G-19. Top 20 recorded rainfall gauges (inches) for the 16–26 April 1973 precipitation event.	625
Table G-20. Top 20 recorded rainfall gauges (inches) for the 19–30 March 1975 precipitation event.	629
Table G-21. Top 20 recorded rainfall gauges (inches) for the 28 June–9 July 1993 precipitation event.	636
Precipitation amounts for the top 20 recorded rainfall gauges are shown in Table G-22. Daily weather maps for 27 February through 10 March are shown in Figures G-65 through G-67. Table G-22. Top 20 recorded rainfall gauges (inches) for the 28 February–12 March 1997 precipitation event.	639
Table G-23. Top 20 recorded rainfall gauges (inches) for 22 April–3 May 2011 precipitation event.	647

Preface

This assessment was conducted for the U.S. Army Corps of Engineers, Mississippi Valley Division, Mississippi River and Tributaries Program, under Project No. 449963, “Mississippi River Flowline Assessment.” The project managers were Mr. Charles A. McKinnie and Mr. Kenneth D. Parrish. Dr. Roger A. Gaines was the Technical Lead.

The work was performed by a collaboration among the U.S. Army Engineer District, Memphis; the National Weather Service, Mississippi Valley Division Liaison; The National Weather Service Arkansas-Red Basin, Lower Mississippi, Missouri Basin, North Central, and Ohio River Forecast Centers; and the Tennessee Valley Authority. Additional support for reservoir regulation was provided by U.S. Army Engineer Districts Nashville, Louisville, Rock Island, St. Louis, Omaha, Kansas City, Little Rock, Tulsa, Fort Worth, and Vicksburg. Valuable assistance was provided by the Mississippi Valley Division (MVD) and Lakes and Rivers Division office staff. The U.S. Army Engineer Research and Development Center, Coastal and Hydraulics Laboratory provided GIS support for converting point precipitation and temperature data into spatial grids.

The report is published through the Mississippi River Geomorphology and Potamology (MRG&P) Program. The MRG&P Program is part of the Mississippi River and Tributaries (MR&T) Program and is managed by the U.S. Army Corps of Engineers (USACE), MVD, and Districts. The MVD Commander was MG Richard G. Kaiser. The MVD Director of Programs was Mr. Jim Bodron. The Vicksburg District (MVK) Commander was COL Michael C. Derosier. The Memphis District (MVM) Commander was COL Michael A. Ellicott. The New Orleans District (MVN) Commander was COL Michael N. Clancy.

Unit Conversion Factors

Multiply	By	To Obtain
acres	4,046.873	square meters
acre-feet	1,233.5	cubic meters
cubic feet	0.02831685	cubic meters
cubic inches	1.6387064 E-05	cubic meters
degrees (angle)	0.01745329	radians
degrees Fahrenheit	$(F-32)/1.8$	degrees Celsius
feet	0.3048	meters
inches	0.0254	meters
miles (U.S. statute)	1,609.347	meters
square miles	2.589998 E+06	square meters

1 Introduction

1.1 Objective

The 2011 Flood tested the Mississippi River and Tributaries¹ (MR&T) System like no flood before; the highest recorded flood stages occurred along much of the Lower Mississippi River. For the first time, three floodways—the Birds Point-New Madrid Floodway, the Morganza Floodway, and the Bonnet Carré Spillway—were operated during a single flood event. River stages and flow rates were comparable to the major floods of 1927 and 1937. However, the 2011 Flood was contained within the MR&T System to a greater extent than those earlier floods. In 2011, the MR&T system prevented massive flood damages by accommodating the river while using approximately 85% of overall peak flow capacity. An estimated \$234 billion in flood damages was prevented in the single event.

The MR&T project is designed to safely contain the Project Design Flood (PDF). The present PDF was developed in 1955 when the Mississippi River Commission made a complete review of the adequacy of the MR&T project (hereafter referred to as the “1955 Study”). The National Weather Service (NWS) was asked to provide the largest storm series considered to have a reasonable chance of occurrence in the season when floods are likely to occur over the Mississippi River Basin. After investigating 35 different hypothetical storm series, the one that produced the greatest discharges from Cairo, IL, to the Gulf of Mexico was selected as the PDF. The development of the PDF is documented in “Mississippi River Project Flood Study – Memorandum No. 1,” USACE, Mississippi River Commission, Dec 1955 (MRC 1955).

Despite the past success of the MR&T system, the results and experience from the 2011 flood revealed some areas that may provide insufficient design elevations to contain the PDF. As a result, the USACE reviewed the Project Design Flowline (based on the PDF event). A key part of the review was to re-validate the PDF hydrology developed in 1955. Following the

¹ The MR&T was originally authorized by the Flood Control Act of 1928 and encompasses levees, floodways, channel improvements, and backwater storage areas to safely pass the PDF from Cairo, IL, to the Gulf of Mexico.
[http://www.mvd.usace.army.mil/About/MississippiRiverCommission\(MRC\)/MississippiRiverTributariesProject\(MRT\).aspx](http://www.mvd.usace.army.mil/About/MississippiRiverCommission(MRC)/MississippiRiverTributariesProject(MRT).aspx)

2011 flood, the Mississippi Valley Division (MVD) completed a review of the meteorology of the PDF (see Appendices G and H). This review concluded that the current 3-storm combination that makes up the PDF is still adequate, but a review of the hydrology of the basin is required to determine if the inflow hydrographs and lateral inflows to the MR&T system (developed in 1955) should be updated to reflect changing hydrologic conditions in the basin from factors such as climate change, land use changes, constructed projects, etc. The PDF is an extreme event and is larger than previous floods of record, including the 2011 event. While it is likely that significant hydrologic changes have occurred in the Mississippi River Basin, the impacts in total runoff for extreme events may not be significantly different today from when the PDF was first developed. The assessment of PDF hydrology became necessary to develop flow inputs required for the Hydrologic Engineering Center-River Analysis System (HEC-RAS) model and was also used to evaluate changes in total runoff.

This effort is a part of the overall MR&T Mississippi River Flowline Assessment to define the maximum design water surface elevations throughout the MR&T domain. Table 1-1 lists the series of reports associated with the overall project, with this report listed in bold font.

Table 1-1. List of reports included in the overall project.

Report Name	Description
Executive Summary	The Executive Summary briefly summarizes the important information from the entire project assessment.
Main Report	The Main Report summarizes the results in each of the aspects of the entire project assessment and shows the combined effects of the PDF event scenarios.
Hydrology Report	The Hydrology Report assesses the flow of water arriving to the MR&T System during the PDF event scenarios.
Hydraulics Report	The Hydraulics Report assesses the water surface elevations in the Mississippi and Atchafalaya rivers during the PDF event scenarios.
Mississippi River Sedimentation Report	The Mississippi River Sedimentation Report assesses how the next 50 years of sedimentation are expected to change the Mississippi River channel; these changes would impact the water surface elevations expected during the PDF event in the future.
Atchafalaya River Sedimentation Report	The Atchafalaya River Sedimentation Report assesses how the next 50 years of sedimentation are expected to

Report Name	Description
	change the Atchafalaya River channel; these changes would impact the water surface elevations expected during the PDF event in the future.

This report documents the development of the hydrology associated with the PDF. Chapter 2 presents a brief explanation of past studies and the need for the current assessment to re-evaluate the PDF hydrology. Chapter 3 provides background information from the 1955 Study, which includes descriptions of the original storms used to build the hypothetical storm series (known as the HYPO storms). HYPO storms, which are described in Chapter 3, produce HYPO floods. Methodologies for routing the HYPO storms through the basin in the 1955 Study are described and include both unregulated and regulated scenarios. Chapter 4 introduces the current (2016) assessment and presents the methodology for re-development of the precipitation datasets, hydrologic models, reservoir regulation effects, HYPO storm combinations, and transpositioning methodology. Chapter 5 presents model results for the governing HYPO storm.

Appendices A-K give additional details. The subject of each appendix is indicated by the titles listed in the Table of Contents.

1.2 Background

1.2.1 Statement of Problem

The 2011 flood on the Lower Mississippi River produced peak stages that approached PDF stages at some locations with peak discharges being within 78% to 91% of the 1955 PDF flows from Cairo, IL, to Natchez, MS. Although stages and flows approached previously estimated PDF flows, the total precipitation from the 2011 storms was approximately 40% lower than the HYPO 58A¹ rainfall.

The USACE in cooperation with the U.S. Weather Bureau (now the National Weather Service [NWS]) last reviewed the hydrology of the MR&T PDF in 1955. This review analyzed past storms of record throughout the United States and compiled extensive information regarding the intensity, distribution, etc., in connection with these storms. Considerably more

¹ The hypothetical storm used to define the MR&T PDF for the main stem Mississippi River between Cairo, IL, and the Gulf of Mexico is referred to as the HYPO 58A storm.

information was available in 1955 than when the previous analysis was conducted in 1941. The 1955 Study determined that the economic value and economic development in the Lower Mississippi valley protected area had increased tremendously since 1941 and warranted a re-study of the PDF to ensure that adequate protection was provided.

Extreme storm events have occurred since 1955; the two storms that produced the 2011 flood provide but one recent example. Following the 2011 flood, a storm meteorology review was completed (Appendix H) and concluded that the maximized precipitation (actual precipitation increased to reflect the maximized available moisture that could have occurred given prevailing climatic conditions) from the 2011 storms were only within 70% to 75% of the HYPO 58A rainfall. The original HYPO 58A storm did not include direct consideration of significant snowmelt contributions; snowmelt was represented in antecedent stream flow in the initial routing calculations. This is in contrast to the significant snowmelt contribution to runoff that was observed during the 2011 flood. The meteorology study recommended that increased snowmelt should be considered during future PDF assessments; however, the scope and funding of the present assessment does not include efforts to adjust the seasonality or changed snowmelt contribution to the individual storms comprising the PDF¹.

Consideration for re-assessment of the PDF storm hydrology stems from current hydraulic and hydrologic tools that are based on different methodologies. Prior studies, which include PDF Flowline assessments following the 1973 and 1975 floods, utilized 1-dimensional (1D) steady-state hydraulics models (HEC-2). The current approach utilizes 1D unsteady hydrodynamic models (HEC-RAS) with some regions included as 2-dimensional (2D) models. Unsteady hydrodynamics require different routing methods than the earlier studies, and boundary conditions for unsteady models require data that are not available from the 1955 hydrology.

1.2.2 Limitations

Original scoping identified a need to develop a hydrologic model that could be used to evaluate both the historic events used to assemble the

¹ The influence of temperature on snow pack and snow melt was included in continuous simulation hydrologic models used in the 2016 study; however, no systematic adjustment was made in the development of HYPO storm sequences.

HYPO storms as well as the four HYPO storms. This scope proved to be beyond the available time and budget originally identified for this assessment. A data call to all USACE districts within the Mississippi River Basin to expedite the hydrologic evaluation identified few available existing hydrologic models that, in total, comprised a limited number of relatively small sub-basins. As an alternative to expedite the assessment, the development of entirely new basin-wide hydrologic models was considered but was determined to be infeasible from time and cost limitations. USACE then opened discussions with the NWS about the use of their existing forecast models to perform the hydrologic modeling for this assessment. This would leverage the extensive work done by NWS in developing and calibrating those models and reduce the investment required to develop new hydrologic models. An inherent risk in following this collaborative approach would be in maintaining the schedule because the NWS would utilize real-time operational staff to perform the work, and their priority would continue to be forecasting real-time weather events. Using the NWS operational models would also eliminate any ability to calibrate to prior periods of time, which would forgo addressing changes in model parameterization for infiltration, routing, land use, and snowmelt over time. The use of NWS models and personnel to conduct the hydrological assessment was ultimately adopted. The USACE and NWS scope of work is provided in Appendix A.

1.2.3 1955 Study for the Mississippi River and Tributaries (MR&T) Project Design Flood (PDF)

Due to the relatively short period of record within the Mississippi River basin available at the time, the 1955 Study assumed that all of the critical storm combinations and run-off events had not yet been observed. Therefore, extreme storms of record were placed in combination, shifted in time, and/or transposed, to develop hypothetical flood magnitudes that were deemed to have a possible, though rare, chance of occurrence. Use of storms of record was limited to the same season of the year in which they occurred. For the 1955 Study, the seasons were as follows: winter floods – December, January, and February; early spring floods – March, April, and the first half of May; and late spring floods – the last half of May, June, and July. Contributions to winter floods were mainly from the Ohio River with moderate to small contributions from the Upper Mississippi and Missouri Rivers, where freezing weather reduces runoff. Early spring floods resulted from moderate to high contributions from all tributaries. Late spring floods were generally caused by high flows in the

Upper Mississippi and Missouri Rivers, moderate Ohio River flows, and moderate to high contributions from the lower tributaries.

The material in this section does not intend to give complete details of the methods used to develop the 1955 PDF. These details are described in the 1955 report documentation (primarily *Memorandum Report No. 1, Appendix J—Mississippi River Basin: Meteorological Study* [MRC (1955)]). Rather, a synopsis of information central to conducting the 2016 analysis is given.

1.2.3.1 *Historic record*

The annual crest stages for various seasons at Evansville (Ohio River), St. Louis (Mississippi River), and Cairo (Mississippi River) from 81 years of available records and the mean monthly contribution by the Upper Mississippi and Ohio at Cairo for 50 years of record were analyzed to evaluate seasonal distributions of flood flows between the Ohio and Mississippi Rivers. The review of crest stages indicated that the Ohio River floods occur mainly in the winter and early spring with very few occurring in late spring; the Missouri and Upper Mississippi floods occur mainly in early and late spring with few occurring in winter. Figure 1-1 illustrates this pattern with a plot of flow contribution in percent of daily flow between Thebes (Mississippi River upstream of Ohio River) and Smithland (Ohio River). Figure 1-1 shows that average and maximum daily flows from the Ohio are highest in January through February while the Mississippi River contribution is highest in June and July. The magnitude of seasonal flow variability is less in recent decades, 1954–2015, than during the 1955 analysis, 1933–1954. For example, the Ohio River has a lower percentage of flow, and the Mississippi River has a higher percentage of flow without significant variability from January through April from 1954–2015 as compared to 1933–1954. Figure 1-1 through Figure 1-3 includes percentages for three time periods: early (first available data at a gage through 1954); full (first available data at a gage through 2015); and late (1954–2015). The first available dates were 1928 for locations on the Arkansas and White, and Mississippi Rivers and 1933 for locations on the Ohio River.

Except for minor differences between the early, full, and late period percentages, Figure 1-1 through Figure 1-3 illustrate that the seasonal distribution has not changed appreciably since the earlier analysis. There is a slight shift between the flow distribution between the Upper

Mississippi and Missouri Rivers in the later decades (Figure 1-2) with a small increase in the percentage of flow coming from the Upper Mississippi River during April, May, and June.

Figure 1-1. Seasonal distribution of flow as a percentage between the Mississippi and Ohio Rivers (Chester and Metropolis, IL, respectively).

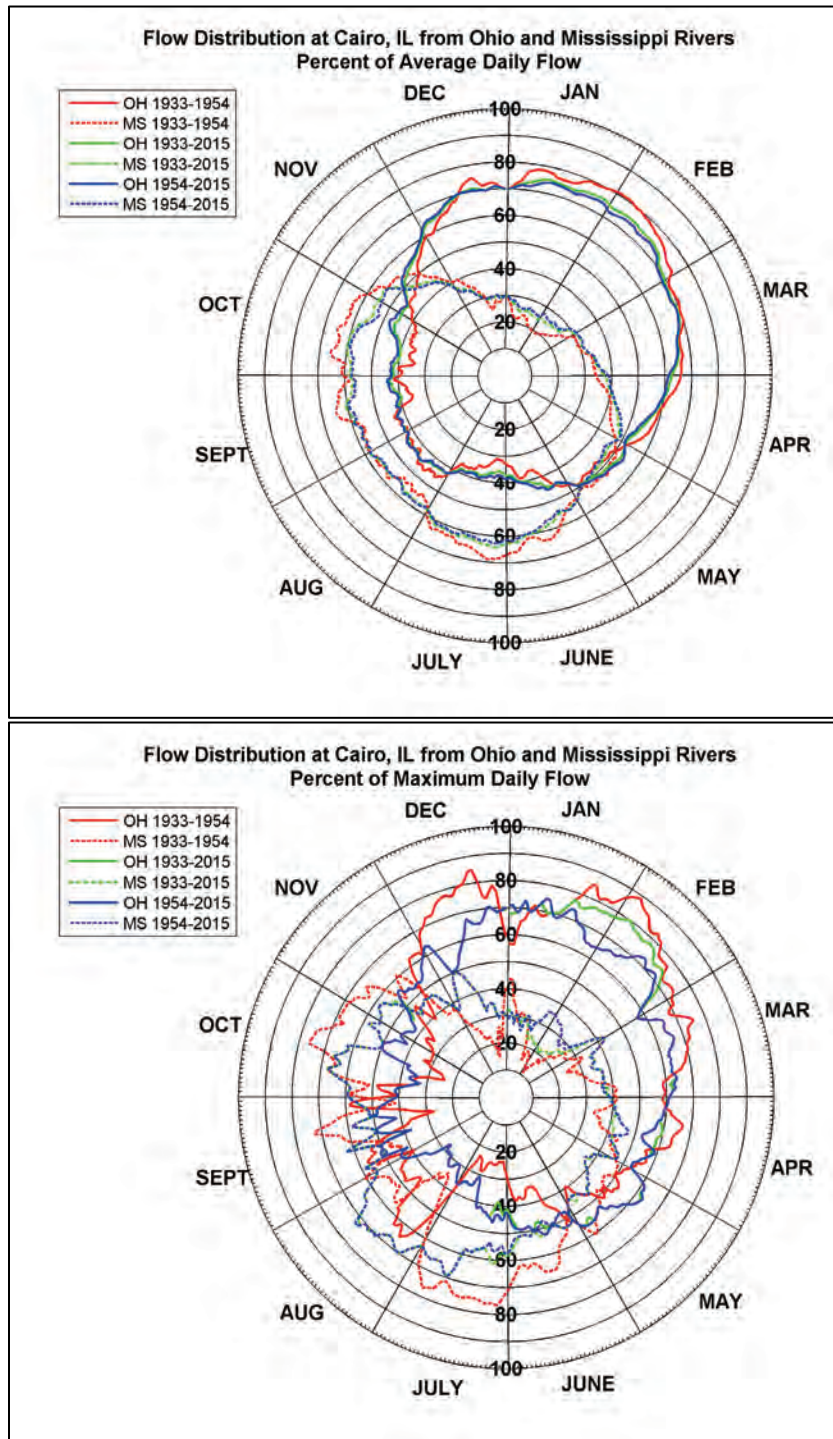


Figure 1-2. Seasonal distribution of flow as a percentage between the Missouri and Mississippi Rivers (Hermann, MO, and Grafton, IL, respectively).

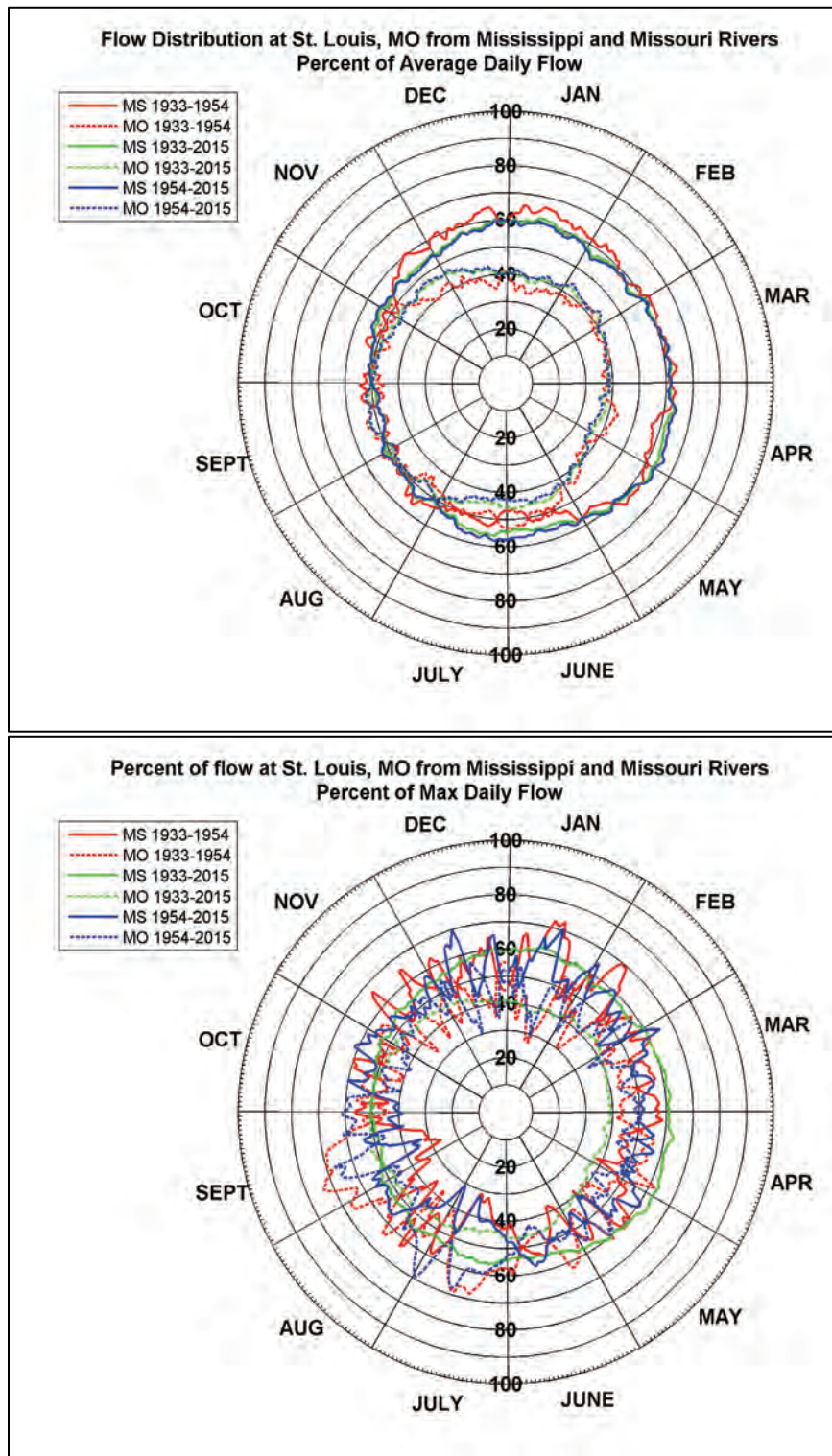
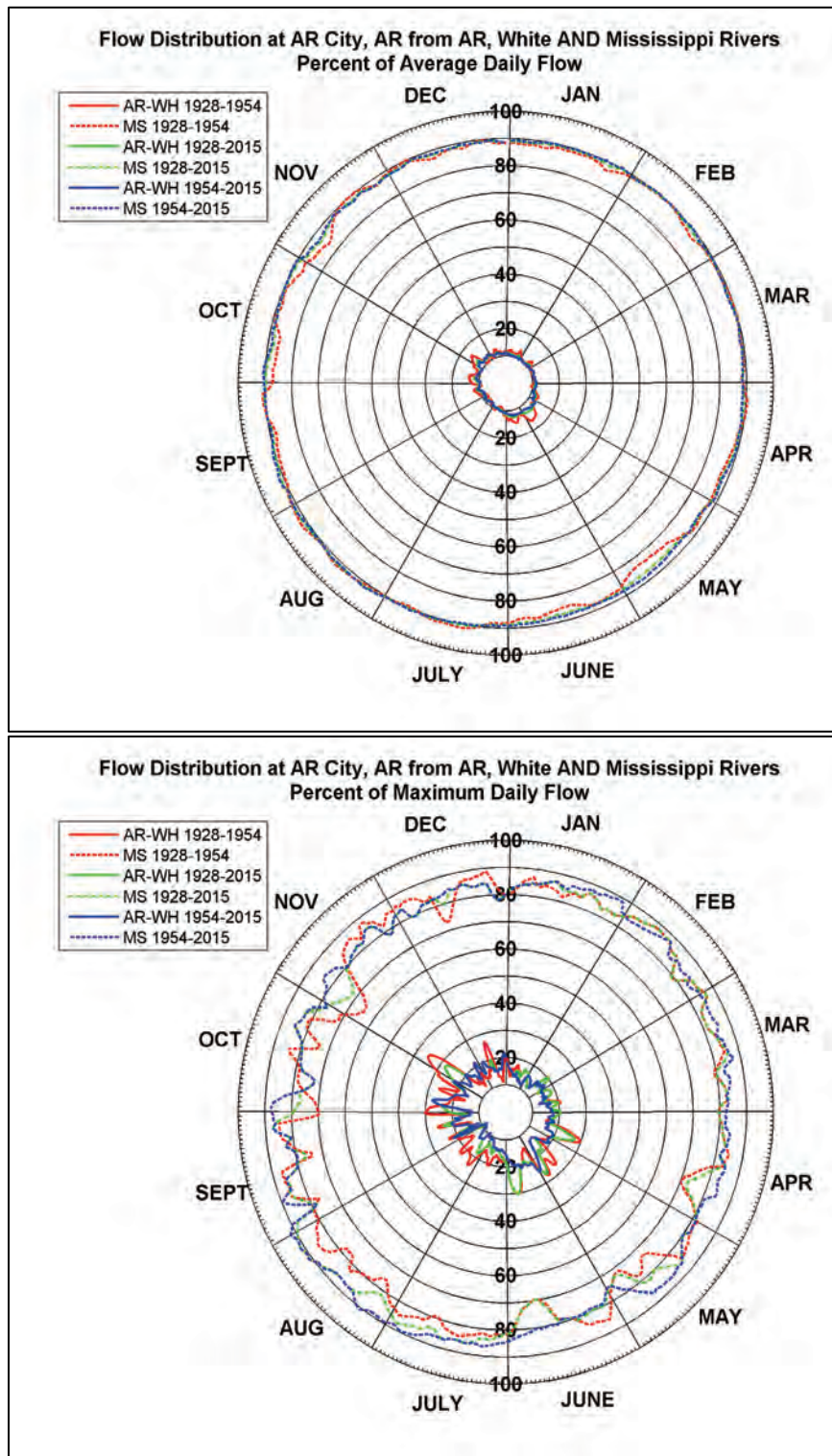


Figure 1-3. Seasonal distribution of flow as a percentage between the Arkansas and White Rivers and the Mississippi River (Pine Bluff, AR; Clarendon, AR; and Arkansas City/Greenville, respectively).



1.2.3.2 Prior project flood studies on Lower Mississippi River

Flood protection on the Lower Mississippi River dates back to 1727 with the completion of small levees around the settlement of New Orleans, LA. Early levee construction along the river was hampered by a lack of an effective organization to function as an integrated system. Early levees were generally deficient in both height and section. The overall goal at that time was to protect against the highest observed river levels. The first detailed, system-wide studies were made in 1861 with subsequent updates in 1899, 1914, 1927, 1928, 1934, 1937, 1941, and 1955 as listed in Table 1-2.

Table 1-2. PDFs for Lower Mississippi River from 1858 to 2016.

Previous Studies of Lower Mississippi River PDF, in cfs*			
Year	Cairo, IL (combined)	Arkansas City, AR	Latitude Red River Landing
1858/1861	1,478,000 ^a	1,418,000 ^b	1,338,000
1899	1	1	1
1914	1	1	1
1927	2,250,000	2,850,000	2,650,000
1928	2,400,000	1,950,000 ²	3,000,000
1934	2,400,000	3,200,000	3,000,000
1937	2,250,000	NA	NA
1941	2,600,000 ³	3,000,000 to 3,065,000	3,000,000
1955	2,450,000	3,065,000	3,000,000
1973	Used 1955 flow values		

^a Columbus, KY

^b Napoleon, AR

¹ Only stage is available for this year.

² Remaining water bypassed through Boeuf Basin.

³ Value with reservoir effects is 2,450,000 cubic feet per second (cfs).

NA = Not Applicable

* = cubic feet per second

In 1941, the calculated PDF flows included reservoir effects, which reduced the PDF peak flow by 150,000 cfs between Cairo, IL, and the mouth of the Arkansas River. The 1941 update was the first to include reservoir effects. The 1955 Study provided the basis for setting the current design flows and levee grades.

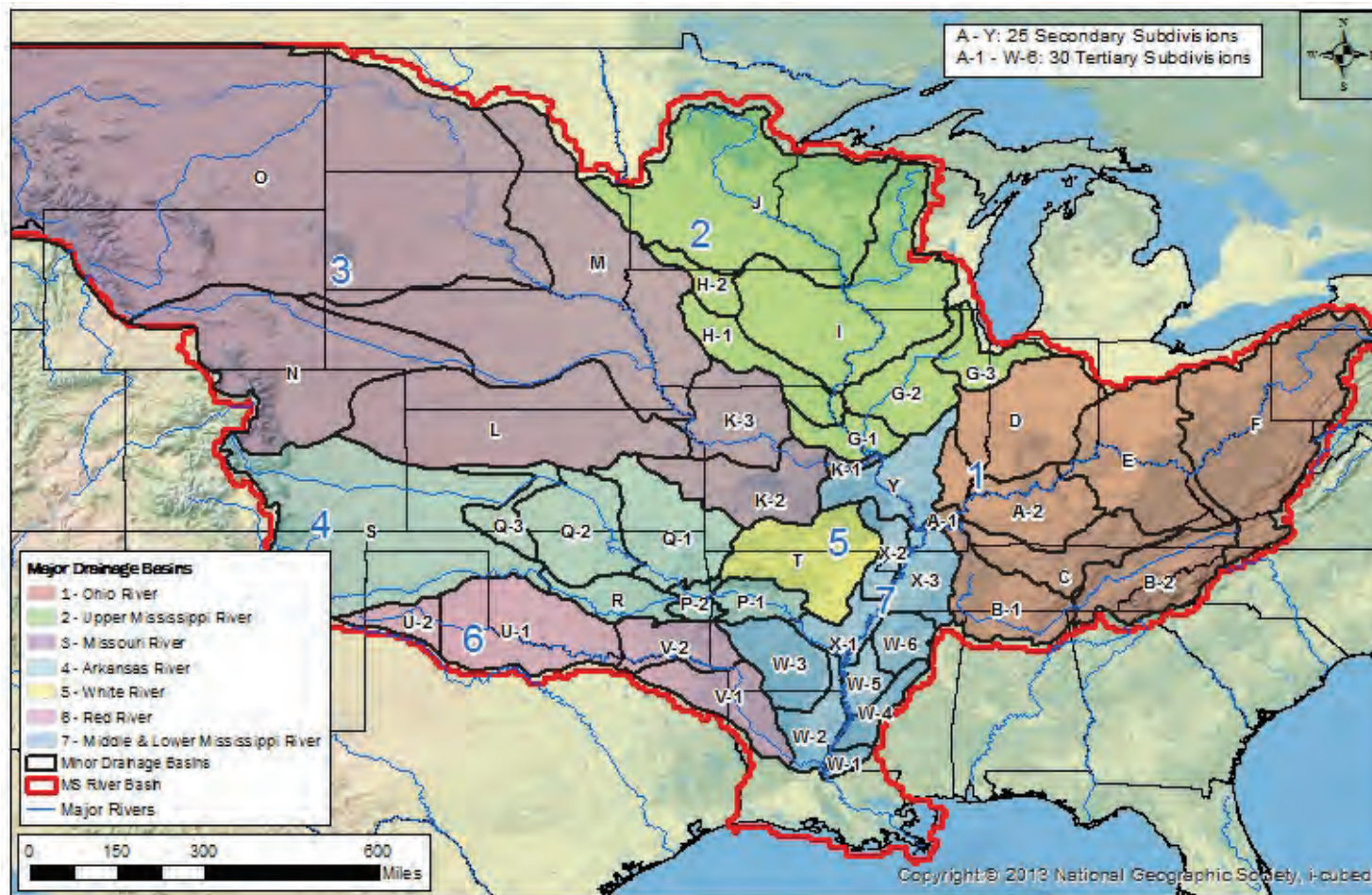
1.2.3.3 Drainage basin description

The Mississippi River Basin was subdivided into areas of the largest practicable size to minimize the time involved in determining tributary

flow for the natural conditions (unregulated) and the modified conditions (regulated) with reservoirs operating. The subdivisions were based on the natural watershed divide and major stream discharge gaging stations. Seven major drainage basin divisions (1–7 in Figure 1-4) were made — one for each of the major tributary streams and one that contains all the minor tributaries and local areas along the main stem. The major divisions were then subdivided into 25 secondary divisions (labeled A through Y in Figure 1-4), and these secondary divisions were further divided into 30 tertiary divisions for convenience in determining runoff (labeled as A-1, etc., in Figure 1-4). Quadrangle areas bounded by 1° lines of latitude and longitude were used to determine average rainfall for the drainage subareas for transposed storms or for subareas where discharge records were not available (MRC 1955).

Figure 1-4 shows the major drainage area divisions selected for the study.

Figure 1-4. Watershed map from 1955 analysis of the MR&T PDF.



1.2.3.4 Extreme storms selected for detailed analysis

In the early 1950s, an analysis of historical records suggested that storms that produced floods on the Lower Mississippi River occurred chiefly during January, February, March, and April and to a lesser extent in May and June. These storms extended over large areas. Summer storms were thought to be limited to smaller areas and would not produce flood stages on the Lower Mississippi.

Table 1-3 details some of the major storms selected in the development of hypothetical floods for the 1955 Study.

Table 1-3. Major storms selected for the 1955 Study (MRC 1955).

Storm			Maximum Average Rainfall Depth in Inches for 100,000 Square Miles		
Assignment No.	Date	Location	1 Day	2 Days	3 Days
OR 1-15 ¹	Mar 1913	Arkansas-New York	3.20	4.80	6.00
LMV 4-8 ¹	Apr 1927	South Central States	3.00	4.30	4.70
OR 5-6 ¹	Jan 1937	Arkansas, Tennessee, and Kentucky	2.70	4.70	6.20
SW 2-17	Feb 1938	South Central States	2.40	4.00	4.80
SW 2-20	May 1943	N. Texas-Great Lakes	3.40	5.80	6.40
SW 2-21 ¹	May 1943	Oklahoma-Great Lakes	2.60	4.10	5.40
SW 3-5	Mar-Apr 1945	Texas, Arkansas, and Missouri	2.50	4.20	4.60
OR 7-10 ¹	June 1928	Missouri – North Carolina	-	-	-
---	Jan 1950	Southern Central States	-	-	-

¹ Tributary storms of record selected based on flood magnitudes and season when the storm occurred.

The storms listed in Table 1-3 did not necessarily represent the largest of record but were chosen on the basis of the floods they produced and their adaptability for meteorological analysis. At the time, major floods on the Lower Mississippi River generally resulted from large floods on the Ohio River augmented by lesser contributions from other major tributaries. Based on recorded data, the flood season prior to 1955 usually occurred from the middle of December through July. Major floods on the

Ohio River at that time typically occurred between the middle of January and the middle of April; between the middle of April and the last of July on the Upper Mississippi and Missouri Rivers,; and between the first of April and the end of June on the Arkansas and White Rivers.

Storm transpositions

Based on storm-rainfall intensities, depths, areal coverage, and seasons of occurrence, the following storms (Table 1-4) were transposed to locations that would produce critical floods and were used in combinations with PDF flood studies listed above (MRC 1955; USACE, Weather Bureau 1959).

Table 1-4. Storm transpositions applied in the 1955 Study.

Storm Transpositions (H-05) (MRC 1955)			
Date of Storm	Storm Assignment Number	Storm Transposed over Area Number ²	Storm Transposition Number
10-12 Jan 1913	LMV 1-9	1, 3, 4, 5, 7Y and 7X	1
10-12 Jan 1913	LMV 1-9	1 and 7Y	1
21-27 Dec 1932	SW 2-9	4, 5, and 7X	2
18-21 Jan 1935	LMV 1-19	1 and 7Y	3
14-19 Feb 1938 ¹	SW 2-17	4, 5, 6, 7X, and 7W	4
6-12 May 1943 ¹	SW 2-20	2 and 3	5
6-12 May 1943 ¹	SW 2-20	4, 5, 6, 7X, and 7W	6

¹ Transposition included in the current analysis

² Area numbers for sub-basins shown in Figure 1-4.

Because only the four critical HYPO storm series pertinent to the Lower Mississippi River system were considered, storm transpositions 1, 2, and 3 were not included in the current 2016 assessment. Descriptions of the transpositions required to assemble data for the four HYPO storm combinations included in the 2016 analysis are as follows:

1. **Transposition Number 4** (Storm of 14–19 February 1938 – SW 2-17): This storm was transposed 90 miles north and rotated 20° clockwise about Calvin, OK, as a center. There was no adjustment made in the rainfall depths.

2. **Transposition Number 5** (Storm of 6–12 May 1943—SW 2-20):
This storm centered at Warner, OK, and was transposed 430 miles north and rotated 14.5° clockwise about the center. Rainfall depths were reduced by 20% for HYPO 52A.
3. **Transposition Number 6** (Storm of 6–12 May 1943—SW 2-20).
This storm was transposed 105 miles north and rotated 21° clockwise about the center of Warner, OK. No adjustment was made in rainfall depths.

Data taken from time periods within Transposition Numbers 4, 5, or 6 were used to assemble the HYPO storm sequences defined in Figure 1-5 and in Section 2.4.

1.2.3.5 Storm combinations selected for detailed analysis in the 1955 Study

Storm study data sheets from the Weather Bureau archives were reviewed in detail, and 44 storms were selected on the basis that their areal extent, duration, season of occurrence, and rainfall amount indicated that they may be used in storm combinations to evaluate the Lower Mississippi River PDF. The Weather Bureau examined these storms and furnished their determination of the minimum time interval necessary between storm events that would allow realistic storm combinations to be generated. Based on the Weather Bureau's determination, 35 storm combinations were developed, and 13 of the combinations were selected for preliminary study after the Weather Bureau made some final adjustments in the rainfall (increases and decreases) for transposed storms and in timing between storms. Run-off hydrographs were computed for tributary areas for all of these combinations, and these hydrographs were routed to key stations on the Mississippi River by the progressive average-lag method. Four of the thirteen storm combinations were selected for detailed study based on the floods they produced and the season in which they occurred.

Hypothetical floods (HYPO floods) are the result of a hypothetical combination of actual storm events, known as HYPO storms. The original storms were evaluated by the Weather Bureau to determine if a potential existed to modify (scale or transpose) the storm precipitation amounts to produce greater floods on the Lower Mississippi River. This evaluation determined that certain storms could be scaled and or transposed with a reasonable expectation that such events could naturally occur.

Development of the HYPO flood estimates utilized two methods to assemble the storm sequences:

Method I: Combinations of storms (or floods) of record, arranged in critical sequence and adjusted for time of occurrence.

Method II: Combinations of storms (or floods) of record with storm transpositions, arranged in critical sequence and adjusted for time of occurrence.

The preliminary results of the 13 HYPO floods were used for comparative purposes only in selecting major flood combinations for detailed study. In selecting the floods, consideration was given to storms from areas that produced the highest contribution of flows and to the seasons of occurrence. Four HYPO floods were selected for detailed study; their order of magnitude of peak flows, determined in the preliminary study in relation to the 13 floods, is shown in Table 1-5.

Table 1-5. Peak flow order of magnitudes in relation to the 13 floods selected in the 1955 report.

Drainage Area or Gaging Station	Ranking Relative to 13 Flood Combinations Numbered 51-63			
	HYPO 58 (winter)	HYPO 56 (early spring)	HYPO 63 (early spring)	HYPO 52 (late spring)
Ohio River Basin	1	10	11	12
Upper Miss. River Basin	12	4	3	2
Missouri River Basin	7	4	3	1
Arkansas River Basin	2	3	1	7
White River Basin	4	1	2	12
Red River Basin	2	1	6	7
St. Louis, MO	12	4	3	2
Cairo, IL	2	9	12	1
Arkansas City, AR	1	2	3	12
Latitude of Red River Landing	1	2	3	12

Of the HYPO floods selected for detailed study, the storm combinations and arrangements for HYPO 56 and HYPO 63 were the same as used in the preliminary study. HYPO 52 and HYPO 58 storms were modified and

designated HYPO 52A and HYPO 58A, respectively. HYPO 52 was modified by decreasing the rainfall depth for the transposed storm, and for HYPO 58 the rainfall depth for the 1937 storm was increased, and the time interval between the two major storms was reduced by 1 day. The HYPO combinations below were determined to be the critical storms for detailed evaluation.

- **HYPO 52A** (late spring season) consists of the combination of one transposed storm and two storms as they actually occurred. The rainfall for the 7–11 May 1943 storm was reduced by 20%, and the storm was rotated 14.5° clockwise about Warner, OK, and transposed 430 miles north over the Missouri and Upper Mississippi River Basins¹. This storm was followed by the 15–20 May 1943 storm 3 days after with the greatest rainfall hitting the Arkansas Basin. Then, 2 days later, the 28–30 June 1928 storm followed, which primarily hit the Ohio Basin followed 3 days later by the actual 15–20 May 1943 storm over all areas, and 2 days later by the actual 28–30 June 1928 storm over all areas above Cairo, IL. HYPO 52A has the same storm combination as HYPO 52; however, the rainfall depth adjustment for the transposed 7–11 May 1943 storm was reduced 20% for HYPO 52A instead of the 4% reduction for HYPO 52. Sequencing of the storm is shown in Figure 1-5.
- **HYPO 56** (early spring season) consists of the combination of two storms as they actually occurred. The 2–30 March 1945 storm was sequenced prior to the main event period to establish the intended antecedent conditions. The main event consisted of the 23–26 March 1913 storm over the Ohio, Upper Mississippi, Arkansas, and White Basins and over the drainage area of the Mississippi River from St. Louis, MO, to Cairo, IL, which was followed 3 days later by the 12-16 April 1927 storm over all areas. This flood gave the largest flows from the White and Red River Basins and the second largest flows for the Mississippi River at Arkansas City and Latitude of Red River Landing. The combination of the March 1913 and April 1927 storms, as used in the preliminary studies, was used in the detailed study without any modifications. Sequencing of the storm is shown in Figure 1-5.
- **HYPO 58A** (winter season) consists of the combination of one storm as it actually occurred with a rainfall depth increase of 10%, one storm as it

¹ Memorandum Report No. 1 (MRC 1955) states that Storm SW2-20, 7–11 May 1943, was transposed “5degrees West.” This notation for the transposition was determined to be an error during the replication of the storm for the 2016 study as a 5° shift west would have placed the storm outside of the Mississippi River Basin. Maps from Memorandum Report No. 1 substantiate use of the transposition without the westward shift.

- actually occurred, and one transposed storm. The actual 6–24 January 1937 storm over all areas with rainfall depth increased by 10% was followed 4 days later by the 3–16 January 1950 storm over all areas above Cairo, IL, and 3 days later by the 14–18 February 1938 storm rotated 20° clockwise about Calvin, OK, and transposed 90 miles northwest over all areas downstream from Cairo, IL¹. This flood gave the largest flows from the Ohio River Basin and for the Mississippi River at Arkansas City and Latitude of Red River Landing. It yielded the second largest flows from the Arkansas and Red River Basins and for the Mississippi River at Cairo. This flood was modified from HYPO 58 by reducing the time interval between the 1937 and 1950 storms from 5 days to 4 days. Sequencing of the storm is shown in Figure 1-5.
- **HYPO 63** (early spring season) consists of two storms as they actually occurred and one transposed storm. The actual 12–16 April 1927 storm over all areas was followed 2 days later by the actual 15–20 May 1943 storm over all areas, and 3 days later by the 7–12 May 1943 storm rotated 21° about Calvin, OK, and transposed 105 miles north over all areas downstream from Cairo, IL². This flood gave the largest flows from the Arkansas River Basin, the second largest flows from the White River Basin, and the third largest flows from the Missouri and Upper Mississippi River Basins, and for the Mississippi River at St. Louis, Arkansas City, and Latitude of Red River Landing. Sequencing of the storm is shown in Figure 1-5.

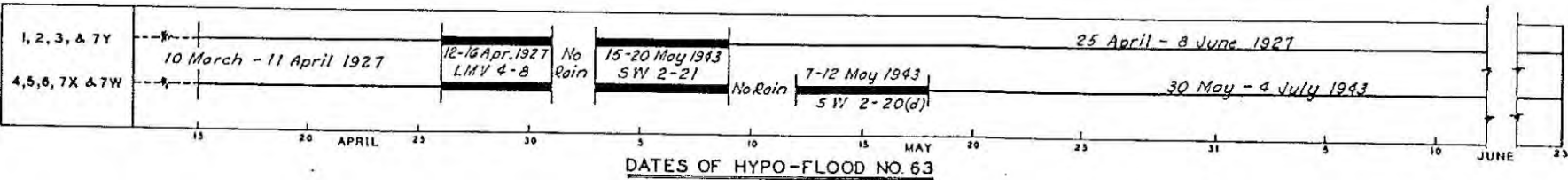
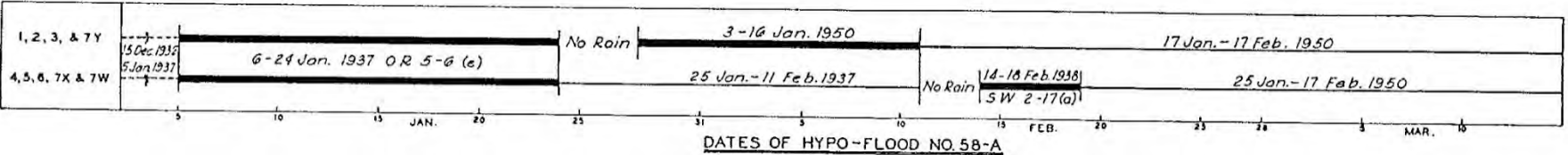
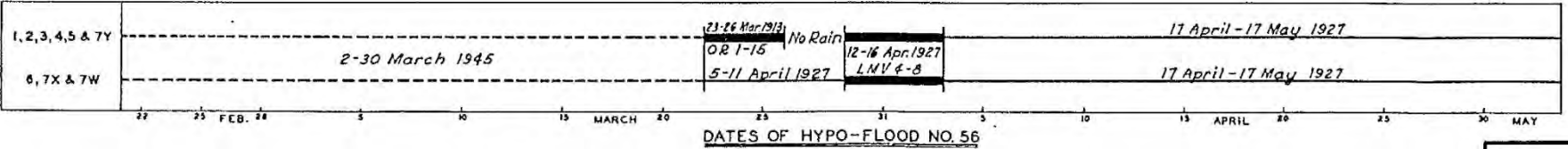
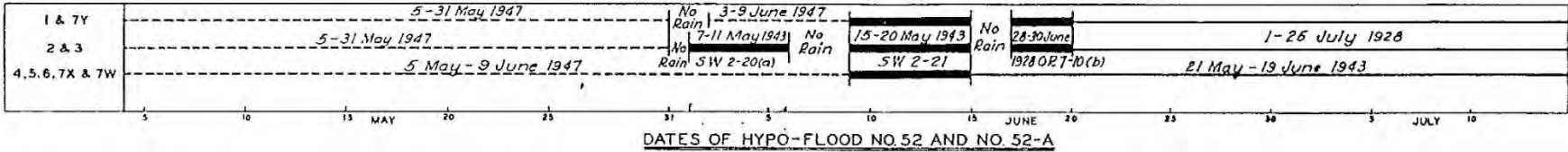
Appendix G of this report describes storm meteorology in more detail. In the 1955 Study, meteorological sequencing was given with individual storms across their entire spatial extent; however, the computation of runoff from storm combinations was selectively applied to designated sub-basins (Figure 1-4) across the watershed as shown in Figure 1-5.

¹ Memorandum Report No. 1 (MRC 1955) states that storm SW2-17, 14–18 February 1938, was transposed 17.5° west. This transposition was determined to be an error during the replication of the storm for the 2016 study as a 17.5° shift west would have placed the storm outside of the Mississippi River Basin. Maps from Memorandum Report No. 1 substantiate use of the transposition without the westward shift.

² Memorandum Report No. 1 (MRC 1955) states that storm SW2-20, 7–12 May 1943, was transposed 55° west in the 1955 Report. This transposition was determined to be an error during the replication of the storm for the 2016 study as a 55° shift west would have placed the storm outside of the Mississippi River Basin. Maps from Memorandum Report No. 1 substantiate use of the transposition without the westward shift.

The 1955 Study did not include continuous snow water equivalent (SWE) accounting, and temperature data were not required for the HYPO storm sequences.

Figure 1-5. HYPO 52A, 56, 58A, and 63 sequence from Memorandum Report No. 1 (MRC 1955, Appendix J).



1.2.3.6 Infiltration and base flow considerations for 1955 Study

Loss rates were applied in the 1955 Study using standard hydrologic procedures. The 1955 Study reduced the total precipitation (P_{Total}) by the losses to determine an effective precipitation depth ($P_{\text{Effective}}$) to be applied.

$$P_{\text{Total}} - \text{LOSS} = P_{\text{Effective}} \quad (1)$$

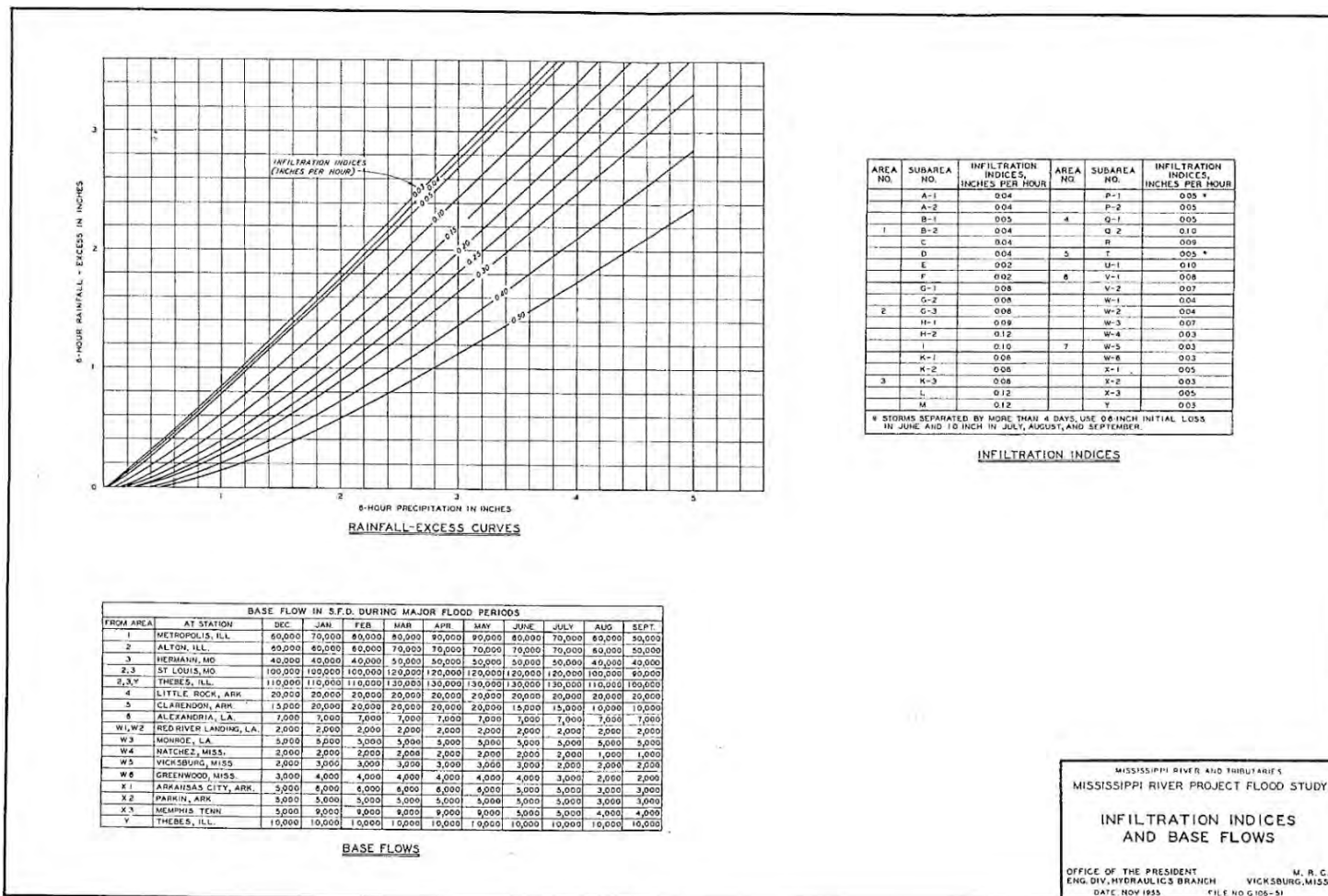
$$\text{Loss} = \text{initial loss} + \text{Infiltration Index} * \text{duration} \quad (2)$$

The effective precipitation was applied using Unit Hydrograph theory to develop flow hydrographs for each basin. Infiltration indices were calculated using contemporary engineering manuals at the time of the 1955 Study and were developed from storms and floods of record with adequate hydrologic data. Infiltration indices (Figure 1-6) range from 0.02 to 0.12 inches (in.) per hour and were defined as average rates of loss such that excess rainfall volume would equal the direct runoff volume. The infiltration indices for each subarea were the minimum to be expected during major storms in the respective areas. Since the study was based primarily on major storms of record with high rainfall intensities, it was assumed that where runoff had to be determined from rainfall, initial losses had occurred for all areas except Areas 4 and 5 (Figure 1-4) prior to the beginning of the storm under consideration. The runoff calculation for Areas 4 and 5 included an adjustment for initial losses.

The hydrographs were adjusted to eliminate runoff from antecedent rainfall. Normal recession curves were developed from observed discharge hydrographs of major floods for each of the key tributary stations. Base flow was defined as that portion of the stream flow occurring from other than direct surface runoff. The base flow adopted for each major subdivision or tributary was determined from natural discharge hydrographs and was segregated by season to coincide with seasons of the year when each of the historical storm events occurred and was considered to represent average conditions during major floods.

The rainfall-excess curves, infiltration indices for all areas, base flows for 17 areas for each month from December through September, and the initial-loss values for Areas 4 and 5 are shown in Figure 1-6.

Figure 1-6. Infiltration indices, rainfall-excess curves, and base flows from the 1955 Study (MRC 1955).



1.2.3.7 Unit hydrograph analysis from 1955 Study

Unit hydrographs were developed for 37 separate drainage areas, varying in size from 1,060 to 80,000 square miles, to compute flood hydrographs of surface runoff from transposed storms and storms of record in places where discharge records were not available. The 1955 Study stated that the largest practicable size of drainage areas was used to minimize the time involved in determining flows at key stations. Unit hydrographs for 30 areas were determined from floods of record, and synthetic unit hydrographs were computed for 7 areas where there was insufficient recorded hydrologic data. The 24-hour unit hydrographs from the gaging stations where the discharges were computed were tabulated on Plate E-1 of Memorandum Report No. 1 (MRC 1955), and an example of unit-hydrograph determination from a flood of record was given on Plate E-2 of the report.

1.2.3.8 Flood routing methods used in 1955 Study

Appendix F from Memorandum Report No. 1 (MRC 1955) used the progressive average-lag method for the preliminary study and the Puls method for the detailed study. Only the Puls method will be addressed in this section since the current assessment only considers the four HYPO storms that were included in the detailed study. The Puls method of routing was used in developing hydrographs of unregulated and regulated flows for four HYPO floods. Reach outflow curves and reach storage curves for each selected reach below St. Louis, MO, were developed from data observed during the occurrence of the 1950 high water period. During this flood, none of the floodways or backwater leveed areas were operated. These curves, which refer to the gages at the lower ends of the reaches, were average curves rather than loop curves. Consequently, their use resulted in discharges that may have been higher or lower than the actual observed flows depending on whether the stages at the lower end of the reach were rising or falling. Therefore, the curves developed were extended above the upper limits of the 1950 high water by comparison with data from other floods, previous computations, and model studies. These curves were used to develop routing tables for 1950 flow conditions in seven reaches (Table 1-8).

The routing tables developed were then used to route the 1950 flood through the basin. Comparisons of the routed discharge hydrographs with the actual hydrographs for the stations at the lower ends of the several reaches are shown in Plate F-2 of Memorandum Report No. 1 (MRC 1955).

A portion of the routing table developed for the Cairo to Memphis reach and the procedure followed in routing the 1950 flood through this reach are also presented on the referenced Plate F-2.

To route the HYPO floods, modification of some of the routing tables developed for 1950 conditions was necessary to reflect the effects of operating various flood-control features in the routed hydrographs. Modifications made to the routing tables are listed in Table 1-6.

Table 1-6. Modifications to 1950 routing tables (Memorandum Report No. 1 [MRC 1955]).

Reach	Modification to Routing Tables
St. Louis-Metropolis to Cairo	Adjusted based on data observed during 1937 flood to reflect Birds Point-New Madrid Floodway operation
Helena to Arkansas City	Adjusted to include effects of operating the White River backwater leveed area
Natchez to Latitude of Red River Landing	Developed several new routing tables to reflect Old River Control Structures near mile 312

The operation of flood control features during the 1955 analysis followed the guidelines established at the time as described in Table 1-7.

Table 1-7. Operation of flood control features (Memorandum Report No. 1 [MRC 1955]).

Flood Control Feature	Operation Utilized in 1955 Study
Birds Point-New Madrid Floodway	Operation begun at 58.0 stage at Cairo Full operation achieved at 59.0 on Cairo gage
White River Backwater Leveed area	Activated when crest stage exceeded 59.5 at Arkansas City, AR gage Levee crevasse was started on 5th day before the predicted crest for 1955 Study
Atchafalaya Basin Control	Old River Control project assumed to be complete and fully opened during operation Morganza floodway assumed to commence operation when stage of 59.5 at River Mile (RM) 310.9 with full operation attained in 3 days Fuseplug levee of Tensas-Cocodrie leveed area assumed to crevasse at stage of 59.5 at Barbre Landing gage West Atchafalaya Floodway assumed to commence operation when stage of 61.1 at Barbre Landing is reached with full operation being achieved in 7 days

The routing of HYPO floods 58A, 52A, 56, and 63 through the seven reaches from St. Louis to the Latitude of Red River Landing assumed that the existing levees would not be overtopped and the flood-control features would be operated as described above.

The Puls routing was performed as described in Table 1-8.

Table 1-8. Puls routing method for seven reaches (Memorandum Report No. 1 [MRC 1955]).

St. Louis-Metropolis to Cairo	Flows at St. Louis and Metropolis added to those from the local area of this reach without travel time. Total inflow was routed to obtain the total outflow hydrograph at Cairo.
Cairo to Memphis	Outflows from Cairo were lagged 1 day for travel time and added to those from the local area to obtain total inflows. Total inflows were routed to Memphis.
Memphis to Helena	Outflows from Memphis were added, without travel time, to those from local areas to obtain total inflows. Total inflows were routed to Helena.
Helena to Arkansas City	Flows of White River at Clarendon and the Arkansas River at Little Rock were lagged 2 days for travel time and added to local flows and outflows from Helena without travel time to obtain total inflows. Combined inflows were routed to Arkansas City.
Arkansas City to Vicksburg	Flows of Yazoo River at Greenwood were lagged 4 days for travel time and added to those from the local area and outflows from Arkansas City without travel time to obtain total inflows. Total inflows routed to Vicksburg.
Vicksburg to Natchez	Outflows from Vicksburg were added without travel time to those from the local area to obtain total inflows. Total inflows routed to Natchez.
Natchez to Latitude of Red River Landing	Two simultaneous routings for Red-Atchafalaya Basin and Mississippi River Basin Stages at RM 310.9 determined by quantities of water passing from Old River Control and Morganza Floodway Structures and down the Mississippi River. Stages at Barbre Landing determined by quantities of water passing through Old River Control were stored in the Red River backwater and Tensas-Cocodrie leveed area, pass down the West Atchafalaya Floodway and down the Atchafalaya River itself. Iterative routings required until stage balance at Barbre Landing and RM 310.9 was achieved.

1.2.3.9 Reservoir regulation influences in the 1955 Study

In the early 1950s, a large number of flood control and multipurpose reservoirs were in operation, under construction, or expected to be constructed in the Mississippi River Basin. The majority of these reservoirs were designed primarily for local flood protection; however, the operation of these existing or future reservoirs were considered to provide benefits along the main stem of the Mississippi River. The 240 reservoirs considered were divided into the following groups:

Group E – Existing reservoirs and those under construction at the time of the study.

Group N – Near future reservoirs (excluding Group E) expected to be completed within 20 years from the time of the study.

Group D – Distant-future reservoirs (excluding Group EN) that were authorized, recommended to Congress, and likely to be proposed in studies under preparation.

The corresponding flood storage and area controlled upstream of the reservoirs are listed in Table 1-9.

Table 1-9. Reservoir groups for 1955 Study (Memorandum Report No. 1 [MRC 1955]).*

	Group E	Group EN	Group END
Number of reservoirs	107	151	240
Usable flood-control storage (1,000 acre-feet)	61,300	84,400	116,700
Area controlled (1,000 square miles)	472	685	740

***Notes**

Group END reservoir summaries are available in section G-03 in Memorandum Report No. 1 (1955); however, Group END hydrographs were never completed in the 1955 Study.

Unregulated (without consideration of reservoirs) flows near the mouth of the main tributaries that were computed for the four HYPO floods selected for detailed study were furnished to the divisions along with the associated unit hydrographs, the isohyetal maps of the HYPO storms, and the computed average rainfall excess for each area. Preliminary estimates of reservoir reductions at the mouths of main tributaries were requested for the various reservoir groups. These preliminary estimates of reductions were furnished for the Group E and Group EN reservoirs; however, the Ohio River Division was unable to furnish the modified hydrographs for Group END reservoirs, so hydrographs were not produced for key stations along the Mississippi River for Group END. Note that the maximum possible reductions were determined for each reservoir instead of estimating reductions using standard operational rule curves. Maximum reductions reflect use of available flood control storage to achieve the greatest reduction in peak flows on the main-stem Mississippi River at Cairo, IL, and below without consideration of local project authorization or operational rule curves. The only way to achieve the maximum reduction from reservoir storage requires knowing the entire storm event beforehand, a priori. Possible operational reductions based on applicable water control manuals would have been lower than those values calculated for this study.

Figure 1-7 shows the HYPO 58A flow hydrographs that compare the unregulated flows with corresponding flows considering the effects of the

E and EN reservoirs for the Mississippi River reach between Cairo, IL, and Memphis, TN. In Figure 1-7 the unregulated hydrograph (blue line) has the highest peak while the hydrographs for E reservoirs (red line) and EN reservoirs (green line) are successively lower due to the amount of reduction that results from increased reservoir storage effects from E and EN reservoirs, respectively.

Figure 1-7. Plot of regulation effects from Cairo to Memphis reach of Mississippi River.

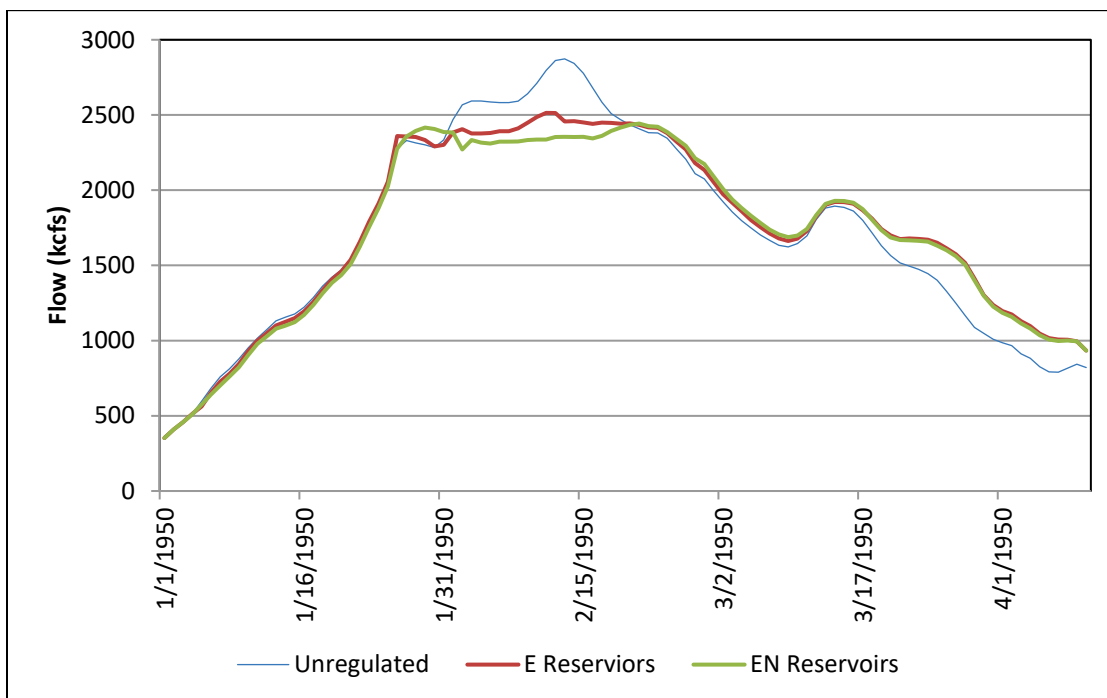


Table 1-10 itemizes the number of EN reservoirs, flood control storage, and drainage area controlled in each drainage basin.

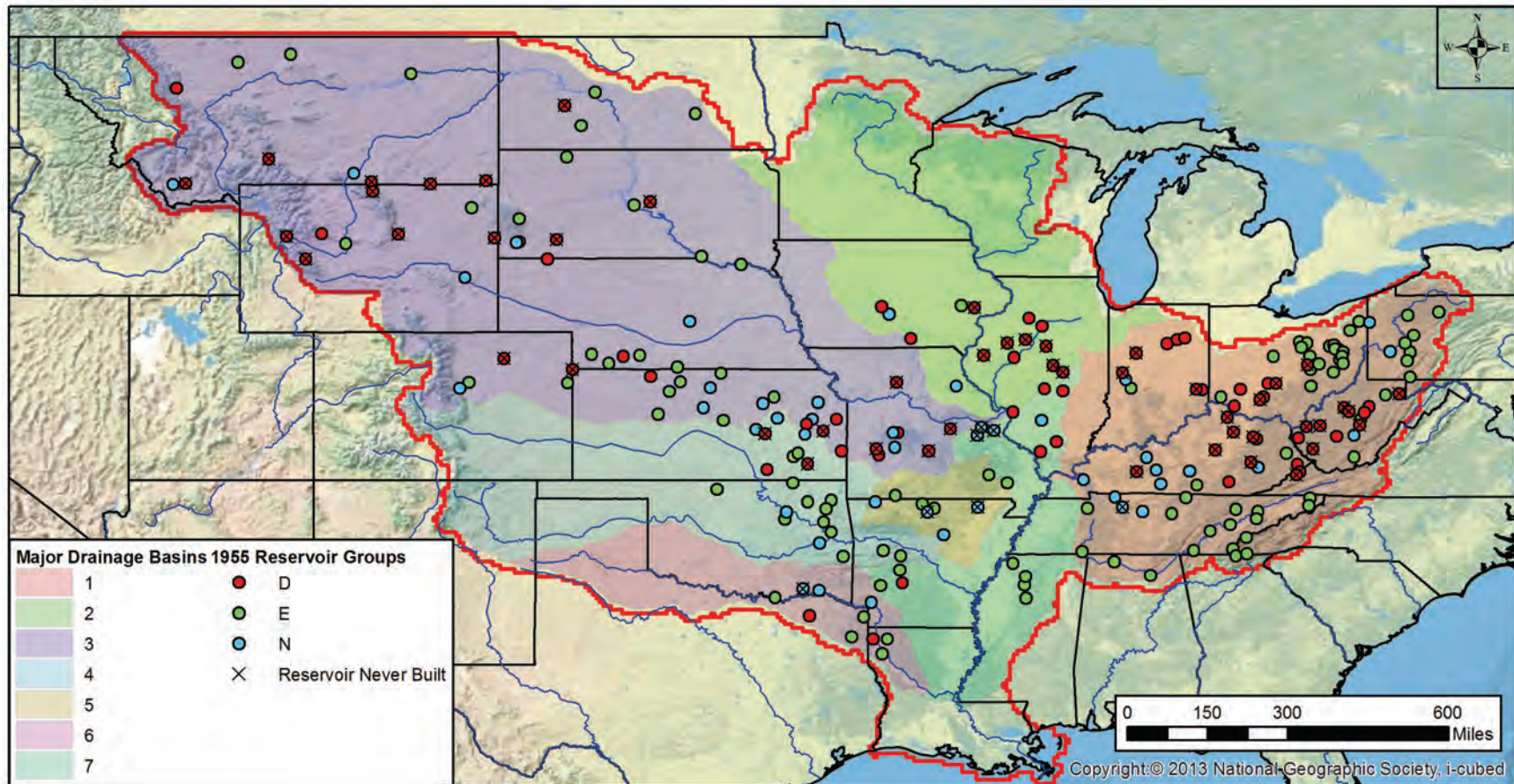
Reservoir locations for Groups E, N, and D projects are shown in Figure 1-8, including those reservoirs that were never built.

Table 1-10. Group EN reservoir data by basin (from Table G-1 Memorandum Report No. 1 [MRC 1955]).

Drainage Basin	Area No.	Number of Reservoirs	Usable Flood-Control Storage (1,000,000 acre-feet)	Drainage Area Controlled (1,000 square miles)
Ohio River above mouth	1	64	24.9	79.1
Mississippi River above Alton, IL	2	3	3.2	17.7
Missouri River above mouth	3	39	22.7	365

Arkansas River above Little Rock, AR	4	18	8.2	143.5
White River above Clarendon, AR	5	8	7.7	13.6
Red River above Alexandria, LA	6	8	10.3	53
Mississippi River local	7	11	7.4	12.9
Mississippi River above Latitude of Red River Landing	7	151	84.4	684.8

Figure 1-8. E, N, and D reservoirs listed in Memorandum Report No. 1 (MRC 1955).



Reservoir maps by state are shown in Appendix I. Table 1-11 lists each reservoir by group and basin. Reservoir names in parentheses are the current reservoir names that were assigned after reservoir completion. Crossed-out reservoirs are those that were never constructed.

Table 1-11. Group E, N, and D reservoirs from Memorandum Report Number 1 (MRC 1955).*

Ohio River Basin – Drainage Basin 1			
Group E			
Atwood	Beach City	Berlin	Bluestone
Bolivar	Burr Oak (Tom Jenkins)	Cagles Mill	Center Hill
Charles Mill	Chatuge	Cherokee	Chickamauga
Clendening	Conemaugh	Crooked Creek	Dale Hollow
Delaware	Dewey	Dillon	Douglas
Dover	East Branch (Clarion)	Fontana	Fort Loudoun
Guntersville	Hiwassee	Kentucky	Leesville
Loyalhanna	Mahoning	Mohawk	Mohicanville
Mosquito Creek	Norris	Nottely	Pickwick
Piedmont	Pleasant Hill	Senecaville	South Holston
Sutton	Tappan	Tionesta	Tygart
Watauga	Watts Bar (Mill Creek)	Wheeler	Wills Creek
Wolf Creek	Youghiogheny		
Group N			
Allegheny	Barren No. 2	Buckhorn	Green No. 2
Lower Cumberland (Barkley)	Mansfield (CM Harden)	Nolin	Rossvie
Rough River	Shenango	Stewarts Ferry (J. Percy Priest)	Summersville
Three Islands			
Group D			
Big Bend	Big Darby	Bireh	Booneville
Brookville	Burnsville	Caesar Creek	Cave Run
Clintwood	Deer Creek	East Fork (William H. Harsha)	East Lynn
Falmouth	Fishtrap	Frazeyburg	Haysi (John W Flannagan)
Huntington (JE Roush)	Jessamine	Laurel Branch	Logan
Metamora	Millersburg	Mining City	Mississinewa
Moore's Ferry	Mud River	Paint Creek	Poca
Rocky Fork	Rowlesburg	Salamonie	Steer Creek
Sugar Creek	West Fork L. Kanawha (London Lock and Dam)	West Fork Mon. (Stonewall Jackson)	Wildcat Creek

Mississippi River Basin above Alton, IL – Drainage Basin 2			
Group E			
Coralville			
Group N			
Joanna (Mark Twain)	Red Rock		
Group D			
Chain of Rocks	Hennepin	Jubilee	Kenney
Lake Senachwine	London Mills	Mackinaw-Dolls	Oakley
Recheater	Saylorville	St. Marys	Taylorville
Thompson Lake			
Missouri River Basin – Drainage Basin 3			
Group E			
Bonny	Boysen	Bull Hook	Cedar Bluff
Cherry Creek	Cold Brook	Enders	Fort Peck
Fort Randall	Garrison	Gavins Point	Harlan County
Heart Butte	Jamestown	Kanopolis	Keyhole
Kirwin	Lovewell	Medicine Creek	Oahe
Pactola	Shadehill	Tiber	Trenton
Tuttle Creek	Webster		
Group N			
Chatfield	Clark Canyon	Cottonwood Springs	Glendo
Glen Elder (Waconda)	Kasinger Bluff (Harry S. Truman)	Perry	Pomme de Terre
Pomona	Milford	Sherman	Wilson
Yellowtail			
Group D			
Absaroka	Alzada	Anchor	Blunt
Bronche	Chillicothe	Colwell	DuNoir
Edgemont	Fort Scott	Garnet	Hackleman Corner
Hillsdale	Hole in the Wall	London	Little Bighorn
Melvern	Moorhead	Narrows	Norton (Keith Sebelius)
Pioneer	Raft Lake	Rathbun	Red Willow
Rich Fountain	Richland	Rockyford	South Fork
Stockton	Sun Butte (Gibson)	Wray	
Arkansas River Basin above Little Rock – Drainage Basin 4			
Group E			
Blue Mountain	Fall River	Fort Gibson	Great Salt Plains
Heyburn	Hulah	Markham Ferry	Nimrod
Oologah	Pensacola	Tenkiller Ferry	Toronto
Wister			

Group N			
Council Grove	Eufaula	Keystone	Marion
Strawn (John Redmond)			
Group D			
Cedar Point	Elk City	Needesha	
White River Basin above Clarendon, Arkansas – Drainage Basin 5			
Group E			
Bull Shoals	Clearwater	Norfork	Table Rock
Group N			
Beaver	Greers Ferry	Lone Rock	Water Valley
Group D			
-	-	-	-
White River Basin above Clarendon, Arkansas – Drainage Basin 6			
Group E			
Bayou Bodcau	Denison	Ferrells Bridge	Texarkana (Wright Patman)
Wallace Lake			
Group N			
Boswell	Hugo	Millwood	
Group D			
Cooper (Jim Chapman)	Mooringsport (Cado Lake)		
Mississippi River Local – Drainage Basin 7			
Group E			
Arkabutla	Blakely Mountain	Enid	Grenada
Narrows	Sardis	Wappapello	
Group N			
Carlyle	Cedar Hill	Meremac Park	Union
Group D			
DeGray	Murfreesboro (Rend Lake)	Murphysboro	Shelbyville

***Notes**

Reservoir Names in parentheses are the current (2016) reservoir names that were selected after construction was completed.

Reservoirs that have been crossed out were never constructed.

1.2.3.10 Other flood reduction feature effects considered in the 1955 Study

Levees, floodwalls, and channel conditions for the 1955 Study conformed to those existing in 1950, except for levees on the main stem of the Lower Mississippi River, where levees and floodwalls were assumed to confine all flows and that the old River Control Structures were complete and operating (excluding the newer auxiliary structure that was added subsequent to the 1973 flood).

1.2.3.11 1955 Study results

At key locations along the main stem of the Mississippi River, Table 1-12 lists the estimated historical peak flows, the 1941 computed PDF peak flows, and the computed peak flows for the unregulated, regulated with E reservoirs, and regulated with EN reservoirs conditions for each of the four HYPO storms carried to detail design as presented in the 1955 Study. From the table, the peak flow from the 1937 flood at Cairo, IL, was estimated to be 2,002,000 cfs, and the peak estimated flow considering EN reservoirs for HYPO 58A at Arkansas City, AR, was computed to be 2,890,000 cfs.

Table 1-12. Summary of peak flows from Table H-2 (Memorandum Report No. 1 [MRC 1955]).

Peak Flows for Mississippi River (in 1,000 cfs)				
Description	St. Louis, MO	Cairo, IL	Arkansas City, AR	Latitude of Red River Landing
Maximum Flood of Record				
Q	1,040	2,002	2,615	2,345
Month	June	February	April	May
Year	1903	1937	1927	1927
Lower Mississippi River Design-Project Flood (1941)				
Q	---	2,450	3,065	3,000
HYPO 52A (May-June)				
Unregulated	1,920	2,600 ¹	2,490 ¹	2,250 ¹
E Regulated	1,840	2,490	2,320 ¹	2,050 ¹
EN Regulated	1,650	2,190	2,090 ¹	1,900 ¹
HYPO 56 (March-April)				
Unregulated	782	2,560	3,190 ¹	3,180 ¹
E Regulated	760	2,280	2,850 ¹	2,970 ¹
EN Regulated	661	2,090 ¹	2,750 ¹	2,670 ¹

Peak Flows for Mississippi River (in 1,000 cfs)				
Description	St. Louis, MO	Cairo, IL	Arkansas City, AR	Latitude of Red River Landing
HYPO 58A (January-February)				
Unregulated	255	2,850 ¹	3,210 ¹	3,320 ¹
E Regulated	255	2,500	2,950 ¹	3,130 ¹
EN Regulated	241	2,360	2,890	3,030 ¹
HYPO 63 (April-May)				
Unregulated	1,300	2,390	2,900 ¹	2,730 ¹
E Regulated	1,210	2,280 ¹	2,740 ¹	2,650 ¹
EN Regulated	1,090	2,120 ¹	2,480 ¹	2,480 ¹
Unregulated = Flows with no reservoir operations				
EN Regulated = Flows regulated by Group EN reservoirs				

¹Peak values from hydrographs in Annex C (USACE 1959).

Table 1-13 presents a comparison of the peak flows between the unregulated conditions and the EN reservoir conditions at key locations along the main stem of the Mississippi River for each of the HYPO storms carried to detailed design in the 1955 Study. From the table, the peak unregulated flow from the HYPO 58A flood at Cairo, IL, was estimated to be 2,850,000 cfs, and the peak estimated flow considering EN reservoirs for HYPO 58A at Cairo was computed to be 2,360,000 cfs; therefore, there was a 17% reduction due to reservoir effects.

Table 1-13. Reservoir group EN reductions by HYPO storm.

Item	Location (discharges given in 1,000 cfs)									
	Metropolis, IL; Ohio River	Alton, IL; Mississippi River	Hermann, MO; Missouri River	Little Rock, AR; Arkansas River	Clarendon, AR; White River	Alexandria, MO; Red River	St. Louis, MO; Mississippi River	Cairo, IL MS/OH; River Confluence	Arkansas City, AR; Mississippi River	Latitude of Red River Landing, MO; MS/Red River Combined
52A-U	783	710	1260	534	113	124	1920	2600	2490	2250
52A-EN	706	614	1070	369	81	106	1650	2190	2090	1900
% Reduction	10%	14%	15%	31%	28%	15%	14%	16%	16%	16%
56-U	1810	359	490	685	459	332	782	2560	3190	3180
56-EN	1460	341	387	386	341	208	661	2090	2750	2670
% Reduction	19%	5%	21%	44%	26%	37%	15%	18%	14%	16%
58A-U	2460	153	139	691	309	208	255	2850	3210	3320
58A-EN	2250	153	123	403	223	146	241	2360	2890	3030
% Reduction	9%	0%	12%	42%	28%	30%	5%	17%	10%	9%
63-U	1010	451	853	1060	379	155	1300	2390	2900	2730
63-EN	960	445	642	986	288	130	1090	2120	2480	2480
% Reduction	5%	1%	25%	7%	24%	16%	16%	11%	14%	9%

1.2.3.12 No frequency assignments for PDF Flood

Considerable variability exists in events that occur across the Mississippi River Basin, which encompasses over 1,246,000 square miles (40% of the continental United States). It is entirely possible to have different discharge probabilities across this area for a given event. For example, statistical analysis of annual peak flows may define annual exceedance probability (AEP) for an event that has a different AEP at some point upstream or downstream. Estimating the probability of a HYPO storm is problematic owing to the hypothetical combinations of multiple historic events, some of which were transposed and scaled up or down.

The 1941 study included frequency computations at Columbus, KY; Arkansas City, AR; and Vicksburg, MS, as a means to compare the degree of protection afforded by the levee system in the northern and middle sections of the Lower Mississippi River. The short historical period available at the time of the 1941 study could not be expected to accurately forecast the average frequency of occurrence of a flood of any given magnitude.

The 1955 Study also included frequency computations using extreme-value methods. The annual flow frequency data were plotted at four locations: St. Louis, MO; Cairo, IL; Arkansas City, AR; and Latitude of Red River Landing, LA. The reported values provide no correlation with the estimated HYPO peak discharges, presumably because the annual series used to develop the frequencies was not representative of the HYPO storm combinations.

1.2.3.13 Summary

The Lower Mississippi Valley has benefited from protective measures that have contained all Mississippi River floods since 1927, and this protection has afforded extensive growth in both farming and industry. The damage that would occur from the failure or overtopping of any of the major flood protective measures would be extensive. Therefore, an accurate estimate of the PDF is essential because it represents the maximum flood that can be reasonably expected to occur.

The four HYPO flood hydrographs were developed from a combination of events that are considered plausible in terms of time, areal extent, and specific location from a meteorological viewpoint, judging from past floods and storm sequences. A possibility exists that the occurrence of an unusual

combination of meteorological and hydrological events could produce a much larger flood than one of the four selected HYPO floods. However, the occurrence of such a sequence is considered highly improbable. To assure reasonably conservative estimates of reservoir capabilities in reducing major flood flows, the transposed storms used in the 1955 HYPO computations were assumed to be located at the downstream portion of the major tributaries, thus placing a substantial proportion of the rainfall downstream from reservoir sites.

On the basis of the 1955 Study, the HYPO 58A flood with EN reservoirs operating was adopted as the PDF for the Lower Mississippi River.

There was some question during the 1955 Study as to whether reductions by EN reservoirs should be assumed as fully effective in reducing the natural flood hydrographs of the adopted hypothetical flood. Certainly, Group E reservoirs had been built, but future construction of the Group N reservoirs was not assured. However, it was considered that the reservoir construction program would continue and that even though there may be changes in the timing of construction for individual reservoirs, it was quite likely that other reservoirs would have been built that would yield approximately the same effect as the near future group (Group N reservoirs).

1.3 Approach

The evaluation of the PDF hydrology for this investigation is described in the following sections.

2 Current Flowline Assessment (2016)

Re-evaluation of the PDF was instigated by the magnitude of the 2011 flood that broke peak stage and flow records along significant portions of the Lower Mississippi River. The current PDF is based on hypothetical storm combinations (from the 1955 Study) that produce the greatest storm with a reasonable chance of occurring.

Initially, a HEC-RAS unsteady model was developed following the 2011 flood to evaluate system performance during the flood. This model was expanded for the 2016 Mississippi River Flowline Assessment to develop a PDF flowline. During HEC-RAS model development for PDF conditions, it became clear that hydrologic data available from the 1955 Study were not sufficient to define flow inputs required for model simulations. The need for additional flow inputs precipitated the need to update the hydrologic analysis.

Updating the 1955 vintage hydrology involved developing a strategy for performing the required analysis. The general strategy involved the following steps:

1. Defining meteorological conditions
2. Defining required outputs
3. Developing model of rainfall-runoff processes
4. Calculating reservoir reduction effects.

A review of PDF meteorology was performed following the 2011 flood event (Appendix H). This review concluded that the existing PDF, HYPO 58A, remained the appropriate design event. This assessment did not redefine the original meteorological inputs. Instead, as prescribed in HMR 52 (Ely and Peters 1984), several assumptions were made relative to how full reservoirs are prior to a Probable Maximum Flood and the associated antecedent soil conditions. Each storm event included a warm-up period to set up reservoir and soil moisture states that would have been commensurate with the initial extreme storms used in the HYPO series. The HYPO rainfall was then applied on top of that. Therefore, the current assessment used the characteristics of the extreme storms and the associated hypothetical combinations of those storms from the detailed 1955 Study. This included HYPO 58A as the primary focus of analysis. The current assessment also evaluated a new HYPO storm combination based

on more recent storm events. The new storm combination, HYPO 11-73, utilized the 1973 and 2011 storms in a sequence developed following the procedures used to assemble the 1955 HYPO storms.

The required inflow and internal boundaries from the HEC-RAS unsteady model determined required locations for hydrologic outputs. Based upon schedule and budget constraints, a joint effort between USACE and NWS determined that the NWS operational hydrologic model would be used. The NWS operational forecast model became the model that would be used to perform all hydrologic analysis. These models are used on a daily basis for producing river forecasts throughout the Mississippi River Basin, including forecasts relied upon for making critical decisions during flood events.

A significant component of the current assessment sought to evaluate how current methodology differed from that used for the 1955 Study. The major difference involved use of the NWS numerical models that apply continuous hydrologic processes across the entire Mississippi River Basin, whereas the computations were manually performed in 1955 and included manipulations to reduce the number of hand calculations necessary. For example, hydrologic engineers used experience-based judgment in the 1955 Study to determine which storms were applied to different parts of the watershed over the HYPO storm sequences to maximize the effect from specific sub-watersheds. Because of the major differences in hydrologic computations between 1955 and the current assessment, it was necessary to consider more than the HYPO 58A storm. Therefore, HYPO storms 52A, 56, and 63 were included to help evaluate differences in methodologies.

To assess the adequacy of the 1955-vintage PDF hydrology, the 2016 hydrologic assessment had to provide the following:

1. The required boundary conditions for the HEC-RAS unsteady model
2. Hydrologic computations for antecedent conditions, rainfall-runoff, and reservoir effects that were based on current practice
3. A means to assess how the current methodology compared to the original methods

4. Output hydrographs that were comparable in magnitude and volume to the original 1955 Study¹.

2.1 General criteria

The current hydrologic analysis addressed the four areas of concern listed above, as follows.

1. A HEC-RAS unsteady model² was developed to meet computational requirements for the Mississippi River Flowline analysis. External limits at primary inflow points were used to identify locations where inflow boundary hydrographs were required. Additional internal boundary hydrographs needed for intervening flow areas were also identified during HEC-RAS model development. The hydrologic model results were defined so that these external (inflow) and internal boundary hydrographs were available for direct input to the HEC-RAS model. Section 2.2 describes the connection between the hydrologic models and the HEC-RAS model.
2. Evaluation of hydrologic model computations relative to the 1955 analysis included comparisons of storm isohyetal maps and precipitation depth-area relationships, evaluation of land use changes, and comparison of computed hydrographs against hydrographs resulting from the HYPO 58A storm (Section 2.8 and 2.5) . Reservoir effects as discussed in Section 2.10 were modeled based on current practice (by the project water control manuals), which differed from how reservoir storage was utilized in the 1955 analysis.
3. Comparing the effects of current methodology with that used in the 1955 analysis was primarily accomplished by comparing hydrologic model outputs with published results from 1955. This included the HYPO 58A unregulated and regulated hydrograph simulations as well as for the HYPO 52A, 56, and 63 simulations (Section 3).
4. Digitized and tabulated hydrographs from the 1955 results were compared with model simulation results to assess agreement between computed peak discharge rates and hydrograph shape (Section 3).

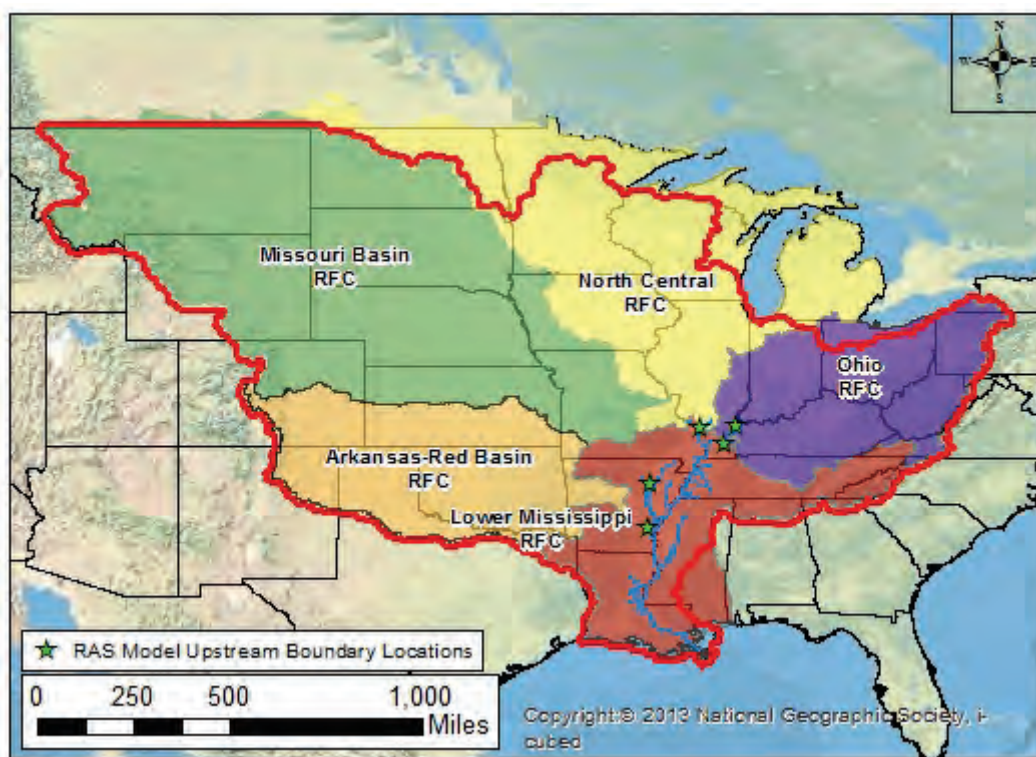
¹ It was not initially known how the 2016 assessment results would compare with previous results. However, the 1941 and 1955 updates yielded somewhat similar flows. Because the same 1955 HYPO storms were to be used for precipitation inputs, it was assumed that the 2016 results should also be similar.

² See separate report volume (USACE 2018) that documents the HEC-RAS model and its development.

2.2 Analysis framework

Previous studies utilized steady-state hydraulics to calculate water surface elevations using peak discharges developed using unit hydrograph theory and various methods for routing hydrographs. The 2016 analysis utilized an unsteady hydrodynamic model. This unsteady flow model included changes in flow and river dynamics through time and required continuous flow hydrographs at upstream boundaries and for other areas that required internal flow contributions. Figure 2-1 shows the Mississippi River Basin with the limits of the unsteady HEC-RAS model extent shown along with NWS River Forecast Centers (RFC).

Figure 2-1. Mississippi River Basin with HEC-RAS extent shown.*



*Note: Red line indicates the USACE area of responsibility for the Mississippi River watershed.

To develop the required hydrologic inputs, the entire watershed was simulated using NWS hydrologic models.

2.2.1 Unsteady hydrodynamic model (HEC-RAS)

The HEC-RAS model was built to include the mainstem Mississippi River as well as significant tributary streams. The model extended from Chester, IL, to the Gulf of Mexico on the Mississippi River with the Ohio River

reach extending upstream to Smithland. The model was extended up significant tributaries, those having a contribution that influenced model calibration for the 2011 event, to locations that had NWS model sub-basin computation points or at the end of model routing reaches. A separate, companion report details HEC-RAS model development (USACE 2018). Inflow hydrographs were directly input at boundaries where the HEC-RAS model started on river channels. Besides upstream boundaries that represent where the model connects to the main river channels, a number of internal connections were required to achieve HEC-RAS model calibration to the 2011 event. Figure 2-2 illustrates the HEC-RAS model reaches and primary inflow boundary locations.

Figure 2-2. HEC-RAS model extent and inflow boundary locations.

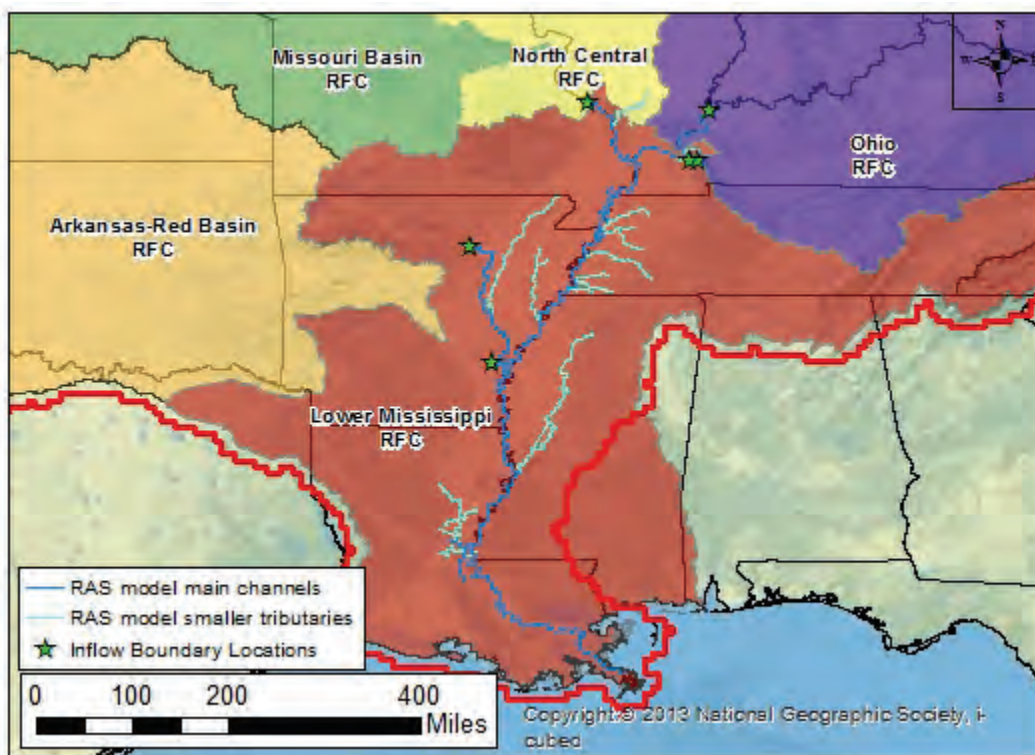
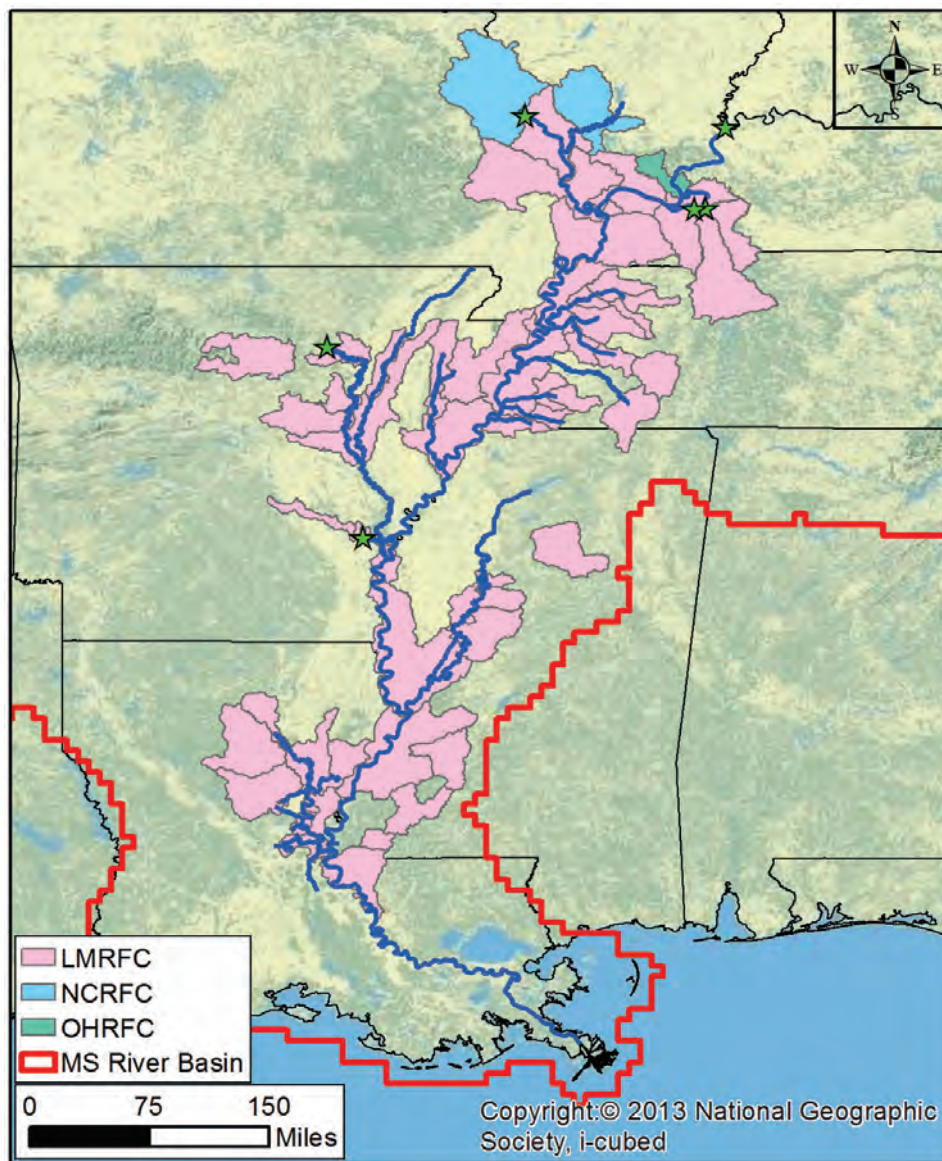


Figure 2-3 illustrates the sub-basins from the hydrologic model that provide internal inputs to the HEC-RAS model. Internal inputs were defined as areas that provide local flow within a reach or a minor tributary that provides a relatively small percentage of overall flow to the total Mississippi River.

Figure 2-3. Hydrologic sub-basins providing local inputs to HEC-RAS model.

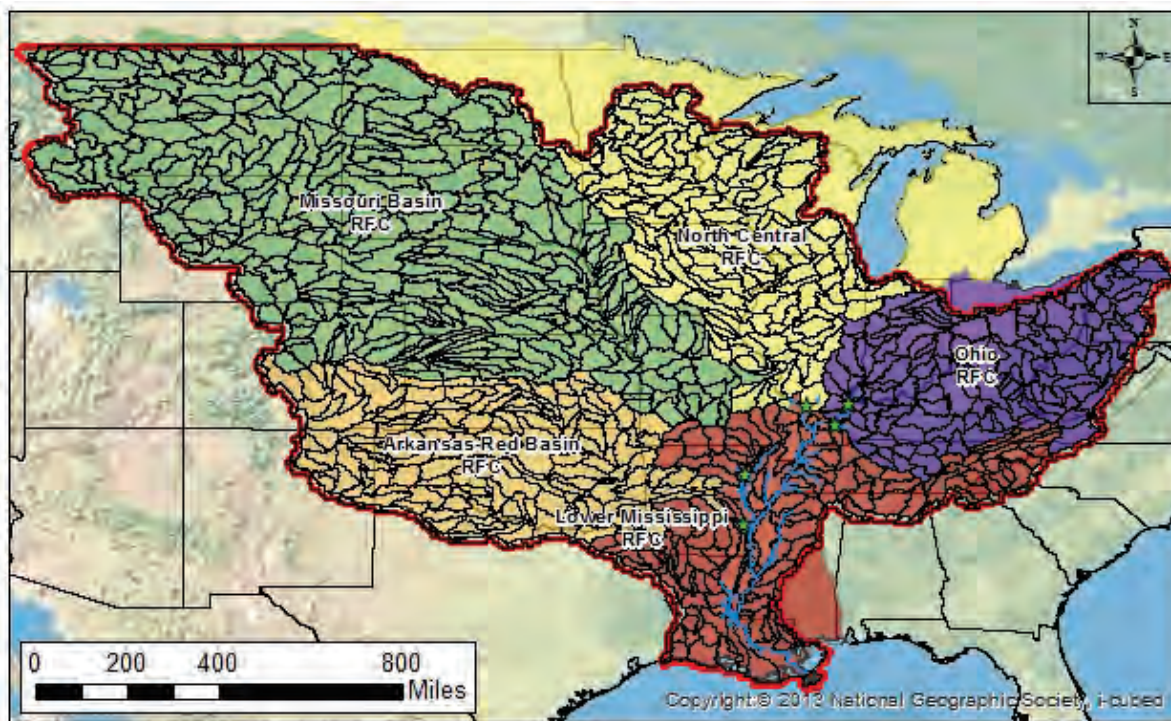


2.2.2 Hydrologic model linkages

The hydrologic model used for the current assessment produced outputs for all modeled sub-areas and computation points in the NWS Community Hydrologic Prediction System-Flood Early Warning System (CHPS-FEWS) configurations.

Figure 2-4 shows that the hydrologic model included 7,066 sub-basins, significantly more sub-basins than the 44 from the 1955 Study. The methods used within the models are described in the following sections of this report. Additional details on the CHPS-FEWS model schematization and computation algorithms can be found in Section 2.4.

Figure 2-4. Mississippi River Basin showing NWS RFC sub-basins.



After each RFCs model run was completed, results were passed successively to downstream RFCs to use as inflows until simulations for the entire Mississippi River Basin were complete. The hand-off process from upstream to downstream for unregulated simulations is described as follows:

1. Missouri Basin River Forecast Center (MBRFC) imported HYPO storm data and completed model simulations; results were passed to North Central River Forecast Center (NCRFC).
2. NCRFC imported HYPO storm data and MBRFC results then completed model simulations; results were passed to the Lower Mississippi River Forecast Center (LMRFC).
3. Ohio River Forecast Center (OHRFC) imported HYPO storm data and completed model simulations; results were passed to LMRFC.
4. Arkansas Basin River Forecast Center (ABRFC) imported HYPO storm data and completed model simulations; results were passed to LMRFC.
5. (OPTIONAL) Tennessee Valley Authority (TVA) imported HYPO storm data and completed CHPS-FEWS and RiverWare model simulations; results passed to LMRFC.
6. LMRFC imported HYPO storm data, NCRFC results, OHRFC results, and ABRFC (OPTIONAL plus TVA) results and completed model simulations.

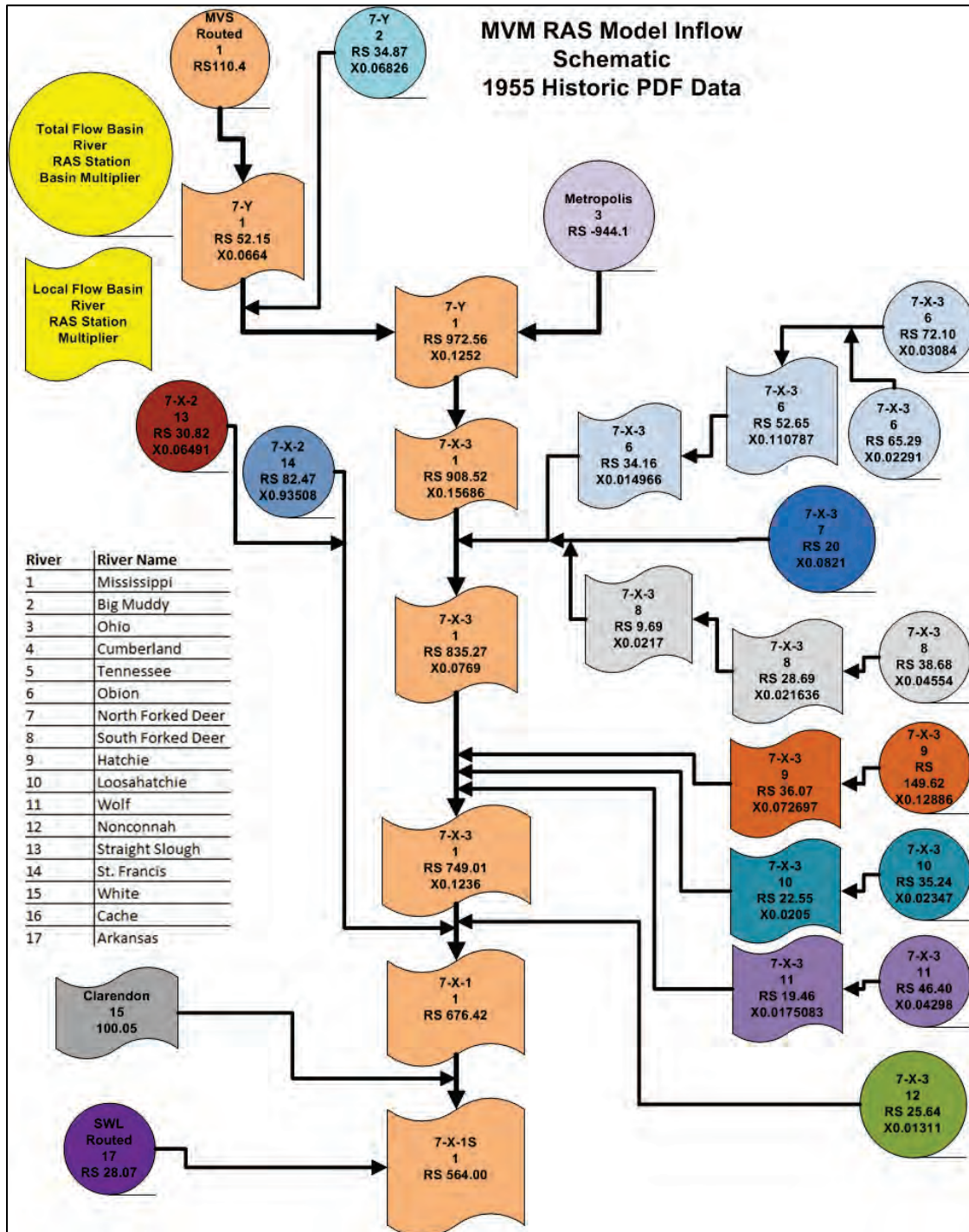
Once a complete simulation from all CHPS-FEWS model segments was finished, LMRFC exported the specific output locations needed for the HEC-RAS model. The extraction process included conversion of a selected list of sub-basin and computation point outputs into the Hydrologic Engineering Center-Data Storage System Visual Utility Engine (HEC-DSSVue) for import into the HEC-RAS model.

2.2.2.1 Replication of 1955 Study

The HEC-RAS unsteady model was configured to run using the limited hydrologic data from the 1955 Study. This coarser resolution of tributary inflows was not desirable for sufficient unsteady modeling of the tributary connections, but it provided a direct means to compare results with prior analyses. HEC-RAS inputs were developed directly from the Memorandum Report No. 1 (MRC 1955) and related computation tabulations from the MRC archives.

Figure 2-5 provides a diagram of the HEC-RAS boundaries for these model runs. The HEC-RAS 1955 PDF model obtained all required inputs directly from Memorandum Report No. 1 (MRC 1955) and did not require any outputs from the hydrologic model. The sub-basin names from the 1955 analysis that are shown in Figure 2-5 (for example 7-Y or 7-X-3) reflect sources of boundary inflows.

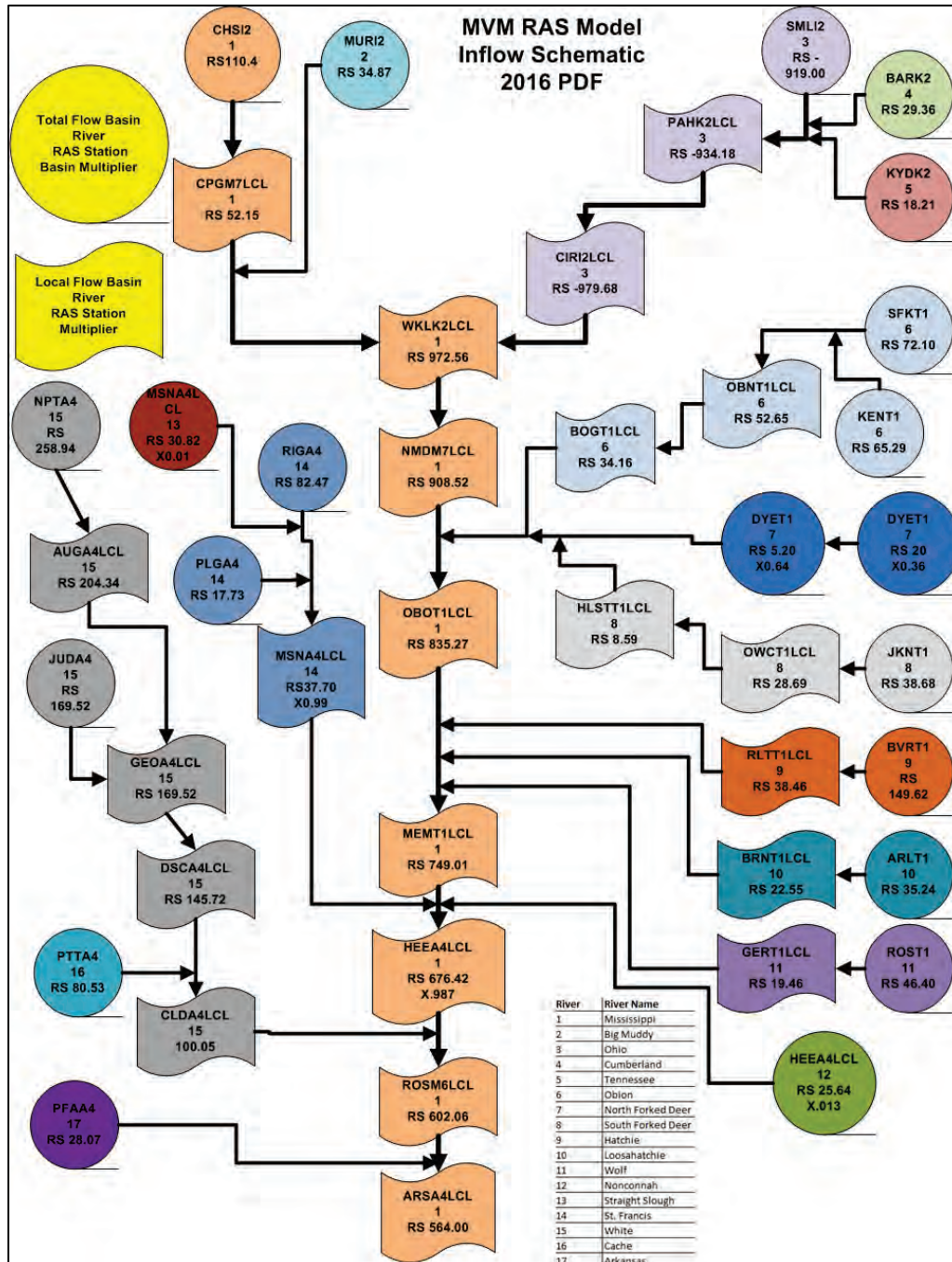
Figure 2-5. HEC-RAS Model schematization for 1955 hydrologic inputs.



2.2.2.2 Current assessment

The HEC-RAS model was reconfigured to run using the current hydrologic data available from NWS RFC model outputs. Figure 2-6 provides a diagram of the HEC-RAS connections for the 2016 analyses. The sub-basin names given in Figure 2-6 correspond to the NWS model output IDs.

Figure 2-6. HEC-RAS Model schematization for 2016 hydrologic inputs.



2.3 Procedural approach

Two scenarios were identified for determining the effects of different methodology used between the 1955 analysis and the current NWS forecast models.

Scenario I developed the PDF inflow hydrographs using the 1955 PDF report antecedent climatic conditions. This scenario utilized precipitation and temperature data from the historic period prior to the first storm in each HYPO sequence as initial forcings¹ in the NWS hydrologic models. To warm up the model simulation, a period of 6 to 9 months was simulated to produce flows and run-off characteristics consistent with the period used in the 1955 analysis. The warm-up period varied in length to capture a full winter season prior to start of the actual HYPO sequence. This was necessary to develop snow water equivalents for the entire winter season that would be available to contribute to flood hydrographs.

Scenario II would have developed the PDF inflow hydrographs using antecedent conditions reflecting spring (April/May, i.e., 2011 event) snowmelt and precipitation. Study objectives, schedule, and funding prohibited the execution of Scenario II.

Each scenario included analysis of HYPO storms 58A, 56, 52A, and 63 as described in Section 1.2.3.5. A description of the seasonality and predominant area impacted by each HYPO is given below:

- HYPO 58A (winter season) storm combination for Mouth of Ohio River to Gulf of Mexico
- HYPO 63 (early-spring season) storm combination for Middle Mississippi from Mouth of Ohio River to Cape Girardeau, MO
- HYPO 52A (late-spring season) storm combination for Arkansas-White Tributaries
- HYPO 56 (early-spring season) storm combination for White and Red River tributaries.

River Forecast Centers

Running these scenarios with the NWS CHPS-FEWS model suite required coordination across five different NWS River Forecast Centers (RFC):

ABRFC = Arkansas Basin RFC
 LMRFC = Lower Mississippi RFC
 MBRFC = Missouri Basin RFC
 NCRFC = North Central RFC
 OHRFC = Ohio RFC

Figure 2-4 shows the area of coverage for each RFC.

¹ Forcings are state conditions imposed on the model at start-up. Model state conditions include antecedent soil moisture, stream flow, temperature, precipitation, and snow pack state at the first model time-step.

The 1955 Study determined that HYPO 58A was the governing combination that defines the PDF for the Lower Mississippi River. This determination was confirmed by a Meteorological Assessment following the 2011 flood (see Appendix H). Therefore, the current assessment used HYPO 58A to develop required inputs for the HEC-RAS unsteady hydrodynamic model. For each HYPO storm simulation, warm temperature-induced snowmelt was also included by using prevailing temperatures from the time of each historical storm used in developing the HYPO storm sequence.¹ Analysis using HYPO 52A, 56, and 63 was included only to provide a means to evaluate and to check the methodology using current practice against the 1955 Study results.

Team dynamics

HYPO storm events were used to develop inflow hydrographs needed for the HEC-RAS unsteady model of the Lower Mississippi River to assess the PDF Flowline. The HYPO storm events that define the 1955 PDF include the effects of Groups E and N reservoirs. The specific HYPO event for the 1955 PDF was labeled as 58A-EN. HYPO 58A-EN flows defined the water surface profile used to establish levee design grades beginning in 1956. The CHPS-FEWS model simulations were first run including reservoirs that existed in the model configurations to assess the regulated condition. While reservoir configurations existed in the CHPS-FEWS models, the NWS simulations for this assessment used automated routing through the reservoirs and did not include any operator over-rides (see Section 2.4.1 for description of the CHPS-FEWS model). In general, the automated reservoir routing from the NWS models was more than approximately 10% higher than when using manual routing. Because the initial regulated CHPS-FEWS runs did not include manual over-rides at specific projects, it was necessary to expand the analysis group to include 10 USACE districts to perform more detailed reservoir routing. The more detailed reservoir routing was done only for projects identified by the USACE districts to have a possible influence on flows at Cairo, IL. The TVA also assisted in detailed regulation calculations for reservoirs on the Tennessee River system. The NWS automated reservoir routing continued to be used for projects that were considered to have no influence on flows at Cairo, IL. Detailed reservoir routing by the USACE districts and TVA followed

¹ Temperature sequences for each HYPO event were developed using historic temperature data in similar fashion to how precipitation sequences were developed (see Section 2.8 for details).

published operational rule curves with regulator adjustment for the current assessment.

The designation for the 2016 regulated PDF HYPO was 58A-R. The new designation, 58A-R, was necessary because the EN condition represented a specific list of reservoirs that was different than used in the 2016 analysis. The 2016 analysis used reservoirs that existed at the beginning of the investigation (circa 2014). Section 2.10 provides specific details on the regulated model simulations. The work was a collaboration among 10 USACE districts, the TVA, and 5 NWS RFCs.

Figure 2-7 shows the general team and their respective roles. Each RFC prepared and executed model simulations for each historic event coordinating with other RFC offices just as in preparing their daily forecast. LMRFC provided a gateway between USACE data and CHPS-FEWS modelers. LMRFC has developed procedures for exchange of data between the CHPS-FEWS model format and the USACE HEC DSSVUE format. USACE coordinated with the U.S. Geological Survey (USGS), TVA, and various USACE district offices to obtain the necessary reservoir release data for event simulations. The process for generating regulated results is shown in Figure 2-8.

It was envisioned that simulation of the HYPO storm events with CHPS-FEWS may have been best accomplished through a table-top exercise. This was only partly accomplished because of the large number of offices involved. The table-top format was considered desirable because CHPS-FEWS simulations for HYPO storm inputs required iterative operator manipulation of reservoir releases in some cases. Two locations where iterative regulation computations could have significant influence on regulated flows at Cairo, IL, were Kentucky Dam on the Tennessee River and Barkley Dam on the Cumberland River, both of which required consultation with TVA and Great Lakes and Ohio River Division for use of their models to develop *forecasted* project releases.

Figure 2-7. Team alignment and general roles for simulation of historic events.

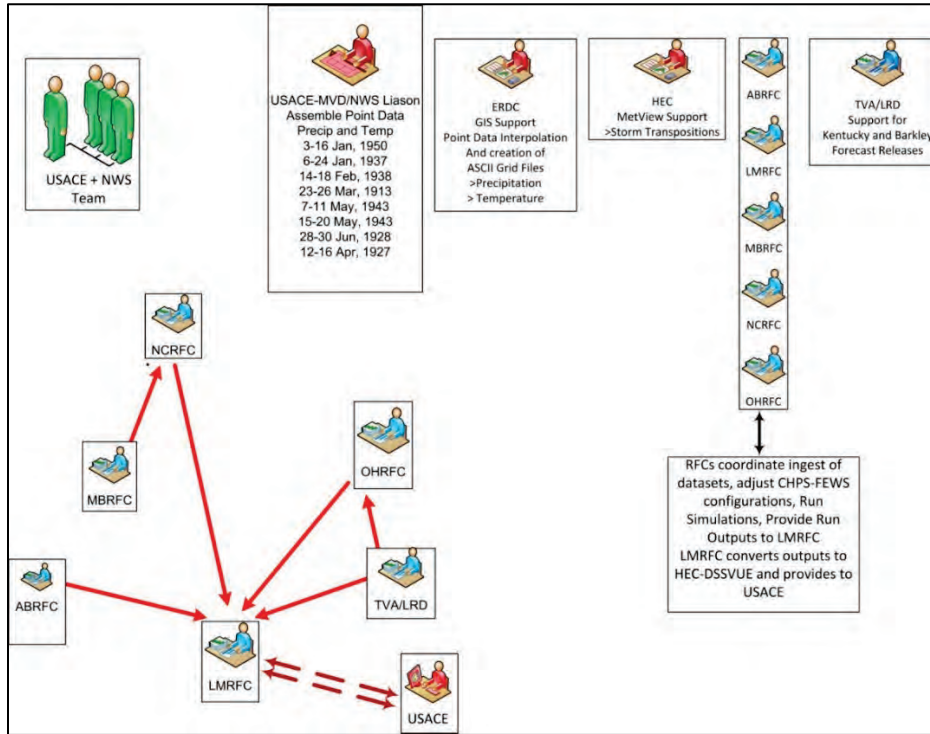
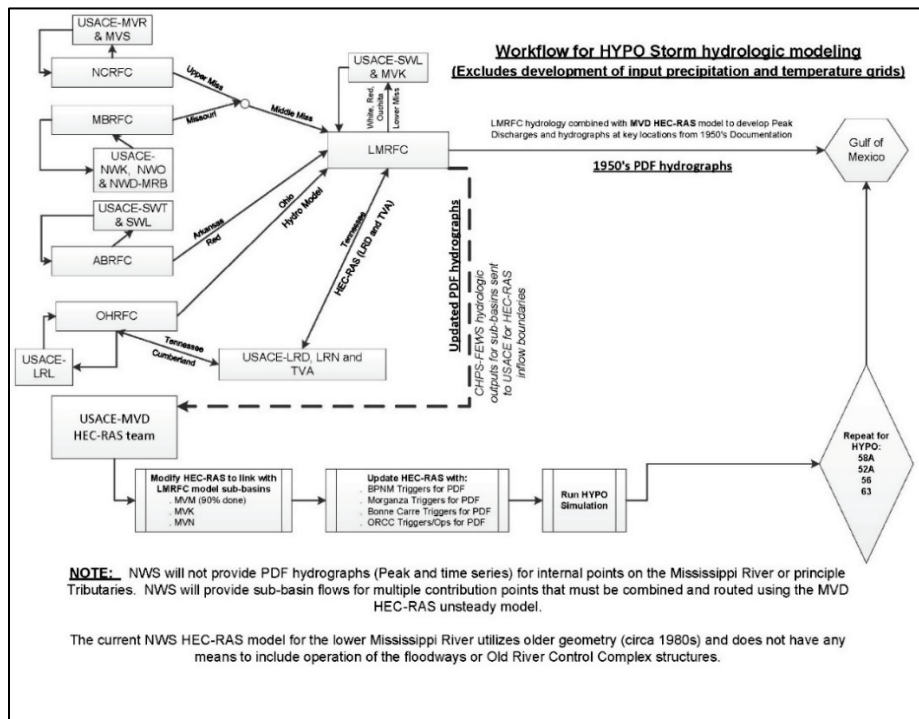


Figure 2-8. General team process to generate regulated results for HYP0 storm modeling.



The 1955 Study results centered on analysis of peak flows with limited information defining complete hydrographs. These results yielded only a few locations where hydrographs existed to compare with 2016 model results. Further, the 1955 Study documents did not provide specific details defining how regulation effects were calculated. To maximize use of available data for comparisons, it was necessary to simulate both unregulated and regulated conditions to evaluate hydrologic model outputs against the previous results.

The unregulated results provided a direct way to compare model results for 1955 calculations and 2016 simulations with the only difference being basic hydrologic parameterization and calculations. No additional assumptions or configurations related to reservoir regulation were needed for direct comparison with 1955 unregulated results. For example, had the only simulation been for regulated conditions, any difference between new model outputs and 1955 results could have been due to assumed hydrologic model parameters, hydrologic computation techniques, reservoir routing assumptions, or any combination thereof. Excluding the reservoir routing assumptions with the unregulated simulations provided a means to assess the differences in methodology (parameterization and computation technique) employed in development of the hydrologic models.

2.4 Hydrologic model

Due to limitations discussed in Section 1.2, it was not feasible to develop new basin-wide hydrologic models required for the present assessment. Therefore, the USACE collaborated with the NWS to leverage its existing hydrologic forecast CHPS-FEWS¹ models to simulate scenarios that examined how hydrologic changes within a watershed impact the PDF runoff and, by extension, the PDF Flowline.

CHPS-FEWS operational models included calibration measures² that best reproduced existing 2010–2014 conditions. This does not imply that all sub-basins within each RFC model domain had been calibrated in the same level of detail; rather, the overall model performance at NWS forecast points

¹ The NWS Community Hydrologic Prediction System (CHPS) utilizes the DELTARES Flood Early Warning System (FEWS) model to simulate rainfall-runoff events and develop river forecasts throughout the United States. This suite of modeling tools is referred to CHPS-FEWS.

² NWS forecast models are calibrated empirically to historical streamflow records, using historical precipitation and temperature forcings, with a tendency to weight more recent periods of history more heavily when basin characteristics show evidence of change. This is done to provide the best parameterization for current event forecasting.

had been used to adjust model parameters to achieve reliable forecast values for each RFC. These adjustments are continuously made as part of routine forecast operations to refine the model's ability to predict flow and stage throughout each RFCs area of responsibility. Therefore, land use, overland and channel routing, as well as any channel ratings used in the CHPS-FEWS models, likely had significant differences from the conditions that existed at the time of each historic event considered in this analysis (1913–1950). The historic data needed to calibrate the NWS operational model to prior periods of time were not available, which made it impossible to address changes in model parameterization for infiltration, routing, land use, and snow melt over time.

2.4.1 Basic CHPS-FEWS model

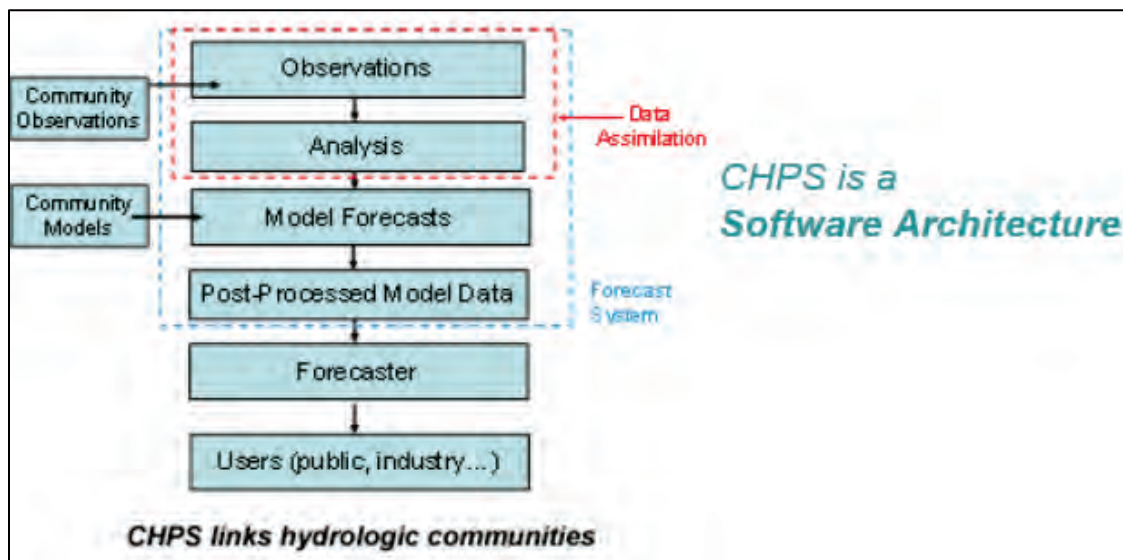
In 2010, the NWS began full implementation of their Community Hydrologic Prediction System (CHPS). CHPS, part of the NWS modernization plan, was developed on the base platform of the Delft Hydraulics Flood Early Warning System (FEWS).

FEWS is a suite of infrastructure software maintained and supported by Deltares. On its own it does very little; it is primarily a generic mechanism to pass data from one place (e.g., a user interface) to another (e.g., a hydraulic model), and it performs some basic time-series data transformations. Only when FEWS is configured for the user's specific domain does it transform into a functioning system. A user would supply the necessary modeling operations or acquire them from a source that shares (open source) or sells FEWS-compatible models.

CHPS is National Oceanic and Atmospheric Administration (NOAA) customized application of FEWS. CHPS runs models that are compatible with FEWS — including those migrated from the National Weather Service River Forecast System (NWSRFS). NWSRFS was the NWS legacy modeling framework that provided extra user capabilities not available via FEWS, such as model calibration. In the future, NOAA will make CHPS models available to other FEWS users.

CHPS assists the growing community of hydrologic users sharing data and computer models as shown in Figure 2-9.

Figure 2-9. CHPS schematic.



This requires improved cooperation and coordination within NOAA, as well as with other federal, state, municipal, academic, and private institutions. Better coordination among water agencies was sought to improve the accuracy and utility of the entire community's water-based forecasts. CHPS provided a new business model in which members of the hydrometeorological community operate more collaboratively through the sharing and infusion of advances in science and new data, without each member having to build or take ownership of the entire system.

FEWS provided only an interface to run models in a forecast environment. There were no inherent modeling capabilities. All models linked through FEWS followed the same approach. Data were exported from the interface to the model using a defined format known as Published Interface (PI). Model runs were made in their own native environment and data formats. Data were imported to the models using the same PI exchange. Model outputs were passed back to FEWS and exported using the same PI exchange.

Figure 2-10 and Figure 2-11 present the concept and management of model inputs and outputs.

Most hydrological forecast models are initial state type models; that is, they require a known state from which to start. CHPS required initial forcings (data inputs) to define the model start state. This includes climatic and meteorological inputs as well as any reservoir regulation states that should exist at the start of a run.

Figure 2-10. FEWS concept for managing inputs, modeling, and outputs.

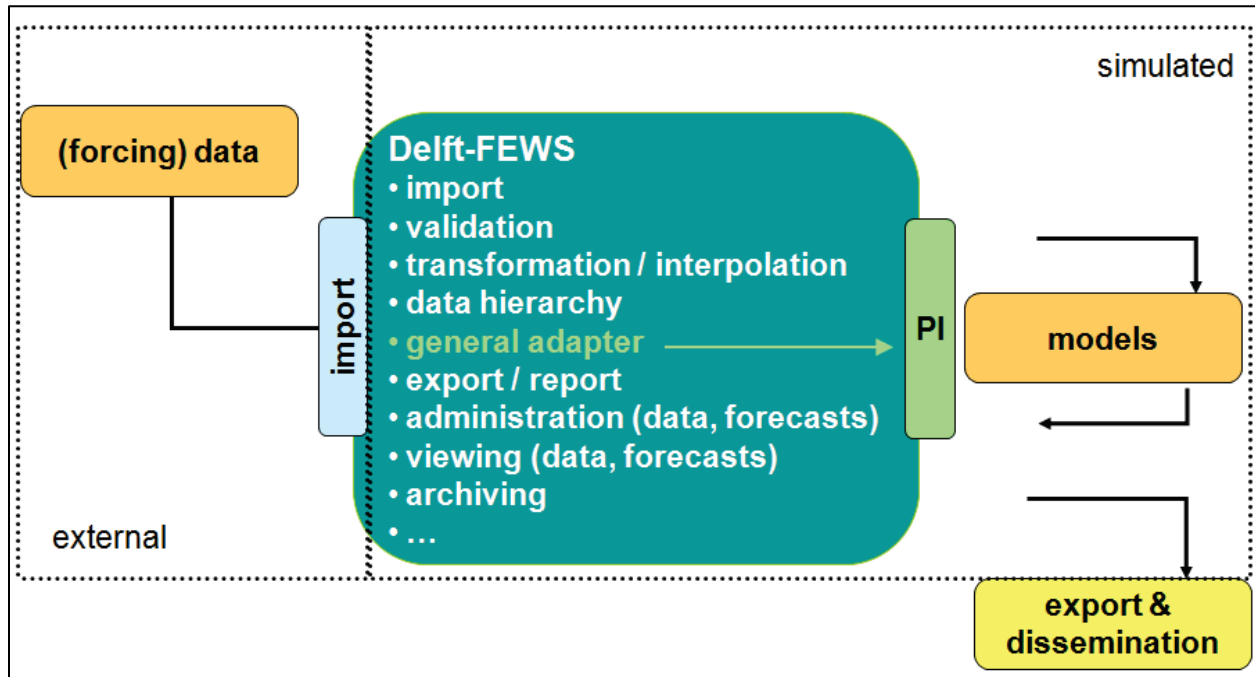
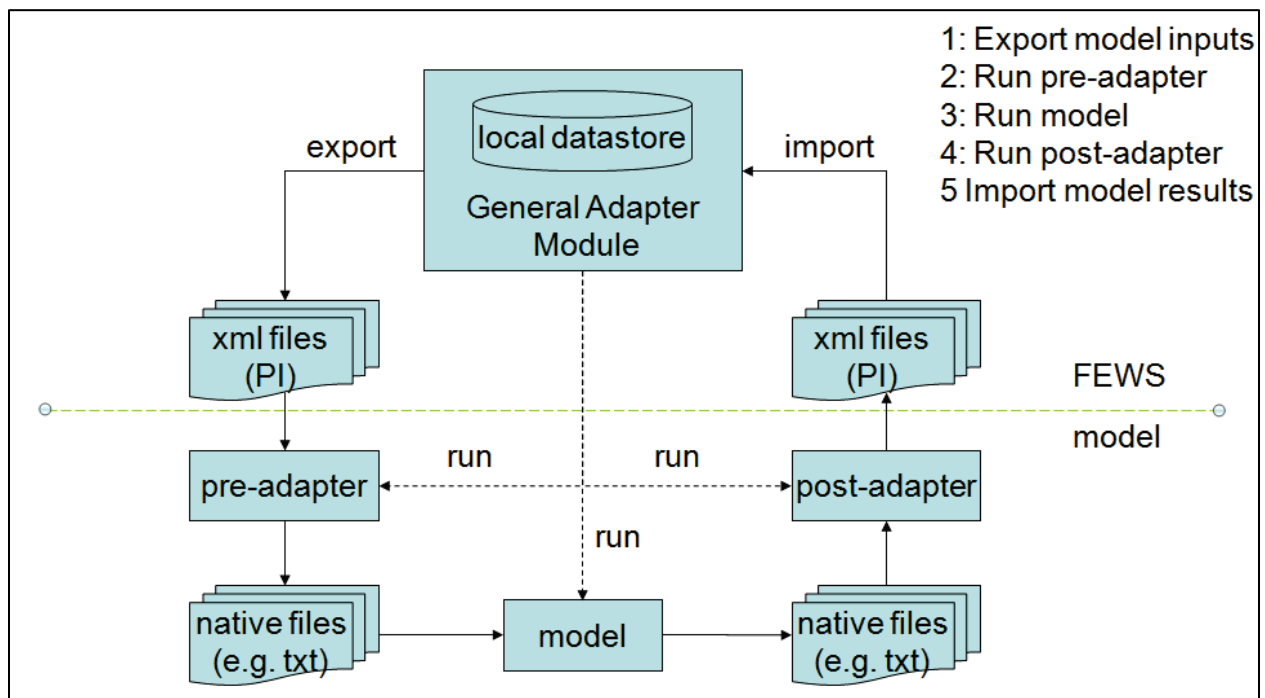


Figure 2-11. FEWS management of model input and output.



The NWS CHPS models run entirely on Linux on the NWS Advanced Weather Interactive Processing System. A general description of the primary NWS models that are run in CHPS follows in the next sections¹.

The TVA also uses a version of CHPS-FEWS to simulate hydrology over the Tennessee River basin as part of their daily operations. TVA operations included hydro power generation, navigation, and flood risk reduction. TVA also uses RiverWare² to assess regulation needs and release requirements based on hydropower, navigation, flooding, and environmental requirements.

2.4.2 Primary NWS hydrologic operations

Snow Accumulation and Ablation (SNOW-17) Model³

The NWS uses the SNOW-17 snow accumulation and ablation model as a component of the CHPS system. SNOW-17 is a conceptual model that uses precipitation and temperature as inputs to maintain an accounting of the water equivalents and depth. All of the RFCs participating in the Flowline assessment use the SNOW-17 model with the exception of the LMRFC, which typically does not have much snow to contend with.

Sacramento Soil Moisture Accounting (SAC-SMA) Model⁴

The SAC-SMA is a conceptually based soil moisture accounting model that computes the runoff derived from rainfall inputs and evaporation losses. The model is characterized by two layers (zones) with tension and free water components. The soil moisture parameters making up the SAC-SMA model are not tied to any physically measured soil characteristics; rather, they are manually calibrated along with the SNOW-17 model (where used) and a unit hydrograph operation to time-distribute the generated runoff to produce simulated flows that reproduce historical flows as closely as possible⁵. All of the RFCs in the Flowline assessment area including the TVA used the SAC-SMA model.

¹ <http://www.nws.noaa.gov/oh/hrl/general/indexdoc.htm>

² RiverWare™ is a general river basin modeling tool developed by CADSWES that includes reservoir operations and optimization components (<http://riverware.org/>).

³ <http://www.nws.noaa.gov/oh/hrl/general/chps/Models/SNOW-17.pdf>

⁴ http://www.nws.noaa.gov/oh/hrl/general/chps/Models/Sacramento_Soil_Moisture_Accounting.pdf

⁵ http://www.nws.noaa.gov/oh/hrl/general/chps/Models/Unit_Hydrograph.pdf

Lag and K Routing (LAG/K) Model¹

The LAG/K routing is widely used by the NWS as a method of storage routing between flow-points. It is configured to accommodate either constant or variable Lag and K elements that can be used together or separately to account for lag with no attenuation or attenuation with negligible lag. LAG/K routing was the predominant lumped routing method used by NWS offices within the Flowline assessment area.

Tatum Routing Model²

Tatum coefficient routing is a numerical non-storage method of routing a hydrograph through a channel. Tatum coefficient routing is not closely tied to the physical processes of river hydraulics. Coefficients at specific ordinates are used to route flow. These coefficients are usually empirically derived through examination of inflow and outflow hydrographs. The NCRFC uses Tatum routing extensively.

Single Reservoir Regulation (RES-SNGL) Operation³

The NWS RES-SNGL operation is designed for the simulation of single independently operated reservoirs. The operation is set up so that it may be calibrated with rules and seasonal guide curves to replicate real-world reservoir operation objectives such as flood control and power generation. The RES-SNGL operation is designed to accommodate simulation of reservoir outputs with or without forecast releases.

Joint Reservoir Regulation (RES-J) Model⁴

The RES-J model can simulate either a single reservoir or a system of reservoirs.

2.4.3 Running NWS CHPS for the Flowline project

The NWS RFC models are operationally run as a continuous model and typically store model states for soil moisture, unit hydrographs, routings, and reservoirs for each model time-step so that the model is prepared for

¹http://www.nws.noaa.gov/oh/hrl/general/chps/Models/Lag_and_K_Routing.pdf

²http://www.nws.noaa.gov/oh/hrl/nwsrfs/users_manual/part2/pdf/24tatum.pdf

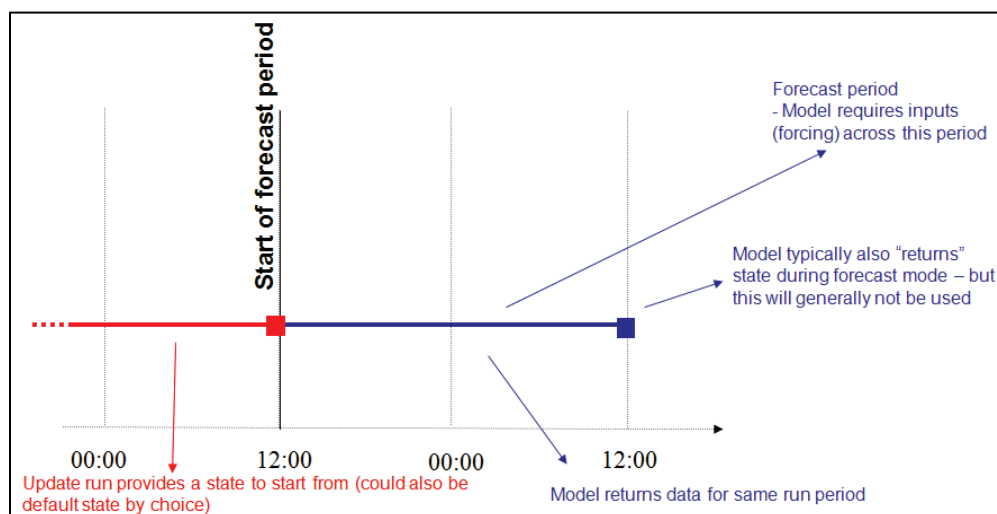
³http://www.nws.noaa.gov/oh/hrl/general/chps/Models/Single_Reservoir_Regulation.pdf

⁴http://www.nws.noaa.gov/oh/hrl/general/chps/Models/Joint_Reservoir_Regulation.pdf

operations using live *warm model states* (Figure 2-12). These models can also be initiated at other times using a *cold state*, which contains initial conditions to start the model. However, these cold states can represent any variety of starting conditions from wet to dry depending upon when and how the original model was developed.

The RFC models had anywhere from 500 to over 1,000 model segments each, and it was not feasible for the RFCs to modify all of the model states to represent a specified initial condition across an RFC sized domain. It was discussed among the RFCs and USACE that a period of at least 6 months of forcings data (i.e., precipitation and temperature) would be prepared for ingest into the RFC models to *warm* the model up to a state close to equilibrium prior to introducing the historical or hypothetical floods.

Figure 2-12. Forecast model initial state considerations.

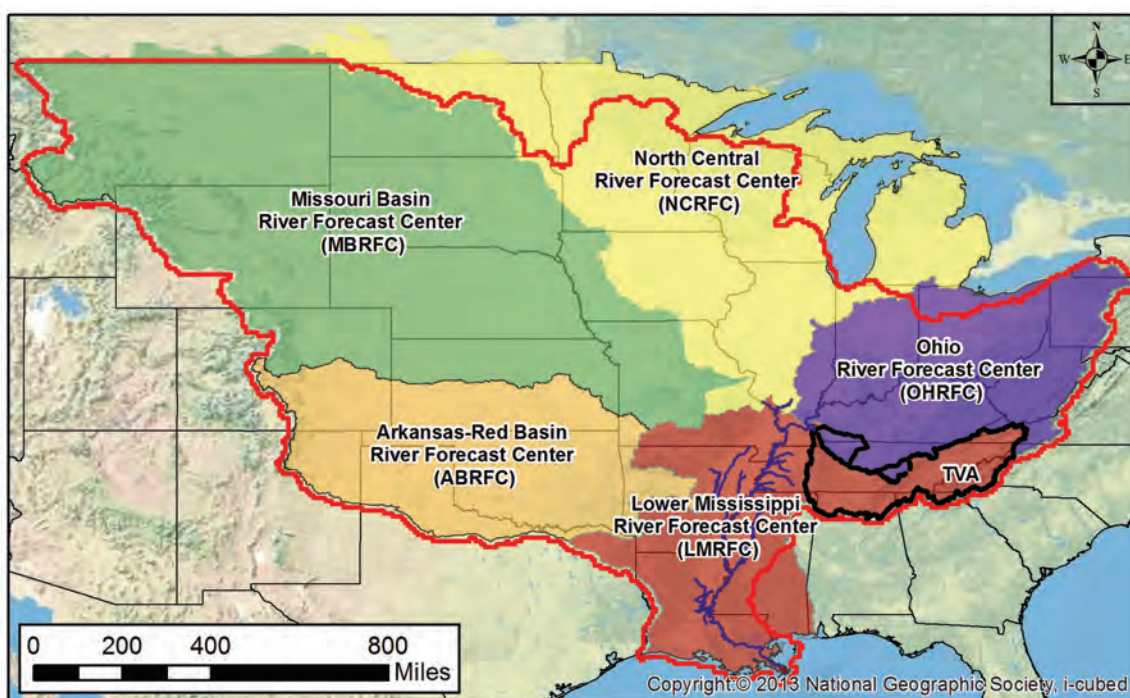


The RFC models ran on a 6-hour time-step and required continuous data during the simulation period for reasonable results. During the preparation of the precipitation and temperature grids for the historical runs, care was taken to ensure that a continuous record of ASCII grid data was available for each 6-hour period. In some cases for the older historical runs in which the time distribution could not be determined from the 24-hour reports, the rainfall was placed into one 6-hour period at 00Z, with the other periods (06, 12, and 18Z) using a *0-inch* rainfall grid to fill in missing periods. Likewise, offices requiring temperature grids used either the historical grids for the period of record available or in some cases had to revert to climatology to extend the forecast runs. The preparation of the forcings data and running of them in the RFC models is discussed in more detail in the following sections.

2.4.4 NWS RFCs in the Flowline assessment area

The Mississippi River Basin, which represents the assessment area of the Flowline assessment, covers an area of approximately 1,245,000 square miles or approximately 41% of the 48 contiguous states of the United States. Coordination of this project required the collaboration of five NWS RFCs and the TVA to generate inflows for the USACE hydraulic model used in the Flowline assessment (Figure 2-13).

Figure 2-13. Map of the NWS RFCs and TVA hydrologic service areas participating in the Flowline assessment.



Each of these RFCs utilized the existing CHPS-FEWS models to ingest the HYPO storm precipitation (and where applicable the corresponding temperatures) to develop flow hydrographs at points needed for the assessment. LMRFC served as the focal point for exchange of data between the RFCs and USACE-MVD. The following section describes the LMRFC model as an example of the models used by all five RFCs.

2.4.4.1 LMRFC CHPS model

The LMRFC hydrologic service area (HSA) covered an area of approximately 220,000 square miles across 12 states. Approximately 500 catchments were modeled by the LMRFC ranging in size from 7 square miles to over 2,500 square miles. The LMRFC domain included

all the catchments below the Lower Ohio River at Smithland, OH, Lock and Dam; the Upper Mississippi River at Chester, IL; the Arkansas River at Pine Bluff, AR; and the Red River at Fulton, AR. The LMRFC also had models for the Tennessee River to the Ohio but obtained the releases for Kentucky dam from TVA to support modeling on the Lower Ohio River unless Cairo was above flood, in which the USACE takes over the regulation of Barkley and Kentucky dams.

Catchment basins throughout the LMRFC area had undergone recalibration over the past 10 years focusing mainly on the headwaters and tributary routings to support flood operations. Many of the reservoirs in the LMRFC area had also been calibrated during this time period with seasonal guide curves and operational rules to replicate the normal operating procedures. The reservoir calibrations had been done primarily to help support short- and long-term ensemble forecasts that were completed for large groups of runs without user interaction.

With the TVA migration to CHPS, the Tennessee River Basin had undergone significant calibration development over the past 2 years. The LMRFC and TVA collaborated on calibration development to synchronize the catchment basins, SAC-SMA, Unit Hydrograph (UNIT-HG), and LAG/K operations so that they are mirrored between offices. The main difference between LMRFC and TVA models was the reservoir operations. The TVA used CHPS to generate local inflows for the reservoir inputs that were then used in RiverWare to generate regulation whereas the LMRFC used the NWS RES-J and RES-SNGL models. At the time of the Flowline assessment, the LMRFC had implemented recently calibrated reservoir models that encompassed regulation to the major storage reservoirs on the Upper Tennessee River basin including Norris (Clinch-Powell Rivers), Douglas (French Broad River), Fontana (Little Tennessee River), Appalachia (Hiwassee River), and Cherokee (Holston River). Low-head dams exist on the main stem of the Tennessee River that were not explicitly modeled as reservoirs in the LMRFC CHPS system. Rather, they were modeled as rivers using LAG/K routings calibrated to replicate historical attenuation from these dams that tend to pass most of the flow and were not designed as storage reservoirs. The LMRFC was able to model regulated versus unregulated systems down to and including the major storage reservoirs in the Tennessee River but could not turn off the LAG/K routings on the lower main stem Tennessee River to completely model the regulation. Given this scenario, the LMRFC generated

unregulated outputs that do have some additional attenuation on the Lower Tennessee River due to the LAG/K calibration for the Flowline assessment. TVA generated regulated outputs at Pickwick Dam for the regulated scenarios for input to the Barkley and Kentucky Dam simulations.

- LMRFC Runoff Model: SAC-SMA Soil Moisture Model
- Reservoir Models: RES-SNGL/RES-J
- Routings: LagK

2.4.4.2 NCRFC CHPS model

The NCRFC HSA covered an area of approximately 340,000 square miles across portions of nine states. NCRFC models included 1,172 catchments that ranged from 7 square miles to 3,060 square miles. With exception of the Missouri River Basin, NCRFC models include the Mississippi River Basin upstream of Chester, IL. NCRFC received Missouri River inflows at Hermann, MO, from the MBRFC.

NCRFC area does use some LAG/K routing in the Mississippi River Basin. However, a vast majority of the NCRFC area uses the Tatum Coefficient Routing method of routing¹.

2.4.4.3 OHRFC CHPS model

The OHRFC area of responsibility covered an area of over 200,000 square miles across portions of 11 states and includes the entire Ohio River basin drainage above Smithland Lock and Dam, the Cumberland River basin above Barkley Dam, and tributaries to Lake Erie that terminate in Ohio and Pennsylvania. The OHRFC hydrologic model for the Ohio and Cumberland basins included 657 catchments ranging from 14 to 1,195 square miles.

Routing of water through the Ohio River basin was accomplished with three different algorithms. LAG/K routing was by far the most common technique used. In flatter terrain — particularly in the Wabash River basin in Indiana and the Green River basin in Kentucky — Tatum routing schemes were used as well. In particular locations with significant backwater impacts, both

¹ http://www.nws.noaa.gov/oh/hrl/general/chps/Models/Tatum_Coefficient_Routing.pdf

LAG/K and Tatum were used together. In a few basins in Ohio, Kentucky, and West Virginia, the Muskingum Routing method was used¹.

There were 96 RES-SNGL or RES-J reservoir models used by the Ohio RFC CHPS configuration to account for the activities of federal, state, and privately owned reservoirs within the Ohio and Cumberland Rivers basins.

2.4.4.4 MBRFC CHPS model

The MBRFC covered an area of approximately 520,000 square miles across nine states. Approximately 1,370 catchments were modeled by the MBRFC, ranging in size from 6 square miles to 8,500 square miles. The MBRFC model included the Missouri River Basin above St. Charles, MO, and the small drainage area of the St. Mary's River that drains into Canada. MBRFC transferred flows to NCRFC at Hermann, MO.

MBRFC used TATUM routing in approximately two-thirds of the reaches and used LAG/K routing in approximately one-third. Muskingum routing method was also used in a limited number of reaches. TATUM routing was used almost exclusively for the Missouri River below Gavins Point Dam except for one reach.

2.4.4.5 ABRFC CHPS model

ABRFC area used LAG/K routing in its basins. The Channel Loss (CHANLOSS) function was also used to account for losses due to evaporation. A large caveat with the Arkansas River was that flows from Colorado/Western Kansas rarely make it to Eastern Kansas. Groundwater losses along with consumptive use caused the Arkansas River to be dry around Dodge City, KS.

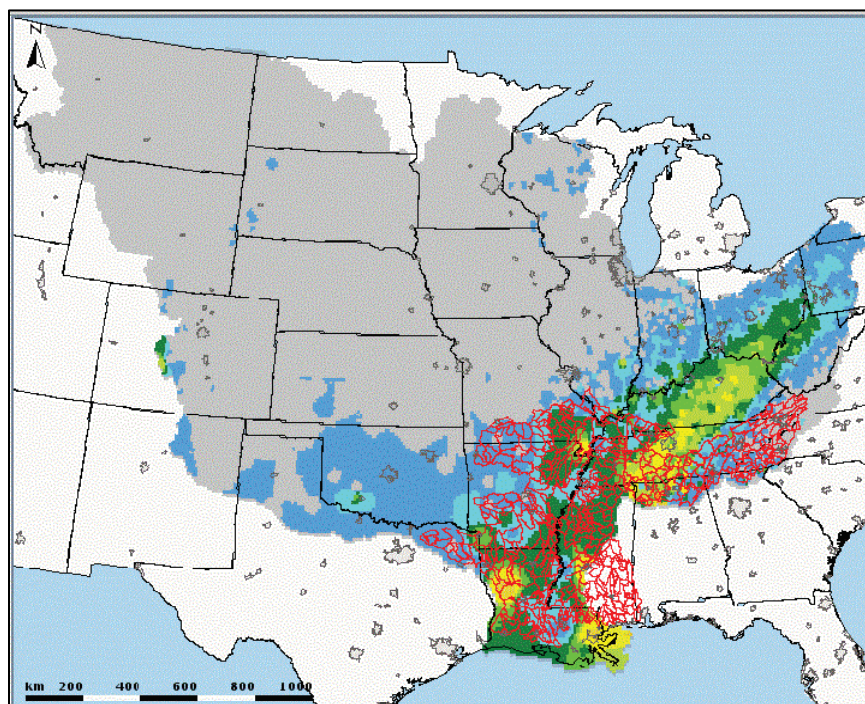
The ABRFC HAS covered an area of approximately 208,000 square miles across portions of seven states. ABRFC model included 450 catchments that ranged from around 30 square miles to 900 square miles. The ABRFC model included the entire Arkansas River basin from Leadville, CO, to Pine Bluff, AR, where it handed off the data to the LMRFC. The ABRFC also modeled the upper part of the Red River from New Mexico to Fulton, AR, where it handed off flow to the LMRFC.

¹ http://www.nws.noaa.gov/oh/hrl/general/chps/Models/Muskingum_Routing.pdf

2.4.5 CHPS precipitation and temperature forcings import process

The primary forcings used in the NWS CHPS models consisted of precipitation and temperature datasets (development of these datasets is discussed in Section 2.8). These datasets were prepared by the USACE and provided to the RFCs in ESRI ASCII format on a 6-hour time-step to match the model time-step used. The CHPS system offers a variety of import/export format options, and the use of ESRI ASCII is a common format that can be readily generated with ArcGIS and configured in CHPS (Figure 2-14).

Figure 2-14. Display of precipitation dataset imported into CHPS. The RFCs used the same import configuration so that a single set of ESRI ASCII grid parameters could be used.



A standard projection was used for all of the datasets, which allowed the RFCs to use a single import configuration in CHPS common to all of the RFCs. The ASCII grid specifics¹ decided on prior to the initiation of the official RFC model runs were the following:

- NCOLS 370
- NROWS 210

¹ An ASCII grid is defined by the number of columns (east-west) and rows (north-south) and the corresponding cell size (in degrees). A grid origin is also defined using the lower left X and Y latitude and longitude.

- XLLCORNER -114.5000
- YLLCORNER 28.5000
- CELLSIZE¹ .100 (degrees)
- NODATA_VALUE -9999.0000

The coordinate system used by the USACE for the precipitation and temperature datasets was WGS 1984 such that the RFC CHPS import configuration looked like the following:

```
<regular locationId="MissRiverBasin">
<rows>210</rows>
<columns>370</columns>
<geoDatum>WGS 1984</geoDatum>
<firstCellCenter>
<x>-114.5</x>
<y>49.5</y>
<z>0.0</z>
</firstCellCenter>
<xCellSize>0.1</xCellSize>
<yCellSize>0.1</yCellSize>
</regular>
```

The units used for the precipitation datasets were English (inches) and for the temperature (Celsius), though it was the responsibility of each RFC to ensure that the correct units were maintained throughout the RFC workflow from import, to preprocessing, and ingest into the runoff calculations used by the RFC hydrologic models.

2.4.6 Other required RFC forcings

Some RFCs required additional datasets beyond precipitation and temperature, and in those cases local expertise was used to determine the most appropriate route to generate required data.

In the LMRFC area, Mean Areal Potential Evaporation (MAPE) is a required parameter. The operational RFC model uses MAPE data calculated from a local application using Real-Time Mesoscale Analysis (RTMA) data. In this case, the RTMA data are not available for the

¹ Approximate cell size area ranges from 32 to 42 square miles depending on the corresponding projection distortion.

historical and hypothetical runs that are required for this project. To accommodate the historical and hypothetical runs, the LMRFC modified the CHPS configuration to use MAPE monthly mean climatology data derived from the Calibration Assistance Program instead of the gridded RTMA MAPE, which could then be applied for any given month of the run period¹. The ABRFC also has a similar requirement and employed similar means to provide the model climatologic data for runtime.

2.4.7 Data exchange

Early discussions during the planning phase of this project considered suitable data formats to exchange datasets between the NWS and USACE. The Hydrologic Engineering Center-Data Storage System (HEC-DSS) format was decided upon with the LMRFC serving as the central collection point to convert the CHPS outputs from all RFCs to HEC-DSSVue format. Several RFCs, including the LMRFC, had prior experience testing a beta version of the HEC-DSSVue program provided by the HEC, which has a Java plug-in to import and export the FEWS PI-xml². Information and sample configurations were shared among the RFCs to set up CHPS configurations to produce a PI-xmloutput with the correct parameters and units for conversion to HEC-DSS. Minor modifications were required to rename the exported CHPS parameters such as CFS (representing cubic feet per second) to FLOW (clarifying that the data type is a flow value) and internal RFC parameters such as pool elevation (PELV), tailwater elevation (TWEL), stage (STG), and SSTG (another label for stage) to HEC-DSS elements such as ELEV (clarifying that the data type is an elevation value) and STAGE (clarifying that the data type is a stage value). The LMRFC served as a central collection point for the RFC model exports for the conversion from PIXML to HEC-DSS and later transfer to the USACE.

During later stages of the project, the NWS also received flow data representing regulated outputs from USACE reservoirs in HEC-DSS format. The same DSSVue application was again used to convert from HEC-DSS format back to FEWS PIXML for import back into CHPS.

¹ <http://www.nws.noaa.gov/oh/hrl/calb/esrihtmlfinal/p1082.htm>

² published interface xml-encoding

2.4.8 RFC flowline modeling procedure

2.4.8.1 LMRFC

The NWS CHPS model has the flexibility to set the date/time to historical and hypothetical future dates and can run for these scenarios as long as corresponding data and model states are provided. As a general procedure, the LMRFC used the following steps:

1. Copy the hourly ASCII precipitation grids to the configured ASCII import folder.
2. Set the Current System Time (To) to the end of the simulation period.
3. Import workflows using the “Manual Forecast” option in CHPS (Grids and Scalar) and set the initial state selection to use a “Cold State” with the “Run start time” set to the beginning of the simulation period (i.e., when the data starts) and run the import. Once the imports complete, run the “Preprocess RRS” workflow to calculate the mean areal precipitation required for the model and process any historical flow data.
4. Confirm the data imports then re-set to 1 day after the first data value (i.e., June 2nd for data beginning on June 1st). Then, set the “Run Options” for the first forecast group to initialize with a “Cold State” and set the “Forecast Length” out to the end of the simulation period (Ex: 303 days). This runs the model in a forecast mode so that modifiers can be applied where needed such as reservoir outflow overrides.
5. Run each forecast.
6. Exports to PIXML were run from the “Manual Forecast” option using the “Cold State” corresponding to the initial simulation T0 and setting the “Forecast Length” out through to the end of the simulation period (Ex: 303 days). Convert the PIXML to HEC-DSS using the DSSVue Beta software with CHPS Export/Import Java plug-in on the PC.

Each historical and hypothetical scenario required running both *regulated* and *unregulated* scenarios. The simulation of the unregulated scenarios was accomplished by using time series change modifiers in CHPS to match the reservoir outflow with the simulated inflow, bypassing any reservoir operations that might attenuate the flow.

The simulation of regulated scenarios was more complex. Older historical runs did not have any historical flow regulation to use for model simulations. In these scenarios, modeling team members allowed the reservoir models in CHPS to attenuate the flow. About two-thirds of

LMRFCs reservoir models have prior calibration using seasonal guide curves, rules, and control points to try to replicate normal operating procedures (Table 2-1). These reservoir models were allowed to run as designed to route simulated regulated flows downstream. Other reservoirs that did not have an actual reservoir calibration had to be monitored on a case-by-case basis to see whether the model operated reasonably. In some cases, the reservoir has a spillway and just passes flow at a certain elevation and was allowed to run using the simulation to route flows to downstream basins. In other cases, the resulting outflow from the reservoir model stayed at a constant value based upon the original cold state and never went into a regulation mode. In these cases, the model inflows were passed as outflows for routing downstream (Table 2-1).

The regulated scenarios for the hypothetical runs required additional assistance with the USACE and TVA to generate a set of regulated flows. The column titled “Assisted Regulation” in Table 2-1 denotes how the regulation was performed for the HYPO scenarios. Stations denoted by USACE <district> were dams where required inflows, locals, and tributary inputs were generated by the RFC and shared with the USACE offices that in turn manually generated the projected regulation outputs from those projects. Some areas had multiple reservoirs on a single reach. In these cases, a special CHPS simulation was run to produce reservoir releases set to “0 CFS” so that the inflows into the next downstream reservoir had only local and tributary flows into it and no regulation from upstream reservoirs. The resulting release data were in turn re-ingested into CHPS and routed to downstream locations.

Stations in Table 2-1 noted as “LMRFC Model Override” indicate that the reservoir model was run, but user overrides were performed in CHPS on the output to match the guidance provided by the USACE, which was the case for Texarkana Dam. Sites noted as “LMRFC Calibration” were locations that the LMRFC had calibrated reservoir models that were allowed to generate simulated regulated flows for downstream routings.

There were some sites that were not calibrated for regulation and not USACE, or TVA locations that had manual regulation. If, in these cases, the reservoir model did not produce reasonable simulations, the outflow was matched with the inflow and is labeled “Matched Outflow/Inflow” in Table 2-1. Most of these were smaller reservoirs on the mainstem Tennessee River tributaries, and the outflow from them is captured farther

downstream in larger regulated dams that did have calibrations or manual regulation applied to them.

Table 2-1 also includes a group of locations that are “additional reservoir segments, not modeled as a reservoir.” These are sites that have catchments defined for locations corresponding to a dam but do not have a reservoir model defined for them. Rather, they are modeled as a river segment with LAG/K routings. The Caddo Lake segment was one that the LMRFC has modeled with LAG/K routing for many years but, in the case of the HYPO regulation scenario, was able to obtain manually routed outflows from MVK to override the model outputs. In the case of sites on the Tennessee River as mentioned prior, they are mostly low-head dams that have been calibrated to replicate historical attenuation since they tend to pass the flow and are not designed as storage reservoirs. In terms of regulated versus unregulated simulations, the LAG/K routing could not be modified to generate truly different regulation scenarios for those reaches.

In the case of the Tennessee River, the TVA generated the HYPO 58A Straight Sequence inflows and regulated hydrograph for Pickwick Dam, which is primary input from the Tennessee River into the joint Barkley/Kentucky reservoir regulation conducted by LRN. The regulation performed by TVA was done by manual routing of the flows to produce the hydrograph shown in Figure 2-15. The RFC model regulated flows generated by the calibrated ResJ models in CHPS are plotted on the same chart for comparison. It was noted that the TVA regulation shaves the peaks off of the hydrographs but that the volume is conserved between methods. The flow difference between methods is less than ~10% of the total flow on the Lower Ohio River and ~3% of the total flow on the Lower Mississippi River below Cairo.

Figure 2-15. Plot showing the difference between RFC simulated regulated outflows at Pickwick Dam on the Lower Tennessee River vs. the hand-adjusted regulation performed by TVA using RiverWare.

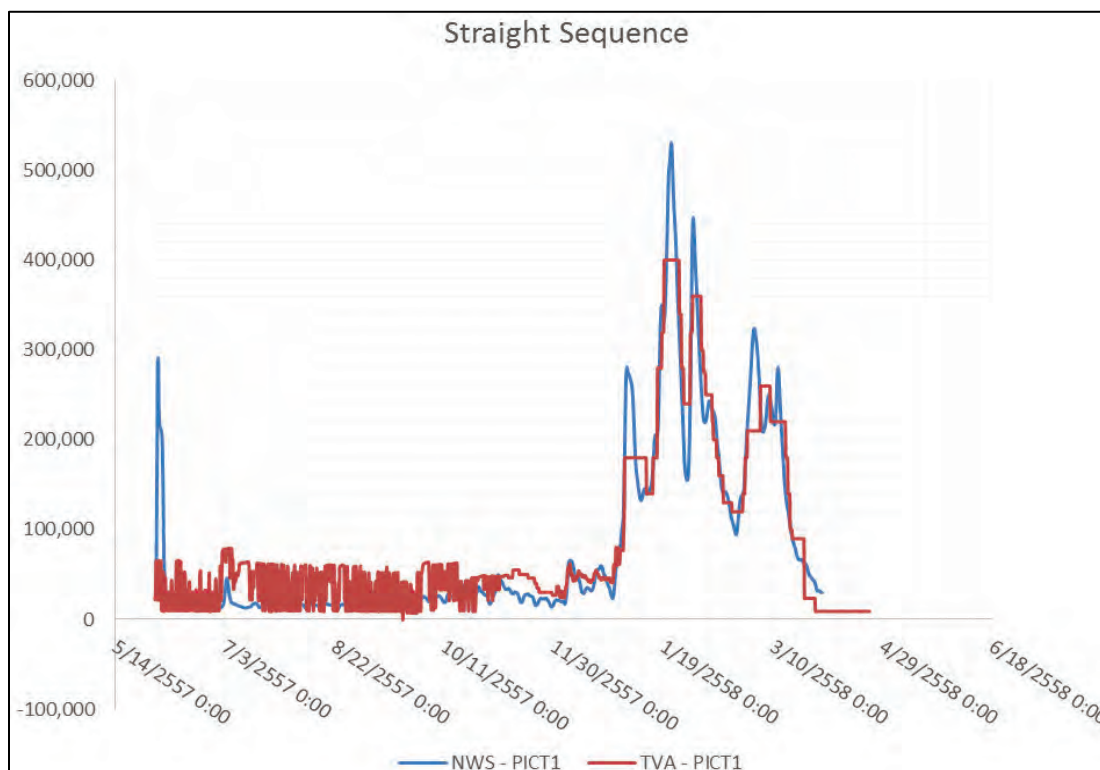


Table 2-1. LMRFC reservoir models.

Dam	River	Owner	NWS 5CharID	NWS Model	NWS Calibrated	Assisted Regulation
Appalachia	Hiwassee River	TVA Dam	HADT1	Res-J	Y	LMRFC Calibration
Arkabutla	Coldwater	USACE MVK	ARKM6	Res-J	Y	USACE MVK
Blakely Mountain	Ouachita	USACE MVK	BMDA4	Res-J	Y	USACE MVK
Boone Dam	South Fork Holston River	TVA Dam	BOOT1	Res-J	Y	LMRFC Calibration
Calderwood	Little Tennessee River	TVA Dam	CALT1	Res-J	Y	LMRFC Calibration
Chatuge	Hiwassee River	TVA Dam	CHAN7	Res-J	Y	LMRFC Calibration
Cheoah	Little Tennessee River	TVA Dam	CHEN7	Res-J	Y	LMRFC Calibration
Cherokee	Holston River	TVA Dam	CRKT1	Res-J	Y	LMRFC Calibration

Dam	River	Owner	NWS 5CharID	NWS Model	NWS Calibrated	Assisted Regulation
Clearwater	Black	USACE SWL	CLRM7	Res-J	Y	LMRFC Calibration
Cooper (Jim Chapman)	South Sulphur	USACE SWF	SCLT2	Res-J	Y	LMRFC Calibration
Degray	Caddo	USACE MVK	DGDA4	Res-J	Y	USACE MVK
Douglas	French Broad River	TVA Dam	DUGT1	Res-J	Y	LMRFC Calibration
Enid	Yocona	USACE MVK	ENDM6	Res-J	Y	USACE MVK
Ferrels Bridge	Lake O' the Pines	USACE SWF	JFNT2	Res-J	Y	LMRFC Calibration
Fontana	Little Tennessee River	TVA Dam	FONN7	Res-J	Y	LMRFC Calibration
Fort Patrick Henry	South Fork Holston River	TVA Dam	FPHT1	Res-J	Y	LMRFC Calibration
Grenada	Yalobusha	USACE MVK	GRNM6	Res-J	Y	USACE MVK
Hiwassee	Hiwassee River	TVA Dam	HIWN7	Res-J	Y	LMRFC Calibration
Narrows	Little Missouri	USACE MVK	NADA4	Res-J	Y	USACE MVK
Normandy	Duck River	TVA Dam	NRMT1	Res-J	Y	LMRFC Calibration
Norris	Clinch River	TVA Dam	NRST1	Res-J	Y	LMRFC Calibration
Nottely	Nottely River	TVA Dam	NOTG1	Res-J	Y	LMRFC Calibration
Santeelah	Cheoah River	APGI Dam	SNTN7	Res-J	Y	LMRFC Calibration
Sardis	Tallahatchie	USACE MVK	SRDM6	Res-J	Y	USACE MVK
South Fork Holston Dam	South Fork Holston River	TVA Dam	SHDT1	Res-J	Y	LMRFC Calibration
Tims Ford	Elk River	TVA Dam	TMFT1	Res-J	Y	LMRFC Calibration
Wappapello	St. Francis	USACE MVS	WPPM7	Res-J	Y	USACE MVS
Bayou Bodcau	Bodcau Bayou	USACE MVK	LBBL1	RES-SNGL	Y	USACE MVK
Bayou D'arbonne	Bayou D'arbonne	Local Dam	LDBL1	RES-SNGL	Y	LMRFC Calibration
Bear Creek	Bear Creek	TVA Dam	BCRA1	RES-SNGL	N	Matched Outflow/Inflow
Beaver	White	USACE SWL	BVGA4	RES-SNGL	N	USACE SWL

Dam	River	Owner	NWS 5CharID	NWS Model	NWS Calibrated	Assisted Regulation
Bistineau	Lake Bistineau	Local Dam	LBUL1	RES-SNGL	Y	LMRFC Calibration
Blue Ridge	Toccoa	TVA Dam	BRDG1	RES-SNGL	Y	LMRFC Calibration
Bob Sandlin Lake	Lake Bob Sandlin	Local Dam	BSLT2	Res-J	Y	LMRFC Calibration
Bull Shoals	White	USACE SWL	BSGA4	RES-SNGL	N	USACE SWL
Cedar Cliff	Tuckasegee River	Duke Power Dam	ICCN7	RES-SNGL	N	Matched Outflow/Inflow
Cedar Creek	Cedar Creek	TVA Dam	CCRA1	RES-SNGL	N	Matched Outflow/Inflow
Greers Ferry	Little Red	USACE SWL	GRR44	RES-SNGL	Y	USACE SWL
Lake Claiborne	Lake Claiborne	Local Dam	LCAL1	RES-SNGL	Y	LMRFC Calibration
Little Bear Creek	Little Bear Creek	TVA Dam	LBRA1	RES-SNGL	N	Matched Outflow/Inflow
Nantahala	Nantahala River	Duke Power Dam	NANN7	RES-SNGL	N	Matched Outflow/Inflow
Norfolk	White	USACE SWL	NFDA4	RES-SNGL	N	USACE SWL
Ocoee Dam #3	Ocoee River	TVA Dam	OCCT1	RES-SNGL	Y	LMRFC Calibration
Table Rock	White	USACE SWL	FORM7	RES-SNGL	N	USACE SWL
Texarkana	Wright Patman Lake	USACE SWF	TXKT2	RES-SNGL	N	LMRFC Model Override
Thorpe	West Fork Tuckasegee River	Duke Power Dam	THPN7	RES-SNGL	N	Matched Outflow/Inflow
Upper Bear Creek	Bear Creek	TVA Dam	UBRA1	RES-SNGL	N	Matched Outflow/Inflow
Wallace Lake	Wallace Lake	USACE MVK	WAGL1	RES-SNGL	Y	USACE MVK
Walters	Pigeon River	Duke Power Dam	WTDN7	RES-SNGL	N	Matched Outflow/Inflow
Additional Reservoir Segments, Not Modeled as a Reservoir						
Calderwood	Little Tennessee River	APGI Dam	CALT1	River Routing	Y	River Routing
Chilhowee	Little Tennessee River	APGI Dam	CLTT1	River Routing	Y	River Routing
Tellico	Little Tennessee River	TVA Dam	TDTT1	River Routing	Y	River Routing

Dam	River	Owner	NWS 5CharID	NWS Model	NWS Calibrated	Assisted Regulation
Watauga	Watauga River	TVA Dam	WTGT1	River Routing	Y	River Routing
Ocoee Dam #1	Ocoee River	TVA Dam	OCAT1	River Routing	Y	River Routing
Fort Loudoun	Tennessee River	TVA Dam	FLDT1	River Routing	Y	River Routing
Melton	Clinch River	TVA Dam	MHDT1	River Routing	Y	River Routing
Watts Bar	Tennessee River	TVA Dam	WBOT1	River Routing	Y	River Routing
Chickamauga	Tennessee River	TVA Dam	CKDT1	River Routing	Y	River Routing
Nickajack	Tennessee River	TVA Dam	NKJT1	River Routing	Y	River Routing
Guntersville	Tennessee River	TVA Dam	GVDA1	River Routing	Y	River Routing
Wheeler	Tennessee River	TVA Dam	WHLA1	River Routing	Y	River Routing
Wilson	Tennessee River	TVA Dam	WLSA1	River Routing	Y	River Routing
Pickwick Landing	Tennessee River	TVA Dam	PICT1	River Routing	Y	River Routing
Kentucky	Tennessee River	TVA Dam	KYDK2	River Routing	Y	River Routing
Caddo Lake	Caddo River	USACE MVK	LCOL1	River Routing	N	USACE MVK

2.4.8.2 NCRFC Regulated flows

During periods when regulation is possible, NCRFC provides inflows to a number of USACE-regulated reservoirs and pools. In return, the USACE provides NCRFC with forecast releases for several locations. Dam locations that NCRFC does not receive forecast outflows are handled either by RES-SNGL, RES-J or assumed *run of river*. In some instances, NCRFC knows target pool levels for various times of the year for federal and non-federal regulated dams. In these situations, NCRFC can use a *modifier* to balance the pool in an effort to estimate the planned releases. For the regulated historical and hypothetical simulations in the Flowline project, NCRFC handed off inflows to the Rock Island Corps of Engineers and the St. Louis Corps of Engineers offices to provide outflows for the following locations:

- Iowa River at Coralville Dam (CRVI4)
- Des Moines River at Saylorville Dam (SAYI4)
- Des Moines River at Red Rock Dam (PELI4)
- Salt River at Clarence Cannon Dam (CDAM7)
- Kaskaskia River at Shelbyville Dam (SLVI2)
- Kaskaskia River at Carlyle Dam (CAYI2).

All other dam locations in the NCRFC area used the operational RES-SNGL or RES-J models where it was possible. If no reservoir regulation model was available, run of river was assumed.

2.4.8.3 OHRFC regulated flows

Reservoirs within the OHRFC area were primarily simulated using the calibrated in-house RES-J and RES-SNGL models. Ninety-six reservoirs are modeled within the OHRFC domain, with the vast majority of the lakes having nominal impact on crest reductions at the Ohio-Mississippi River confluence. To facilitate the study, it was determined to only utilize USACE model outflows within the Wabash and Green Rivers basins within the Louisville District (LRL). Inflows upstream of each of these reservoirs, as well as local flows downstream in each basin, were provided to LRL for their simulations. In other LRL basins, as well as for projects in the Huntington District and Pittsburgh District, NWS model output was used.

Table 2-2 below outlines each dam model used during regulated runs within the OHRFC CHPS system.

Due to issues with spillway releases triggered during the LRL simulations of the Upper Wabash lakes (Rousch, Mississinewa, and Salamonie Dams) during the Hypo 56 event, the RES-J modeled outflows were used in place of USACE overrides. This output was reviewed and verified by LRL staff before final Smithland flow hydrographs were provided to LMRFC and MVD for use on the lower Ohio River.

Table 2-2. Regulation within OHRFC.

HB5	Location	Basin Name	CHPS Model	USACE Overrides Provided
CMDP1	Conemaugh Dam	Lower Allegheny	RESJ	No
CCDP1	Crooked Creek Dam	Lower Allegheny	RESJ	No
SLTP1	Loyalhanna Dam	Lower Allegheny	RESJ	No
MHDP1	Mahoning Dam	Lower Allegheny	RESJ	No
GHDP1	East Branch Dam	Lower Allegheny	RESJ	No
PNDP1	Piney Dam	Lower Allegheny	RESJ	No *
TIOP1	Tionesta	Upper Allegheny	RESSNGL	No
FLCN6	Chataqua Lake	Upper Allegheny	RESSNGL	No *
KNZP1	Kinzua Dam	Upper Allegheny	RESSNGL	No
WDRP1	Woodcock Dam	Upper Allegheny	RESSNGL	No
UCYP1	Union City	Upper Allegheny	RESSNGL	No
BRW01	Berlin Dam	Beaver	RESJ	No
SHDP1	Shenango Dam	Beaver	RESSNGL	No
MSQ01	Mosquito Creek Dam	Beaver	RESJ	No
KIT01	Kirwan Dam	Beaver	RESJ	No
MONI3	Monroe Res	East Fork White	RESJ	Yes
NOLK2	Nolin Lake Dam	Green	RESJ	Yes
GRLK2	Green River Lake	Green	RESJ	Yes
RRLK2	Rough River Dam	Green	RESJ	Yes
BRRK2	Barren River Lake	Green	RESJ	Yes
TJD01	Tom Jenkins Dam	Hocking	RESJ	No
HINW2	Bluestone Dam	Kanawha	RESJ	No
SUMW2	Summersville Dam	Kanawha	RESSNGL	No
SUTW2	Sutton Lake	Kanawha	RESSNGL	No
CLLV2	Claytor Lake	Kanawha	RESSNGL	No *
SHPK2	Taylorville Lake (COE)	Kentucky (Salt)	RESJ	No
BUCK2	Buckhorn Lake	Kentucky	RESJ	No
CFLK2	Carr Fork Lake	Kentucky	RESJ	No

HB5	Location	Basin Name	CHPS Model	USACE Overrides Provided
DIXK2	Dix Dam	Kentucky	RESSNGL	No *
FRMK2	Cave Run Dam	Licking (KY)	RESSNGL	No
BULW2	Burnsville	Little Kanawha	RESSNGL	No
GERO1	Germantown Dam	Miami	RESSNGL	No *
CCL01	Caesar Ck Dam	Miami	RESSNGL	No
TAYO1	Taylorville Dam (MCD)	Miami	RESSNGL	No *
LOC01	Lockington Dam	Miami	RESSNGL	No *
MRD01	Huffman Dam	Miami	RESSNGL	No *
ENGO1	Englewood Dam	Miami	RESSNGL	No *
BKVI3	Brookville Dam	Miami (Whitewater)	RESSNGL	No
BHDO1	Harsha Dam	Miami	RESSNGL	No
CJB01	C J Brown	Miami	RESSNGL	No
SNC01	Senecaville Dam	Lower Muskingum	RESJ	No
NBK01	N Branch Kokosing Dam	Lower Muskingum	RESSNGL	No
SIL01	Salt Fork Lake	Lower Muskingum	RESJ	No
CHAO1	Charles Mill Dam	Lower Muskingum	RESJ	No
PTH01	Pleasant Hill Lake	Lower Muskingum	RESJ	No
DLL01	Dillon Dam	Lower Muskingum	RESJ	No
BCK01	Buckeye Lake	Lower Muskingum	RESSNGL	No *
WLL01	Wills Creek Dam	Lower Muskingum	RESJ	No
NLL01	Mohawk Dam	Lower Muskingum	RESJ	No
MCH01	Mohicanville Dam	Lower Muskingum	RESJ	No
BHL01	Beach City Dam	Upper Muskingum	RESJ	No
DVL01	Dover Dam	Upper Muskingum	RESJ	No
CLK01	Clendening Lake	Upper Muskingum	RESJ	No
PIEO1	Piedmont Dam	Upper Muskingum	RESJ	No
TAP01	Tappan Lake	Upper Muskingum	RESJ	No
YGOP1	Youghiogheny Dam	Lower Monongahela	RESJ	No
FRDM2	Deep Creek Lake	Lower Monongahela	RESJ	No *
SWJW2	Stonewall Jackson	Upper Monongahela	RESJ	No
TYGW2	Tygart Dam	Upper Monongahela	RESSNGL	No
PMAW2	Lake Lynn Dam	Upper Monongahela	RESSNGL	No *
ELSW2	East Lynn	Ohio (Twelvepole)	RESSNGL	No
GYLK2	Grayson Dam	Ohio (Little Sandy)	RESSNGL	No
BFOW2	Beech Fork Dam	Ohio (Twelvepole)	RESSNGL	No
YTVK2	Yatesville Dam	Sandy	RESJ	No

HB5	Location	Basin Name	CHPS Model	USACE Overrides Provided
FLAV2	Flannagan Lake	Sandy	RESJ	No
FTLK2	Fishtrap Lake	Sandy	RESJ	No
DWYK2	Dewey Lake	Sandy	RESJ	No
RDBW2	R D Bailey Dam	Sandy (Guandotte)	RESJ	No
NOFV2	North Fork Pound Lake	Sandy	RESJ	No
PNTK2	Paintsville Lake	Sandy	RESJ	No
BBR01	Paint Creek Lake	Scioto	RESSNGL	No
PCB01	Deer Creek Lake	Scioto	RESSNGL	No
AFR01	Alum Creek Lake	Scioto	RESSNGL	No
DELO1	Delaware Dam	Scioto	RESSNGL	No
CSC01	Hoover Reservoir	Scioto	RESSNGL	No *
DUB01	O'Shaughnessy Lake	Scioto	RESSNGL	No *
PRLI3	Patoka Lake	Lower Wabash	RESJ	Yes
COXI3	Cecil Hardin Lake	Lower Wabash	RESJ	Yes
LYNI3	Grand Lake St Mary	Upper Wabash	RESJ	No *
OAKI3	Oakdale Dam	Upper Wabash	RESSNGL	No *
WABI3	Rousch Dam (Huntington)	Upper Wabash	RESJ	Yes
PRUI3	Mississinewa	Upper Wabash	RESJ	Yes
SALI3	Salamonie	Upper Wabash	RESJ	Yes
ECRI3	Eagle Creek Dam	White	RESSNGL	No *
MANI3	Cagles Mill	White	RESJ	Yes

* Denotes non-USACE project.

Within the Cumberland River basin, OHRFC provided inflows to tributary projects and local flows for all sub-basins within the basin for use by LRN in constructing regulated flow hydrographs from each of their reservoirs (Table 2-3). No overrides were used in the OHRFC analysis for the smaller projects located upstream of large storage reservoirs.

Table 2-3. Coordination between OHRFC and Nashville District, USACE.

HB5	Location	Basin Name	Model	Data Provided
CORT1	Great Falls (TVA)	Lower Cumberland	RESJ	Inflow
CORT1	Cordell Hull Dam	Lower Cumberland	RESJ	Inflow
BARK2	Barkley Dam	Lower Cumberland	RESSNGL	Local flows

HB5	Location	Basin Name	Model	Data Provided
OHIT1	Old Hickory Dam	Lower Cumberland	RESJ	Local flows
PPDT1	J. Percy Priest Dam	Lower Cumberland	RESJ	Inflow
CHET1	Cheatham Lock and Dam	Lower Cumberland	RESJ	Local Flows
MNLK2	Martins Fork Dam	Upper Cumberland	RESSNGL	Inflow
DAHT1	Dale Hollow Dam	Upper Cumberland	RESJ	Inflow
LCLK2	Laurel River Dam	Upper Cumberland	RESJ	Inflow
WLCK2	Wolf Creek Dam	Upper Cumberland	RESJ	Inflow

2.4.8.4 MBRFC regulated flows

During periods when regulation is possible, MBRFC provides inflows to a number of USACE-regulated reservoirs and pools. In return, the USACE provides MBRFC with forecast releases for several locations. Dam locations that MBRFC does not receive forecast outflows are handled either by RES-SNGL, RES-J, or assumed run of river.

For the regulated historical and hypothetical simulations in the Flowline project, MBRFC transferred inflows and flows or gains below the reservoirs to the appropriate USACE office, which in return provided outflows from a reservoir regulation model. To operate USACE reservoir models for releases, downstream gains below the reservoirs at certain river gage locations (control points) were also provided along with the inflows. For each of the regulated historical and hypothetical simulations, a separate model run was made but with the releases from the reservoirs in the list below were set to zero. This allowed MBRFC CHPS model to compute river flow contributions without any reservoir releases, and the USACE reservoir models were able to simulate the releases.

For Kansas City District, USACE, Hydrologic Engineering Branch, Water Management, the following reservoir inflows and gains at control points were provided.

Osage River Basin Reservoirs

- Pomona (PLKK1)
- Melvern (MLVK1)
- Hillsdale (HILK1)

- Stockton (STXM7)
- Pomme De Terre (PTXM7)
- Harry S. Truman (TKZM7)

Osage River Basin River/Control Point flow locations with upstream reservoir release set to zero

- Marias Des Cygnes River at Pomona, KS (PMNK1)
- Marias Des Cygnes River at Ottawa, KS (OTWK1)
- Marias Des Cygnes River at KS-MO State Line (TPOK1)
- Sac River at Hwy J below Stockton, MO (SJZM7)
- Sac River at Caplinger Mills, MO (CMZM7)
- Osage River at St. Thomas, MO (STTM7)

Kansas River Basin Reservoirs

- Wilson (WLSK1)
- Kanopolis (KANK1)
- Waconda (GLNK1)
- Milford (MLFK1)
- Tuttle Creek (MTTK1)
- Perry (PRRK1)
- Clinton (CLIK1)

Kansas River Basin River/Control Point flow locations with upstream reservoir release set to zero

- Saline River at Tescott, KS (TSCK1)
- Solomon River at Niles, KS (NLSK1)
- Smoky Hill River at Mentor, KS (MTRK1)
- Smoky Hill River at New Cambria, KS (NCMK1)
- Smoky Hill River at Enterprise, KS (ENTK1)
- Kansas River at Fort Riley, KS (FTRK1)
- Kansas River at Wamego, KS WMGK1)
- Kansas River at Topeka, KS (TPAK1)
- Kansas River at LeCompton, KS (LCPK1)
- Kansas River at DeSoto, KS (DSOK1)

Platte River Basin Reservoirs

- Smithville (SLKM7)

Platte River Basin River/Control Point flow locations with upstream reservoir release set to zero

- Little Platte River at Smithville, MO (SMHM7)
- Platte River at Agency, MO (AGYM7)
- Platte River at Sharps Station, MO (SSTM7)

Chariton River Basin Reservoirs

- Rathbun (RADI4)

Chariton River Basin River/Control Point flow locations with upstream reservoir release set to zero

- Chariton River at Moulton, IA (MOLI4)
- Chariton River at Livoinia, MO (LVZM7)
- Chariton River at Novinger, MO (NVZM7)
- Chariton River at Prairie Hill, MO (PRIM7)

For the Missouri River Basin Water Management Division, the following reservoir inflows were provided:

- Missouri River Basin Reservoirs
- Gavins Point Dam (GPDN1)

Missouri River Basin River/Control Point flow locations with upstream reservoir release set to zero

- Missouri River at St. Joseph, MO (SJSM7)
- Missouri River at Kansas City, MO (KCDM7)
- Missouri River at Waverly, MO (WVYM7)
- Missouri River at Hermann, MO (HRNM7)

These reservoirs above were the major downstream control points for the Missouri River basin, except for the Platte River basin. All other dams upstream of these reservoir locations or in the Platte River basins used RES-SNGL or RES-J models where it was possible with built-in functions

to determine outflows. If no reservoir regulation model was available, run of river was assumed, including Bagnell Dam/Lake of the Ozarks.

2.4.8.5 ABRFC regulated flows

Reservoir inflows were provided to the Tulsa District (SWT). The Arkansas River and its tributaries are highly regulated above Van Buren, AR. These reservoirs are regulated in tandem during high flows. The SWT provided forecast releases based on their rules. Other smaller reservoirs on Arkansas River tributaries are modeled in RES-SNGL based on seasonal and a few downstream regulations. The SWT also provided regulated flows for a few points on the Red River as well. The Little Rock District (SWL) regulates a large reservoir at Millwood, AR, as a tributary for the Red River. This reservoir is regulated to limit flows at Fulton, AR, to be 100,000 cfs or below if possible. For these cases, the ABRFC was able to manually regulate the modeled flows in this manner.

Inflows from SWT for the Arkansas

- Caney River at Copan Dam (CPLO2)
- Caney River at Hulah Dam (HULO2)
- Canadian River at Eufala Dam (EUFO2)
- Grand River at Fort Gibson (GIBO2)
- Polecat Creek at Heyward Dam (HEYO2)
- Arkansas River at Keystone Dam (KEYO2)
- Verdigris River at Oologah Dam (OOLO2)
- Bird Creek at Skiatook Dam (SKLO2)
- Illinois River at Tenkiller Dam (TEN02)
- Poteau River at Wister Dam (WSLO2)

Inflows from SWT for the Red River

- Red River at Lake Texoma (DSNT2)
- Kiamichi River at Hugo Dam (HGLO2)

2.4.9 Storm simulations

HYP0 58A is comprised of the 1937, 1938, and 1950 storms that produced historical floods throughout the Mississippi River Basin. These storms were simulated separately based on the dates shown below, which allowed a 6-month warm-up period with forcings inputs prior to the primary flood of interest.

- **1937 Simulation Dates:** 1 June 1936 through 1 March 1937
- **1938 Simulation Dates:** 1 July 1937 through 1 April 1938
- **1950 Simulation Dates:** 1 June 1949 through 1 March 1950

The 1950 simulation had historical regulation for Clearwater, Norfork and Kentucky Dams. The regulation was converted to PIXML formats to import into CHPS and override reservoir releases for downstream routings. For the other simulations and reservoirs, there was no available historical regulation available to incorporate into the regulated scenarios generated by the LMRFC. In this case, the model was allowed to run with the Res-J operations turned on to generate outflows based upon the guide curves and rules in the model calibration, noted in Table 2-1 as “Y” in the column labeled “NWS Calibrated.” Outflow was set equal to inflow for some locations where model calibrations were not available or outputs were unreasonable, noted as “N” in the “NWS Calibrated” column of Table 2-1. As mentioned prior, most of these locations were smaller dams on tributaries of the mainstem Tennessee River basin, which did have larger projects further downstream where regulation could be applied.

2.4.9.1 HYPO 58A clipped-merged

The HYPO 58A clipped-merged scenario (Section 2.7.1) ran from 1 June 2657 through 1 April 2658 allowing a 6-month warm-up period with forcings inputs prior to the primary flood of interest. Although the rainfall for this scenario ends prior to April 1, the simulation was extended by inserting additional zero precipitation into the models to permit routing the entire flood hydrograph to the Gulf of Mexico.

Reservoir outflows were developed by USACE and TVA in collaboration with the respective RFCs. Flows were determined using existing regulation models. Outputs were provided in HEC-DSSVUE. These were converted to PIXML formats to import into CHPS and override reservoir releases for downstream routings.

2.4.9.2 HYPO 58A straight sequence

The HYPO 58A straight sequence scenario (Section 2.7.1) was run on CHPS from 1 June 2557 through 1 April 2558. The rainfall/temperature forcings for this scenario actually ended on 14 March 2558, but the routings were extended through April 1 to allow time for the routed flow to

make its way down to the mouth of the Mississippi River. This assumes no additional rainfall inputs and climatological inputs for temperature.

The unregulated scenarios were run as described previously where the outflows were set equal to the inflows. Data from completed runs were exported and converted to HEC-DSSVUE to be shared with the USACE.

The regulated scenarios were run including reservoir outflows that were developed by USACE and TVA in collaboration with the respective RFCs. Flows were determined using existing regulation models. Outputs were provided in HEC-DSS. These were converted to PIXML formats to import into CHPS and override reservoir releases for downstream routings.

2.4.10 TVA Flowline modeling procedure

The TVA is a federally owned corporation, signed into existence on 18 May 1933 by President Franklin Delano Roosevelt. The purpose of the TVA, as stated in the act, is “To improve the navigability and to provide for the flood control of the Tennessee River...; to provide for reforestation and the proper use of marginal lands in the Tennessee Valley; to provide for the agricultural and industrial development of said valley; to provide for the national defense by the creation of a corporation for the operation of Government properties at and near Muscle Shoals in the State of Alabama, and for other purposes” (TVA 1933). While TVA is now the largest public power company in the United States, demonstrating the flexibility in the original act to steer its mission towards “Energy,” its service commitment¹ continues to reflect the high priority of flood control of the Tennessee River Valley.

TVA owns and operates 49 dams — 29 that are power producing, 1 that is a pumped-storage facility, and 5 that are “non-power” but have controllable spill gates and valves. The other 14 dams provide flood control and recreational benefits. Spanning nearly 41,000 square miles and stretching from the western divide of the Appalachian Mountains to its drainage point into the Ohio River near Paducah, KY, the Tennessee River Valley is a major resource and asset to the regional economy. These 30 power-producing hydroelectric facilities can provide as much as 10% of the maximum-possible power produced by all TVA generation facilities. The 49 TVA dams

¹ Tennessee Valley Authority: (accessed July 10, 2018) <https://www.tva.com/About-TVA/Our-Service-Commitment>.

are designated as multi-use dams that in addition to hydropower and flood control are also responsible for maintaining a navigable pool for barge traffic and providing enough flow for water use and recreation while meeting all applicable environmental and nuclear regulations.

2.4.10.1 Flood operations

Because the Tennessee River is a major tributary of the Mississippi River and is largely regulated and controlled, TVA has an opportunity and an obligation to help mitigate flooding in downstream, non-TVA locations. The USACE Flood Risk Management Program main mission is to reduce, mitigate, and prevent flooding. To accommodate the USACE mission, TVA is required to surrender operations of Kentucky Dam to the Great Lakes and Ohio River Division of the USACE under “Flood Operations.” This designated event ensures that the TVA primary mission becomes flood control and that all other priorities, including power-price optimization, become second.

River operations and decision-making are performed by staff, working 24 hours a day, 7 days a week, at the RFC in Knoxville, TN. Under *normal* operations, modelers and schedulers are incorporating all required targets (recreation, flood control, megawatt price, hydrothermal concerns, etc.) into several optimization models that help the forecaster solve the optimal amount of flow to release out of any one dam, in any number of ways — turbine, spill, sluice, valve, etc. This ongoing mathematical optimization requires careful analysis of weather forecasts, power market changes, and other enviro-economic conditions that could change the outcome of an optimization result.

2.4.10.2 Operational river forecasting system

Beginning in September 2013, a project was initiated to update the operational river forecast system in terms of the overarching framework, the hydrologic and hydraulic models, and the practice and processes of scheduling the Tennessee River. The TVA switched to the new system in February 2017.

The new framework is called Delft-FEWS, which is used by the NWS as well as other federal hydro-power entities such as the Department of Energy Bonneville Power Administration. This new system will incorporate and connect all primary models used by the RFC including

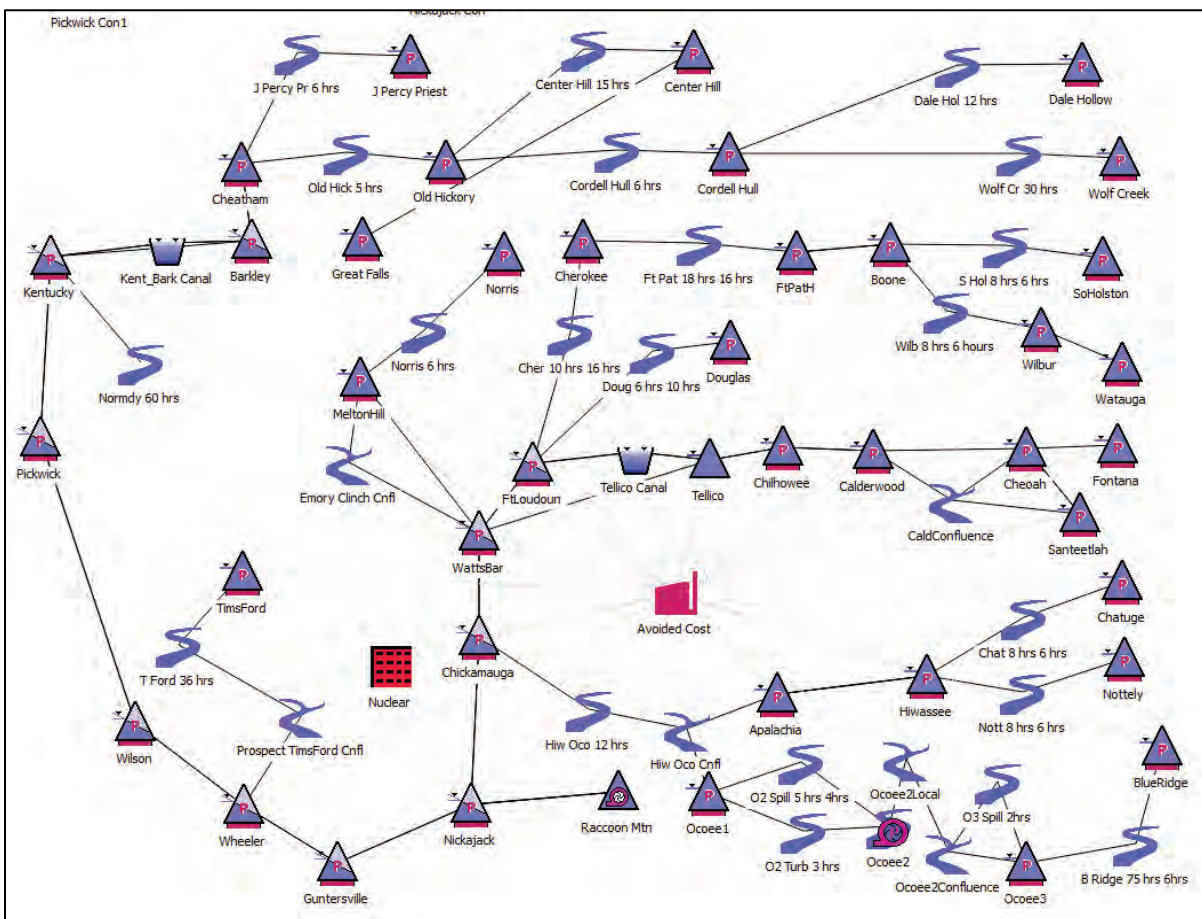
HEC-RAS, the NWS hydrologic model suite, and RiverWare. The development implementation of the NWS hydrologic model suite and RiverWare, inside the Delft-FEWS framework, are used in this assessment. The RiverWare model included both reservoir operational rules and guide curves and river routing components as shown in Table 2-4 and Figure 2-16.

Table 2-4. TVA reservoirs.

Dam	Tributary Dam 1	Tributary Dam 2	River System	Model	Method
Pickwick			Tennessee	RiverWare	Reservoir routing
Wilson			Tennessee	RiverWare	Reservoir routing
Wheeler			Tennessee	RiverWare	Reservoir routing
	Tims Ford		Tennessee	RiverWare	Reservoir plus channel routing
Guntersville			Tennessee	RiverWare	Reservoir routing
Nickajack			Tennessee	RiverWare	Reservoir routing
	Chickamauga		Tennessee	RiverWare	Reservoir routing
		Appalachia	Tennessee	RiverWare	Reservoir plus channel routing
		Hiwassee	Tennessee	RiverWare	Reservoir routing
		Chatuge	Tennessee	RiverWare	Reservoir plus channel routing
		Nottely	Tennessee	RiverWare	Reservoir plus channel routing
		Ocoee 1	Tennessee	RiverWare	Reservoir routing
		Ocoee 2	Tennessee	RiverWare	Reservoir plus channel routing
		Ocoee 3	Tennessee	RiverWare	Reservoir plus channel routing
		Blue Ridge	Tennessee	RiverWare	Reservoir plus channel routing
	Watts Bar		Tennessee	RiverWare	Reservoir routing
		Melton Hill	Tennessee	RiverWare	Reservoir plus channel routing
		Norris	Tennessee	RiverWare	Reservoir plus channel routing
	Ft Loudoun		Tennessee	RiverWare	Reservoir routing
		Cherokee	Tennessee	RiverWare	Reservoir plus channel routing

Dam	Tributary Dam 1	Tributary Dam 2	River System	Model	Method
		Ft Pat H	Tennessee	RiverWare	Reservoir plus channel routing
		Boone	Tennessee	RiverWare	Reservoir routing
		Wilbur	Tennessee	RiverWare	Reservoir plus channel routing
		Watauga	Tennessee	RiverWare	Reservoir routing
		So Holston	Tennessee	RiverWare	Reservoir plus channel routing
		Tellico	Tennessee	RiverWare	Reservoir plus channel routing
		Chihowee	Tennessee	RiverWare	Reservoir routing
		Calderwood	Tennessee	RiverWare	Reservoir routing
		Cheoah	Tennessee	RiverWare	Reservoir plus channel routing
		Fontanna	Tennessee	RiverWare	Reservoir routing
		Santeetlah	Tennessee	RiverWare	Reservoir routing
Chetham			Cumberland	RiverWare	Reservoir routing
	J. Percy Priest		Cumberland	RiverWare	Reservoir plus channel routing
	Old Hickory		Cumberland	RiverWare	Reservoir plus channel routing
		Great Falls	Cumberland	RiverWare	Reservoir routing
		Center Hill	Cumberland	RiverWare	Reservoir plus channel routing
	Cordell Hull		Cumberland	RiverWare	Reservoir plus channel routing
		Dale Hollow	Cumberland	RiverWare	Reservoir plus channel routing
		Wolf Creek	Cumberland	RiverWare	Reservoir plus channel routing

Figure 2-16. TVA reservoir system modeled in RiverWare.



2.4.10.3 MR&T modeling for HYPO 58A

The Sacramento Soil Moisture Accounting model in conjunction with LAG-K and Unit-hydrograph theory only required qualitative precipitation estimates. Operationally, snow was not considered in TVA models because of the latitude extent of the Tennessee Valley River system and the lack of measurable snow that could affect operations.

Data preparation

Using the ArcInfoAscii importer in Delft-FEWS, developed by Deltares, each storm was imported individually. To maintain consistent naming conventions and operational structure of the precipitation import, the parameter was renamed to quantitative precipitation forecast (QPF), and the precipitation was treated as a forecast. Once imported, timeshifts were performed on each time series using the timeshift module in Delft-FEWS.

The time series was shifted to the same month and day within the current year to keep reasonable antecedent soil moisture conditions.

Inflow modeling

Treating hypothetical precipitation as QPF, time was set back to 1 June 2015, to include a warm-up period, and the forecast period was set to end at 13 April 2016 (approximately a month past the end date of the hypothetical precipitation). This allowed the resident soil moisture/precipitation enough time to be released into the river and recede to base flow conditions.

RiverWare optimization modeling

After local inflows were calculated for the length of the modeling period, these inflows were mapped to RiverWare nodes using previously developed connecting configuration. Since non-policy flow did not start until approximately January 2016, optimization modeling began starting in January and simply provided historical data for points of interest for that initial time period.

Modeling involved using the operational 6-hour model. A typical RiverWare run requires manual routing by adjusting gate settings, abiding by policy and regulating zones, mitigating flooding at various *damage centers*, and having some idea of the requirements for potential downstream flooding on the Ohio and Mississippi Rivers. For the purposes of this assessment, forecasters operated dams to reduce flooding at a few of the major damage centers as well as kept headwaters below the top of the gates to prevent overtopping. Other policies were kept in place but not modeled to the detail of an operational run.

2.4.10.4 Modeling for HYPO 52A, 56, and 63

The same methodology was utilized to develop computed regulated flows for TVA reservoirs for HYPOs 52A, 56, and 63.

2.5 Land use considerations

A general land use comparison between 1949 and 2007 was available (Figure 2-17) and indicated minimal land use change as listed in Table 2-5.

Figure 2-17. Land use comparison within Mississippi River Basin.

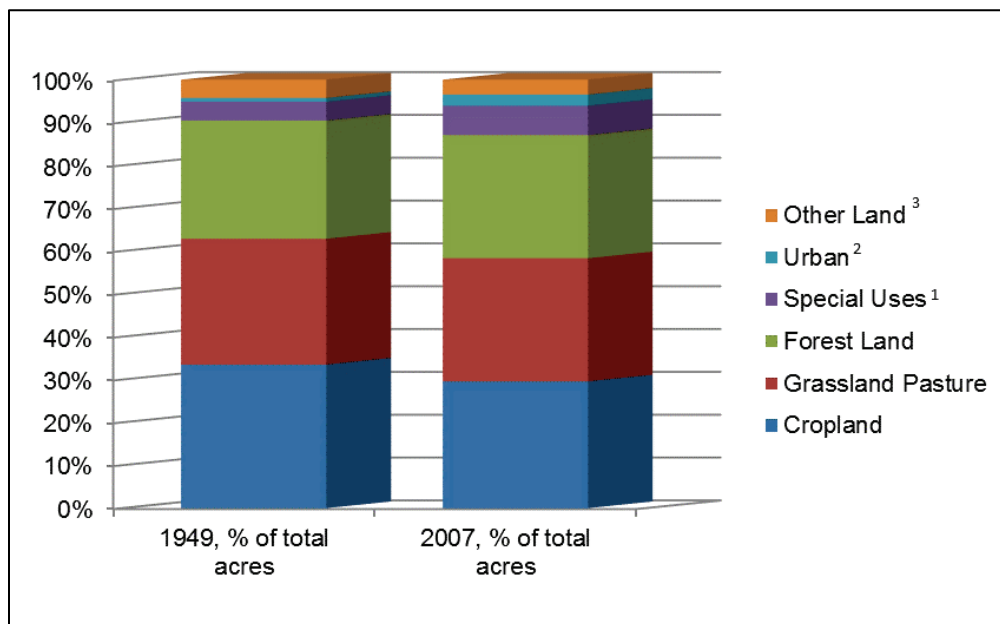


Table 2-5. Land use within the Mississippi River Basin obtained from the U.S. Department of Agriculture.

Land Use	By Land Use Category			By Total Area		
	1949 (1,000 acres)	2007 (1,000 acres)	% Difference	1949, % of total acres	2007, % of total acres	Change from 1949, %
Cropland	362,307	317,890	-13	34%	30%	-4%
Grassland pasture	317,462	308,948	-3	29%	29%	-1%
Forest land	298,476	308,938	3	28%	29%	1%
Special uses ¹	47,669	74,023	43	4%	7%	2%
Urban ²	9,546	27,598	97	1%	3%	2%
Other land ³	45,995	37,366	-21	4%	3%	-1%

¹ Special uses includes rural transportation, parks and wildlife areas, defense installations, and farmsteads.

² In 1969, urban areas shifted from areas of 1,000 acres to areas of 2,500 acres or more.

³ Marshes, swamps, bare rock, deserts, tundra plus other uses not estimated, classified, or inventoried.

While these land use categories failed to depict drainage alterations¹ and improvements within each category, the data still indicated minimal change over the large drainage basin (1,245,000 square miles).

¹ Drainage alterations (i.e., tile drainage and ditching) have changed the hydrologic responses in lower flow regimes and snowmelt; however, this assessment only considers large rain events, and these drainage alterations have minimal impact.

2.6 Infiltration and base flow considerations

Section 1.2.3.6 describes how the 1955 analysis utilized simplified loss coefficients across 44 relatively large sub-basins (Figure 1-4) to adjust rainfall depths in run-Off calculations (Table 2-6). This method grouped large portions of the watershed into a few loss rates. This grouping limited the spatial resolution applied in the calculations and had very minor allowances for temporal change in infiltration. Base flows used during 1955 calculations were derived from discharge observations using standard separation techniques. Resulting values were given for monthly average flows.

Table 2-6. Infiltration coefficients from 1955 Study.*

Area No	Sub Area	Infiltration Indices (in./hr)
1	A-1	0.04
	A-2	0.04
	B-1	0.05
	B-2	0.04
	C	0.04
	D	0.04
	E	0.02
2	F	0.02
	G-1	0.06
	G-2	0.06
	G-3	0.06
	H-1	0.09
	H-2	0.12
3	I	0.1
	K-1	0.08
	K-2	0.08
	K-3	0.08
	L	0.12
4	M	0.12
	P-1	0.05*

Area No	Sub Area	Infiltration Indices (in./hr)
	P-2	0.05
	Q-1	0.05
	Q-2	0.1
	R	0.09
5	T	0.05*
6	U-1	0.1
	V-1	0.08
	V-2	0.07
7	W-1	0.04
	W-2	0.04
	W-3	0.07
	W-4	0.03
	W-5	0.03
	W-6	0.03
	R-1	0.05
	X-2	0.03
	X-3	0.05
	Y	0.03

***Notes**

Storms separated by more than 4 days, use 0.8 in. initial loss in June and 1.0 in. in July, August, and September.

The 2016 analysis utilized the SAC-SMA model, which included continuous soil moisture accounting and evaporation losses. The NWS models had a cumulative total of 7,066 sub-basins that were each individually adjusted to calibrate the SAC-SMA parameters. The more physically based SAC-SMA method and greater spatial resolution in the NWS models would be a significant improvement in accounting for losses over the earlier analysis. Base flow was not inherently required by the NWS models because stream flow at index points was continually computed using routing algorithms within the models. Ideally, the effects of parameter calibration on computed peak flows would be investigated using multiple model simulations to evaluate sensitivity and possibly to estimate uncertainty. The high degree of complexity in generating one individual model simulation and the limited time available for the analysis precluded such sensitivity runs. Future analysis should explore model sensitivity to different infiltration calibration parameters.

2.7 HYPO storm combinations

This assessment reconstructed the 1955 HYPO 58A storm event. Individual precipitation datasets were rebuilt for each storm by converting tabular precipitation data from the 1955 Study or from NOAA national archives into spatial data with continual coverage over the entire Mississippi River Basin. Similarly, the hydrologic models also required temperature data obtained from NOAA national archives for the individual storm periods. The point data for precipitation and temperature were interpolated to develop values over the entire basin. This process is described in Section 2.8. In addition to the HYPO 58A storm event, precipitation datasets were reconstructed from NOAA archives for the 1955 HYPO 52A, 56, and 63 storm events. The latter three HYPO events were included to assess the new methodology being used.

Reassessment of appropriate storms and storm combinations was not evaluated during this review as considerable effort was spent during the 1955 Study to evaluate severe storms and storm combinations. Sections 3.2 and 3.3 give a basic overview of methods used for selection of the HYPO storm combinations. Table 1-12 shows the historical peaks determined from the 1955 Study. More extensive coverage of the procedures can be found in Memorandum Report No. 1 (MRC 1955; Appendix J) and NOAA Hydrological Report Number 34 (USACE Weather Bureau 1956).

There were concerns that more recent extreme storms (those occurring after approximately 1950 and subsequent to the 1955 analysis) might produce higher flood peaks than HYPO 58A. The meteorological analysis required to assess extreme storm events and combinations thereof are extensive and highly complex. Because this complex meteorological analysis was beyond the scope and schedule available for the present analysis, it was not possible to consider extreme storm events and combinations of more recent storms. However, it was determined that one additional combination for the 1973 and 2011 events could be included based on the following (criteria given in the original meteorological assessment):

1. Storms were considered within the general season in which they occurred.
2. The storm combination had a reasonable chance of occurring.
3. There was a period of no rain included between the different historic events.

Fictional Year Assignment – Clipped Merged

The storms were given fictional future dates that used a century of 26 for Clipped-Merged (CM) sequences plus the HYPO storm number:

58A CM = 2658

52A CM = 2652

56 CM = 2656

63 CM = 2663

This gave a unique time property for the resulting model outputs that helped to keep track of the different runs.

2.7.1 Storm sequencing

Each HYPO storm combination prescribed an order for sequencing the historic events. The sequence order was developed as part of the meteorology study described in the 1955 Study (Section 1.2.3). In general terms, the combinations include antecedent rainfall with a core period of intense

rainfall (two or three historic storms coupled with one or more blocks of time with no rain) immediately followed by another period of rainfall. To facilitate use of continuous simulation hydrologic models, a warm-up period was included prior to the core period. This allowed initial model forcings at the start of simulations to develop an antecedent state based on period input data that lead up to the core period. The model warm-up period was 6 to 9 months for original HYPO sequences with an exception of 10 months for the new HYPO 11-73. The actual length of warmup depended on the start date for the core period because the simulation needed to entirely span the preceding winter to fully capture water stored as snow pack. A recession period of 60 days following the core period was included to provide sufficient time for flood peaks to route through the Lower Mississippi River to the Gulf of Mexico.

As discussed in Section 1.2.3, the 1955 Study divided the Mississippi River Basin into seven sub-basins to allow hydrologic hand computations to be completed at a manageable level. This included selectively applying storm sequences across the watershed. The individual storms comprising each HYPO storm were applied to selected sub-basins within the Mississippi River Basin, which allowed separate rainfall/runoff calculations for different sub-basins. This, however, resulted in discontinuous precipitation across adjacent sub-basin boundaries where different rainfall sequences were applied.

The current hydrologic method applies the individual storms across all sub-basins in the time sequence in which they appeared in the HYPO storm. In other words, a storm would begin to develop and then move across the watershed according to the precipitation patterns defined by the underlying historical events and as combined to make up the HYPO storms (just as a radar animation shows storm tracks). There would be no

discontinuities in precipitation amounts across adjacent sub-basin boundaries as was the case for the 1955 Study.

Figure 2-18 through Figure 2-21 illustrate the way precipitation was applied during the 1955 analysis (multiple storm sequences given below the dashed line). The 1955 precipitation sequences required selective extraction of precipitation and temperature data grids to match the multiple sequences shown in these figures. Once input data grids had been extracted for the select sub-basins, they had to be merged back into a single input grid needed by the hydrologic models. This was referred to as the clipped-merged (CM) sequence.

Fictional Year Assignment – Straight Sequence

The storms were given fictional future dates that used a century of 25 for Straight Sequence (SS) simulations plus the HYPO storm number:

- 58A SS = 2558
- 52A SS = 2552
- 56 SS = 2556
- 63 SS = 2563

This gave a unique time property for the resulting model outputs that helped to keep track of the different runs.

The figures below also show how precipitation was applied for the current analysis (single continuous sequence given above the dashed line). The single continuous sequence was referred to as the straight sequence (SS).

Figure 2-18. HYPO 58A flow chart representation of meteorological combination (above dashed line) and computation approach used for Memorandum Report No. 1 (MRC 1955).

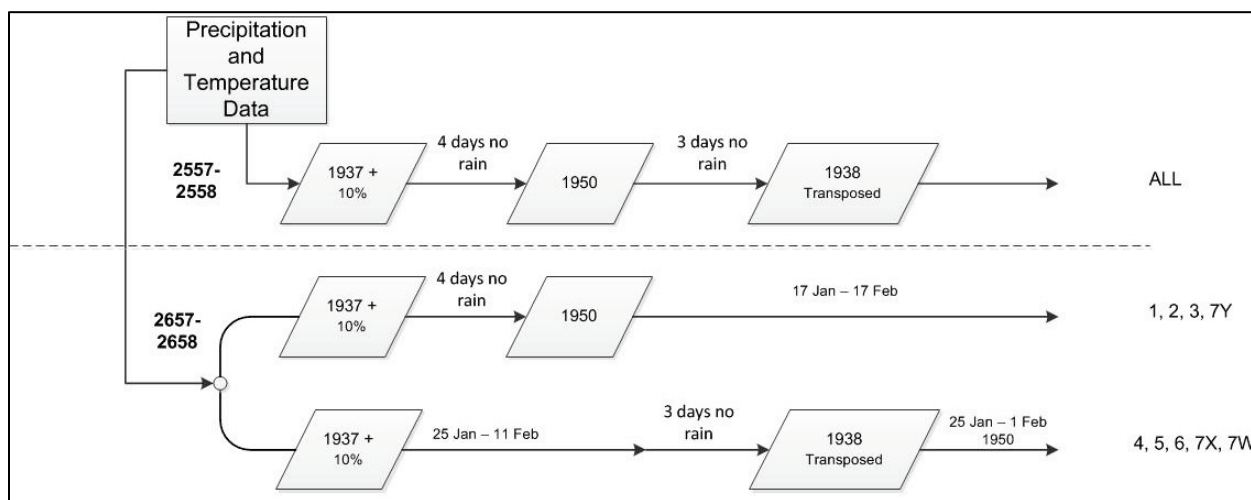


Figure 2-19. HYPO 52A flow chart representation of meteorological combination (above dashed line) and computation approach used for Memorandum Report No. 1 (MRC 1955).

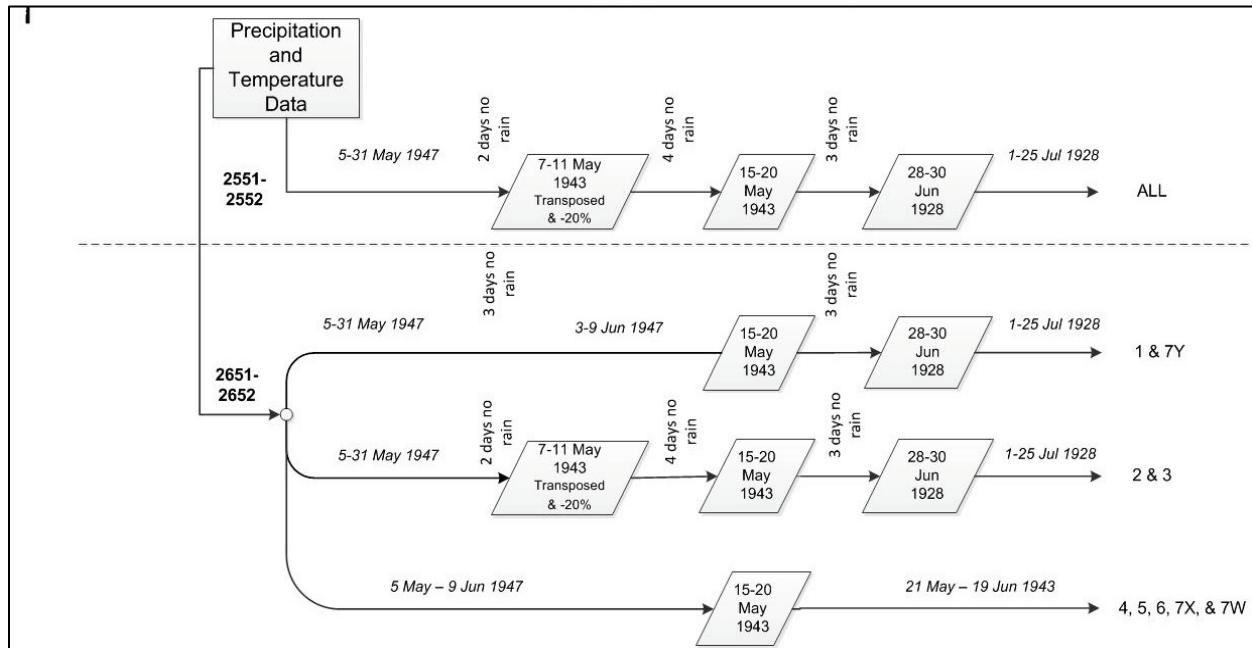


Figure 2-20. HYPO 56 flow chart representation of meteorological combination (above dashed line) and computation approach used for Memorandum Report No. 1 (MRC 1955).

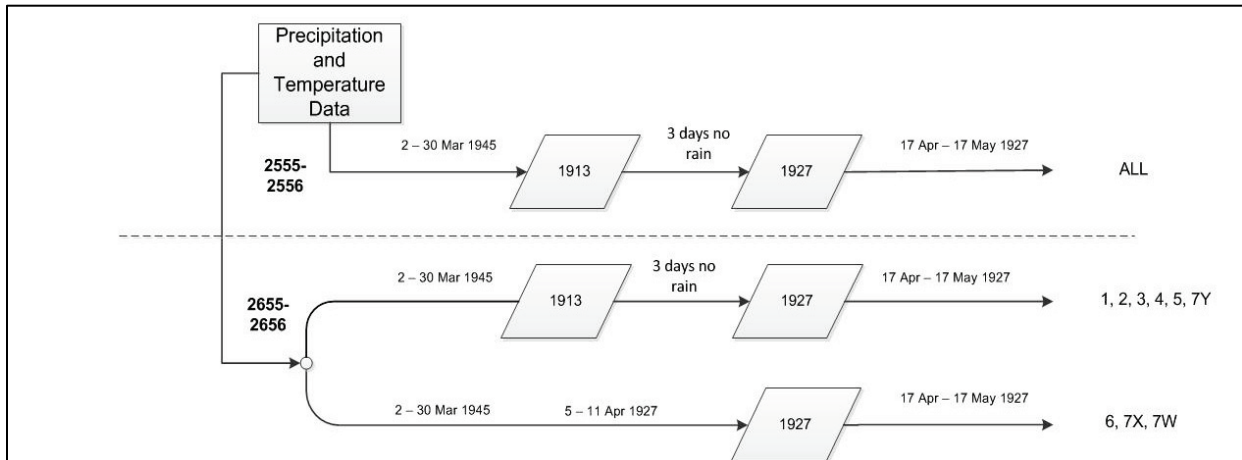
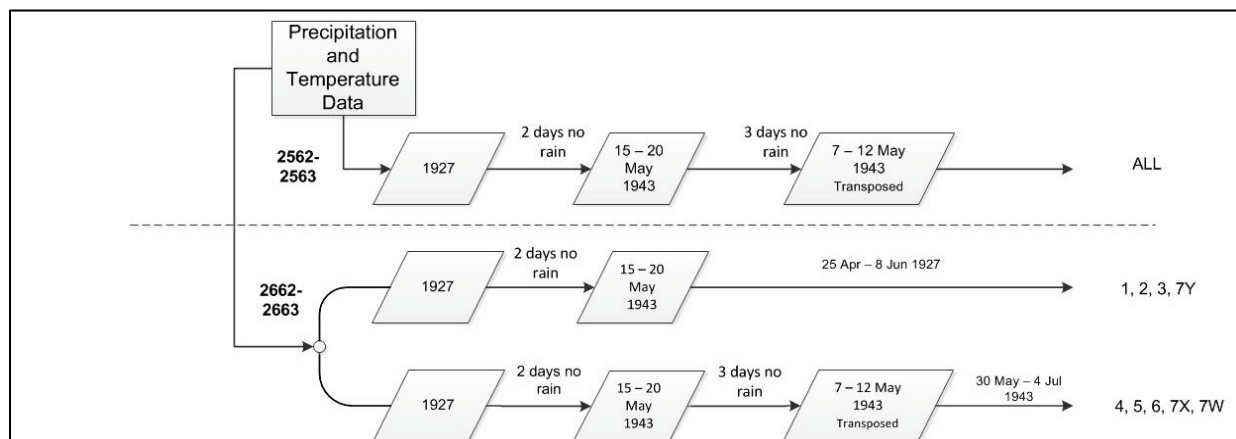


Figure 2-21. HYPO 63 flow chart representation of meteorological combination (above dashed line) and computation approach used for Memorandum Report No. 1 (MRC 1955).



2.7.1.1 CM sequence – 1955 methodology

To create the spatial precipitation grids that match the exact sequence presented in the 1955 Study, each time series of storm grids was clipped to match its respective coverage area (e.g., sub-areas 1, 2, 3, and 7Y; 4, 5, 6, 7W; and 7X for HYPO 58A) as detailed in the 1955 report (MRC 1955). Each HYPO storm combination was comprised of two sequences except for HYPO 52A that had three sequences. Once each clipping operation was completed for each region, the regions were merged to compile a full grid input for each time-step. This process is referred to as the CM sequence.

For example, HYPO 58A consists of the following:

- The January 1937 and January 1950 storms over Areas 1, 2, 3, and 7Y (Figure 3-4); purple area shown in Figure 2-22.
- The January 1937 and transposed February 1938 storm over all remaining areas: Areas 4, 5, 6, 7X, and 7W; green area shown in Figure 2-22.

For this assessment, only the HYPO 58A CM sequence was regenerated for comparison purposes. CM sequences for the other three HYPO events are depicted in Figure 2-23 (HYPO 52A), Figure 2-24 (HYPO 56), and Figure 2-25 (HYPO 63).

Figure 2-22. Map showing different regions of precipitation for the HYPO 58A CM sequence.

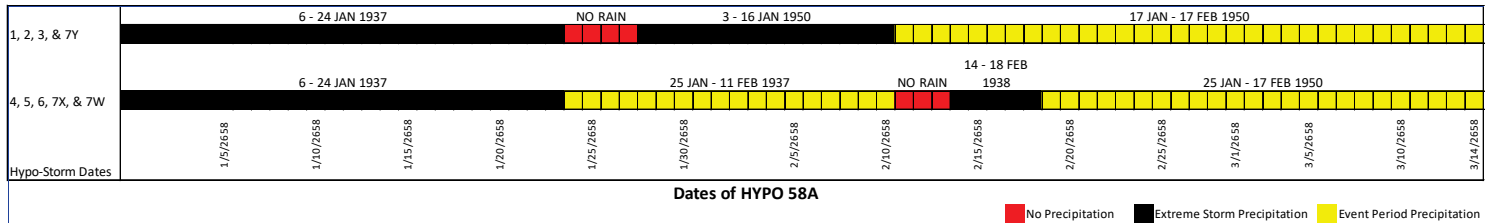
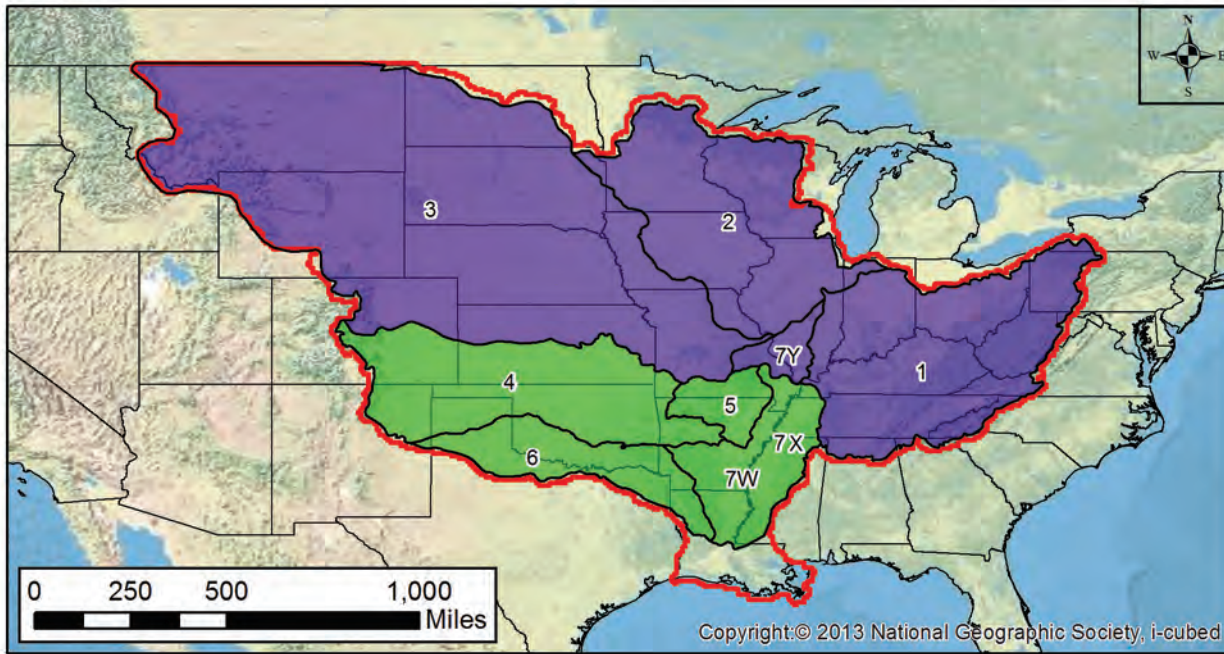


Figure 2-23. Map showing different regions of precipitation for the HYPO 52A CM sequence.

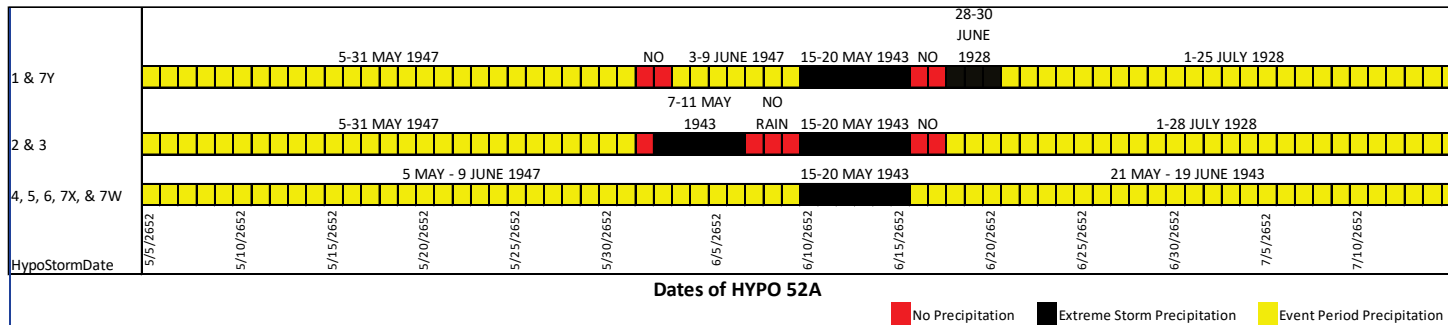
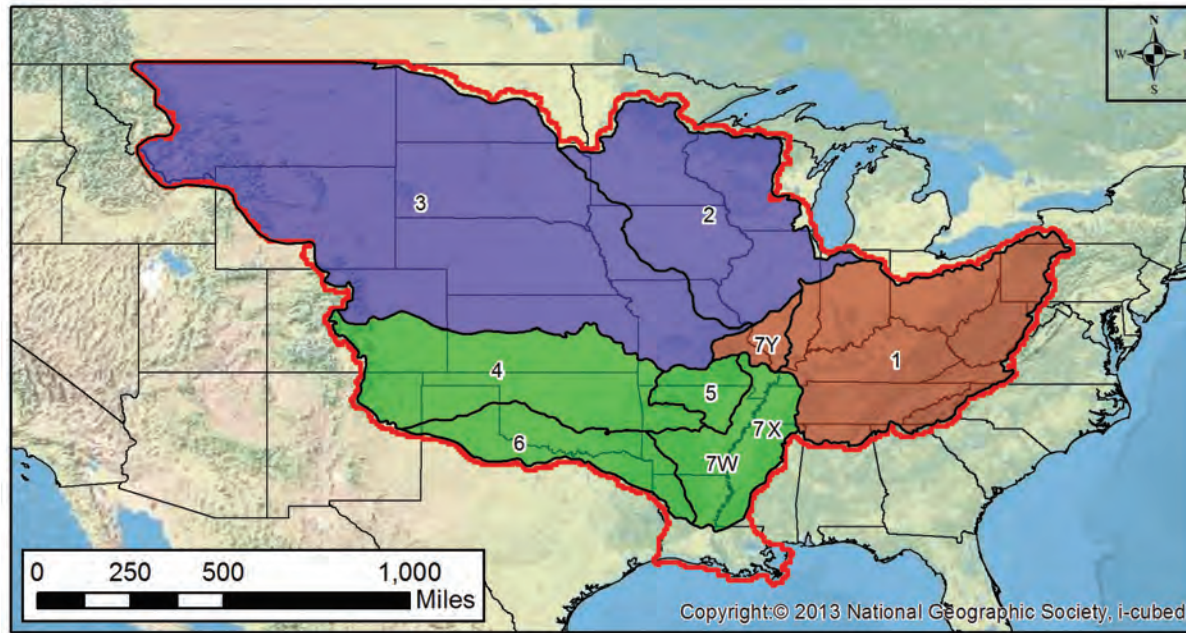


Figure 2-24. Map showing different regions of precipitation for the HYPO 56 CM sequence.

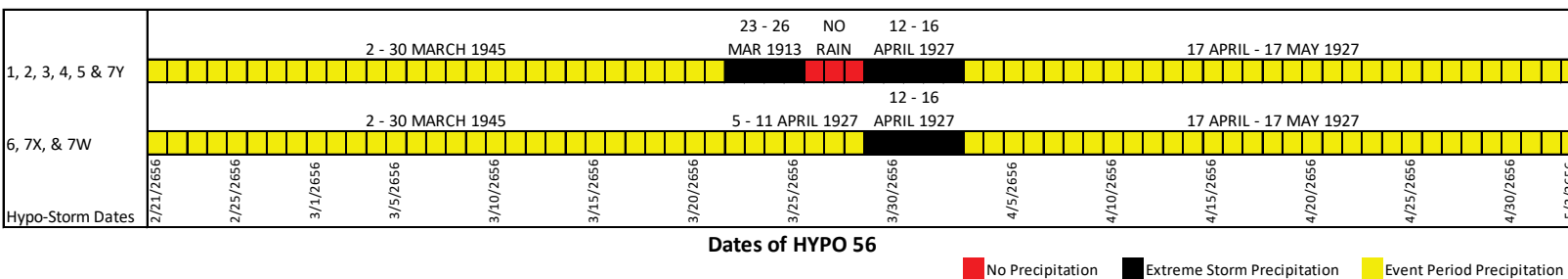
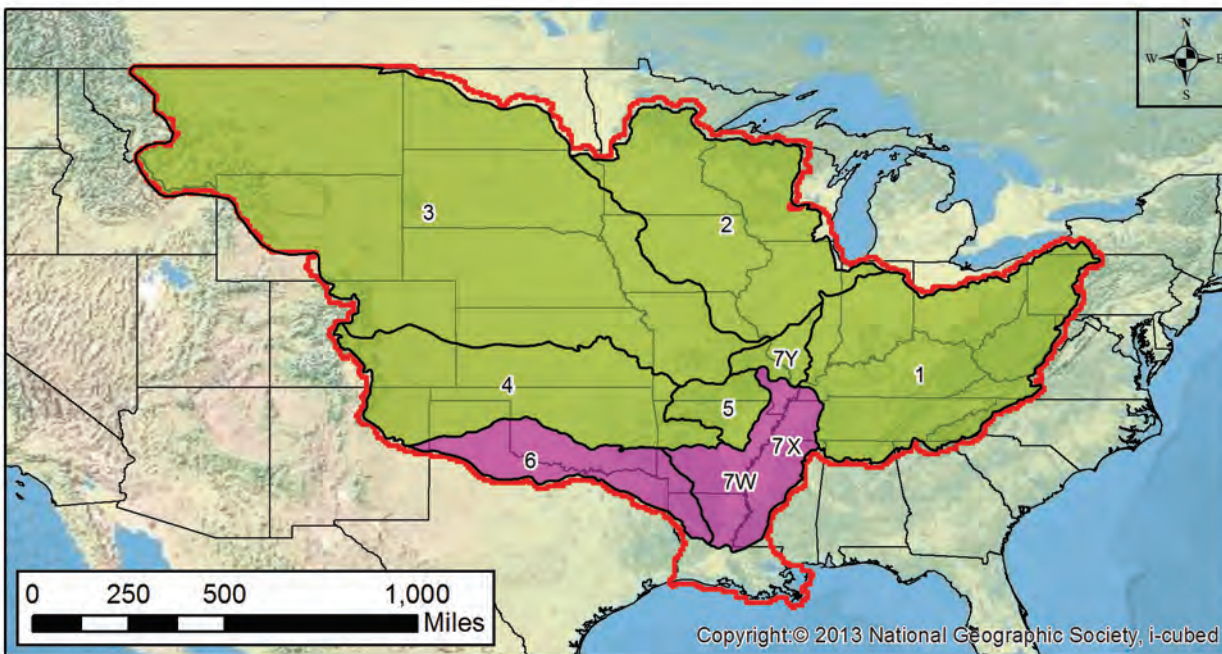
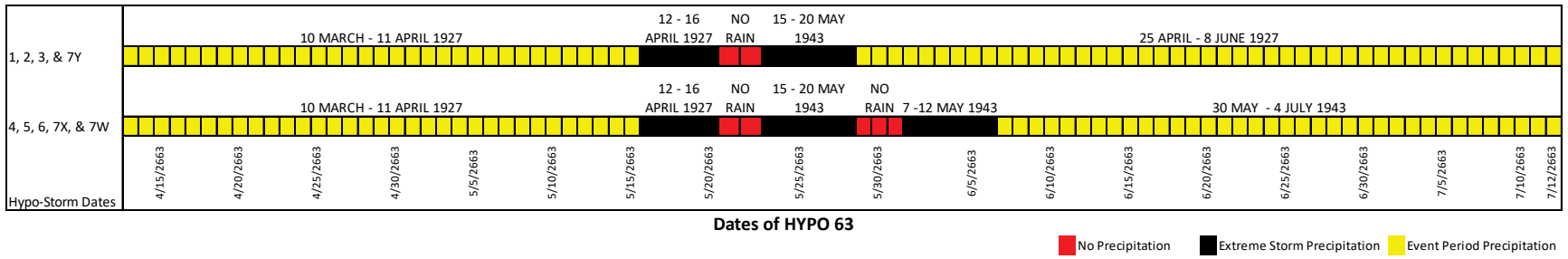
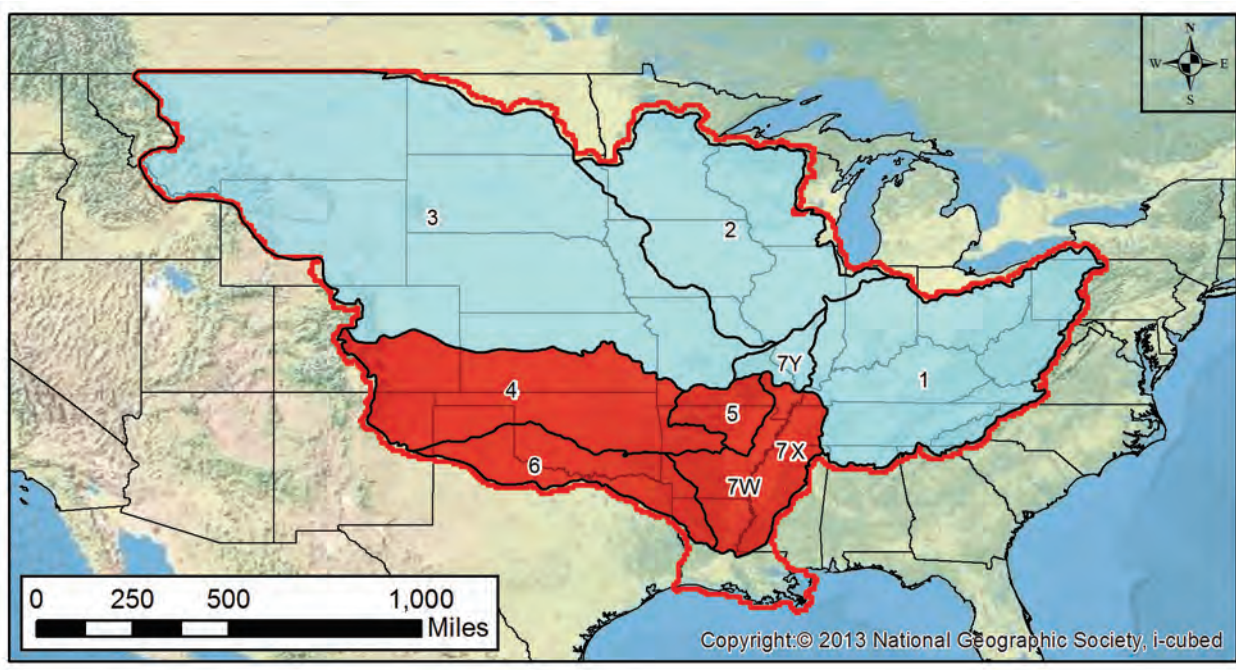


Figure 2-25. Map showing different regions of precipitation for the HYPO 63 CM sequence.



2.7.1.2 SS - 2016 methodology

Point precipitation data were interpolated¹ to produce a continuous spatial representation and then converted into ASCII grids that cover the entire Mississippi River Basin as shown in Figure 2-26. This process is referred to as the SS.

For example, HYPO 58A consists of the following:

- The January 1937, January 1950, and the transposed February 1938 storms over all Areas 1, 2, 3, 4, 5, 6, 7X, 7W, and 7Y (see Figure 2-27).

Initial results from HYPO 58A unregulated and regulated simulations showed that CM results were slightly lower than computed using the SS. The difference between SS peak flow and CM peak flow immediately below the Mississippi/Ohio River confluence was approximately +5% (SS being higher) for both unregulated and regulated simulations. This level of difference is within the standard accuracy given for flow discharge measurement on the Mississippi River, which is $\pm 5\%$. A recommendation to adopt the current standard methodology following the SS approach was made to the Executive Steering Committee (ESC). The ESC subsequently approved this recommendation, and no further analysis was done using the CM approach (see Appendix F).

¹ Interpolation was performed using inverse distance weighted (IDW) methods with bias correction to the observed point data values (see Section 2.8.3).

Figure 2-26. Map showing the spatial representation of precipitation for HYPO 52A, 56, 58A, 63, and 11-73 SS.

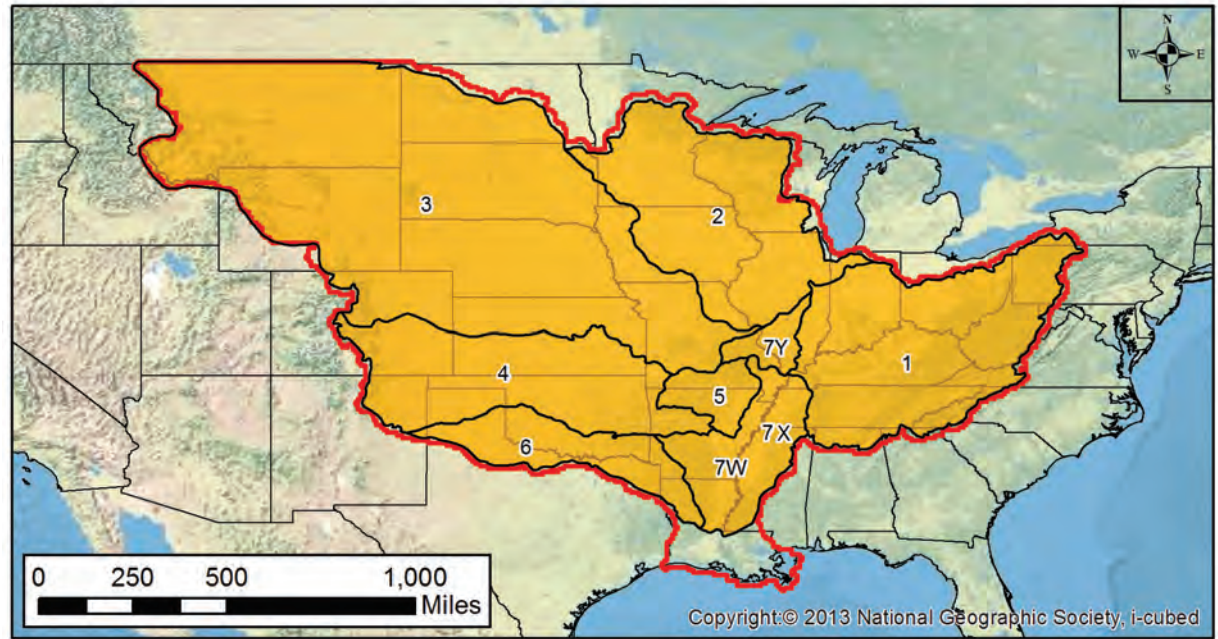
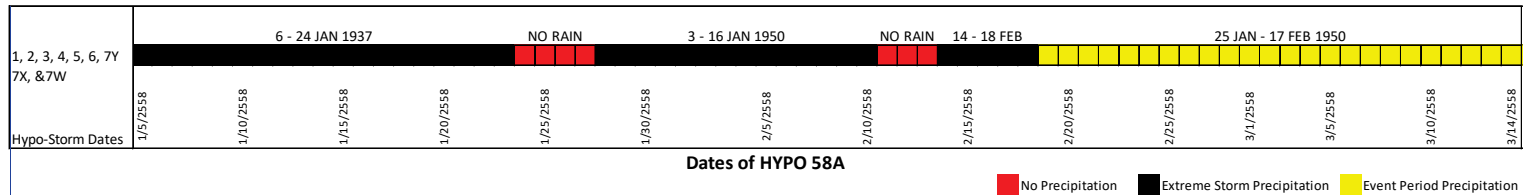


Figure 2-27. HYPO 58A SS.



2.7.1.3 CM and SS comparison

Both the CM and SS were evaluated for HYPO 58A to assess how well the new methodology developed spatially continuous hypothetical storms. Table 2-7 compares the HEC-RAS SS (58A-U) and CM (58A-U-CM) peak flow results at various points along the Mississippi River within the Memphis District against the peak flow values provided in USACE (1955) and WES (1957). The 1955 Study values are labeled as 58A and 58A-EN in the table.

Table 2-7. SS and CM peak flow results compared to historic peak flow values.

Location	Project Design Flood				
	Unregulated Discharge (U), cfs			Regulated Discharge (Existing and Near-term Reservoirs, EN), cfs	
	58A ¹	58A-U	58A-U-CM	58A-EN ¹	58A-R
Ohio at Cairo, IL	2,460,000	2,458,000	2,392,678	2,250,000	2,326,000
Miss/Ohio Confluence (combined)	2,850,000	2,937,000	2,785,000	2,360,000	2,791,000
New Madrid, MO	NA	2,751,000	2,628,000	NA	2,660,000
Caruthersville, MO	NA	2,391,000	2,353,000	NA	2,342,000
Osceola, AR	NA	2,915,000	2,628,000	NA	2,833,000
Memphis, TN	2,770,000	2,956,000	2,758,000	2,410,000	2,863,000
Helena, AR	2,710,000	2,862,000	2,684,000	2,460,000	2,788,000
Arkansas City, AR	3,210,000	3,366,000	3,065,000	2,890,000	3,263,000

¹ Values obtained from USACE (1955) and WES (1957).

Generally, the CM sequence results had peak discharges that were lower than authorized peak PDF flows from Memorandum Report No. 1 (MRC 1955). The SS results had peak discharges that were higher than authorized peak PDF flows. Table 2-8 shows the percent difference between the peak flow values.

Table 2-8. Percent differences from the historic 58A peak flow values.

Location	Percent Differences (For peak flows in Table 2-7)		
	Unregulated Discharges		
	58A-U to 58A	58A-U-CM to 58A	58A-U to 58A-U-CM
Ohio at Cairo, IL	0%	-3%	3%
Miss/Ohio Confluence (combined)	3%	-2%	5%
New Madrid, MO	NA	NA	5%
Caruthersville, MO	NA	NA	2%
Osceola, AR	NA	NA	10%
Memphis, TN	6%	0%	7%
Helena, AR	5%	-1%	6%
Arkansas City, AR	5%	-5%	9%

The differences (Table 2-8) between unregulated peaks for the CM and SS were not significantly different than the unregulated peak values¹. Using the 2016 SS methodology generally resulted in higher unregulated peak flows coming from the Upper Mississippi, shown in Table 2-7. However, this represented only a small fraction of the total combined confluence flow of the Mississippi and Ohio Rivers. The combined difference represented 3%-6% increases in unregulated peak flow compared to the 1955 unregulated peak values for the Memphis District reach. Since the SS follows current methodologies and has values within an acceptable range of the authorized peak flows from the 1955 analysis, only the SS approach was used for the remaining HYPO storm simulations.

Plots of the SS and CM output flow hydrographs indicate that the SS had higher discharge volumes for both unregulated and regulated scenarios. Examples from key HEC-RAS inflow boundary locations (modeled by the corresponding RFCs) follow in Figure 2-28 through Figure 2-35.

¹ Significant difference was defined by expert opinion of the Executive Steering Committee as deviations greater than 10%.

Figure 2-28. Smithland unregulated discharge hydrograph, HYPO 58A.

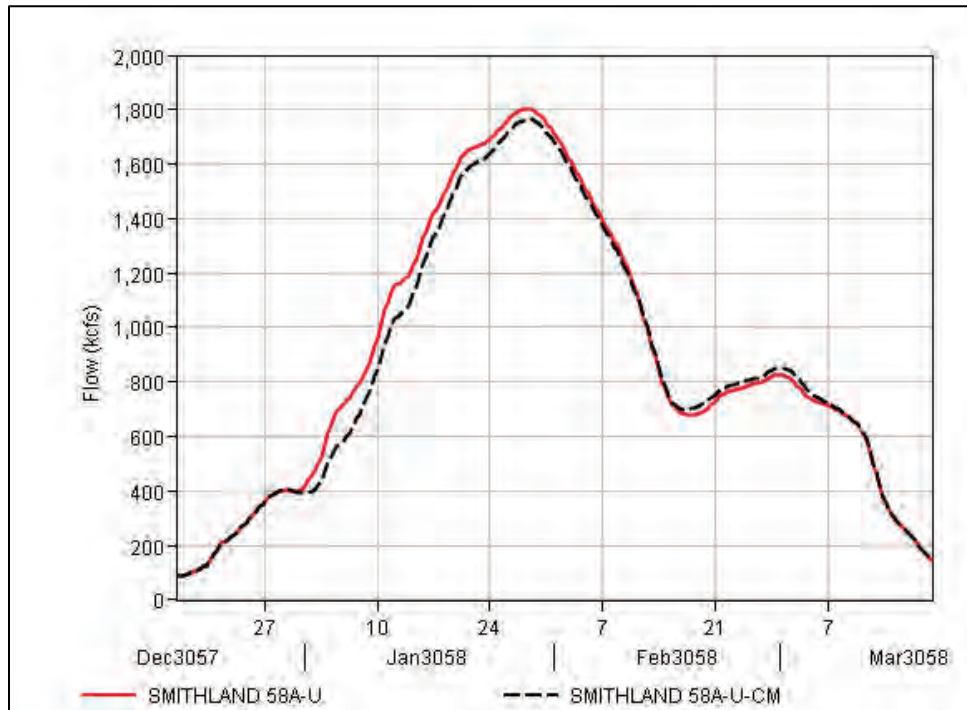


Figure 2-29. Smithland regulated discharge hydrograph, HYPO 58A-R.

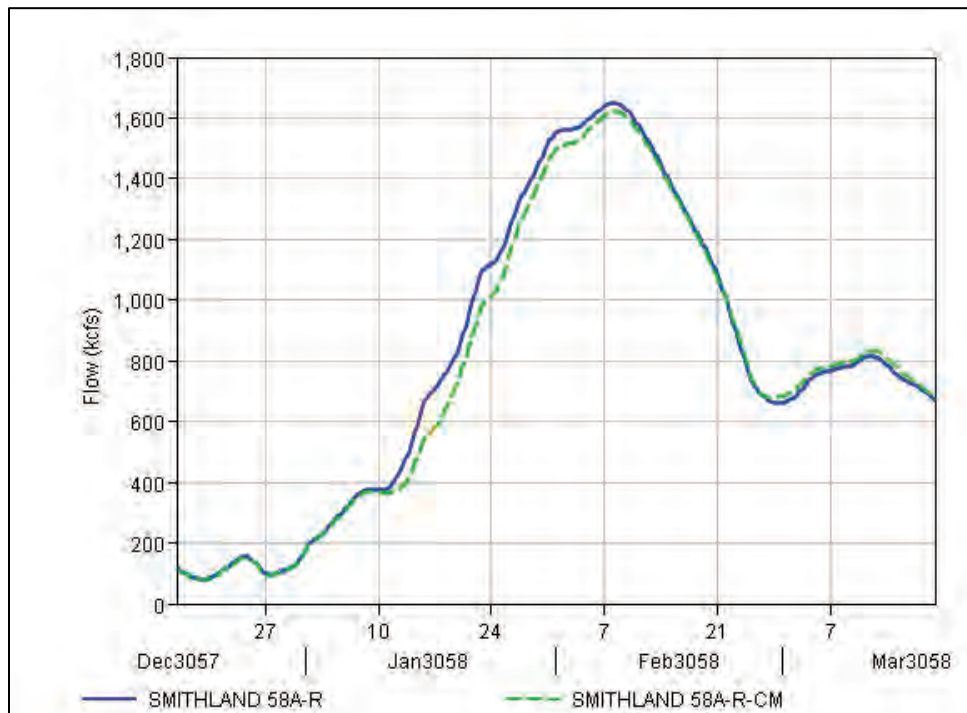


Figure 2-30. Chester unregulated discharge hydrographs, HYPO 58A.

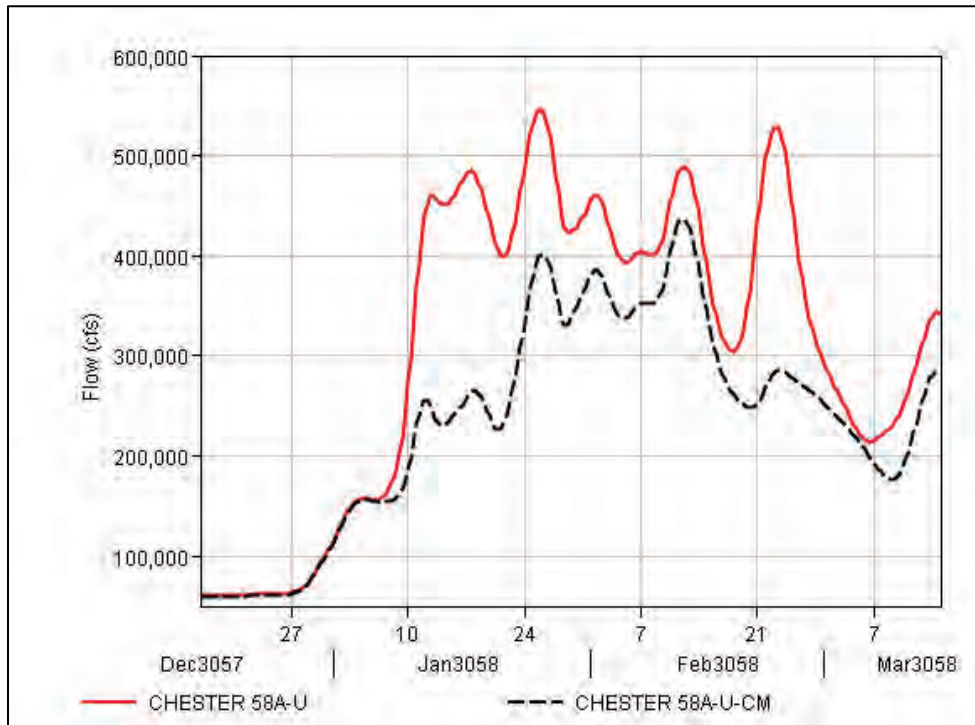


Figure 2-31. Chester regulated discharge hydrographs, HYPO 58A.

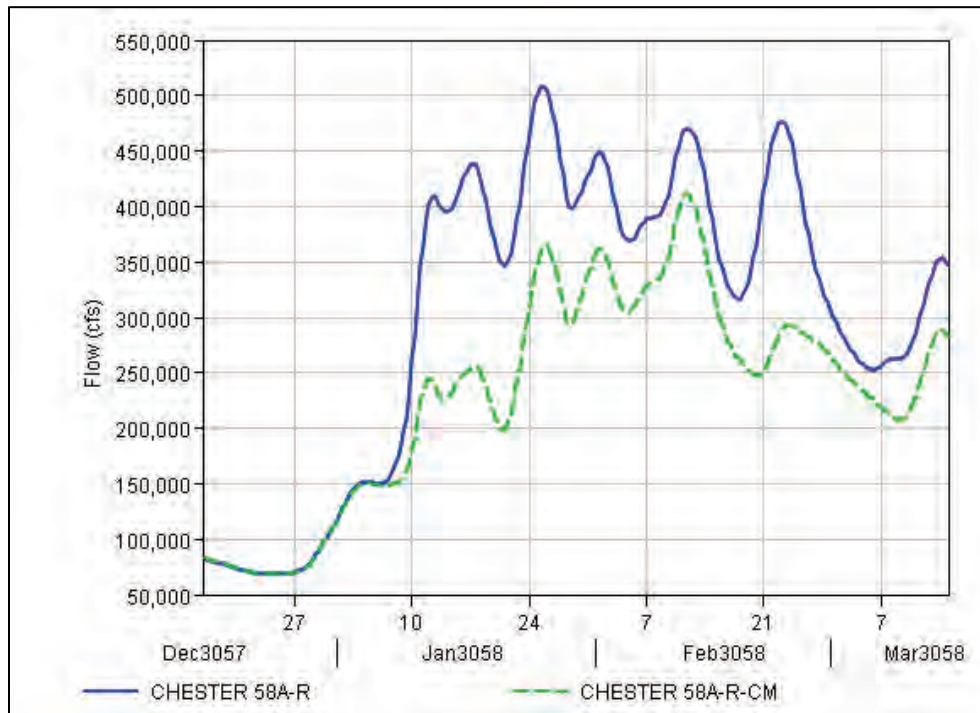


Figure 2-32. Clarendon unregulated discharge hydrographs, HYPO 58A.

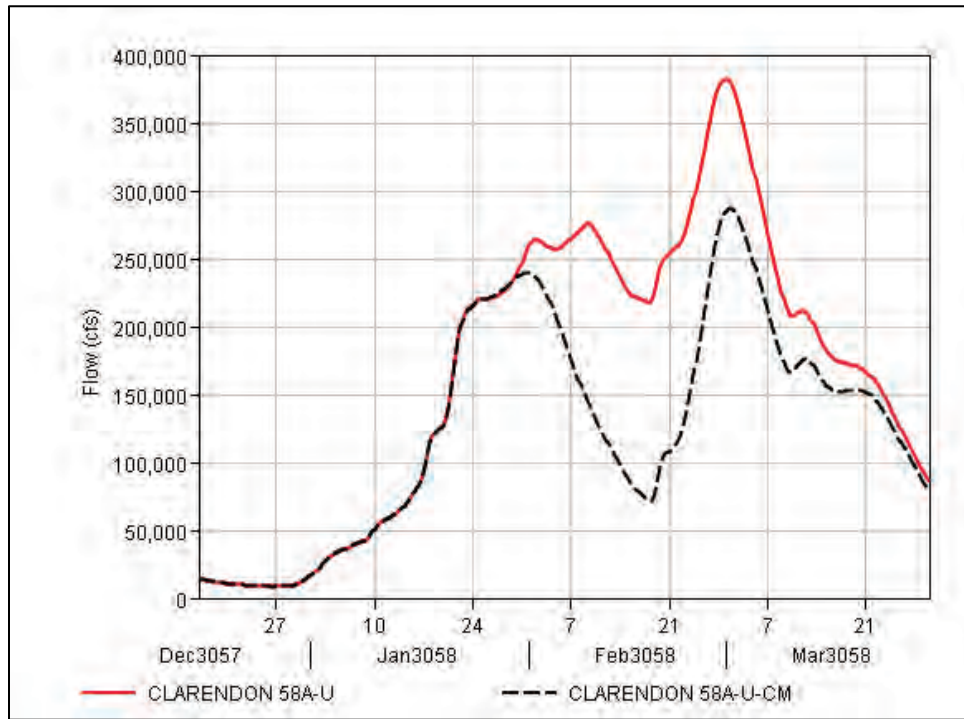


Figure 2-33. Clarendon regulated discharge hydrographs, HYPO 58A.

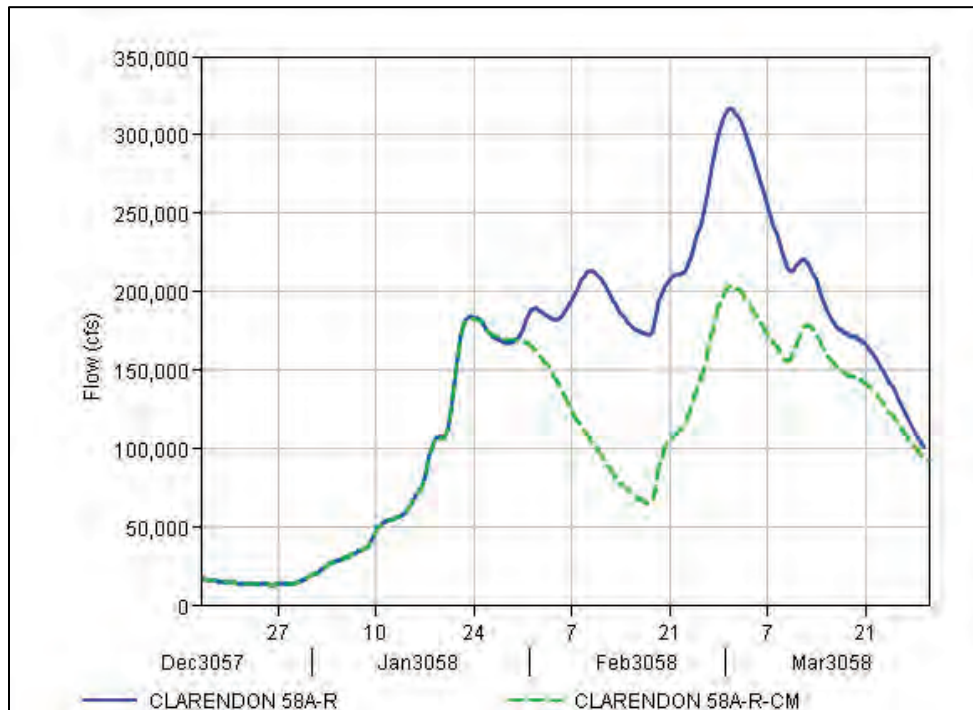


Figure 2-34. Shreveport unregulated discharge hydrographs, HYPO 58A.

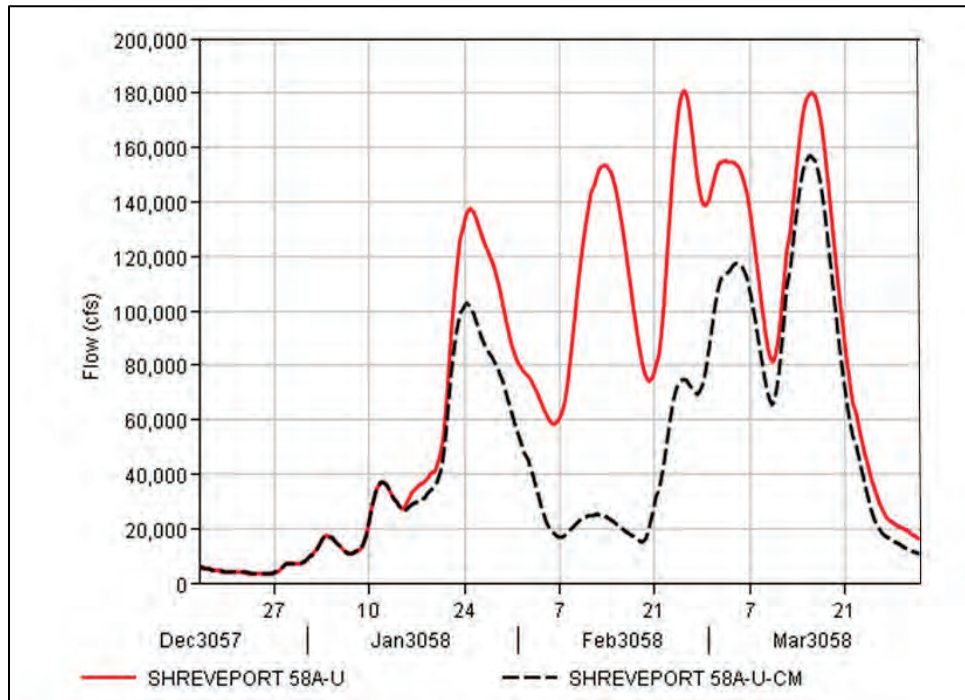
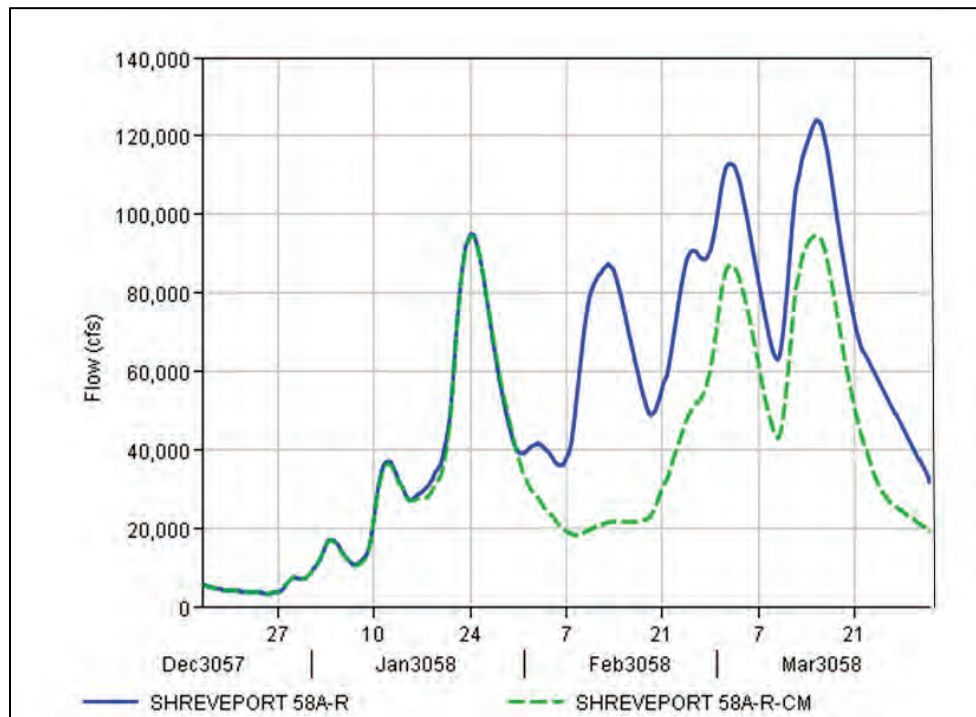


Figure 2-35. Shreveport regulated discharge hydrographs, HYPO 58A.



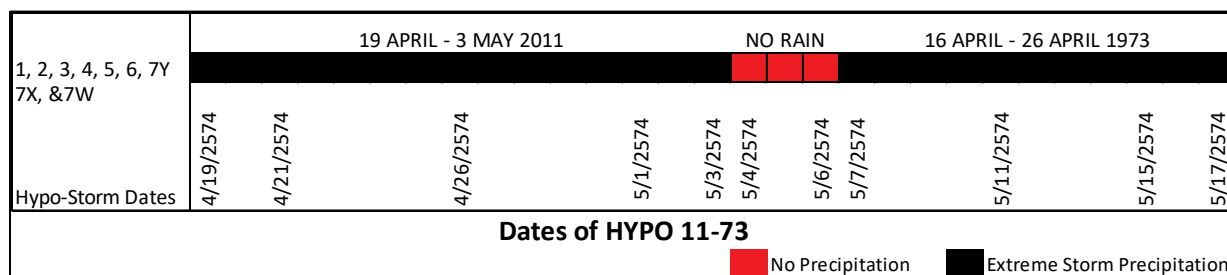
2.7.2 Evaluation of new HYPO storm sequence

Recent major floods have occurred during early spring while the HYPO 58A storm (current PDF storm) produces a winter flood. For this reason, there were concerns about (1) the need to include extreme storms that have occurred since 1950 and (2) if another storm with a new higher peak flood might result from a combination from more recent extreme events.

The meteorological analysis required to evaluate multiple extreme events and combinations was outside the scope and schedule available for the present assessment. Because there were concerns that more recent extreme storms in a different season might produce higher flood peaks than HYPO 58A, the current assessment developed one additional storm combination that was prepared following the methodology outlined in HMR 35 (USACE, Weather Bureau 1959) and Memorandum Report No. 1 (MRC 1955). The new storm combination, named HYPO 11-73, was based on events that produced the 1973 and 2011 floods on the Lower Mississippi River as detailed in Appendix G. The 2011 and 1973 storms could be combined under general meteorological criteria applied for the 1955 HYPO storms.

This new HYPO 11-73 storm combined those events and consisted of three distinct periods of intense rainfall placed in sequence. Individual precipitation datasets were built for each storm for point precipitation and temperature data that covered the entire Mississippi River Basin. The point data were interpolated to develop values over the entire basin following the same methodology used to develop the other HYPO gridded data sets. HYPO 11-73 consists of the 16–26 April 1973 and the 19 April – 3 May 2011 over all areas 1, 2, 3, 4, 5, 6, 7X, 7W, and 7Y as shown in Figure 2-36.

Figure 2-36. HYPO 11-73 SS.



The HYPO 11-73 storm was simulated in the CHPS-FEWS hydrologic models to produce boundary hydrographs for the HEC-RAS unsteady model. The results show that HYPO 58A is still the governing storm event

for the PDF as the resulting peak flows from HYPO 11-73 were lower than determined for HYPO 58A as shown in Table 2-9.

Table 2-9. HYPO 11-73 results compared to 1955 HYPO storm results.

River	Location	Peak Flow (kcfs)	
		HYPO 58A-U	HYPO 11-73-U
Mississippi	St Louis, MO	433	1024
Missouri	Hermann, MO	220	668
Ohio	Metropolis, IL	2461	1734
Mississippi	Cairo, IL	2937	2806
Mississippi	Arkansas City, AR	3367	3286
White	Clarendon, AR	271	311

2.8 Storm development

Historic precipitation data to develop the storms needed for inclusion in the HYPO storm events were obtained from the original working files and from old reports like Memorandum Report No. 1 (MRC 1955). Generally, the data were 6-hour point values for the storm duration. To facilitate the conversion of point data to a spatial representation of the data, the point values were entered into Excel to build a database for each separate historic event. Once the database had been completed, the data were interpolated using ESRI's Arcmap. The interpolation was first tried using Kriging techniques. Each interpolated 6-hour interval was then summed over the storm period. Isohyetal contours were generated for the interpolated data. The resulting isohyets were then compared to maps of isohyets in the published reports. The comparison was visual by the NWS and USACE meteorologists. As the process developed, a more rigorous comparison method was adopted to check areas within each isohyet.

An extended simulation period was necessary to allow the NWS CHPS models to arrive at the appropriate antecedent state at the beginning of the actual storm. The team determined that a 6-month warm-up period would be sufficient and there needed to be a post event period to permit the unsteady model sufficient time to fully route the event all the way to the Gulf of Mexico. This proved sufficient except for events beginning in April or later; for these events, the warm-up period was extended so that the

model could account for SWE from when the first snowfall occurred. The post-event period was first set to 1 month past the last day of the event but was later extended an additional month — 2 months total. This required extending the point datasets to cover an approximate 10-month simulation period.

With an extended simulation period, it became necessary to enhance the checks employed to test agreement of interpolated rainfall grids with the original storm maps from the 1955 Study. The additional testing involved re-sampling the interpolated grids to determine *point* values at select gage locations that could be compared. This process revealed that values obtained from the interpolated grids did not return the published storm totals at known gage locations. Generally, the interpolated values were lower than observed values. Possible reasons for the difference were the sparse network of point gage readings used as input to the interpolation process and the interpolation scheme used. Nothing could be done to significantly improve the number of gages available. The historic events ranged from 1913 to 1950, so there was a lack of point data, especially in the earliest storm events. For example, the 1913 dataset included approximately 400 point locations spread over the entire Mississippi River Basin. The 1950 dataset ultimately consisted of approximately 6,200 point locations, still relatively few to cover such a large watershed. Prior to 1950, the 6-hour data were taken directly from the PDF Flowline Study found at the National Archives. It was only for the storm event. The warm-up and post-storm data were derived from daily data and placed into the 00 Coordinated Universal Time (UTC) time frame. Any of the other periods could have been chosen (06, 12, or 18UTC) to put all of the daily data into, but 00UTC was picked since it was the first one. Hourly data were sparse prior to 1948.

As an example, 1950 rainfall data were derived from hourly and daily data with the hourly data providing the breakdown for the 6-hour periods for the daily data. The hourly-only dataset included only approximately 1,500 sites while the daily data allowed for 6,400 sites, thus reducing interpolation inaccuracies. The quality assurance/quality control (QA/QC) for 1950 rainfall data focused primarily on the storm event rainfall totals. If they were a few hours off, it did not affect the total. The key was to get the totals correct, which turned out to be Inverse Distance Weighted (IDW) interpolation with bias to observed point values. Daily and hourly data were reviewed to ensure the individual time period values matched

published values, but the storm totals were the key (see Figure 2-37 for published isohyet contours and Figure 2-38 for isohyet contours derived from interpolated grids).

Figure 2-37. Published map of 1950 cumulative storm isohyets.

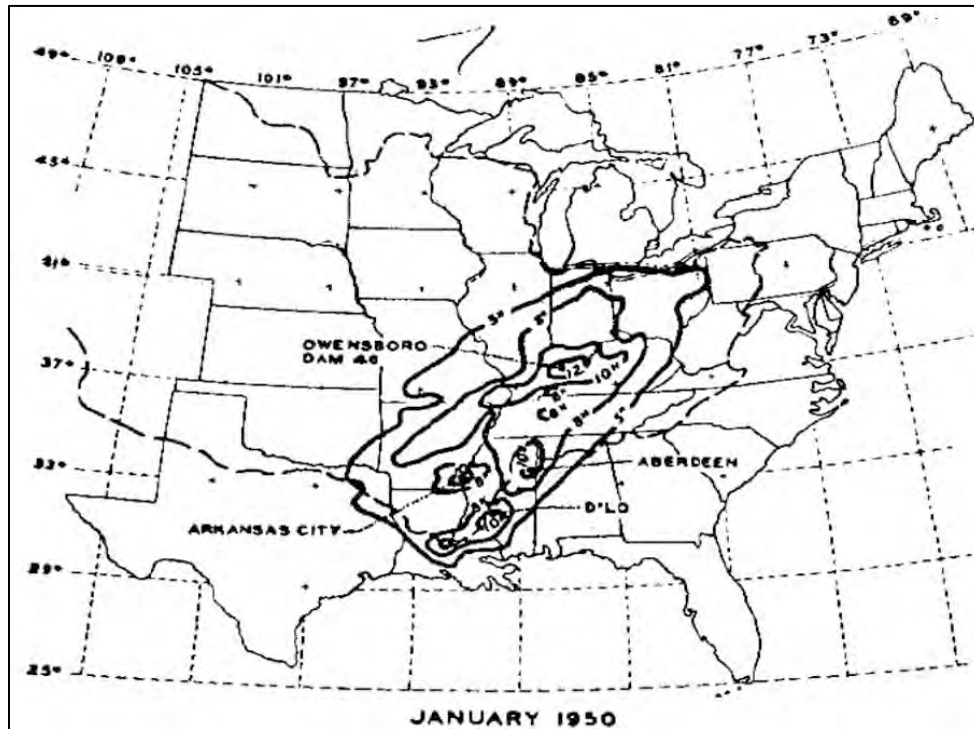
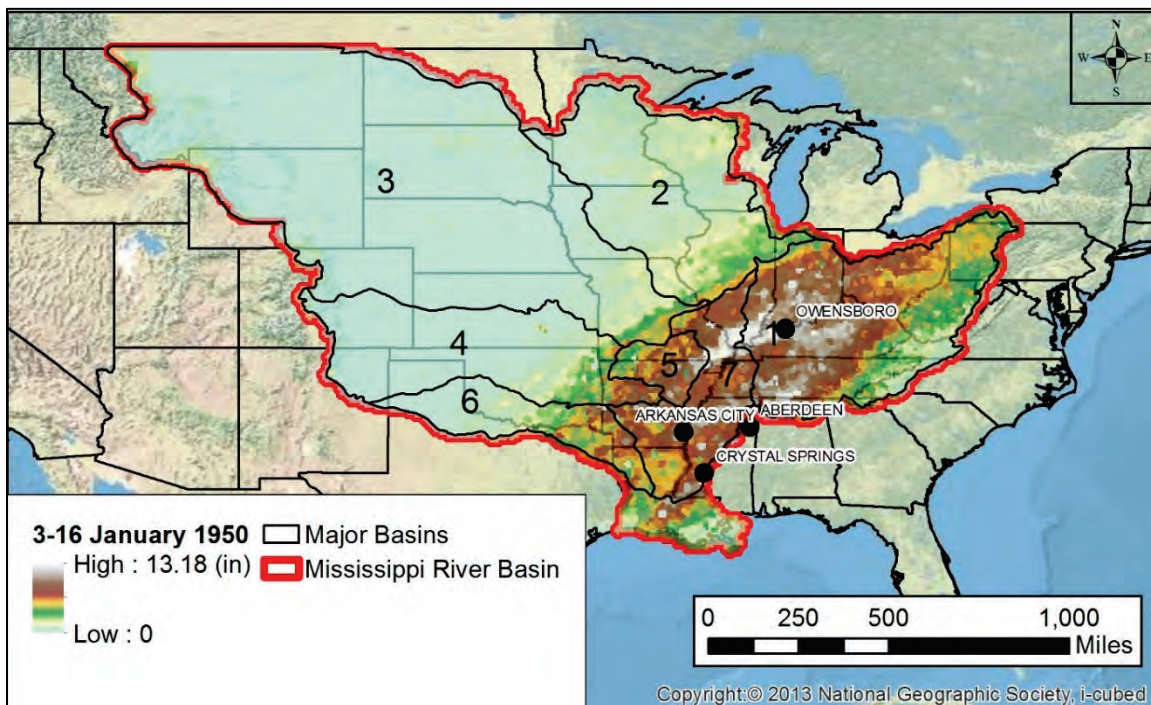


Figure 2-38. Interpolated map of 1950 cumulative storm isohyets.



2.8.1 Precipitation

The assessment of the PDF flowline is driven by the accuracy of the precipitation inputs developed for the hydraulic model. Re-compiling the data used to generate the individual storms that make up the HYPO 58A, 52A, 56, and 63 was no small feat. HYPO 58A was the PDF storm for the 1955 Study; thus, it was the most documented storm. Still, compiling data for each storm event was an arduous process that required mining precipitation data from multiple sources (MRC 1955; National Climate Data Center [NCDC]¹) and converting data times to consistent time intervals. Once the NWS compiled each storm event, those storm text files were provided to USACE to convert to the ESRI ASCII grid format. USACE developed Python scripts to automate the conversion. These scripts also included several checks to ensure all of the data transferred properly. The final ASCII grid files were sequenced based on the HYPO storm pattern and sent to the RFCs for ingest into their CHPS-FEWS hydrologic models.

Extensive QA/QC measures were taken to ensure the precipitation input values were correctly transferred and that the interpolated ASCII grids were comparable to published isohyetal maps, depth area curves, and cumulative precipitation curves from the 1955 Study. The 2016 isohyetal maps, depth area curves, and cumulative precipitation curves are presented for HYPO 58A in this section with additional supporting information provided in Appendix B. The other HYPO storms can be found in Appendix C–Appendix E.

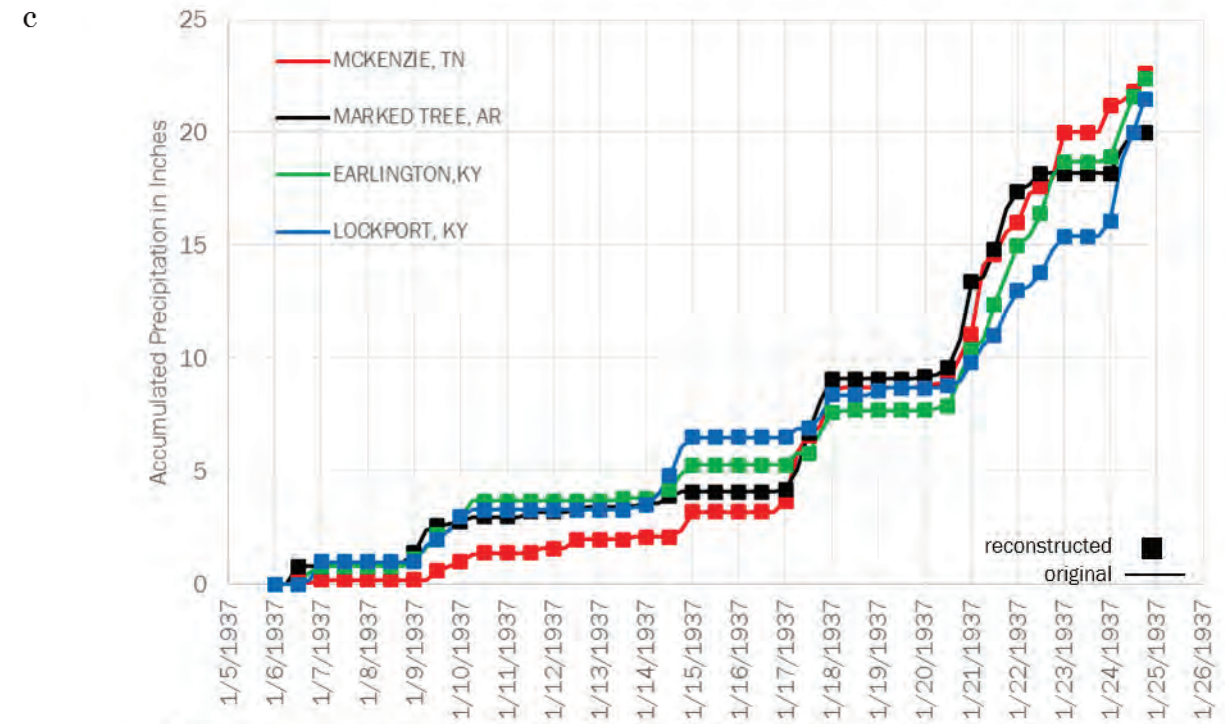
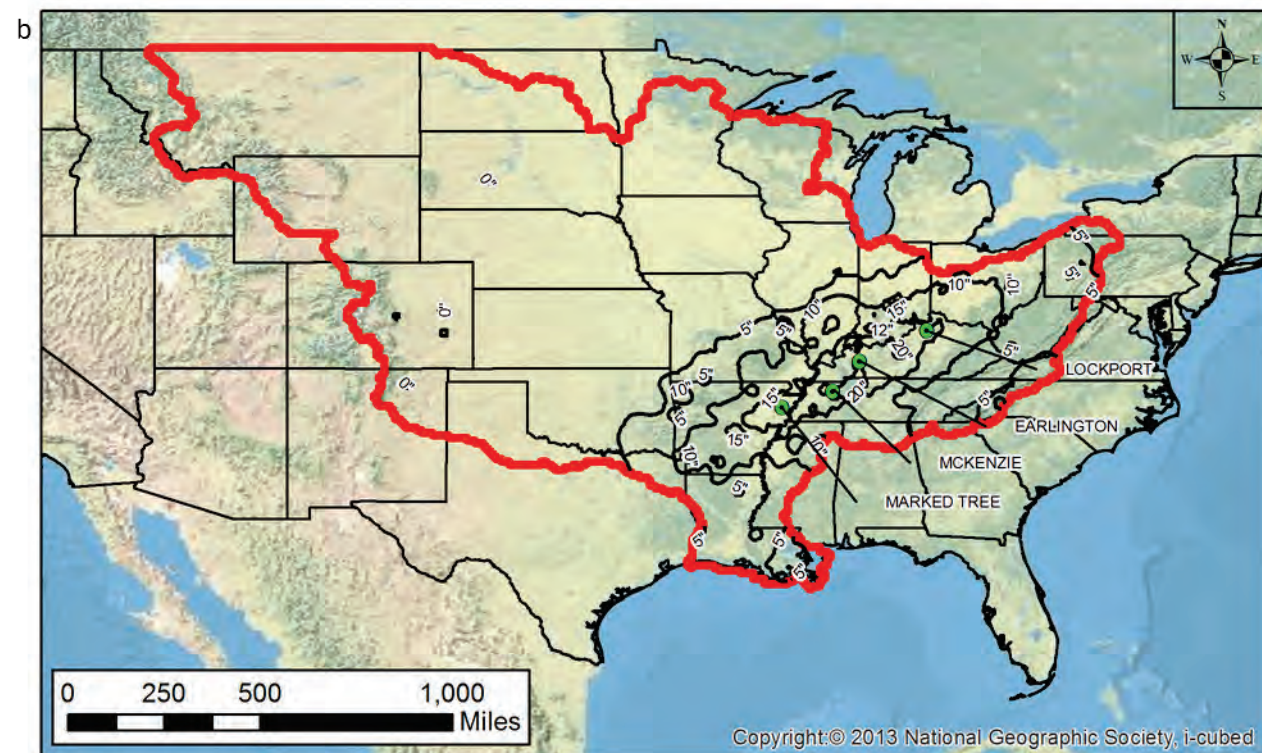
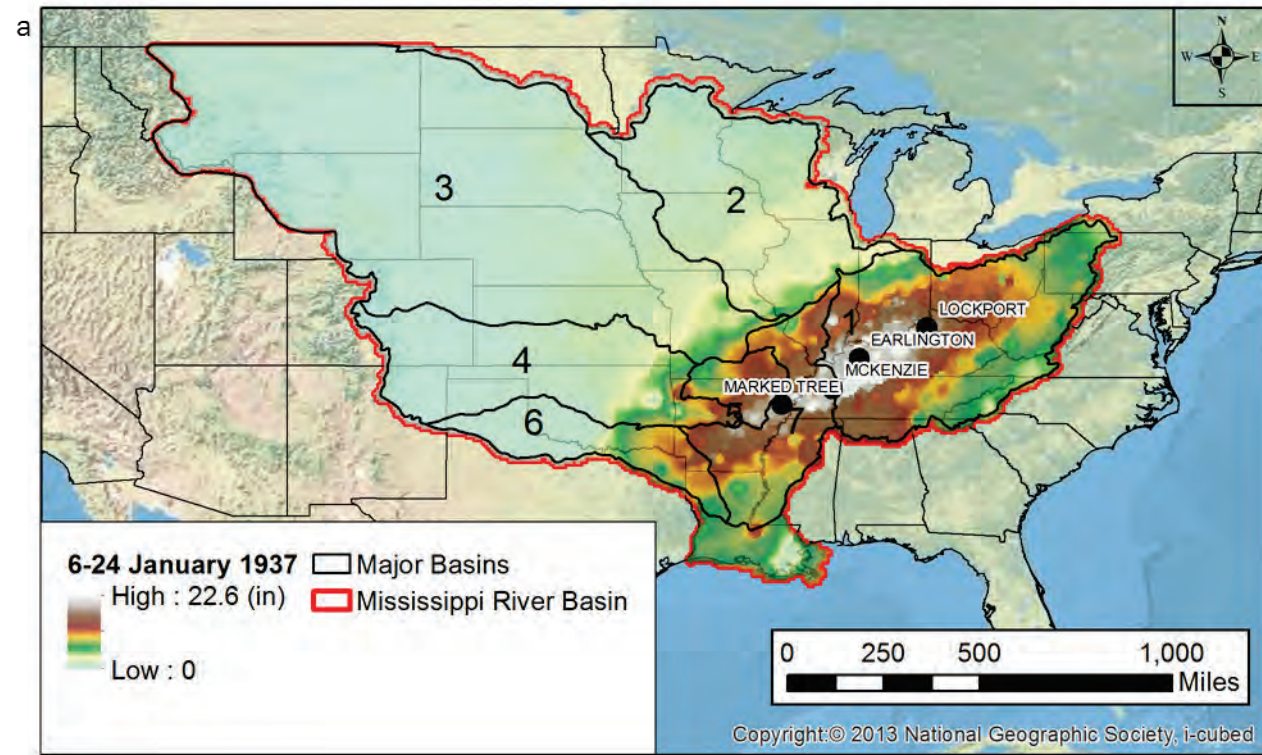
HYPO 58A storm precipitation

HYPO Storm 58A is composed of three historical storm events centered primarily over the Ohio, Red, and White River Basins. The Hydrologic Engineering Center (HEC) transposed one storm in this HYPO event according to parameters given in the 1955 documentation (MRC 1955) (Section 2.9). Figure 2-39 through Figure 2-41 depict the total precipitation and coverage of each storm event that compiles HYPO 58A. Figure (a) in each of the figures depicts the storm coverage of the storm event. Figure (b) depicts the isohyetal for the original storm event. Figure (c) looks at several locations and compares the original precipitation

¹ NCDC: <https://www.ncdc.noaa.gov/data-access>.

inputs against the processed inputs after they were converted to a raster. Table (d) tabulates the 1955 values, the original 2016 inputs, the processed 2016 inputs, and (if applicable) the transposed 2016 processed inputs. Each HYPO storm in the 2016 simulations included a warm-up period to capture the snow pack that would have been lost otherwise. A recession period following the storm sequence was included to provide sufficient time to route the hydrograph peak downstream to the Gulf of Mexico. Figure 2-42 shows the warm-up and recession period for HYPO 58A.

Figure 2-39. HYPO 58A - 6-24 January 1937 (a) (top left) storm coverage over the Mississippi River Basin; (b) (bottom left) isohyetal for unadjusted January 1937 storm; (c) (top right) comparison of mass rainfall curves for original point precipitation data versus the processed/interpolated precipitation data for the unadjusted storm; and (d) (bottom right) comparison of 1955 precipitation, 2016 precipitation, and 2016 post-processed precipitation at select locations.



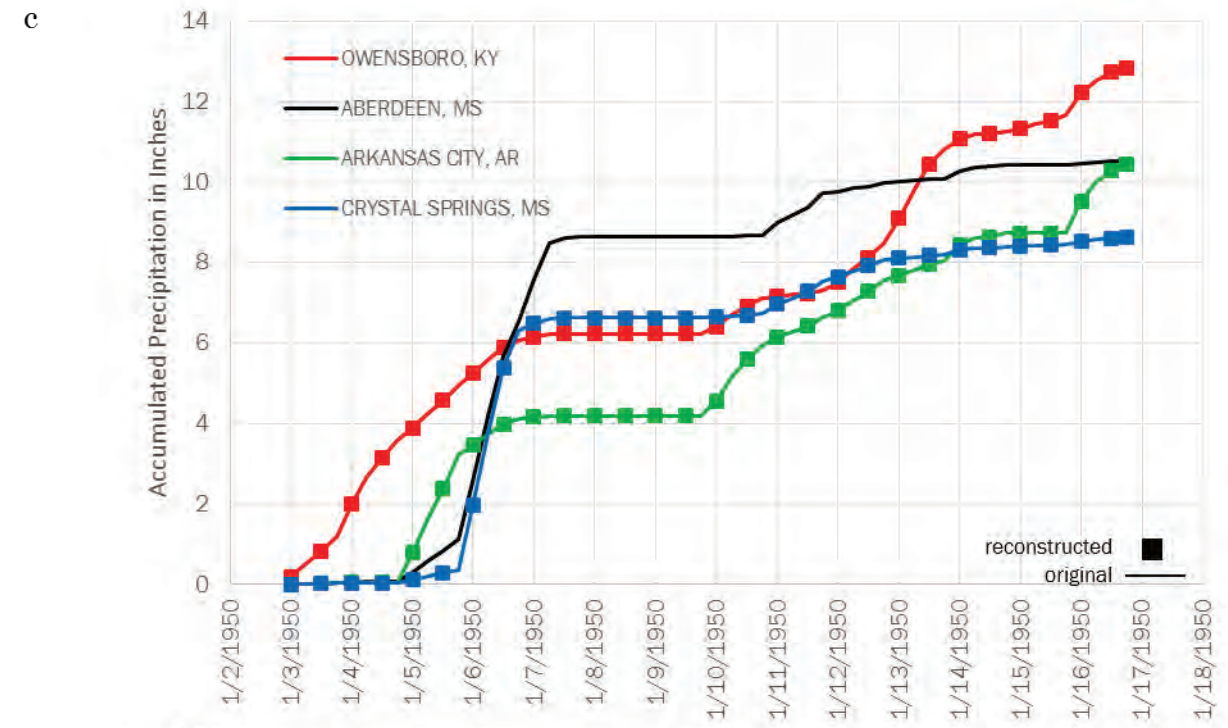
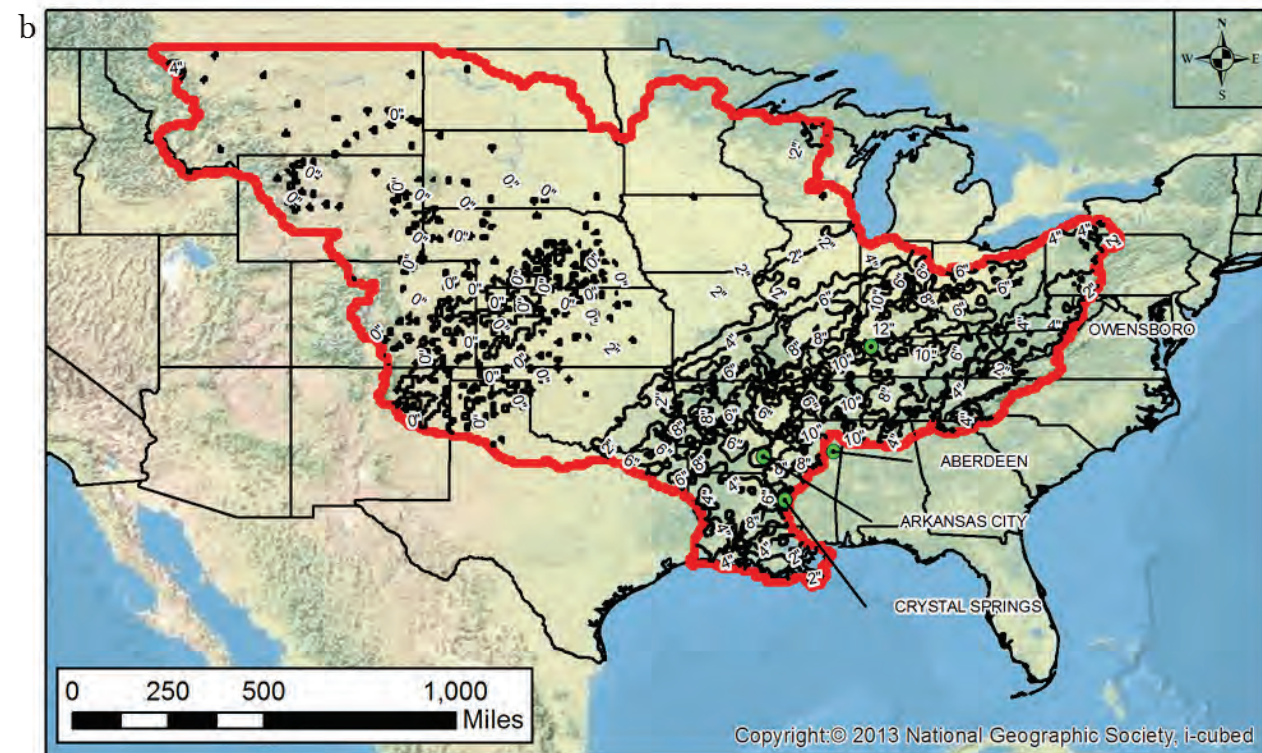
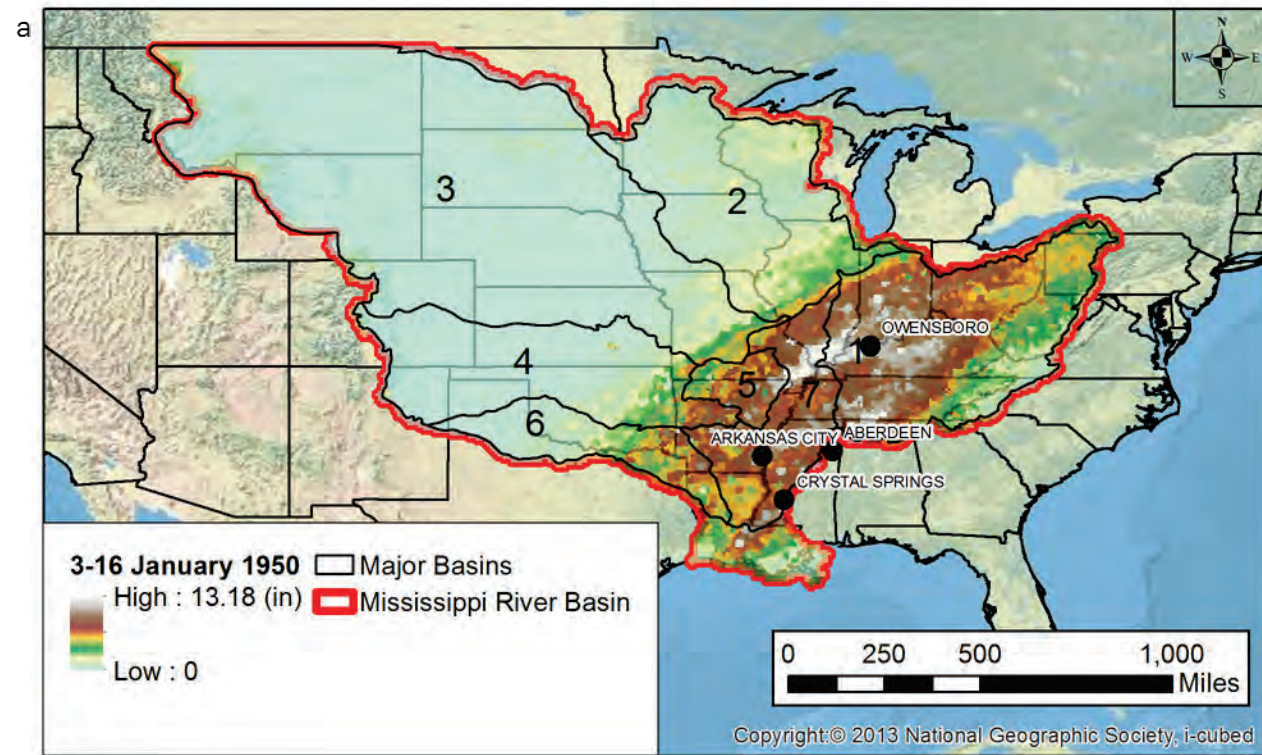
Notes:
 Reconstructed cumulative precipitation data is represented by square symbols.
 Original cumulative precipitation data is represented by a solid line.

d

Location	6-26 January 1937 Precipitation ² (in)		
	1955 ¹	2016	2016 Reconstructed
McKenzie, TN	22.60	22.60	22.60
Marked Tree, AR	20.00	20.00	20.00
Earlington, KY	22.40	22.40	22.40
Lockport, KY	21.60	21.50	21.50

Notes:
 1 = Derived by digitizing the 1955 isohyet map and interpolating to obtain values.
 2 = Values are compared against the original values, not the 10% increase.

Figure 2-40. HYPO 58A - 3-16 January 1950 (a) (top left) storm coverage over the Mississippi River Basin; (b) (bottom left) isohyetal for storm; (c) (top right) comparison of mass rainfall curves for original point precipitation data versus the processed/ interpolated precipitation data; and (d) (bottom right) comparison of 1955 precipitation, 2016 precipitation, and 2016 post-processed precipitation at select locations.



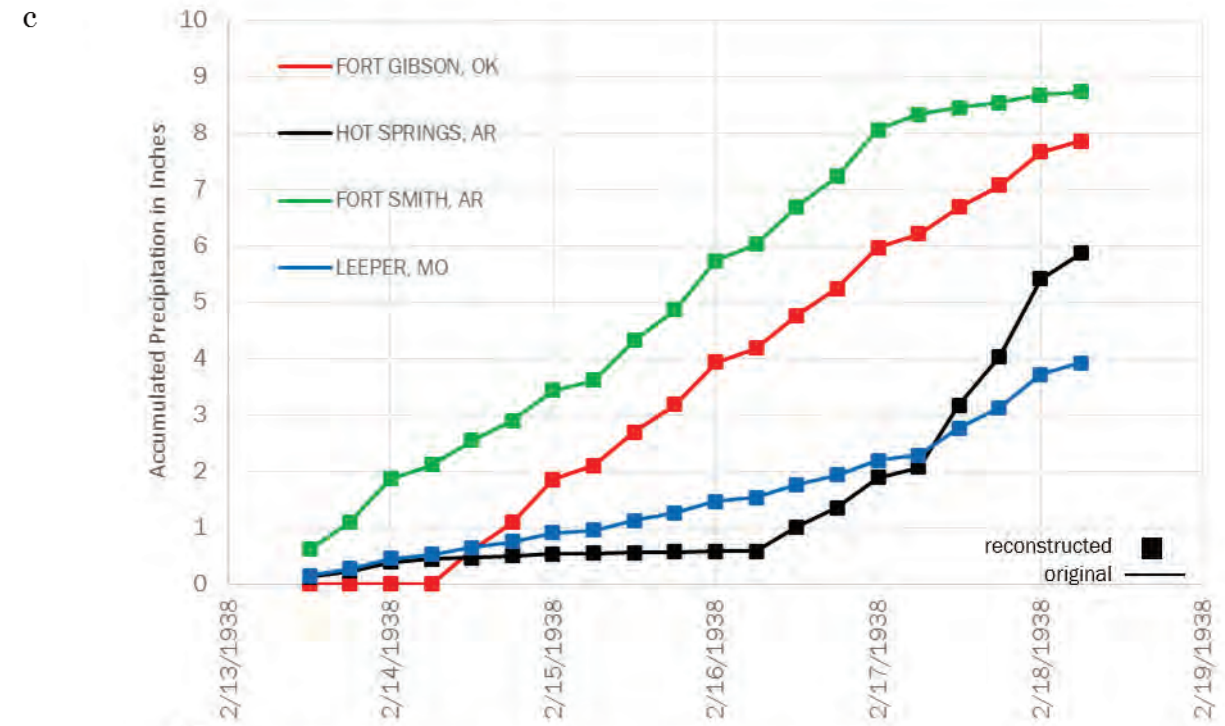
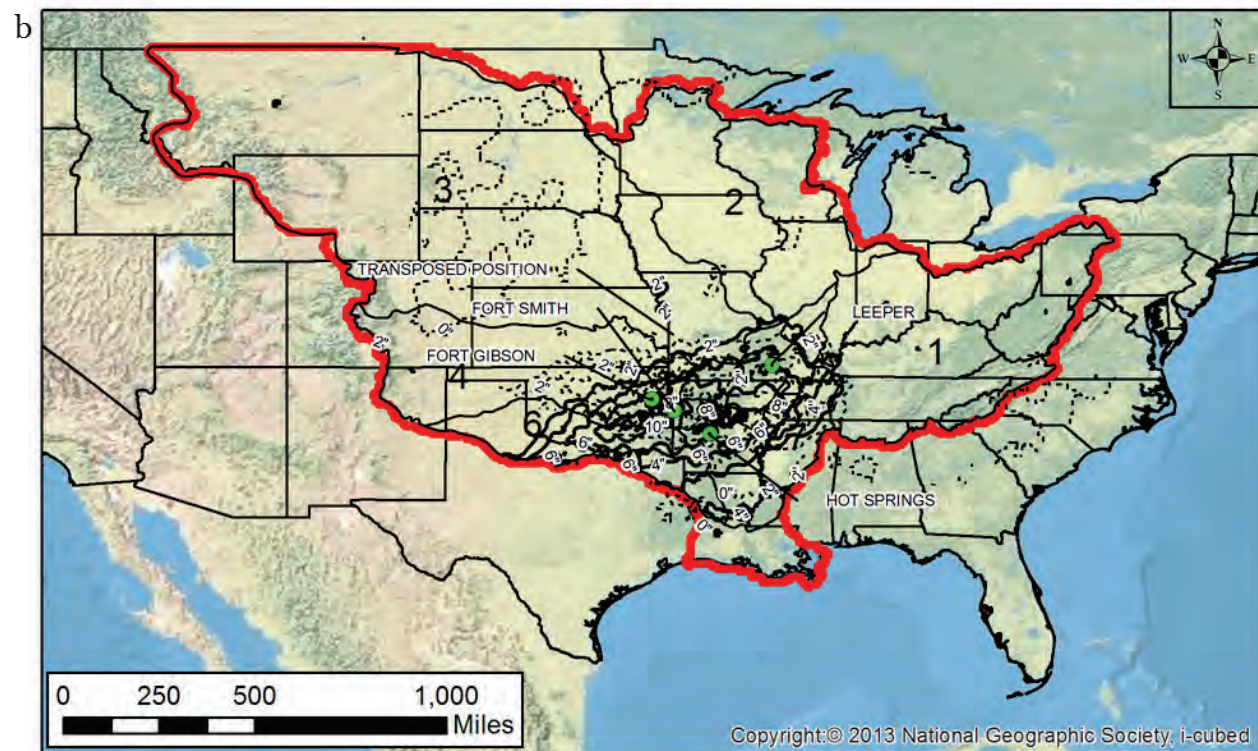
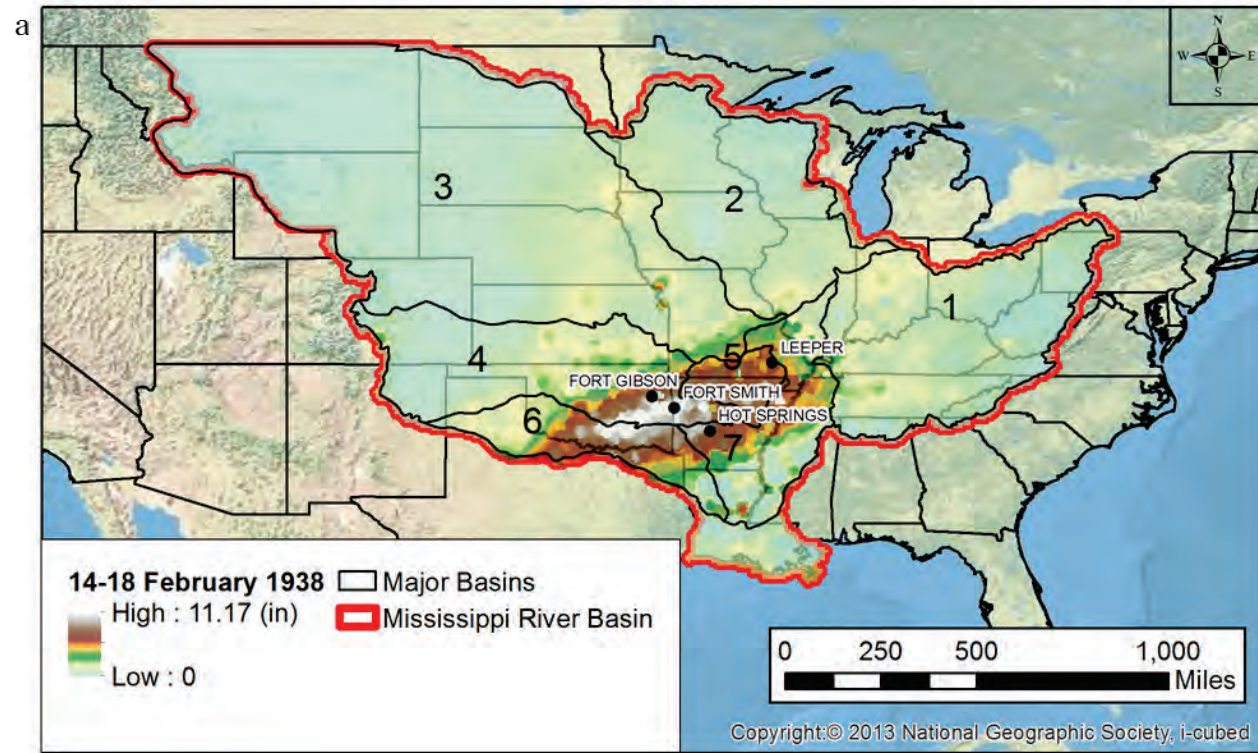
Notes:
 Reconstructed cumulative precipitation data is represented by square symbols.
 Original cumulative precipitation data is represented by a solid line.

d

Location	3-16 January 1950 Precipitation (in)		
	1955 ¹	2016	2016 Reconstructed
Owensboro, KY	13.20	12.83	12.83
Aberdeen, MS	10.6	10.53	NA ²
Arkansas City, AR	10.80	10.44	10.44
Crystal Springs, MS	9.89	8.62	8.62

Notes:
 1 = Derived by digitizing the 1955 isohyet map and interpolating to obtain values.
 2 = Location not included in results as Aberdeen, MS falls outside of the MS River Basin.

Figure 2-41. HYPO 58A – 14–18 February 1938 (a) (top left) storm coverage over the Mississippi River Basin; (b) (bottom left) isohyetal for storm with and without transposition; (c) (top right) comparison of mass rainfall curves for original point precipitation data versus the processed/interpolated precipitation data for the storm with and without transposition; and (d) (bottom right) comparison of 1955 precipitation, 2016 precipitation, 2016 post-processed precipitation, and 2016 transposed precipitation at select locations.



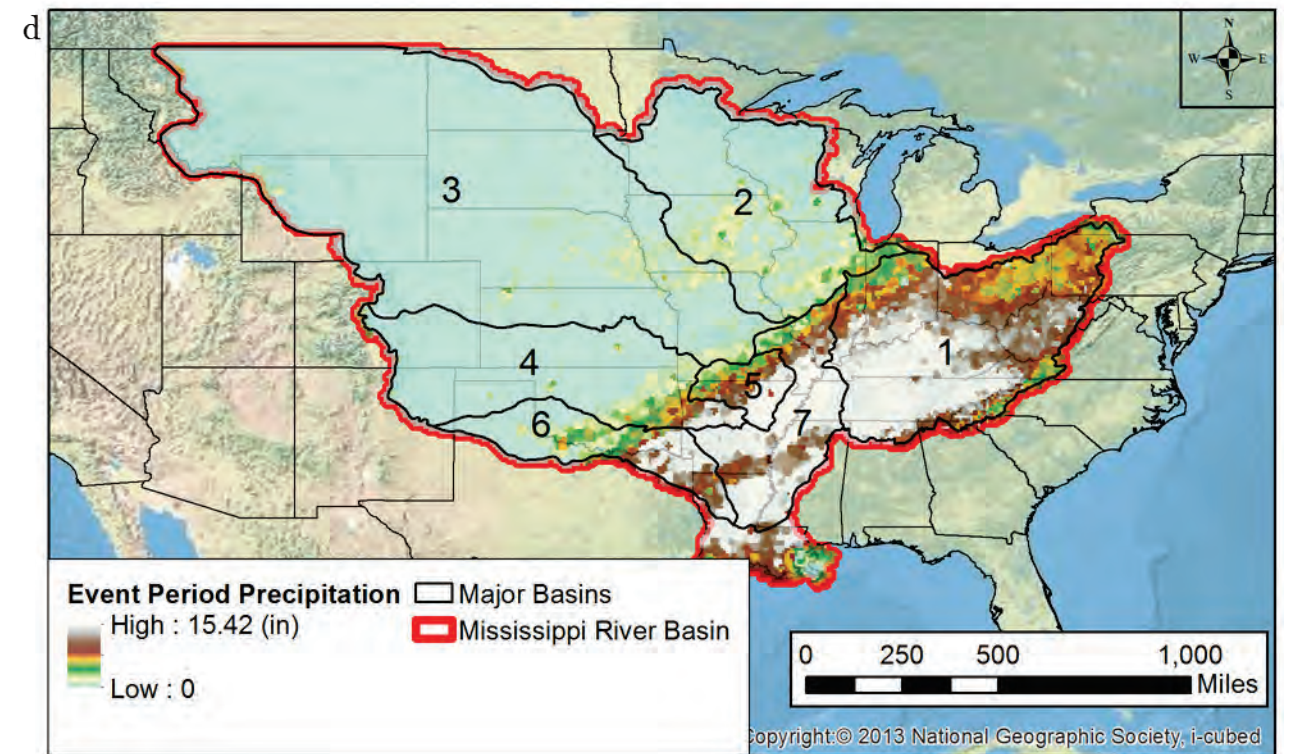
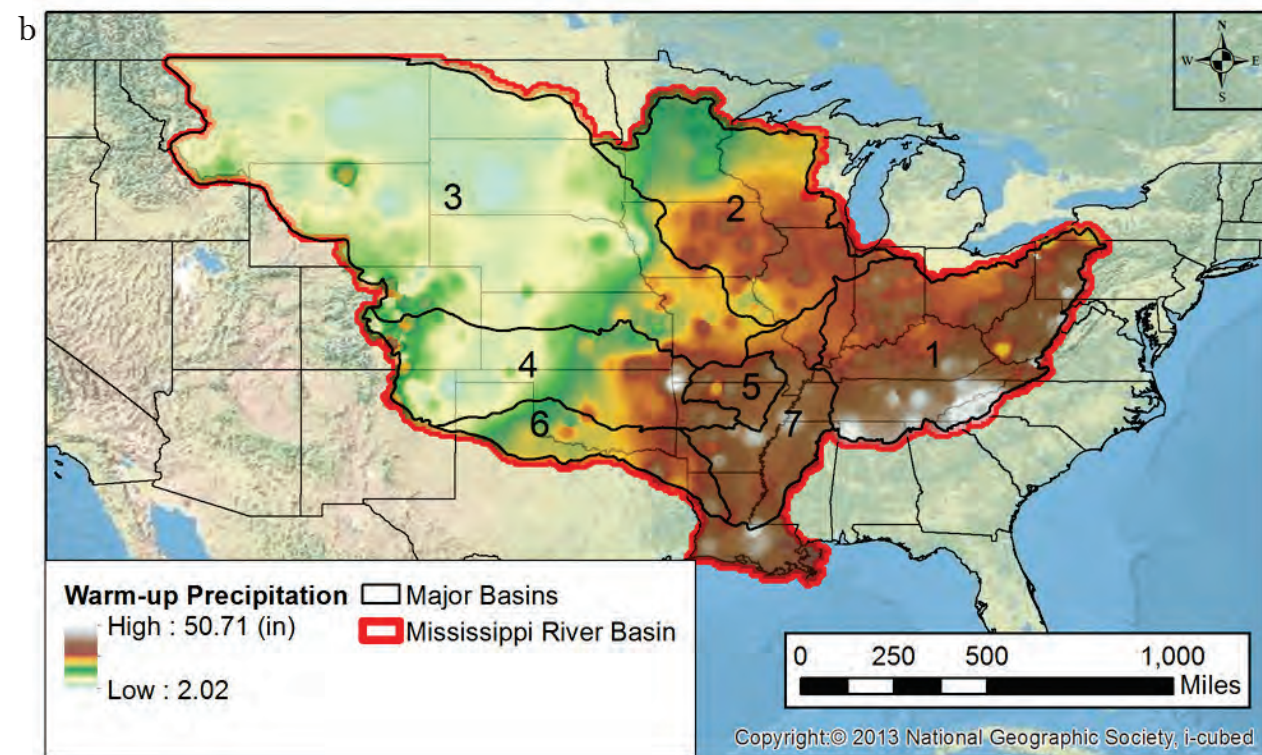
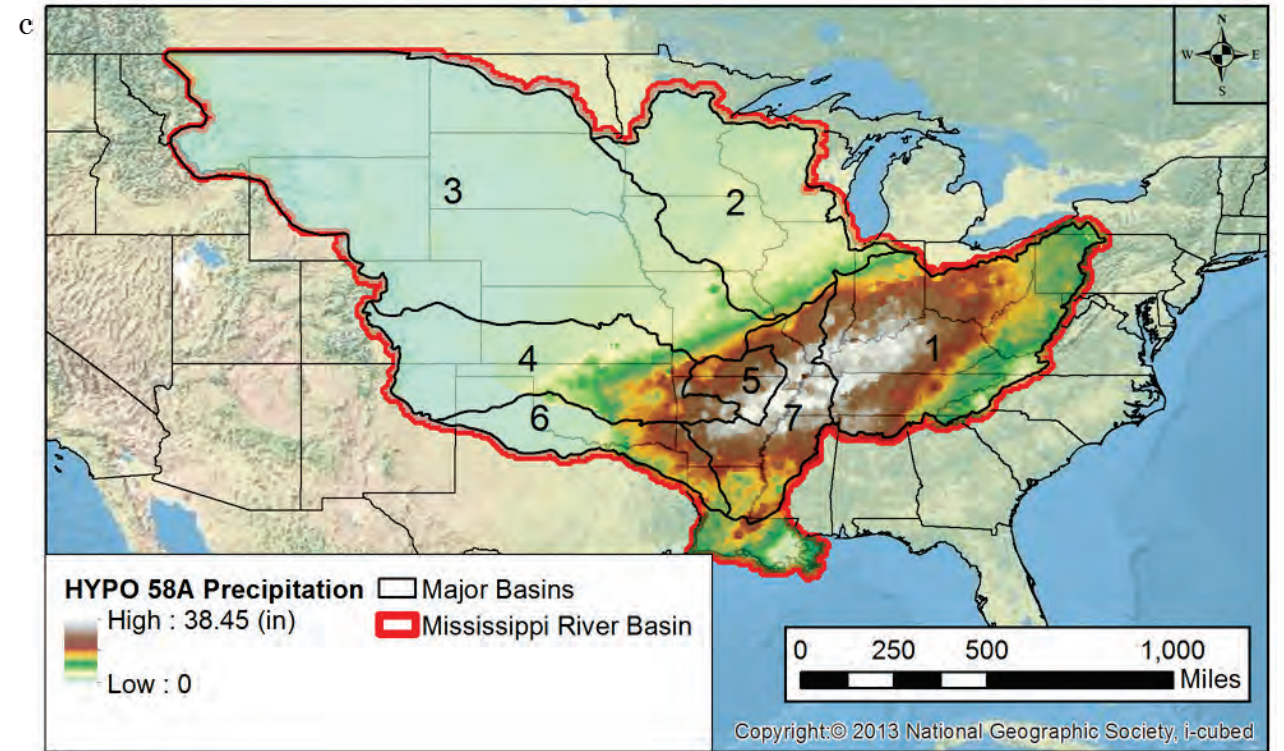
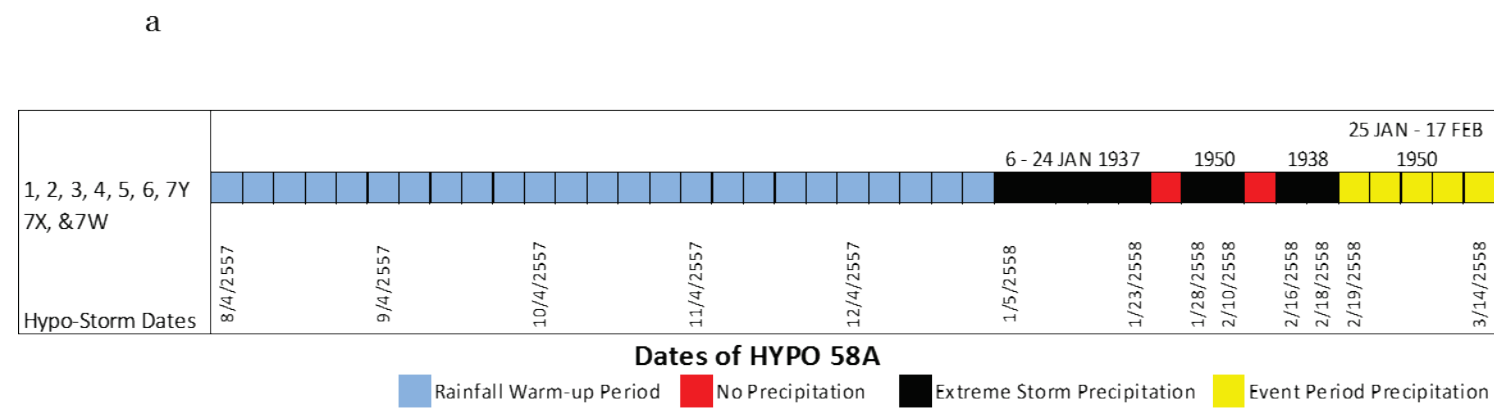
Notes:
 Reconstructed cumulative precipitation data is represented by square symbols.
 Original cumulative precipitation data is represented by a solid line.

d

Location	14-18 February 1938 Precipitation (In)			
	1955 ¹	2016	2016 Reconstructed	2016 Reconstructed and Transposed
Fort Gibson, OK	8.83	7.86	7.86	7.90
Hot Springs, AR	4.28	5.87	5.87	5.80
Fort Smith, AR	6.70	8.73	8.73	8.70
Leeper, MO	4.92	3.92	3.92	3.90

Notes:
 1 = Derived by digitizing the 1955 isohyet map and interpolating to obtain values.

Figure 2-42. HYPO 58A (a) (top left) storm sequencing with warm-up and cool down periods; (b) (bottom left) warm-up precipitation coverage over the Mississippi River Basin; (c) (top right) 1937, 1950, and 1938 combined storm coverage over the Mississippi River Basin; and (d) (bottom right) cool down precipitation coverage over the Mississippi River Basin.



The January 1937 storm had the same gage locations available to make a direct comparison of the 2016 results to the gage locations in the MRC (1955) report. The tabular data and cumulative precipitation plot (Figure 2-39) indicate that the original 1955 values are almost an exact match with the precipitation data used to re-generate this storm for the current assessment at the prescribed locations. After the data were processed and converted to an ASCII grid, the values still matched the 2016 input point data.

The January 1950 storm had three of the same gage locations available to make a direct comparison of the 2016 results to the gage locations in the 1955 report. The tabular data (Figure 2-40) shows slight deviations between the original 1955 values and the 2016 values compiled from the archives; however, once the 2016 data were converted to an ASCII grid, each location matched the input value. The 2016 processed value for Aberdeen, MS, was not included because this location is just outside of the Mississippi River Basin.

The February 1938 storm did not have the gage data available to make a direct comparison of the 2016 results with the gage locations used in the MRC (1955) report, so the isohyetal map in the 1955 report was digitized to obtain the values at select locations (Figure 2-41). The deviation between the 1955 data and the 2016 data ranges from 0.97-in to 2.03-in. Considering the contour lines from the 1955 report are at 2-in, 5-in, and 10-in intervals, the deviations between the 1955 and 2016 values fell within anticipated accuracy ranges given the coarse precision of the historic data. After the 2016 data was processed, the new grids retained the original input gage value. After the raster was transposed (see Section 2.9), the value of that grid cell lost one significant digit and was rounded to the nearest tenth of an inch.

Figure 2-42 shows the complete storm sequence for HYPO 58A that includes the warm-up period, the extreme storm event period, and the event period precipitation.

2.8.2 Temperature data

The 1955 analysis did not include temperature effects in any hydrologic computations. Instead, any snow melt that occurred due to temperature effects was embedded in the measured flow records that were used to estimate base flow and other hydrograph characteristics.

The NWS hydrologic models used for the current assessment included temperature effects using the Snow-17 model that maintained accounting of water equivalents and depths throughout the simulations. Required temperature data for each historical storm event were compiled by USACE from NOAA archives. These point data were then interpolated to generate a complete spatial grid of temperatures needed for CHPS-FEWS simulations. Section 2.8.3 provides the details for point data interpolation.

Temperature effects on peak flow

In the USACE HYPO 58A temperature dataset, temperatures in the upper mid-west and the northern Mississippi River Basin were much warmer than general historic trends for the January/February time frame. NCRFC noted the higher temperatures as one possible reason for why CHPS model results produced higher flows than in the 1955 analysis. After thorough checks and an extensive review of the data, it was confirmed that the higher-than-expected temperatures during late January and early February agreed with observed temperature data for the 1937 event. Meteorologists at least partially attributed the unusually warm period during January and February 1937 as a causal factor that produced the major flood that occurred in that year.

To assess the influence of temperature on model results, the NCRFC and MBRFC simulated the HYPO 58A precipitation inputs with two different temperature datasets in the CHPS model for each region. Figure 2-43 presents a sample map for one time-step based on original USACE temperatures derived from historical 1937 data; Figure 2-44 presents a sample map developed using historical average temperatures for the identical simulation time-step. The original USACE temperatures derived using actual storm event data were the first dataset used. For the second temperature dataset, both NCRFC and MBRFC applied a correction factor to those periods where temperatures were outside the normal expected range of values. The correction factor lowered the grid values as much as 40 °F, which was derived from a best fit line over historical average temperature data.

The USACE dataset temperatures for 1937 from the national archives for the 24th to 27th of January and for the 11th to 13th of February resulted in no Snow Water Equivalent (SWE) going into February for the NCRFC area. With the modified temperatures, SWE accumulated throughout the

winter season until March. MBRFC reported similar results with the exception that HYPO 58A precipitation amounts over their region did not produce significant SWE even with the modified temperatures. Table 2-10 compares the original USACE temperature dataset flow results with the RFC modified temperature flow results at various locations within the NCRFC region. Minimal difference exists between the peak flows at St. Louis, MO, and Chester, IL (within approximately $\pm 3\%$). However, Figure 2-45 shows that the timing of the peak is significantly different. The USACE temperature dataset, which included actual temperature data from the 1937 event, produced a peak much earlier than occurred when using historic normal temperatures.

Figure 2-43. Sample map of temperatures from HYPO 58A: USACE dataset developed from NOAA Archives for 1937 period.

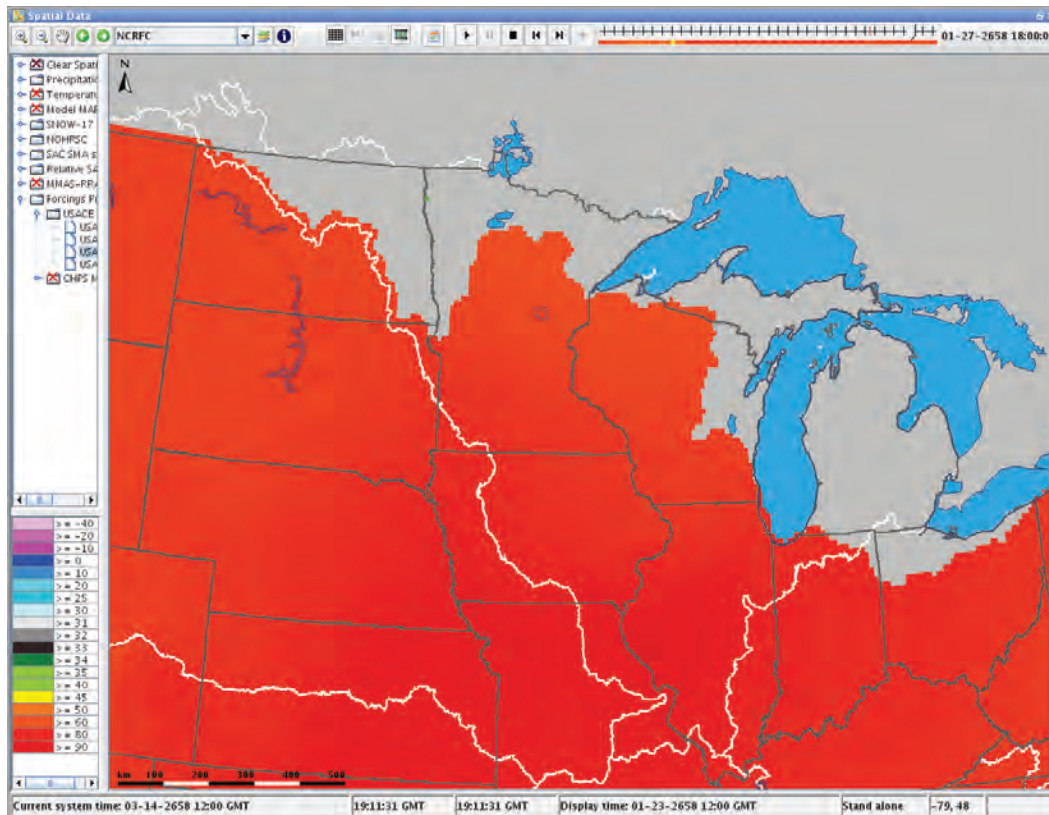


Figure 2-44. Sample map of temperatures from HYPO 58A: NCRFC historical average temperatures.

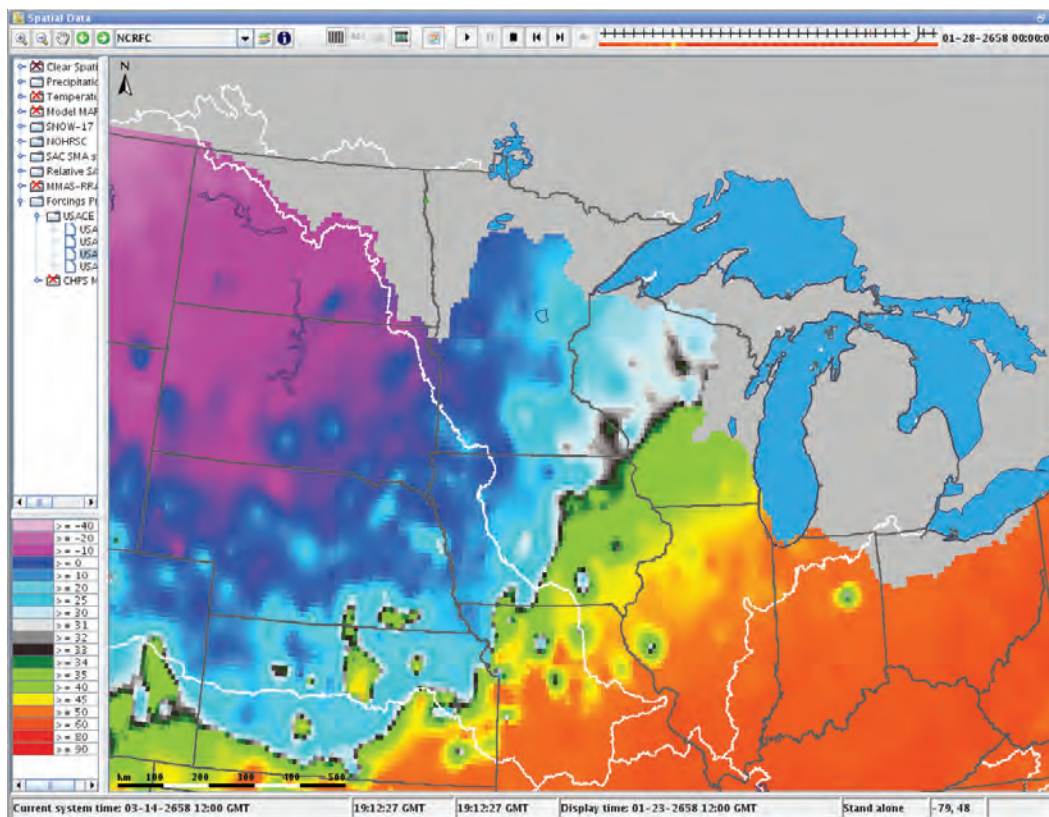


Table 2-10. Temperature effects on computed peak unregulated flows at select locations for HYPO 58A.

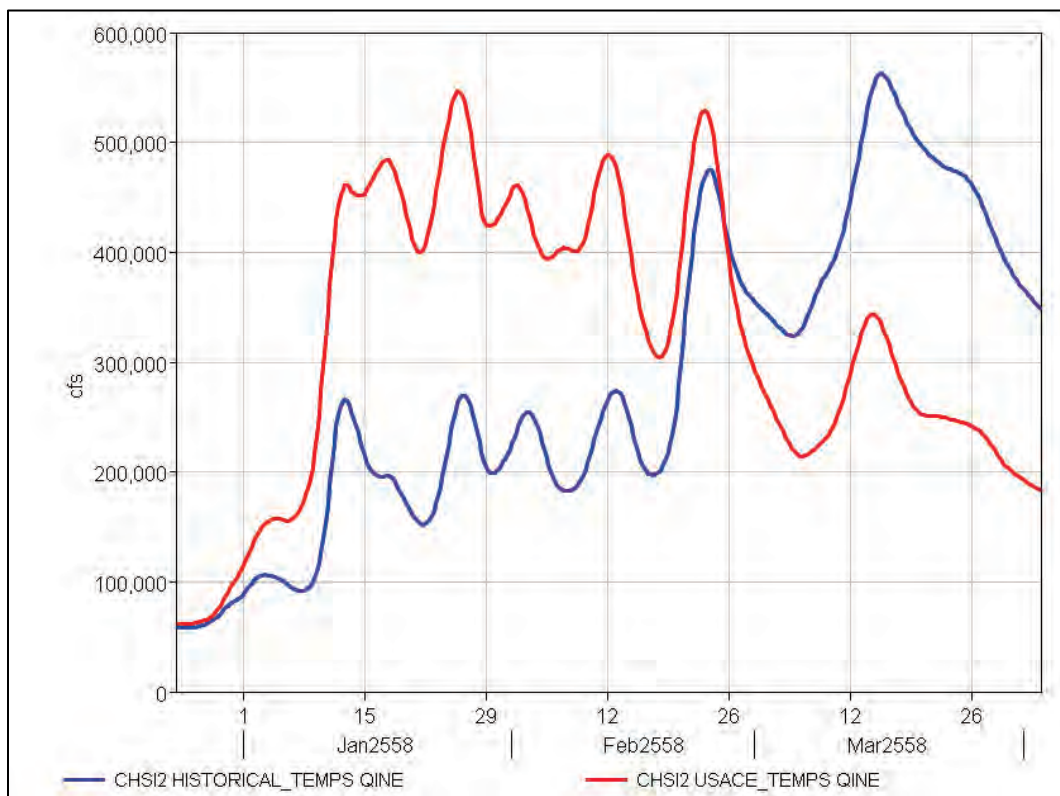
River Forecast Center	Location	Gage Name	River	Peak UNREGULATED Flow in 1,000 cfs (CHPS)		
				HYPO 58A USACE Temperature Dataset	HYPO 58A RFC Modified Temperatures	Difference ¹ (percent)
NCRFC	L/D 20		Mississippi	106	63	41%
NCRFC	L/D 21		Mississippi	107	67	37%
NCRFC	L/D 22		Mississippi	109	74	32%
NCRFC	L/D 24		Mississippi	111	80	28%
NCRFC	L/D 25		Mississippi	111	80	28%
NCRFC	GRFI2		Mississippi	195	175	10%
NCRFC	EADM7	St. Louis, MO	Mississippi	321	316	2%
NCRFC	CHSI2	Chester, IL	Mississippi	546	562	-3%
NCRFC	VALI2		Illinois	102	102	0%

River Forecast Center	Location	Gage Name	River	Peak UNREGULATED Flow in 1,000 cfs (CHPS)		
				HYP0 58A USACE Temperature Dataset	HYP0 58A RFC Modified Temperatures	Difference ¹ (percent)
NCRFC	AGSI4		Skunk	5	5	0%
NCRFC	MLLI2		Rock	15	16	-7%
NCRFC	WAPI4		Iowa	13	8	38%
NCRFC	KEQI4		Des Moines	2	3	-50%
NCRFC	ERKM7		Meramec	41	47	-15%
NCRFC	MURI2		Big Muddy	31	31	0%
NCRFC	NASI2		Kaskaskia	37	38	-3%

¹ Percent differences shown are greatest in Iowa and Minnesota or where computed peak values are small.

Figure 2-45 shows discharge hydrographs for the Mississippi River at Chester, IL, for the NCRFC outputs using the USACE temperature dataset and RFC modified temperatures. The flow from the USACE HYP0 storm sequence temperature dataset (USACE_TEMPS QINE in Figure 2-45 legend) for 1937 peaks on January 25. There is a significant increase in flow between January 8 and 12 with a lesser peak on January 17, which leads up to the second larger peak on January 25. The RFC modified temperature simulation (HISTORICAL_TEMPS QINE in Figure 2-45 legend) produced a peak flow on March 15 at Chester, IL, well after the USACE HYP0 peak with only relatively minor flows occurring until approximately February 20. There is a maximum 276,000 cfs difference between flows computed at Chester, IL, using the two different temperature inputs for the January 1 to February 15 period.

Figure 2-45. NCRFC computed flows for Mississippi River at Chester, IL, using two different temperature inputs; HYPO 58A unregulated flow.



The 1955 analysis did not directly consider temperature effects on SWE accumulation relying instead on gage flow data or synthetic methods to calculate runoff. Using this approach biased outcomes toward normal historic conditions and did not directly consider abnormal effects of individual extreme storms such as evident in the temperatures from the 1937 event. It is therefore likely that flow contributions from the upper Mississippi and Missouri River basins were understated in 1955 results given for HYPO 58A. The current assessment utilized historic temperatures that captured the unique aspects of the actual extreme events thereby providing a better representation.

2.8.3 Interpolation schemes

Several iterations were made using different interpolation algorithms including Kriging and IDW. The best agreement between sampled interpolation grids and observed gage data was obtained using IDW with a bias toward the observed point values. The interpolation with bias toward observed point values simply performed the interpolations by fixing values at locations where observed data existed and then generated surrounding

values relative to those observed points. To verify this interpolation approach for the rainfall data, five known gage locations were excluded from the interpolation and then compared to values determined from the final interpolation grid for that location.

The intent of picking five known gage locations for use in benchmarking interpolation results was to use locations that were within the storm extent across all extreme historical storms, which ranged from 1913 to 1950. Significantly fewer gage locations were available in the older datasets than existed in 1950.

NWS and USACE staff debated the appropriateness of using IDW interpolation over Kriging. Citations from the literature suggested that Kriging was the preferred method for dealing with stochastic data such as precipitation. Attempts to use Kriging for the present analysis did not achieve agreement with the historical isohyetal maps from the original design/analysis reports. Therefore, IDW with the bias toward observed data was adopted. During this debate, there were questions regarding the validity and influence of the underlying data values.

To resolve concerns over data validity, the 1950 dataset was selected for detailed scrutiny because it had the best spatial coverage by point gages. The point rainfall database built by USACE was broken into the 6-hour periods based on data from the NCDC and paper archives. The NWS also took published data from their network of observers and built a separate database that was separated into 6-hour intervals. The two databases (USACE and NWS) were then compared in Excel. There were some locations where the daily precipitation totals did not match, but there was no systematic error apparent in the data. After several iterations of comparing data values over different periods, it became apparent that there was an issue in how data values were represented in time. Accounting for the correct time when both observer and data reported in the NCDC database resulted in a good comparison in point values with most differences being zero. Details of the QA/QC are given in section 2.8.4.

Precipitation data conversion process

ERDC developed a Python script to convert the point precipitation text files to ESRI grids. The script rounded the latitude and longitude of each gage location to the nearest tenth of a degree and assigned the

precipitation value to the center of the cell corresponding to that location. Cell size was 0.1° latitude by 0.1° longitude. If more than one gage existed in the cell, the first gage that the script looped through had its precipitation value retained in that cell. Remaining gages with the same location were retained in an adjacent cell. The 1950 storm had areas with dense gage coverage where the script was not able to locate an adjacent cell without a gage already assigned to it; therefore, some gage data were lost in the process.

The process to convert the gaged precipitation data to gridded data proceeded in several stages.

Step 1: Obtain NCDC Data

- NCDC data are set up in files that have data for all the gages, one file for every 6-hour period. For example, the file might be called “1937PREC_19370106060000.txt,” which had precipitation measurements for 06 January 1937. The values are total rainfall depths from 0000 hours to 0600 hours. A single line in the file would follow this format:

```
LOCKPORT, KY,38.44, -84.96, 19370106,0
```

- With the gage name, state, latitude/longitude coordinates (WGS84), a date code, and finally the total rainfall depth (0 in.).
- For years that have only daily values recorded, the total daily rainfall depth is in the “0000” hour file. The “0600,” “1200,” and “1800” hour files all contain depth values of 0.00. Rainfall units are in inches.
- The number of gages in each file varies over time as gages were added or removed by the agencies in charge of them.

Step 2: Automated Quality Control

- The second step was an automated filtering process to ensure only high-quality gages were being included in the analysis. Gages were filtered out of the raw list based on poorly formatted lines (e.g., had extra fields), missing values in the lines (e.g., no rain depth or no latitude or longitude), duplicate gages in the file, or if the gage did not report any rainfall over the entire period of record associated with each storm event (e.g., 1946–1947). This last case was taken to indicate a

faulty gage that was not actually in service but was reported to be in service. Any files with bad dates (e.g., September 31) were also removed.

- The gages removed were reported, and the operators verified the reasons for removing the gages. This quality-controlled data set was taken to be the *best available data* for use in the conversion process.

Step 3: Prepare Datasets for Processing

- The third step was to create four additional data sets. The first version was a copy of the quality-controlled data. The second version was a *verification* data set. To test the quality of the data conversion process (from point data to gridded data), a *Leave N Out* methodology was employed. Similar to a *Leave 1 Out* method where one data point is left out of the conversion process and the results checked against it, the *Leave N Out* methodology was employed to strategically remove a few (typically five) key gages near, but not the center of, major rainfall areas of concern. This method allowed for the engineers to check the interpolation methodologies at various key locations across the United States.
- As the actual gages in each location varied over time, slightly different sets of gages were used for verification. The same gages for verification were used whenever feasible. When it was not feasible to re-use a verification gage, typically because the gage was removed, a gage was chosen that was both nearby the original gage as well as present for an extended period of time (to minimize future changes in verification).
- The third and fourth versions were subsets of the full data and full verification data. These two data sets were for only the actual event days. All of the data sets had several months of data before the actual event to allow for model warm-up. It was desired, though, to verify the data both for the full time period and just the event time period. This enabled the engineers to check that the event magnitudes themselves were reasonably correct as well as the full period rainfall values were correct.

Step 4: Process the Data Sets

- For the precipitation data sets, an IDW algorithm was created specifically for this task. Several commercially available IDW, Kriging, and other spatial interpolation methodologies were tested. However, the rainfall data exhibited several characteristics that effectively violated

- assumptions and strained the credibility of the results of the algorithms. These included strong gradients, widely varying spatial distributions of points, portions of data sets that exhibited high variability and low correlation and others that exhibited high correlation, even to the point of having different clusters of values that demonstrated regional behavior very different from neighboring regions. These many characteristics taxed the ability of the many commonly used spatial interpolation algorithms to provide realistic results.
- After much development and testing, a specialized IDW algorithm was chosen. The IDW algorithm used the four nearest gages, one from each north/south/east/west quadrant, or whichever of those were available. This would occasionally result in a boundary effect where a stripe in the data would appear. The stripes would indicate a strong change of precipitation values that are indicative of an algorithm artifact as they would be oriented along the quadrant lines. The more traditionally used IDW or Kriging algorithms in those same situations, however, would tend to greatly over- or underestimate the values in those areas.
 - The IDW algorithm operated on a pre-defined grid. The grid was a 0.1° by 0.1° grid of the continental United States. The centroid of each cell was taken as the point of reference for the IDW algorithm, and the algorithm worked along cell by cell, selected the (up to) four nearest gages, and used a linear distance-weighted averaging algorithm on the values.
 - The IDW interpolation routine was carried out on all four gage data sets (full, full-verification, event, and event-verification).

Step 5: Analyze the Results

- Several analysis methods were conducted to assess the quality and effectiveness of the work. First, a graphical depiction of the data was created for visual inspection by the engineers. Various depths were color coded to facilitate rapid identification of anomalies. Next, all the grids for each time-step were summed together to create a total rainfall depth grid. This was also mapped. Then the values of the gages used for verification were summed together to create total rainfall depths at a point. This was done for both the event and full time scales. These gage values were then compared to the summed values of the grid cell where the verification data sets had been established by their latitude and longitude. This tested the sensitivity of the interpolation algorithms to missing data points. Finally, the full set of gage points was summed

and checked against the values in the complete grid summation to determine biases or errors.

- The verification results in general showed errors that were small and well within reasonable ranges. The bias results were almost always zero. The bias test errors that did show up were traced back to having multiple gages in a single grid cell. Obviously the grid cell could only have one value while the individual gages within a gage cluster within that cell could vary, at times dramatically. These differences were taken to be attributable to the local variability of the storm and were not treated further.
- The final deliverables of this process provided input precipitation grids needed by the hydrologic models. These were the set of grids of the full quality-controlled data for the duration of each storm period.
- Point temperature data were developed and processed to produce ASCII grid files following the same method used for precipitation. Interpolated temperature grids were checked using the same approach as described in Steps 3 and 4 above. Validation of temperature data was done as part of the data ingest process where climatic averages in CHPS-FEWS were compared to the imported datasets.

2.8.4 Quality assurance

The NWS completed a compilation of all the January 1950 rainfall observations for the MR&T collected by NWS cooperative observers. This included the states of Alabama, Arkansas, Colorado, Georgia, Iowa, Illinois, Indiana, Kansas, Kentucky, Louisiana, Minnesota, Missouri, Mississippi, North Carolina, Nebraska, New Mexico, Ohio, Oklahoma, Pennsylvania, South Carolina, Tennessee, Texas, Virginia, and West Virginia. Wyoming, North Dakota, and South Dakota were ready to add if needed. A spreadsheet was used to manually quality control the published values with the NWS Monthly Climatological data taking precedence over data digitized for the NWS Office of Hydrology database when discrepancies were found.

Each of the NWS monthly climatological data publications was used to gather the observation times for each of the stations. This was done to calculate a 24-hour total from the 6-hour totals on the team Google Drive. This way the value to the actual observation could be correlated. In the spreadsheet titled "FULL150.csv," if the station observation time was noted as MID (midnight), then the FULL150 spreadsheet denoted this with a "24." For an observation time of 7 p.m., the spreadsheet denoted

“19,” for an observation time of 7 a.m. the spreadsheet denoted “7,” etc., using military time conventions.

Once the observation time for the station from the NWS Monthly Climatological publication had been verified, the locations were totaled for the 6-hour values to compare them with actual observations. For example, if a station reported at midnight January 4, then the 6-hour values from January 4, 12UTC; January 4, 18UTC; January 5, 00UTC; and January 5, 06 UTC were totaled. Likewise for a station that reported at approximately daybreak (5–8 a.m.) January 5, then the values for January 4, 18UTC; January 5, 00UTC; January 5 06UTC; and January 5, 12UTC were added. In doing this, an offset in observations was added on January 4 for Iowa stations that report in the evening (5 p.m.–9 p.m.) or approximately 00UTC. Upon inspection of the t-hour totals for the Indiana stations, it was discovered that 6-hour totals were under-reporting on January 5 for stations that reported at midnight. This issue led the team to compare IDW and Kriging interpolation methods. Observations also indicated an area of above-normal values in the southeast portion of Oklahoma, which would be missed if one did not add in stations from the actual printed publication and just used the NWS digital database. The USACE-tabulated precipitation data from PDF investigation archives were also inserted into the spreadsheets containing the NWS Monthly Climatological data.

After the initial cross-check between the USACE and NWS databases was made, USACE verified the original input values and evaluated the time intervals used in calculating the 24-hour/daily totals. It was found that there was a 6-hour offset between the two databases. Aligning the datasets time intervals resulted in less than a 0.01 in. difference in daily values 99.5% of the time.

USACE evaluated the NWS spreadsheets and identified some large discrepancies in the point data values. There were numerous errors, generally in the January 12, 1800Z column for Illinois and Kentucky. These errors were corrected and calculations updated. The adjustment caused the differences to diminish greatly. The comparison in the spreadsheet used 06, 12, 18Z totals from one day and 00Z totals from the next day to compare with the NCDC value. If the columns for 00, 06, 12, and 18Z for the same day were added and compared to the NCDC total for that day, the values were within 0.1 in. 99.9% of the time in Kentucky and 99.6% of the time in Illinois. If the range was changed to 0.02 in., it was within that range 99.4% of the time in Kentucky and 97.5% of the time in Illinois.

Upon further reviewing the NWS spreadsheets, the COOP¹ values the NWS used were not all aligned with midnight readings. The NWS values were aligned with the corresponding four 6-hourly values that would best match the 24 hours proceeding when the COOP observation was taken. For example, if the COOP reading were 0600, then the 0600, previous 0000, previous 1800, and previous 1200 values were summed for the comparison.

In the 6 January 1950 tabulation, it was noted that columns containing the USACE 6-hour data were totaled using times of 1800 + 0000 + 0600 + 1200. The total thus shown had 24 hours ending at 1200 UTC to match the observer's report time. Using the USACE 0600 + 1200 + 1800 + 0000 sum produced essentially the same value (+/- 0.01) as the NCDC 24-hour COOP values. Those appeared to be verified as a reasonable match using an allowable criteria of +/- 0.02 in. difference.

2.8.4.1 Concurrence on acceptable quality assurance.

The analysis team evaluated quality checks for precipitation data and agreed that with the minor corrections of USACE 6-hour values that storm totals checked (within 0.01 in.) and NCDC 2-hour values could be matched by summing 0000–1800 6-hour USACE values.

2.8.4.2 Depth area relationships

To further validate the precipitation inputs developed by interpolation, depth-area relationships were generated using ArcGIS. Isohyetal maps for each original storm event were georeferenced, digitized in ArcMap, converted from a polyline to a triangulated irregular network (TIN), converted from a TIN to a raster, and projected with USA Contiguous Albers Equal Area Conic to obtain an equal area grid size of 2,000 meters (m) × 2,000 m. For the total original HYPO storm comparisons, the projected rasters were then aggregated with the mosaic tool. The interpolated rainfall grids were clipped to the spatial extent of each original HYPO storm or to the original individual storm events. With equal area grids, a zonal histogram was generated that compares a defined precipitation interval against area. These zonal histograms were exported to a spreadsheet to plot against each other.

¹ COOP values were readings reported by the NWS cooperative observer network.

While Figure 2-46 indicates deviations within an inch of the original precipitation, Figure 2-47 shows that the interpolated precipitation grid follows the original precipitation shape with a maximum 3 in. deviation for basin area greater than approximately 350,000 square miles. Breaking each storm down by each drainage basin shows more fluctuation between the original and interpolated precipitation as the area of coverage within each drainage basin plummets. This is expected with large grid data covering a smaller extent.

Figure 2-48 through Figure 2-54 show the depth-area curves for the entire storm total precipitation over the Mississippi River Basin as well as the totals falling over each of the seven major sub-basins.

Figure 2-46. Depth-area curves for 1955 and 2016 individual storms composing HYPO 58A.

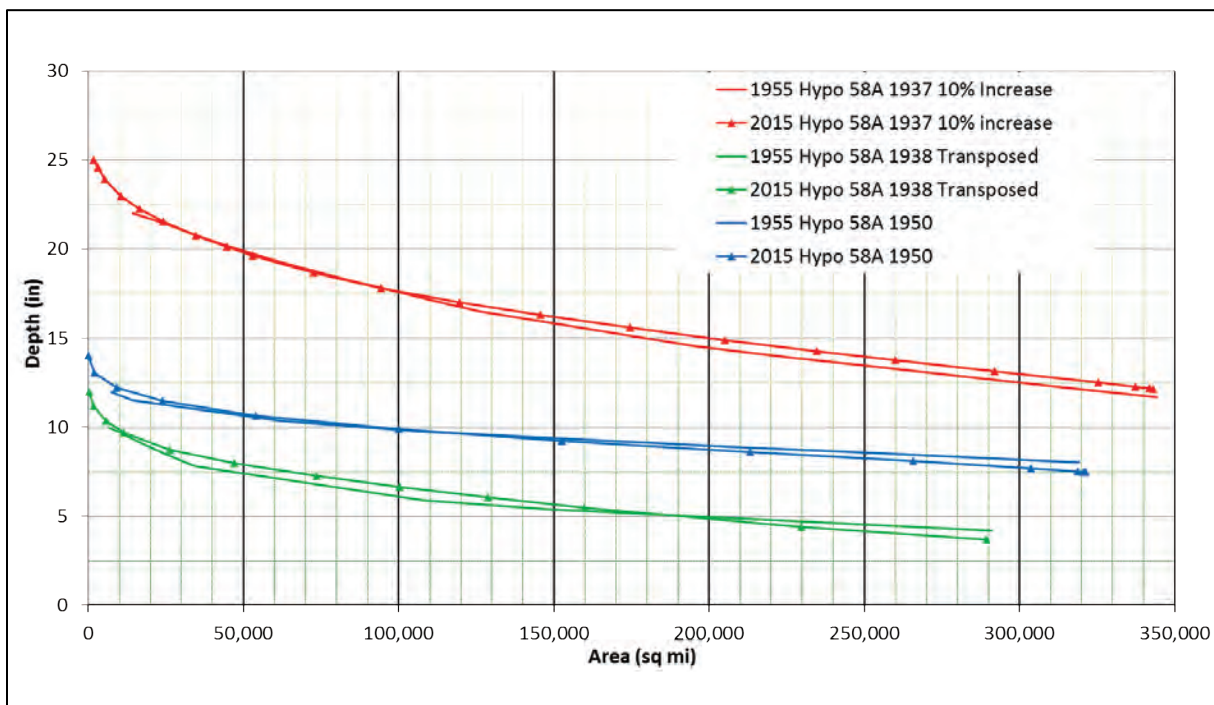


Figure 2-47. Depth-area curves for 1955 and 2016 total HYPO 58A event.

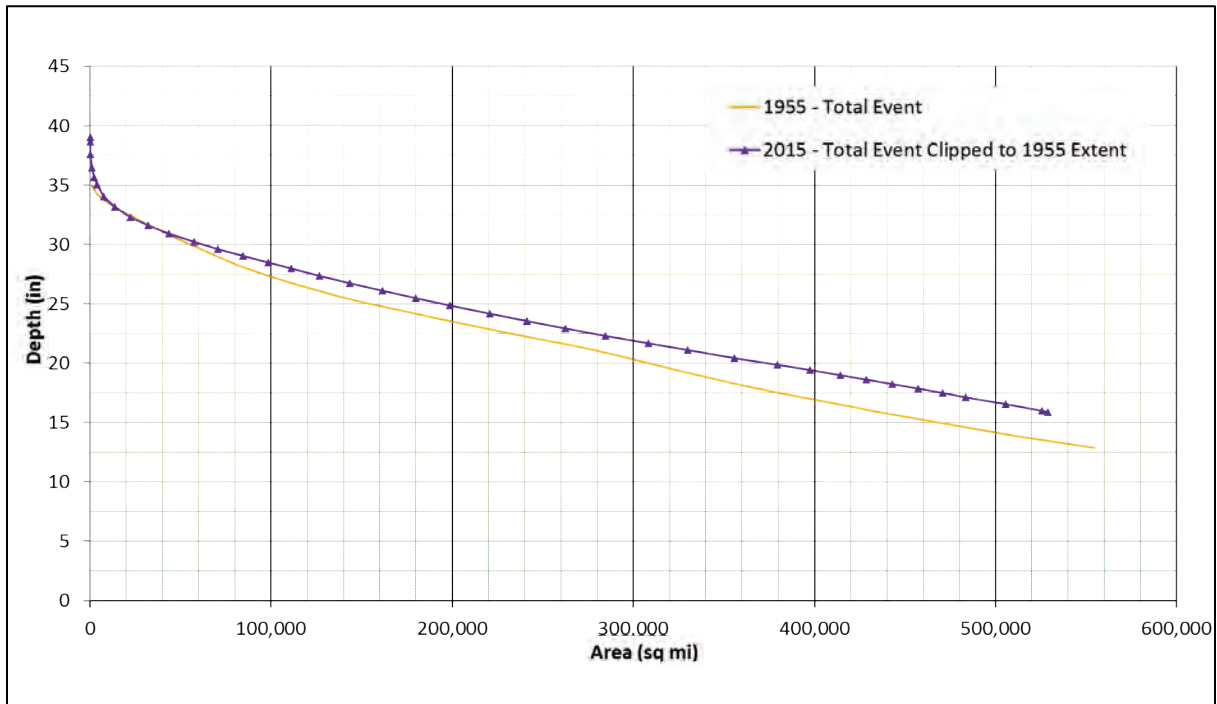


Figure 2-48. Depth-area curve for 1955 and 2015 individual storm events composing HYPO 58A over Drainage Basin 1.

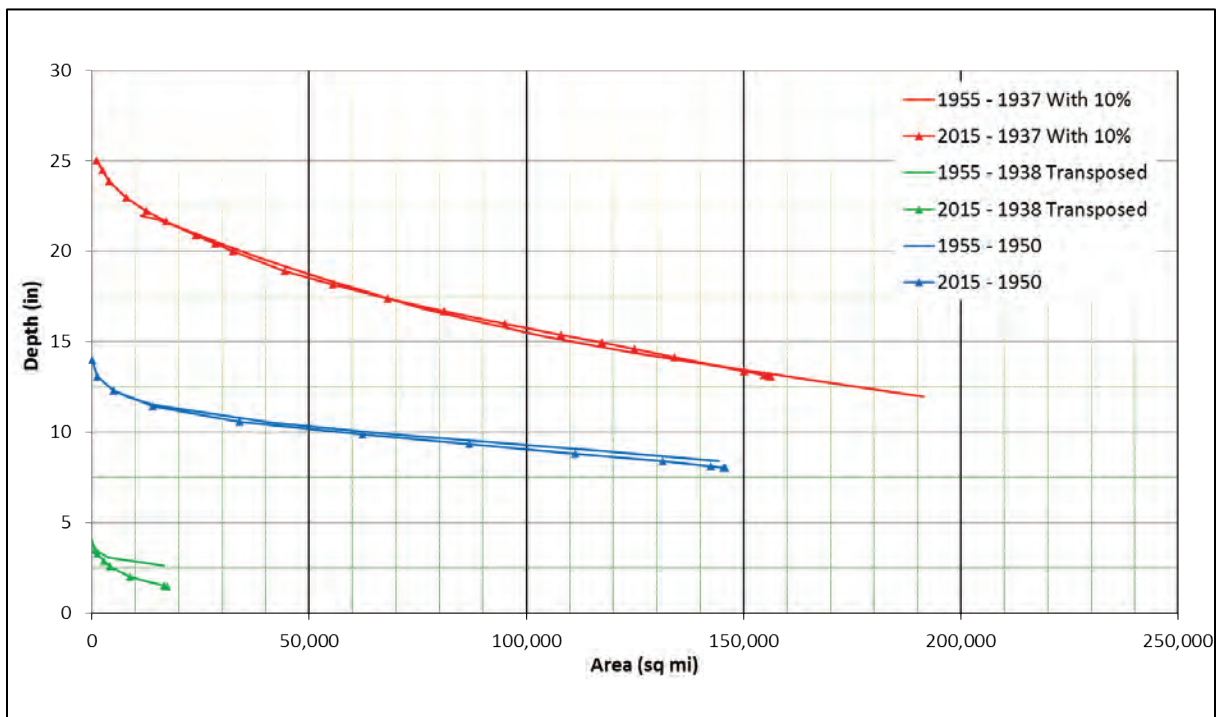


Figure 2-49. Depth-area curve for 1955 and 2015 individual storm events composing HYPO 58A over Drainage Basin 2.

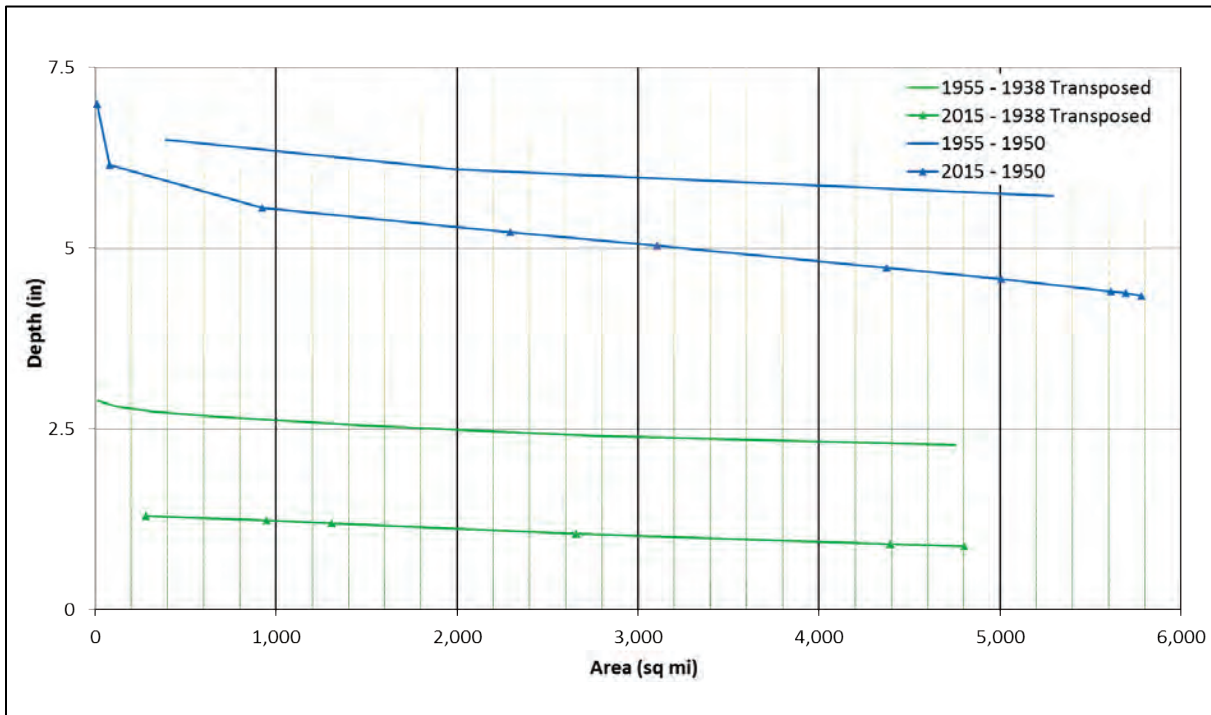


Figure 2-50. Depth-area curve for 1955 and 2015 individual storm events composing HYPO 58A over Drainage Basin 3.

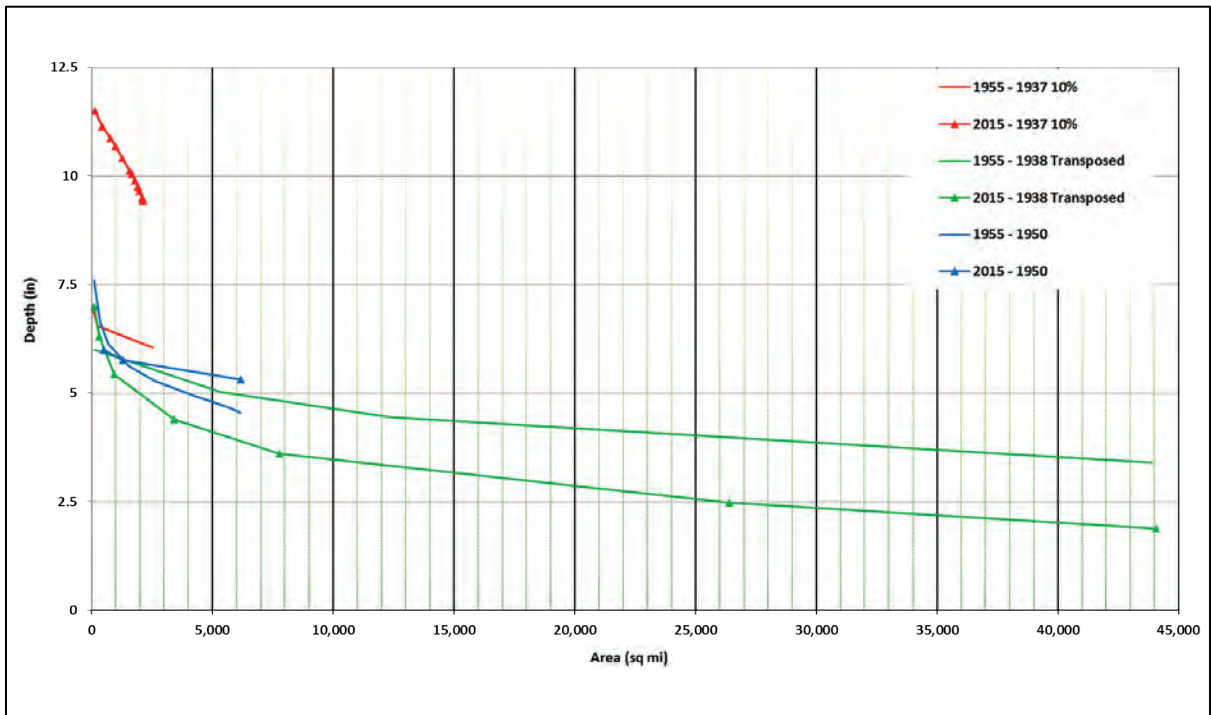


Figure 2-51. Depth-area curve for 1955 and 2015 individual storm events composing HYPO 58A over Drainage Basin 4.

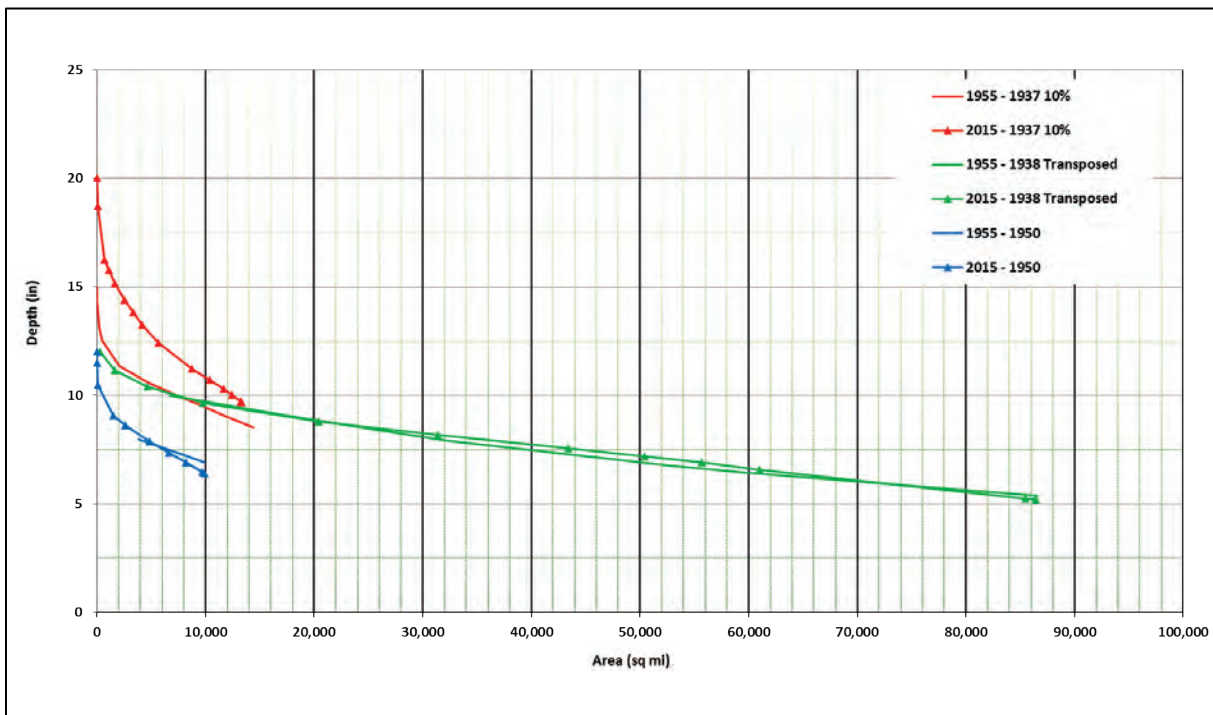


Figure 2-52. Depth-area curve for 1955 and 2015 individual storm events composing HYPO 58A over Drainage Basin 5.

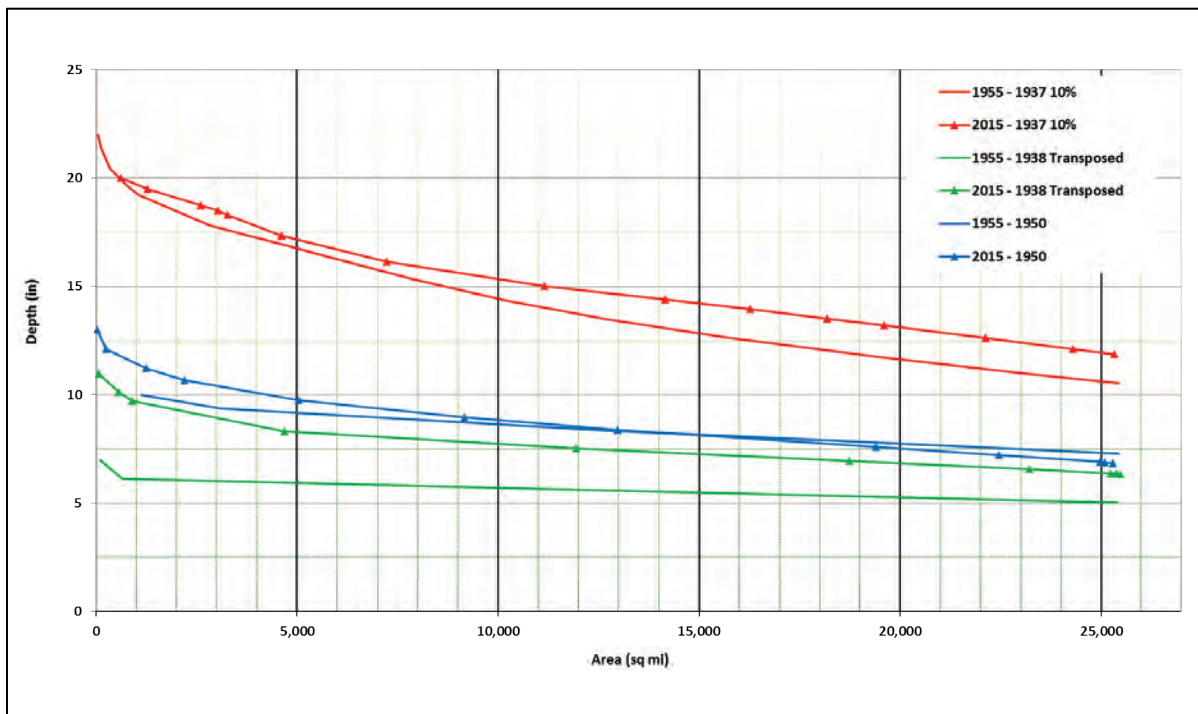


Figure 2-53. Depth-area Curve for 1955 and 2015 individual storm events composing HYPO 58A over Drainage Basin 6.

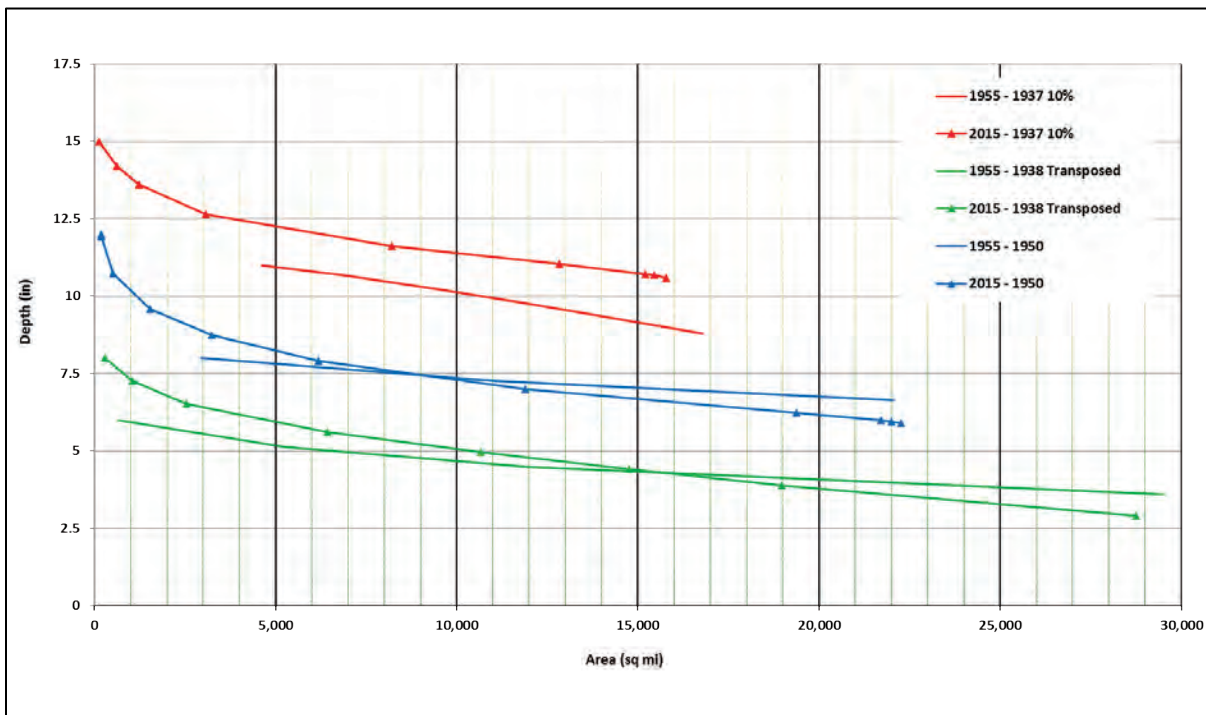
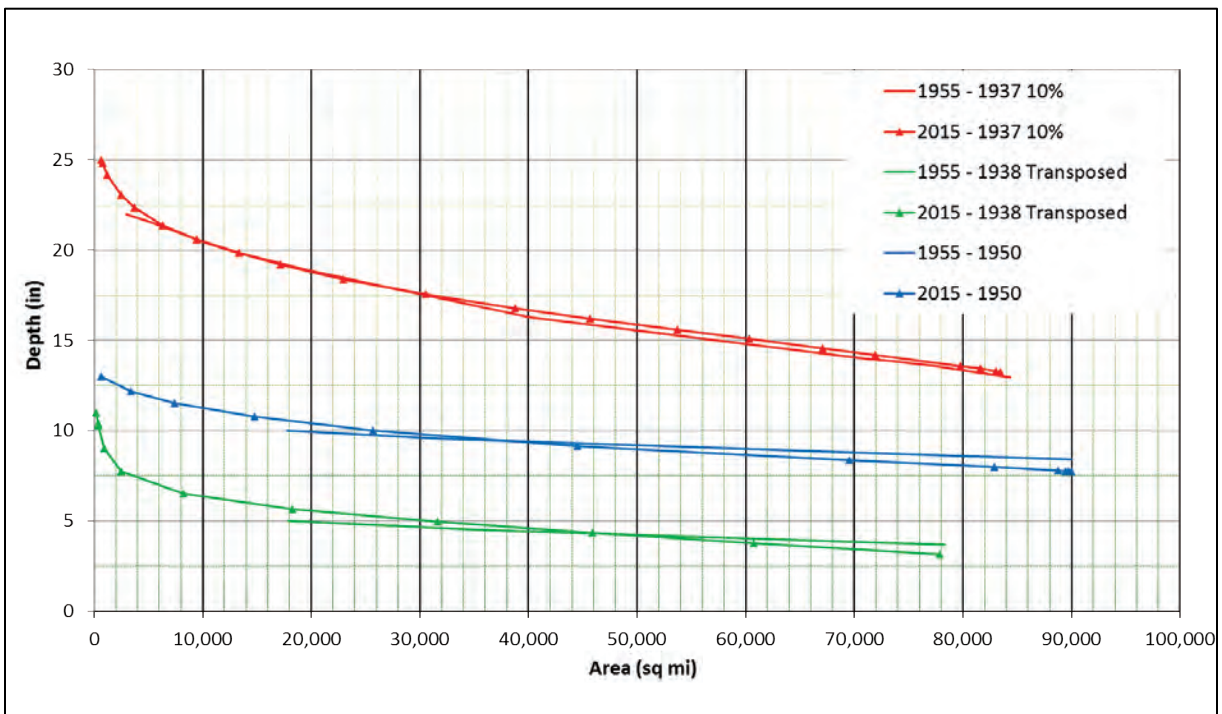


Figure 2-54. Depth-area curve for 1955 and 2015 individual storm events composing HYPO 58A over Drainage Basin 7.



Overall, the depth-area curves for 2016 precipitation inputs matched the previous 1955 rainfall maps. There were variations across each of the seven major sub-basins where 2016 depth-area curves were higher or lower than 1955 depth-area curves, but these deviations were compensated over the entire storm basin for each storm event and for the HYPO 58A storm event.

2.8.5 An overview of digitized precipitation events

To reproduce the HYPOs used to develop the PDF, this assessment first attempted digitization of the 6- or 12-hour isohyet maps located in HMR 34 (USACE, Weather Bureau 1956). The original paper copies of the isohyet maps were georeferenced, and GIS shapefiles were created for the final output. These shapefiles were then converted to ASCII grids that could be readily used as input in current hydrologic river models. The final goal was to attempt to simulate the PDF flood event.

The MR&T Flowline Study ESC determined that four HYPOs should be re-generated (52A, 56, 58A, and 63). This required digitization of isohyetal maps for eight storm events. During May and June 2014, the NWS Office in Jackson, MS (the developer of the digitization process used), and the USACE ERDC in Vicksburg, MS, performed this task by geo-referencing the paper copies and producing 6- or 12-hour shapefiles for each storm event. Storm total precipitation shapefiles were also generated for verification with observational data from the actual storm events.

Because of difficulties encountered with use of digitized isohyet contours, the approach was not used to produce the final ASCII grid files needed to run the CHPS-FEWS models. Digitized isohyet contour maps were used to check interpolated grids. Some of the major difficulties with using the digitized precipitation maps are described in the next sections.

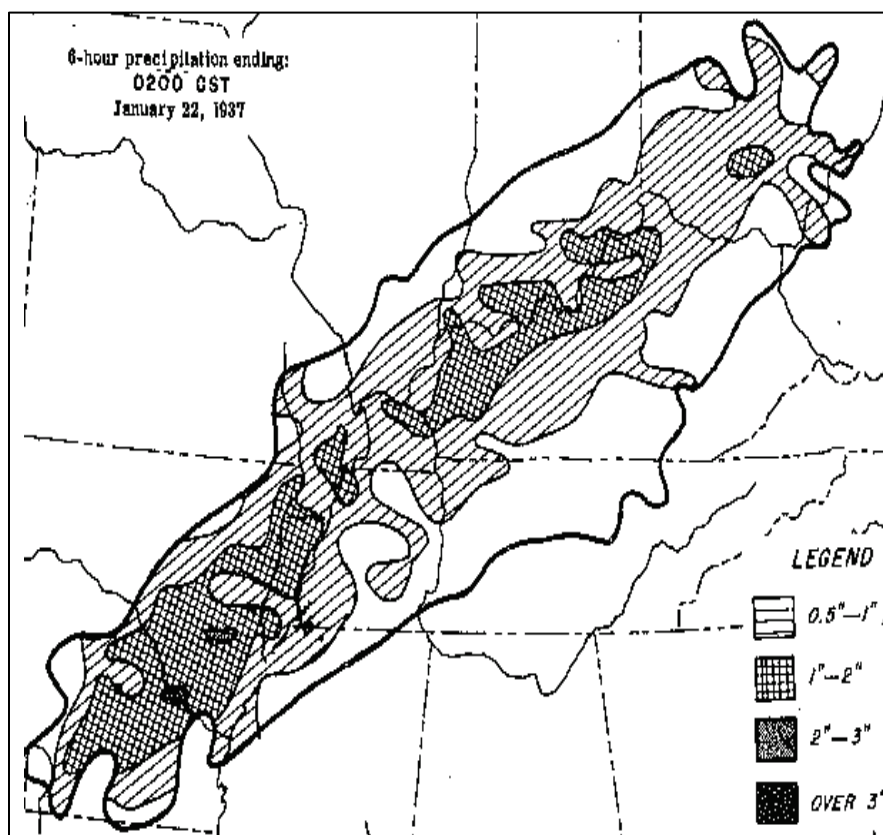
2.8.5.1 Challenges that occurred during the digitization process

While reproducing the initial precipitation event for the assessment (1937 event was used), it became apparent that several decisions were necessary to produce the most accurate product. Some of the challenges faced were the following:

1. While comparing the storm totals from the original 1937 storm contained in the Mississippi River Project Flood Study (MRPFS) (MRC 1955), with the generated storm totals from the digitization process,

discrepancies in the total amounts were quite evident. One of the reasons for the discrepancies was determined to be the wide incremental range between isohyet contours (Figure 2-55) in the paper copy isohyets maps from HMR 34 (USACE, Weather Bureau 1956).

Figure 2-55. Example of 6-hour isohyets map from 1937 storm event from HMR 34.



Due to the sparseness of the network of actual hourly observations for historical storms in the early twentieth century and the fact that HMR 34 did not contain a table of values, a decision had to be made as to what values should be used at locations within a given incremental range. Several options were discussed and evaluated with a subset of the findings contained in Table 2-11. It is noted from this table that although the results were not precise, the best results at all locations were achieved by using the midpoint of the range. For example, 1.5 in. was used for all values within the 1–2 isohyets increment. Taking Louisville, KY, as a test site, observational data showed a storm total of 12.24 in. fell during the 17–25 January 1937 storm. If the lower limit (e.g., 1 in. of the 1–2 in. increment) was used, a deficiency in the storm totals of 34.6% would occur. If the upper limit (e.g., 2 in. of the 1–2 in. increment) was chosen, an excess of 18.5% occurred. Last, the midpoint value of the 1–2 in. increment only

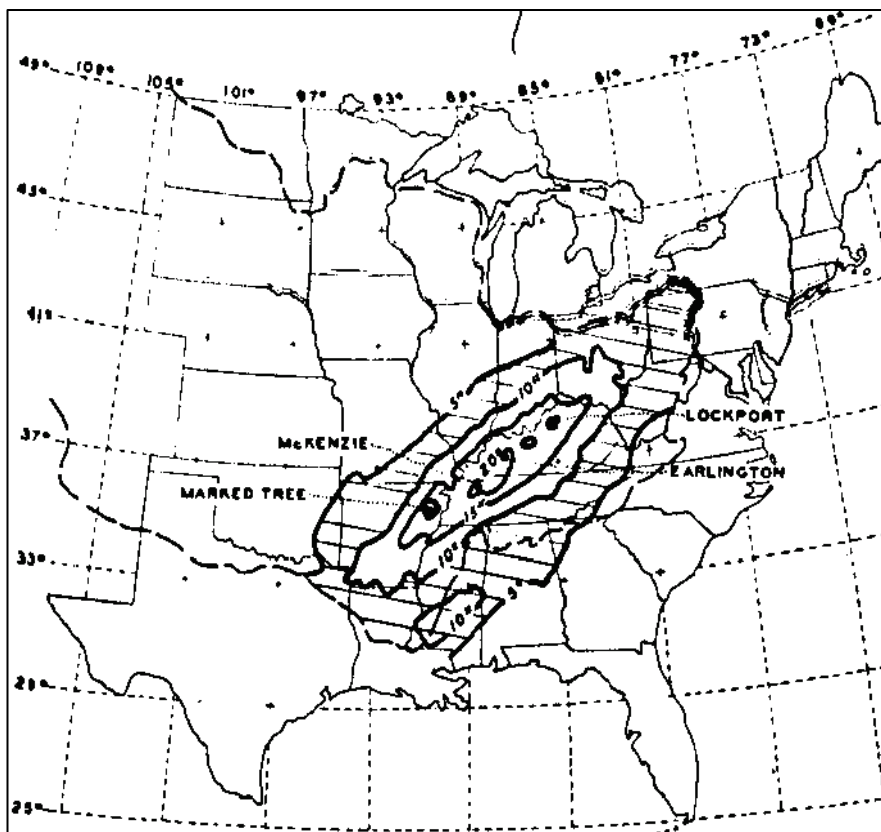
produced a deficiency of 8.1%. Thus, it was determined to use the midpoint value to populate the dataset within each incremental range to produce the 6- or 12-hour shapefiles.

Table 2-11. Comparison of incremental values from the legend in Figure 2-56 to observational data (inches).

	Lower	Midpoint	Upper
Pittsburgh, PA	-1.26	0.74	2.74
Cincinnati, OH	-2.64	0.61	3.86
Louisville, KY	-4.24	-0.99	2.26
Paducah, KY	-2.84	0.16	2.66
Leavenworth, KS	-0.21	0.34	1.29
Peoria, IL	-0.49	0.51	1.51
St Louis, MO	-1.1	0.15	1.4
Cairo, IL	-2.81	0.19	3.19
Jackson, KY	-1.16	2.09	5.34
Knoxville, TN	-2.08	0.42	2.92
Clarksville, TN	-4.31	-0.56	2.69
Memphis, TN	-3.11	0.14	2.89
Sikeston, MO	-2.5	-0.25	1.5
Little Rock, AR	-3.09	-0.09	2.41
Alexandria, LA	-2.1	0.15	2.4
Greenville, MS	-2.29	-0.04	2.21
Black Rock, AR	-2.74	-0.49	1.76
New Madrid, MO	-3.8	-0.8	2.2
Vinita, OK	-0.55	0.2	0.95
Clarendon, AR	-3.88	-0.88	2.12
Newport, AR	-3.01	0.24	2.99
St Frances, AR	-2.12	0.63	2.88
Union City, TN	-4.1	-0.85	1.9
Bethany, MO	-0.34	-0.09	0.16
Bowling Green, KY	-2.74	0.26	2.76

2. The 6- or 12-hour maps also contained variable amounts of white space within the storm area noted in Figure 2-55. The legend contains only values of 0.50 in. or more with the white space denoting anything less than 0.50 in. of precipitation. It was unclear what value should be used for the white space. Without sufficient data, it was determined to use 0 in. for this increment based on the premise that most of the precipitation falling in the period could have been lost to infiltration and not realized as runoff.
3. Similarly, the upper bound of 3 in. within a 6- or 12-hour period forced another decision about what value should be used. Based on the reasoning for the remainder of the increments, a mid-point value between adjacent 1-in. isohyets of 3.5 in. were used for any 6- or 12-hour period that exceeded 3 in.
4. When examining the total of the 6- or 12-hour maps compiled from the HMR 34 (USACE, Weather Bureau 1956) for the 1937 storm event and the storm total graphics contained in Memorandum Report No. 1 (MRC 1955) (Figure 2-56), the geographic extent was not the same in both graphics. The 6- and 12-hour maps contained a much smaller areal extent than the storm total graphics published in Memorandum Report No. 1 (MRC 1955). In fact, storm total precipitation amounts that totaled 10 in. or less were not included in the 6- or 12-hour maps in HMR 34. Since the original intent was to produce the greatest magnitude flood, a reason for this discrepancy could be that it was determined for the 1955 Study that anything outside of the 10 in. values would not immediately impact the height of the crest and thus was eliminated. It could have been determined that the rainfall outside of the 10 in. isohyets would only impact volume and not crest height. This is purely speculation because there was no documentation found that explains why there is a difference in the areal extent.

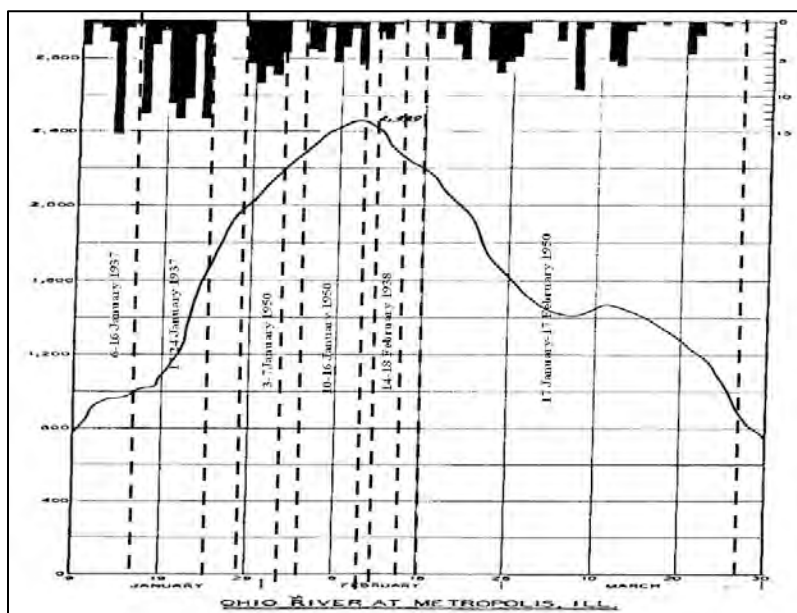
Figure 2-56. Storm total precipitation from the January 6–24 precipitation event from MRPFS (MRC 1955).



5. HMR 34 (USACE, Weather Bureau 1956) recorded a summary of the individual storms that were used in the development of HYPO 52A, 56, 58A, and 63. The summarized storms were determined to have produced the greatest impact to flows during the flood of the given year they occurred. While examining the storms used to produce HYPO 58A, it was noted that the duration of the storms was different in the HMR 34 and in Memorandum Report No. 1 (MRC 1955). The 1937 event was bounded by 17–25 January 1937 in HMR 34 and 6–24 January 1937 in Memorandum Report No. 1. No explanation was given in the documentation of either report that would describe why the periods were different. The resulting problem was that the 6- or 12-hourly data were not available for digitization in HMR 34; thus, the storm totals were inherently low. To solve this issue, a database of daily data was developed over the storm area contained in HMR 34 to produce the shapefiles for the period January 6–16. This process is in agreement with HMR 34, which also supplemented daily data for locations where hourly data were unavailable.

A similar disparity occurred in the 1950 event. When examining the storm total values digitized from HMR 34 (USACE, Weather Bureau 1956), it was noted that the values were about one-half of the values recorded in Memorandum Report No. 1 (MRC 1955) at many locations. Further examination revealed that the HMR 34 6- or 12-hourly storm data occurred from 3–7 January 1950 while Memorandum Report No. 1 storm data occurred from 3-16 January 1950. HMR 34 clearly stated that the main storm ended on 7 January 1950 with a second storm beginning 10 January 1950. Without 6- or 12-hourly data readily available, a database for the January 10–16 storm based on daily data was also compiled and used in the development of the shapefiles used for the 1950 event. Plate H-11 from Memorandum Report No. 1 (Figure 2-57) displayed the hydrograph from HYPO 58A at Metropolis, IL, along the Ohio River including the daily rainfall amounts. Subdivisions (denoted by dashed lines in Figure 2-57) were made for this assessment to denote the impacts of the various precipitation events. It was noted that the 6–16 January 1937 precipitation event produced the initial rise in the hydrograph at Metropolis, IL. Omission of the 10–16 January 1950 precipitation impacted the crest and volume. Also, when calculating the volume of the hydrographs for the inflow points, it was noted that daily precipitation data from January 17 through February 17 needed to be included since it was in the original HYPO 58A calculation.

Figure 2-57. Simulated hydrograph for HYPO 58A from MRPFS (MRC 1955).



6. To develop the HYPO storms studied, transposition of the 7–11 May 1943 and 14–19 February 1938 storms was required. This was accomplished by using the same geo-referencing technique used to produce the original storm graphics for the 6- or 12-hourly precipitation events. Transposition locations were derived from MRPFS Plates MRC 1955).
7. Some adjustments to the storm total precipitation amounts were documented in Memorandum Report No. 1 (MRC 1955), which were not included in HMR 34 (USACE, Weather Bureau 1956). According to HMR 34 (page 24), “The representative 12-hour surface dew point for the 1937 storm was 66°F, while the maximum observed dew point in January at the same location was 68°F. This allowed for an increase of 10% in the rainfall values on the basis of surface moisture adjustment only.” Thus, the 1937 rainfall totals were increased by 10% in the final precipitation amounts used for input into the hydrologic models for the 1955 Study and the current assessment.
8. According to Memorandum Report No. 1 (MRC 1955), “Since the largest of the thirteen preliminary floods at Cairo [HYPO 52] was in late spring and its estimated frequency in years is beyond the realm of practicability, it was considered unreasonable to use this flood without reducing the peak flow that would be equal to or less than the winter and early spring floods selected for detailed study.” With respect to floods that have occurred since the time of the writing of Memorandum Report No. 1, it is not apparent as to whether this statement is still valid. However, the transposition for the 8–10 May 1943 storm resulted in a shift northward by 430 miles, which would limit the availability of moisture. The HYPO 52 storm combination recognized this reduction by decreasing precipitation from the transposed 8–10 May 1943 by 4%. To satisfy the statement in Memorandum Report No. 1, the rainfall of the transposed storm of 8–10 May 1943 was adjusted by a reduction factor of 20% in developing HYPO 52A. While reproducing the graphics for the current assessment, rainfall amounts were also reduced 20%. The current assessment considered this northward shift and resulting reduction in available moisture and concluded that the original HYPO 52 should have been reduced by more than the 4% used. An appropriate adjustment was on the order of a 20% decrease. This was consistent with the formulation for HYPO 52A. An assessment of more recent combinations will occur later.
9. Compilation of additional rainfall data not provided in HMR 34 (USACE, Weather Bureau 1956) was required to produce total volumes

for the various HYPO storm events. For instance, HYPO 58A required data compilation from 15 December 1936 through 5 January 1937 to provide antecedent conditions for the flood and 17 January through 17 February 1950 to fill in the flood after the crest. Daily point data were used to develop the shapefiles that were used as input to the hydrologic models.

2.8.5.2 Digitized data versus interpolated point data

The difficulties encountered in developing the digitized precipitation amounts, especially considering the uncertainty in interpretation of appropriate precipitation depths from the few available isohyet contours, led to developing an alternate method for preparing the required input precipitation grids. The alternate method, described in Section 2.8.3, utilized tabulated point data and an interpolation scheme to produce the precipitation grids required for input to the hydrologic models. The digitized precipitation maps were used as a cross-check for the interpolated values.

2.9 Storm transpositioning

The original development of the HYPO storm series included meteorological adjustment of historic extreme storms to maximize their effects on parts of the Mississippi River Basin. This included transposing, that is rotating and moving, storms over different parts of the watershed from where they actually occurred. The purpose of transpositioning storm events was to shift the location where precipitation fell over the watershed. All transpositioning adjustments only applied to location of rainfall and storm extent; there was no impact on the size or extent of the watershed boundaries or their characteristics.

The HEC designed and implemented enhancements to the HEC-MetVue program (Version 2.2.8.10) to provide a command-line utility for rotation and translation of ESRI ASCII precipitation grids to rotate and translate two historical storm events.

2.9.1 HEC-MetVue enhancements

HEC-MetVue transformed the original grid into an equal-area projection to preserve the original precipitation volume, then rotated the grid about the center of the specified coordinates, translated the rotated grid in the

specified east-west and/or north-south direction(s), and re-sampled the rotated and translated grid back into the original coordinate system. The HEC-MetVue enhancements allowed the user to specify, from a command line or script, the center, rotation angle, and translation and output new ASCII grids with the same georeferencing and spacing as the source data. The rotation angle was specified in decimal degrees with positive numbers denoting counterclockwise rotation and negative numbers denoting clockwise rotation. The translation distance may be specified in degrees or linear units, such as miles. HEC-MetVue triangulated the input data to a TIN and, by default, resampled the values using bi-linear interpolation.

To best preserve the original maximum and minimum precipitation values, an option was added to HEC-MetVue to perform nearest neighbor resampling, selecting the value from the nearest grid cell within a specified range, expressed as a multiple of the input grid cell size. The user controlled this interpolation option by specifying a search radius as a multiplier of the cell size, or specifying “NONE” to use bilinear interpolation to set all output values.

2.9.2 Post-processing

HEC developed a Python (www.python.org) script to automate the processing of a large number of ASCII grids. The script can process all ASCII grids in a specified folder or a sub-set of these grids using a specified time window. HEC-MetVue determined boundaries for the output grids to include the original data as well as any necessary increase in extents to accommodate the rotated and translated data. To meet model requirements, the transposed grids must have the same bounds as the original grids; HEC developed a Python script to clip or fill the boundary with nulls to match the boundaries of the original grids.

2.9.3 Data source and specifications

The Memphis District provided HEC with ESRI-style ASCII grids of historical precipitation depths in 6-hour increments for a February 1938 storm event near Calvin, OK, and a 1943 event near Warner, OK. The grid files were named using a convention that includes date and time as part of the file name. For example, the file “PREC_19370701000000.asc” contained precipitation data for a 6-hour interval beginning on 7 July 1937 at 0000 hours. The spatial reference of the grids was unprojected

longitude and latitude, and the grid was composed of values spaced at 0.1° . Longitude and latitude were assumed to be relative to NAD 83.

2.9.4 Data processing

HEC applied the HEC-MetVue enhancements to rotate and translate the grids in the 1938 and 1943 data sets as prescribed below:

- **1938** – Transposed 90 miles north and rotated 20° clockwise about Calvin, OK ($34.96777778^\circ\text{N}$, $96.24861111^\circ\text{W}$), the defined center point of the storm.
- **1943** – Transposed 430 miles north and rotated 14.5° clockwise about Warner, OK ($35.494166667^\circ\text{N}$, $-95.305555556^\circ\text{W}$), the defined center point of the storm.
- **1943** – Transposed 105 miles north and rotated 21° clockwise about Warner, OK ($35.494166667^\circ\text{N}$, $-95.305555556^\circ\text{W}$), the defined center point of the storm.

The longitude and latitude for each transposition was provided to the program as decimal degrees, where the grids were processed using nearest neighbor resampling with a constraint of 1.15 grid cells and then written to ESCRI ASCII grids. With this specification, if a value were available within 1.15 grid cells from a given location, the value of the nearest neighbor was used for that location. Otherwise, the value was determined from the surrounding points using bilinear interpolation. The value of 1.15 was determined through analysis of several options, as detailed in the proceeding sections. These grids were then clipped to the original grid extents, using a Python script to trim the data and create a new header, generating a new set of clipped transformed grids. The unclipped grids were used for the QA/QC below, and the clipped grids were the final product for use in storm modeling and analysis.

2.9.5 Spatial analysis of results

2.9.5.1 Spatial analysis of preservation of feature shapes: ArcMap

A qualitative spatial analysis was performed for the 1938 storm to ensure that the shapes of the precipitation features of the original grids were preserved during rotation and translation. Figure 2-58 shows the original (as received) 6-hour accumulated precipitation for 15 February 1938 at 0000 UTC, summarized in ArcMap. The maps are displayed in

unprojected latitude and longitude. The precipitation depths are shown as filled contours at 0.25 in. intervals. The maximum precipitation accumulation within a single cell for this grid is 3.0 in. The watershed boundaries of the original precipitation grid are denoted by a black line. The watershed boundaries of the translated and rotated precipitation grid are denoted by a red line. The white rectangular area shows the extents of the original grid as well as the clipped rotated and translated grid. The white pixels of the rectangular region denote undefined (null) values, which are located outside the watershed boundaries that were used to define the original historical grid. Figure 2-59 shows the rotated and translated grid for 15 Feb 1938 at 0000 GMT. The shapes of the features in the precipitation as well as the values are preserved.

Figure 2-60 and Figure 2-61 show the results for 15 Feb 1938 at 0600 GMT, at the peak of this storm. Figure 5.3 shows the original historical grid for 15 Feb 1938 at 0600 GMT. The maximum precipitation depth for this grid is 3.3 in. Figure 2-58 shows the rotated and translated grid for 15 Feb 1938 at 0600 GMT. As with the data for 0000 GMT shown in Figure 2-58 and Figure 2-59, the shapes of the features in the precipitation as well as the values are preserved. Areas that fell outside the transposed boundary (red outline in the figures) were assigned a value of zero (0). This maintained the primary storm extent over the original basin.

Figure 2-58. Original precipitation grid, 15 February 1938 at 0000 GMT.

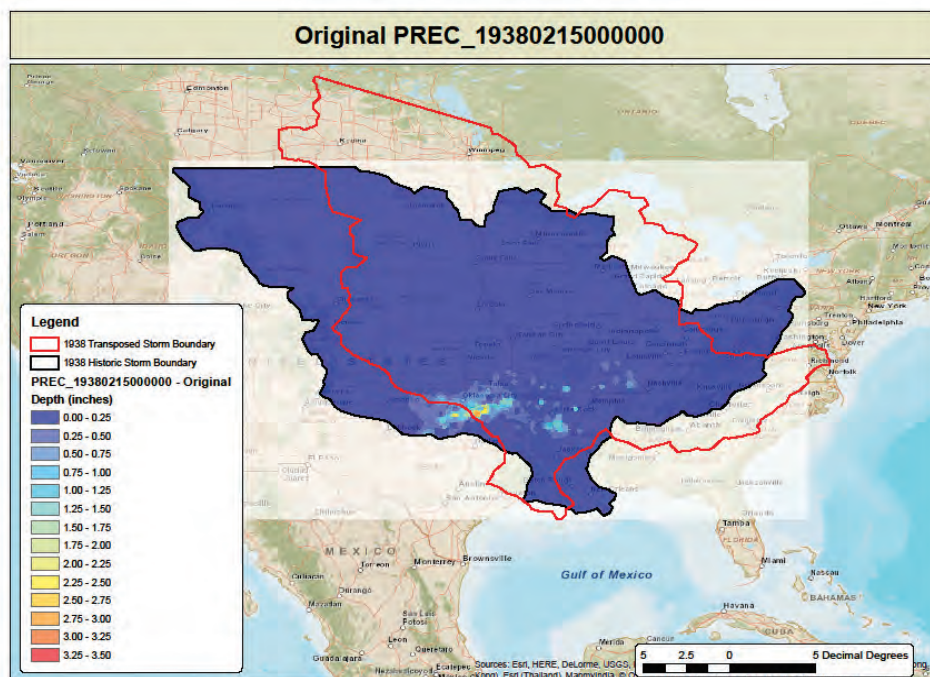


Figure 2-59. Transposed precipitation grid, 15 February 1938 at 0000 GMT.

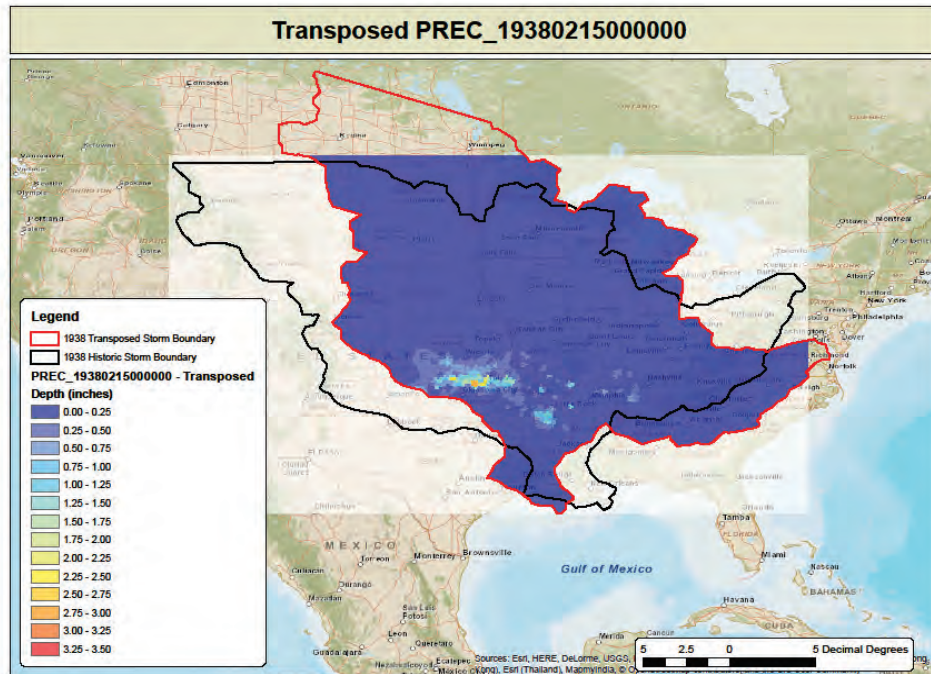


Figure 2-60. Original precipitation grid, 15 February 1938 at 0600 GMT.

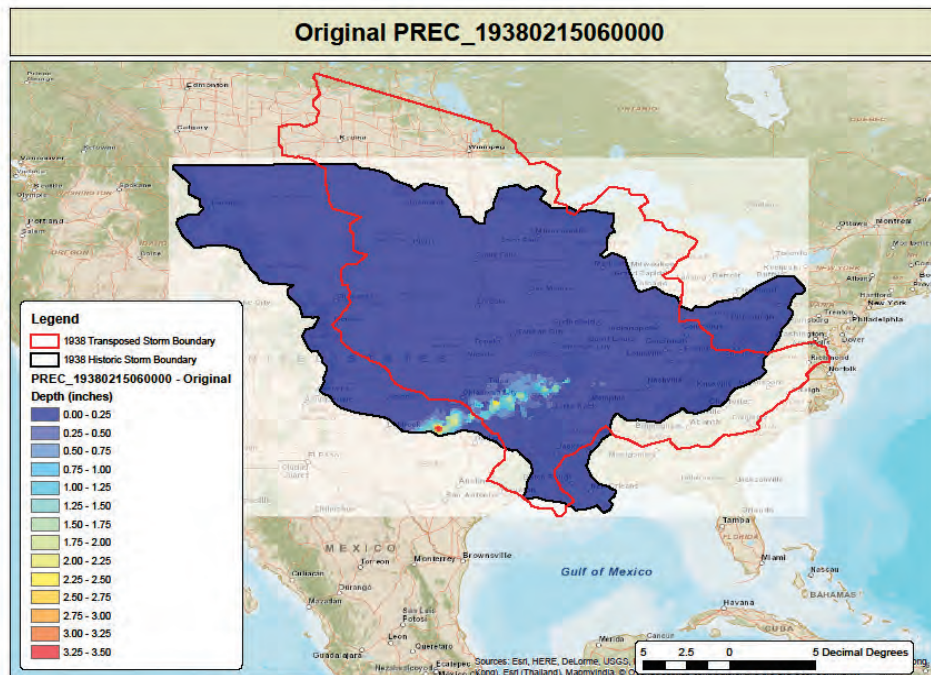
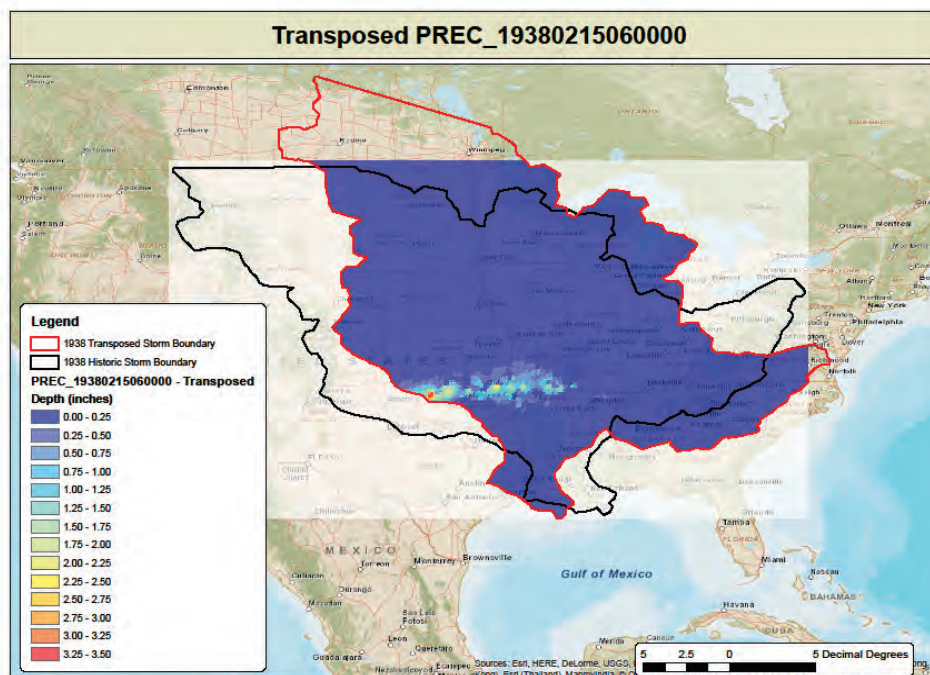


Figure 2-61. Transposed precipitation grid, 15 February 1938 at 0600 GMT.



2.9.5.2 Spatial analysis of preservation of feature shapes: Precipitation maps

The qualitative analysis in ArcMap is labor intensive, so it was only performed for the limited set of grids above. To obtain a complete and high-quality qualitative analysis that was flexible, adjustable, objective, and repeatable, HEC prepared Python scripts to plot and animate all of the precipitation grids, including the original grids, the unclipped transformed grids, and the clipped transformed grids. The same grid extents and precipitation range were used for all grids. This enabled multiple grids for each hour to be viewed in succession, allowing users to readily identify differences from one grid to another. These scripts were applied to prepare individual *.png image files of all grids from all processing steps of the 1938 and 1943 storm events. Figure 2-62 shows the original precipitation grid from 09 May 1943 at 0600 GMT. Figure 2-63 shows this grid after rotating it 21° clockwise about Warner, OK (35° 29' 39" N, 95° 18' 20" W) and translating it 105 miles north. Figure 2-64 shows the grid after trimming to the watershed boundaries and grid extents of the original grid. The precipitation grid maps for all processing levels of the 1938 and 1943 storm events are provided as *.png image files in the supplemental data to this report. An animation of these grid maps was prepared for each transformation and processing level (original, transformed, and clipped) of the 1938 and 1943 storm events.

Figure 2-62. Grid map of original grid, 09 May 1943 at 0600 GMT.

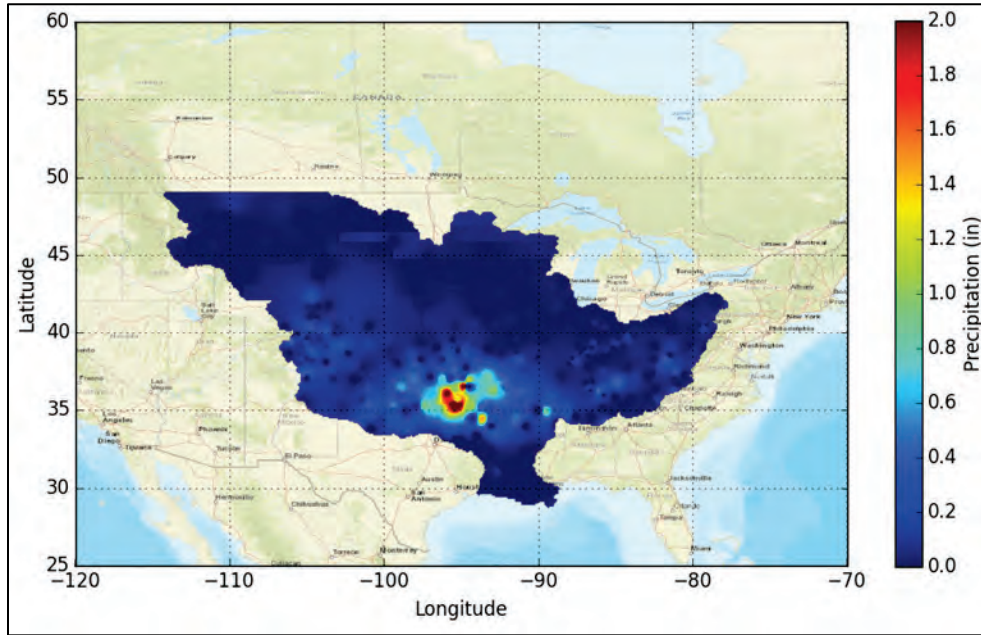


Figure 2-63. Grid map of transformed grid, 09 May 1943 at 0600 GMT.

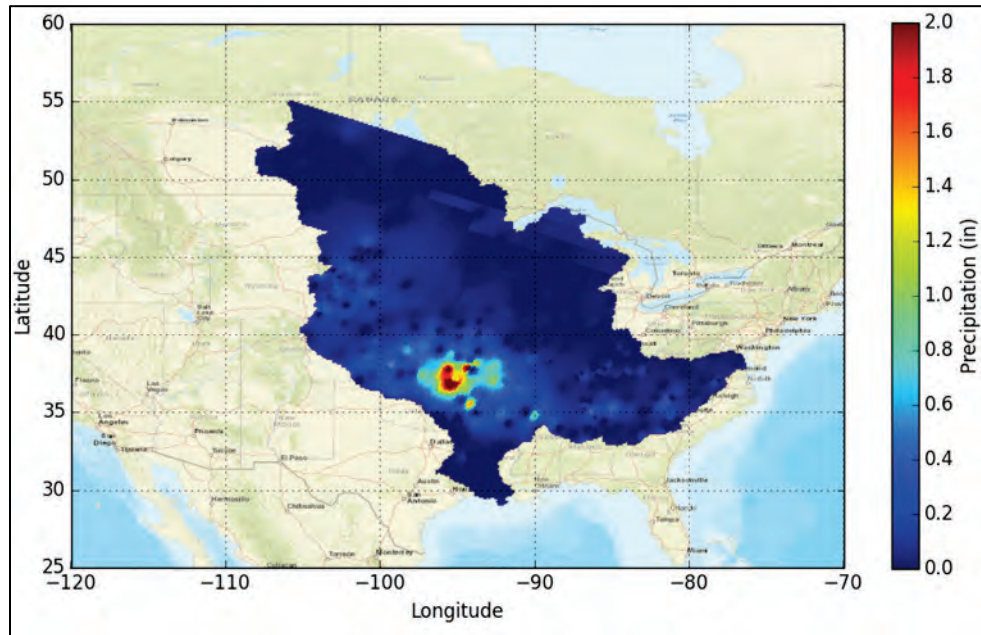
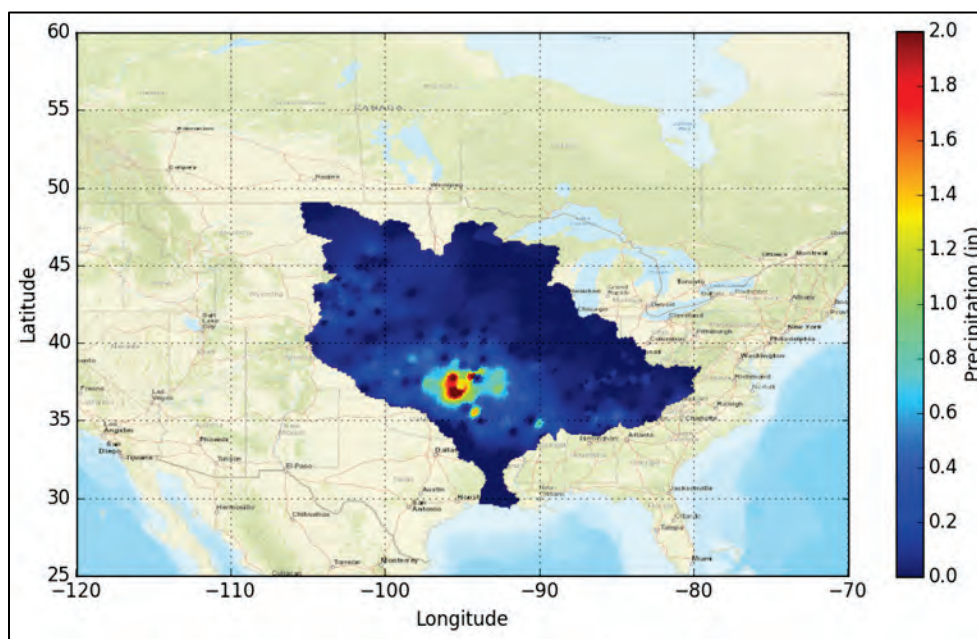


Figure 2-64. Grid map of transformed grid, 09 May 1943 at 0600 GMT, trimmed to the original watershed boundaries and grid extents.



2.9.6 Quantitative analysis: Volume conservation

A quantitative numerical analysis was performed to identify the best interpolation option to use for the grid rotation and translation. The interpolation option can be set to use the default bilinear interpolation or nearest-neighbor resampling. The nearest-neighbor option then requires a numerical value to specify a search radius as a multiple of the grid cell size. If a cell center in the input grid can be identified within the specified radius of the output cell center, nearest-neighbor resampling will be used for that cell. If not, bilinear interpolation will be used to generate a value for that cell.

2.9.6.1 Count-based analysis

To identify the best overall interpolation option that best preserved the original numerical values, bilinear interpolation and 10 nearest-neighbor options (0.25, 0.50, 0.75, 1.00, 1.10, 1.15, 1.20, 1.30, 1.50, and 2.00) were evaluated for all of the transformed grids for the 1938 and 1943 storm events. Options at the center of this range varied by a smaller number of units (1.10, 1.15, 1.20) to fine-tune the results.

Histograms were computed for each grid, counting the number of grid cells occurring in each 0.25 in. bin from 0.00 to 12.00 in. The grid spacing

is 0.1° in each of the north-south and east-west directions. Therefore, the area of each grid cell is 0.01° squared. To perform volume comparisons using common units of acre-feet, the approximate area of each grid cell was computed in acres using a mid-latitude estimate of 6.9 miles per 0.1° and using the conversion factor of 640 acres per square mile. Volumes were computed for each grid cell in each bin by multiplying the upper precipitation level of that bin by the area in acres. The differences in area and volume for each bin were then computed between the rotated/translated grid and the original grid. The percent difference for each bin was computed by dividing this difference by the corresponding area or volume in the corresponding bin of the original grid.

The absolute values of the maximum percent differences were computed and summarized to identify the best resampling option. Table 2-12 summarizes the absolute maximum percent difference of cell counts computed between each rotated/translated grid and the original grid. The 1.10 option performed the best of all of the options in preserving counts; however, it resulted in significant error in the 2.75 and 3.00 bins. The 1.15 option preserved counts well for these bins and generally performed well for all bins.

Table 2-13 summarizes the absolute maximum percent difference of volume computed between each rotated/translated grid and the original grid. The 1.15 option achieved the best overall preservation of volume. Therefore, the 1.15 option was selected for producing the final data set of rotated and translated grids for the 1938 storm event. Note in Table 2-13 that there is minimal difference reported for the highest precipitation amounts, and thus, any potential error is less for high levels of precipitation that occur near the storm peak.

Table 2-12. Absolute maximum of the percent difference of cell counts between each transposed grid and the original grid (1938).*

Precip Level (in)	Interp	NN, opt 0.25	NN, opt 0.50	NN, opt 0.75	NN, opt 1.00	NN, opt 1.10	NN, opt 1.15	NN, opt 1.20	NN, opt 1.30	NN, opt 1.50	NN, opt 2.00	Minimum
0.00	0.0%	0.0%	0.0%	0.0%	0.0%	0.0%	0.0%	0.0%	0.0%	0.0%	0.0%	--
0.25	6.0%	6.0%	4.0%	4.0%	2.0%	1.0%	2.0%	1.0%	1.0%	2.0%	2.0%	1.0%
0.50	16.0%	15.0%	12.0%	8.0%	3.0%	3.0%	4.0%	4.0%	4.0%	4.0%	4.0%	3.0%
0.75	19.0%	19.0%	19.0%	6.0%	10.0%	14.0%	14.0%	14.0%	14.0%	14.0%	14.0%	6.0%
1.00	46.0%	46.0%	38.0%	23.0%	8.0%	5.0%	15.0%	15.0%	15.0%	15.0%	15.0%	5.0%
1.25	45.0%	45.0%	45.0%	9.0%	11.0%	10.0%	9.0%	9.0%	7.0%	7.0%	7.0%	7.0%
1.50	13.0%	13.0%	15.0%	20.0%	15.0%	15.0%	20.0%	12.0%	12.0%	12.0%	12.0%	12.0%
1.75	33.0%	33.0%	22.0%	11.0%	8.0%	8.0%	10.0%	11.0%	11.0%	11.0%	11.0%	8.0%
2.00	600.0%	600.0%	600.0%	300.0%	25.0%	25.0%	25.0%	25.0%	25.0%	25.0%	25.0%	25.0%
2.25	100.0%	100.0%	100.0%	14.0%	10.0%	0.0%	0.0%	0.0%	0.0%	0.0%	0.0%	0.0%
2.50	300.0%	300.0%	300.0%	200.0%	100.0%	0.0%	0.0%	0.0%	0.0%	0.0%	0.0%	0.0%
2.75	100.0%	100.0%	100.0%	75.0%	50.0%	50.0%	25.0%	25.0%	25.0%	25.0%	25.0%	25.0%
3.00	600.0%	500.0%	400.0%	300.0%	100.0%	100.0%	17.0%	17.0%	17.0%	17.0%	17.0%	17.0%
3.25	75.0%	62.0%	50.0%	38.0%	12.0%	12.0%	12.0%	12.0%	12.0%	12.0%	12.0%	12.0%
3.50	0.0%	0.0%	0.0%	0.0%	0.0%	0.0%	0.0%	0.0%	0.0%	0.0%	0.0%	0.0%
3.75	0.0%	0.0%	0.0%	0.0%	0.0%	0.0%	0.0%	0.0%	0.0%	0.0%	0.0%	0.0%
4.00	0.0%	0.0%	0.0%	0.0%	0.0%	0.0%	0.0%	0.0%	0.0%	0.0%	0.0%	0.0%
4.25	0.0%	0.0%	0.0%	0.0%	0.0%	0.0%	0.0%	0.0%	0.0%	0.0%	0.0%	0.0%
4.50	0.0%	0.0%	0.0%	0.0%	0.0%	0.0%	0.0%	0.0%	0.0%	0.0%	0.0%	0.0%
4.75	0.0%	0.0%	0.0%	0.0%	0.0%	0.0%	0.0%	0.0%	0.0%	0.0%	0.0%	0.0%
5.00	0.0%	0.0%	0.0%	0.0%	0.0%	0.0%	0.0%	0.0%	0.0%	0.0%	0.0%	0.0%
5.25	0.0%	0.0%	0.0%	0.0%	0.0%	0.0%	0.0%	0.0%	0.0%	0.0%	0.0%	0.0%
5.50	0.0%	0.0%	0.0%	0.0%	0.0%	0.0%	0.0%	0.0%	0.0%	0.0%	0.0%	0.0%
5.75	0.0%	0.0%	0.0%	0.0%	0.0%	0.0%	0.0%	0.0%	0.0%	0.0%	0.0%	0.0%
6.00	0.0%	0.0%	0.0%	0.0%	0.0%	0.0%	0.0%	0.0%	0.0%	0.0%	0.0%	0.0%
6.25	0.0%	0.0%	0.0%	0.0%	0.0%	0.0%	0.0%	0.0%	0.0%	0.0%	0.0%	0.0%
6.50	0.0%	0.0%	0.0%	0.0%	0.0%	0.0%	0.0%	0.0%	0.0%	0.0%	0.0%	0.0%
6.75	0.0%	0.0%	0.0%	0.0%	0.0%	0.0%	0.0%	0.0%	0.0%	0.0%	0.0%	0.0%
7.00	0.0%	0.0%	0.0%	0.0%	0.0%	0.0%	0.0%	0.0%	0.0%	0.0%	0.0%	0.0%
7.25	0.0%	0.0%	0.0%	0.0%	0.0%	0.0%	0.0%	0.0%	0.0%	0.0%	0.0%	0.0%
7.50	0.0%	0.0%	0.0%	0.0%	0.0%	0.0%	0.0%	0.0%	0.0%	0.0%	0.0%	0.0%
7.75	0.0%	0.0%	0.0%	0.0%	0.0%	0.0%	0.0%	0.0%	0.0%	0.0%	0.0%	0.0%
8.00	0.0%	0.0%	0.0%	0.0%	0.0%	0.0%	0.0%	0.0%	0.0%	0.0%	0.0%	0.0%
8.25	0.0%	0.0%	0.0%	0.0%	0.0%	0.0%	0.0%	0.0%	0.0%	0.0%	0.0%	0.0%
8.50	0.0%	0.0%	0.0%	0.0%	0.0%	0.0%	0.0%	0.0%	0.0%	0.0%	0.0%	0.0%
8.75	0.0%	0.0%	0.0%	0.0%	0.0%	0.0%	0.0%	0.0%	0.0%	0.0%	0.0%	0.0%
9.00	0.0%	0.0%	0.0%	0.0%	0.0%	0.0%	0.0%	0.0%	0.0%	0.0%	0.0%	0.0%
9.25	0.0%	0.0%	0.0%	0.0%	0.0%	0.0%	0.0%	0.0%	0.0%	0.0%	0.0%	0.0%
9.50	0.0%	0.0%	0.0%	0.0%	0.0%	0.0%	0.0%	0.0%	0.0%	0.0%	0.0%	0.0%
9.75	0.0%	0.0%	0.0%	0.0%	0.0%	0.0%	0.0%	0.0%	0.0%	0.0%	0.0%	0.0%
10.00	0.0%	0.0%	0.0%	0.0%	0.0%	0.0%	0.0%	0.0%	0.0%	0.0%	0.0%	0.0%
10.25	0.0%	0.0%	0.0%	0.0%	0.0%	0.0%	0.0%	0.0%	0.0%	0.0%	0.0%	0.0%
10.50	0.0%	0.0%	0.0%	0.0%	0.0%	0.0%	0.0%	0.0%	0.0%	0.0%	0.0%	0.0%
10.75	0.0%	0.0%	0.0%	0.0%	0.0%	0.0%	0.0%	0.0%	0.0%	0.0%	0.0%	0.0%
11.00	0.0%	0.0%	0.0%	0.0%	0.0%	0.0%	0.0%	0.0%	0.0%	0.0%	0.0%	0.0%
11.25	0.0%	0.0%	0.0%	0.0%	0.0%	0.0%	0.0%	0.0%	0.0%	0.0%	0.0%	0.0%
11.50	0.0%	0.0%	0.0%	0.0%	0.0%	0.0%	0.0%	0.0%	0.0%	0.0%	0.0%	0.0%
11.75	0.0%	0.0%	0.0%	0.0%	0.0%	0.0%	0.0%	0.0%	0.0%	0.0%	0.0%	0.0%
12.00	0.0%	0.0%	0.0%	0.0%	0.0%	0.0%	0.0%	0.0%	0.0%	0.0%	0.0%	0.0%

*Notes

NN = nearest neighbor resampling method in MetVue

Opt = nearest neighbor option specified

Interp = default interpolation method in MetVue

Minimum absolute percent difference highlighted in yellow

Table 2-13. Absolute maximum of the percent difference of volume between each transposed grid and the original grid (1938).*

Precip Level (in)	Interp	NN, opt 0.25	NN, opt 0.50	NN, opt 0.75	NN, opt 1.00	NN, opt 1.10	NN, opt 1.15	NN, opt 1.20	NN, opt 1.30	NN, opt 1.50	NN, opt 2.00	Minimum
0.00	0.000%	0.000%	0.000%	0.000%	0.000%	0.000%	0.000%	0.000%	0.000%	0.000%	0.000%	--
0.25	0.150%	0.125%	0.100%	0.088%	0.027%	0.025%	0.027%	0.025%	0.025%	0.050%	0.050%	0.0%
0.50	0.108%	0.097%	0.075%	0.043%	0.022%	0.032%	0.043%	0.043%	0.043%	0.043%	0.043%	0.0%
0.75	0.072%	0.068%	0.052%	0.020%	0.024%	0.023%	0.023%	0.023%	0.023%	0.023%	0.023%	0.0%
1.00	0.046%	0.039%	0.033%	0.013%	0.007%	0.005%	0.014%	0.014%	0.018%	0.018%	0.018%	0.0%
1.25	0.013%	0.013%	0.013%	0.006%	0.027%	0.024%	0.022%	0.022%	0.017%	0.017%	0.017%	0.0%
1.50	0.030%	0.030%	0.030%	0.018%	0.014%	0.014%	0.014%	0.017%	0.017%	0.017%	0.017%	0.0%
1.75	0.022%	0.022%	0.014%	0.005%	0.005%	0.005%	0.005%	0.005%	0.005%	0.005%	0.005%	0.0%
2.00	0.016%	0.016%	0.016%	0.008%	0.003%	0.003%	0.003%	0.003%	0.003%	0.003%	0.003%	0.0%
2.25	0.011%	0.011%	0.011%	0.005%	0.003%	0.000%	0.000%	0.000%	0.000%	0.000%	0.000%	0.0%
2.50	0.008%	0.008%	0.008%	0.005%	0.003%	0.000%	0.000%	0.000%	0.000%	0.000%	0.000%	0.0%
2.75	0.011%	0.011%	0.011%	0.008%	0.003%	0.003%	0.003%	0.003%	0.003%	0.003%	0.003%	0.0%
3.00	0.016%	0.014%	0.011%	0.008%	0.003%	0.003%	0.003%	0.003%	0.003%	0.003%	0.003%	0.0%
3.25	0.016%	0.013%	0.011%	0.008%	0.003%	0.003%	0.003%	0.003%	0.003%	0.003%	0.003%	0.0%
3.50	0.000%	0.000%	0.000%	0.000%	0.000%	0.000%	0.000%	0.000%	0.000%	0.000%	0.000%	0.0%
3.75	0.000%	0.000%	0.000%	0.000%	0.000%	0.000%	0.000%	0.000%	0.000%	0.000%	0.000%	0.0%
4.00	0.000%	0.000%	0.000%	0.000%	0.000%	0.000%	0.000%	0.000%	0.000%	0.000%	0.000%	0.0%
4.25	0.000%	0.000%	0.000%	0.000%	0.000%	0.000%	0.000%	0.000%	0.000%	0.000%	0.000%	0.0%
4.50	0.000%	0.000%	0.000%	0.000%	0.000%	0.000%	0.000%	0.000%	0.000%	0.000%	0.000%	0.0%
4.75	0.000%	0.000%	0.000%	0.000%	0.000%	0.000%	0.000%	0.000%	0.000%	0.000%	0.000%	0.0%
5.00	0.000%	0.000%	0.000%	0.000%	0.000%	0.000%	0.000%	0.000%	0.000%	0.000%	0.000%	0.0%
5.25	0.000%	0.000%	0.000%	0.000%	0.000%	0.000%	0.000%	0.000%	0.000%	0.000%	0.000%	0.0%
5.50	0.000%	0.000%	0.000%	0.000%	0.000%	0.000%	0.000%	0.000%	0.000%	0.000%	0.000%	0.0%
5.75	0.000%	0.000%	0.000%	0.000%	0.000%	0.000%	0.000%	0.000%	0.000%	0.000%	0.000%	0.0%
6.00	0.000%	0.000%	0.000%	0.000%	0.000%	0.000%	0.000%	0.000%	0.000%	0.000%	0.000%	0.0%
6.25	0.000%	0.000%	0.000%	0.000%	0.000%	0.000%	0.000%	0.000%	0.000%	0.000%	0.000%	0.0%
6.50	0.000%	0.000%	0.000%	0.000%	0.000%	0.000%	0.000%	0.000%	0.000%	0.000%	0.000%	0.0%
6.75	0.000%	0.000%	0.000%	0.000%	0.000%	0.000%	0.000%	0.000%	0.000%	0.000%	0.000%	0.0%
7.00	0.000%	0.000%	0.000%	0.000%	0.000%	0.000%	0.000%	0.000%	0.000%	0.000%	0.000%	0.0%
7.25	0.000%	0.000%	0.000%	0.000%	0.000%	0.000%	0.000%	0.000%	0.000%	0.000%	0.000%	0.0%
7.50	0.000%	0.000%	0.000%	0.000%	0.000%	0.000%	0.000%	0.000%	0.000%	0.000%	0.000%	0.0%
7.75	0.000%	0.000%	0.000%	0.000%	0.000%	0.000%	0.000%	0.000%	0.000%	0.000%	0.000%	0.0%
8.00	0.000%	0.000%	0.000%	0.000%	0.000%	0.000%	0.000%	0.000%	0.000%	0.000%	0.000%	0.0%
8.25	0.000%	0.000%	0.000%	0.000%	0.000%	0.000%	0.000%	0.000%	0.000%	0.000%	0.000%	0.0%
8.50	0.000%	0.000%	0.000%	0.000%	0.000%	0.000%	0.000%	0.000%	0.000%	0.000%	0.000%	0.0%
8.75	0.000%	0.000%	0.000%	0.000%	0.000%	0.000%	0.000%	0.000%	0.000%	0.000%	0.000%	0.0%
9.00	0.000%	0.000%	0.000%	0.000%	0.000%	0.000%	0.000%	0.000%	0.000%	0.000%	0.000%	0.0%
9.25	0.000%	0.000%	0.000%	0.000%	0.000%	0.000%	0.000%	0.000%	0.000%	0.000%	0.000%	0.0%
9.50	0.000%	0.000%	0.000%	0.000%	0.000%	0.000%	0.000%	0.000%	0.000%	0.000%	0.000%	0.0%
9.75	0.000%	0.000%	0.000%	0.000%	0.000%	0.000%	0.000%	0.000%	0.000%	0.000%	0.000%	0.0%
10.00	0.000%	0.000%	0.000%	0.000%	0.000%	0.000%	0.000%	0.000%	0.000%	0.000%	0.000%	0.0%
10.25	0.000%	0.000%	0.000%	0.000%	0.000%	0.000%	0.000%	0.000%	0.000%	0.000%	0.000%	0.0%
10.50	0.000%	0.000%	0.000%	0.000%	0.000%	0.000%	0.000%	0.000%	0.000%	0.000%	0.000%	0.0%
10.75	0.000%	0.000%	0.000%	0.000%	0.000%	0.000%	0.000%	0.000%	0.000%	0.000%	0.000%	0.0%
11.00	0.000%	0.000%	0.000%	0.000%	0.000%	0.000%	0.000%	0.000%	0.000%	0.000%	0.000%	0.0%
11.25	0.000%	0.000%	0.000%	0.000%	0.000%	0.000%	0.000%	0.000%	0.000%	0.000%	0.000%	0.0%
11.50	0.000%	0.000%	0.000%	0.000%	0.000%	0.000%	0.000%	0.000%	0.000%	0.000%	0.000%	0.0%
11.75	0.000%	0.000%	0.000%	0.000%	0.000%	0.000%	0.000%	0.000%	0.000%	0.000%	0.000%	0.0%
12.00	0.000%	0.000%	0.000%	0.000%	0.000%	0.000%	0.000%	0.000%	0.000%	0.000%	0.000%	0.0%

***Notes**

- NN = nearest neighbor resampling method in MetVue
- Opt = nearest neighbor option specified
- Interp = default interpolation method in MetVue
- Minimum absolute percent difference highlighted in yellow

2.9.6.2 Volume-based analysis

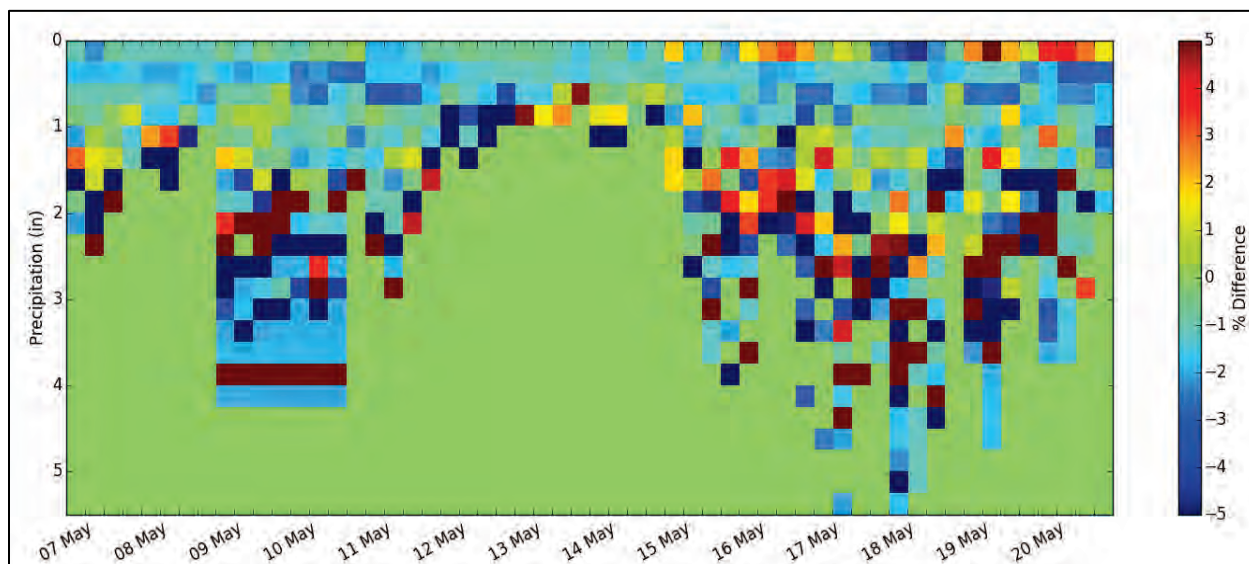
The second transformation of the 1943 event required a 430-mile northward translation. This translation was large enough to require accounting for the convergence of meridians as the north coordinate increased. As a storm is translated northward in an equal-area projection, its original areal extent (using Albers Equal Area Projection) is preserved, but it covers an increasing number of 0.1° grid cells that are in un-projected latitude and longitude. When the grid is resampled back to 0.1° postings, a single depth value can influence more than one 0.1° grid cell.

This spreading occurs because an equal-area cell moved northward across the converging meridians covers more than a single 0.1° cell. When a constant-area feature is translated northward over a distance of 430 miles, it requires almost 10% more 0.1° cells to represent its east-west extent. Therefore, up to a 10% increase in cell count can be expected for this grid transformation without a change in area of the feature, and a cell-count-based analysis was inadequate for analysis of the 1943 event.

Instead, a volume-based analysis was selected, computing the precipitation volume (cubic meters) for each cell in the grid (multiplying the area by the depth). A Python program was written to compute the areas of the grid cells and resulting precipitation volumes. The program then summed the volume occurring within each 0.25 in. bin from 0.00 to 5.00 in., presenting the results in cubic meters.

The differences in volume for each bin were then computed between the rotated and translated grid and the original grid. The percent difference for each bin was computed by dividing this difference by the corresponding volume in the corresponding bin of the original grid. Plots were created for each storm that summarized the percent difference of volume between each transformed grid and original grid over each storm event. A sample is shown in Figure 2-65.

Figure 2-65. Summary of percent volume difference between the transformed and original grids for the 1943 event.



This figure shows percent difference of volume rather than total volume. The highest absolute values in each grid represented very small percentages of the total area and total volume of the grid. The errors shown near the horizontal axis correspond to large precipitation values. However, the total volume of those individual grid cells is small, resulting in a small total volume error for each grid. Summary statistics computed for the 1943 event are shown in Table 2-14.

Table 2-14. Volume percent difference summary statistics for 1943 event transposition.*

	1943 Event: 430 miles, 14.5°	1943 Event: 105 miles, 21.0°
Minimum	-2.51%	-2.21%
25% percentile	-1.53%	-1.68%
50% percentile (median)	-1.31%	-1.43%
75% percentile	-0.98%	-1.14%
Maximum	-0.56%	-0.67%

***Note**

The maximum value represents the minimum absolute error (i.e., the best volume conservation).

Analysis of these plots, while showing some scatter, confirmed that the resampling option using the 1.15 search radius option yielded the best overall results (lower bias and reduced outliers) when using the volume-based comparison method. Note: the interpolation method was not changed, only the analysis method. Either count-based or volume-based methods are sufficient to choose the best interpolation option.

2.9.7 Quality assurance: Volume conservation

Analysis of the data for the 1938 and 1943 storms found that the HEC-MetVue rotation and translation process performed very well, preserving the shapes and magnitudes of the precipitation features, and therefore preserving the volumes. Volume conservation within individual cells was generally within 1%. The transformations performed particularly well during the storm peaks, when volume conservation matters most. Toward the end of the storms, as the clouds break up, the original and transformed precipitation grid maps show spatial fragmentation of the precipitation patterns. Rather than a smooth spatial trend toward one or more large peaks, many small peaks are spread across the grid. Any interpolation method will tend to slightly attenuate peaks, particularly where a grid cell contains a larger precipitation value, surrounded by lower

precipitation values in the neighboring cells. Therefore, the grids during these periods result in transformations that do not perform as well as during the storm peaks. However, the relatively small volume error contributed to the full storm event is negligible.

The analysis outlined above was applied to the full data set for the 1938 and 1943 storm events using nearest neighbor resampling and the 1.15 option. The results for each grid were written to an ASCII file, named PREC_YYYYMMDDHH000000_PercentVolumeDifferences_NNmi_NNdegCW.dat. These files are available in the supplemental data to this report. The minimum and maximum error for each grid, along with the best interpolation option are summarized for each bin level in one file per each grid. These files are named PREC_YYYYMMDDHH000000_MaxPercentVolumeDifferences_NNmi_NNdegCW.dat.

Finally, a single summary file, VolumeSummary.txt, was prepared, extracting total computed volume from each file of percent volume differences. A VolumeSummary.txt file was prepared for the original grids and for each (unclipped) transformation data set. These appear at the end of the file lists in each data set's directory. The VolumeSummary.txt files were then used to compute the percent volume differences for the full data sets of the 1938 and 1943 storms. The total precipitation volumes and the percent volume differences for each event are shown in Table 2-15. Total volume conservation was 1.84% for the 1938 event and within 1.41% for the 1943 event.

Table 2-15. Summary of total precipitation volume conservation.*

Event	Grid	Total Event Volume (m ³)	Volume Difference (m ³)	Percent Volume Difference (%)
1938	Original	1.65939E+11	--	--
1938	Transformed: 90 miles N, 20 deg clockwise (CW)	1.62882E+11	-3.06000E+09	-1.84
1943	Original	3.37531E+11	--	--
1943	Transformation #5: 430 miles N, 14.5 deg CW	3.32786E+11	-4.74000E+09	-1.41
1943	Transformation #6: 105 miles N, 21.0 deg CW	3.33268E+11	-4.26000E+09	-1.26

*Note: Volumes computed for the 1938 and 1943 events (original and transformed grids) using nearest neighbor resampling and the 1.15 option).

Summary of Python modules and scripts

A list of python scripts developed for the analysis and post processing of the transposed ASCII grids are described in Table 2-16.

Table 2-16. Python scripts developed to transpose storms.

Python Script Name	Description
animateGrids.py	Generate animations of precipitation grids. This program reads in grids stored in ESRI ASCII grid format, plots the grids, and saves an animation file in *.mp4 or *.avi format.
asc2grid.py	Module that reads and writes ESRI ASCII grids and performs a number of useful grid functions. ASCII grids loaded into Python are stored in an "ascgrid" object that contains a gridded data array and information from the ASCII header, including grid extents and coordinates. Latitude and longitude coordinate arrays are created to facilitate extracting, plotting, and analyzing data.
checkGrids.py	This module contains basic QA functions to verify grids. The compare function compares two grids to see if they are identical. The stats function computes basic grid statistics.
clipGrids.py	This module contains functions to trim ESRI ASCII grid files to specified extents. The user inputs the desired header info. This module then generates a new file with this header and a subset of the data extracted to match the extents specified in the new header.
extractVolumePctDiffOption.py	Compute percent volume differences between original and transformed grids.
gridTranslateRotateMetVue.py	This script automates HEC-MetVue to perform grid rotation and translation.
makeComparisonSummary.py	Generate summaries of the individual comparisons.
plotGrids.py	Plot precipitation grid maps for a specified precipitation range and a date/time window.
qaGrids.py	Perform QA/QC on transformed precipitation grids. This compares the transformed grids to the original grids, computing volumes of precipitation by bin for a specified range of bins and a specified date/time window.
volumeSummary.py	Compute volume summaries of a set of grids for a specified date/time window. This script generates a file named VolumeSummary.txt

The workflow for processing grid files follows the sequence below.

1. Create translated and rotated grids.
 - a. gridTranslateRotateMetVue.py (creates translated and rotated grids)
2. Perform QA/QC on the grids. Perform this step before clipping (trimming) the grids to the original grid and watershed boundaries.
 - a. qaGrids.py (operates on untrimmed transformed grids)
3. Clip the grids transformed grids to the original grid and watershed boundaries.
 - a. clipGrids.py (creates final trimmed transformed grids)
4. Compute the percent volume differences between the original and transformed grids. This step depends on having run qaGrids.py.
 - a. extractVolumePctDiffOption.py
 - b. This generates files named
PREC_<date>_PercentVolumeDifferences_<options>.dat
5. Compute the volume summaries.
 - a. volumeSummary.py

USACE Districts

LRL	= Louisville District
LRN	= Nashville District
MVK	= Vicksburg District
MVR	= Rock Island District
MVS	= St. Louis District
NWD-MR	= Northwestern Division Missouri River
NWK	= Kansas City District
NWO	= Omaha District
SWF	= Fort Worth District
SWL	= Little Rock District
SWT	= Tulsa District
TVA	= Tennessee Valley Authority

2.10 Reservoir regulation effects

PDF hydrology from the 1955 Study began using unregulated flows calculated by applying unit hydrograph theory, observed historic flow data, and hydrologic routing. The outputs from this analysis were generally in the form of peak discharges with some hydrographs documented at key locations along the main-stem Mississippi River. Reservoir effects were based on a determination of the percentage reduction that would result from the EN Group described in Section 3.9. The MRC (1955) report did not document development of regulated outflow values from each reservoir listed under the EN Group (151 reservoirs in total). However, each USACE entity at the time was asked to provide percentage reductions from each major tributary system, which included any effects from reservoirs in the EN Group. Of the original 151 reservoirs listed in the EN Group, some were not constructed while others that were in the D group (distant future) have actually been constructed (Table 1-9). For this reason, current analyses considered only reservoirs that have been constructed to date, circa 2014.

For the 2016 PDF assessment, reservoir effects were assessed by coordinating with each USACE region. While using percentage reductions as a way to capture reservoir effects was plausible for adjusting peak flow, this method was not appropriate where continuous flow hydrographs are required for unsteady flow models. Therefore, reservoir routings were performed to provide the full hydrographs needed by the unsteady flow models.

2.10.1 Reservoir Selection

Each USACE region made a qualitative evaluation to determine which reservoirs should be included in routing computations to determine regulated outflows for each HYPO storm combination based on the HYPO storm precipitation maps and known tributary travel time to the Lower Mississippi River/Gulf of Mexico. Reservoirs were selected based on their flood storage capacity, location relative to major rivers and other reservoirs, and release travel time to the Lower Mississippi River. The reservoirs identified in this manner were included in detailed routing computations by each respective USACE District. Reservoirs located outside of a 30-day tributary travel time to the Gulf of Mexico were deemed unlikely to have any reduction effect on a flood occurring on the Lower Mississippi River; however, CHPS-FEWS, RES-SNGL, and RES-J configurations were utilized to model reservoirs beyond the 30-day travel time to generate hydrograph inputs needed for the hydraulic model of the Lower Mississippi River. Some reservoirs were included in the detailed USACE routing computations even though they were screened out as having no expected impact on main-stem Mississippi River flows. Such is the case for several large reservoirs located on the Upper Missouri River.

Models

CWMS	= Corps Water Management System
HEC-ResSim	= Reservoir System Simulation
HEC-HMS	= Hydrologic Modeling System
MFP	= Meteorological Forecast Processor
CHPS	= Community Hydrologic Prediction System
FEWS	= Deltares Flood Early Warning System

These reservoirs were included because of their perceived impacts to capture any possible effects from their operation.

Reservoir effects for the updated hydrology were calculated using available models and techniques. Reservoirs expected to have significant potential to reduce flood peaks were modeled by the respective USACE or TVA offices as indicated in Table 2-17. USACE and NWS reservoirs modeled in the current analysis are shown in Figure 2-66 along with the travel time to the Gulf of Mexico. State-by-state reservoir maps are available in Appendix I.

Table 2-17. Reservoirs modeled to determine regulated outflows for HYPO storms.

Reservoir	1955 Group	Drainage Basin	Flood Control Storage (acre-feet)	Tributary	USACE District	NWS-RFC	Model or Techniques to Produce Reservoir Outflow
Barren River	N	1	749,080	Barren River	LRL	OHRFC	CWMS HEC-ResSim Model
Cagles Mill	E	1	200,961	Mill Creek	LRL	OHRFC	CWMS HEC-ResSim Model
CM Harden	N	1	116,615	Big Raccoon Creek	LRL	OHRFC	CWMS HEC-ResSim Model
Green River	N	1	532,925	Green River	LRL	OHRFC	CWMS HEC-ResSim Model
JE Roush	D	1	153,100	Wabash River	LRL	OHRFC	CWMS HEC-ResSim Model
Mississinewa	D	1	345,044	Mississinewa River	LRL	OHRFC	CWMS HEC-ResSim Model
Monroe	-	1	258,760	Salt Creek	LRL	OHRFC	CWMS HEC-ResSim Model
Nolin River	N	1	545,559	Nolin River	LRL	OHRFC	CWMS HEC-ResSim Model
Patoka	-	1	153,170	Patoka River	LRL	OHRFC	CWMS HEC-ResSim Model
Rough River	N	1	306,880	Rough River	LRL	OHRFC	CWMS HEC-ResSim Model
Salamonie	D	1	252,393	Salamonie River	LRL	OHRFC	CWMS HEC-ResSim Model
Barkley	N	1	1,429,440	Cumberland River	LRN	OHRFC	CWMS (HEC-ResSim)
Center Hill	E	1	1,253,890	Cumberland River	LRN	LMRFC	CWMS (MFP, HMS, and HEC-ResSim)
Cheatham	-	1	104,000	Cumberland River	LRN	LMRFC	CWMS (MFP, HMS, and HEC-ResSim)
Cordell Hull	-	1	310,900	Cumberland River	LRN	LMRFC	CWMS (MFP, HMS, and HEC-ResSim)
Dale Hollow	E	1	849,266	Cumberland River	LRN	LMRFC	CWMS (MFP, HMS, and HEC-ResSim)
J. Percy Priest	-	1	383,404	Cumberland River	LRN	LMRFC	CWMS (MFP, HMS, and HEC-ResSim)

Reservoir	1955 Group	Drainage Basin	Flood Control Storage (acre-feet)	Tributary	USACE District	NWS-RFC	Model or Techniques to Produce Reservoir Outflow
Kentucky	E	1	4,008,000	Tennessee River	LRN	LMRFC	CWMS (HEC-ResSim)
Old Hickory	-	1	467,000	Cumberland River	LRN	LMRFC	CWMS (MFP, HMS, and HEC-ResSim)
Wolf Creek	E	1	4,236,323	Cumberland River	LRN	LMRFC	CWMS (MFP, HMS, and HEC-ResSim)
Arkabutla	E	7	493,800	Yazoo River	MVK	LMRFC	HEC-ResSim
Blakely Mt	E	7	617,400	Ouachita River	MVK	LMRFC	HEC-ResSim
Degray	D	7	227,200	Caddo River	MVK	LMRFC	HEC-ResSim
Enid	E	7	602,400	Yazoo River	MVK	LMRFC	HEC-ResSim
Grenada	E	7	1,251,700	Yazoo River	MVK	LMRFC	HEC-ResSim
Narrows	E	7	128,200	Little Missouri River	MVK	LMRFC	HEC-ResSim
Sardis	E	7	1,461,900	Yazoo River	MVK	LMRFC	HEC-ResSim
Coralville	E	2	461,200	Iowa River	MVR	NCRFC	HEC-ResSim
Red Rock	N	2	1,436,000	Des Moines River	MVR	NCRFC	HEC-ResSim
Saylorville	D	2	567,400	Des Moines River	MVR	NCRFC	HEC-ResSim
Carlyle	N	7	699,900	Kaskaskia River	MVS	NCRFC	HEC-ResSim
Mark Twain	N	2	884,000	Salt River	MVS	NCRFC	HEC-ResSim
Shelbyville	D	7	474,000	Kaskaskia River	MVS	NCRFC	HEC-ResSim
Wappapello	E	7	582,200	St. Francis River	MVS	LMRFC	HEC-ResSim
Big Bend	D	1	177,000	Missouri River	NWD-MR	MBRFC	Legacy Program to Balance 6 Reservoir System

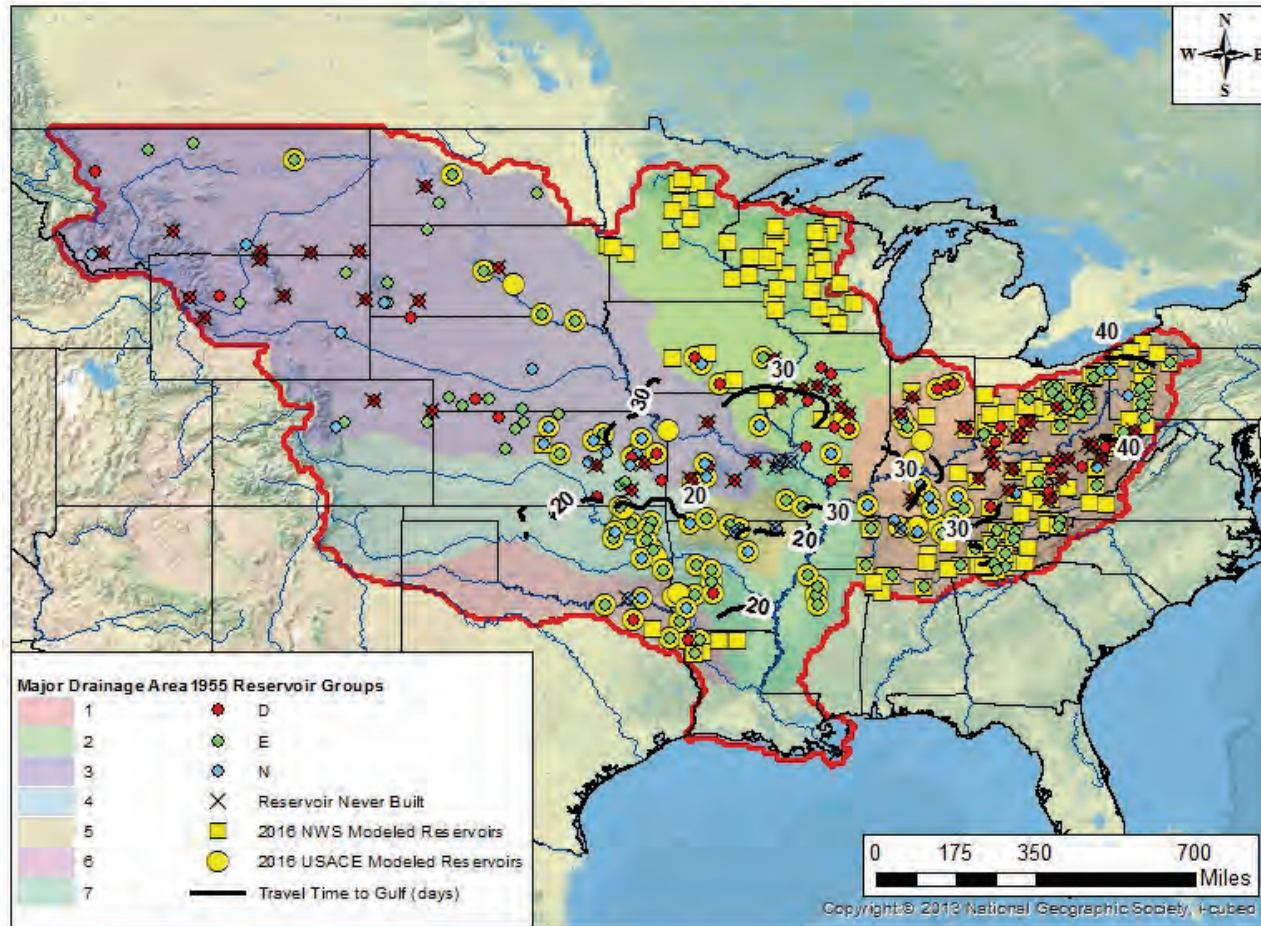
Reservoir	1955 Group	Drainage Basin	Flood Control Storage (acre-feet)	Tributary	USACE District	NWS-RFC	Model or Techniques to Produce Reservoir Outflow
Fort Peck	E	3	3,675,000	Missouri River	NWD-MR	MBRFC	Legacy Program to Balance 6 Reservoir System
Fort Randall	E	3	2,294,000	Missouri River	NWD-MR	MBRFC	Legacy Program to Balance 6 Reservoir System
Garrison	E	3	5,711,000	Missouri River	NWD-MR	MBRFC	Legacy Program to Balance 6 Reservoir System
Gavins Point	E	3	143,000	Missouri River	NWD-MR	MBRFC	Legacy Program to Balance 6 Reservoir System
Oahe	E	3	4,303,000	Missouri River	NWD-MR	MBRFC	Legacy Program to Balance 6 Reservoir System
Clinton	-	3	292,500	Kansas River	NWK	MBRFC	HEC-ResSim
Hillsdale	D	3	86,500	Osage River	NWK	MBRFC	HEC-ResSim
Kanopolis	E	3	365,000	Kansas River	NWK	MBRFC	HEC-ResSim
Melvern	D	3	209,000	Osage River	NWK	MBRFC	HEC-ResSim
Milford	N	3	758,000	Kansas River	NWK	MBRFC	HEC-ResSim
Perry	N	3	515,500	Kansas River	NWK	MBRFC	HEC-ResSim
Pomme de Terre	N	3	406,800	Osage River	NWK	MBRFC	HEC-ResSim
Pomona	N	3	184,000	Osage River	NWK	MBRFC	HEC-ResSim
Rathbun	D	3	349,500	Chariton River	NWK	MBRFC	HEC-ResSim
Smithville	-	3	101,800	Little Platte River	NWK	MBRFC	HEC-ResSim
Stockton	D	3	776,000	Osage River	NWK	MBRFC	HEC-ResSim
Truman	N	3	4,009,000	Osage River	NWK	MBRFC	HEC-ResSim
Tuttle Creek	E	3	884,000	Kansas River	NWK	MBRFC	HEC-ResSim

Reservoir	1955 Group	Drainage Basin	Flood Control Storage (acre-feet)	Tributary	USACE District	NWS-RFC	Model or Techniques to Produce Reservoir Outflow
Waconda	N	3	723,000	Kansas River	NWK	MBRFC	HEC-ResSim
Wilson	N	3	530,000	Kansas River	NWK	MBRFC	HEC-ResSim
Cooper	D	6	130,361	Red River	SWF	LMRFC	SWF does not have to perform routing: provided simple outflow relationships applicable for the Mississippi River PDF storms.
Lake O' the Pines	-	6	580,000	Red River	SWF	LMRFC	SWF does not have to perform routing: provided simple outflow relationships applicable for the Mississippi River PDF storms.
Wright Patman	E	6	2,509,000	Red River	SWF	LMRFC	SWF does not have to perform routing: provided simple outflow relationships applicable for the Mississippi River PDF storms.
Beaver	N	5	300,000	White River	SWL	LMRFC	Legacy Spreadsheet
Bull Shoals	E	5	2,360,000	White River	SWL	LMRFC	Legacy Spreadsheet
Greers Ferry	N	5	934,000	White River	SWL	LMRFC	Legacy Spreadsheet
Norfork	E	5	732,000	White River	SWL	LMRFC	Legacy Spreadsheet
Table Rock	E	5	760,000	White River	SWL	LMRFC	Legacy Spreadsheet
Copan	-	4	184,075	Little Caney River	SWT	ABRFC	Spreadsheet
Eufaula	N	4	1,350,326	Canadian River	SWT	ABRFC	Spreadsheet
Fort Gibson	E	4	919,200	Arkansas River	SWT	ABRFC	Spreadsheet
Heyburn	E	4	49,144	Polecat Creek	SWT	ABRFC	Spreadsheet
Hula	E	4	246,955	Caney River	SWT	ABRFC	Spreadsheet
Hugo	N	6	809,100	Red River	SWT	ABRFC	Spreadsheet

Reservoir	1955 Group	Drainage Basin	Flood Control Storage (acre-feet)	Tributary	USACE District	NWS-RFC	Model or Techniques to Produce Reservoir Outflow
Keystone	N	4	1,219,000	Arkansas River	SWT	ABRFC	Spreadsheet
Oologah	E	4	966,000	Arkansas River	SWT	ABRFC	Spreadsheet
Pensacola	E	4	525,000	Arkansas River	SWT	ABRFC	Spreadsheet
Skiatook	-	4	182,000	Arkansas River	SWT	ABRFC	Spreadsheet
Tenkiller	E	4	576,700	Arkansas River	SWT	ABRFC	Spreadsheet
Texoma	E	6	2,660,000	Red River	SWT	ABRFC	Spreadsheet
Wister	E	4	365,960	Arkansas River	SWT	ABRFC	Spreadsheet
Boone	-	1	216,147	South Fork Holston River	TVA	LMRFC	Riverware and CHPS-FEWS (TVA version)
Cherokee	E	1	749,400	Holston River	TVA	LMRFC	Riverware and CHPS-FEWS (TVA version)
Chickamauga	E	1	347,000	Tennessee River	TVA	LMRFC	Riverware and CHPS-FEWS (TVA version)
Douglas	E	1	1,081,900	French Broad River	TVA	LMRFC	Riverware and CHPS-FEWS (TVA version)
Fort Loudoun	E	1	231,000	Tennessee River	TVA	LMRFC	Riverware and CHPS-FEWS (TVA version)
Fort Patrick Henry	-	1	31,728	South Fork Holston River	TVA	LMRFC	Riverware and CHPS-FEWS (TVA version)
Great Falls	-	1	64,800	Caney Fork River	TVA	LMRFC	Riverware and CHPS-FEWS (TVA version)
Guntersville	E	1	162,100	Tennessee River	TVA	LMRFC	Riverware and CHPS-FEWS (TVA version)
Melton Hill	-	1	150,708	Clinch River	TVA	LMRFC	Riverware and CHPS-FEWS (TVA version)
Nickajack	-	1	402,549	Tennessee River	TVA	LMRFC	Riverware and CHPS-FEWS (TVA version)
Norris	E	1	1,113,000	Clinch River	TVA	LMRFC	Riverware and CHPS-FEWS (TVA version)
Ocoee1	-	1	79,320	Ocoee River	TVA	LMRFC	Riverware and CHPS-FEWS (TVA version)
Ocoee2	-	1		Ocoee River	TVA	LMRFC	Riverware and CHPS-FEWS (TVA version)

Reservoir	1955 Group	Drainage Basin	Flood Control Storage (acre-feet)	Tributary	USACE District	NWS-RFC	Model or Techniques to Produce Reservoir Outflow
Ocoee3	-	1	7,932	Ocoee River	TVA	LMRFC	Riverware and CHPS-FEWS (TVA version)
Pickwick	E	1	1,546,740	Tennessee River	TVA	LMRFC	Riverware and CHPS-FEWS (TVA version)
South Holston	E	1	252,700	South Holston River	TVA	LMRFC	Riverware and CHPS-FEWS (TVA version)
Tims Ford	-	1	183,000	Elk River	TVA	LMRFC	Riverware and CHPS-FEWS (TVA version)
Watauga	E	1	152,800	Watauga River	TVA	LMRFC	Riverware and CHPS-FEWS (TVA version)
Watts Bar	E	1	379,000	Clinch River	TVA	LMRFC	Riverware and CHPS-FEWS (TVA version)
Wheeler	E	1	326,000	Tennessee River	TVA	LMRFC	Riverware and CHPS-FEWS (TVA version)
Wilbur	-	1	873	Watauga River	TVA	LMRFC	Riverware and CHPS-FEWS (TVA version)
Wilson	N	3	530,000	Saline River	TVA	LMRFC	Riverware and CHPS-FEWS (TVA version)

Figure 2-66. 2016 reservoirs modeled in current analysis.*



*Note: Symbols illustrate which agency's modeling efforts addressed regulation effects of reservoirs; they do not indicate the agency responsible for daily operations of those projects.

Other reservoirs that were expected to have minor or no impact were modeled by the NWS using its existing RES-SNGL (single reservoirs) or RES-J (single reservoirs and systems of reservoirs) configurations in CHPS-FEWS.

2.10.2 Reservoir routing

Detailed reservoir routing was accomplished using current water management plans to determine gate and pool operations. Antecedent pool conditions assumed the project was at the established guide curve at the start of the event. Each project was evaluated to develop regulated releases by applying the established rule curves in a general sense. While it would have been possible to route each event with the intention of maximizing or optimizing the regulation effect, it was determined that such analysis would not be consistent with how a water manager would operate the project during an actual event. This was because a water manager would effectively know the future for the PDF simulations; that would not be the case should an actual event occur that might have characteristics of the PDF.

There was a multi-step process required to produce the final regulated outputs from the NWS hydrologic models. First, the NWS RFCs produced model outputs at each reservoir for project inflow and local contributions. These outputs were then provided to each USACE office for use as input to their regulation computations. Each USACE office had water management staff members perform the regulation based on their experience with floods and the projects' operating guide curves. For projects in sequence, the regulation included joint operations. Finally, the regulated outflows from each USACE office were then passed to the respective RFC for input to models and simulation of the final regulated run. Each respective entity provided the regulation and routing for reservoirs under their control.

The current CHPS-FEWS models include various reservoirs with configurations that vary by RFC. Some of the configurations provided a simplified means to route events through the outlets; others required input of observed reservoir releases. Many of the reservoirs that exist today did not exist when the historic storms occurred. Table 2-18 gives a list of reservoirs and the dates when regulation began for select reservoirs, where historical and actual project release data are required for the three storms that make up the HYPO 58A storm.

Table 2-18. Reservoirs and impoundment dates for ABRFC and MBRFC.*

River	Reservoir	Date Impoundment Started	Owner/Operator
North Platte River	Pathfinder	1909	USBR
North Platte River	Seminole Dam	1939	USBR
Fourche La Fave River	Nimrod	1942	SWL
White River	Norfork	1944	SWL
Petit Jean River	Blue Mountain	1947	SWL
Black River	Clearwater	1948	SWL
Heart River	Heart Butte Dam	1949	USBR
White River	Bull Shoals	1951	SWL
White River	Table Rock	1957	SWL
Little Red River	Greers Ferry	1965	SWL
White River	Beaver	1966	SWL
Missouri River	Fort Peck	Jun-37	NWO
Wolf Creek	Fort Supply	May-42	SWT
Red River	Colbert & Texoma	Jan-44	SWT
Tennessee River	Kentucky Dam	Aug-44	TVA
Smoky Hill River	Kanopolis	Feb-48	NWK
North Canadian River	Canton	Apr-48	SWT
Fall River	Fall	Aug-48	SWT
Neosho River	Ft. Gibson (FGIB)	Jun-49	SWT
Poteau River	Wister	Oct-49	SWT
Cumberland River	Barkley Dam	Jul-64	LRN
Neosho River	Langly (Pensacola Dam)	? 1941	SWT

***Notes**

USBR = United States Bureau of Reclamation
 SWL = Little Rock District
 NWO = Omaha District
 SWT = Tulsa District
 LRN = Nashville District

Reservoir routings performed for the current assessment were done using a general approach based upon each project's Water Control Manual. The reservoir routings were not optimized to achieve the maximum possible reduction in peak flow as represented in the 1955 report. This approach was used because it mimics what might occur during an actual event. Without a priori knowledge of future rainfall (as is the case for the HYPO

storms used in the 2016 analyses), it is not possible to optimize reservoir operations. The following sections provide details of reservoir regulation utilized for the current analysis.

2.10.2.1 NWK USACE

NWK utilized an existing HEC-ResSim model to route inflows provided by MBRFC to develop reservoir releases. NWK and MBRFC developed the procedure for a two-phase exchange between USACE and NWS modelers. This procedure included use of unregulated local and inflow hydrographs from the NWS as well as a secondary NWS model output that captured zero releases from the reservoirs to calculate local flows for the HEC-ResSim model. Unregulated inflows and local flows were used to develop regulated releases for joint reservoir operations.

The Osage River Basin has six USACE reservoirs: Melvern, Pomona, Hillsdale, Stockton, Pomme De Terre, and Truman. The first five lakes operate in tandem with Truman. Flood control releases are based on phase 1, 2, and 3 release targets at each dam and specific downstream targets, which are Marais Des Cygnes River near Pomona, KS, and Marais Des Cygnes River near Ottawa, KS (targets for Melvern and Pomona); Marais Des Cygnes River near Kansas-Missouri State Line, KS (target for Melvern, Pomona, and Hillsdale); Pomme de Terre River near Hermitage, MO (target for Pomme de Terre); Sac River at Highway J below Stockton, MO and Sac River near Caplinger Mills, MO (targets for Stockton); Osage River below Saint Thomas, MO, and Missouri River at Hermann, MO (targets for Truman). In addition, the five upstream lake projects must operate according to a tandem balance curve with Truman.

The Kansas River Basin includes the Lower Kansas River projects (Milford, Tuttle Creek, Perry, and Clinton Lakes) and the most downstream Smoky Hill River Basin projects (Kanopolis, Wilson, and Waconda Lakes). The Lower Kansas River projects and Smoky River Basin projects are operated as distinctly separate systems within the model. The Smoky Hill Basin lakes are believed too far upstream to provide significant flood management operation for the downstream Lower Kansas Basin. Therefore, the most downstream control point designated for Kanopolis, Wilson, and Waconda is the Enterprise gage on the Smoky Hill River. The Lower Kansas River projects are operated primarily for a Waverly control point on the Missouri River downstream of Kansas City.

The Little Platte Basin includes only one reservoir project with a relatively simple operation methodology. Smithville Dam is at RM 13.5 of the Little Platte River. The river flows to a confluence with the Platte River. The Platte River flows southeast to a confluence with the Missouri River near Leavenworth, KS. Two control points, one on the Little Platte River at Smithville and one on the Platte River at Sharp Station, are considered during flood operation. There are also backwater effects at the Platte, Little Platte confluence that may restrict flood water evacuation.

The Chariton River Basin includes one USACE reservoir that operates independently of the Missouri River. Rathbun Dam is located at RM 142.3 on the Chariton River, a left bank tributary of the Missouri River. There are three control points downstream of the dam at the following locations: Moulton, IA; Novinger, MO; and Prairie Hill, MO.

2.10.2.2 NWO USACE

NWO used an existing reservoir operations model to route inflows through the Missouri River mainstem projects to develop reservoir releases. The legacy FORTRAN program includes the six Missouri River mainstem dams; Fort Peck, Garrison, Oahe, Big Bend, Fort Randall, and Gavins Point. Unregulated, incremental inflows were developed by the NWS for each reservoir reach. The program balances inflow, storage, and releases for the six reservoirs based upon joint operational guide curves and project objectives. Releases from Gavins Point Dam, the lowermost reservoir in the mainstem system, were provided to the NWS for continued routing down the Lower Missouri River.

2.10.2.3 MVR USACE

MVR used an existing HEC-ResSim model for the Des Moines and Iowa River Basins. Both of these models have been in use by the district for over a decade to help communicate operational decisions. These models are commonly referred to as the district's *full-basin* models and include inflow junctions for all major tributaries as well as all control points outlined in the corresponding regulation manuals. For this analysis, Coralville Reservoir was evaluated on the Iowa River while Saylorville and Red Rock were evaluated on the Des Moines River.

To run the events for the Flowline assessment, inflows for each of the three reservoirs and all tributaries were used from the NCRFC. The HEC-ResSim

models were mapped to use these flows, and the models were run to compute the resulting flows throughout each basin. Due to MVR being situated along the northern part of the Mississippi River Basin, the HYPO events were not necessarily very large within the district. The model results showed no problem in maintaining normal pool elevations as well as normal flows throughout the Iowa and Des Moines Basins. In fact, downstream constraints were rarely engaged in any of the many events that were evaluated. These results were then sent back to the NCRFC so further modeling could be performed. The final results were then given to the Flowline assessment team.

The models used in this analysis have been used for many years and have been calibrated over many events in real-time. For this reason the data were simply run through the model without the need for any major assumptions or manual overrides performed by the modeler. The results were plotted and visually evaluated and were found to be very reasonable.

2.10.2.4 MVK USACE

MVK used existing HEC-ResSim models to develop reservoir outflows using LMRFC local and reservoir inflow hydrographs. Arkabutla, Sardis, Enid, and Grenada Lakes are operated using seasonal guide curves with maximum release rates depending upon the time of year as shown in Table 2-19.

Table 2-19. Vicksburg reservoir maximum release rates by season.

Reservoirs	Crop Season Release Rates, cfs (March 15 - November 1)	Non-Crop Season Release Rates, cfs (November 1- March 15)
Arkabutla	1,500	5,000
Sardis	4,500	6,350
Enid	1,500	2,400
Grenada	3,000	5,100

The only way releases would be higher than what is listed above is if the pool rose above the spillway elevations where uncontrolled releases would begin.

The Ouachita Basin reservoirs are all operated for hydropower production. The reservoirs are operated to release water only through the hydropower

turbines unless the pool rises into the flood control pools at which time the flood control gates would be utilized to get the pool back into the hydropower pool. Turbine capacities are 7,000 cfs at Blakely; 6,000 cfs at Degray; and 6,000 cfs at Narrows unless the spillways are overtopped. The model is set up to release up to flood control capacity if the pool rises into the flood control pool.

2.10.2.5 LRL USACE

Reservoir regulation for the Green River Basin was performed using the HEC-ResSim model that resides within the Green River Basin CWMS model. This model includes Barren River, Green River, Rough River, and Nolin River reservoirs. The HEC-ResSim model contains the same sub-basin delineation utilized by the Ohio RFC. Inflows into the projects and uncontrolled downstream flows were provided by the Ohio RFC and imported into the HEC-ResSim model. Inflows were routed through each of the projects using the rules established in the HEC-ResSim model that are based on the criteria specified in each project's water control plan. Antecedent pool elevations at each of the projects were determined based on the time-series data provided by the OHRFC and the corresponding target pool elevation shown on each project's guide curve. Reservoir routing results were reviewed internally by LRL water management staff, revised if necessary, and the routed outflows from each project were provided to the OHRFC for further routing downstream.

Reservoir regulation for the Wabash River Basin was performed using the HEC-ResSim model that resides within the Wabash River Basin CWMS model. This model includes J. E. Roush, Salamonie, Mississenewa, Cagles Mill, C. M. Harden, Monroe, and Patoka Reservoirs. The HEC-ResSim model contains the same sub-basin delineation utilized by the OHRFC. Inflows into the projects and uncontrolled downstream flows were provided by the OHRFC and imported into the HEC-ResSim model. Inflows were routed through each of the projects using the rules established in the HEC-ResSim model, which are based on the criteria specified in each project's water control plan. Antecedent pool elevations at each of the projects were determined based on the time-series data provided by the OHRFC and the corresponding target pool elevation shown on each project's guide curve. Reservoir routing results were reviewed internally by LRL water management staff, revised if necessary, and the routed outflows from each project were provided to the OHRFC for further routing downstream.

2.10.2.6 LRN USACE

LRN utilized CWMS (MFP, HEC-HMS, and HEC-ResSim) to route flows through the Cumberland River System, including regulation at Wolf Creek, Dale Hollow, Cordell Hull, Center Hill, Old Hickory, J. Percy Priest, and Cheatham Dams. To run CWMS, LRN used the unregulated inflows from the OHRFC model as inputs into the CWMS model. These inflows essentially served as the MFP and HEC-HMS inputs and were routed through the system through the list of dams provided above using HEC-ResSim.

For the reaches below Cheatham Dam on the Cumberland River and below Pickwick Dam on the Tennessee River, LRN used the CWMS (based on HEC-ResSim) outflows from Cheatham Dam as the upstream input in the Barkley Dam reach. LRN also used outflows from Pickwick Dam (provided by TVA) as the input to the Kentucky Dam Reach. These two inputs were routed through a HEC-HMS model of the Barkley and Kentucky Dam local areas along with local inflows provided by the OHRFC and LMRFC. The results of this HEC-HMS model were then used as inputs into an HEC-RAS model of the Barkley and Kentucky Dam reaches, which is connected by a canal just upstream of each of these dams. Using a Navigation Dams method within HEC-RAS for the Barkley and Kentucky Dam inline structures, the inflows were routed downstream to the Cumberland and Tennessee River reaches flowing into the Ohio River.

An assumption was made that flooding was occurring throughout the event on the Ohio and Mississippi Rivers. Therefore, the Navigation Dams method was optimized to store water at and minimize outflows from these two dams to keep water out of the Ohio and Mississippi Rivers. The problem with this approach was that this ignores the timing of flooding occurring on the Ohio and Mississippi Rivers. Historically, Barkley and Kentucky Dams have been used to release water downstream ahead of Ohio and Mississippi flooding and hold water while flooding is occurring. Ultimately, the assumption and approach may not optimize the use of storage at Barkley and Kentucky Dams, but it does produce the lowest peak outflows from these two dams using a reasonable amount of storage without inducing major damages upstream.

2.10.2.7 SWF USACE

Wright-Patman (Sulphur River) has a simple operation that generally closes the gates once a day. When the elevation is above 240 ft, 10,000 cfs is released.

Table 2-20 shows the release flows for Wright-Patman.

Table 2-20. Daily flow values to use for Wright-Patman releases during HYPO storms.

Date	Reservoir Discharge, cfs
Minimum or starting day's flow	108
Day 1	230
Day 2	550
Day 3	1,100
Day 4	2,000
Day 5	2,825
Day 6	4,000
Day 7	6,000
Day 8	10,000
Subsequent through start of recession	10,000 (maximum)

For HYPO 58A simulations, Wright-Patman immediately released 10,000 cfs at the beginning of the run. Releases remained at 10,000 cfs until the pool was back to an elevation of 226 ft (winter) or 228 ft (summer). Releases stayed at 10,000 cfs for the rest of the simulation unless the Shreveport gage (Red River) was above 31 ft stage. If the Shreveport gage went above a 31 ft stage, Table 2-20 is applied in reverse order until the Shreveport gage is below 31 ft stage.

Lake O' the Pines also operates reservoir releases by stepping up (or down) flows each day. Table 2-21 shows release flows used each day until achieving 2,700 cfs.

Table 2-21. Daily flow values to use for Lake O' the Pines releases during HYPO storms.

Date	Reservoir Discharge, cfs
Current day's flow	50
Day 1 change	275
Day 2	550
Day 3	1,100
Day 4	1,925
Day 5	2,700 (maximum)

Cooper Dam releases could go up to 3,000 cfs Day 1. It also regulates to 6,000 cfs on the South Sulphur River and 34,000 cfs on the Sulphur River at Talco. The elevation of Cooper Dam requires 3,000 cfs releases unless one of the two controls presented above is exceeded. If they are exceeded, the releases will be stopped, and the project will only release when it exceeds an elevation of 446.2 ft.

2.10.2.8 SWT USACE

Hydraulic routing was performed in a simplified manner using spreadsheets for each reservoir. The reservoirs that were modeled — Copan, Hulah, Skiatook, Oologah, Keystone, Pensacola, Fort Gibson, Tenkiller, Wister, Heyburn, and Eufaula on the Arkansas River and Hugo and Denison (Texoma) on the Red River — were included because they were deemed critical to the downstream flows. In other words, releases from these projects have particular influence on flows along the downstream reach of the Arkansas and Red Rivers, respectively. A look-up table was included that incorporated the elevation-volume curve for each of the projects. Inflow hydrographs (obtained from the ABRFC) were then routed through each project using a mass balance approach. Regulation rules for each project were incorporated from the appropriate water control manual.

A 6-hour time-step was used for each computation. During each step, the inflow value was compared with the elevation-volume table, and the corresponding pool elevation was explicitly computed. Both the inflow value and the pool elevation were then compared with the regulation rules

to determine the outflow. The computation was then performed again for each successive time-step.

Computations were performed for each project instead of for the system as a whole. However, the output was then examined by water management staff to ensure that it was consistent with a system operation, and adjustments were made to reflect these recommendations. None of the reservoirs that were modeled were in series with any of the other projects with the exception of Pensacola and Fort Gibson. Since an adjusted hydrograph was provided for Fort Gibson by the ABRFC, no further modification of any of the inflow hydrographs was made. Once outflow hydrographs were computed for each of the reservoirs, they were then returned to the ABRFC for downstream routing.

2.10.2.9 SWL USACE

The White River Reservoirs (Beaver Lake, Table Rock Lake, Bull Shoals Lake, Norfolk Lake, and Greers Ferry Lake) were operated using modified Legacy Spreadsheets for flood routing. The operation of the system followed the current water control plan described in Table 2-22. The inflows provided by the NWS were treated as forecasted inflows that are typically developed by applying forecasted rainfall to the design Unit Hydrographs. Hydropower release requirements, storage balancing, downstream control stages, and surcharge operation rulesets were followed using the spreadsheets while treating the provided inflows as forecasted inflows. Induced surcharge operations commenced when the pool elevation was projected to exceed the top of flood control pool. Reservoir routing and operations were developed using a 6-hour time-step.

Table 2-22. Little Rock District reservoir minimum, maximum, and routine flood control releases.

BEAVER		
Time	Elevation	Criteria
Any time	1120.43 to 1130.00	Release a minimum of firm power when flood control storage is in use at Table Rock and/or Bull Shoals. When minor flood control storage (less than 2 ft) is in use at Table Rock and/or Bull Shoals, greater weight will be given to secondary power generation at Beaver based on powerload conditions at the time. Release a maximum of 15,000 cfs less the tributary inflow between Beaver and Table Rock when flood control storage is not in use at Table Rock and Bull Shoals.
Any time	Above or predicted to exceed 1130.00	Let outflow equal inflow when the flood pool fills, subject to the use of surcharge storage to reduce peak discharges and delay inflow to Table Rock.
Any time	Between firm power rule curve and 1120.43	Release a minimum of firm power when flood control storage is in use at Table Rock and/or Bull Shoals when needed for system peaking purposes, otherwise release zero.
TABLE ROCK		
Time	Elevation	Criteria
Any time	915.0 to 920.0 and Bull Shoals below 684.0	Release 15,000 cfs.
Any time	920.0 to 931.0 and Bull Shoals below 684.0	Release 20,000 cfs.
Any time	Above 915.0 and Bull Shoals above 684.0	Limit release to maintain equal amounts of remaining flood control storage (in acre-feet) in Table Rock and Bull Shoals, insofar as practicable, subject to the minimum release required for firm power.
Any time	Above, or predicted to exceed, 931.0	Regulate to obtain the most effective flood modification with the designated surcharge storage space.
Any time	915.0 to 931.0	Release a minimum of firm power.
BULL SHOALS AND NORFORK		
Time	Elevation	Criteria
1 December to 14 April	Any elevation in flood pool	Regulate Newport to 21 ft. If the natural crest exceeds 21 ft, regulate to the lower of 24 ft or the natural crest.

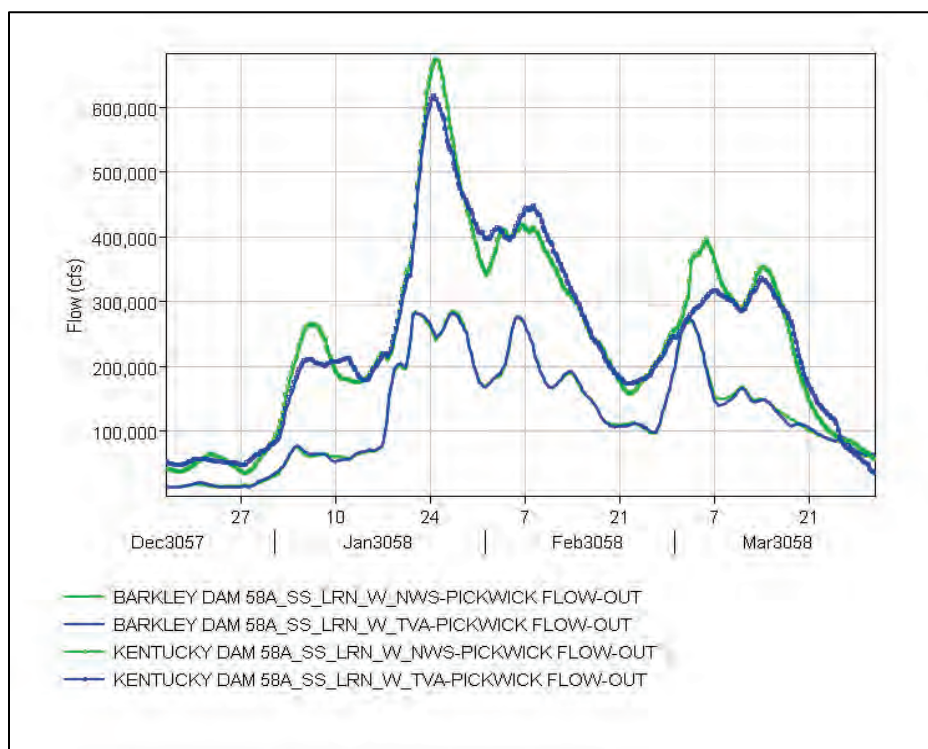
15 April to 30 April	Any elevation in flood pool	Regulate Newport to 14 ft. If the 4-lake system has 50% or more flood storage in use, regulate to 21 ft.
1 May to 7 May	Any elevation in flood pool	Regulate Newport to 14 ft. If the 4-lake system has 50% or more flood storage in use, regulate to 18 ft.
8 May to 14 May	Any elevation in flood pool	Regulate Newport to 12 ft. If the 4-lake system has 50% or more flood storage in use, regulate to 18 ft.
15 May to 30 November	Any elevation in flood pool	Regulate Newport to 12 ft. If the 4-lake system has 70% or more flood storage in use, regulate to 14 ft.
Any time	Any elevation in flood pool	Release a minimum of firm power and in extreme cases zero if a significant reduction in critical downstream flood conditions is possible. Prorate flood control releases between Bull Shoals and Norfolk to maintain equal percentages of available flood control storage in Norfolk and the Beaver - Table Rock - Bull Shoals system, insofar as practicable. Release a maximum of 32,500 cfs from Bull Shoals and 10,500 cfs from Norfolk, subject to a 50,000 cfs flow limit at Batesville. Curtail secondary power generation until 6 days after the crest at Newport (secondary power releases should provide that stages above the regulating stage continue to recede until the regulating stage is reached).
Any time	Above or predicted to exceed the top of the spillway gates	Regulate to obtain the most effective flood modification with the designated surcharge storage space.
GREERS FERRY		
1 December to 14 April	Any elevation in flood pool	Regulate Georgetown to 21 ft. If Newport is being regulated to 24 ft, regulate to 22 feet.
15 April to 30 April	Any elevation in flood pool	Regulate Georgetown to 16 ft. If the 4-lake system has 50% or more flood storage in use, regulate to 21 ft.
1 May to 7 May	Any elevation in flood pool	Regulate Georgetown to 16 ft. If the 4-lake system has 50% or more flood storage in use, regulate to 19 ft.
8 May to 14 May	Any elevation in flood pool	Regulate Georgetown to 13 ft. If the 4-lake system has 50% or more flood storage in use, regulate to 19 ft.
15 May to 30 November	Any elevation in flood pool	Regulate Georgetown to 13 ft. If the 4-lake system has 70% or more flood storage in use, regulate to 16 ft.
Any time	Any elevation in flood pool	Release a minimum of 3,000 cfs or 15,000 cfs less the tributary inflow between Greers Ferry and Judsonia, whichever is less, subject to the minimum release required for firm power. Releases in excess of 10,500 cfs must be used with caution and require prior coordination with the Greers Ferry Project Office. In extreme cases release zero if a significant reduction in critical downstream flood conditions is possible.
Any time	Above or predicted to exceed 487.0	Regulate to obtain the most effective flood modification with the designated surcharge storage space.

2.10.2.10 TVA

TVA utilized an existing RiverWare model to develop HYPO 58A regulated outflows for their reservoir system. The routings were performed using manual regulation for each model time-step to obtain the regulated releases from Pickwick Dam. Pickwick Dam discharges into Kentucky Lake, which was routed in combination with Barkley Dam by the LRN USACE. TVA was only able to route storms through HYPO storm 58A due to time constraints. Fortunately, NWS-LMRFC models the Tennessee River with basic reservoir options for TVA projects but does not include intricate operational rules or joint operation considerations that are included in the TVA modeling.

The LMRFC made runs to generate the Pickwick releases for only the straight sequence HYPO 58A. Their results were then passed to LRN, which made additional runs of the combined Kentucky/Barkley reservoir model. Resulting Kentucky/Barkley outflows using the LMRFC model Pickwick flows were approximately 10% higher than when using the TVA-generated Pickwick flows. Figure 2-67 illustrates the difference in Kentucky/Barkley outflows for the two methods.

Figure 2-67. Kentucky and Barkley LMRFC and TVA routing results.



The two simulations were run in the HEC-RAS unsteady model to see how changes might result along the mainstem Mississippi River. The 10% increase in Kentucky Dam outflow translates into very minor changes at Cairo, IL, and below. The changes are given in Table 2-23. The relative differences between peak flows for NWS and TVA routings on the Ohio and Mississippi Rivers quickly decreases below Kentucky and Barkley Dams because of timing and attenuation due to channel storage. The times when peak outflows at Kentucky and Barkley occur do not align with peak times on the Ohio and Mississippi Rivers. There is also a lag due to travel time along each river.

Table 2-23. Peak flows from HEC-RAS simulation for TVA and NWS regulation methods for Tennessee River, HYPO 58A.

	MVM 58 Regulated StraightSeq A (NWS Pickwick Outflows)	MVM 58 Regulated StraightSeq B (TVA Pickwick Outflows)	Percent Change (NWS vs. TVA)
Tennessee River at Downstream of Kentucky Dam	672,210	617,490	8.86
Cumberland River at Downstream of Barkley Dam	286,371	282,235	1.47
Mississippi at Chester	501,451	501,448	0.00
Mississippi at Cape Girardeau	512,824	513,010	(0.04)
Mississippi at Thebes	514,539	514,854	(0.06)
Ohio River at Cairo	2,303,676	2,331,371	(1.19)
Mississippi at MS OH Confluence	2,767,225	2,793,557	(0.94)
Mississippi at Hickman	2,007,986	1,963,755	2.25
Mississippi at New Madrid	2,543,957	2,526,756	0.68
Mississippi at Tiptonville	2,771,887	2,790,620	(0.67)
Mississippi at Caruthersville	2,330,311	2,332,402	(0.09)
Mississippi at Osceola	2,727,595	2,748,706	(0.77)
Mississippi at Memphis	2,727,899	2,738,423	(0.38)

Further details for TVA models can be found in Section 2.4.10.

2.10.2.11 MVS USACE

MVS used existing HEC-ResSim models to develop reservoir outflows using NCRFC and LMRFC local and reservoir inflow hydrographs. Water control manuals for each reservoir were referenced for guidance and summarized in Table 2-24.

Table 2-24. MVS reservoir release guidance.

Date	Pool Elevation Range (ft) NGVD	Maximum Release (cfs)	Minimum Release (cfs)
Shelbyville			
May 1 - Nov 1	599.7 - 610.0	1,800	10
	610.0 - 626.5	1,800 - 4,500	10
Nov 1 - Dec 15	599.7 - 626.5	4,500	10
Dec 15 - Apr 1	594.0 - 626.5	4,500	10
Apr 1 - May 1	596.0 - 626.5	4,500	10
Carlyle			
May 1 - Nov 1	445.0 - 450.0	4,000	50
	450.0 - 462.5	4,000-10,000	50
Nov 1 - Dec 1	445.0 - 462.5	10,000	50
Dec 1 - Apr 1	443.0 - 462.5	10,000	50
Apr 1 - May 1	444.0 - 462.5	10,000	50
Rend			
Rend Lake is unregulated.			
Wappapello			
Apr 1 - Dec 15	359.7 - 379.7	4,200	40
	379.7 - 394.7	constant 10,000	40
Dec 15 - Apr 1	354.7 - 379.7	10,000	40
	379.7 - 394.7	constant 10,000	40
Mark Twain			
Apr 1 - Nov 1	606.0 - 615.0	10,000 dsf	50
	615.0 - 638.0	12,000 dsf	50
Nov 1 - Apr 1	606.0 - 638.0	12,000 dsf	50

2.10.3 Reductions from standard reservoir operations

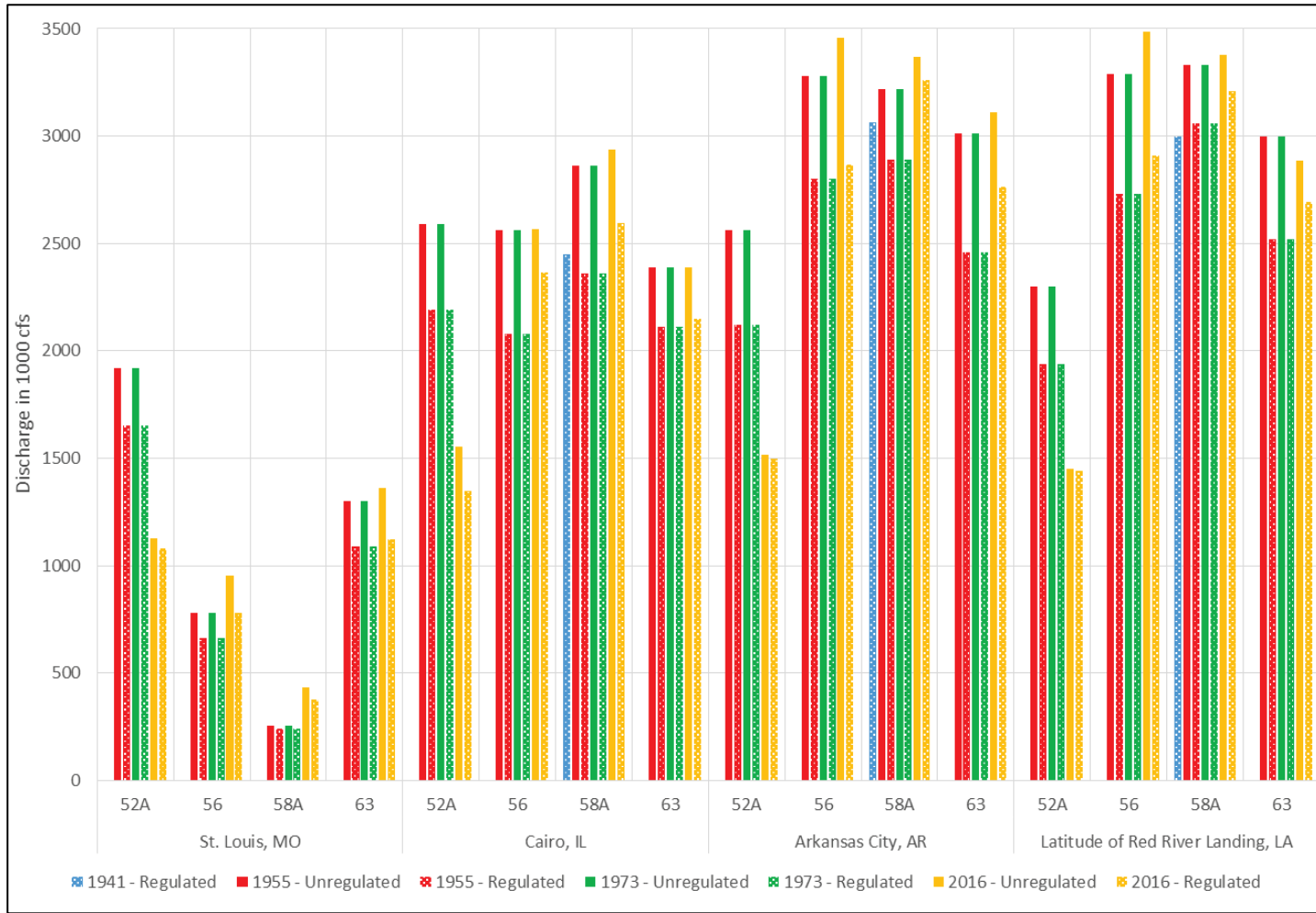
The reductions due to reservoir regulation were evaluated by calculating the difference between peak flows (regardless of times when peaks actually occurred) for the unregulated and regulated discharge hydrographs. This calculation was made for peaks published in USACE MRC (1955) and at those same locations for the current assessment. Table 2-25 lists the calculated percent reductions and differences between the 1955 and 2016 flow reductions.

Figure 2-68 shows the differences calculated for each of the four HYPO storms for each location.

Table 2-25. Reservoir peak flow reductions in percent for four HYPO storms.

Reductions from EN Regulation										
HYPO	Description	Based on Peak Flows (cfs)								
		Alton, IL Miss R.	Hermann, MO Missouri R.	Little Rock (Pine Bluff), AR Arkansas R.	Clarendon, AR White R.	Alexandria, LA Red R.	St. Louis, MO Miss R.	Metropolis, IL Ohio R.	Cairo, IL Combined Ohio and Miss R.	Arkansas City, AR Miss R.
1955										
52A	% Reduction	14%	15%	31%	28%	15%	14%	10%	16%	16%
58A	% Reduction	0%	12%	42%	28%	30%	5%	9%	17%	10%
56	% Reduction	5%	21%	44%	26%	37%	15%	19%	18%	14%
63	% Reduction	1%	25%	7%	24%	16%	16%	5%	11%	14%
2016										
52A	% Reduction	3%	10%	6%	19%	20%	3%	20%	11%	1%
58A	% Reduction	7%	12%	7%	17%	19%	13%	5%	5%	2%
56	% Reduction	10%	32%	22%	42%	61%	12%	5%	5%	10%
63	% Reduction	6%	28%	10%	38%	15%	16%	8%	0%	8%
Difference between 1955 Reductions and 2016 Reductions										
Change in % Reduction: 1955 versus 2016 [negative = decrease in 2016; plus = increase in 2016]										
52A	% Reduction	-11%	-5%	-25%	-9%	5%	-11%	10%	-5%	-15%
58A	% Reduction	7%	0%	-35%	-11%	-11%	8%	-4%	-12%	-8%
56	% Reduction	5%	11%	-22%	16%	24%	-3%	-14%	-13%	-4%
63	% Reduction	5%	3%	3%	14%	-1%	0%	3%	-11%	-6%

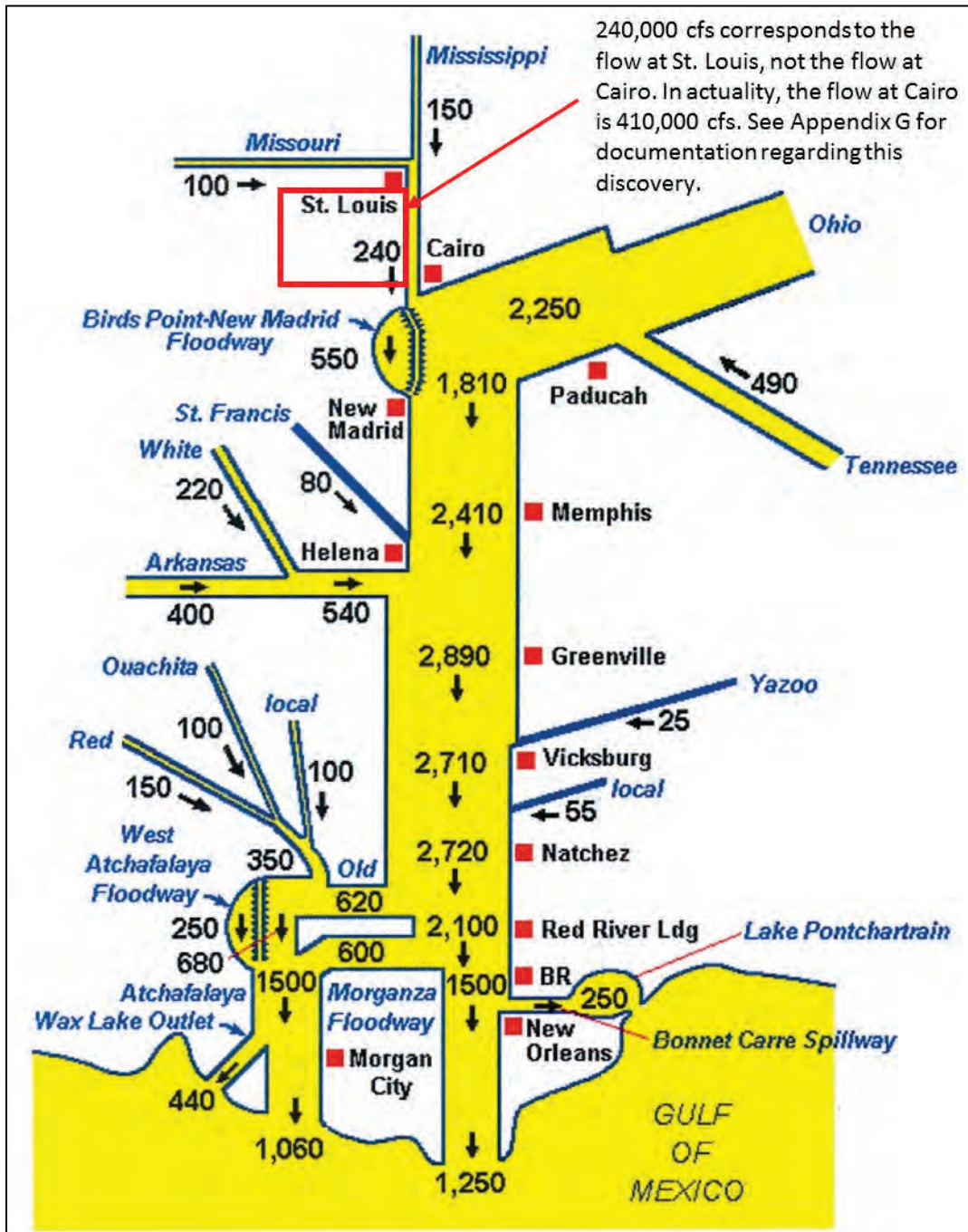
Figure 2-68. Regulation flow reductions for HYPO 58A, 52A, 56, and 63 in the 1955 and 2016 hydrology studies.



2.11 Alternative regulation effects

New hydrologic model results appear to show significant increases in peak flows for the Middle Mississippi River when compared to values given in the 1955 HYPO 58A-EN flow diagram as shown in Figure 2-69.

Figure 2-69. Flow Diagram developed from 1955 Study showing 240 kcfs flow from Middle Mississippi River at Cairo, IL.



A review of the tabulated hydrographs used in the 1955 routing computations revealed that the flow given for the Middle Mississippi River (240,000 cfs) was the flow at St. Louis, MO, and did not include flow contributed by the local area between St. Louis and the Ohio River confluence. This local contributing area was designated sub-basin 7-Y in the 1955 Study. When the St. Louis hydrograph was routed and combined with the local sub area, 7-Y, the peak flow was found to be 410,000 cfs.

For example, peak flows for HYPO 58A-U were 3% higher than 1955 HYPO 58A peak unregulated flows at the confluence of the Mississippi and Ohio Rivers while regulated peak flows for HYPO 58A-R were 17% higher at this location than were the 1955 HYPO 58A-EN peaks.

Factors identified as contributing causes of this difference were the following:

1. The total volume of computed unregulated flow is greater than the 1955 Study utilizing the 2016 methodologies, which may have limited the ability of reservoirs to reduce releases since they had to account for additional volumes of water.
2. Operation of reservoir projects to achieve maximum reductions at Cairo, IL, as for the HYPO 58A-EN results is not achievable during regular flood operations because this type of operation requires a priori knowledge of the entire event. It is not possible to know future storage requirements for a major flood like HYPO 58A beforehand in the event such a storm event occurs.
3. The HYPO 58A-EN results included reservoirs that were not constructed, which reduces the amount of storage available to reduce flood peaks routed downstream to Cairo, IL.

To demonstrate how reservoir operations effect downstream flows, Kentucky and Barkley Dam operations were analyzed as detailed in the following section.

Kentucky and Barkley Dam operations

1955 Study results were based on maximizing the use of storage in Groups E and N reservoirs to achieve the greatest reduction in peak flows at Cairo, IL. Kentucky and Barkley Dams (located on tributaries to the Ohio River which have a significant impact on flow at Cairo) were included in the

Groups E and N analysis. Storage utilization was managed to have the greatest reduction in flow at Cairo regardless of local impacts at each project. Specifically, locally induced flooding due to this regulation scheme was not considered in the decision process with respect to conditions on the main-stem Ohio River at Cairo, IL.

The present investigation utilized project operation manuals to determine regulation effects. Guide curves (or rule curves) from each project's Water Management Manual were used to develop regulated releases from each impoundment that had flood storage. There is a significant difference between operating a reservoir project solely for the maximum effect at a single downstream target location and following a set of guide curves developed to balance multiple objectives such as flood risk management, environmental sustainment, recreation, hydropower, and water supply.

The base regulated model simulation (HYPO 58A-R) for the 2016 investigation utilized standard reservoir operation protocols. This represented how Kentucky and Barkley projects would be operated during a normal flood scenario. This approach did not include extraordinary measures typically employed by joint regulation efforts by USACE, TVA, and NWS during critical floods to reduce stages at Cairo, IL. The joint regulation component was excluded because those operations depend heavily on forecasted information that has uncertainty built in. Using an event that is known, such as a design event like the PDF, removes the uncertainty and results in decisions that are biased due to the known characteristics of the full event.

To estimate the difference between operating Kentucky and Barkley Dams using the *maximized effect* approach and what would be possible with current guide curve regulation during the HYPO 58A PDF event, several different combinations of project storage utilization, release rates, and pool elevations were back-calculated to determine a new release hydrograph. Five combinations were considered. The operating combinations were labeled Mod 1 through Mod 5 (Mod for Modified Regulation Operations as compared to the base HYPO 58-R).

Regulated outflow hydrographs from Mod 1 through Mod 4 were used as inputs to the HEC-RAS unsteady model to assess computed hydrographs at Metropolis, IL, and to compare them with the unmodified HYPO 58A-R outputs (Figure 2-70). HYPO 58A was used here to demonstrate the

effects of reservoir regulation. Table 2-26 provides tabulated peak flows and the associated reductions from the base regulated model output for HYPO 58A-R.

Figure 2-70. HYPO 58A Hydrographs for Ohio River at Metropolis, IL: Unregulated, Regulated, and Modified Kentucky and Barkley reservoir releases.

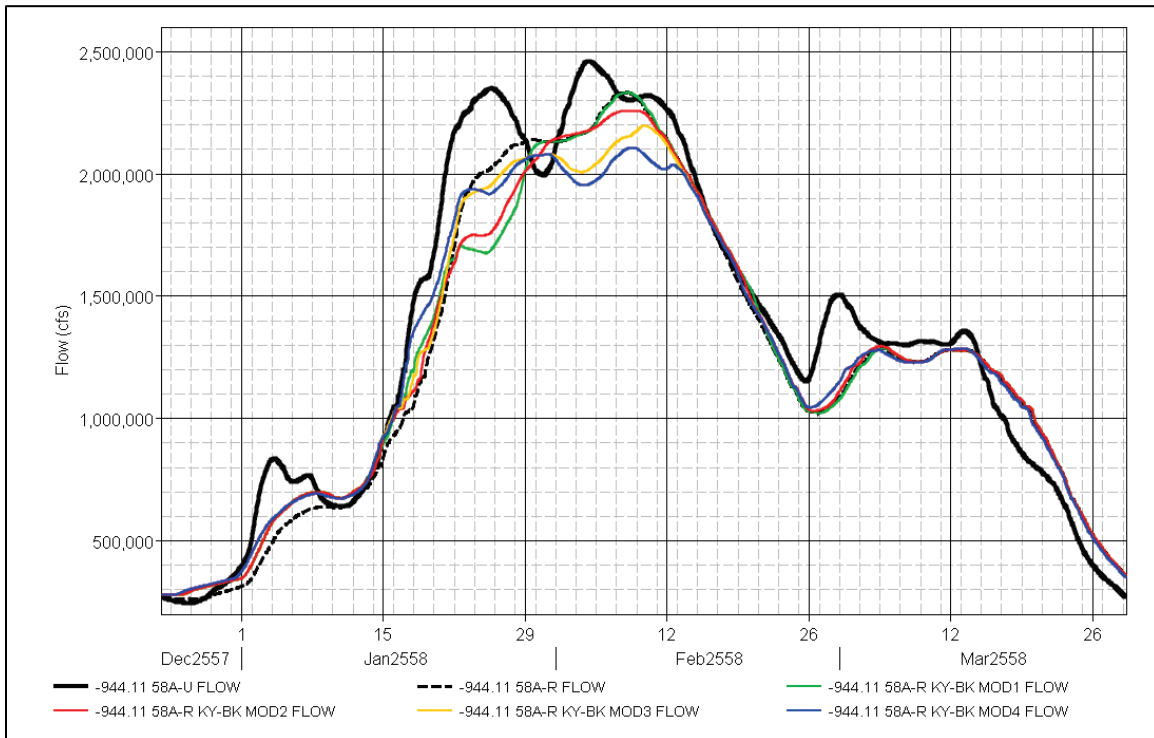


Table 2-26. Tabulated peak discharges for Ohio River at Metropolis, IL, with changes from the base regulated model result.

Run	Res Operation at Kentucky and Barkley Dams	Peak Flow at Metropolis, IL (cfs)	Date of Peak	Change from H58A-R (cfs)
H58A-U	Unregulated	2,461,083	4-Feb-58	-
H58A-R (Base)	Regulated	2,332,557	8-Feb-58	-
H58A-R M1	Mod-1	2,332,770	8-Feb-58	213
H58A-R M2	Mod-2	2,257,680	8-Feb-58	(74,877)
H58A-R M3	Mod-3	2,196,429	9-Feb-58	(136,128)
H58A-R M4	Mod-4	2,107,750	8-Feb-58	(224,806)

2.11.1.1 Description of modified reservoir operations

Mod 1 through Mod 4 regulation adjusted outflow while balancing storage and pool level using project guide curves. Mod 1 made minor changes in outflow, storage, and pool level. Each successive modification—Mod 2, Mod 3, and Mod 4—made more significant changes to alter the project outflows, each modification building on knowledge gained from the previous modification result. Mod 5 attempted to increase peak reductions in reservoir outflows further than achieved with Mod 4; however, no combination could be found to yield improvements without violating storage utilization and pool level guide curves.

2.11.1.2 Base regulation for 58A-R

The base regulation modeling applied basic guide curve constraints with no manual over-rides by the operator. This approach utilized an available HEC-RAS model for Kentucky and Barkley reservoirs. The HEC-RAS model is used by USACE in developing planned releases during flood events. The model configuration follows guide curves when operated in an unsupervised simulation. Note that USACE regulation of these projects during flood events seeks to pre-evacuate storage volume prior to each successive rise thereby making room to store flood waters later in the flood sequence. There are operational constraints on how much and how quickly drawdown can occur for real-time operations. For the modified reservoir calculations for the known HYPO 58A event, it was determined that drawdown to the allowable minimum pool could be accomplished in 1 or 2 days.

All modified regulation calculations took the base regulated model run and altered outflow to maximize storage in a way that maximized peak flow reductions on the Ohio River at Metropolis, IL. Routing calculations were made by simple routing computations based on the following equation.

$$\text{Inflow} - \text{Outflow} = \Delta\text{Storage}/\text{time} \quad (3)$$

The inflows were the same as used for the base regulated model run. The outflow from both Kentucky and Barkley Dams directly impacts the Ohio River discharge and became the variable that was adjusted. Storage calculated from the equation above was combined with project storage-elevation curves to determine changes in water level. Computed water levels and storage utilization were evaluated at each time period, 1 day in this analysis, for compliance with project guide curves.

2.11.1.3 Mod 1

The first modification, Mod 1, made to Kentucky and Barkley releases attempted to release a greater quantity of water beginning in late December with more severe cutbacks during the crest. The increased releases were evaluated against storage utilization and pool guide curves at each time-step. If the release resulted in a condition that violated the guide curves, then an adjustment was made to remain within the guide curve constraints. The higher release rates were continued until the pool level dropped to the guide curve; after that point, discharges followed those in the base regulation. Regulated outflows from Mod 1 were used as input to the HEC-RAS model to obtain the flow hydrograph for the Ohio River at Metropolis, IL. Results from the Mod 1 computations are shown in Figure 2-71 and Figure 2-72.

Figure 2-71. Plot of Mod 1 Kentucky and Barkley Reservoir operations for HYPO 58A-R.

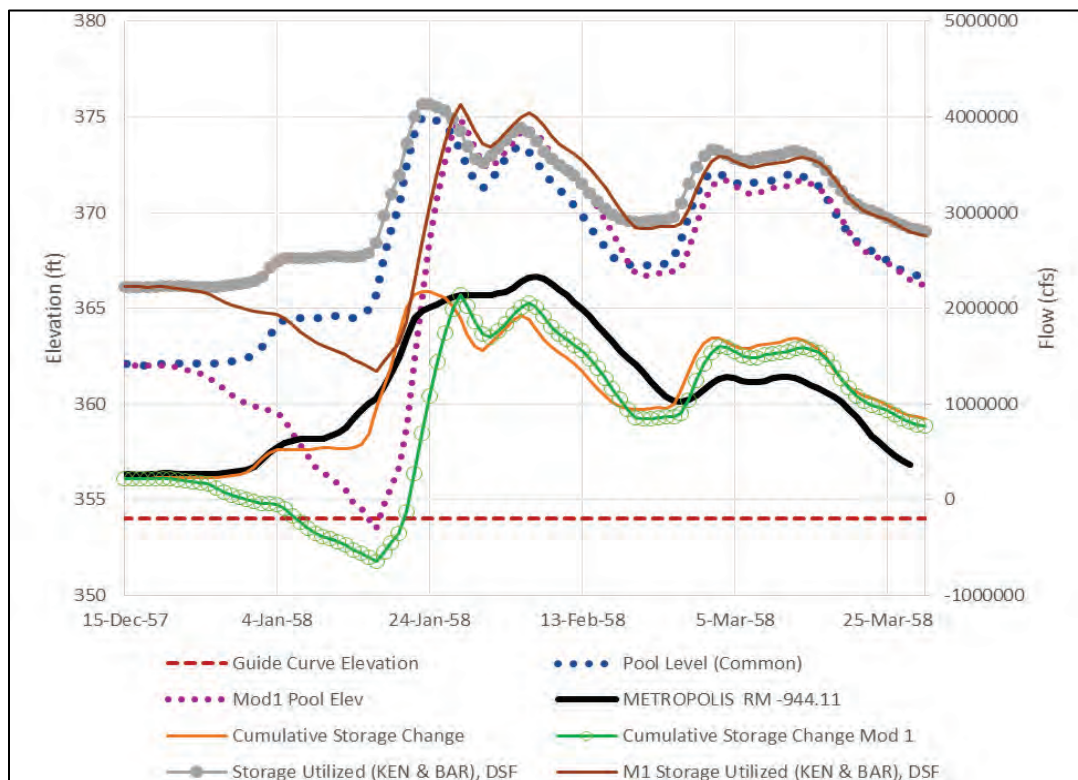
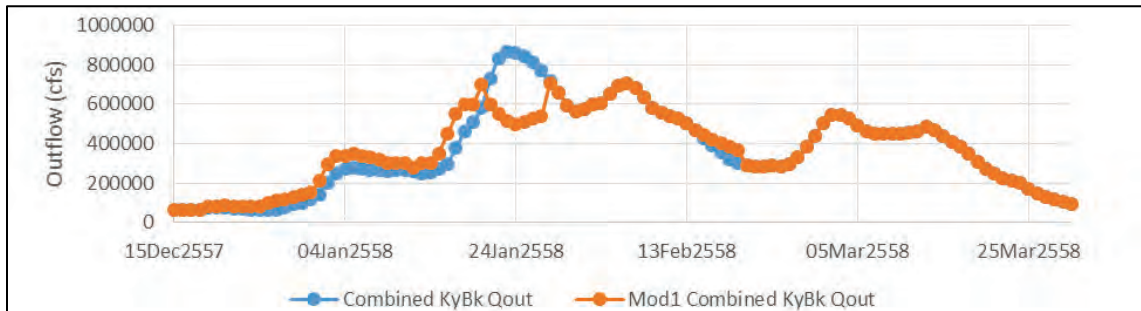


Figure 2-72. Mod 1 regulation outflows compared to the base regulation outflows.



2.11.1.4 Mod 2

The second modification, Mod 2, made to Kentucky and Barkley releases attempted to release a greater quantity of water beginning in late December as done for Mod 1. However, combined releases from Kentucky and Barkley were held nearly constant at approximately 600,000 cfs through the peak period. The increased releases were evaluated against storage utilization and pool guide curves at each time-step. If the release resulted in a condition that violated the guide curves then an adjustment was made to remain within the guide curve constraints. Regulated outflows from Mod 2 were used as input to the HEC-RAS model to obtain the flow hydrograph for the Ohio River at Metropolis, IL. Results from the Mod 2 computations are shown in Figure 2-73 and Figure 2-74.

Figure 2-73. Plot of Mod 2 Kentucky and Barkley Reservoir operations for HYPO 58A-R.

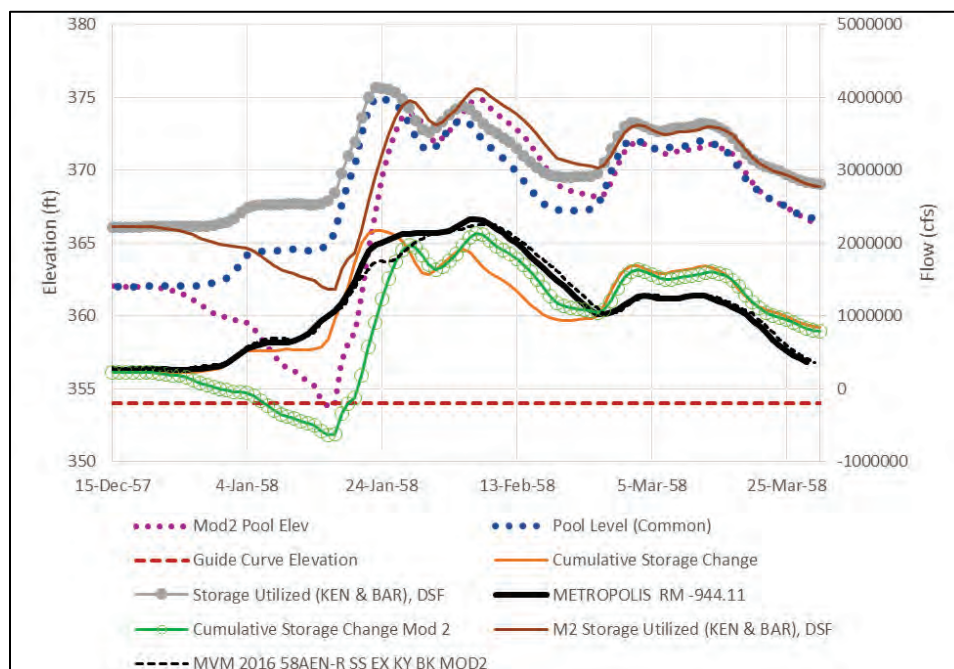
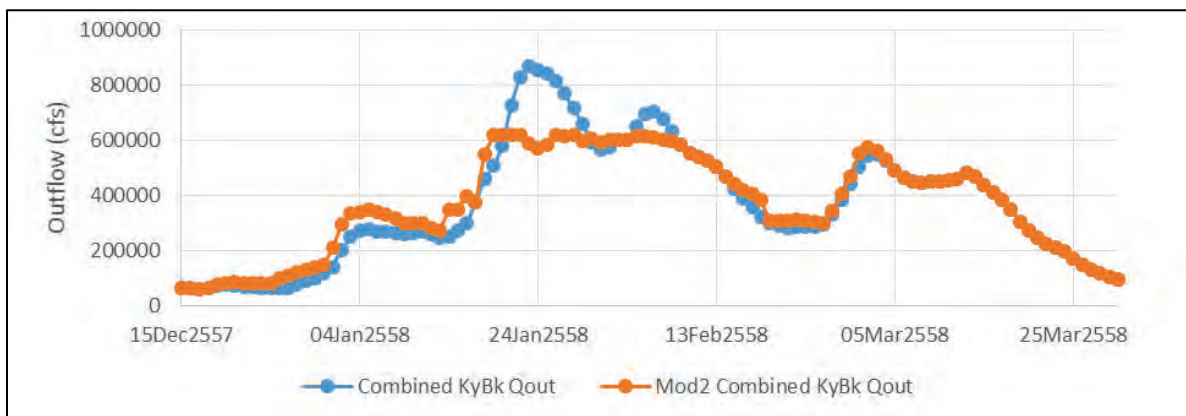


Figure 2-74. Mod 2 regulation outflows compared to the base regulation outflows.



2.11.1.5 Mod 3

The third modification, Mod 3, made to Kentucky and Barkley releases, attempted to release a greater quantity of water beginning in late December as done for Mod 1. Results from the Mod 2 regulation run at Metropolis, IL, indicated that lowering the peak to a constant 600,000 cfs did not yield the desired effect on the Ohio River flows. As a result, Mod 3 regulation closely tracked the base regulated outflows between January 20 and January 22, slightly decreased outflows from the base January 23 to January 31, then had significantly lower outflows from February 1 through February 8. The altered releases were evaluated against storage utilization and pool guide curves at each time-step. If the release resulted in a condition that violated the guide curves, then an adjustment was made to remain within the guide curve constraints. Regulated outflows from Mod 3 were used as input to the HEC-RAS model to obtain the flow hydrograph for the Ohio River at Metropolis, IL. Results from the Mod 3 computations are shown in Figure 2-75 and Figure 2-76.

Figure 2-75. Plot of Mod 3 Kentucky and Barkley Reservoir operations for HYPO 58A-R.

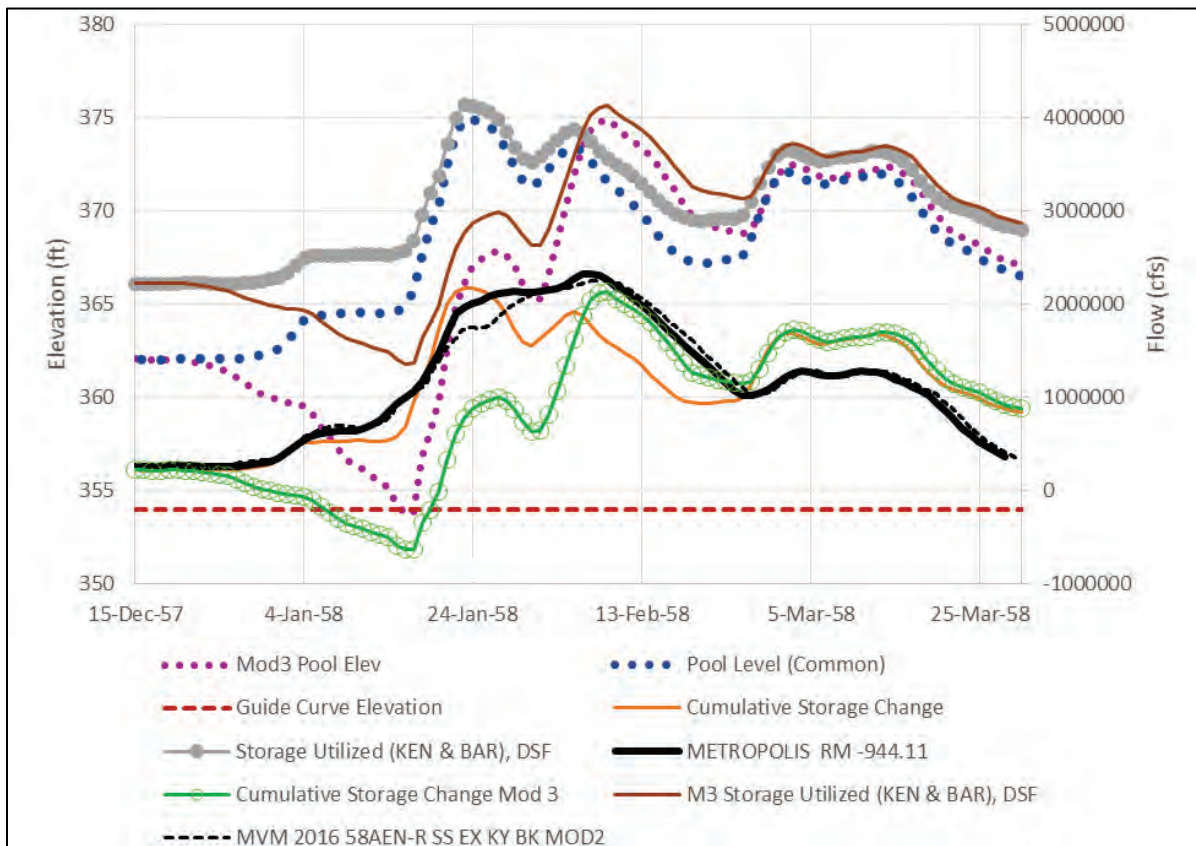
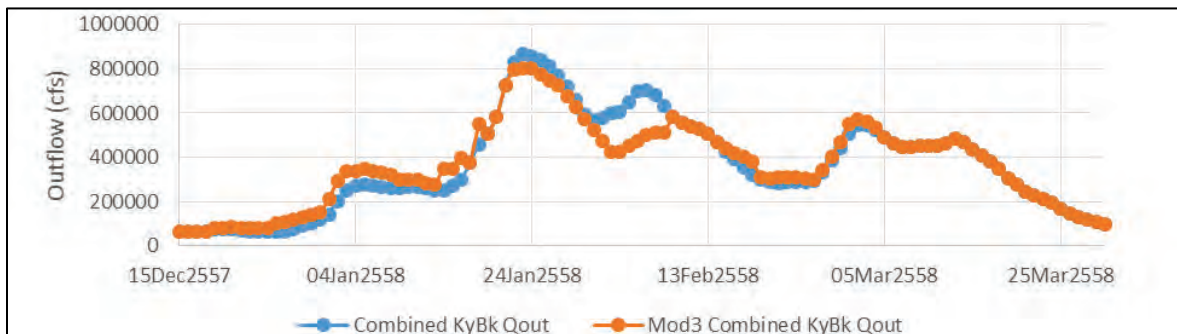


Figure 2-76. Mod 3 regulation outflows compared to the base regulation outflows.



2.11.1.6 Mod 4

The fourth modification, Mod 4, made to Kentucky and Barkley releases, attempted to build on results obtained from the Mod 3 regulation. The primary objective was to evacuate additional storage volume before January 21 that would increase the storage available that allowed for lower releases between January 30 and February 11. The altered releases were evaluated against storage utilization and pool guide curves at each time-

step. If the release resulted in a condition that violated the guide curves, then an adjustment was made to remain within the guide curve constraints. Regulated outflows from Mod 4 were used as input to the HEC-RAS model to obtain the flow hydrograph for the Ohio River at Metropolis, IL. Results from the Mod 4 computations are shown in Figure 2-77 and Figure 2-78.

Figure 2-77. Plot of Mod 4 Kentucky and Barkley Reservoir operations; HYPO 58A-R.

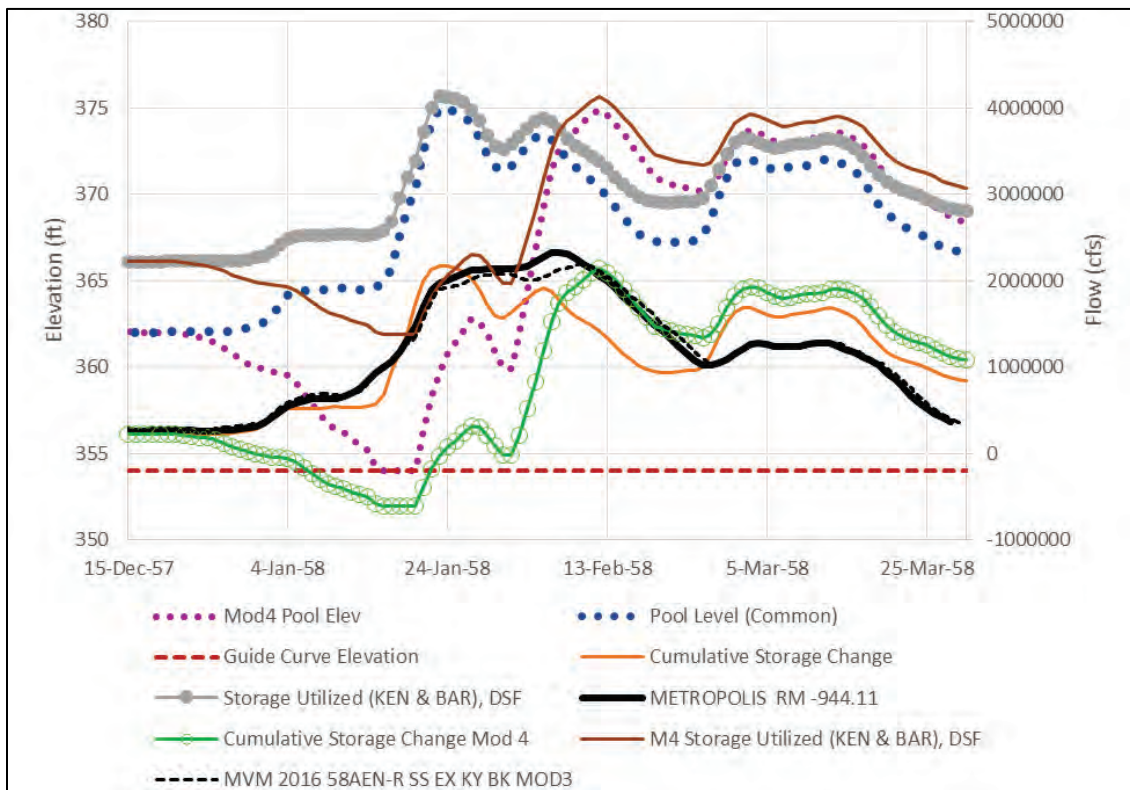
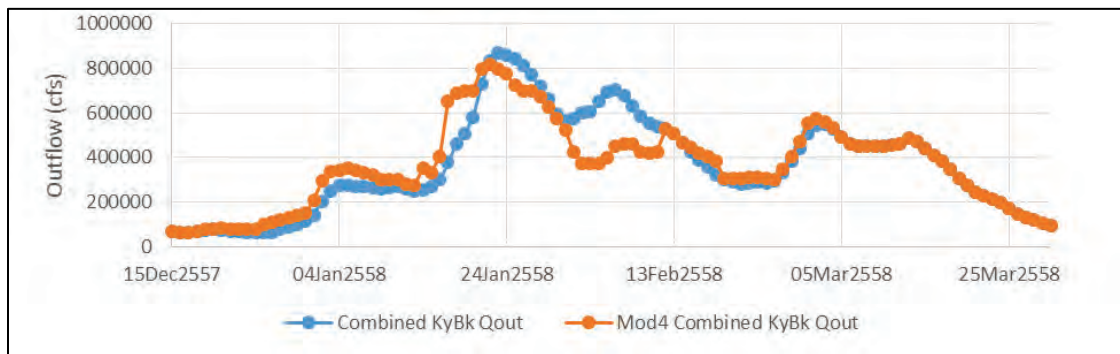


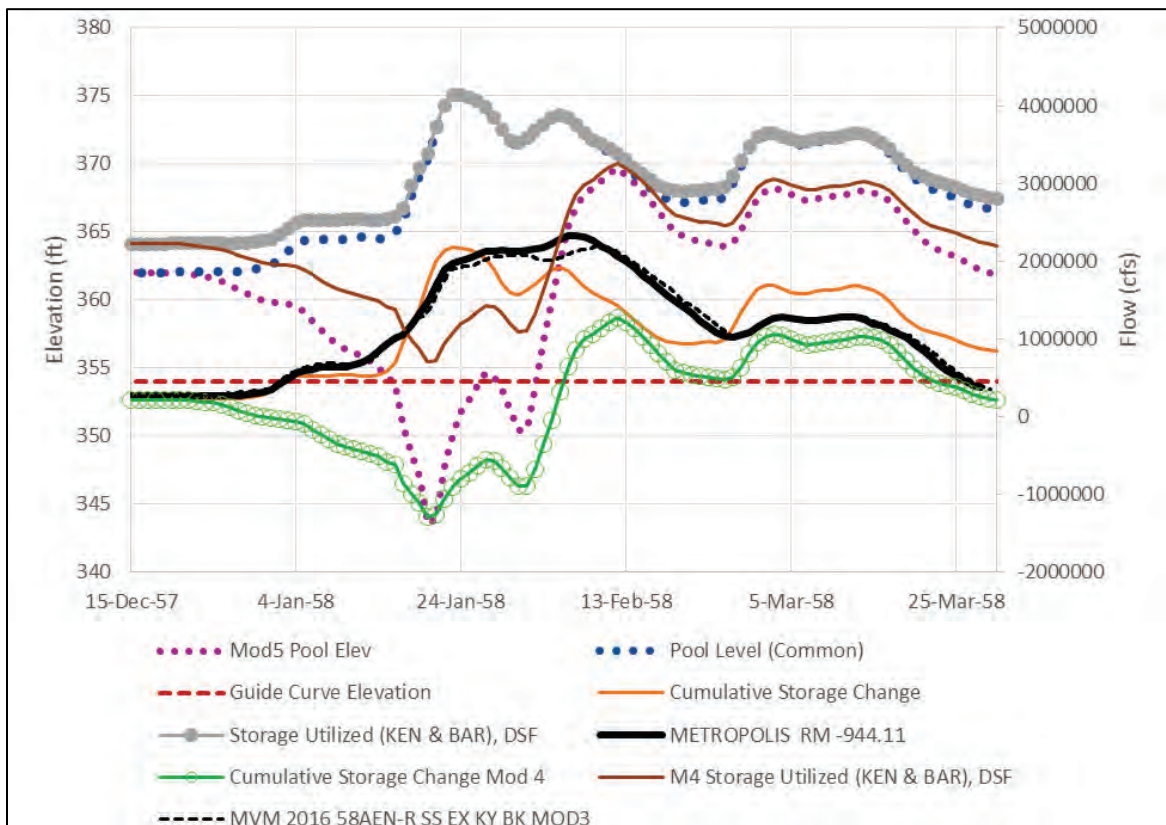
Figure 2-78. Mod 4 regulation outflows compared to the base regulation outflows.



2.11.1.7 Mod 5

The fifth modification, Mod 5, made to Kentucky and Barkley releases attempted to build on results obtained from the Mod 4 regulation. The primary objective was to evacuate significantly more storage volume before January 21 that would increase the storage available for use later. The altered releases were evaluated against storage utilization and pool guide curves at each time-step. There were no combinations that permitted early evacuation of storage beyond what was achieved by Mod 4 without drawing the pool level below the guide curve. The outflow developed for Mod 5 was not simulated in HEC-RAS to assess flows at Metropolis, IL, because there was no improved outcome from Mod 5 over results from Mod 4 without deviating from the guide curves. The interim calculations from the Mod 5 computations are shown in Figure 2-79 to illustrate how pool levels drop below the guide curve.

Figure 2-79. Plot of Mod 5 Kentucky and Barkley Reservoir operations for HYPO 58A-R.



2.12 Synopsis of methodology differences, 2016 versus 1955

The combined CHPS and USACE hydrologic modeling was an extensive effort. There was good overall agreement between model results for the HYPO 58A results within the focus reach for the MR&T Project. The agreement for HYPO 52A, HYPO 56, and HYPO 63 varied.

HYPO 58A flows provided the design condition for the mainstem Mississippi River from Cairo, IL, to the Gulf with few exceptions as noted in House Document 308 (H.R. Doc. No. 308). The 2016 re-evaluation of hydrologic conditions resulted in minor changes in the unregulated flow hydrographs needed for developing the PDF water surface profile from HEC-RAS. The unregulated combined peak flow calculated for the Mississippi River at the Ohio/Miss confluence was within 3% of the previous peak values published in USACE MRC (1955) report. Given the significant differences between the 1955 and 2016 methodologies, a 3% difference in peak unregulated flows instills confidence in how the 1955 input parameters and calculations were translated to the more refined current assessment process.

The other three HYPO storms analyzed, 52A, 56, and 63, provided a check on the methodology. The 2016 unregulated peak flows for HYPO 56 and HYPO 63 were in fair agreement with prior 1955 values, which provided further validation of the methodology. However, computed HYPO 52A unregulated peak values were significantly lower than those from 1955. Various elements of the analysis were checked in an effort to determine why this one model run produced lower flow. The precipitation inputs for HYPO 52A had greater variation from the 1955 precipitation depth-area curves indicating that the precipitation inputs were the primary source of difference. Multiple measures were employed to resolve the discrepancy in precipitation inputs without success. The analysis team concluded that the problem with HYPO 52A results arose because the precipitation inputs for the 2016 analysis were different than used in the 1955 analysis; it was not due to the methodology.

The following lists provide a summary of principal differences in the current modeling approach and that used for 1955 analysis.

Meteorology (climatic inputs)

- Same historical extreme events from 1937, 1950, and 1938
- Same HYPO 58A storm sequence: 1937 + 1950 + 1938

- Same storm scaling factors and transpositions
- Combined Historic events into HYPO sequence using 2016
- SS methodology (different from 1955 methodology replicated by the CM sequence)

Hydrology (rainfall-runoff)

- 2016 analysis used NWS production forecast models
- 2016 model calibration was based on 2010 to 2014 data and daily operational adjustments
- 2016 model used 7,066 sub-basins versus 44 from 1955 Study
- 2016 analysis included temperature effects (not part of 1955 Study)
- 2016 model utilized continuous soil moisture and snow pack/snow melt accounting (not part of 1955 Study)
- 2016 regulated simulations employed joint NWS/USACE/TVA modeling of reservoir releases
- 2016 regulation included reservoirs that existed as of 2014 (different than Groups E and N list used in 1955 Study)
- 2016 regulation was based on standard operating rule curves (different that maximized reduction used in 1955 Study)
- 2016 analysis included both Unregulated and Regulated Runs completed for comparison with 1955 Study
- 2016 routing included both hydrologic methods (upper watershed) and unsteady HEC-RAS model* (Flowline analysis reach)

* The 1955 Study did not consider unsteady hydrodynamic routing.

2.12.1 Climatic inputs

Meteorology components of the analysis followed the methods used in 1955 except for how the HYPO storm sequences were applied. A comparison was made between the current approach that used the SS versus the 1955 approach that used different precipitation depths for portions of the watershed, as represented by the CM sequence. There were minor differences, approximately +5%, between the SS results and those obtained using the CM sequencing.

Some differences in precipitation inputs were inevitable because not all of the original point data from 1955 report archives could be obtained (Section 2.8). This required use of other sources of information including the NOAA national archive database. The sensitivity of results to

precipitation inputs was not evaluated as this task fell outside of the study's scope and schedule. Future investigations should include an evaluation of model sensitivity to precipitation and temperature inputs.

2.12.2 Hydrologic modeling

The current investigation included significantly higher resolution of watershed characteristics than used in 1955 (7,066 versus 44 sub-basins). There were also improved calculations for rainfall/runoff through continuous soil moisture accounting, snow melt, and routing. The improvements in routing included higher resolution through more and shorter reaches and through unsteady hydrodynamic modeling.

Two noteworthy factors that affected model results were calibration period and reservoir regulation. Use of the NWS forecast models meant that calibration was based on modern data, 2010–2014, which may be considerably different than if model parameters been developed based on conditions from the 1950s. Even though broad-scale land use had not changed between approximately 1950 and 2007 (see Table 2-5), channel and floodplain rating curves were different; therefore, model parameterization required to calibrate to historic conditions (stages and discharges) would be different. Such differences had localized effects on model outputs; however, aggregate results for the Lower Mississippi River were similar. The impacts of calibration state were not determined because it was not possible to back-calibrate the models to a 1950s state within available timeframes.

Reservoir regulation effects in the current analysis were based on current Water Management Manuals while the 1955 analysis maximized utilization of available flood control storage. The 1955 Study maximized use of total flood storage including prior evacuation of water to make storage available during the peak period which would require foreknowledge of the entire event. While desirable to leverage all available storage to reduce peak flows during a PDF level event, this objective is not achievable since the timing and spatial distribution of the event are not known beforehand. Operating reservoirs according to their standard operating plans was considered achievable and was the approach adopted for model simulations. The best representation of reservoir regulation effects lies between the maximized use of storage and use of daily guide curves and procedures. Section 2.10 gives details of reservoir regulation for the current analysis. It is recommended that additional model

simulations be performed to develop several scenarios that could be used to guide operational decisions for extreme floods. These additional simulations would be similar to the assessment of the effects of upstream reservoirs on the PDF performed for the MRC in WES (1957).

2.13 Paleoflood considerations

Although not part of the original PDF studies, paleoflood information has been introduced as a means for supplementing available gage data to assess flood probabilities. While paleoflood information can lead to potentially useful hydraulics and hydrologic information, this should be weighed against the underlying uncertainties and assumptions. Citing ETL 1100-2-2 (USACE 2014), paleoflood analysis is not suitable for watersheds that have been altered through time, either by geologic or by anthropogenic processes. Paleoflood information is mostly useful when the channel and surrounding watershed have remained stable. Additionally, there is limited evidence to support the application of paleoflood information when using multiple hydrologic events or the use of flood volumes and durations.

Paleoflood analysis is most appropriate in arid to semi-arid regions. The Mississippi Valley is not within a semi-arid or arid region.

With 60 years of additional data since the 1955 study, more dependable peak flow frequency estimates could be derived. However, the available historical dataset is a mixed population of annual peaks created from events with various levels of regulation from upstream reservoirs over the period of record. Use of this dataset in a frequency analysis would require an incorrect assumption that the dataset is part of a naturally occurring population that fits an assumed statistical distribution. Discharge frequency estimates would only be valid with a complete record of unregulated events and a corresponding record of regulated flows that were based on a consistent regulation scheme over time, neither of which is available. An estimated frequency of the PDF peak discharge at given locations could be developed from statistical analysis using only the recorded peaks, but given the inherently inappropriate assumptions in such an analysis, no such estimates have been made as part of the current assessment.

2.14 Climate change considerations

Although climate change was not considered in the 1955 Study, potential climate change impacts over the Mississippi River Basin were considered in this assessment, as any change in hydrologic input could have adverse impacts to the updated Flowline analysis. USACE (2016) provides guidance, regional documentation on climate change analyses, and a Climate Hydrology Assessment Tool (CHAT) to determine potential climate change trends. The tool analyzes flowrate trends across hydrologic unit code 4 (HUC 4) watersheds, which represent large river basins at the subregional level.

2.14.1 Regional documentation on climate change

The National Climate Assessment summarizes changing climate conditions in each of eight regions within the United States. The Lower Mississippi River flows through the Midwest Region and the Southeast and Caribbean Region. The key regional topics of interest in the Southeast and Caribbean Region are outlined below:

- **Sea Level Rise Threats** — Sea level rise poses a widespread and continuing threat to the natural and built environments and to the regional economy.
- **Increasing Temperatures** — Increasing temperatures and the associated increase in frequency, intensity, and duration of extreme heat events will affect public health, natural and built environments, energy, agriculture, and forestry.
- **Water Availability** — Decreased water availability, exacerbated by population growth and land-use change, will continue to increase competition for water and affect the region's economy and unique ecosystems.

The key regional topics of interest in the Midwest Region are outlined below:

- **Impacts to Agriculture** — In the next few decades, longer growing seasons and rising carbon dioxide levels will increase yields of some crops, though those benefits will be progressively offset by extreme weather events. Though adaptation options can reduce some of the detrimental effects, in the long term, the combined stresses associated with climate change are expected to decrease agricultural productivity.

- **Forest Composition** — The composition of the region's forests is expected to change as rising temperatures drive habitats for many tree species northward. The role of the region's forests as a net absorber of carbon is at risk from disruptions to forest ecosystems, in part due to climate change.
- **Public Health Risks** — Increased heat wave intensity and frequency, increased humidity, degraded air quality, and reduced water quality will increase public health risks.
- **Fossil-Fuel Dependent Electricity System** — The Midwest has a highly energy-intensive economy with per capita emissions of greenhouse gases more than 20% higher than the national average. The region also has a large and increasingly utilized potential to reduce emissions that cause climate change.
- **Increased Rainfall and Flooding** — Extreme rainfall events and flooding have increased during the last century, and these trends are expected to continue, causing erosion, declining water quality, and negative impacts on transportation, agriculture, human health, and infrastructure.
- **Increased Risk to the Great Lakes** — Climate change will exacerbate a range of risks to the Great Lakes, including changes in range and distribution of certain fish species, increased invasive species and harmful blooms of algae, and declining beach health. Ice cover declines will lengthen the commercial navigation season.

The USACE Institute for Water Resources (IWR) summarizes the available climate change literature available for each of the smaller regions within the Mississippi River Basin (USACE 2015a–f). The report series uses available data to determine observed trends at various gages and to project trends. Summaries for each region are detailed in Table 2-27 and Table 2-28.

Table 2-27. Observed climate trends within the six major basins in the Mississippi River Basin as summarized in USACE (2015a–f).

Region	Observed Trend		
	Streamflow	Precipitation	Temperature
Ohio Region 05	Streamflow data was collected to study the trends in the Ohio Region. The general consensus for the Ohio Region is an increase in streamflow. Data from 1948–2004 showed an increase in annual runoff between .2 and 1.8 millimeters (mm) per year.	A clear consensus is lacking about the precipitation in the Ohio Region. Multiple studies conclude an increase in precipitation while others show a decrease or no change at all. Grundstien (2009) has found increasing trends in soil moisture for several climate stations in the Ohio region.	The Ohio Region has been recognized as a transition zone due to a warming trend toward the north and a cooling trend toward the south. Research concludes that there has been a linearly increasing trend between 0 °C and 0.4 °C per century.
Tennessee Region 06	No trend has been observed in the streamflow data for the region.	Annual precipitation totals have become more variable in recent years compared to earlier in the twentieth century. Evidence has also been presented, but with limited consensus, of mildly increasing trends in the magnitude of annual and seasonal precipitation for parts of the study region.	Evidence has been presented in the recent literature of mild increases in annual temperature in the Tennessee Region over the past century, particularly since the 1970s. Consensus, and the number of available region specific studies, is low, however.
Upper Mississippi Region 07	A mild upward trend in mean streamflow in the study region has been identified by multiple authors but a clear consensus is lacking.	A mild upward trend in precipitation in the study region has been identified by multiple authors.	Increasing trends in observed air temperature in the study basin, including daily mean and minimum temperatures, were reported by multiple authors.
Lower Mississippi River Region 08	A mild upward trend in mean streamflow in the study region has been identified by multiple authors but a clear consensus is lacking.	A mild upward trend in precipitation in the study region has been identified by multiple authors but a clear consensus is lacking.	No significant trend in observed mean air temperature in the study region, though extreme minimum daily air temperatures may be increasing.
Missouri River Region 10	A mild upward trend in mean streamflow in the Missouri River Region has been identified by multiple authors, but a clear consensus is lacking in the upper portion of the region.	A mild upward trend in annual and extreme precipitation in the lower portion of the Missouri River Region has been identified by multiple authors while the upper portion has been identified to have a decreasing trend for annual and extreme precipitation.	An increasing trend in observed mean and daily minimum air temperature in the study region was observed; however, a trend in daily maximum air temperature is lacking.
Arkansas, White and Red Rivers Region 11	Streamflow data was collected to study the trends in Region 11. Water runoff increased 140 mm for the lower portion and increased 20 mm for the upper portion of the region in a study done by Qian et al. (2007). A general consensus amongst recent peer reviewed literature indicates an upward trending for average streamflow.	A general consensus amongst recent peer-reviewed literature indicates a mild upward trending for average precipitation and extreme precipitation events.	Studies were conducted on mean temperatures and extreme temperatures in Region 11. Slight warming trends occurred during the winter and spring months while mild cooling trends occurred for the summer and fall months for mean temperatures. One day extreme minimum temperatures have begun to increase since 1995.

Table 2-28. Projected climate trends within the six major basins in the Mississippi River Basin as summarized in USACE (2015a-f).

Region	Projected Trends		
	Streamflow	Precipitation	Temperature
Ohio Region 05	Projected changes in streamflow in the Ohio Region vary significantly.	Although precipitation is projected to increase in most studies surveyed, there are no clear trends in the literature indicating the magnitude or geographic distribution of future changes to average or extreme precipitation.	Although there is a strong consensus that temperatures will increase, the amount of projected increase varies between studies. Several studies also show considerable variation within the Ohio Region.
Tennessee Region 06	Variability exists with projected streamflow changes in the Tennessee Region.	Strong consensus exists in the literature that the intensity and frequency of extreme storm events will increase in the future for the Tennessee Region. Low consensus exists with respect to projected changes in total annual precipitation for the region.	Strong consensus exists in the literature that projected temperatures in the study region show a sharp increasing trend over the next century.
Upper Mississippi Region 07	Clear consensus in the literature is lacking, with some studies projecting an increase in future streamflow (as a result of increased precipitation) in the study region, while others project a decrease in flows (a result of increased evapotranspiration). Seasonally, multiple studies suggest increased flows in the winter and spring and decreased flows in the summer.	General consensus exists in the literature with respect to projected increasing trends in future annual and extreme precipitation in the study basin.	Strong consensus exists in the literature that projected temperatures in the study region will rise over the next century.
Lower Mississippi River Region 08	Although consensus is lacking, a small number of reviewed studies indicate a mild decreasing trend in streamflow for the study region through the next century.	Little consensus exists in the literature with respect to projected trends in future precipitation in the study region.	Strong consensus exists in the literature that projected temperature in the study region show a sharp increasing trend over the next century.
Missouri River Region 10	Consensus amongst recent literature is lacking regarding the direction of projected trends in streamflow and related variable such as runoff and water yield. The trend direction seems to be dependent on selection of Global Climate Model (GCM), emissions scenario, and hydrologic model.	A general consensus exists in the literature with respect to an increasing trend in future precipitation in the study region.	Strong consensus exists in the literature that projected temperature trends in the study region show a steady increase over the next century.

Region	Projected Trends		
	Streamflow	Precipitation	Temperature
Arkansas, White and Red Rivers Region 11	There is limited consensus that projected streamflow will decrease for portions of Water Resources Region 11; however, projected trends are highly dependent on GCM selection.	A general consensus amongst recent peer-reviewed literature indicates no change in projected annual precipitation levels within the Water Resources Regions 11. However, there is consensus that the projected occurrence of extreme precipitation events will increase as well as the number of consecutive dry days.	A large consensus amongst recent peer-reviewed literature indicates a moderate upward trending for projected mean temperature and a significant upward trend for maximum temperature within the Water Resources Region 11.

Although these results indicate an overall streamflow increase throughout the next century, the studies do not pinpoint critical sub-basins within each region that are most impacted and those sub-basins that may have a greater effect on the MR&T Flowline.

2.14.2 Discharge as a surrogate for precipitation

The present tools available from USACE IWR evaluate available and projected stream discharge data to evaluate potential changes to river discharge due to climate change or other changes. Two tools are presently available for this purpose: the nonstationarity detection tool (NDT) evaluates observed streamflow data for trends and change-points while the CHAT assesses modeled future streamflows based on downscaled general circulation model outputs and scenarios of future climate. Changes in streamflow and temperature that are projected by the general circulation models are manifested as changes in streamflow through simplified hydrologic and routing models.

2.14.3 NDT and CHAT

The USACE NDT detects nonstationarities in annual instantaneous peak streamflow data in flow records of 30 years or more for one gage location (Friedman et al. 2016). A change point in the data record is defined by two or more periods within the record that are described by different statistical distributions, mean, and/or variance. Change points can be used to identify those periods of record that violate the stationarity assumption that is implicit in traditional statistical methods in hydrology (i.e., the assumption that the mean and standard deviation do not change over time). Nonstationarity is useful in water management planning on a local or regional level when the cause of the nonstationarity is understood and

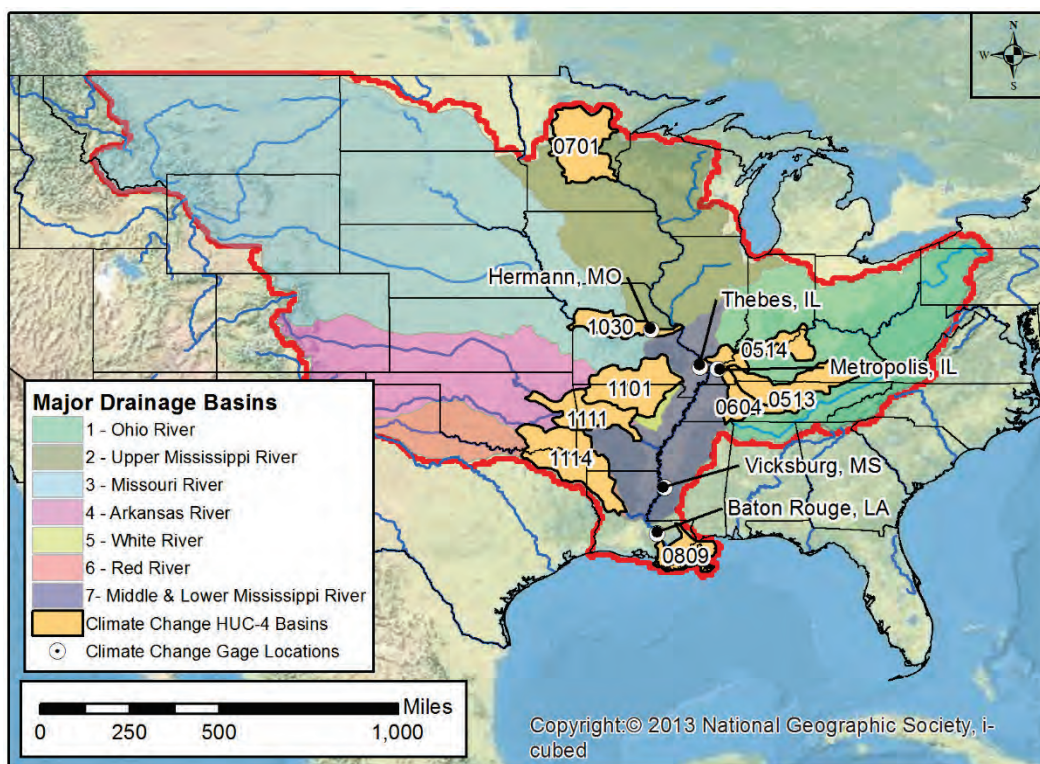
there is a way to describe the shift (Hirsch 2011). Otherwise, the detected change point could lead to erroneous conclusions with little meaning. USACE guidance prescribes running a nonstationarity analysis; however, the scale of this assessment, which spans over 40% of the contiguous United States and two Canadian provinces, is such that a nonstationarity analysis would have little meaning over the entire watershed. On a localized scale, locations at key points with major sub-basins can be analyzed for nonstationarity to obtain a general signal for the watershed.

CHAT is able to analyze the observed streamflow trend at a single gage location by running a simple linear regression. In the future, the user will be able to select multiple gage locations to analyze the observed streamflow trend for the entire HUC-4. At its current state, the current observed trend at a single location within a HUC-4 for this assessment would have little meaning. CHAT is able to generate future climate change trends based on available historic observed data as it incorporates the Representative Concentration Pathways 4.5 (RCP4.5) emissions model and the ACCESS1.0 climate model generated by the Commonwealth Scientific and Industrial Research Organisation's Bureau of Meteorology¹. The CHAT database includes all available USGS gage flowrate data on record. These flowrate observations then feed into 93 different hydrologic climate models for a period of 2000–2099. Since the Mississippi River Basin encompasses a large number of HUC-4 basins, only HUC-4 basins that represent main areas of concern, those areas along main tributaries to the Mississippi River and directly impacted by HYPO 58A, were selected for the Flowline assessment. Since NDT is primarily useful on a localized scale, consideration was taken to evaluate the appropriate USGS gage locations on tributaries just above the confluence to the Mississippi River and several locations along the Lower Mississippi River. Figure 2-80 displays the HUC-4 basins and gage locations selected for the climate change analysis.

¹ The RCP4.5 scenario has a mean global surface temperature increase of 1.4 °Celsius between 2046 to 2065 and an increase of 1.8 °Celsius between 2081 to 2100 relative to the reference period of 1986–2005.

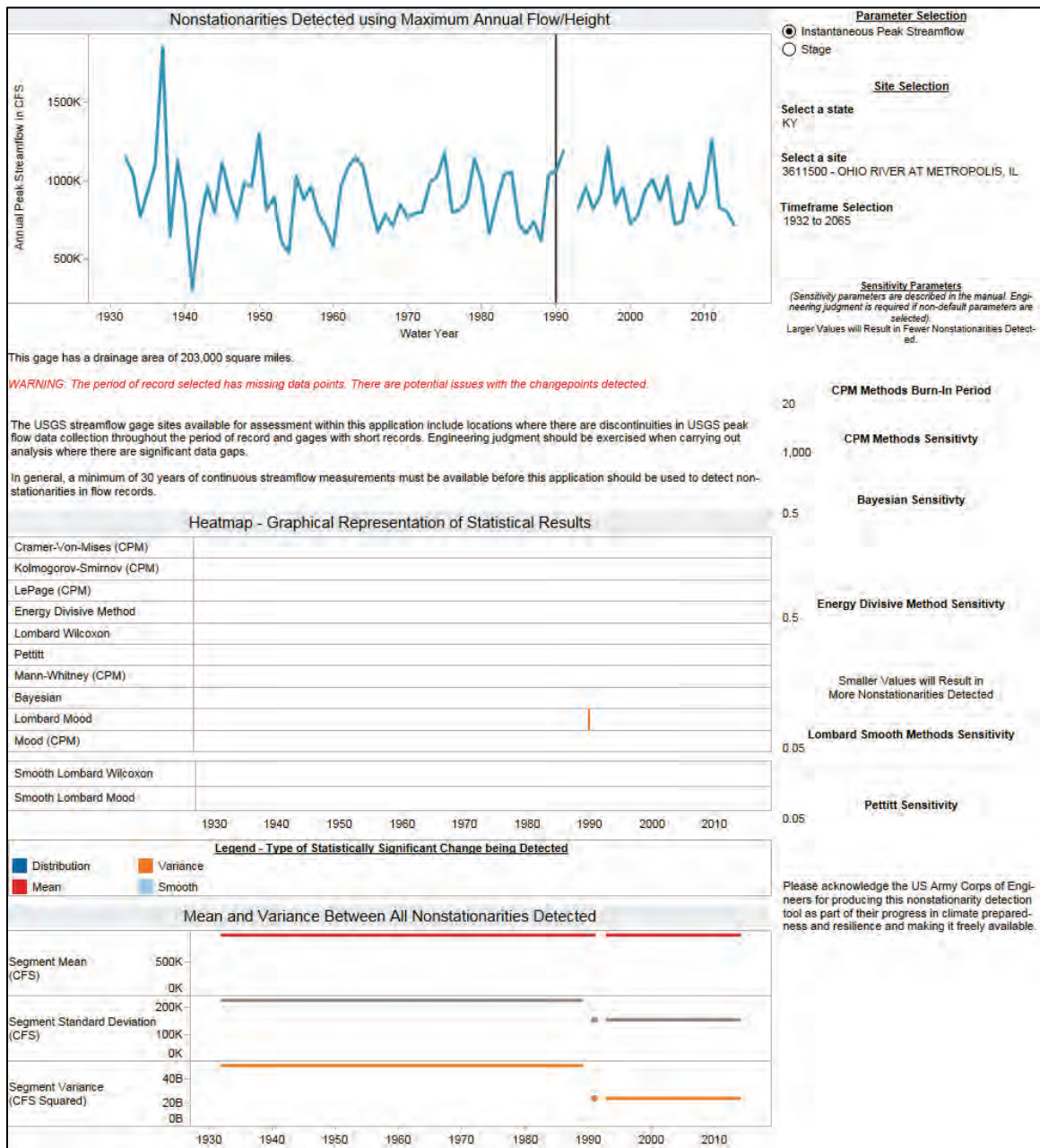
ACCESS1.0 uses the UK MetOffice UM atmosphere model, the GFDL MOM4p1 ocean model, the LANL CICE4.1 sea-ice model, and the MOSES2 land surface model to simulate the global climate between 1850–2006 using historical forcings.

Figure 2-80. HUC-4 drainage basins and gage locations selected for climate change analysis.



Streamflow data prior to 1933 were excluded from the analysis as discharge measurements prior to 1933 were proven to be unreliable and inconsistent as advances in streamflow measurement tools were becoming standardized (Watson et al. 2013). Significant nonstationarity is defined as one in which a change point has statistical consensus within a 5-year period or a known event (e.g., reservoir construction/completion) caused nonstationarity. Figure 2-81 – Figure 2-90 show the results of the nonstationarity detection analysis and the corresponding trend analysis.

Figure 2-81. USGS Gage 3611500, Ohio River at Metropolis, IL, nonstationarity detection.



The nonstationarity point detected in 1990 lacks consensus between statistical tests.

Figure 2-82. USGS Gage 3611500, Ohio River at Metropolis, IL, stationarity trend analysis.

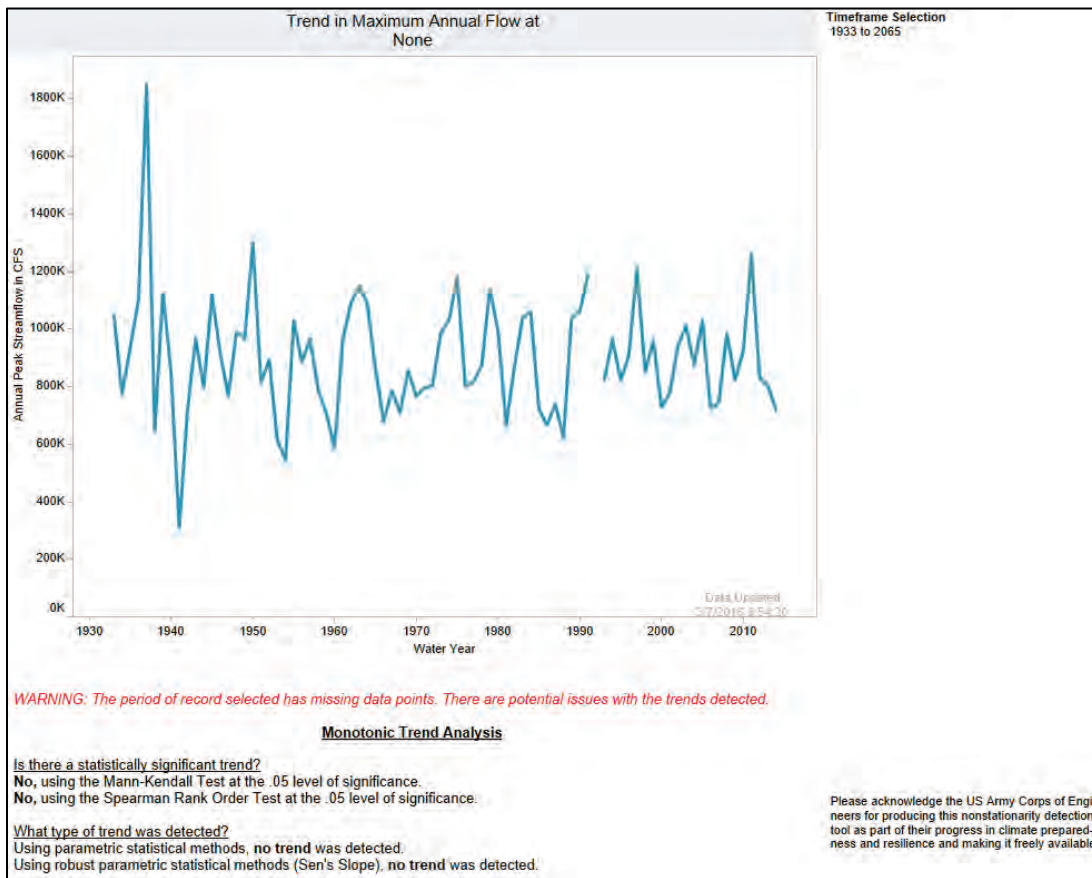
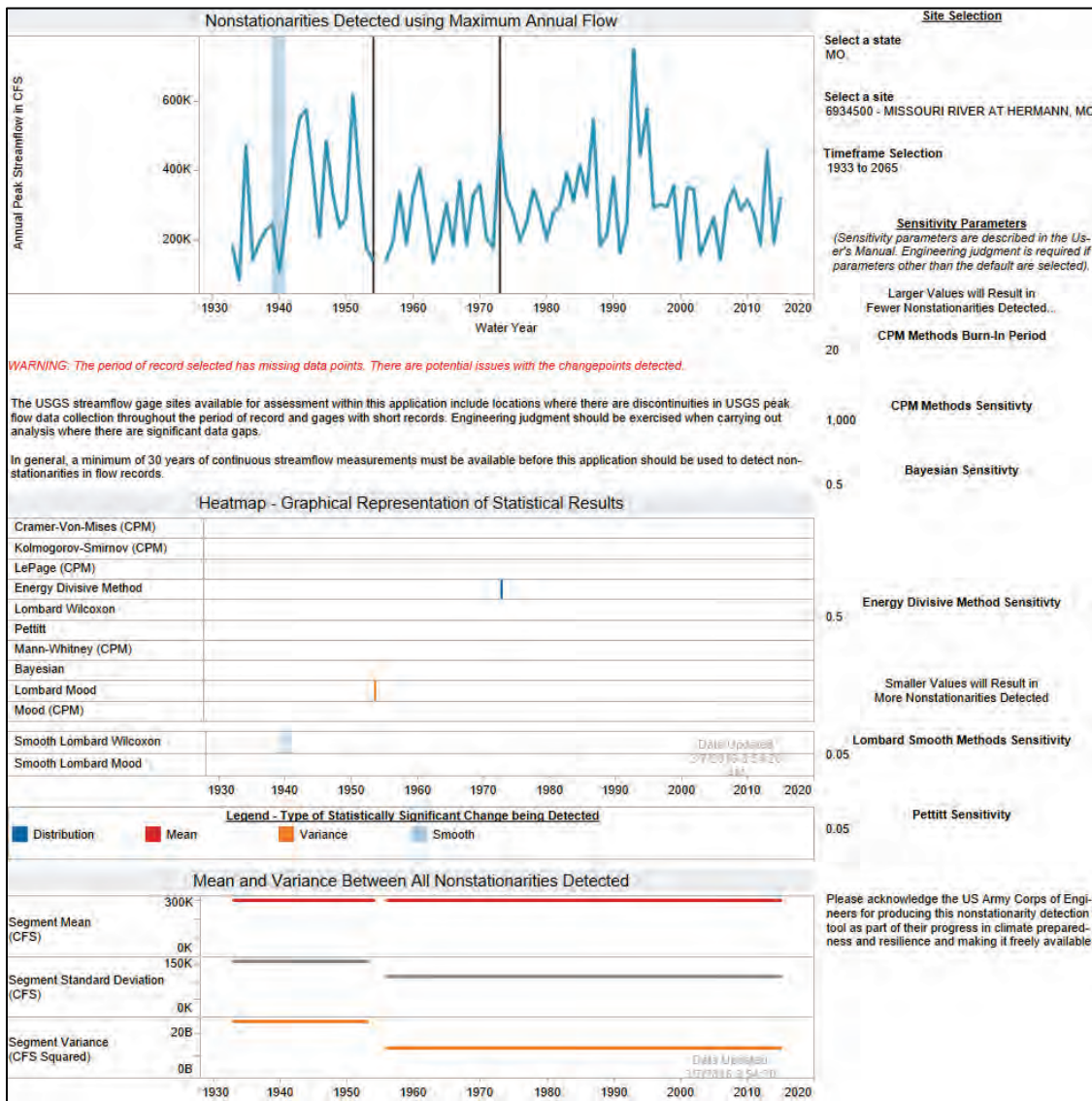


Figure 2-83. USGS Gage 6934500, Missouri River at Hermann, MO, nonstationarity detection.



The nonstationarity points detected in 1939 through 1941, 1954, and 1973 lack consensus between statistical tests. When the timeframe selection is adjusted to 1956–2065 to remove the gap in data, nonstationarity points are not detected.

Figure 2-84. USGS Gage 6934500, Missouri River at Hermann, MO, stationarity trend analysis.

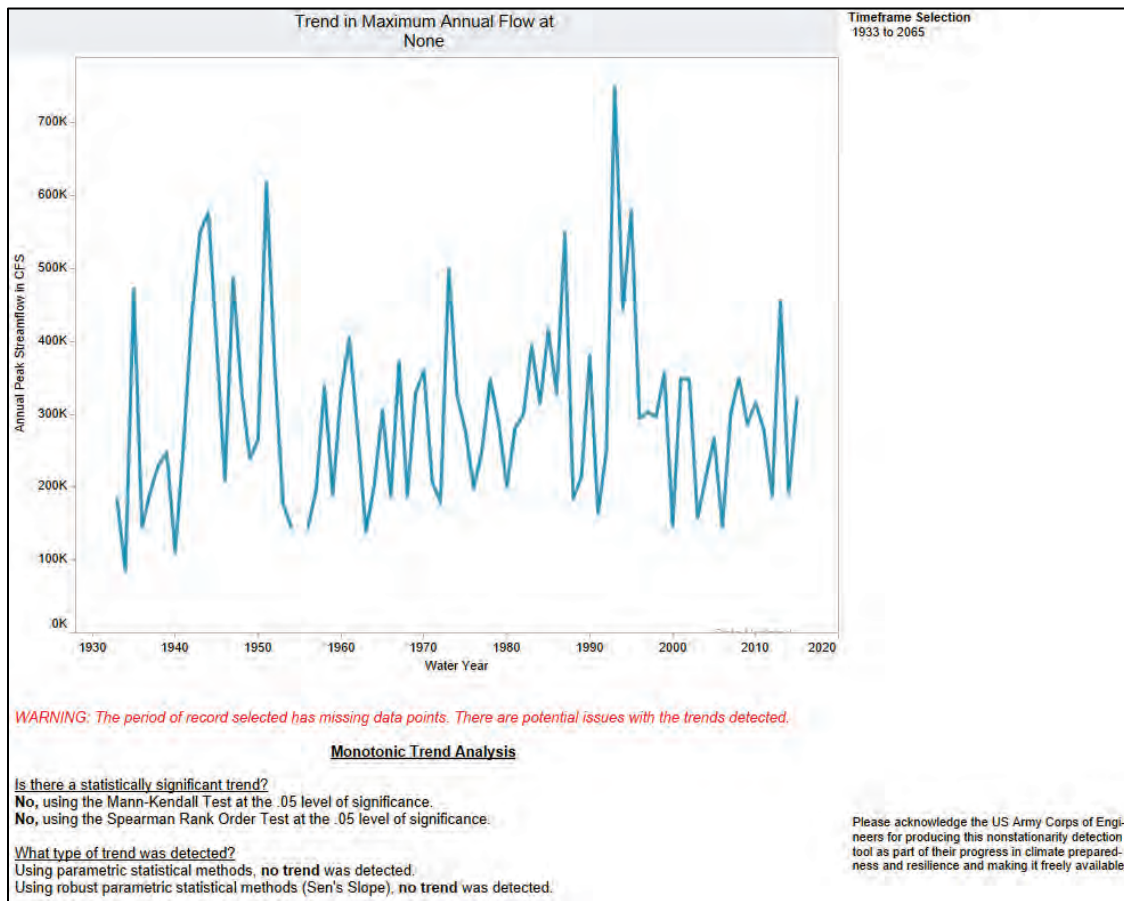
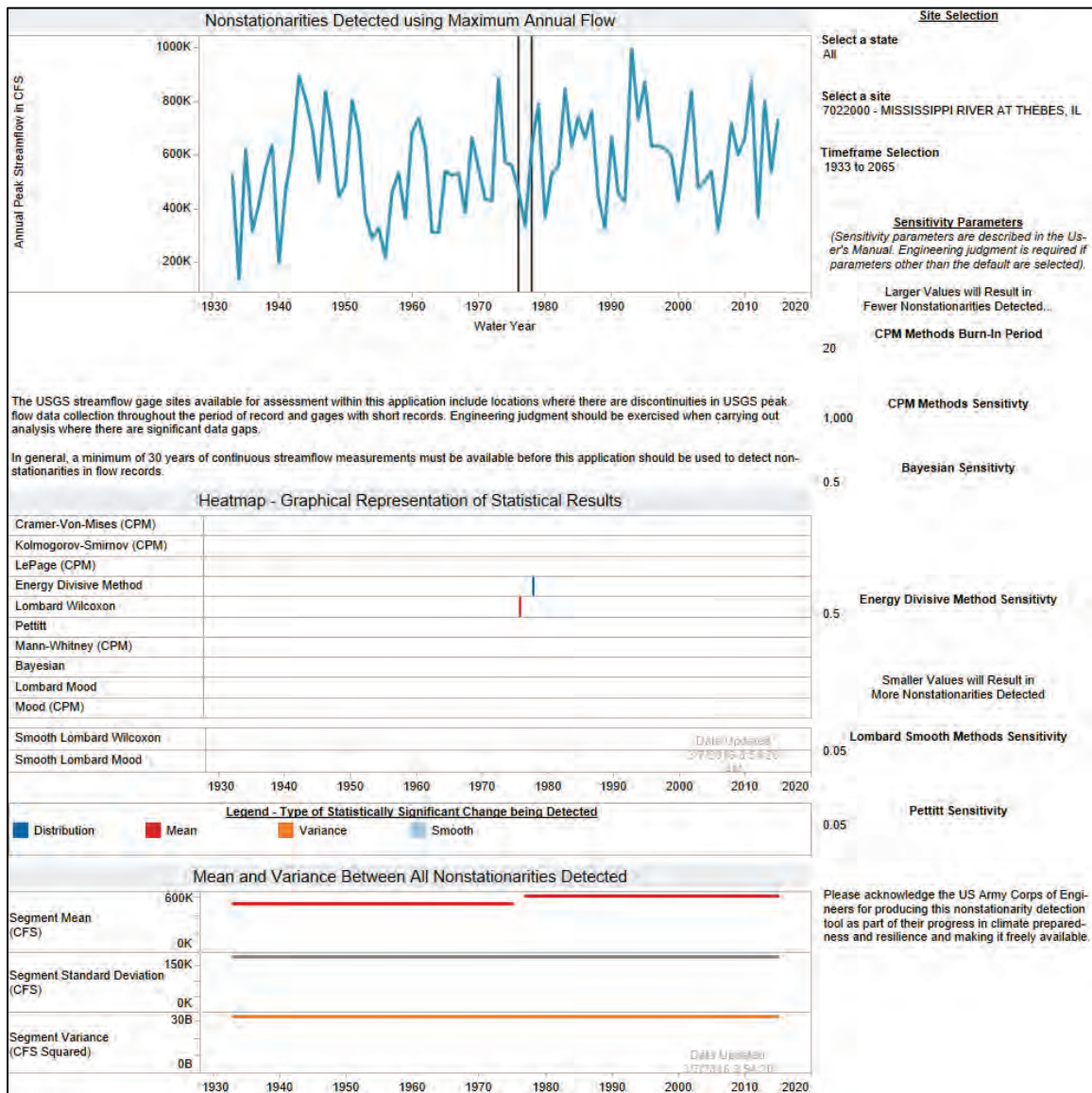


Figure 2-85. USGS Gage 7022000, Mississippi River at Thebes, IL, nonstationarity detection.



The nonstationarity points detected in 1976 and 1978 lack consensus between statistical tests.

Figure 2-86. USGS Gage 7022000, Mississippi River at Thebes, IL, stationarity trend analysis.

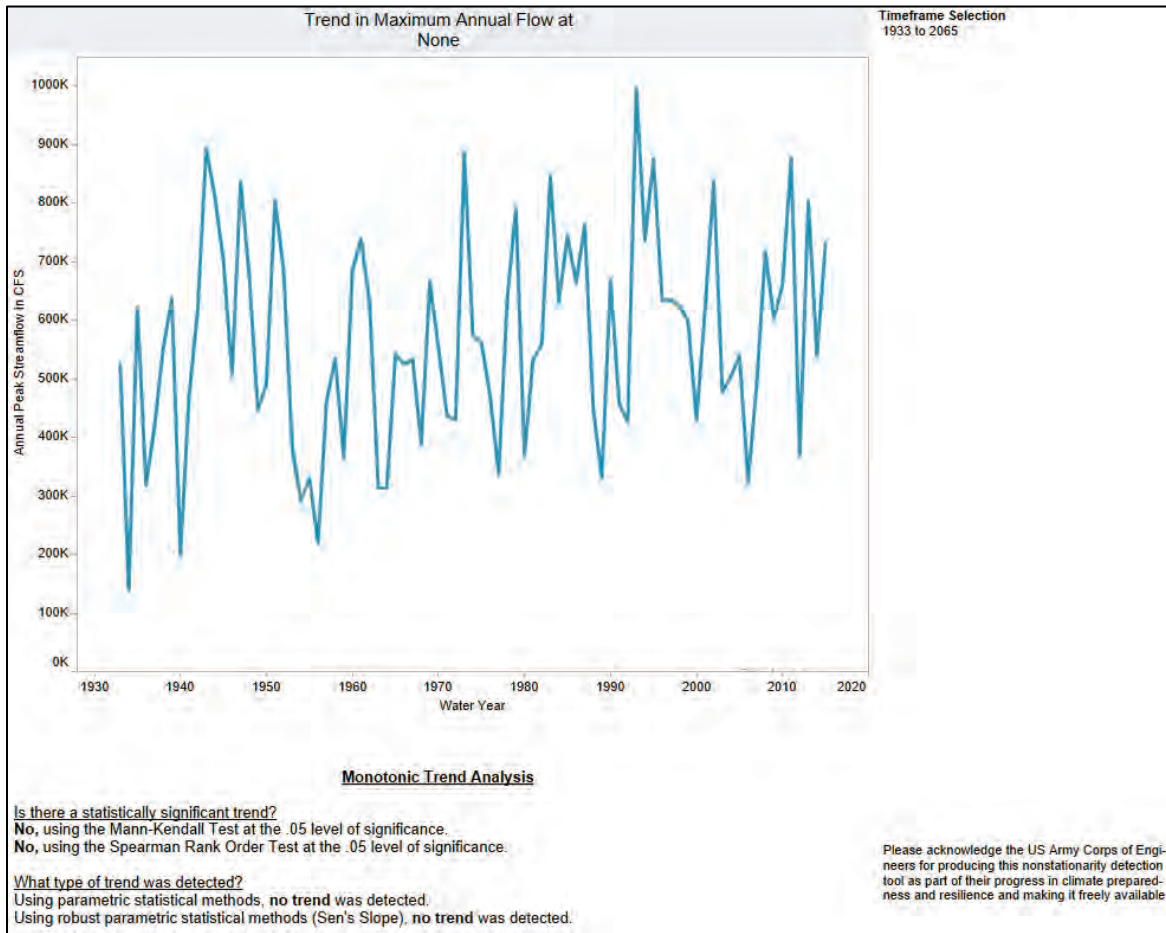


Figure 2-87. USGS Gage 7289000, Mississippi River at Vicksburg, MS, nonstationarity detection.

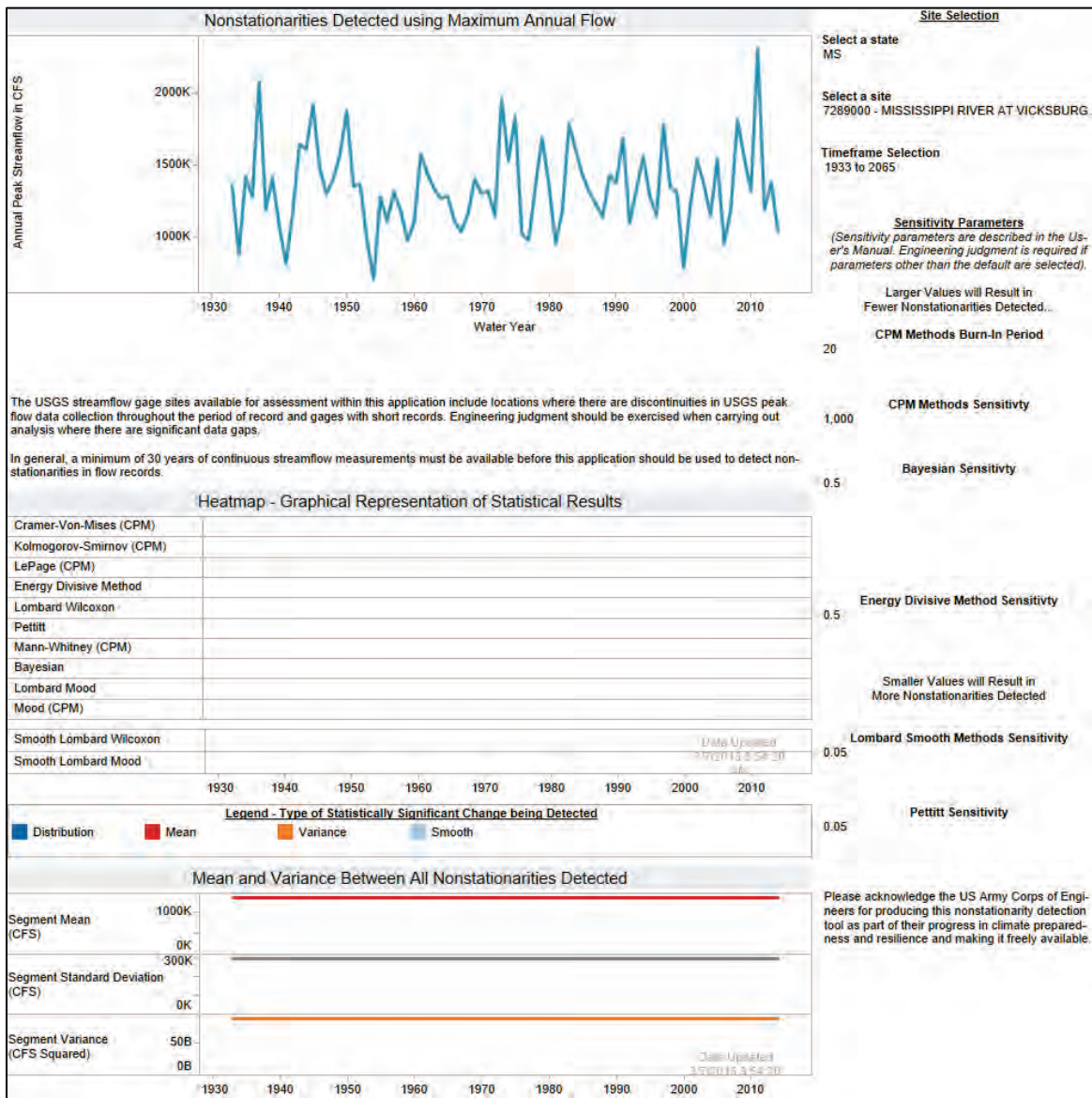


Figure 2-88. USGS Gage 7289000, Mississippi River at Vicksburg, MS, stationarity trend analysis.

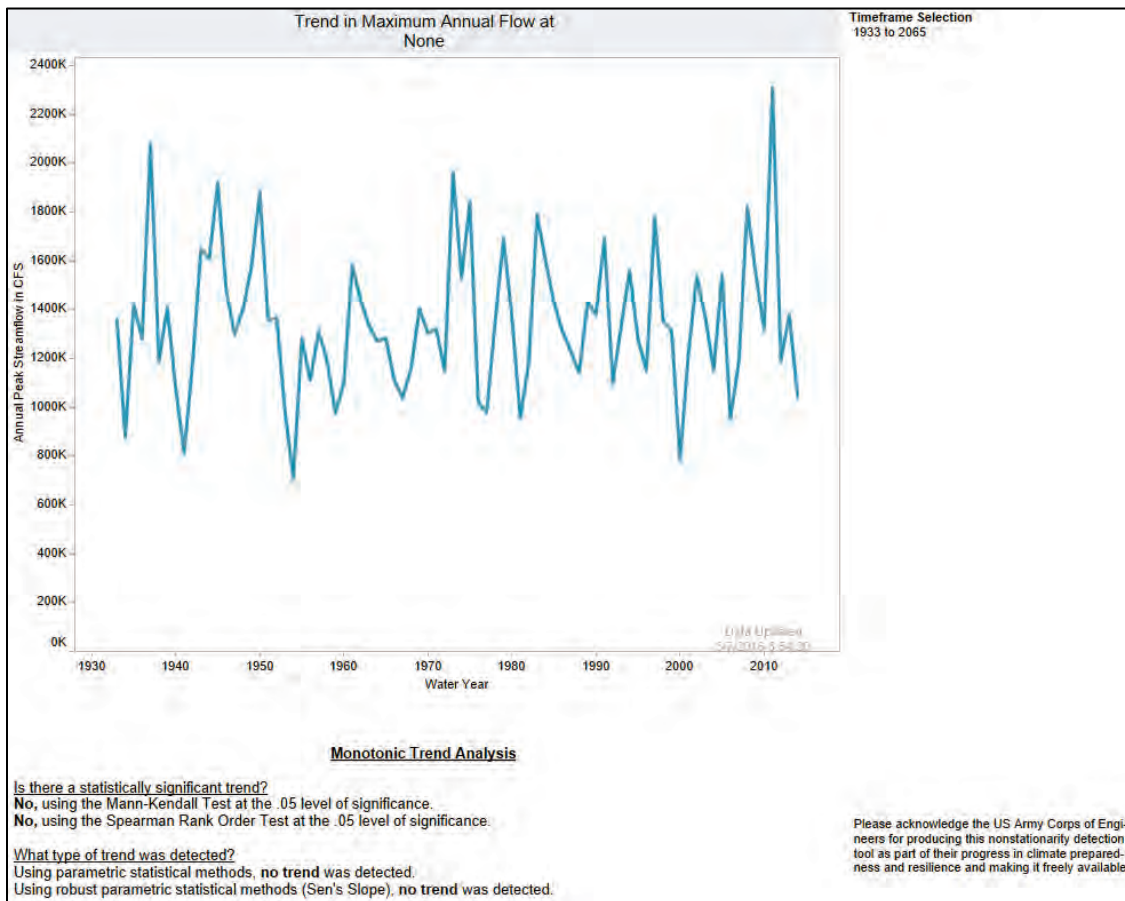
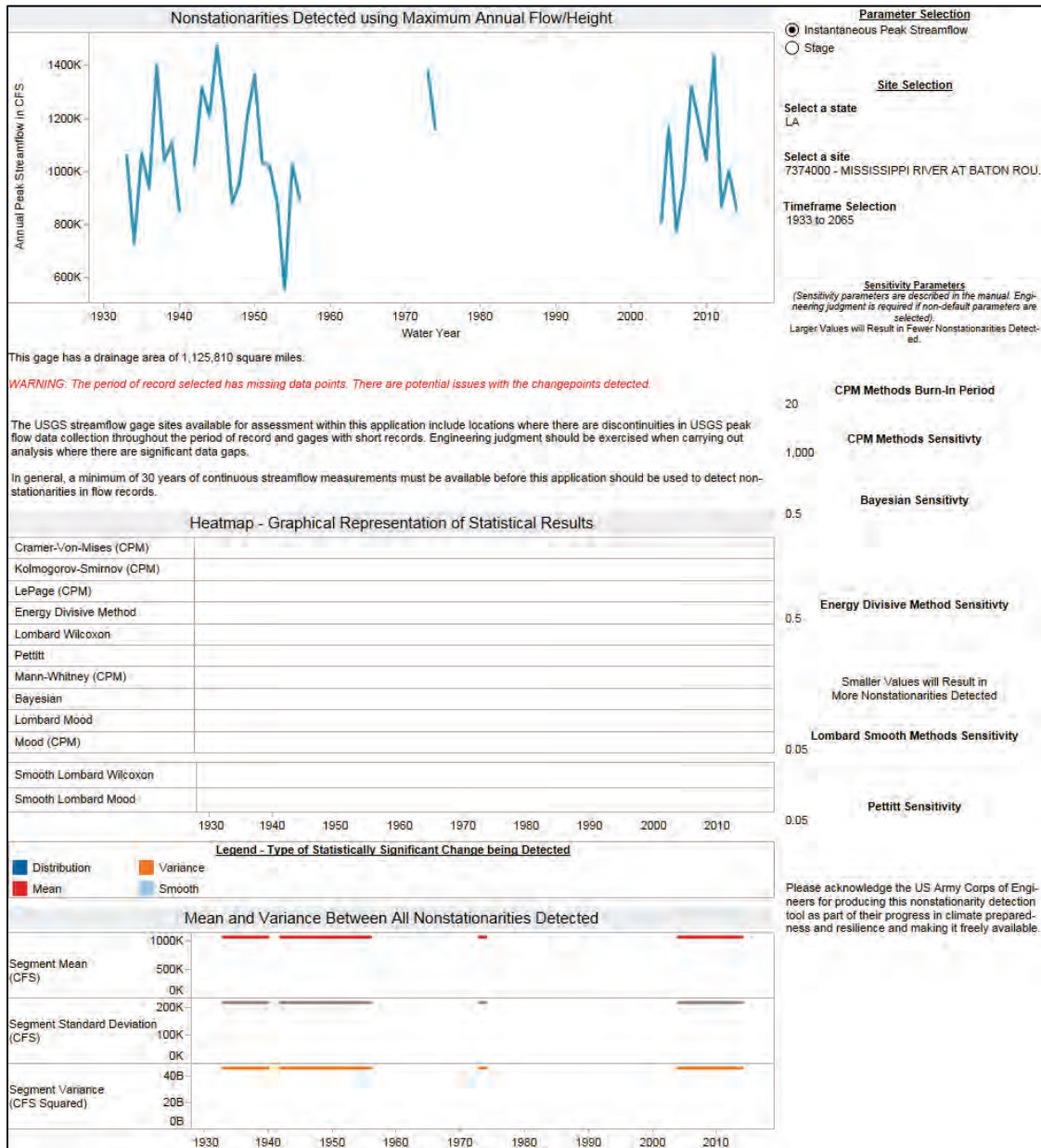
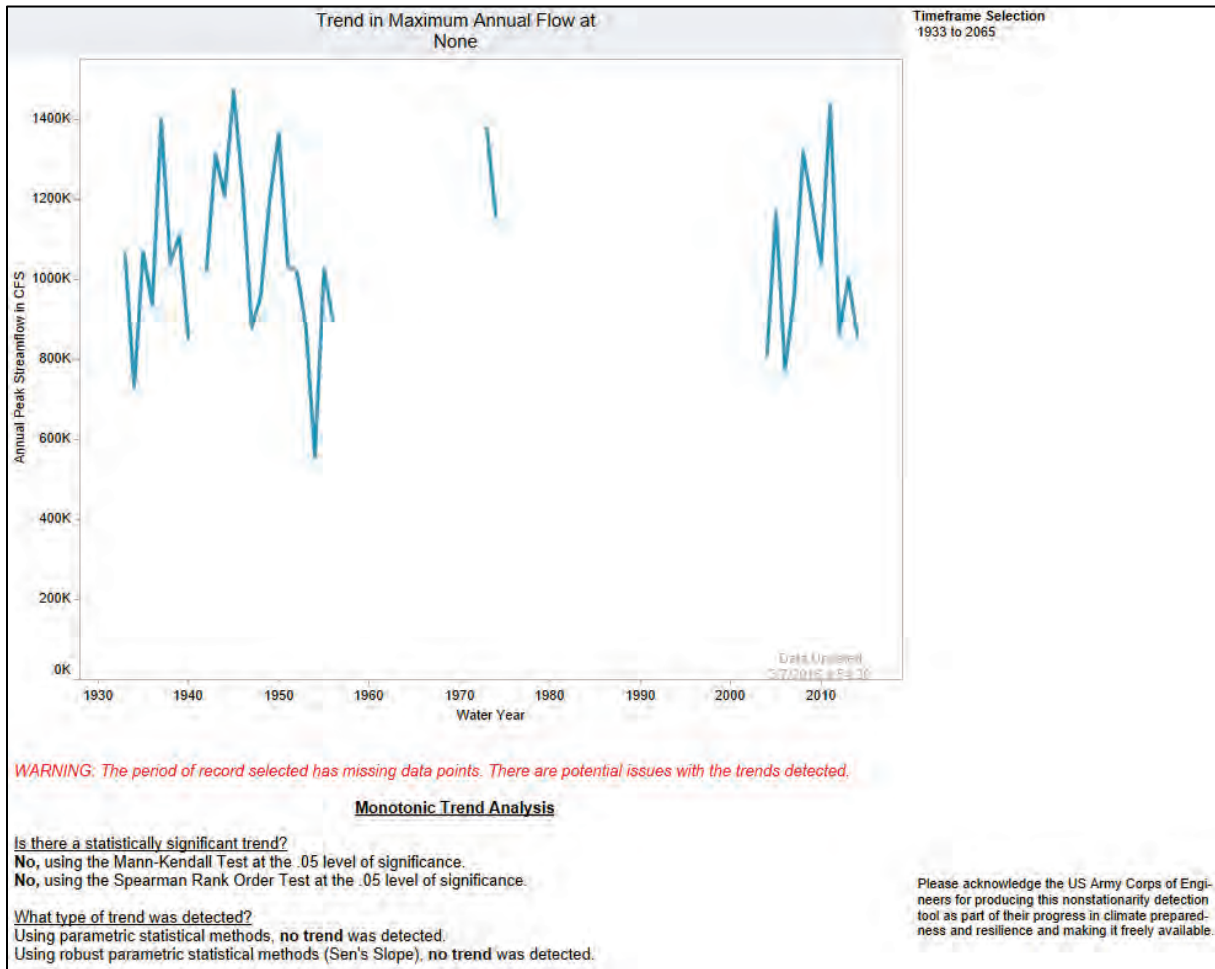


Figure 2-89. USGS Gage 7374000, Mississippi River at Baton Rouge, LA, nonstationarity detection.



The results from this gage location may be affected by the significant amount of missing data and should be considered with extreme caution. This is the only gage available on the Mississippi River in Louisiana.

Figure 2-90. USGS Gage 7374000, Mississippi River at Baton Rouge, LA, stationarity trend analysis.



Results of the analysis are summarized in Table 2-29.

Table 2-29. Stationarity analysis on selected gage locations that impact the Lower Mississippi River.

USGS Gage	Nonstationarity Detected (Y/N) ¹	Significant Trend Detected (Y/N)
3611500 - Ohio River at Metropolis, IL	N	N
6934500 - Missouri River at Hermann, MO	N	N
7022000 - Mississippi River at Thebes, IL	N	N
7289000 - Mississippi River at Vicksburg, MS	N	N
7374000 ² - Mississippi River at Baton Rouge, LA	N	N

¹ Significant nonstationarity is defined as a change point where statistical consensus is reached within a 5-year period or a known event caused nonstationarity.

² The results from this gage location may be affected by the significant amount of missing data.

While the analysis is not robust enough to understand stationarity in the entire Mississippi River Basin, the NDT analysis does provide a snapshot of the trends (or lack of trends) along the main reach of concern for the MR&T PDF. There were no significant nonstationarities or significant trends between 1933 to 2014 detected at any of the USGS gage locations examined.

With numerous climate change models to choose from, CHAT streamlines the selection process and allows USACE to consider climate change in a reproducible and comparable manner for all domestic projects by allowing climate change trends to be analyzed with one model that produces the projected annual maximum monthly flow trend line for year 2000–2099 and the climate-modeled annual maximum monthly flow range from 93 different climate models as shown in Figure 2-91–Figure 2-108.

Figure 2-91. Range of annual maximum monthly flow for 1111-Lower Arkansas River Basin.

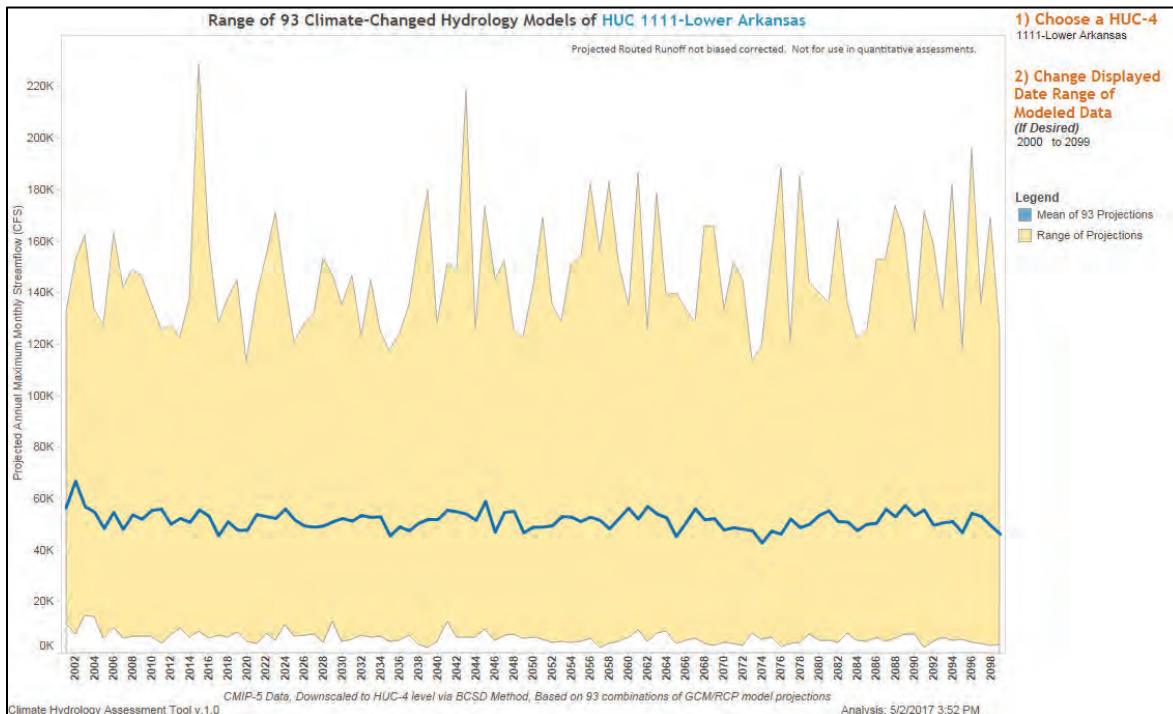


Figure 2-92. Annual maximum monthly flow for 1111-Lower Arkansas River Basin.
Trendline Equation: $Q = -25.8837 * (\text{Water Year}) + 104718, p = 0.04.$

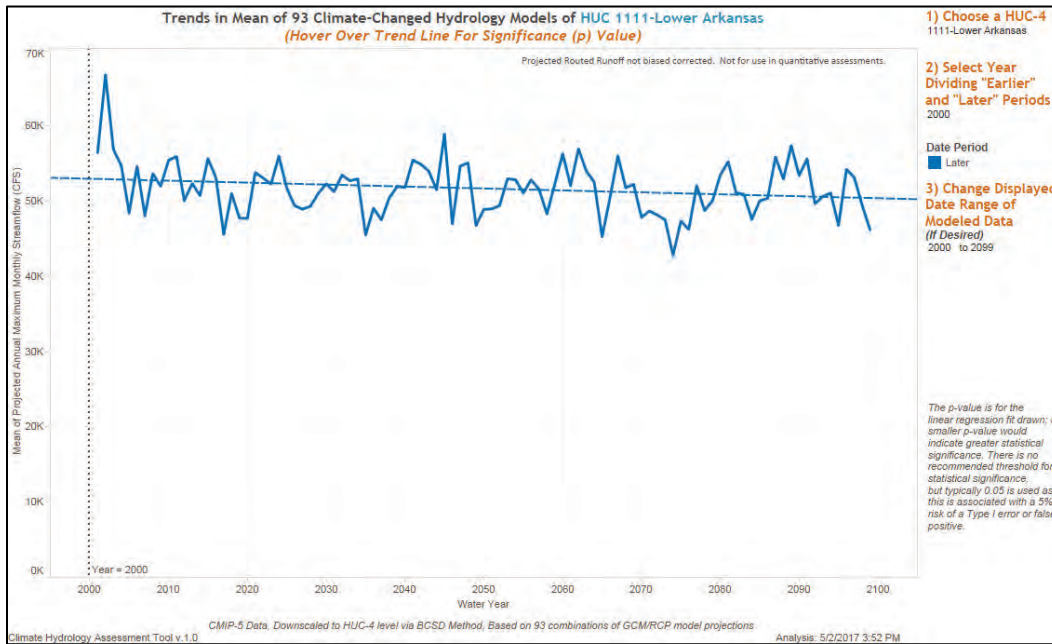


Figure 2-93. Range of annual maximum monthly flow for 1101-Upper White River Basin.

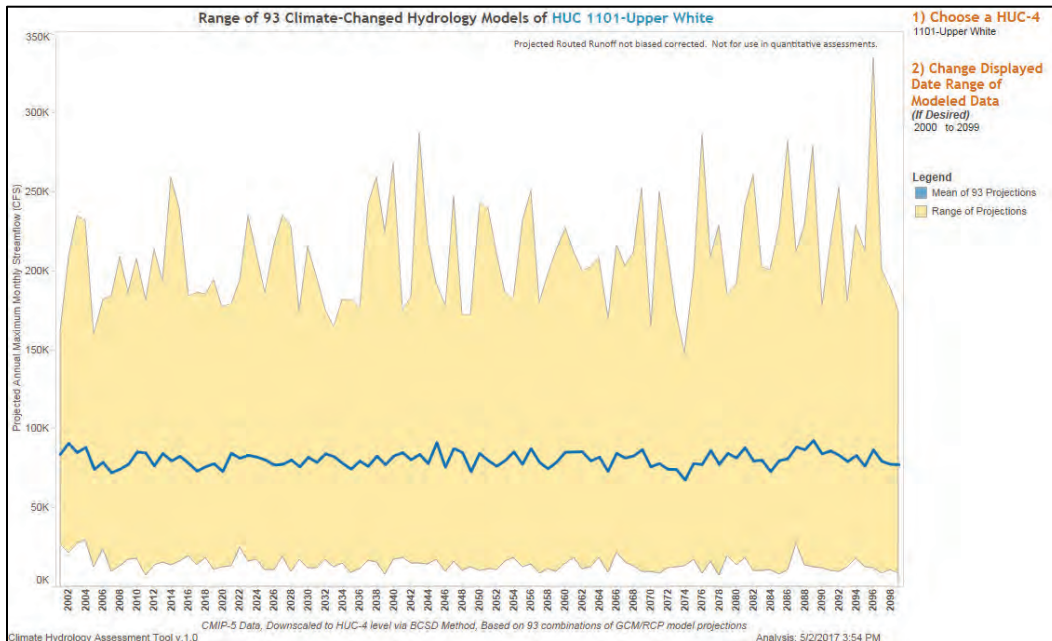


Figure 2-94. Annual maximum monthly flow for 1101-Upper White River Basin.
Trendline Equation: $Q = 13.1126 * (\text{Water Year}) + 53765.7, p = 0.44.$

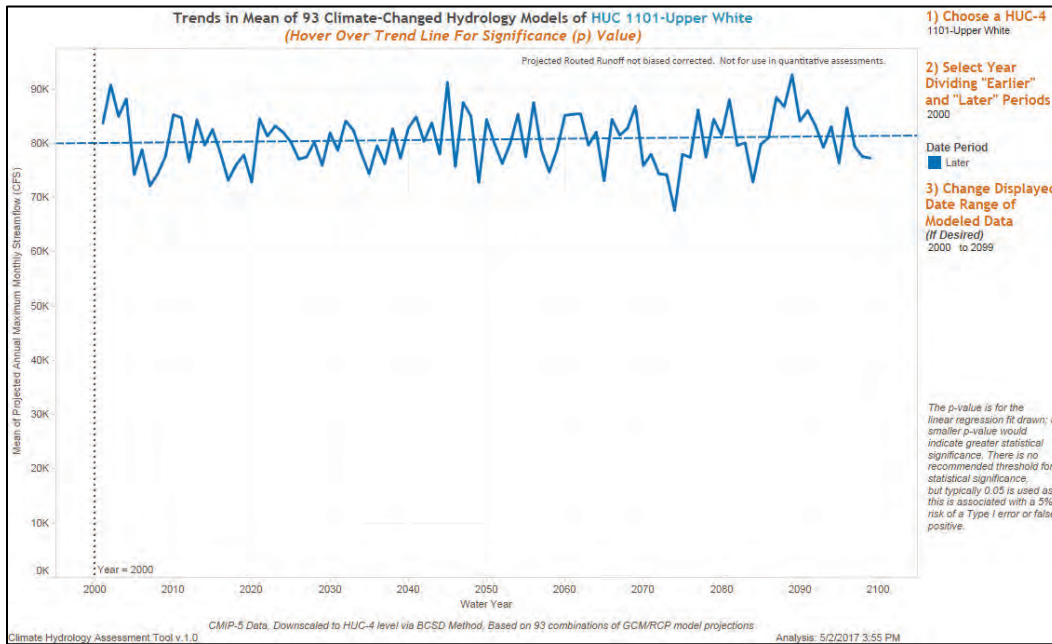


Figure 2-95. Range of annual maximum monthly flow for 0701-Mississippi River Headwaters.

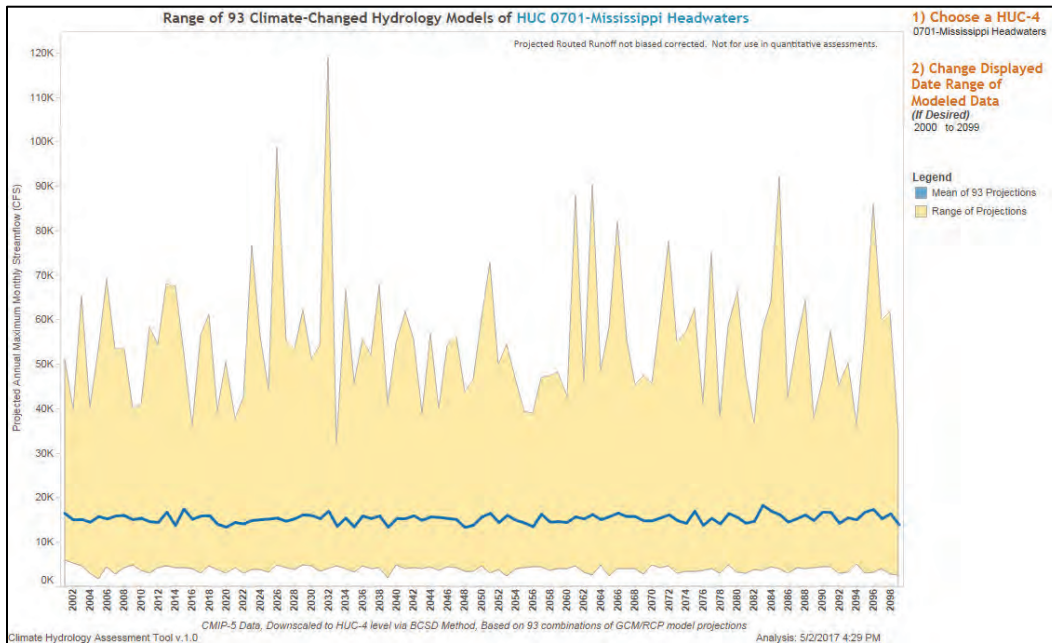


Figure 2-96. Annual maximum monthly flow for 0701-Mississippi River Headwaters.
Trendline Equation: $Q = 5.00965 * (\text{Water Year}) + 5041.06, p = 0.16.$

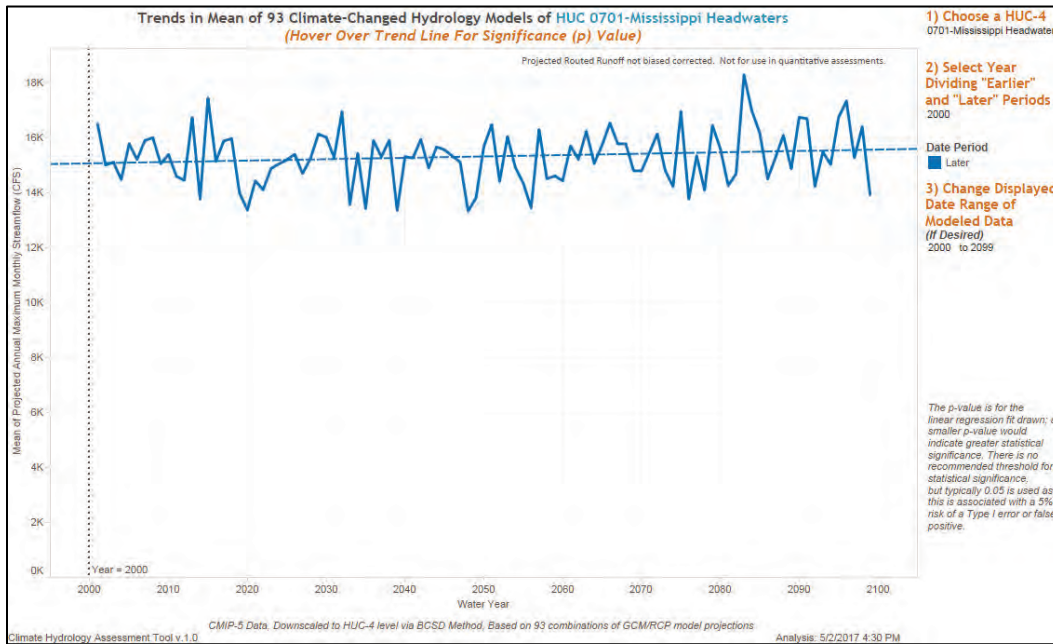


Figure 2-97. Range of annual maximum monthly flow for 0809-Lower Mississippi River Basin.

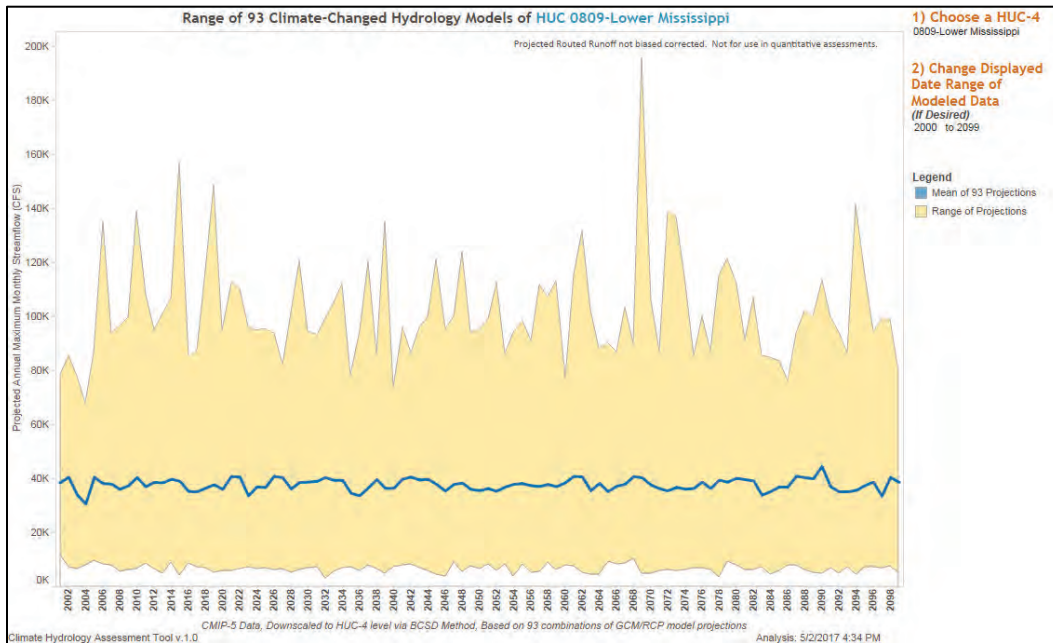


Figure 2-98. Annual maximum monthly flow for 0809-Lower Mississippi River Basin.
 Trendline Equation: $Q = 2.35076 * (\text{Water Year}) + 32968$, $p = 0.76$.

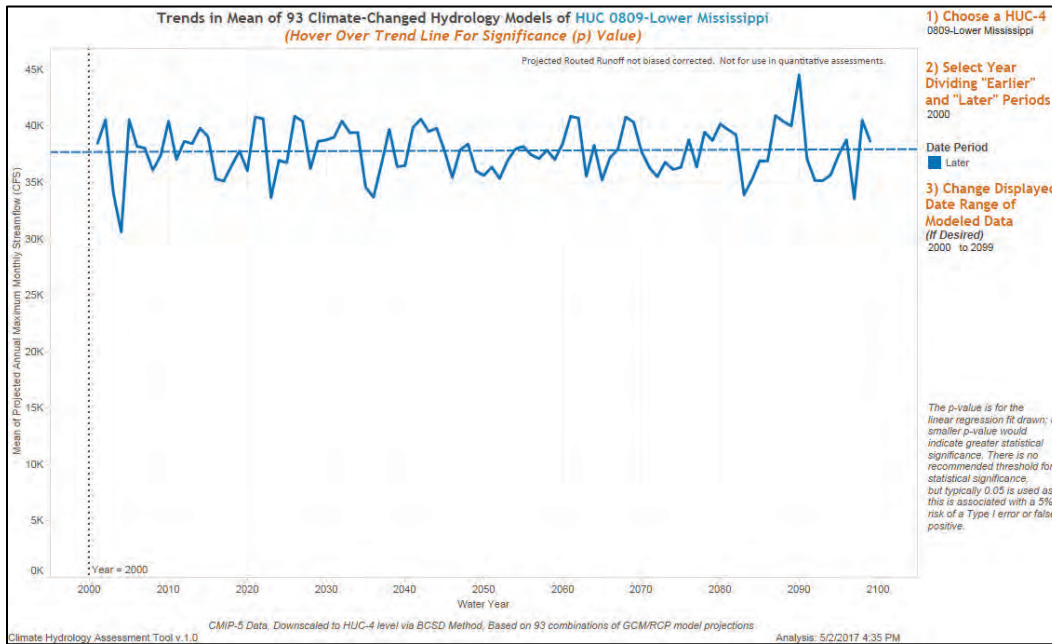


Figure 2-99. Range of annual maximum monthly flow for 1030-Lower Missouri River Basin.

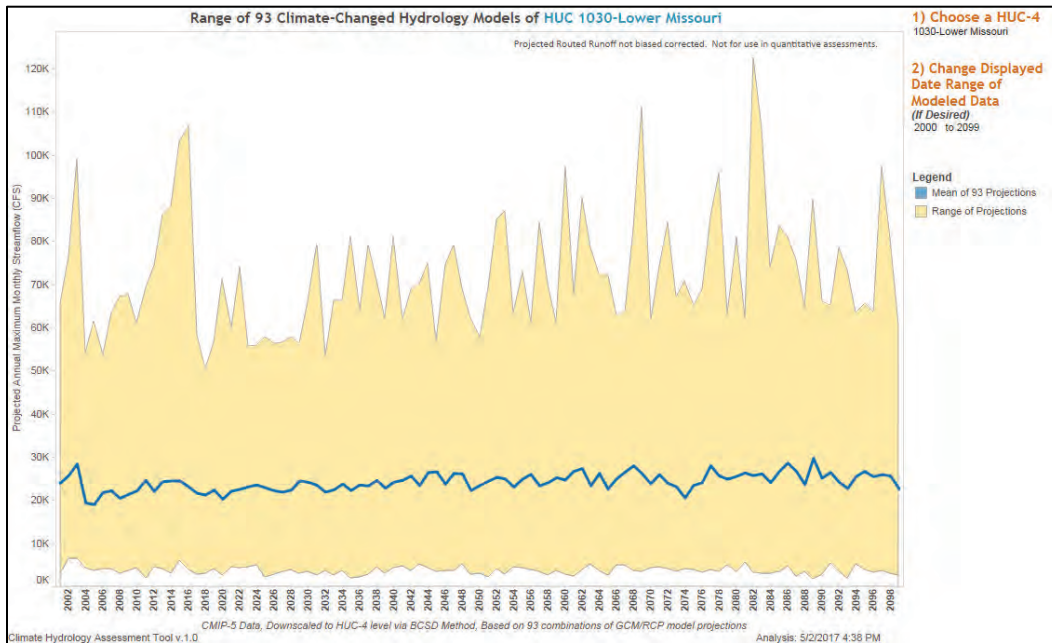


Figure 2-100. Annual maximum monthly flow for 1030-Lower Missouri River Basin.
Trendline Equation: $Q = 37.2536 * (\text{Water Year}) + - 52125.6, p < 0.0001$.

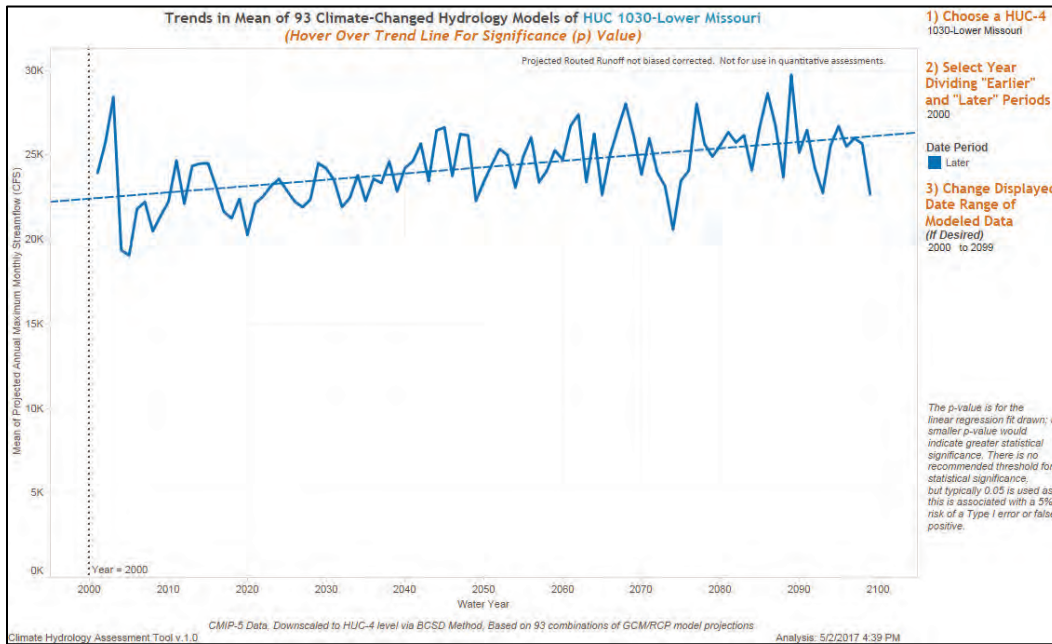


Figure 2-101. Range of annual maximum monthly flow for 0604-Lower Tennessee River Basin.

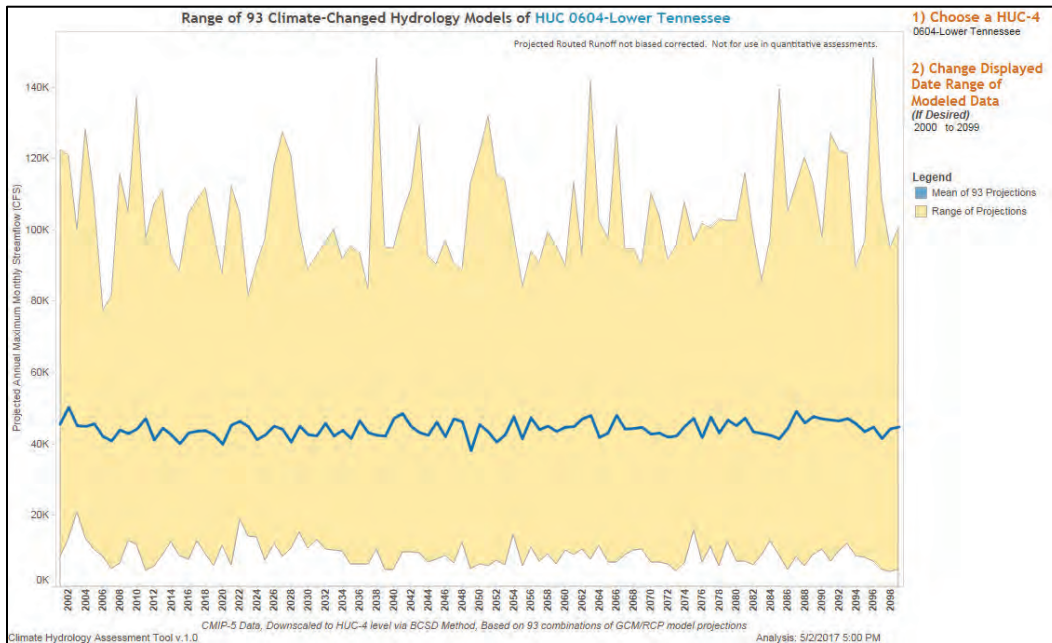


Figure 2-102. Annual maximum monthly flow for 0604-Lower Tennessee River Basin.
Trendline Equation: $Q = 14.876 * (\text{Water Year}) + 13754.2$, $p = 0.07$.

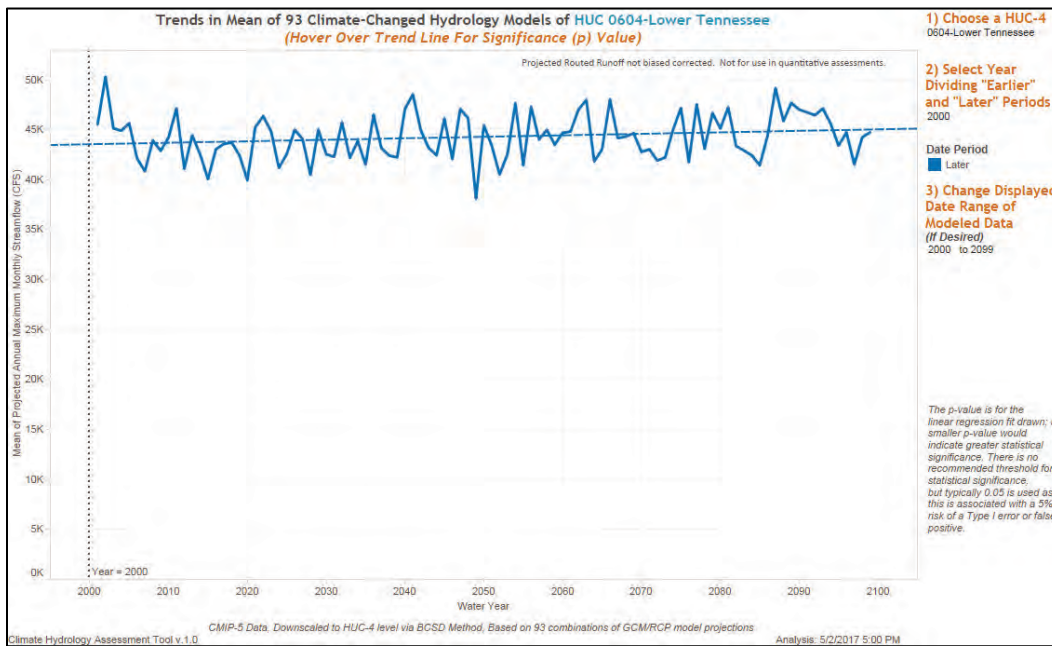


Figure 2-103. Range of annual maximum monthly flow for 0513-Cumberland River Basin.

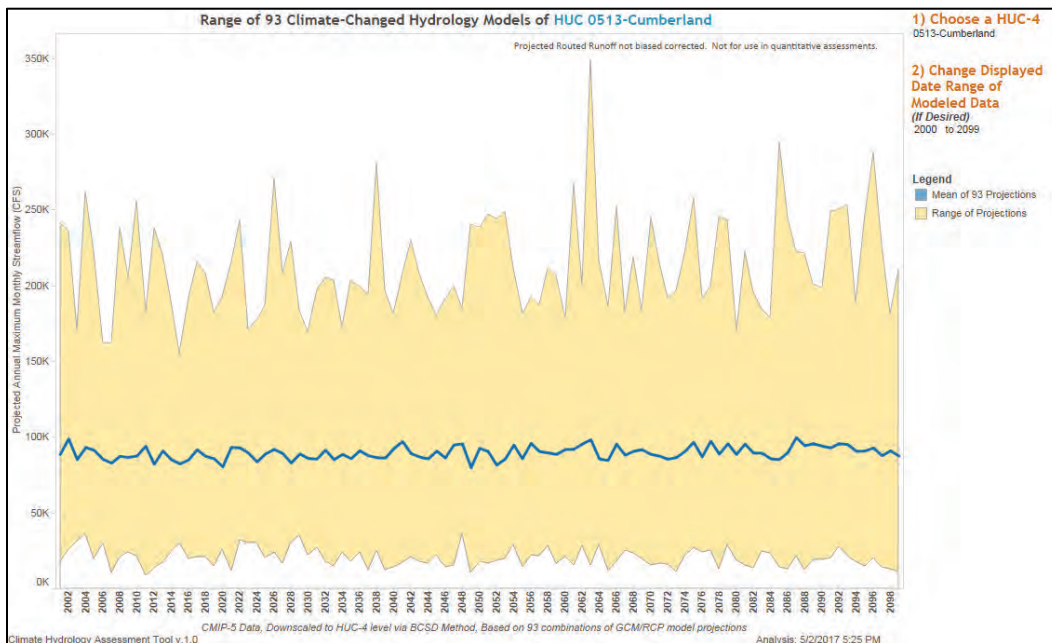


Figure 2-104 Annual maximum monthly flow for 0513-Cumberland River Basin.
 Trendline Equation: $Q = 47.6113 * (\text{Water Year}) + -52125.6, p = 0.002.$

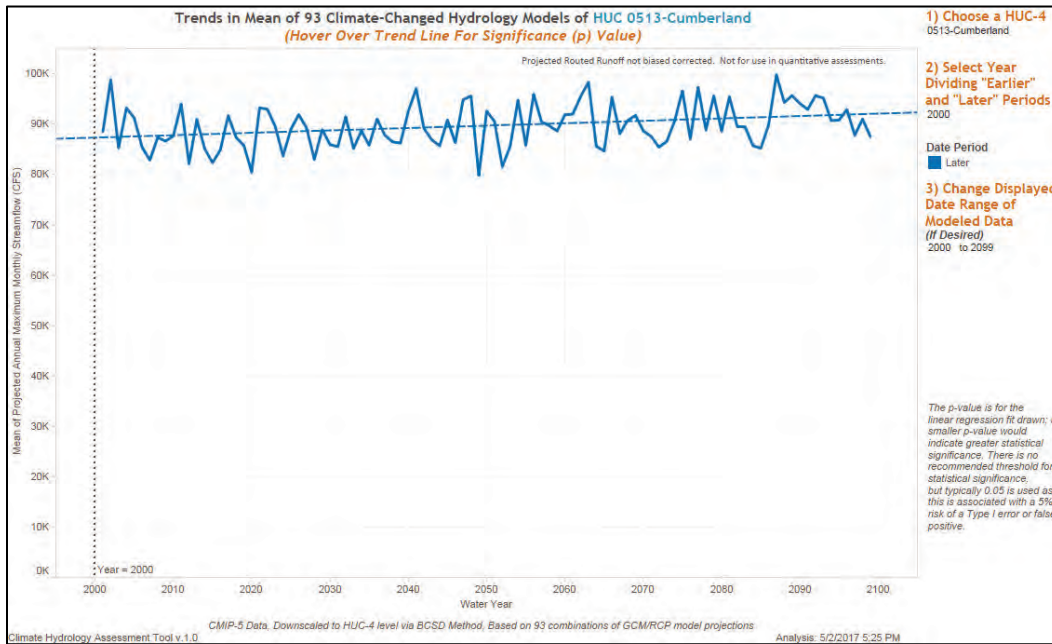


Figure 2-105. Range of annual maximum monthly flow for 0514-Lower Ohio River Basin.

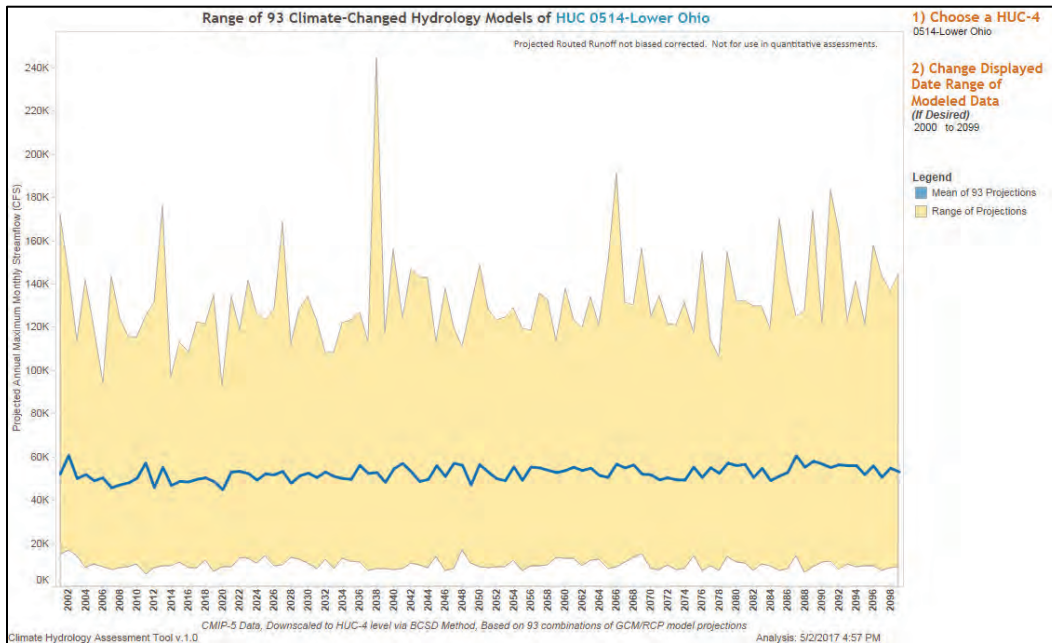


Figure 2-106. Annual maximum monthly flow for 0514-Lower Ohio River Basin.
Trendline Equation: $Q = 47.9137 * (\text{Water Year}) + -45758.8, p < 0.0001.$

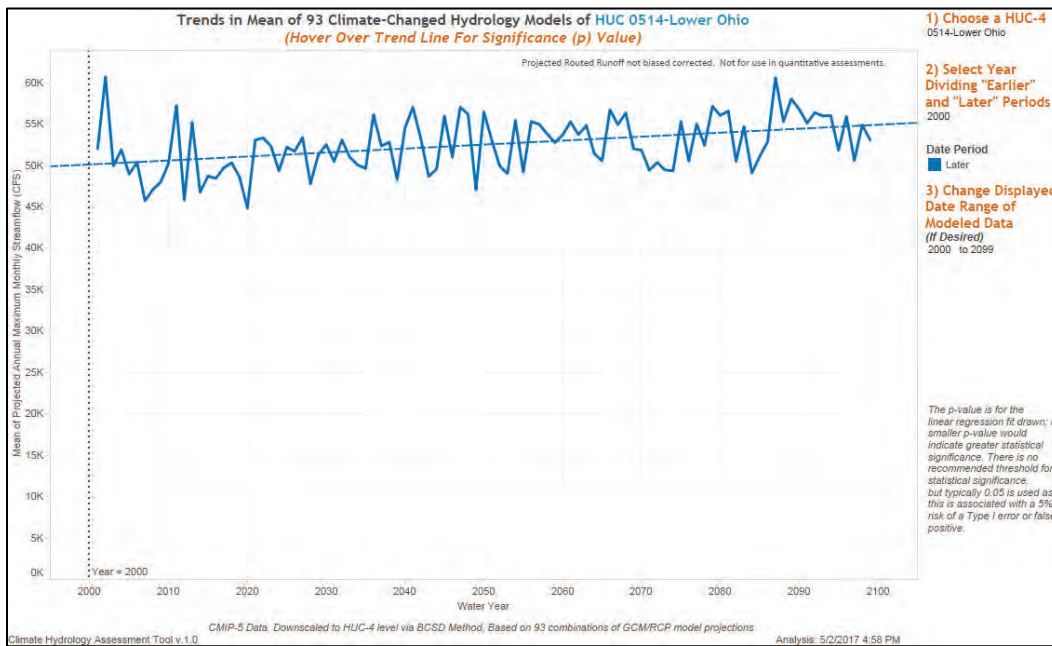


Figure 2-107. Range of annual maximum monthly flow for 1114-Red Sulfur.

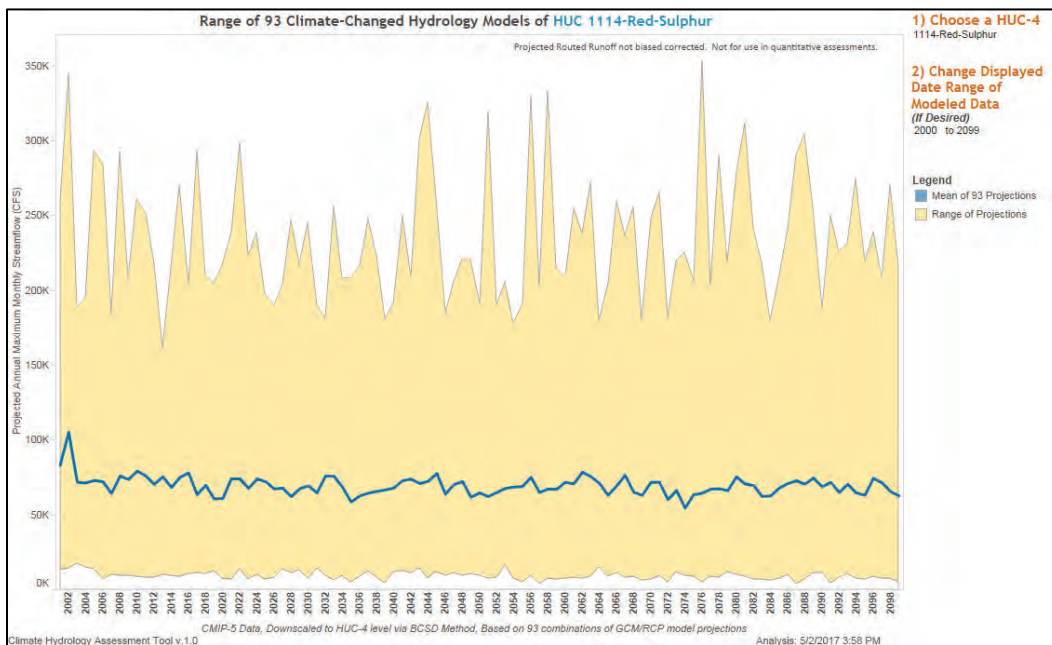
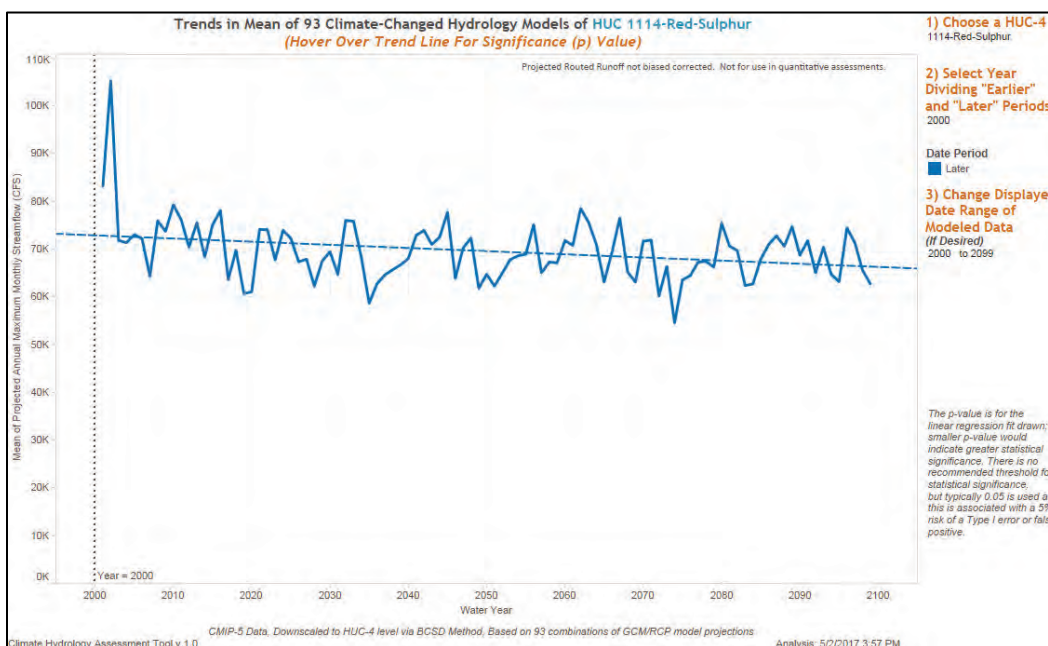


Figure 2-108. Annual maximum monthly flow for 1114-Red Sulfur. Trendline Equation: $Q = - 6.0463 * (\text{Water Year}) + 204856$, $p = 0.003$.



Each graph includes statistical significance (p) as shown in Table 2-30.

Table 2-30. HUC 4 basins from USACE Climate Change Web Analysis Tool with calculated significance, p .

HUC–Basin Name	Projected Annual Maximum Monthly Flow, p (2000–2099)
1111–Lower Arkansas River	0.04 -
1101–Upper White River	0.44 +
0701–Mississippi River Headwaters	0.16 +
0809–Lower Mississippi River	0.76 +
1030–Lower Missouri River	<0.0001 +
0514–Lower Ohio River Basin	<0.0001 +
0604–Lower Tennessee River	0.07 +
0513–Cumberland River	0.002 +
1114–Red Sulfur	0.003 -

- = downward trend

+ = upward trend

Climate Change Web Analysis Tool accessed on 05/02/2017 with the Demo Tool v.1.0.

The data show that the projected trends in the Lower Missouri River, Lower Ohio River, and Cumberland River Basin have a significant positive trend ($p < 0.05$) in discharge for increasing maximum monthly flows over the next century while the Red Sulfur and Lower Arkansas Rivers show a significant decreasing trend. The Upper White River, Mississippi River Headwaters, Lower Tennessee River, and Lower Mississippi River do not have a statistically significant trend for maximum monthly flows over the next century. The goodness-of-fit for all of the analyses is low indicating that little of the variability in flow can be explained by change over time.

2.14.4 Watershed vulnerability assessment (VA) tool

The USACE VA tool evaluates climate change vulnerabilities at the HUC-4 level by using a weighted order weighted average that assigns vulnerability scores based on numerous indicators. These indicators assess eight business line vulnerabilities critical to the USACE mission for two scenarios (dry and wet) over two epochs (2050 and 2085). This tool was used to determine which HUCs in the MVD have business line vulnerabilities for both the wet and dry 2085 conditions.

Each of the eight business lines — flood risk reduction, navigation, ecosystem restoration, emergency management, hydropower, recreation, regulatory, and water supply — were evaluated. Flood risk reduction, navigation, and emergency management are of particular interest for this assessment.

The VA tool identifies flood risk vulnerabilities are determined by the tool based on the following indicators:

- Acres of urban area within the 500-year floodplain
- Coefficient of variation of cumulative annual flow
- Streamflow elasticity, or ratio of streamflow response to precipitation
- Flood magnification: ratio of 10% exceedance flow in the future to the 10% exceedance flow in the base flow period, for cumulative monthly flows
- Flood magnification: ratio of 10% exceedance flow in the future to the 10% exceedance flow in the base flow period, for local monthly flows.

The VA tool identifies Navigation risk vulnerabilities are determined by the tool based on the following indicators:

- The ratio of the change in the sediment load in the future to the present load
- Land area that is urban or suburban as a percentage of the total U.S. land area
- Measure of the short-term variability in the region's hydrology: 75th percentile of annual ratios of the standard deviation of monthly runoff to the mean of monthly runoff. Includes upstream freshwater inputs (cumulative).
- Median of deviation of runoff from monthly mean times average monthly runoff to the mean of monthly runoff. Excludes upstream freshwater inputs (local).
- Acres of urban area within the 500-year floodplain
- Flood magnification: ratio of 10% exceedance flow in the future to the 10% exceedance flow in the base flow period, for cumulative monthly flows
- Low runoff: monthly runoff that is exceeded 90% of the time, including upstream freshwater (cumulative and local)
- Change in low runoff: ratio of indicator exceeded 90% of the time
- Greatest precipitation deficit: The most negative value calculated by subtracting potential evapotranspiration from precipitation over any 1-, 3-, 6-, or 12- month period.

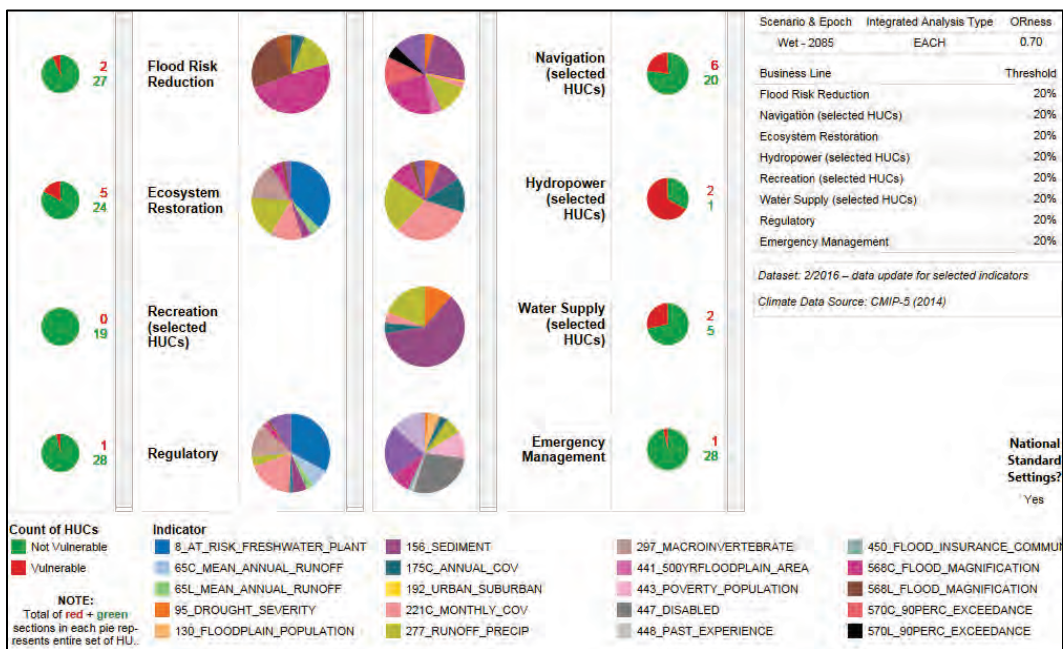
The VA tool identifies Emergency management risk vulnerabilities are determined by the tool based on the following indicators:

- Population within the 500-year floodplain
- Ratio of the standard deviation of annual runoff to the annual runoff mean. Includes upstream freshwater (cumulative).
- Median of deviation of runoff from monthly mean times average monthly runoff divided by deviation of precipitation from monthly mean times average monthly precipitation.
- Number of people living below the poverty line
- Percent of people who are disabled
- Experience with declared disasters in the past
- Number of communities enrolled in the National Flood Insurance Program

- Flood magnification: ratio of 10% exceedance flow in the future to the 10% exceedance flow in the base flow period, for cumulative monthly flows
- Change in low runoff: ratio of indicator exceeded 90% of the time.

Indicators for the other business lines are available for review in the tool. Figure 2-109 displays each of the eight USACE business lines for the wet scenario 2085 epoch.

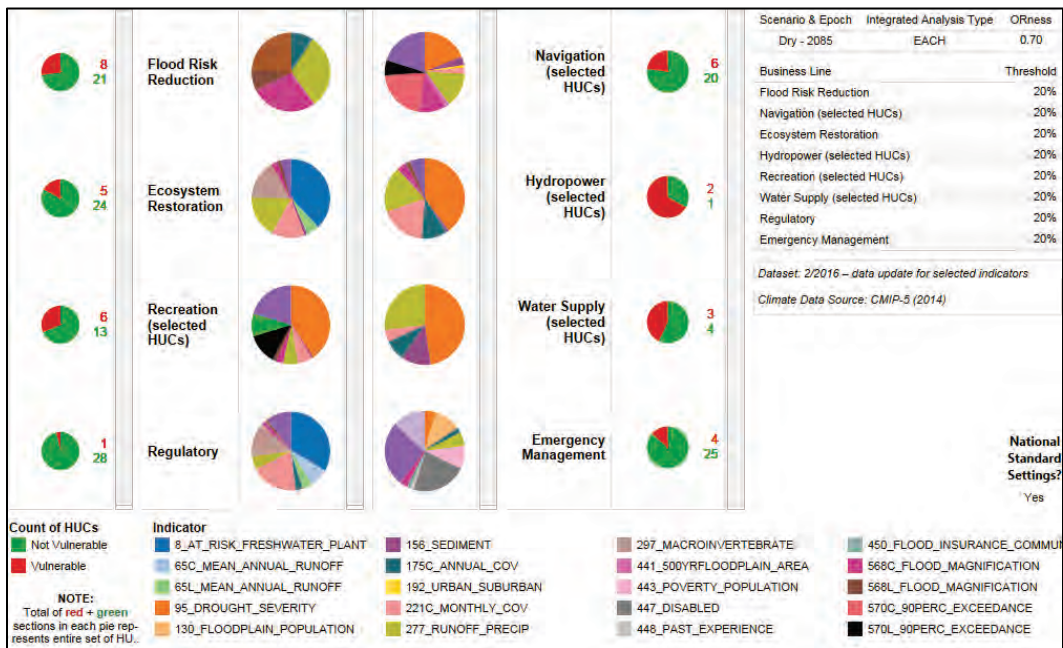
Figure 2-109. MVD business line vulnerability assessment for the wet scenario 2085 epoch.



There are two HUCs vulnerable for flood risk, six HUCs vulnerable for navigation, and one HUC vulnerable for emergency management.

Figure 2-110 displays each of the eight USACE business lines for the dry scenario 2085 epoch.

Figure 2-110. MVD business line vulnerability assessment for the dry scenario 2085 epoch.



There are eight HUCs vulnerable for flood risk, six HUCs vulnerable for navigation, and four HUCs vulnerable for emergency management.

The USACE IWR summarizes the available literature to summarize business line vulnerabilities in each region within the Mississippi River Basin (USACE 2015a-f). Summaries for each region are detailed in Figure 2-111 through Figure 2-116.

Figure 2-111. Summary of projected climate trends and impacts on USACE business lines for Region 05 – Ohio (USACE 2015a).



































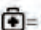
CLIMATE VARIABLE	VULNERABILITY
 <p>Increased Ambient Temperatures</p>	<p>Increased ambient air temperatures throughout the century, and over the next century are expected to create the following vulnerabilities on the business lines in the region:</p> <ul style="list-style-type: none"> • Loss of vegetation from increased periods of drought and reduced streamflows may have impacts on vegetation within the region, which is important for sediment stabilization in the watershed. Loss of non-drought resistant vegetation may result in an increase in sediment loading, potentially causing geomorphic changes in the tributaries to the river system. • Decrease in flows may result from periods of drought and reduced streamflow has implications for maintain water levels in the rivers. <p>BUSINESS LINES IMPACTED:      </p>
 <p>Increased Maximum Temperatures</p>	<p>Air temperatures are expected to increase 2-6°C in the latter half of the century with the number of heat wave days increasing as much as 75 days. This is expected to create the following vulnerabilities on business lines in the region:</p> <ul style="list-style-type: none"> • Increased water temperatures leading to water quality concerns, particularly for the dissolved oxygen (DO) levels, growth of nuisance algal blooms and influence wildlife and supporting food supplies. • Increased evapotranspiration. • Human health risk increases from extended heat waves, impacting recreational visitors and increasing the need for emergency management. <p>BUSINESS LINES IMPACTED:    </p>
 <p>Increased Annual Precipitation</p>	<p>By the middle of the century, annual precipitation is expected to increase in the region which are expected to influence the following vulnerabilities on business lines in the region:</p> <ul style="list-style-type: none"> • Increased flows and runoff, which may carry pollutants to receiving water bodies, decreasing water quality. • Increased erosion with subsequent changes in sediment accumulation rates and creating water quality concerns. • Increased flooding, which may have negative consequences for all infrastructure, habitats, and people in the area. <p>BUSINESS LINES IMPACTED:       </p>
 <p>Streamflow Variability</p>	<p>Streamflow will have more extreme variability, which greatly depends on where the area of the region. This may result in:</p> <ul style="list-style-type: none"> • Increased flows and runoff, which may carry pollutants to receiving water bodies, decreasing water quality. • Increased erosion with subsequent changes in sediment accumulation rates and creating water quality concerns. • Increased flooding, which may have negative consequences for all infrastructure, habitats, and people in the area. • Loss of vegetation from increased periods of drought and reduced streamflows may have impacts on vegetation within the region, which is important for sediment stabilization in the watershed. Loss of non-drought resistant vegetation may result in an increase in sediment loading, potentially causing geomorphic changes in the tributaries to the river system. • Decrease in flows may result from periods of drought and reduced streamflow has implications for maintain water levels in the rivers. <p>BUSINESS LINES IMPACTED:       </p>
<p><i>NOTE: The Regulatory and Military Program business lines may be impacted by all climate variables</i></p>	
<p> = Navigation  = Flood Risk Management  = Ecosystem Restoration  = Hydropower  = Recreation  = Water Supply  = Emergency Management</p>	

Figure 2-112. Summary of projected climate trends and impacts on USACE business lines for Region 06 – Tennessee (USACE 2015b).



























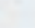
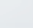







CLIMATE VARIABLE	VULNERABILITY
 Increased Ambient Temperatures	<p>Increased ambient air temperatures throughout the century, and over the next century are expected to create the following vulnerabilities on the business lines in the region:</p> <ul style="list-style-type: none"> • Loss of vegetation from increased periods of drought and reduced streamflows may have impacts on vegetation within the region, which is important for sediment stabilization in the watershed. Loss of non-drought resistant vegetation may result in an increase in sediment loading, potentially causing geomorphic changes in the tributaries to the river system. • Decrease in flows may result from periods of drought and reduced streamflow has implications for maintain water levels in the rivers. • Flora and fauna that are not drought resistant can also be impacted by longer drought conditions, which may reduce opportunities for recreational wildlife viewing. <p>BUSINESS LINES IMPACTED:      </p>
 Increased Maximum Temperatures	<p>Air temperatures are expected to increase, including maximum high and low temperatures in each season. This is expected to create the following vulnerabilities on business lines in the region:</p> <ul style="list-style-type: none"> • Increased water temperatures leading to water quality concerns, particularly for the dissolved oxygen (DO) levels, growth of nuisance algal blooms and influence wildlife and supporting food supplies. • Increased evapotranspiration. • Human health risk increases from extended heat waves, impacting recreational visitors and increasing the need for emergency management. <p>BUSINESS LINES IMPACTED:    </p>
 Increased Storm Intensity and Frequency	<p>Extreme storm events may become more intense and frequent over the coming century which are expected to influence the following vulnerabilities on business lines in the region:</p> <ul style="list-style-type: none"> • Increased flows and runoff, which may carry pollutants to receiving water bodies, decreasing water quality. • Increased erosion with subsequent changes in sediment accumulation rates and creating water quality concerns. • Change in engineering design standards to accommodate new extreme storms magnitudes. • Increased groundwater recharge rates, as residence times are shortened within areas where evapotranspiration takes place during high intensity events. • Increased flooding, which may have negative consequences for all infrastructure, habitats, and people in the area. <p>BUSINESS LINES IMPACTED:       </p>
 Streamflow Variability	<p>The changes in streamflow may be positive or negative, depending on local conditions.</p> <p>BUSINESS LINES IMPACTED:       </p>
<p><i>NOTE: The Regulatory and Military Program business lines may be impacted by all climate variables</i></p>	
<p> = Navigation  = Flood Risk Management  = Ecosystem Restoration  = Hydropower  = Recreation  = Water Supply  = Emergency Management</p>	

Figure 2-113. Summary of projected climate trends and impacts on USACE business lines for Region 07 – Upper Mississippi (USACE 2015c).












































CLIMATE VARIABLE	VULNERABILITY
 Increased Ambient Temperatures	<p>By mid-century, increased ambient air temperatures are expected to create the following vulnerabilities on the business lines in the region:</p> <ul style="list-style-type: none"> Loss of vegetation from increased periods of heat and variable streamflows may have impacts on vegetation within the region, which is important for sediment stabilization in the watershed. Loss of non-drought resistant vegetation may result in an increase in sediment loading, potentially causing geomorphic changes in the tributaries to the river system. Variable flows, have implications for maintain water levels in the rivers and lakes. Risk of wildfires during hot and dry conditions may cause an increased risk of wildfires, especially in heavily forested and dry areas. Flora and fauna that are not drought resistant can also be impacted by longer drought conditions, which may reduce opportunities for recreational wildlife viewing. <p>BUSINESS LINES IMPACTED:       </p>
 Increased Maximum Temperatures	<p>Air temperatures are expected to increase 1–4.5°C by mid century, with the number of heat wave days per year increasing by 15-50 days. This is expected to create the following vulnerabilities on business lines in the region:</p> <ul style="list-style-type: none"> Increased water temperatures leading to water quality concerns, particularly for the dissolved oxygen (DO) levels, growth of nuisance algal blooms and influence wildlife and supporting food supplies. Increased evapotranspiration. Human health risk increases from extended heat waves, impacting recreational visitors and increasing the need for emergency management. <p>BUSINESS LINES IMPACTED:   </p>
 Increased Annual Precipitation	<p>Annual precipitation is expected to increase in the region which are expected to influence the following vulnerabilities on business lines in the region:</p> <ul style="list-style-type: none"> Increased flows and runoff, which may carry pollutants to receiving water bodies, decreasing water quality. Increased erosion with subsequent changes in sediment accumulation rates and creating water quality concerns. Increased flooding, which may have negative consequences for all infrastructure, habitats, and people in the area. <p>BUSINESS LINES IMPACTED:       </p>
 Increased Storm Intensity and Frequency	<p>Extreme storm events may become more frequent and intense over the coming century which are expected to influence the following vulnerabilities on business lines in the region:</p> <ul style="list-style-type: none"> Increased runoff during an event, which may carry pollutants to receiving water bodies, decreasing water quality. Increased erosion with subsequent changes in sediment accumulation rates and creating water quality concerns. Change in engineering design standards to accommodate new extreme storms magnitudes. Increased flash flooding, which may have negative consequences for all infrastructure, habitats, and people in the area. <p>BUSINESS LINES IMPACTED:       </p>
 Streamflow Variability	<p>Streamflow is expected to increase by the end of the century. This includes an increase in overall flow and an increase of peak flow:</p> <ul style="list-style-type: none"> Increased flows and runoff, which may carry pollutants to receiving water bodies, decreasing water quality. Increased erosion with subsequent changes in sediment accumulation rates and creating water quality concerns. Increased flooding, which may have negative consequences for all infrastructure, habitats, and people in the area. Loss of vegetation from increased periods of drought and reduced streamflows may have impacts on vegetation within the region, which is important for sediment stabilization in the watershed. Loss of non-drought resistant vegetation may result in an increase in sediment loading, potentially causing geomorphic changes in the tributaries to the river system. Decrease in flows may result from periods of drought and reduced streamflow has implication for maintaining water levels in the rivers. <p>BUSINESS LINES IMPACTED:       </p>
<p>NOTE: The Regulatory and Military Program business lines may be impacted by all climate variables</p>	
<p> = Navigation  = Flood Risk Management  = Ecosystem Restoration  = Hydropower  = Recreation  = Water Supply  = Emergency Management</p>	

Figure 2-114. Summary of projected climate trends and impacts on USACE business lines for Region 08 – Lower Mississippi (USACE 2015d).








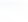




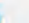
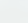
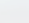
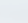















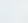













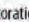









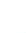












CLIMATE VARIABLE	VULNERABILITY
 Increased Ambient Temperatures	<p>Increased ambient air temperatures throughout the century, and over the next century are expected to create the following vulnerabilities on the business lines in the region:</p> <ul style="list-style-type: none"> Loss of vegetation from increased periods of drought and reduced streamflows may have impacts on vegetation within the region, which is important for sediment stabilization in the watershed. Loss of non-drought resistant vegetation may result in an increase in sediment loading, potentially causing geomorphic changes in the tributaries to the river system. Decrease in flows may result from periods of drought and reduced streamflow has implications for maintain water levels in the rivers. Risk of wildfires during hot and dry conditions may cause an increased risk of wildfires, especially in heavily forested and dry areas. Flora and fauna that are not drought resistant can also be impacted by longer drought conditions, which may reduce opportunities for recreational wildlife viewing. <p>BUSINESS LINES IMPACTED:       </p>
 Increased Maximum Temperatures	<p>Air temperatures are expected to increase 2-4°C in the latter half of the 21st century, especially in the summer months. This is expected to create the following vulnerabilities on business lines in the region:</p> <ul style="list-style-type: none"> Increased water temperatures leading to water quality concerns, particularly for the dissolved oxygen (DO) levels, growth of nuisance algal blooms and influence wildlife and supporting food supplies. Increased evapotranspiration. Human health risk increases from extended heat waves, impacting recreational visitors and increasing the need for emergency management. <p>BUSINESS LINES IMPACTED:       </p>
 Increased Annual Precipitation	<p>By the middle of the century, annual precipitation is expected to increase in the region which are expected to influence the following vulnerabilities on business lines in the region:</p> <ul style="list-style-type: none"> Increased flows and runoff, which may carry pollutants to receiving water bodies, decreasing water quality. Increased erosion with subsequent changes in sediment accumulation rates and creating water quality concerns. Increased flooding, which may have negative consequences for all infrastructure, habitats, and people in the area. <p>BUSINESS LINES IMPACTED:       </p>
 Increased Storm Intensity and Frequency	<p>Extreme storm events may become more intense and frequent over the coming century which are expected to influence the following vulnerabilities on business lines in the region:</p> <ul style="list-style-type: none"> Increased flows and runoff, which may carry pollutants to receiving water bodies, decreasing water quality. Increased erosion with subsequent changes in sediment accumulation rates and creating water quality concerns. Increased groundwater recharge rates, as residence times are shortened within areas where evapotranspiration takes place during high intensity events. Increased flooding, which may have negative consequences for all infrastructure, habitats, and people in the area. <p>BUSINESS LINES IMPACTED:       </p>
 Streamflow Variability	<p>The changes in streamflow may be positive or negative, depending on local conditions. This variability requires that multiple plausible streamflow futures be considered to adequately plan, design, and operate projects and programs.</p> <p>BUSINESS LINES IMPACTED:       </p>
 Sea Level Rise	<p>Sea level rise may exacerbate saltwater intrusion into fresh water supplies.</p> <p>BUSINESS LINES IMPACTED: </p>
<p><i>NOTE: The Regulatory and Military Program business lines may be impacted by all climate variables</i></p>	
<p> = Navigation  = Flood Risk Management  = Ecosystem Restoration  = Hydropower  = Recreation  = Water Supply  = Emergency Management</p>	

Figure 2-115. Summary of projected climate trends and impacts on USACE business lines for Region 10 – Missouri River (USACE 2015e).

CLIMATE VARIABLE	VULNERABILITY
 <p>Increased Ambient Temperatures</p>	<p>Increased ambient air temperatures throughout the century, and over the next century are expected to create the following vulnerabilities on the business lines in the region:</p> <ul style="list-style-type: none"> • Loss of vegetation from increased periods of drought and reduced streamflows may have impacts on vegetation within the region, which is important for sediment stabilization in the watershed. Loss of non-drought resistant vegetation may result in an increase in sediment loading, potentially causing geomorphic changes in the tributaries to the river system. • Decrease in flows may result from periods of drought has implications for maintain water levels in the rivers; however hydrological models show little concenseous on streamflow. • Risk of wildfires during hot and dry conditions may cause an increased risk of wildfires, especially in heavily forested and dry areas. Flora and fauna that are not drought resistant can also be impacted by longer drought conditions, which may reduce opportunities for recreational wildlife viewing. <p>BUSINESS LINES IMPACTED:      </p>
 <p>Increased Maximum Temperatures</p>	<p>Air temperatures are expected to increase 4-8°C in the latter half of the 21st century, especially in the summer months. This is expected to create the following vulnerabilities on business lines in the region:</p> <ul style="list-style-type: none"> • Increased water temperatures leading to water quality concerns, particularly for the dissolved oxygen (DO) levels, growth of nuisance algal blooms and influence wildlife and supporting food supplies. • Increased evapotranspiration. • Human health risk increases from extended heat waves, impacting recreational visitors and increasing the need for emergency management. <p>BUSINESS LINES IMPACTED:   </p>
 <p>Increased Annual Precipitation</p>	<p>By the middle of the century, annual precipitation is expected to increase in the region which are expected to influence the following vulnerabilities on business lines in the region:</p> <ul style="list-style-type: none"> • Times of increased streamflows and runoff, which may carry pollutants to receiving water bodies, decreasing water quality. • Increased erosion with subsequent changes in sediment accumulation rates and creating water quality concerns. • Increased flooding, which may have negative consequences for all infrastructure, habitats, and people in the area. <p>BUSINESS LINES IMPACTED:       </p>

NOTE: The Regulatory and Military Program business lines may be impacted by all climate variables





















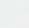
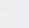
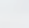















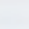







 = Navigation
  = Flood Risk Management
  = Ecosystem Restoration
  = Hydropower
  = Recreation
  = Water Supply
  = Emergency Management

Figure 2-116. Summary of projected climate trends and impacts on USACE business lines for Region 11 – Arkansas, White, and Red Rivers (USACE 2015f).

CLIMATE VARIABLE	VULNERABILITY
 Increased Ambient Temperatures	<p>Increased ambient air temperatures throughout the century, and over the next century are expected to create the following vulnerabilities on the business lines in the region:</p> <ul style="list-style-type: none"> • Loss of vegetation from increased periods of drought and reduced streamflows may have impacts on vegetation within the region, which is important for sediment stabilization in the watershed. Loss of non-drought resistant vegetation may result in an increase in sediment loading, potentially causing geomorphic changes in the tributaries to the river system. • Decrease in flows may result from periods of drought and reduced streamflow has implications for maintain water levels in the rivers. • Risk of wildfires during hot and dry conditions may cause an increased risk of wildfires, especially in heavily forested and dry areas. Flora and fauna that are not drought resistant can also be impacted by longer drought conditions, which may reduce opportunities for recreational wildlife viewing. <p>BUSINESS LINES IMPACTED:       </p>
 Increased Maximum Temperatures	<p>Air temperatures are expected to increase 2-4°C in the latter half of the 21st century, especially in the summer months. This is expected to create the following vulnerabilities on business lines in the region:</p> <ul style="list-style-type: none"> • Increased water temperatures leading to water quality concerns, particularly for the dissolved oxygen (DO) levels, growth of nuisance algal blooms and influence wildlife and supporting food supplies. • Increased evapotranspiration. • Human health risk increases from extended heat waves, impacting recreational visitors and increasing the need for emergency management. <p>BUSINESS LINES IMPACTED:       </p>
 Increased Storm Intensity and Frequency	<p>Extreme storm events may become more intense and frequent over the coming century which are expected to influence the following vulnerabilities on business lines in the region:</p> <ul style="list-style-type: none"> • Increased flows and runoff, which may carry pollutants to receiving water bodies, decreasing water quality. • Increased erosion with subsequent changes in sediment accumulation rates and creating water quality concerns. • Increased groundwater recharge rates, as residence times are shortened within areas where evapotranspiration takes place during high intensity events. • Increased flooding, which may have negative consequences for all infrastructure, habitats, and people in the area. <p>BUSINESS LINES IMPACTED:       </p>
 Streamflow Variability	<p>The changes in streamflow may be positive or negative, depending on local conditions. This variability requires that multiple plausible streamflow futures be considered to adequately plan, design, and operate projects and programs.</p> <p>BUSINESS LINES IMPACTED:       </p>

NOTE: The Regulatory and Military Program business lines may be impacted by all climate variables*

 = Navigation
  = Flood Risk Management
  = Ecosystem Restoration
  = Hydropower
  = Recreation
  = Water Supply
  = Emergency Management

The results show that the Mississippi River Basin will continue to be vulnerable in business lines related to flood risk management, navigation, emergency management, and other business lines across the twenty-first century, with higher vulnerability under a drier future scenario. This information should be considered during future analysis to increase resiliency of proposed project alternatives and reduce vulnerabilities. Vulnerabilities consist primarily of uncertainty in basic hydrologic parameters such as temperature and rainfall inputs, infiltration, land use, rainfall-runoff characteristics, and snowmelt. There is also vulnerability in the way reservoirs are operated over time with changing climatic conditions. Because there is no defined approach for quantitative

assessment of climate change or its effects for a large complex watershed such as the Mississippi River Basin, each of the hydrologic parameters should undergo sensitivity testing to determine the significance of each relative to future climate change scenarios. Additionally, various reservoir regulation schemes should be evaluated with the sensitivity analysis to provide insight how the MR&T system might perform given different operational regulation controls over a range of possible PDF hydrologic inputs. Once climate-change methodology matures, potential impacts to the different business lines should be evaluated because the USACE (2015a-f) regional analysis indicated that nearly every business line has a vulnerability by the end of the mid-century.

2.14.5 Climate-change summary

The regional literature review indicates an overall increase in streamflow over the next century. The Lower Missouri River Basin, Lower Ohio River Basin, Lower Tennessee River Basin, and Cumberland River show a significant upward trend that indicates increased streamflow over the next century, but the results are conflicting with other studies that show both an upward and downward trend for the same basins. The Mississippi River 2011 Post Flood Assessment (Appendix H) concludes that a projected increase in maximum dew point temperature would require a revision to the rainfall used for the PDF, but current precipitation values are valid for the climate trend data available. Therefore, the meteorological and hydrological underpinnings of the MR&T PDF are found to be adequate for the present climate. As climate-change understanding, methodology, and tools develop in the coming years and decades, the effects of climate change on the Mississippi River Basin hydrology should be monitored, and future PDF flowline computations should reassess the observed and potential changes due to climate change.

3 Results

This section presents the results of the 2016 hydrologic assessment of the HYPO 58A flowline. To assess the adequacy of the 1955-vintage hydrology for the PDF, this hydrologic assessment provided (1) a means to compare current (SS) and original (CM) methodology by running both methods through the CHPS-FEWS model; (2) upstream inflow and local contributing hydrographs needed for the boundary conditions in the HEC-RAS unsteady model; (3) output hydrographs; and (4) the hydrologic computations for antecedent conditions, rainfall-runoff, and reservoir effects based on current practice.

The 1955 methodology (CM) was reproduced with current tools/technology and was compared to the 2016 methodology (SS). The SS represented the standard method to apply storms across the Mississippi River Basin according to current practice. Local USACE Districts and the NWS RFCs were provided with precipitation and temperature grid files from the SS to simulate rainfall-runoff processes through their sub-basins and reservoirs. HEC-RAS inflow boundary and local contribution hydrographs are included in this section. Finally, the resulting 2016 peak flow values at several locations along the Lower Mississippi River are presented.

HYPO Storm Naming Convention

58A	= 1955 Unregulated
58A-EN	= 1955 Regulated (Group EN)
58A-U	= 2016 Unregulated
58A-R	= 2016 Regulated
58A-U-CM	= 2016 Clipped-Merged Unregulated
58A-R-CM	= 2016 Clipped-Merged Regulated

In the appendices, HYPO 52A, 56, and 63 results follow the same naming convention for each respective HYPO event.

Additional hydrographs are presented in Appendix B, and the results for HYPO 52A, 56, and 63 are presented in Appendix C through Appendix E.

3.1 Comparison of peak flows for HYPO storms

Peak flows at select locations are given in Table 3-1. This table includes peak flow values resulting from the hydrologic modeling and from the HEC-RAS unsteady flow routing.

Table 3-1. HYPO peak unregulated flow comparisons at select locations.

River	Location	Peak Flow (kcfs)				
		HYPO 58A-U	HYPO 52A-U ¹	HYPO 56-U	HYPO 63-U	HYPO 11-73-U
Missouri	Hermann, MO	220	675	575	946	668
Mississippi	Cairo, IL	2937	1555	2568	2387	2806
Mississippi	Arkansas City, AR	3366	1516	3455	3115	3286
Mississippi	St Louis, MO	433	1125	955	1362	1024
Ohio	Metropolis, IL	2458	566	1540	1078	1734
White	Clarendon, AR	271	40	316	213	311

¹ Results from HYPO 52A simulations were not comparable to other HYPO simulations. Precipitation and temperature inputs were determined as the cause for the discrepancy, but problems could not be resolved within study schedule.

HYPO 58A remains the governing storm event for the PDF on the lower Mississippi River even considering the new HYPO 11-73. Note that Table 3-1 shows peak unregulated flow. Peak flows from HYPO 11-73 results were lower than determined for HYPO 58A for Cairo, IL; Metropolis, IL; and Arkansas City, AR.

HYPO 11-73 has the second highest magnitude of flow compared to HYPO 58A as shown in Figure 3-1.

Figure 3-1. HYPO storm event comparison for HYPO 52A, 56, 58A, and 63 plus the 2016 HYPO 11-73 storm for Cairo, IL, for the combined confluence flows.

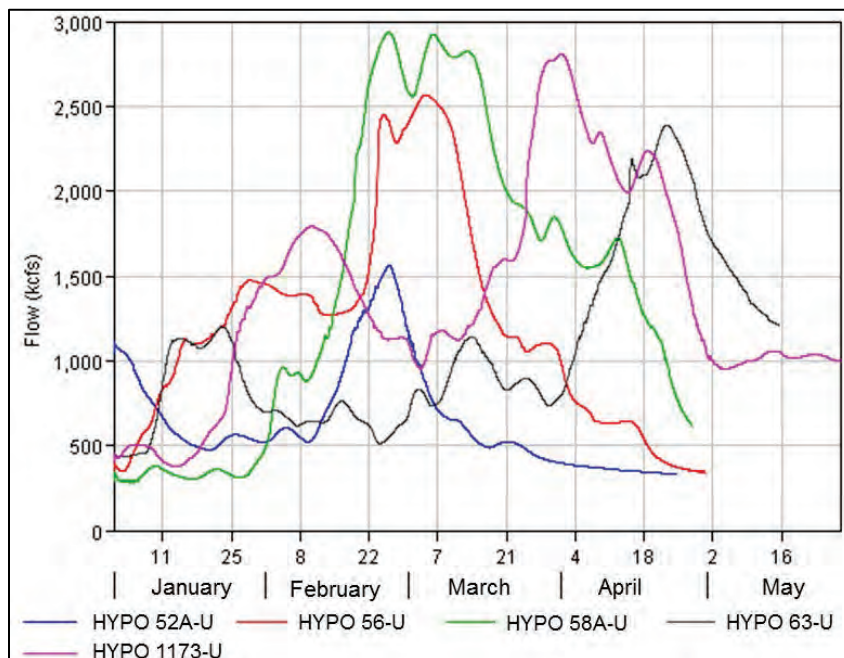


Table 3-2 compares the peak flows for the HYPO 58A storm event.

3.1.1 Hydrograph shape and volume

In addition to comparing peak discharges and a visual comparison of hydrograph plots, hydrograph shape was assessed using volume and mean discharge over 3-, 15-, and 30-day periods. Table 3-2 shows that results from the current assessment yielded higher 1-day peaks as well as larger volumes than obtained from the MRC (1955) report analysis. For example, at Cairo IL (combined confluence), 2016 58A-R values of 2,791 kcfs, 2,776 kcfs, 2,687 kcfs, and 2,518 kcfs are shown for the 1-day peak flow, 3-day mean flow, 15-day mean flow, and 30-day mean flow, respectively. Corresponding values for 1955 58A-EN were 2,336 kcfs, 2,336 kcfs, 2,318 kcfs, and 2,303 kcfs, which illustrates that 2016 results produced higher values throughout the 30-day flood crest period. This means a larger volume of flow actually passed through the system for the 2016 simulations than indicated from the 1955 Study. This may have limited the ability of reservoirs to reduce releases since they had to account for additional volumes of water.

Note that the table includes an additional simulation, labeled 58A-EN-2016HECRAS, that utilized the 1955 discharge hydrographs (see Section

2.2.2.1). More information about this run, which used the existing elevations of the backwater areas, can be found in the Hydraulics Report (USACE 2018). The additional run provided a means to directly compare hydrodynamic routing effects from HEC-RAS with the 1955 Study results. No 58A-EN-2016HECRAS values were given at St. Louis, MO, because that location was outside the HEC-RAS model domain. Peak and 3-day, 15-day, and 30-day mean flows from the HEC-RAS 58A-EN-2016HECRAS results were only slightly higher than the corresponding 1955 58A-EN values. This suggested that hydrodynamic effects had no appreciable effect on the computed peak flows; however, the timing of the peak values were different. The 2016 peaks occurred approximately 6 days later than indicated in the 1955 Study.

Table 3-2. Hydrograph volume and shape comparisons for HYPO 58A.

Mississippi River HYPO Flood Flows are in 1,000 cfs and sfd															
	Storm	Peak Flow	Peak Flow Date	3 Days				15 Days				30 days			
				Start	End	Volume (sfd)	Mean (cfs)	Start	End	Volume (sfd)	Mean (cfs)	Start	End	Volume (sfd)	Mean (cfs)
St. Louis	58A-R	378	24-Jan	23-Jan	25-Jan	1,112	371	11-Jan	25-Jan	5,015	334	14-Jan	12-Feb	9,684	323
	58A-U	433	22-Feb	20-Feb	22-Feb	1,254	418	10-Jan	24-Jan	5,342	356	10-Jan	8-Feb	9,874	329
	58A-EN	241	11-Feb	10-Feb	12-Feb	695	232	7-Feb	21-Feb	2,514	168	31-Jan	1-Mar	4,747	158
	58A	255	11-Feb	10-Feb	12-Feb	738	246	7-Feb	21-Feb	2,779	185	31-Jan	1-Mar	5,126	171
Combined Confluence	58A-R	2,791	8-Feb	7-Feb	9-Feb	8,327	2,776	29-Jan	12-Feb	40,311	2,687	21-Jan	19-Jan	75,546	2,518
	58A-U	2,937	26-Jan	24-Jan	26-Jan	8,735	2,912	23-Jan	6-Feb	41,932	2,795	19-Jan	17-Feb	80,480	2,683
	58A-EN-2016HE CRAS	2,393	30-Jan	17-Feb	19-Feb	7,160	2,387	7-Feb	21-Feb	35,236	2,349	26-Jan	24-Feb	69,683	2,323
	58A-EN	2,336	12-Feb	11-Feb	13-Feb	7,008	2,336	2-Feb	16-Feb	34,800	2,318	27-Jan	25-Feb	69,096	2,303
	58A	2,856	12-Feb	11-Feb	13-Feb	8,520	2,840	2-Feb	16-Feb	39,989	2,666	27-Jan	25-Feb	74,026	2,468
Arkansas City	58A-R	3,263	22-Feb	21-Feb	23-Feb	9,772	3,257	11-Feb	25-Feb	47,930	3,195	2-Feb	3-Mar	92,216	3,074
	58A-U	3,366	22-Feb	20-Feb	22-Feb	10,086	3,362	10-Feb	24-Feb	49,732	3,315	1-Feb	2-Mar	97,101	3,237
	58A-EN-2016HE CRAS	2,874	4-Mar	2-Mar	4-Mar	8,607	2,869	22-Feb	8-Mar	42,220	2,815	10-Feb	11-Mar	80,730	2,691
	58A-EN	2,880	2-Mar	1-Mar	3-Mar	8,620	2,873	21-Feb	7-Mar	42,070	2,805	9-Feb	10-Mar	80,195	2,673
	58A	3,220	2-Mar	1-Mar	3-Mar	9,640	3,213	21-Feb	7-Mar	46,560	3,104	9-Feb	10-Mar	88,170	2,939
Latitude of Red River Landing	58A-R	3,211	2-Mar	28-Feb	2-Mar	9,926	3,309	22-Feb	8-Mar	49,029	3,269	13-Feb	14-Mar	95,346	3,178
	58A-U	3,376	1-Mar	27-Feb	1-Mar	10,589	3,530	20-Feb	6-Mar	52,246	3,483	13-Feb	14-Mar	101,983	3,399
	58A-EN-2016HE CRAS	2,788	6-Mar	5-Mar	7-Mar	8,359	2,786	27-Feb	13-Mar	41,494	2,766	23-Feb	24-Mar	81,651	2,722
	58A-EN	2,956	13-Mar	12-Mar	14-Mar	8,738	2,913	7-Mar	21-Mar	43,800	2,920	28-Feb	29-Mar	86,100	2,870
	58A	3,325	13-Mar	12-Mar	14-Mar	9,967	3,322	7-Mar	21-Mar	49,030	3,269	28-Feb	29-Mar	93,946	3,132

3.1.2 Hydrograph timing

The timing between hydrographs at different locations affected the way peak values could be related at different locations. The travel time of the flood crest as it moves downstream can be clearly seen in Table 3-2. While this phenomena is straightforward between locations separated by some distance, like Cairo and Arkansas City, considering peak values at points near the Mississippi and Ohio River confluence was not as clear. For example, estimating the flow contribution for the Mississippi River immediately upstream of the Ohio River could not be done using the individual peak values for the Ohio River and the Lower Mississippi River (below the mouth of the Ohio River). Figure 3-2 and Table 3-3 show hourly computed flows for four locations that are near the Mississippi/Ohio River confluence: Thebes, IL; Birds Point, MO; Metropolis, IL; and a location on the Mississippi River just below the Ohio River.

Figure 3-2. Comparing peak flows near the Mississippi/Ohio River confluence.

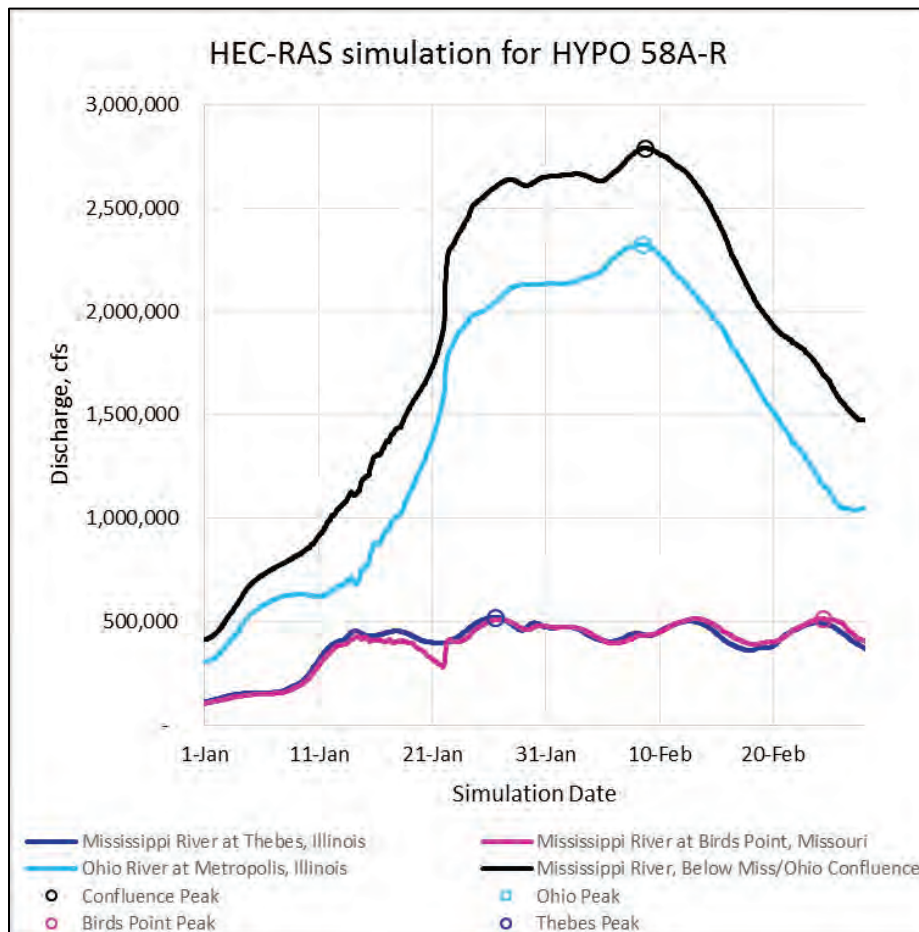


Table 3-3. Comparing peak flows near the Mississippi/Ohio River confluence.

HEC-RAS Simulation HYPO 58A-R	Mississippi River at Thebes, Illinois	Mississippi River at Birds Point, Missouri	Ohio River at Metropolis, Illinois	Mississippi River, Below Miss/Ohio Confluence
	HEC-RAS River Mile 43.7	HEC-RAS River Mile 4.6	HEC-RAS River Mile -979.7	HEC-RAS River Mile 973.8
Simulation date and time	Flow in cfs	Flow in cfs	Flow in cfs	Flow in cfs
1/26/58 6:00	519,000	504,000	2,033,000	2,592,000
1/26/58 7:00	520,000	505,000	2,035,000	2,594,000
1/26/58 8:00	520,000	506,000	2,037,000	2,596,000
1/26/58 9:00	520,000	506,000	2,038,000	2,597,000
1/26/58 10:00	520,000	507,000	2,040,000	2,599,000
1/26/58 11:00	520,000	508,000	2,042,000	2,600,000
1/26/58 12:00	520,000	508,000	2,043,000	2,602,000
1/26/58 13:00	520,000	509,000	2,045,000	2,603,000
1/26/58 14:00	520,000	509,000	2,047,000	2,605,000
1/26/58 15:00	520,000	510,000	2,049,000	2,606,000
1/26/58 16:00	520,000	510,000	2,051,000	2,608,000
1/26/58 17:00	520,000	510,000	2,053,000	2,609,000
2/8/58 6:00	440,000	432,000	2,325,000	2,786,000
2/8/58 7:00	439,000	432,000	2,326,000	2,787,000
2/8/58 8:00	439,000	432,000	2,326,000	2,788,000
2/8/58 9:00	438,000	432,000	2,326,000	2,788,000
2/8/58 10:00	438,000	433,000	2,326,000	2,789,000
2/8/58 11:00	437,000	433,000	2,326,000	2,790,000
2/8/58 12:00	437,000	433,000	2,326,000	2,790,000
2/8/58 13:00	436,000	433,000	2,326,000	2,791,000
2/8/58 14:00	436,000	433,000	2,325,000	2,791,000
2/8/58 15:00	435,000	434,000	2,325,000	2,791,000
2/8/58 16:00	435,000	434,000	2,324,000	2,791,000
2/8/58 17:00	435,000	434,000	2,324,000	2,791,000
2/24/58 6:00	493,000	515,000	1,166,000	1,705,000
2/24/58 7:00	493,000	515,000	1,162,000	1,702,000
2/24/58 8:00	492,000	515,000	1,159,000	1,699,000
2/24/58 9:00	492,000	514,000	1,157,000	1,696,000
2/24/58 10:00	491,000	514,000	1,155,000	1,693,000
2/24/58 11:00	491,000	513,000	1,154,000	1,691,000

For example, the peak computed flow below the Mississippi/Ohio confluence (2,791,000 cfs) and the peak computed flow on the Ohio River at Metropolis, IL (2,326,000), by basic continuity for steady flow where volume is preserved (flowrate in – flowrate out = zero; or change in storage per time interval is zero) suggests that flow from the upper Mississippi River would be 465,000 cfs ($2,791,000 - 2,326,000 = 465,000$). However, the table shows that flow from the upper Mississippi River was actually 435,000 cfs at the time when the combined Mississippi/Ohio flow was 2,791,000 cfs. This is due to the unsteady routing used in the HEC-RAS model. In other words, the unsteady hydrodynamic routing effects from HEC-RAS must be considered when analyzing peak flow values, particularly near major tributary junctions. Additionally, the peak flow of 515,000 cfs on the Mississippi River at Birds Point, MO, occurred 16 days after the peak at the confluence due to the unsteady flow and hydrodynamics of the reach.

Corresponding values (Table 3-4) from 1955 obtained from the MRC archives¹ were 2,250,000 cfs (Ohio River at Metropolis), 2,384,000 cfs (below Mississippi/Ohio confluence), and in this case, 134,000 cfs (Mississippi upstream of the Ohio River). The estimated peak on the Mississippi River upstream of the Ohio River was 410,000 cfs, which occurred 6 days prior to the peak at the confluence. Routing calculations from the 1955 Study were based on a simple lag approach as described in Section 1.2.3.8 where total flows were determined by summing all contributing flows for a time-step.

Peak regulated flow for HYPO 58A on the Ohio River was computed in 2016 as 2,326,000 cfs compared to 2,250,000 cfs from the 1955 Study. Peak flow on the Mississippi River near Birds Point, MO, was computed in 2016 as 515,000 cfs compared to 410,000 cfs from the 1955 Study. The combined peak flow for the Mississippi and Ohio Rivers was computed in 2016 as 2,791,000 cfs compared to 2,360,000 cfs from the 1955 Study. At the time of the main flood crest, computed flows were 435,000 cfs versus 134,000 cfs (Mississippi) and 2,324,000 cfs versus 2,250,000 (Ohio) for 2016 and 1955 results, respectively. Differences between the 2016 and 1955 results were +300,000 cfs (Mississippi) and +71,000 cfs (Ohio). The increase on the Ohio River for the current assessment can be attributed to differences in how regulation effects were calculated. The large increase on

¹ MRC archives: Files containing original tabulated routing calculations.

the Mississippi River for the current assessment can likewise be attributed to differences in regulation effects.

Table 3-4. Tabulated flows from 1955 routing calculations.

MISSISSIPPI RIVER PROJECT FLOOD STUDY					
Flood Routing of Hypo_Flood No. 58-A					
Condition EN_Reservoirs					
Reach St Louis-Metropolis to Cairo					
NOTE: New Madrid FloodWay Operating					
INFLOW in 1,000 cfs					
HYPO 58A- EN (1955) Date	Ohio River @ Metropolis, Illinois	Mississippi River @ St. Louis, Missouri	Local Contribution St. Louis to Ohio River (Area 7-Y)	Mississippi River Upstream of Ohio River 58A-EN St Louis + 7Y local	Mississippi and Ohio River Combined (downstream of confluence)
8-Feb	2,130	156	48	204	2,334
9-Feb	2,050	193	78	271	2,321
10-Feb	1,970	235	123	358	2,328
11-Feb	1,940	241	169	410	2,350
12-Feb	1,950	218	164	382	2,332
13-Feb	1,990	214	132	346	2,336
14-Feb	2,050	177	109	286	2,336
15-Feb	2,120	145	41	186	2,306
16-Feb	2,200	125	11	136	2,336
17-Feb	2,250	124	10	134	2,384
18-Feb	2,240	130	10	140	2,380
19-Feb	2,220	132	10	142	2,362
20-Feb	2,180	142	18	160	2,340

3.2 HEC-RAS inflow boundary discharge hydrographs

The hydrologic modeling produced discharge hydrographs at the same key locations used from computations in the 1955 Study. The hydrologic modeling also produced discharge hydrographs at upstream stream boundary points required by the HEC-RAS model. Plots of unregulated (U – shown in red) and regulated (EN – shown in blue) model simulations are presented in Figure 3-3 through Figure 3-14. Plots of local inflow hydrographs for minor tributaries and intervening areas are not included in this report.

Figure 3-3. HYPO 58A hydrographs: Missouri River at Hermann, MO.

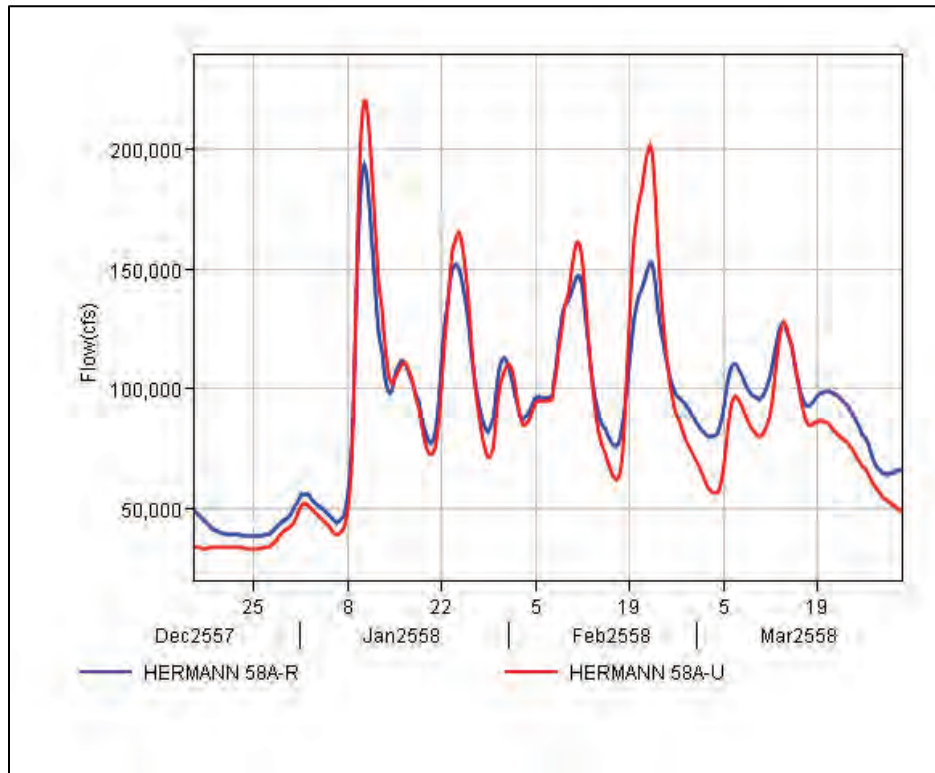


Figure 3-4. HYPO 58A hydrographs: Mississippi River at St. Louis, MO.

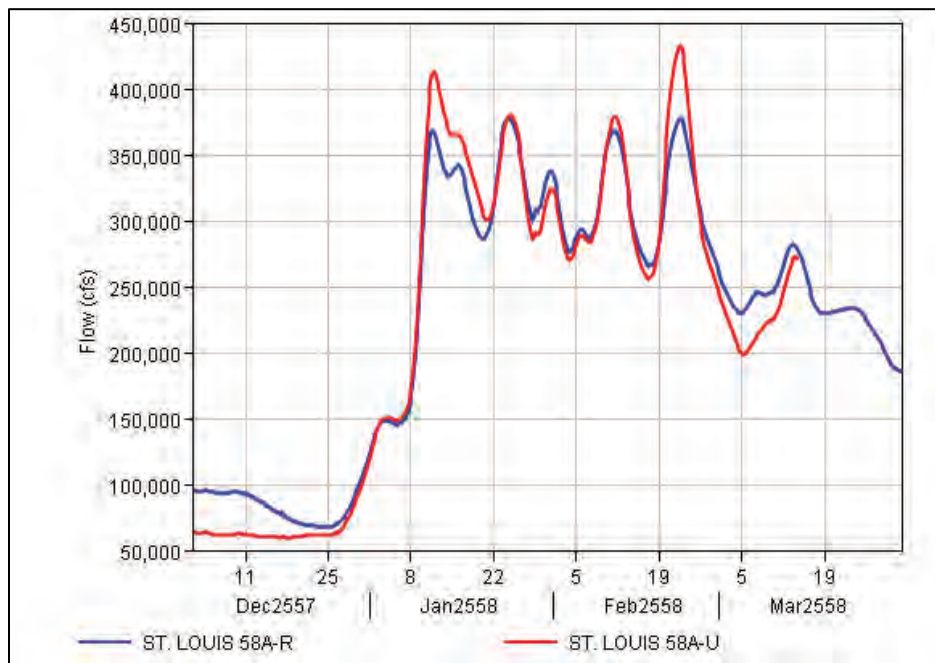


Figure 3-5. HYPO 58A hydrographs: Mississippi River at Chester, IL.¹

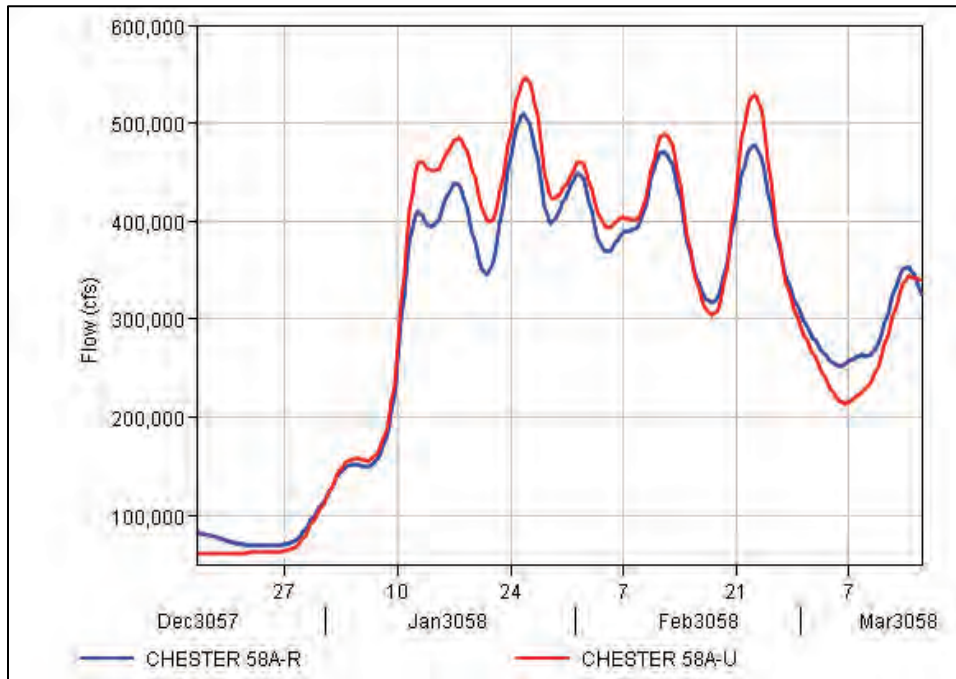
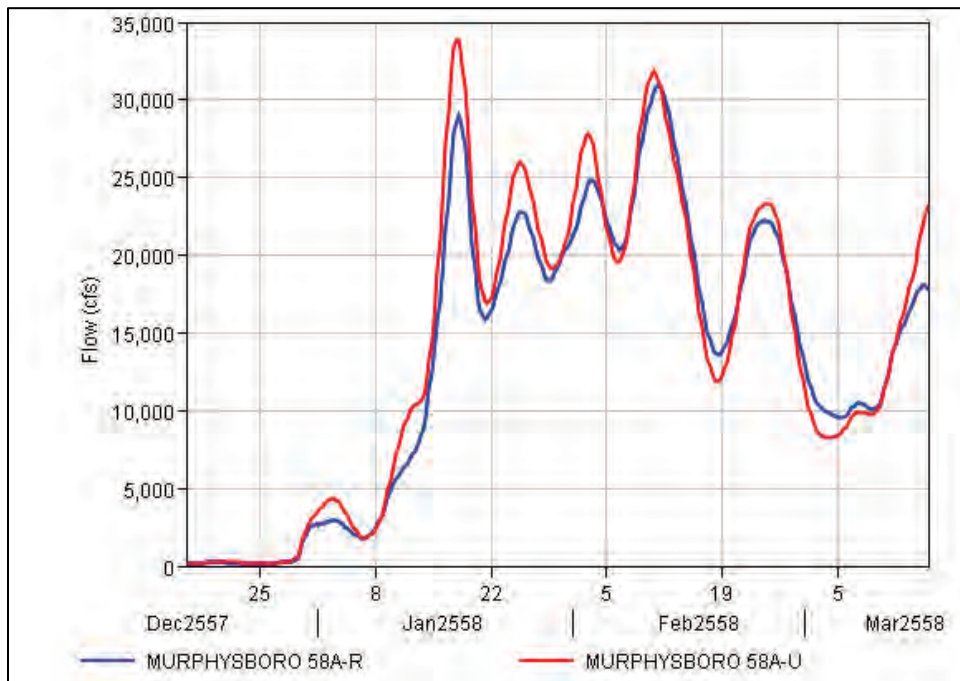


Figure 3-6. HYPO 58A hydrographs: Big Muddy River at Murphysboro, IL.



¹ The NWS model simulation for Mississippi River at Chester, IL, ended on March 14. To extend this hydrograph to March 31, the recession was manually estimated to follow the daily average recession for the additional 17 days required to allow routing the full hydrograph to the Gulf of Mexico in HEC-RAS.

Figure 3-7. HYPO 58A hydrographs: Cumberland River at Barkley Dam.

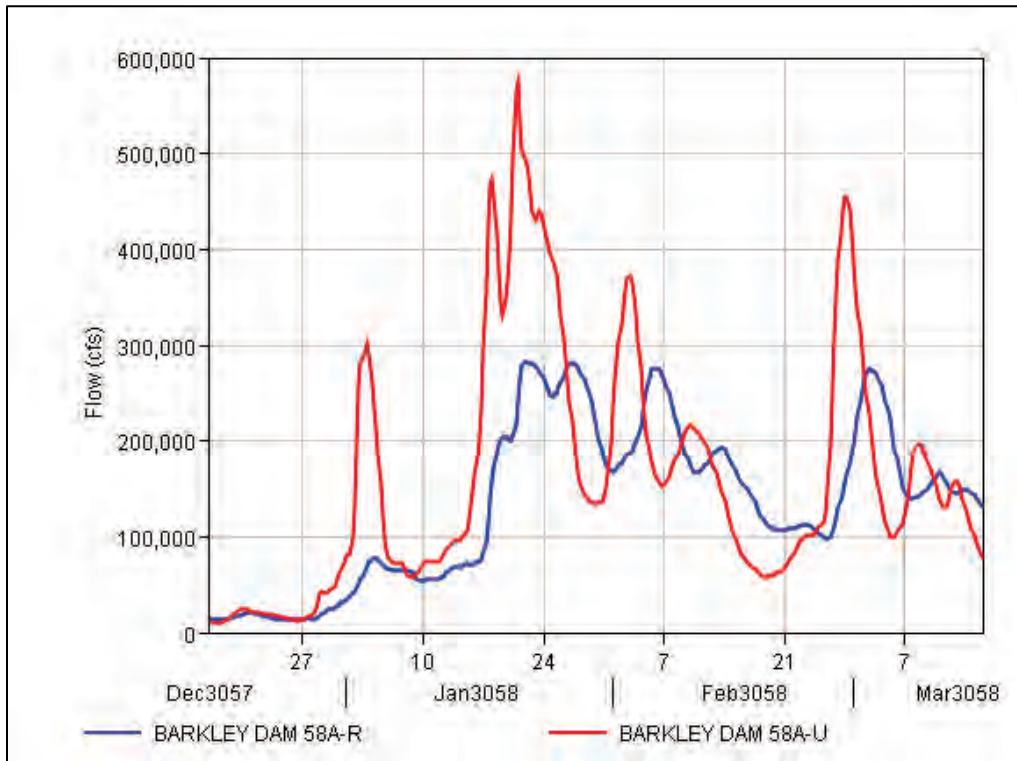


Figure 3-8. HYPO 58A hydrographs: Tennessee River at Kentucky Dam.

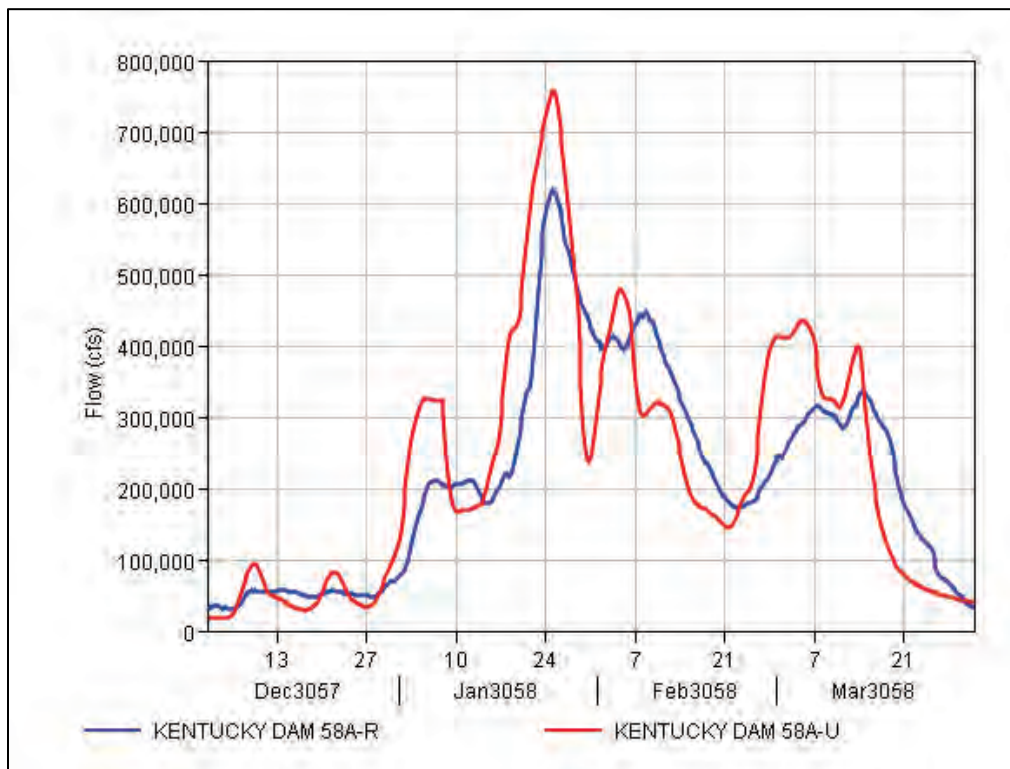


Figure 3-9. HYPO 58A hydrographs: Ohio River at Smithland, IL.

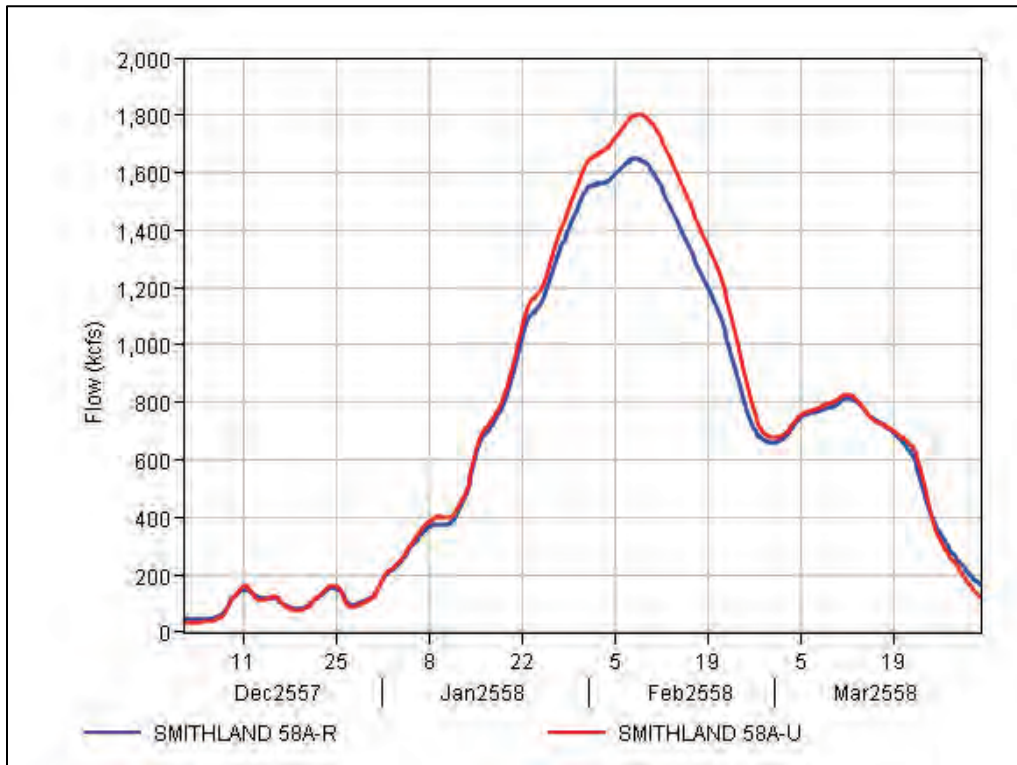


Figure 3-10. HYPO 58A hydrographs: Arkansas River at Pine Bluff, AR.

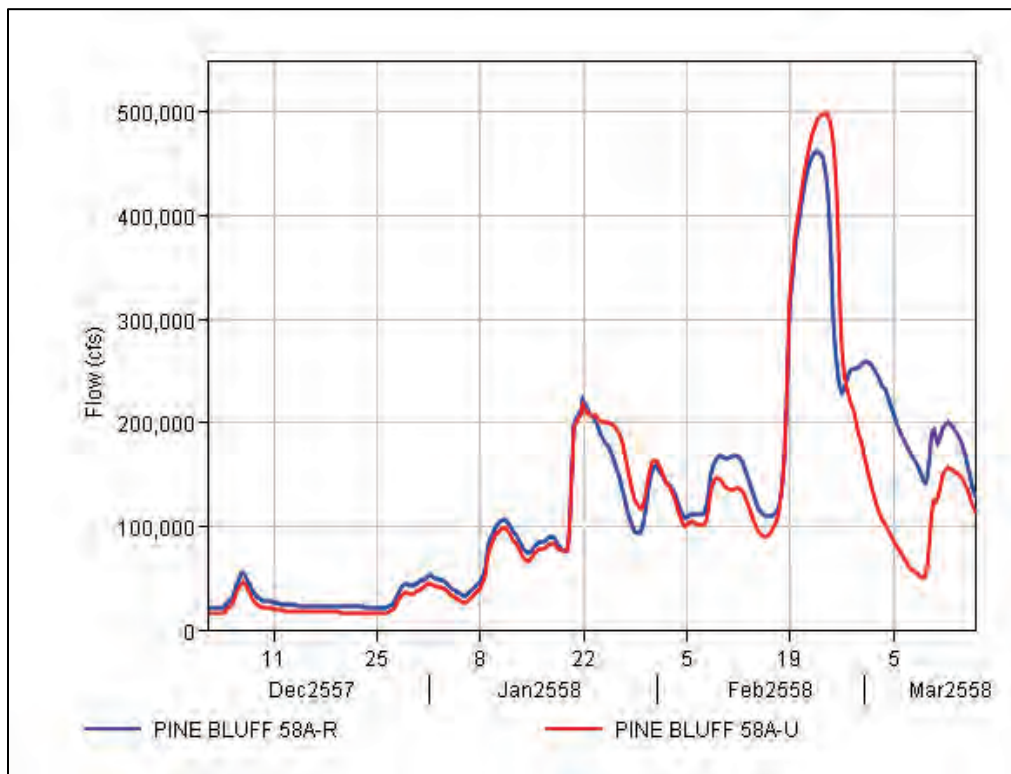


Figure 3-11. HYPO 58A hydrographs: Red River at Shreveport, LA.

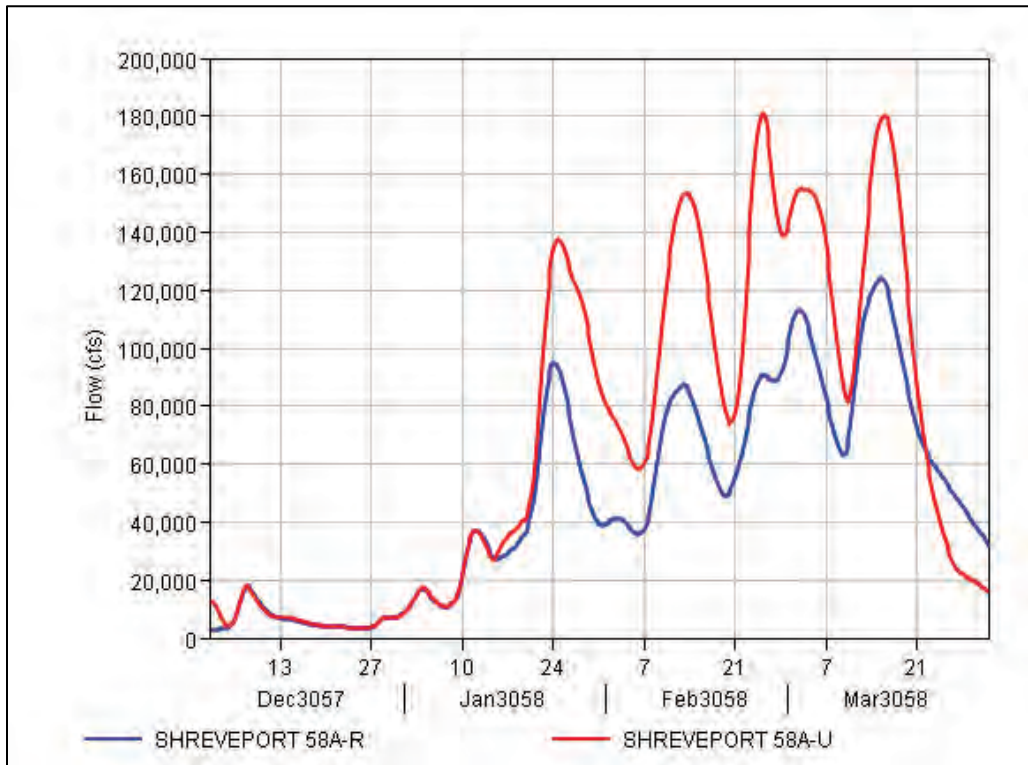


Figure 3-12. HYPO 58A hydrographs: Ouachita River at Monroe, LA.

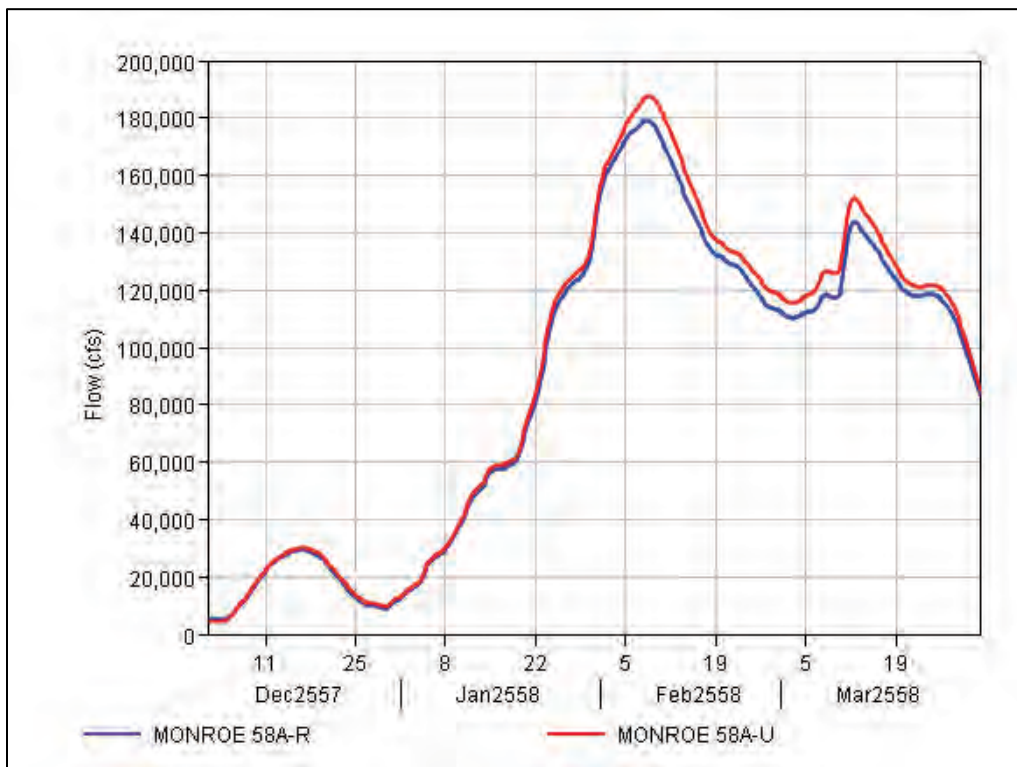


Figure 3-13. HYPO 58A hydrographs: Red River at Alexandria, LA.

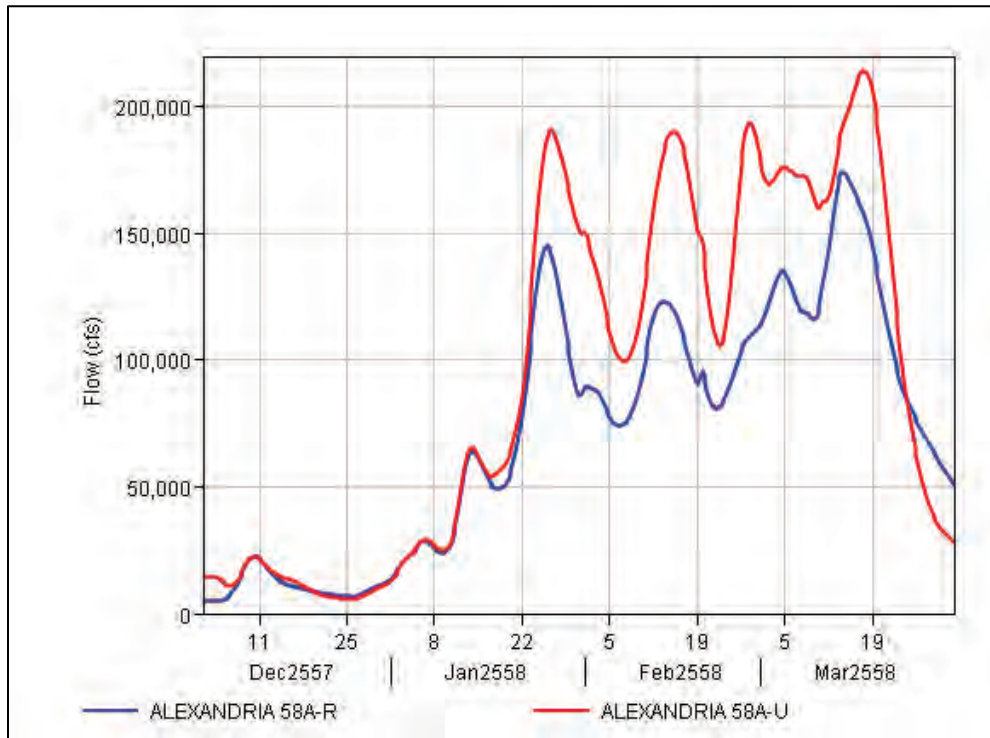
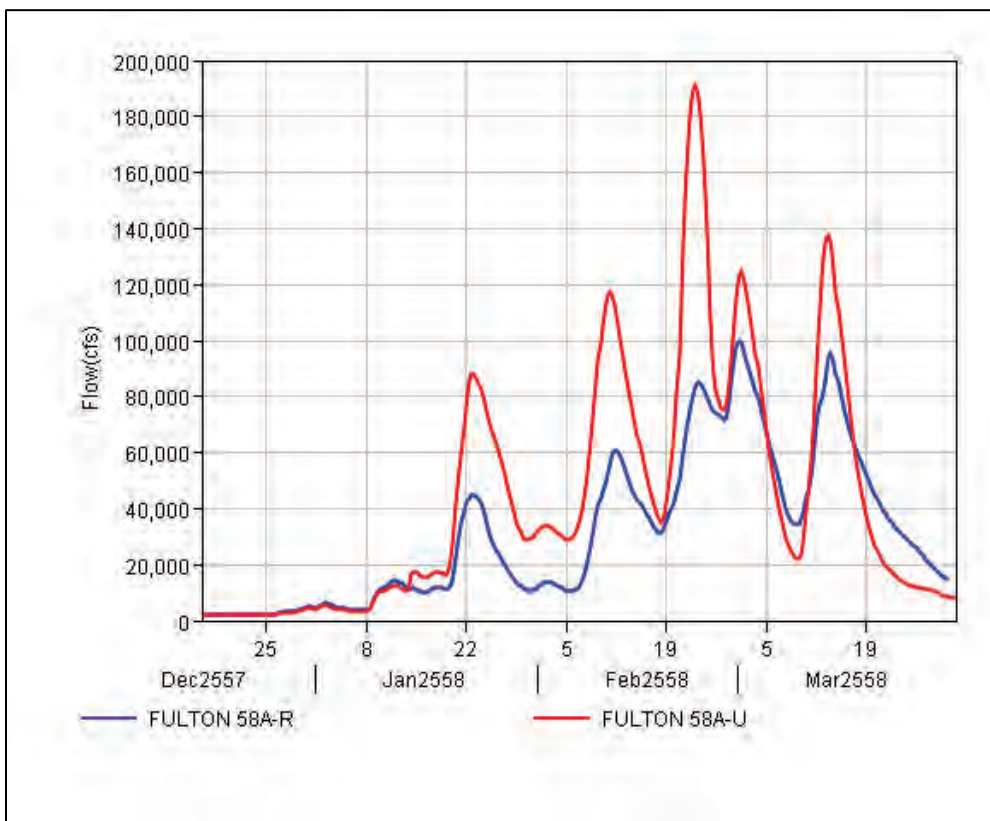


Figure 3-14. HYPO 58A hydrographs: Fulton, LA.



3.3 Peak flows for the Lower Ohio and Mississippi Rivers

The combined MVD HEC-RAS model developed for the current assessment provided unsteady hydrodynamic flood routing along the main river channels within the assessment area. Peak flow for the Ohio and Lower Mississippi Rivers (points downstream of the Ohio/Mississippi confluence) are direct outputs from the HEC-RAS unsteady calculations. Table 3-5 provides the HEC-RAS results for HYPO 58A under existing conditions of the Yazoo Backwater levee and authorized conditions of the Yazoo Backwater levee¹.

Table 3-5. Comparison of peak flow values for HYPO 58A.

Location	Project Design Flood (PDF) (from Table 7 WES [1957])					
	Unregulated Discharge, cfs			Regulated Discharge, cfs		
	58A	58A-U Existing Yazoo	58A-U Authorized Yazoo	58A-EN	58A-R Existing Yazoo	58A-R Authorized Yazoo
Ohio at Cairo, IL	2,460,000	2,458,000	2,458,000	2,250,000	2,326,000	2,326,000
Miss/Ohio Confluence (Combined)	2,850,000	2,937,000	2,937,000	2,360,000	2,791,000	2,791,000
Hickman, KY	NA	1,988,000	1,988,000	NA	1,973,000	1,973,000
Memphis, TN	2,770,000	2,956,000	2,956,000	2,410,000	2,863,000	2,863,000
Helena, AR	2,710,000	2,861,000	2,862,000	2,460,000	2,788,000	2,788,000
Arkansas City, AR	3,210,000	3,366,000	3,367,000	2,890,000	3,263,000	3,263,000
Greenville, MS	NA	3,362,000	3,364,000	NA	3,259,000	3,260,000
Lake Providence, MS	NA	3,357,000	3,361,000	NA	3,253,000	3,257,000
Vicksburg, MS	2,960,000	3,245,000	3,122,000	2,710,000	3,076,000	3,087,000
Natchez, MS	2,970,000	3,242,000	3,135,000	2,720,000	3,072,000	3,099,000
Red River Landing, LA	2,240,000	2,618,000	2,514,000	2,100,000	2,449,000	2,475,000
Baton Rouge, LA	NA	2,007,000	1,910,000	NA	1,838,000	1,869,000
Donaldsonville, LA	NA	2,007,000	1,910,000	NA	1,837,000	1,868,000
Carrollton, LA	NA	1,613,000	1,654,000	NA	1,581,000	1,613,000
Empire, LA	NA	1,675,000	1,583,000	NA	1,513,000	1,543,000
Venice, LA	NA	1,204,000	1,142,000	NA	1,094,000	1,115,000

The original 1955 hydrographs were digitized and compared to the hydrographs produced from the 2016 RFC models at the boundary

¹ The Yazoo Backwater levee was constructed after the WES (1957) report was published; therefore, the 1957 peak flow values are comparable to the Yazoo Backwater authorized condition. The authorized condition has a design grade of elevation 112.8 while the existing levee height is at elevation 107.0.

locations for the HEC-RAS model. Figure 3-15 through Figure 3-19 show the hydrographs comparing the 1955 data and 2016 hydrologic model results, where the label 58A represents 1955 unregulated values and 58A-U represents the current (2016) unregulated values. Labels of 58A-R represent the current (2016) regulated values and 58A-EN represent the 1955 regulated values. The shape and/or magnitude between the hydrographs at Alexandria, Alton, St. Louis, and Hermann are significantly different with the 2016 unregulated hydrographs being much higher than the 1955 Study results. Little Rock shows that the 1955 results are much higher than the 2016 results, but the shape of the hydrograph is similar. The source of the differences is not easily identifiable; however, their source most likely lies in the precipitation sequencing (SS versus CM sequence), the inclusion of temperature effect, and differences in hydrologic modeling/routing techniques (see Section 4.4).

Figure 3-15. Alexandria, LA, HYPO 58A 1955 unregulated flow compared to 2016 unregulated flow generated by the RFC.

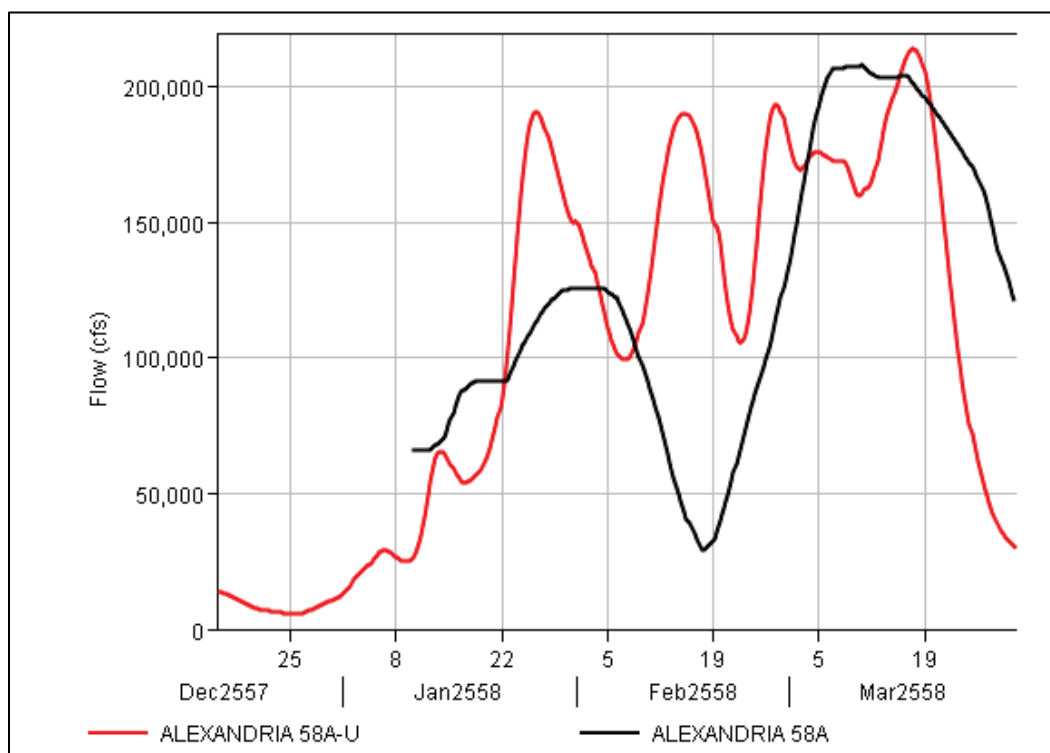


Figure 3-16. Alton, IL, HYPO 58A 1955 unregulated flow compared to 2016 unregulated flow generated by the RFC.

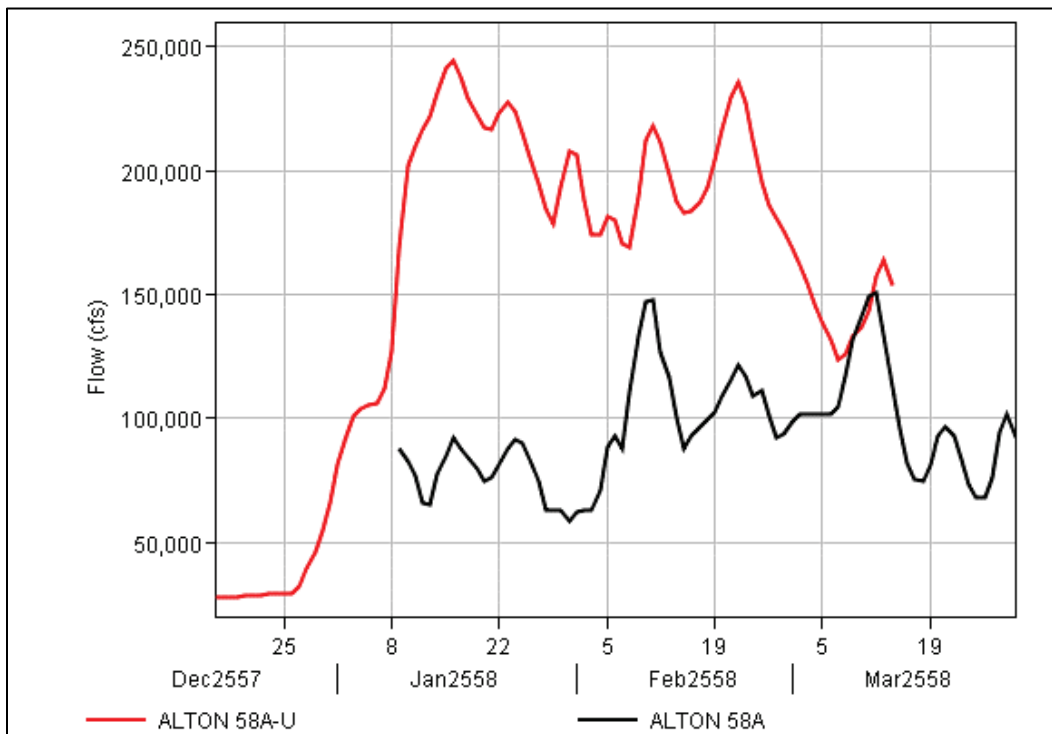


Figure 3-17. Hermann, MO, HYPO 58A 1955 unregulated flow compared to 2016 unregulated flow generated by the RFC.

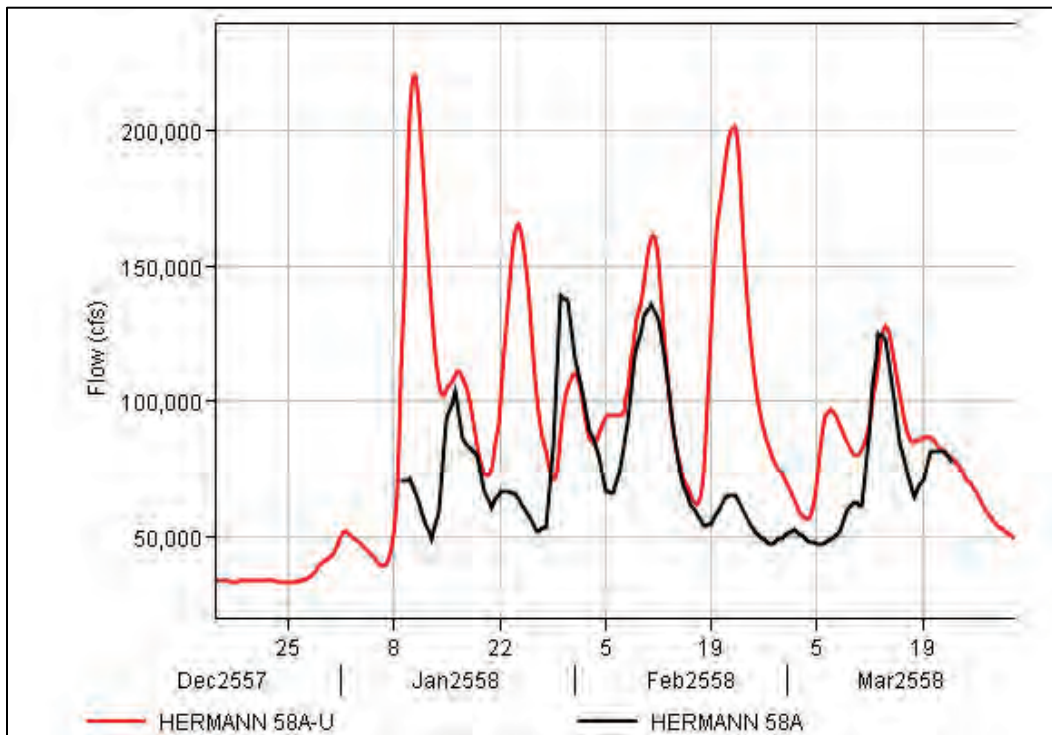


Figure 3-18. Little Rock, AR, HYPO 58A 1955 unregulated flow compared to 2016 unregulated flow generated by the RFC.

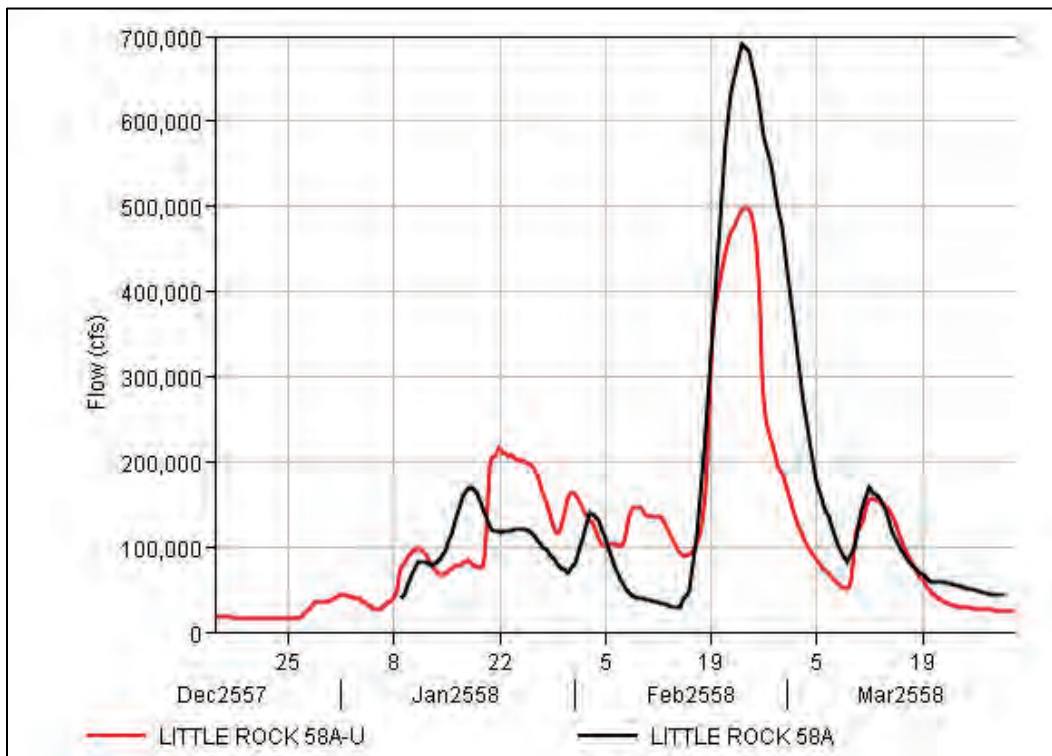
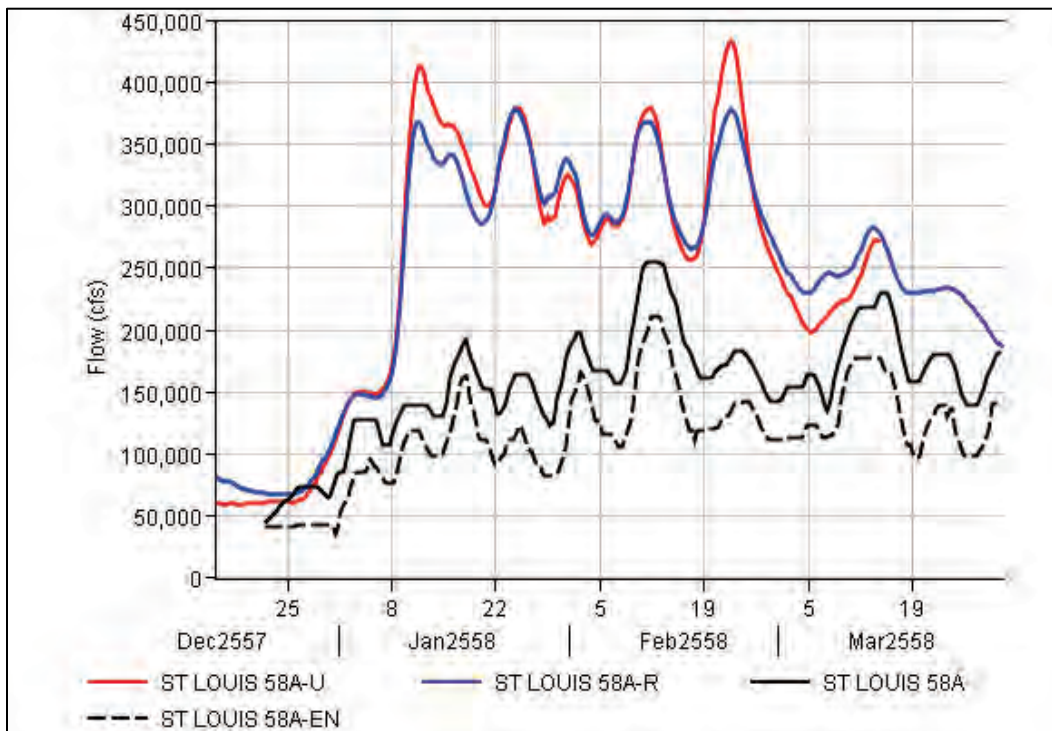
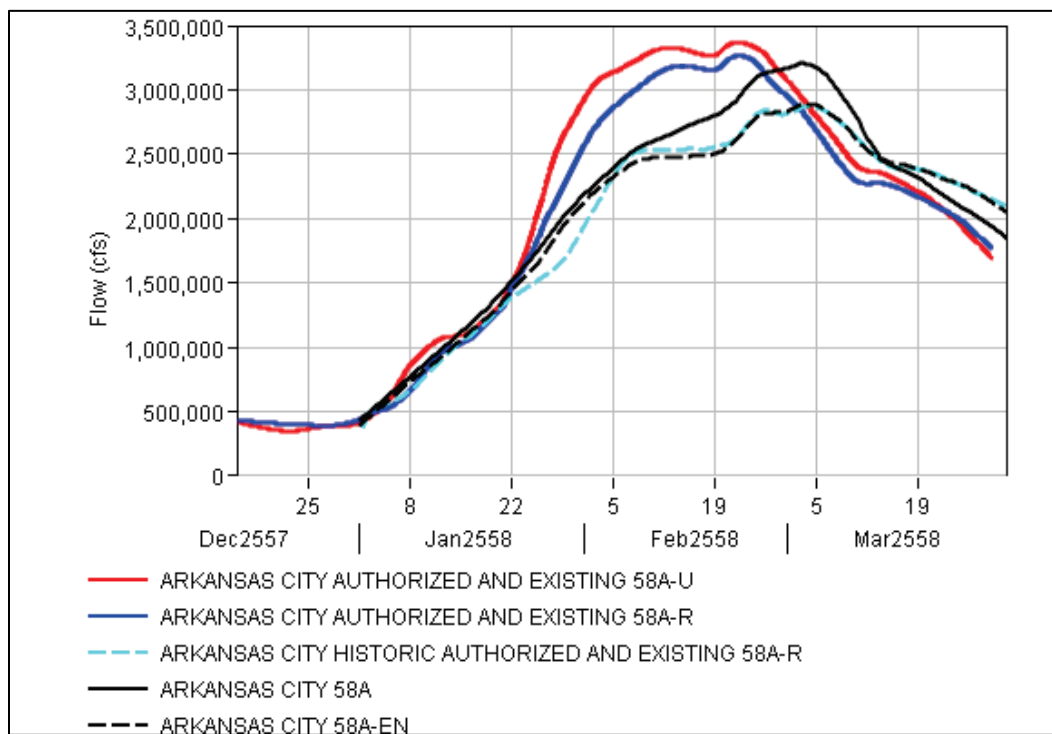


Figure 3-19. St. Louis, MO, HYPO 58A 1955 unregulated and regulated flow compared to 2016 unregulated and regulated flow generated by the RFC.



To compare the magnitude and volume of the hydrographs produced in this assessment, the 1955 hydrographs were digitized and input as the boundary conditions to the 2016 HEC-RAS model. Figure 3-20 through Figure 3-24 compare the digitized 1955 hydrographs, the 2016 HEC-RAS model results, and the 2016 HEC-RAS historic run that used the digitized 1955 hydrographs. The authorized and existing conditions have nearly the same flow values upstream of Vicksburg, MS. At the Latitude of Red River Landing, the authorized and existing condition flow values deviate at the peak. Figure 3-24 shows the entire hydrograph along with a shorter window hydrograph that focuses on the deviation between each condition.

Figure 3-20. Arkansas City, AR, HYPO 58A 1955 and 2016 regulated and unregulated flow compared to the 2016 regulated historic HEC-RAS results.*



*Note: The authorized and existing condition results have a 370 cfs peak flow difference for the regulated run and a 330 cfs peak flow difference for the unregulated run.

Figure 3-21. Cairo, IL, HYPO 58A 1955 and 2016 regulated and unregulated flow compared to the 2016 regulated historic HEC-RAS results.

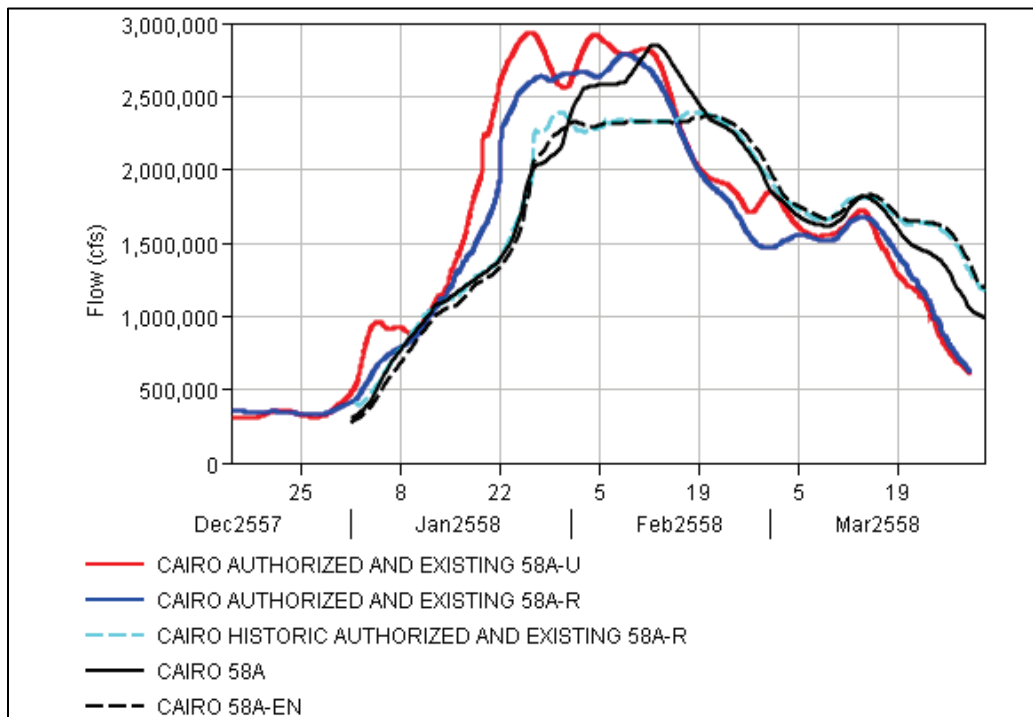
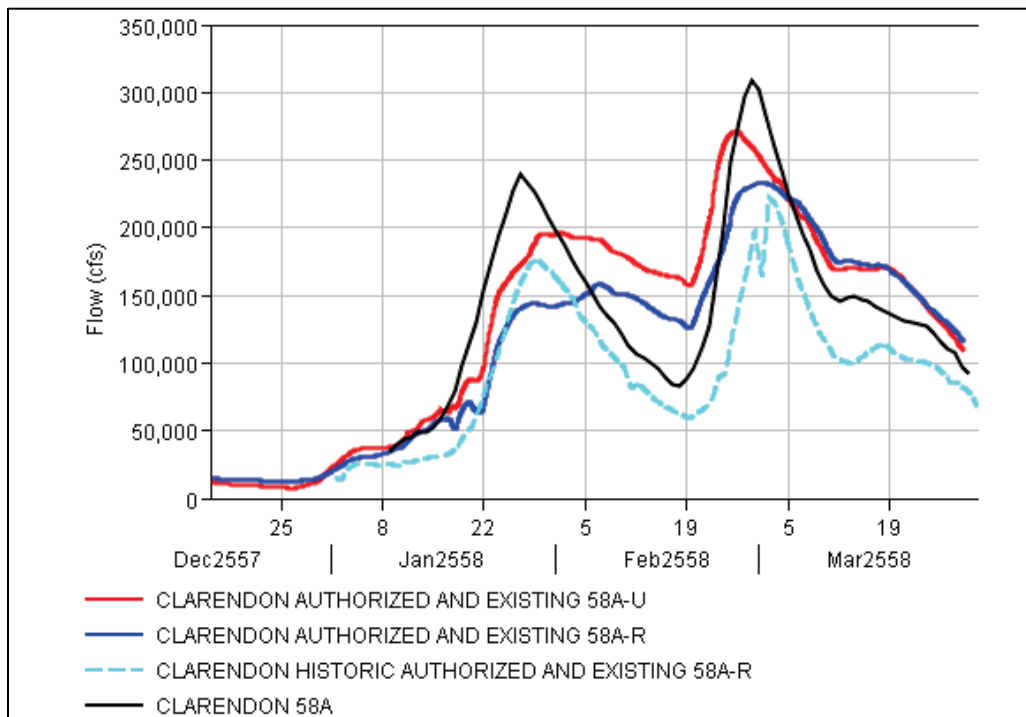


Figure 3-22. Clarendon, AR, HYPO 58A 1955 and 2016 regulated and unregulated flow compared to the 2016 regulated historic HEC-RAS results.*



*Note: The authorized and existing condition results have a 60 cfs peak flow difference for the regulated run and a 5 cfs peak flow difference for the unregulated run.

Figure 3-23. Metropolis, IL, HYPO 58A 1955 and 2016 regulated and unregulated flow compared to the 2016 regulated historic HEC-RAS results.

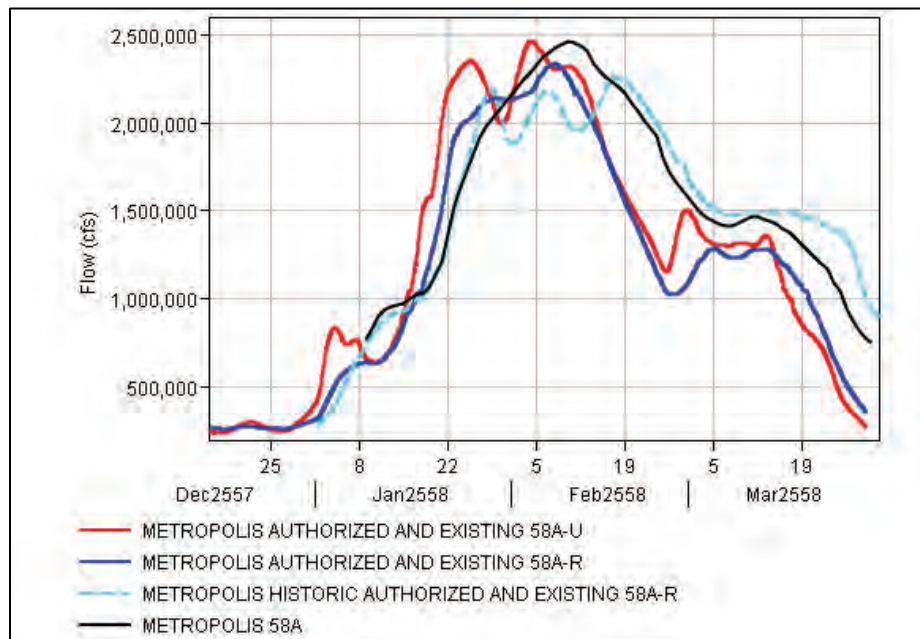
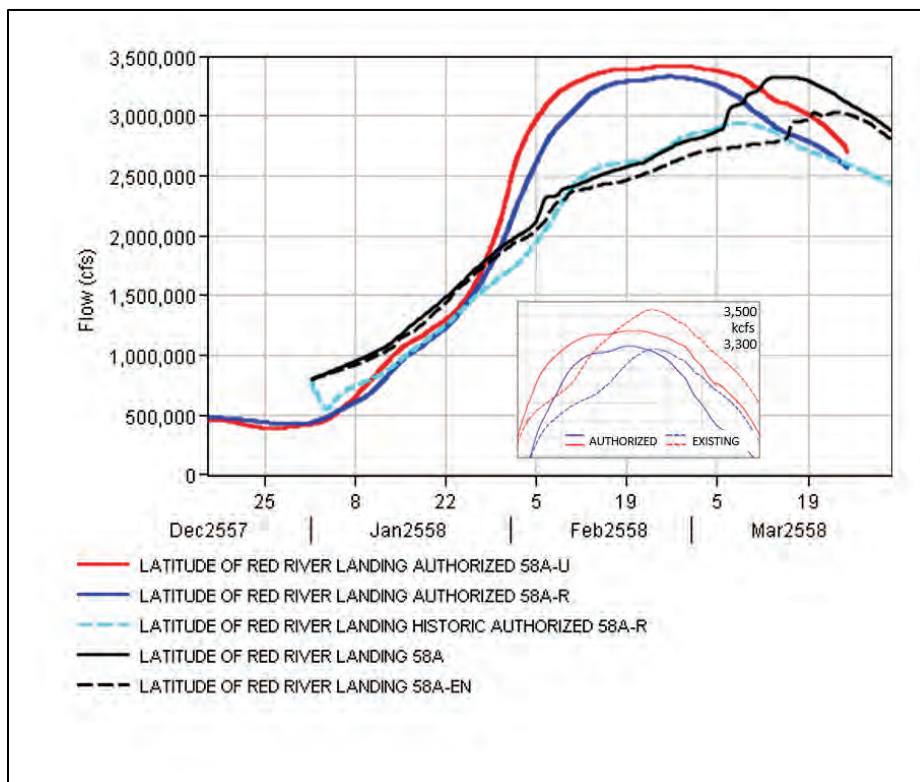


Figure 3-24. Latitude of Red River Landing, LA, HYPO 58A 1955 and 2016 regulated and unregulated flow compared to the 2016 regulated historic HEC-RAS results.*



*Note: Figure 3-24 inset shows slight difference around the peak for Authorized and Existing Yazoo Backwater Levee conditions.

HYPO 58A HEC-RAS unsteady routing

Hydrographs, shown in Figure 3-25 through Figure 3-40, for the Ohio and Lower Mississippi River (points downstream of the Ohio/Mississippi confluence) are direct outputs from the HEC-RAS unsteady calculations. For additional details, see the HEC-RAS volume of the Mississippi River Flowline Assessment (USACE 2018).

Figure 3-25. HYPO 58A HEC-RAS hydrograph: Ohio River at Cairo, IL.

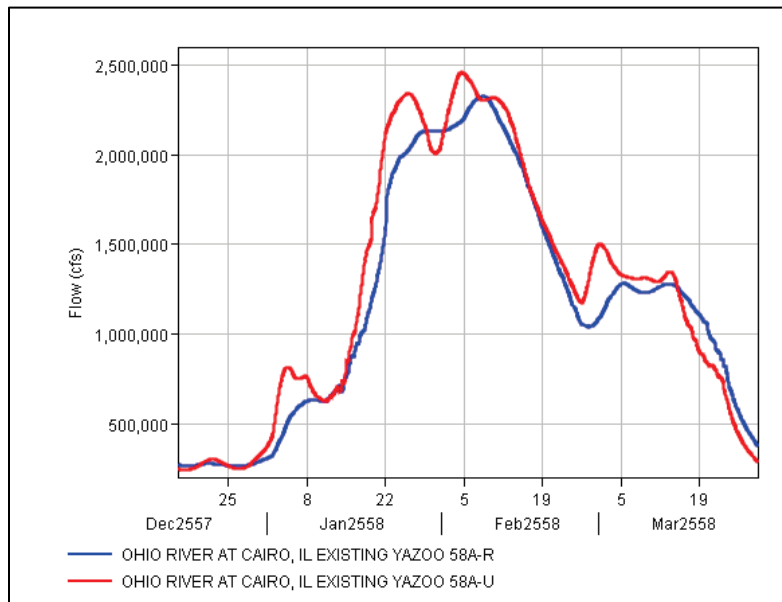


Figure 3-26. HYPO 58A HEC-RAS hydrograph: Combined Ohio and Mississippi River flow near Cairo, IL.

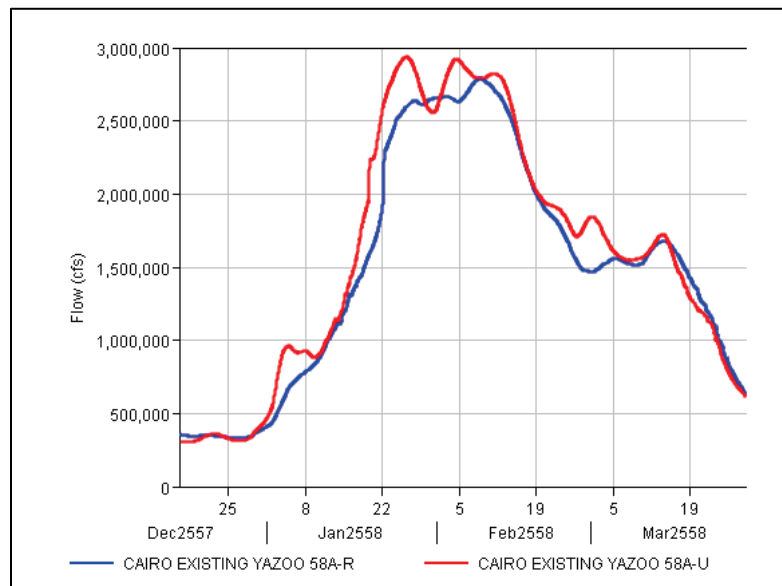


Figure 3-27. HYPO 58A HEC-RAS hydrograph: Mississippi River at Hickman, KY.

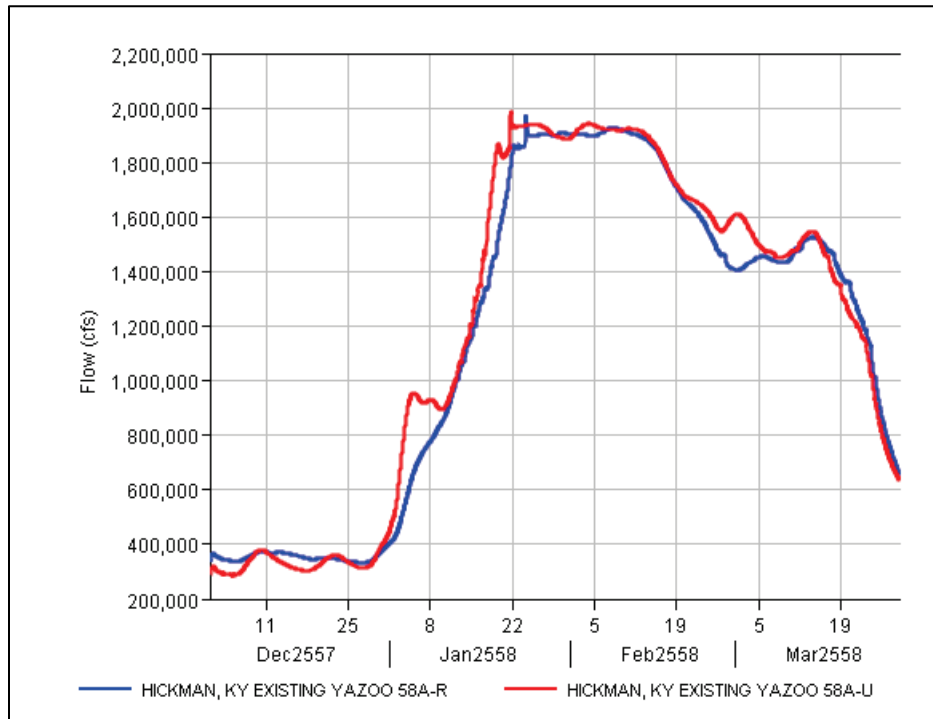


Figure 3-28. HYPO 58A HEC-RAS hydrograph: Mississippi River at Memphis, TN.

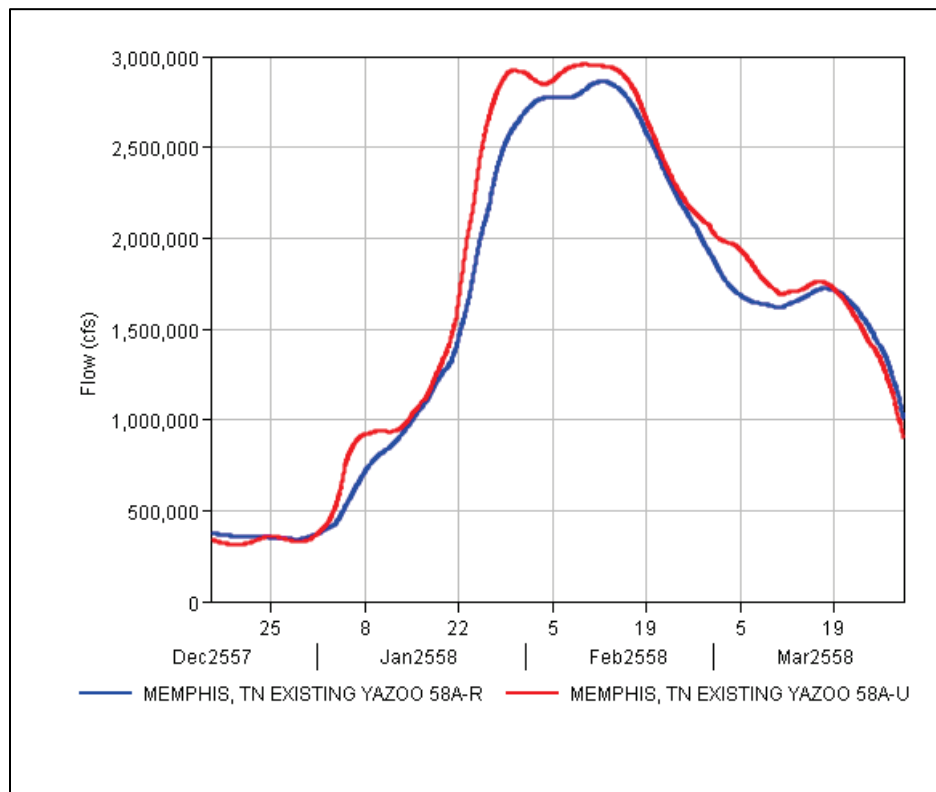


Figure 3-29. HYPO 58A HEC-RAS hydrograph: Mississippi River at Helena, AR.

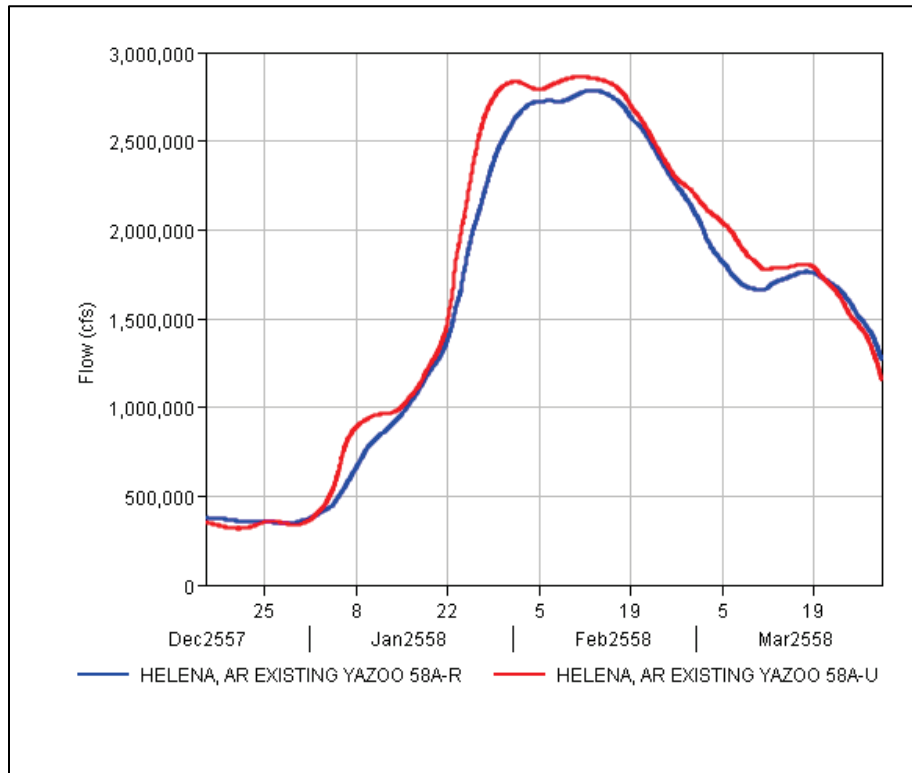


Figure 3-30. HYPO 58A HEC-RAS hydrograph: Mississippi River at Arkansas City, AR.

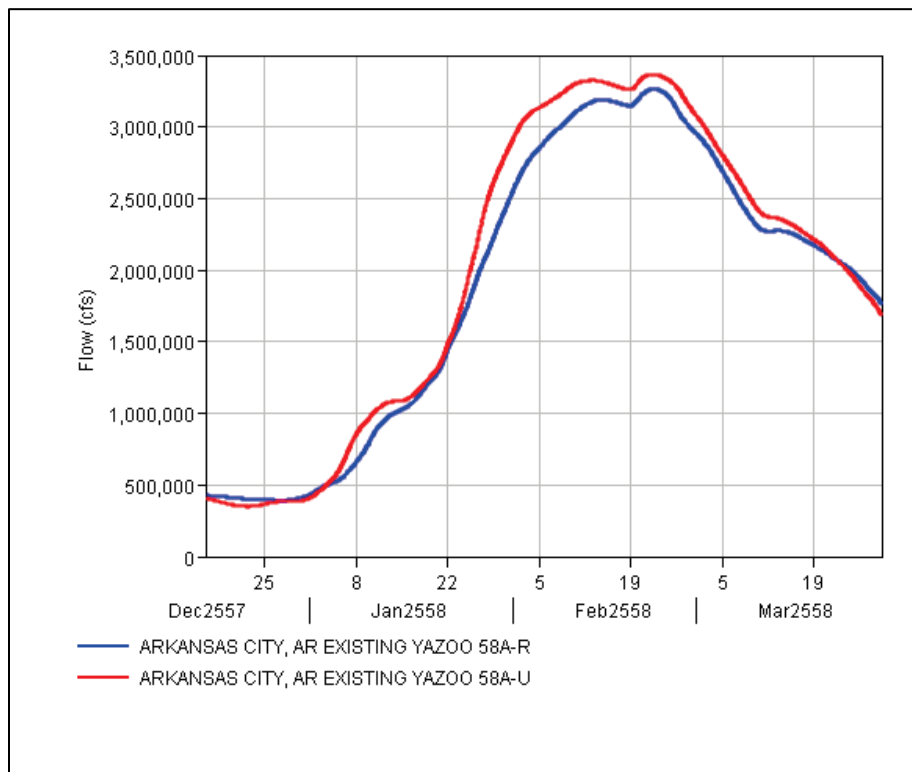


Figure 3-31. HYPO 58A HEC-RAS hydrograph: Mississippi River at Greenville, MS.

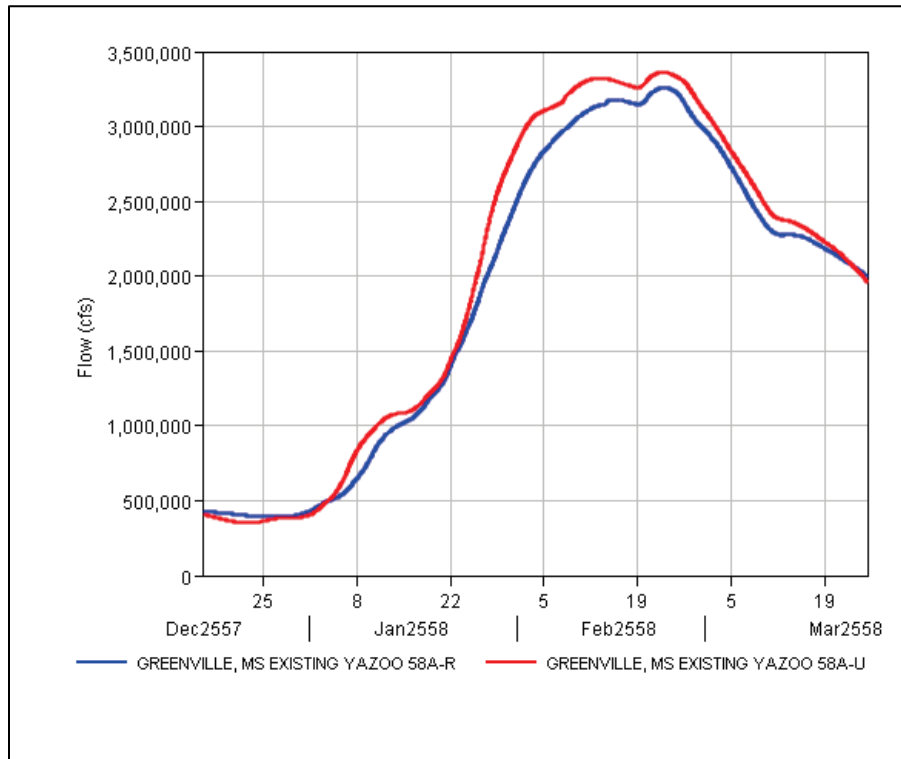


Figure 3-32. HYPO 58A HEC-RAS hydrograph: Mississippi River at Lake Providence, LA.

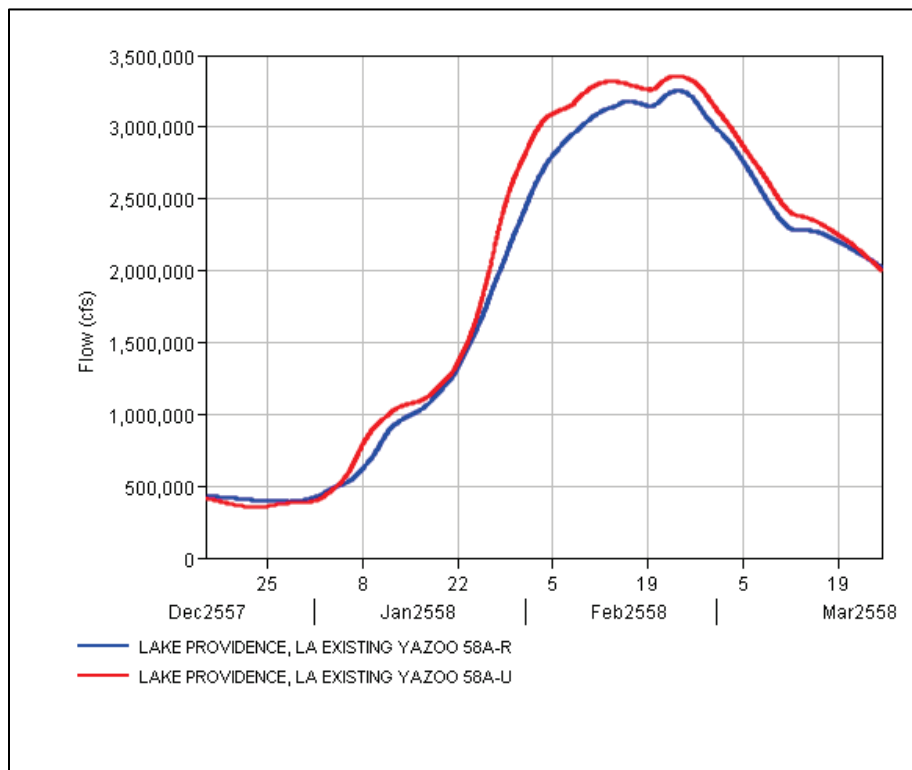


Figure 3-33. HYPO 58A HEC-RAS hydrograph: Mississippi River at Vicksburg, MS.

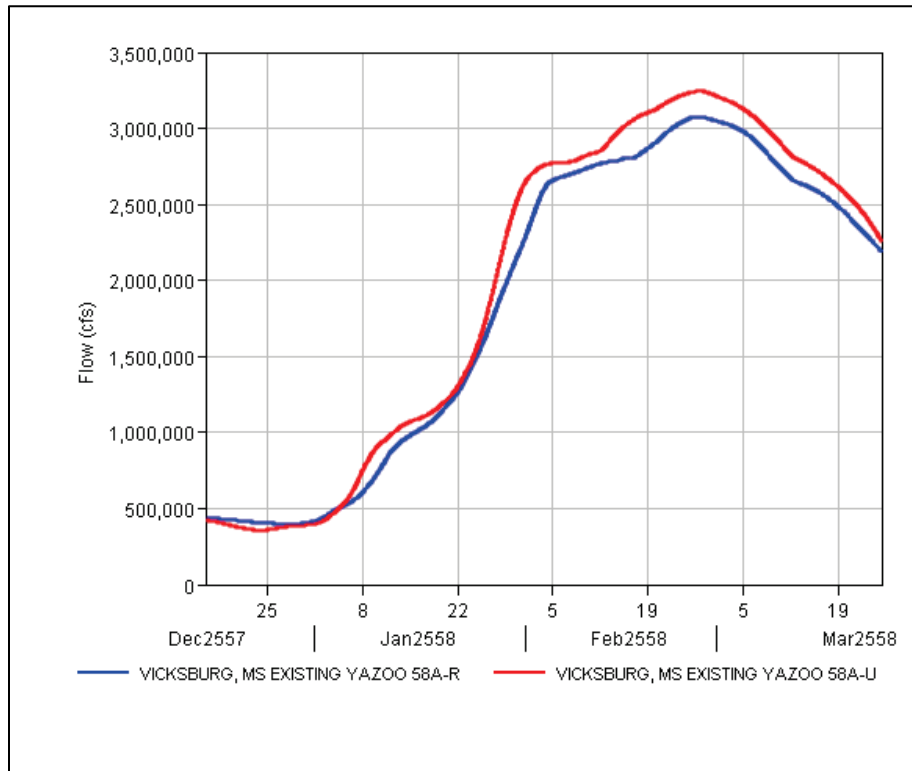


Figure 3-34. HYPO 58A HEC-RAS hydrograph: Mississippi River at Natchez, MS.

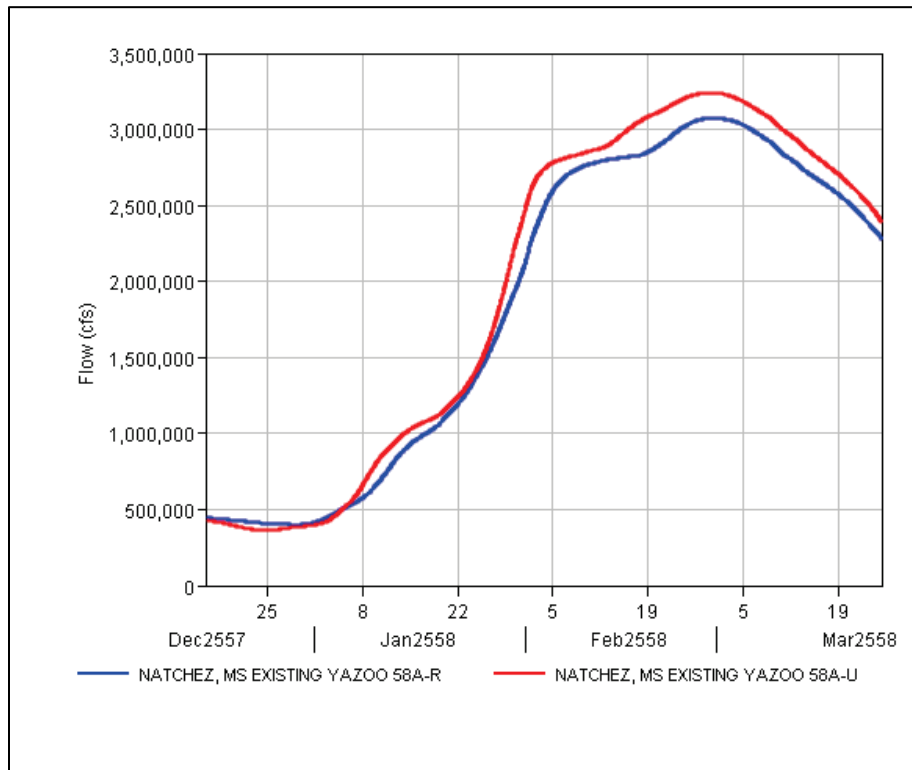


Figure 3-35. HYPO 58A HEC-RAS hydrograph: Mississippi River at Red River Landing, LA.

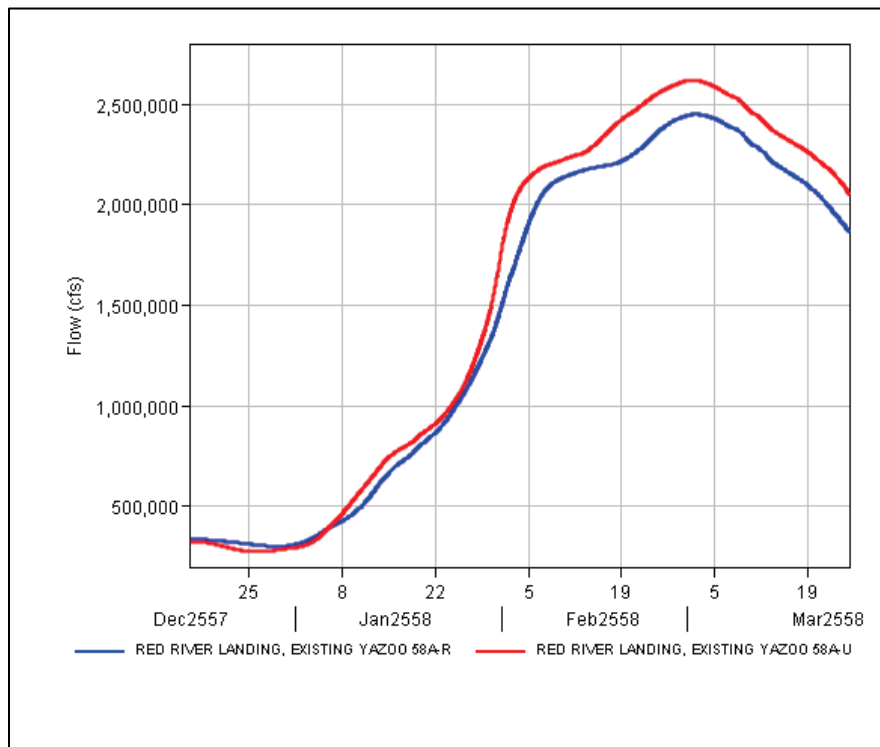


Figure 3-36. HYPO 58A HEC-RAS hydrograph: Mississippi River at Baton Rouge, LA.

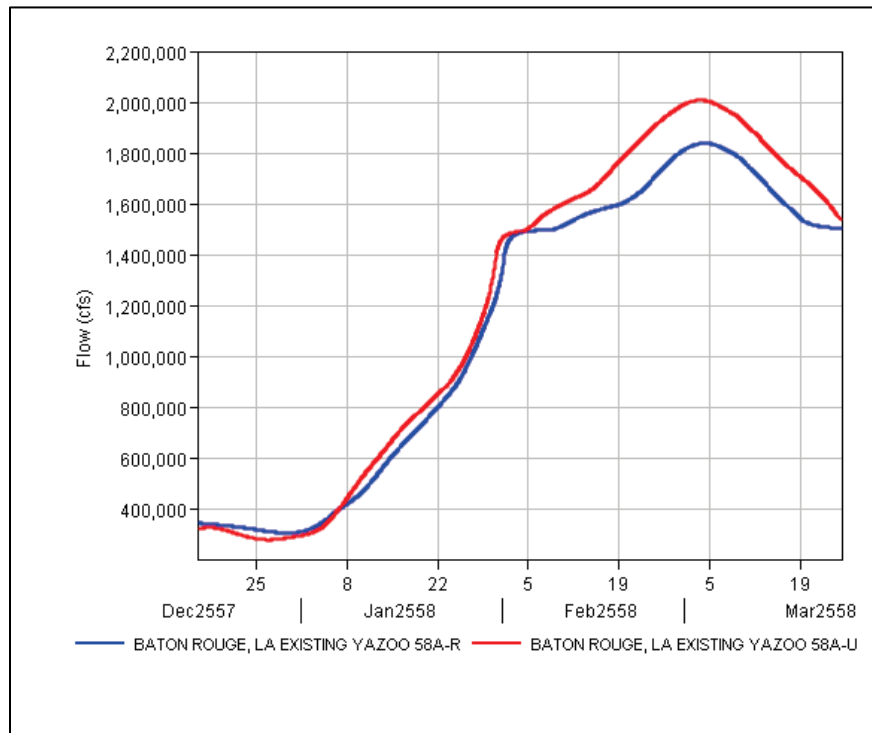


Figure 3-37. HYPO 58A HEC-RAS hydrograph: Mississippi River at Donaldsonville, LA.

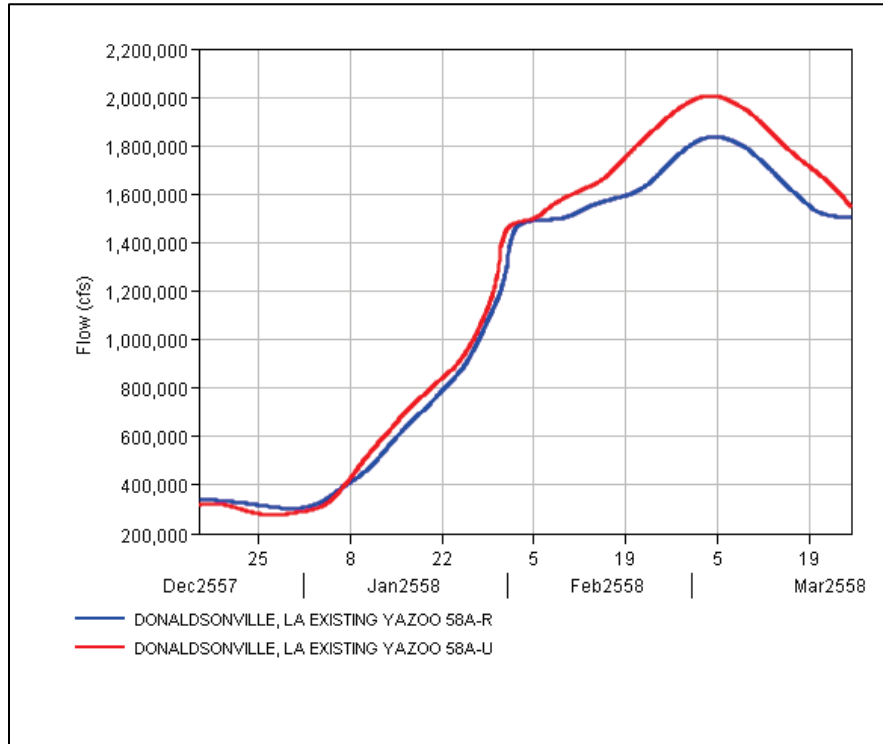


Figure 3-38. HYPO 58A HEC-RAS hydrograph: Mississippi River at Carrollton, LA.

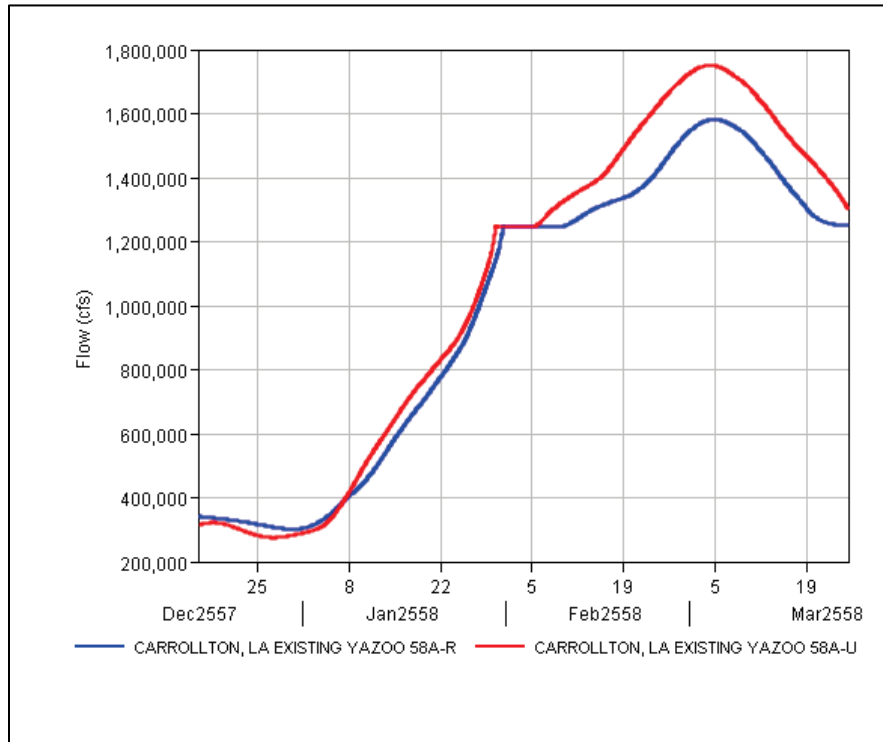


Figure 3-39. HYPO 58A HEC-RAS hydrograph: Mississippi River at Empire, LA.

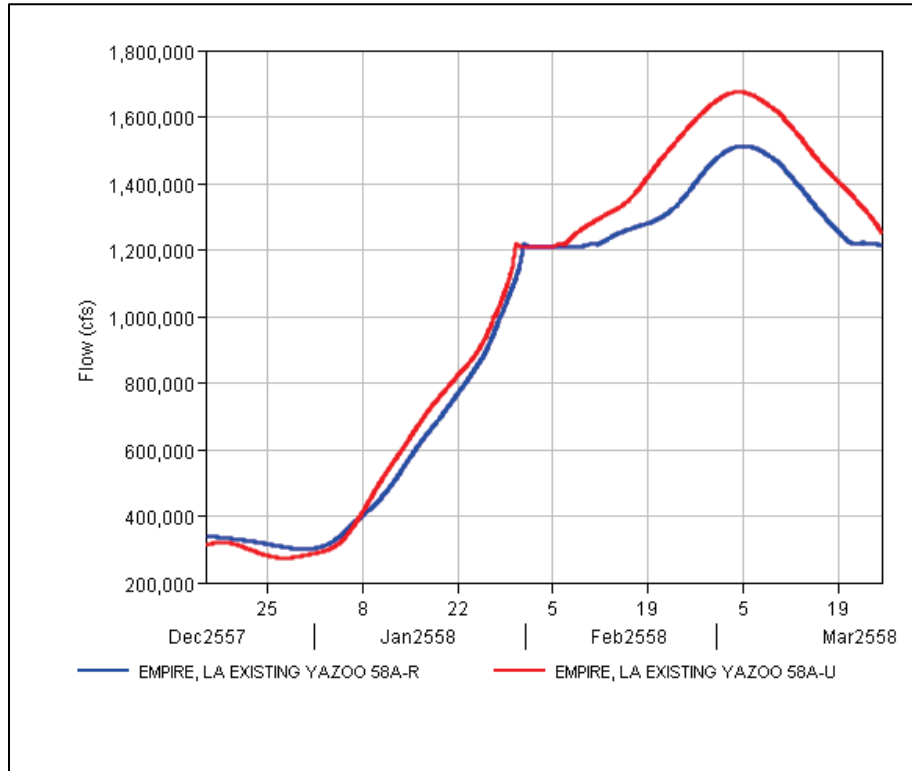
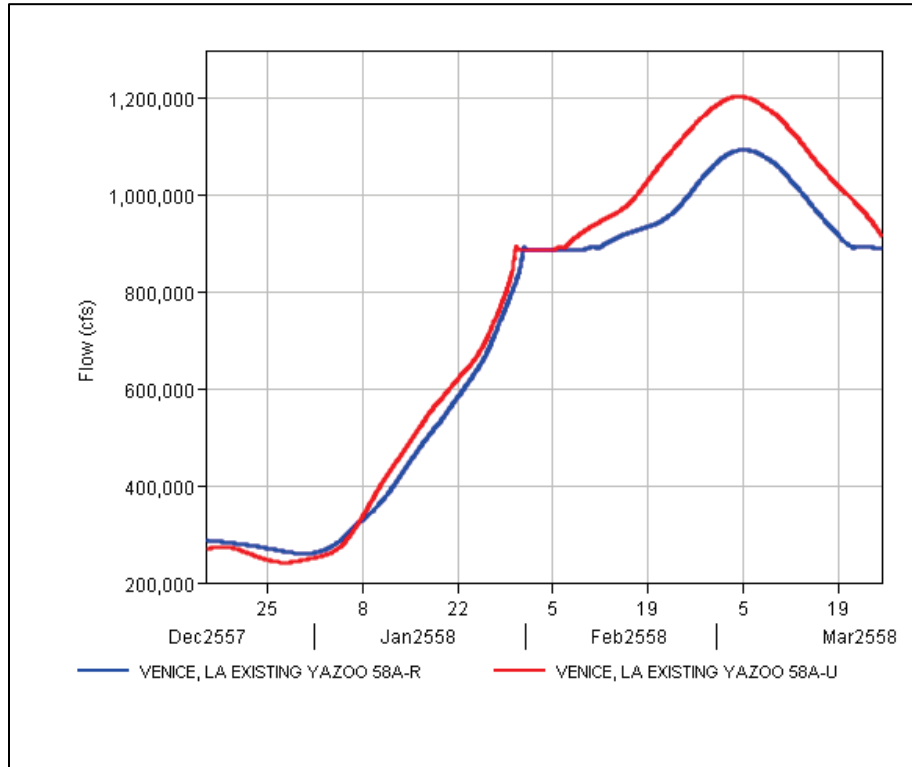


Figure 3-40. HYPO 58A HEC-RAS hydrograph: Mississippi River at Venice, LA.



4 Summary

The combined NWS, TVA, and USACE hydrologic modeling was an extensive effort. There was good overall agreement among model results for the HYPO¹ 58A results within the focus reach for the Mississippi River and Tributaries Project. The agreement for HYPO 52A, HYPO 56 and HYPO 63 varied.

HYPO 58A flows provide the design condition for the main-stem Mississippi River from Cairo, IL, to the Gulf of Mexico except with few exceptions as noted in House Document 308 (H.R. Doc. No. 308). The 2016 re-evaluation of hydrologic conditions resulted in changes in the unregulated flow hydrographs needed for developing the PDF water surface profile from the Hydrologic Engineering Center-River Analysis System (HEC-RAS). The unregulated combined peak flow calculated for the Mississippi River at the Ohio/Mississippi confluence was within 3% of the previous peak values published in USACE MRC (1955) report while changes in calculated total volume were greater.

The other three HYPO storms, 52A, 56, and 63, were also included in the analysis. The unregulated peak flows for HYPO 56 and HYPO 63 were in fair agreement with prior-1955 values. However, computed HYPO 52A unregulated peak values were significantly lower than those from 1955 (see Figure 3-1). Various elements of the analysis were checked in an effort to determine why this one model run produced lower flows. Indications point to differences in precipitation and temperature inputs for HYPO 52A; original data that were used in the 1955 analysis were not available, requiring use of NOAA archive data. Multiple checks with NOAA archive data failed to resolve the issue. Further investigation to resolve the issues was not within time and funding constraints of the current assessment.

The effects of reservoir regulation were different with the 2016 reductions being less than indicated by the prior 1955 Study. There is potential to alter reservoir operations to reduce the amount of regulated flow for HYPO 58A from those indicated by 58A-R results (see Section 4.11). It is not feasible to achieve reductions based on maximum utilization of flood control storage during real-time operations as applied in the 1955 Study. Additional studies using realistic real-time operational considerations

¹ HYPO = hypothetical.

should be conducted to determine best operating procedures and their level of reduction for reservoirs during extreme events like HYPO 58A.

References

- Ely, Paul B., and John C. Peters. 1984. "Probable Maximum Flood Estimation – Eastern United States 1." *Journal of the American Water Resources Association* 20(3): 391–396.
- Friedman, D., J. Schechter, B. Baker, C. Mueller, G. Villarini, and K. D. White. 2016. *US Army Corps of Engineers Nonstationarity Detection Tool User Guide*. U.S. Army Corps of Engineers: Washington, DC.
https://www.engr.colostate.edu/~pierre/ce_old/classes/ce717/Nonstationarity_Detection_Tool_User_Guide.pdf.
- Grundstein, A. 2009. "Evaluation of Climate Change over the Continental United States Using a Moisture Index." *Climatic Change* 93: 103–115.
- Hirsch, Robert M. 2011. "A Perspective on Nonstationarity and Water Management." *Journal of the American Water Resources Association* 47(3): 436–446.
<http://onlinelibrary.wiley.com/doi/10.1111/j.1752-1688.2011.00539.x/abstract>.
- H.R. Doc. No. 308. 1964. *Mississippi River and Tributaries Project*. 88th Congress, 2d Session.
- Klein, William H. 1948. "Winter Precipitation as Related to the 700-Mb Circulation." *Bulletin of the American Meteorological Society* 29(9): 439–453.
- Mississippi River Commission (MRC). 1955. *Memorandum Report No. 1, Appendix J—Mississippi River Basin: Meteorological Study*. Mississippi River Commission, U.S. Army Corps of Engineers.
- National Oceanic and Atmospheric Administration. 1994. *Natural Disaster Survey Report – The Great Flood of 1993*. U.S. Department of Commerce. February 1994. https://www.weather.gov/media/publications/assessments/93_Flood.pdf.
- Qian T, A, Dai, and K. E. Trenberth. 2007. "Hydroclimatic Trends in the Mississippi River Basin from 1948 to 2004." *Journal of Climate* 20: 4,599–4,614.
- Tennessee Valley Authority Act (TVA) of 1933. 16 U.S.C. sec. 831. 48 Stat. 58-59. 18 May 1933.
http://www.ourdocuments.gov/print_friendly.php?flash=true&page=&doc=65&title=Tennessee+Valley+Authority+Act+%281933%29.
- U.S. Army Corps of Engineers (USACE). 1959. *Annex C: Project Design Flood Study, Response to a Resolution by the Committee on Public Works of the United States Senate, Mississippi River Commission*. Vicksburg, MS: U.S. Army Corps of Engineers.
- USACE. 1973. *Mississippi River and Tributaries Post-Flood Report 1973*. Lower Mississippi Valley Division and Mississippi River Commission. Vicksburg, MS: U.S. Army Corps of Engineers.
www.mvd.usace.army.mil/Portals/52/docs/regional_flood_risk_management/Docs/1973_Post_Flood_Report.pdf.

- USACE. 1989. *Flooding in the Lower Mississippi Valley (1973 – 1989)*. Vicksburg, MS: U.S. Army Corps of Engineers.
- USACE. 1999. *1997 Post Flood Report*. New Orleans, LA: U.S. Army Corps of Engineers, New Orleans District.
- USACE. 2014. *Appropriate Application of Paleoflood Information for Hydrology and Hydraulics Decisions*. Engineer Technical Letter 1100-2-2. Washington, D.C: U.S. Army Corps of Engineers.
https://www.publications.usace.army.mil/Portals/76/Publications/EngineerTechnicalLetters/ETL_1100-2-2.pdf.
- USACE. 2015a. *Recent US Climate Change and Hydrology Literature Applicable to US Army Corps of Engineers Missions – Ohio Region*. Civil Works Technical Report CWTS 2015-05. Springfield, VA: National Technical Information Service.
http://www.usace.army.mil/corpsclimate/Recent_CC_HydrologyLit_Applicable_USACE_Missions.aspx.
- USACE. 2015b. *Recent US Climate Change and Hydrology Literature Applicable to US Army Corps of Engineers Missions – Tennessee Region*. Civil Works Technical Report CWTS 2015-05. Springfield, VA: National Technical Information Service.
http://www.usace.army.mil/corpsclimate/Recent_CC_HydrologyLit_Applicable_USACE_Missions.aspx.
- USACE. 2015c. *Recent US Climate Change and Hydrology Literature Applicable to US Army Corps of Engineers Missions – Upper Mississippi Region*. Civil Works Technical Report CWTS 2015-05. Springfield, VA: National Technical Information Service.
http://www.usace.army.mil/corpsclimate/Recent_CC_HydrologyLit_Applicable_USACE_Missions.aspx.
- USACE. 2015d. *Recent US Climate Change and Hydrology Literature Applicable to US Army Corps of Engineers Missions – Lower Mississippi Region*. Civil Works Technical Report CWTS 2015-05. Springfield, VA: National Technical Information Service.
http://www.usace.army.mil/corpsclimate/Recent_CC_HydrologyLit_Applicable_USACE_Missions.aspx.
- USACE. 2015e. *Recent US Climate Change and Hydrology Literature Applicable to US Army Corps of Engineers Missions – Missouri River Region*. Civil Works Technical Report CWTS 2015-05. Springfield, VA: National Technical Information Service.
http://www.usace.army.mil/corpsclimate/Recent_CC_HydrologyLit_Applicable_USACE_Missions.aspx.
- USACE. 2015f. *Recent US Climate Change and Hydrology Literature Applicable to US Army Corps of Engineers Missions – Arkansas, White, and Red Rivers Region*. Civil Works Technical Report CWTS 2015-05. Springfield, VA: National Technical Information Service.
http://www.usace.army.mil/corpsclimate/Recent_CC_HydrologyLit_Applicable_USACE_Missions.aspx.

- USACE. 2016. *Engineering and Construction Bulletin - Guidance for Incorporating Climate Change Impacts to Inland Hydrology in Civil Works Studies, Designs, and Projects*. No. 2016-25. Washington, DC: U.S. Army Corps of Engineers. http://www.iwr.usace.army.mil/Portals/70/docs/Climate%20Change/ecb_2016_25.pdf.
- USACE. 2018. *Mississippi River and Tributaries Flowline Assessment Hydraulics Report*. MRG&P Report No. 24; No. 3. Vicksburg, MS: U.S. Army Research and Development Center.
- USACE, Weather Bureau. 1937. *A Meteorological Analysis of the Possibility of the Coincidence of Maximum Flood Discharges from the Ohio, Mississippi and Missouri Rivers*. Ft. Humphreys, DC: Engineer Reproduction Plant.
- USACE, Weather Bureau. 1956. *Meteorology of Flood-Producing Storms in the Mississippi River Basin*. Hydrometeorological Report No. 34, HMR 34. U.S. Department of Commerce. Washington, DC: U.S. Government Printing Office.
- USACE, Weather Bureau. 1959. *Meteorology of Hypothetical Flood Sequences in the Mississippi River Basin*. Hydrometeorological Report No. 35, HMR 35. Washington, DC: U.S. Department of Commerce.
- Waterways Experiment Station (WES). 1957. *Effects of Upstream Reservoirs on the Project Flood, Vicinity of Confluence, Ohio and Mississippi Rivers: Interim Report*. For Mississippi River Commission, Reservoir Benefit Study, Mississippi Basin Model Comprehensive Testing Program, U.S. Army Corps of Engineers. Vicksburg, MS: Waterways Experiment Station.
- Watson, C. C., R. R. Holmes, Jr., and D. S. Biedenharn. 2013. "Mississippi River Streamflow Measurement Techniques at St. Louis, Missouri." *Journal of Hydraulic Engineering* 139(10): 1062–1070.

Appendix A: Agency Correspondence — National Weather Service Scope of Work

Mississippi River and Tributaries Project

Review of Project Design Flood Inflow Hydrographs

Scope of Work

December 2013

Purpose

The purpose of this scope of work (SOW) is to define the tasks that U.S. Army Corps of Engineers – Mississippi Valley Division (USACE-MVD) requests the National Weather Service (NWS) to accomplish to support the Mississippi River and Tributaries (MR&T) project as it reviews the project's design flows and elevations. This SOW, developed jointly between MVD and the NWS, identifies the tasks required, the division of tasks between MVD and NWS, the deliverables, and the expected schedule to accomplish.

Background

The MR&T project was authorized by the 1928 Flood Control Act. In the wake of the devastating 1927 flood, it was deemed necessary to put into place a comprehensive, unified system of public works within the Lower Mississippi Valley that would provide unprecedented flood risk management and an equally efficient navigation channel. The MR&T project has four major features: 1. Levees/floodwalls; 2. Tributary basin improvements; 3. Floodways; 4. Channel improvement and stabilization. These features work together to provide flood risk management and navigation and foster environmental protection and enhancement.

The 2011 Flood tested the MR&T System like no flood before; it was the largest recorded flood through much of the Lower Mississippi River. Stage and flow rates broke records at several locations, and for the first time, three floodways—Birds Point-New Madrid Floodway, the Morganza Floodway, and the Bonnet Carré Spillway—were operated during a single

flood event. River stages and flow rates were comparable to the major floods of 1927 and 1937. However, the 2011 Flood was contained within the MR&T System to a greater extent than the earlier comparable floods. In 2011, the MR&T system prevented massive flood damages by accommodating the river while using approximately 85 percent of its overall design capacity. An estimated \$230 billion in flood damages was prevented in the single event. Since its inception in 1928, the MR&T system is calculated to have prevented \$612 billion in cumulative flood damages. At an investment level of \$14 billion to date, those savings result in a \$44 return on every \$1 invested. These figures do not include all of the positive economic activity, from farming to towns and factories, plus annual transportation savings of \$3 billion enabled by this unique system.

The MR&T project is designed to control the “project design flood.” The present Project Design Flood (PDF) was developed in 1956 when the Mississippi River Commission made a complete review of the adequacy of the MR&T project. The NWS was asked to provide the largest storm series considered to have a reasonable chance of occurrence in the season when floods are likely to occur over the Mississippi River Basin. After investigating 35 different hypothetical storm series, the one that produced the greatest discharges from Cairo, IL, to the Gulf of Mexico was selected as the PDF. The development of the PDF is documented in “Mississippi River Project Flood Study – Memorandum No. 1” USACE, Mississippi River Commission, December 1955.

Despite the success of the MR&T system, the results and experience from the 2011 flood revealed some areas in which the current design elevations based on the PDF may not be adequate if and when larger events up to the PDF occur. As a result, the USACE is in the process of reviewing the PDF Flowline. A key part of the review is to re-validate the PDF hydrology, which was developed in 1956. A review of the meteorology of the PDF was recently completed and concluded that the current hypothetical three-storm combination is still adequate. A review of the hydrology of the basin is required to determine if the inflow hydrographs and lateral inflows to the MR&T system (developed in 1956) should be updated or revised to reflect changing hydrologic conditions in the basin from factors such as climate change, land use changes, constructed projects, etc. A list of the inflow hydrograph and lateral inflow points are provided as Enclosure 1 to this scope. The PDF is a very extreme event (a frequency cannot be developed for the full event) and is larger than previous floods

of record, including the 2011 event. While it is likely that significant hydrologic changes have occurred in the Mississippi River Basin, the impacts in total runoff for extreme events may or may not be significantly different today from when the PDF was first developed.

Summary of tasks requested from NWS

To assess the adequacy of the 1956-vintage hydrology for the PDF, the NWS is requested to use its existing hydrologic forecast modeling to simulate two scenarios that will be used by the USACE to examine how watershed hydrologic changes impact the PDF runoff and, by extension, the PDF Flowline. Storm events to be modeled for each scenario include HYPO 58A, HYPO 56, HYPO 52A and HYPO 63. This should be accomplished for two scenarios where antecedent conditions are used that (1) match the original PDF antecedent conditions and (2) where antecedent conditions will match an Apr-May storm (similar to 2011 flood). A possible third scenario (characteristics to be determined) may be requested after the results of the first two scenario sets have been reviewed. The two scenario sets will reflect the PDF rainfall/runoff occurring under different antecedent conditions. The original PDF hydrographs were developed using storms with antecedent conditions reflecting a particular time of year. At that time, the NWS and the USACE concluded that winter storms provided the highest runoff flows into the MR&T system downstream of Cairo, IL, and that severe spring storms did not exceed those levels. However, since the early 1970s, the most severe floods in the MR&T systems downstream of Cairo, IL, have occurred predominantly in the spring months of April and May. Thus, a second scenario will be developed placing the PDF rainfall for HYPO storms during an April/May timeframe where antecedent conditions reflect the impacts of significant snowmelt and spring precipitation leading up to the HYPO storm rainfall, much as occurred during the actual 2011 Flood. The USACE will provide the individual HYPO Storms precipitation and orientation data in 6-hour increments by converting the rainfall charts from DM No. 1 into shapefiles and converting to the NWS preferred ARC-ASCII formats. The NWS, via OHRFC and LMRFC, will provide guidance on converting shapefile to ARC-ASCII formats. In addition, the USACE will work with the TVA to assist in modeling the Tennessee River system and operation of Kentucky reservoir. This will be required to complete this portion of the system.

The PDF event for the MR&T Project actually consists of different sets of storm conditions referred to as hypothetical floods or storms (HYPO Flood or HYPO Storm). The primary PDF storm known as HYPO Flood 58A is a winter season three-storm combination that defines the design runoffs and elevations for the MR&T system downstream of Cairo, IL. HYPO Flood 56 is an early-spring season two-storm combination which defines the largest flows contributed from the White and Red River basins. HYPO Flood 63 is an early-spring season three-storm combination that gave the largest flows from the Arkansas River basin. HYPO Flood 52A is a late-spring season three-storm combination that gave the largest flow from the Missouri River basin. All four HYPO Storm sets will have to be modeled by NWS for a complete scenario run.

While the actual approach conducted for each scenario may be adjusted as the work is accomplished to ensure the best available products, discussions between NWS and the USACE envisioned an approach similar to the following:

For first scenario (HYPO 58A): (1) take fall 2010 conditions for simulating the forcings and let come to equilibrium, (2) introduce above-average winter 2010-2011 rainfall to ensure “wet” conditions, (3) apply the HYPO 58A in the forecasting models and compute hydrographs at the required points, and (4) repeat for the HYPO 56, 52A, and 63, respectively. A sensitivity analysis should be conducted on the HYPO 58A event, varying key parameters to identify the level of sensitivity of the models. If necessary, repeat the sensitivity analysis for the one or more of the other HYPO Storm events.

For the second scenario: (1) take winter 2011 conditions for simulating the forcings and let come to equilibrium, (2) introduce 2011 rainfall (March and early April) to ensure wet conditions, (3) apply the HYPO event 58A in the forecasting models and compute hydrographs at the required points, and (4) repeat for the HYPO Storms 56, 52A, and 63, respectively. It is assumed the sensitivity analysis conducted earlier will not need to be repeated for this scenario.

1. Scenario I – Develop PDF Inflow Hydrographs Using Original PDF Report Antecedent Conditions for the following:
 - a. HYPO 58A (winter season) storm combination for Mouth of Ohio River to Gulf of Mexico

- b. HYPO 63 (early-spring season) storm combination for Middle Mississippi from Mouth of Ohio River to Cape Girardeau, MO
- c. HYPO 52A (late-spring season) storm combination for Arkansas-White Tributaries
- d. HYPO 56 (early-spring season) storm combination for White and Red River tributaries.

The NWS forecast models will be used to develop inflow hydrographs and lateral inflows throughout the watershed for the MR&T system using the 1950s PDF precipitation and antecedent conditions as defined in the Mississippi River Project Flood Study Memorandum Report No. 1, December 1955.

- 2. Scenario II – Develop PDF Inflow Hydrographs Using Antecedent Conditions Reflecting Spring (April/May, i.e., 2011 event) snowmelt and precipitations for the following:
 - a. HYPO 58A (winter season) storm combination for Mouth of Ohio River to Gulf of Mexico
 - b. HYPO 63 (early-spring season) storm combination for Middle Mississippi from Mouth of Ohio River to Cape Girardeau, MO
 - c. HYPO 52A (late-spring season) storm combination for Arkansas-White Tributaries
 - d. HYPO 56 (early-spring season) storm combination for White and Red River tributaries.

The NWS will use its forecasting models to develop the inflow hydrographs and lateral inflows throughout the watershed for the MR&T system using the 1950s PDF precipitation and with antecedent conditions reflecting above average spring conditions such as existed prior to the 2011 flood.

The USACE will need the NWS to define the database (input) needs for the PDF rainfall to be applied to NWS models. This will include defining rainfall points and time distribution format requirements.

Outputs should include both tabular and graphical forms of the inflow hydrographs. Outflows should be provided in HEC-DSS format for direct links to the HEC-RAS models.

- 1. Other Items – As this SOW is developed through discussions between NWS and USACE, additional information or tasks required

by either NWS or USACE may be identified and included in this SOW.

- a. USACE Tasks or Products
 - i. Mississippi River Project Flood Study Memorandum Report No. 1, December 1955, PDF precipitation and distribution in 6-hour increments.
 - ii. List of EN reservoirs from Memorandum Report No. 1 (1955) for the NWS to evaluate how they represent the operations of these reservoirs in the NWS models. The USACE will verify the full list of EN reservoirs and coordinate with NWS to ensure they are covered by the NWS modeling.
 - iii. Antecedent Conditions from Memorandum Report No. 1 (1955) for Scenario 1.
 - iv. Define the inflow hydrograph and lateral inflow hydrographs locations required for the Mississippi River and Tributaries system.
 - v. Storm precipitation for each PDF event (6-hr time steps) – USACE will develop shapefiles for each storm’s 6-hr time steps and convert to ARC-ASCII.
 - vi. Milestone meetings – To ensure quality results and to prevent significant rework, two to three collaboration or milestone meetings will be held between key technical NWS and USACE personnel. These meetings will review initial processes and results to ensure the required quality products are produced. As necessary, USACE forecasters/modelers will be embedded at NWS RFCs to review the forecasting/modeling development and results.
- b. NWS Tasks or Products
 - i. Database (input) format needs for the USACE to provide the PDF rainfall to be applied to NWS models to include rainfall points and time distribution format requirements.
 - ii. Scenario 1 runoff hydrographs and lateral inflow hydrographs for the MR&T system.
 - iii. Scenario 2 runoff hydrographs and lateral inflow hydrographs for the MR&T system (Format: All RFCs send the output to DMW at LMRFC for conversion to DSS; RFCs will work with DMW on what format (i.e., PIXML) or other format out of CHPS).
 - iv. NWS discussion of the model’s development and any sensitivity analysis conducted either in prior

calibration/verification of the models or to be conducted to support the PDF runs. In addition, to address reservoir conditions, sensitivity runs will be made for “low,” “medium,” and “high” start levels for each scenario — all reservoirs in a model realization would be set to the same initial condition. Identification of those parameters displaying significant sensitivity and the range of model outputs from this analysis will be discussed. This will be needed for technical review and defend ability of the overall assessment process and results.

- v. Detailed descriptions of how the NWS models incorporate reservoir operations. The original PDF inflow hydrographs reflected unregulated (no reservoir) conditions and were adjusted for the final design to reflect anticipated impacts of the reservoirs). As part of this effort, the USACE needs to understand how NWS models account for the large number of reservoirs in the basin. A list of the reservoirs which should be accounted for in the NWS modeling is provided as Enclosure 2.

2. Deliverables

- a. Scenario I: NWS – PDF hydrograph results for this scenario – electronic tabular and graphical results. Outflows should be provided in HEC-DSS format for direct links to the HEC-RAS models.
 - 1. HYPO 58A
 - 2. HYPO 63
 - 3. HYPO 52A
 - 4. HYPO 56
- b. Scenario II: NWS – PDF hydrograph results for this scenario – electronic tabular and graphical results. Outflows should be provided in HEC-DSS format for direct links to the HEC-RAS models.
 - 1. HYPO 58A
 - 2. HYPO 63
 - 3. HYPO 52A
 - 4. HYPO 56
- c. Documentation
 - i. NWS – Summary report providing results of Scenarios I and II tasks and a discussion of the tasks and efforts required to produce. This will be used as an appendix to the MR&T

Project Flood Flowline Review report and excerpts will be used in the main report to describe this part of the PDF review.

- ii. NWS – Electronic/printable Inputs and Outputs of all final model simulations (not the software itself) to be kept with USACE report as an appendix.
- iii. Discussion of sensitivity analysis conducted and the results.
- iv. Discussion of how reservoirs are incorporated in the NWS models.

3. Schedule

- a. TBD after discussions between USACE and NWS

4. Project POCs

Technical POC (MVD, sponsor)

Chuck Shadie

1400 Walnut St.

Vicksburg, MS 39181

Phone: 601-634-5917

Email: Charles.E.Shadie@usace.army.mil

Financial POC (MVD, sponsor)

Charlie McKinnie, MVK and/or TBD

1400 Walnut St.

Vicksburg, MS 39181

Phone: <phone number>

Email: <email>@usace.army.mil

Technical POC (NWS)

Financial POC (NWS)

5. TBD

Enclosure 1 – PDF Inflow Hydrograph and Lateral Inflow Locations

(See attached spreadsheet titled “MississippiRiver_InflowPoints—PreliminaryList_2014.03.17xlsx

Enclosure 2 – Reservoirs included in the PDF inflows

(See attached excerpts from “Mississippi River Project Flood Study Memorandum Report No. 1, December 1955” – three files which discuss the HYPO floods and reservoirs included in the PDF analysis.)

Appendix B: HYPO 58A

B.1 Local inputs to the RAS model

The HEC-RAS model included local inputs throughout the Lower Mississippi River to ensure those flows not included in the RFC hydrographs were included. Figure B-1 through Figure B-50 show the local flows that were included into the HEC-RAS model at various locations along the Mississippi River.

Figure B-1. HYPO 58A local input at Acme, LA.

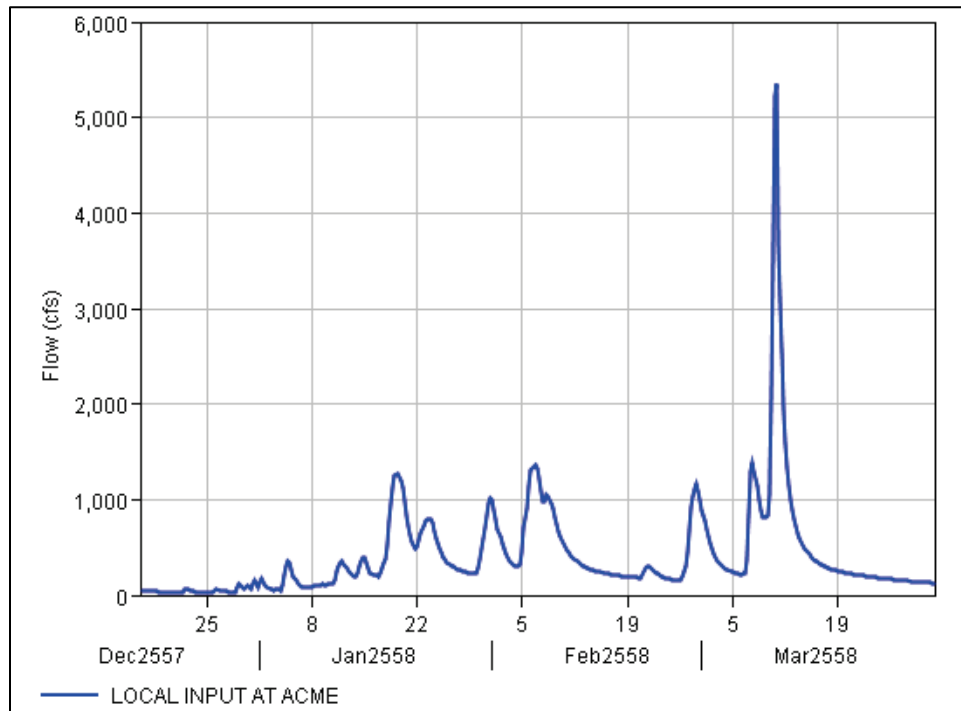


Figure B-2. HYPO 58A local input at Arkansas City, AR.

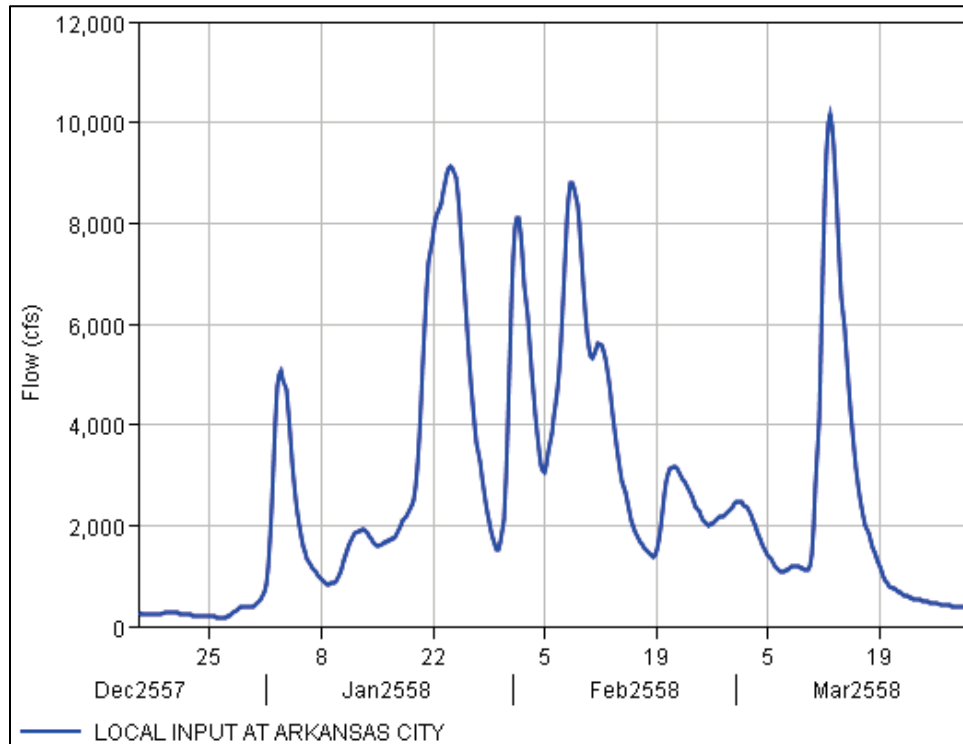


Figure B-3. HYPO 58A local input at Arlington, TN.

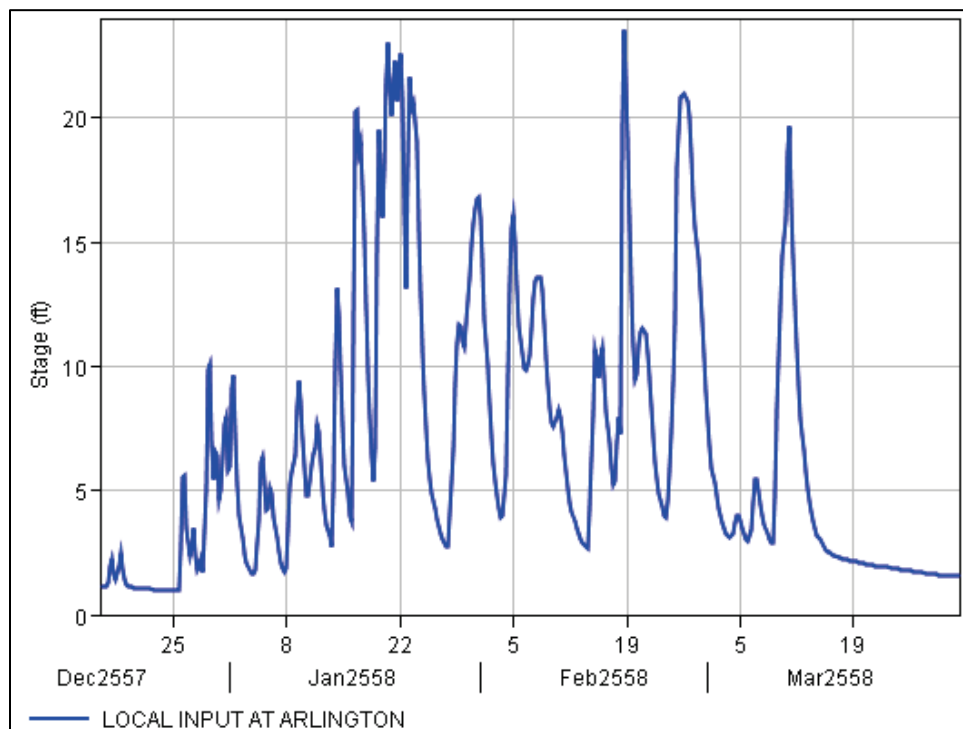


Figure B-4. HYPO 58A local input at Barbre Landing, LA.

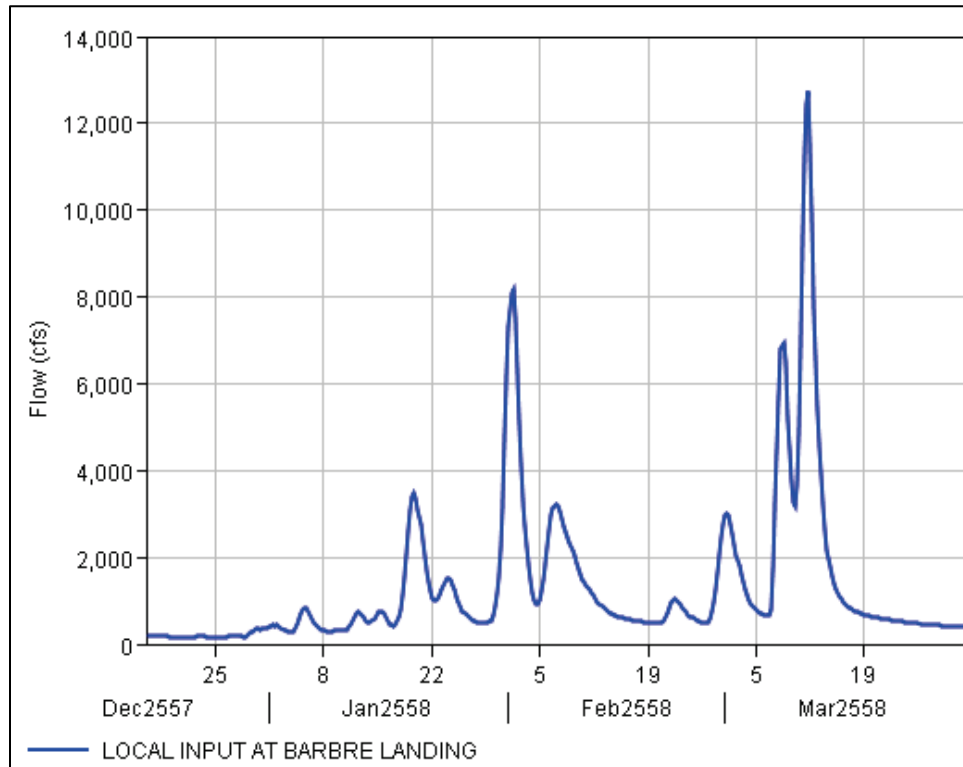


Figure B-5. HYPO 58A local input at Baton Rouge, LA.

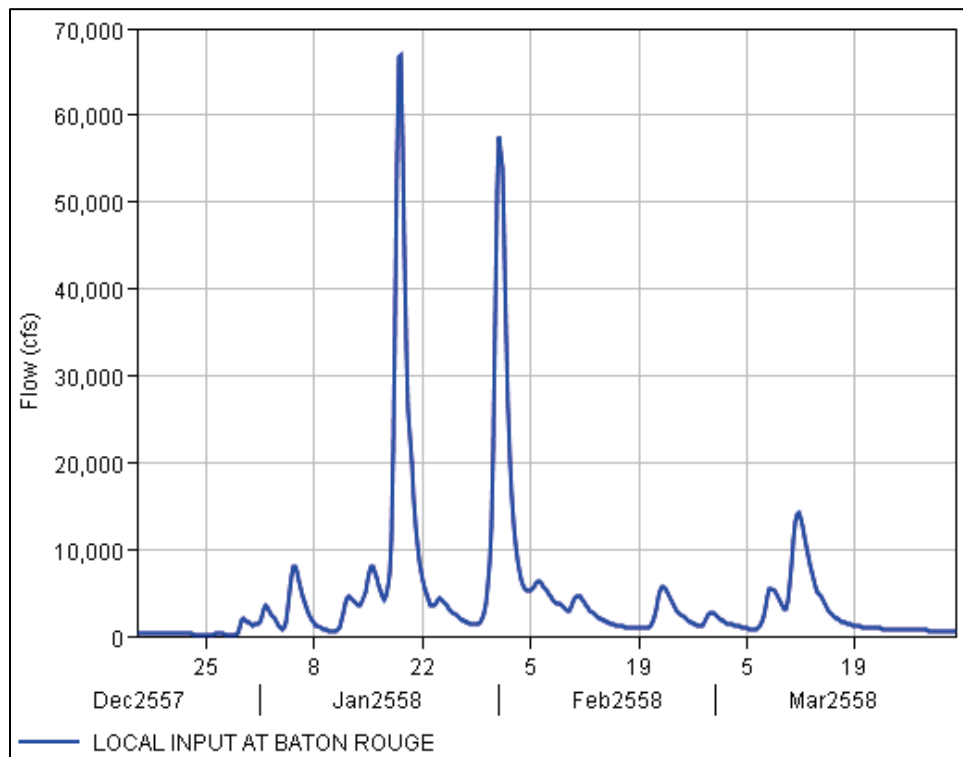


Figure B-6. HYPO 58A local input at Belzoni, MS.

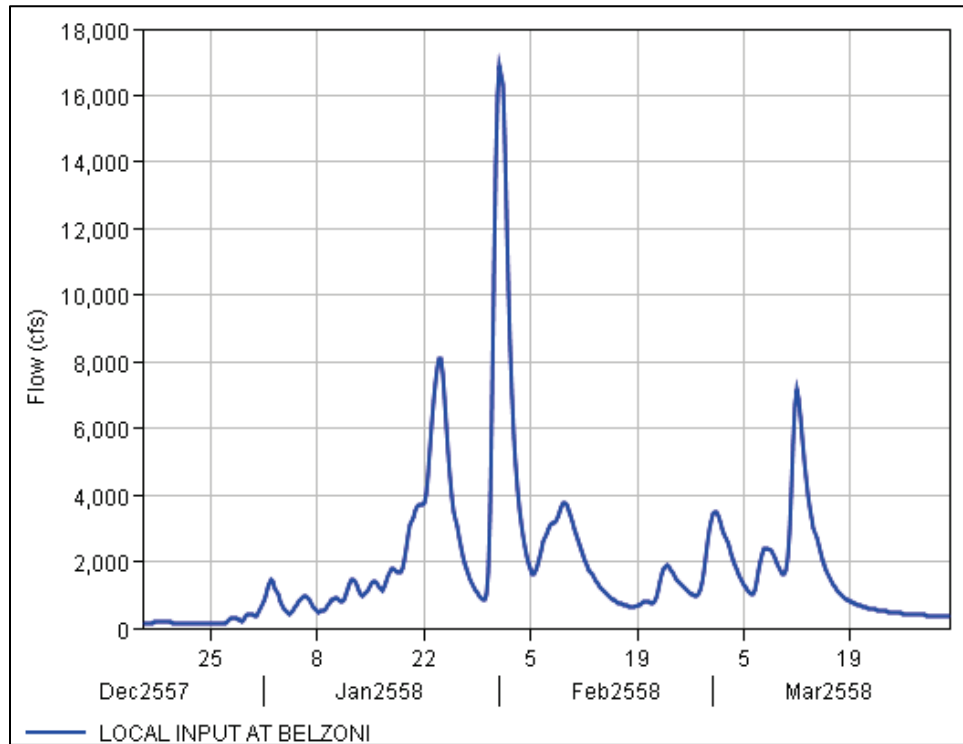


Figure B-7. HYPO 58A local input at Bogota, TN.

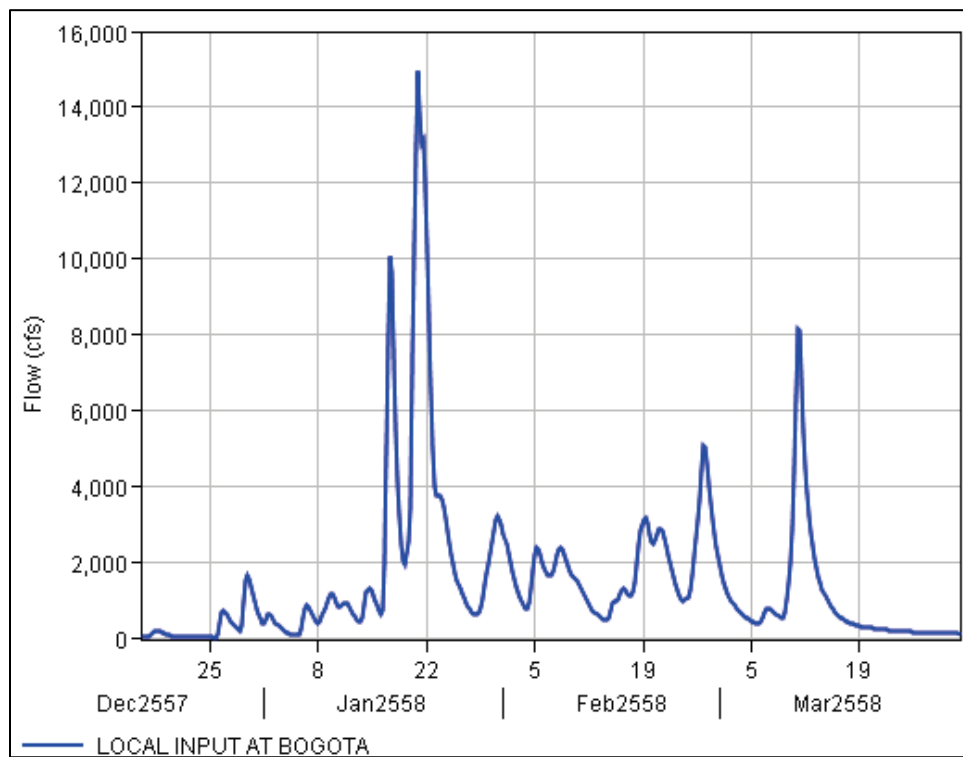


Figure B-8. HYPO 58A local input at Bolivar, TN.

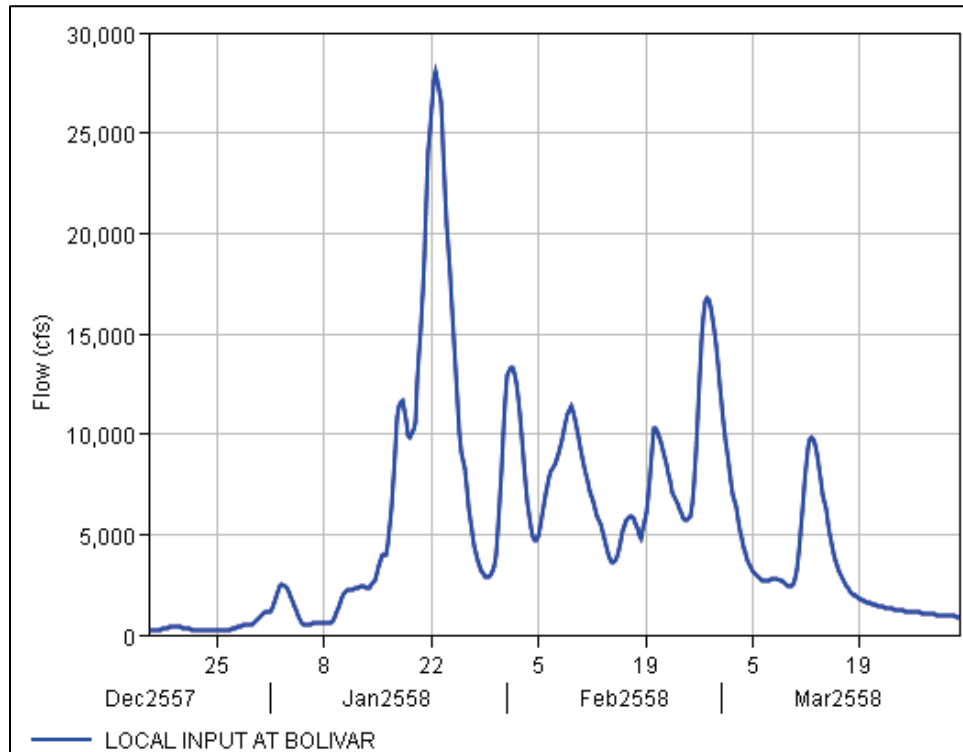


Figure B-9. HYPO 58A local input at Brunswick, TN.

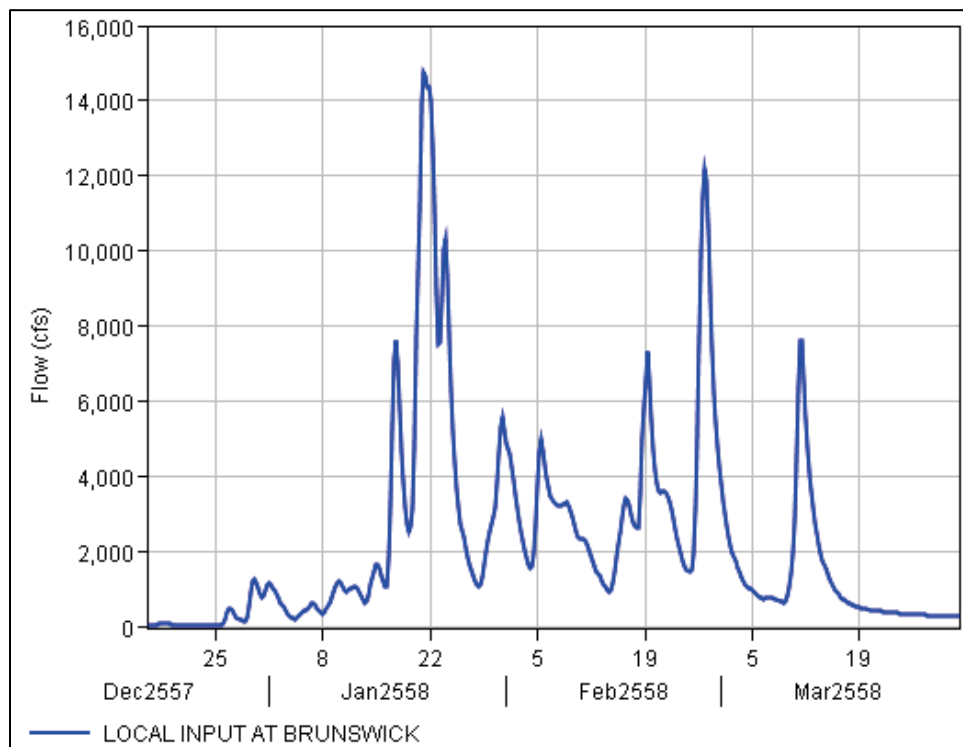


Figure B-10. HYPO 58A local input at Cairo, IL.

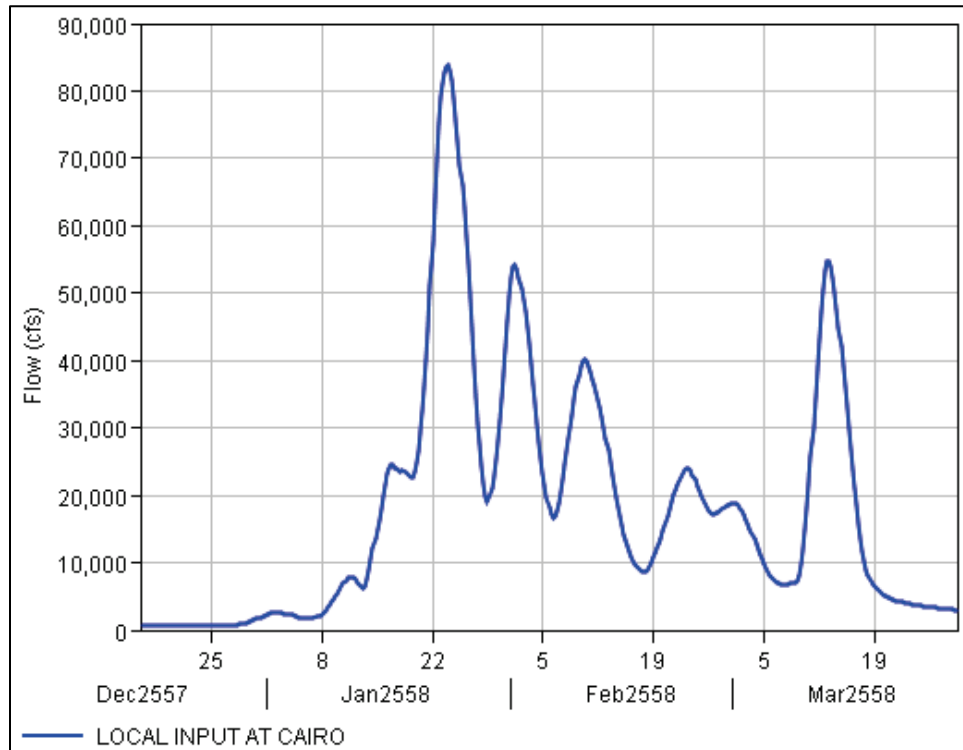


Figure B-11. HYPO 58A local input at Cape Girardeau, MO.

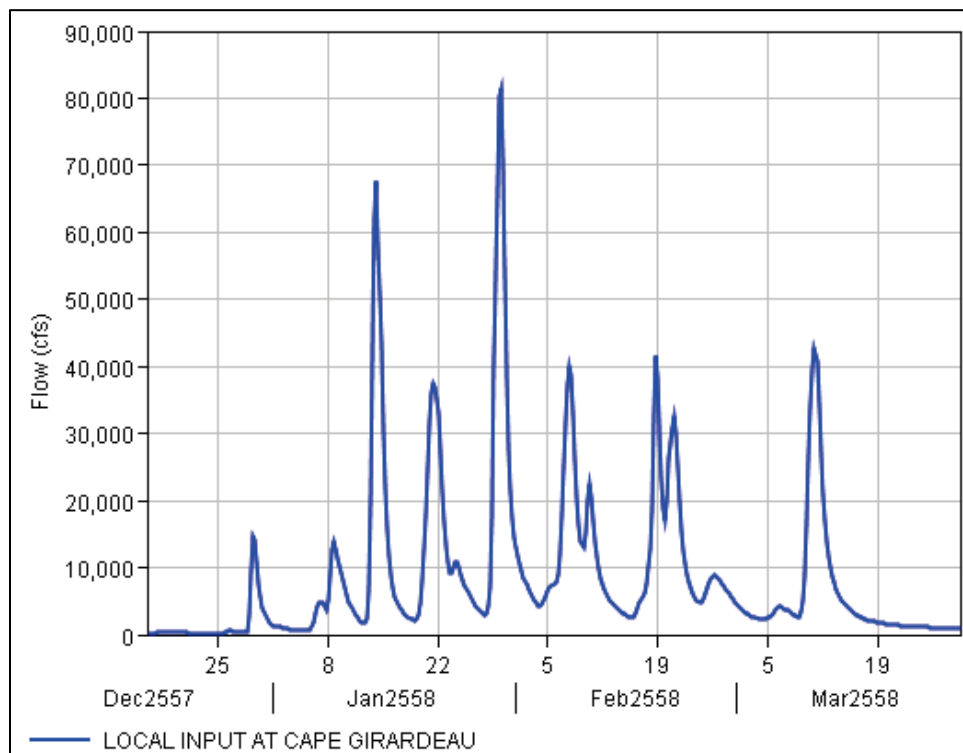


Figure B-12. HYPO 58A local input at Chester, MO.

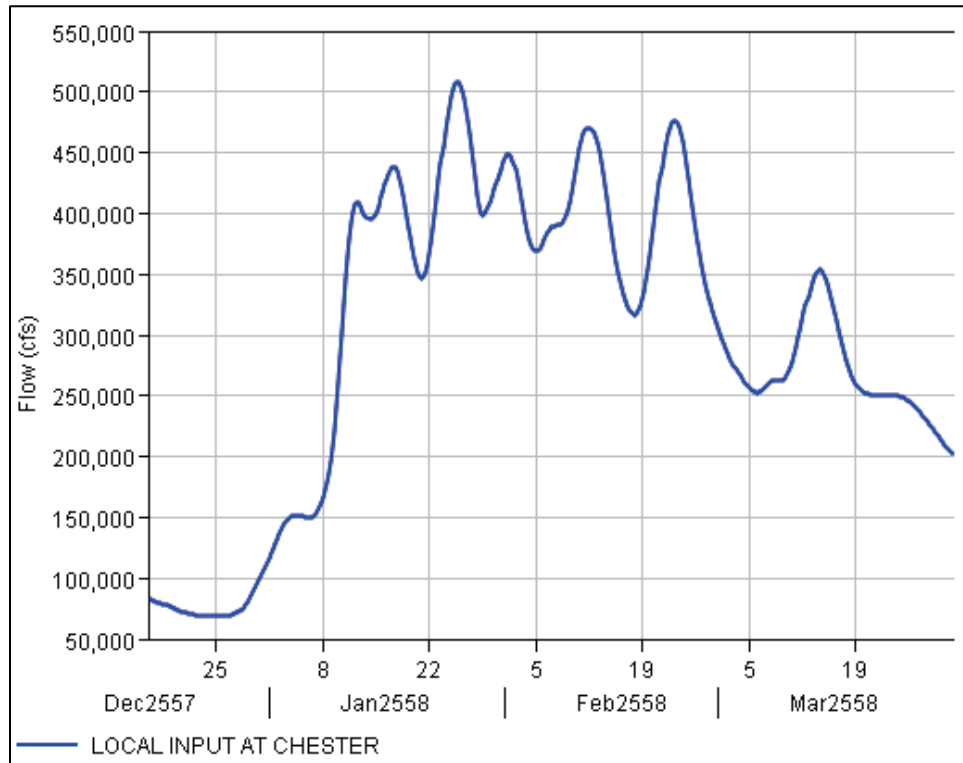


Figure B-13. HYPO 58A local input at Clarendon, AR.

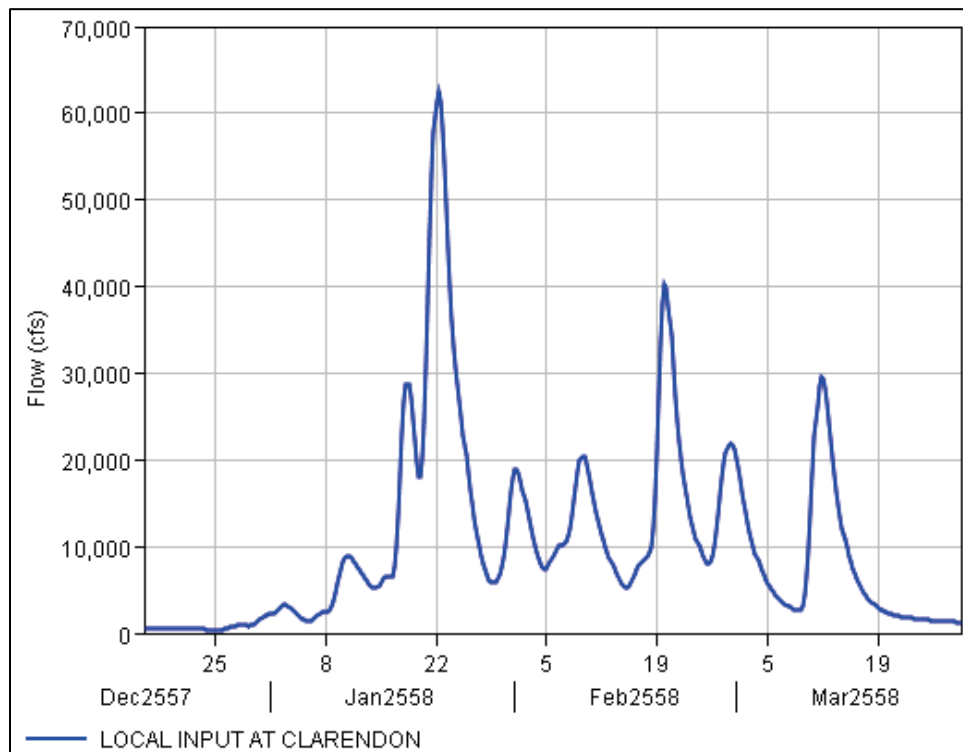


Figure B-14. HYPO 58A local input at Clayton, MS.

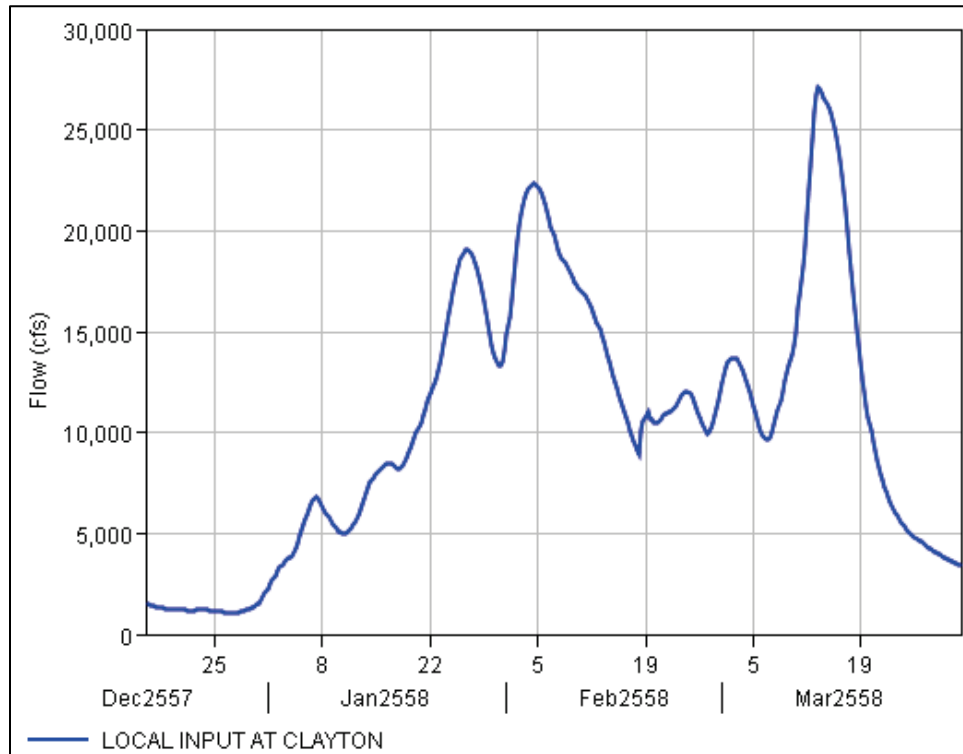


Figure B-15. HYPO 58A local input at Columbia Lock and Dam, LA.

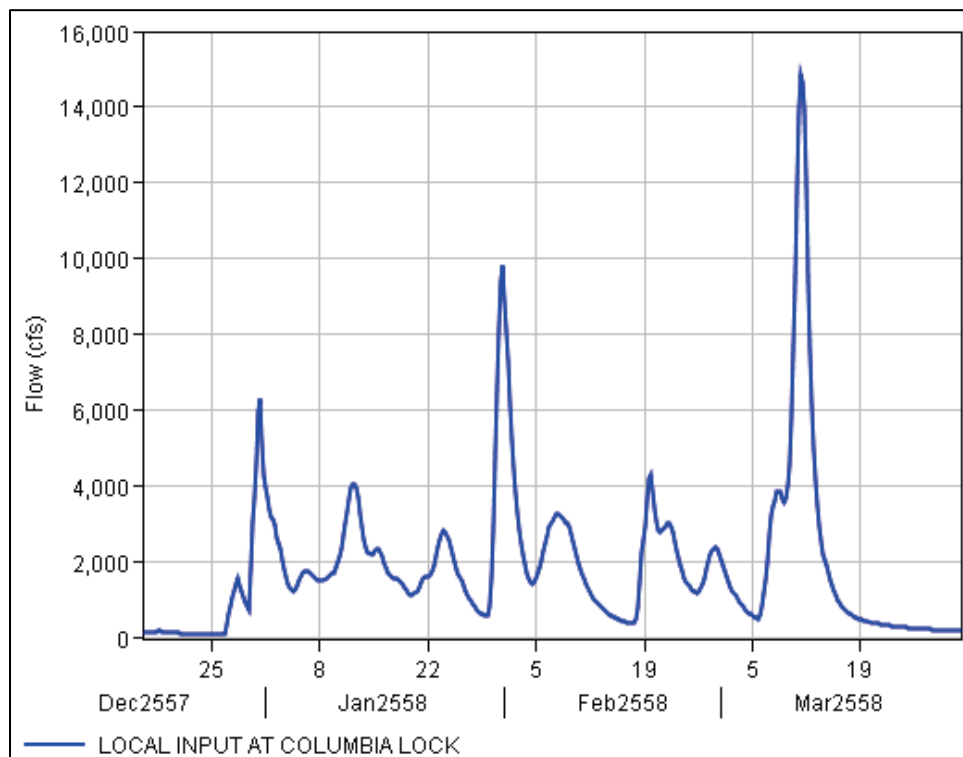


Figure B-16. HYPO 58A local input at Des Arc, AR.

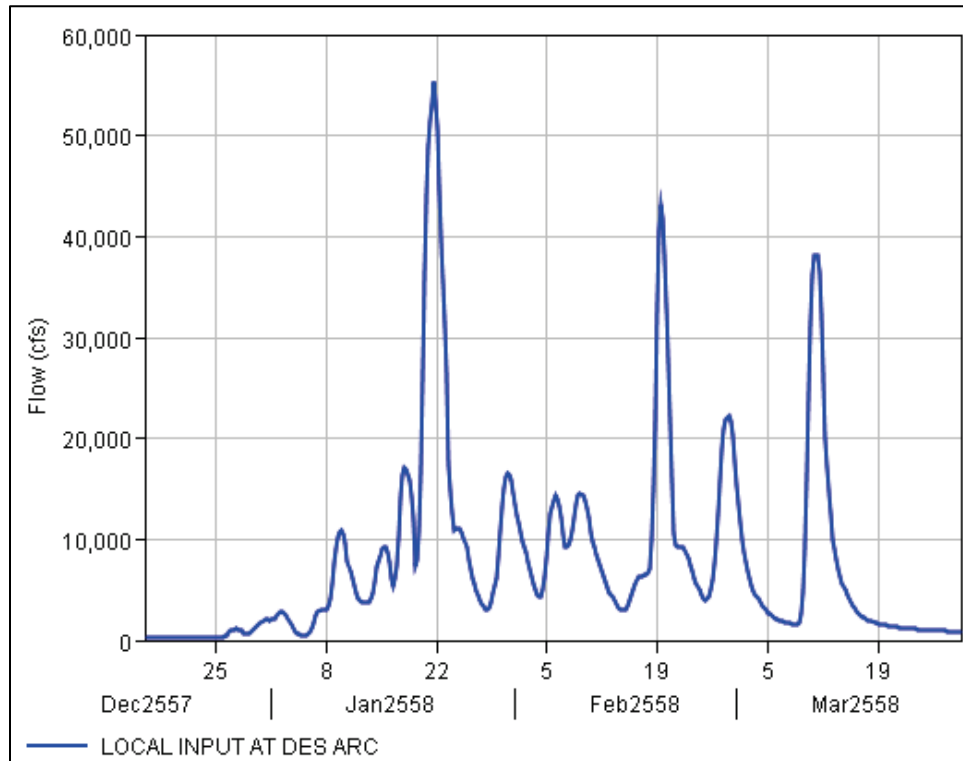


Figure B-17. HYPO 58A local input at Dyersburg, TN.

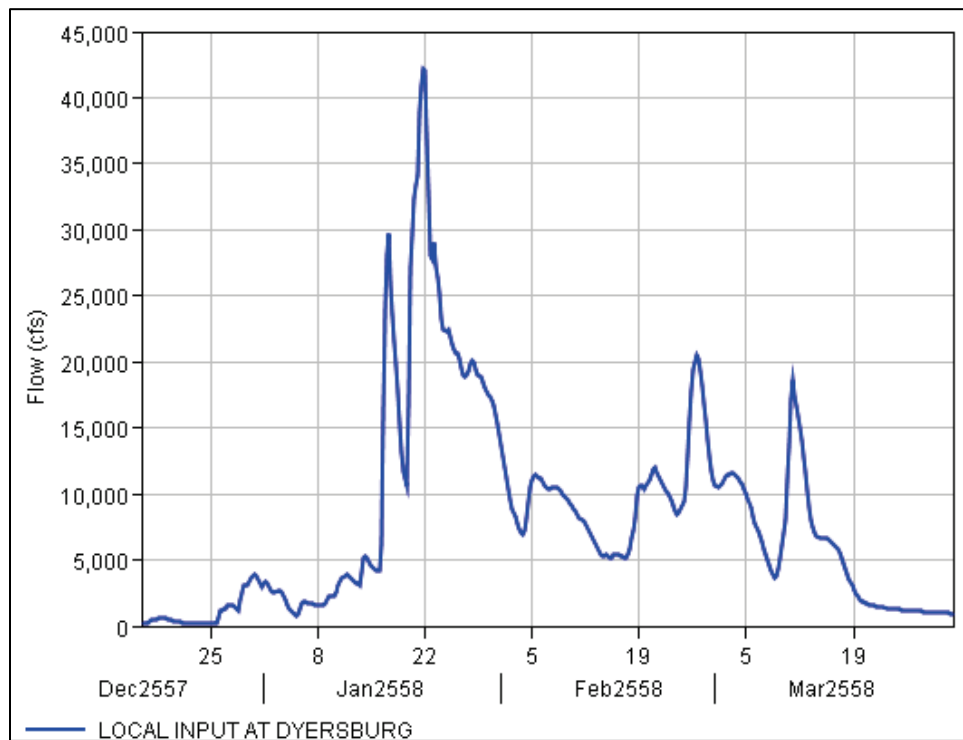


Figure B-18. HYPO 58A local input at Georgetown, AR.

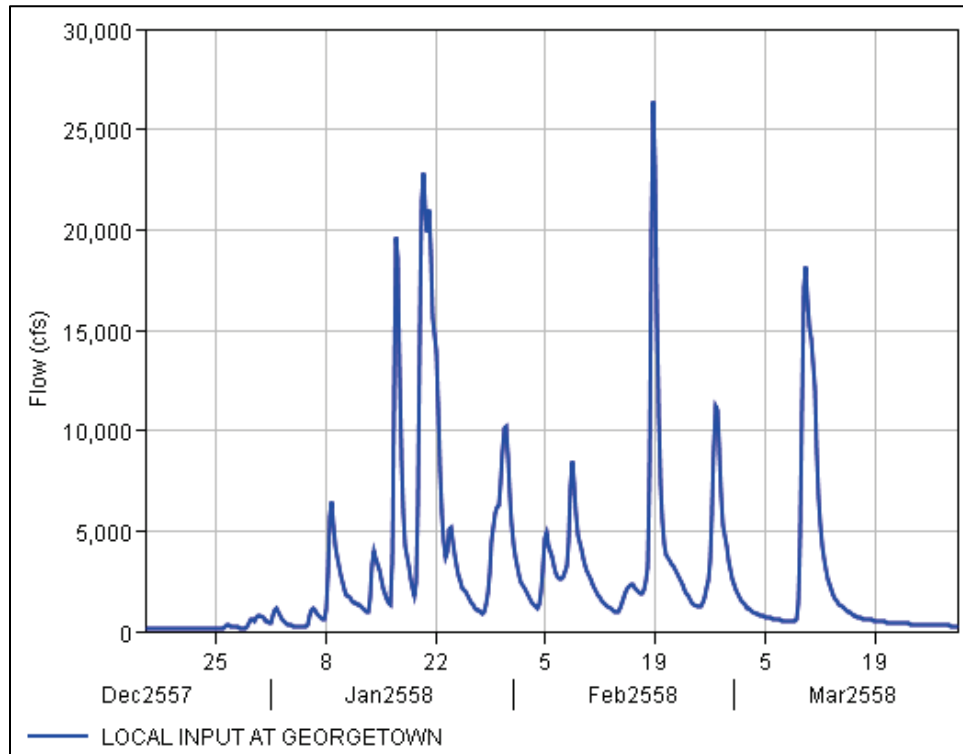


Figure B-19. HYPO 58A local input at Germantown, TN.

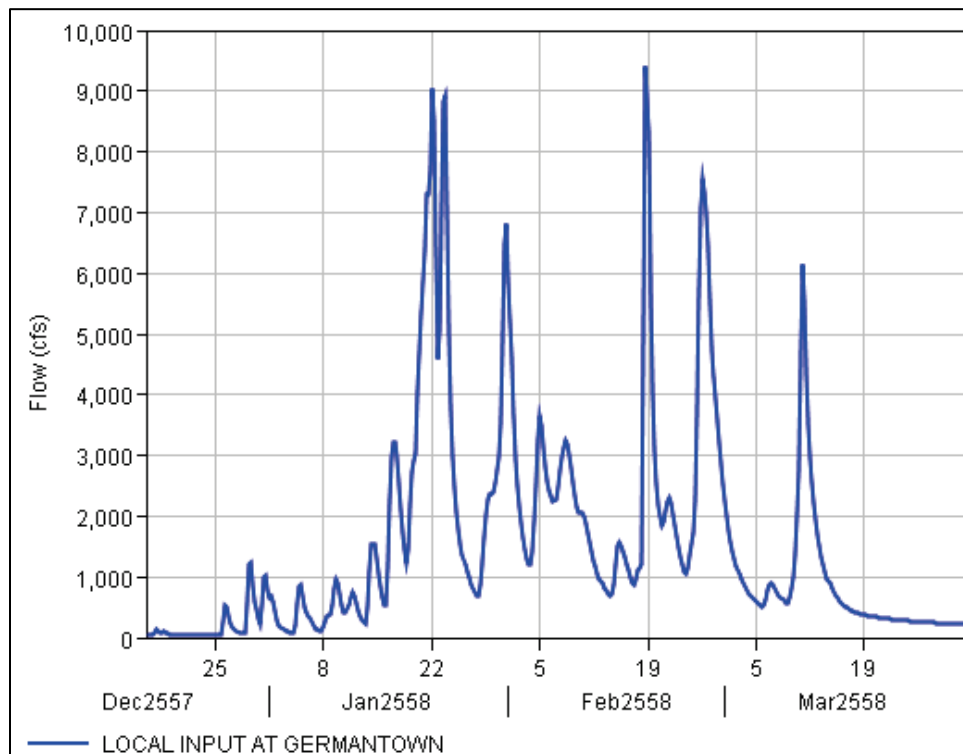


Figure B-20. HYPO 58A local input at Greenwood, MS.

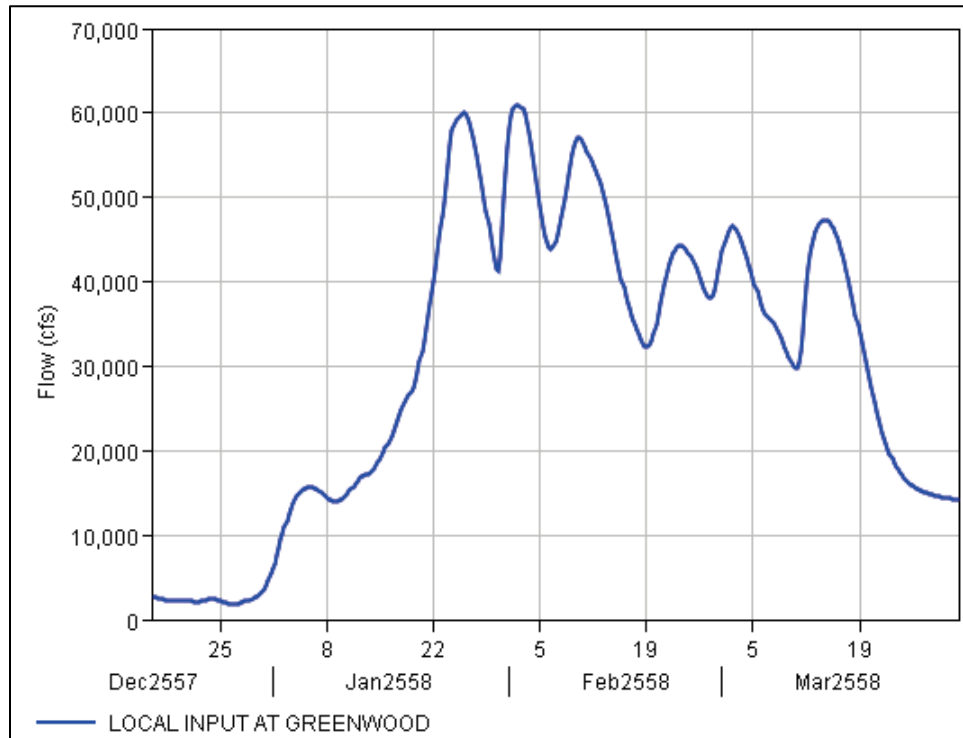


Figure B-21. HYPO 58A local input at Greer's Ferry Dam, AR.

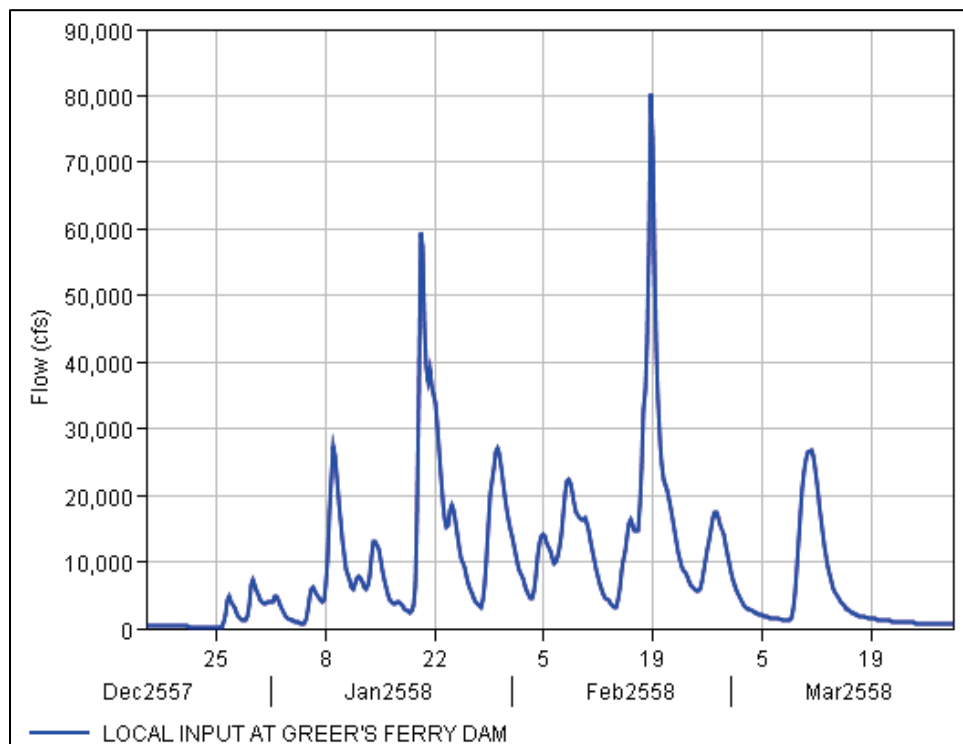


Figure B-22. HYPO 58A local input at Grenada Dam, MS.

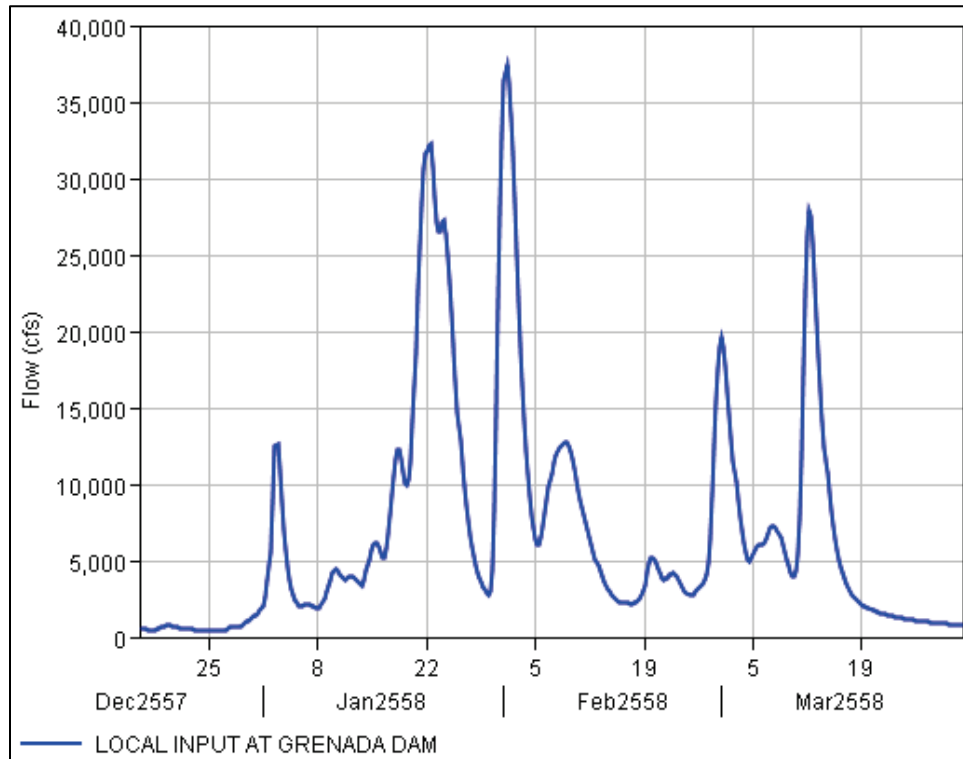


Figure B-23. HYPO 58A local input at Halls, TN.

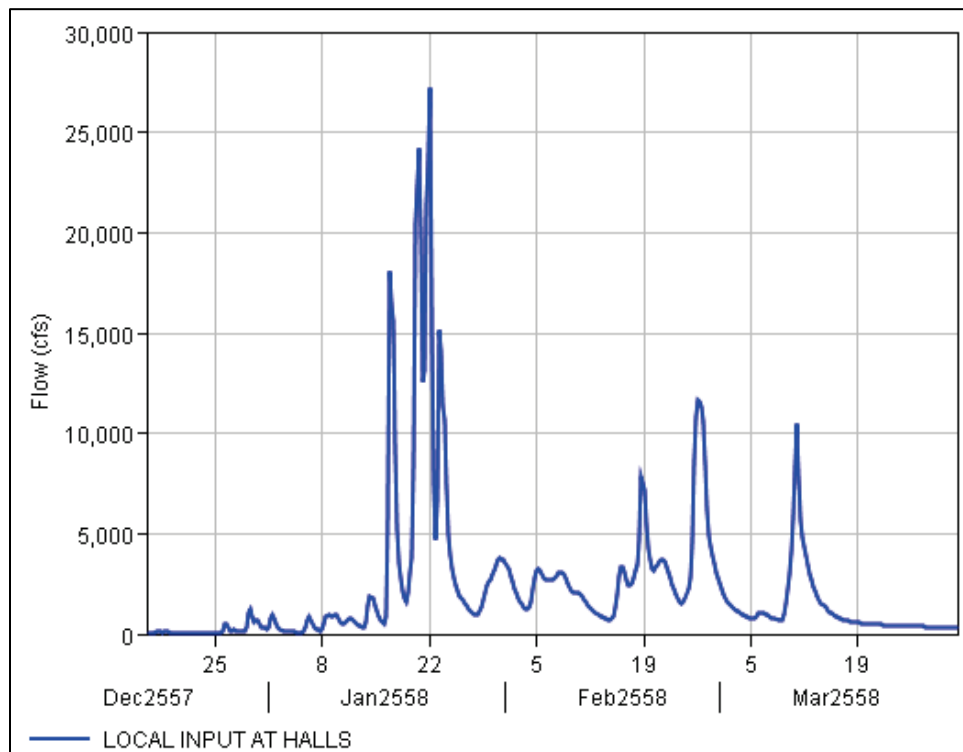


Figure B-24. HYPO 58A local input at Helena, AR.

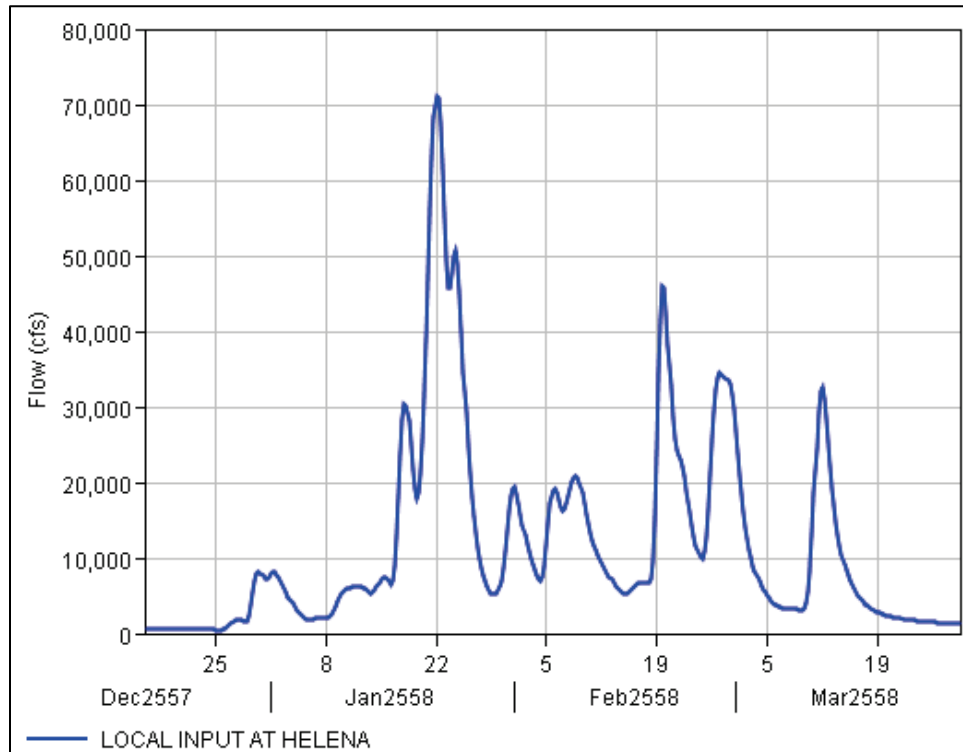


Figure B-25. HYPO 58A local input at Jonesville, MS.

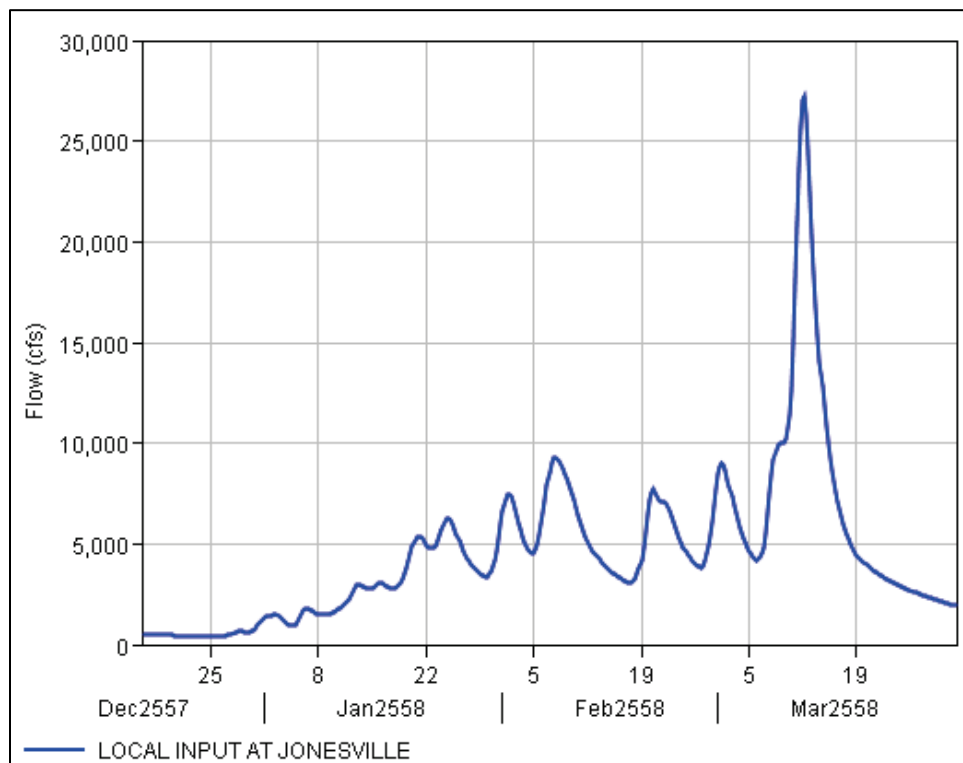


Figure B-26. HYPO 58A local input at Kenton, TN.

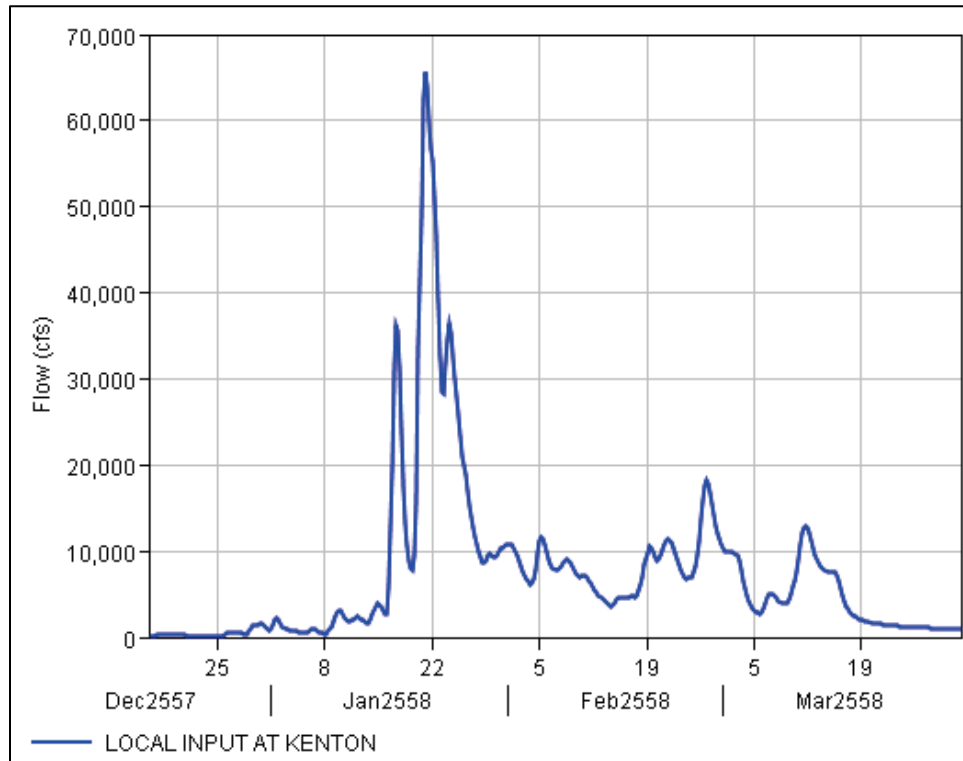


Figure B-27. HYPO 58A local input at Kentucky Dam, KY.

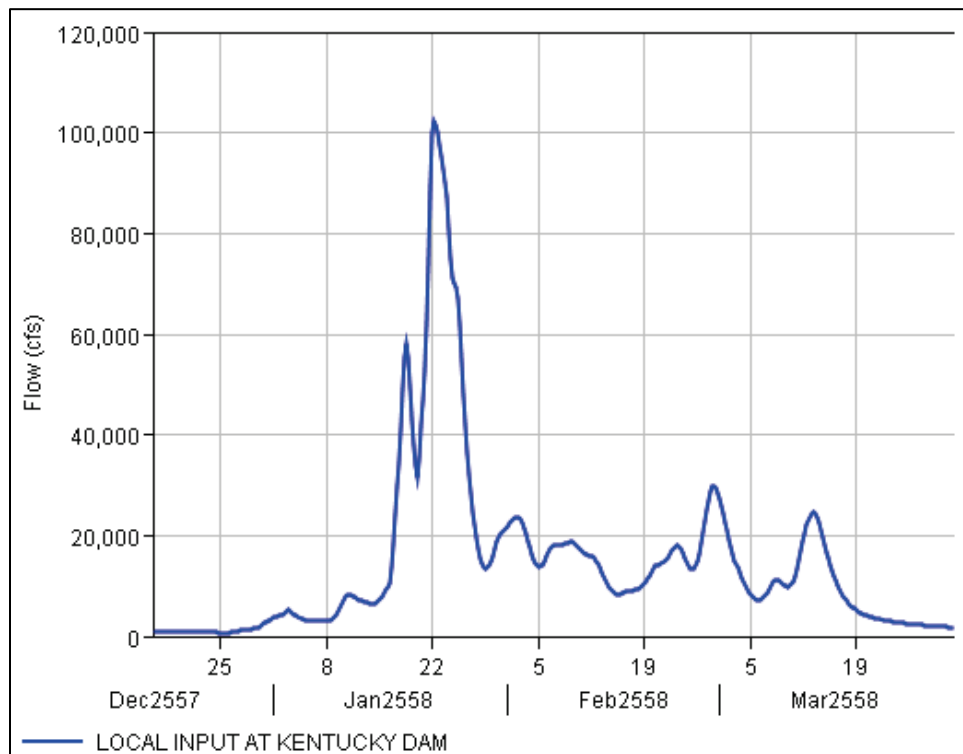


Figure B-28. HYPO 58A local input at Madison, AR.

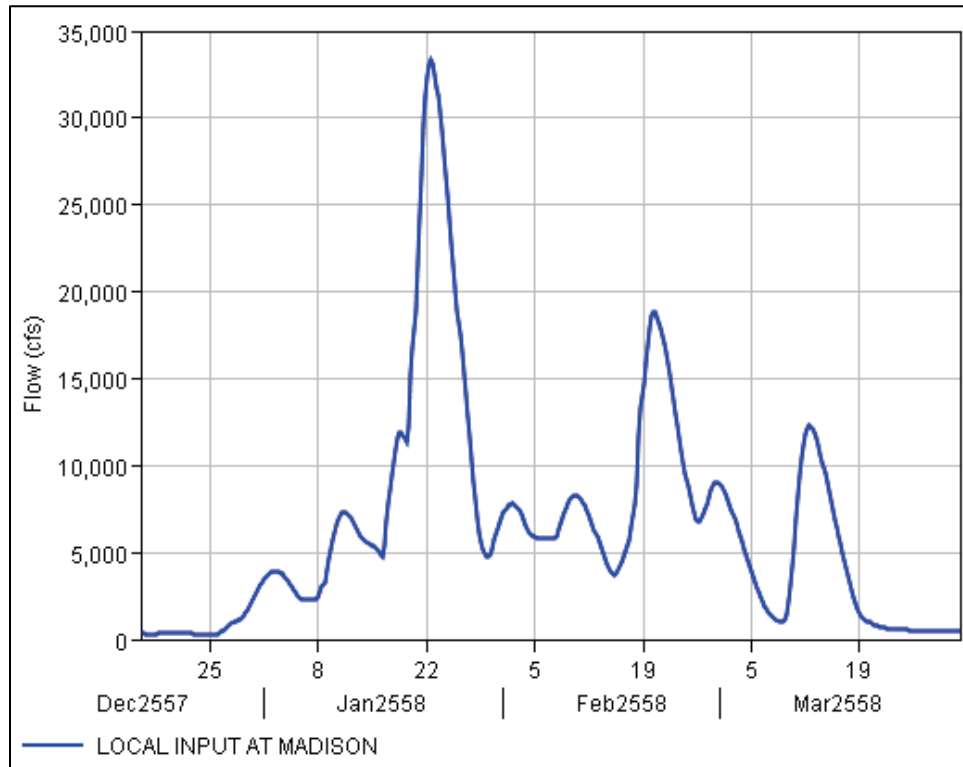


Figure B-29. HYPO 58A local input at Memphis, TN.

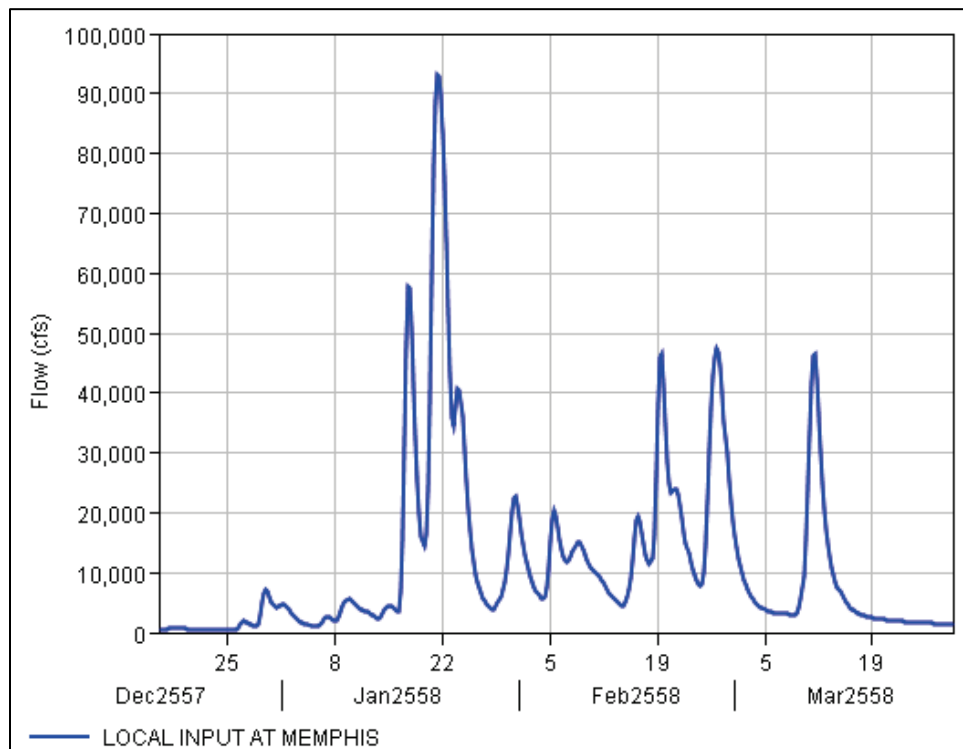


Figure B-30. HYPO 58A local input at Murphysboro, IL.

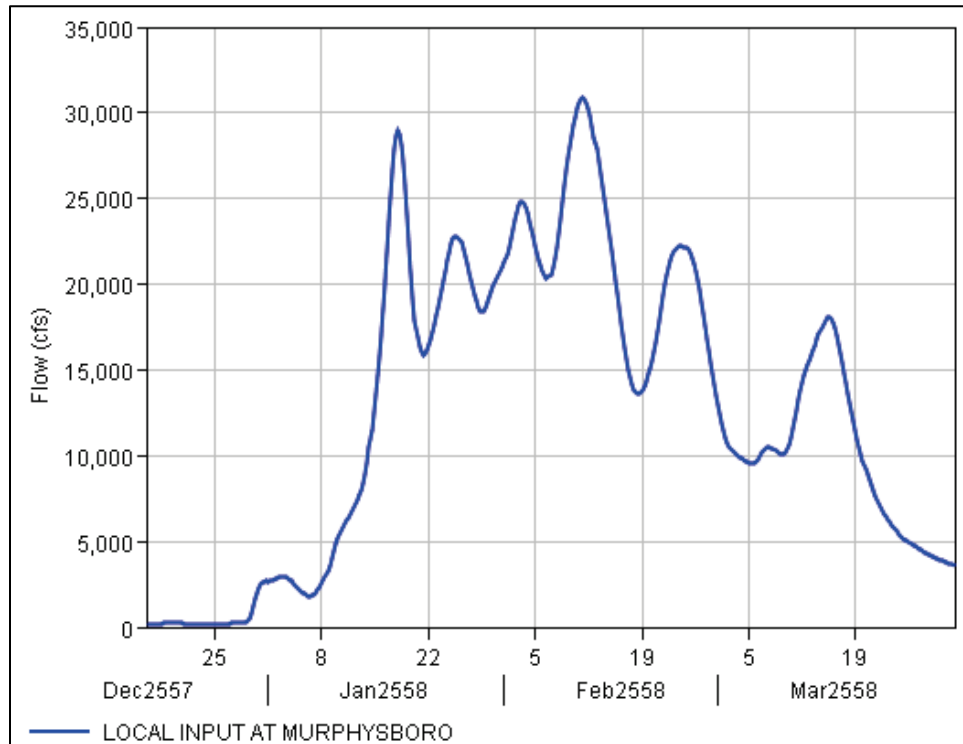


Figure B-31. HYPO 58A local input at Natchez, MS.

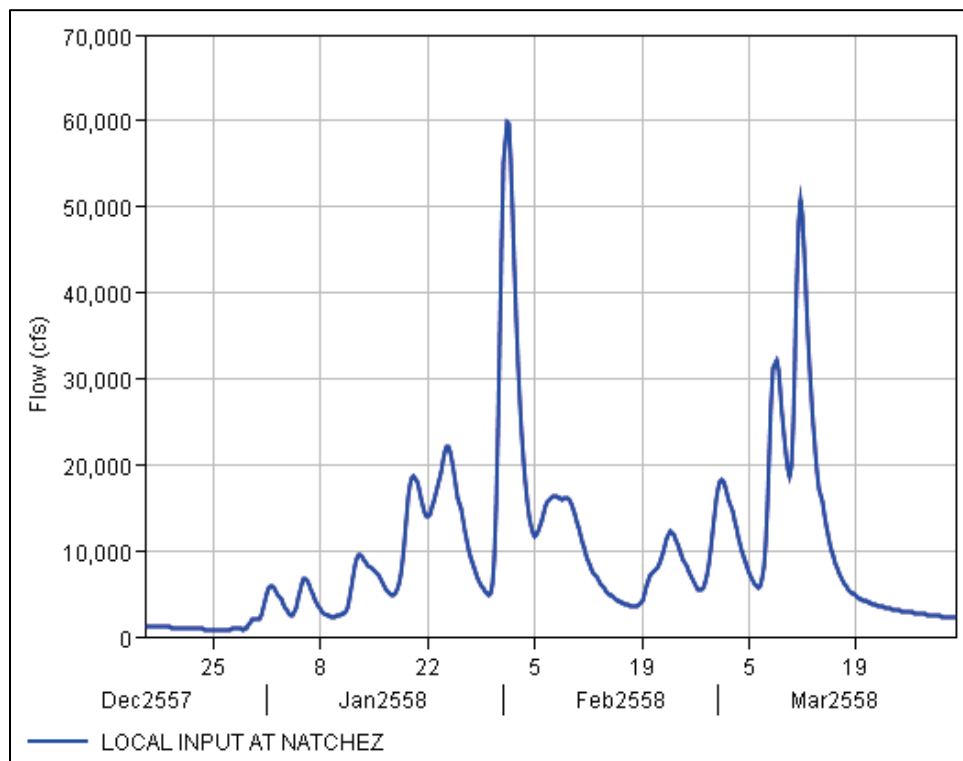


Figure B-32. HYPO 58A local input at New Madrid, MO.

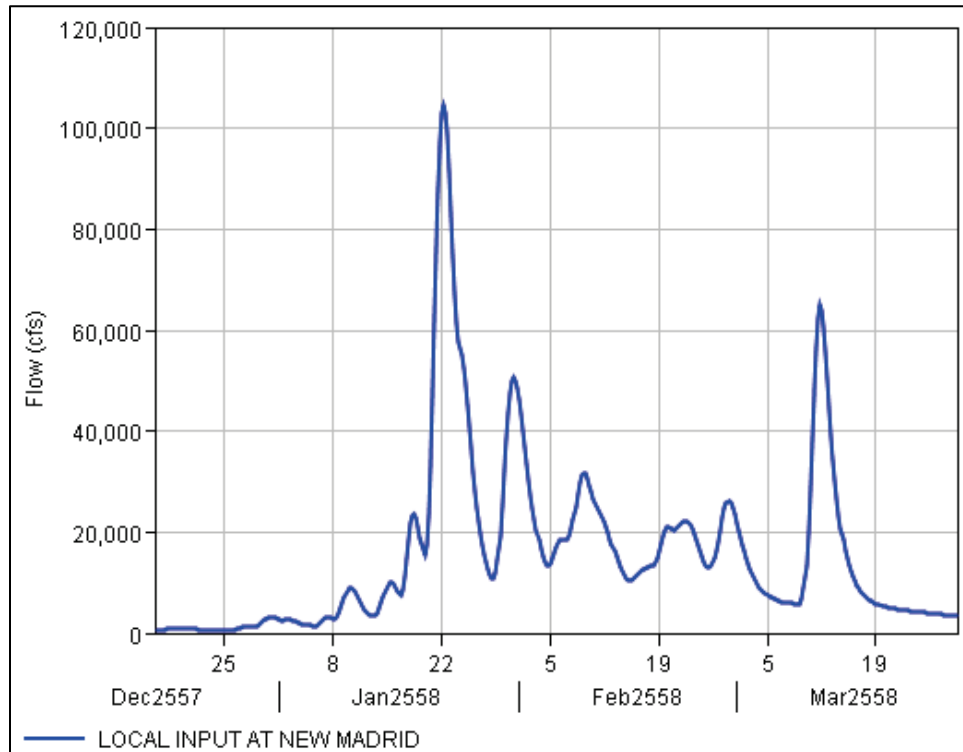


Figure B-33. HYPO 58A local input at Newport, AR.

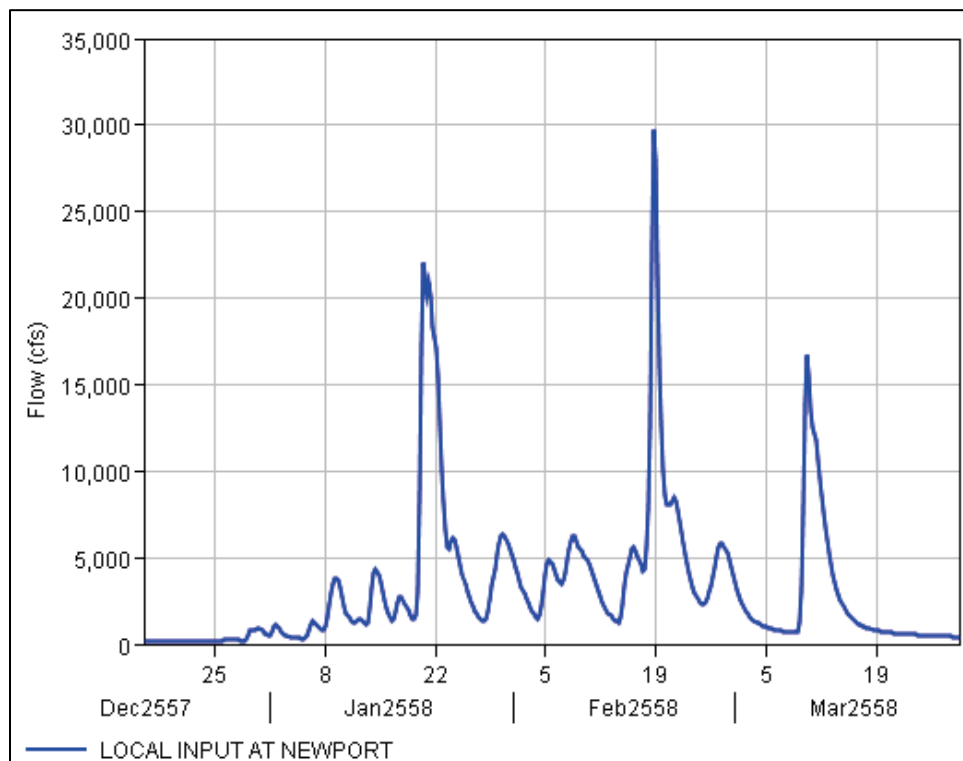


Figure B-34. HYPO 58A local input at Obion, TN.

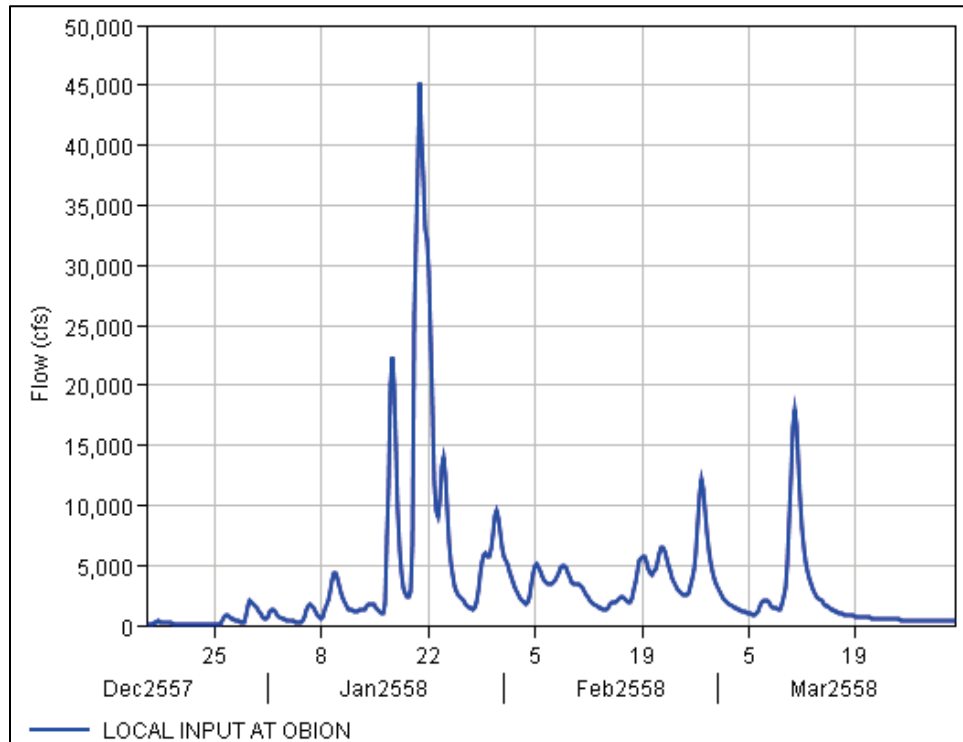


Figure B-35. HYPO 58A local input at Obion, TN, at the Mississippi River confluence.

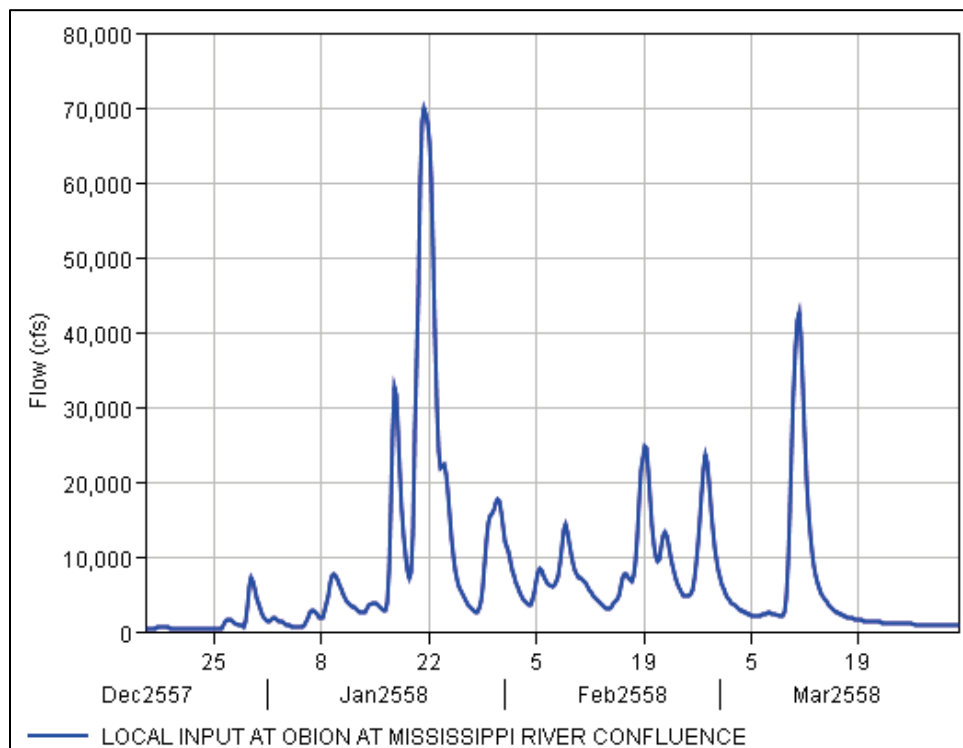


Figure B-36. HYPO 58A local input at Owl City, TN.

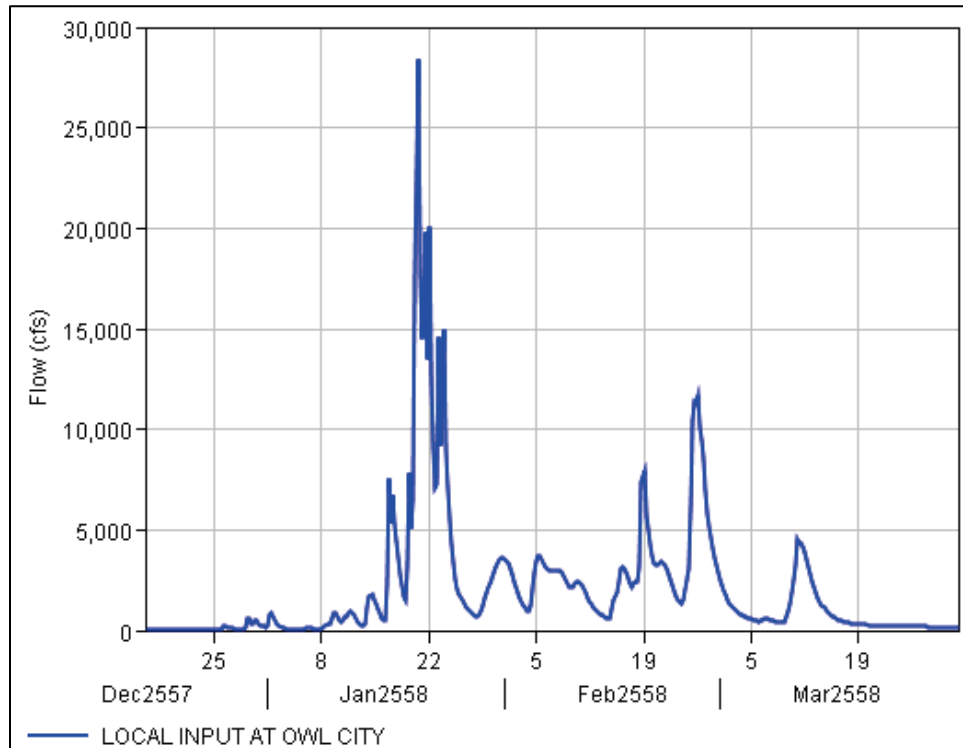


Figure B-37. HYPO 58A local input at Paducah, KY.

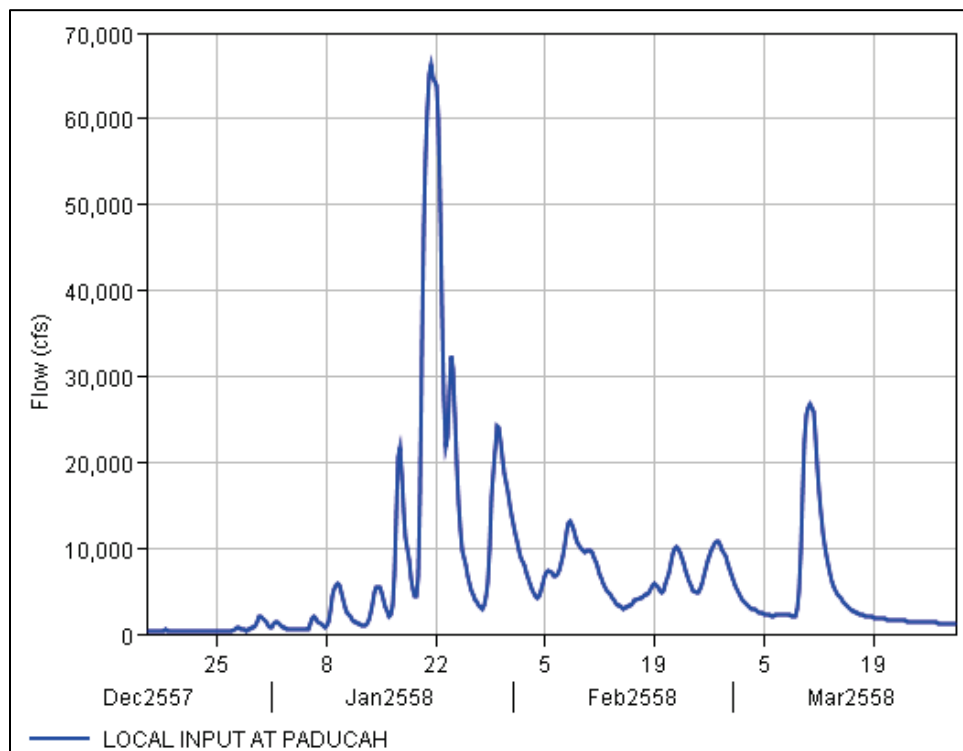


Figure B-38. HYPO 58A local input at Parkin, AR.

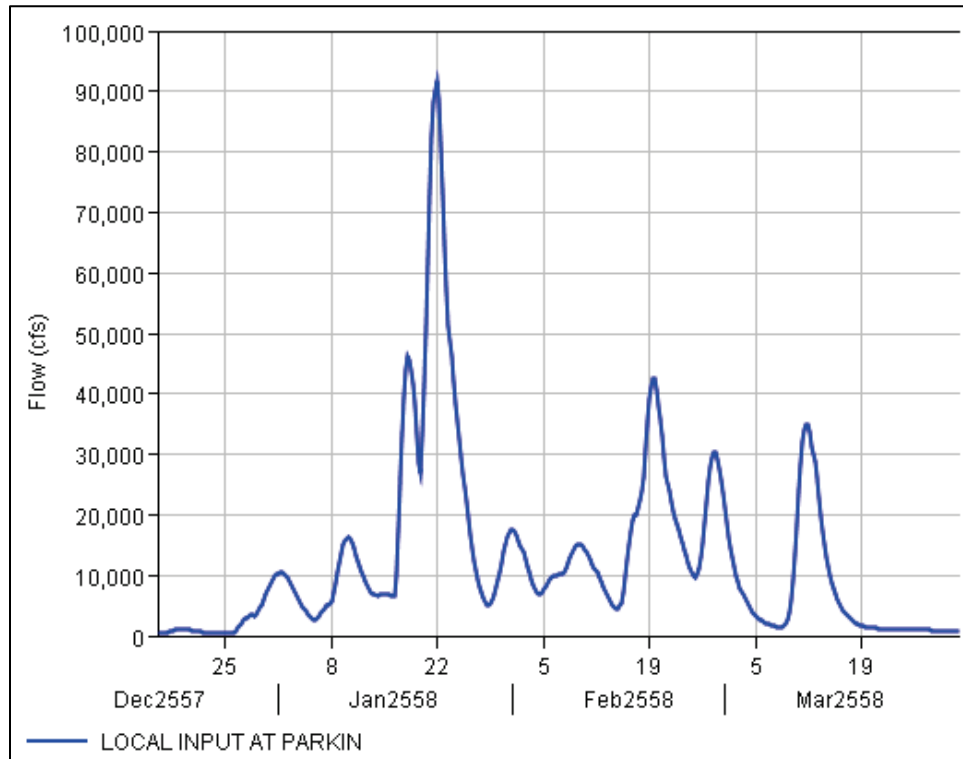


Figure B-39. HYPO 58A local input at Patterson, AR.

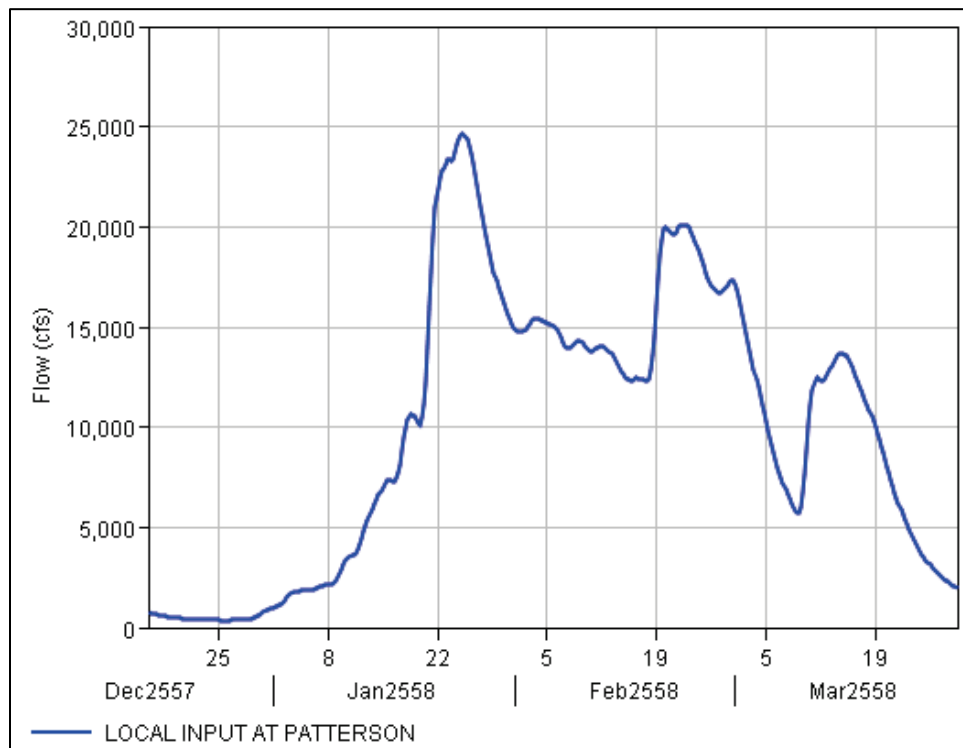


Figure B-40. HYPO 58A local input at Pendleton, AR.

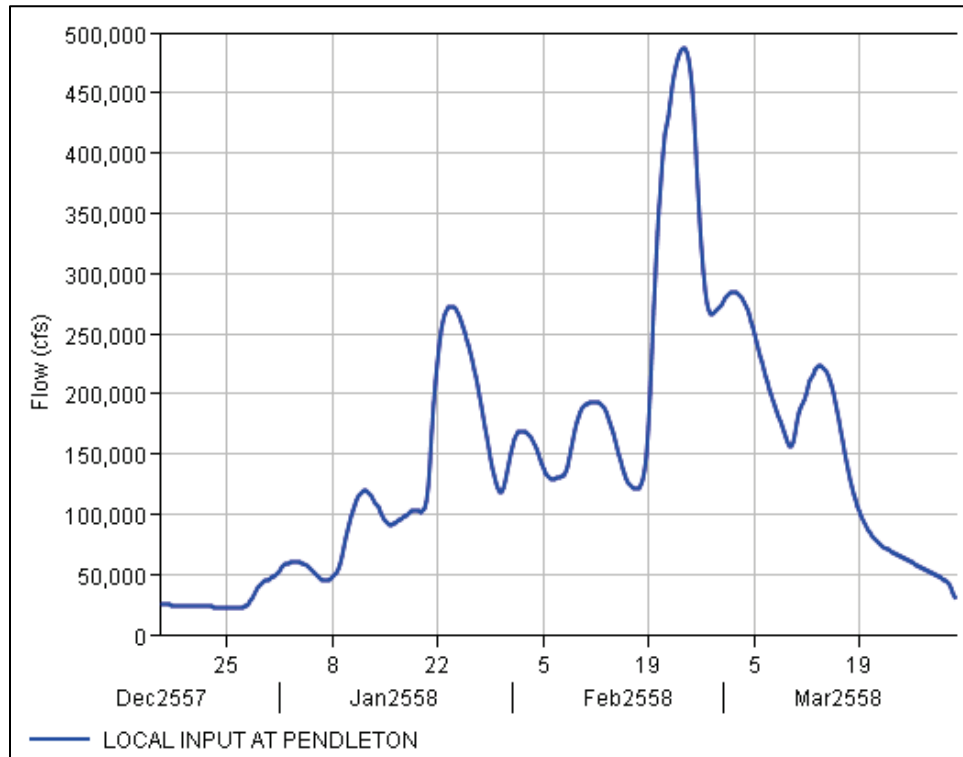


Figure B-41. HYPO 58A local input at Rochelle, LA.

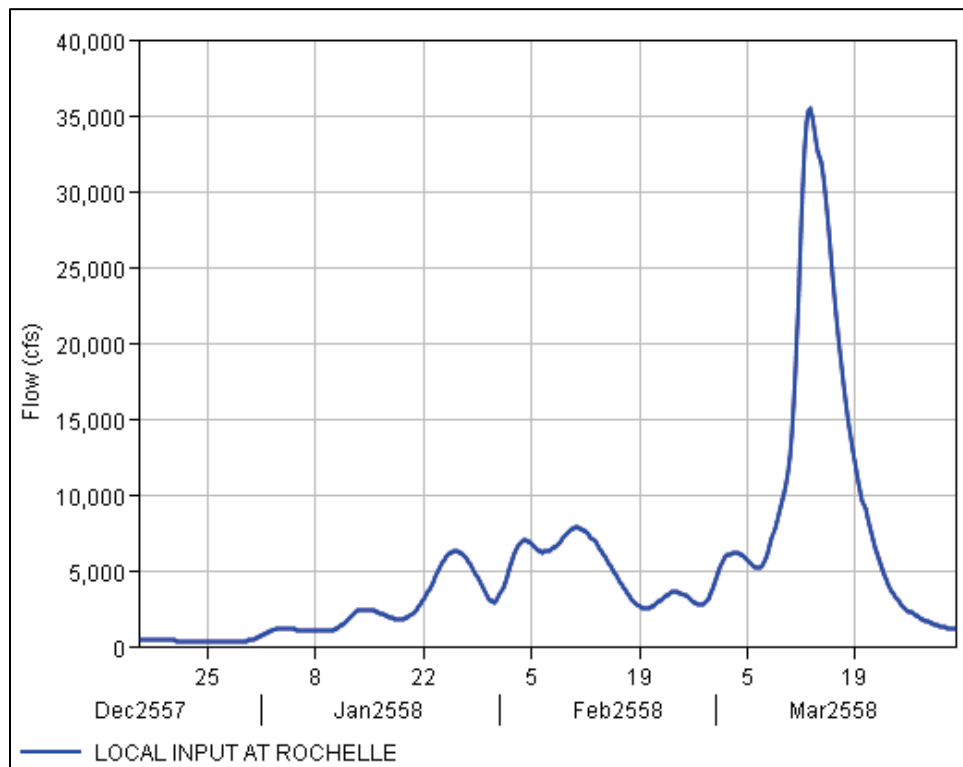


Figure B-42. HYPO 58A local input at Rosetta, MS.

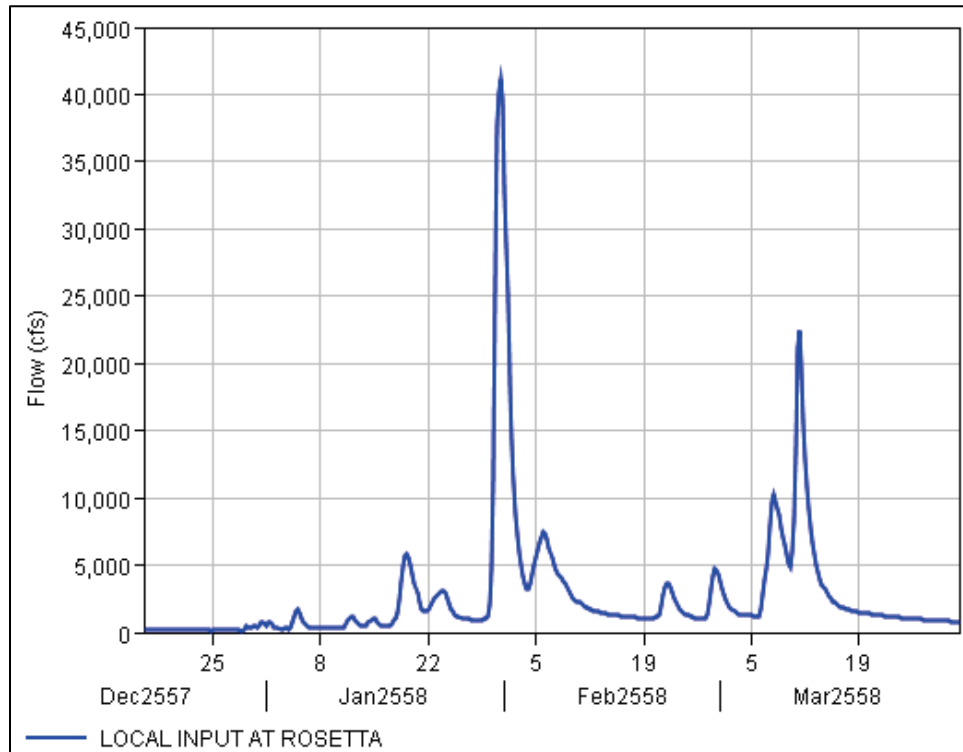


Figure B-43. HYPO 58A local input at Simmesport, LA.

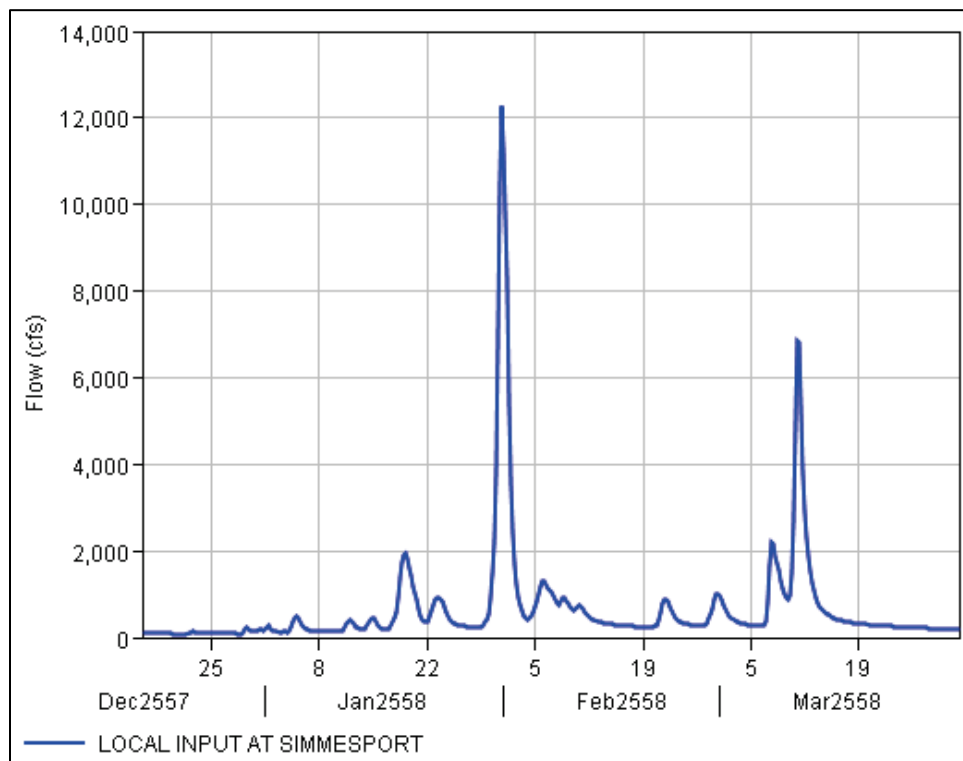


Figure B-44. HYPO 58A local input at Smithland Lock and Dam, IL.

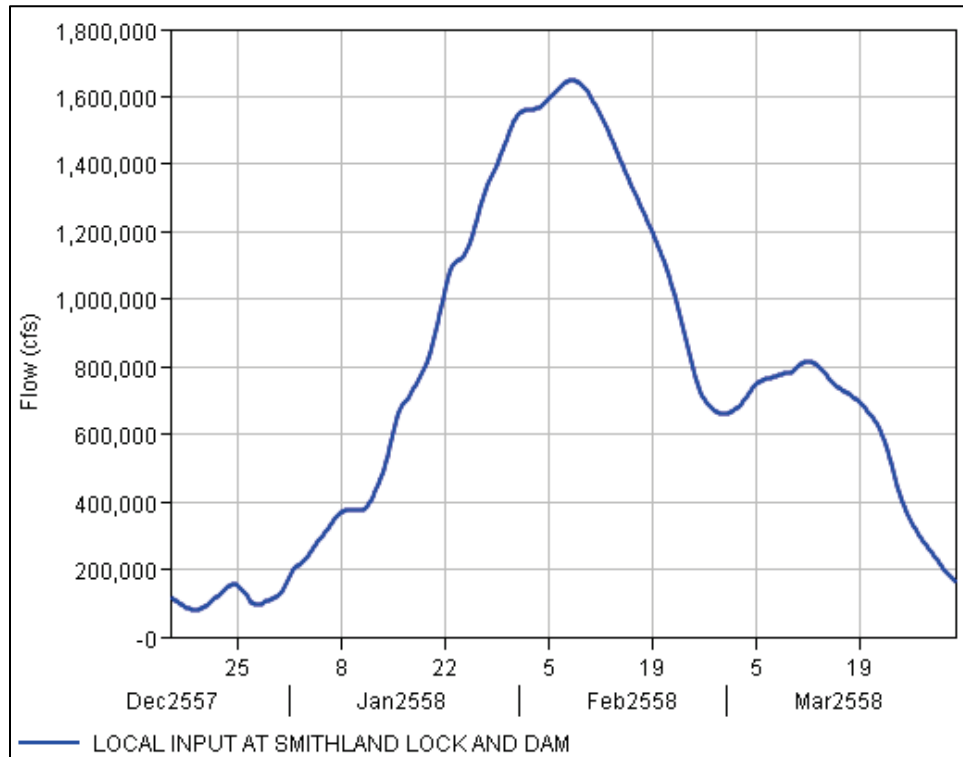


Figure B-45. HYPO 58A local input at Vicksburg, MS.

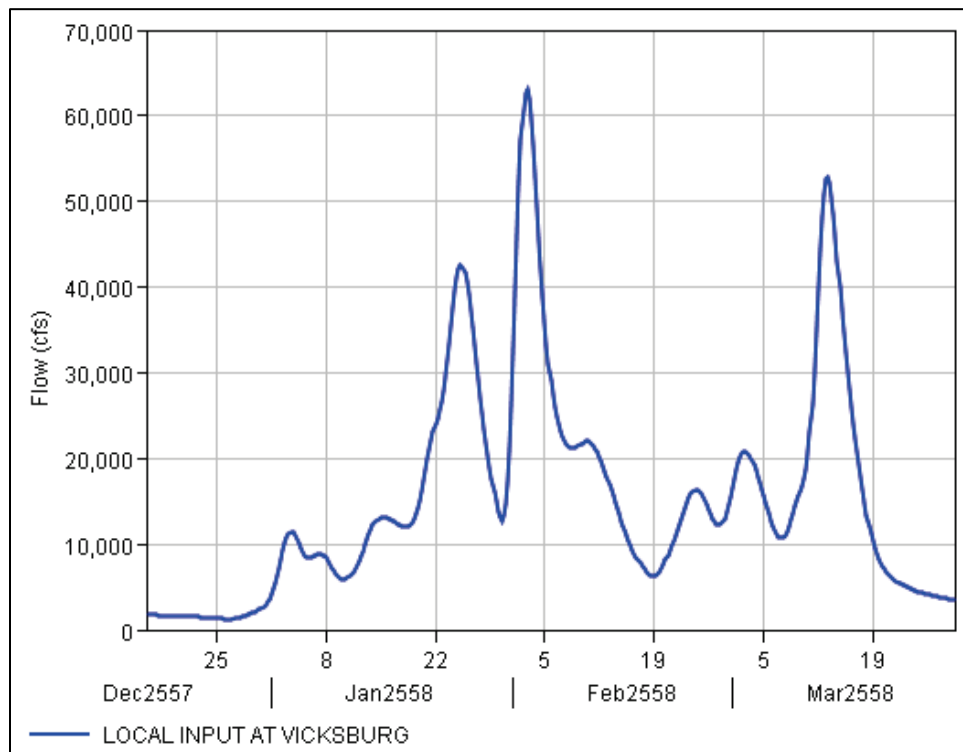


Figure B-46. HYPO 58A local input at Whitehall, LA.

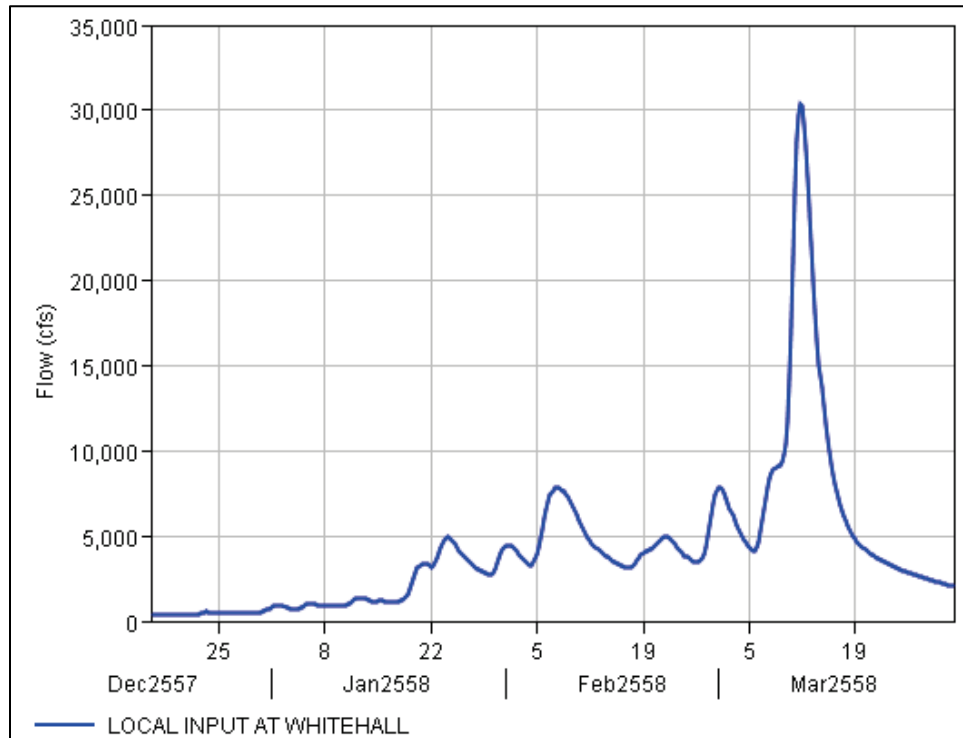


Figure B-47. HYPO 58A local input at Wickliffe, KY.

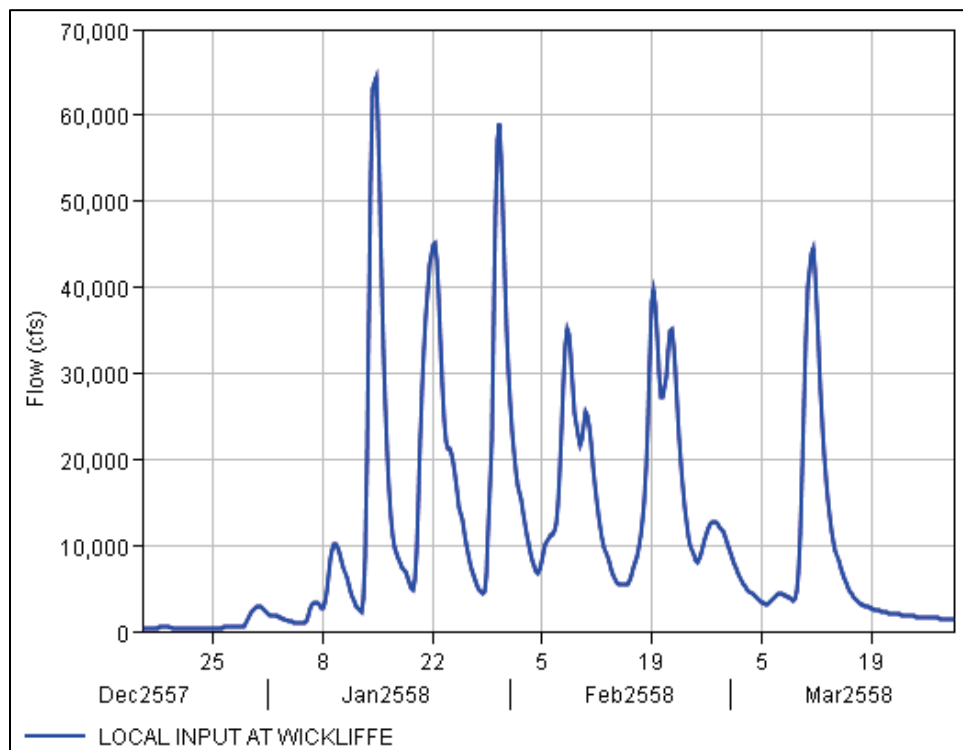


Figure B-48. HYPO 58A local input at Willows, MS.

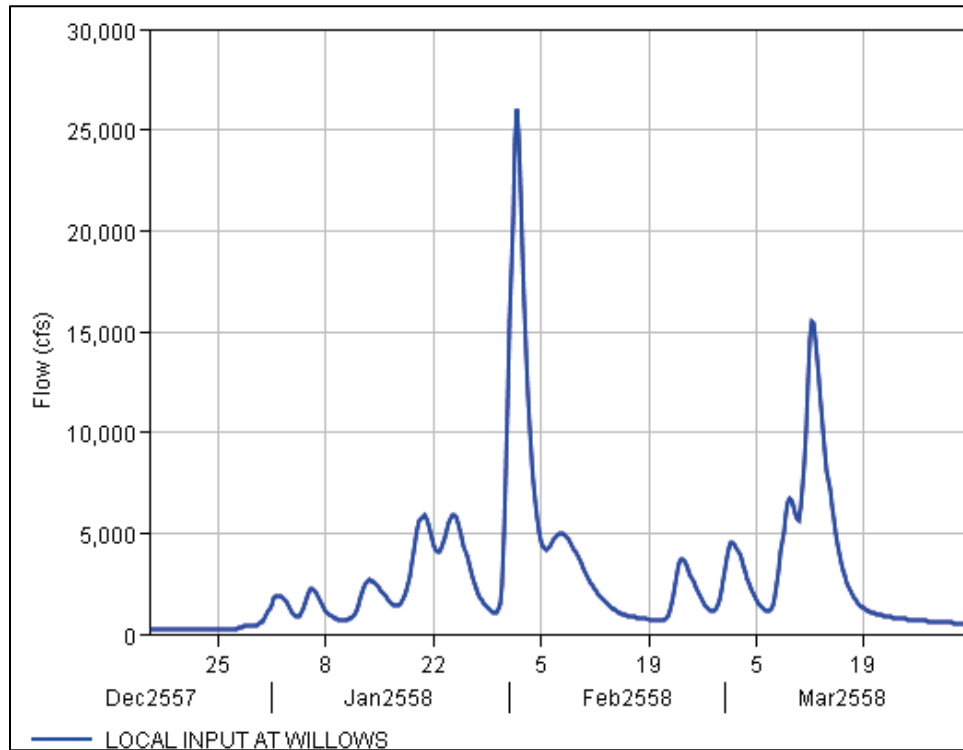


Figure B-49. HYPO 58A local input at Woodville, MS.

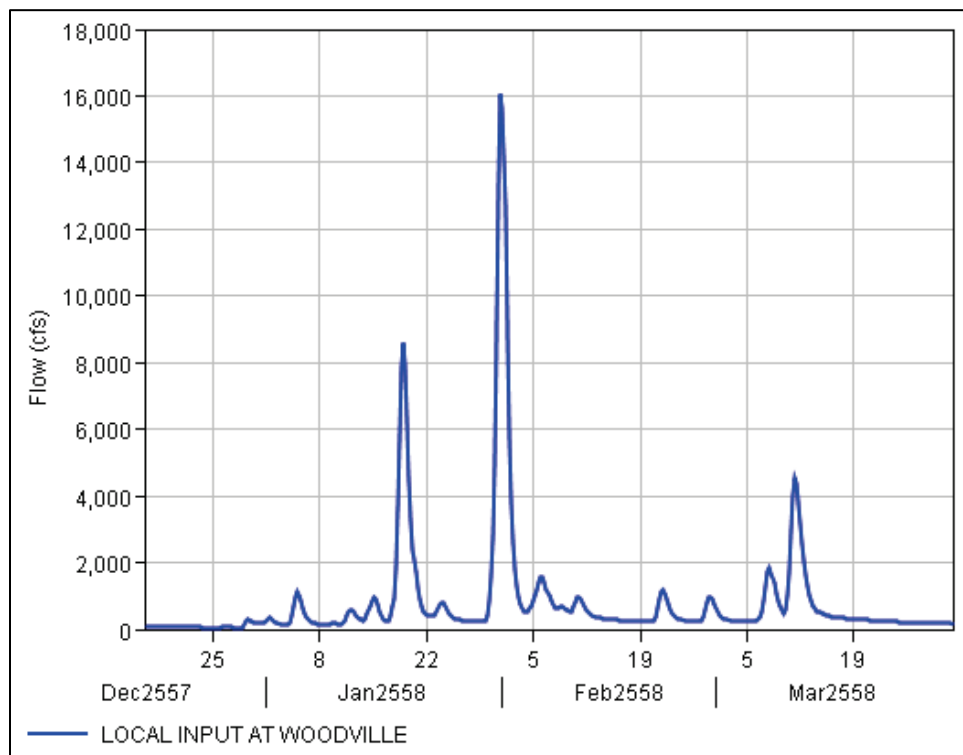
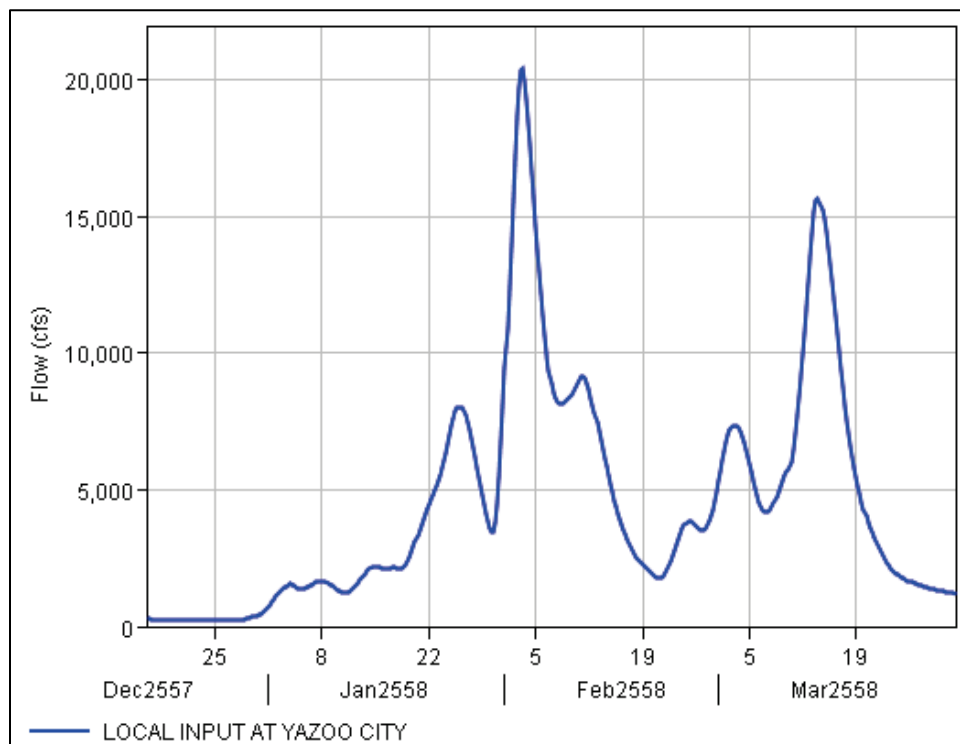


Figure B-50. HYPO 58A local input at Yazoo City, MS.



B.2 Reservoir Routing

Reservoirs along major tributaries to the Mississippi River provide localized flood reductions that contribute to flood reductions along the Lower Mississippi River. Table B-1 shows the unregulated peak flows for given locations, the date when that peak flow event occurs, the corresponding regulated flows for that date, and the percent reduction.

Table B-1. Reductions in peak flows from regulation for HYPO 58A.

HYPO	Description	Peak Flows (cfs)					
		Alton, IL Mississippi River	Hermann, MO Missouri River	Little Rock (Pine Bluff), AR, Arkansas River	Clarendon, AR White River	Alexandria, LA Red River	St. Louis, MO Mississippi River
58A (SS)	Date	15 Jan 2558, 1800	10 Jan 2558, 1200	23 Feb 2558, 1200	28 Feb 2558, 2400	17 Mar 2558, 1200	22 Feb 2558, 1200
	Unregulated	244,653	220,478	499,116	382,045	214,014	432,735
	Regulated	222,604	193,279	449,217	313,341	158,382	377,343
	Reduction	22,049	27,199	49,899	68,704	55,632	55,392
	% Reduction	9%	13%	11%	20%	30%	14%

The time of travel for the river to reach St. Louis from Alton or Hermann is approximately 1 day (notice that the peak flow dates are several days apart, as each location is influenced by other tributaries), and the time of travel for peak flows to reach the Mississippi River from Little Rock, Clarendon, or Alexandria takes approximately 4 days.

Reservoir routing and regulation for each district are described in Section 2 of this report. Plots of the inflow and outflow for USACE regulation computations are shown in the following sections. Dates shown on the inflow/outflow hydrograph plots are simulation dates for the HYPO 58A SS storm.

B.2.1 NWK USACE reservoirs

The inflow/outflow hydrographs for the NWK reservoirs located on tributaries to the Missouri River show localized flood reductions that reduce the peak flow of the Missouri River at Hermann, MO, by 13% (Table B-1). Each plot in Figures B-51 through B-65 states the time of travel for water to reach Hermann, MO, as derived from the 1957 Drainage Area Map (WES 1957).

Figure B-51. HYPO 58A routed through Clinton Dam - ~3 days from Hermann, MO.

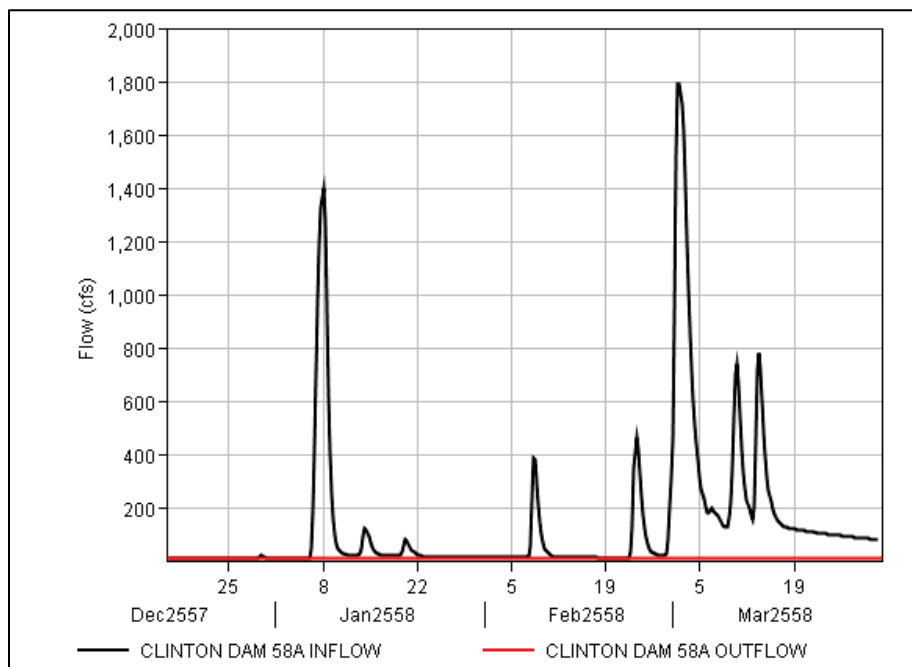


Figure B-52. HYPO 58A routed through Glen Elder Dam - ~8 days from Hermann, MO.

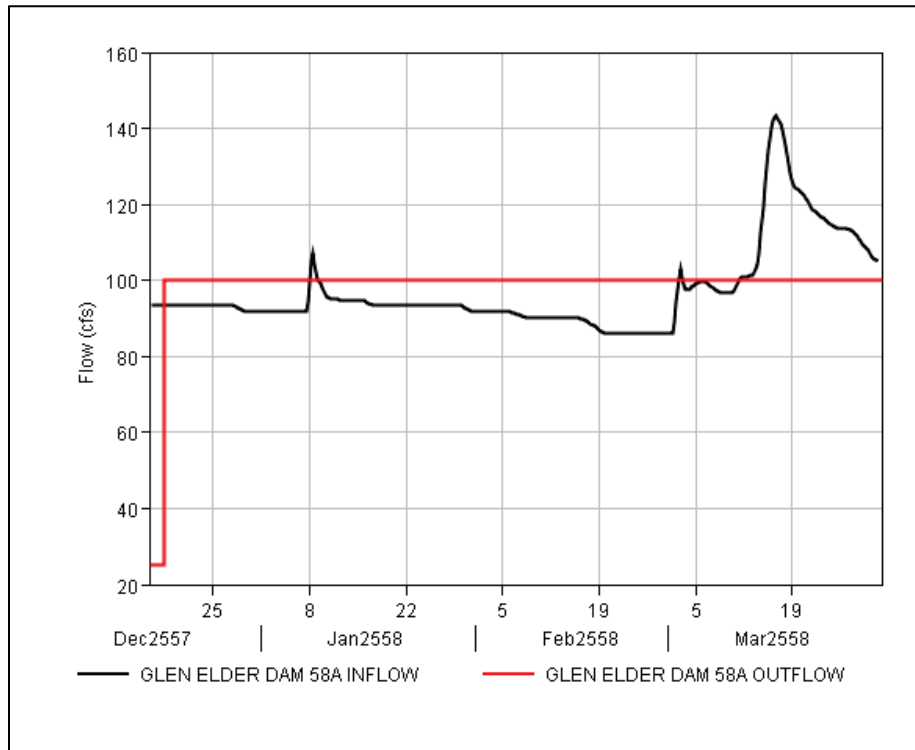


Figure B-53. HYPO 58A routed through Hillsdale Dam - ~3-4 days from Hermann, MO.

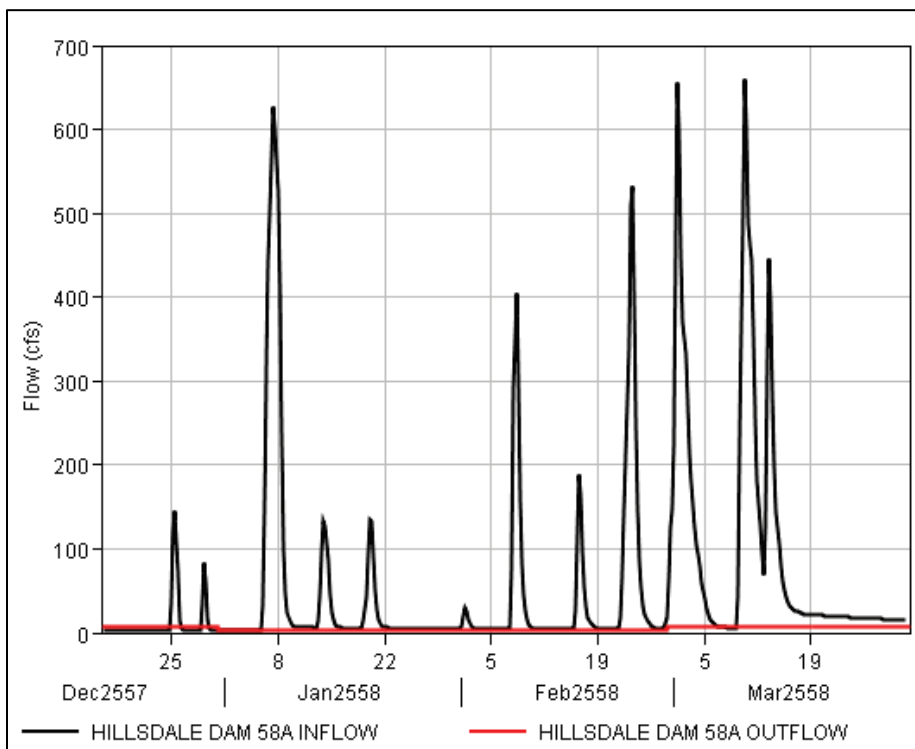


Figure B-54. HYPO 58A routed through Kanopolis Dam - ~9 days from Hermann, MO.

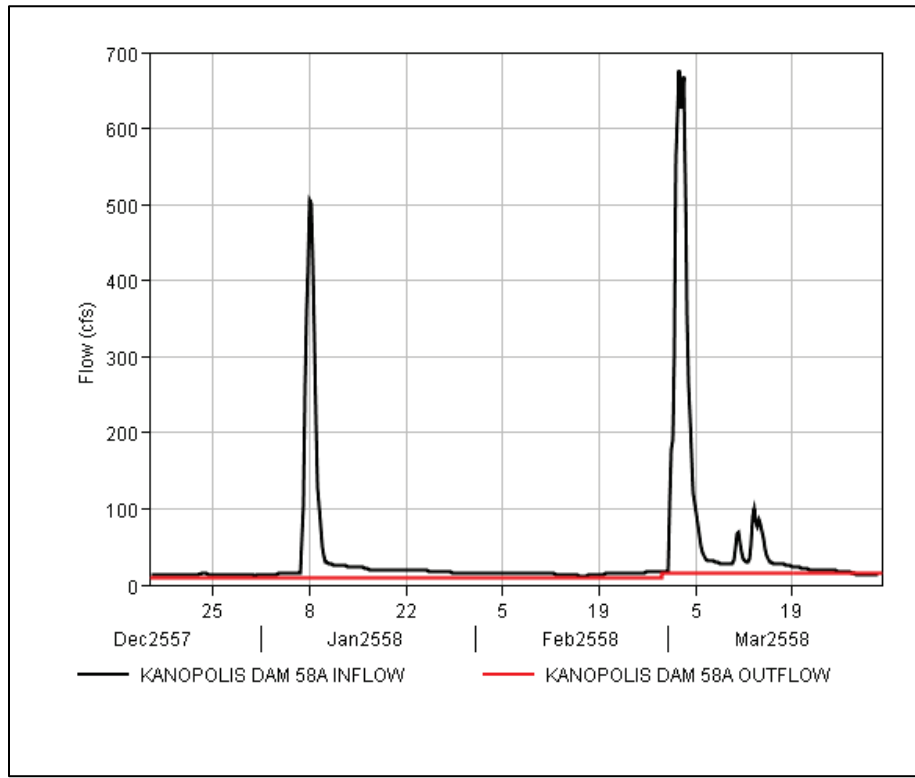


Figure B-55. HYPO 58A routed through Melvern Dam - ~4 days from Hermann, MO.

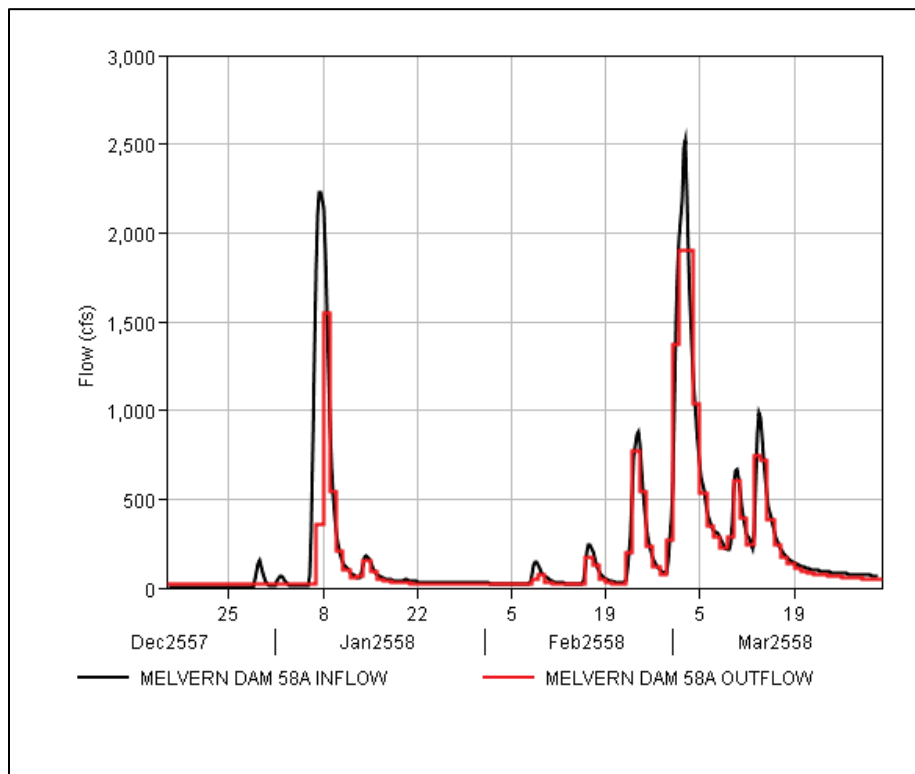


Figure B-56. HYPO 58A routed through Milford Dam - ~6 days from Hermann, MO.

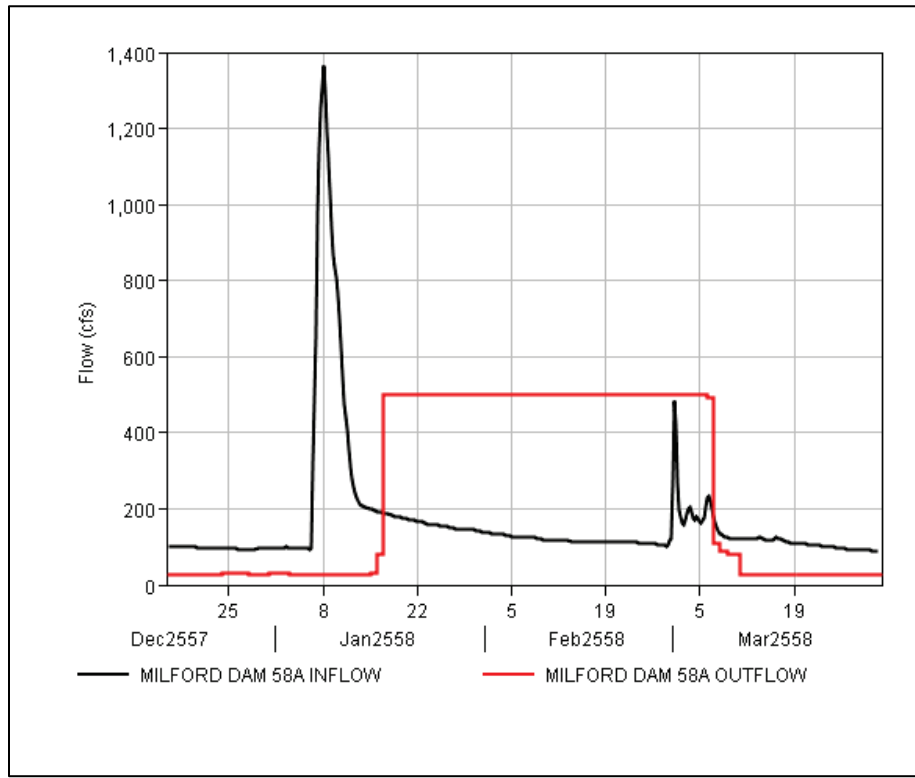


Figure B-57. HYPO 58A routed through Perry Dam - ~4 days from Hermann, MO.

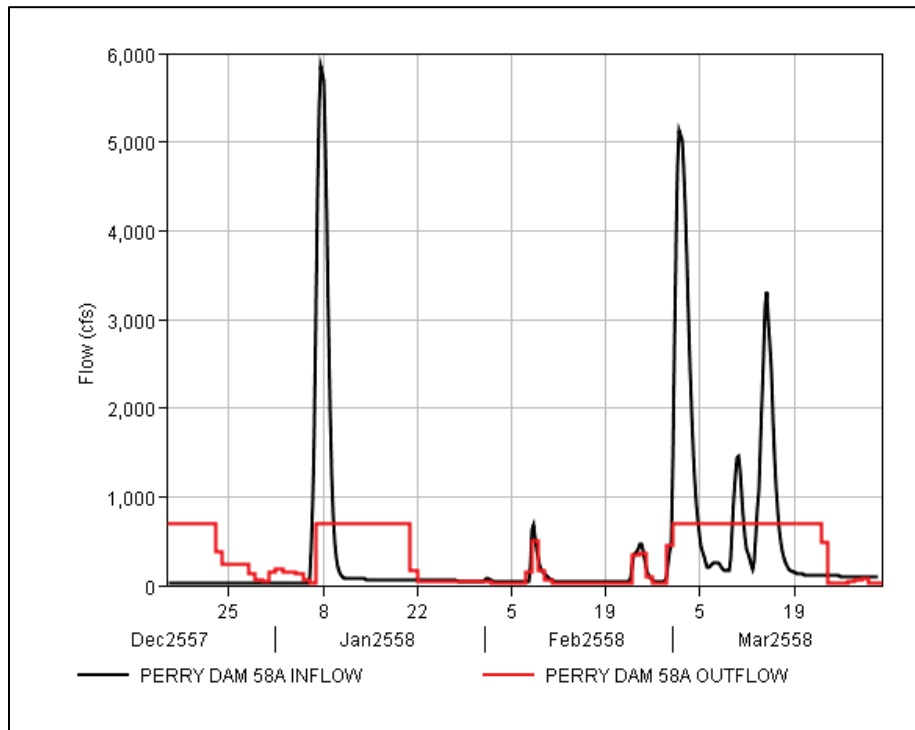


Figure B-58. HYPO 58A routed through Pomme De Terre Dam - ~3 days from Hermann, MO.

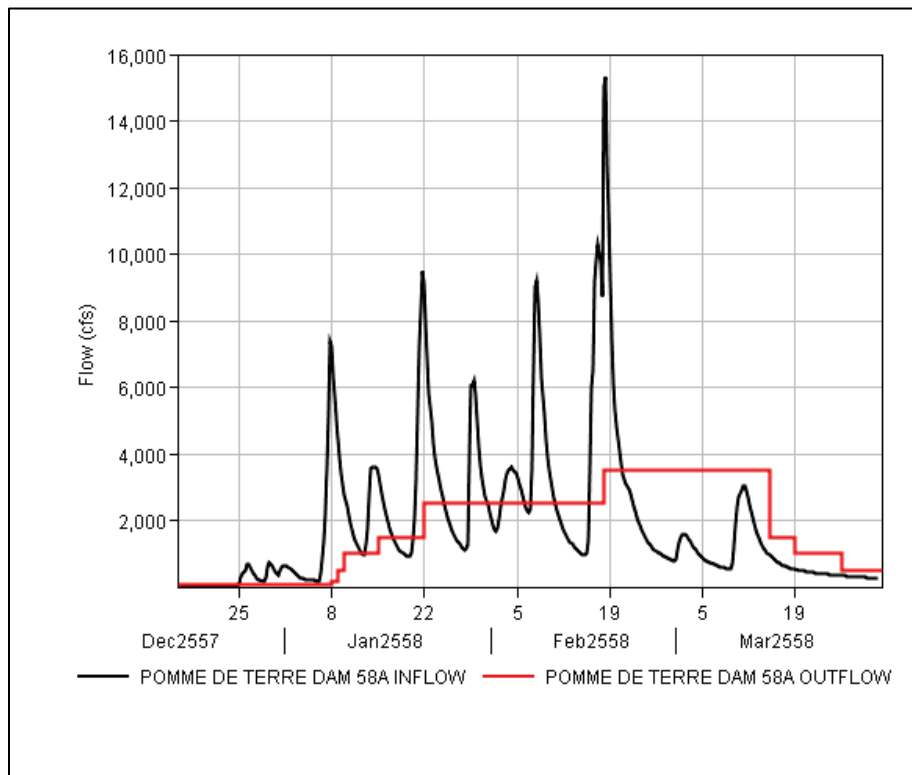


Figure B-59. HYPO 58A routed through Pomona Dam - ~4 days from Hermann, MO.

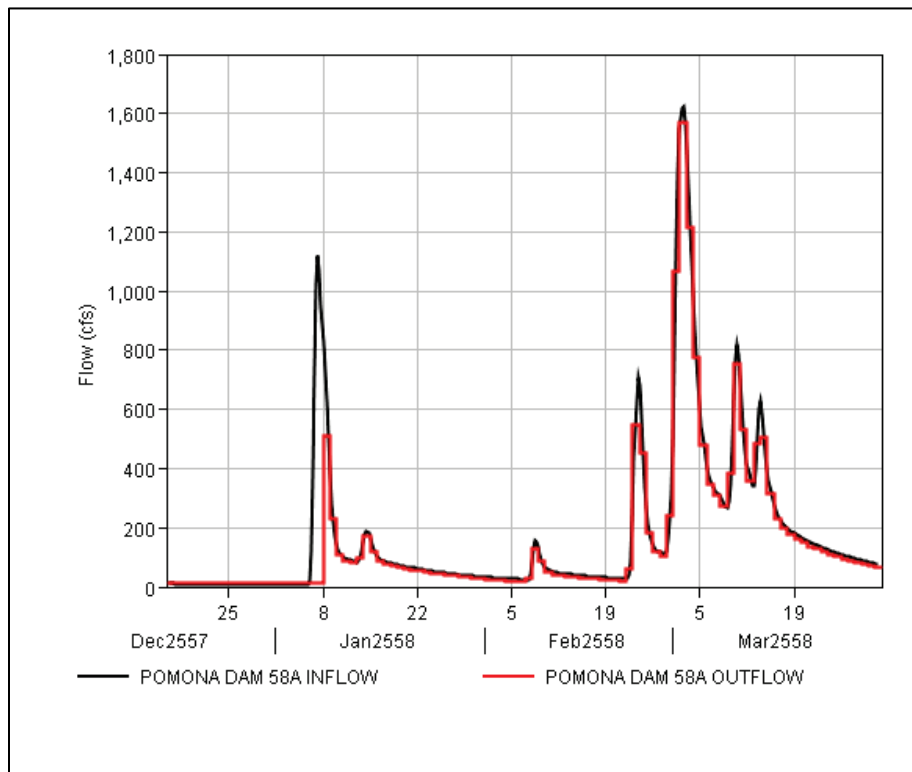


Figure B-60. HYPO 58A routed through Rathbun Dam - ~4 days from Hermann, MO.

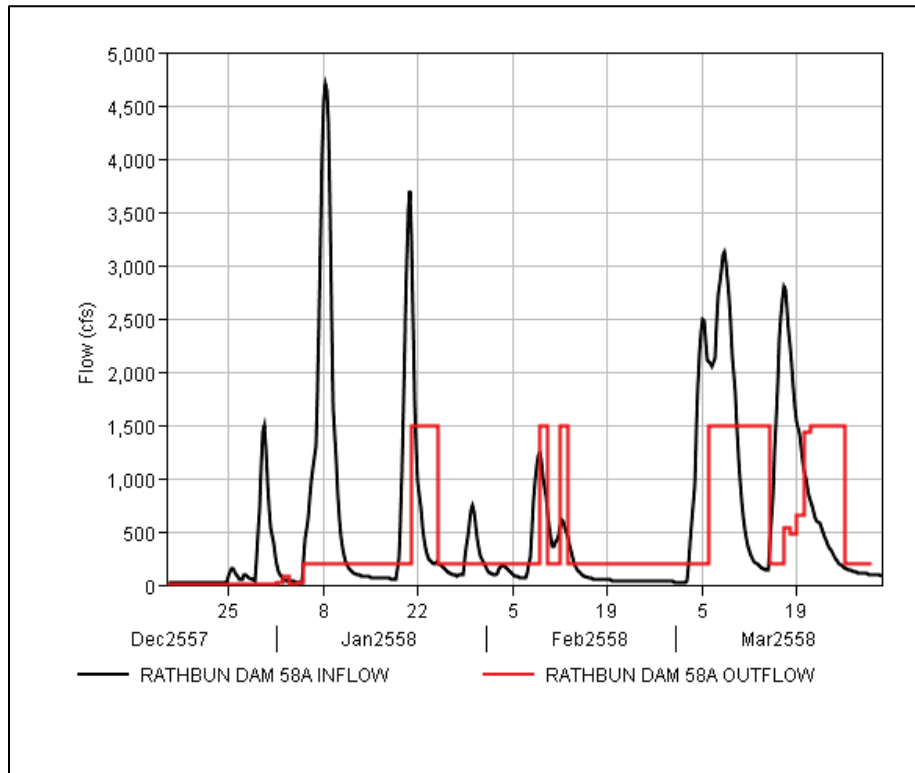


Figure B-61. HYPO 58A routed through Smithville Dam - ~3 days from Hermann, MO.

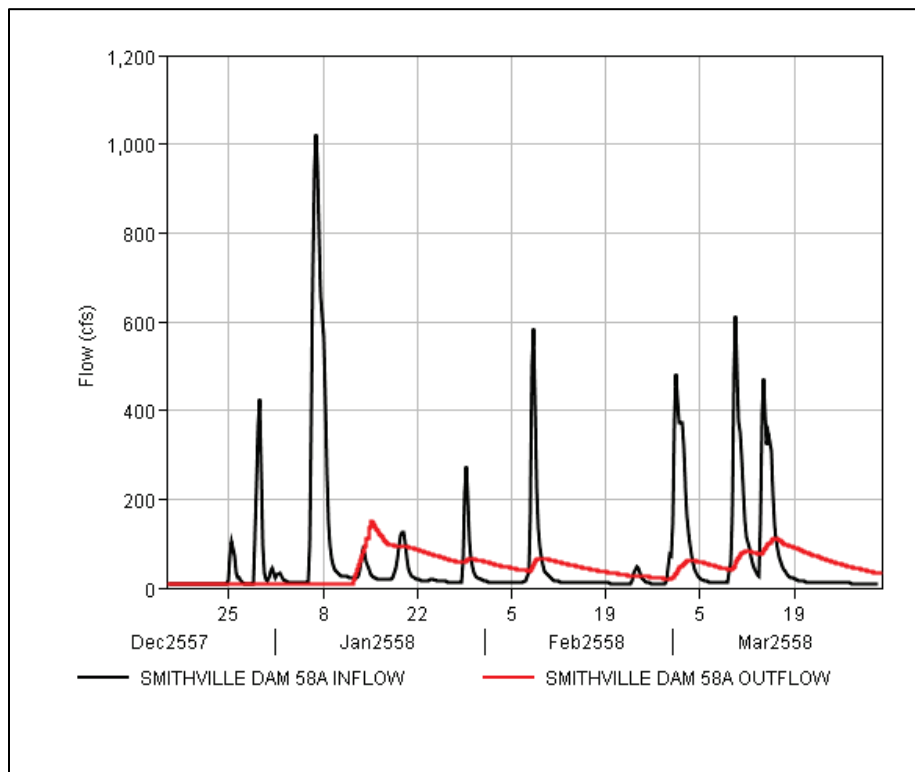


Figure B-62. HYPO 58A routed through Stockton Dam - ~3-4 days from Hermann, MO.

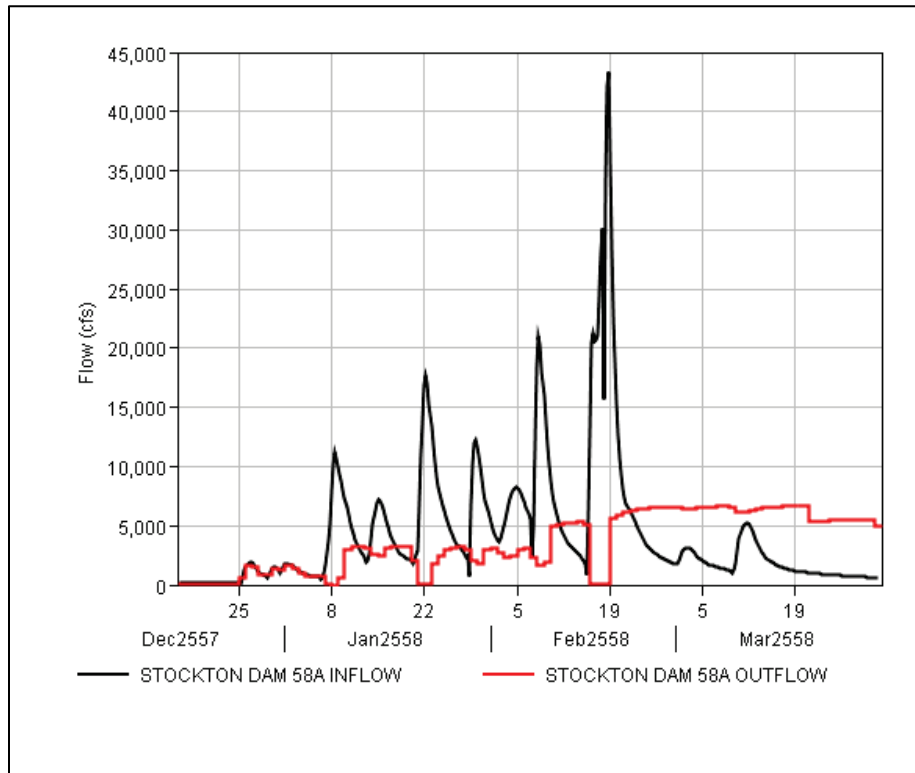


Figure B-63. HYPO 58A routed through Truman Dam - ~2-3 days from Hermann, MO.

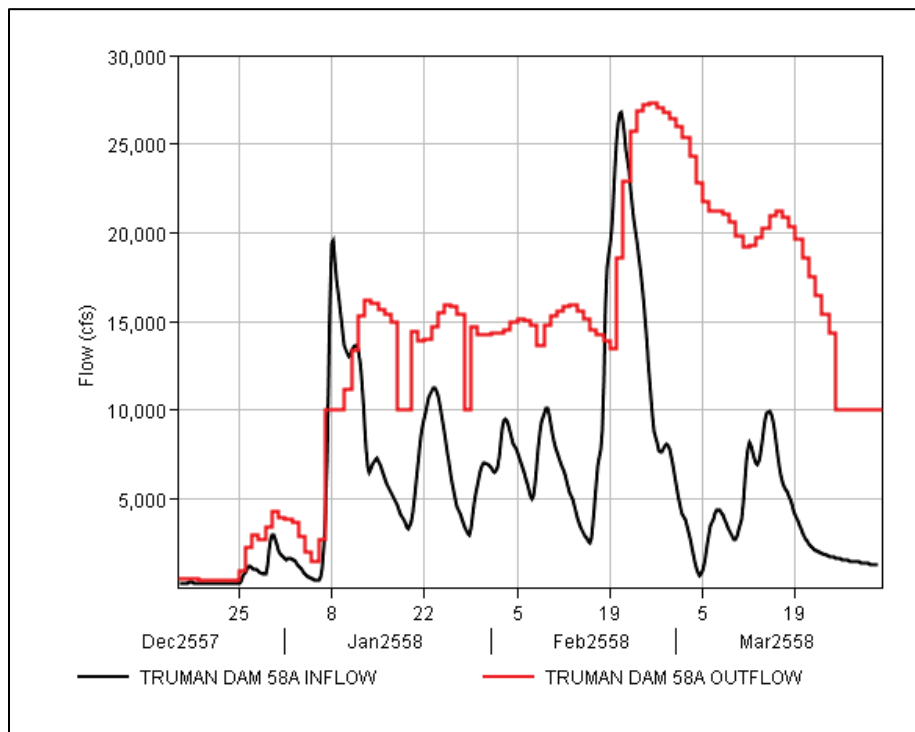


Figure B-64. HYPO 58A routed through Tuttle Creek Dam - ~5 days from Hermann, MO.

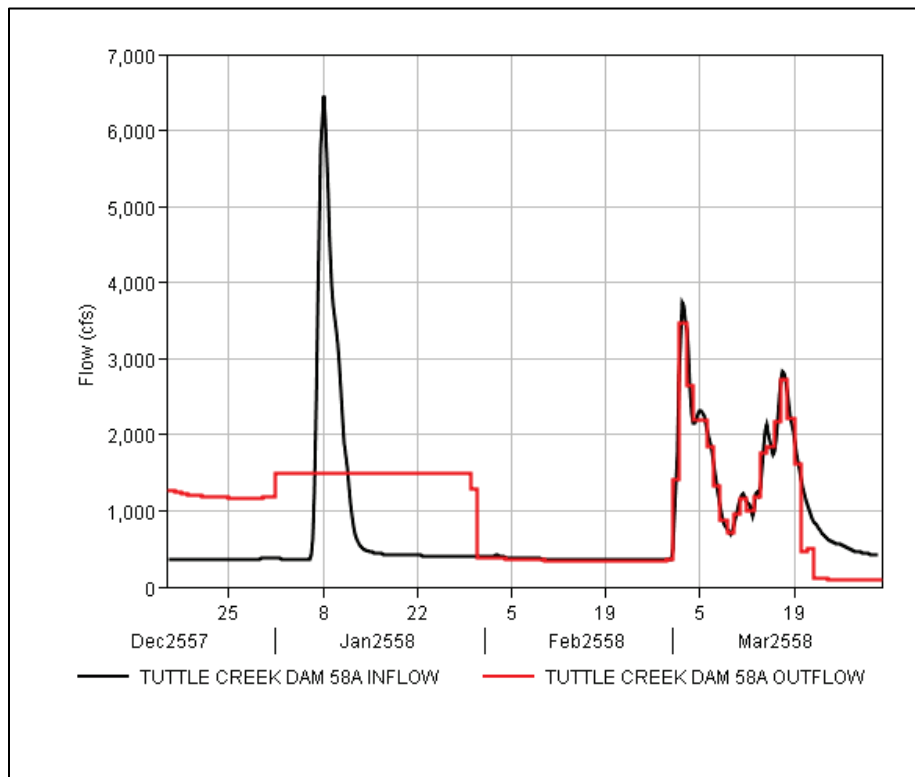
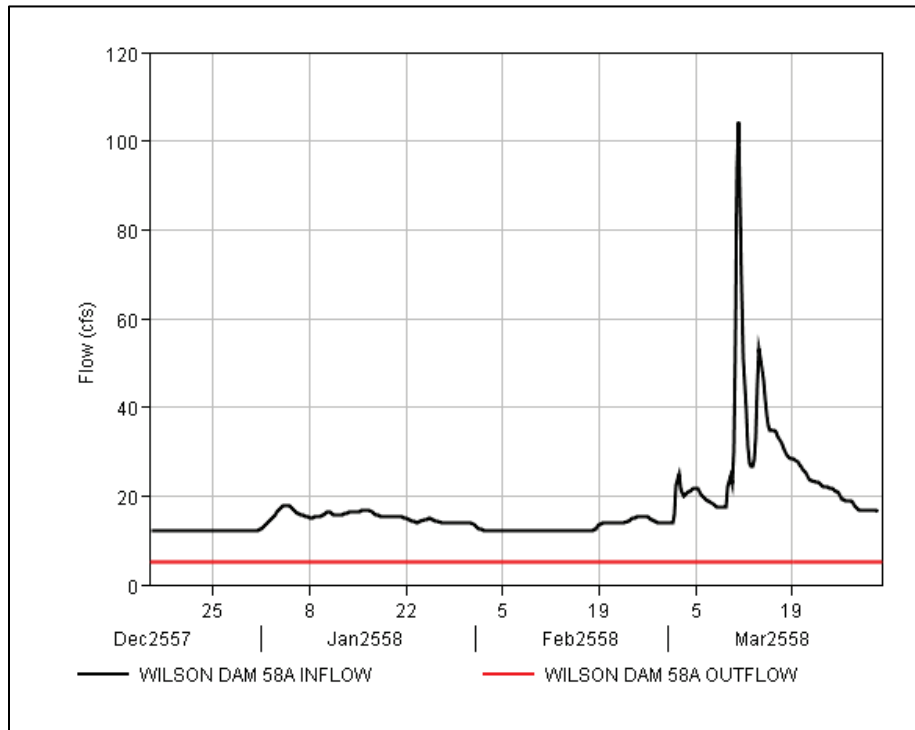


Figure B-65. HYPO 58A routed through Wilson Dam - ~9 days from Hermann, MO.



B.2.2 NWO USACE reservoirs

NWO reservoirs located on the Upper Missouri River were modeled due to their perceived flood reduction impact on the Lower Mississippi River. Gavins Point Dam is located farthest downstream of this reservoir series, but the flow from this point takes 11 days to reach Hermann, MO. By example, the peak flow occurs at Hermann on January 10 which, allowing for the 11-day travel time, corresponds to releases being made on December 29 at Gavins Point Dam. Outflow at this time is greater than the inflow.

The other major mainstem reservoirs in NWO have a longer travel time than Gavins Point Dam. While these reservoirs provide localized flood reductions on the Upper Missouri River, these reservoirs effectively have no immediate flood reduction impact to the Lower Missouri or Lower Mississippi Rivers for HYPO 58A. Figure B-66 through Figure B-71 show the reservoir hydrographs for NWO.

Figure B-66. HYPO 58A routed through Big Bend Dam - 11+ days from Hermann, MO.

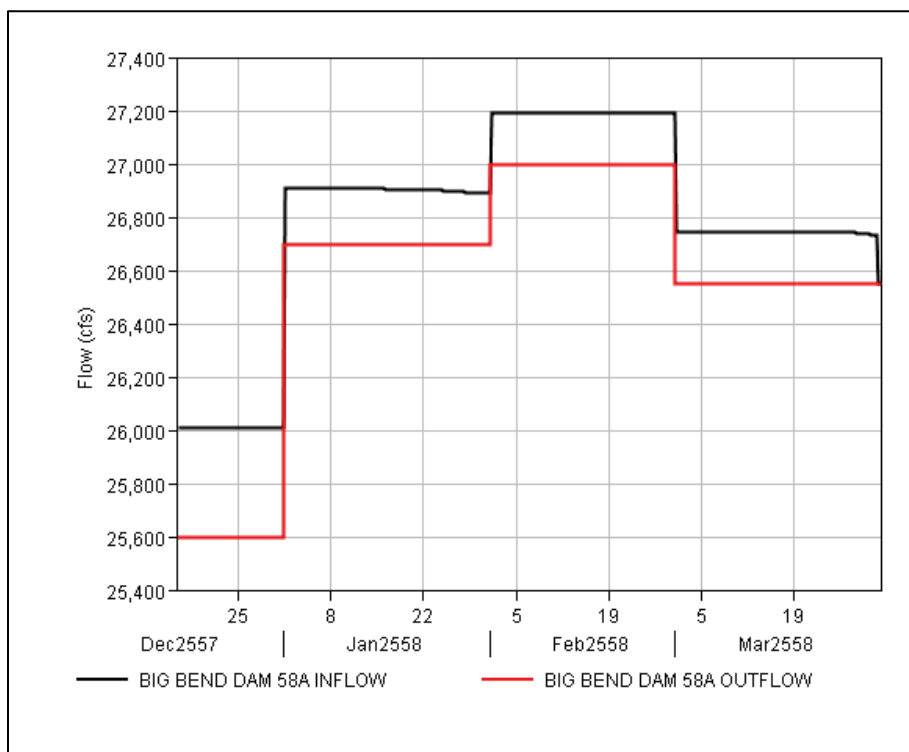


Figure B-67. HYPO 58A routed through Fort Peck Dam - 11+ days from Hermann, MO.

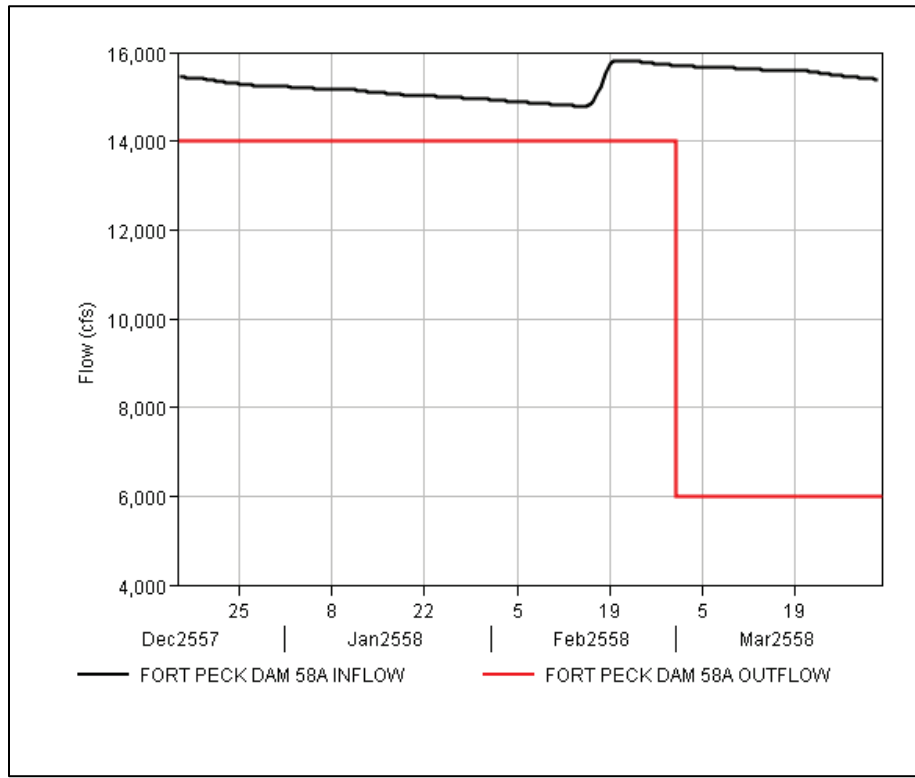


Figure B-68. HYPO 58A routed through Fort Randall Dam - 11+ days from Hermann, MO.

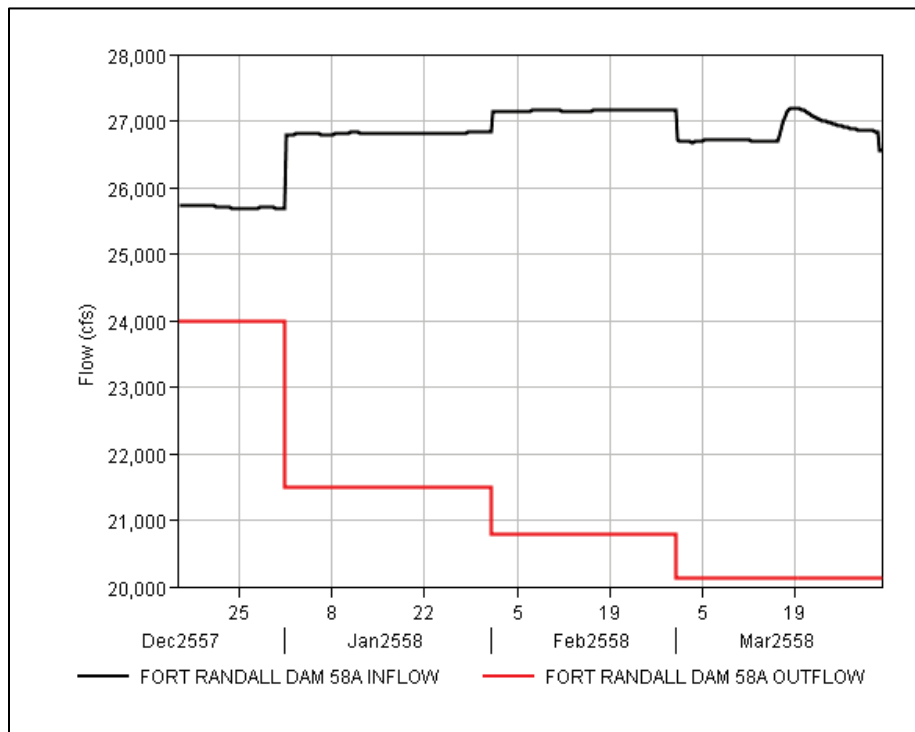


Figure B-69. HYPO 58A routed through Garrison Dam - 11+ days from Hermann, MO.

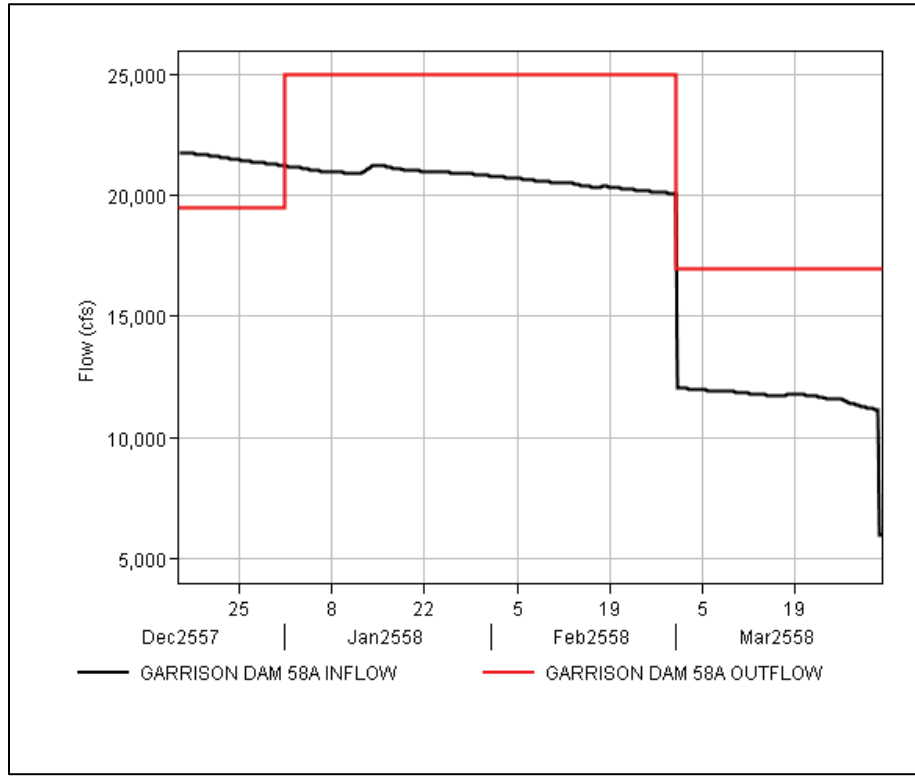


Figure B-70. HYPO 58A routed through Gavins Point Dam - 11+ days from Hermann, MO.

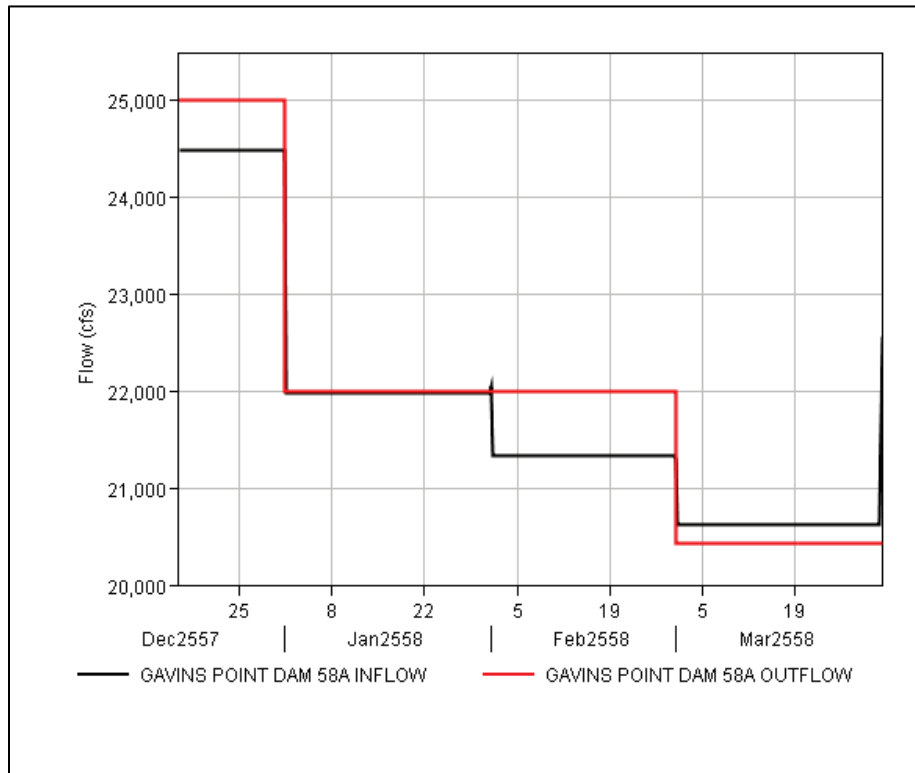
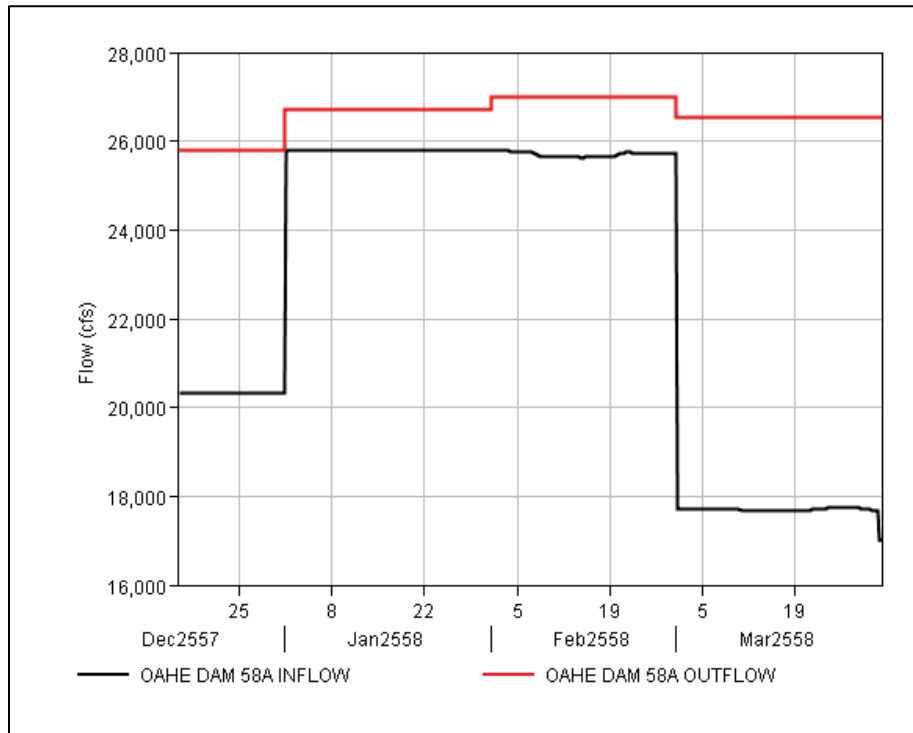


Figure B-71. HYPO 58A routed through Oahe Dam - 11+ days from Hermann, MO.



B.2.3 MVR USACE reservoirs

MVR reservoirs are located on tributaries of the Upper Mississippi River. These reservoirs provide flood reductions to the upstream portion of the Lower Mississippi River by reducing the flood peak at Alton, IL, by 9% (Table 1). Figure B-72 through Figure B-74 show the reservoir hydrographs for MVR.

Figure B-72. HYPO 58A routed through Coralville Dam.

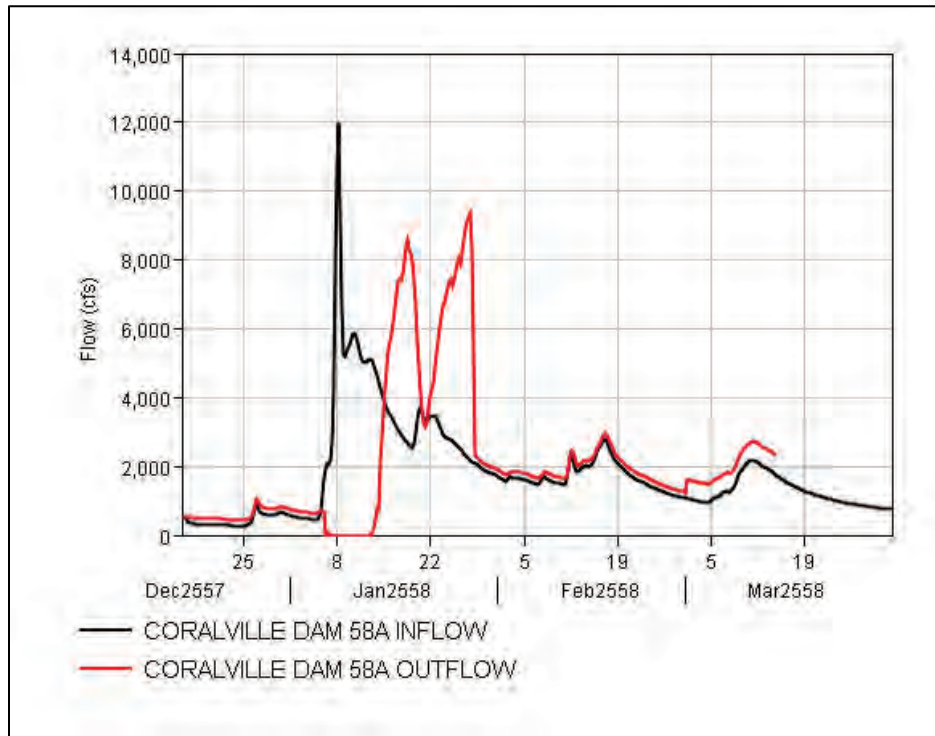


Figure B-73. HYPO 58A routed through Red Rock Dam.

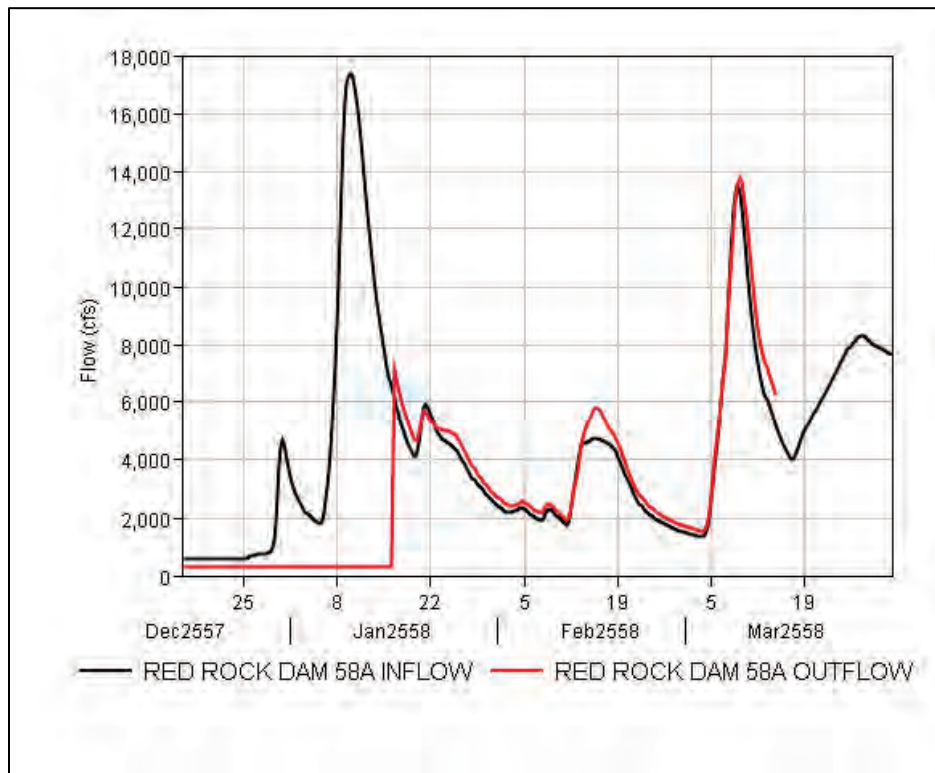
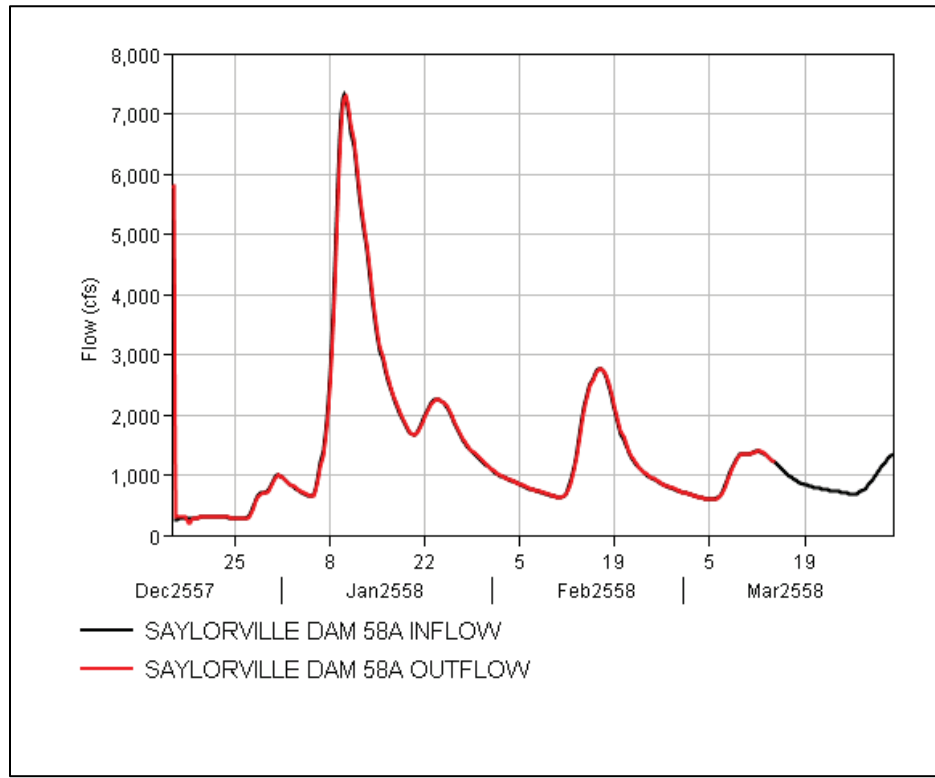


Figure B-74. HYPO 58A routed through Saylorville Dam.



B.2.4 MVK USACE reservoirs

MVK reservoirs are located both east and west of the Mississippi River. The peak flows from the reservoirs on the east side of the Mississippi River take 8–13 days to reach the Mississippi River at Vicksburg. Grenada Dam effects take approximately 5 days to reach the Yazoo River at RM 108 and 8 days to reach the Mississippi River at Vicksburg.

The peak flows from reservoirs on tributaries to the Ouachita River on the west side of the Mississippi River take approximately 20+ days to reach the Lower Mississippi River and have a minimal impact on flood reduction at Monroe, LA. The reservoirs on tributaries to the Red River are approximately 6 days from Alexandria, LA, and do have a significant contribution to flood reduction on the Red River at this location. Figure B-75 through Figure B-84 show the reservoir hydrographs for MVK.

Figure B-75. HYPO 58A routed through Arkabutla Dam - ~13 days from Vicksburg, MS.

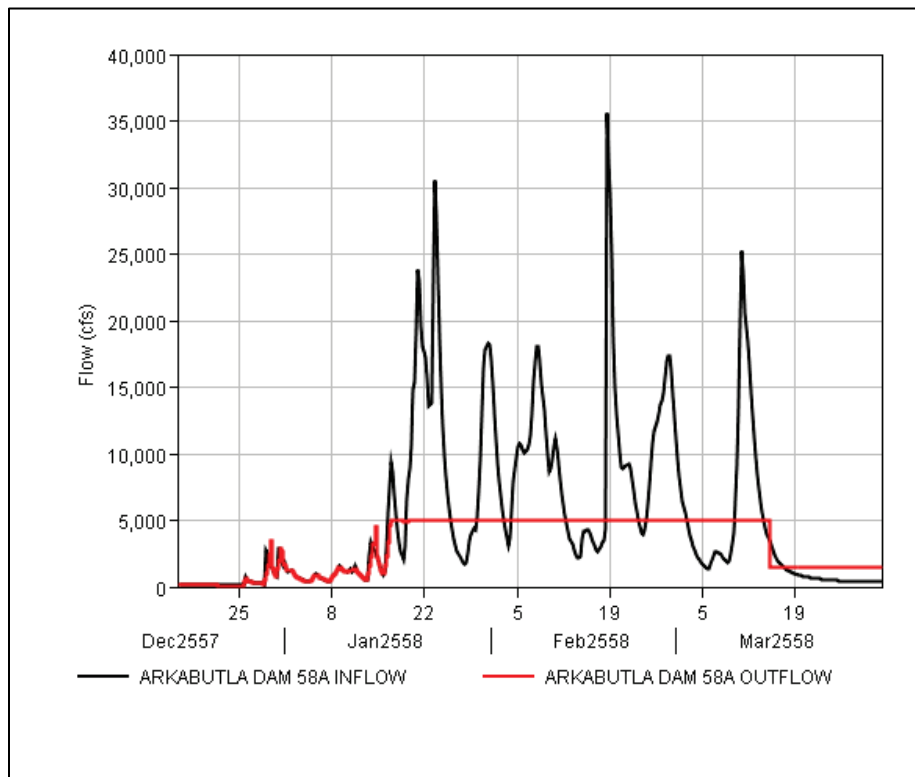


Figure B-76. HYPO 58A routed through Bayou Bodcau Dam - ~6 days from Alexandria, LA.

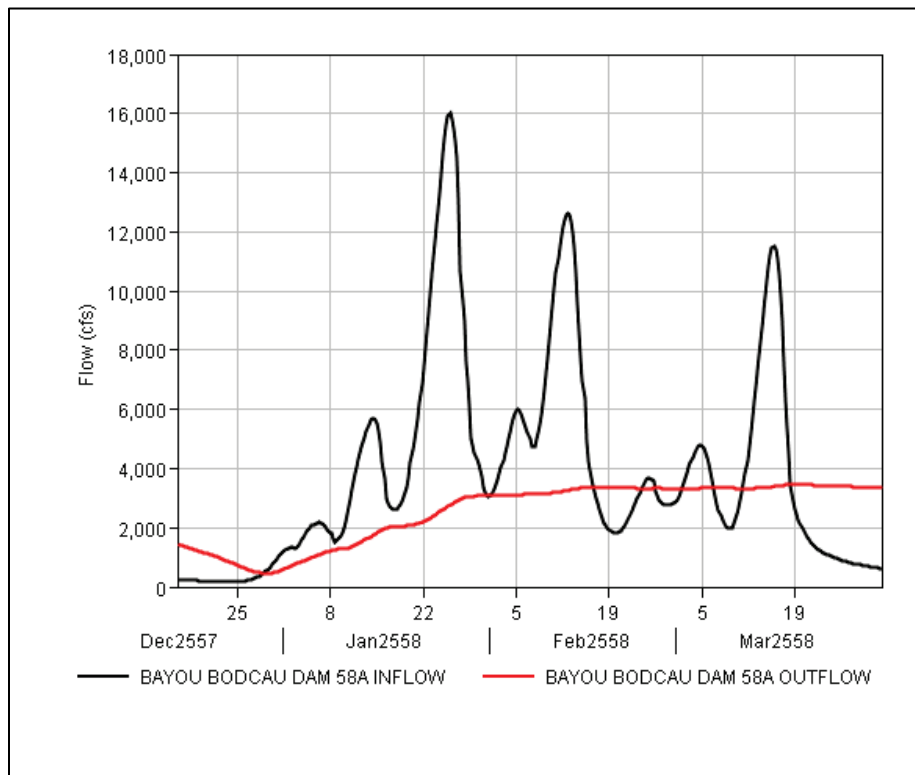


Figure B-77. HYPO 58A routed through Blakely Mountain Dam - ~20+ days from the Mississippi River.

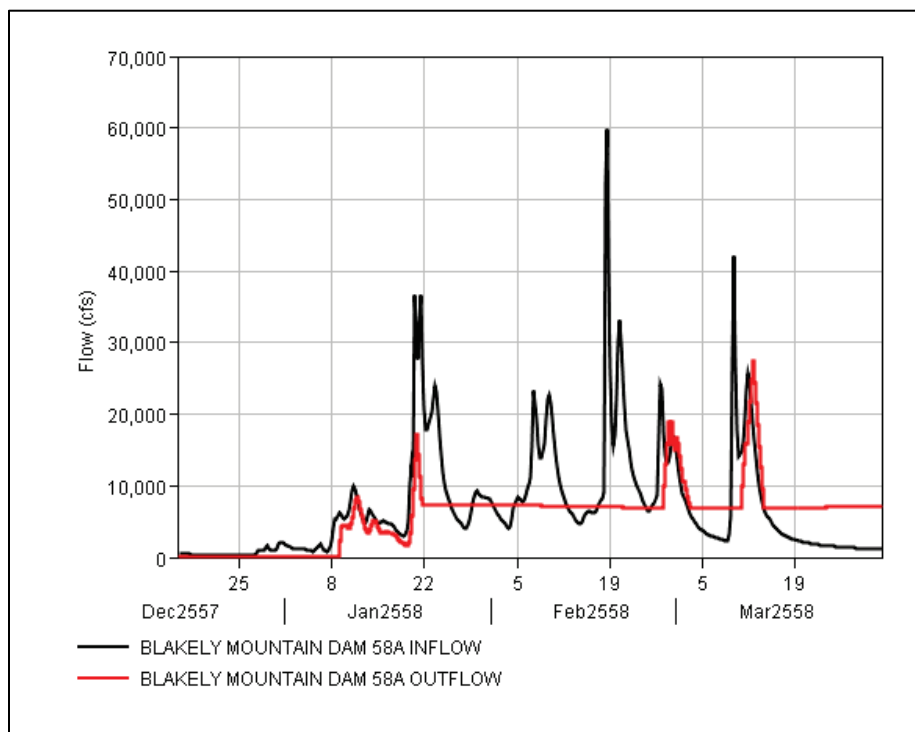


Figure B-78. HYPO 58A routed through Degray Dam - ~20+ days from the Mississippi River.

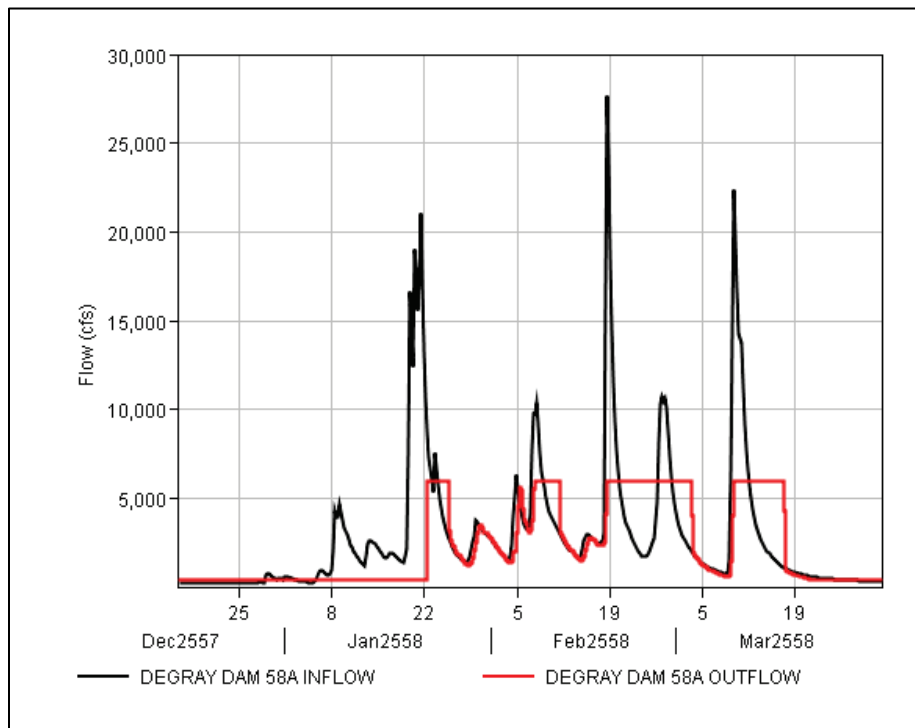


Figure B-79. HYPO 58A routed through Enid Dam - ~12 days from Vicksburg, MS.

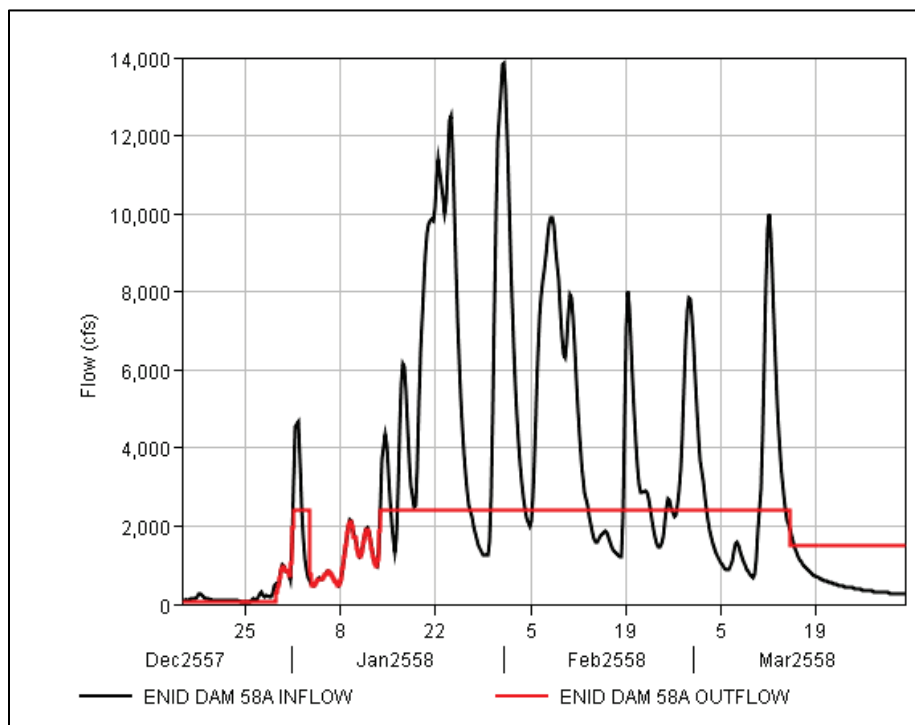


Figure B-80. HYPO 58A routed through Grenada Dam - ~8 days from Vicksburg, MS.

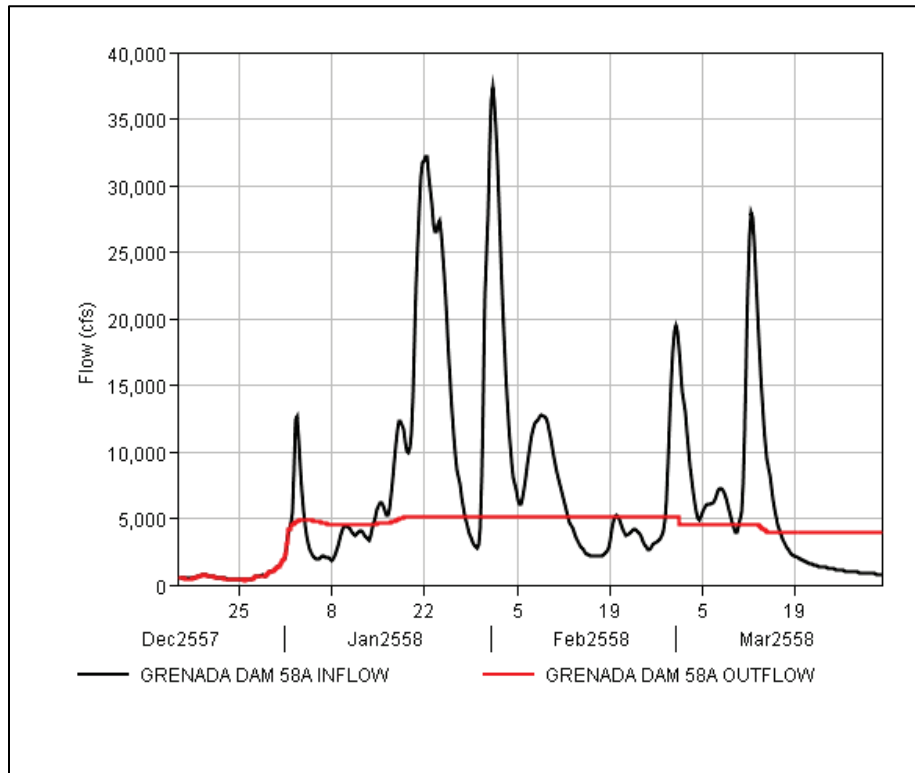


Figure B-81. HYPO 58A routed through Caddo Dam - ~6 days from Alexandria, LA.

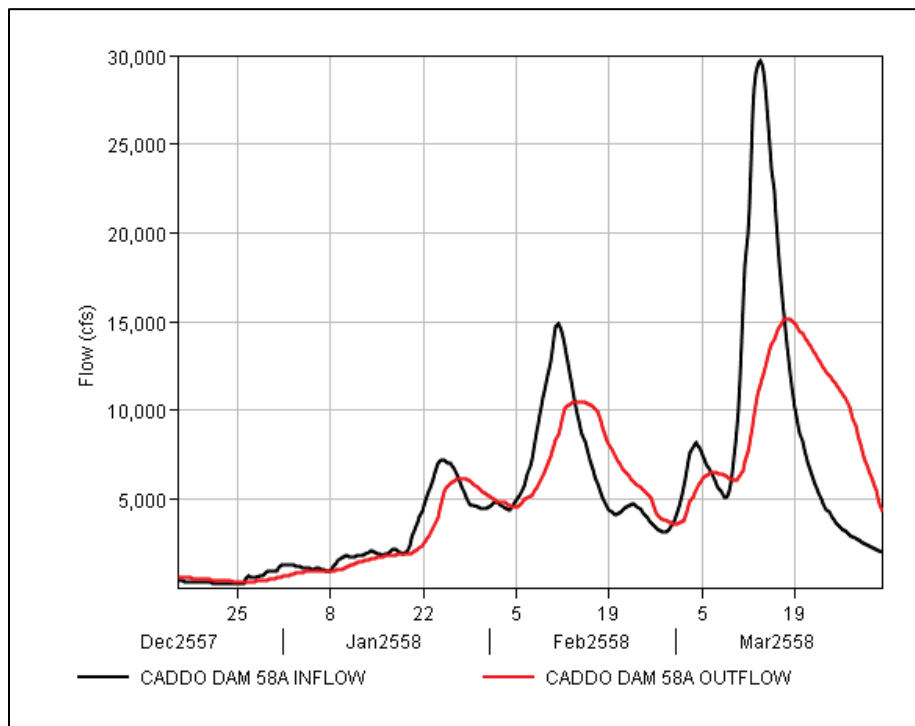


Figure B-82. HYPO 58A routed through Narrows Dam - ~20+ days from the Mississippi River.

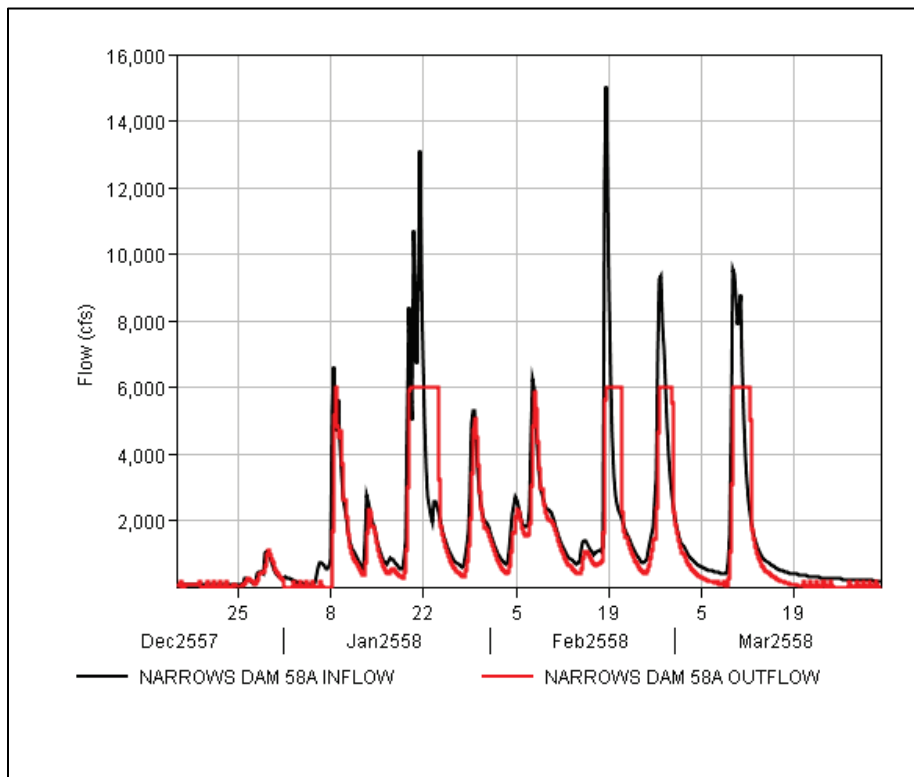


Figure B-83. HYPO 58A routed through Sardis Dam - ~12 days from Vicksburg, MS.

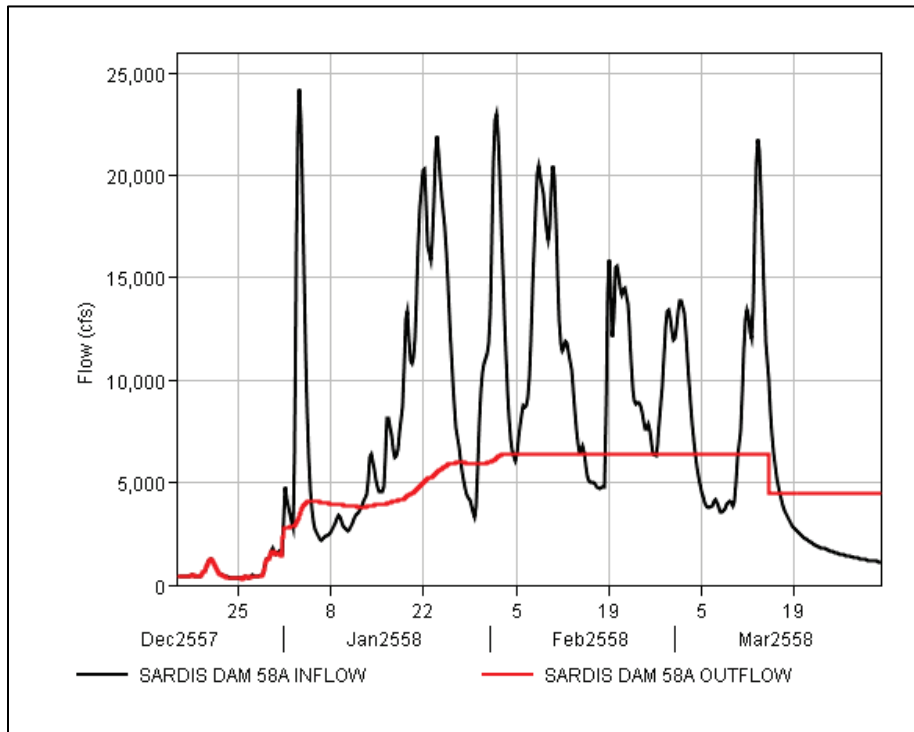
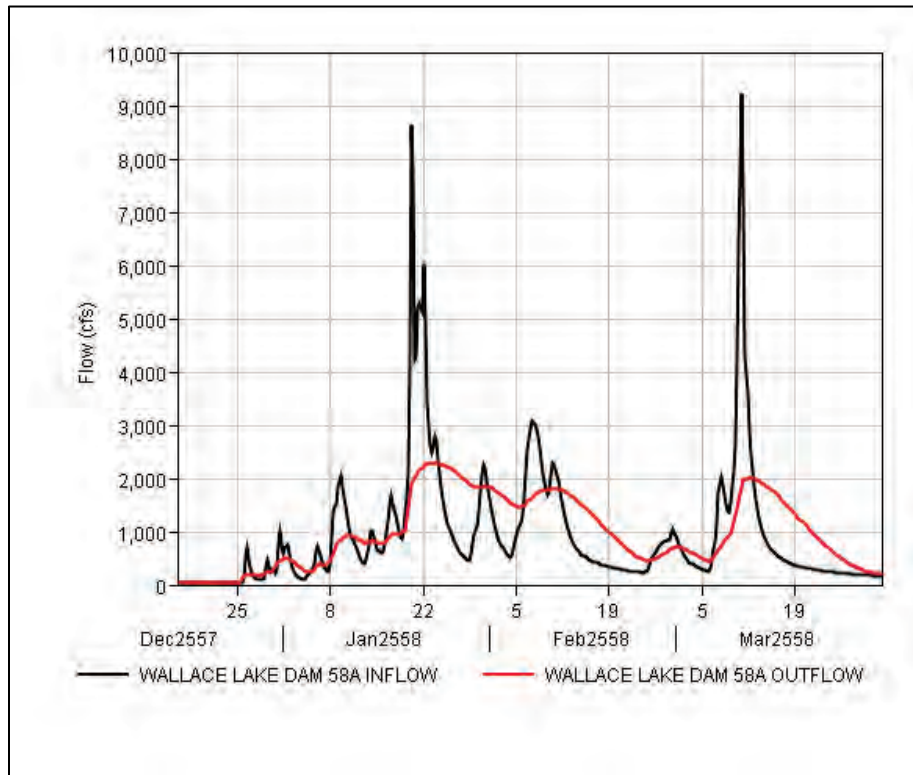


Figure B-84. HYPO 58A routed through Wallace Lake Dam - ~5 days from Alexandria, LA.



B.2.5 LRL USACE reservoirs

LRL reservoirs are located on tributaries of the Lower Ohio River. These reservoirs take 9–12 days to show an effect on the Ohio River at Cairo, IL.

Figure B-85 through Figure B-95 show the reservoir hydrographs for LRL and the time it takes their effects to reach the Ohio River at Cairo.

Figure B-85. HYPO 58A routed through Barren River Lake - ~11 days from Cairo, IL.

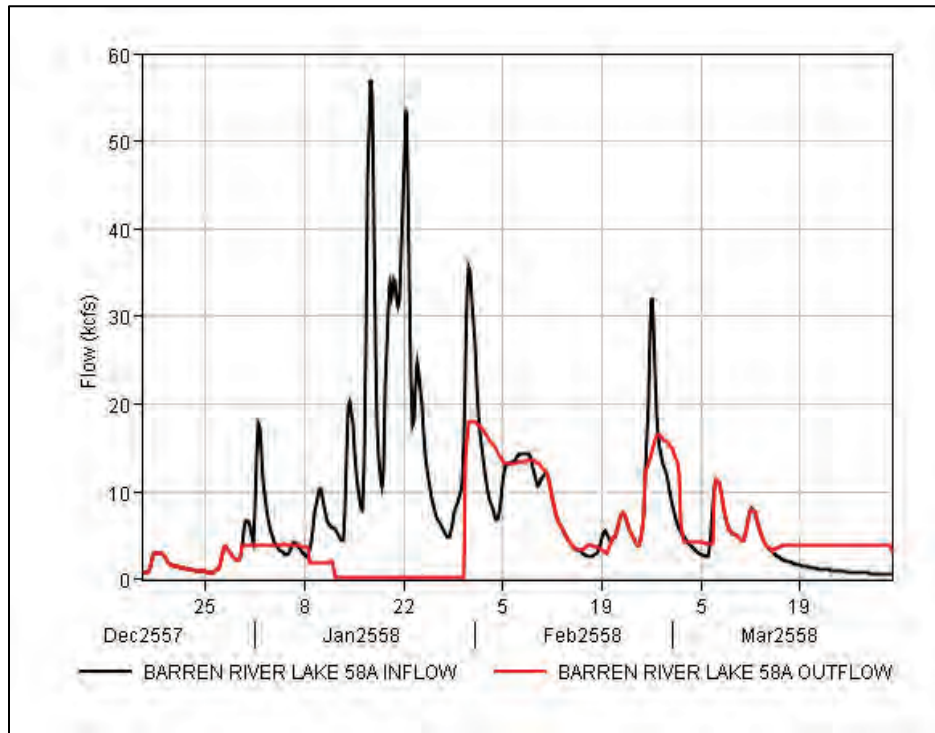


Figure B-86. HYPO 58A routed through Cagles Mill Lake - ~13 days from Cairo, IL.

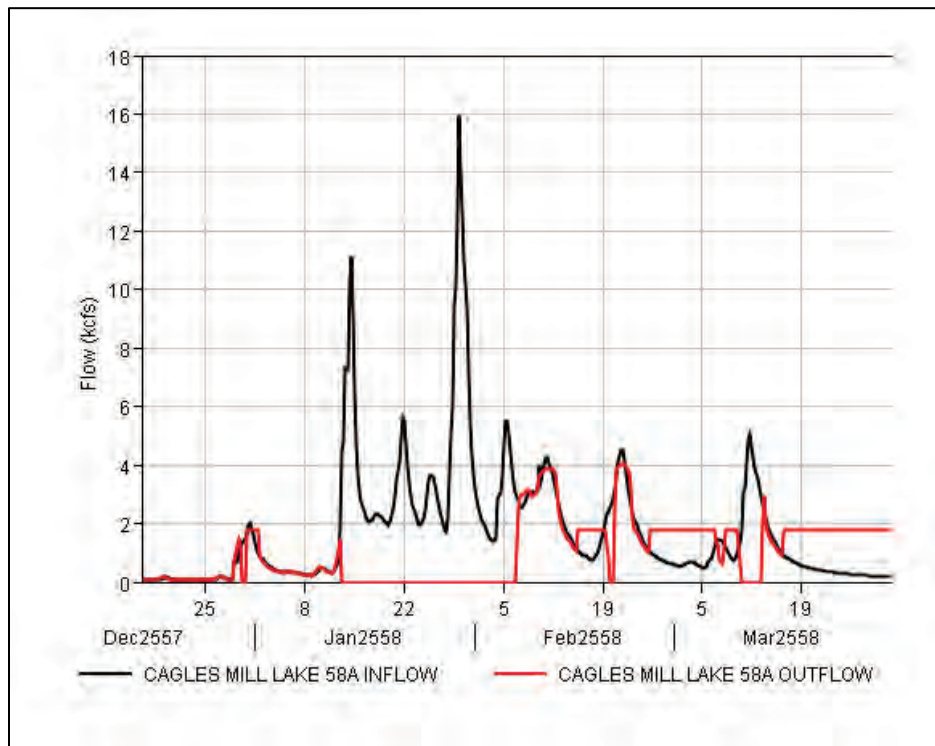


Figure B-87. HYPO 58A routed through CM Harden Lake - ~14 days from Cairo, IL.

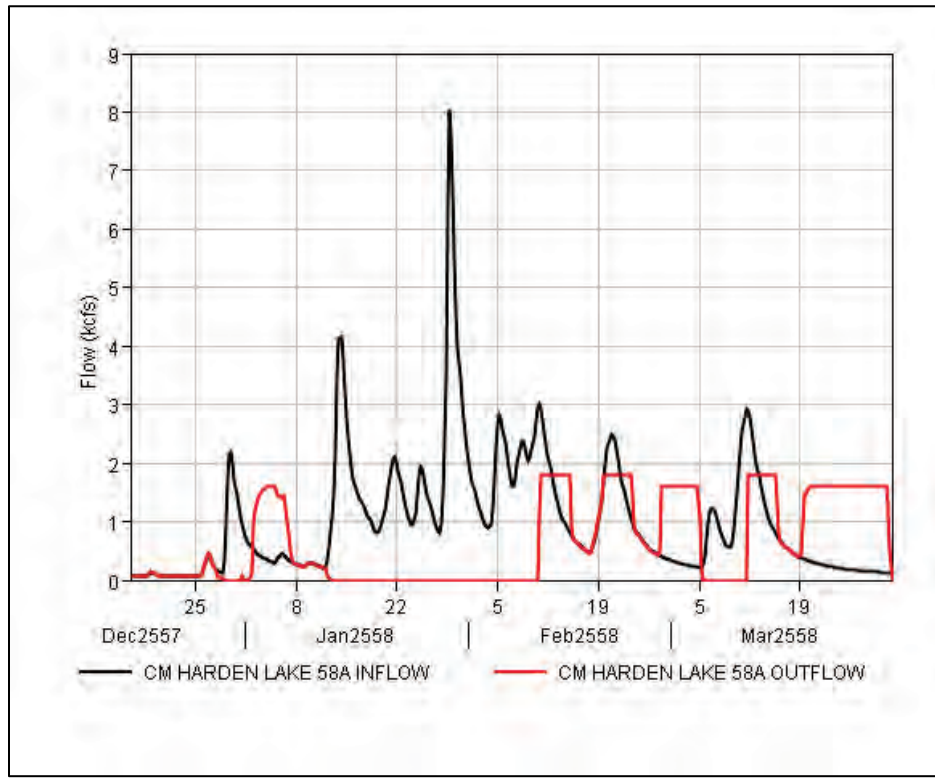


Figure B-88. HYPO 58A routed through Green River Lake - ~13 days from Cairo, IL.

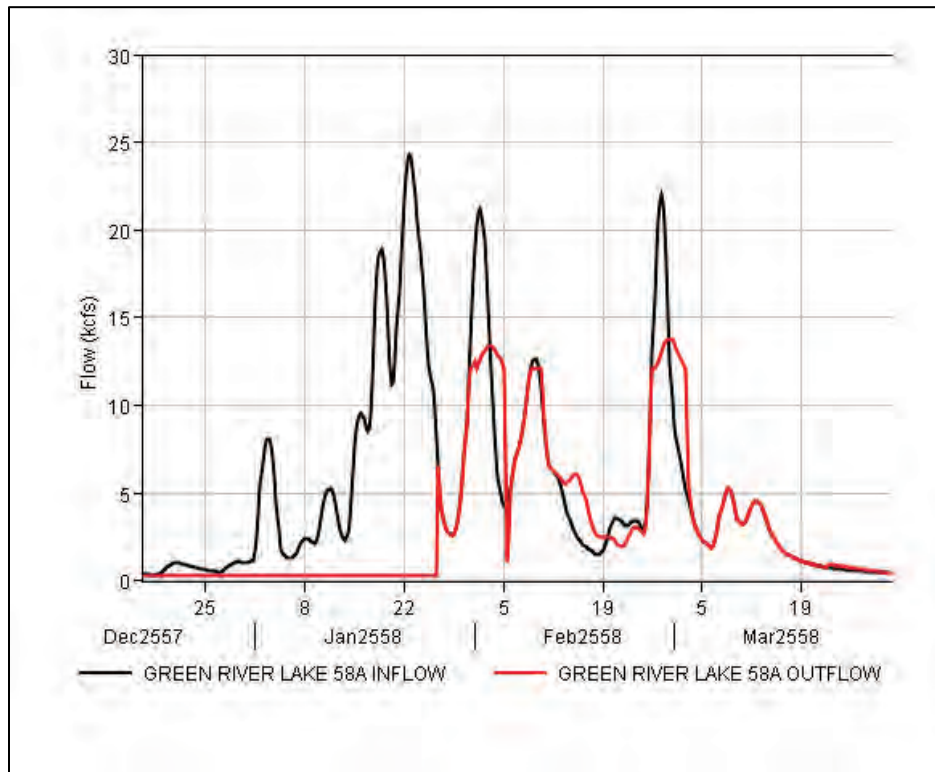


Figure B-89. HYPO 58A routed through J. E. Roush Lake - ~16+ days from Cairo, IL.

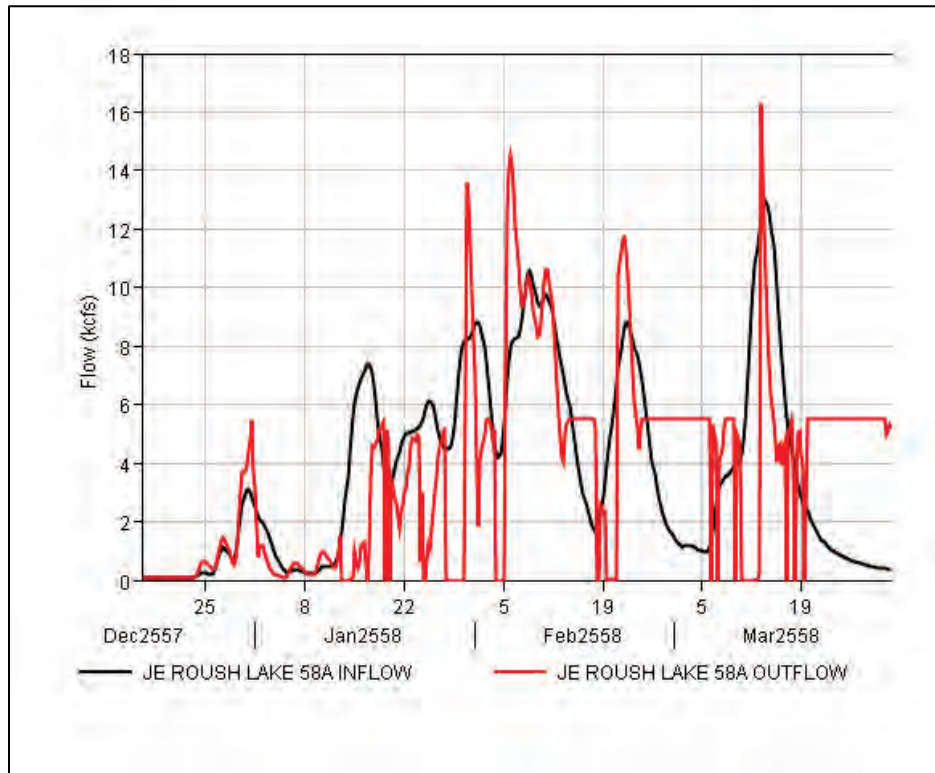


Figure B-90. HYPO 58A routed through Mississinewa Lake - ~15 days from Cairo, IL.

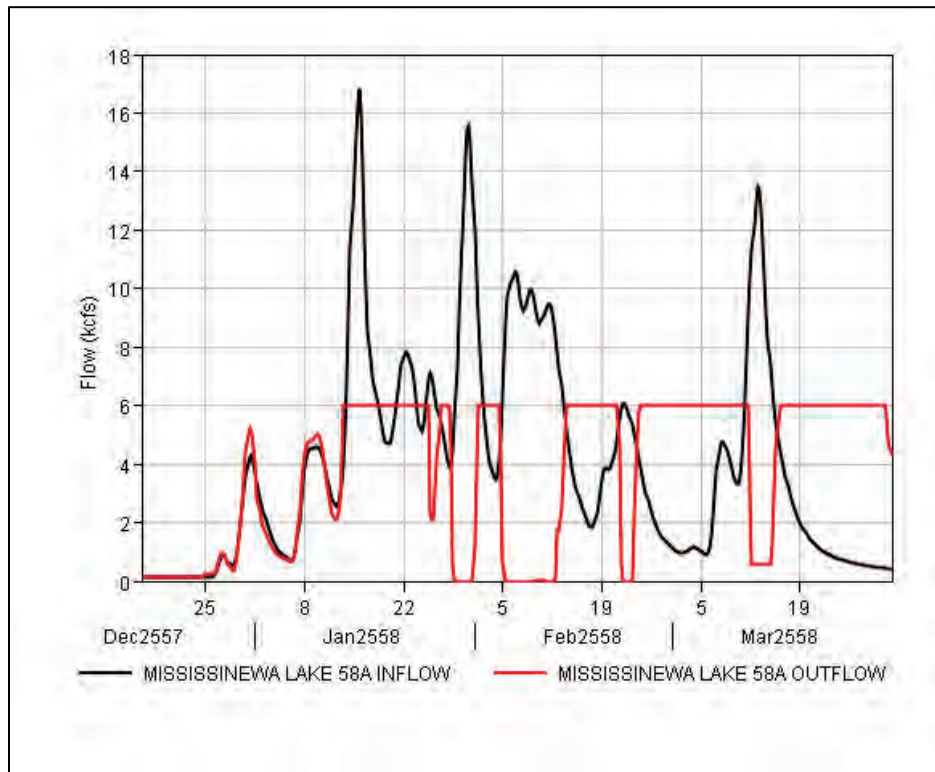


Figure B-91. HYPO 58A routed through Monroe Lake - ~12 days from Cairo, IL.

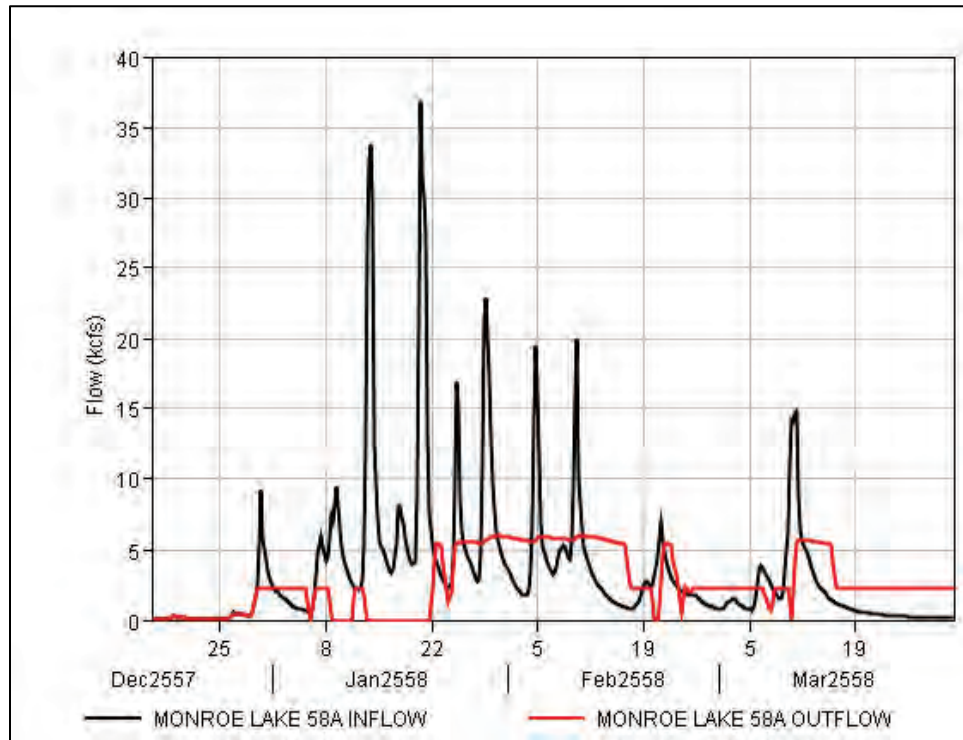


Figure B-92. HYPO 58A routed through Nolin River Lake - ~10 days from Cairo, IL.

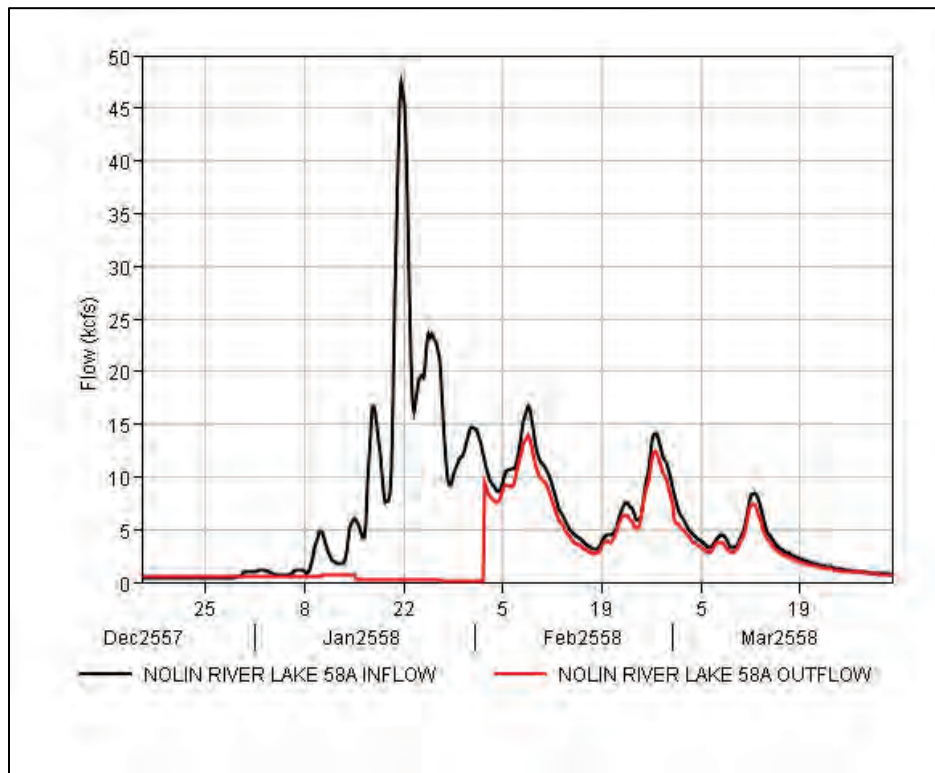


Figure B-93. HYPO 58A routed through Patoka Lake - ~10 days from Cairo, IL.

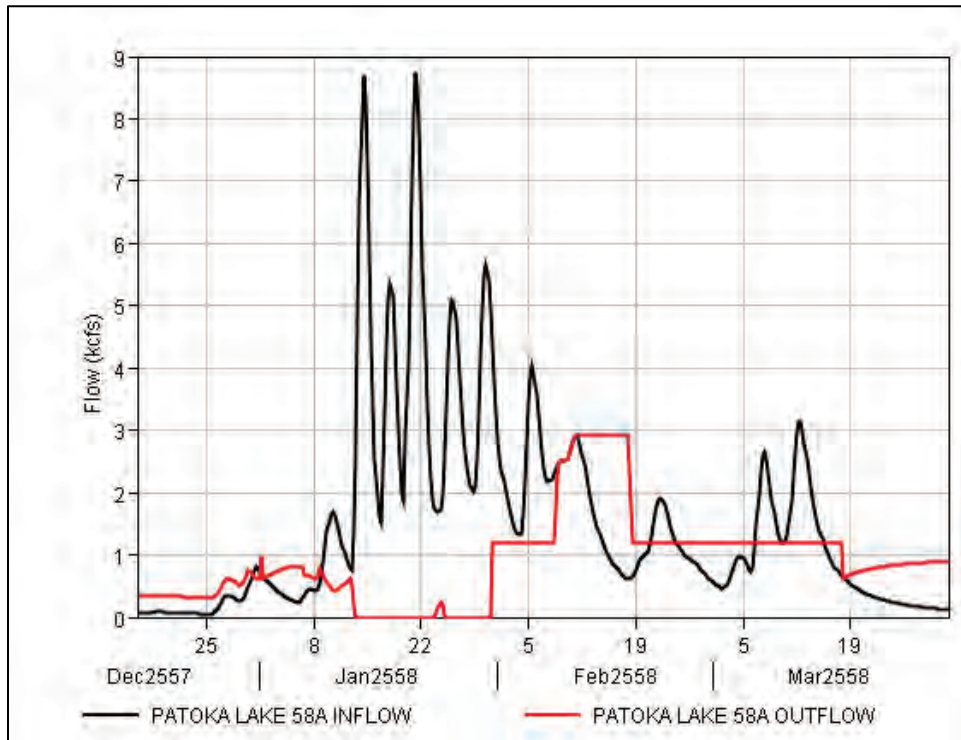


Figure B-94. HYPO 58A routed through Rough River Lake - ~9 days from Cairo, IL.

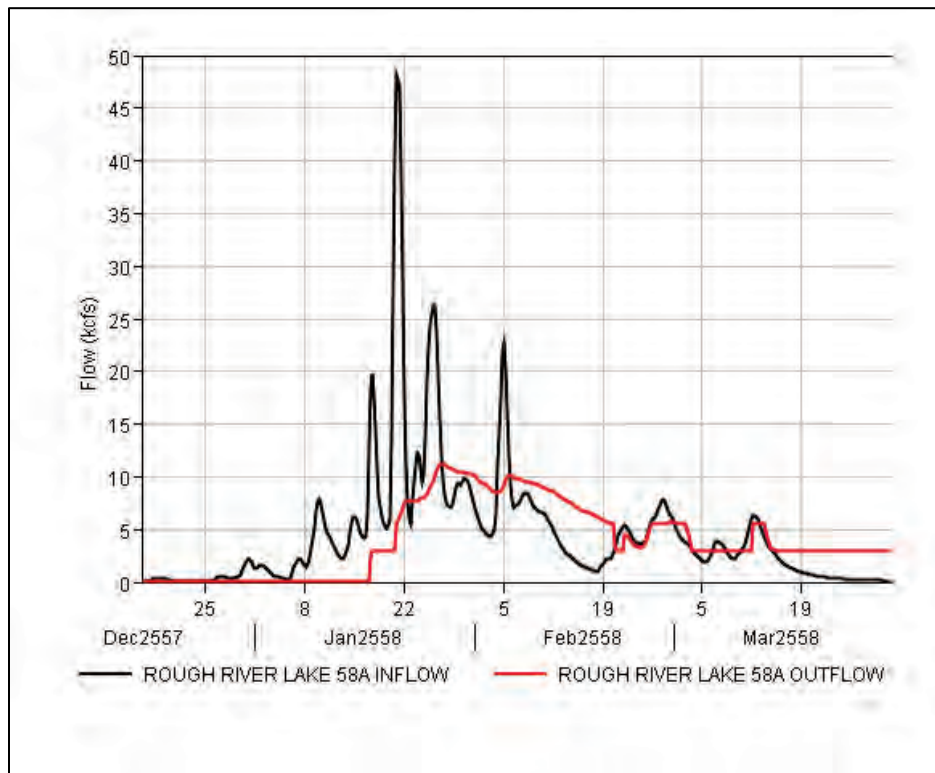
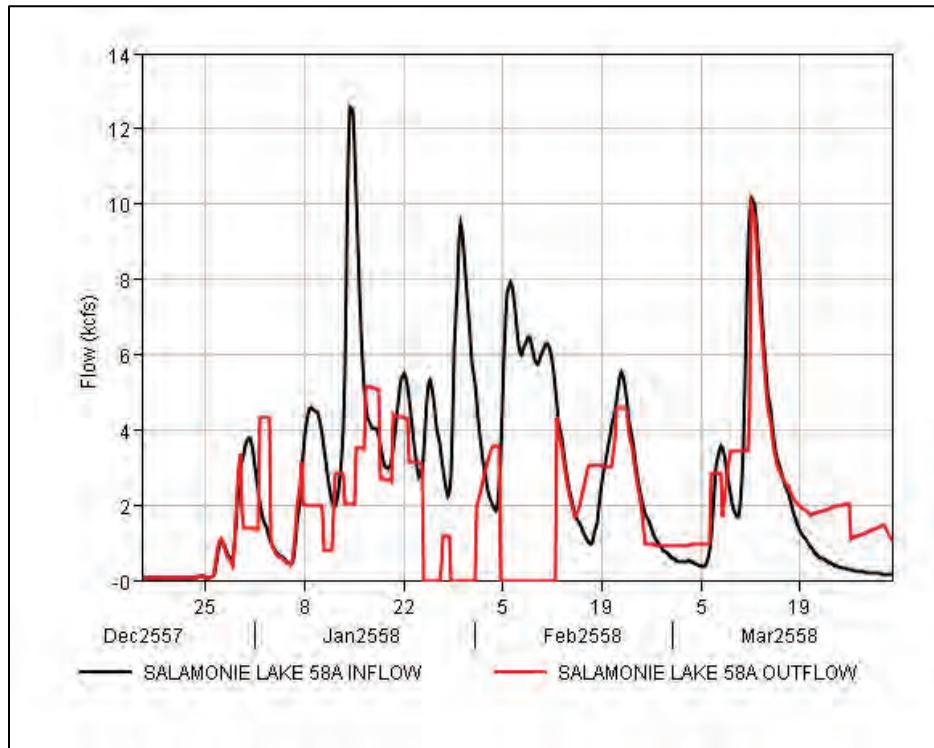


Figure B-95. HYPO 58A routed through Salamonie Lake ~15 days from Cairo, IL.



B.2.6 LRN USACE and TVA reservoirs

LRN reservoirs are located on tributaries of the Lower Ohio River. These reservoirs take 2–8 days to show an effect on the Ohio River at Cairo, IL. Barkley Dam takes approximately 2 days for effects to reach the Ohio River at Cairo.

Figure B-96 through Figure B-105 show the hydrographs for the reservoirs in LRN as well as the time it takes for their effects to reach the Ohio River at Cairo.

Figure B-96. HYPO 58A routed through Barkley Dam - ~2 days from Cairo, IL.

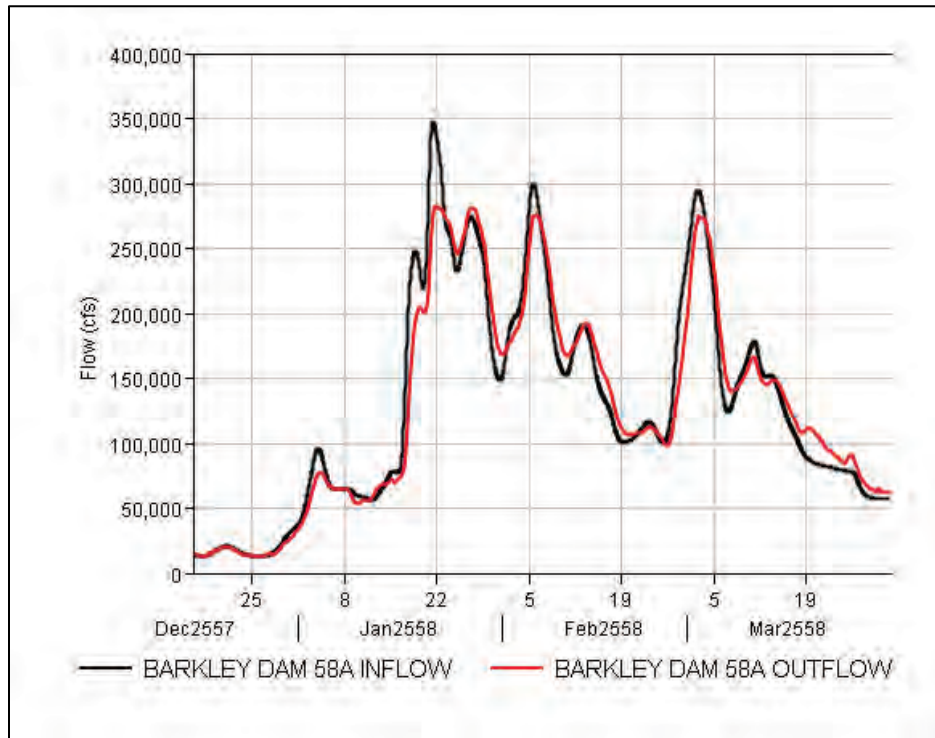


Figure B-97. HYPO 58A routed through Center Hill Dam - ~7 days from Cairo, IL.

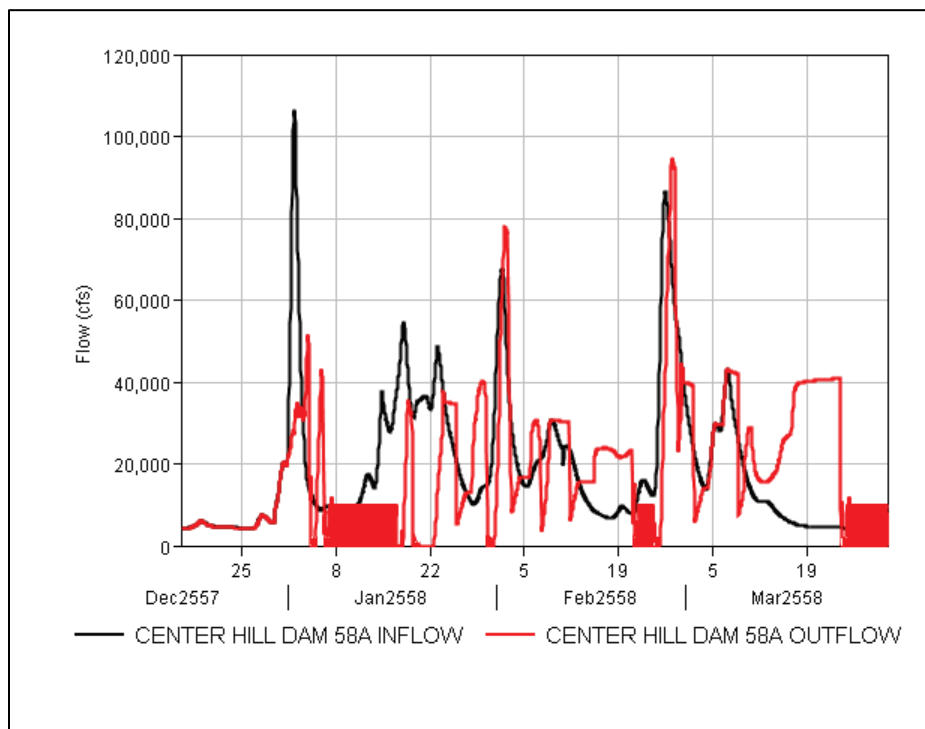


Figure B-98. HYPO 58A routed through Cheatham Dam - ~5 days from Cairo, IL.

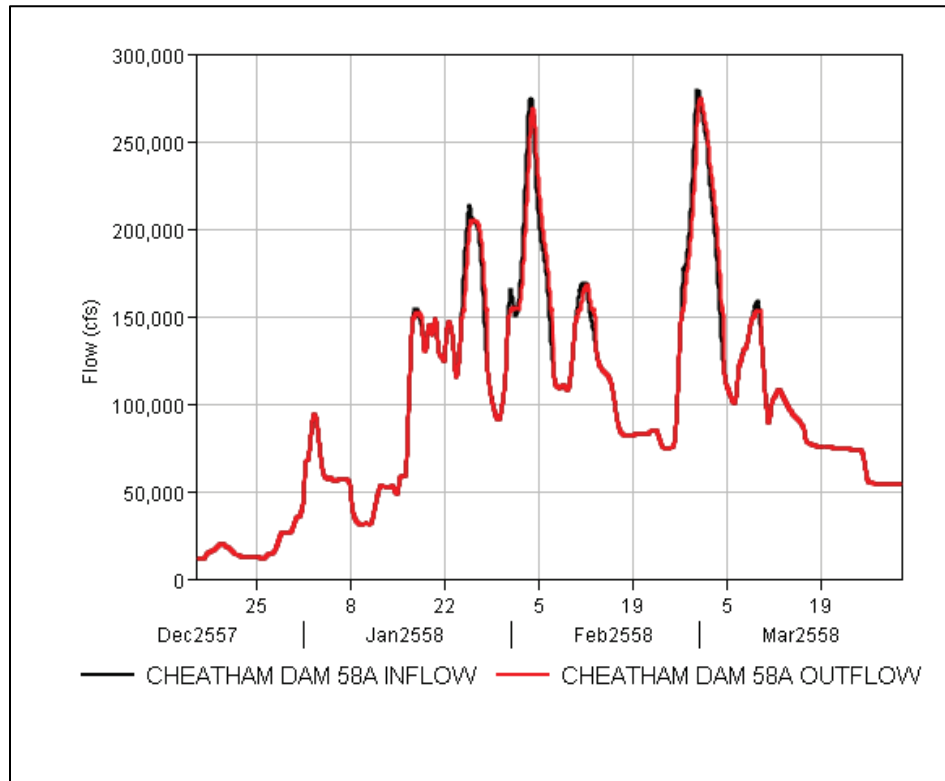


Figure B-99. HYPO 58A routed through Cordell Hull Dam - ~7 days from Cairo, IL.

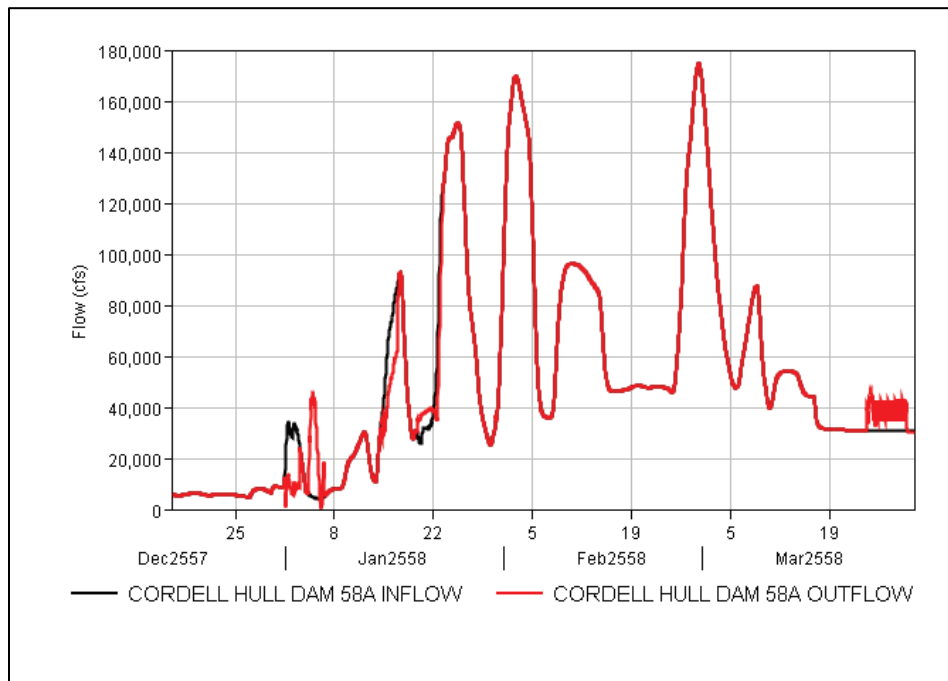


Figure B-100. HYPO 58A routed through Dale Hollow Dam - ~8 days from Cairo, IL.

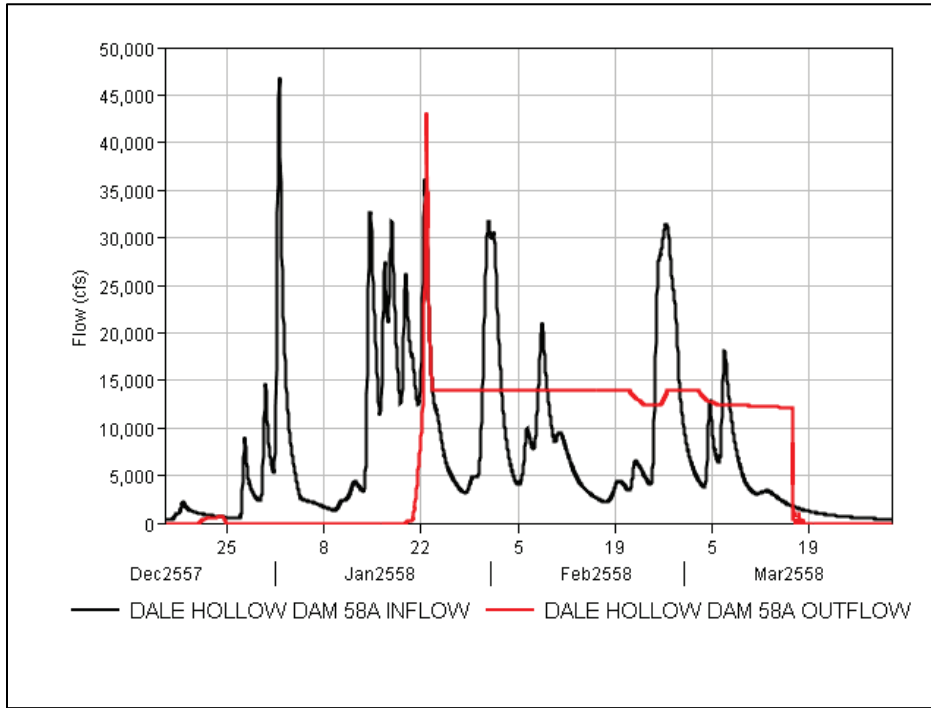


Figure B-101. HYPO 58A routed through Great Falls - ~7 days from Cairo, IL.

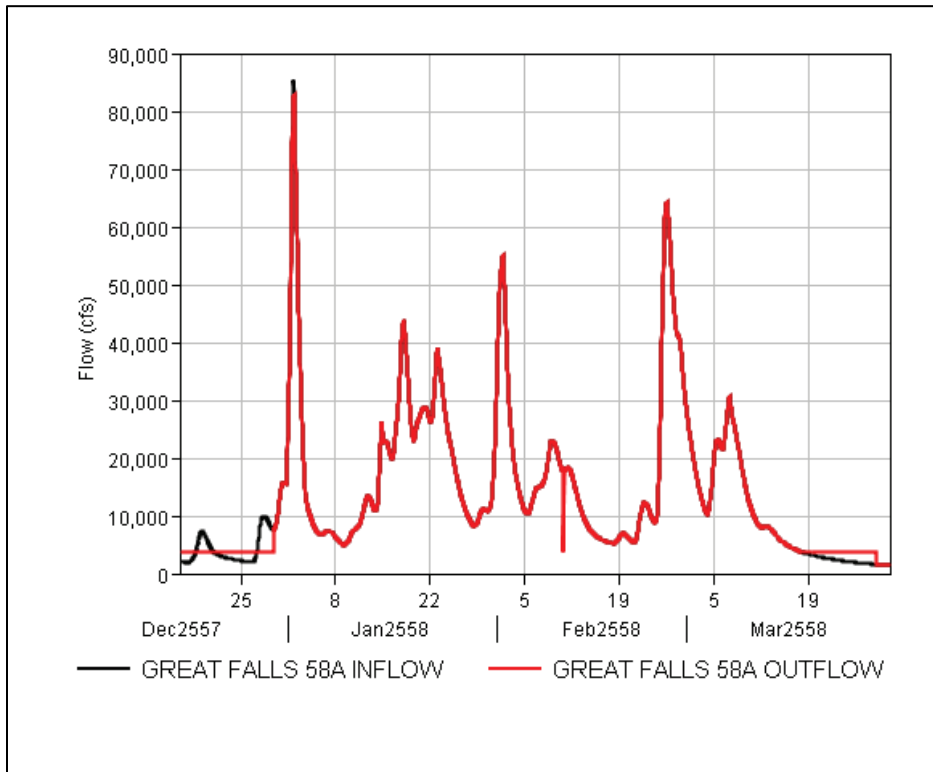


Figure B-102. HYPO 58A routed through J. Percy Priest Dam - ~6 days from Cairo, IL.

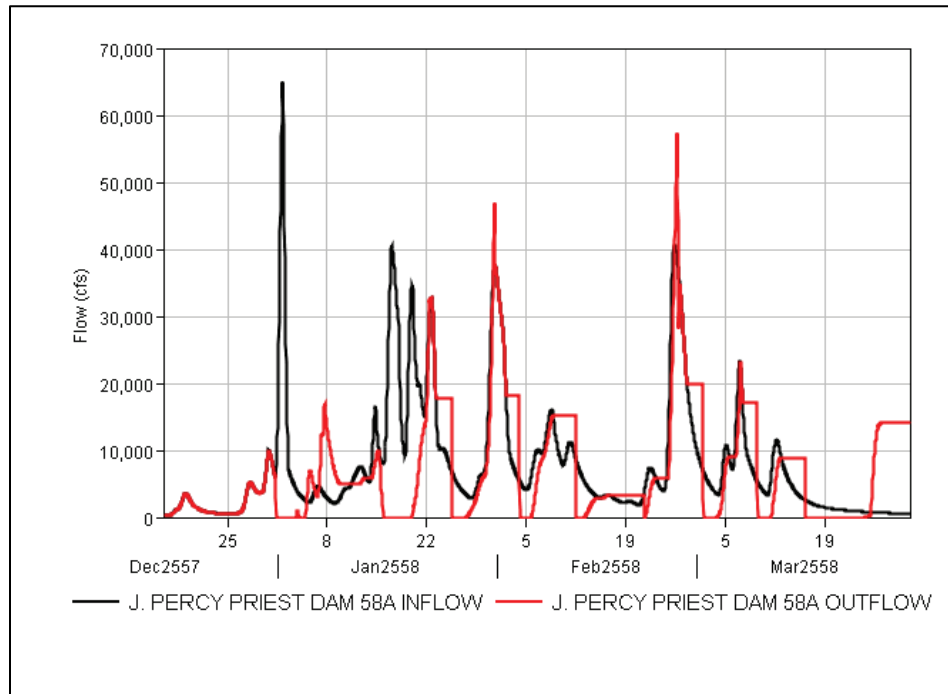


Figure B-103. HYPO 58A routed through Kentucky Dam - ~1 days from Cairo, IL.

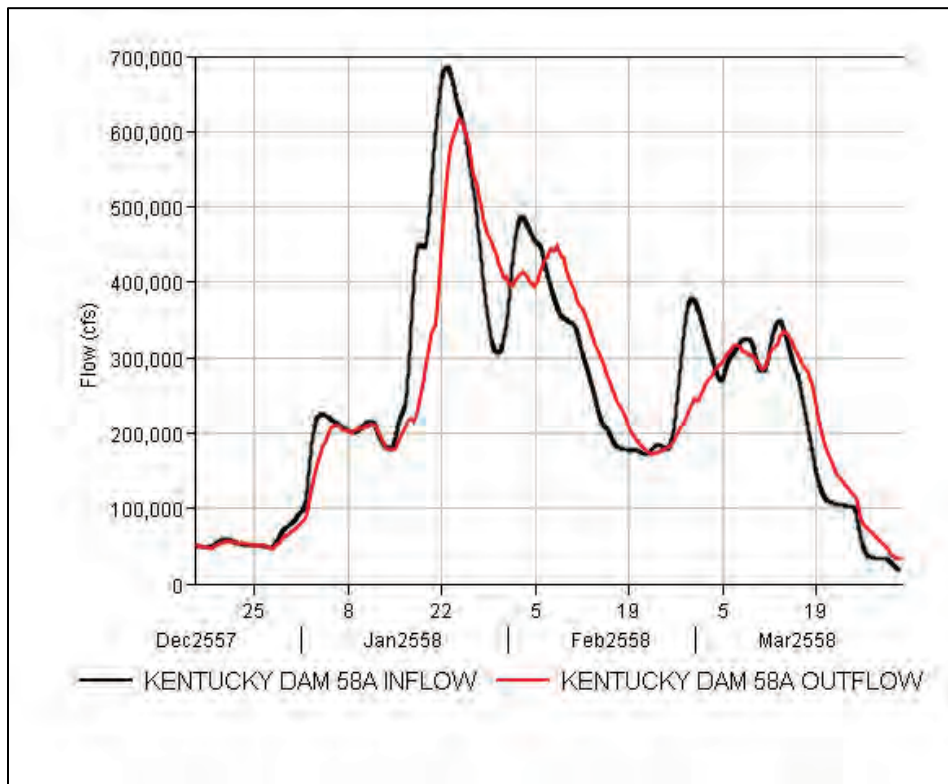


Figure B-104. HYPO 58A routed through Old Hickory Dam - ~6 days from Cairo, IL.

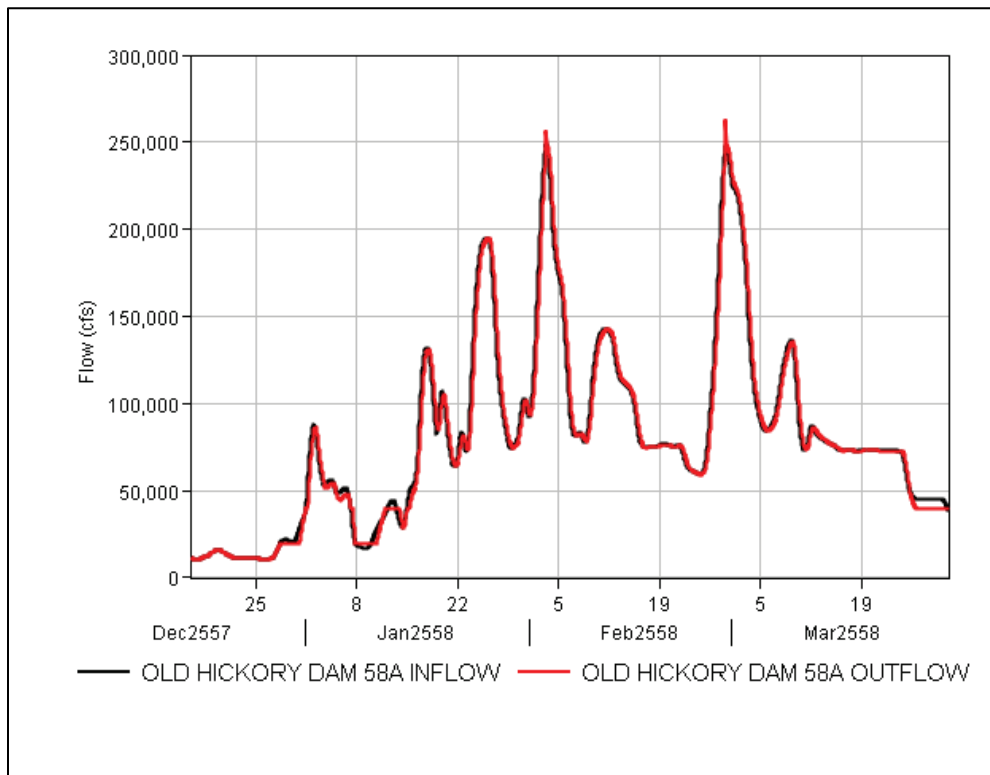
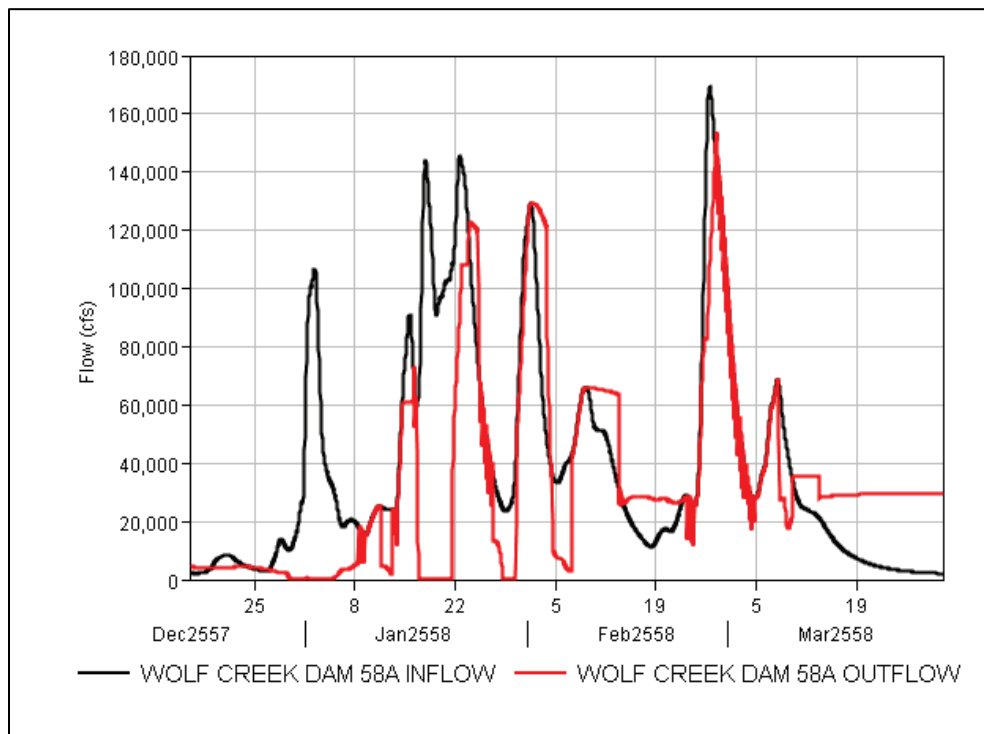


Figure B-105. HYPO 58A routed through Wolf Creek Dam - ~8 days from Cairo, IL.



B.2.7 SWT USACE reservoirs

SWT reservoirs are located on tributaries of the Arkansas and Red Rivers. These reservoirs take 3–6 days to show an effect on the Arkansas River at Pine Bluff (Little Rock), AR, and approximately 13 days to show an effect on the Red River at Alexandria, LA. Tenkiller Lake takes approximately 3 days for effects to reach the Arkansas River at Pine Bluff.

Figure B-106 through Figure B-113 show the hydrographs for the reservoirs in SWT as well as the time it takes for their effects to reach the Arkansas River at Pine Bluff or the Red River at Alexandria.

Figure B-106. HYPO 58A routed through Fort Gibson Dam - ~4 days from Pine Bluff, AR.

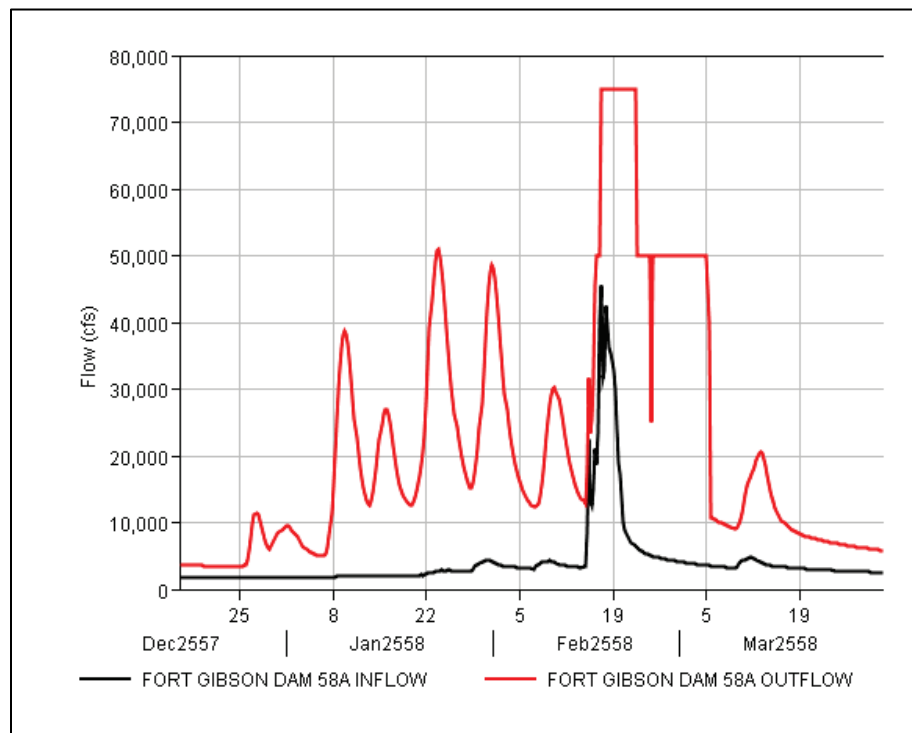


Figure B-107. HYPO 58A routed through Hugo Dam - ~13 days from Alexandria, LA.

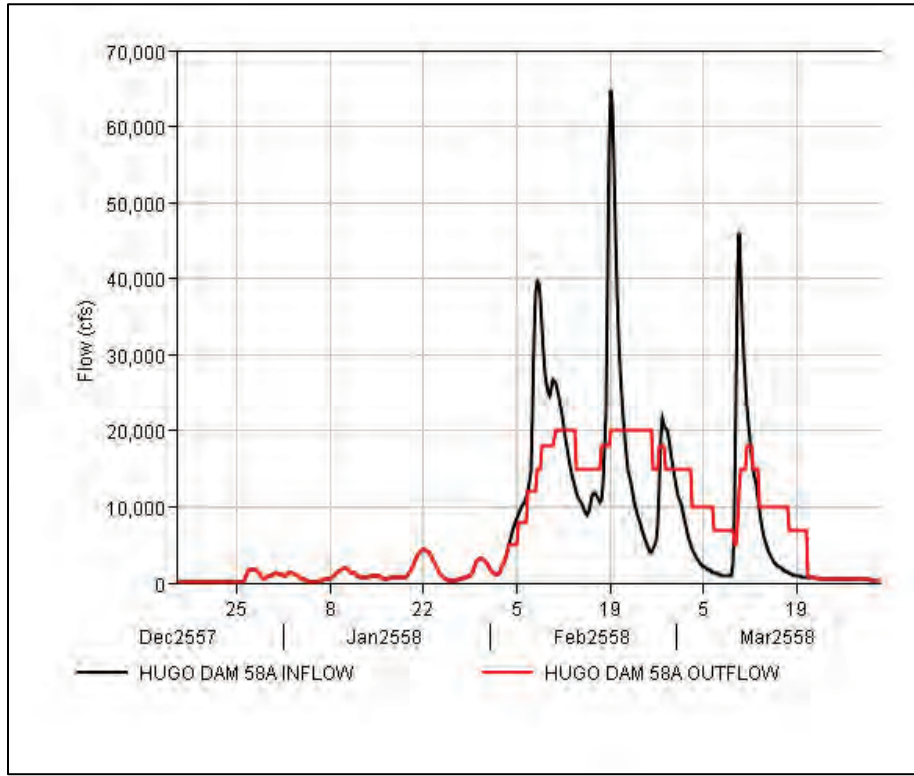


Figure B-108. HYPO 58A routed through Keystone Lake - ~5 days from Pine Bluff, AR.

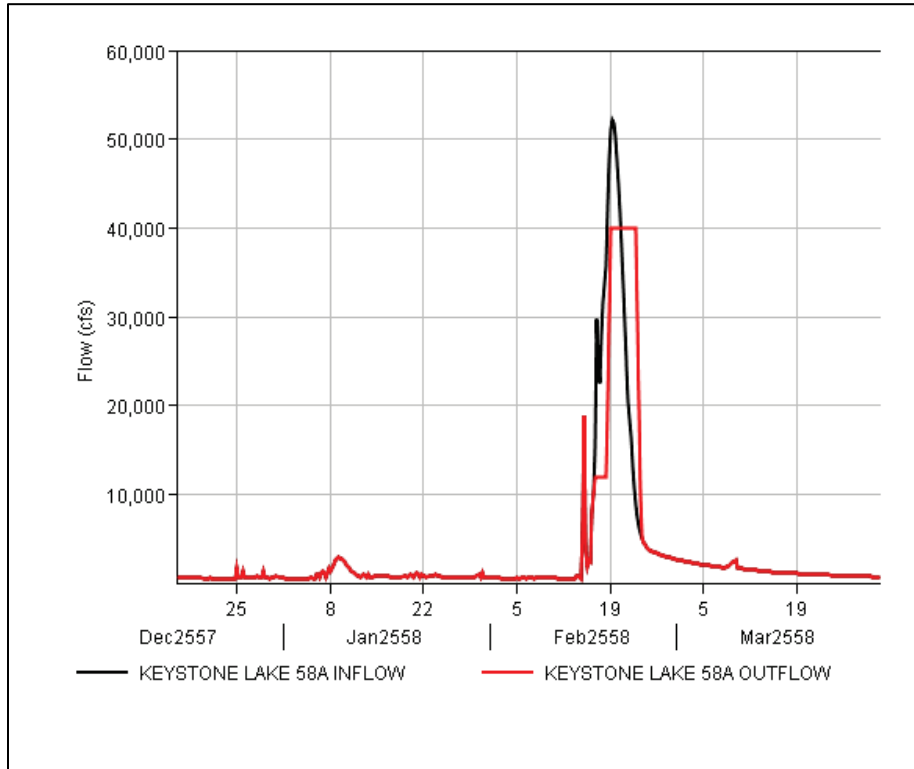


Figure B-109. HYPO 58A routed through Lake Texoma - ~14 days from Alexandria, LA.

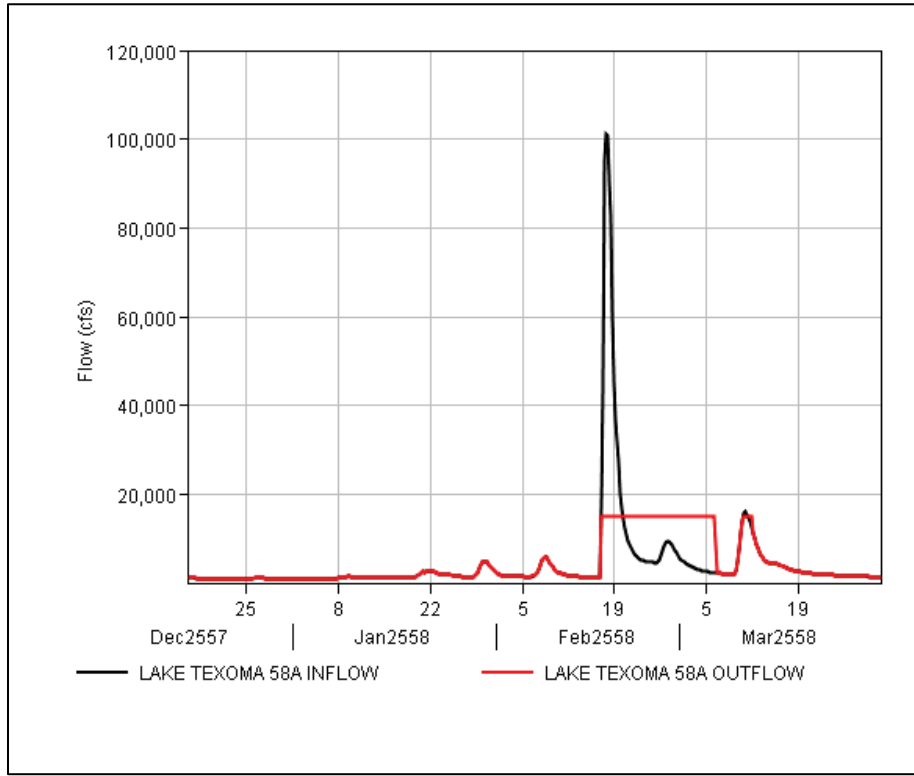


Figure B-110. HYPO 58A routed through Oologah Lake - ~6 days from Pine Bluff, AR.

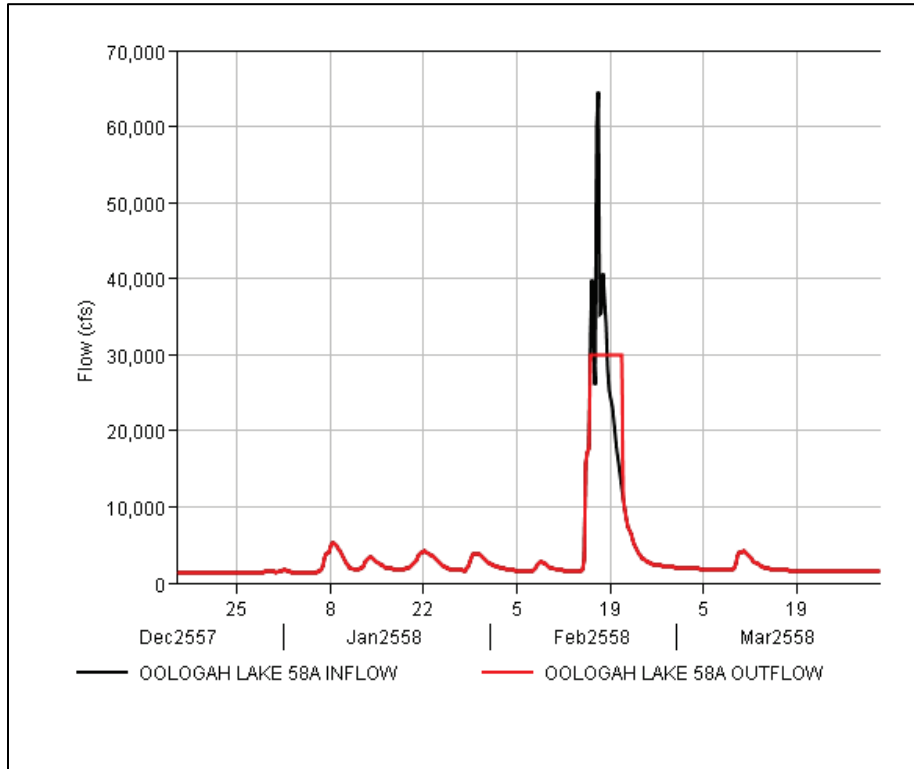


Figure B-111. HYPO 58A routed through Skiatook Lake - ~6 days from Pine Bluff, AR.

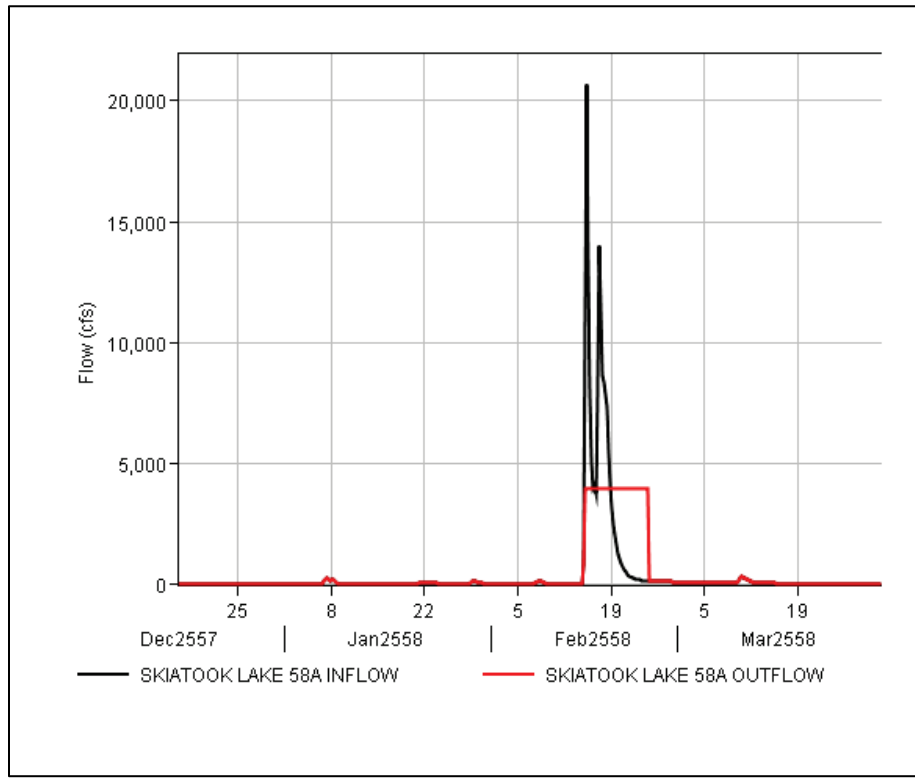


Figure B-112. HYPO 58A routed through Tenkiller Lake - ~3 days from Pine Bluff, AR.

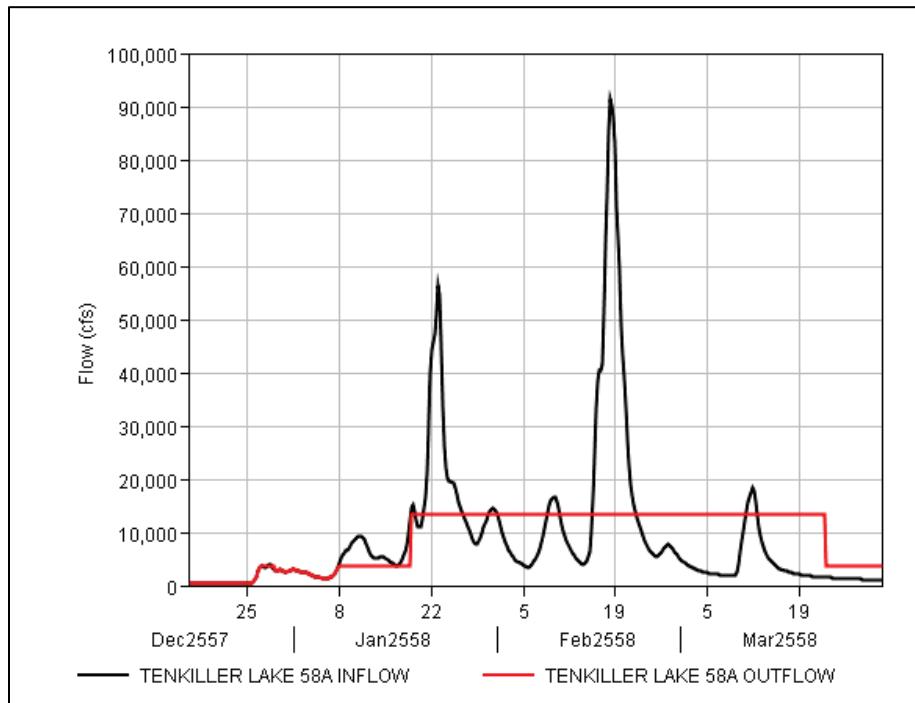
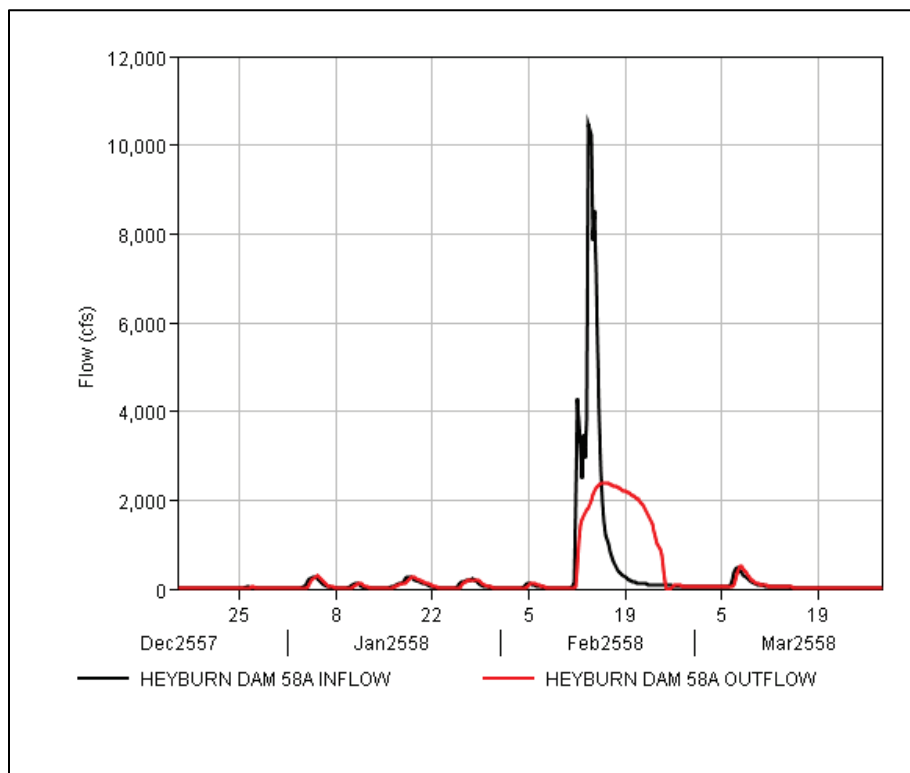


Figure B-113. HYPO 58A routed through Heyburn Dam - ~3 days from Pine Bluff, AR.



B.2.8 SWL USACE reservoirs

SWL reservoirs are located on tributaries to the White River. These reservoirs take 4–7 days to show an effect on the White River at Clarendon, AR. Clarendon reaches its peak flow on February 28 and has a 20% reservoir reduction effect. The flow from Greers Ferry takes approximately 4 days to reach the White River at Clarendon; however, Greers Ferry is only one of four major projects (Norfolk, Bull Shoals, Tablerock, and Greers Ferry) that affect flow on the White River. Regulation at each project can be influenced by the combined effect of these major projects.

Figure B-114 through Figure B-116 show the hydrographs for the reservoirs in SWL as well as the time it takes for their effects to reach the White River at Clarendon, AR.

Figure B-114. HYPO 58A routed through Bull Shoals Dam - ~7 days from Clarendon, AR.

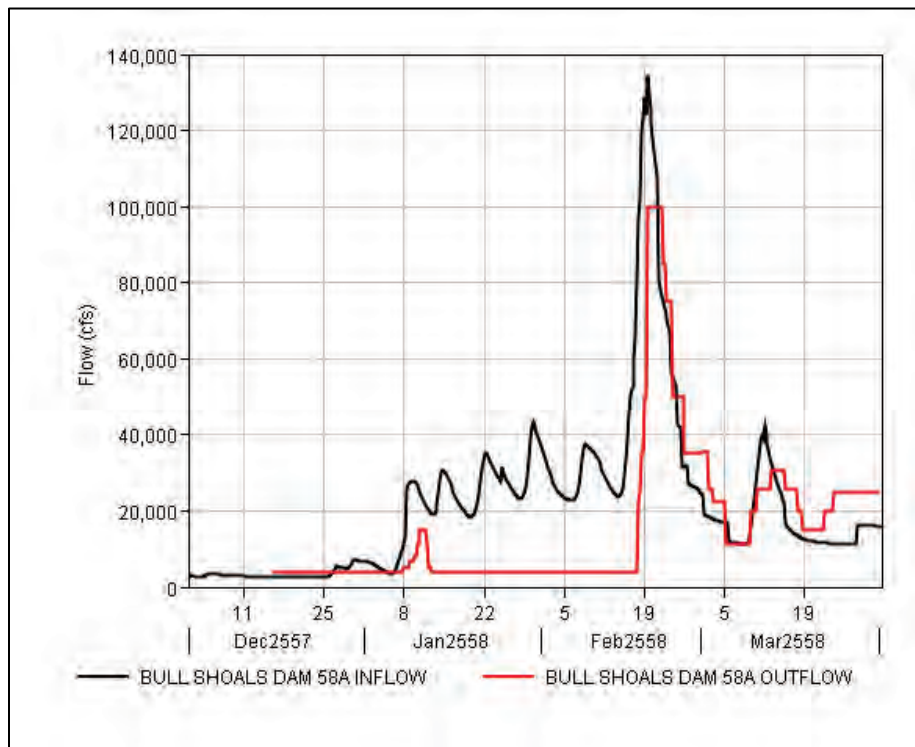


Figure B-115. HYPO 58A routed through Greers Ferry Dam - ~4 days from Clarendon, AR.

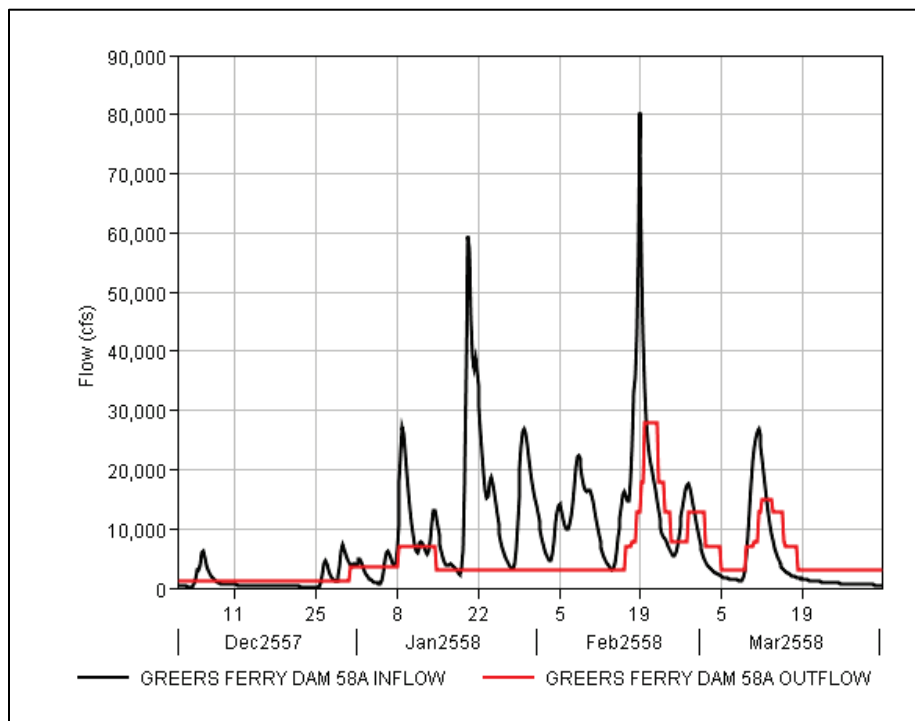
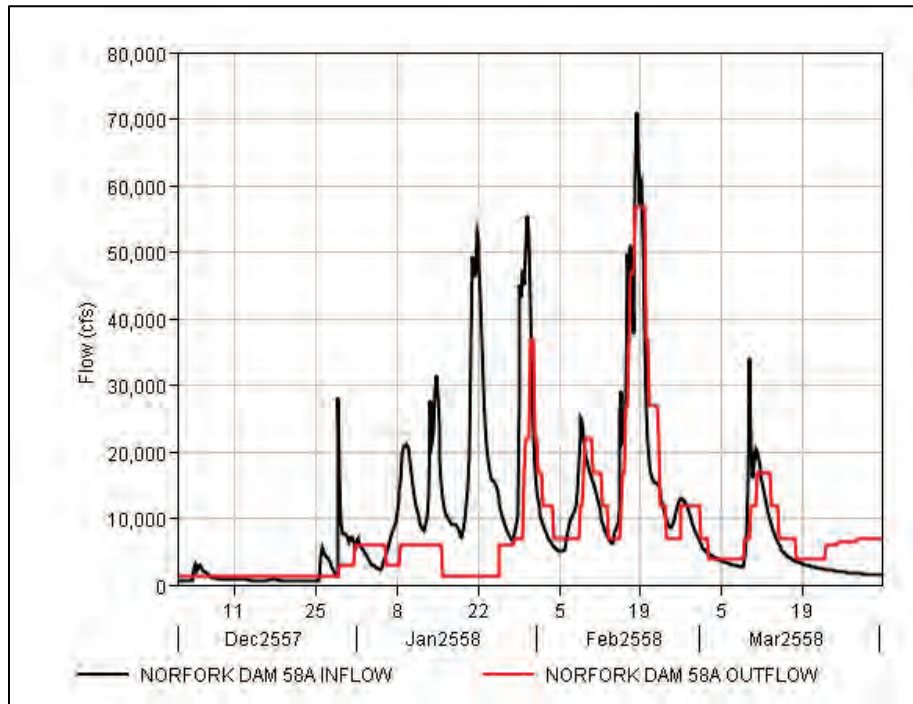


Figure B-116. HYPO 58A routed through Norfolk Dam - ~7 days from Clarendon, AR.



B.2.9 MVS USACE reservoirs

MVS reservoirs are located on tributaries to the Kaskaskia, Saint Francis, and Salt Rivers. The flows from these reservoirs take from 1 to 18 days to reach the Mississippi River. Carlyle Lake flows take approximately 2 days to reach the Mississippi River at Chester, IL.

Figure B-117 through Figure B-120 show the hydrographs for the reservoirs in MVS as well as the time it takes for their effects to reach the Mississippi River at the defined locations.

Figure B-117. HYPO 58A routed through Carlyle Lake Dam - ~2 days from Chester, IL.

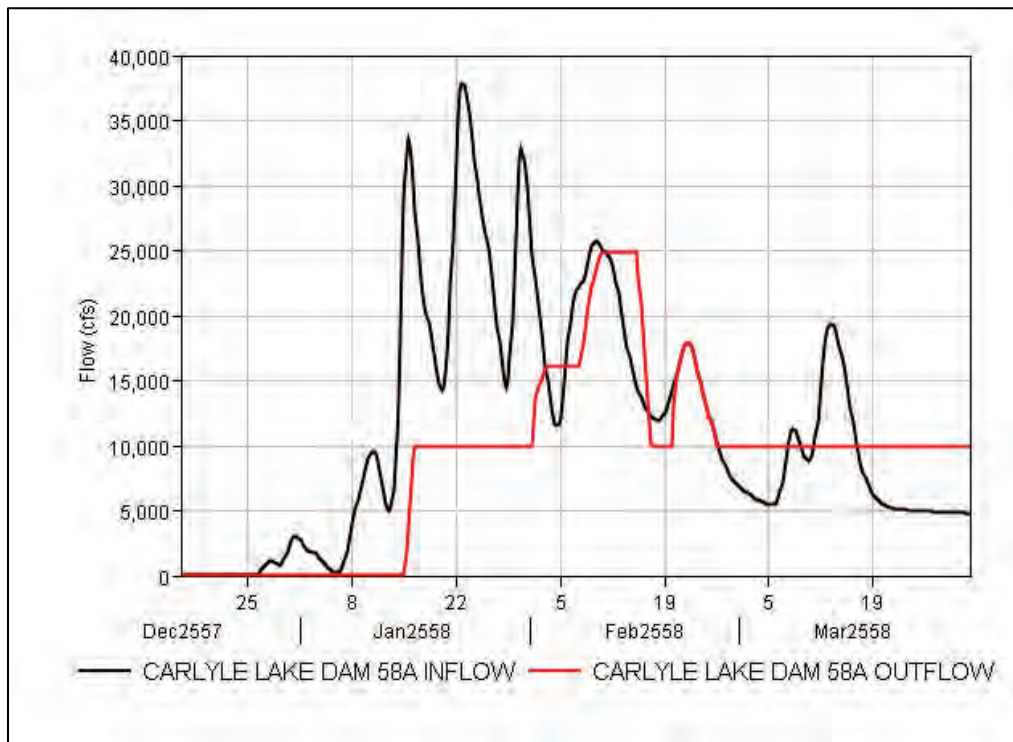


Figure B-118. HYPO 58A routed through Lake Shelbyville Dam - ~5 days from Chester, IL.

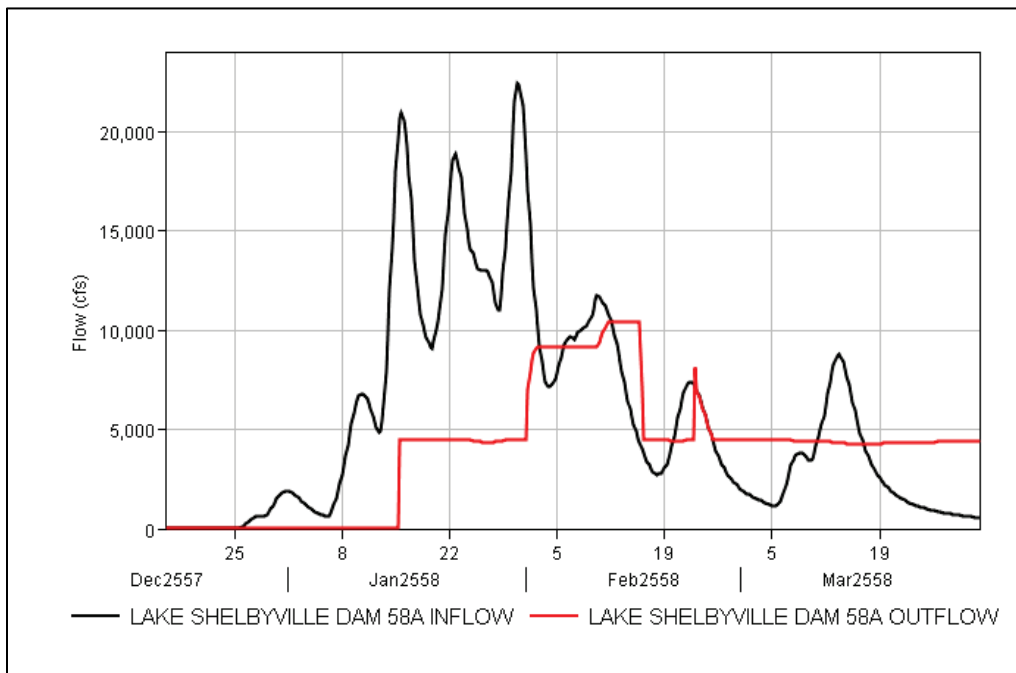


Figure B-119. HYPO 58A routed through Mark Twain Lake - ~2 days from Hermann, MO.

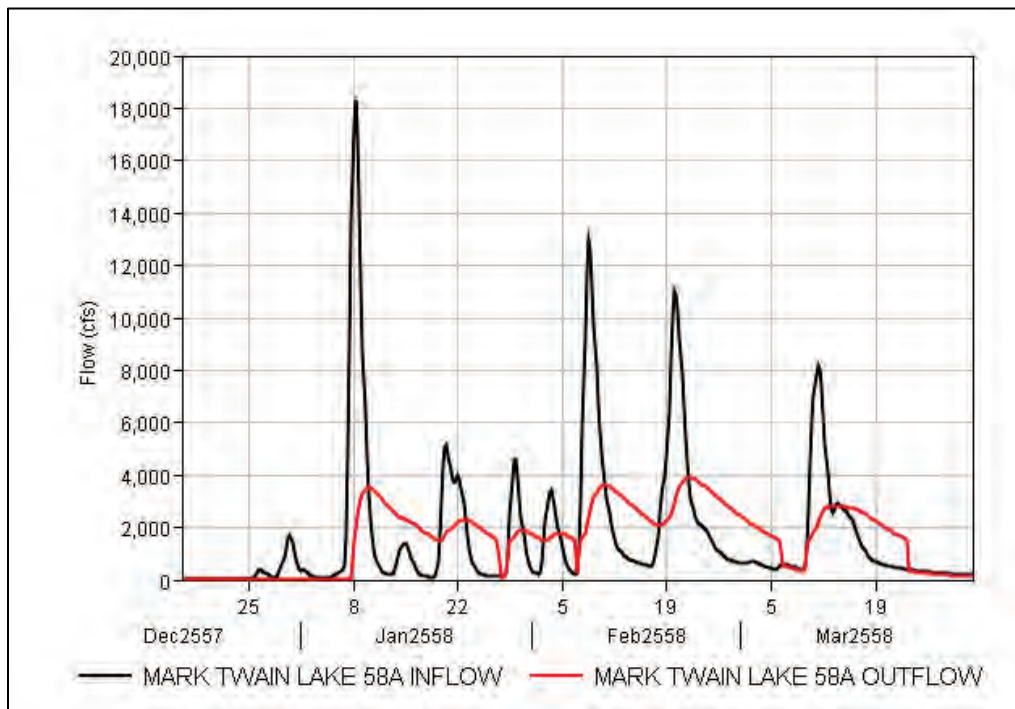
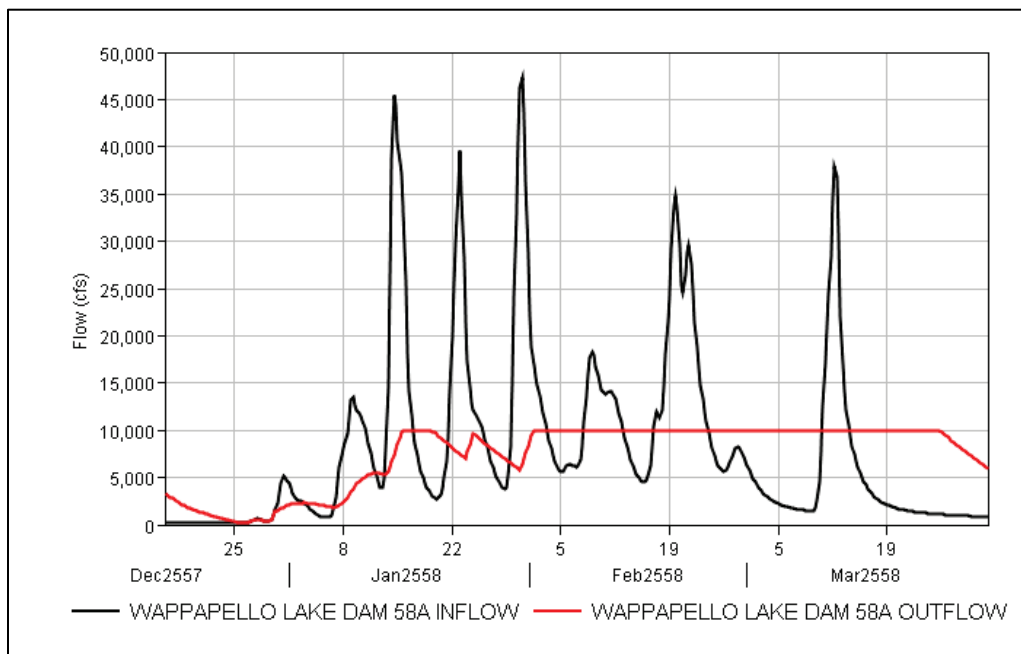


Figure B-120. HYPO 58A routed through Wappapello Lake - ~18 days from the confluence of the Saint Francis and Mississippi Rivers.



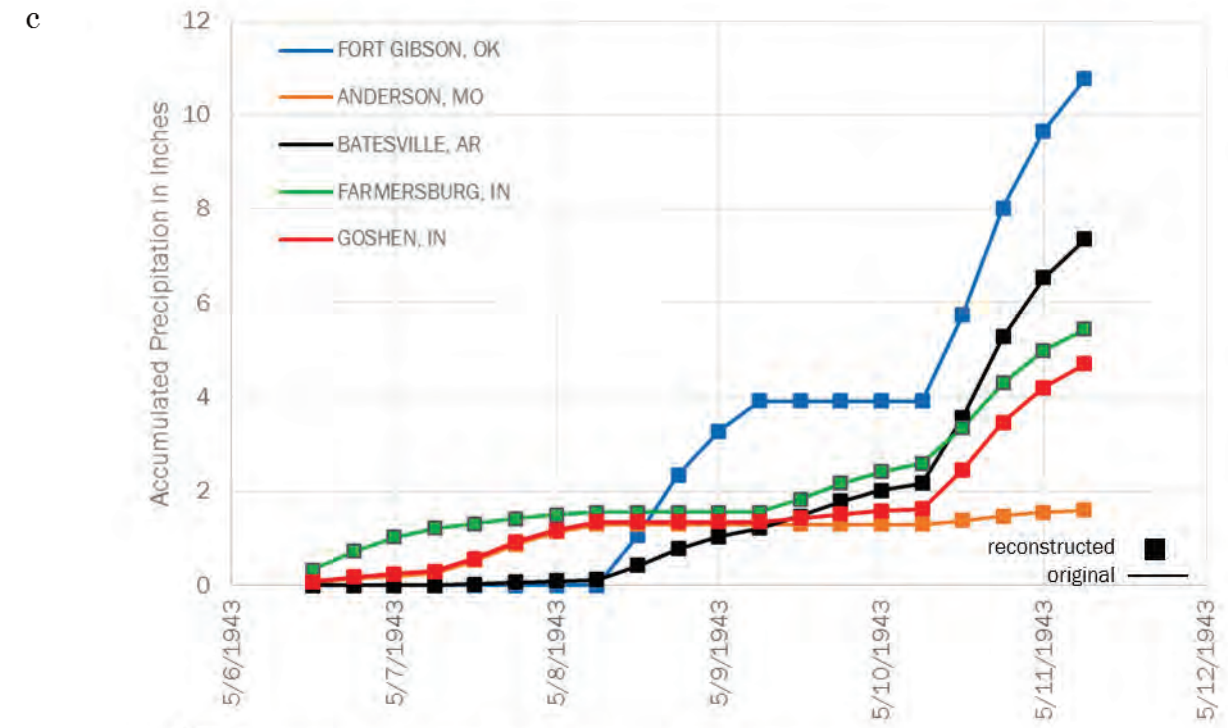
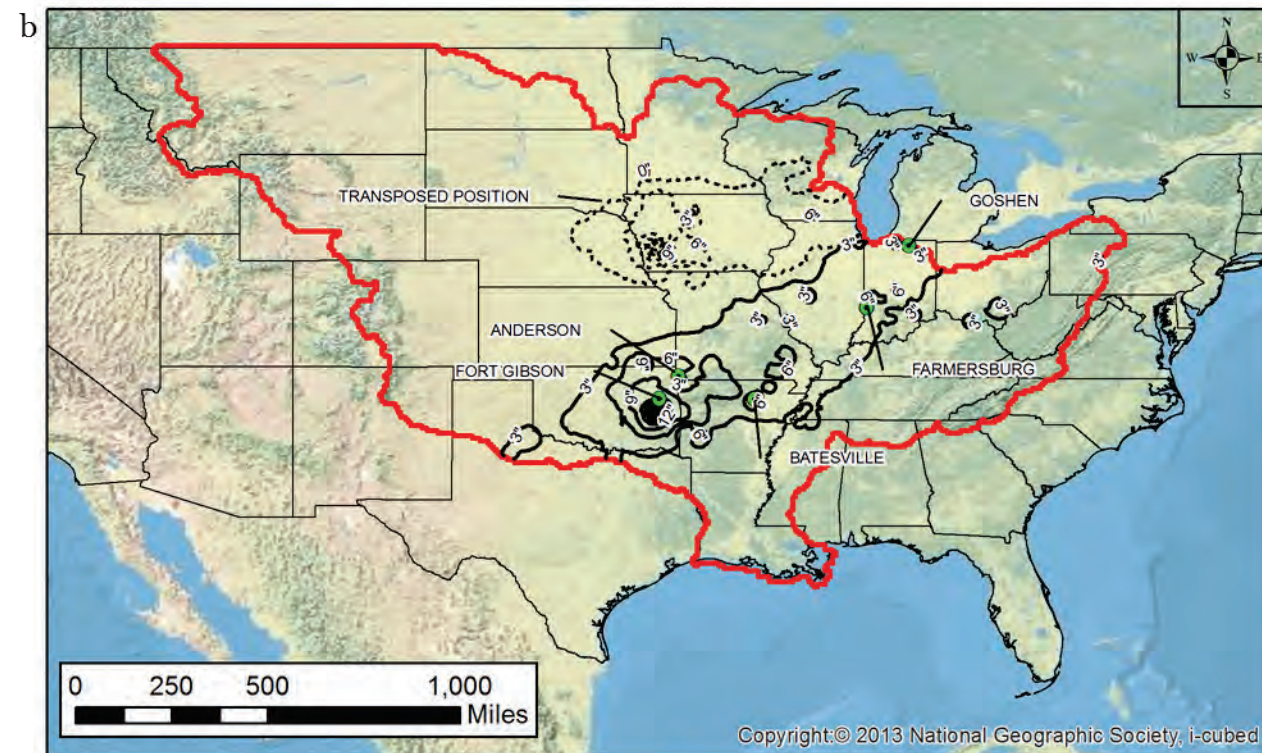
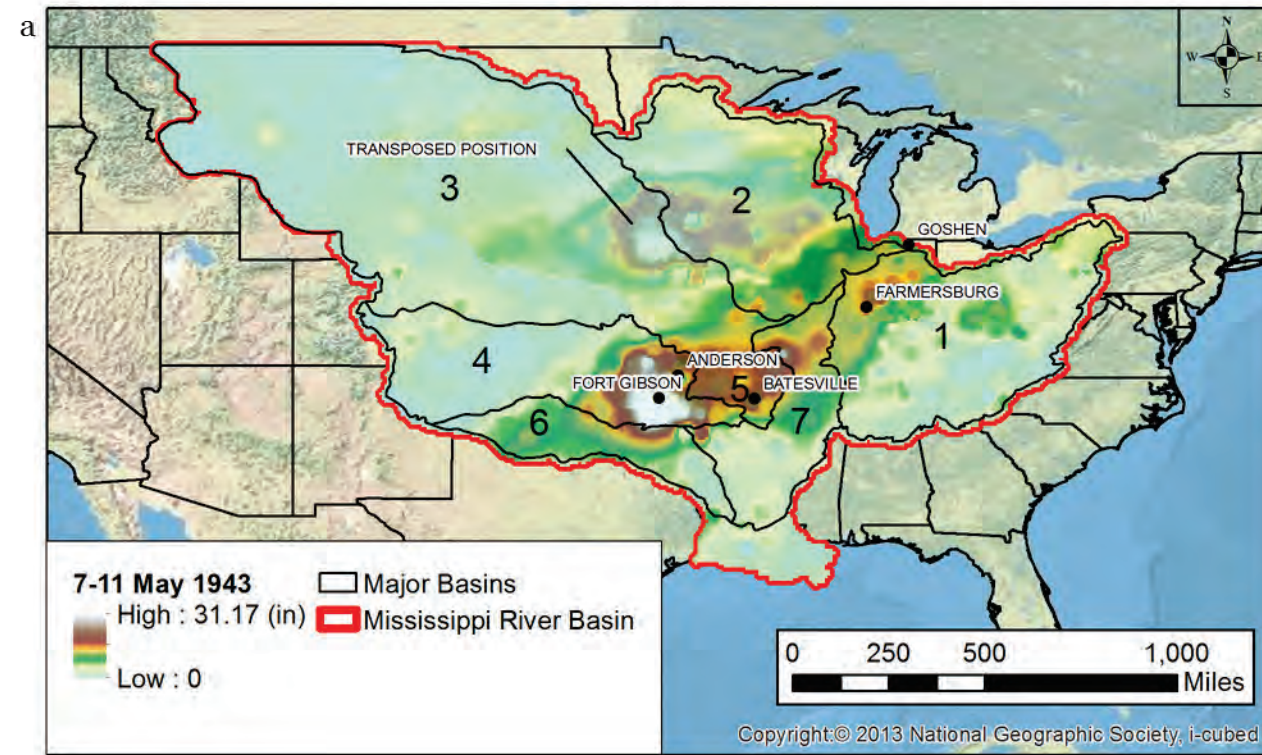
Appendix C: HYPO 52A

C.1 HYPO 52A storm precipitation

HYPO Storm 52A is comprised of three historical storm events centered over the Missouri, Upper Missouri, Arkansas, and Ohio River Basins. Two storms were applied as they actually occurred, and one was transposed and reduced 20%. The 2016 assessment used point rainfall data and IDW interpolation (with bias toward observed point values) to reconstruct the original 1955 storms data. Figure C-1 through Figure C-4 depict the total precipitation and coverage of each storm event that compiles HYPO 52A. Figure (a) in each of the figures depicts the reconstructed storm coverage of the event. Figure (b) depicts the isohyetal contours for the reconstructed storm event. Figure (c) looks at several locations and compares the original 1955 precipitation data against the processed inputs after they were converted to a raster by interpolation. Table (d) tabulates the 1955 values, the initial 2016 point data inputs, the interpolated 2016 grid inputs, and the inputs after transposition (if applicable). Each HYPO storm included a warm-up period to capture the snow pack that would have been lost otherwise. A recession period following the storm sequence was included to provide sufficient time to route the hydrograph peak downstream to the Gulf of Mexico. Figure C-4 shows the warm-up and recession period for HYPO 52A.

The 7–11 May 1943 storm did not have the gage data available to make a direct comparison with the gage locations used in the 1955 report, so the isohyetal map from the 1955 report was digitized to obtain the values at select locations. The deviation between the 1955 data and the 2016 data ranges from 0.34 in. to 8.27 in. After the data were processed and converted to an ASCII grid, all of the locations matched. The 15–20 May 1943 storm had the gage data needed to make a direct comparison with the gage locations used in the MRC (1955) report. At Kokomo, IN, the deviation between the 1955 event and the reconstructed storm event was 0.5 in. All other locations matched. After the data were converted to an ASCII grid, the values at each location matched with the reconstructed data.

Figure C-1. HYPO 52A – 7–11 May 1943 (a) (top left) storm coverage over the Mississippi River Basin; (b) (bottom left) isohyetal for storm; (c) (top right) comparison of mass rainfall curves for original point precipitation data versus the processed/ interpolated precipitation data; and (d) (bottom right) comparison of 1955 precipitation, 2016 precipitation, 2016 processed precipitation, and transposed values at select locations.



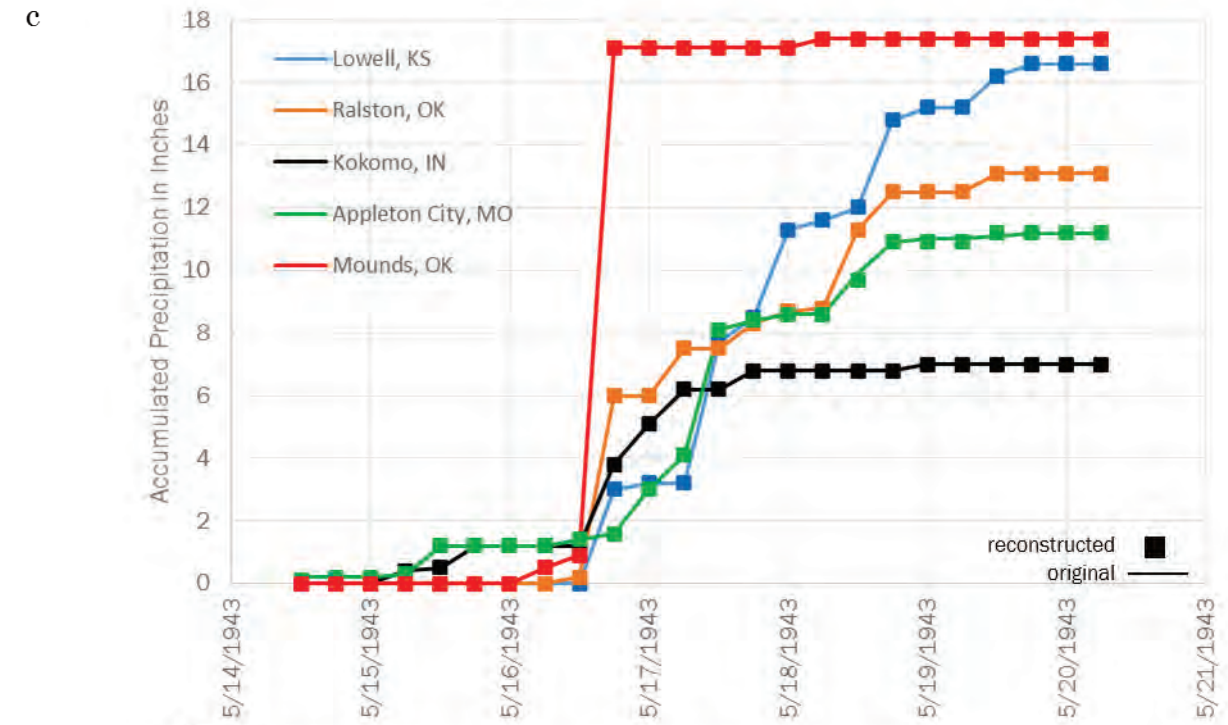
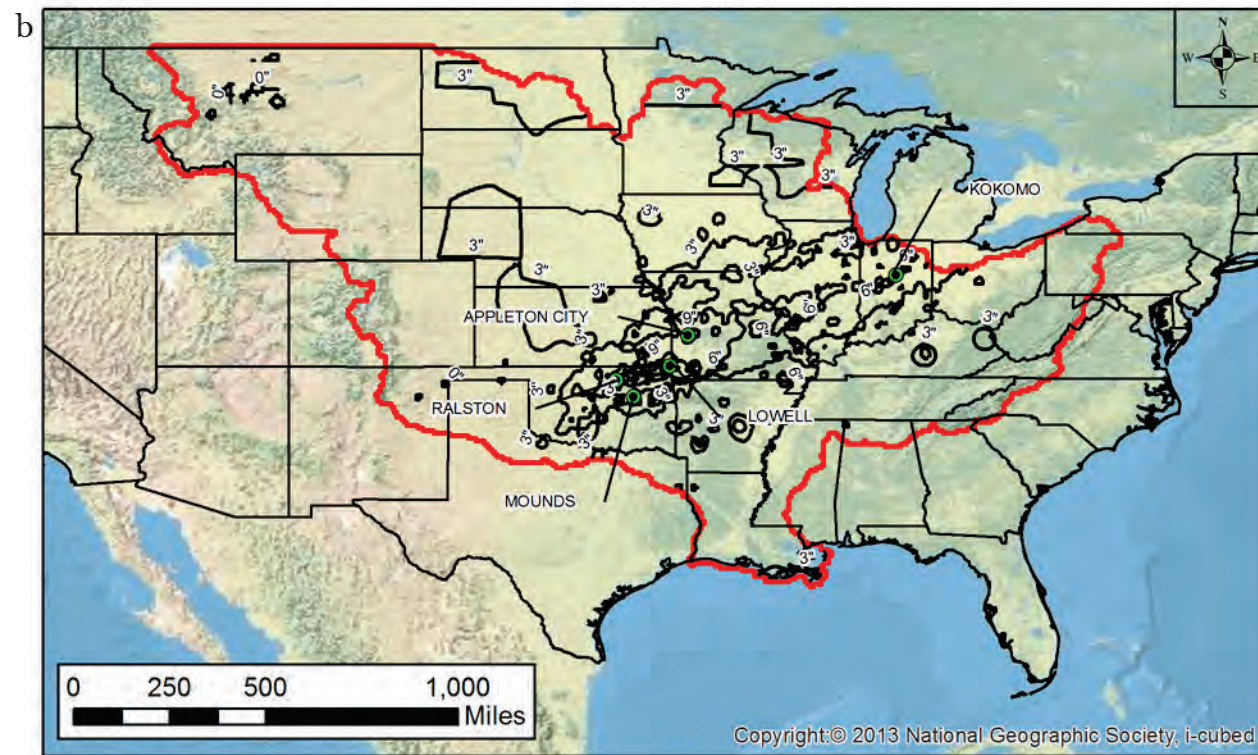
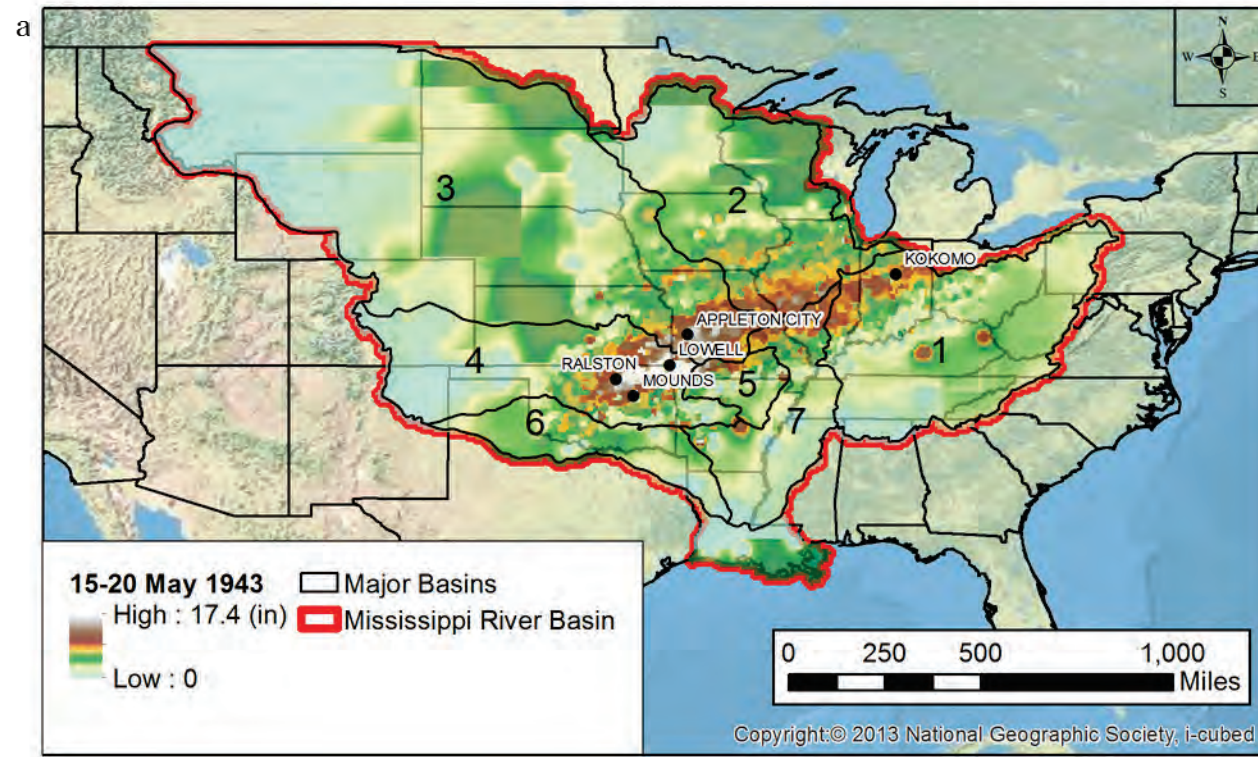
Notes:
 Reconstructed cumulative precipitation data is represented by square symbols.
 Original cumulative precipitation data is represented by a solid line.

d

Location	7-11 May 1943 SW2-20 Precipitation ²			
	1955 ¹	2016	2016 Reconstructed	2016 Reconstructed and Transposed
Fort Gibson, OK	13.00	10.76	10.76	10.05
Anderson, MO	9.87	1.60	1.60	6.94
Batesville, AR	7.02	7.36	7.36	6.36
Farmersburg, IN	5.00	5.45	5.45	na
Goshen, IN	3.81	4.71	4.71	na

Notes:
 1 = Derived by digitizing the 1955 isohyet map and interpolating to obtain values.
 2 = Values are compared against the original values, not the 20% reduction.

Figure C-2. HYPO 52A - 15-20 May 1943 (a) (top left) storm coverage over the Mississippi River Basin; (b) (bottom left) isohyetal for storm; (c) (top right) comparison of mass rainfall curves for original point precipitation data versus the processed/ interpolated precipitation data; and (d) (bottom right) comparison of 1955 precipitation, 2016 precipitation, and 2016 processed precipitation.

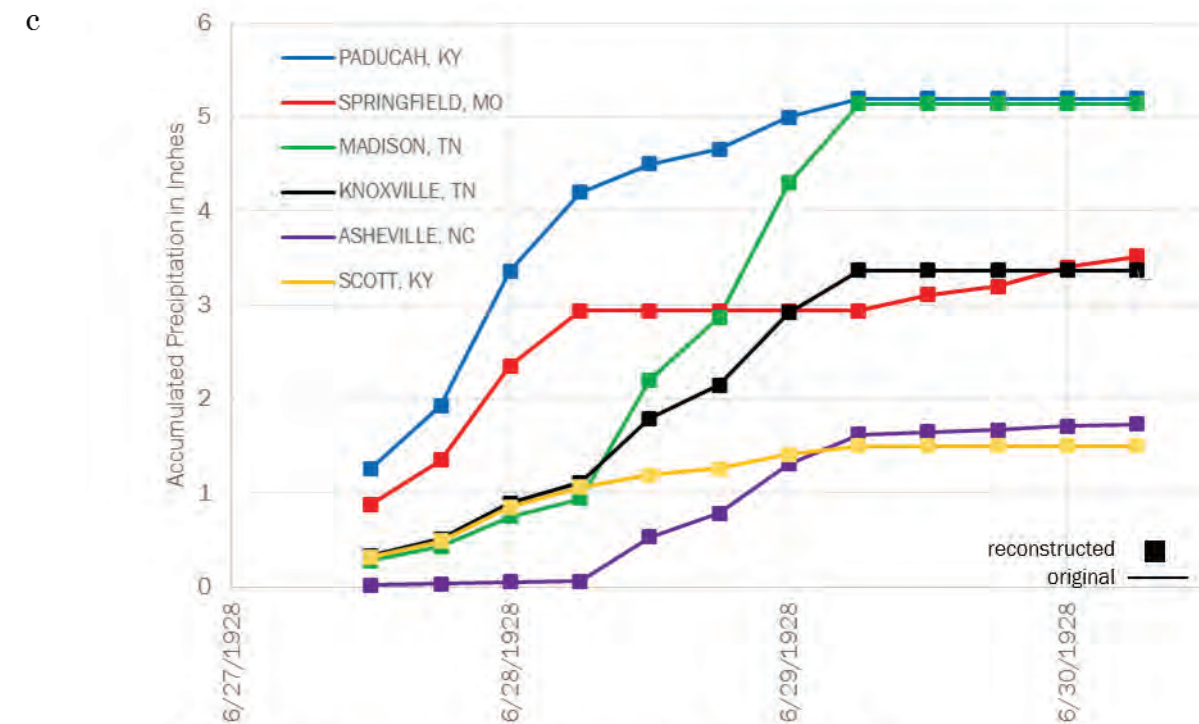
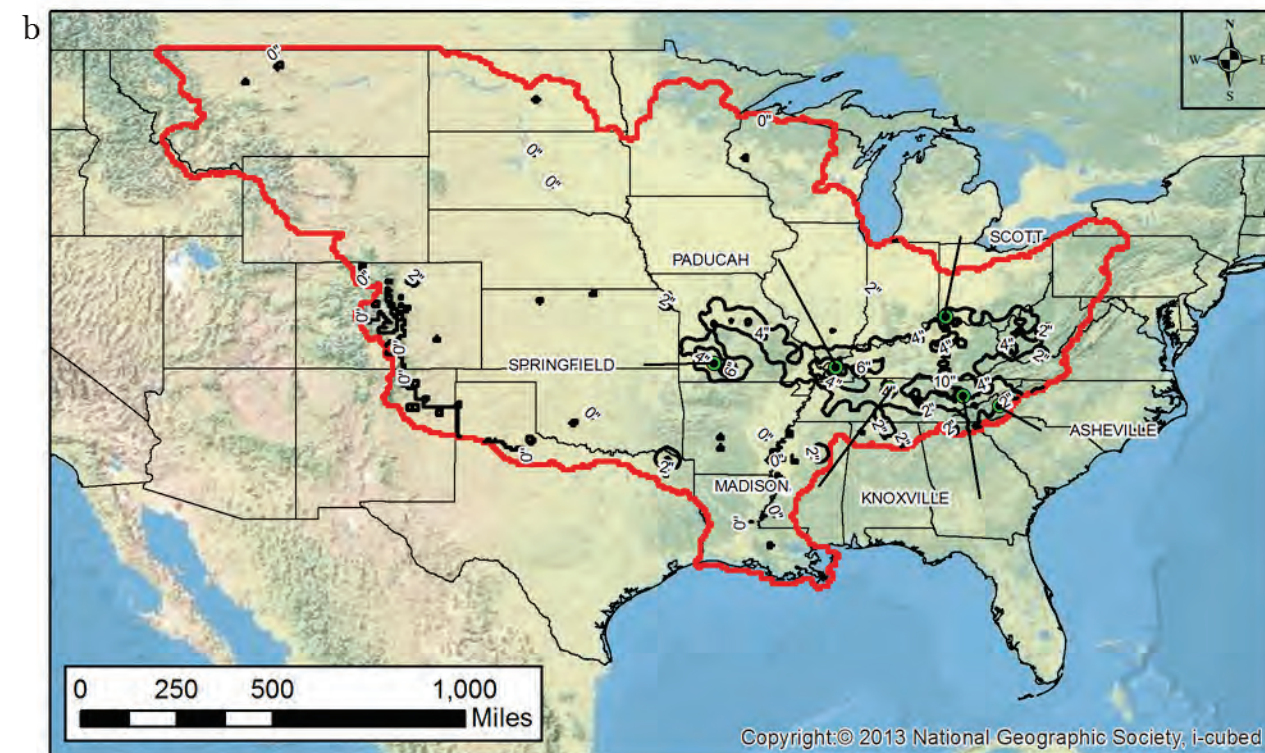
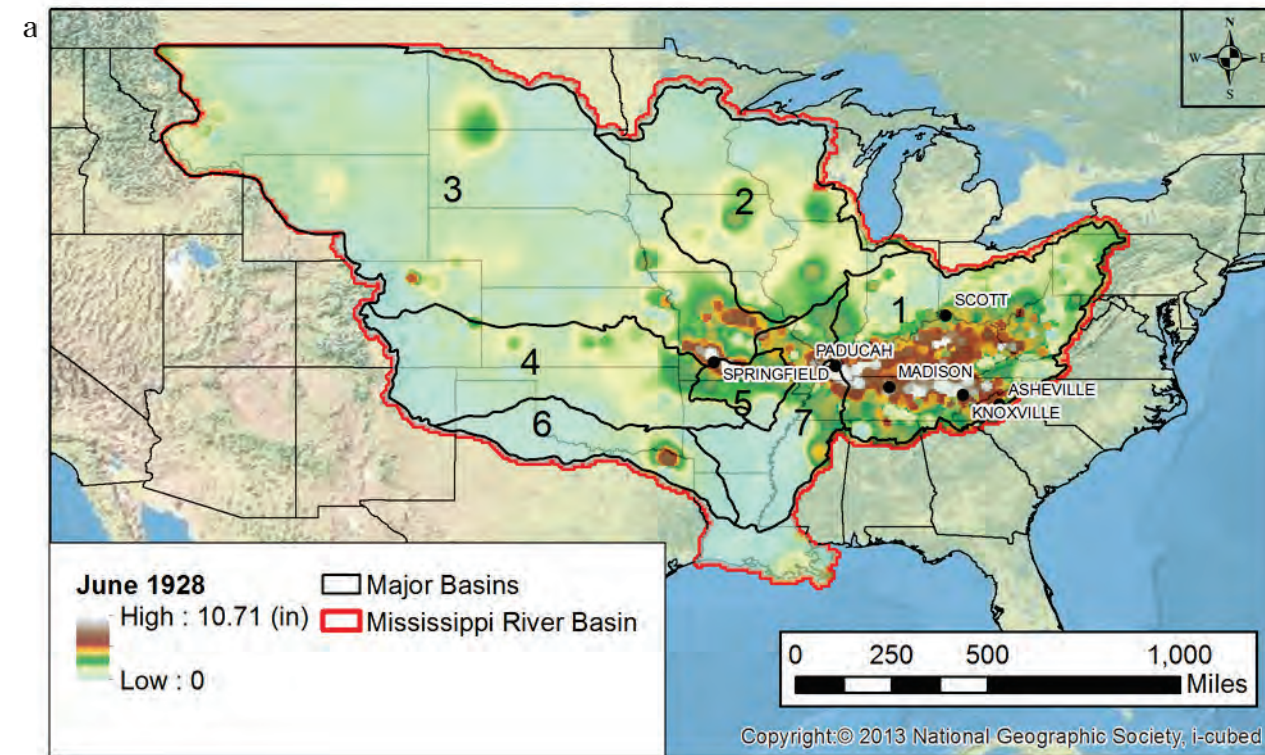


Notes:
 Reconstructed cumulative precipitation data is represented by square symbols.
 Original cumulative precipitation data is represented by a solid line.

d

Location	15-20 May 1943 SW2-21 Precipitation		
	1955	2016	2016 Reconstructed
Lowell, KS	16.5	16.6	16.6
Ralston, OK	13.1	13.1	13.1
Kokomo, IN	7.5	7.0	7.0
Appleton City, MO	11.2	11.2	11.2
Mounds, OK	17+	17.4	17.4

Figure C-3. HYPO 52A – 28–30 June 1928 Figure HYPO 52A – 28–30 June 1928 Figure 4 41 HYPO 52A – 28–30 June 1928 (a) (top left) storm coverage over the Mississippi River Basin; (b) (bottom left) isohyetal for storm; (c) (top right) comparison of mass rainfall curves for original point precipitation data versus the processed/ interpolated precipitation data; and (d) (bottom right) comparison of 1955 precipitation, 2016 precipitation, and 2016 processed precipitation.



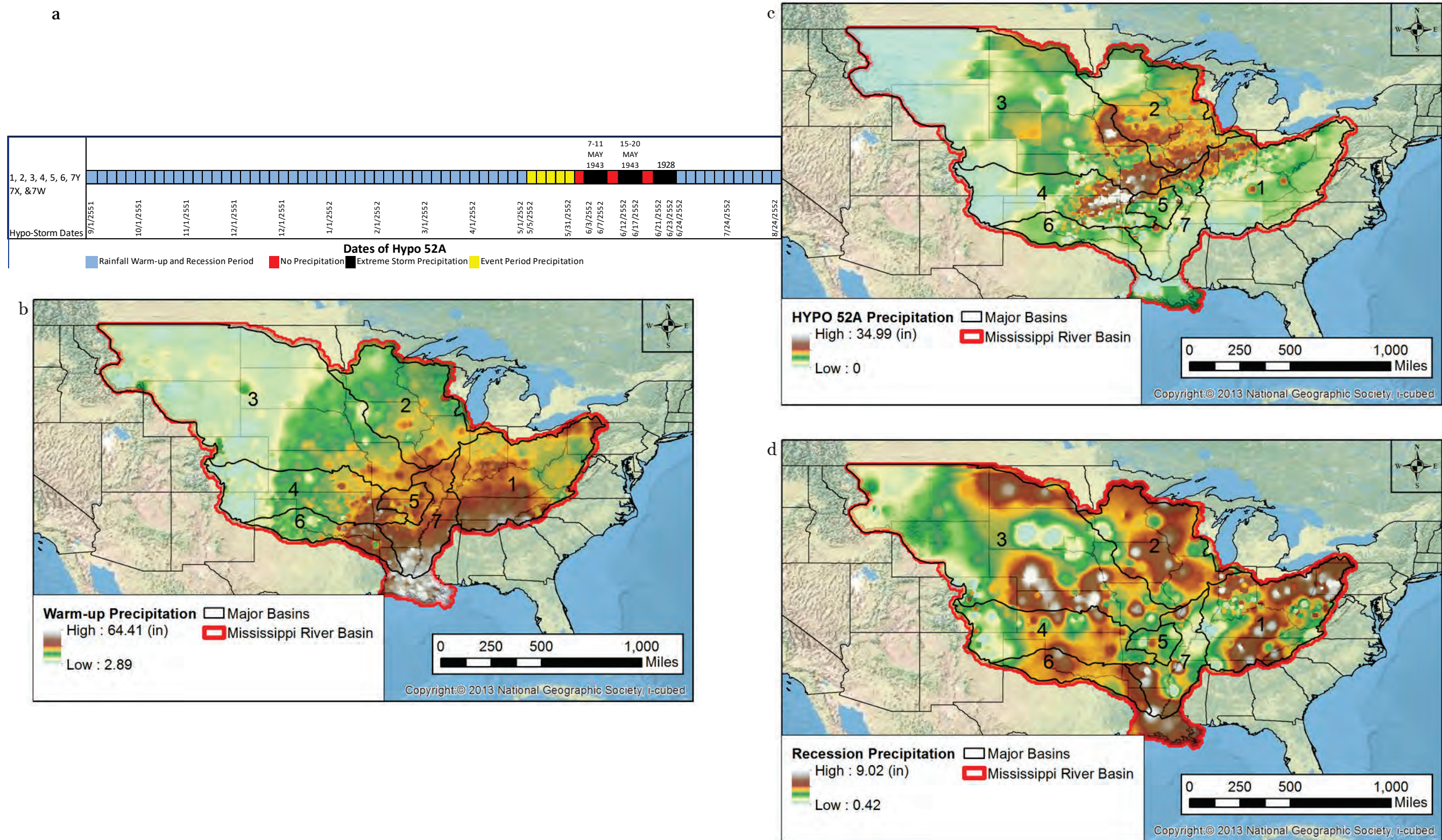
Notes:
 Reconstructed cumulative precipitation data is represented by square symbols.
 Original cumulative precipitation data is represented by a solid line.

d

Location	28-30 June 1928 Precipitation		
	1955 ¹	2016	2016 Reconstructed
Paducah, KY	4.72	5.20	5.20
Springfield, MO	3.92	3.52	3.52
Madison, TN	4.08	5.14	5.14
Knoxville, TN	10.00	3.37	3.37
Asheville, NC	2.85	1.73	1.73
Scott, KY	2.00	1.50	1.50

Notes:
 1 = Derived by digitizing the 1955 isohyet map and interpolating to obtain values.

Figure C-4. HYPO 52A (a) (top left) storm sequencing with warm-up and recession periods; (b) (bottom left) warm-up precipitation coverage over the Mississippi River Basin; (c) (top right) 1943 AND 1928 combined storm coverage over the Mississippi River Basin; and (d) (bottom right) recession precipitation coverage over the Mississippi River Basin.



The June 1928 storm did not have any gage locations available to make a direct comparison to the gage locations in the 1955 report, so the 1955 isohyetal map was digitized and interpolated to estimate the 1955 precipitation values. The tabular data show that the original 1955 values deviate from the regenerated 2016 data by 0.4 in. to 6.63 in. After the regenerated data were processed and converted to an ASCII grid, all of the locations matched with regenerated point precipitation inputs.

C.1.1 Depth area relationships

To further validate the precipitation inputs developed by interpolation, depth-area relationships were generated using ArcGIS. Isohyetal maps for each original storm event were georeferenced, digitized in ArcMap, converted from a polyline to a TIN, converted from a TIN to a raster, and projected with USA Contiguous Albers Equal Area Conic to obtain an equal area grid size of 2,000 m × 2,000 m. For the total original HYPO storm comparisons, the projected rasters were then aggregated with the mosaic tool. The interpolated rainfall grids were clipped to the spatial extent of each original HYPO storm or to the original individual storm events. With equal area grids, a zonal histogram was generated that compares a defined precipitation interval against area. These zonal histograms were exported to excel to plot against each other.

Figure C-5 through Figure C-12 show the depth-area curves for the entire storm total precipitation over the Mississippi River Basin, as well as the totals falling over each of the seven major sub-basins (excluding Drainage Basin 6, where 1955 rainfall coverage did not exist).

Figure C-5. Depth-area curves for 1955 and 2016 individual storms comprising HYPO 52A.

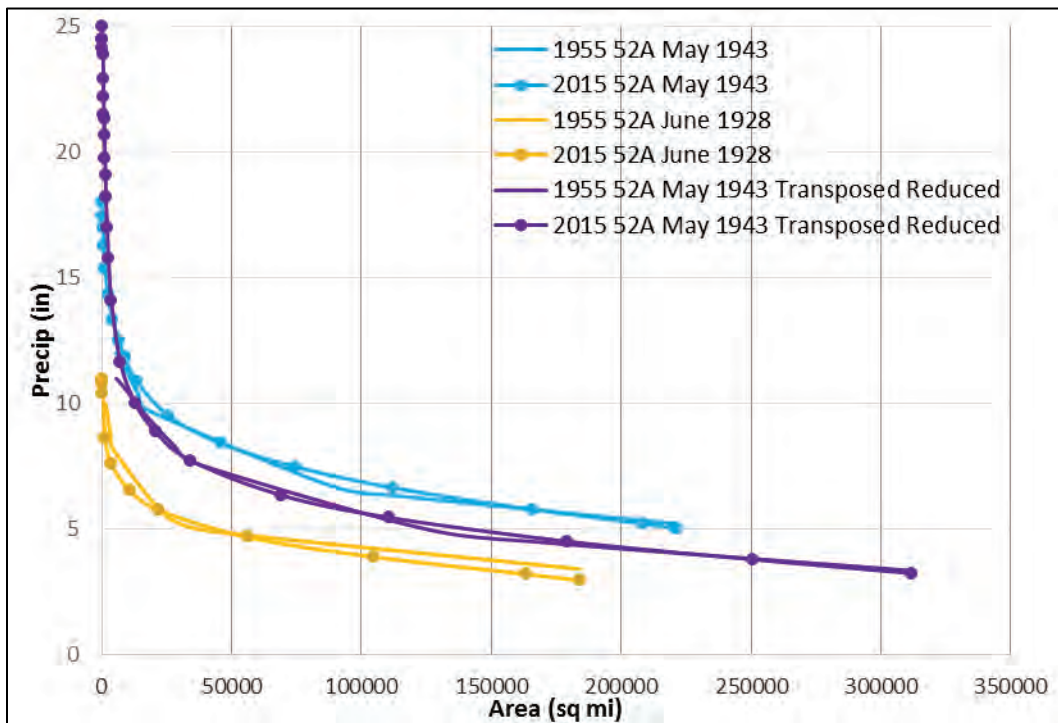


Figure C-6. Depth-area curves for 1955 and 2016 total HYPO 52A event.

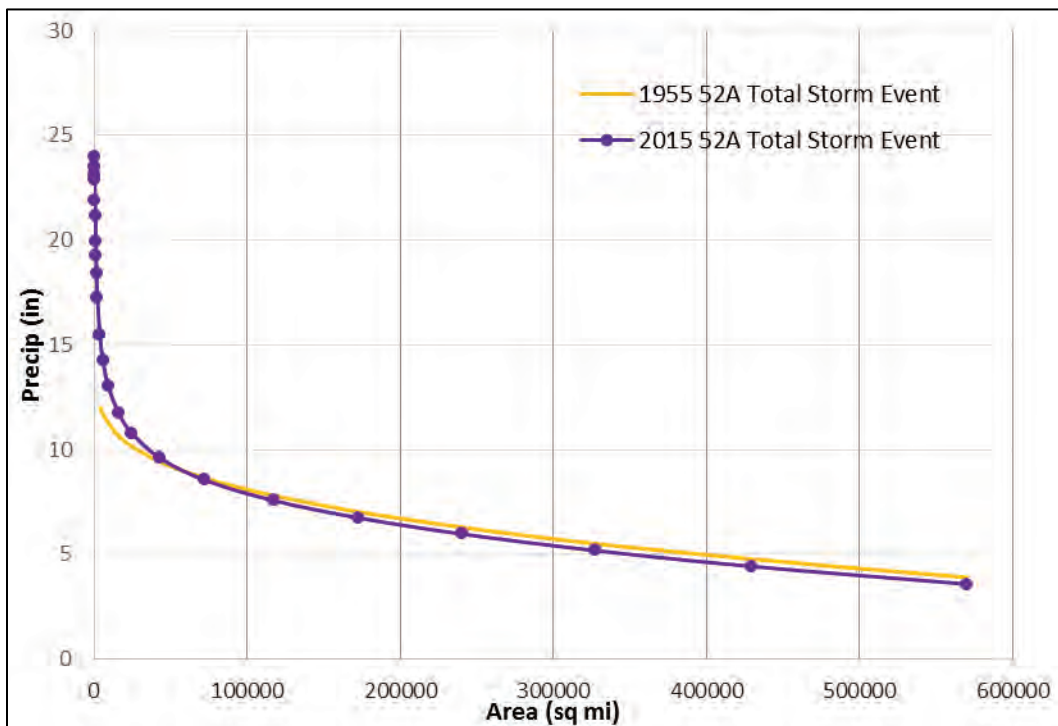


Figure C-7. Depth-area curve for 1955 and 2015 individual storm events comprising HYP0 52A over Drainage Basin 1.

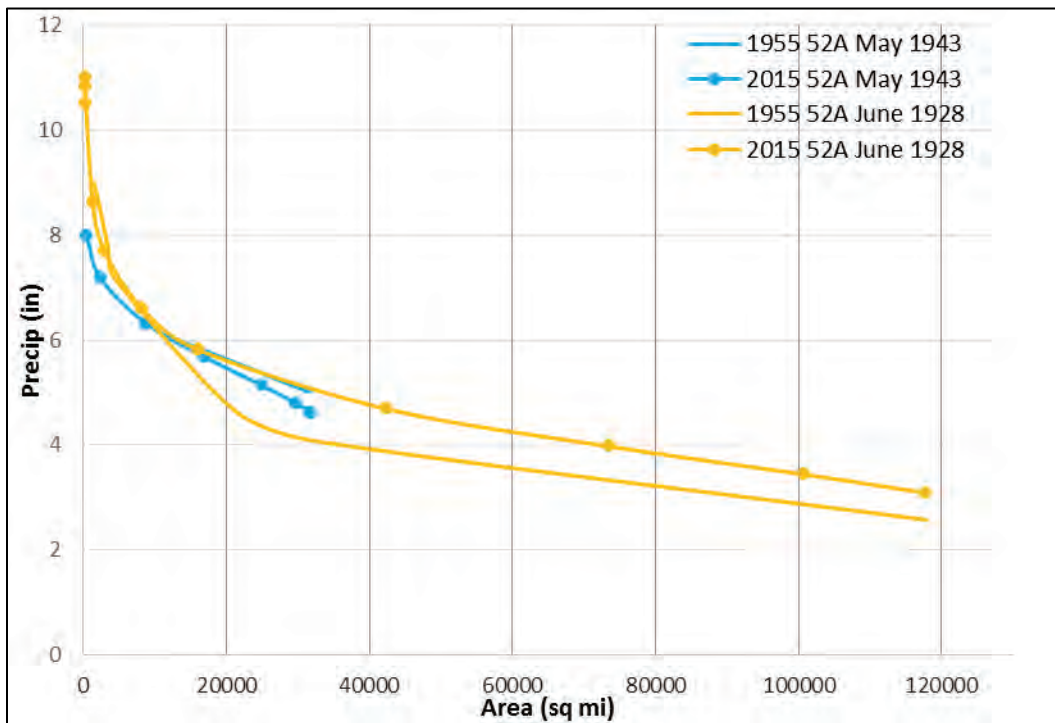


Figure C-8. Depth-area curve for 1955 and 2015 individual storm events comprising HYP0 52A over Drainage Basin 2.

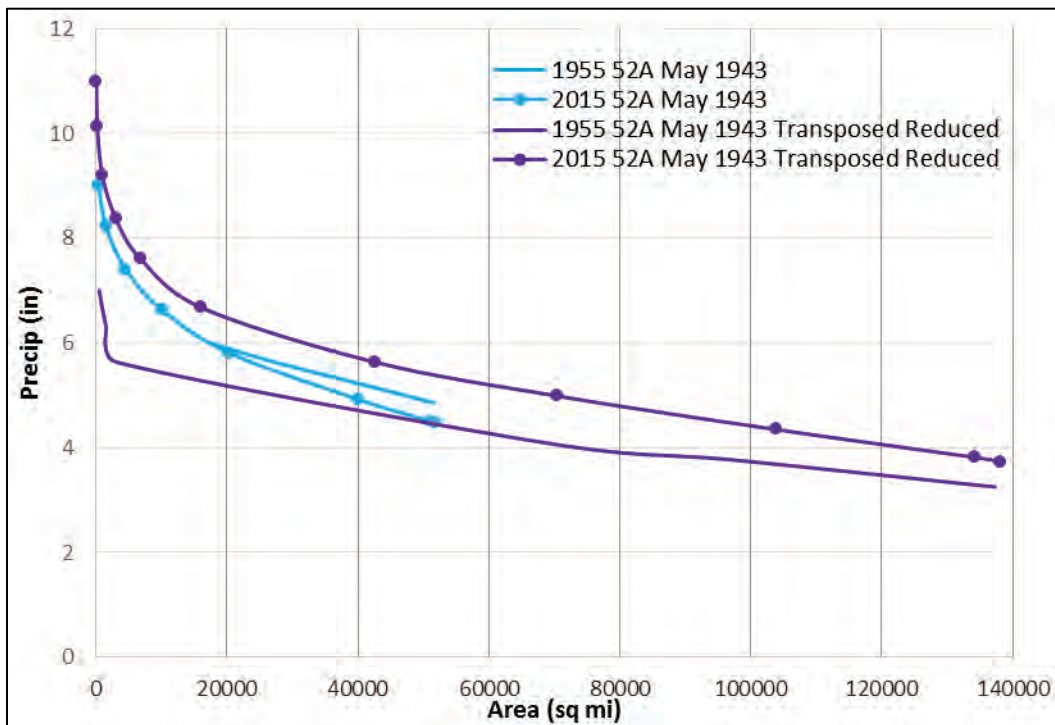


Figure C-9. Depth-area curve for 1955 and 2015 individual storm events comprising HYPO 52A over Drainage Basin 3.

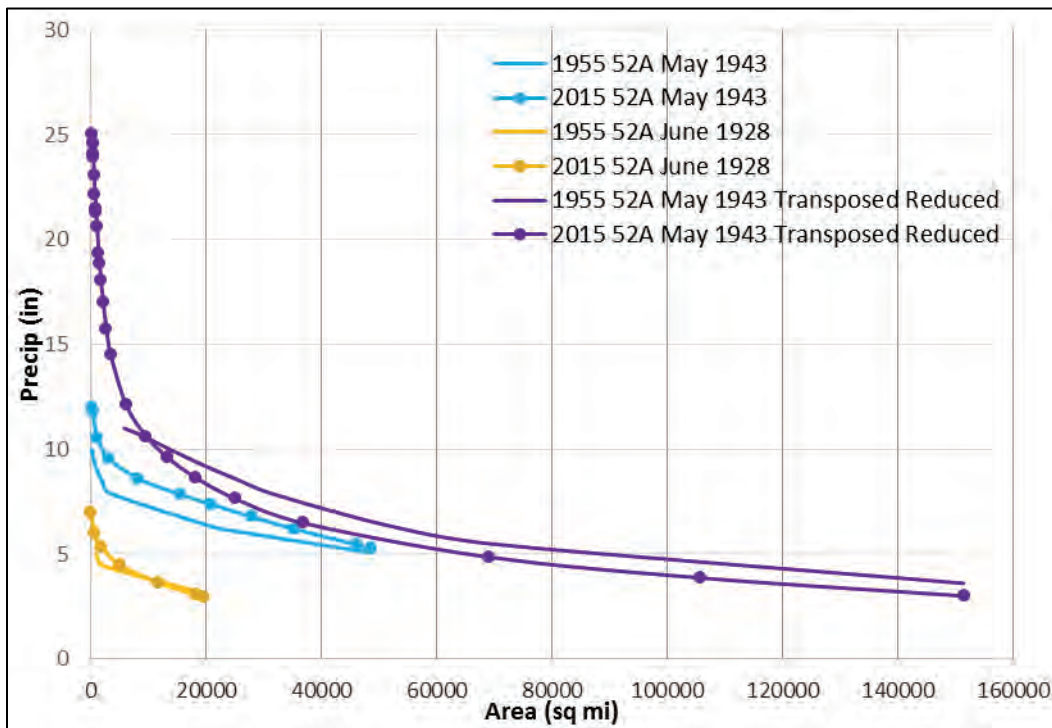


Figure C-10. Depth-area curve for 1955 and 2015 individual storm events comprising HYPO 52A over Drainage Basin 4.

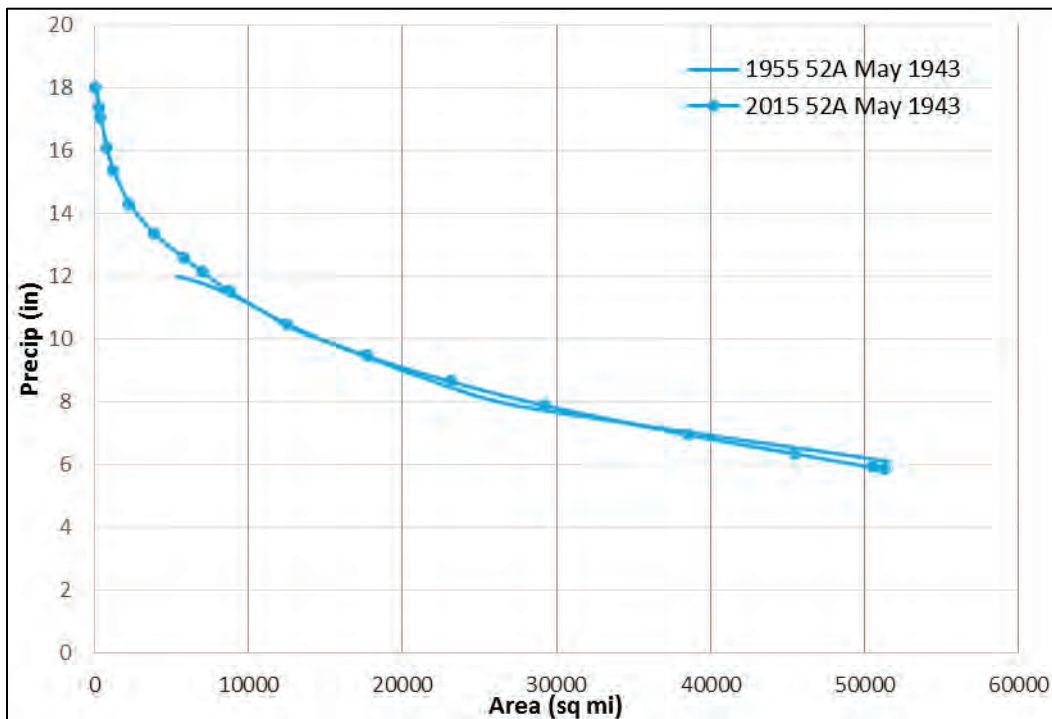


Figure C-11. Depth-Area Curve for 1955 and 2015 individual storm events comprising HYPO 52A over Drainage Basin 5.

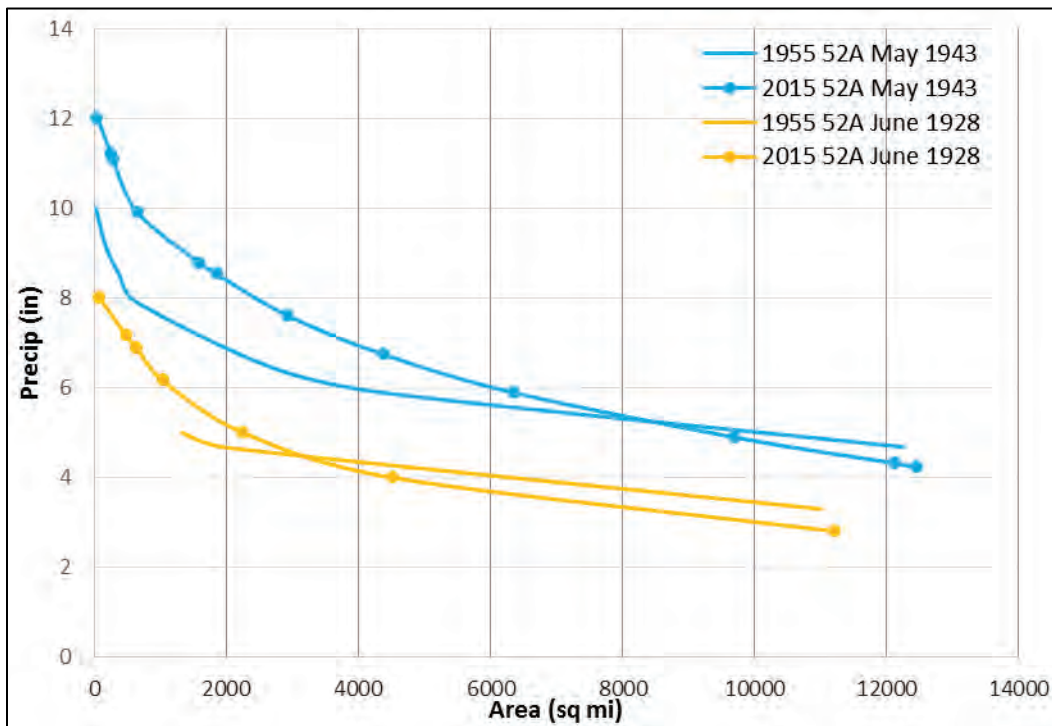
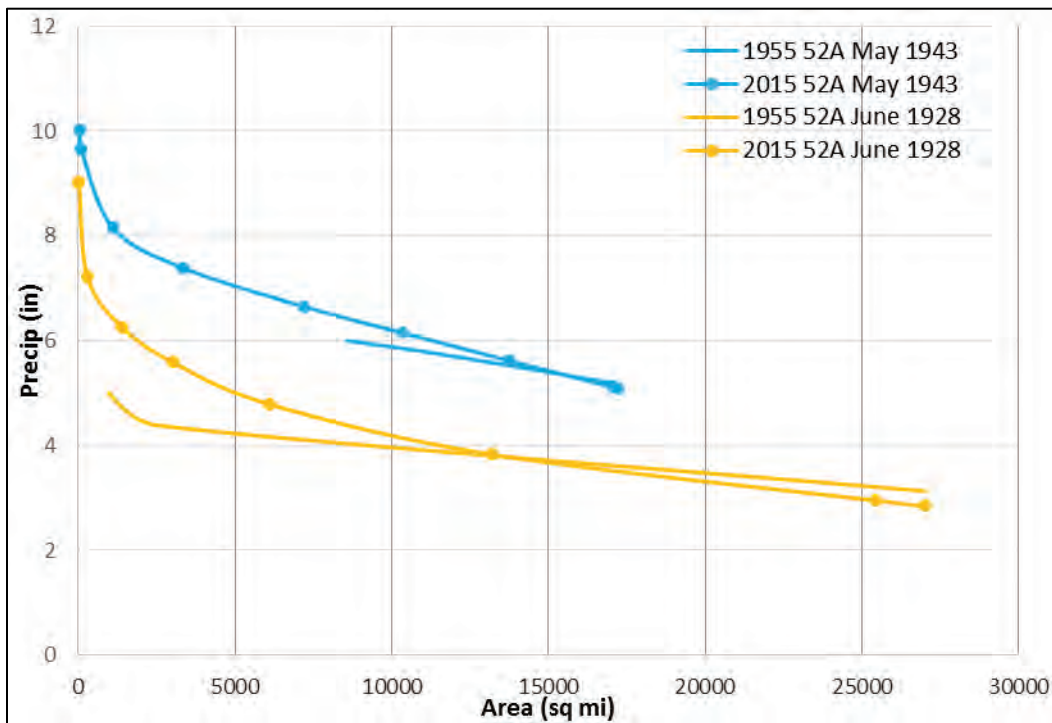


Figure C-12. Depth-area curve for 1955 and 2015 individual storm events comprising HYPO 52A over Drainage Basin 7.



Overall, the depth-area curves for 2016 precipitation inputs matched the previous 1955 rainfall maps. There were variations across each of the seven major sub-basins where 2016 depth-area curves were higher or lower than 1955 depth-area curves, but these deviations were compensated over the entire storm basin for each storm event and for the HYPO 52A storm event.

C.1.2 Hydrograph comparisons

Table C-1 provides a comparison of 1-day (labeled as peak), 3-day, 15-day, and 30-day volumes for HYPO 52A hydrographs. Values for the 1955 hydrographs are labeled 52A and 52A-EN for unregulated and regulated flows, respectively. Values computed for the 2016 hydrographs are labeled 52A-U and 52A-R for unregulated and regulated flows, respectively. The flow and volume comparisons do not show agreement between the unregulated or regulated values; for instance, Cairo, IL, unregulated values are 2,586 kcfs for 1955 and 1,555 kcfs for 2016. Regulated values at Cairo are 2,171 kcfs for 1955 and 1,353 kcfs for 2016. The 2016 values are drastically lower than the 1955, but the cumulative precipitation curves show that the 1955 inputs match relatively well with the 2016 inputs with a few locations being lower than the digitized isohyet values for the 1955 storms. The reason for the values being drastically lower in the 2016 analysis is unknown; this storm was not used to validate the methodology for HYPO 52A.

1

2

Table C-1. Hydrograph volume and shape comparisons for HYPO 52A.

	Storm	Peak Flow	Peak Flow Date	3 Days				15 Days				30 days			
				Start	End	Volume	Mean	Start	End	Volume	Mean	Start	End	Volume	Mean
St. Louis	52A-R	1,095	18-Jun	17-Jun	19-Jun	3,246	1,082	13-Jun	27-Jun	12,884	859	10-Jun	9-Jul	19,978	666
	52A-EN	1,597	18-Jun	17-Jun	19-Jun	4,691	1,564	12-Jun	26-Jun	17,259	1,151	2-Jun	1-Jul	23,395	780
	52A-U	1,125	19-Jun	18-Jun	20-Jun	3,362	1,121	13-Jun	27-Jun	13,925	928	9-Jun	8-Jul	20,232	674
	52A	1,917	18-Jun	17-Jun	19-Jun	5,652	1,884	12-Jun	26-Jun	21,025	1,402	2-Jun	1-Jul	28,419	947
Cairo	52A-R	1,353	26-Jun	24-Jun	26-Jun	4,028	1,343	17-Jun	1-Jul	17,847	1,190	12-Jun	11-Jul	29,067	969
	52A-EN	2,171	20-Jun	19-Jun	21-Jun	6,428	2,143	14-Jun	28-Jun	24,884	1,659	3-Jun	2-Jul	37,208	1,240
	52A-U	1,555	26-Jun	25-Jun	27-Jun	4,543	1,514	17-Jun	1-Jul	18,960	1,264	12-Jun	11-Jul	29,358	979
	52A	2,586	20-Jun	19-Jun	21-Jun	7,667	2,556	14-Jun	28-Jun	30,539	2,036	3-Jun	2-Jul	44,148	1,472
Arkansas City	52A-R	1,498	29-Jun	27-Jun	29-Jun	4,468	1,489	24-Jun	8-Jul	21,396	1,426	18-Jun	17-Jul	35,965	1,199
	52A-EN	2,115	27-Jun	26-Jun	28-Jun	6,320	2,107	21-Jun	5-Jul	28,445	1,896	11-Jun	10-Jul	46,235	1,541
	52A-U	1,516	28-Jun	27-Jun	29-Jun	4,515	1,505	24-Jun	8-Jul	21,593	1,440	17-Jun	16-Jul	35,696	1,190
	52A	2,555	27-Jun	26-Jun	28-Jun	7,630	2,543	21-Jun	5-Jul	34,345	2,290	11-Jun	10-Jul	53,743	1,791
Latitude of Red River Landing	52A-R	1,447	8-Jul	6-Jul	8-Jul	4,335	1,445	30-Jun	14-Jul	20,876	1,392	22-Jun	21-Jul	36,329	1,211
	52A-EN	1,933	3-Jul	2-Jul	4-Jul	5,791	1,930	28-Jun	12-Jul	27,625	1,842	17-Jun	16-Jul	48,649	1,622
	52A-U	1,452	9-Jul	8-Jul	10-Jul	4,349	1,450	29-Jun	13-Jul	21,041	1,403	21-Jun	20-Jul	36,098	1,203
	52A	2,304	3-Jul	2-Jul	4-Jul	6,817	2,272	28-Jun	12-Jul	32,390	2,159	17-Jun	16-Jul	54,923	1,831

3

C.2 HEC-RAS inflow boundary discharge hydrographs

The hydrologic modeling produced discharge hydrographs at the same key locations used in the 1955 Study. Plots of unregulated (U) and regulated (EN) model simulations are presented in Figure C-13 C13 through Figure C-25 C-25. Unregulated hydrographs are shown in red, and regulated hydrographs are shown in blue.

Figure C-13. HYPO 52A hydrographs: Missouri River at Hermann, MO.

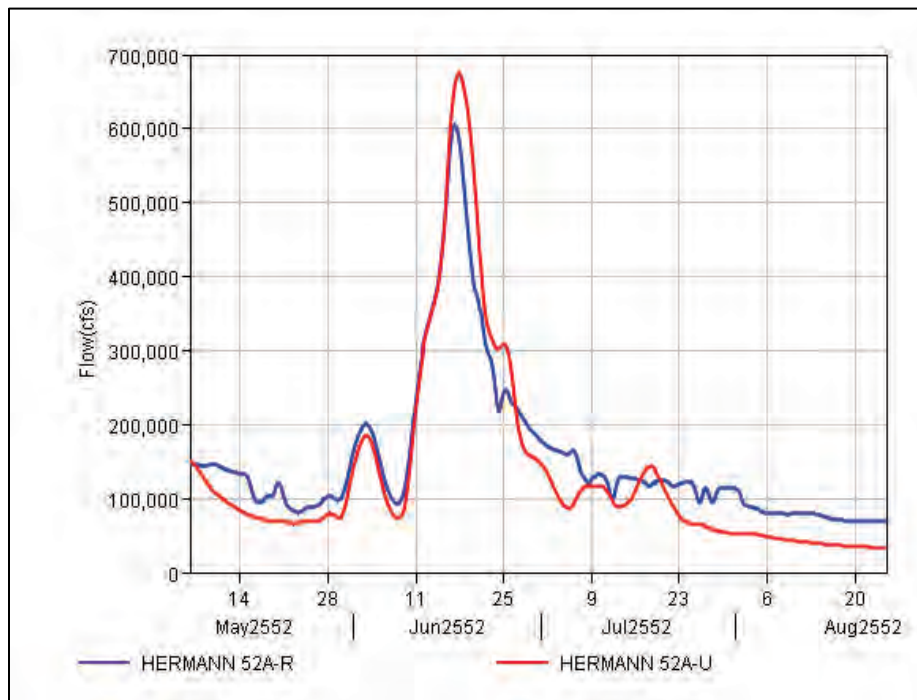


Figure C-14. HYPO 52A hydrographs: Mississippi River at Alton, IL.

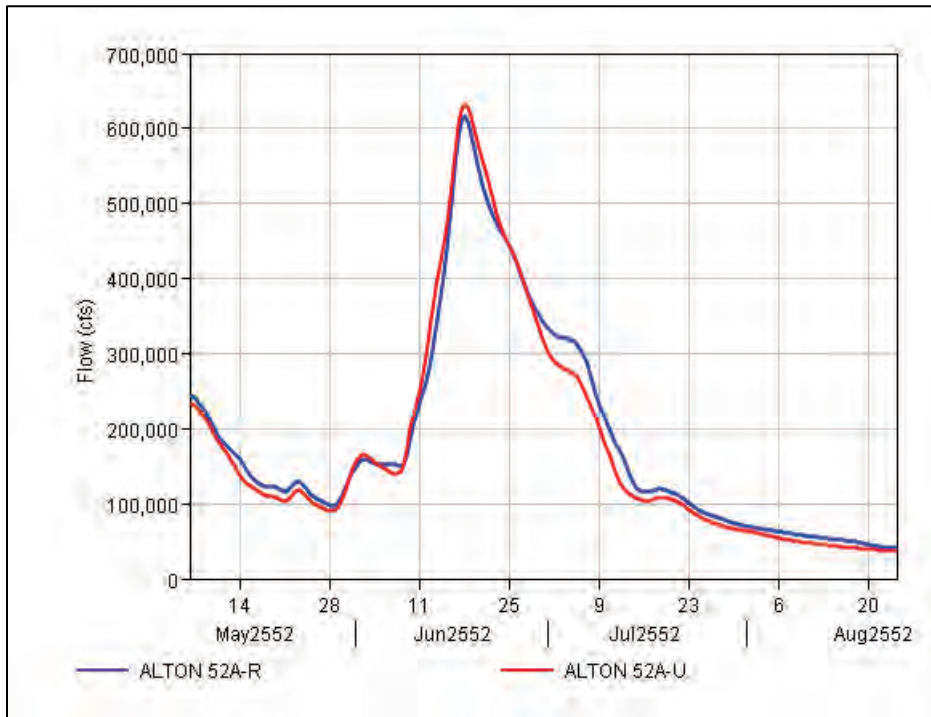


Figure C-15. HYPO 52A hydrographs: Mississippi River at St. Louis, MO.

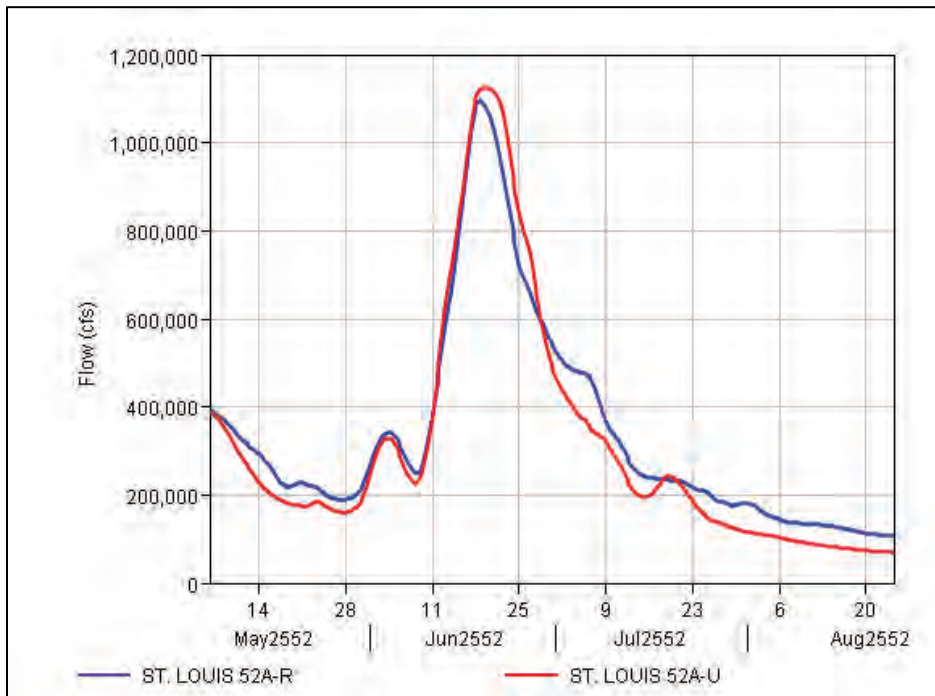


Figure C-16. HYPO 52A hydrographs: Mississippi River at Chester, IL.

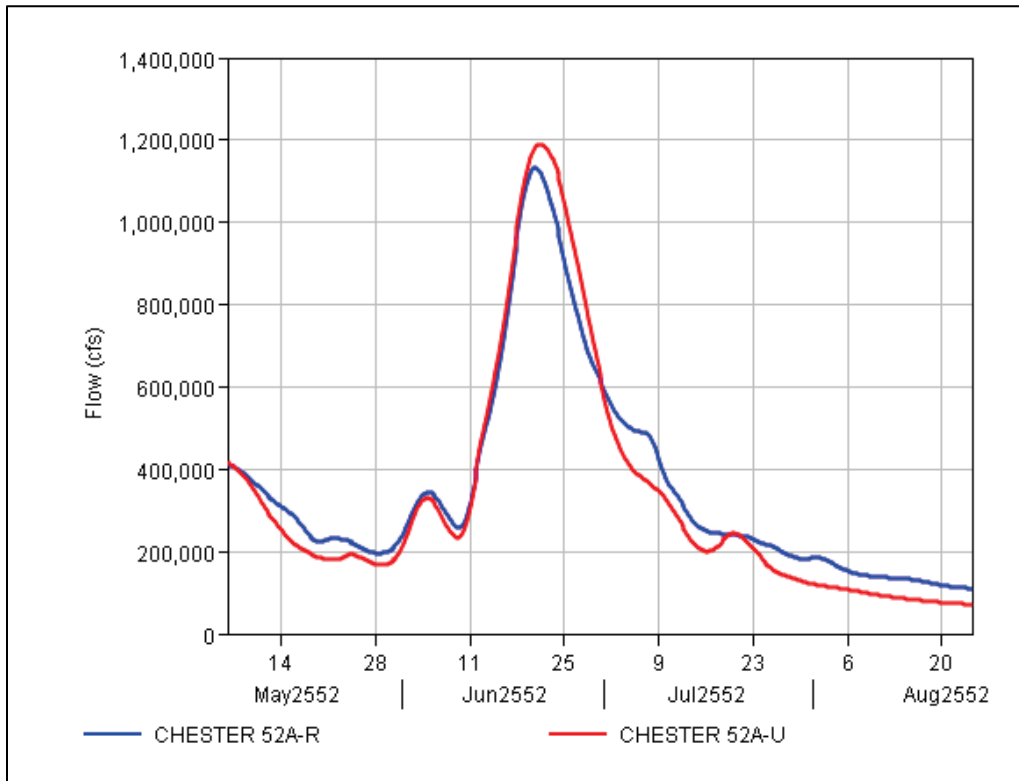


Figure C-17. HYPO 52A hydrographs: Big Muddy River at Murphysboro, IL.

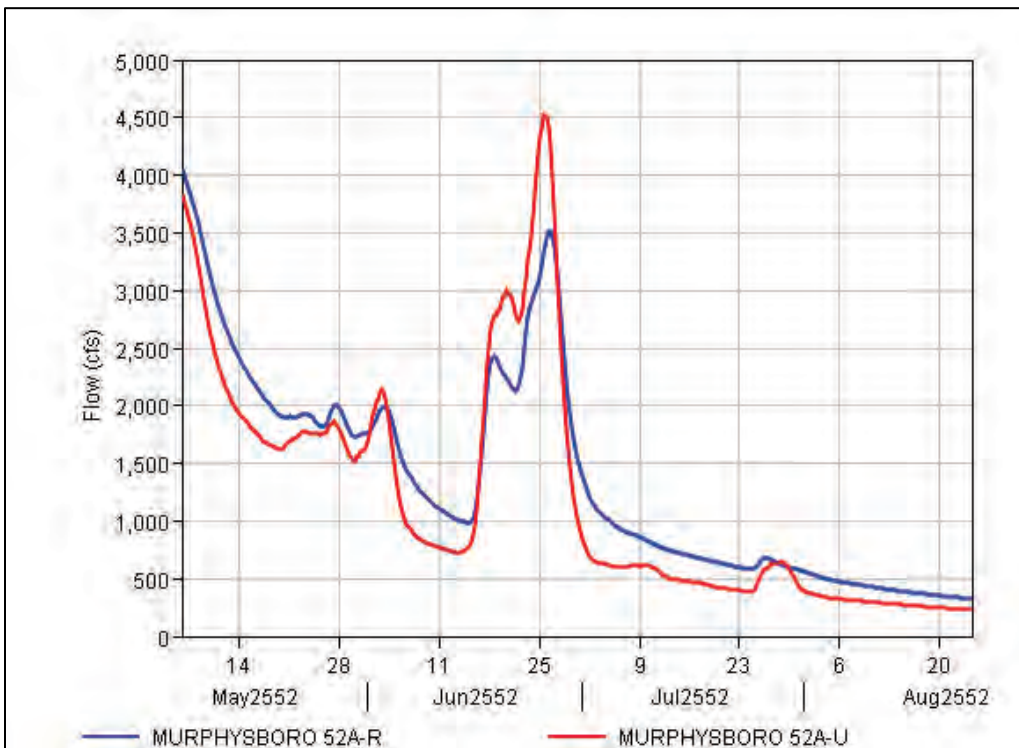


Figure C-18. HYPO 52A hydrographs: Cumberland River at Barkley Dam.

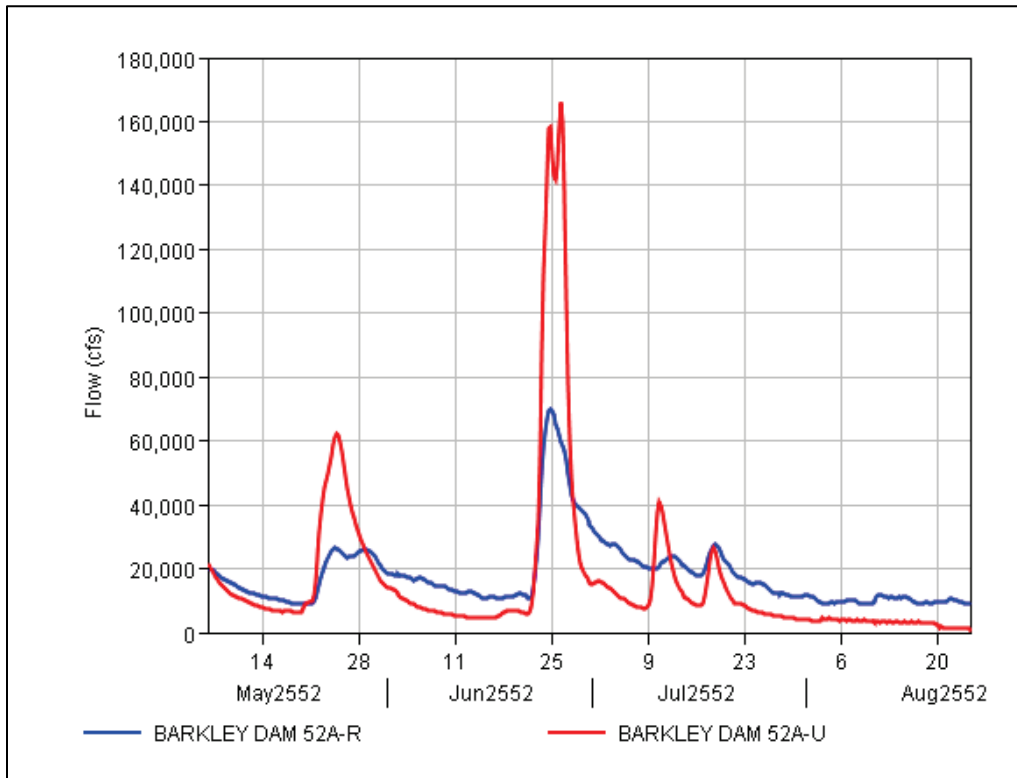


Figure C-19. HYPO 52A hydrographs: Tennessee River at Kentucky Dam.

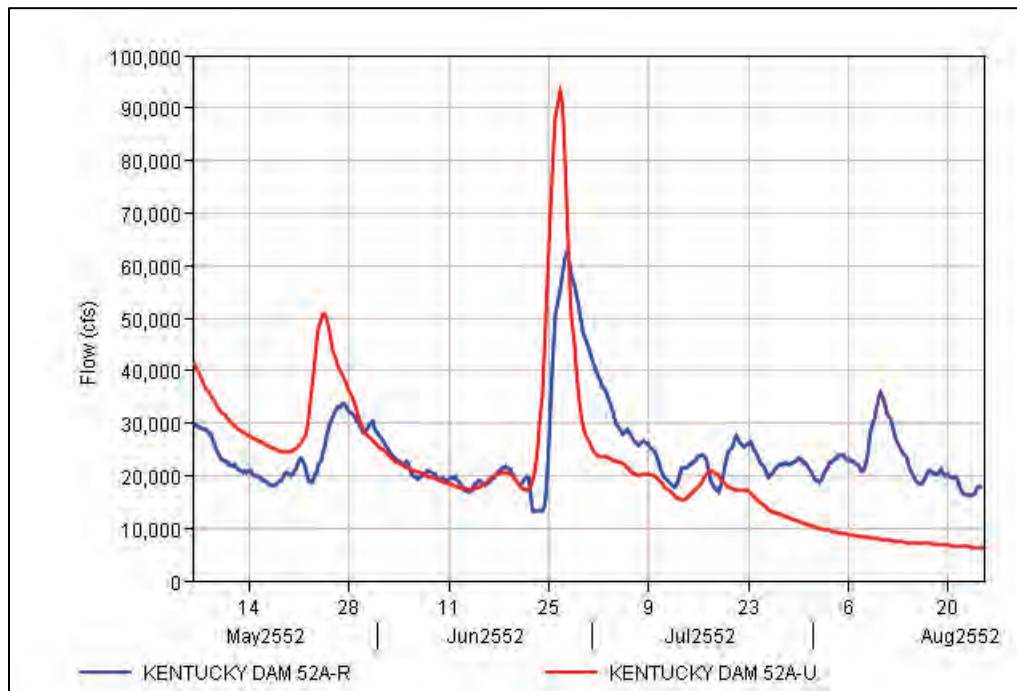


Figure C-20. HYPO 52A hydrographs: Ohio River at Smithland, IL.

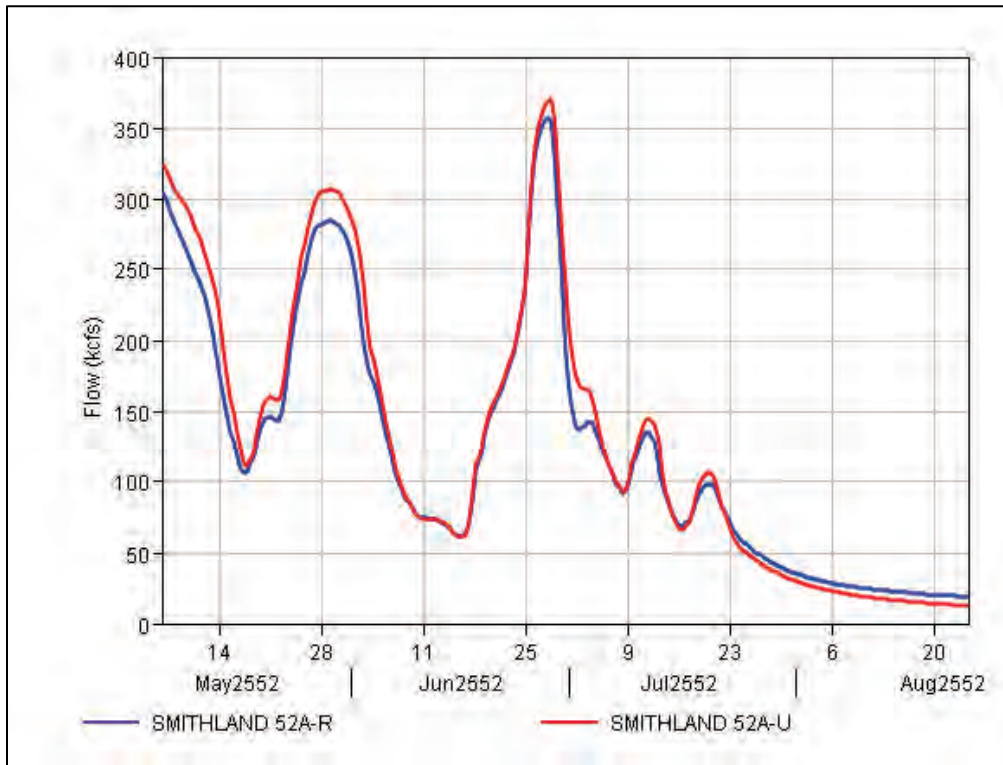


Figure C-21. HYPO 52A hydrographs: Arkansas River at Pine Bluff, AR.

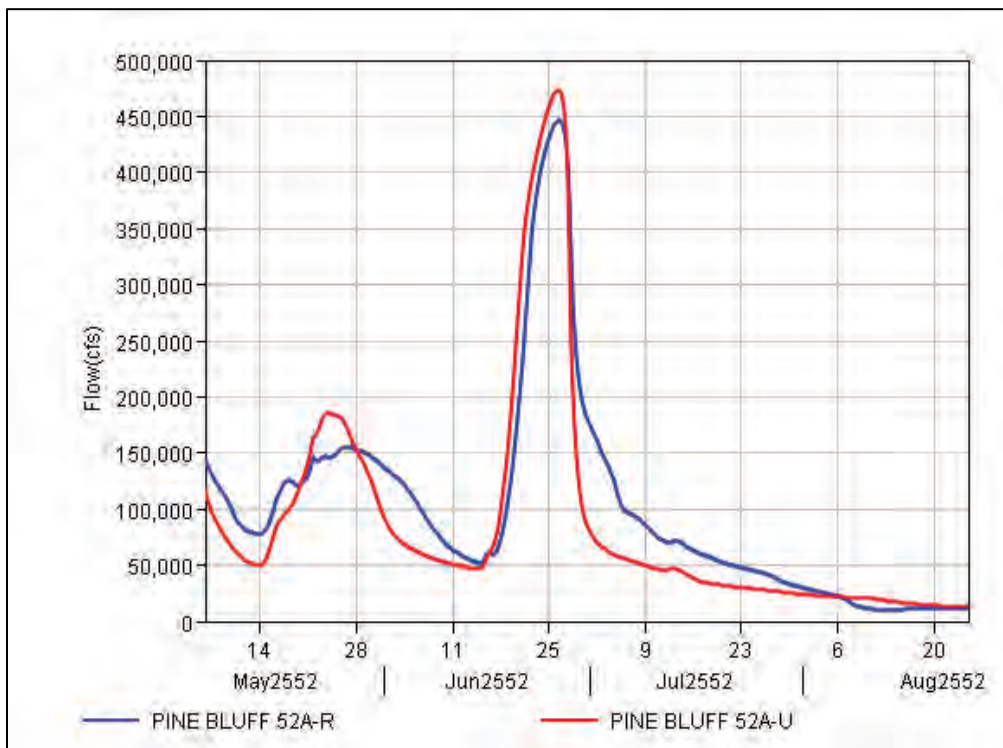


Figure C-22. HYPO 52A hydrographs: Shreveport, LA.

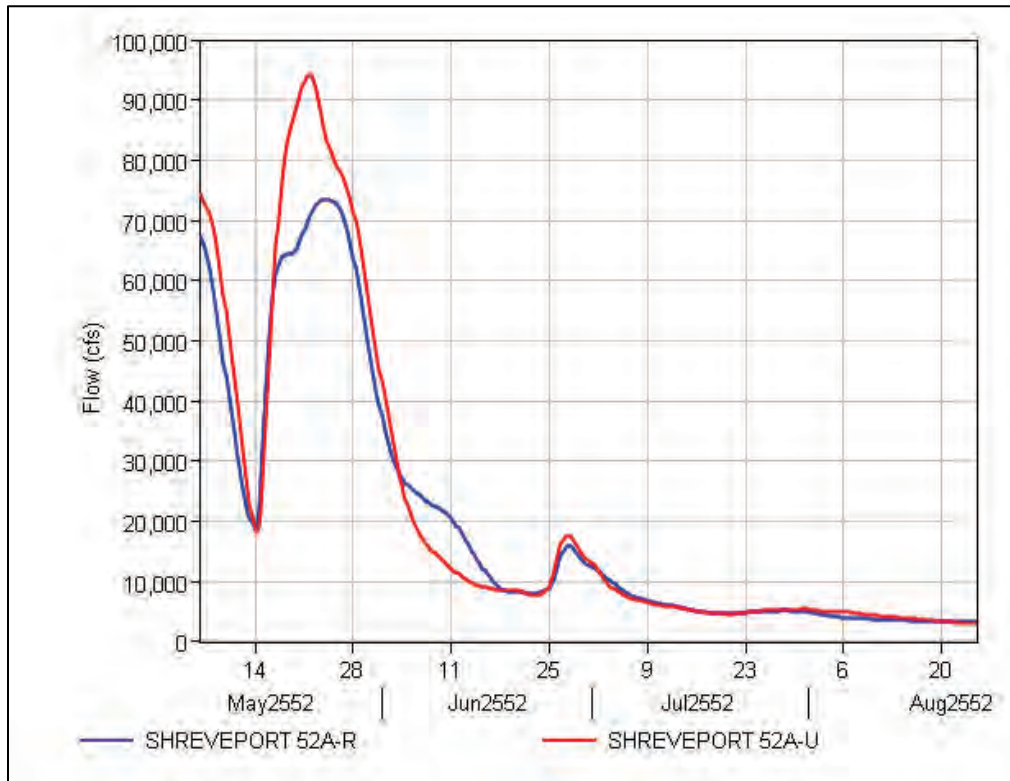


Figure C-23. HYPO 52A hydrographs: Monroe, LA.

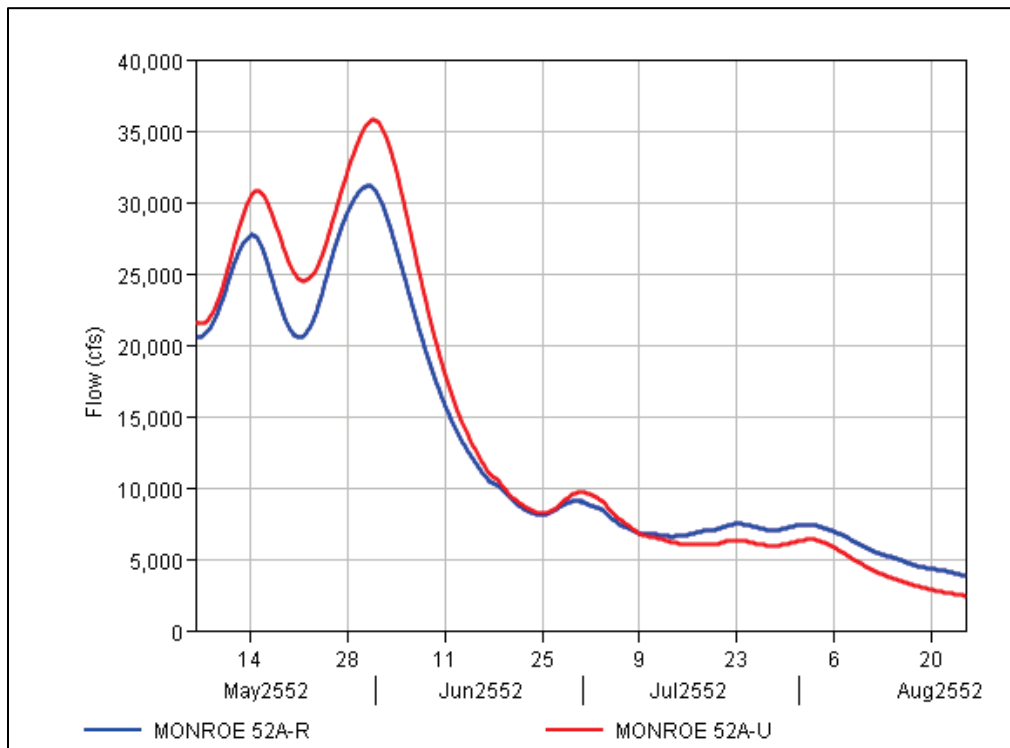


Figure C-24. HYPO 52A hydrographs: Alexandria, LA.

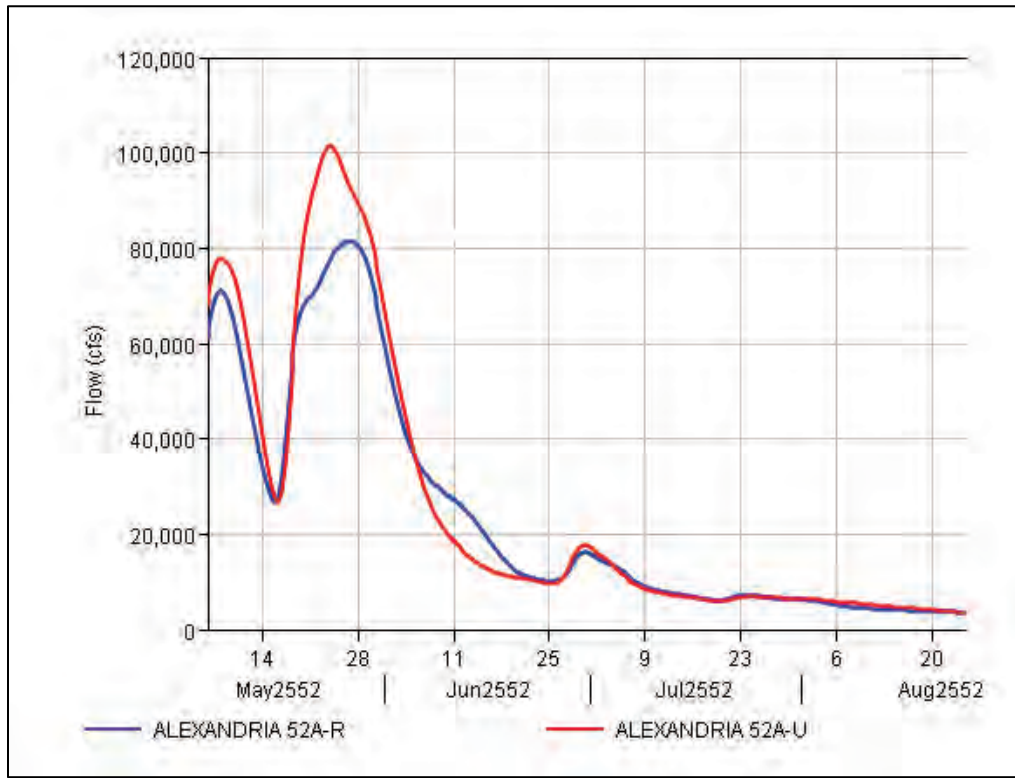
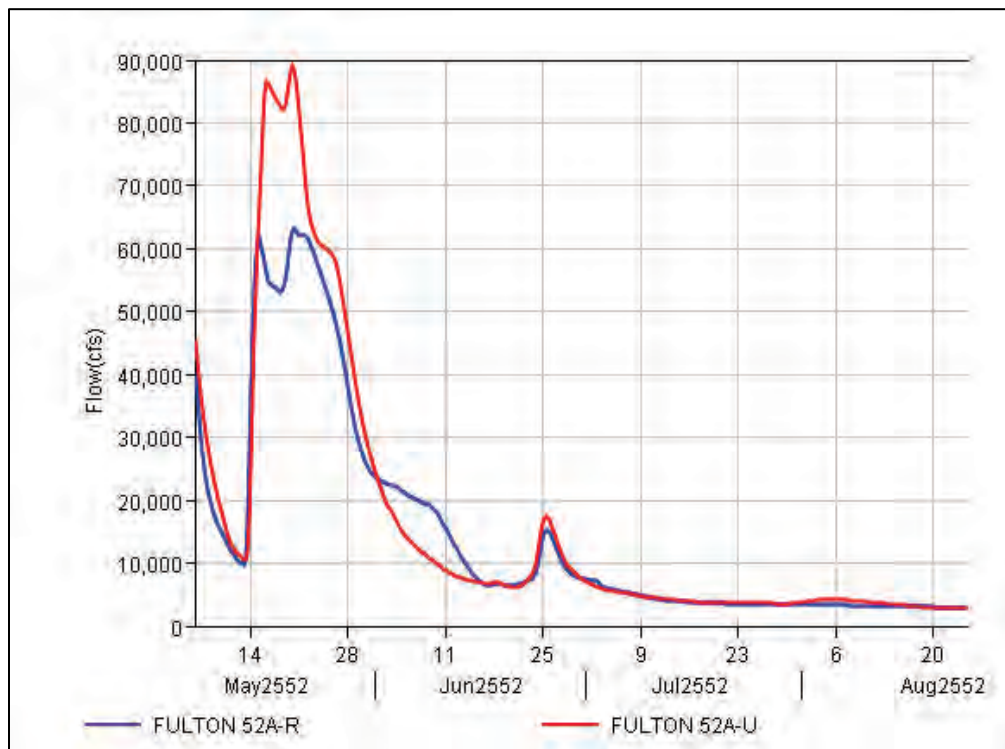


Figure C-25. HYPO 52A hydrographs: Fulton, LA.



C.3 Peak Flows for the Lower Ohio and Mississippi River

A comparison of calculated peak discharges from the 2016 HEC-RAS model with values from the MRC (1955) report is given in Table C-2. Peak flows from the 1955 report are given as historic values in the table. The two HEC-RAS model runs reflect (1) the existing, 2016 conditions for the Yazoo Backwater levee at Elevation 107.0 and (2) the authorized 1973 refined condition for the Yazoo Backwater levee at Elevation 112.8.

Table C-2. Comparison of peak flow values for HYPO 52A.

Location	Project Design Flood (PDF) (from Table 7 WES [1957])					
	Unregulated Discharge (U), cfs			Regulated Discharge (Existing and Near-term Reservoirs, EN), cfs		
	52A	52A-U Existing Yazoo	52A-U Authorized Yazoo	52A-EN	52A-R Existing Yazoo	52A-R Authorized Yazoo
Ohio at Cairo, IL	NA	566,000	566,000	NA	498,000	498,000
Miss/Ohio Confluence (combined)	2,600,000	1,555,000	1,555,000	2,190,000	1,353,000	1,353,000
Hickman, KY	NA	1,536,000	1,536,000	NA	1,339,000	1,339,000
Memphis, TN	2,270,000	1,418,000	1,418,000	1,910,000	1,306,000	1,306,000
Helena, AR	2,030,000	1,395,000	1,395,000	1,740,000	1,294,000	1,294,000
Arkansas City, AR	2,490,000	1,516,000	1,516,000	2,090,000	1,498,000	1,498,000
Greenville, MS	NA	1,507,000	1,507,000	NA	1,489,000	1,489,000
Lake Providence, MS	NA	1,492,000	1,492,000	NA	1,475,000	1,475,000
Vicksburg, MS	2,200,000	1,454,000	1,454,000	1,930,000	1,452,000	1,452,000
Natchez, MS	2,190,000	1,443,000	1,443,000	1,920,000	1,443,000	1,443,000
Red River Landing, LA	1,690,000	1,011,000	1,011,000	1,390,000	1,008,000	1,008,000
Baton Rouge, LA	NA	1,005,000	1,005,000	NA	998,000	998,000
Donaldsonville, LA	NA	1,004,000	1,005,000	NA	997,000	997,000
Carrollton, LA	NA	1,003,000	1,003,000	NA	993,000	993,000
Empire, LA	NA	992,000	992,000	NA	978,000	978,000
Venice, LA	NA	738,000	738,000	NA	727,000	727,000

C.3.1 Comparison of 2016 model output hydrographs with 1955 hydrographs

The following plots provide a comparison of 2016 hydrologic model or HEC-RAS model outputs with available 1955 hydrographs. Both unregulated and regulated hydrographs are compared for the mainstem Mississippi River locations. Only unregulated hydrographs were available for tributary locations from the 1955 Study; therefore, those locations do not include regulated hydrographs.

The HEC-RAS model included two separate runs: (1) Existing, Yazoo Backwater levee at elevation 207.1 and (2) Authorized, Yazoo Backwater levee at elevation 212.8. For most plots, there is no difference between the Existing and Authorized Yazoo Backwater levee results except near the peak of the hydrograph. Where there are differences, an inset is included to show the relative differences between these two runs. Where there are no differences between the existing and authorized Yazoo Backwater runs, only a single line appears in the plot because the lines plot directly on top of each other.

Figure C-26. Alexandria, LA, HYPO 52A 1955 unregulated flow compared to 2016 unregulated flow generated by the RFC.

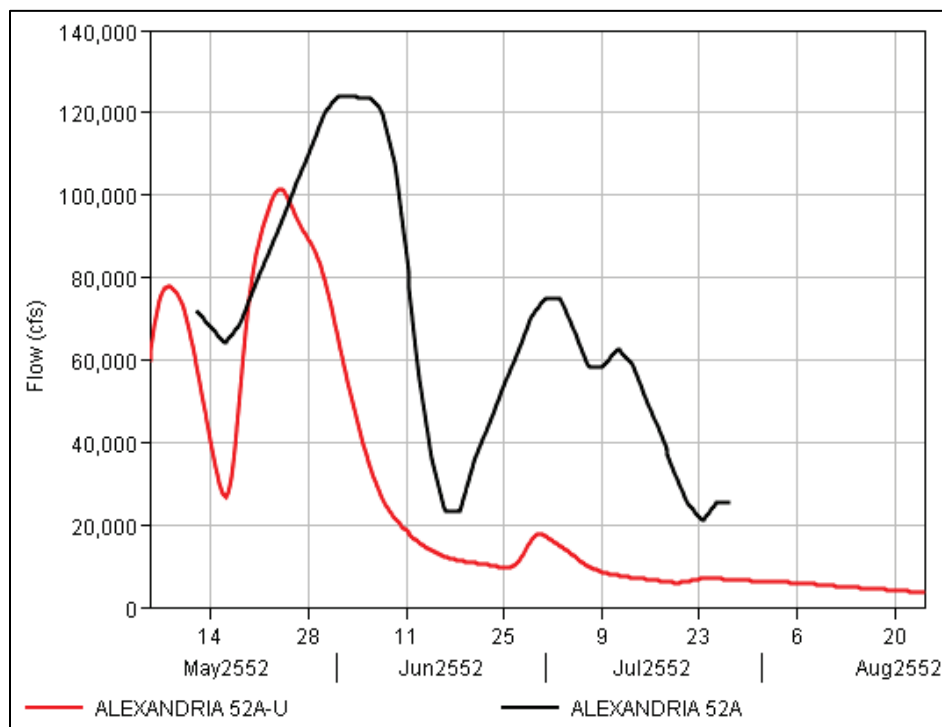


Figure C-27. Alton, IL, HYPO 52A 1955 unregulated flow compared to 2016 unregulated flow generated by the RFC.

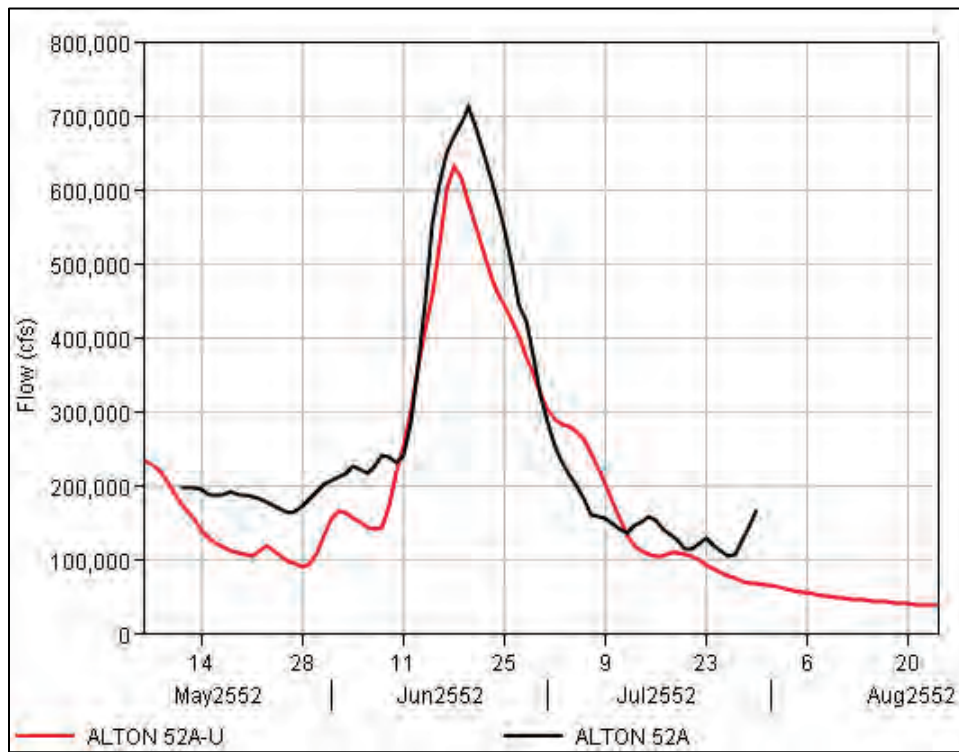


Figure C-28. Hermann, MO, HYPO 52A 1955 unregulated flow compared to 2016 unregulated flow generated by the RFC.

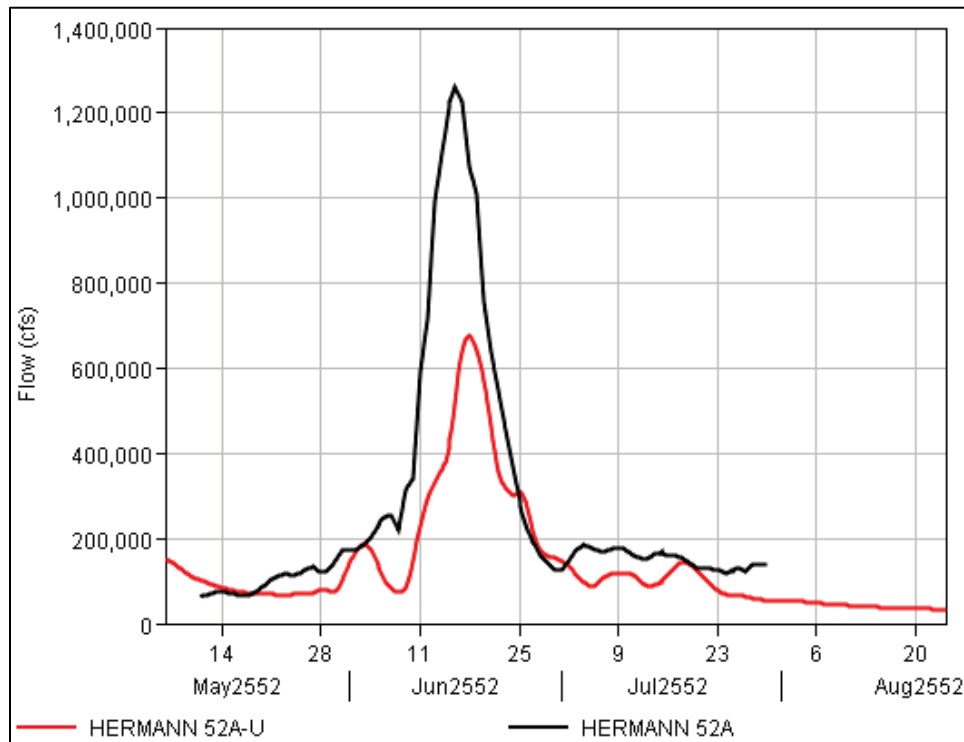


Figure C-29. Little Rock, AR, HYPO 52A 1955 unregulated flow compared to 2016 unregulated flow generated by the RFC.

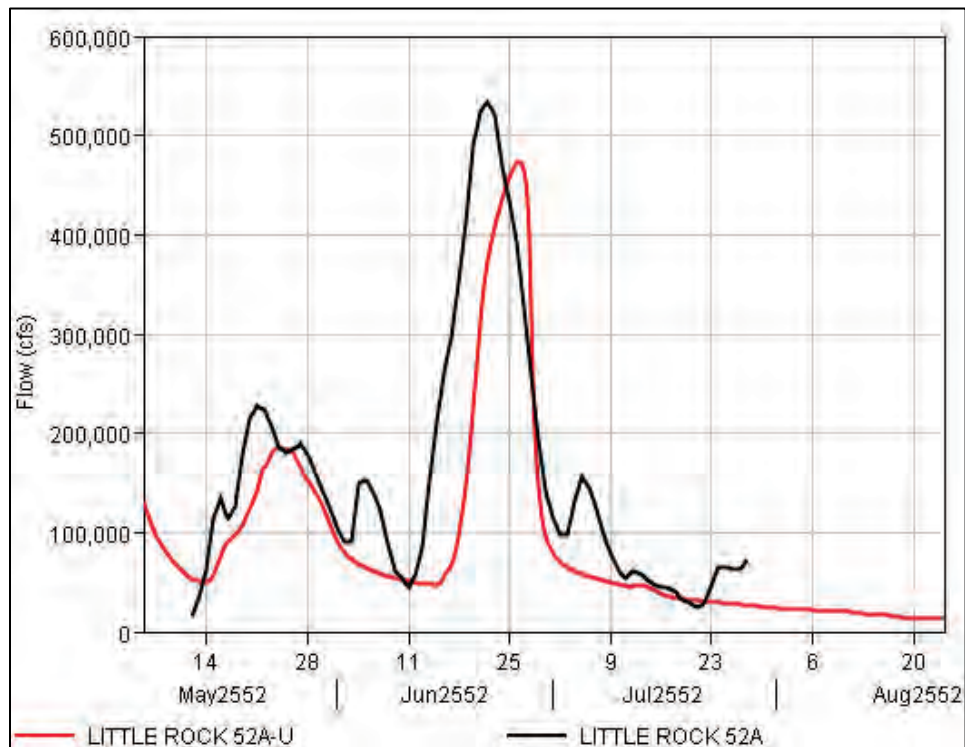


Figure C-30. Arkansas City, AR, HYPO 52A 1955 unregulated flow compared to 2016 unregulated flow generated by the RFC

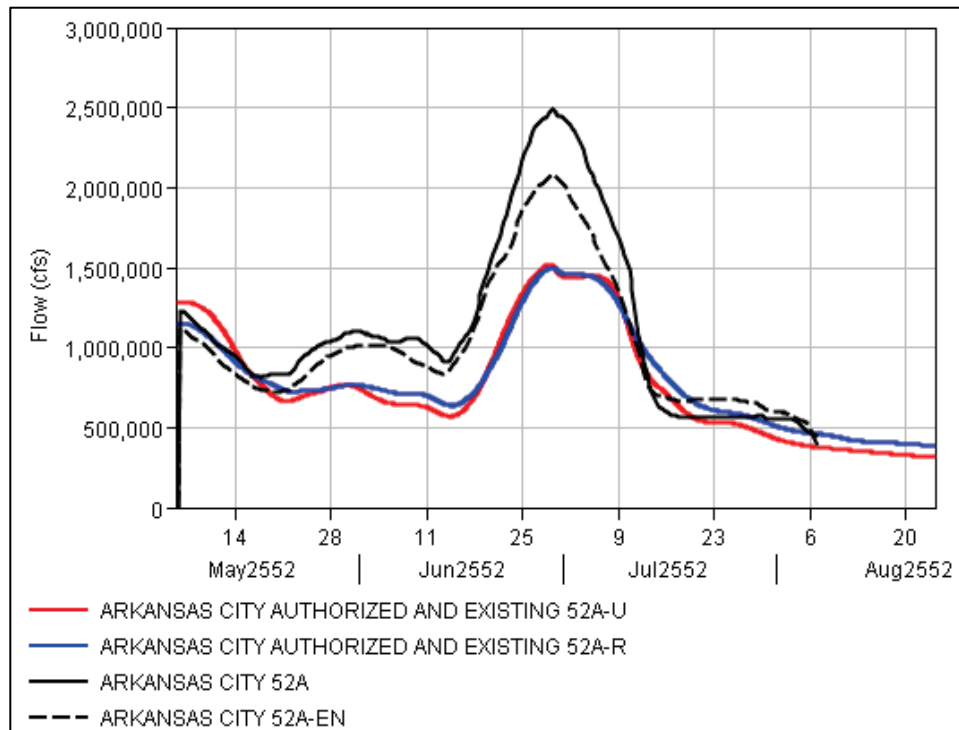


Figure C-31. Cairo, IL, HYPO 52A 1955 unregulated flow compared to 2016 unregulated flow generated by the RFC.

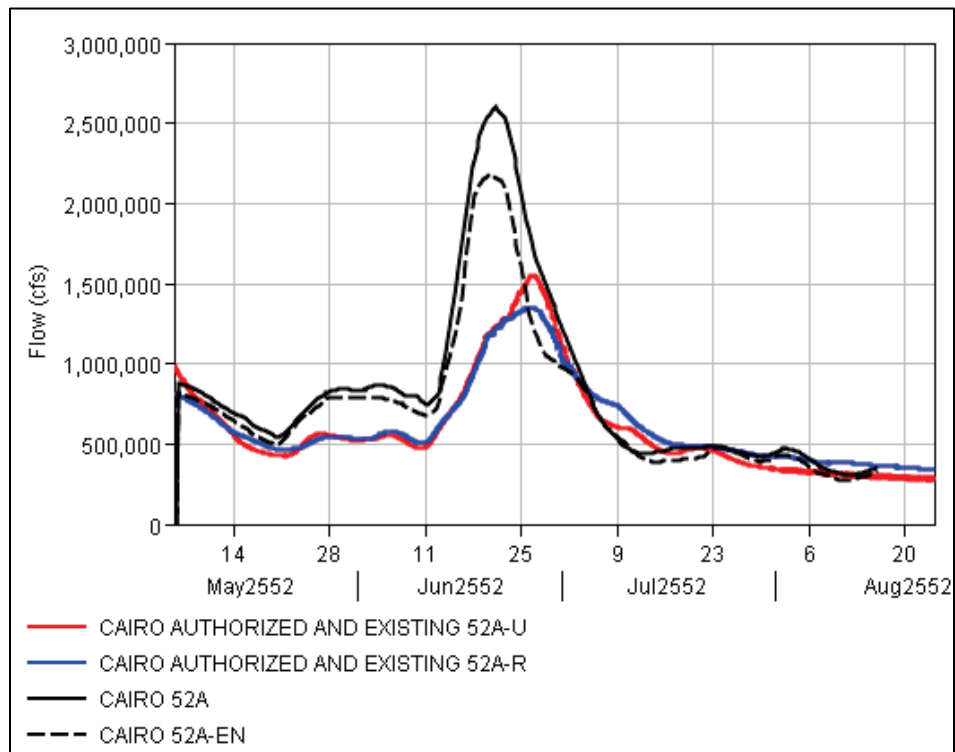


Figure C-32. Clarendon, AR, HYPO 52A 1955 unregulated flow compared to 2016 unregulated flow generated by the RFC.

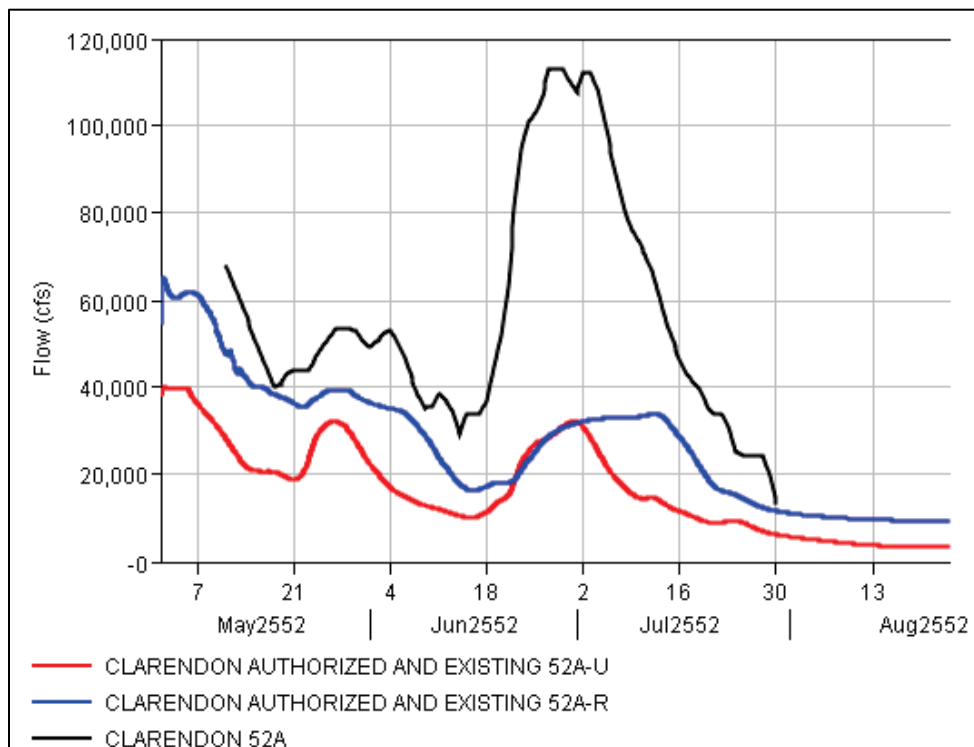


Figure C-33. Metropolis, IL, HYPO 52A 1955 unregulated flow compared to 2016 unregulated flow generated by the RFC.

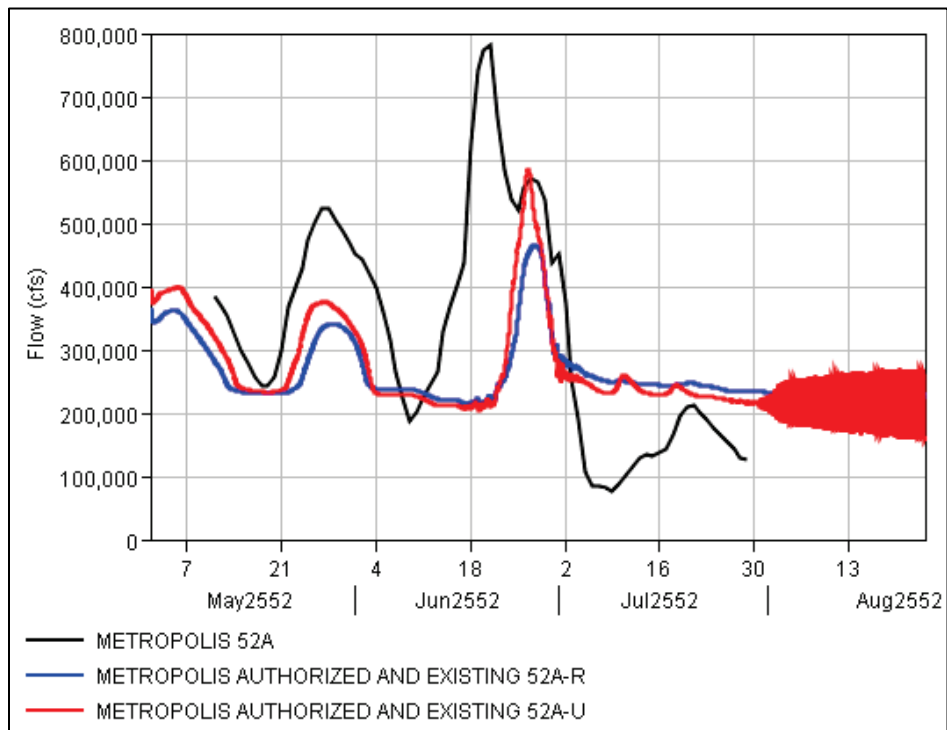


Figure C-34. St. Louis, MO, HYPO 52A 1955 unregulated flow compared to 2016 unregulated flow generated by the RFC.

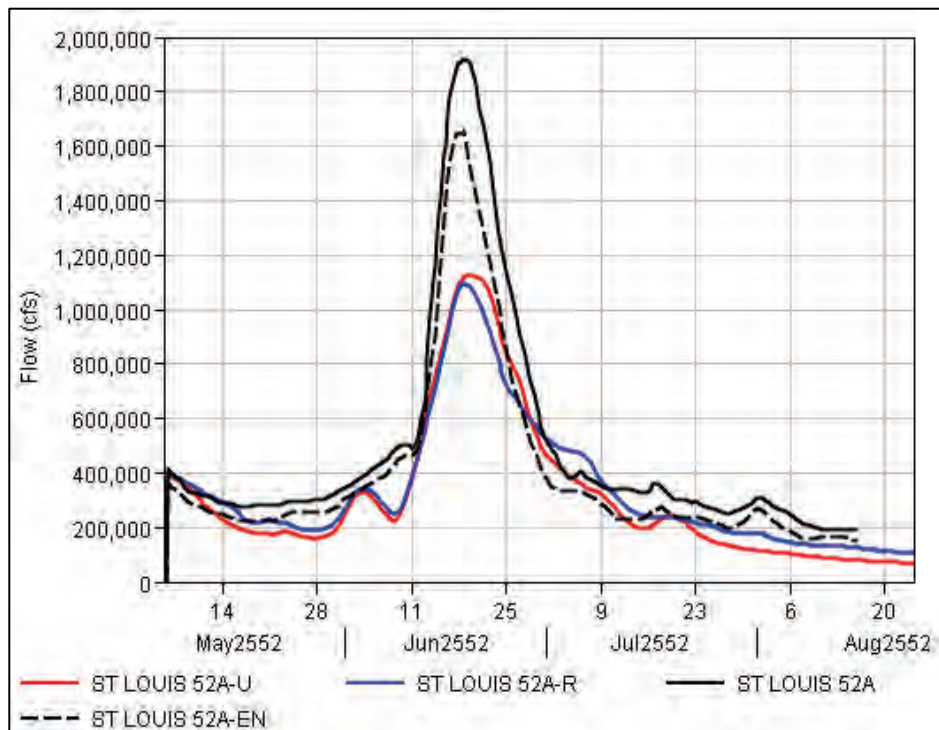
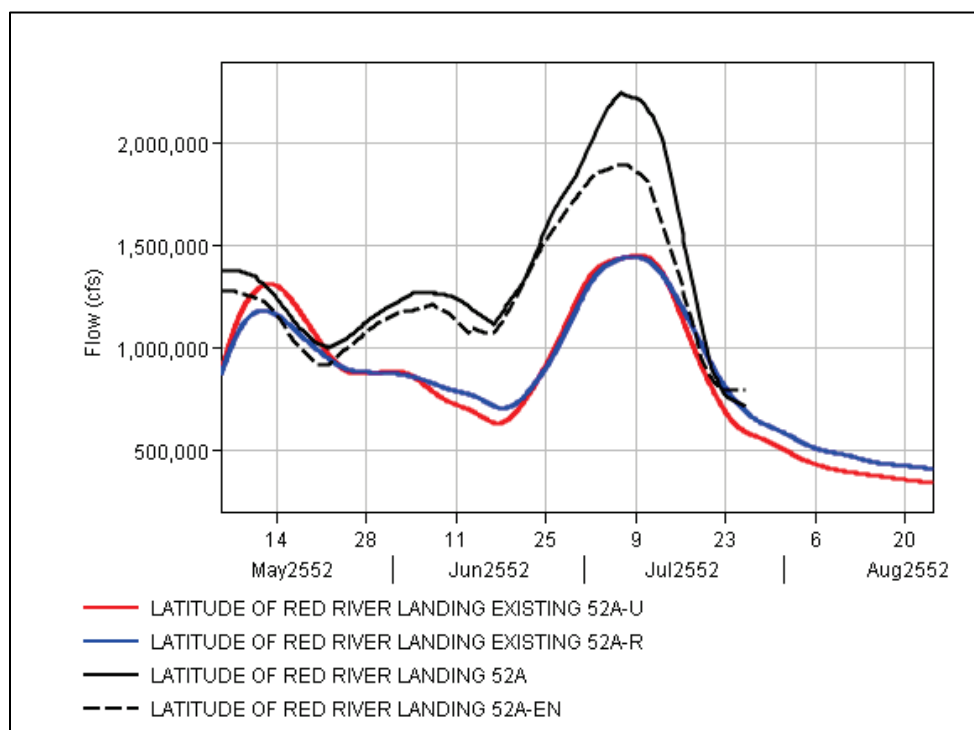


Figure C-35. Red River Landing, LA, HYPO 52A 1955 unregulated flow compared to 2016 unregulated flow generated by the RFC.



C.3.2 HYPO 52A HEC-RAS unsteady model outflows

The combined MVD HEC-RAS model developed for the current assessment provides unsteady hydrodynamic flood routing along the main river channels within the assessment area. However, since the agreement between the 1955 and 2016 flow values is significantly off, the remaining unsteady model outflow hydrographs were not produced as it is known that these hydrographs are incorrect.

C.4 Reservoir inflow and outflow hydrographs for regulated simulations

Figures shown in this section provide data used to develop regulated flows for each reservoir in the LRN. The resulting reservoir outflows for each project were used by the NWS River Forecast Centers to define reservoir outflows in their CHPS-FEWS model simulations. Only the LRN reservoir hydrographs are presented to showcase that the flow for HYPO 52A is much lower than the 1955 values. Figure C-36 through Figure C-45 either show that the reservoir outflow matches the inflow or the reservoir outflow is constant because there is not enough flow to enable flood control rules.

Figure C-36. Barkley Dam HYPO 52A inflow compared to outflow.

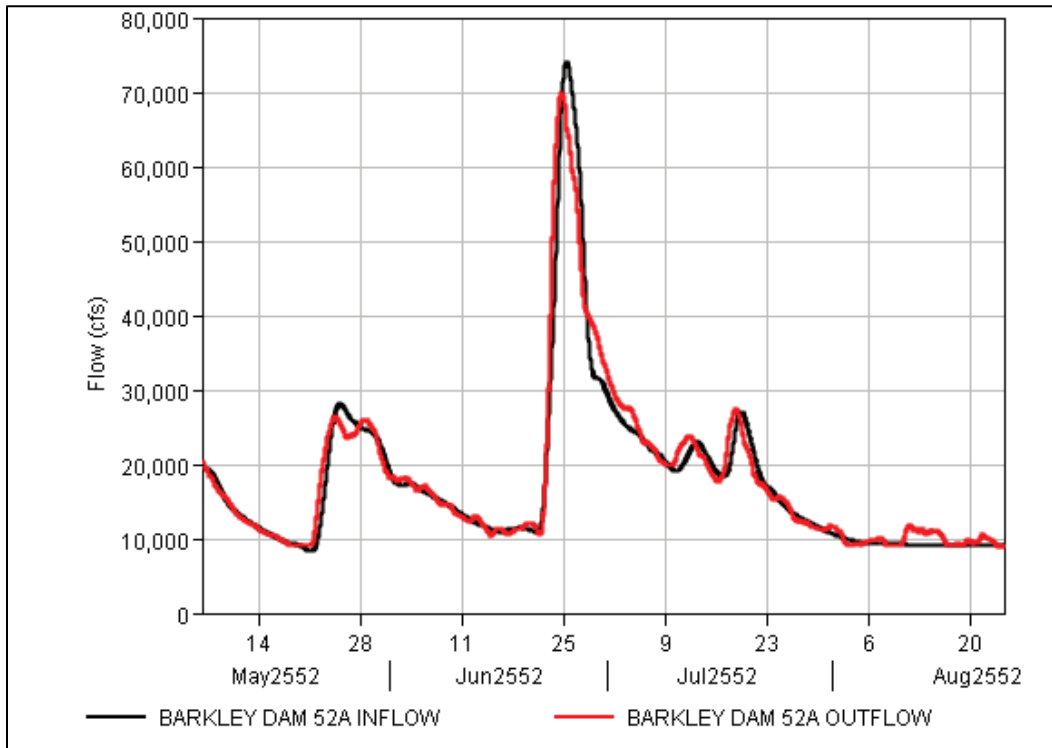


Figure C-37. Center Hill Dam HYPO 52A inflow compared to outflow.

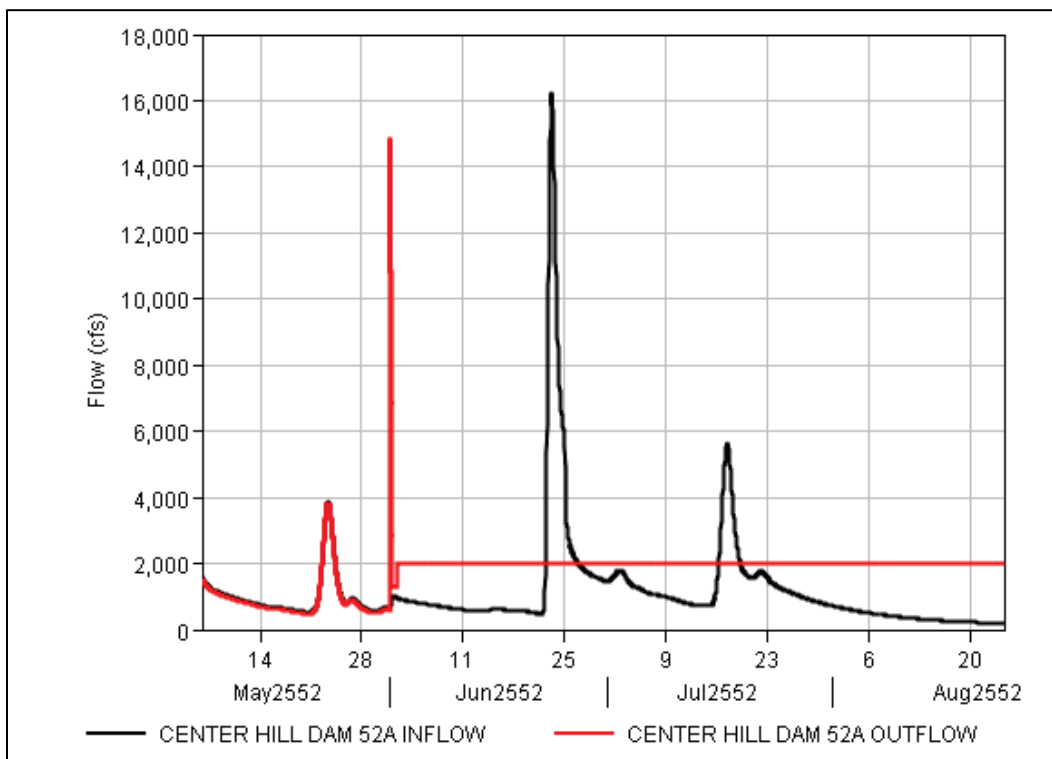


Figure C-38. Cheatham Hill Dam HYPO 52A inflow compared to outflow.

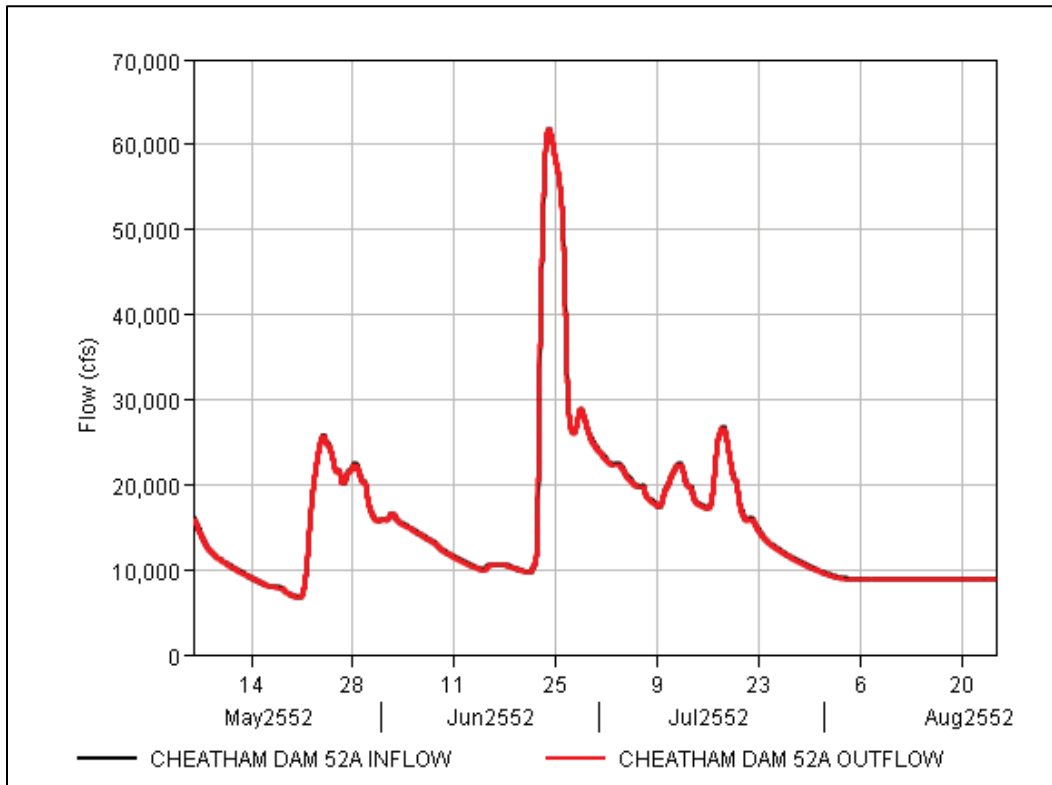


Figure C-39 . Cordell Hull Dam HYPO 52A inflow compared to outflow.

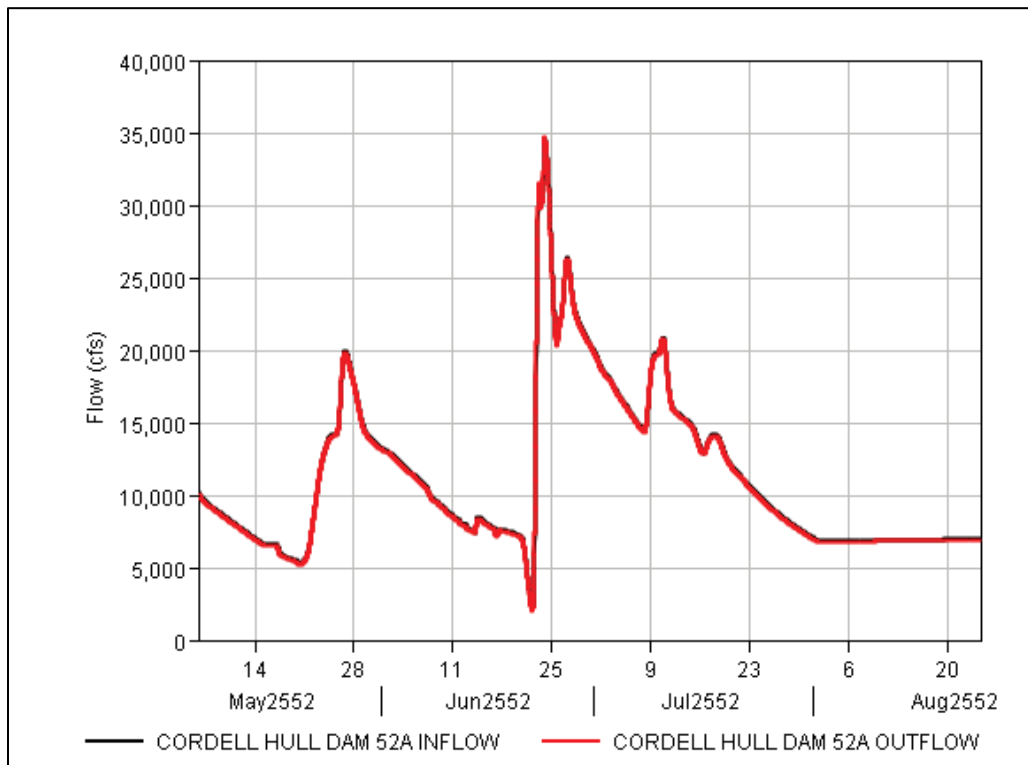


Figure C-40. Dale Hollow Dam HYPO 52A inflow compared to outflow.

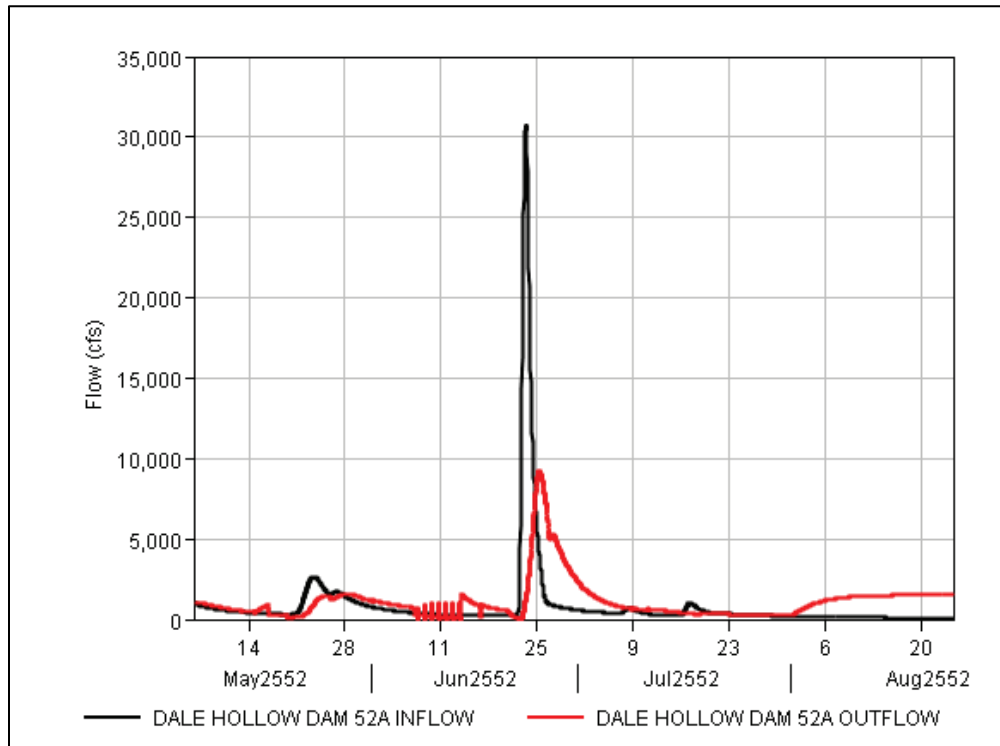


Figure C-41. Great Falls HYPO 52A inflow compared to outflow.

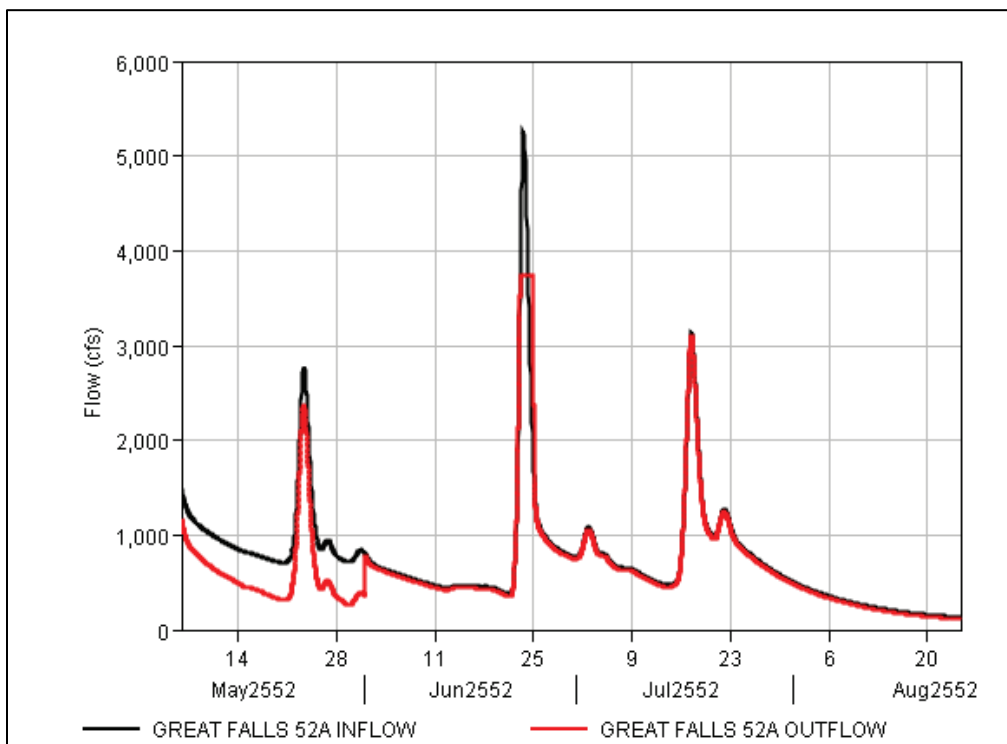


Figure C-42. J. Percy Priest Dam HYPO 52A inflow compared to outflow.

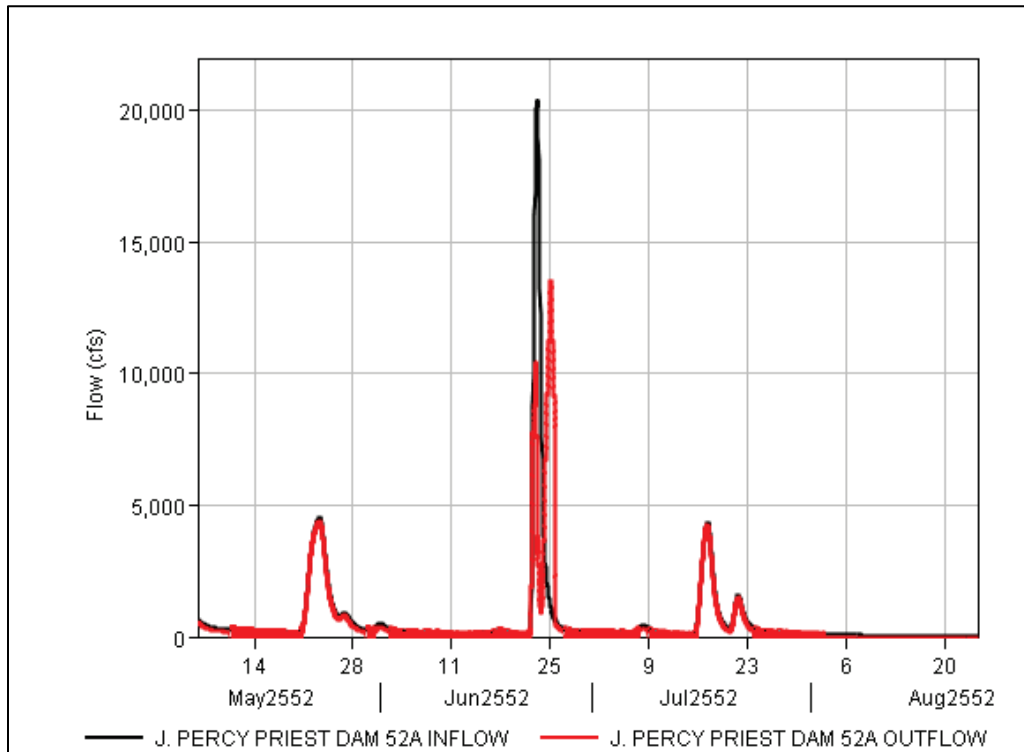


Figure C-43. Kentucky Dam HYPO 52A inflow compared to outflow.

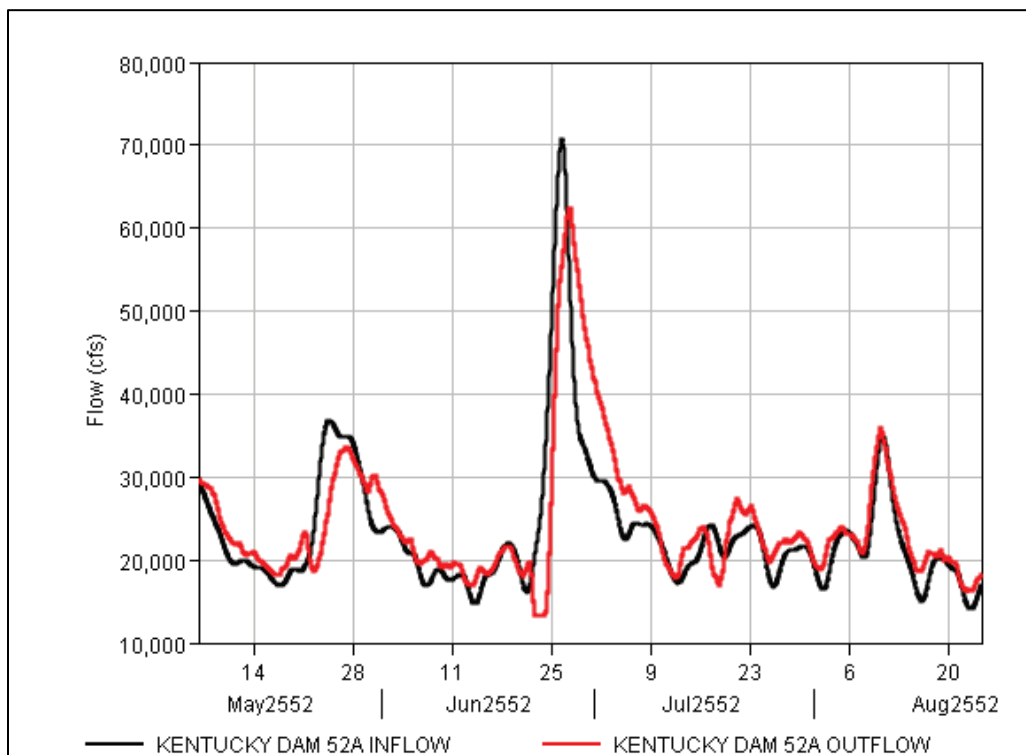


Figure C-44. Old Hickory Dam HYPO 52A inflow compared to outflow.

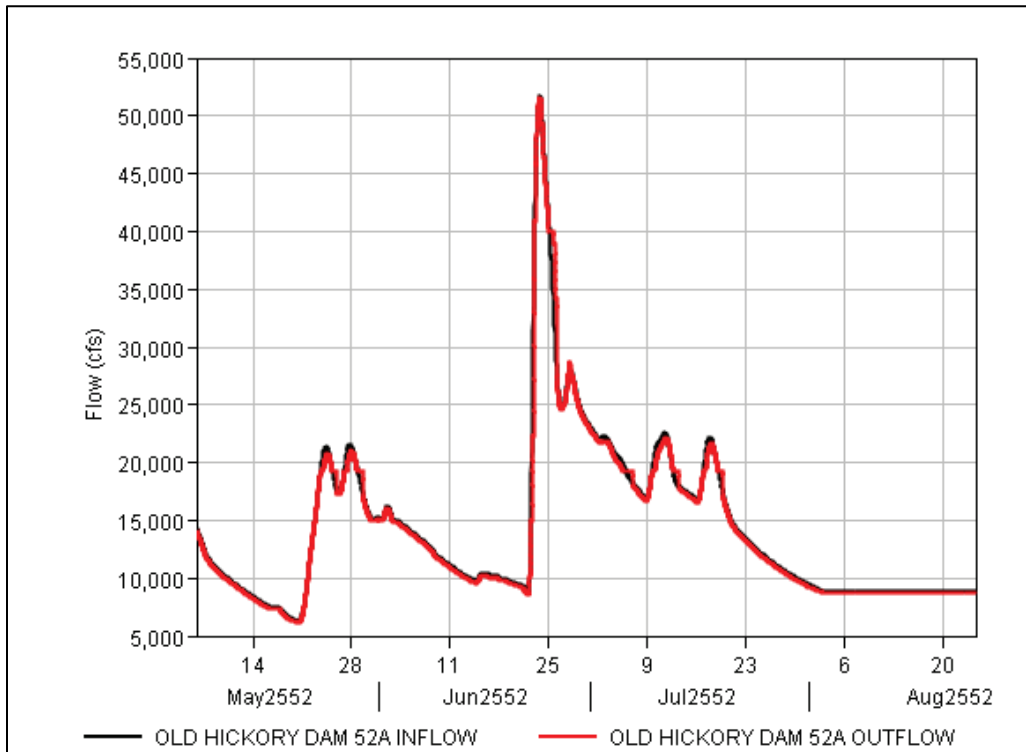
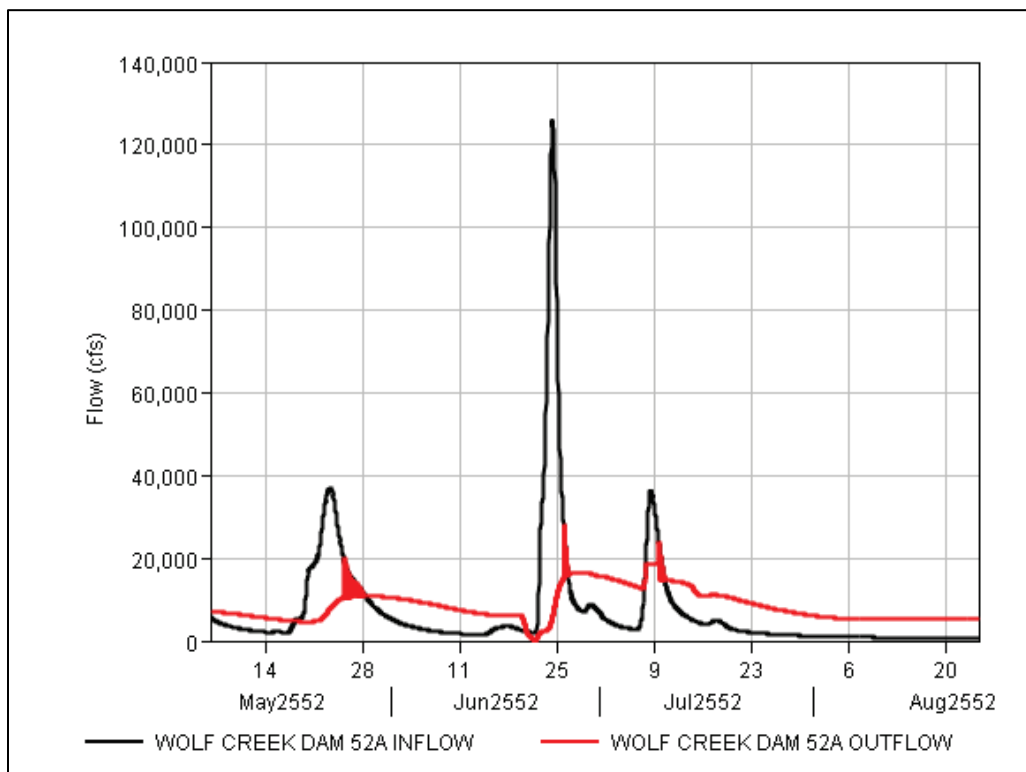


Figure C-45. Wolf Creek Dam HYPO 52A inflow compared to outflow.

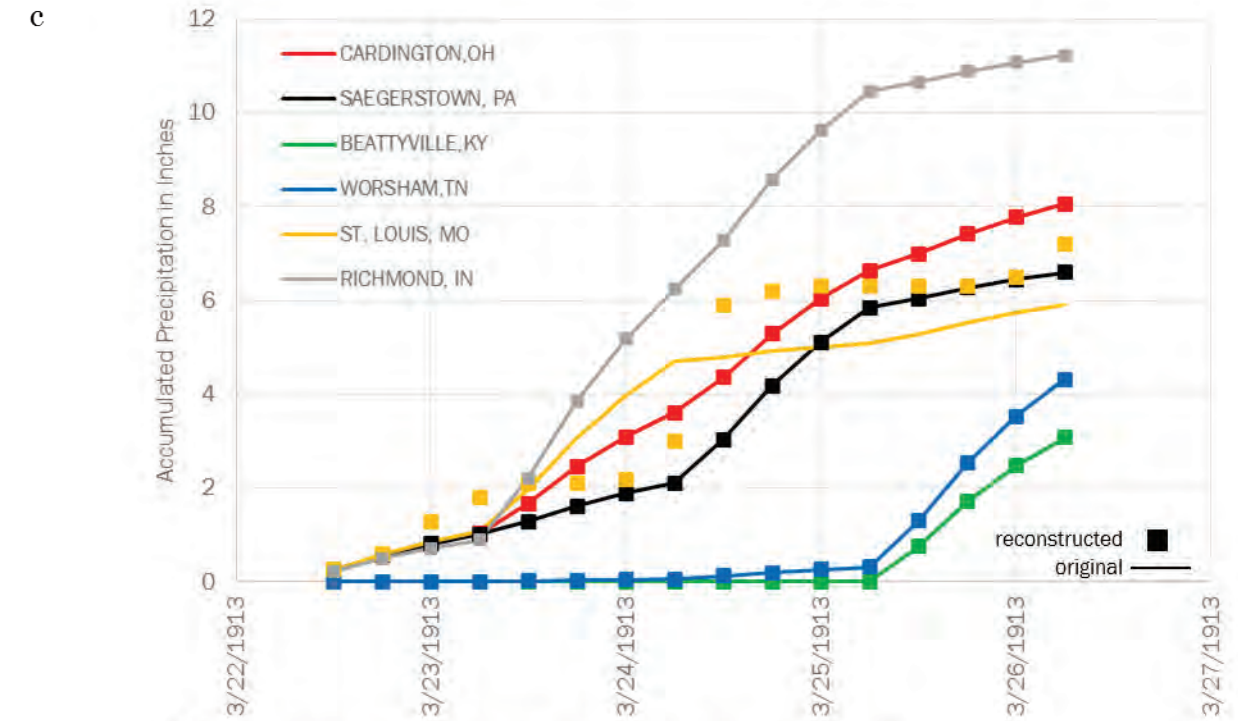
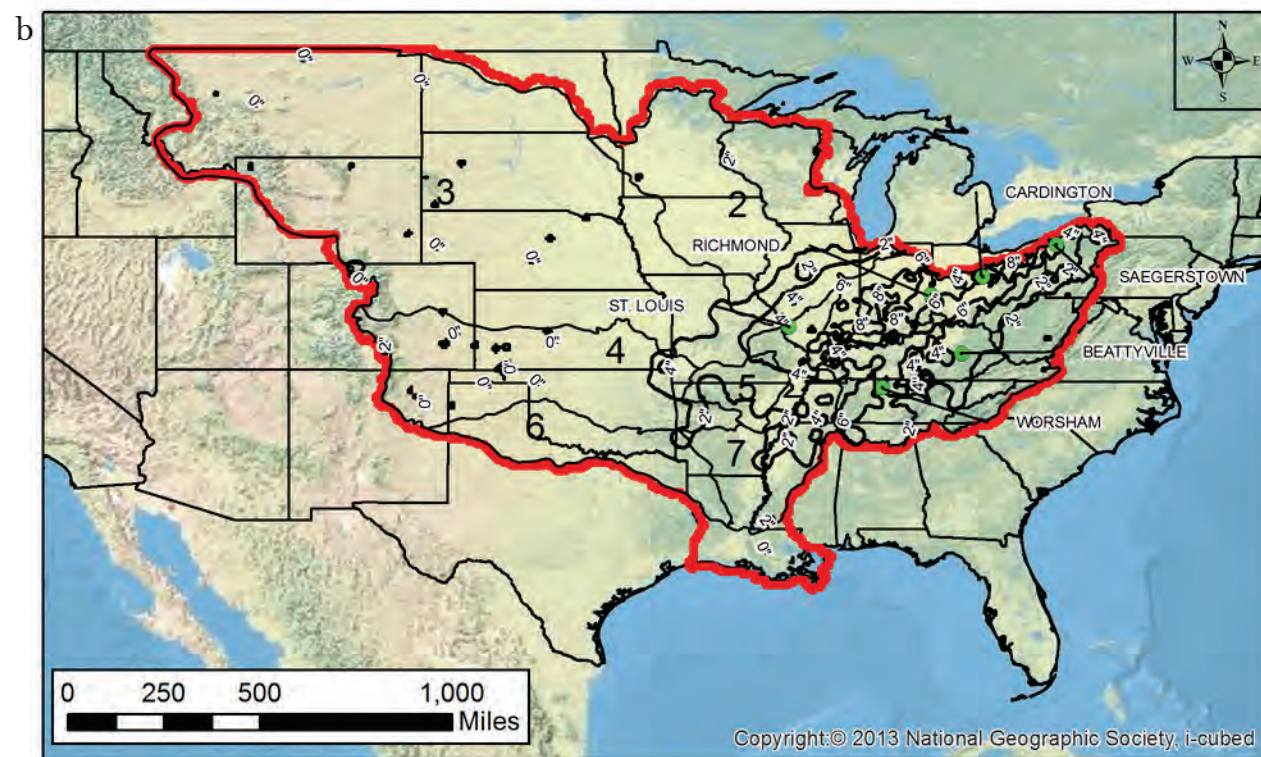
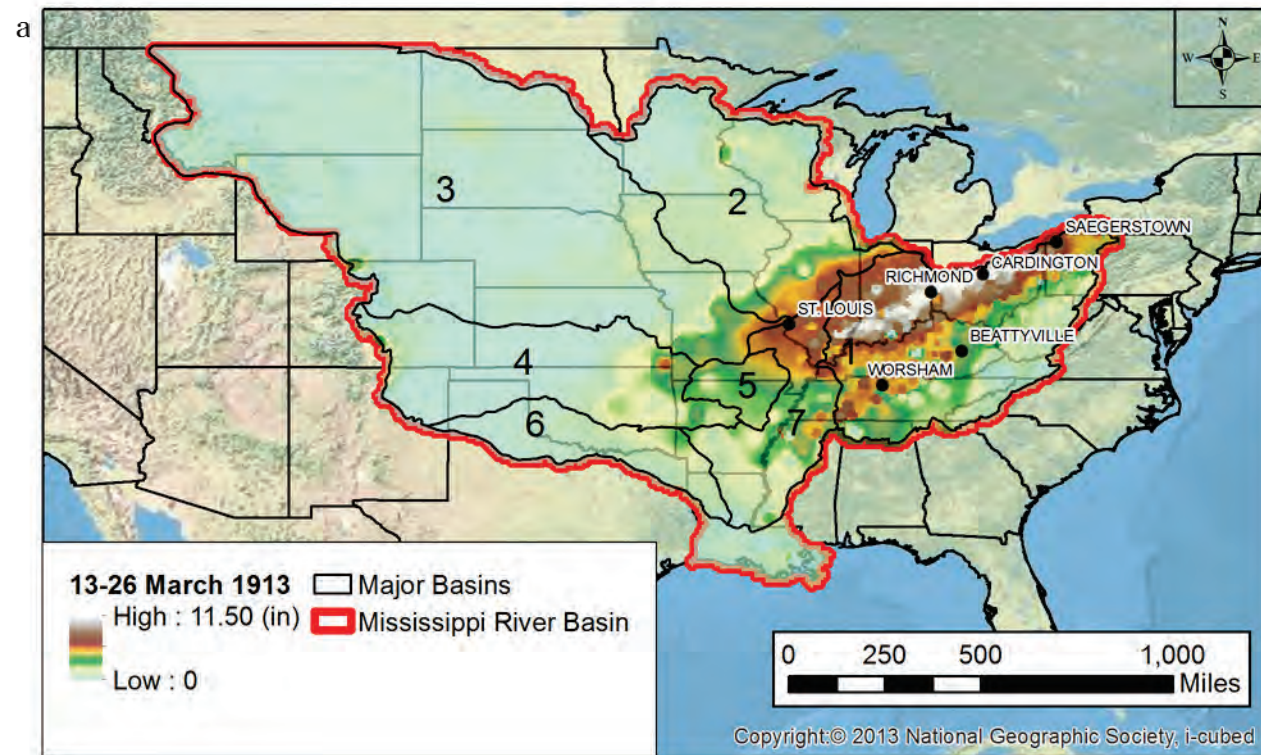


Appendix D: HYPO 56

D.1 HYPO 56 storm precipitation

HYPO Storm 56 is comprised of two historical storm events centered over the Ohio, Upper Mississippi, Arkansas, White, and Red River Basins. The 2016 assessment used point rainfall data and IDW interpolation (with bias toward observed point values) to reconstruct the original 1955 storms data. Figure D-1 and Figure D-2 depict the total precipitation and coverage of each storm event that compiles HYPO 56. Figure (a) in each of the figures depicts the reconstructed storm coverage of the storm event. Figure (b) depicts the isohyetal contours for the reconstructed storm event. Figure (c) looks at several locations and compares the original 1955 precipitation data against the processed inputs after they were converted to a raster by interpolation. Table (d) tabulates the 1955 values, the initial 2016 point data inputs, and the interpolated 2016 grid inputs. Figure D-2 shows the storm coverage that was included in the HYPO 56 hydrology model, but Figure D-3 shows the corrected storm coverage of what should have been included in the model. The precipitation accumulation in the erroneous data is higher than that of the corrected data, so the model results are conservative. Each HYPO storm included a warm-up period to capture the snow pack that would have been lost otherwise. A recession period following the storm sequence was included to provide sufficient time to route the hydrograph peak downstream to the Gulf of Mexico. Figure D4 shows the warm-up and recession period for HYPO 56.

Figure D-1. HYPO 56 – 13–26 March 1913 (a) (top left) storm coverage over the Mississippi River Basin; (b) (bottom left) isohyetal for unadjusted March 1913 storm; (c) (top right) comparison of mass rainfall curves for original point precipitation data versus the processed/interpolated precipitation data for the unadjusted storm; and (d) (bottom right) comparison of 1955 precipitation, 2016 precipitation, and 2016 post-processed precipitation at select locations.



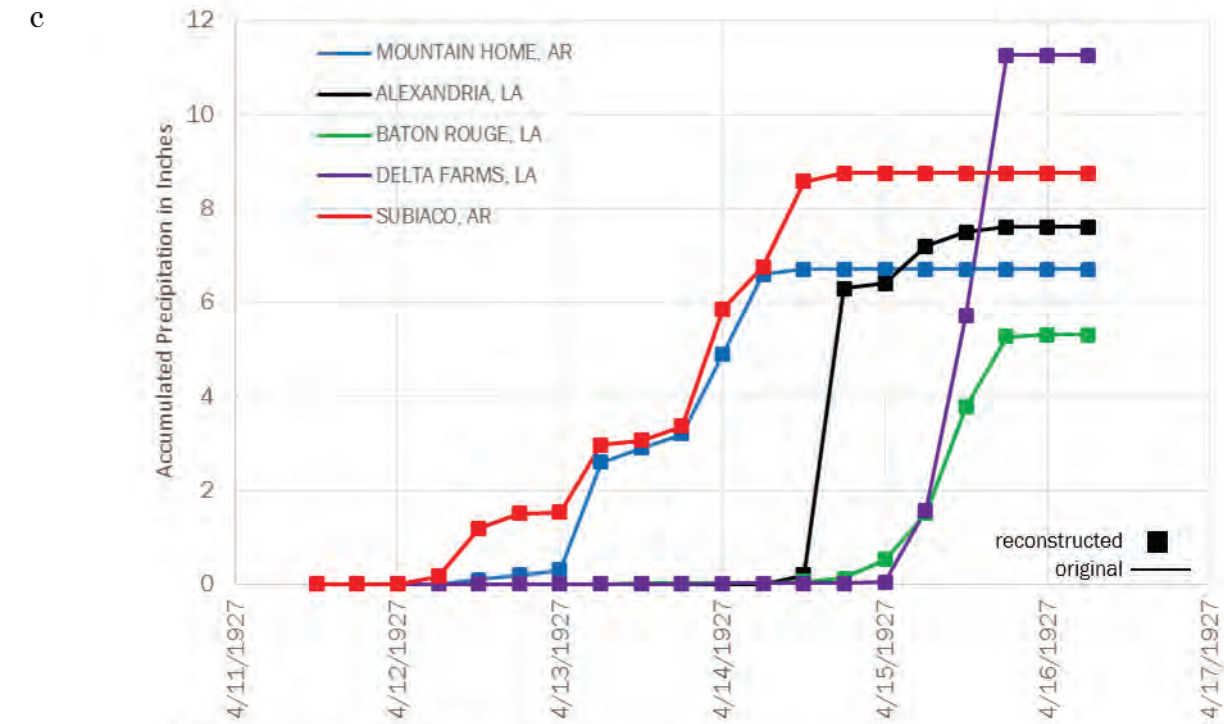
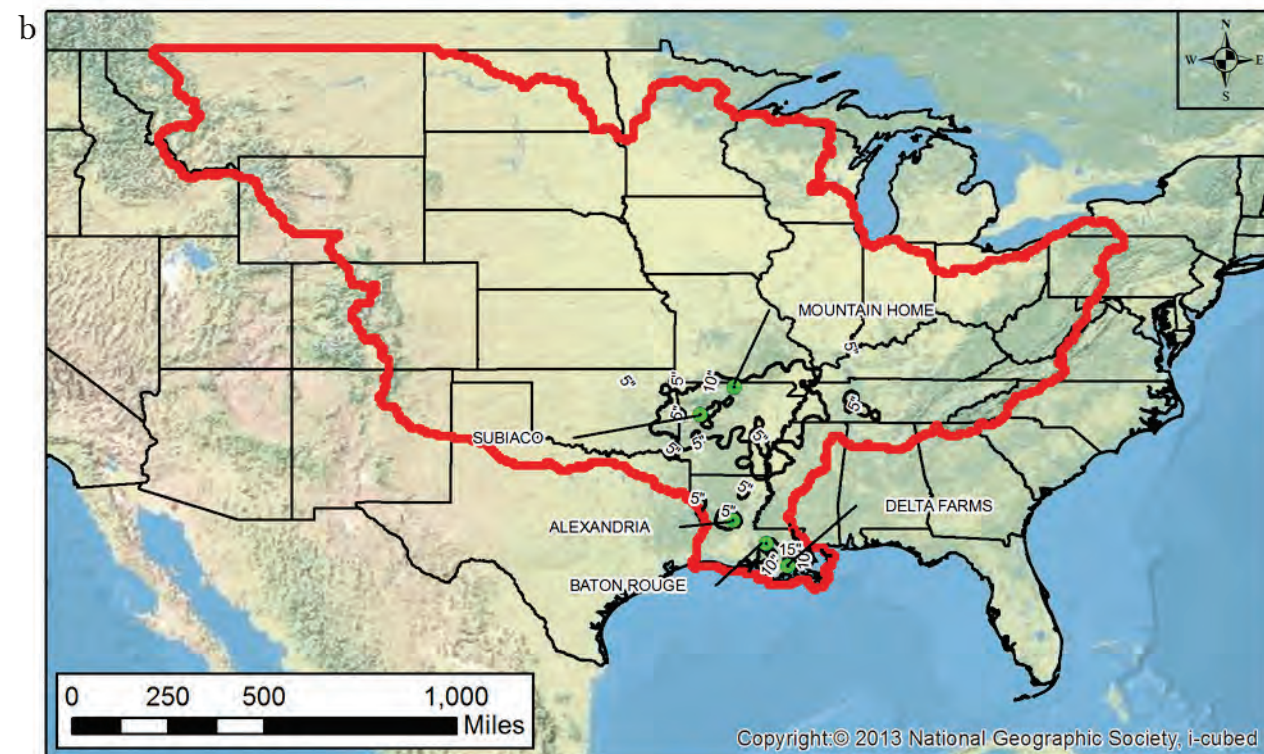
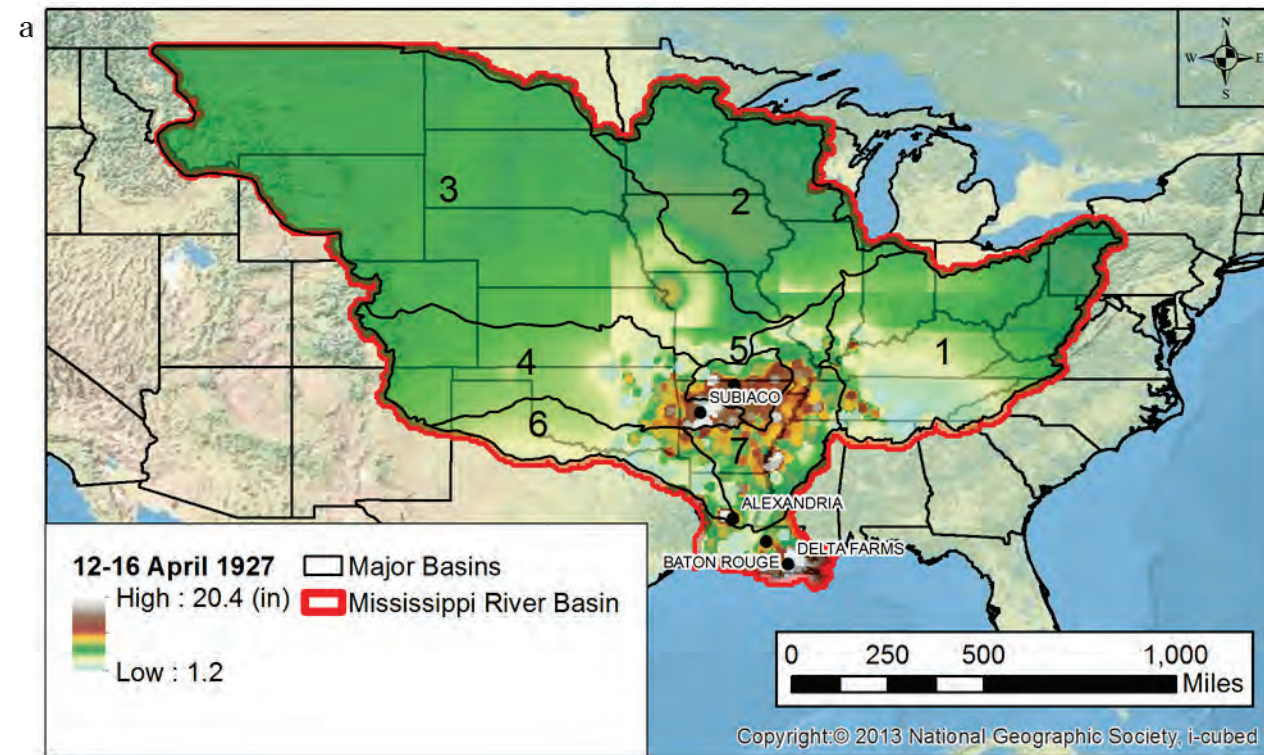
Notes:
Reconstructed cumulative precipitation data is represented by square symbols.
Original cumulative precipitation data is represented by a solid line.

d

Location	23-26 March 1913 Precipitation (in)		
	1955	2016	2016 Reconstructed
Cardington, OH	8.00 ¹	8.05	8.05
Saegerstown, PA	7.51	6.60	6.60
Beattyville, KY	5.00 ¹	3.07	3.07
Worsham, TN	5.00 ¹	4.31	4.31
St. Louis, MO	5.85	5.90	7.19
Richmond, IN	11.15	11.22	11.22

Notes:
1 = Derived by digitizing the 1955 isohyet map and interpolating to obtain values.

Figure D-2. HYPO 56 – 12–16 April 1927 (a) (top left) storm coverage over the Mississippi River Basin; (b) (bottom left) isohyetal for unadjusted April 1927 storm; (c) (top right) comparison of mass rainfall curves for original point precipitation data versus the processed/interpolated precipitation data for the unadjusted storm; and (d) (bottom right) comparison of 1955 precipitation, 2016 precipitation, and 2016 post-processed precipitation at select location.



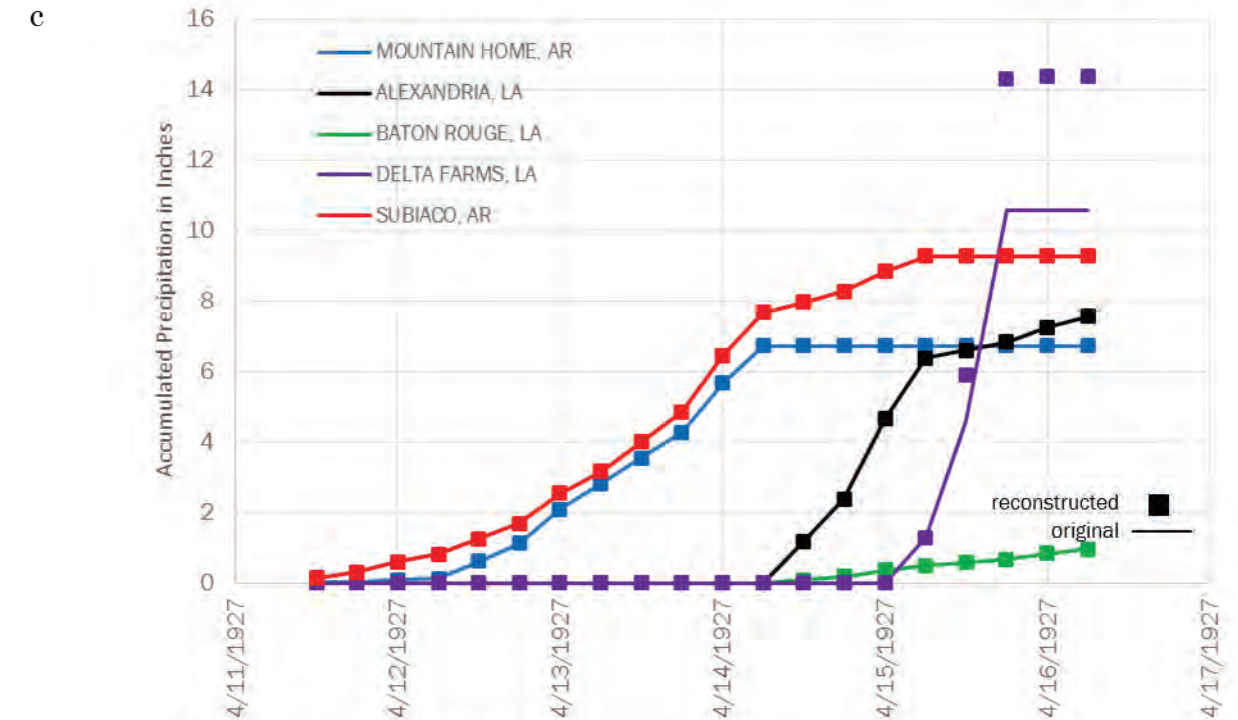
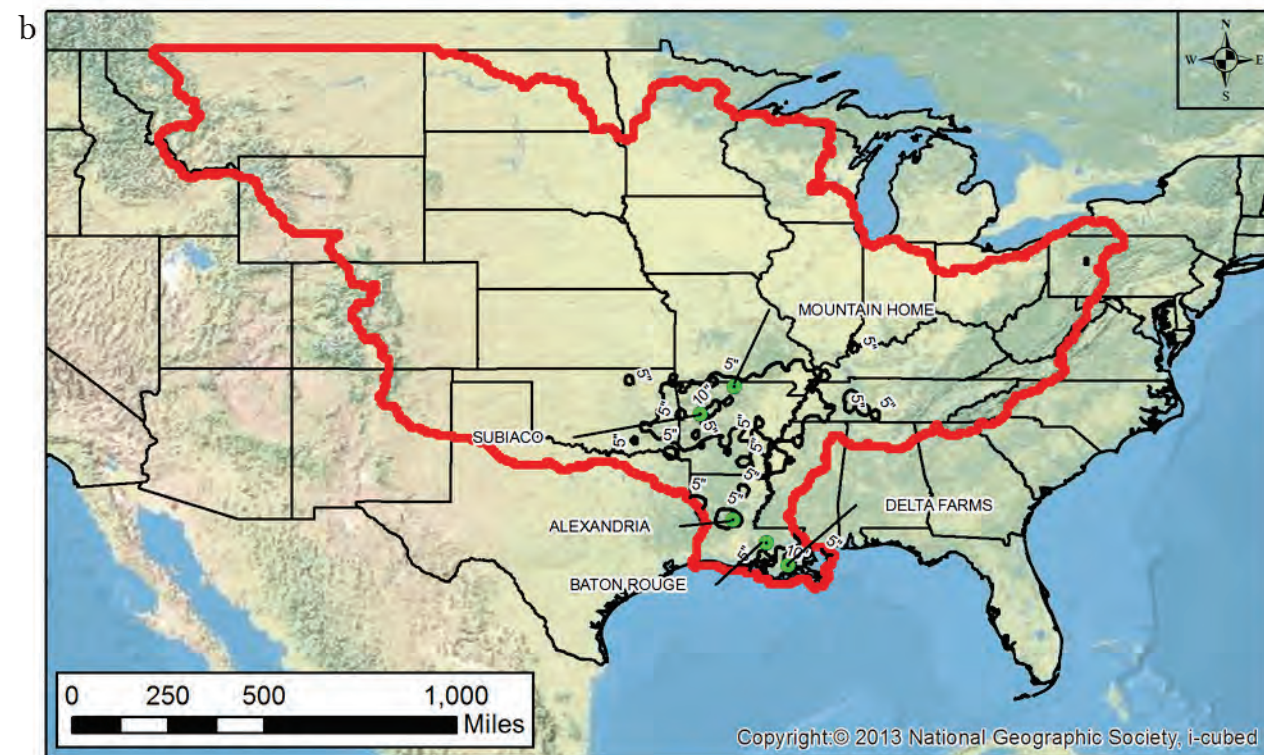
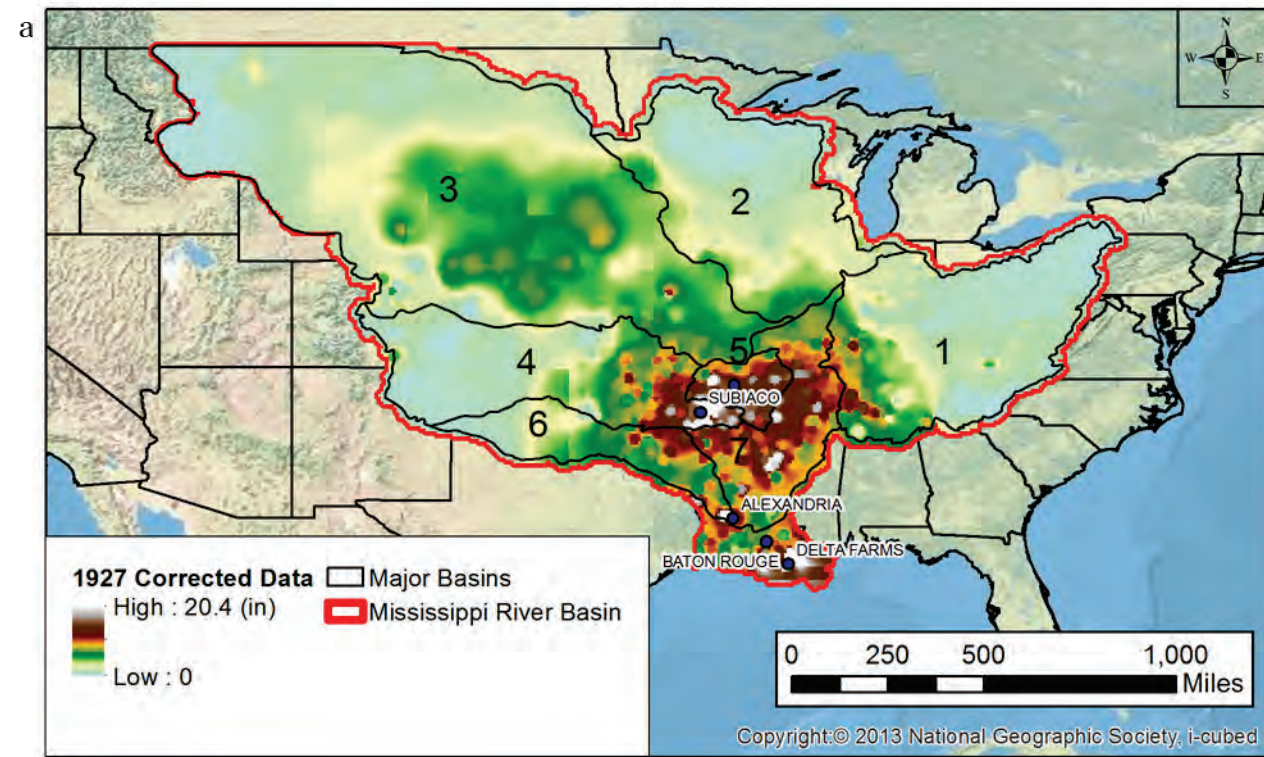
Notes:
 Reconstructed cumulative precipitation data is represented by square symbols.
 Original cumulative precipitation data is represented by a solid line.

d

Location	12-16 April 1927 Precipitation		
	1955 ¹	2016	2016 Reconstructed
Mountain Home, AR	8.88	6.70	6.70
Alexandria, LA	6.00	7.60	7.60
Baton Rouge, LA	4.47	5.32	5.32
Delta Farms, LA	10.00	11.27	11.27
Subiaco, AR	5.00	8.76	8.76

Notes:
 1 = Derived by digitizing the 1955 isohyet map and interpolating to obtain values.

Figure D-3. Corrected 12–16 April 1927 (a) (top left) storm coverage over the Mississippi River Basin; (b) (bottom left) isohyetal for unadjusted April 1927 storm; (c) (top right) comparison of mass rainfall curves for original point precipitation data versus the processed/interpolated precipitation data for the unadjusted storm; and (d) (bottom right) comparison of 1955 precipitation, 2016 precipitation, and 2016 post-processed precipitation at select location.



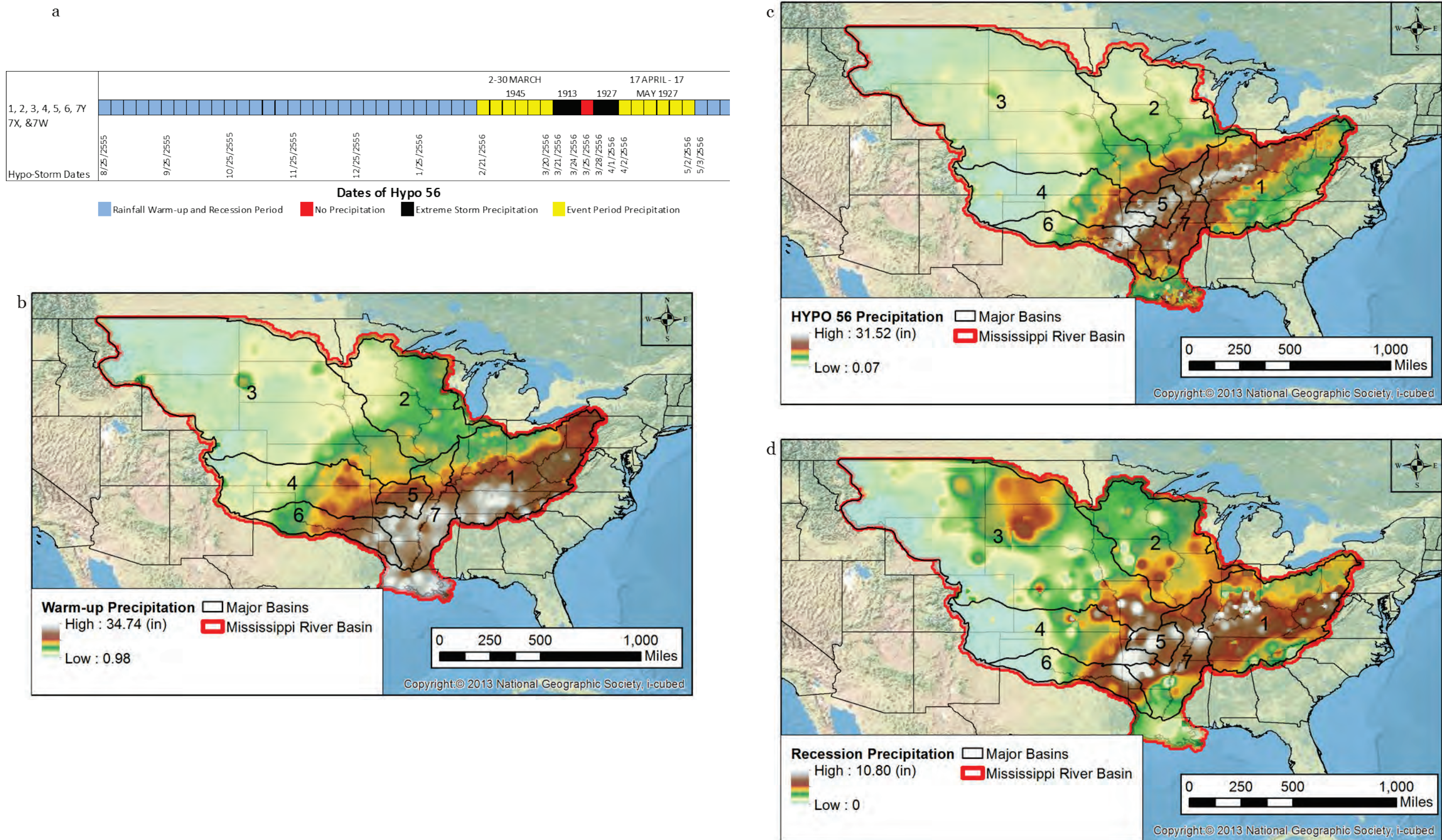
Notes:
Reconstructed cumulative precipitation data is represented by square symbols.
Original cumulative precipitation data is represented by a solid line.

d

Location	12-16 April 1927 Precipitation		
	1955 ¹	2016	2016 Reconstructed
Mountain Home, AR	8.88	6.73	6.73
Alexandria, LA	6.00	7.58	7.58
Baton Rouge, LA	4.47	0.97	0.97
Delta Farms, LA	10.00	10.60	14.40
Subiaco, AR	5.00	9.28	9.28

Notes:
1 = Derived by digitizing the 1955 isohyet map and interpolating to obtain values.

Figure D-4. HYPO 56 (a) (top left) storm sequencing with warm-up and recession periods; (b) (bottom left) warm-up precipitation coverage over the Mississippi River Basin; (c) (top right) 1927 and 1913 combined storm coverage over the Mississippi River Basin; and (d) (bottom right) recession precipitation coverage over the Mississippi River Basin.



The March 1913 storm had some of the same gage locations available to make a direct comparison to the gage locations in the MRC (1955) report; for the remaining locations, the 1955 isohyets were digitized to obtain precipitation values. The tabular data and cumulative precipitation plot show that the original 1955 values are slightly different from the 2016 values. Considering the contour lines in the 1955 report are reported in 2 in., 5 in., and 8 in. intervals, the deviation between the 1955 and 2016 values are insignificant. After the data were processed and converted to an ASCII grid, most of the locations matched well minus the values at St. Louis.

The April 1927 storm did not have the gage data available to make a direct comparison with the gage locations used in the MRC (1955) report, so the isohyetal map in the 1955 report was digitized to obtain the values at select locations. For Figure D-2, the deviation between the 1955 data and the 2016 data ranges from 0.85 in. to 3.76 in. For Figure D-3, the deviation between the 1955 data and the 2016 data ranges from 0.6 in. to 4.28 in. When the April 1927 data were compiled from the archives, several data gaps were discovered. This led to the generation of several versions of the data, and ultimately Figure D-3 is the correct storm event, but Figure D-2 was the storm event included in the 2016 hydrology model. The 2016 precipitation values are higher than the digitized 1955 storm event, which produced conservative runoff values from the model. After the 2016 data were processed, the new grids retained the original gage value, except for the Delta Farms, LA, location from Figure D-3.

D.1.1 Depth area relationships

To further validate the precipitation inputs developed by interpolation, depth-area relationships were generated using ArcGIS. Isohyetal maps for each original storm event were georeferenced, digitized in ArcMap, converted from a polyline to a TIN, converted from a TIN to a raster, and projected with USA Contiguous Albers Equal Area Conic to obtain an equal area grid size of 2,000 m × 2,000 m. For the total original HYPO storm comparisons, the projected rasters were then aggregated with the mosaic tool. The interpolated rainfall grids were clipped to the spatial extent of each original HYPO storm or to the original individual storm events. With equal area grids, a zonal histogram was generated that compares a defined precipitation interval against area. These zonal histograms were exported to excel to plot against each other.

Figure D-5 through Figure D-13 show the depth-area curves for the entire storm total precipitation over the Mississippi River Basin, as well as the totals falling over each of the seven major sub-basins.

Figure D-5. Depth-area curves for 1955 and 2016 individual storms comprising HYPO 56.

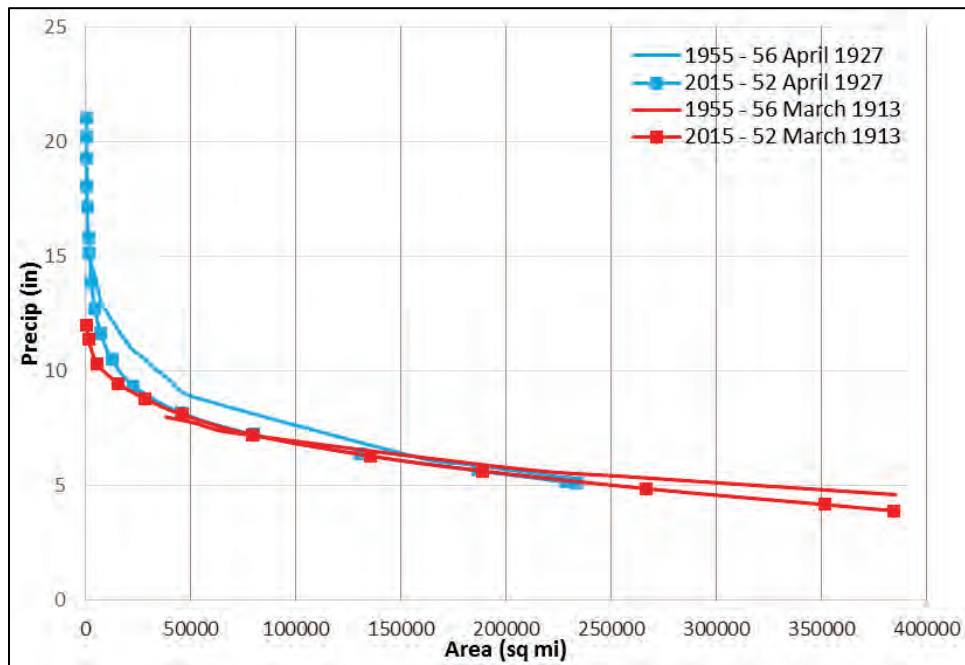


Figure D-6. Depth-area curves for 1955 and 2016 total HYPO 56 event.

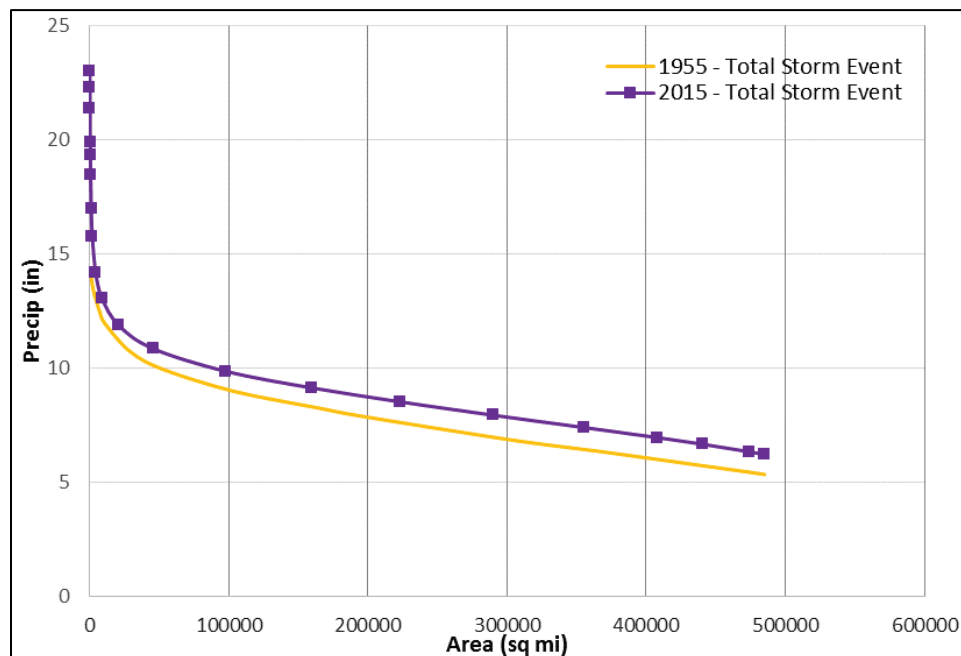


Figure D-7. Depth-area curve for 1955 and 2015 individual storm events comprising HYPO 56 over Drainage Basin 1.

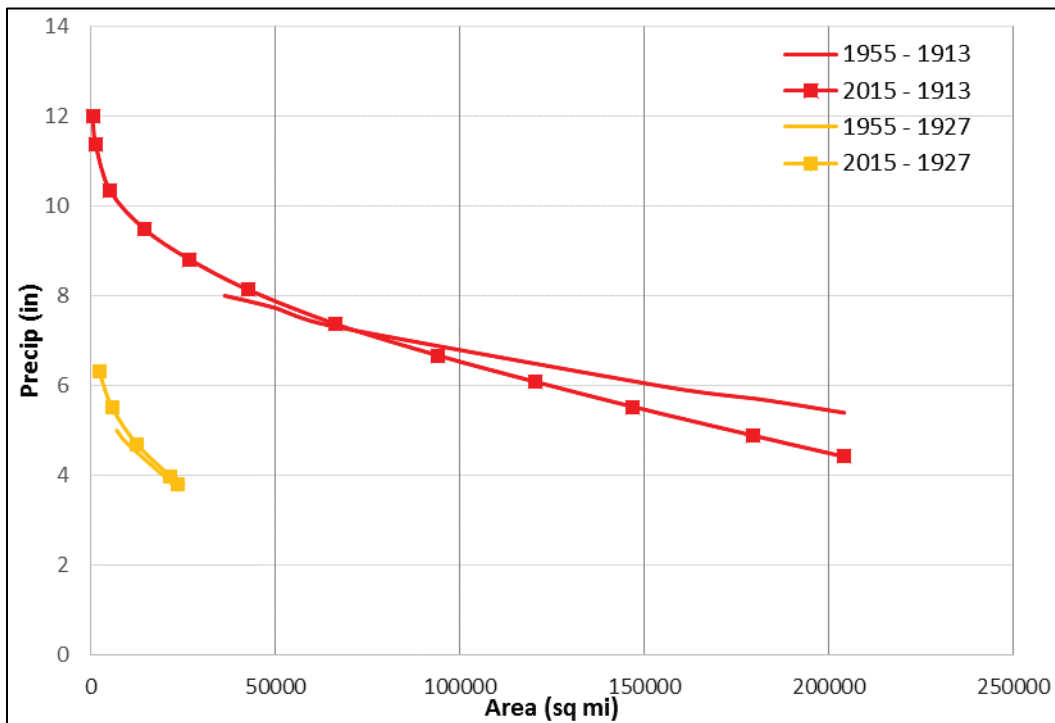


Figure D-8. Depth-area curve for 1955 and 2015 individual storm events comprising HYPO 56 over Drainage Basin 2.

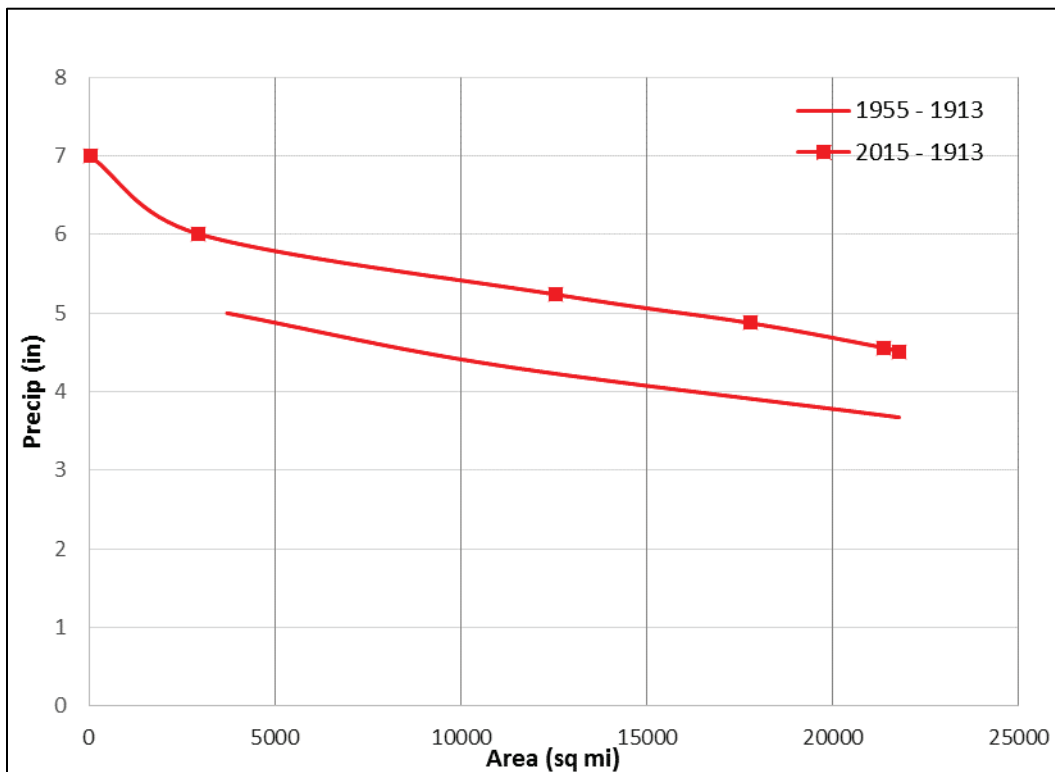


Figure D-9. Depth-area curve for 1955 and 2015 individual storm events comprising HYPO 56 over Drainage Basin 3.

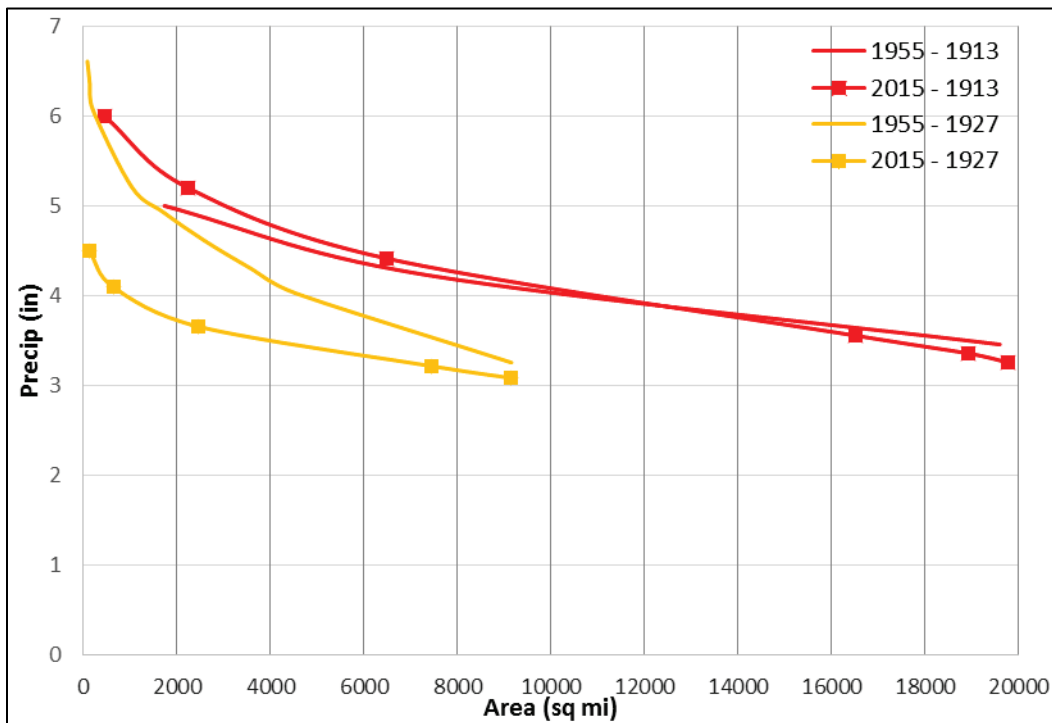


Figure D-10. Depth-area curve for 1955 and 2015 individual storm events comprising HYPO 56 over Drainage Basin 4.

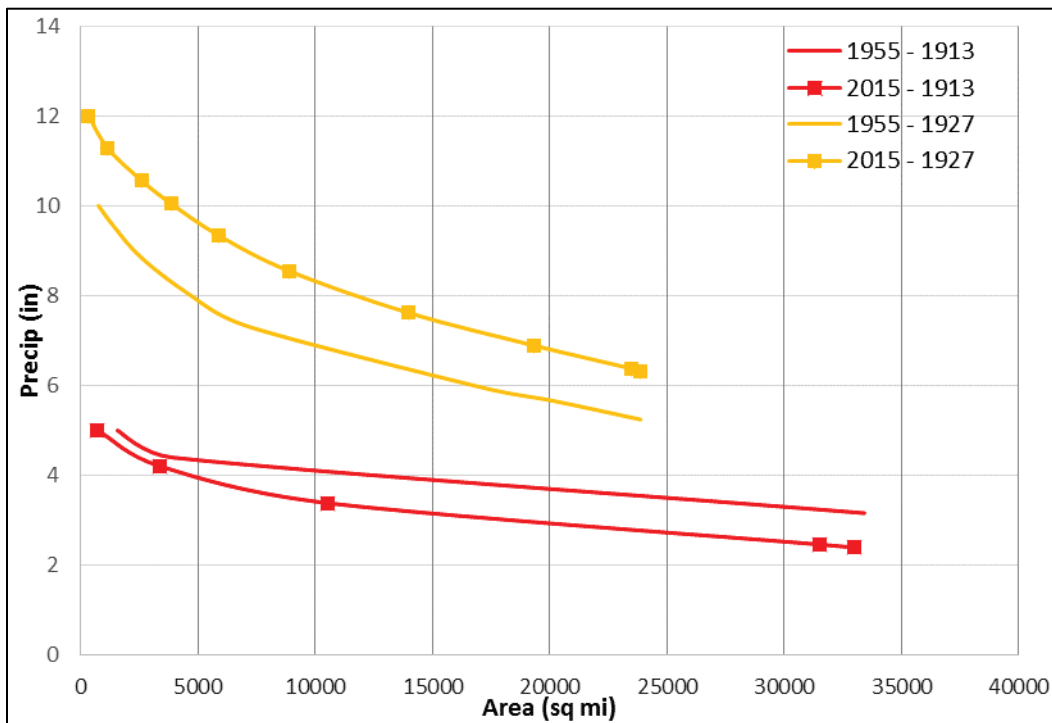


Figure D-11. Depth-area curve for 1955 and 2015 individual storm events comprising HYPO 56 over Drainage Basin 5.

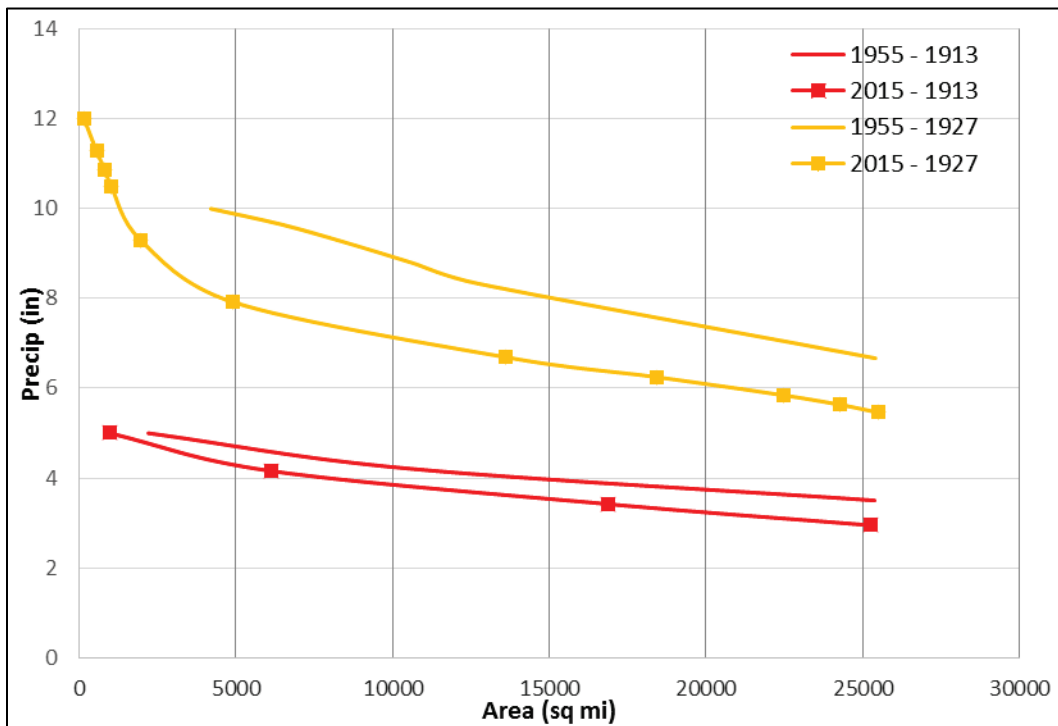


Figure D-12. Depth-area curve for 1955 and 2015 individual storm events comprising HYPO 56 over Drainage Basin 6.

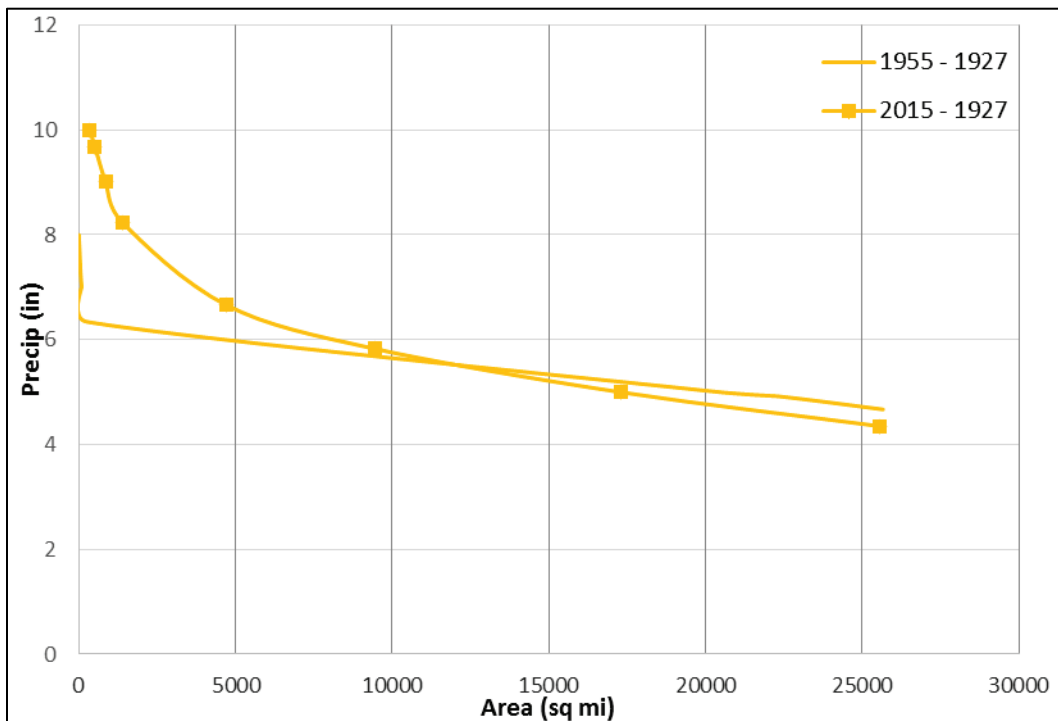
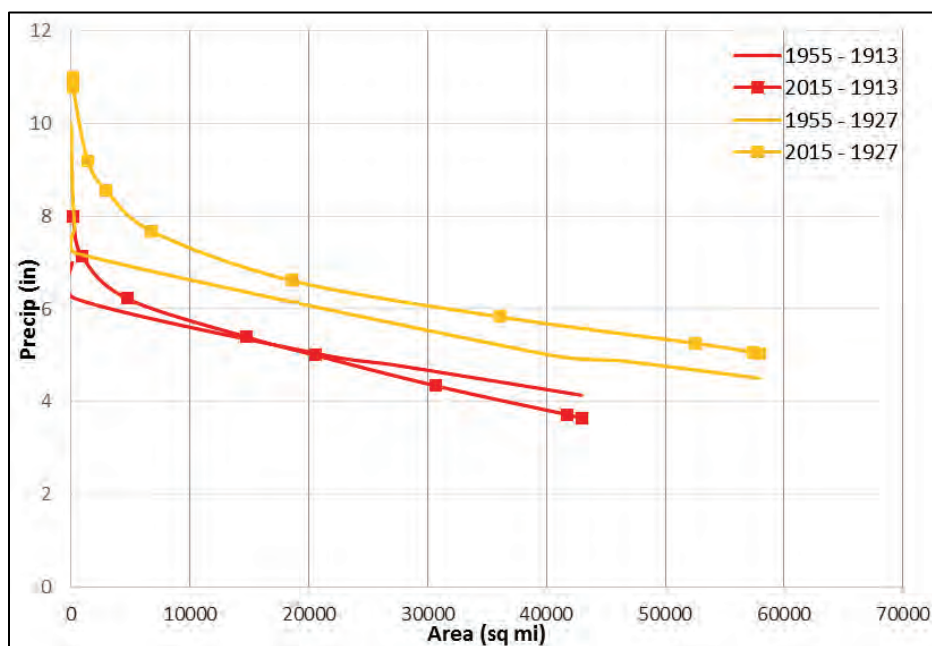


Figure D-13. Depth-area curve for 1955 and 2015 individual storm events comprising HYPO 56 over Drainage Basin 7.



Overall, the depth-area curves for 2016 precipitation inputs matched the previous 1955 rainfall maps. There were variations across each of the seven major sub-basins where 2016 depth-area curves were higher or lower than 1955 depth-area curves, but these deviations were compensated over the entire storm basin for each individual storm event and for the HYPO 56 storm event.

D.1.2 Hydrograph comparisons

Table D-1 provides a comparison of 1-day (labeled as peak), 3-day, 15-day, and 30-day volumes for HYPO 56 hydrographs. Values for the 1955 hydrographs are labeled 56 and 56-EN for unregulated and regulated flows, respectively. Values computed for the 2016 hydrographs are labeled 56-U and 56-R for unregulated and regulated flows, respectively. There appears to be good agreement between peak 1-day values for unregulated values; for instance Cairo, IL, values are 2,558 kcfs for 1955 and 2,568 kcfs for 2016. Regulated values at Cairo, IL, are 2,078 kcfs for 1955 and 2,365 kcfs for 2016, which has a greater difference with 2016 results being higher. This greater difference is consistent with observations for the HYPO 56 results. The larger difference for regulated numbers reflects the difference in how reservoir operations were included in the 1955 and 2016 investigations. The 3-day, 15-day, and 30-day volumes are also comparable for Cairo, Arkansas City, and Latitude of Red River Landing.

Table D-1. Hydrograph volume and shape comparisons for HYPO 56.

Mississippi River HYPO Flood Flow and Volume are in 1,000 cfs and sfd															
	Storm	Peak Flow	Peak Flow Date	3 Days				15 Days				30 days			
				Start	End	Volume	Mean	Start	End	Volume	Mean	Start	End	Volume	Mean
St. Louis	56-R	842	25-Mar	1-Mar	26-Mar	2,441	814	24-Mar	7-Apr	11,237	749	18-Mar	16-Apr	20,543	685
	56-U	661	12-Apr	11-Apr	13-Apr	1,966	655	3-Apr	17-Apr	8,853	590	18-Apr	20-Mar	16,309	544
	56	955	4-Apr	3-Apr	5-Apr	2,846	949	30-Mar	13-Apr	13,416	894	18-Mar	16-Apr	24,460	815
	56-EN	782	12-Apr	11-Apr	13-Apr	2,329	776	3-Apr	17-Apr	10,469	698	20-Mar	18-Apr	18,929	631
Cairo	56-R	2,365	5-Apr	4-Apr	6-Apr	7,064	2,355	27-Mar	10-Apr	33,146	2,210	19-Mar	17-Apr	54,448	1,815
	56-U	2,078	8-Apr	7-Apr	9-Apr	6,226	2,075	2-Apr	16-Apr	30,812	2,054	24-Mar	22-Apr	56,971	1,899
	56	2,568	5-Apr	4-Apr	6-Apr	7,661	2,554	26-Mar	9-Apr	36,714	2,448	19-Mar	17-Apr	61,179	2,039
	56-EN	2,558	8-Apr	7-Apr	9-Apr	7,638	2,546	2-Apr	16-Apr	35,403	2,360	24-Mar	22-Apr	60,937	2,031
Arkansas City	56-R	2,872	12-Apr	10-Apr	12-Apr	8,607	2,869	5-Apr	19-Apr	41,250	2,750	30-Mar	28-Apr	72,706	2,424
	56-U	2,755	16-Apr	15-Apr	17-Apr	8,255	2,752	8-Apr	22-Apr	40,005	2,667	1-Apr	30-Apr	73,700	2,457
	56	3,455	12-Apr	11-Apr	13-Apr	10,351	3,450	5-Apr	19-Apr	49,466	3,298	29-Mar	27-Apr	86,178	2,873
	56-EN	3,280	16-Apr	15-Apr	17-Apr	9,800	3,267	8-Apr	22-Apr	46,630	3,109	1-Apr	30-Apr	82,100	2,737
Latitude of Red River Landing	56-R	2,929	16-Apr	15-Apr	17-Apr	8,782	2,927	10-Apr	24-Apr	43,044	2,870	4-Apr	3-May	80,266	2,676
	56-U	2,712	25-Apr	24-Apr	26-Apr	8,136	2,712	19-Apr	3-May	40,569	2,705	10-Apr	9-May	79,908	2,664
	56	3,567	19-Apr	18-Apr	20-Apr	10,690	3,563	12-Apr	26-Apr	52,256	3,484	4-Apr	3-May	98,565	3,286
	56-EN	3,289	25-Apr	24-Apr	26-Apr	9,860	3,287	19-Apr	3-May	47,949	3,197	10-Apr	9-May	90,011	3,000

D.2 HEC-RAS inflow boundary discharge hydrographs

The hydrologic modeling produced discharge hydrographs at the same key locations used in the 1955 Study. Plots of unregulated (U) and regulated (R) model simulations are presented in Figure D-14 through Figure D-26. Unregulated hydrographs are shown in red, and regulated hydrographs are shown in blue.

Figure D-14. HYPO 56 hydrographs: Missouri River at Hermann, MO.

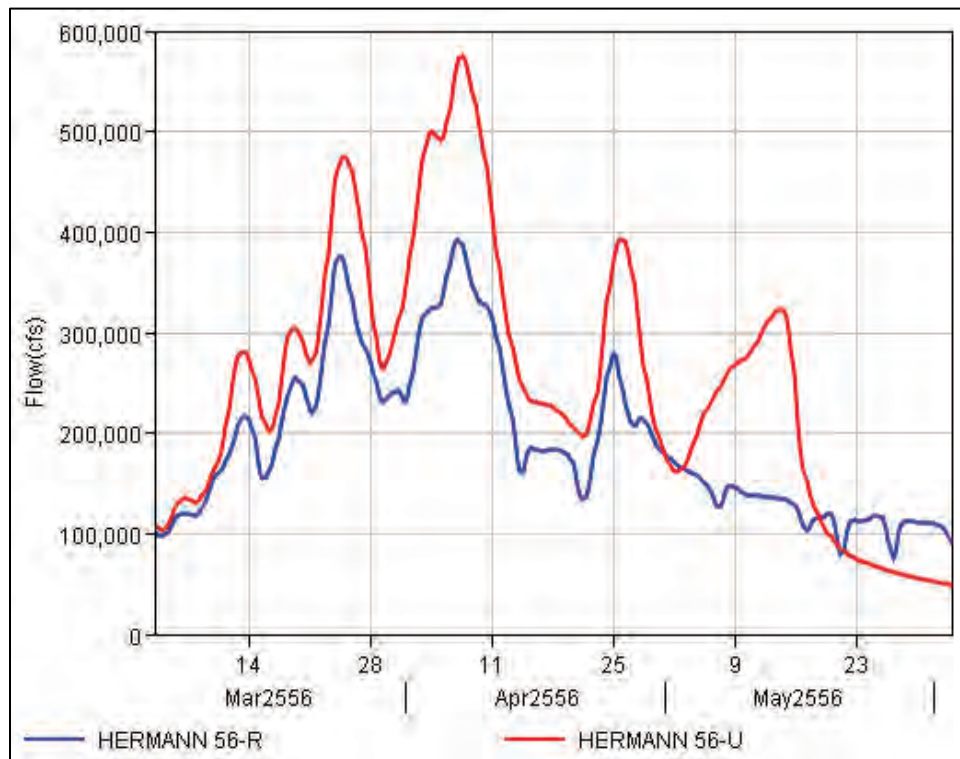


Figure D-15. HYPO 56 hydrographs: Mississippi River at Alton, IL..

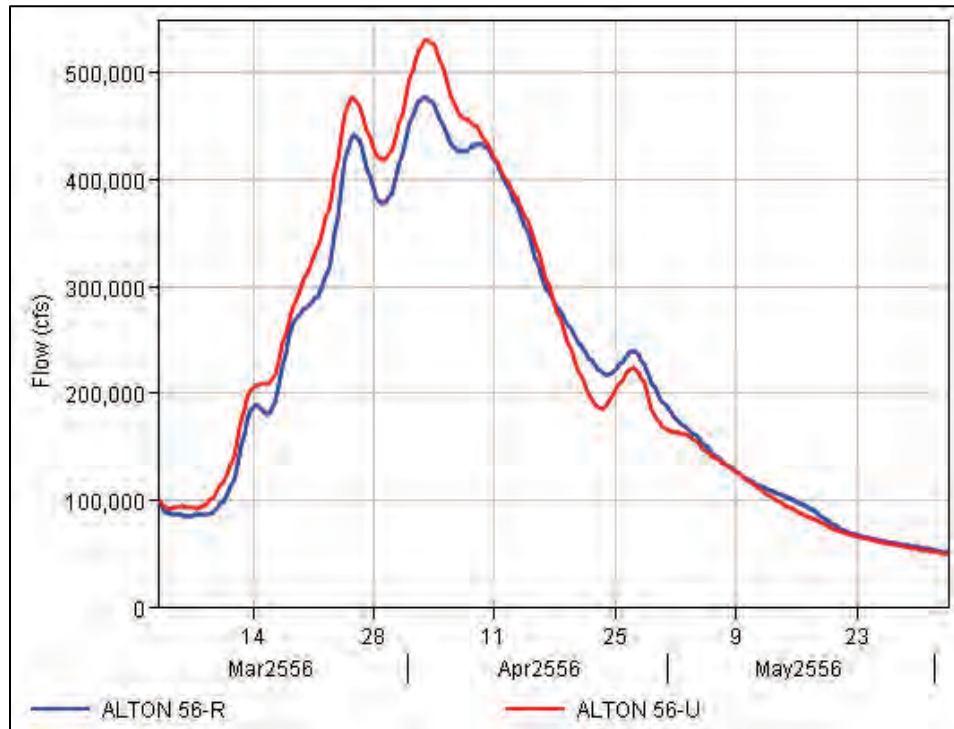


Figure D-16. HYPO 56 hydrographs: Mississippi River at St. Louis, MO.

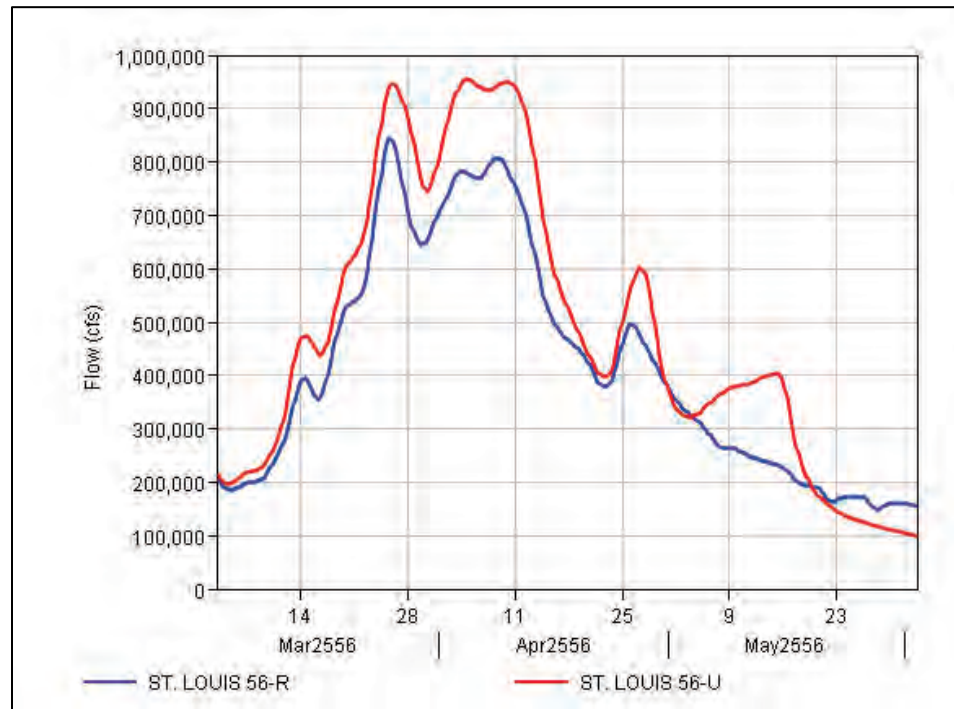


Figure D-17. HYPO 56 hydrographs: Mississippi River at Chester, IL.

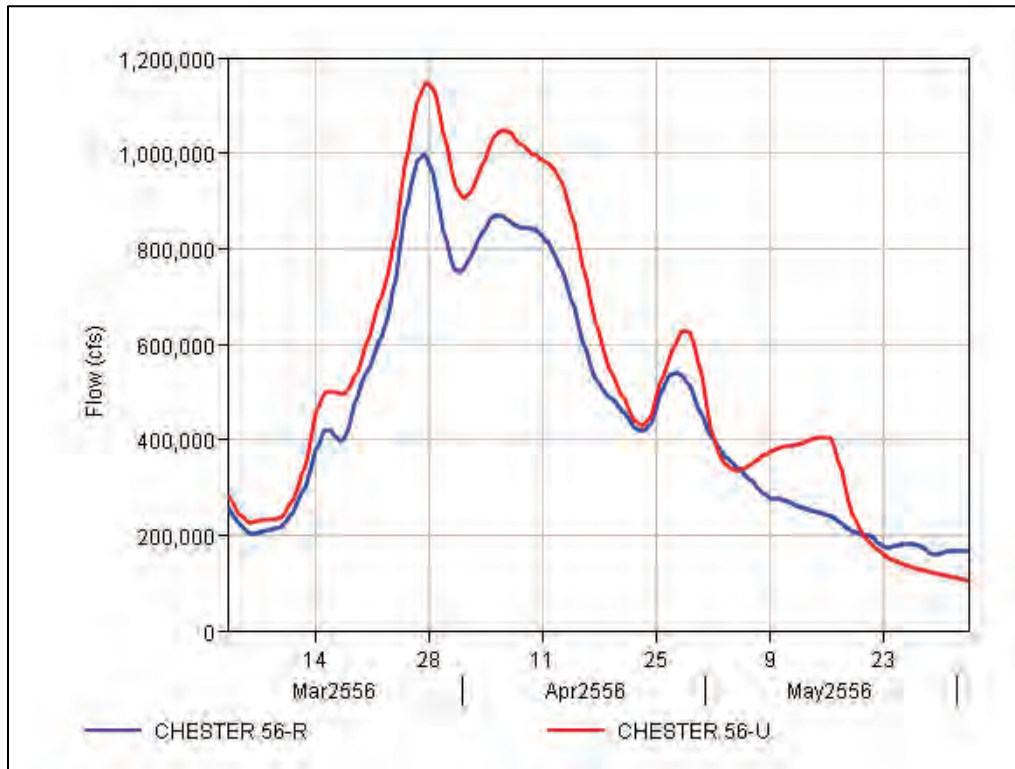


Figure D-18. HYPO 56 hydrographs: Big Muddy River at Murphysboro, IL.

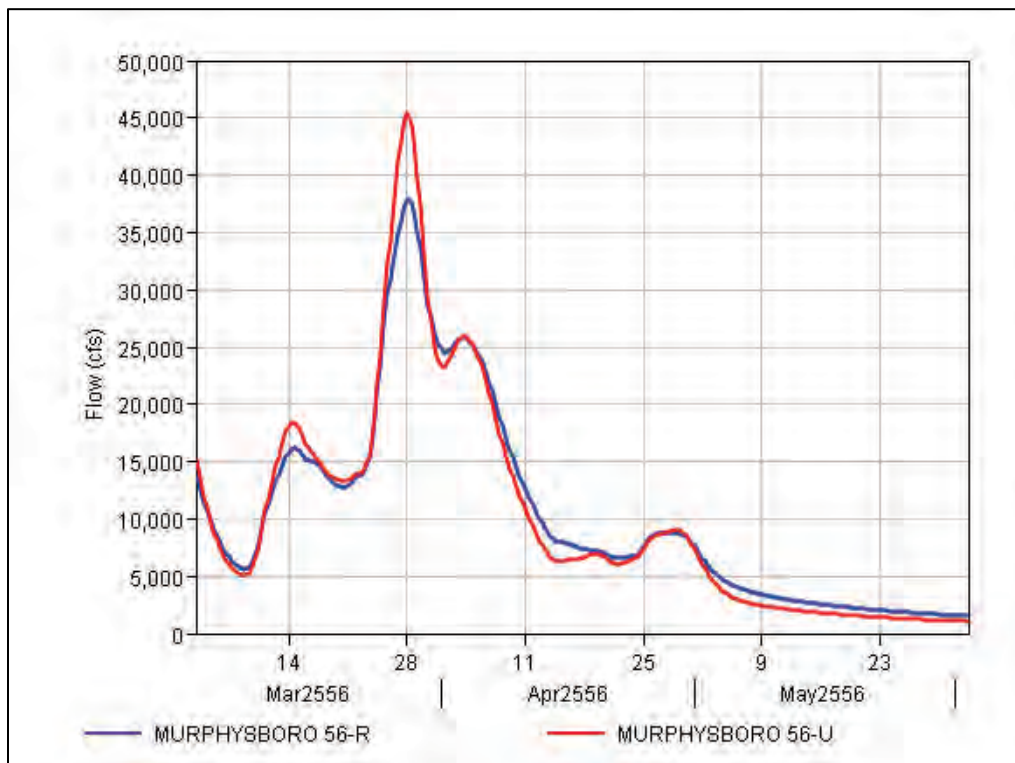


Figure D-19. HYPO 56 hydrographs: Cumberland River at Barkley Dam.

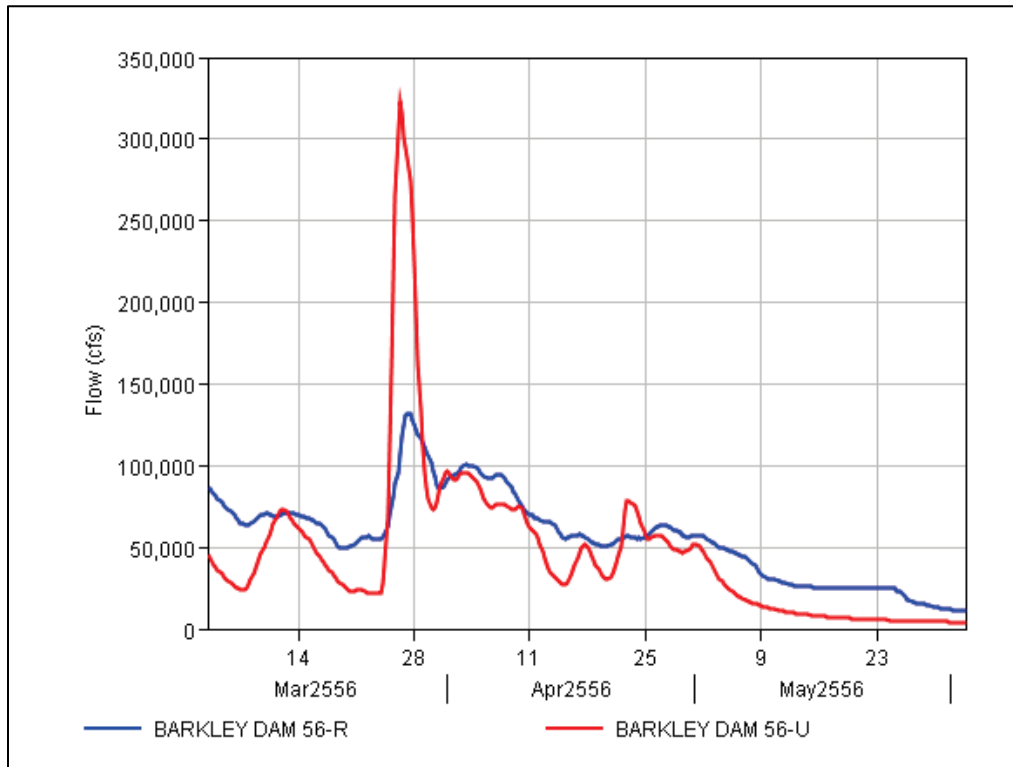


Figure D-20. HYPO 56 hydrographs: Tennessee River at Kentucky Dam.

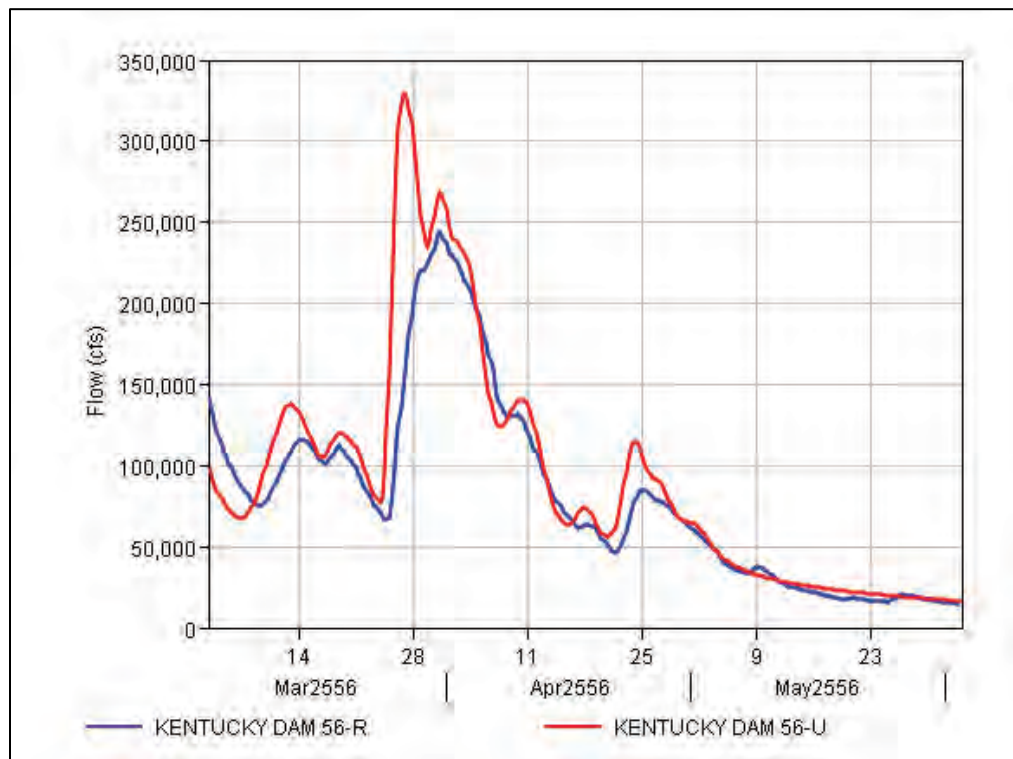


Figure D-21. HYPO 56 hydrographs: Ohio River at Smithland, IL.

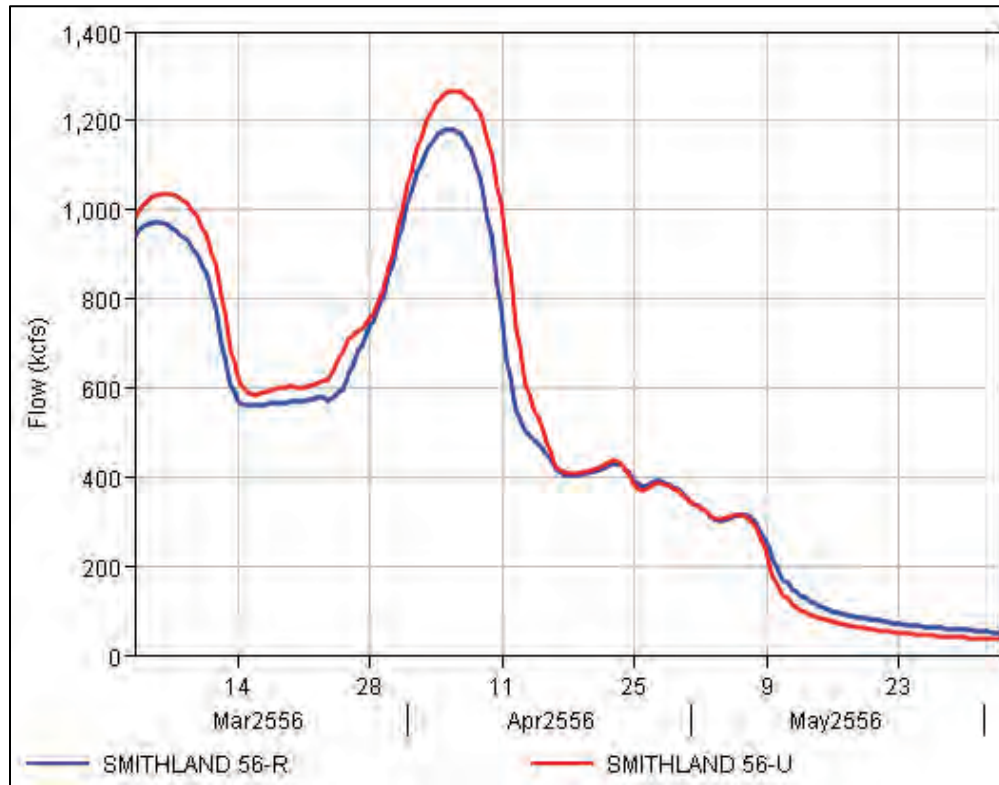


Figure D-22. HYPO 56 hydrographs: Arkansas River at Pine Bluff, AR.

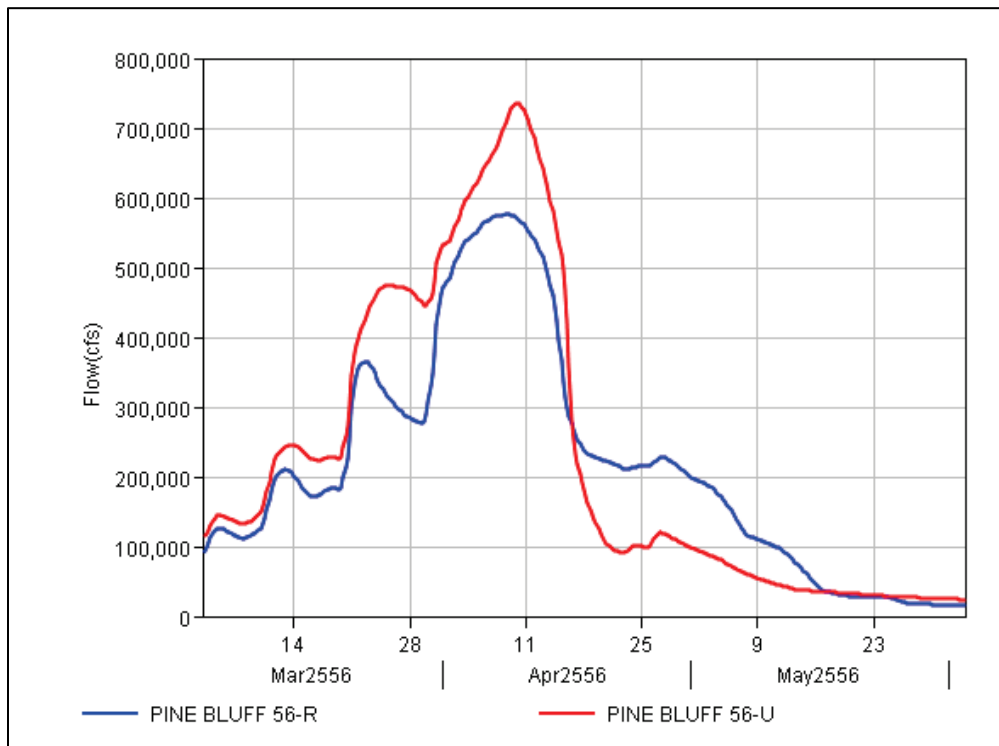


Figure D-23. HYPO 56 hydrographs: Shreveport, LA.

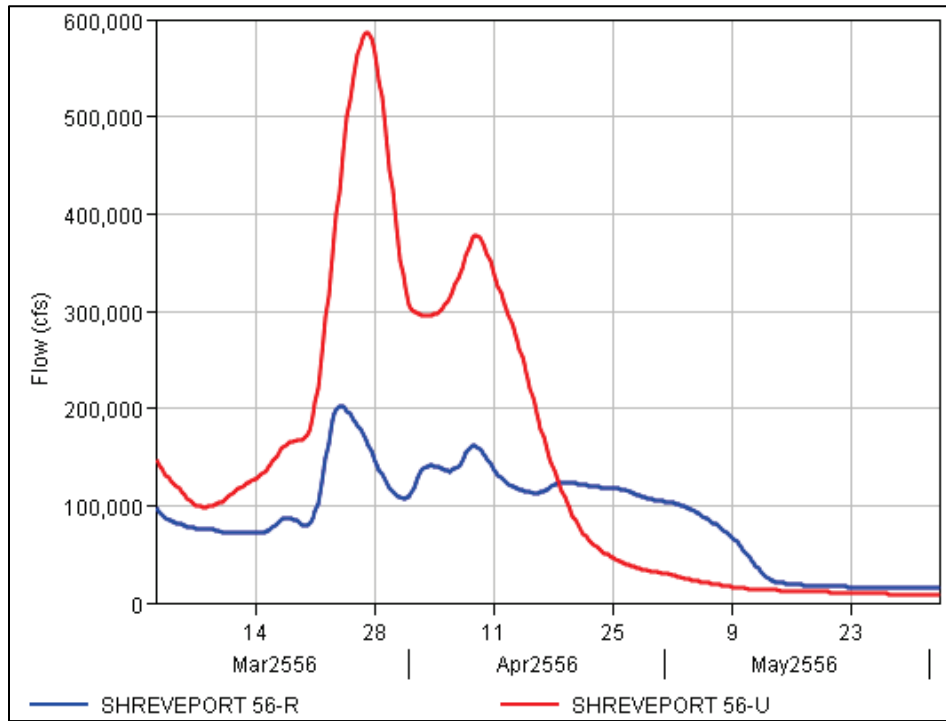


Figure D-24. HYPO 56 hydrographs: Monroe, LA.

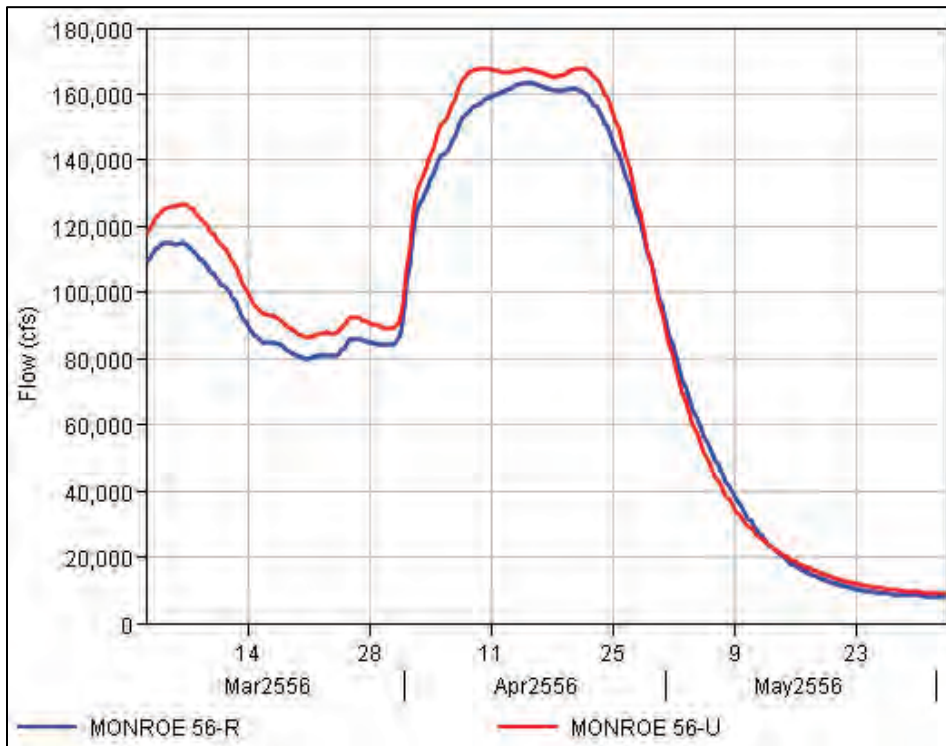


Figure D-25. HYPO 56 hydrographs: Alexandria, LA.

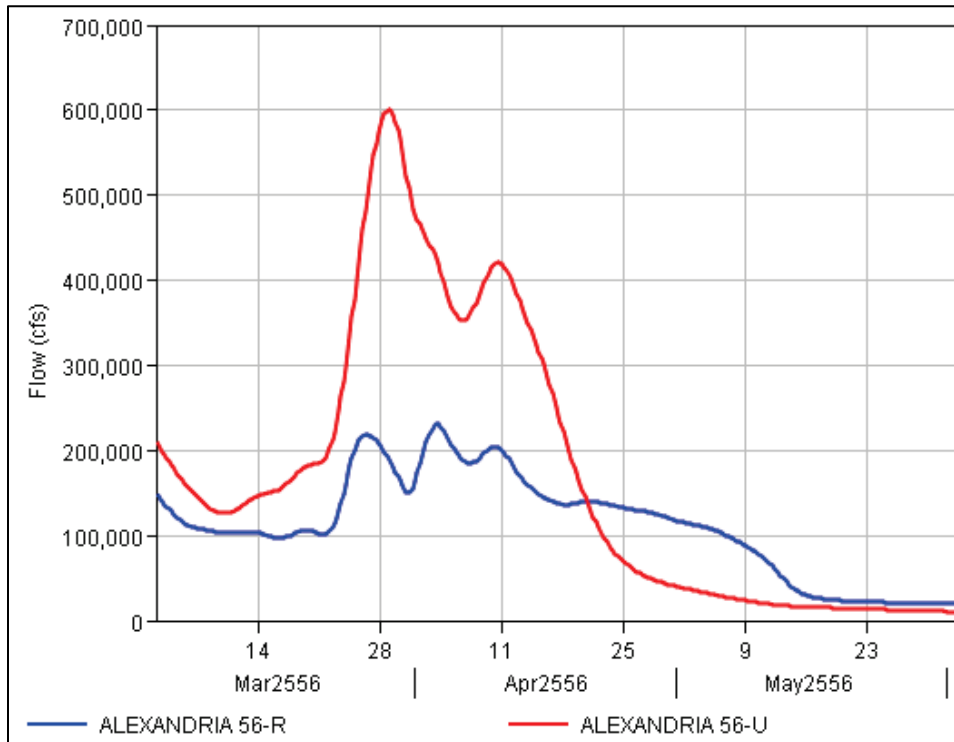
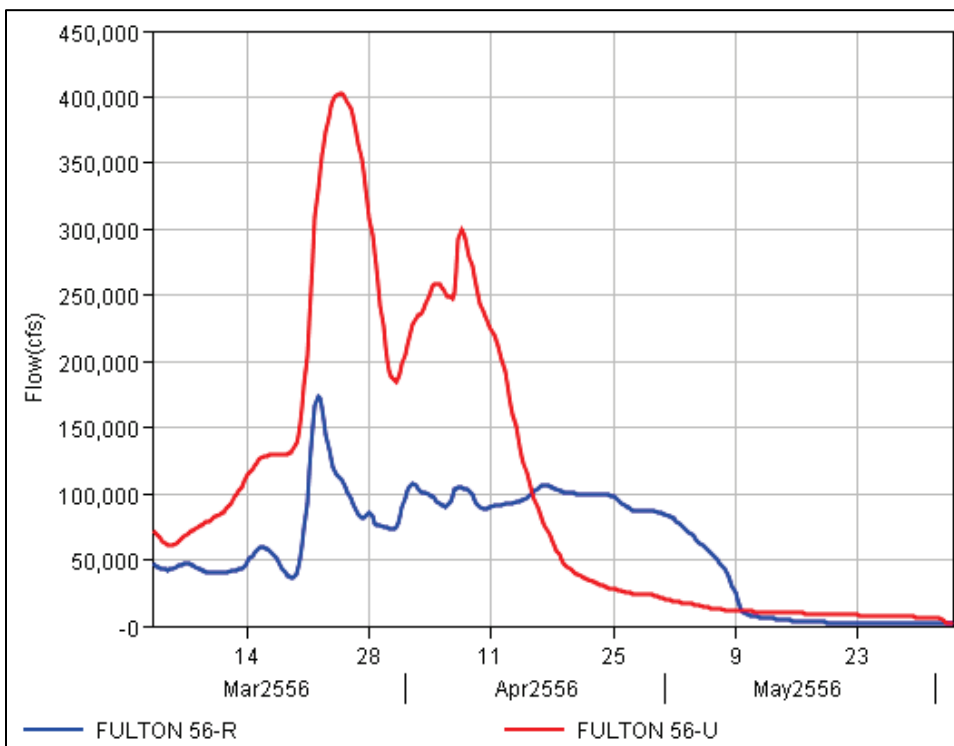


Figure D-26. HYPO 56 hydrographs: Fulton, LA.



D.3 Peak Flows for the Lower Ohio and Mississippi Rivers

A comparison of calculated peak discharges from the 2016 HEC-RAS model with values from the MRC (1955) report is given in Table D- D-2. Peak flows from the 1955 report are given as historic values in the table. The two HEC-RAS model runs reflect (1) the existing (2016) conditions for the Yazoo Backwater levee at Elevation 107.0 and (2) the authorized 1973 refined condition for the Yazoo Backwater levee at Elevation 112.8.

Table D-2. Comparison of peak flow values for HYPO 56.

Location	Project Design Flood (PDF) (from Table 7 WES [1957])					
	Unregulated Discharge (U), cfs			Regulated Discharge (Existing and Near-term Reservoirs, EN), cfs		
	56	56-U Existing Yazoo	56-U Authorized Yazoo	56-EN	56-R Existing Yazoo	56-R Authorized Yazoo
Ohio at Cairo, IL	NA	1,540,000	1,540,000	NA	1,468,000	1,468,000
Miss/Ohio Confluence (Combined)	2,560,000	2,568,000	2,568,000	2,090,000	2,365,000	2,365,000
Hickman, KY	NA	1,930,000	1,930,000	NA	1,881,000	1,881,000
Memphis, TN	2,550,000	2,592,000	2,592,000	2,180,000	2,388,000	2,388,000
Helena, AR	2,500,000	2,552,000	2,552,000	2,200,000	2,377,000	2,378,000
Arkansas City, AR	3,190,000	3,455,000	3,451,000	2,750,000	2,872,000	2,871,000
Greenville, MS	NA	3,450,000	3,448,000	NA	2,867,000	2,865,000
Lake Providence, MS	NA	3,443,000	3,445,000	NA	2,864,000	2,861,000
Vicksburg, MS	2,800,000	3,178,000	3,171,000	2,510,000	2,683,000	2,805,000
Natchez, MS	2,800,000	3,175,000	3,179,000	2,510,000	2,692,000	2,808,000
Red River Landing, LA	2,150,000	2,538,000	2,537,000	1,980,000	2,070,000	2,179,000
Baton Rouge, LA	NA	1,921,000	1,921,000	NA	1,502,000	1,568,000
Donaldsonville, LA	NA	1,920,000	1,920,000	NA	1,502,000	1,567,000
Carrollton, LA	NA	1,664,000	1,664,000	NA	1,252,000	1,312,000
Empire, LA	NA	1,593,000	1,593,000	NA	1,215,000	1,258,000
Venice, LA	NA	1,149,000	1,149,000	NA	892,000	920,000

D.3.1 Comparison of 2016 model outflow hydrographs with 1955 hydrographs

The following plots provide a comparison of 2016 hydrologic model or HEC-RAS model outflows with available 1955 hydrographs. Both unregulated and regulated hydrographs are compared for the mainstem Mississippi River locations. Only unregulated hydrographs were available for tributary locations from the 1955 Study; therefore, those locations do not include regulated hydrographs.

The HEC-RAS model included two separate runs: (1) Existing, Yazoo Backwater levee at elevation 207.1 and (2) Authorized, Yazoo Backwater levee at elevation 212.8. For most plots there is no difference between the Existing and Authorized Yazoo Backwater levee results except near the peak of the hydrograph. Where there are differences, an inset is included to show the relative differences between these two runs. Where there are no differences between the existing and authorized Yazoo Backwater runs, only a single line appears in the plot because the lines plot directly on top of each other.

Figure D-26. Alexandria, LA, HYPO 56 1955 unregulated flow compared to 2016 unregulated flow generated by the RFC.

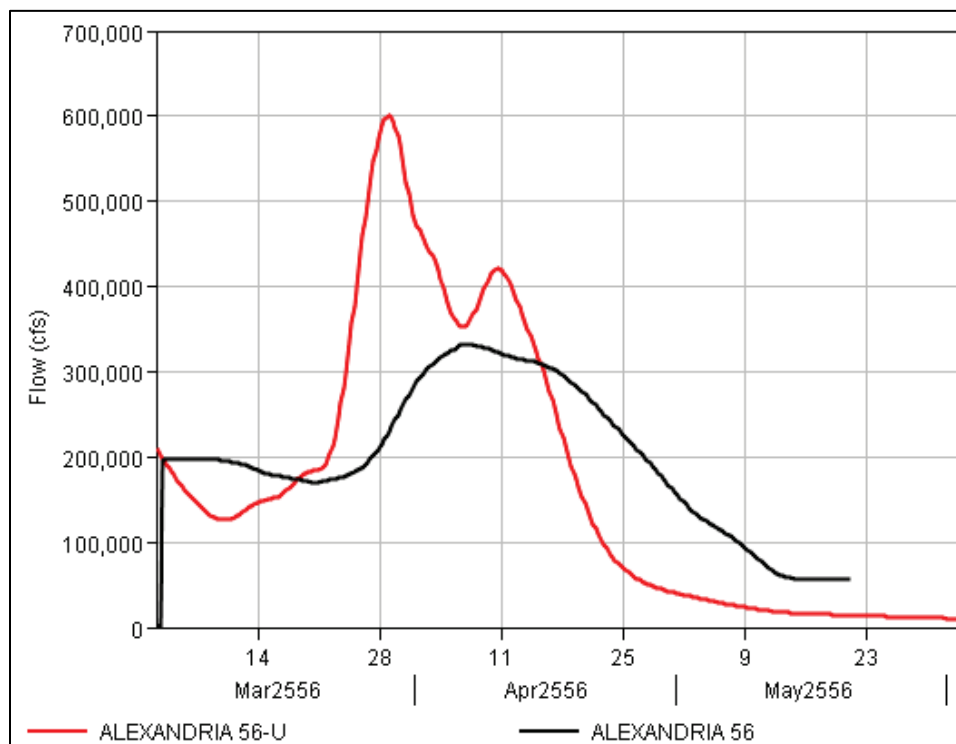


Figure D-27. Alton, IL, HYPO 56 1955 unregulated flow compared to 2016 unregulated flow generated by the RFC.

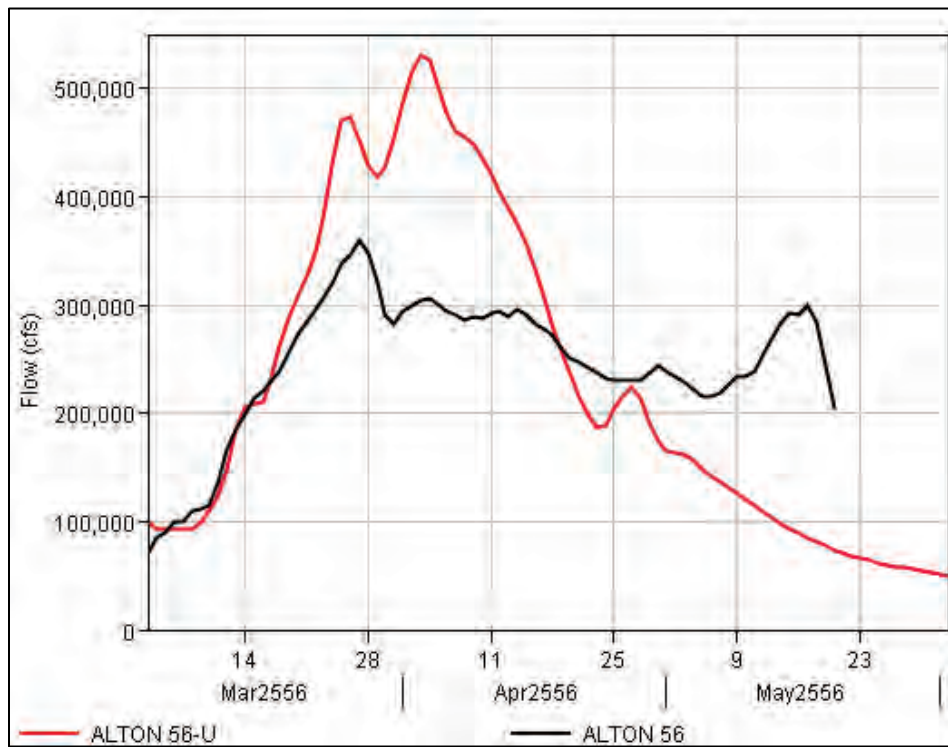


Figure D-28. Hermann, MO, HYPO 56 1955 unregulated flow compared to 2016 unregulated flow generated by the RFC.

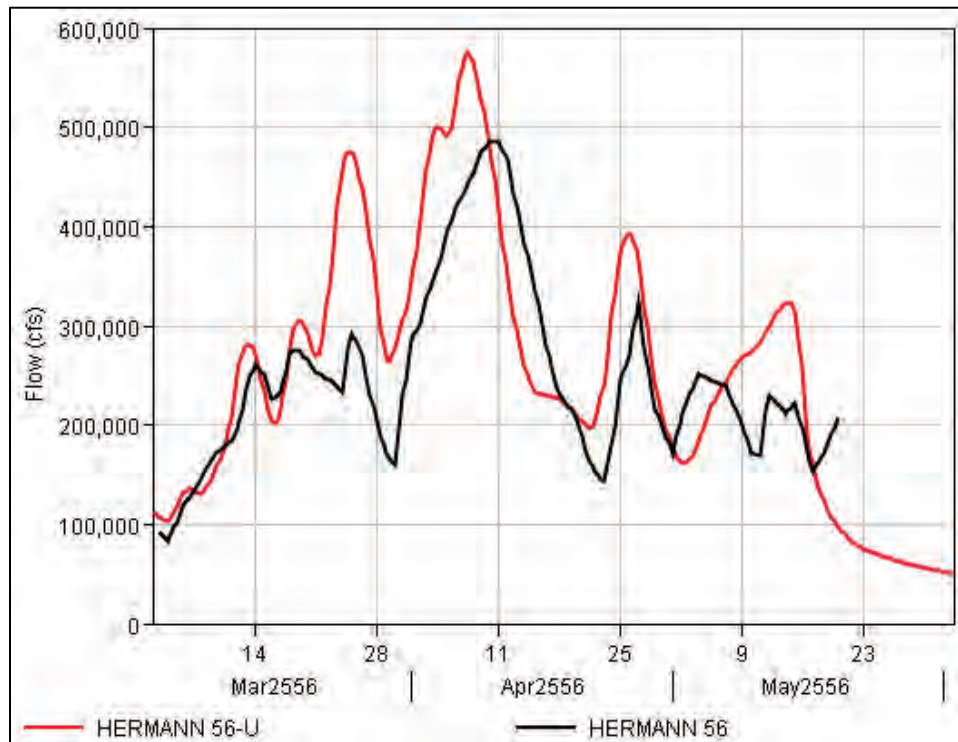


Figure D-29. Little Rock, AR, HYPO 56 1955 unregulated flow compared to 2016 unregulated flow generated by the RFC.

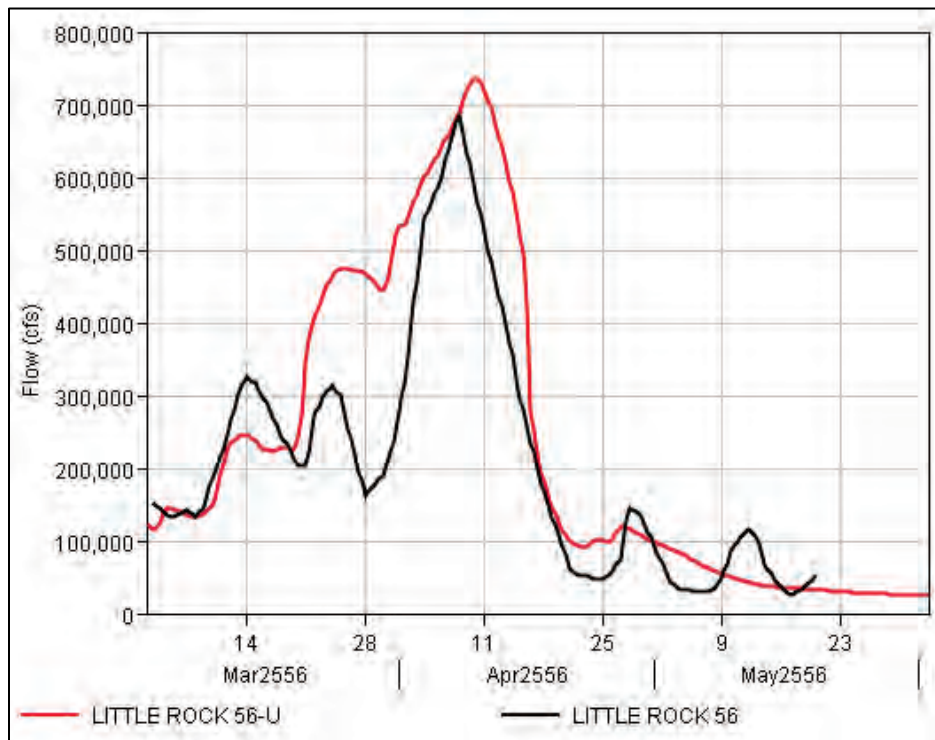


Figure D-30. St. Louis, MO, HYPO 56 1955 unregulated flow compared to 2016 unregulated flow generated by the RFC.

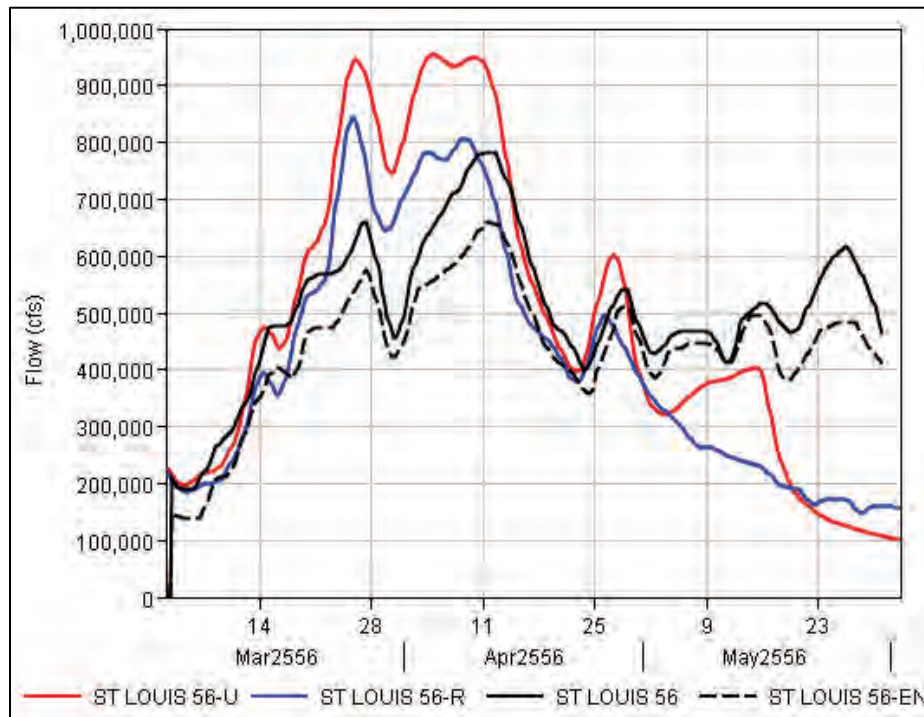


Figure D-31. Arkansas City, AR, HYPO 56 1955 unregulated flow compared to 2016 unregulated flow generated by the RFC.

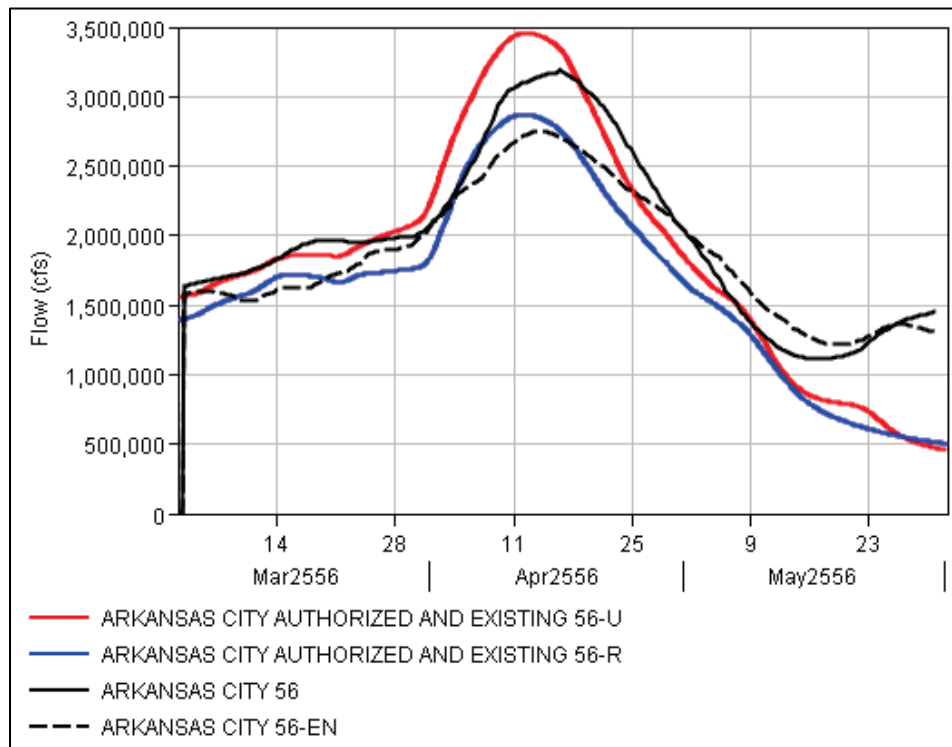


Figure D-32. Cairo, IL, HYPO 56 1955 unregulated flow compared to 2016 unregulated flow generated by the RFC.

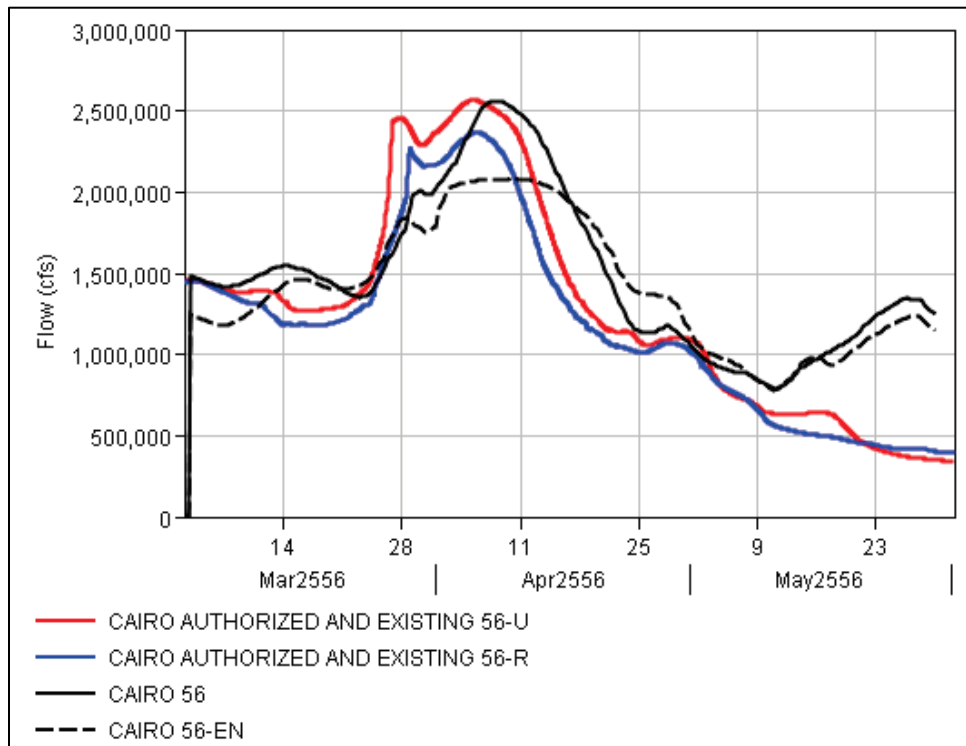


Figure D-33. Clarendon, AR, HYPO 56 1955 unregulated flow compared to 2016 unregulated flow generated by the RFC.

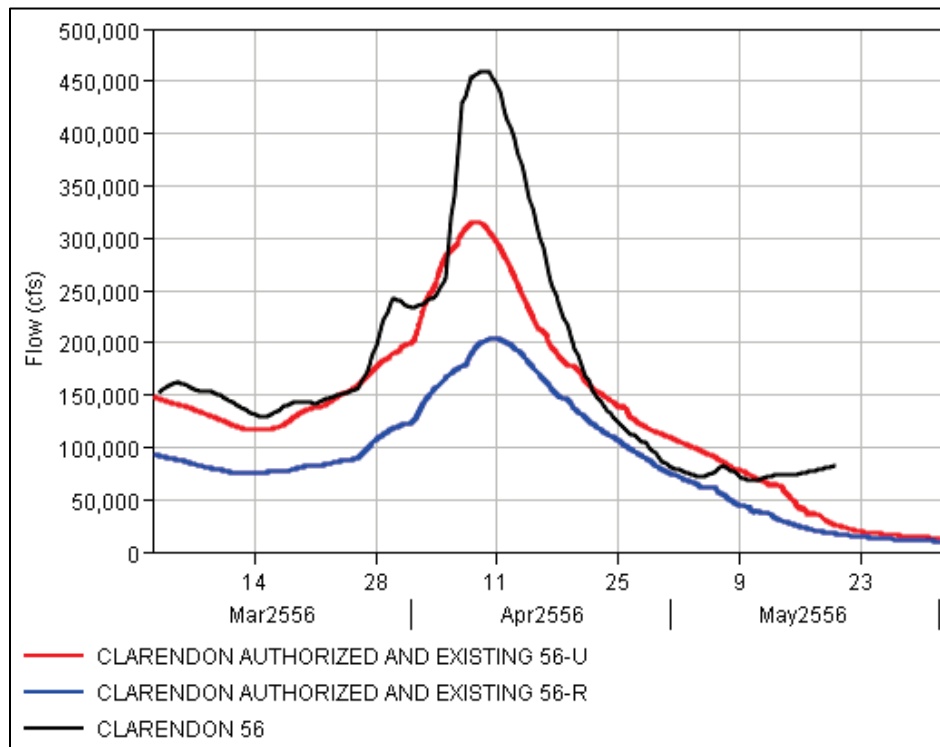


Figure D-34. Metropolis, IL, HYPO 56 1955 unregulated flow compared to 2016 unregulated flow generated by the RFC.

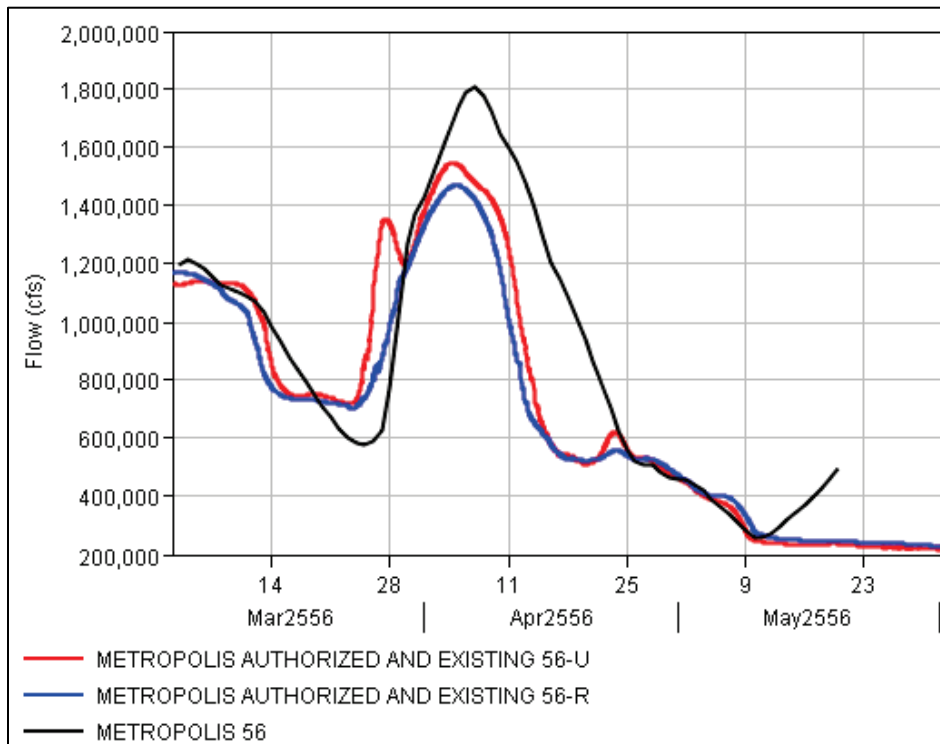
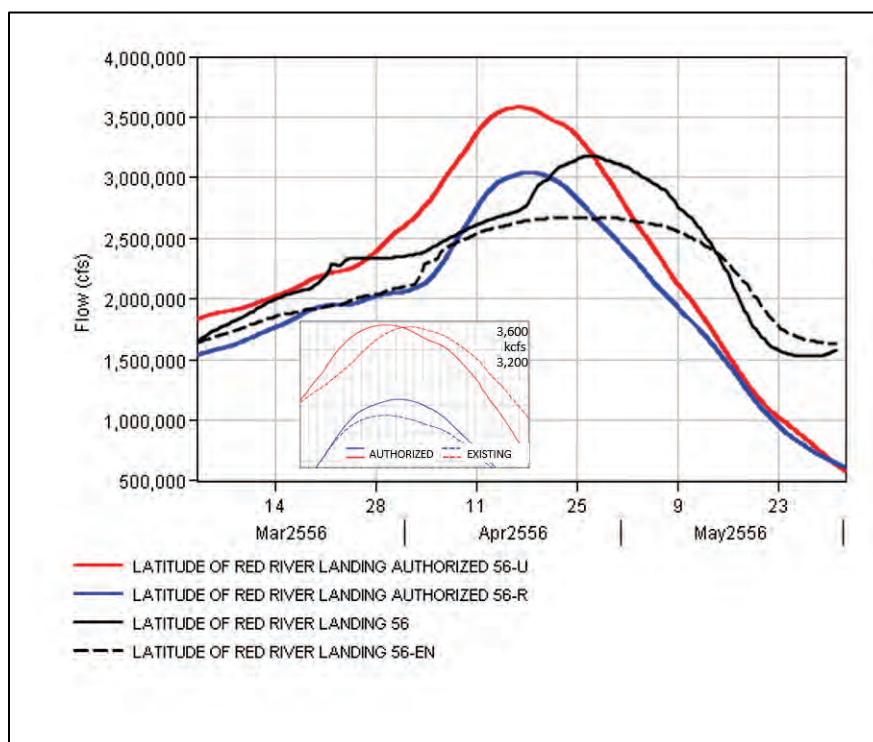


Figure D-35. Latitude of Red River Landing, LA, HYPO 56 1955 unregulated flow compared to 2016 unregulated flow generated by the RFC.



D.3.2 HYPO 56 HEC-RAS unsteady model outflows

The combined MVD HEC-RAS model developed for the current assessment provides unsteady hydrodynamic flood routing along the main river channels within the assessment area. Peak flow and event hydrographs for the Ohio and Lower Mississippi Rivers (points downstream of the Ohio/Mississippi confluence) are direct outflows from the HEC-RAS unsteady calculations. The HEC-RAS model included two separate runs: (1) Existing, Yazoo Backwater levee at elevation 207.1 and (2) Authorized, Yazoo Backwater levee at elevation 212.8. For most plots there is no difference between the Existing and Authorized Yazoo Backwater levee results except near the peak of the hydrograph. Where there are differences, an inset is included to show the relative differences between these two runs. Where there are no differences between the existing and authorized Yazoo Backwater runs, only a single line appears in the plot because the lines plot directly on top of each other.

Figure D-36. HYPO 56 HEC-RAS hydrograph: Ohio River at Cairo, IL.

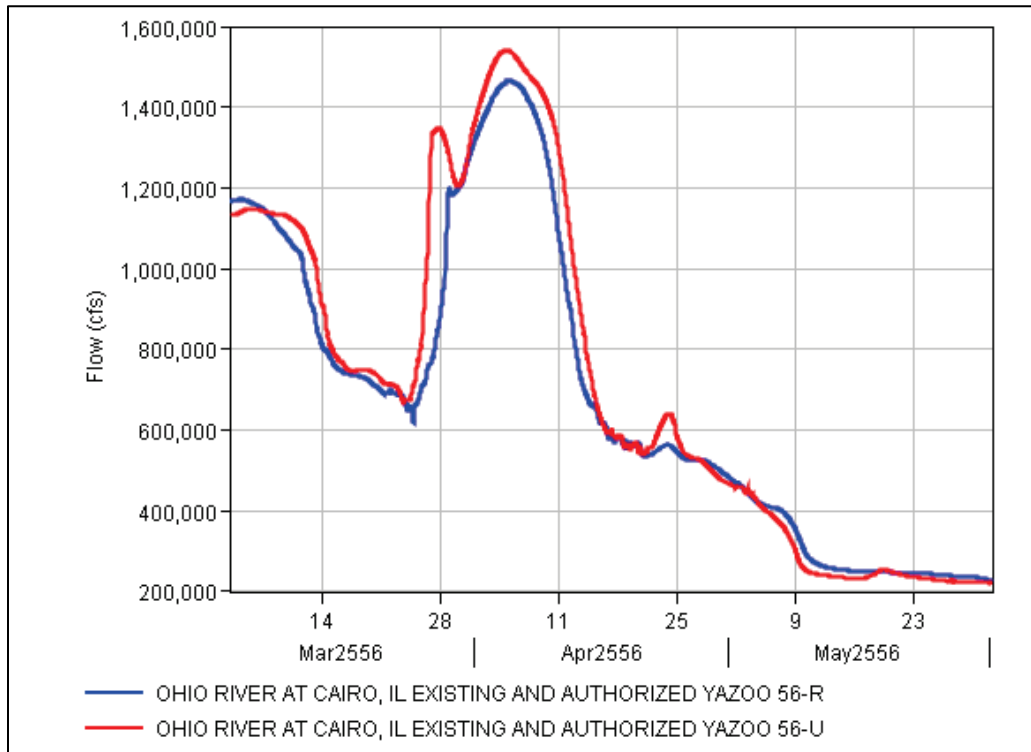


Figure D-37. HYPO 56 HEC-RAS hydrograph: Combined Ohio and Mississippi River flow near Cairo, IL.

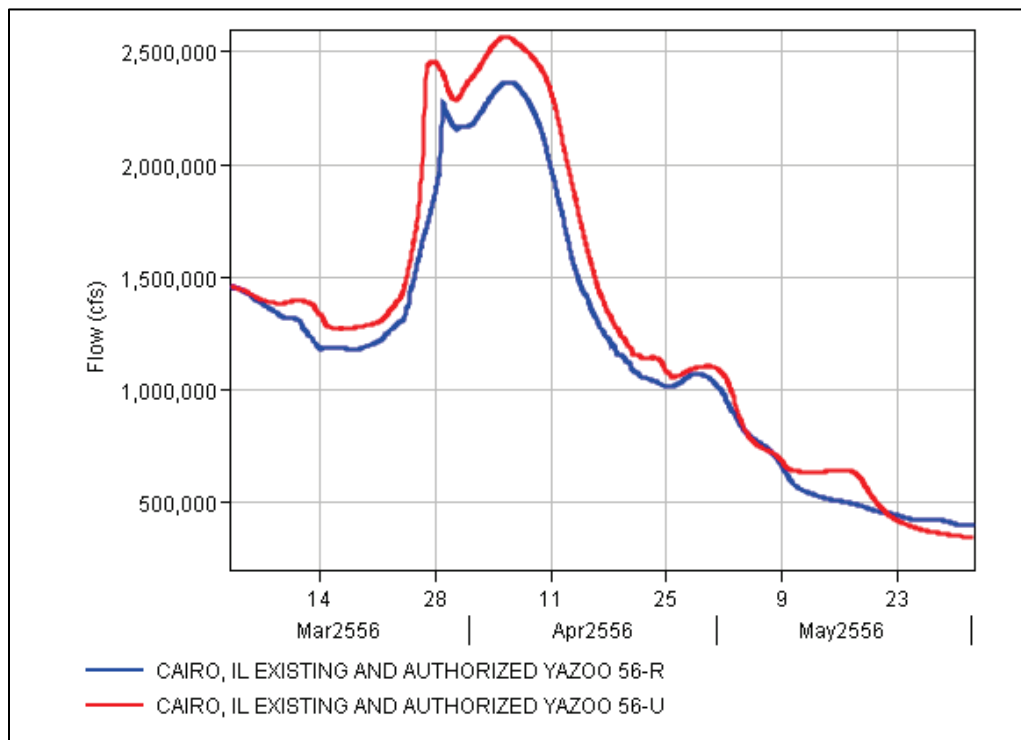


Figure D-38. HYPO 56 HEC-RAS hydrograph: Mississippi River at Hickman, KY.

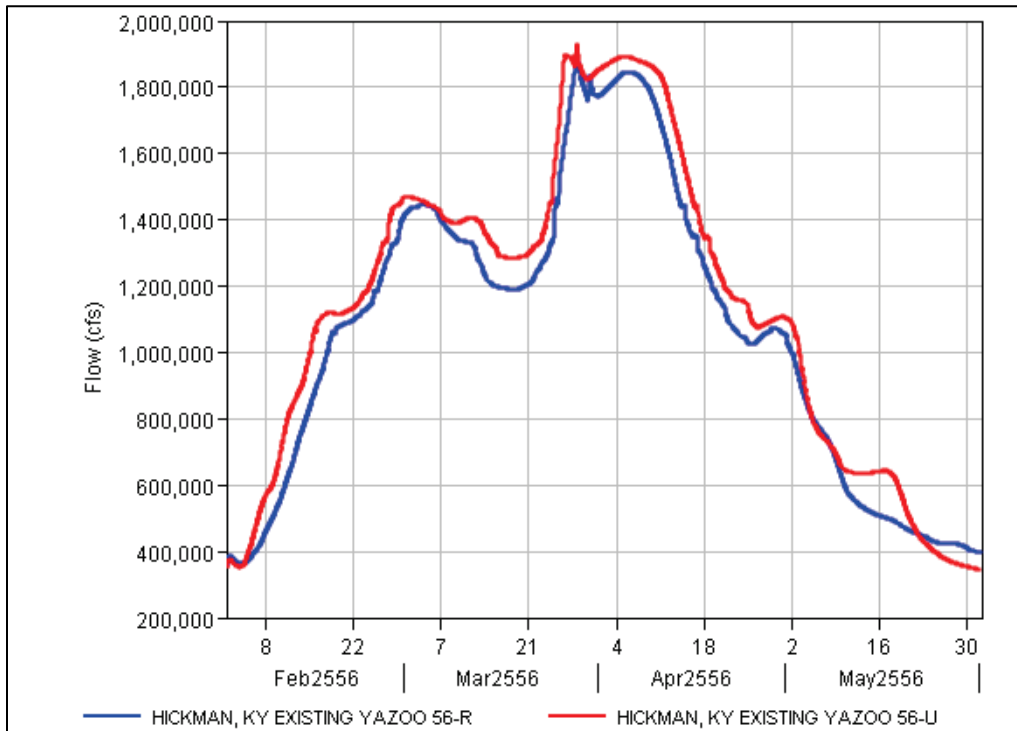


Figure D-39. HYPO 56 HEC-RAS hydrograph: Mississippi River at Memphis, TN.

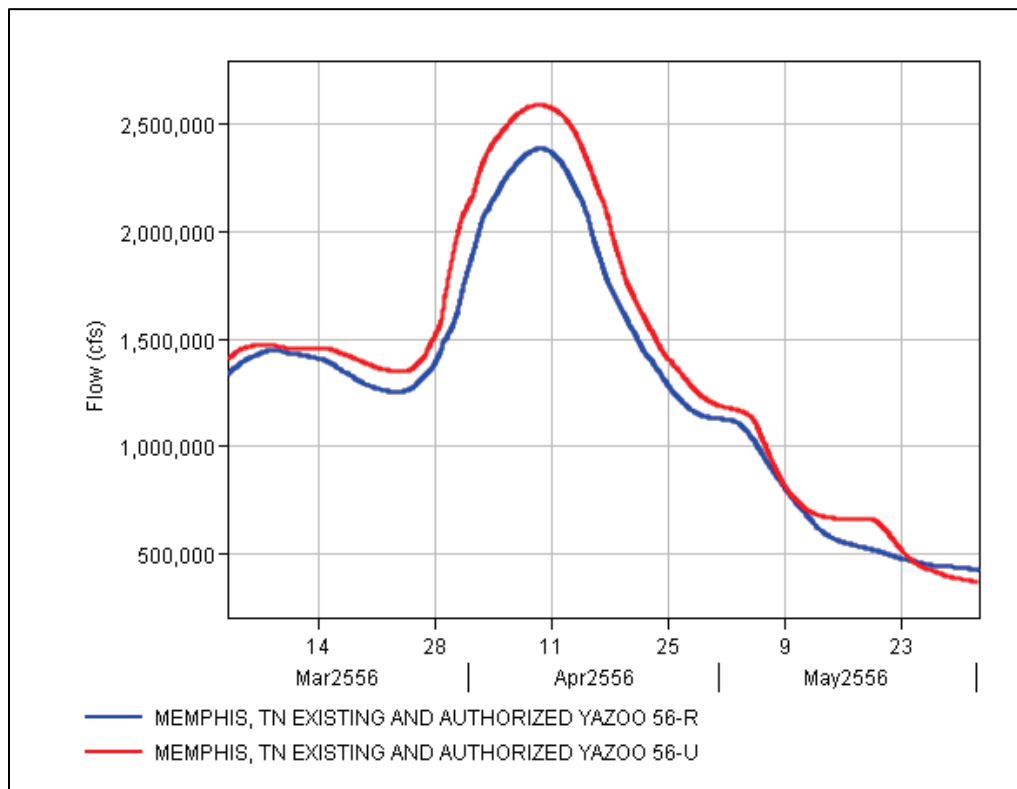


Figure D-40. HYPO 56 HEC-RAS hydrograph: Mississippi River at Helena, AR.

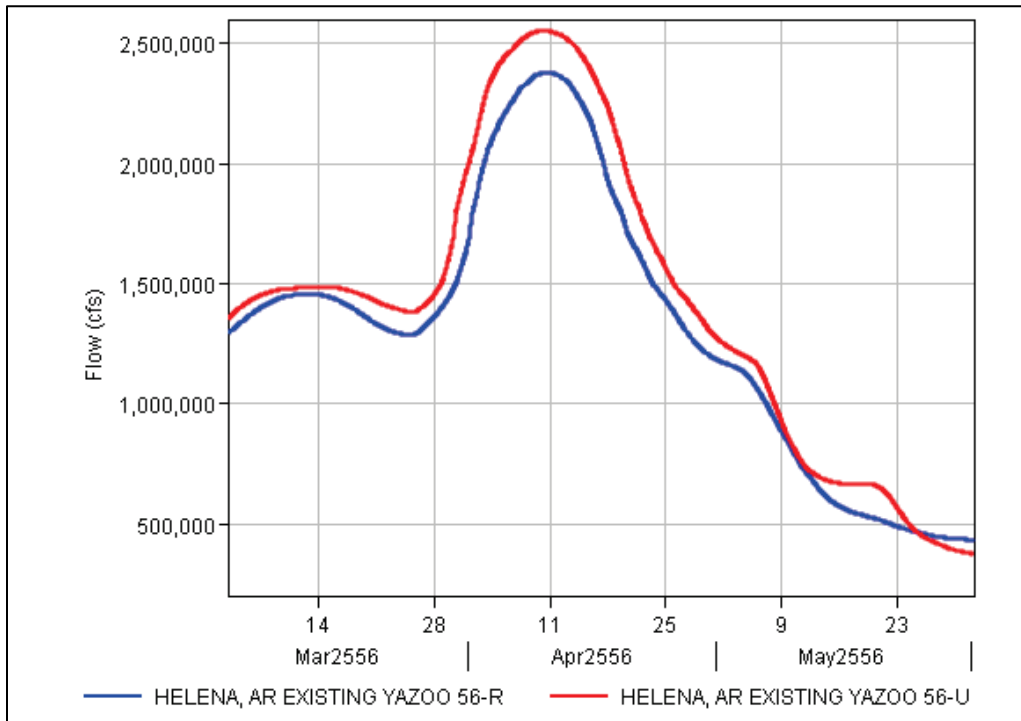
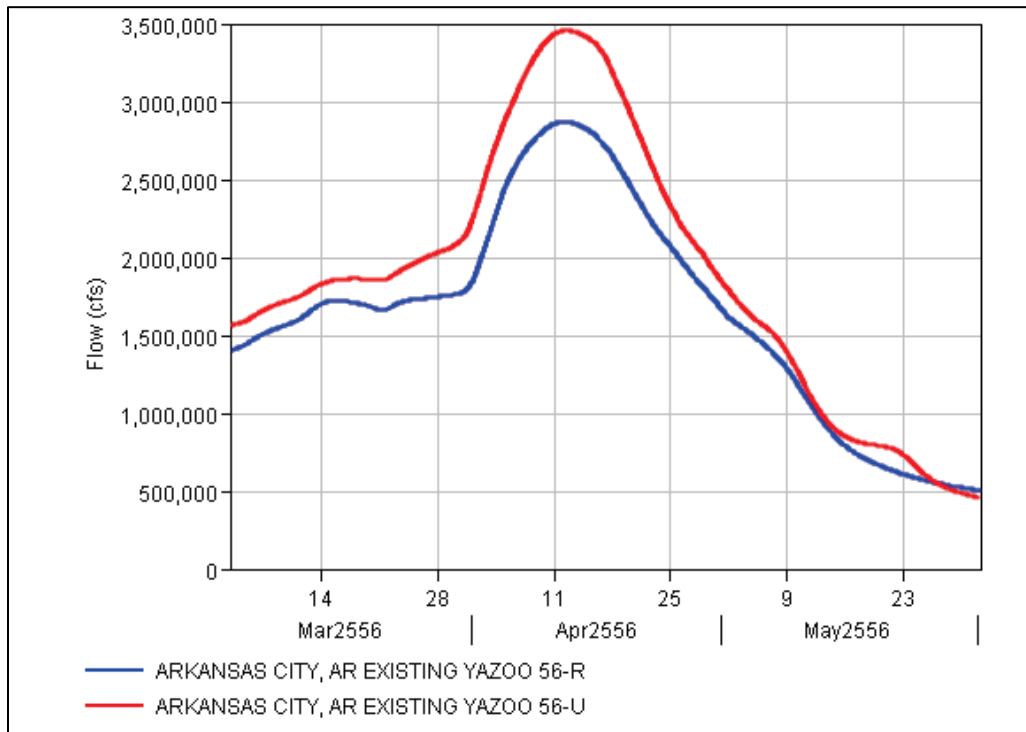


Figure D-41. HYPO 56 HEC-RAS hydrograph: Mississippi River at Arkansas City, AR.*



*Note: The authorized and existing condition results have a 426 cfs peak flow difference for the regulated run and a 3391 cfs peak flow difference for the unregulated run.

Figure D-42. HYPO 56 HEC-RAS hydrograph: Mississippi River at Greenville, MS.

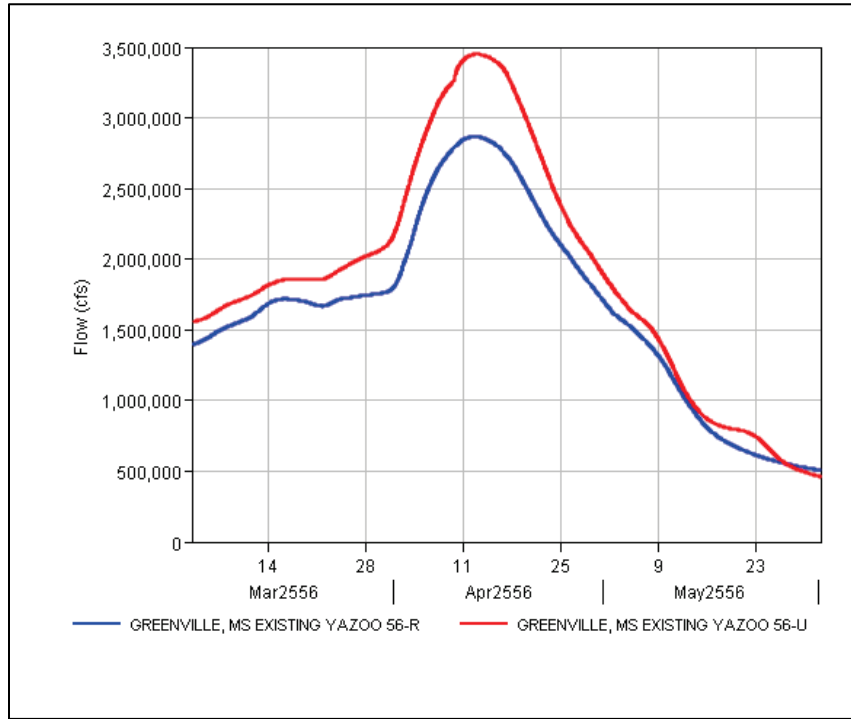
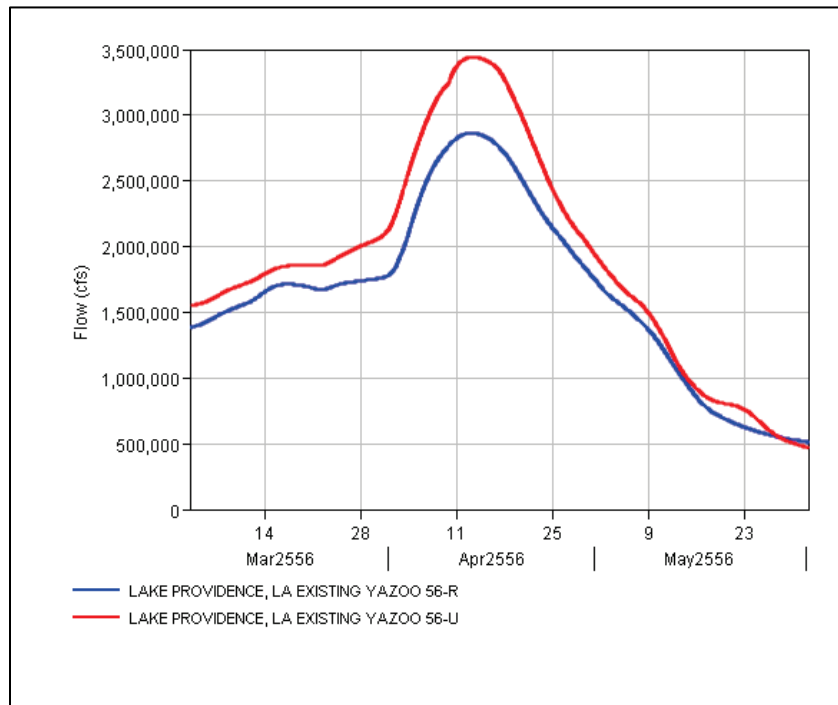


Figure D-43. HYPO 56 HEC-RAS hydrograph: Mississippi River at Lake Providence, LA.*



***Notes:** The authorized and existing condition results have a 2734 cfs peak flow difference for the regulated run and a 1091 cfs peak flow difference for the unregulated run.

Figure D-44. HYPO 56 HEC-RAS hydrograph: Mississippi River at Vicksburg, MS.

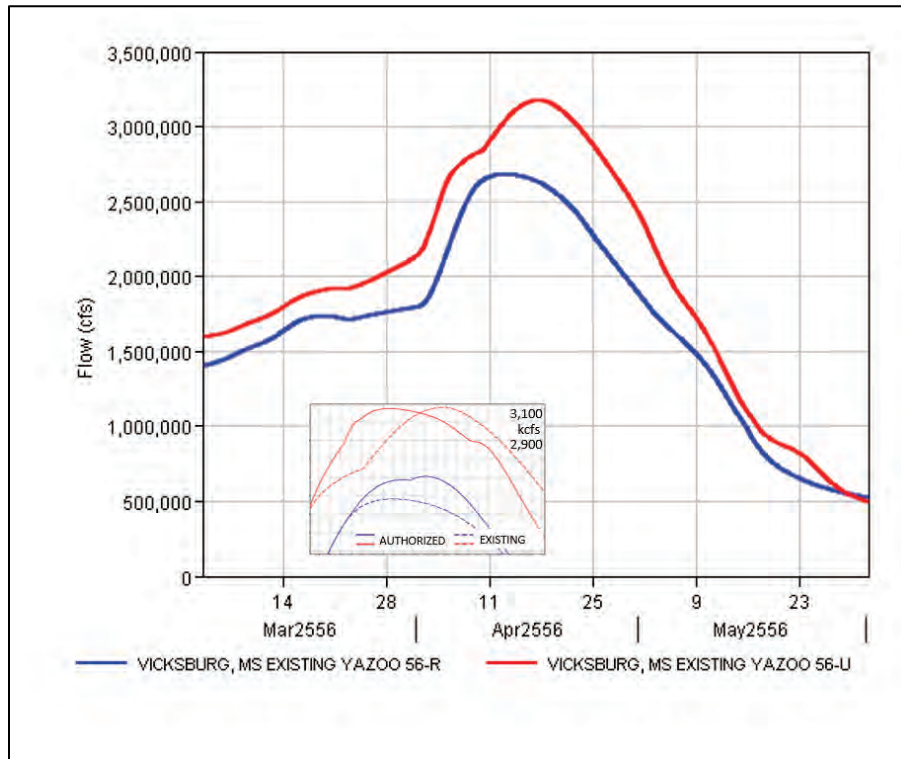


Figure D-45. HYPO 56 HEC-RAS hydrograph: Mississippi River at Natchez, MS.

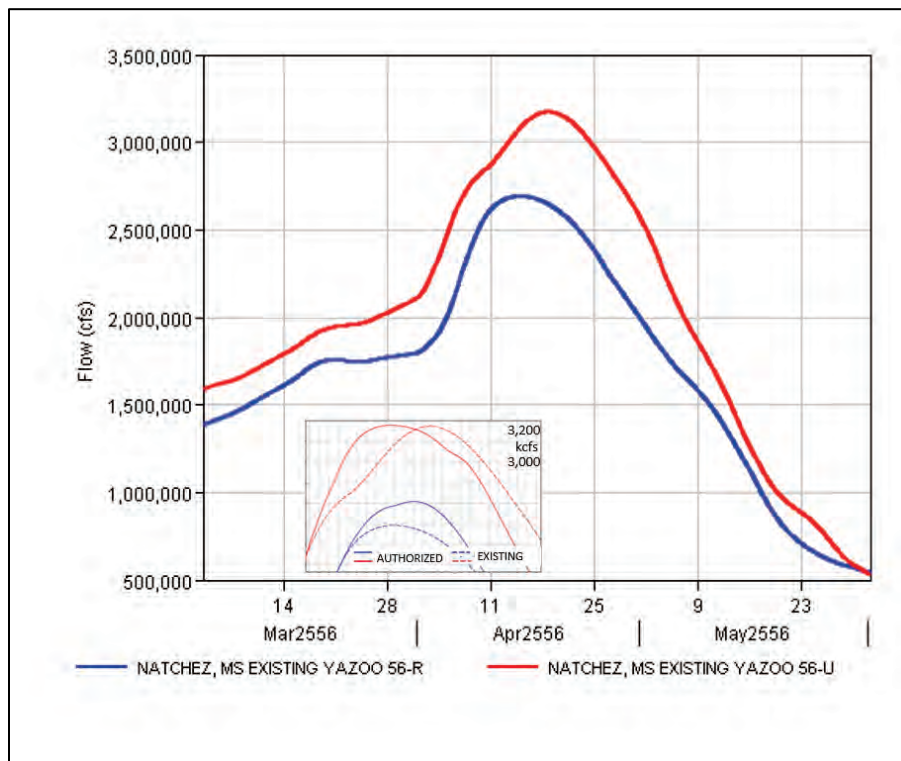


Figure D-46. HYPO 56 HEC-RAS hydrograph: Mississippi River at Red River Landing, LA.

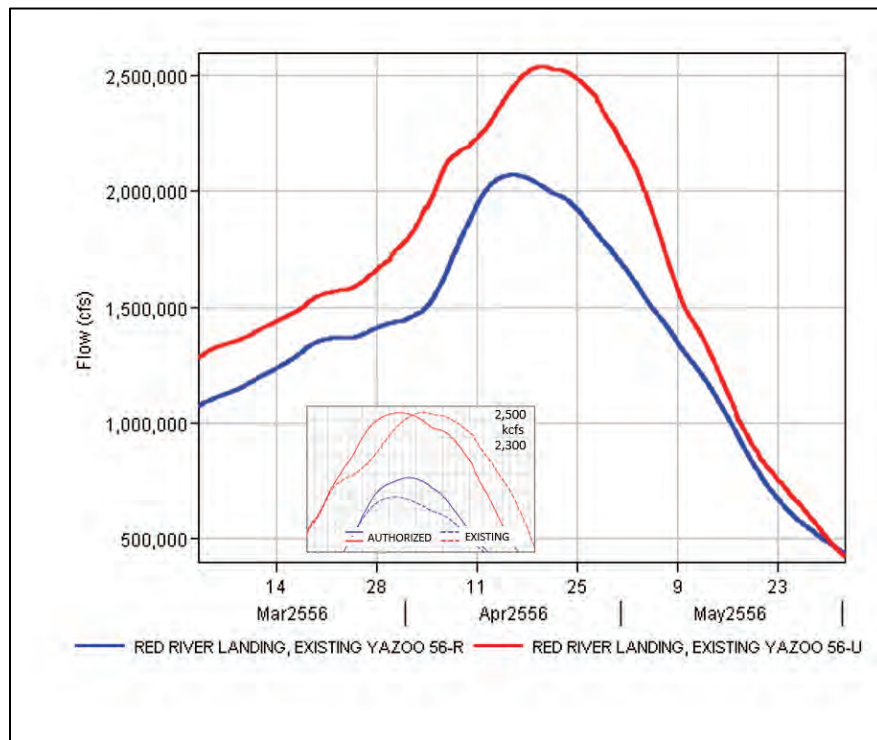


Figure D-47. HYPO 56 HEC-RAS hydrograph: Mississippi River at Baton Rouge, LA.

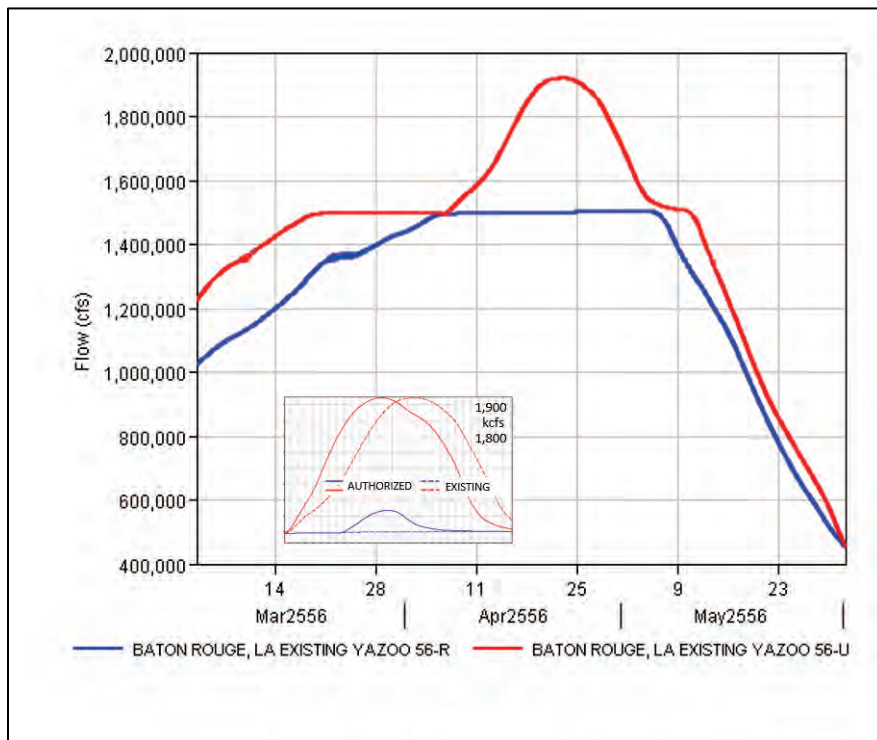


Figure D-48. HYPO 56 HEC-RAS hydrograph: Mississippi River at Donaldsonville, LA.

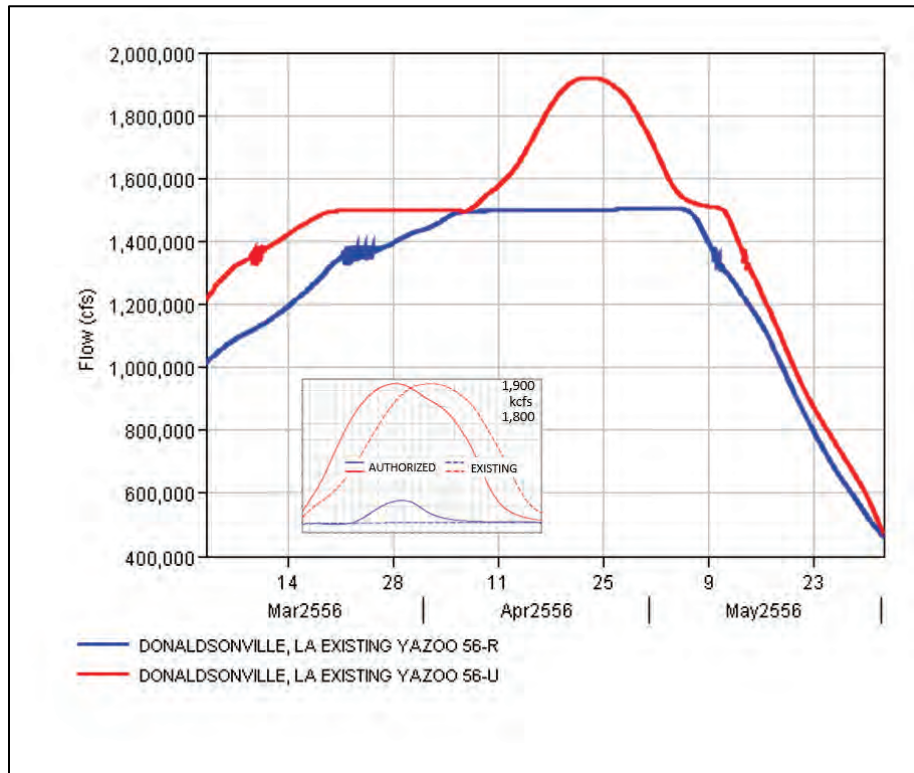


Figure D-49. HYPO 56 HEC-RAS hydrograph: Mississippi River at Carrollton, LA.

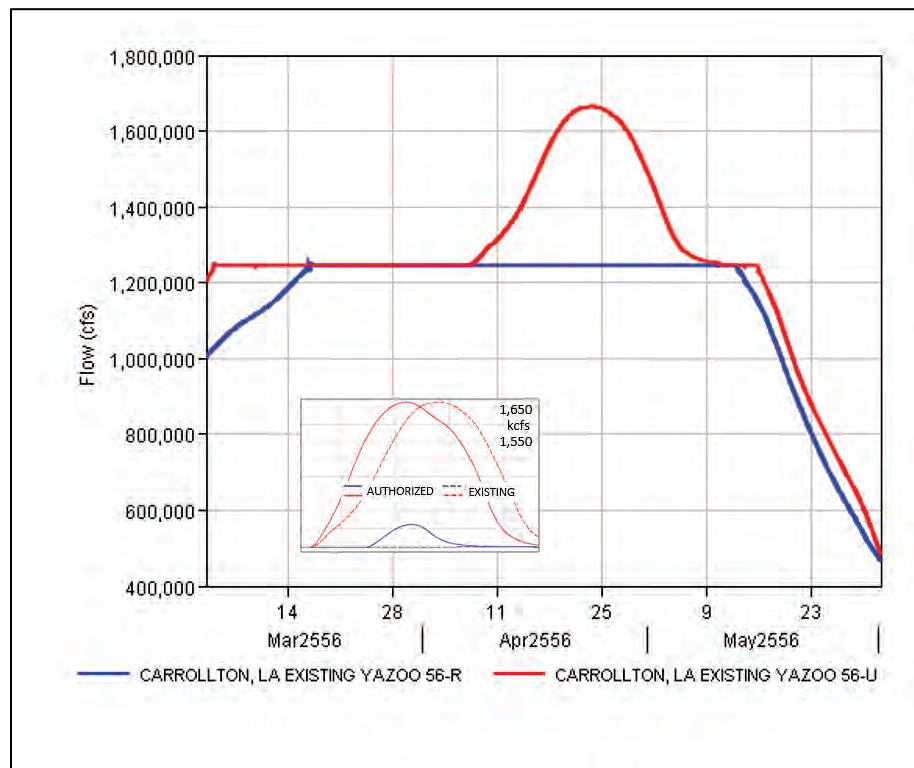


Figure D-50. HYPO 56 HEC-RAS hydrograph: Mississippi River at Empire, LA.

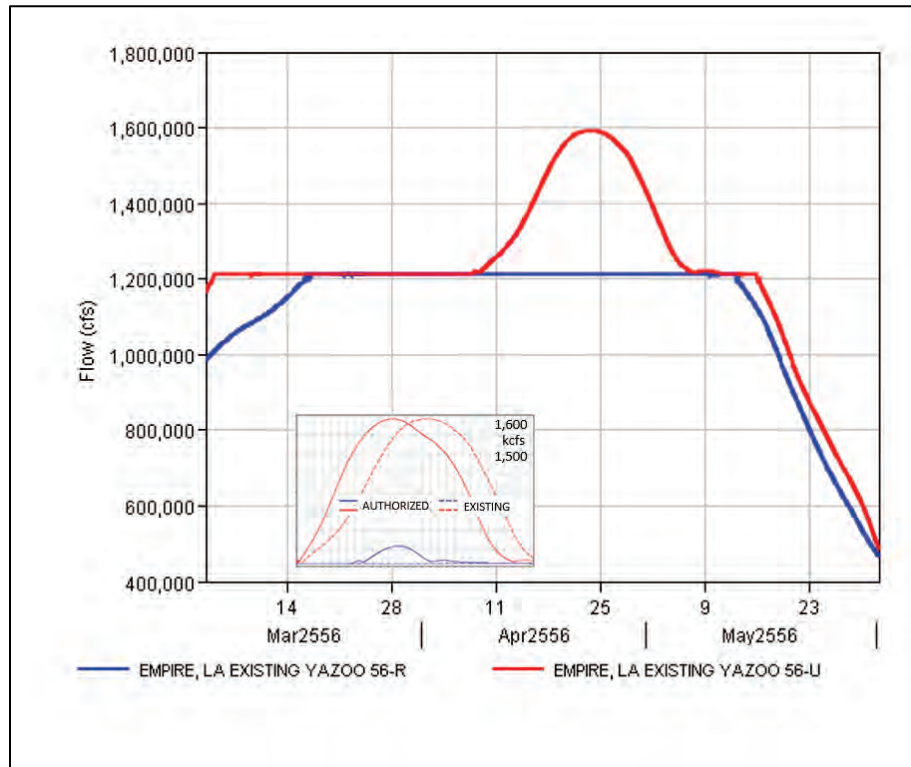
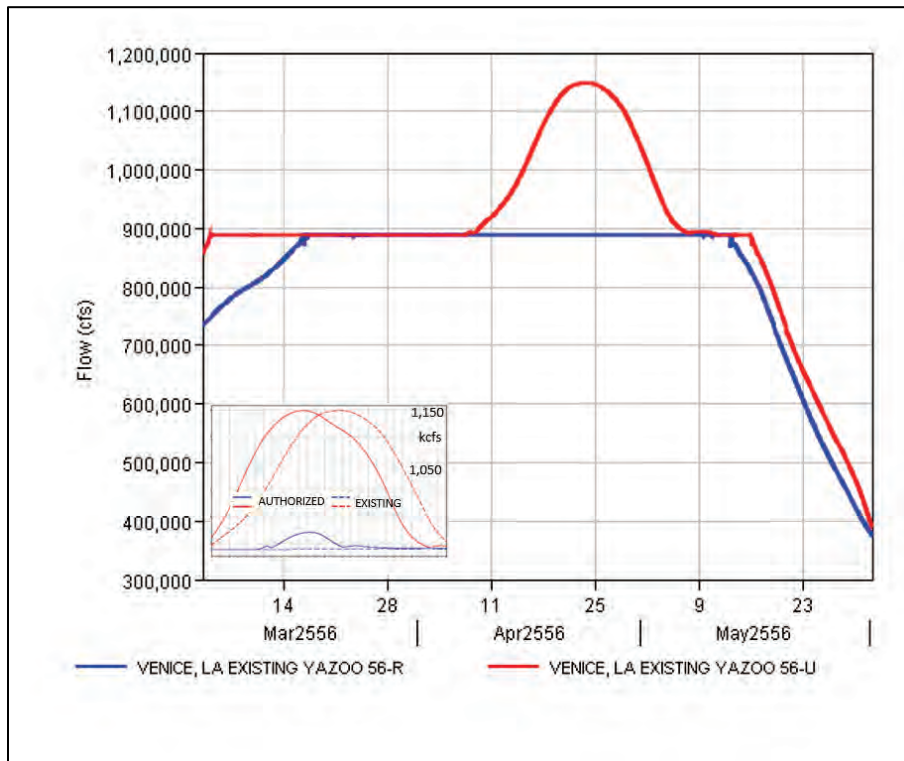


Figure D-51. HYPO 56 HEC-RAS hydrograph: Mississippi River at Venice, LA.



D.4 Reservoir inflow and outflow hydrographs for regulated simulations

Figures shown in this section provide data used to develop regulated flows for each reservoir as computed by the USACE district offices. The resulting reservoir outflows for each project were used by the NWS River Forecast Centers to define reservoir outflows in their CHPS-FEWS model simulations. Some figures shows slight oscillations that were due to model instabilities; these were outside the primary period of analysis and did not impact results obtained for peak flow periods.

D.4.1 LRL reservoir hydrographs

Figure D-52. Barren River Lake HYPO 56 inflow compared to outflow.

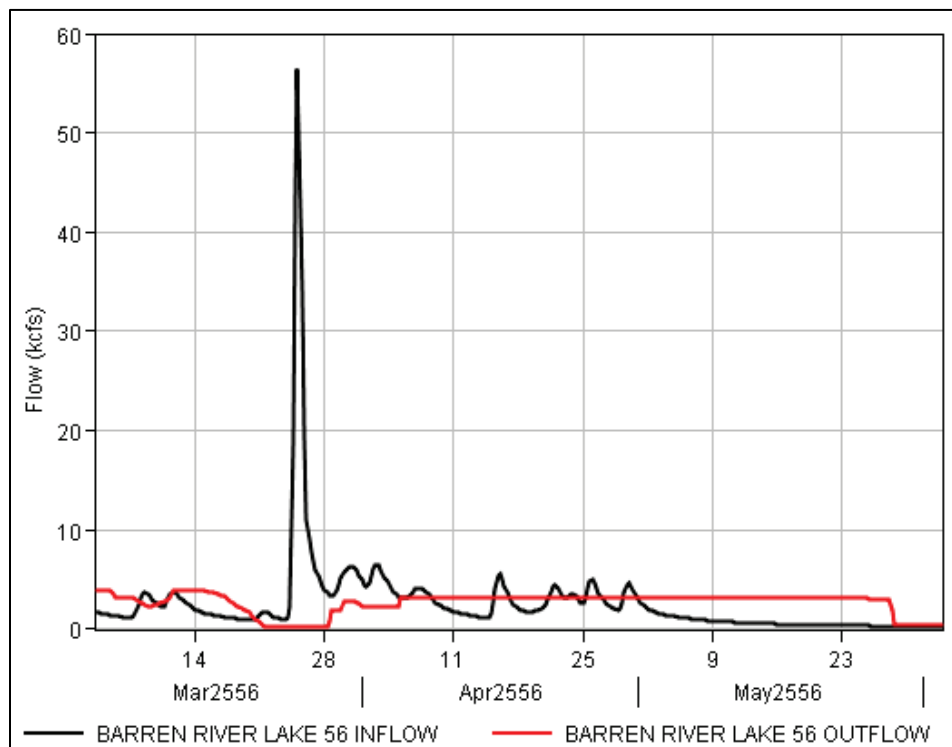


Figure D-53. Cagles Mill Lake HYPO 56 inflow compared to outflow.

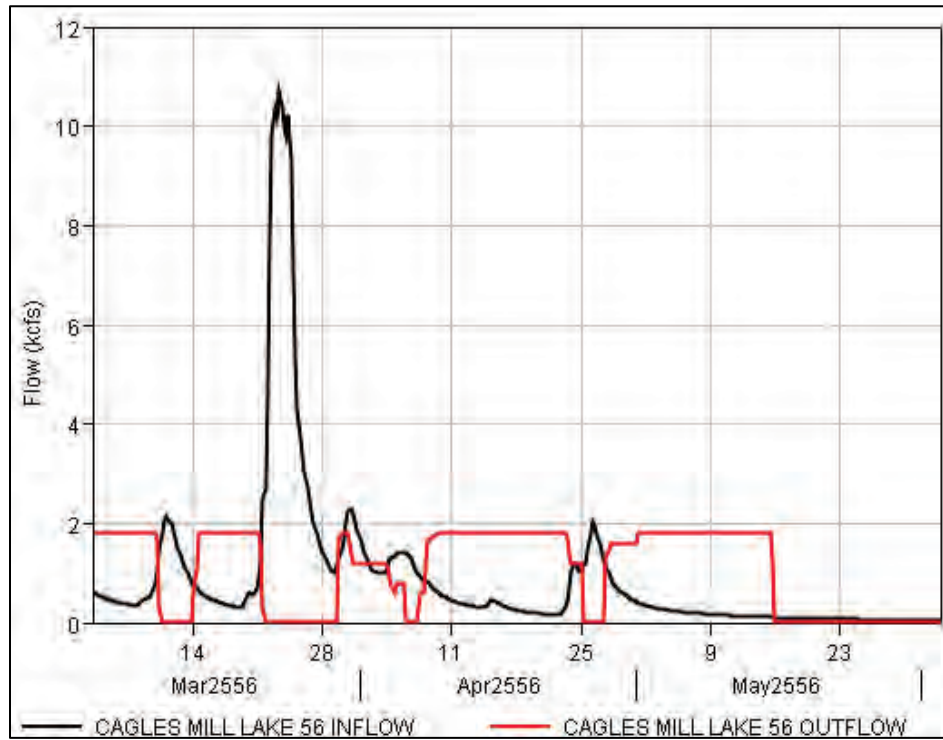


Figure D-54. CM Harden Lake HYPO 56 inflow compared to outflow.

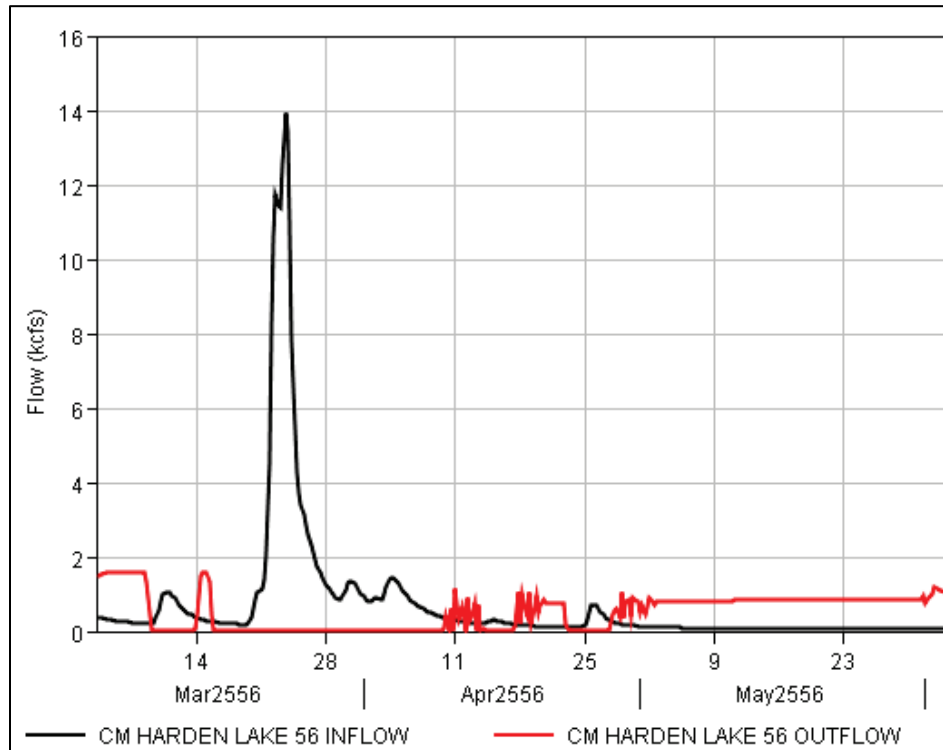


Figure D-55. Green River Lake HYPO 56 inflow compared to outflow.

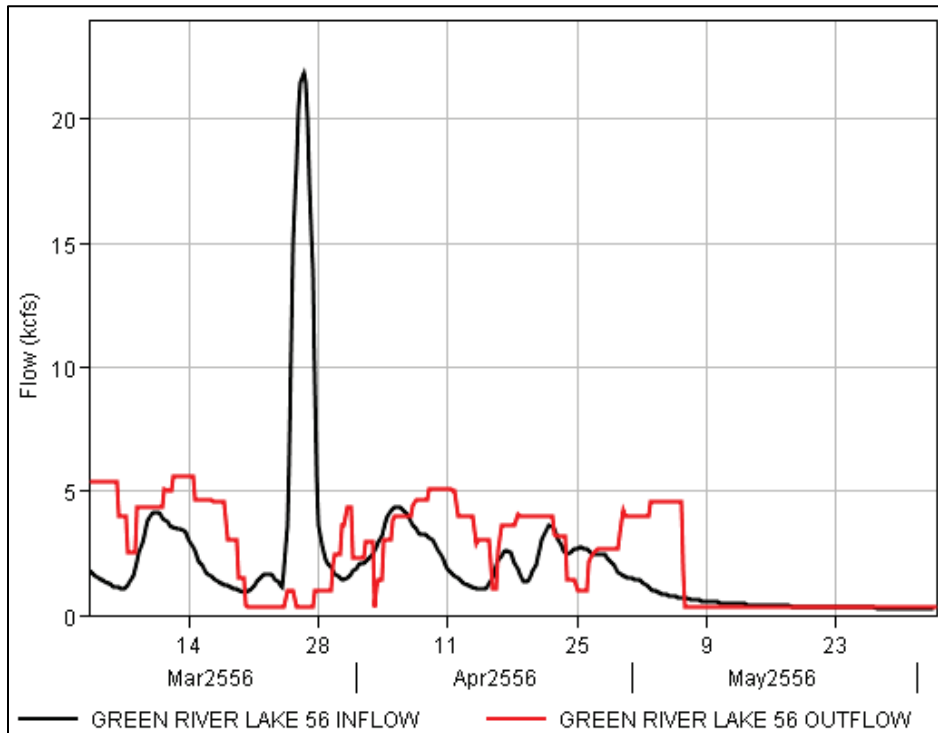


Figure D-56. Je Roush Lake HYPO 56 inflow compared to outflow.

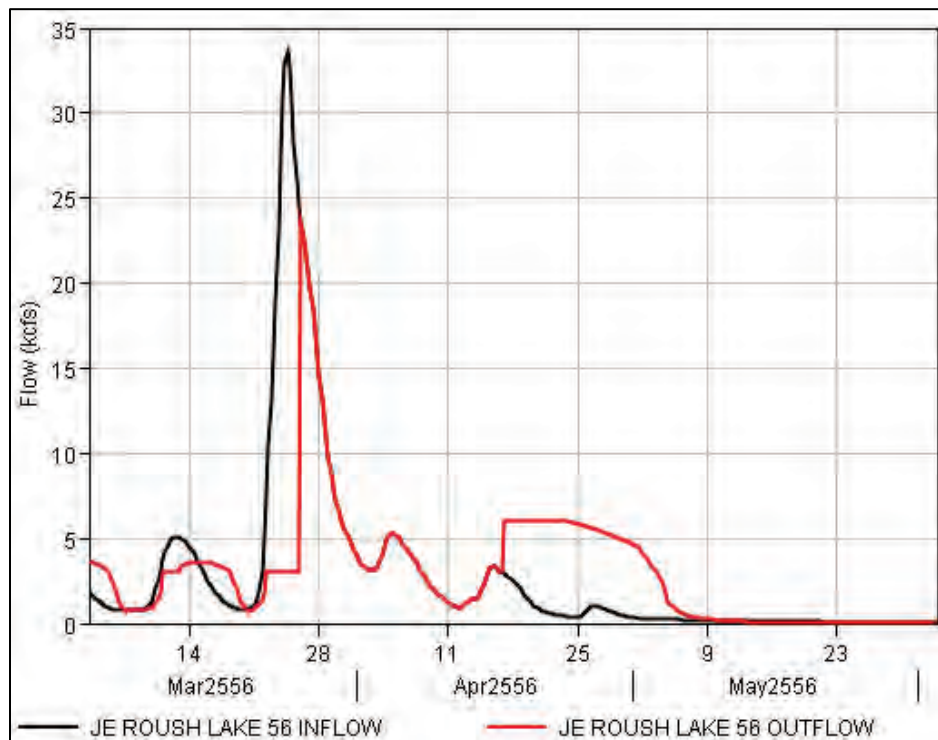


Figure D-57. Mississinewa Lake HYPO 56 inflow compared to outflow.

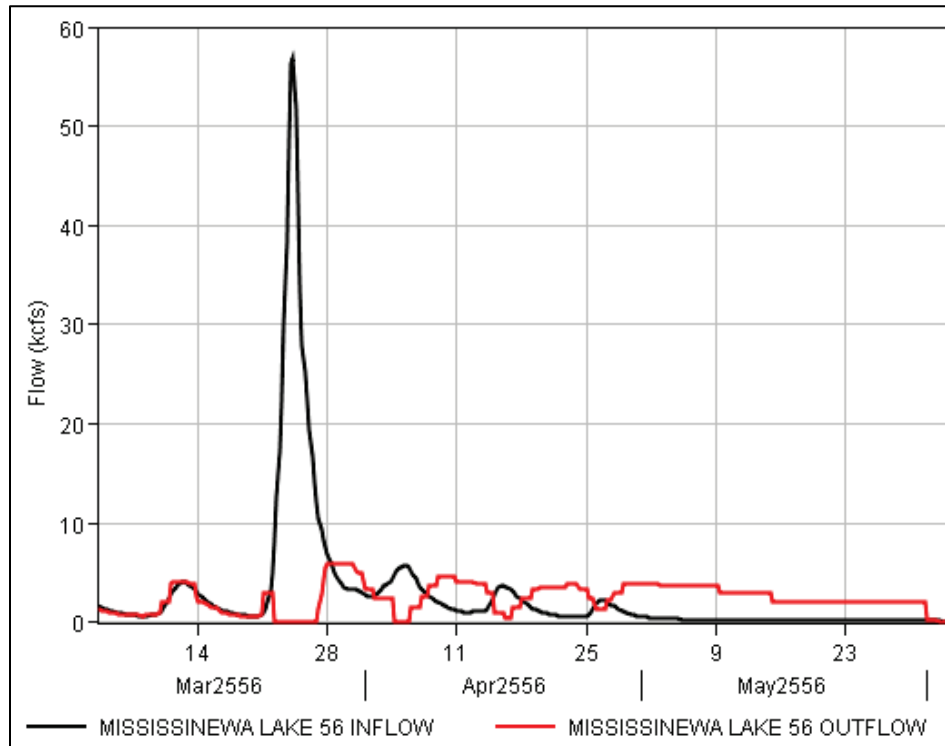


Figure D-58. Monroe Lake HYPO 56 inflow compared to outflow.

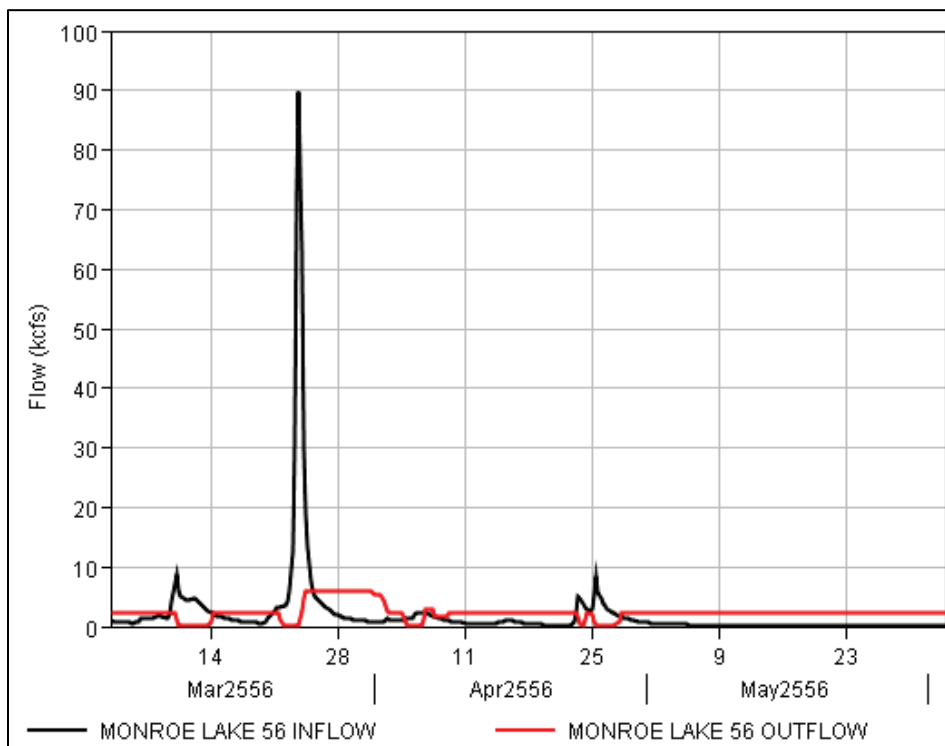


Figure D-59. Nolin River Lake HYPO 56 inflow compared to outflow.

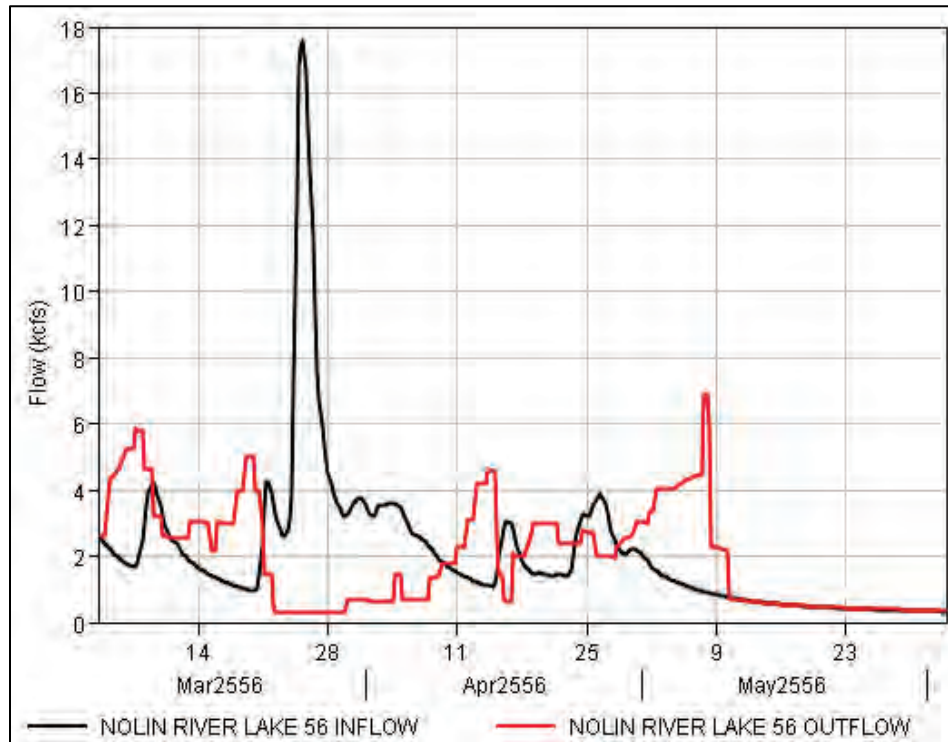


Figure D-60. Patoka Lake HYPO 56 inflow compared to outflow.

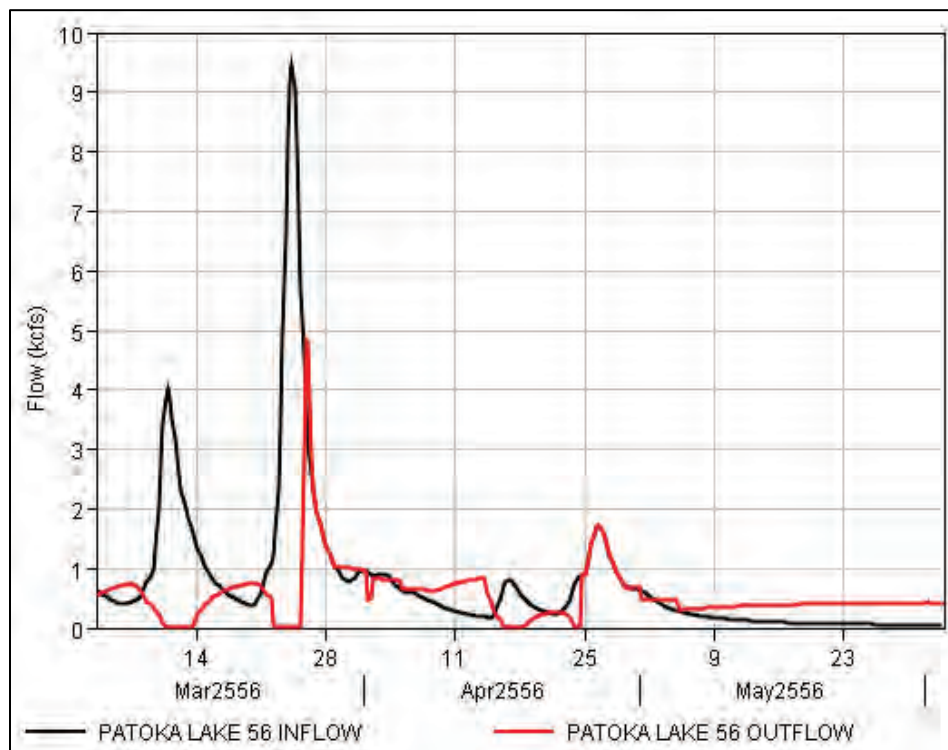


Figure D-61. Rough River HYPO 56 inflow compared to outflow.

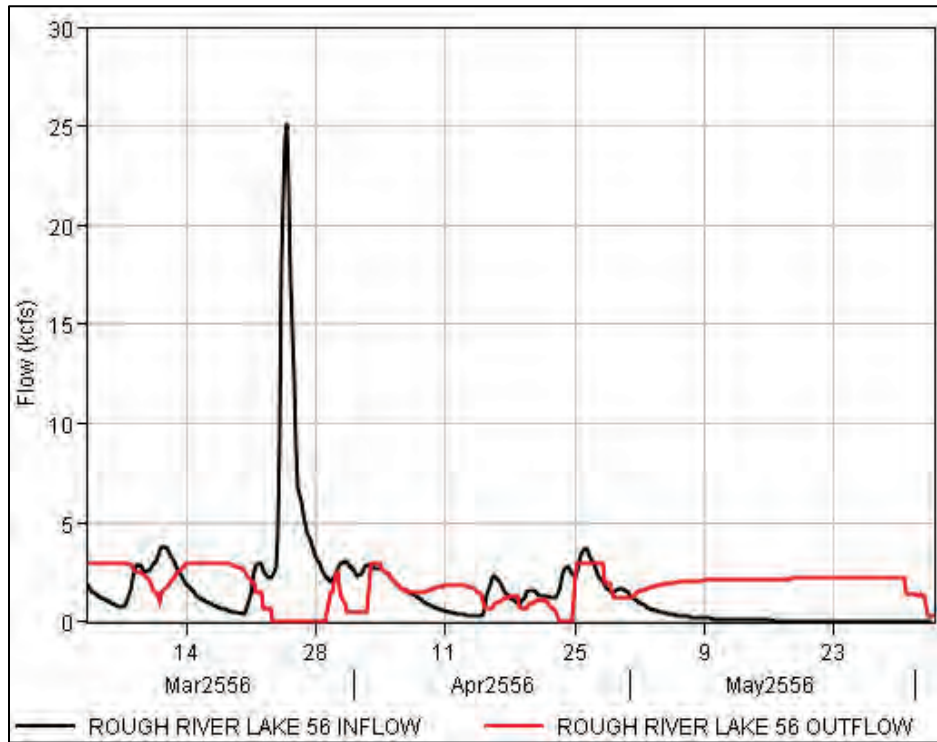
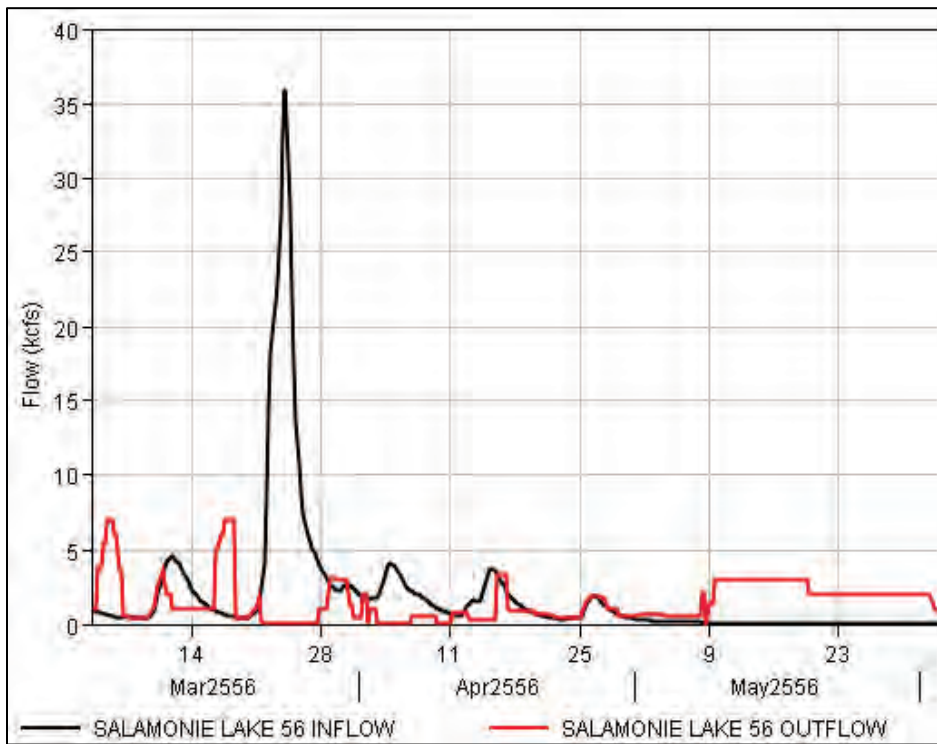


Figure D-62. Salamonie Lake HYPO 56 inflow compared to outflow.



D.4.2 LRN Reservoir Hydrographs

Figure D-63. Barkley Dam HYPO 56 inflow compared to outflow.

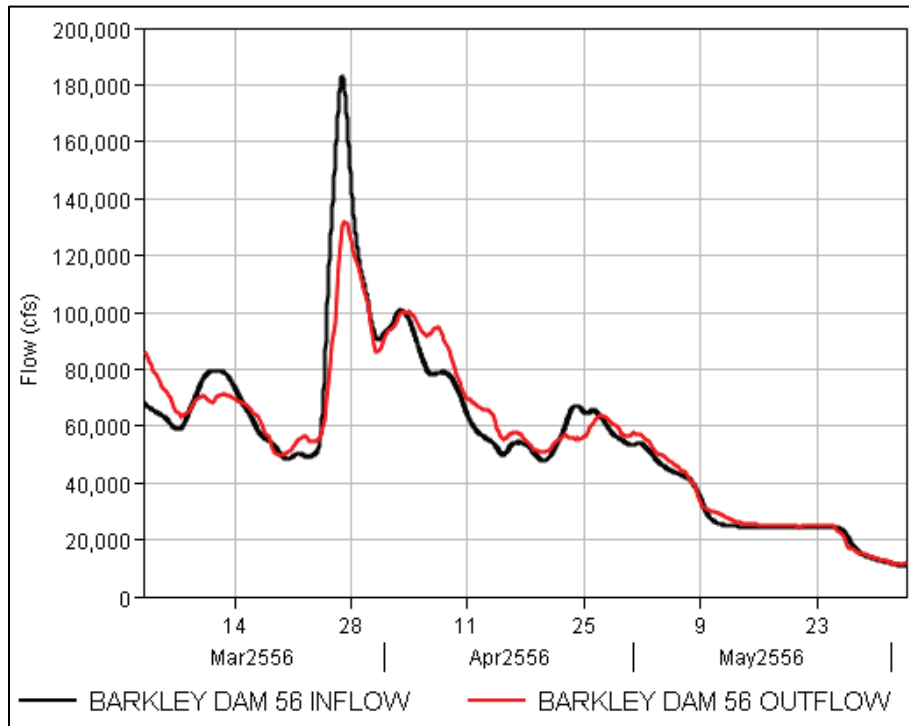


Figure D-64. Center Hill Dam HYPO 56 inflow compared to outflow.

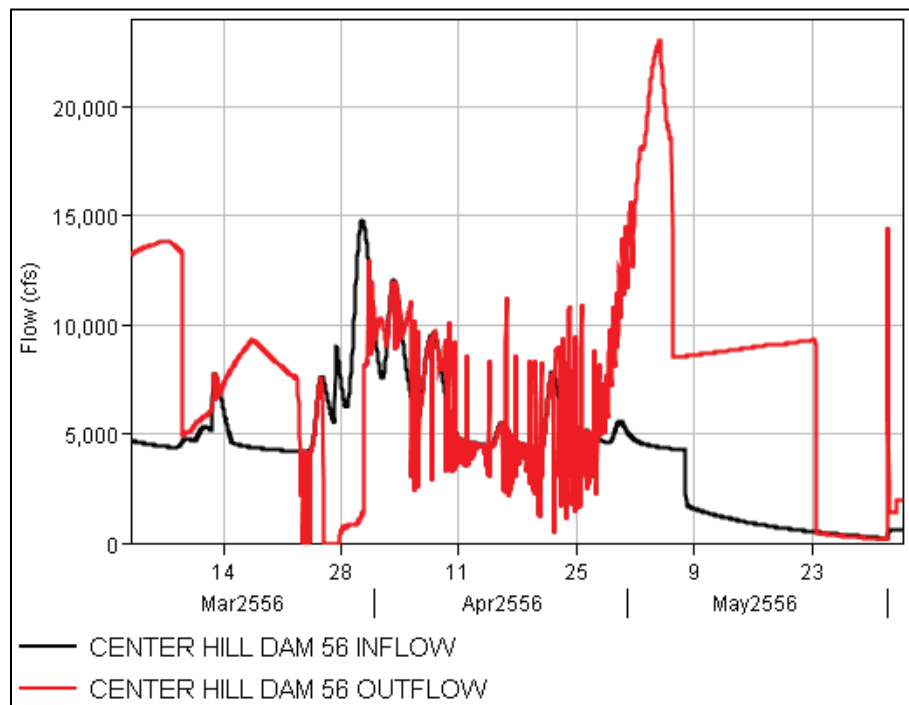


Figure D-65. Cheatham Hill Dam HYPO 56 inflow compared to outflow.

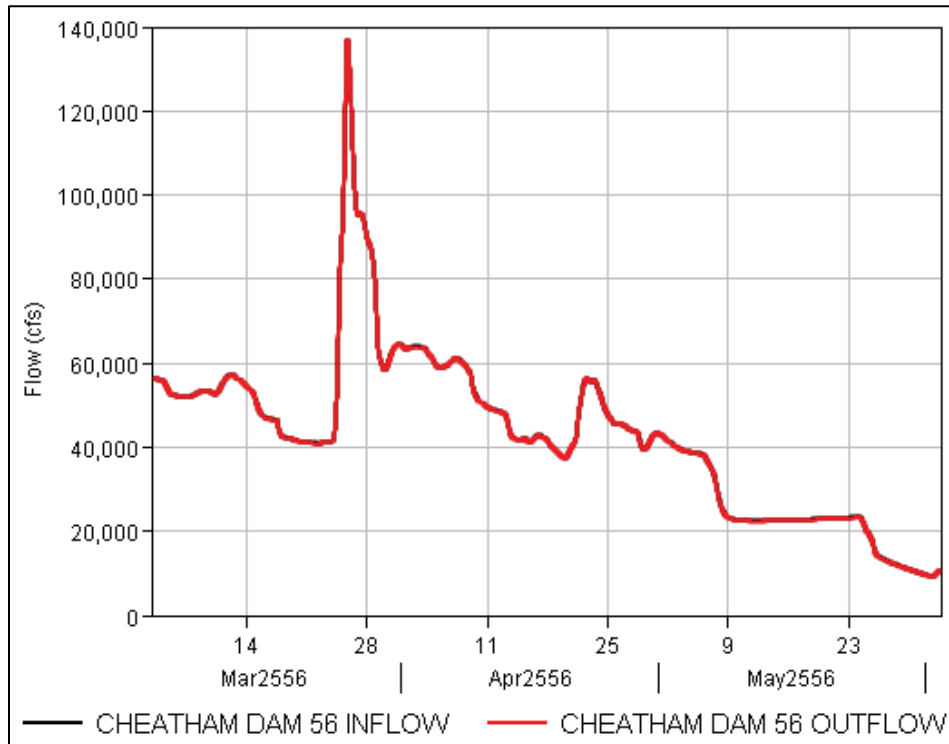


Figure D-66. Cordell Hull Dam HYPO 56 inflow compared to outflow.

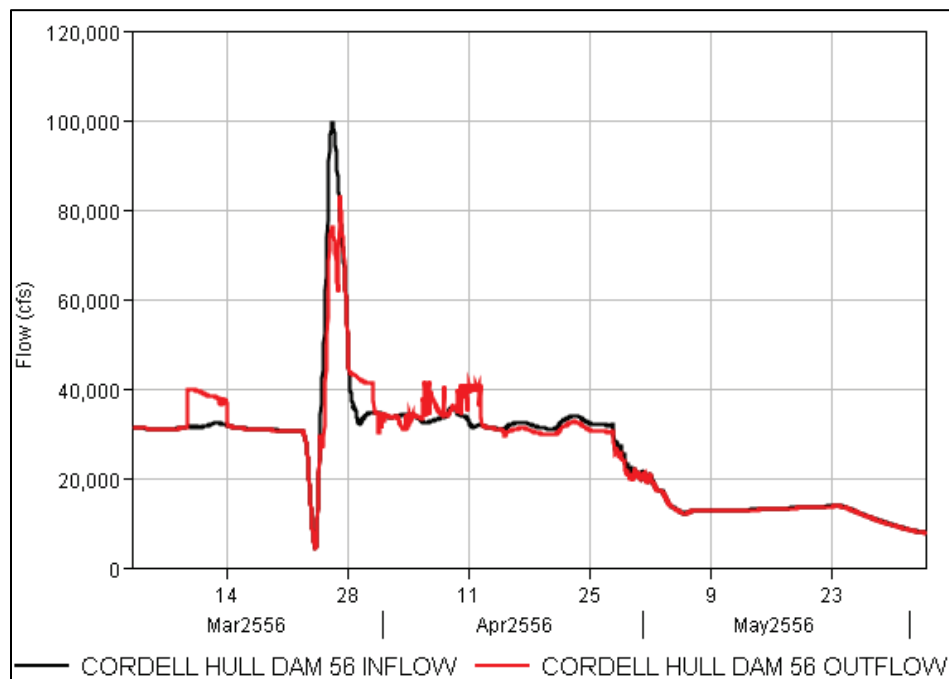


Figure D-67. Dale Hollow Dam HYPO 56 inflow compared to outflow.

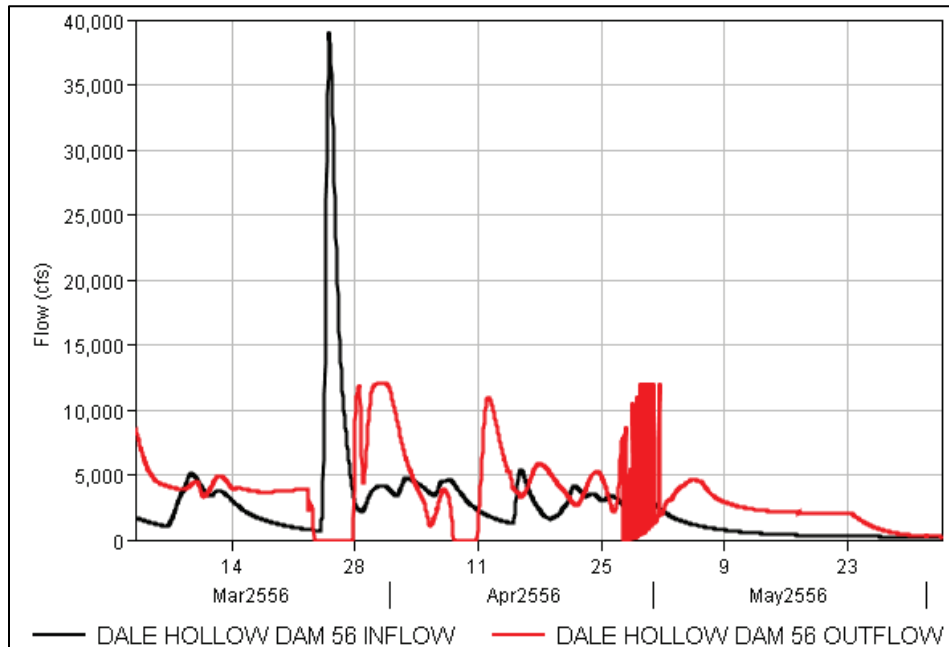


Figure D-68. Great Falls HYPO 56 inflow compared to outflow.

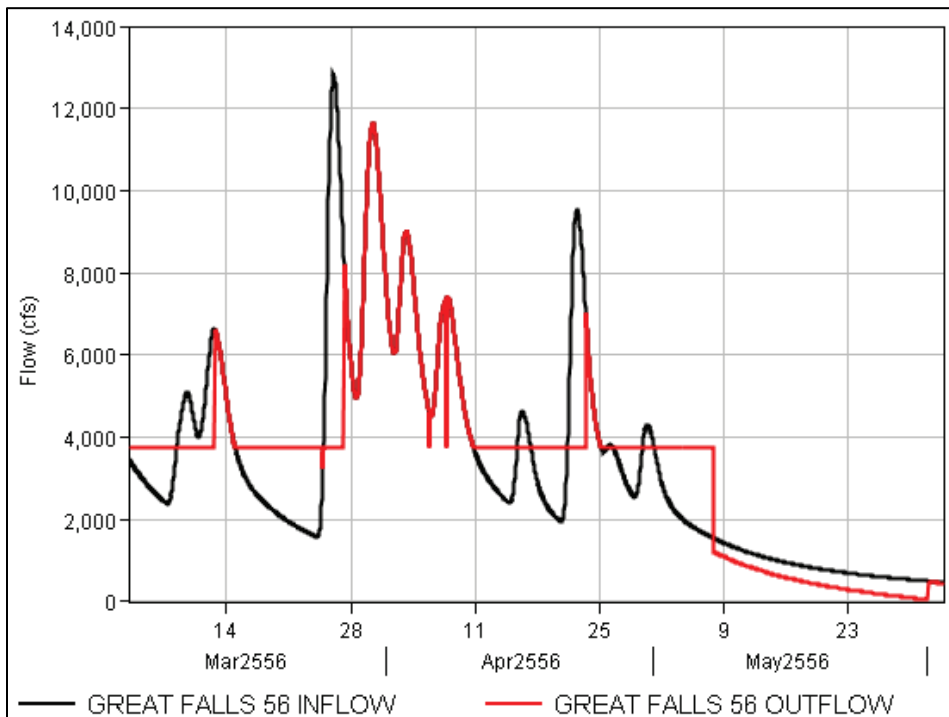


Figure D-69. J. Percy Priest Dam HYPO 56 inflow compared to outflow.

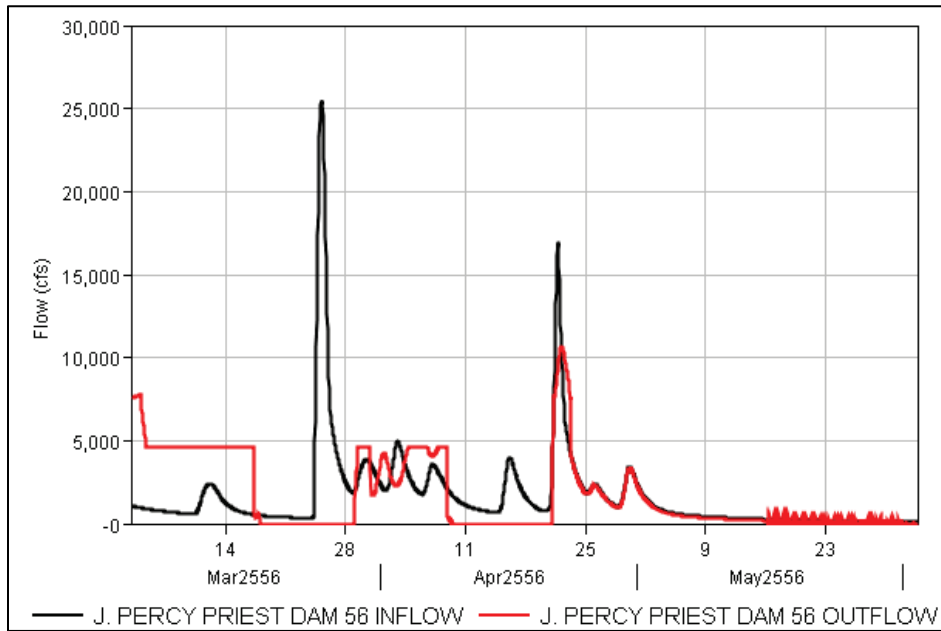


Figure D-70. Kentucky Dam HYPO 56 inflow compared to outflow.

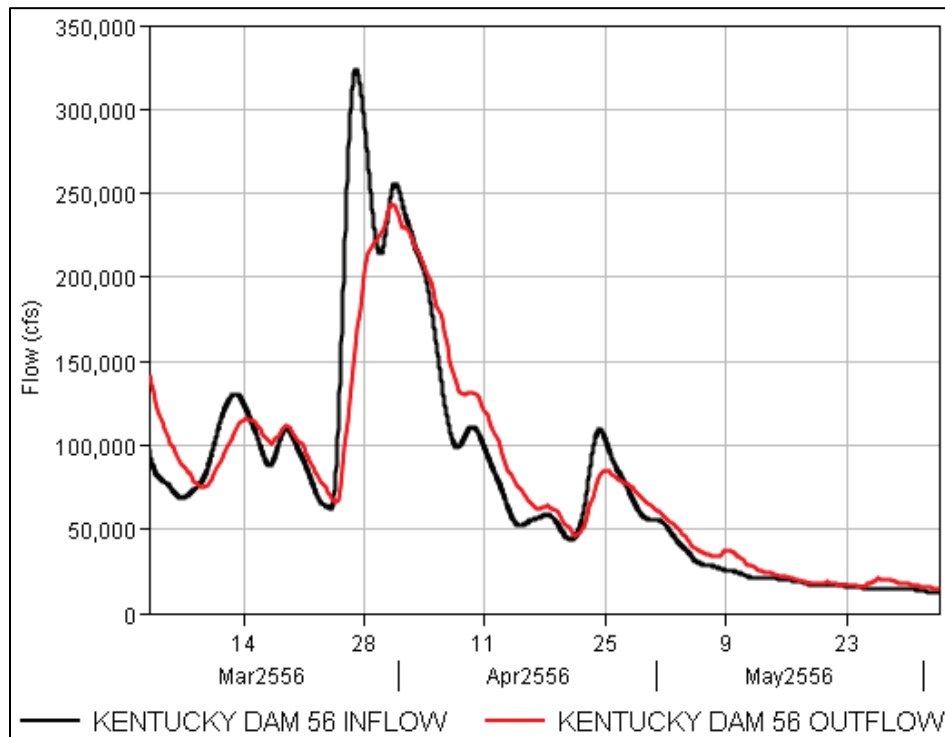


Figure D-71. Old Hickory Dam HYPO 56 inflow compared to outflow.

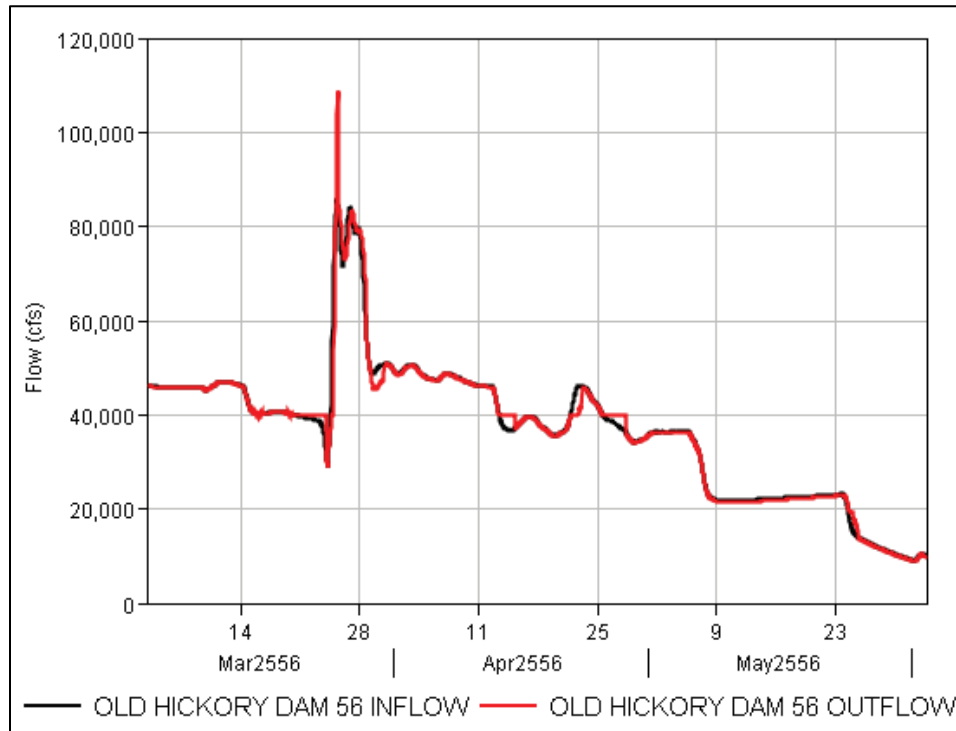
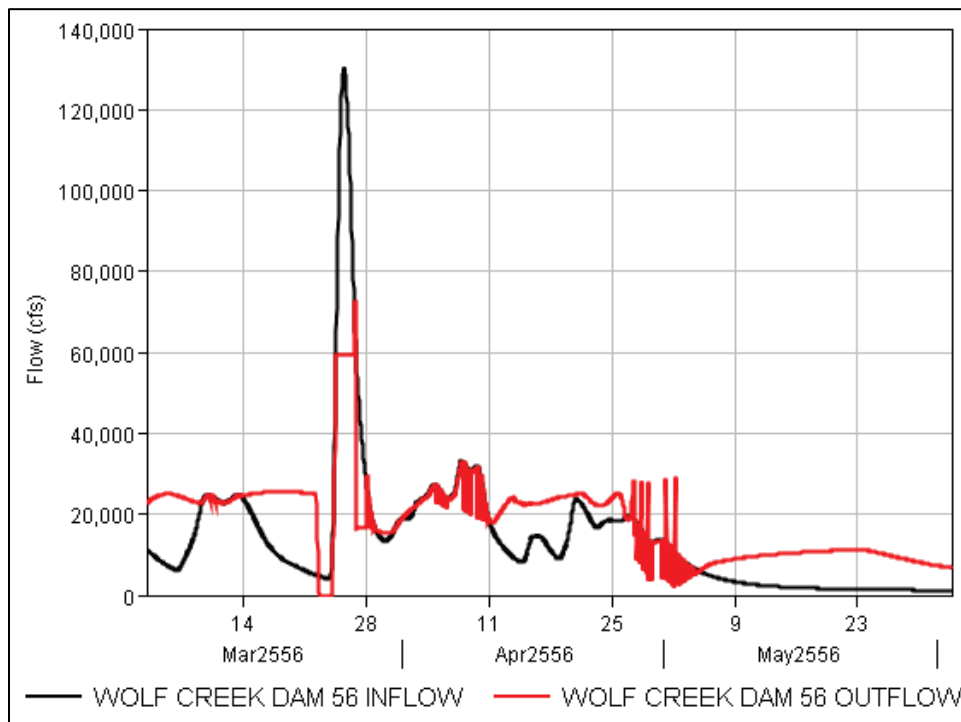


Figure D-72. Wolf Creek Dam HYPO 56 inflow compared to outflow.



D.4.3 MVK Reservoir Hydrographs

Figure D-73. Arkabutla Dam HYPO 56 inflow compared to outflow.

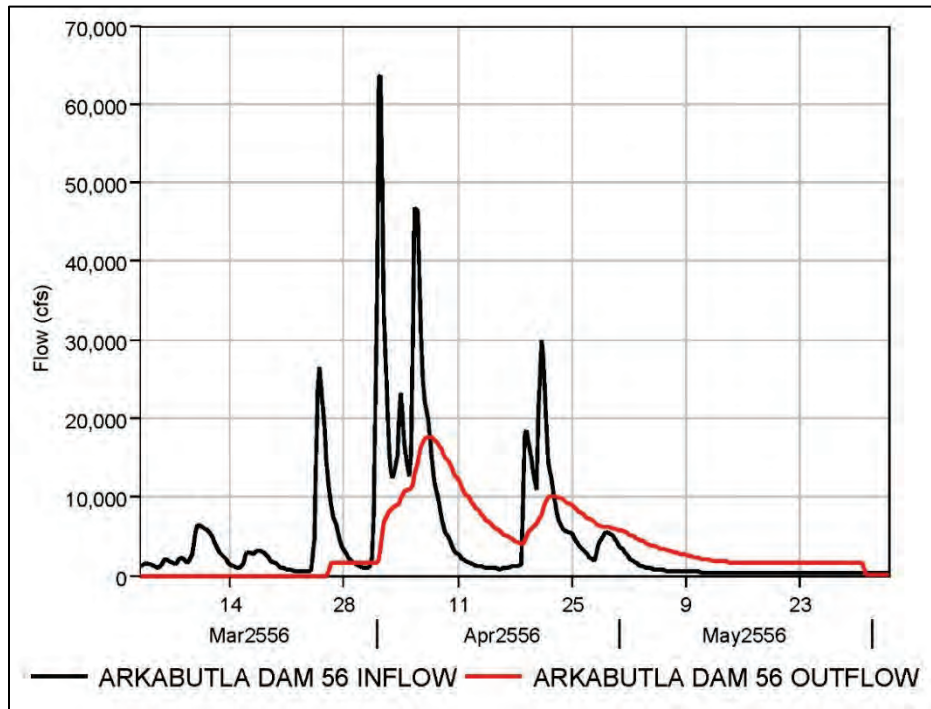


Figure D-74. Sardis Dam HYPO 56 inflow compared to outflow.

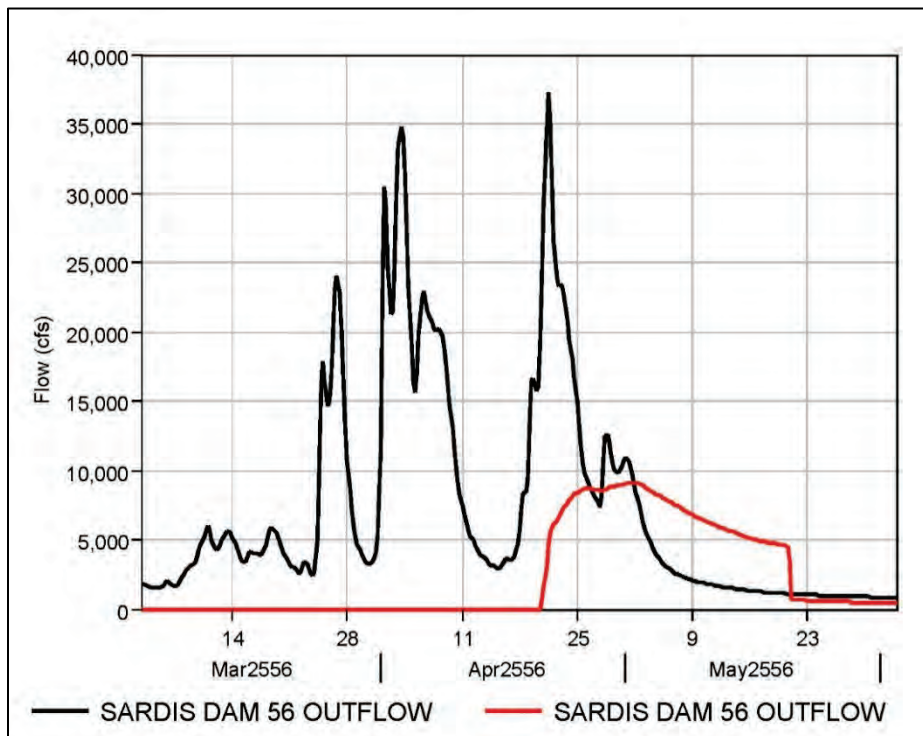


Figure D-75. Enid Dam HYPO 56 inflow compared to outflow.

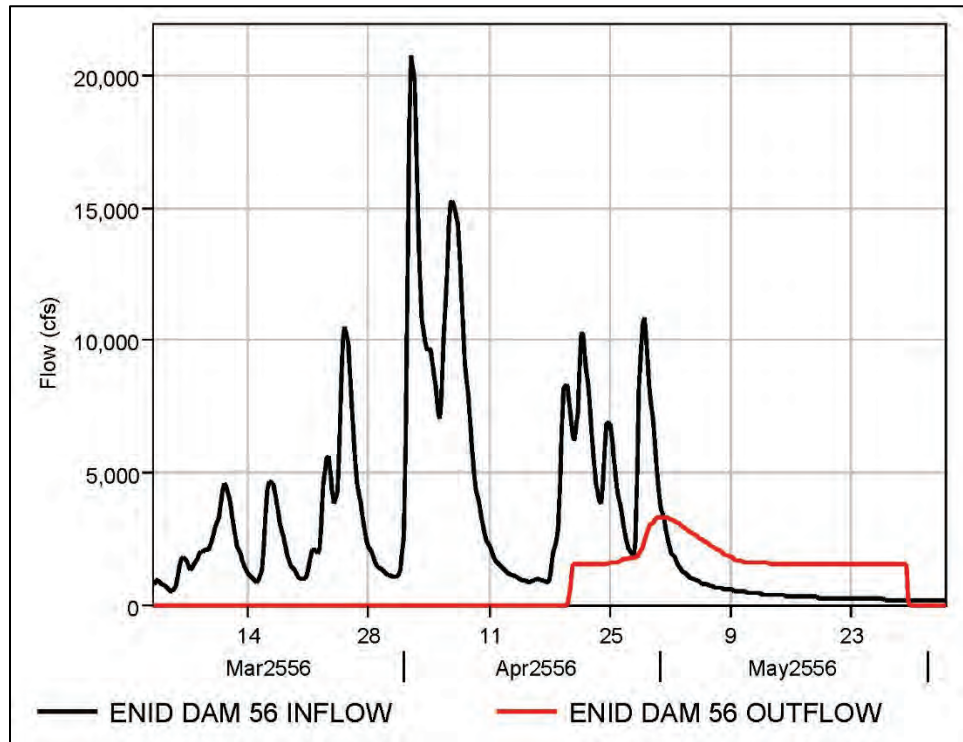


Figure D-76. Grenada Dam HYPO 56 inflow compared to outflow.

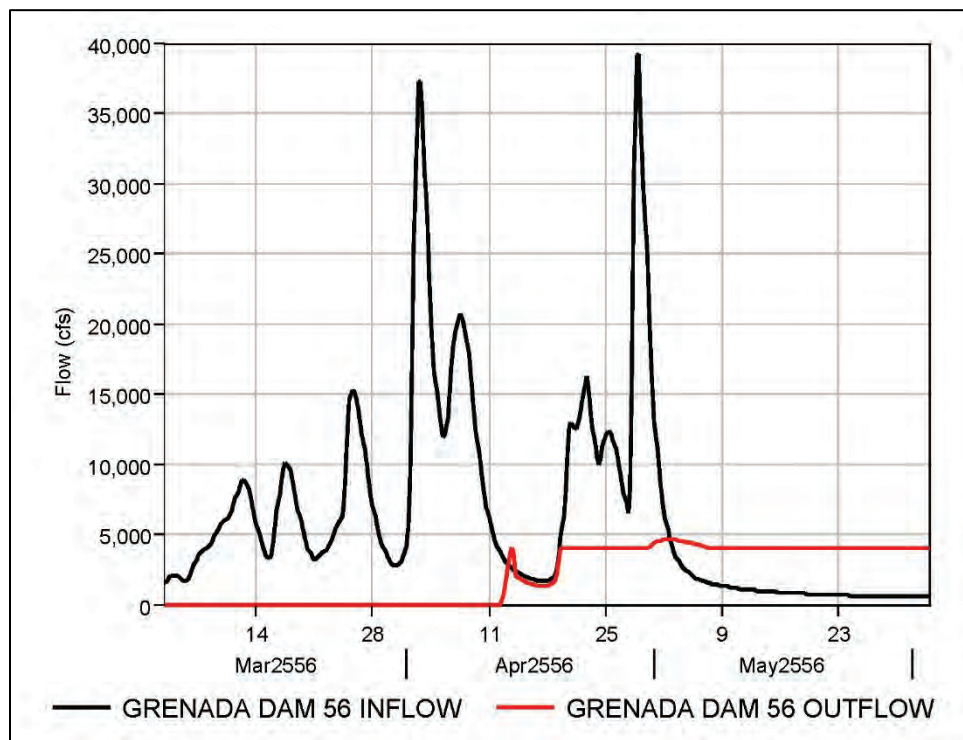


Figure D-77. Bayou Bodcau Dam HYPO 56 inflow compared to outflow.

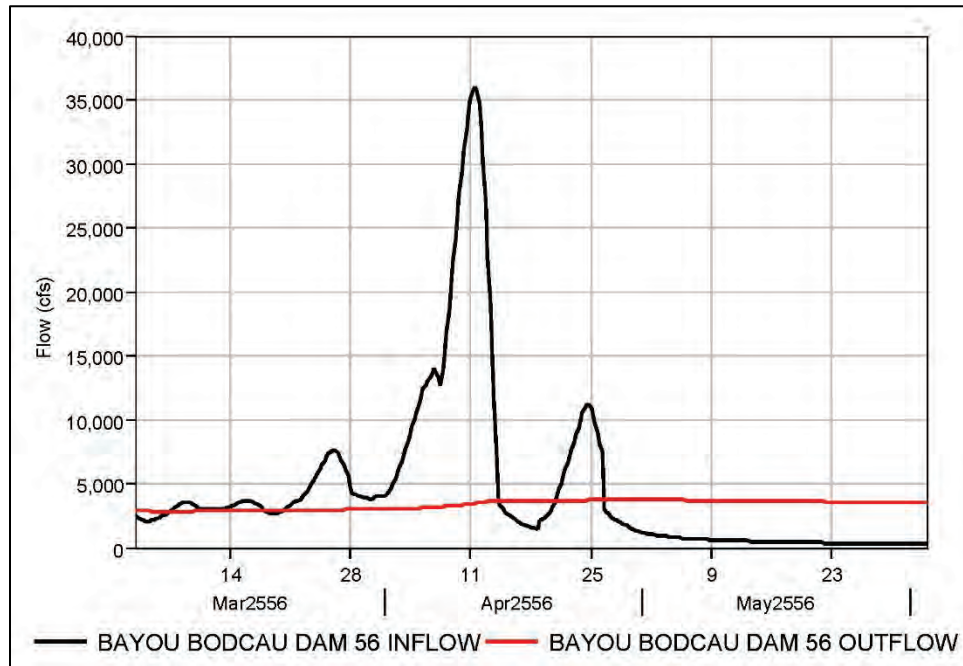


Figure D-78. Caddo Dam HYPO 56 inflow compared to outflow.

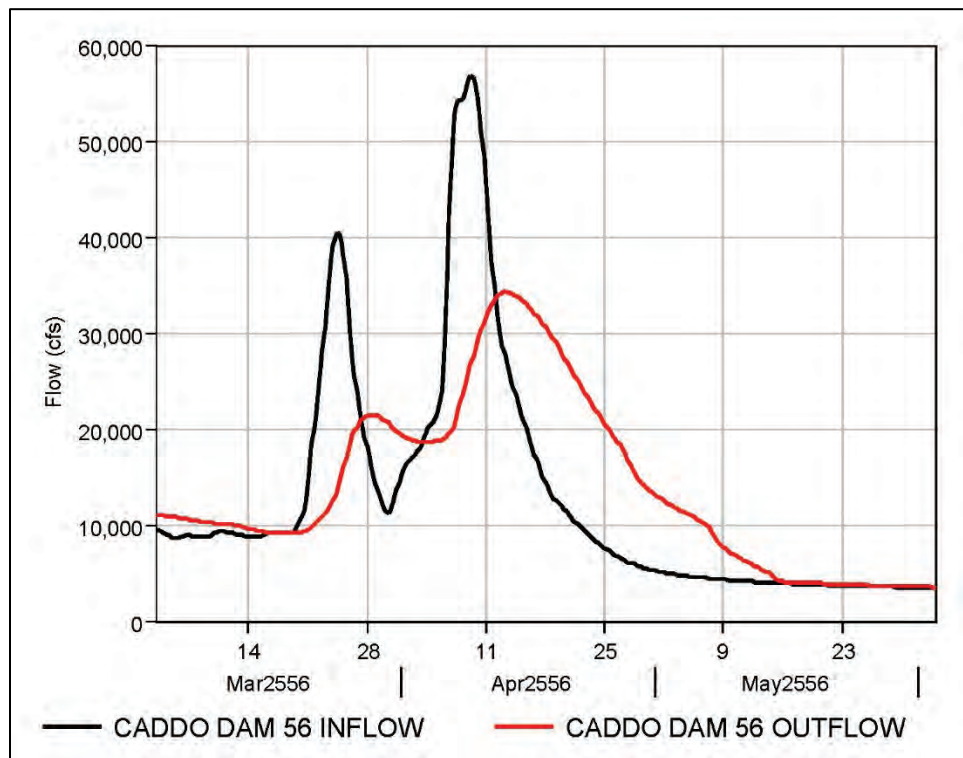


Figure D-79. Wallace Lake dam HYPO 56 inflow compared to outflow.

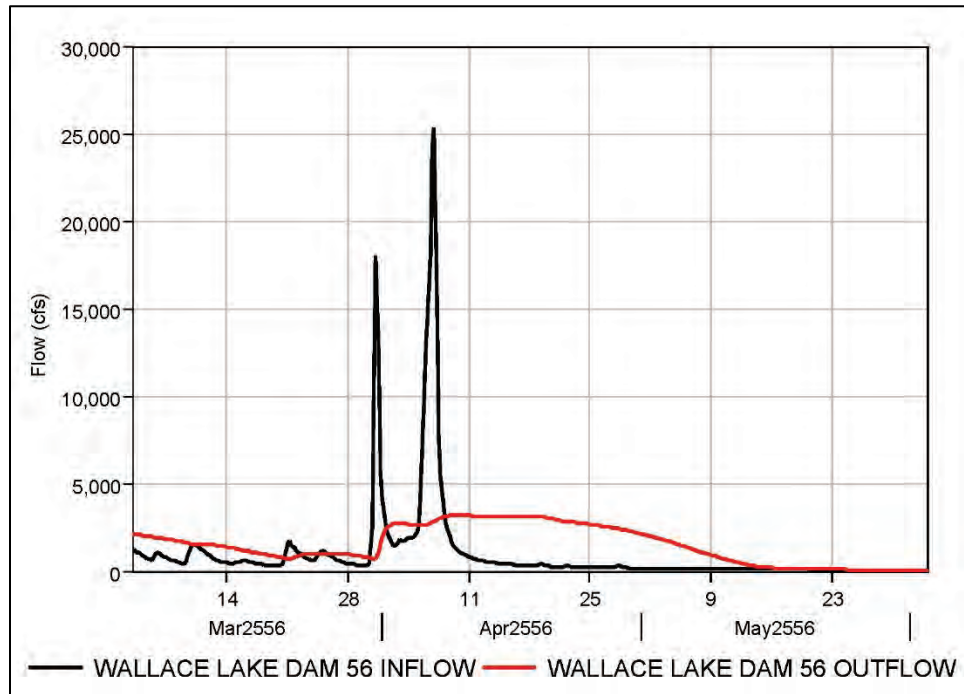


Figure D-80. Narrows Dam HYPO 56 inflow compared to outflow.

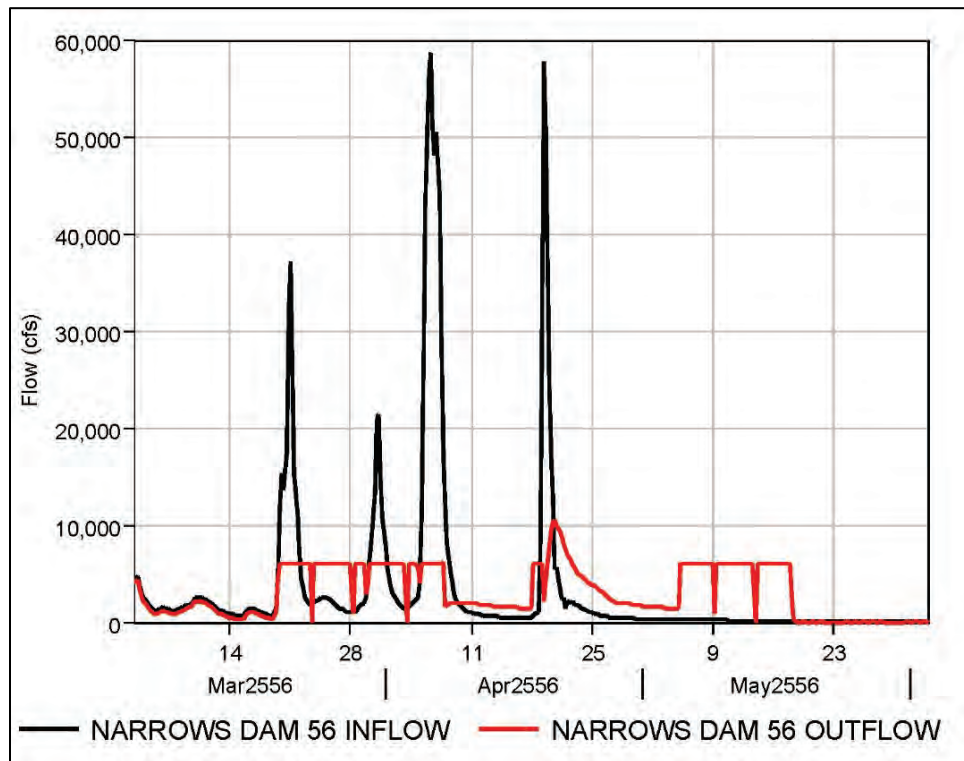


Figure D-81. Degray Dam HYPO 56 inflow compared to outflow.

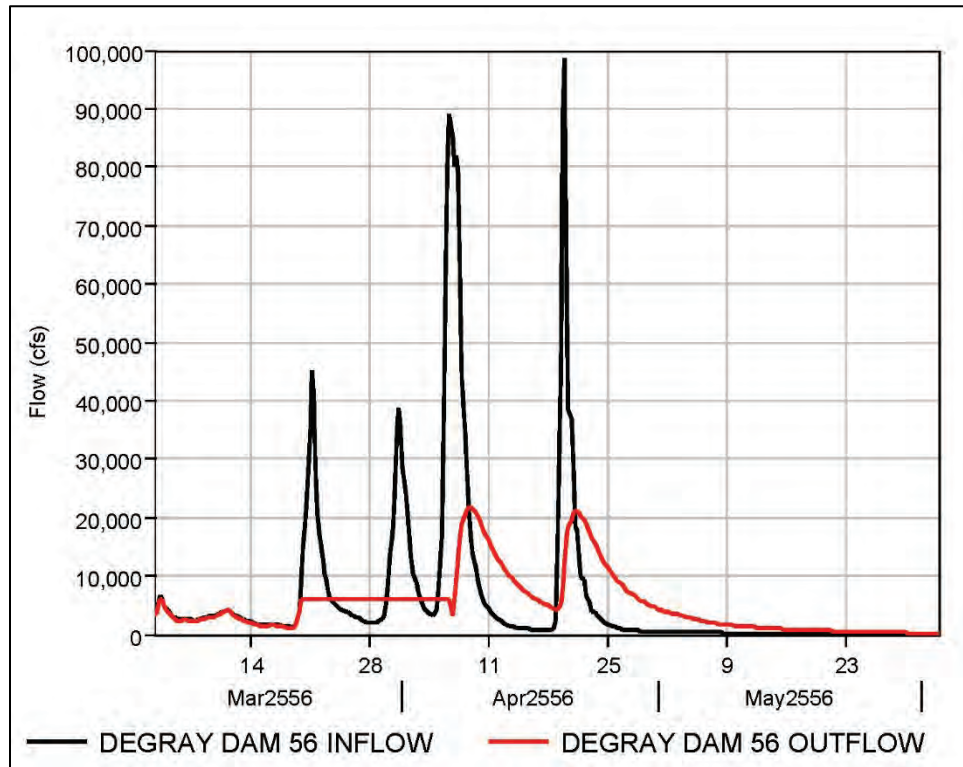
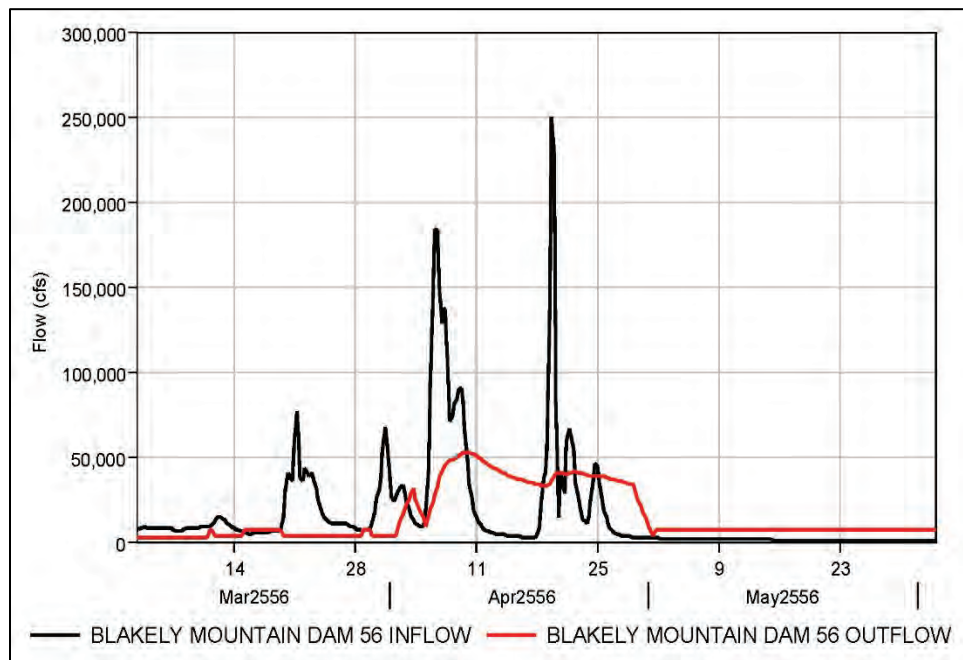


Figure D-82. Blakely Mountain Dam HYPO 56 inflow compared to outflow.



D.4.4 MVR Reservoir Hydrographs

Figure D-83. Coralville Dam HYPO 56 inflow compared to outflow.

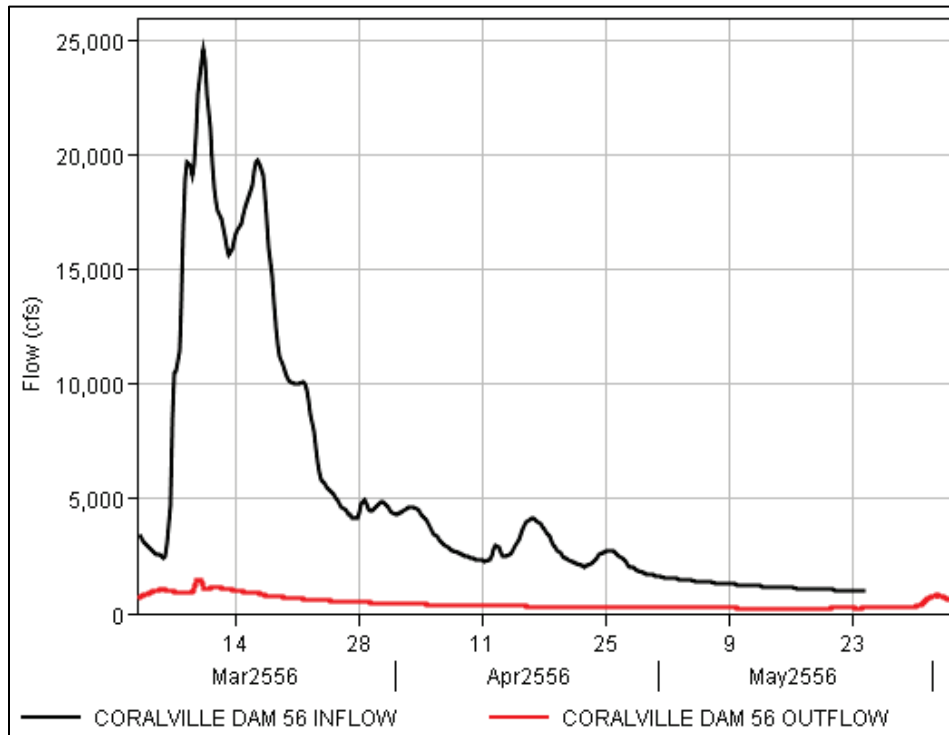
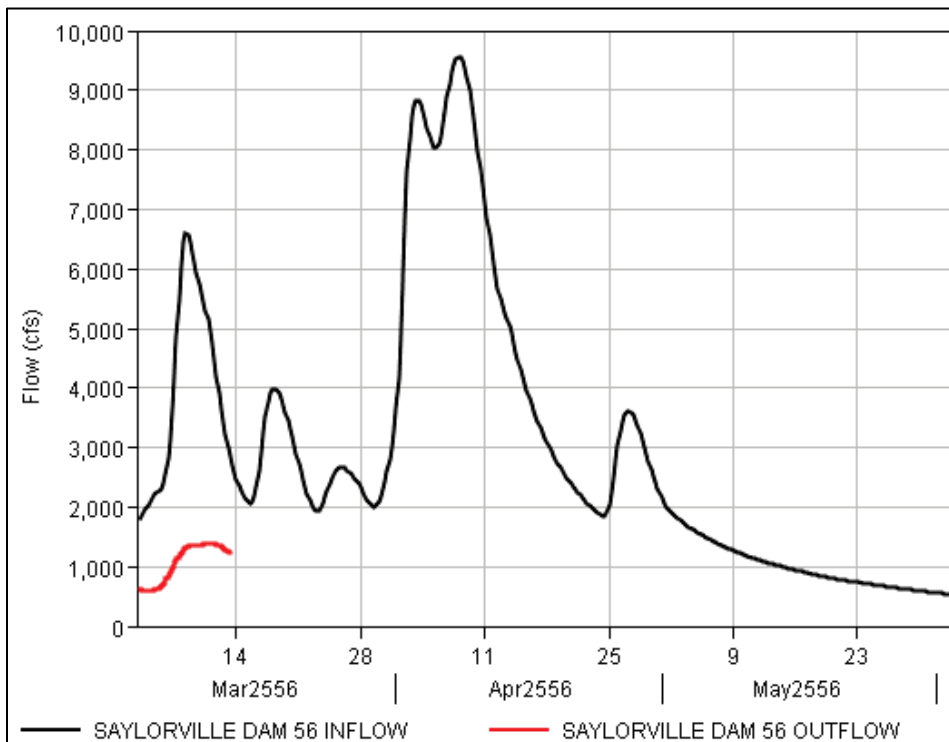


Figure D-84. Saylorville Dam HYPO 56 inflow compared to outflow.



D.4.5 MVS reservoir hydrographs

Figure D-85. Carlyle Lake Dam HYPO 56 inflow compared to outflow.

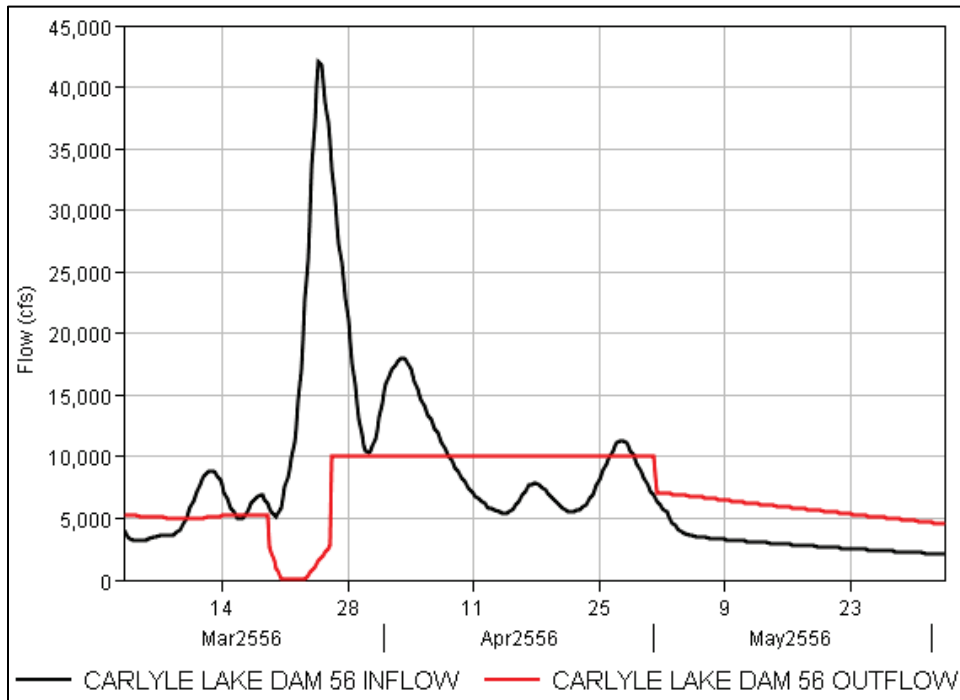


Figure D-86. Lake Shelbyville Dam HYPO 56 inflow compared to outflow.

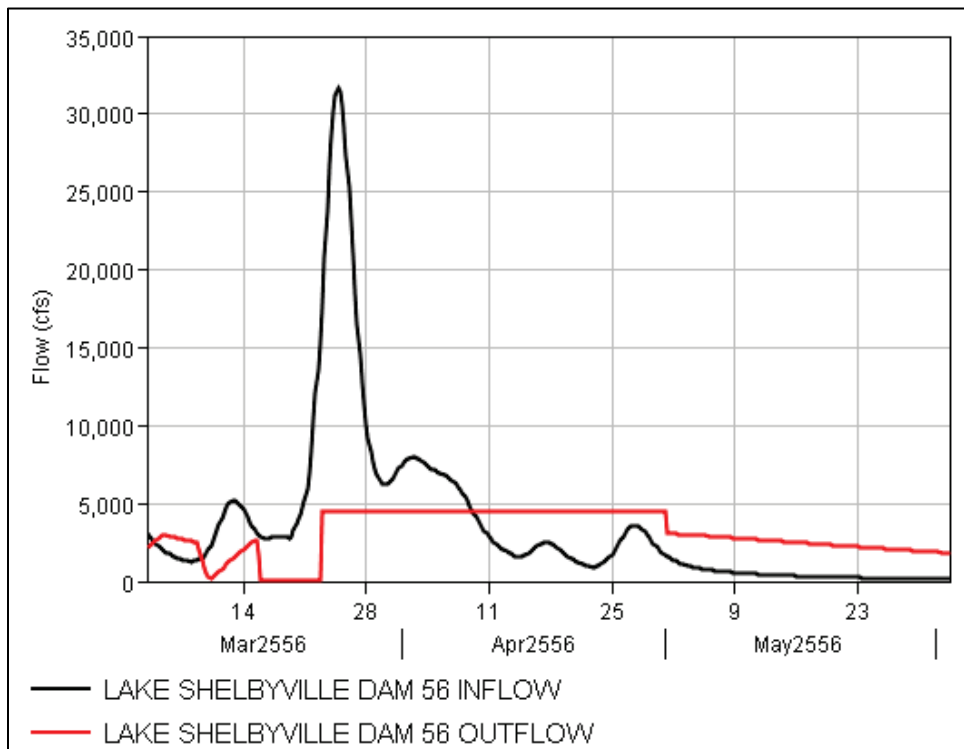


Figure D-87. Mark Twain Lake HYPO 56 inflow compared to outflow.

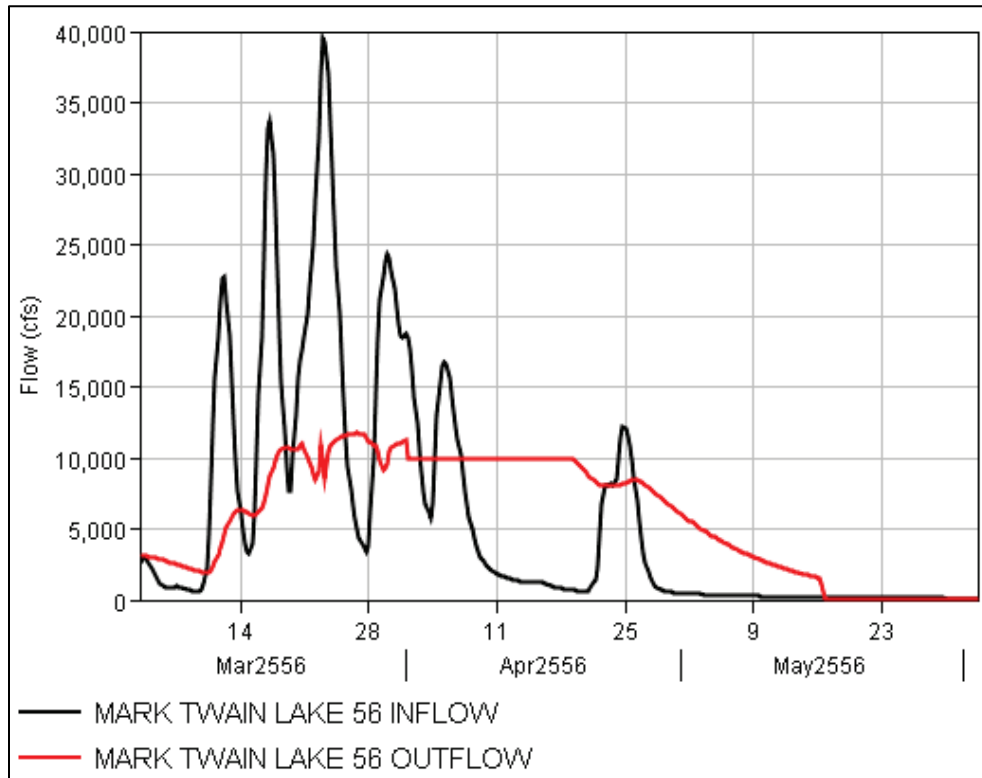
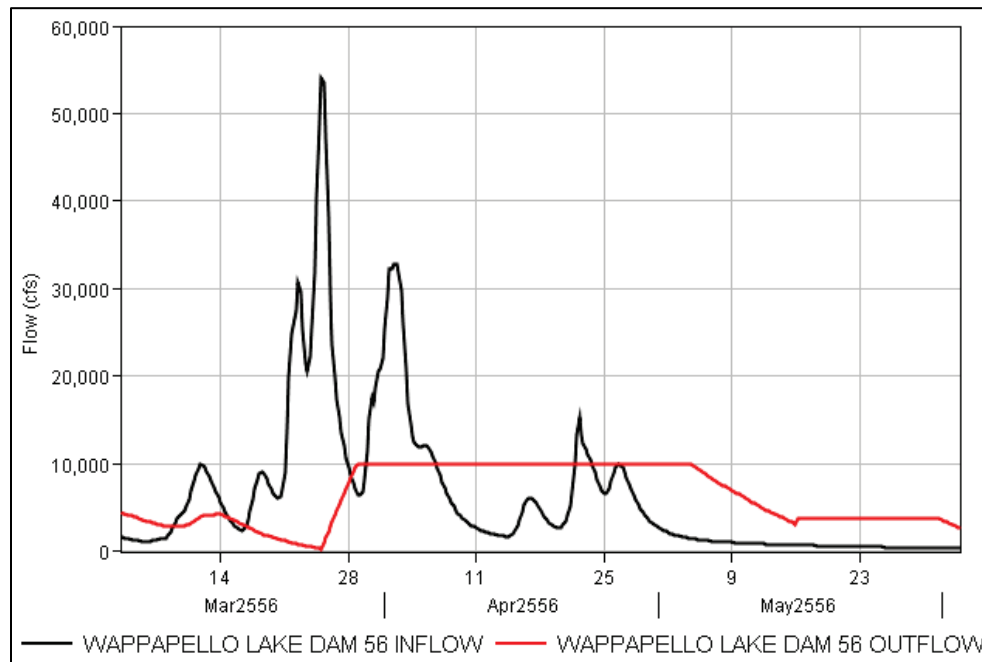


Figure D-88. Wappapello Lake Dam HYPO 56 inflow compared to outflow.



D.4.6 NWO Reservoir Hydrgraphs

Figure D-89. Big Bend DAM HYPO 56 inflow compared to outflow.

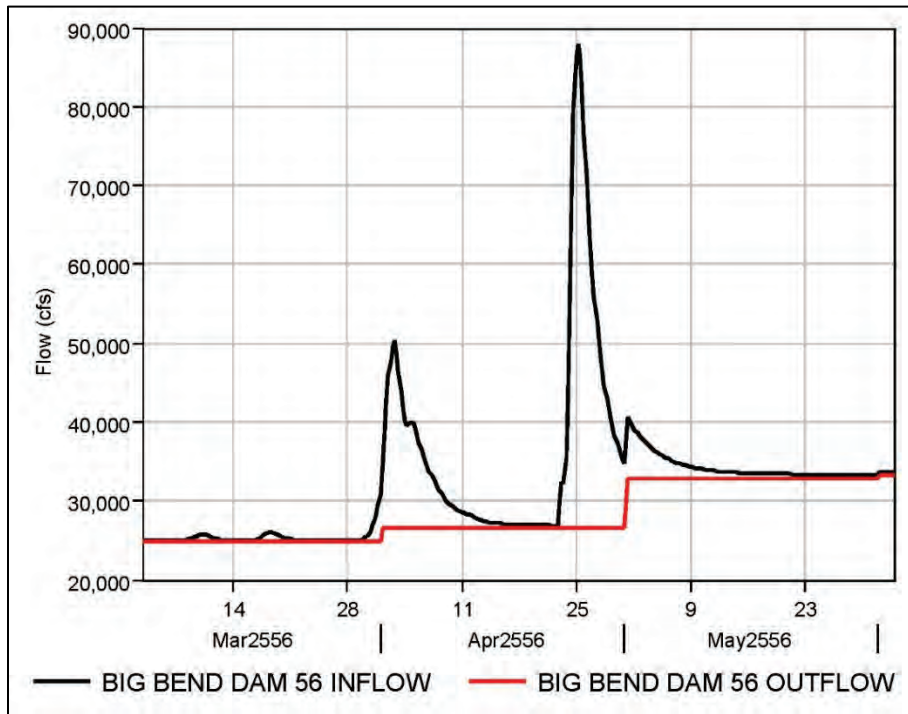


Figure D-90. Fort Peck Dam HYPO 56 inflow compared to outflow.

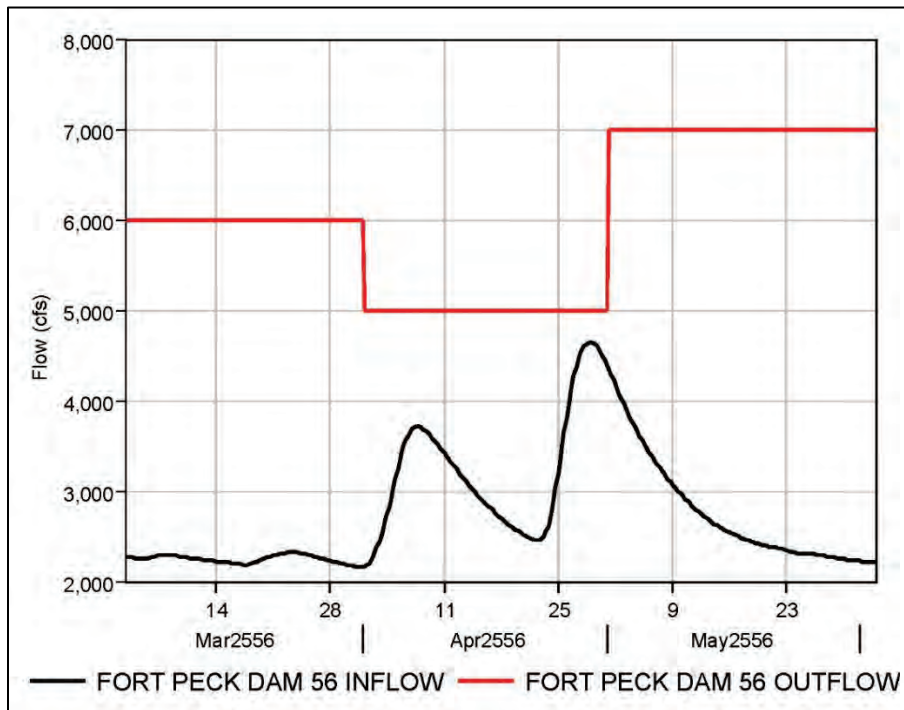


Figure D-91. Fort Randall Dam HYPO 56 inflow compared to outflow.

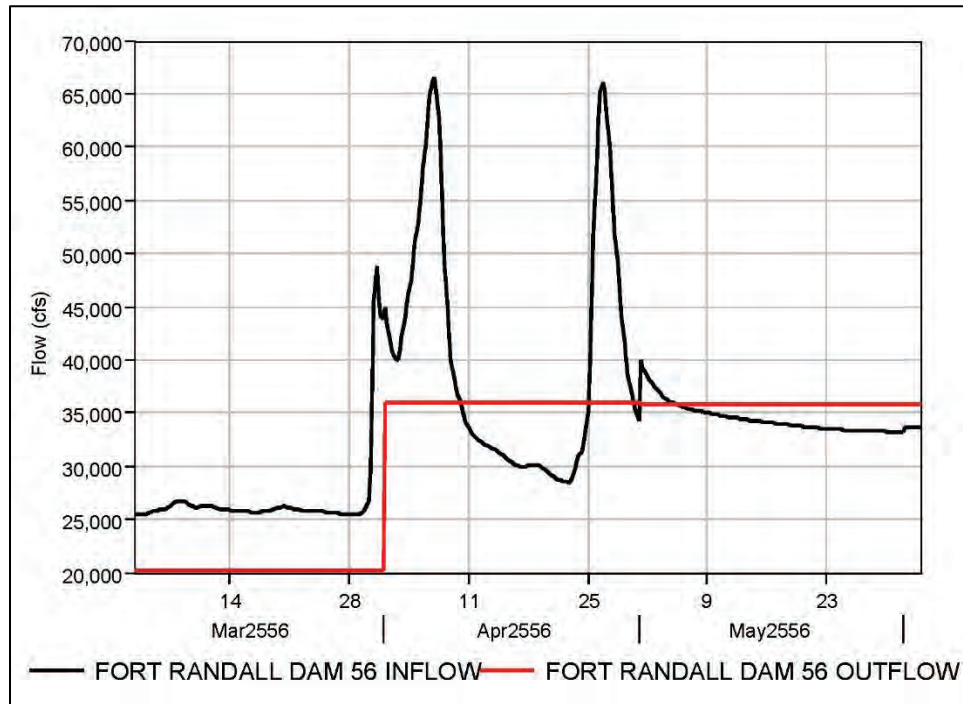


Figure D-92. Garrison Dam HYPO 56 inflow compared to outflow.

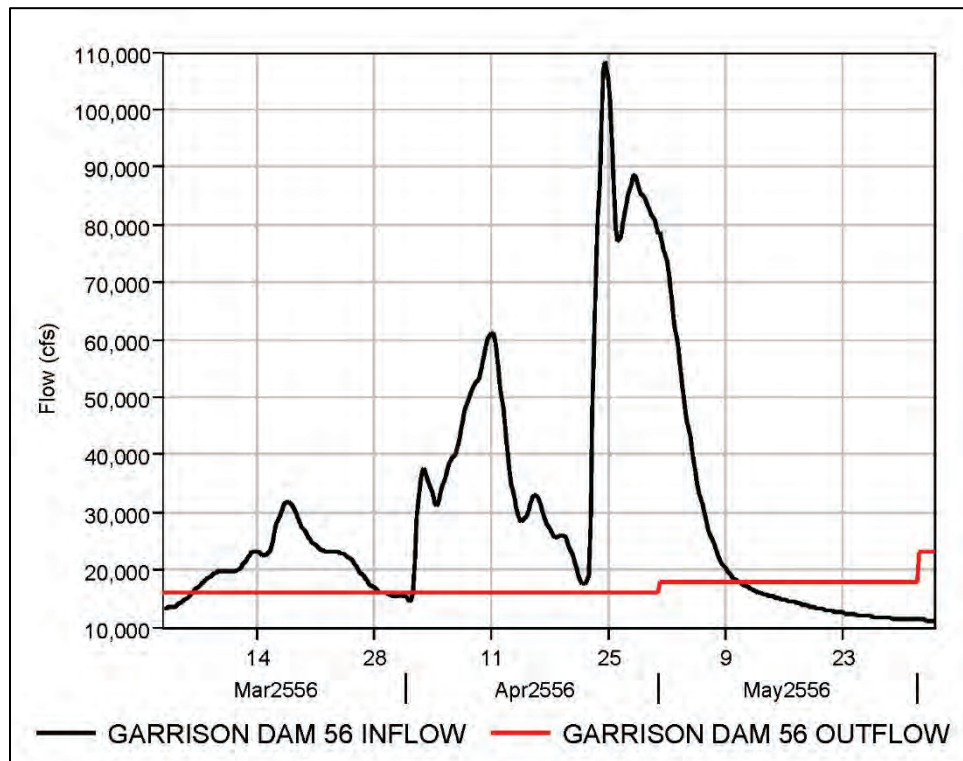


Figure D-93. Gavin's Point Dam HYPO 56 inflow compared to outflow.

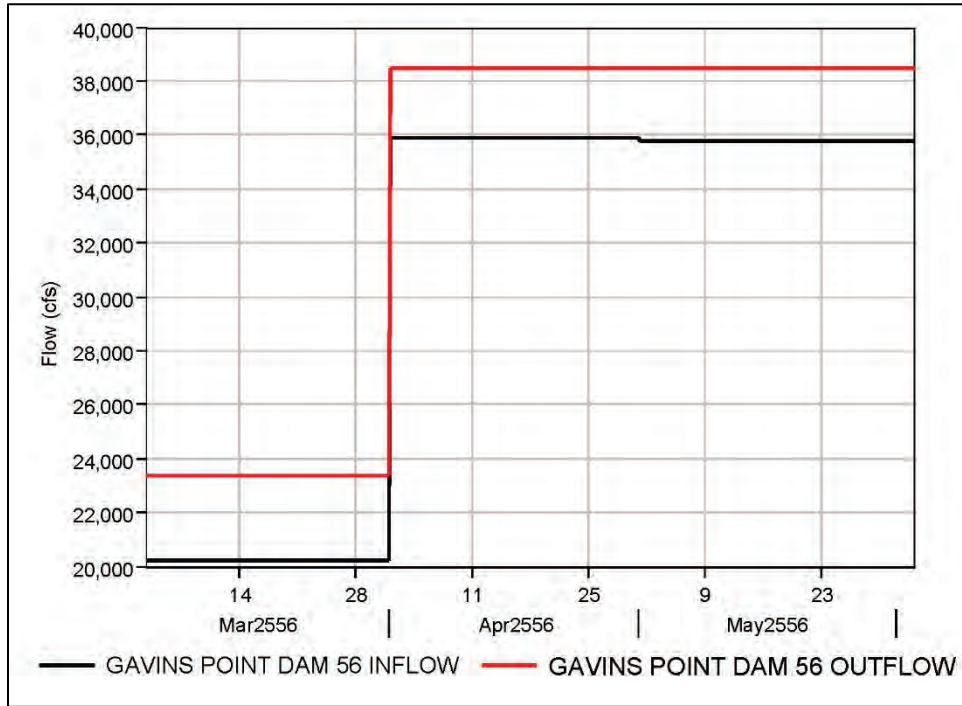
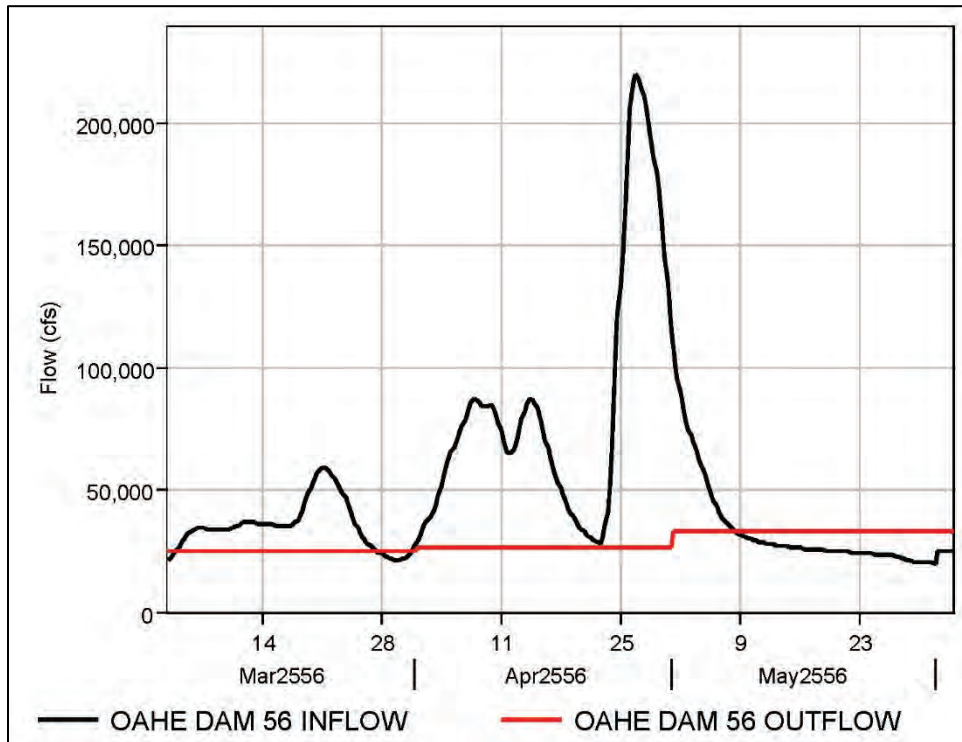


Figure D-94. Oahe Dam HYPO 56 inflow compared to outflow.



D.4.7 NWK Reservoir Hydrographs

Figure D-95. Clinton Dam HYPO 56 inflow compared to outflow.

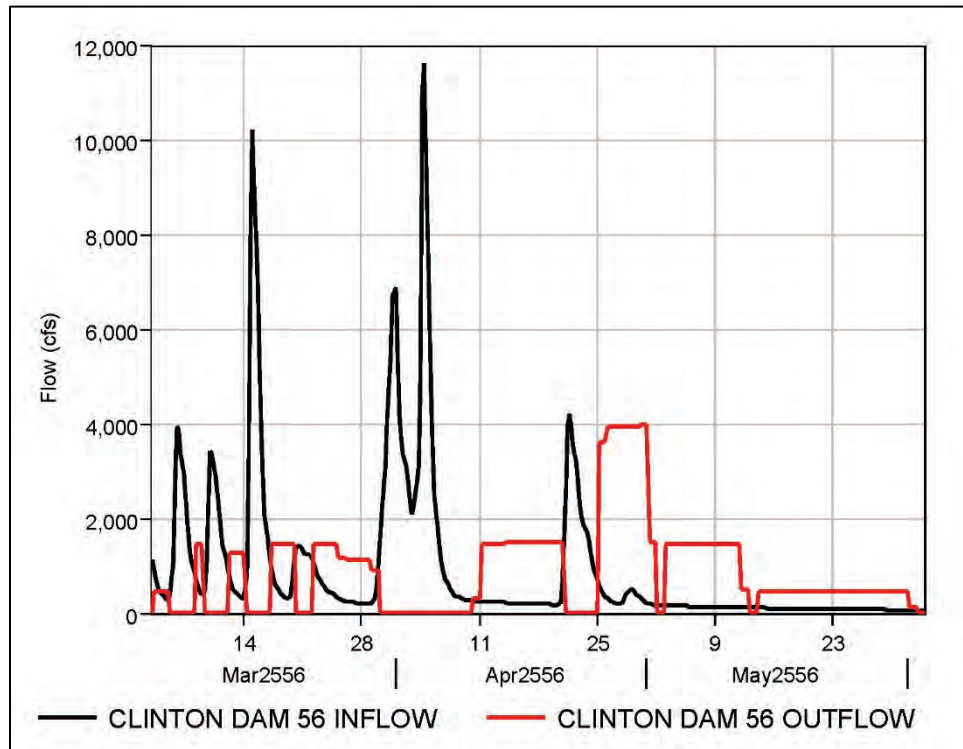


Figure D-96. Glen Elder Dam HYPO 56 inflow compared to outflow.

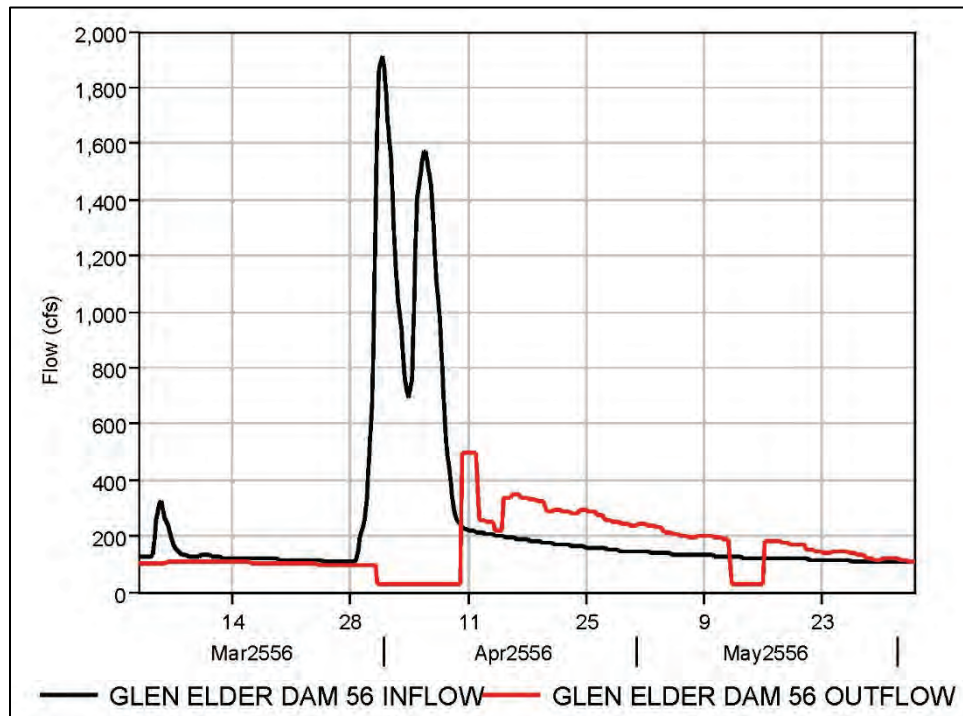


Figure D-97. Hillsdale Dam HYPO 56 inflow compared to outflow.

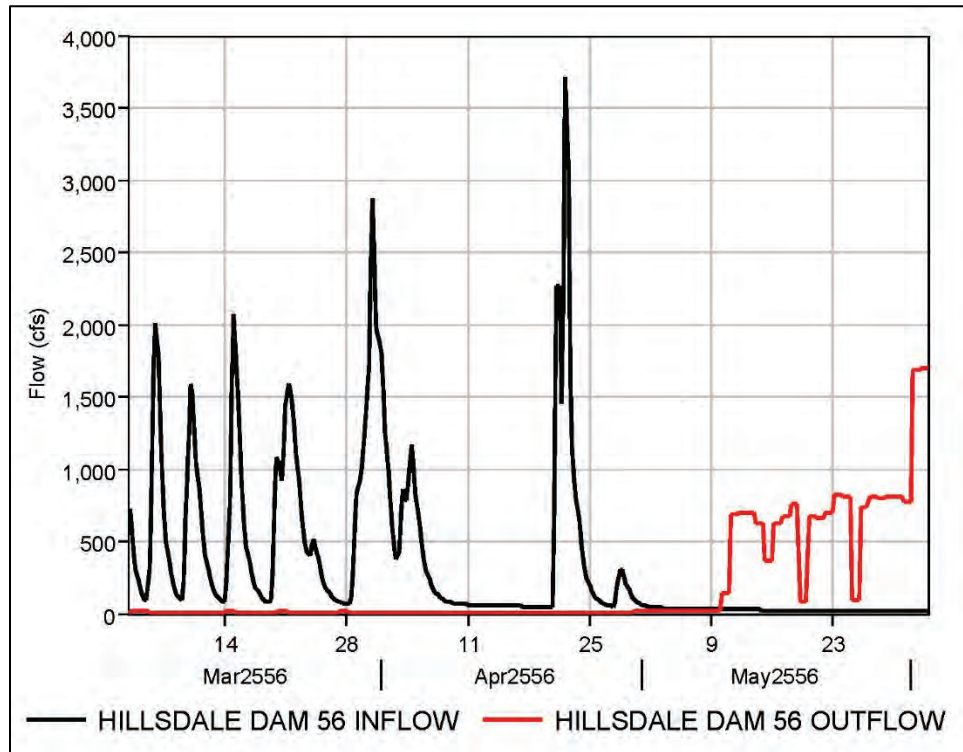


Figure D-98. Kanopolis Dam HYPO 56 inflow compared to outflow.

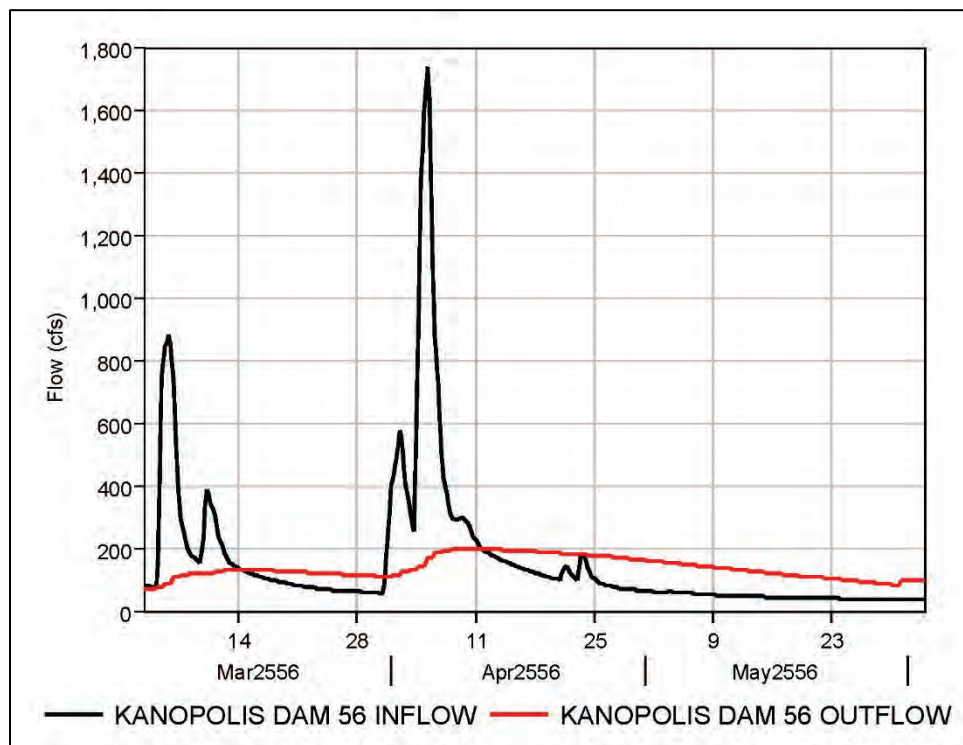


Figure D-99. Melvern Dam HYPO 56 inflow compared to outflow.

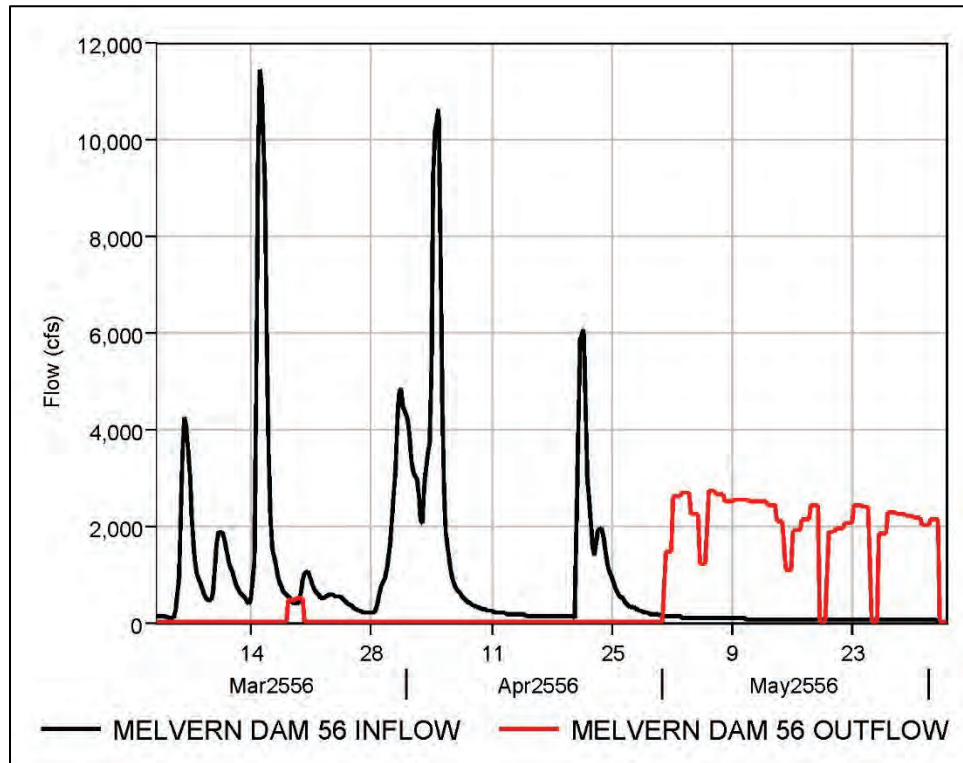


Figure D-100. Milford Dam HYPO 56 inflow compared to outflow.

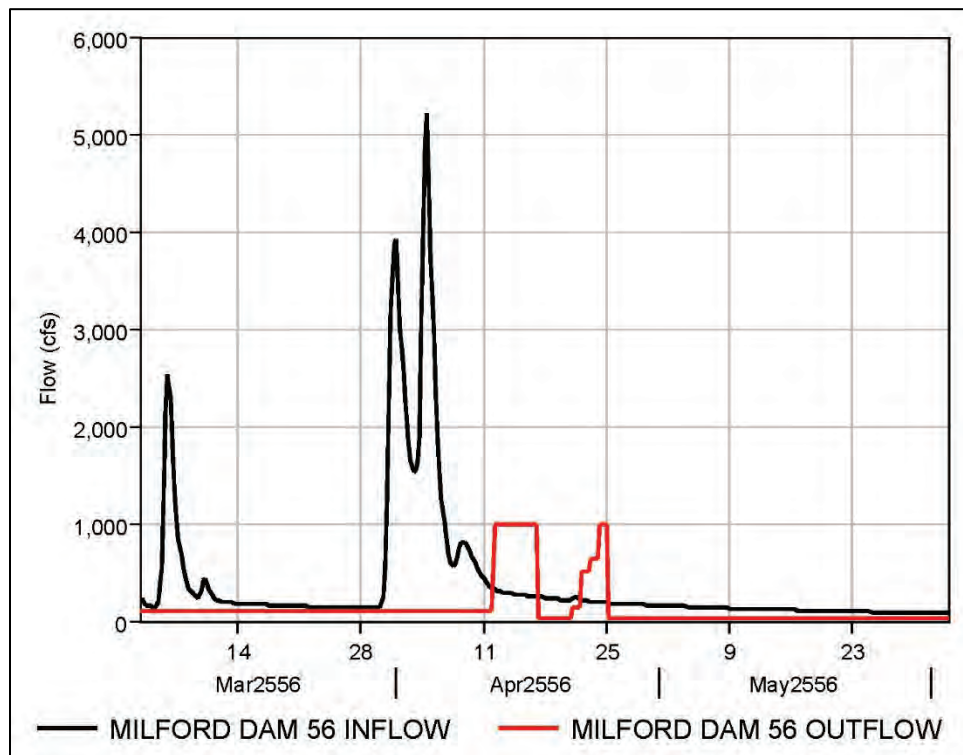


Figure D-101. Perry Dam HYPO 56 inflow compared to outflow.

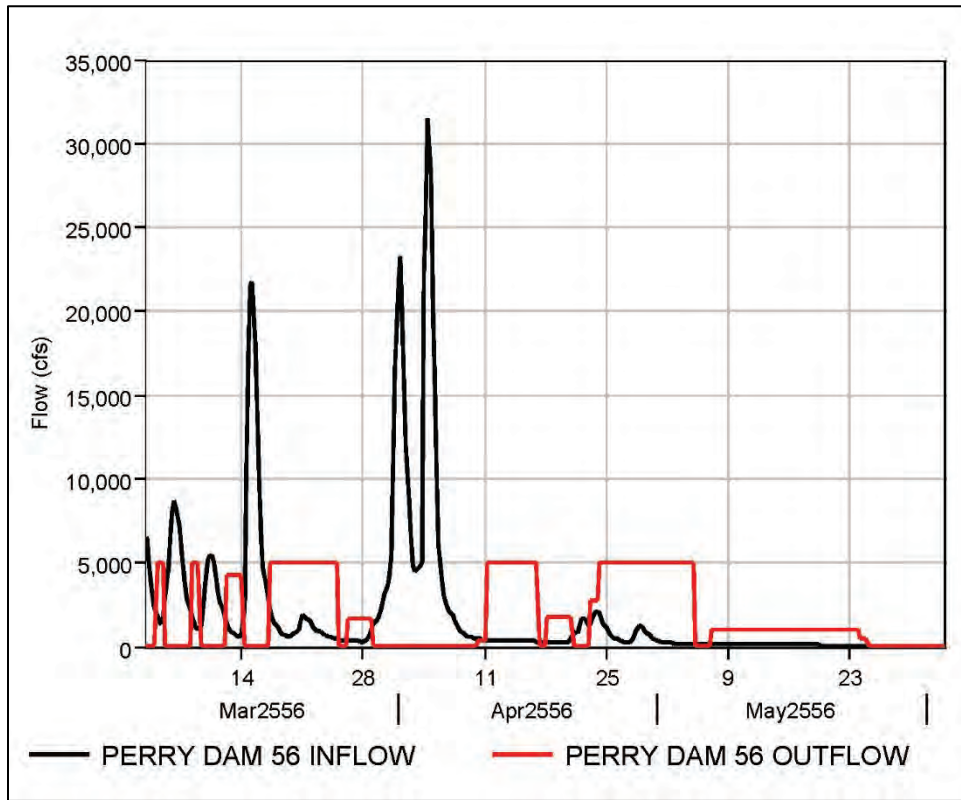


Figure D-102. Pomme De Terre Dam HYPO 56 inflow compared to outflow.

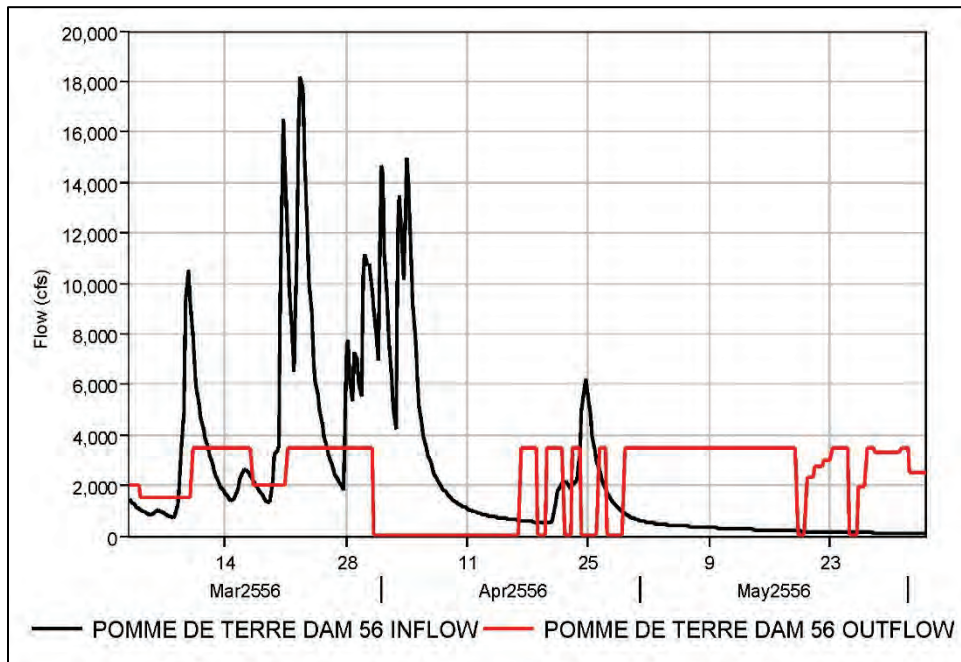


Figure D-103. Pomona Dam HYPO 56 inflow compared to outflow.

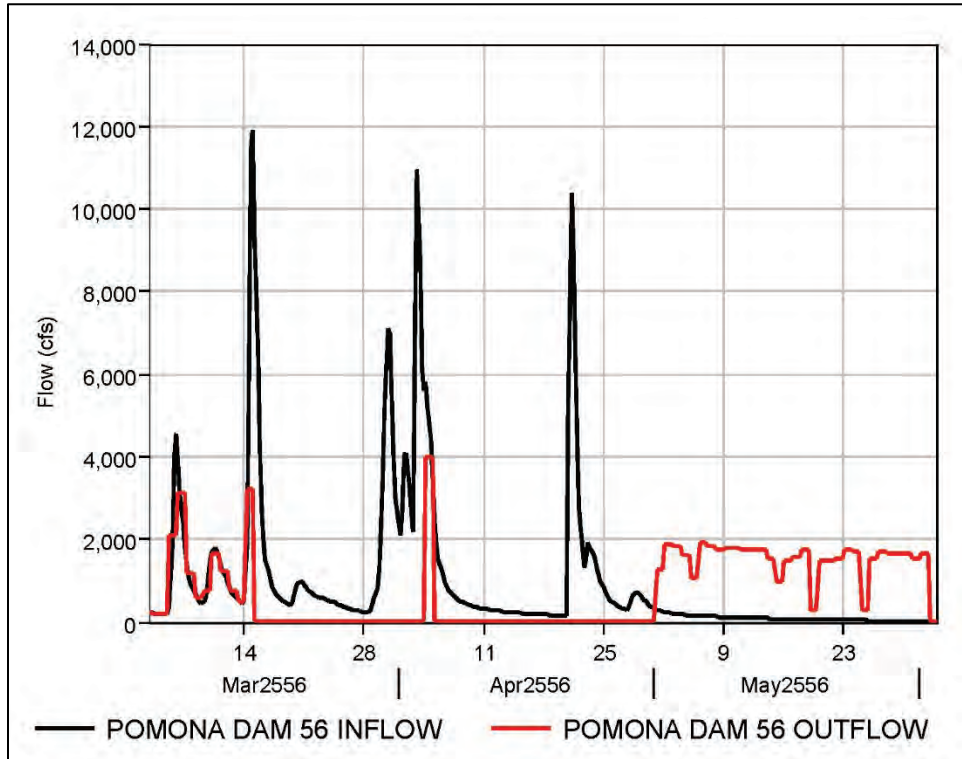


Figure D-104. Rathbun Dam HYPO 56 inflow compared to outflow.

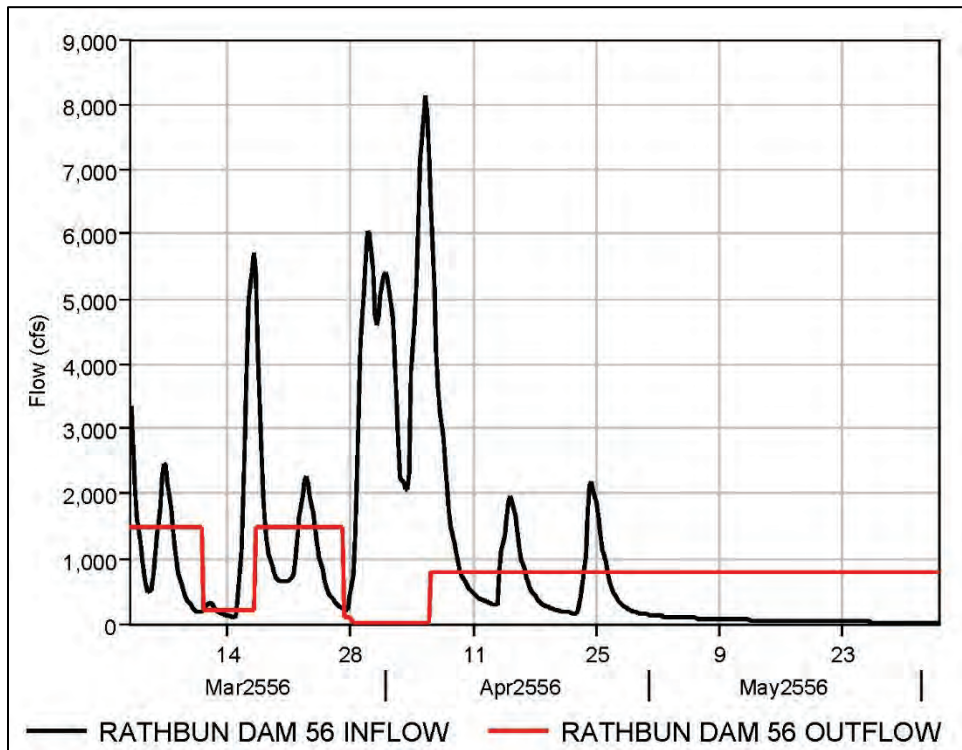


Figure D-105. Smithville Dam HYPO 56 inflow compared to outflow.

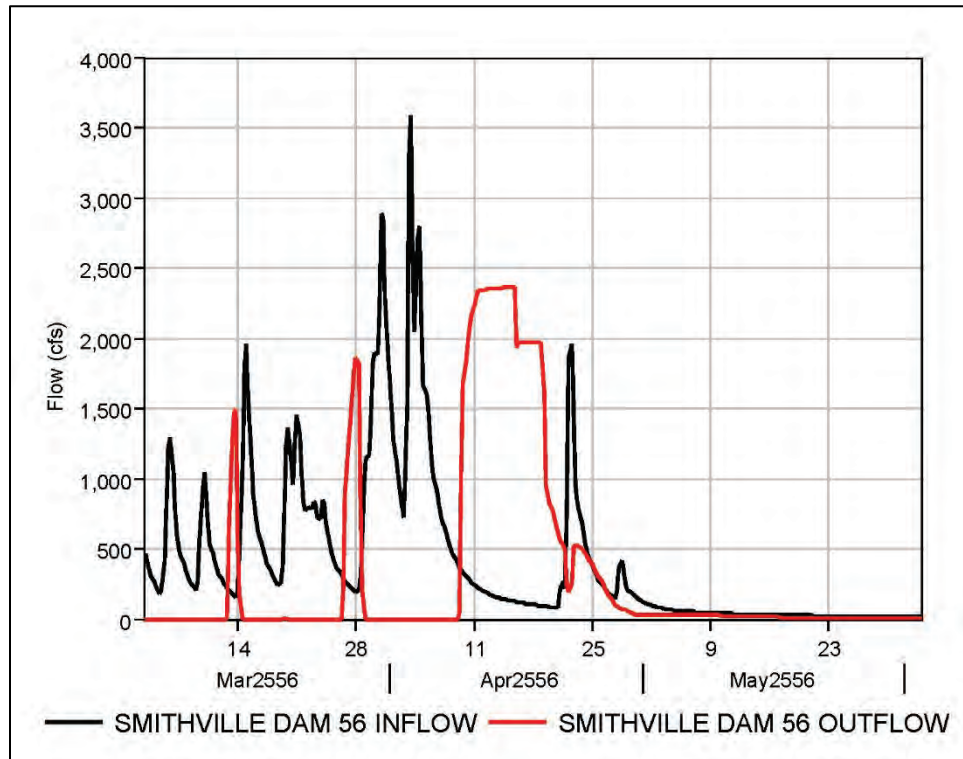


Figure D-106. Stockton Dam HYPO 56 inflow compared to outflow.

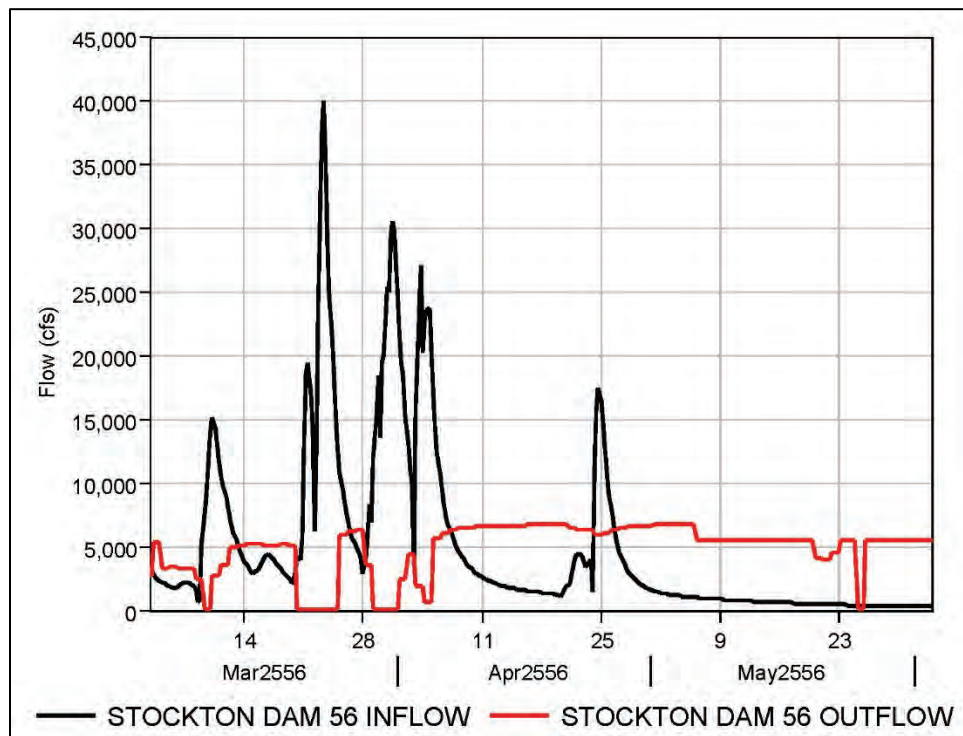


Figure D-107. Truman Dam HYPO 56 inflow compared to outflow.

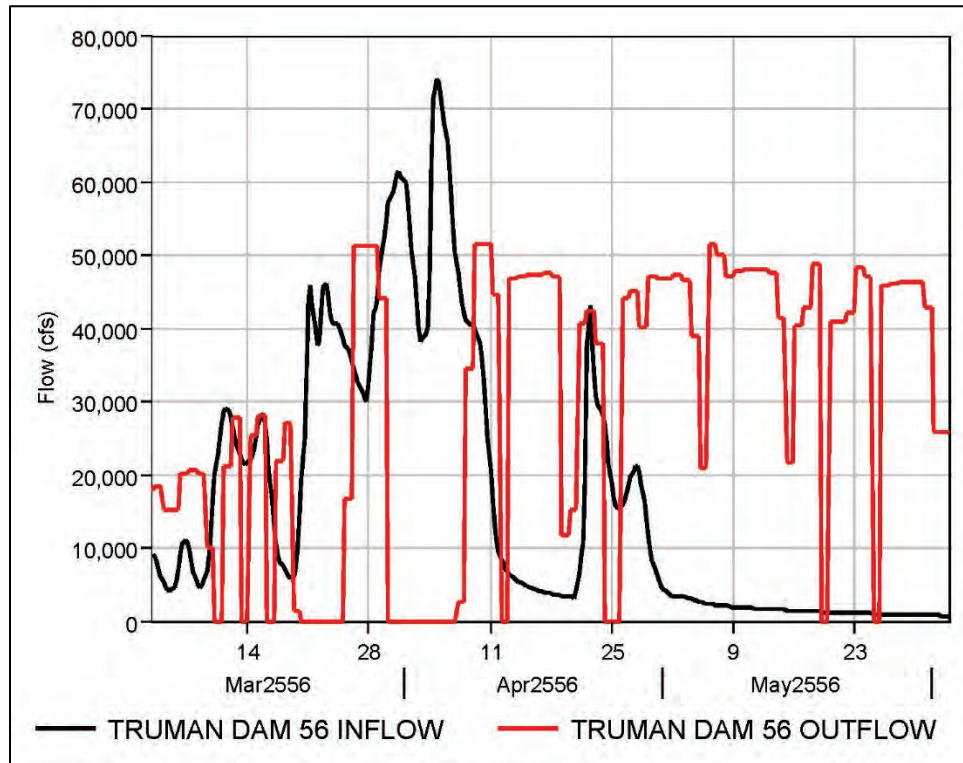


Figure D-108. Tuttle Creek Dam HYPO 56 inflow compared to outflow.

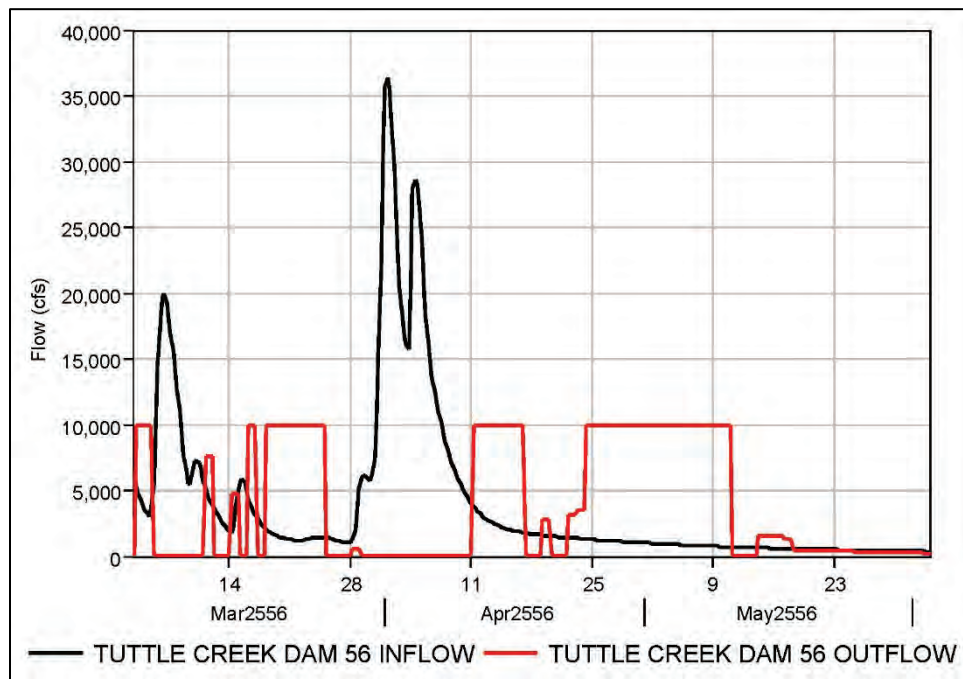
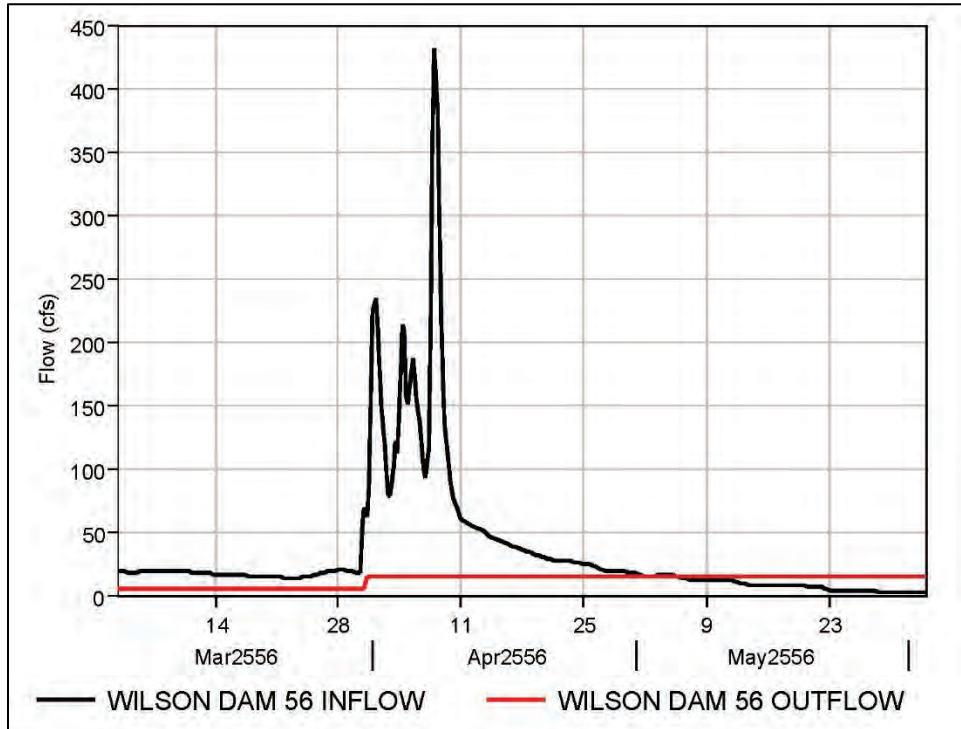


Figure D-109. Wilson Dam HYPO 56 inflow compared to outflow.



D.4.8 SWL Reservoir Hydrographs

Figure D-110. Bull Shoals Dam HYPO 56 inflow compared to outflow.

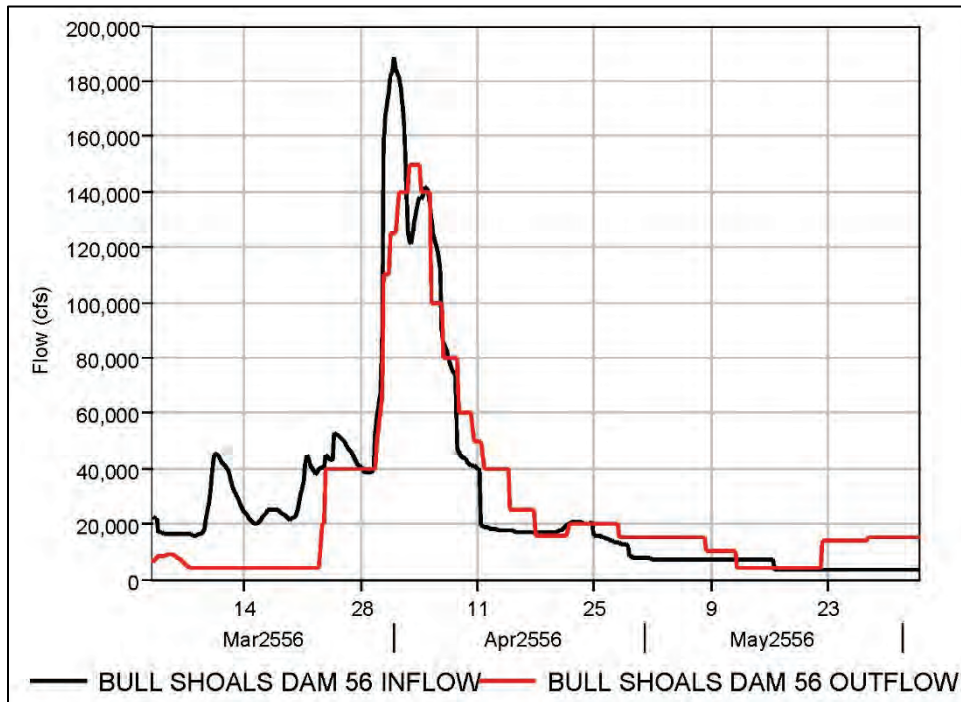


Figure D-111. Greer's Ferry Dam HYPO 56 inflow compared to outflow.

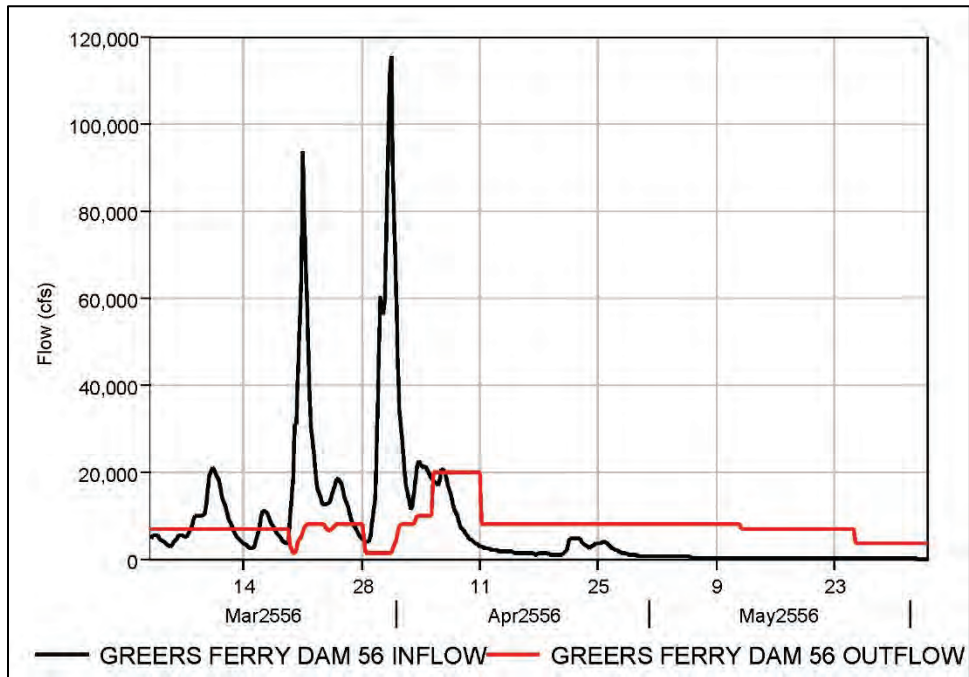
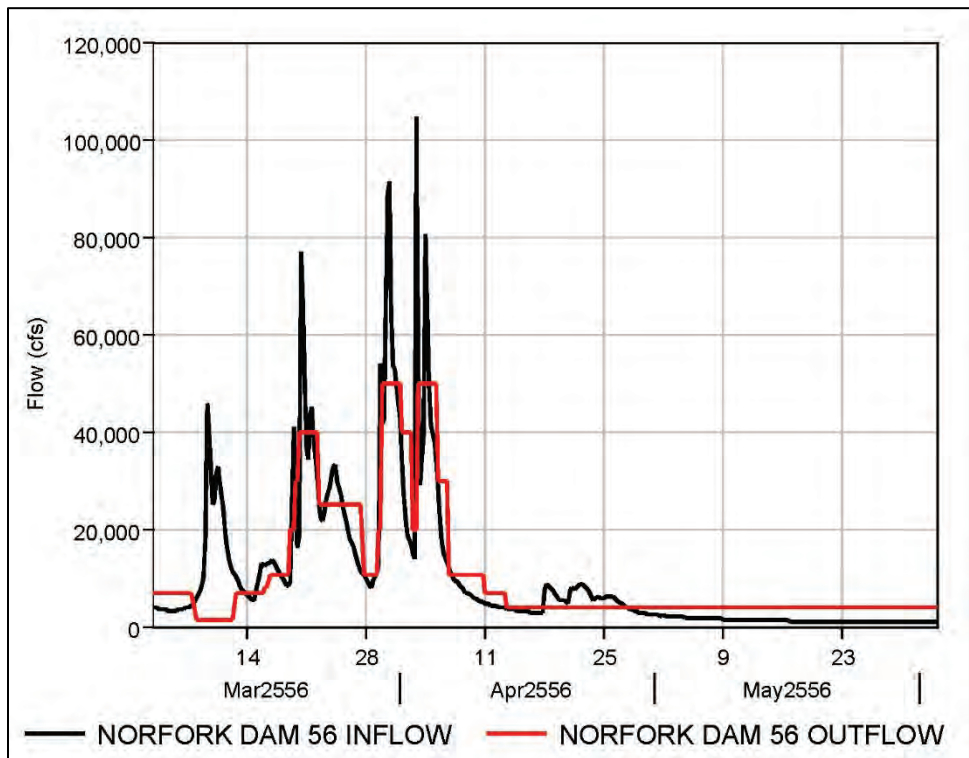


Figure D-112. Norfolk Dam HYPO 56 inflow compared to outflow.



D.4.9 SWT Reservoir Hydrographs

Figure D-113. Fort Gibson Dam HYPO 56 inflow compared to outflow.

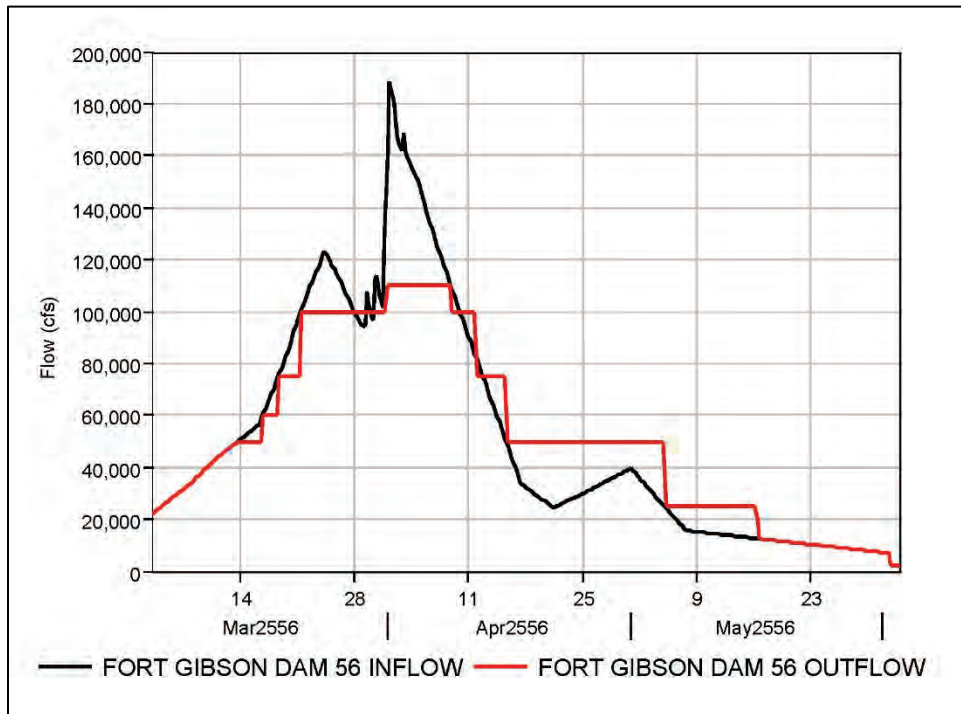


Figure D-114. Hugo Dam HYPO 56 inflow compared to outflow.

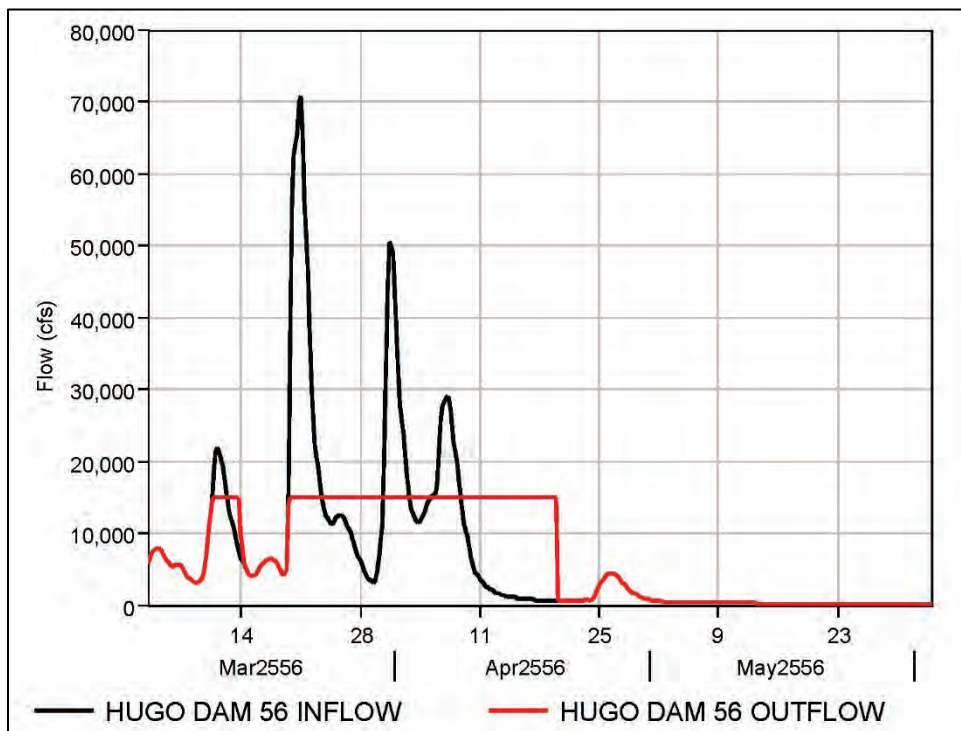


Figure D-115. Keystone Lake HYPO 56 inflow compared to outflow.

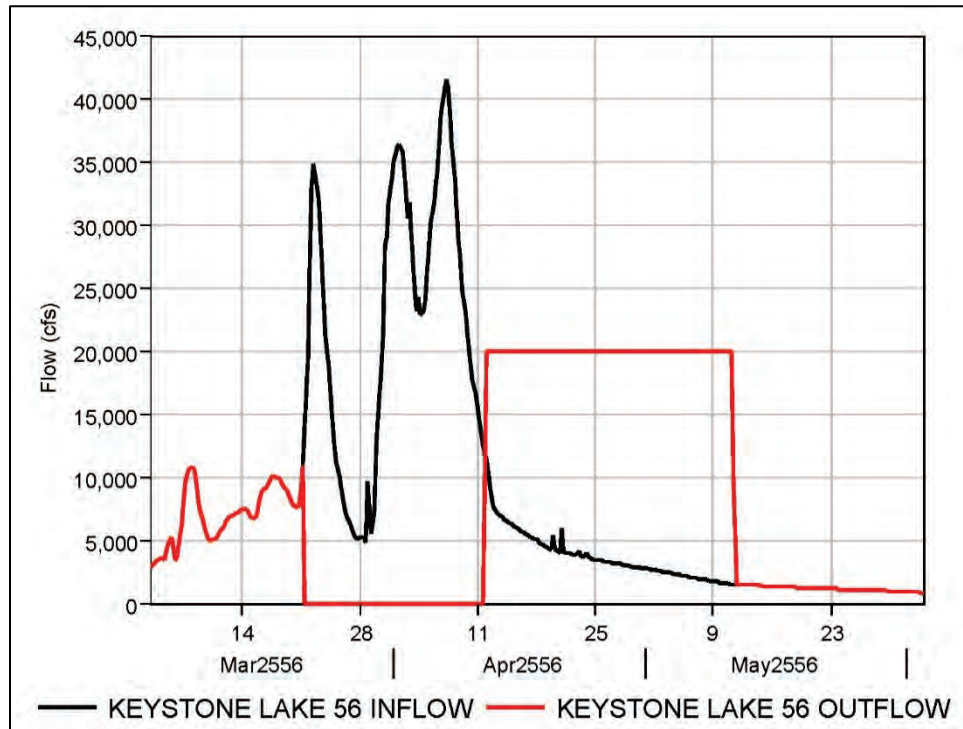


Figure D-116. Lake Texoma HYPO 56 inflow compared to outflow.

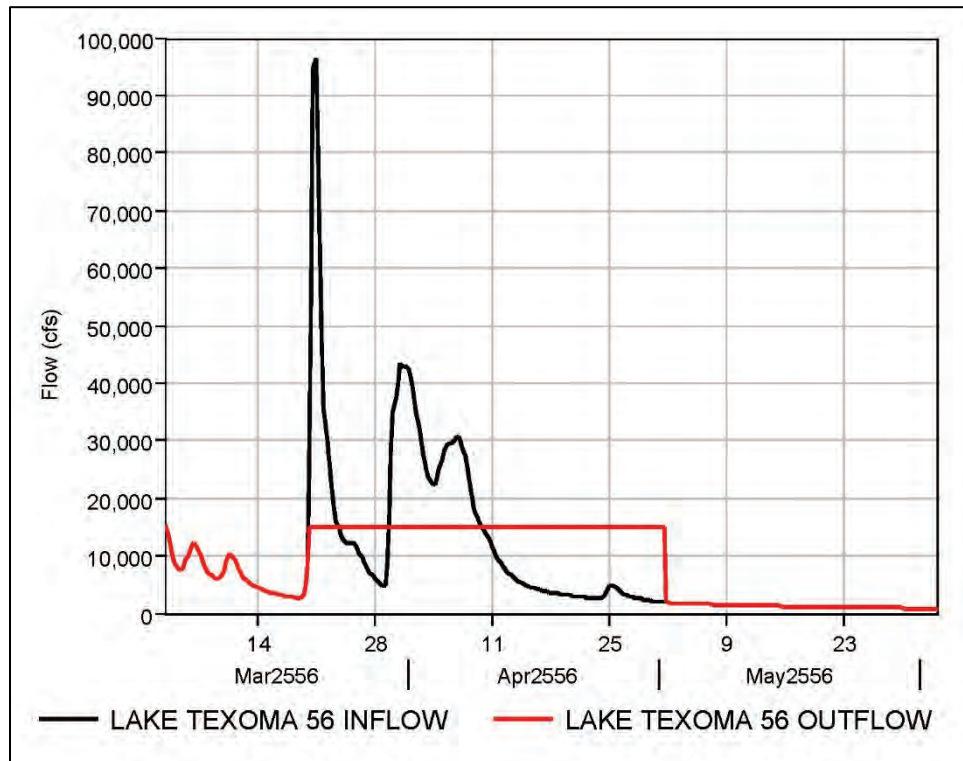


Figure D-117. Oologah Lake HYPO 56 inflow compared to outflow.

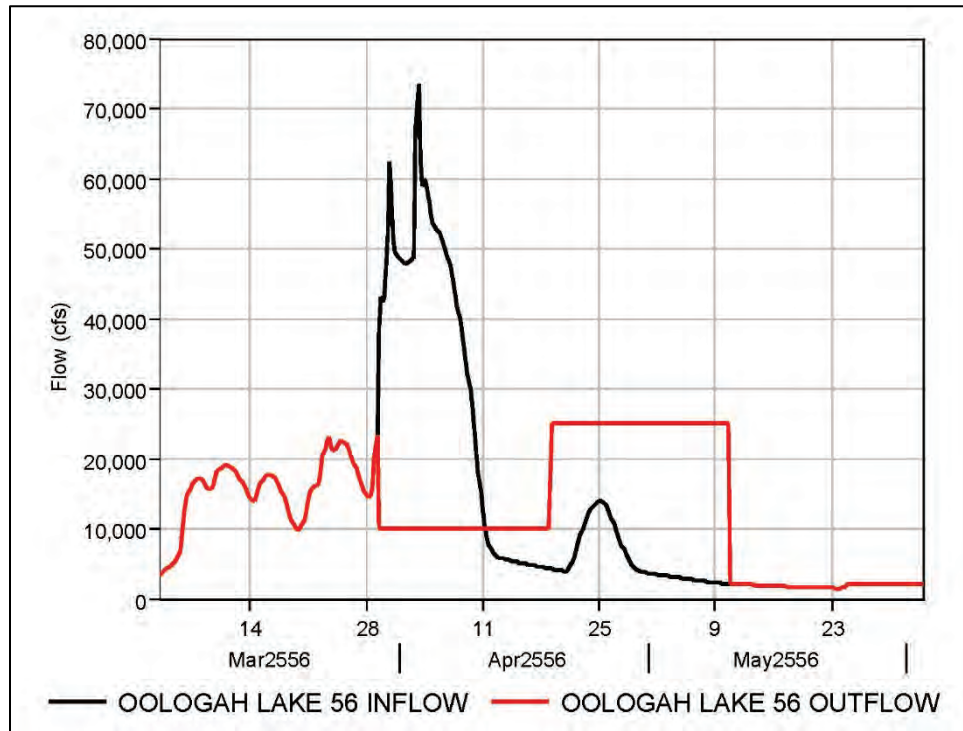


Figure D-118. Skiatook Lake HYPO 56 inflow compared to outflow.

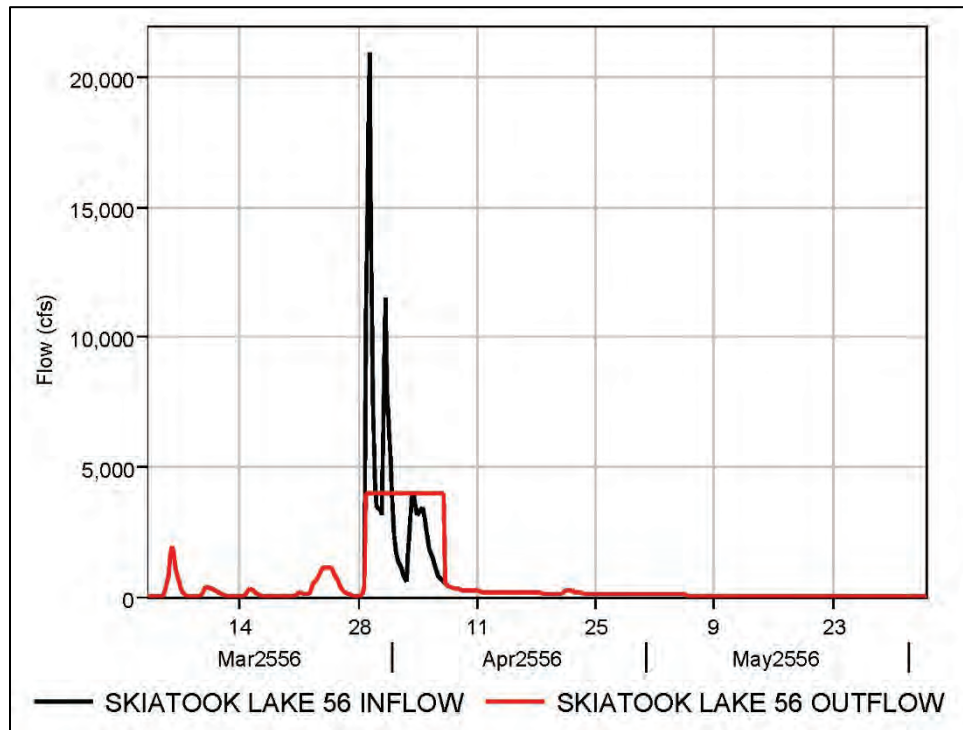


Figure D-119. Tenkiller Lake HYPO 56 inflow compared to outflow.

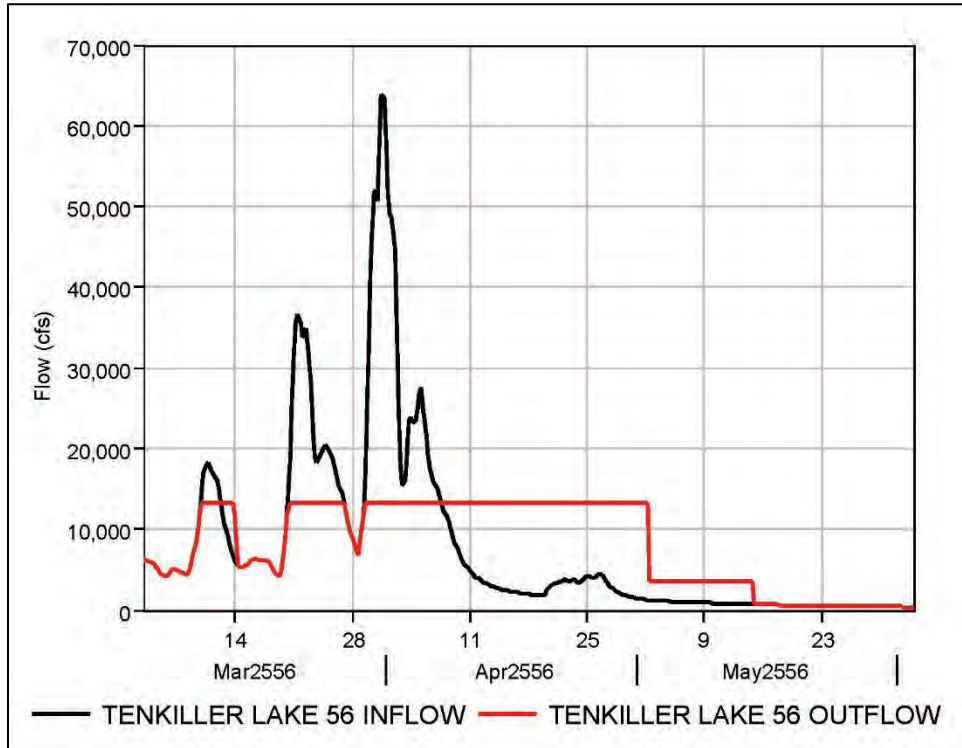
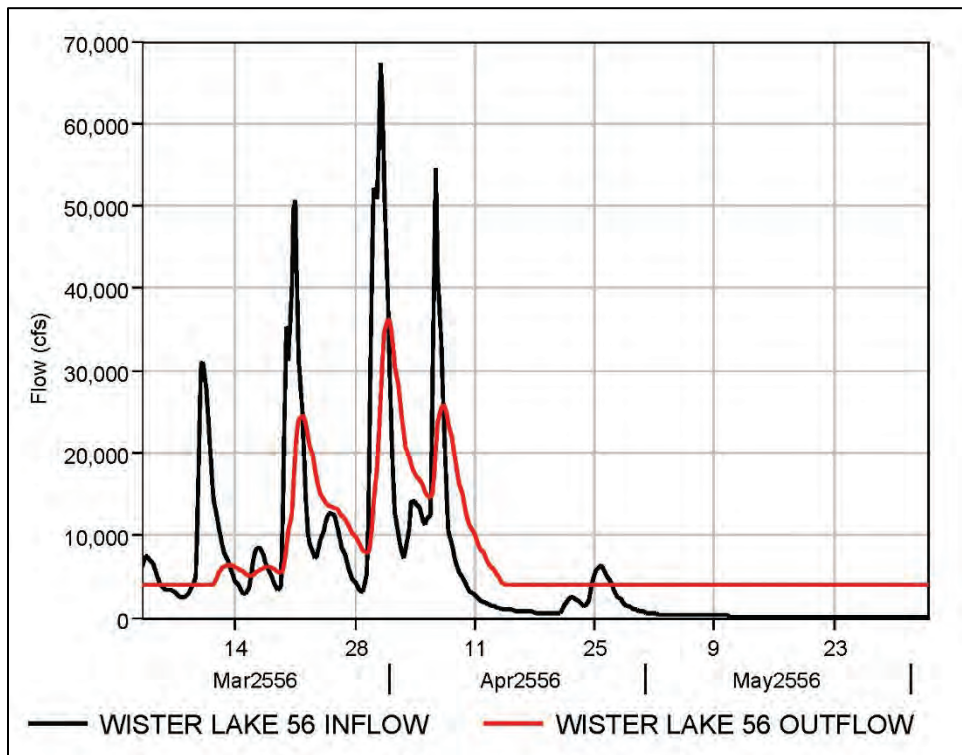


Figure D-120. Wister Lake HYPO 56 inflow compared to outflow.

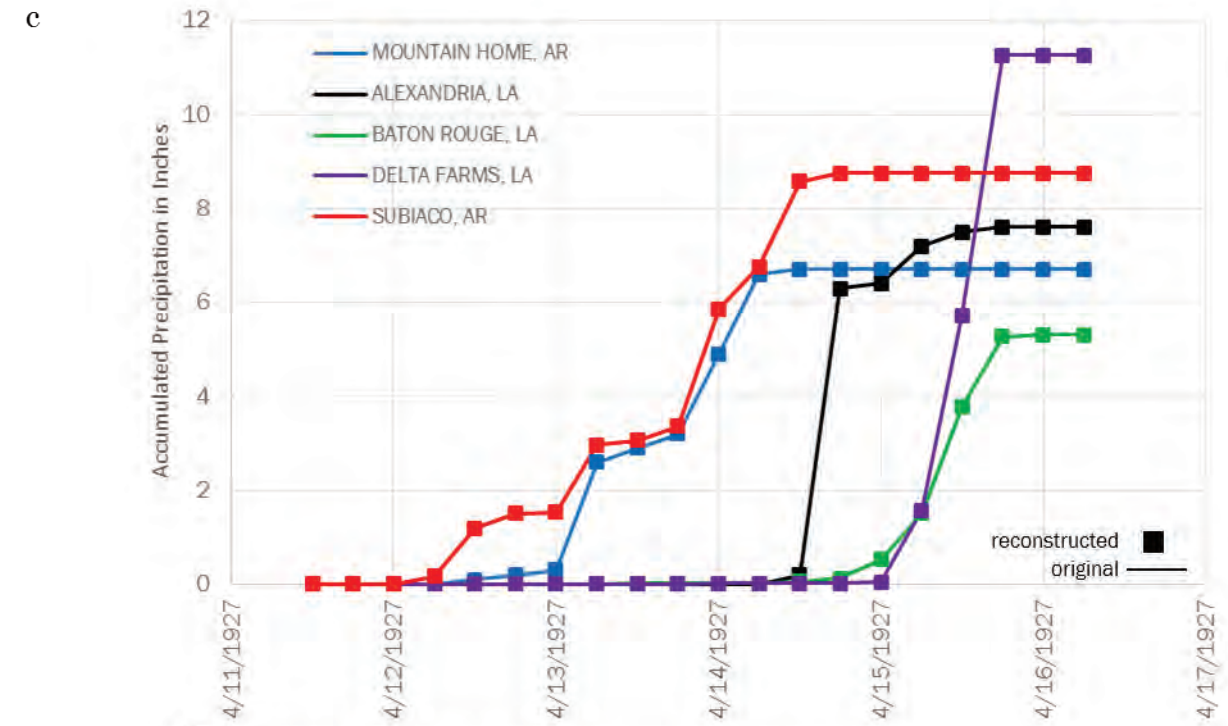
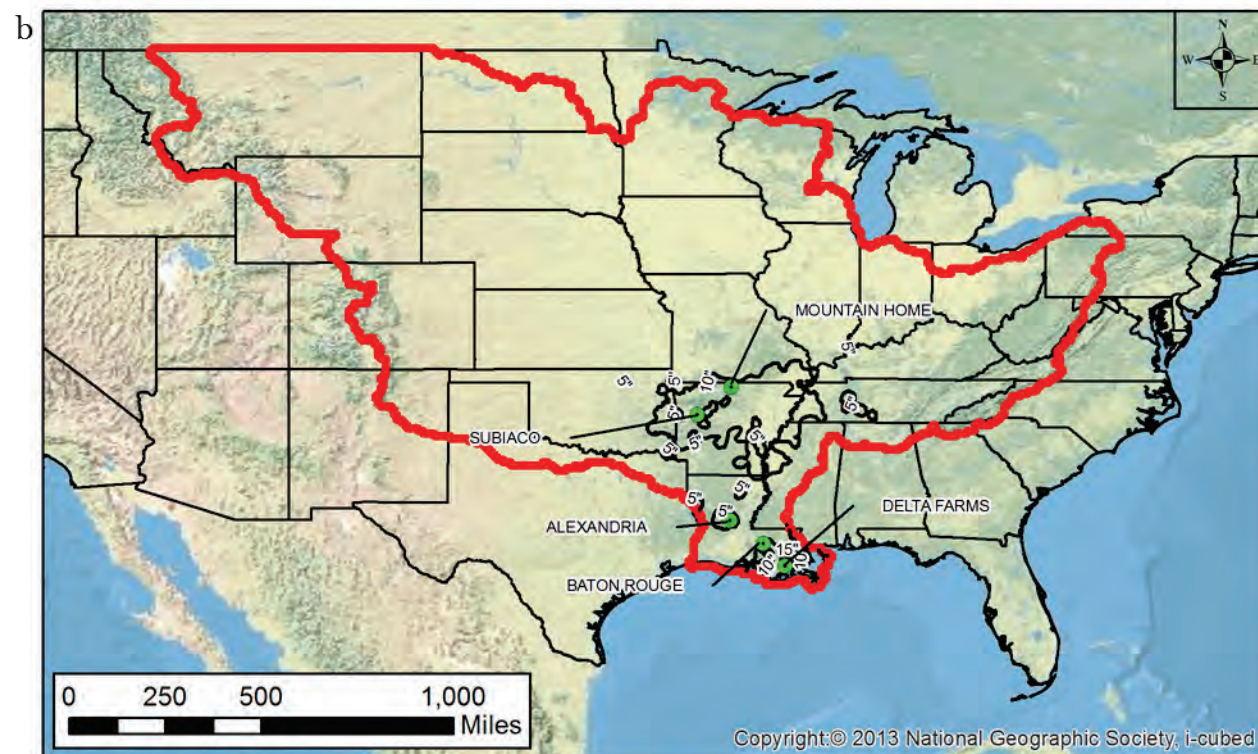
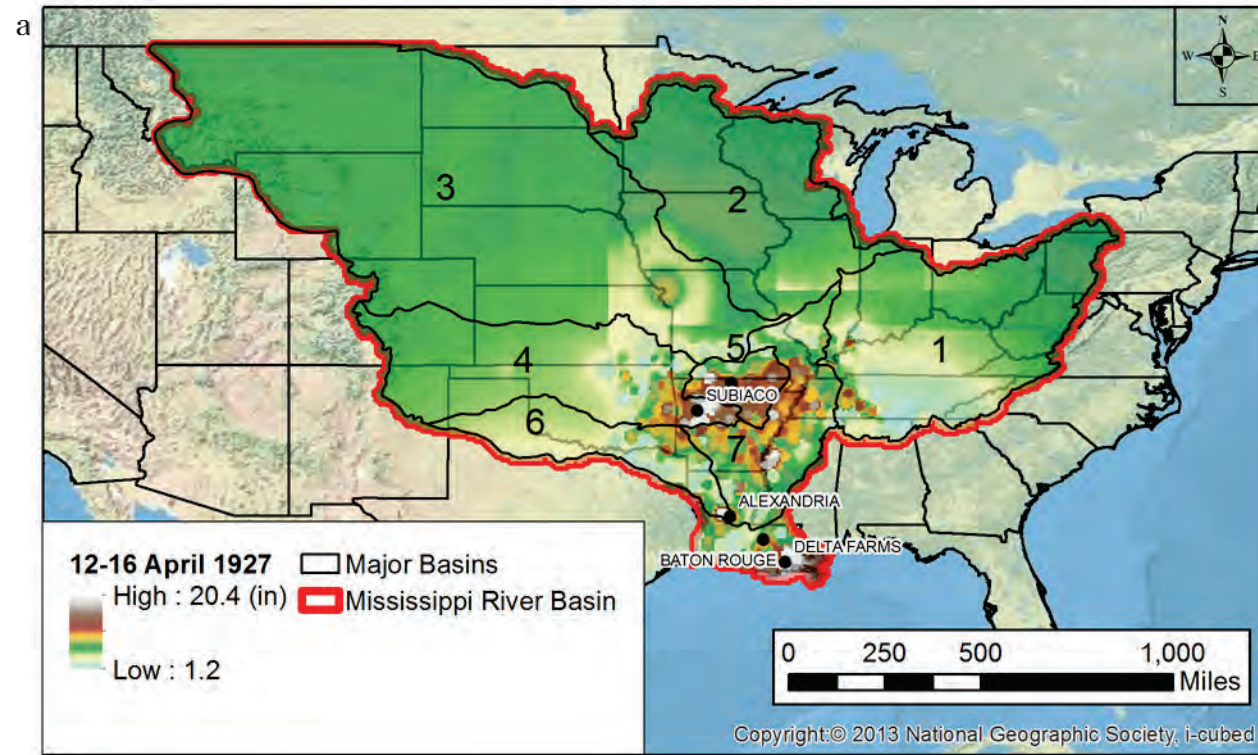


Appendix E: HYPO 63

E.1 HYPO 63 storm precipitation

HYPO Storm 63 is comprised of two historical storm events as they actually occurred and one transposed storm. Two of the storms centered over all areas north of the Latitude of Red River Landing and the transposed storm is centered between Cairo, IL, and the Latitude of Red River Landing, LA. The 2016 assessment used point rainfall data and IDW interpolation (with bias toward observed point values) to reconstruct the original 1955 storms data. Figure E-1, Figure E-3, and Figure E-4 depict the total precipitation and coverage of each storm event that compiles HYPO 63. Figure (a) in each of the figures depicts the reconstructed storm coverage of the storm event. Figure (b) depicts the isohyetal contours for the reconstructed storm event. Figure (c) looks at several locations and compares the original 1955 precipitation data against the processed inputs after they were converted to a raster by interpolation. Table (d) tabulates the 1955 values, the initial 2016 point data inputs, and the interpolated 2016 grid inputs. Figure E-1 shows the storm coverage that was included in the HYPO 63 hydrology model, but Figure E-2 shows the corrected storm coverage of what should have been included in the model. The precipitation accumulation in the erroneous data is higher than that of the corrected data, so the model results are conservative. Each HYPO storm included a warm-up period to capture the snow pack that would have been lost otherwise. A recession period following the storm sequence was included to provide sufficient time to route the hydrograph peak downstream to the Gulf of Mexico. Figure E-5 shows the warm-up and recession period for HYPO 63.

Figure E-1. HYPO 63 – 12–16 April 1927 (a) (top left) storm coverage over the Mississippi River Basin; (b) (bottom left) isohyetal for unadjusted April 1927 storm; (c) (top right) comparison of mass rainfall curves for original point precipitation data versus the processed/interpolated precipitation data for the unadjusted storm; and (d) (bottom right) comparison of 1955 precipitation, 2016 precipitation, and 2016 post-processed precipitation at select location.



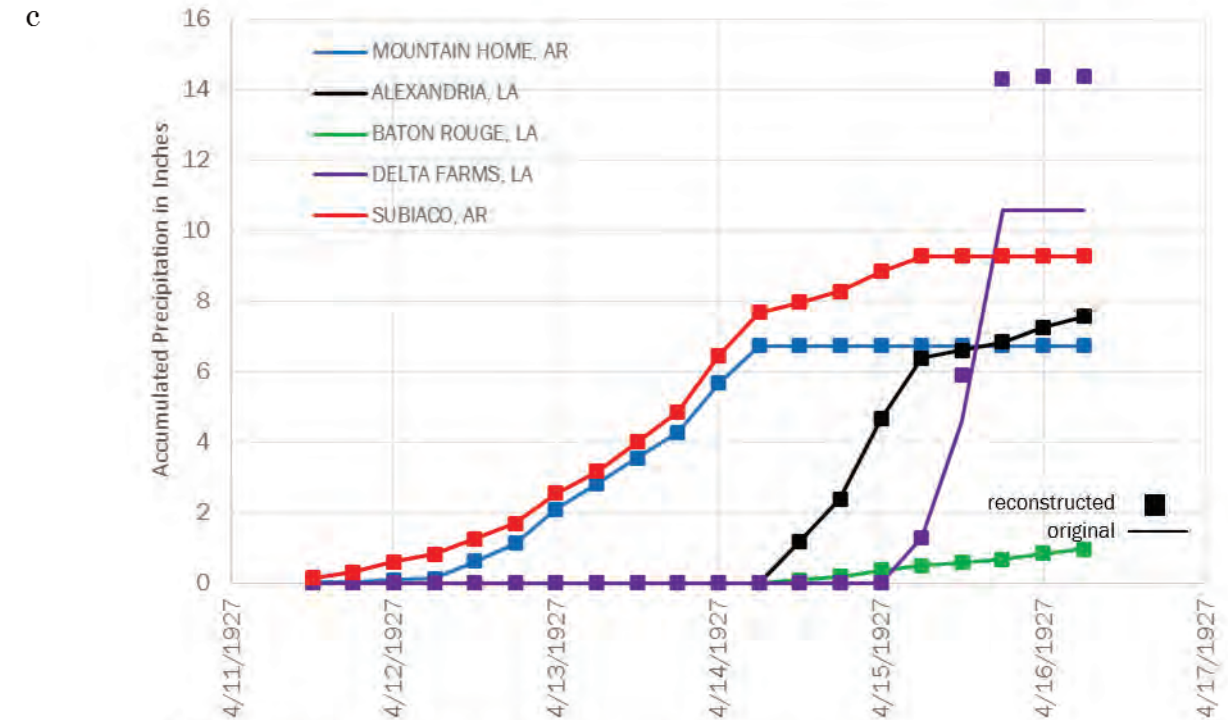
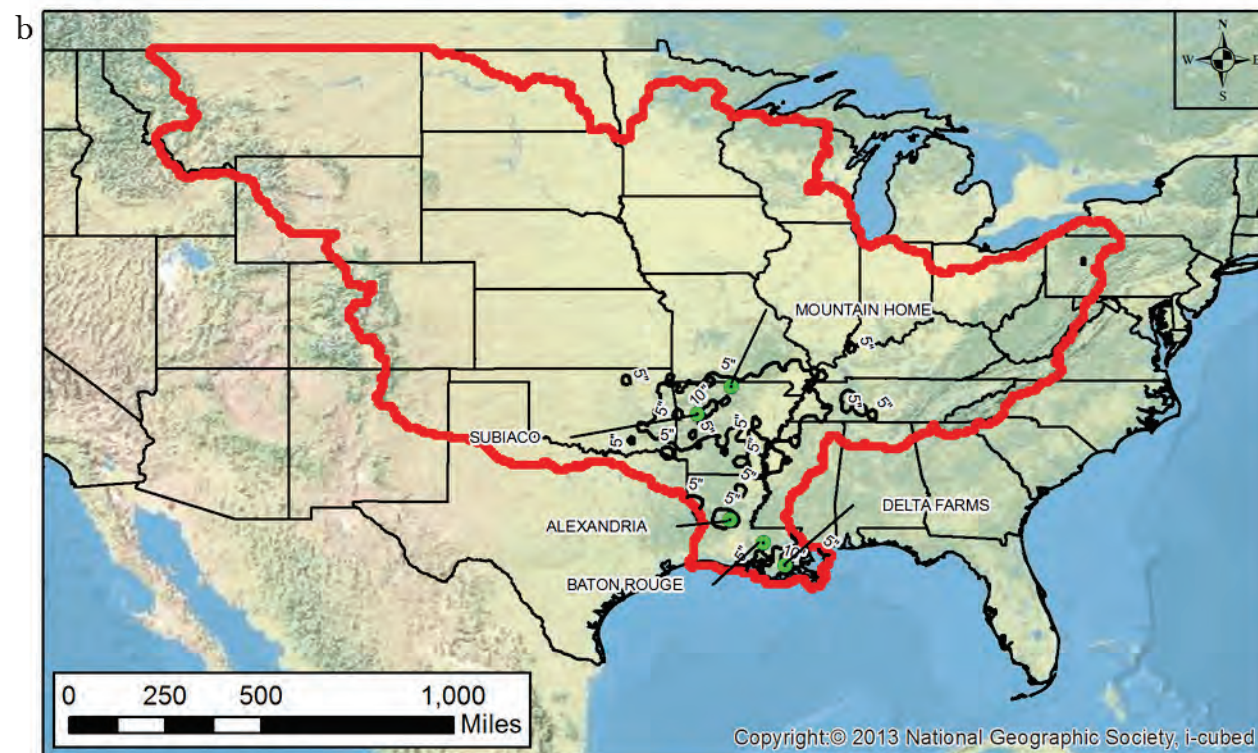
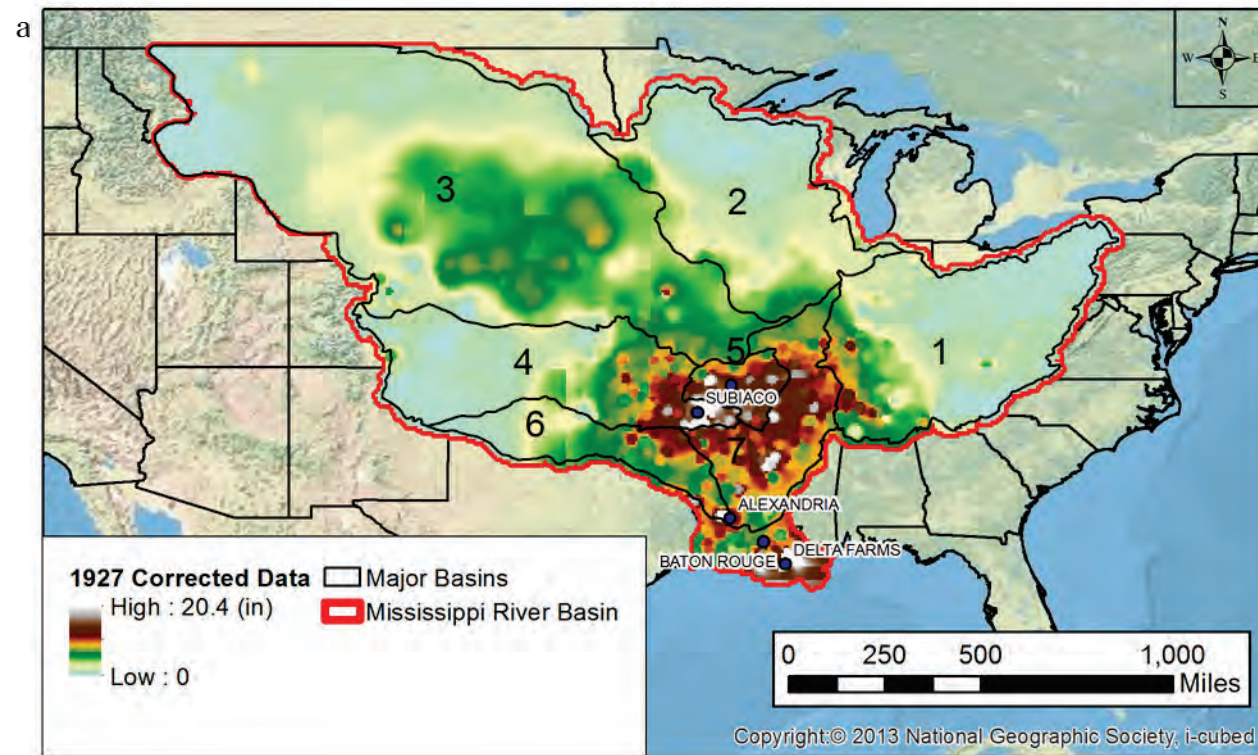
Notes:
Reconstructed cumulative precipitation data is represented by square symbols.
Original cumulative precipitation data is represented by a solid line.

d

Location	12-16 April 1927 Precipitation		
	1955 ¹	2016	2016 Reconstructed
Mountain Home, AR	8.88	6.70	6.70
Alexandria, LA	6.00	7.60	7.60
Baton Rouge, LA	4.47	5.32	5.32
Delta Farms, LA	10.00	11.27	11.27
Subiaco, AR	5.00	8.76	8.76

Notes:
1 = Derived by digitizing the 1955 isohyet map and interpolating to obtain values.

Figure E-2. Corrected 12–16 April 1927 (a) (top left) storm coverage over the Mississippi River Basin; (b) (bottom left) isohyetal for unadjusted April 1927 storm; (c) (top right) comparison of mass rainfall curves for original point precipitation data versus the processed/interpolated precipitation data for the unadjusted storm; and (d) (bottom right) comparison of 1955 precipitation, 2016 precipitation, and 2016 post-processed precipitation at select location.



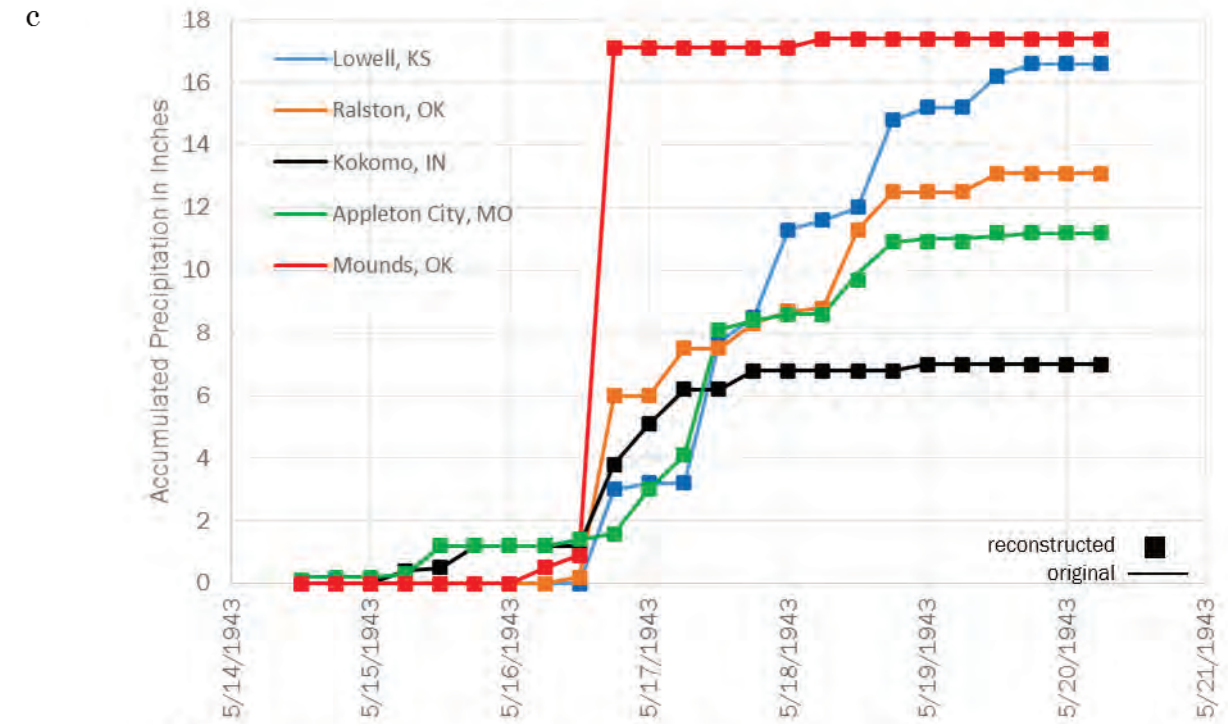
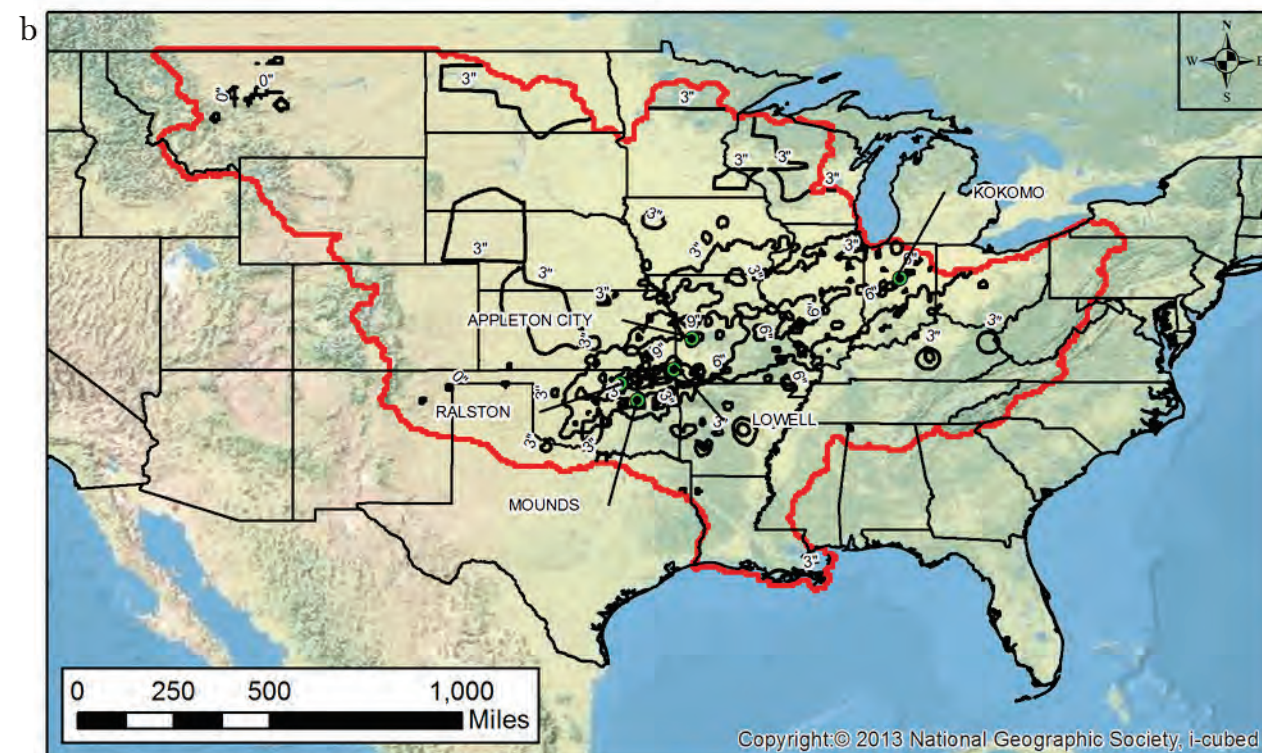
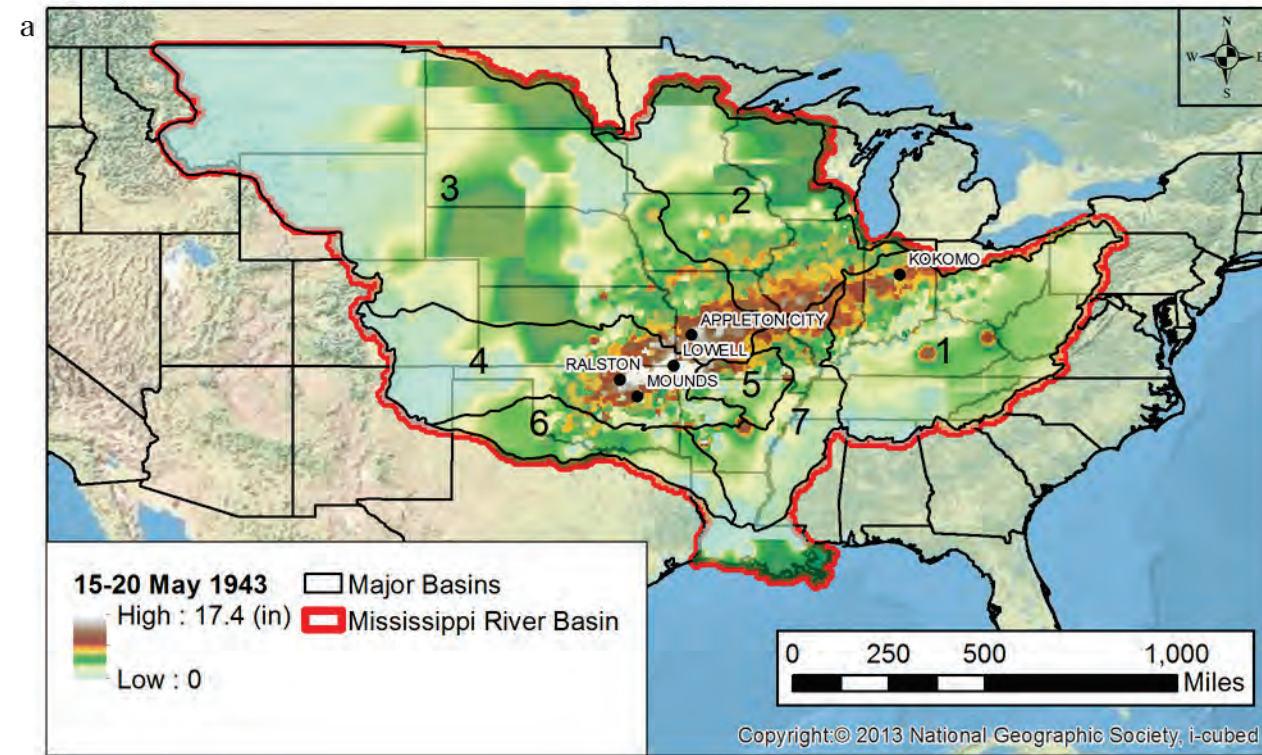
Notes:
Reconstructed cumulative precipitation data is represented by square symbols.
Original cumulative precipitation data is represented by a solid line.

d

Location	12-16 April 1927 Precipitation		
	1955 ¹	2016	2016 Reconstructed
Mountain Home, AR	8.88	6.73	6.73
Alexandria, LA	6.00	7.58	7.58
Baton Rouge, LA	4.47	0.97	0.97
Delta Farms, LA	10.00	10.60	14.40
Subiaco, AR	5.00	9.28	9.28

Notes:
1 = Derived by digitizing the 1955 isohyet map and interpolating to obtain value

Figure E-3. HYPO 63 – 15–20 May 1943 (a) (top left) storm coverage over the Mississippi River Basin; (b) (bottom left) isohyetal for storm; (c) (top right) comparison of mass rainfall curves for original point precipitation data versus the processed/ interpolated precipitation data; and (d) (bottom right) comparison of 1955 precipitation, 2016 precipitation, and 2016 processed precipitation.

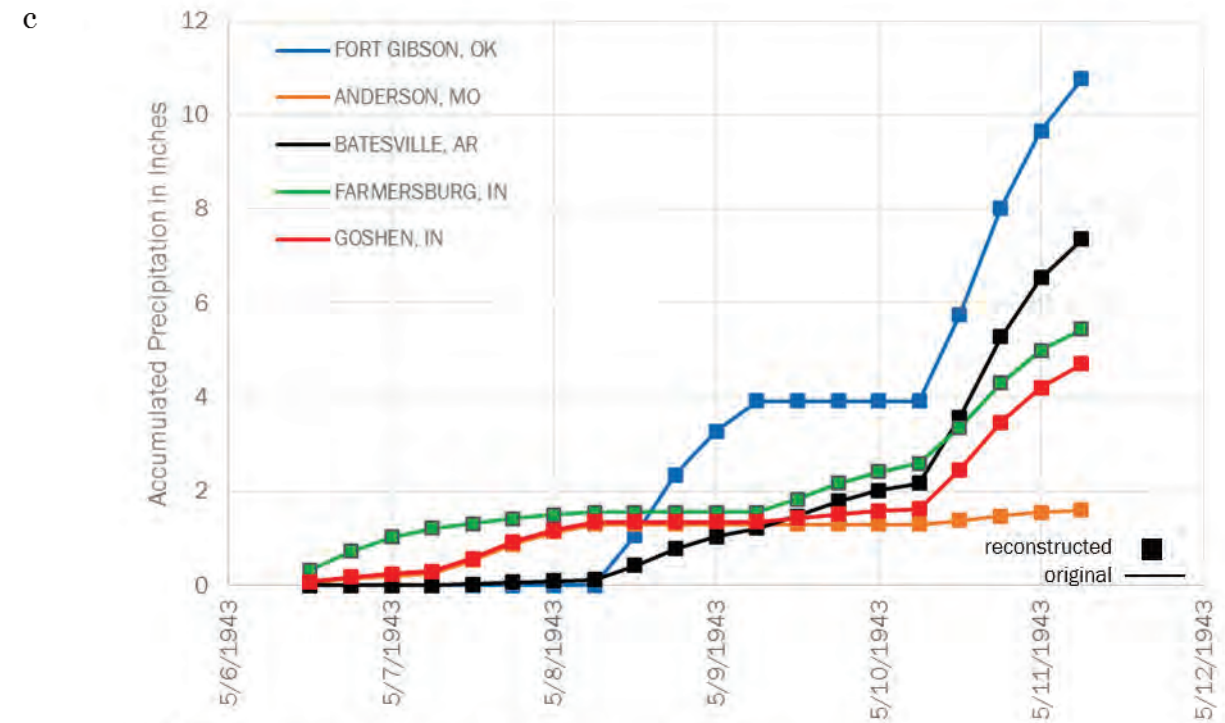
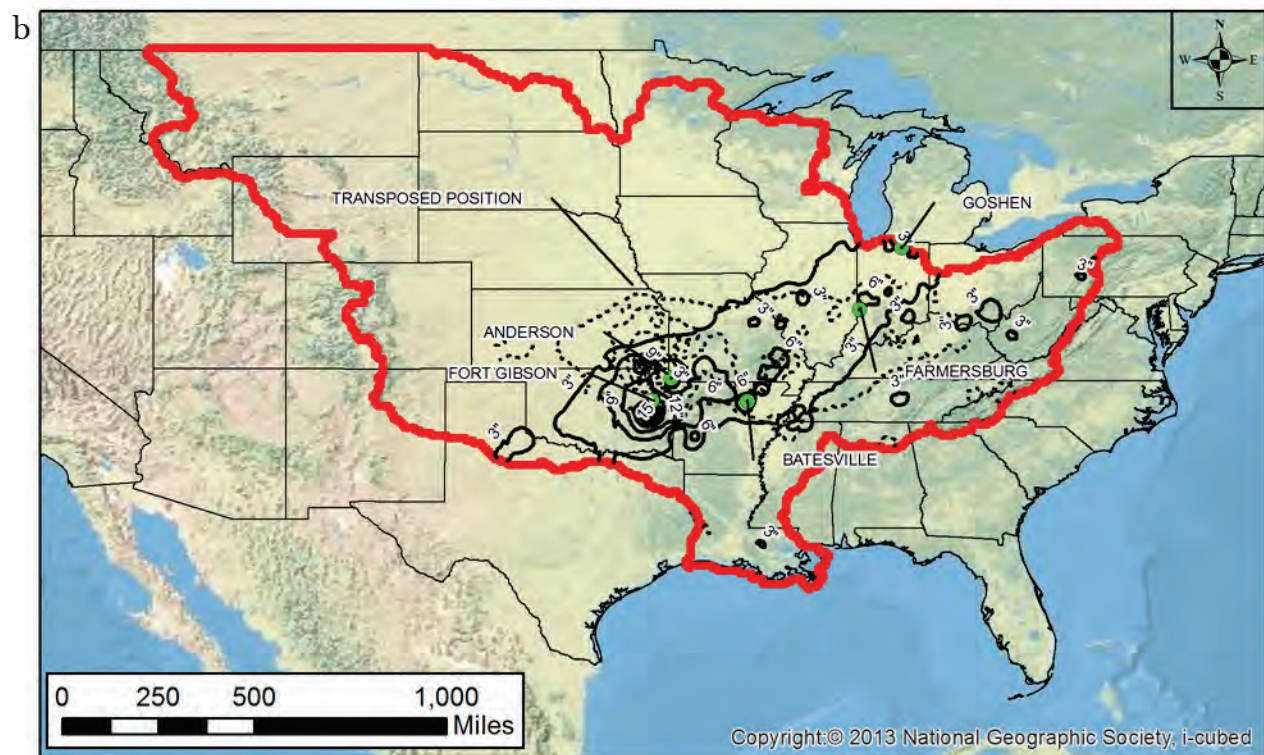
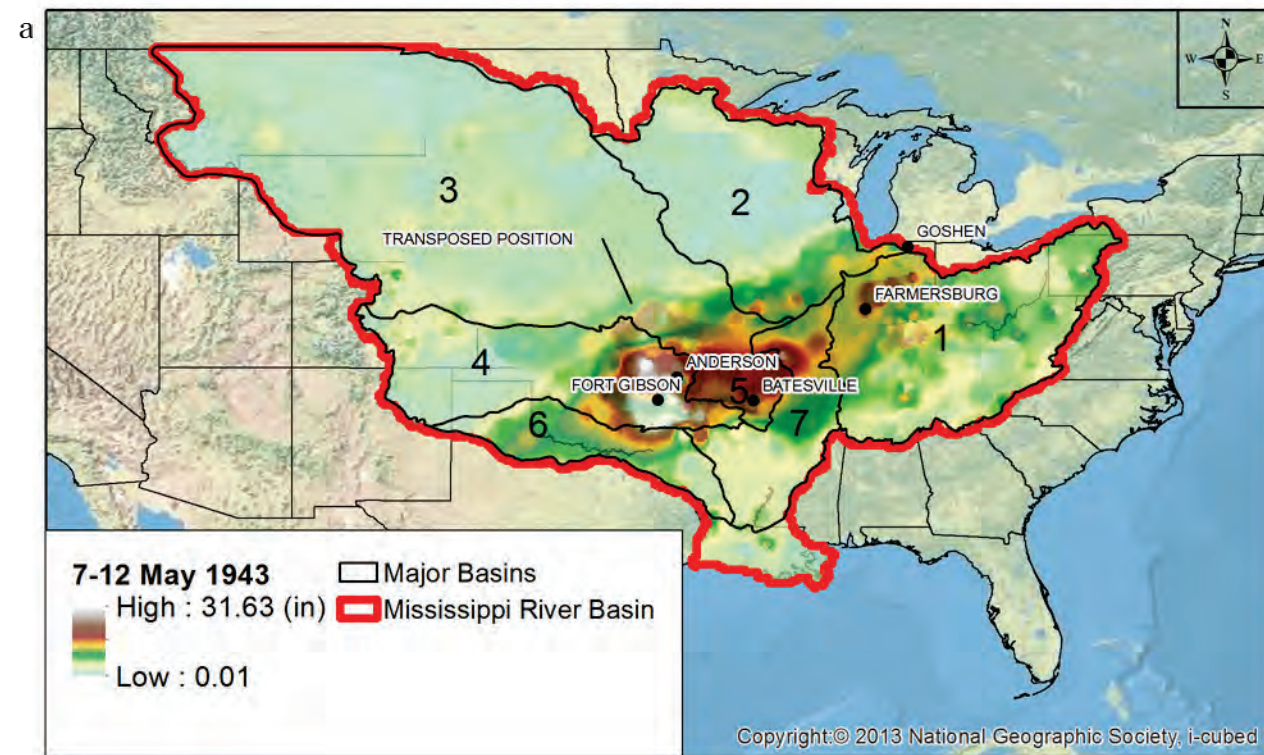


Notes:
 Reconstructed cumulative precipitation data is represented by square symbols.
 Original cumulative precipitation data is represented by a solid line.

d

Location	15-20 May 1943 SW2-21 Precipitation		
	1955	2016	2016 Reconstructed
Lowell, KS	16.5	16.6	16.6
Ralston, OK	13.1	13.1	13.1
Kokomo, IN	7.5	7.0	7.0
Appleton City, MO	11.2	11.2	11.2
Mounds, OK	17+	17.4	17.4

Figure E-4. HYPO 63 – 7–12 May 1943 (a) (top left) storm coverage over the Mississippi River Basin; (b) (bottom left) isohyetal for storm; (c) (top right) comparison of mass rainfall curves for original point precipitation data versus the processed/ interpolated precipitation data; and (d) (bottom right) comparison of 1955 precipitation, 2016 precipitation, and 2016 processed precipitation.



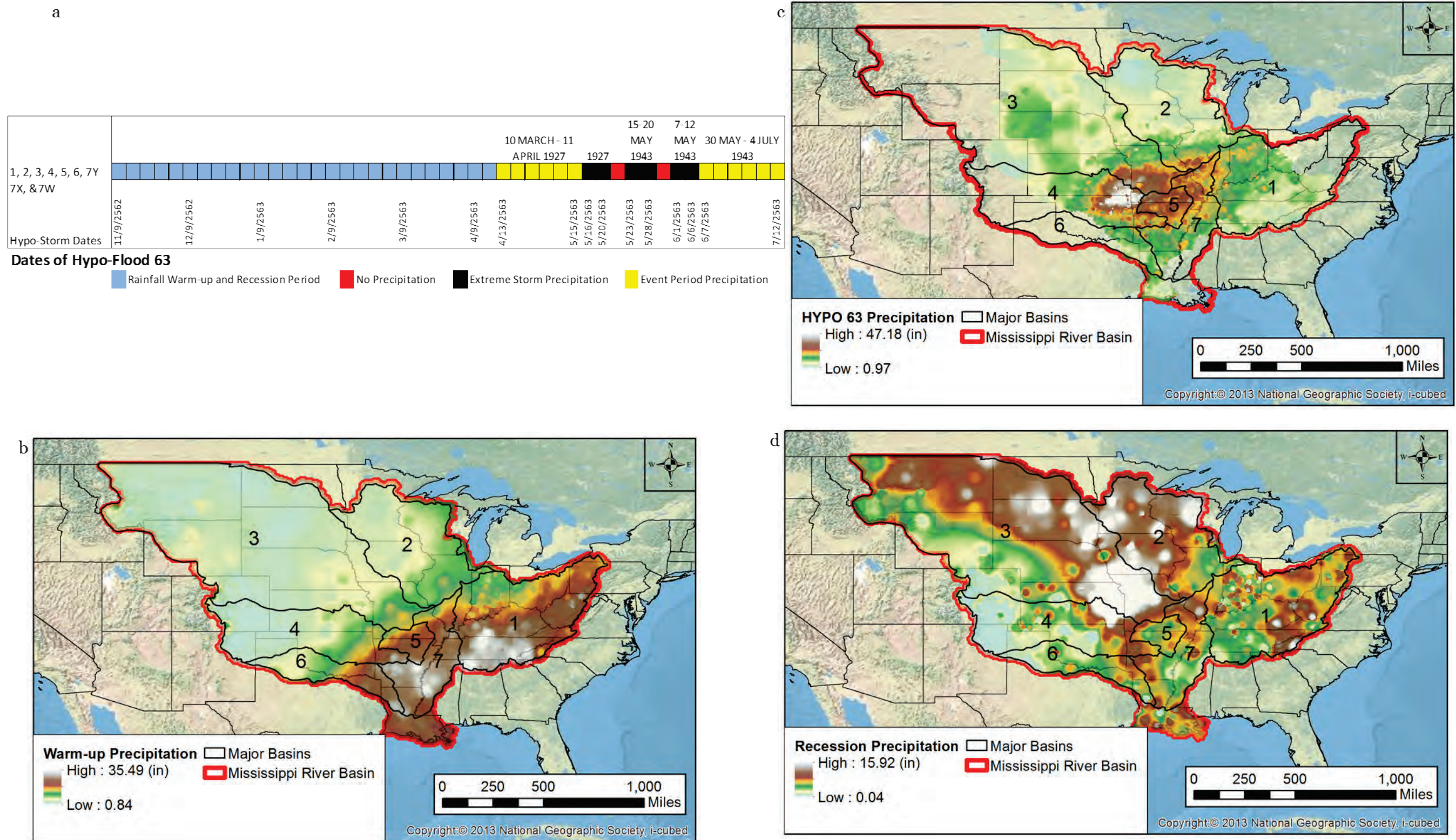
Notes:
 Reconstructed cumulative precipitation data is represented by square symbols.
 Original cumulative precipitation data is represented by a solid line.

d

Location	7-12 May 1943 SW2-20 Precipitation ²			
	1955 ¹	2016	2016 Reconstructed	2016 Reconstructed and Transposed
Fort Gibson, OK	13.00	11.27	11.27	11.27
Anderson, MO	9.87	1.6	1.60	1.60
Batesville, AR	7.02	7.36	7.36	7.36
Farmersburg, IN	5.00	5.45	5.45	5.45
Goshen, IN	3.81	4.75	4.75	NA

Notes:
 1 = Derived by digitizing the 1955 isohyet map of the 7-11 May 1943 storm and interpolating to obtain values.
 2 = Values are compared against the original precipitation values, not the 20% reduction.

Figure E-5. HYPO 63 (a) (top left) storm sequencing with warm-up and recession periods; (b) (bottom left) warm-up precipitation coverage over the Mississippi River Basin; (c) (top right) 1943 AND 1927 combined storm coverage over the Mississippi River Basin; and (d) (bottom right) recession precipitation coverage over the Mississippi River Basin.



The 7–12 May 1943 storm did not have the gage data available to make a direct comparison with the gage locations used in the 1955 report, so the isohyetal map from the MRC (1955) report was digitized to obtain the values at select locations. The deviation between the 1955 data and the 2016 data ranges from 0.34 in. to 8.27 in. After the data were processed and converted to an ASCII grid, all of the locations matched. The 15–20 May 1943 storm had the gage data needed to make a direct comparison with the gage locations used in the 1955 report. At Kokomo, IN, the deviation between the 1955 event and the reconstructed storm event was 0.5 in. All other locations matched. After the data were converted to an ASCII grid, the values at each location matched with the reconstructed data.

The April 1927 storm did not have the gage data available to make a direct comparison with the gage locations used in the MRC (1955) report, so the isohyetal map in the 1955 report was digitized to obtain the values at select locations. For Figure E-1, the deviation between the 1955 data and the 2016 data ranges from 0.85 in. to 3.76 in. For Figure E-2, the deviation between the 1955 data and the 2016 data ranges from 0.6 in. to 4.28 in. When the April 1927 data were compiled from the archives, several data gaps were discovered. This led to the generation of several versions of the data, and ultimately Figure E-2 is the correct storm event, but Figure E-1 was the storm event included in the 2016 hydrology model. The 2016 precipitation values are higher than the digitized 1955 storm event, which produced conservative runoff values from the model. After the 2016 data were processed, the new grids retained the original gage value, except for the Delta Farms, LA, location from Figure E-2.

E.1.1 Depth area relationships

To further validate the precipitation inputs developed by interpolation, depth-area relationships were generated using ArcGIS. Isohyetal maps for each original storm event were georeferenced, digitized in ArcMap, converted from a polyline to a TIN, converted from a TIN to a raster, and projected with USA Contiguous Albers Equal Area Conic to obtain an equal area grid size of 2,000 m × 2,000 m. For the total original HYPO storm comparisons, the projected rasters were then aggregated with the mosaic tool. The interpolated rainfall grids were clipped to the spatial extent of each original HYPO storm or to the original individual storm events. With equal area grids, a zonal histogram was generated that compares a defined precipitation interval against area. These zonal histograms were exported to Excel to plot against each other.

Figure E-6 through Figure E-14 show the depth-area curves for the entire storm total precipitation over the Mississippi River Basin, as well as the totals falling over each of the seven major sub-basins.

Figure E-6. Depth-area curves for 1955 and 2016 individual storms comprising HYPO 63.

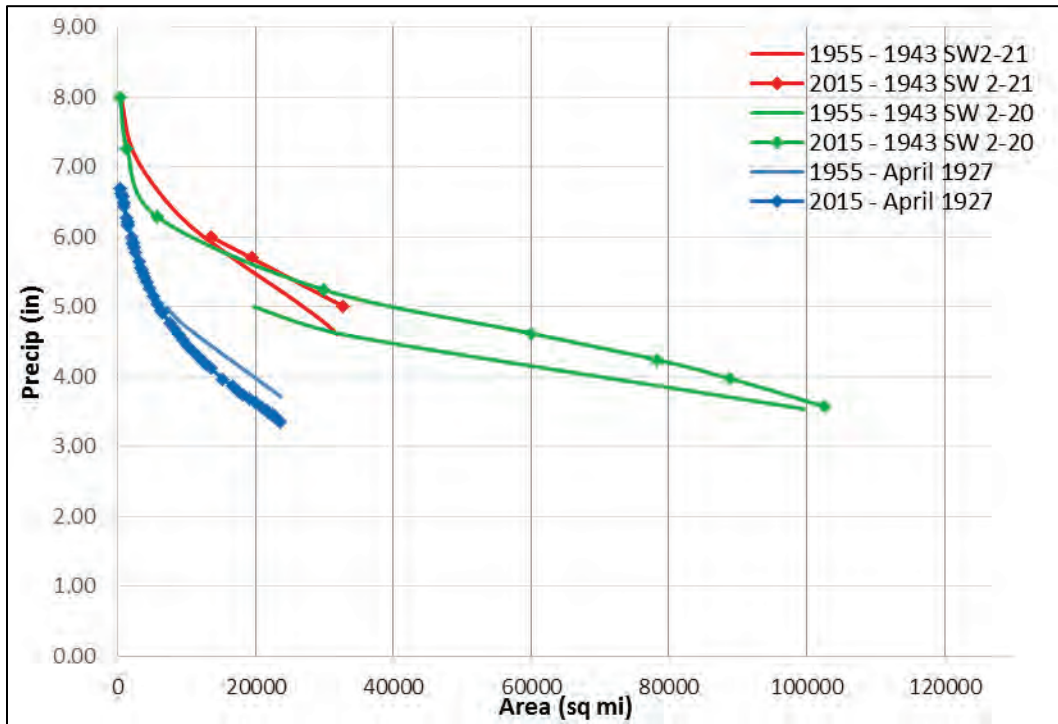


Figure E-7. Depth-area curves for 1955 and 2016 total HYPO 63 event.

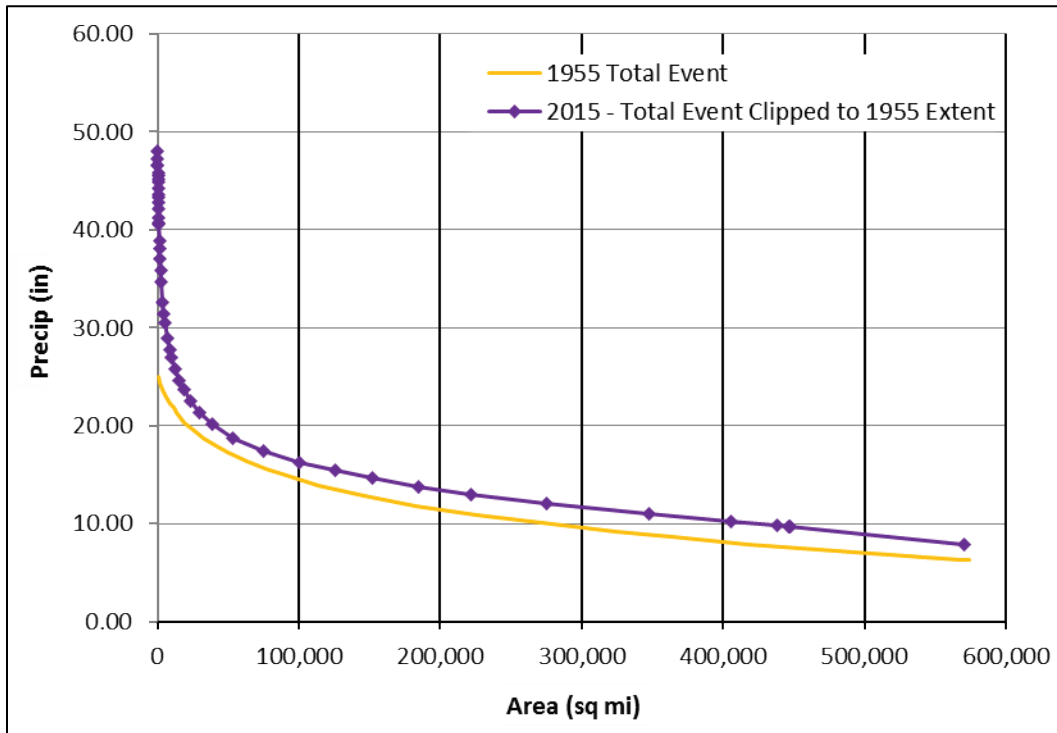


Figure E-8. Depth-area curve for 1955 and 2015 individual storm events comprising HYPO 63 over Drainage Basin 1.

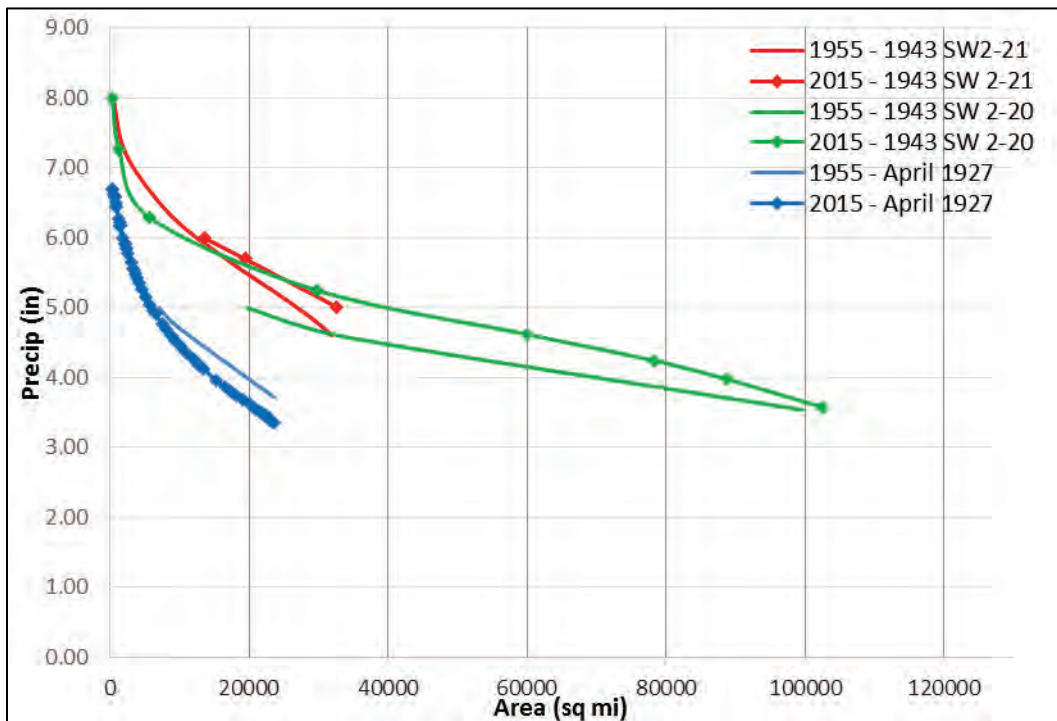


Figure E-9. Depth-area curve for 1955 and 2015 individual storm events comprising HYP0 63 over Drainage Basin 2.

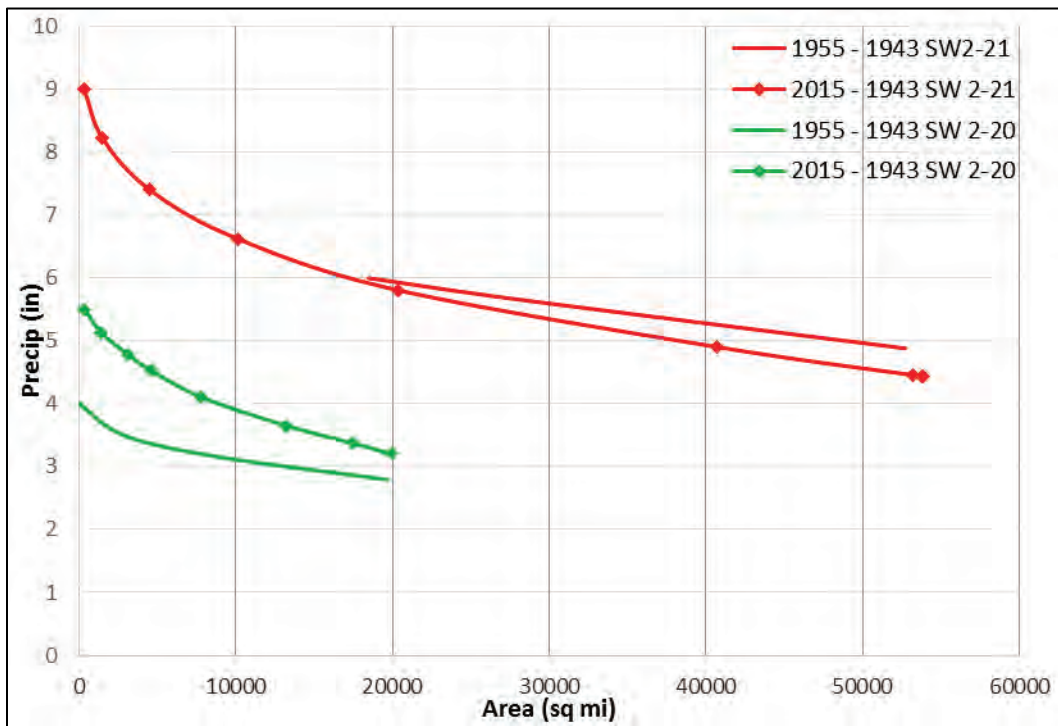


Figure E-10. Depth-area curve for 1955 and 2015 individual storm events comprising HYP0 63 over Drainage Basin 3.

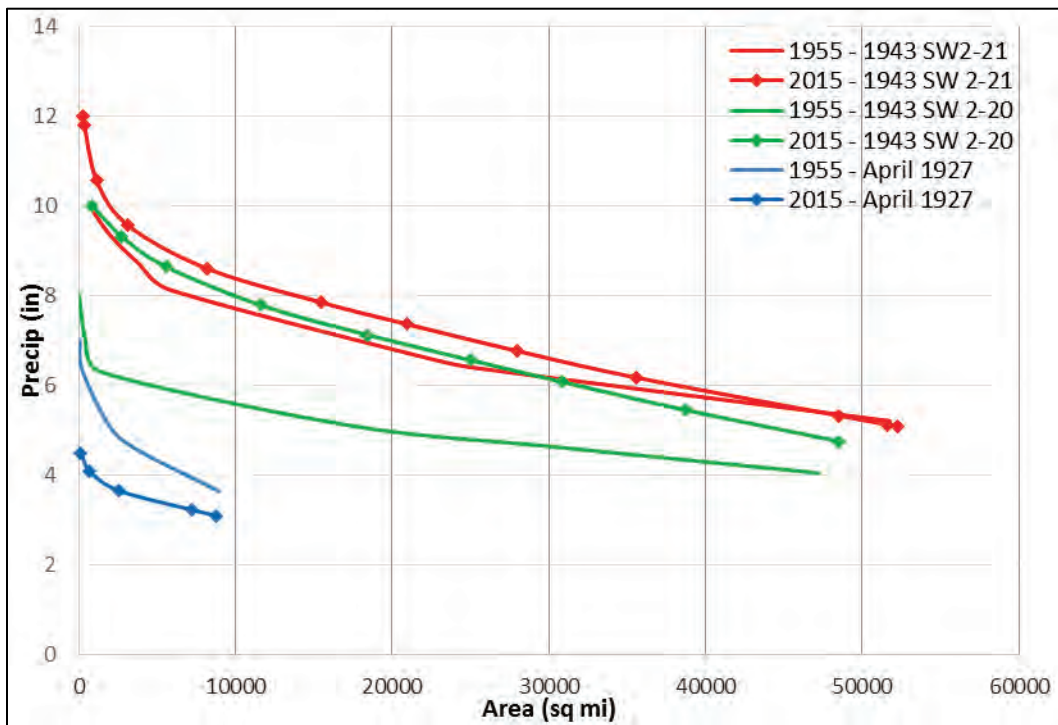


Figure E-11. Depth-area curve for 1955 and 2015 individual storm events comprising HYP0 63 over Drainage Basin 4.

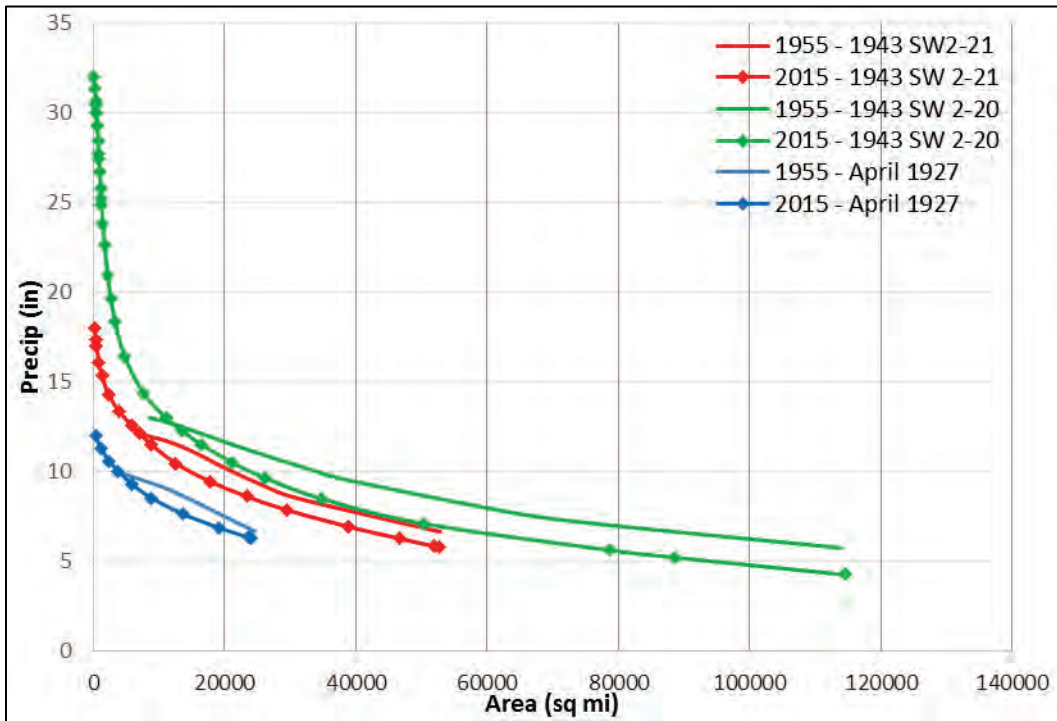


Figure E-12. Depth-area curve for 1955 and 2015 individual storm events comprising HYP0 63 over Drainage Basin 5.

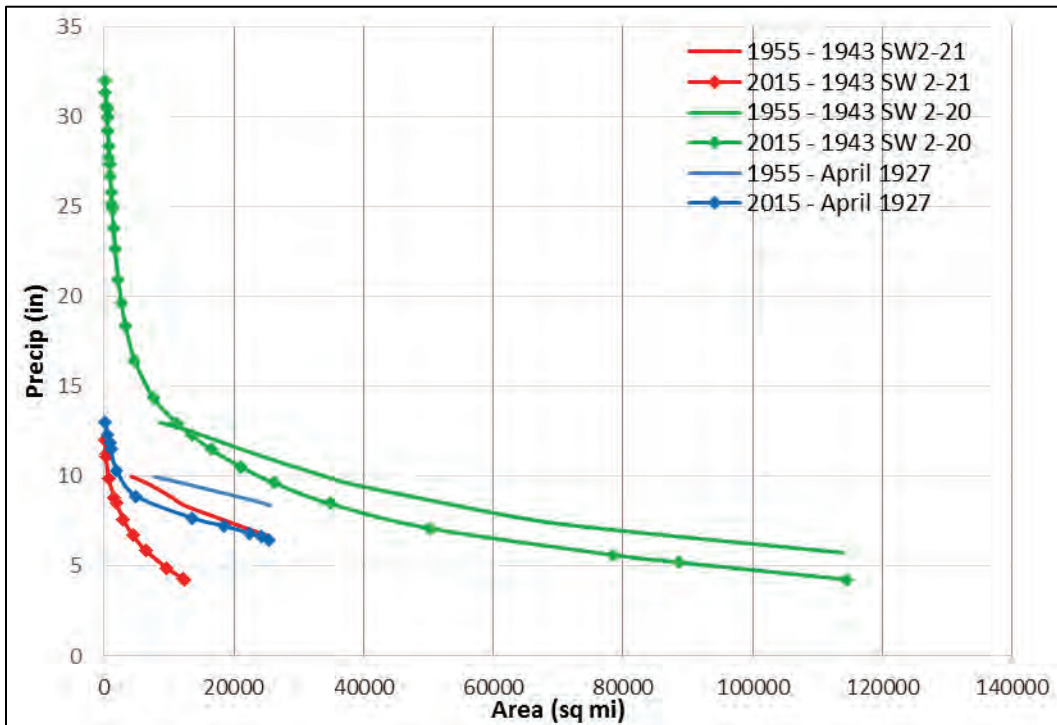


Figure E-13. Depth-area curve for 1955 and 2015 individual storm events comprising HYPO 63 over Drainage Basin 6.

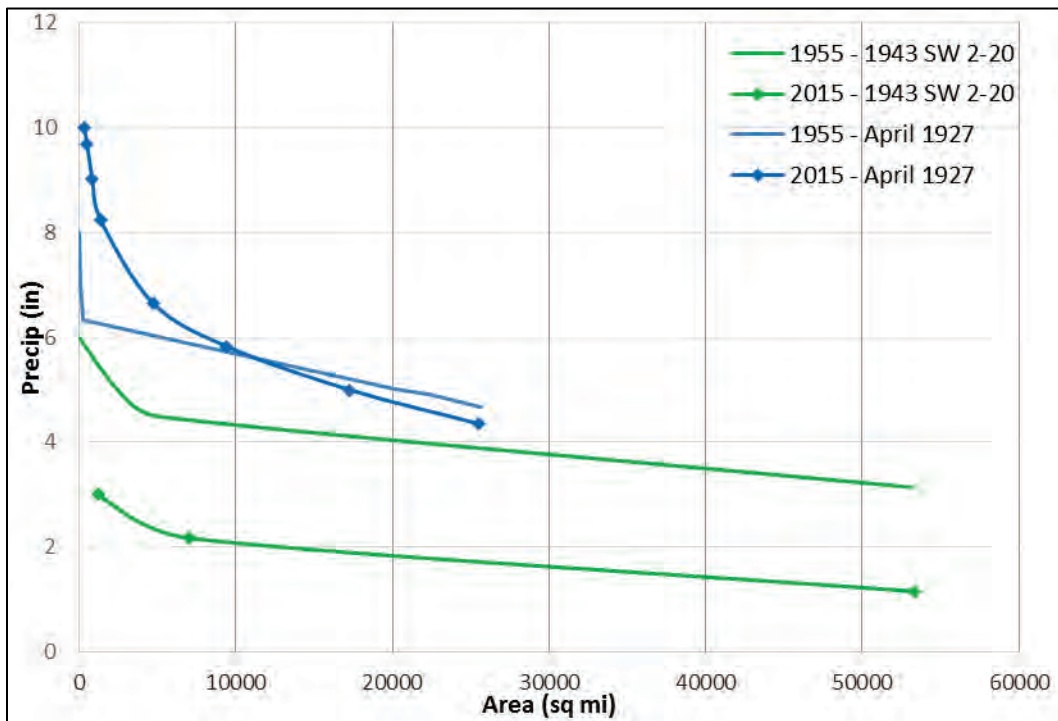
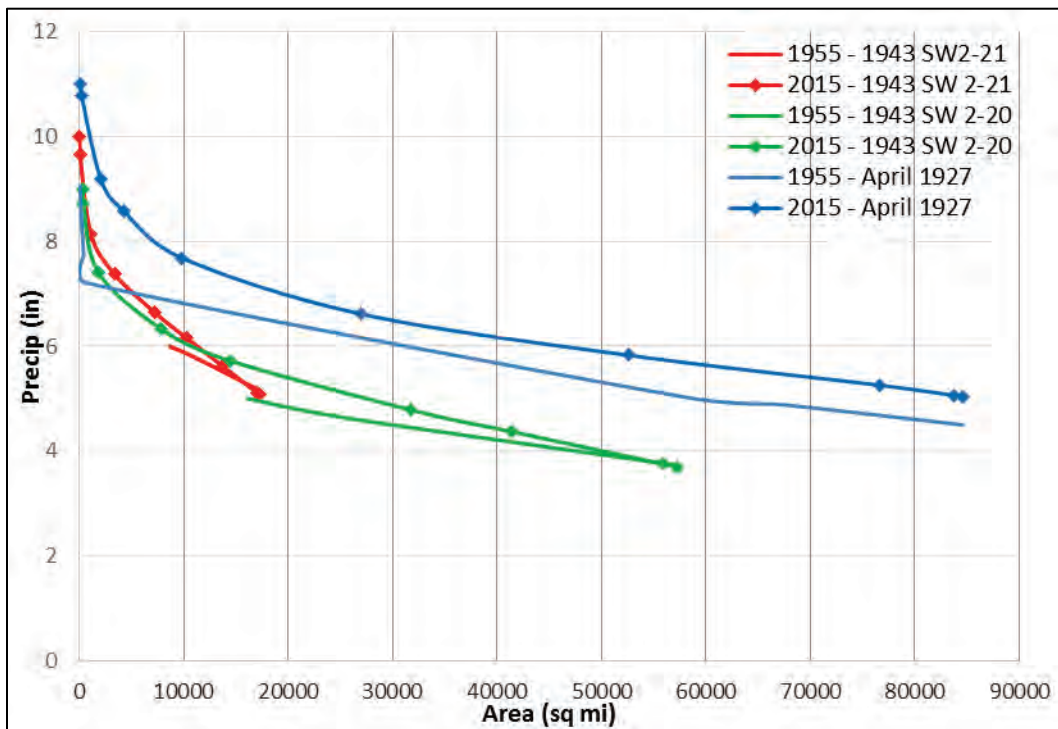


Figure E-14. Depth-area curve for 1955 and 2015 individual storm events comprising HYPO 63 over Drainage Basin 7.



Overall, the depth-area curves for 2016 precipitation inputs matched the previous 1955 rainfall maps. There were variations across each of the seven major sub-basins where 2016 depth-area curves were higher or lower than 1955 depth-area curves, but these deviations were compensated over the entire storm basin for each individual storm event and for the HYPO 63 storm event.

E.1.2 Hydrograph comparisons

Table E-1 provides a comparison of 1-day (labeled as peak), 3-day, 15-day, and 30-day volumes for HYPO 56 hydrographs. Values for the 1955 hydrographs are labeled 56 and 56-EN for unregulated and regulated flows, respectively. Values computed for the 2016 hydrographs are labeled 56-U and 56-R for unregulated and regulated flows, respectively. There appears to be good agreement between peak 1-day values for unregulated values; for instance Cairo, IL, values are 2,558 kcfs for 1955 and 2,568 kcfs for 2016. Regulated values at Cairo, IL, are 2,078 kcfs for 1955 and 2,365 kcfs for 2016, which has a greater difference with 2016 results being higher. This greater difference is consistent with observations for the HYPO 58A results. The larger difference for regulated numbers reflects the difference in how reservoir operations were included in the 1955 and 2016 investigations. The 3-day, 15-day, and 30-day volumes are also comparable for Cairo, Arkansas City, and Latitude of Red River Landing.

Table E-1. Hydrograph volume and shape comparisons for HYPO 63.

Mississippi River HYPO Flood Flows are in 1,000 cfs and sfd															
	Storm	Peak Flow	Peak Flow Date	3 Days				15 Days				30 Days			
				Start	End	Volume	Mean	Start	End	Volume	Mean	Start	End	Volume	Mean
St. Louis	63-R	1,142	4-Jun	3-Jun	5-Jun	3,416	1,139	27-May	10-Jun	16,464	1,098	24-May	22-Jun	28,629	954
	63-EN	1,078	11-May	10-May	12-May	3,147	1,049	2-May	16-May	11,023	735	19-Apr	18-May	18,045	602
	63-U	1,362	7-Jun	5-Jun	7-Jun	4,078	1,359	31-May	14-Jun	19,481	1,299	27-May	25-Jun	35,701	1,190
	63	1,298	11-May	10-May	12-May	3,818	1,273	2-May	16-May	14,297	953	19-Apr	18-May	23,218	774
Cairo	63-R	2,208	1-Jun	6-Jun	8-Jun	6,408	2,136	30-May	13-Jun	30,742	2,049	22-May	20-Jun	52,547	1,752
	63-EN	2,078	11-May	10-May	12-May	6,153	2,051	2-May	16-May	24,206	1,614	19-Apr	18-May	42,979	1,433
	63-U	2,387	8-Jun	7-Jun	9-Jun	7,087	2,362	31-May	14-Jun	32,659	2,177	25-May	23-Jun	56,986	1,900
	63	2,388	11-May	10-May	12-May	7,078	2,359	2-May	16-May	30,170	2,011	19-Apr	18-May	51,782	1,726
Arkansas City	63-R	2,777	18-Jun	16-Jun	18-Jun	8,319	2,773	9-Jun	23-Jun	39,209	2,614	1-Jun	30-Jun	68,992	2,300
	63-EN	2,455	23-May	22-May	24-May	7,345	2,448	13-May	27-May	35,210	2,347	4-May	2-Jun	65,165	2,172
	63-U	3,115	17-Jun	15-Jun	17-Jun	9,333	3,111	9-Jun	23-Jun	43,972	2,932	1-Jun	30-Jun	77,265	2,576
	63	3,010	23-May	22-May	24-May	9,010	3,003	13-May	27-May	43,710	2,914	4-May	2-Jun	80,590	2,686
Latitude of Red River Landing	63-R	2,704	22-Jun	20-Jun	22-Jun	8,106	2,702	15-Jun	29-Jun	38,994	2,600	1-Jun	30-Jun	68,541	2,285
	63-EN	2,471	2-Jun	1-Jun	3-Jun	7,410	2,470	25-May	8-Jun	36,506	2,434	14-May	12-Jun	70,280	2,343
	63-U	2,896	23-Jun	21-Jun	23-Jun	8,678	2,893	15-Jun	29-Jun	42,596	2,840	1-Jun	30-Jun	75,940	2,531
	63	3,003	2-Jun	1-Jun	3-Jun	8,932	2,977	25-May	8-Jun	43,462	2,897	14-May	12-Jun	83,045	2,768

E.2 HEC-RAS inflow boundary discharge hydrographs

The hydrologic modeling produced discharge hydrographs at the same key locations used in the 1955 Study. Plots of unregulated (U) and regulated (R) model simulations are presented in Figure E-15 through Figure E-27. Unregulated hydrographs are shown in red, and Regulated hydrographs are shown in blue.

Figure E-15. HYPO 63 hydrographs: Missouri River at Hermann, MO.

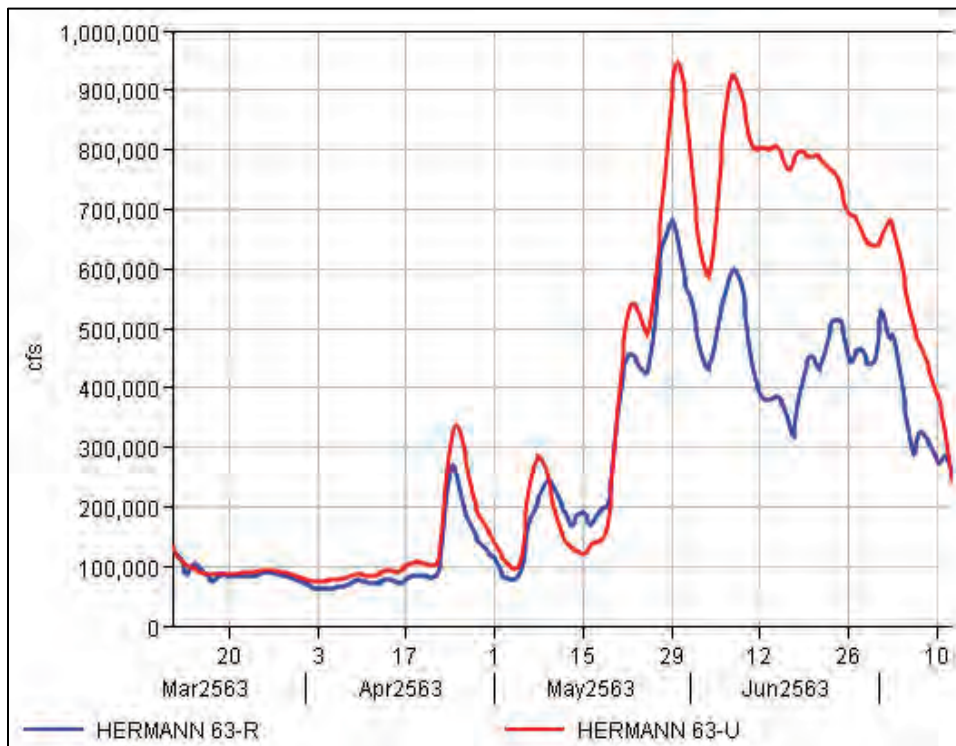


Figure E-16. HYPO 63 hydrographs: Mississippi River at Alton, IL.

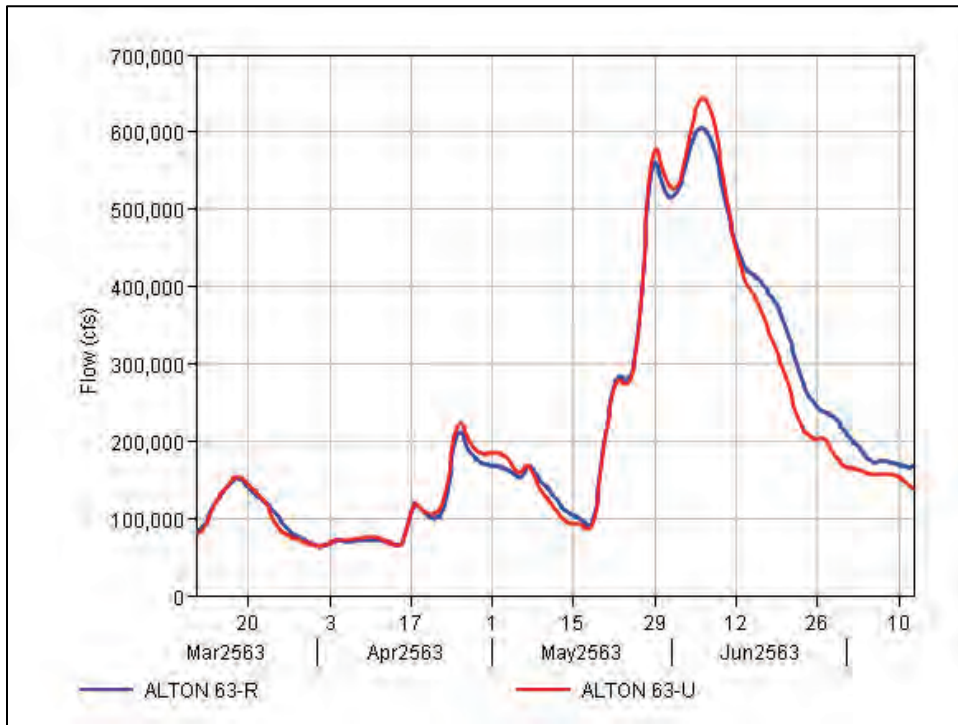


Figure E-17. HYPO 63 hydrographs: Mississippi River at St. Louis, MO.

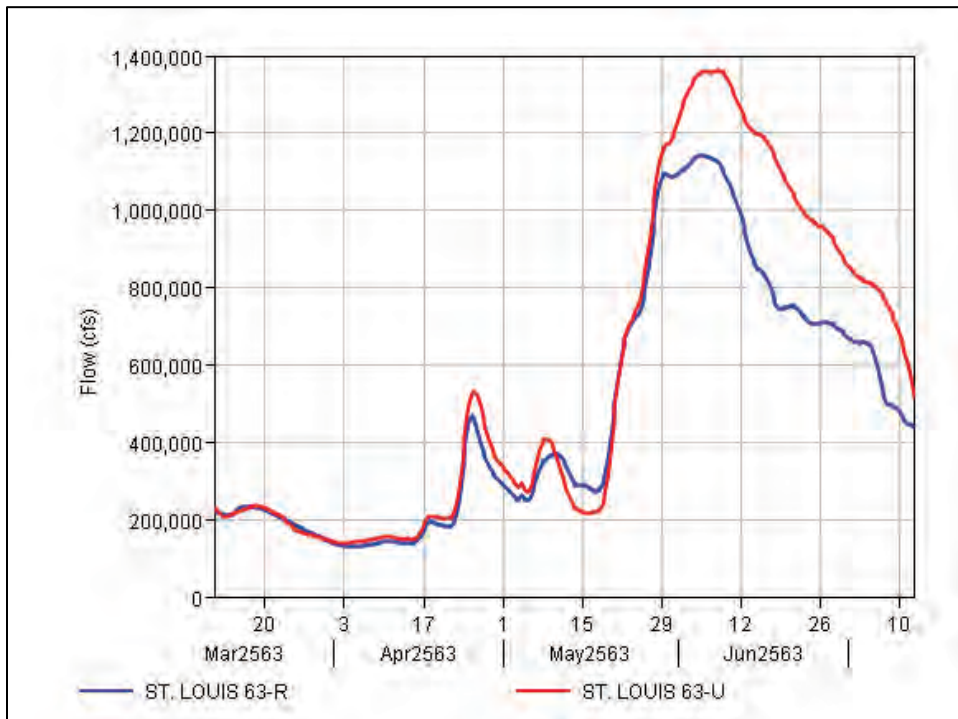


Figure E-18. HYPO 63 hydrographs: Mississippi River at Chester, IL.

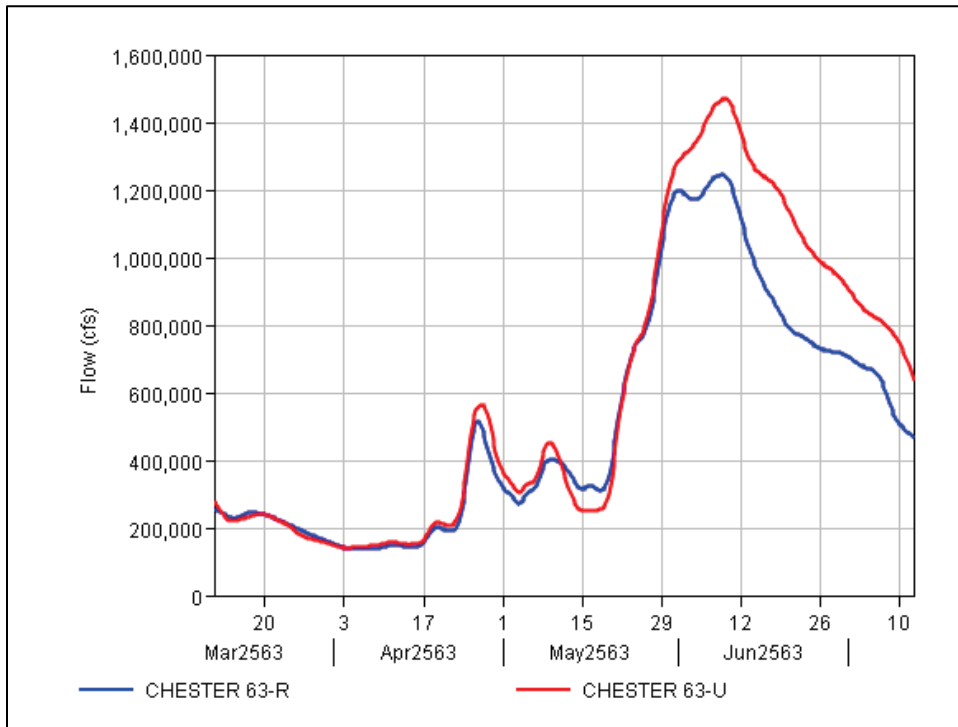


Figure E-19. HYPO 63 hydrographs: Big Muddy River at Murphysboro, IL.

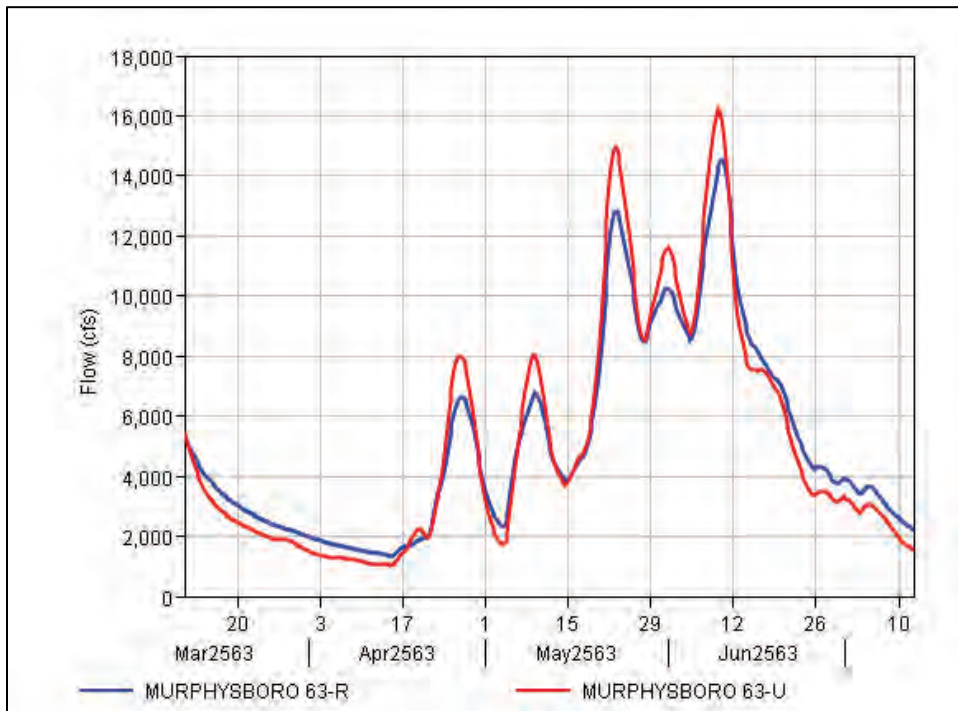


Figure E-20. HYPO 63 hydrographs: Cumberland River at Barkley Dam.

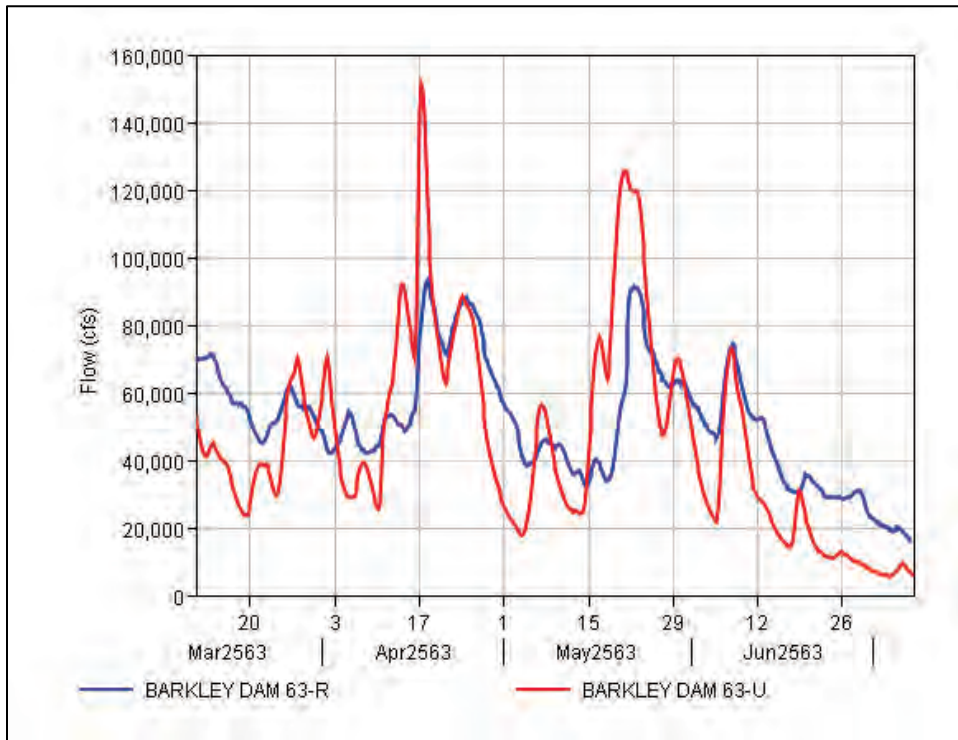


Figure E-21. HYPO 63 hydrographs: Tennessee River at Kentucky Dam.

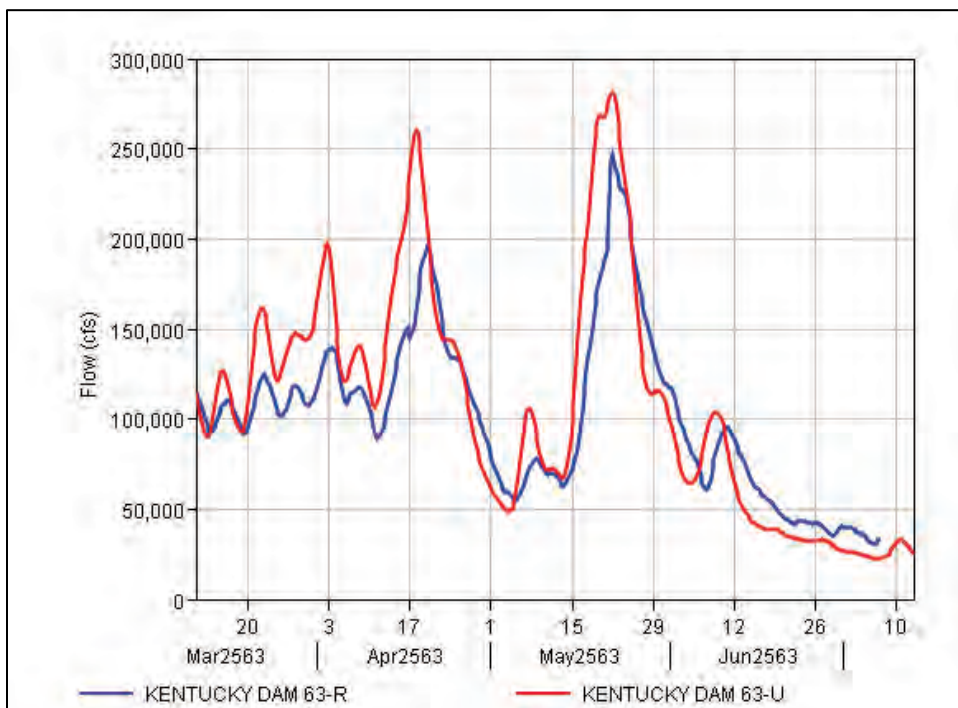


Figure E-22. HYPO 63 hydrographs: Ohio River at Smithland, IL.

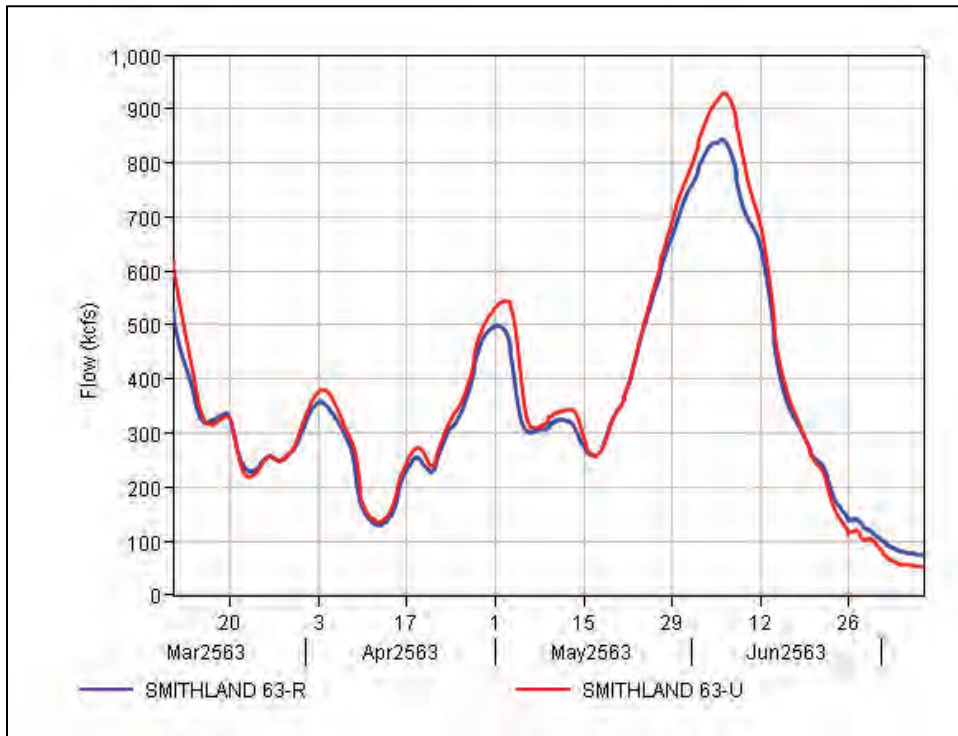


Figure E-23. HYPO 63 hydrographs: Arkansas River at Pine Bluff, AR.

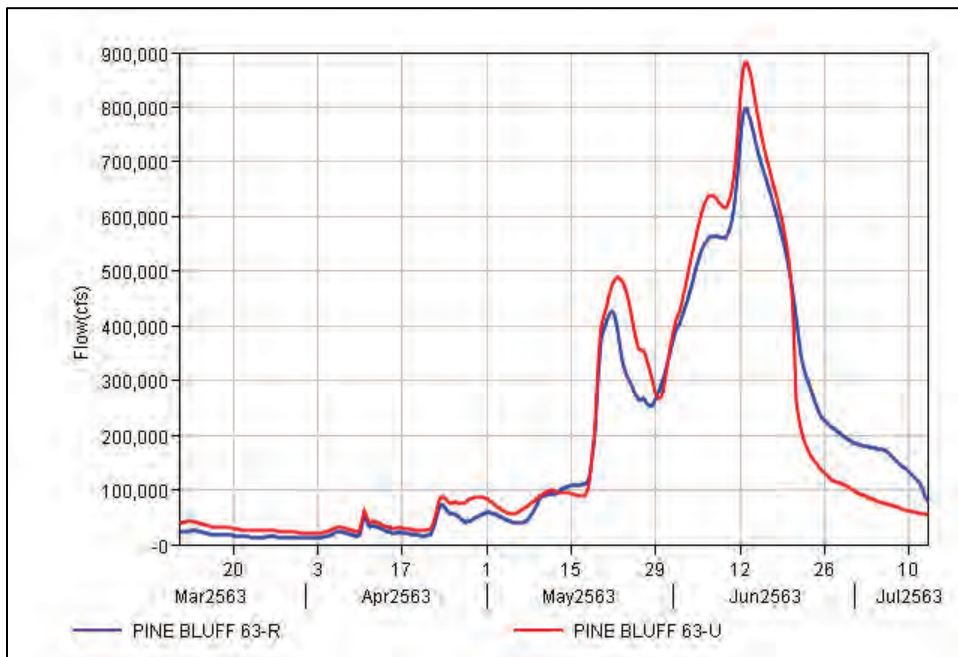


Figure E-24. HYPO 63 hydrographs: Shreveport, LA.

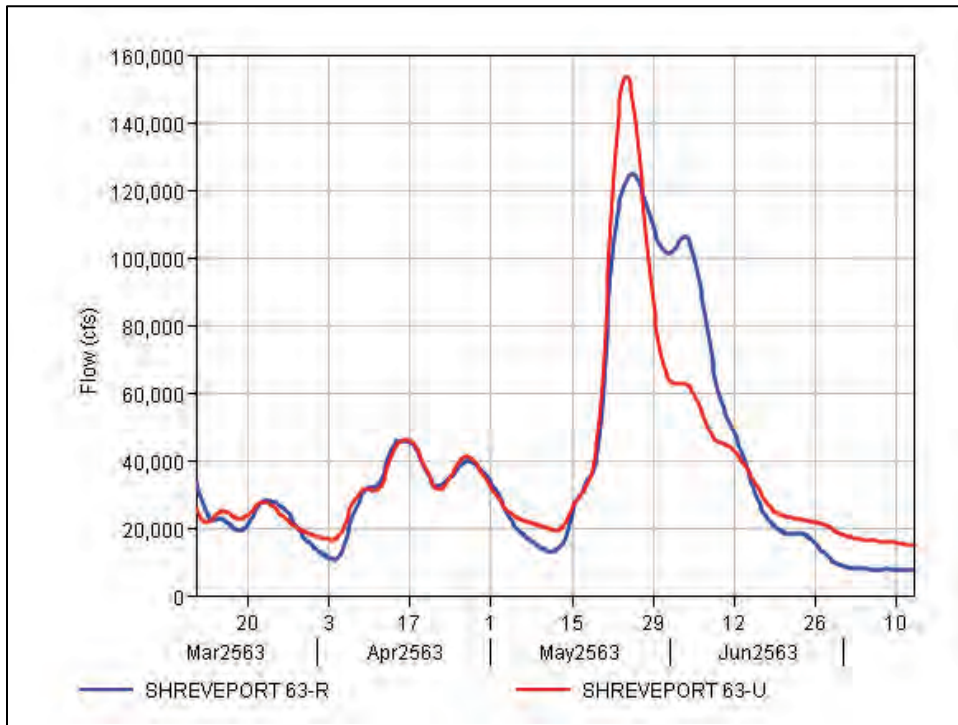


Figure E-25. HYPO 63 hydrographs: Monroe, LA.

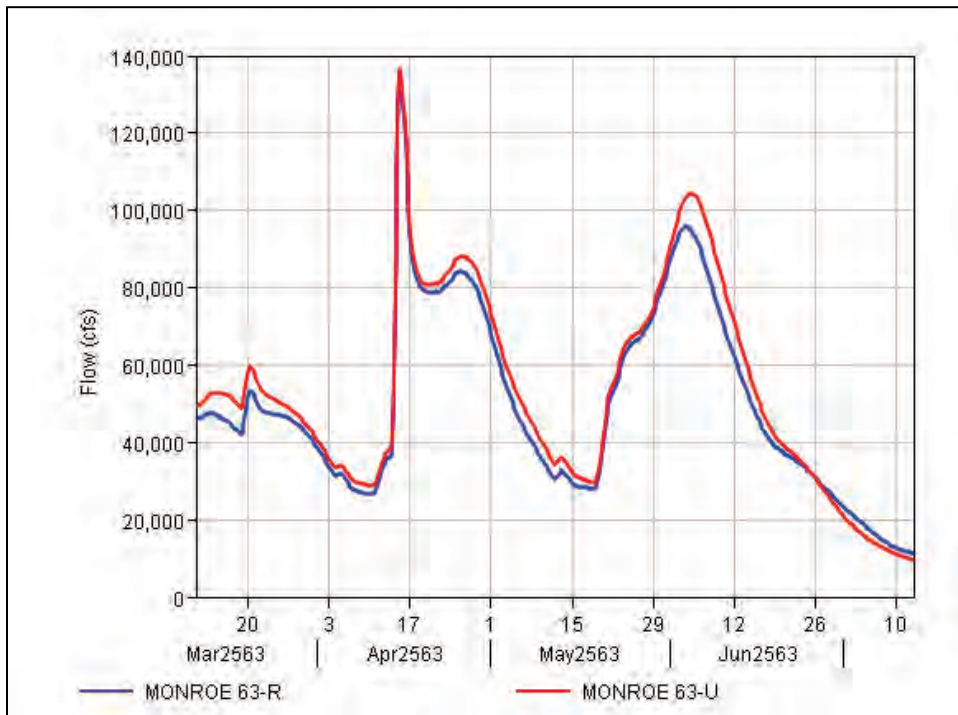


Figure E-26. HYPO 63 hydrographs: Alexandria, LA.

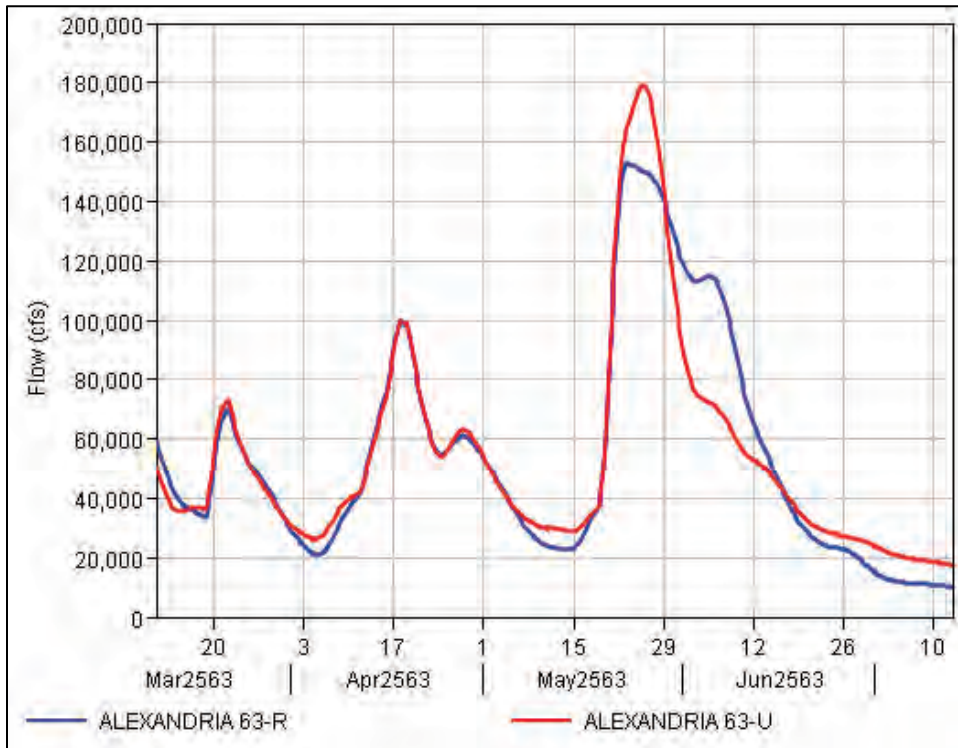
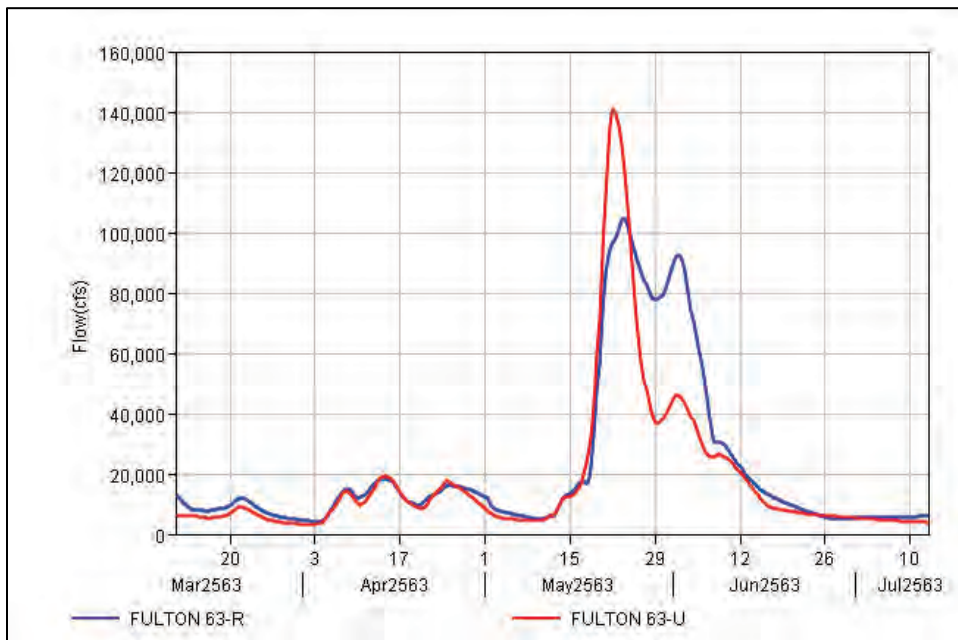


Figure E-27. HYPO 63 hydrographs: Fulton, LA.



E.3 Peak Flows for the Lower Ohio and Mississippi River

A comparison of calculated peak discharges from the 2016 HEC-RAS model with values from the MRC (1955) report is given in Table E-2. Peak flows from the 1955 report are given as historic values in the table. The two HEC-RAS model runs reflect (1) the existing, 2016 conditions for the Yazoo Backwater levee at Elevation 107.0 and (2) the authorized 1973 refined condition for the Yazoo Backwater levee at Elevation 112.8.

Table E-2. Comparison of peak flow values for HYPO 63.

Location	Project Design Flood (PDF) (from Table 7 WES [1957])					
	Unregulated Discharge (U), cfs			Regulated Discharge (Existing and Near-Term Reservoirs, EN), cfs		
	63	63-U Existing Yazoo	63-U Authorized Yazoo	63-EN	63-R Existing Yazoo	63-R Authorized Yazoo
Ohio at Cairo, IL	NA	1,078,000	1,078,000	NA	1,078,000	1,078,000
Miss/Ohio Confluence (Combined)	2,390,000	2,387,000	2,387,000	2,120,000	2,208,000	2,208,000
Hickman, KY	NA	1,884,000	1,884,000	NA	1,884,000	1,884,000
Memphis, TN	2,220,000	2,335,000	2,335,000	1,880,000	2,152,000	2,152,000
Helena, AR	2,120,000	2,307,000	2,307,000	1,780,000	2,152,000	2,152,000
Arkansas City, AR	2,900,000	3,115,000	3,114,000	2,480,000	2,777,000	2,777,000
Greenville, MS	NA	3,092,000	3,088,000	NA	2,772,000	2,771,000
Lake Providence, MS	NA	3,088,000	3,082,000	NA	2,768,000	2,765,000
Vicksburg, MS	2,690,000	2,816,000	2,969,000	2,310,000	2,642,000	2,702,000
Natchez, MS	2,680,000	2,810,000	2,952,000	2,300,000	2,628,000	2,685,000
Red River Landing, LA	2,040,000	2,183,000	2,313,000	1,830,000	2,005,000	2,060,000
Baton Rouge, LA	NA	1,574,000	1,693,000	NA	1,503,000	1,503,000
Donaldsonville, LA	NA	1,573,000	1,692,000	NA	1,503,000	1,503,000
Carrollton, LA	NA	1,318,000	1,436,000	NA	1,252,000	1,252,000
Empire, LA	NA	1,264,000	1,373,000	NA	1,214,000	1,215,000
Venice, LA	NA	924,000	999,000	NA	891,000	891,000

E.3.1 Comparison of 2016 model outflow hydrographs with 1955 hydrographs

The following plots provide a comparison of 2016 hydrologic model or HEC-RAS model outflows with available 1955 hydrographs. Both unregulated and regulated hydrographs are compared for the mainstem Mississippi River locations. Only unregulated hydrographs were available for tributary locations from the 1955 Study; therefore, those locations do not include regulated hydrographs.

The HEC-RAS model included two separate runs: (1) Existing, Yazoo Backwater levee at elevation 207.1 and (2) Authorized, Yazoo Backwater levee at elevation 212.8. For most plots there is no difference between the Existing and Authorized Yazoo Backwater levee results except near the peak of the hydrograph. Where there are differences, an inset is included to show the relative differences between these two runs. Where there are no differences between the existing and authorized Yazoo Backwater runs only a single line appears in the plot because the lines plot directly on top of each other.

Figure E-28. Alexandria, LA, HYPO 63 1955 unregulated flow compared to 2016 unregulated flow generated by the RFC.

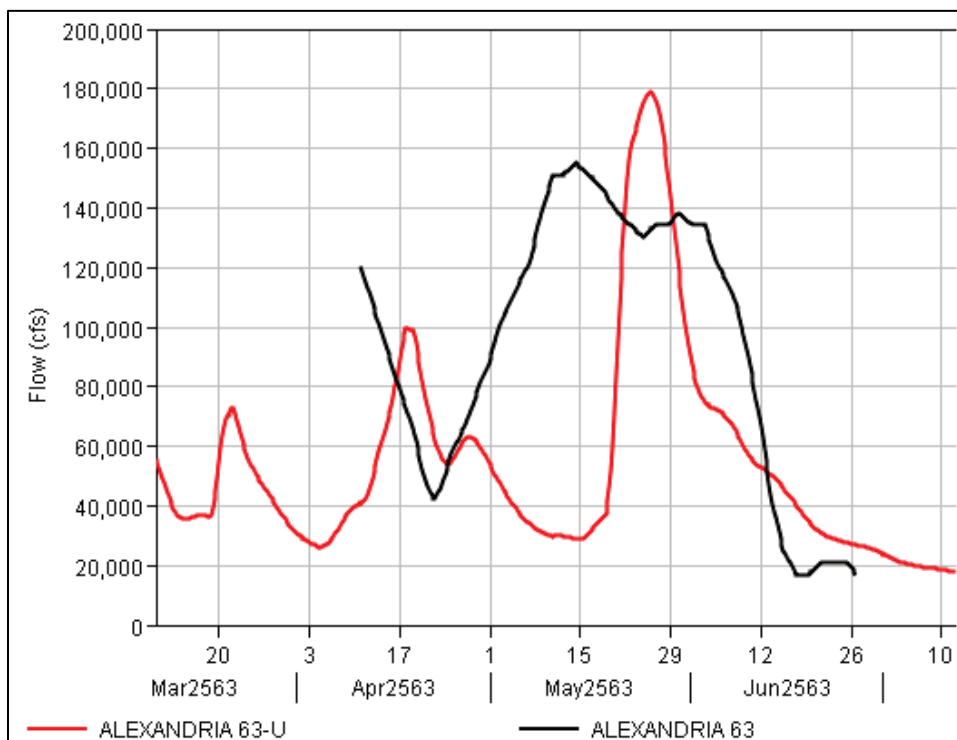


Figure E-29. Alton, IL, HYPO 63 1955 unregulated flow compared to 2016 unregulated flow generated by the RFC.

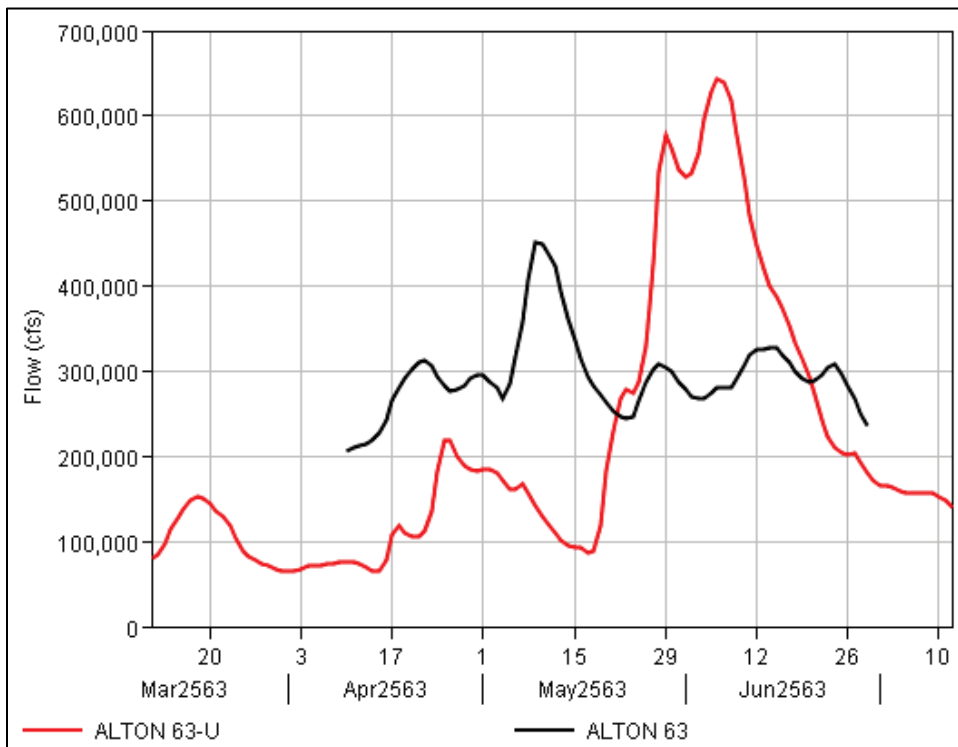


Figure E-30. Hermann, MO, HYPO 63 1955 unregulated flow compared to 2016 unregulated flow generated by the RFC.

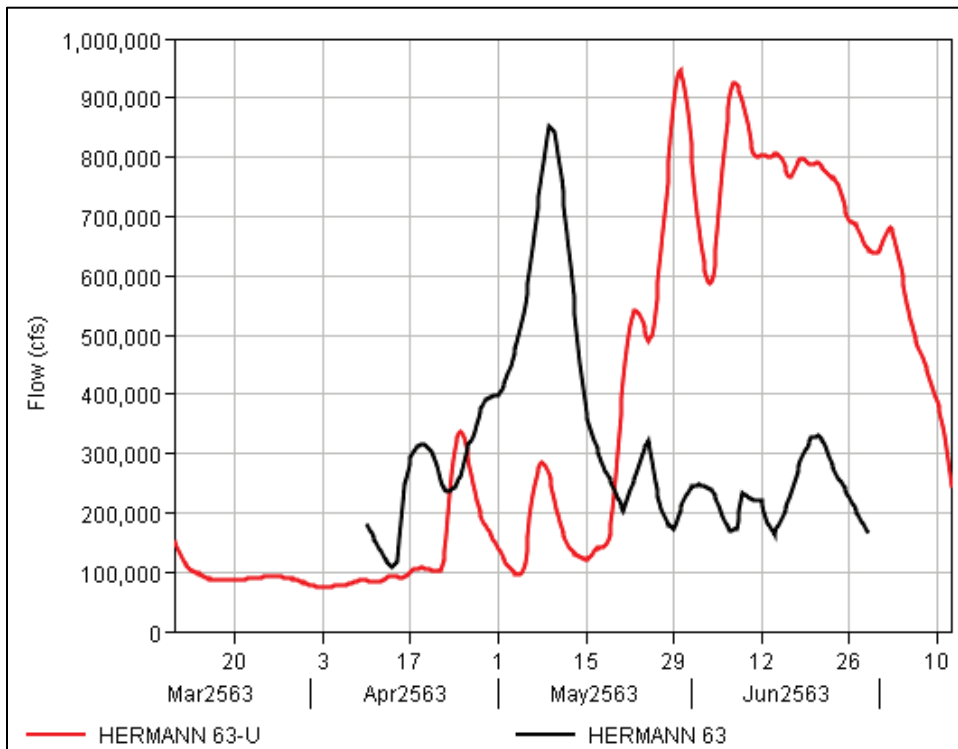


Figure E-31. Little Rock, AK, HYPO 63 1955 unregulated flow compared to 2016 unregulated flow generated by the RFC

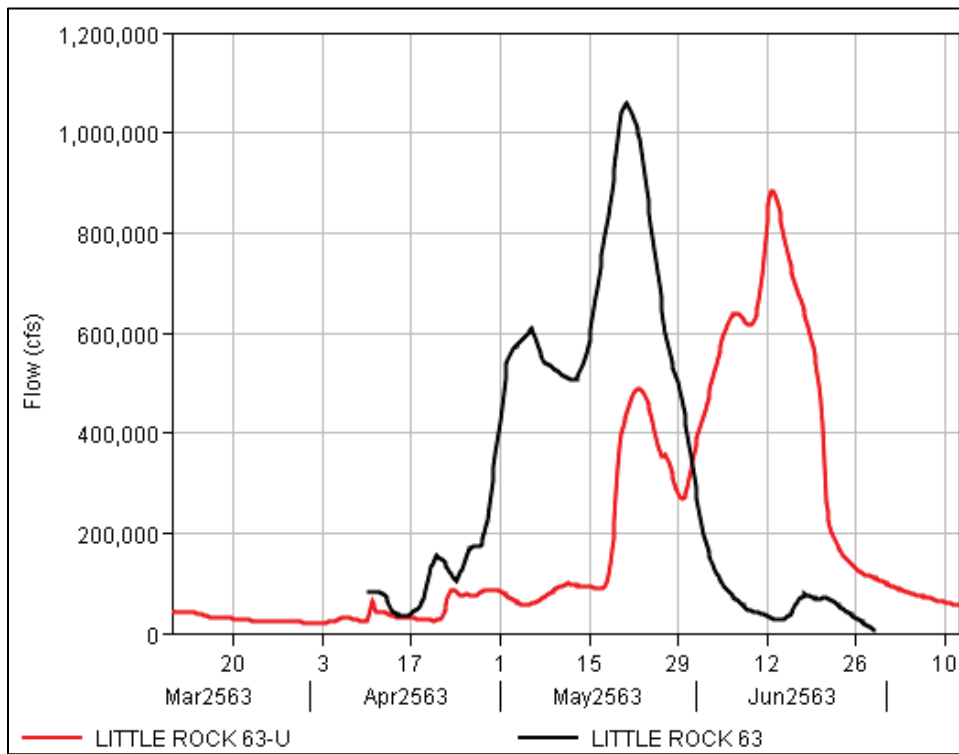


Figure E-32. Arkansas City, AR, HYPO 63 1955 unregulated flow compared to 2016 unregulated flow generated by the RFC.

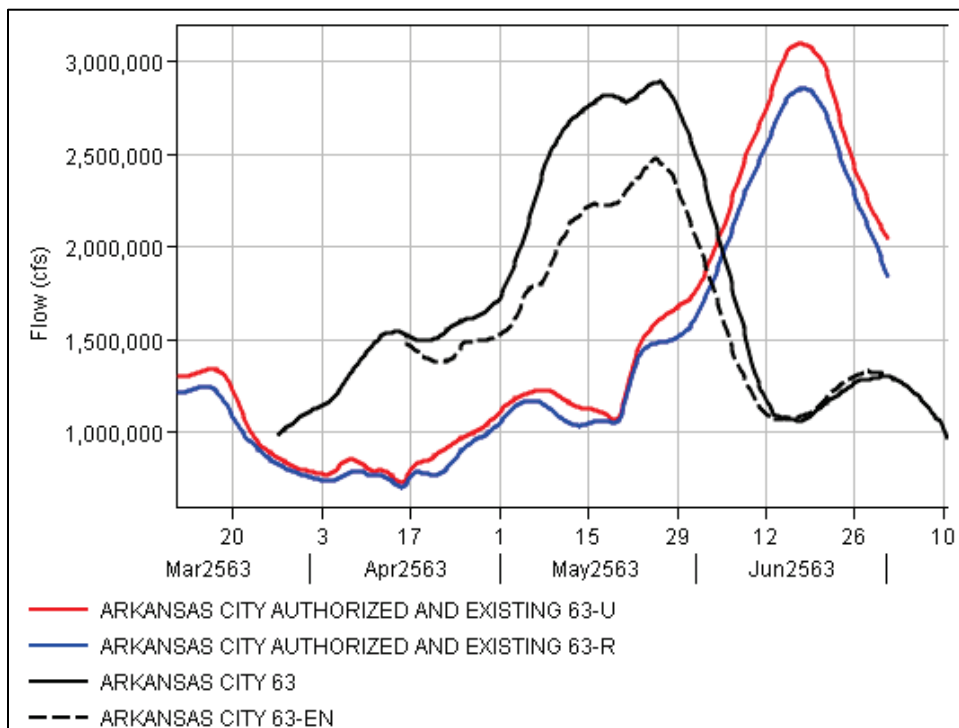


Figure E-33. Cairo, IL, HYPO 63 1955 unregulated flow compared to 2016 unregulated flow generated by the RFC.

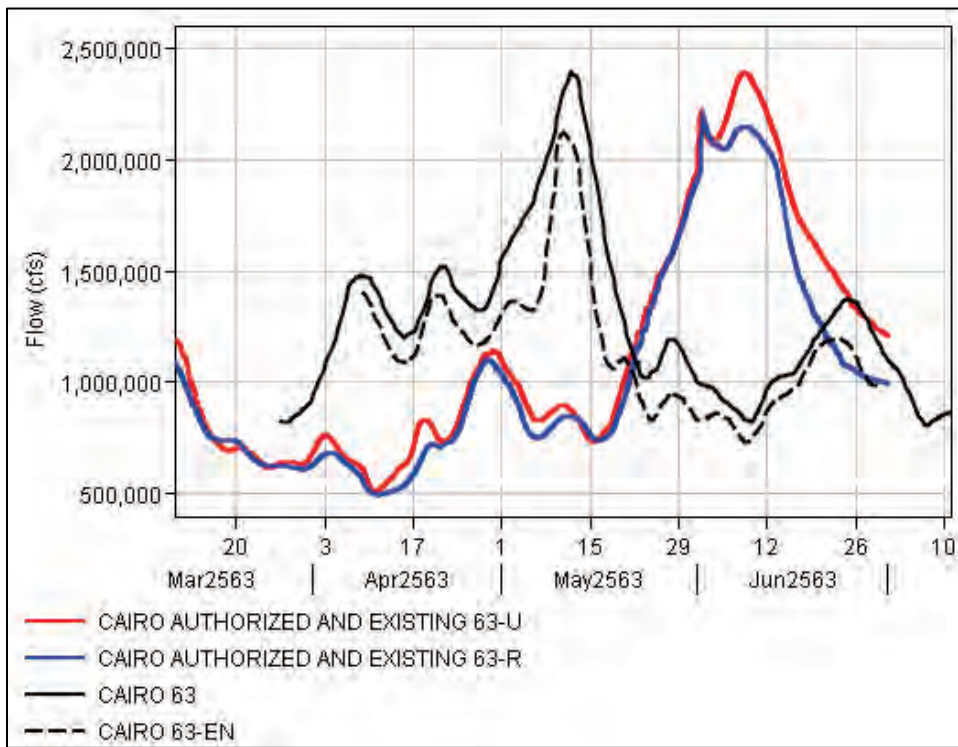


Figure E-34. Clarendon, AR, HYPO 63 1955 unregulated flow compared to 2016 unregulated flow generated by the RFC.

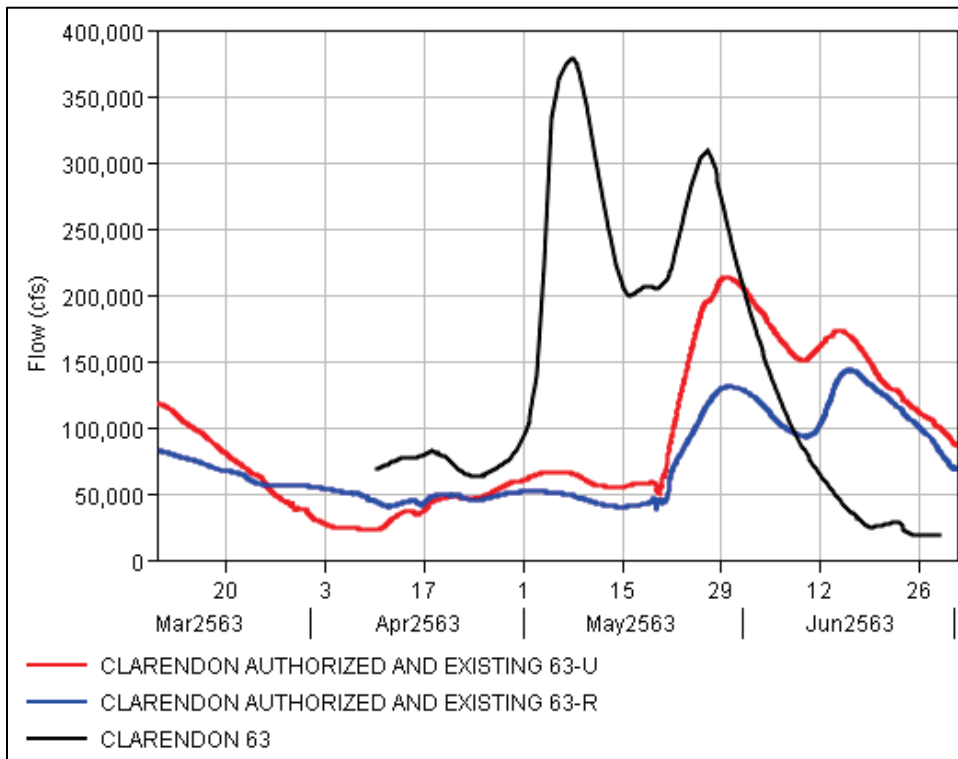


Figure E-35. Metropolis, IL, HYPO 63 1955 unregulated flow compared to 2016 unregulated flow generated by the RFC.

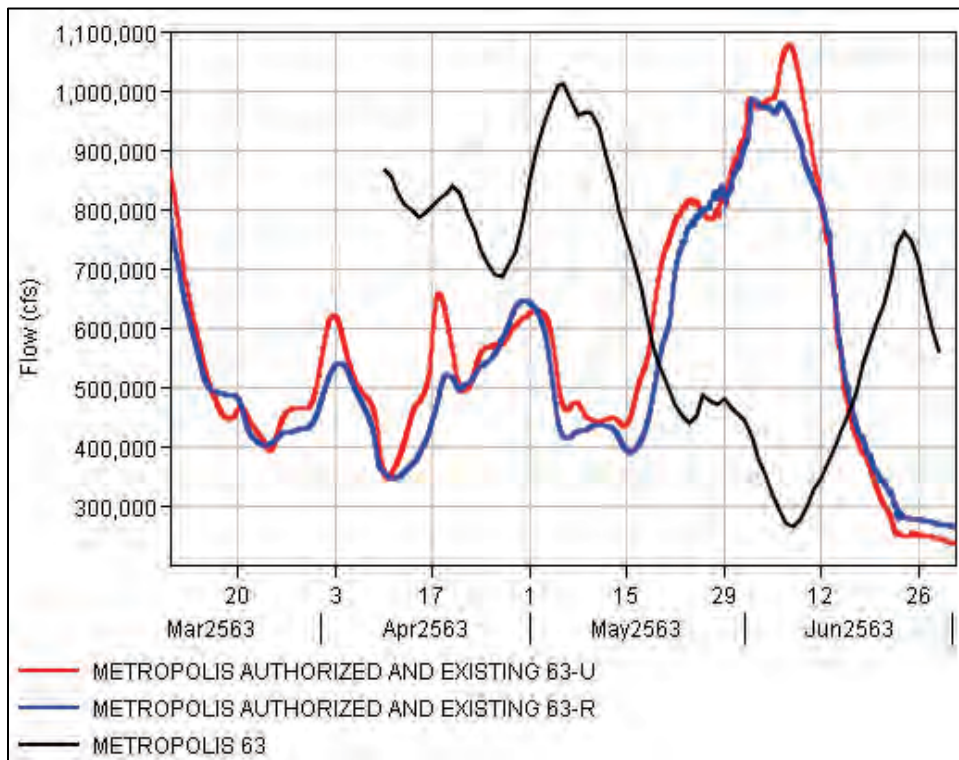


Figure E-36. St. Louis, MO, HYPO 63 1955 unregulated flow compared to 2016 unregulated flow generated by the RFC.

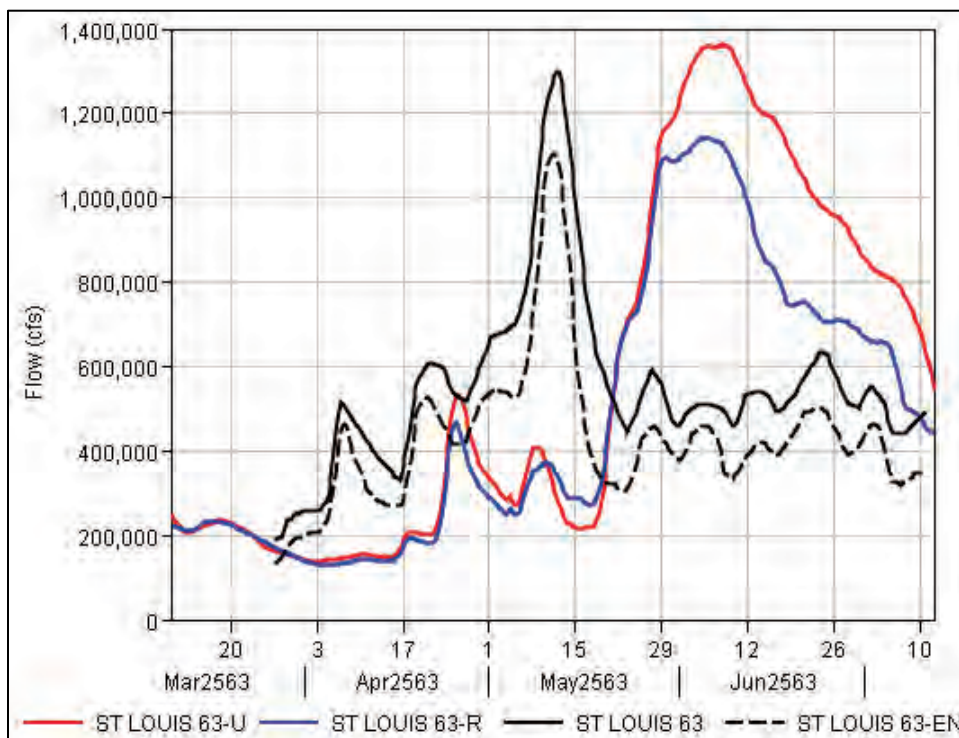
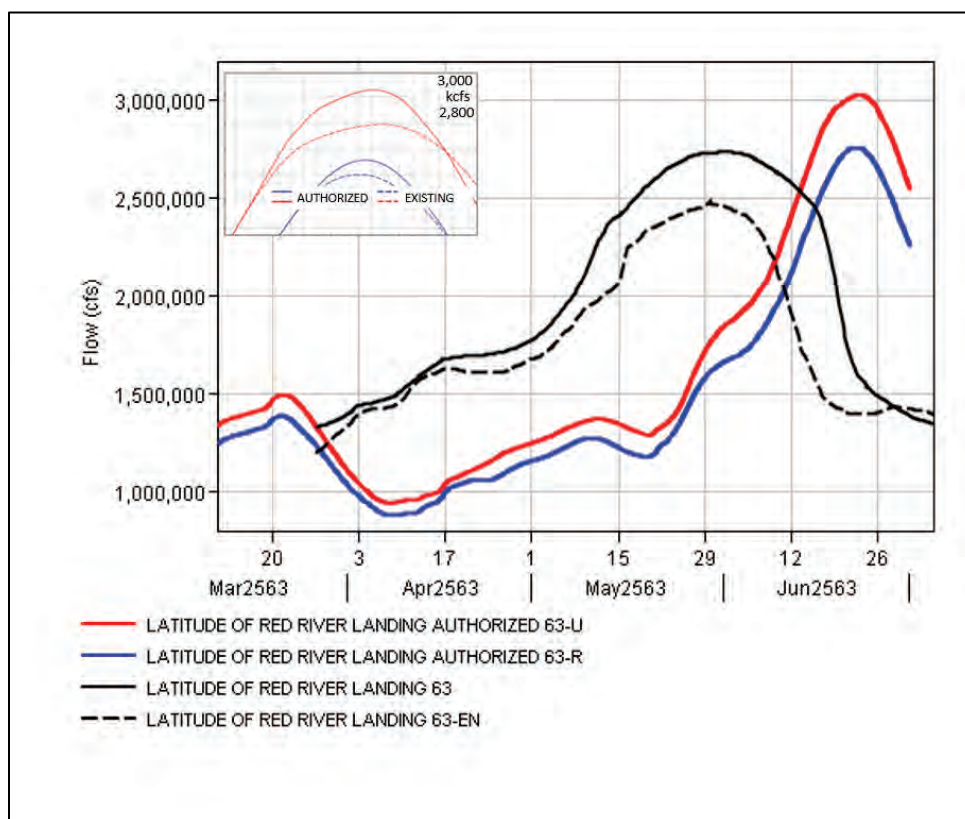


Figure E-37. Red River Landing, LA, HYPO 63 1955 unregulated flow compared to 2016 unregulated flow generated by the RFC.



E.3.2 HYPO 63 HEC-RAS unsteady model outflows

The combined MVD HEC-RAS model developed for the current assessment provides unsteady hydrodynamic flood routing along the main river channels within the assessment area. Peak flow and event hydrographs for the Ohio and Lower Mississippi Rivers (points downstream of the Ohio/Mississippi confluence) are direct outflows from the HEC-RAS unsteady calculations. The HEC-RAS model included two separate runs: (1) Existing, Yazoo Backwater levee at elevation 207.1 and (2) Authorized, Yazoo Backwater levee at elevation 212.8. For most plots there is no difference between the Existing and Authorized Yazoo Backwater levee results except near the peak of the hydrograph. Where there are differences, an inset is included to show the relative differences between these two runs. Where there are no differences between the existing and authorized Yazoo Backwater runs only a single line appears in the plot because the lines plot directly on top of each other.

Figure E-38. HYPO 63 HEC-RAS hydrograph: Ohio River at Cairo, IL.

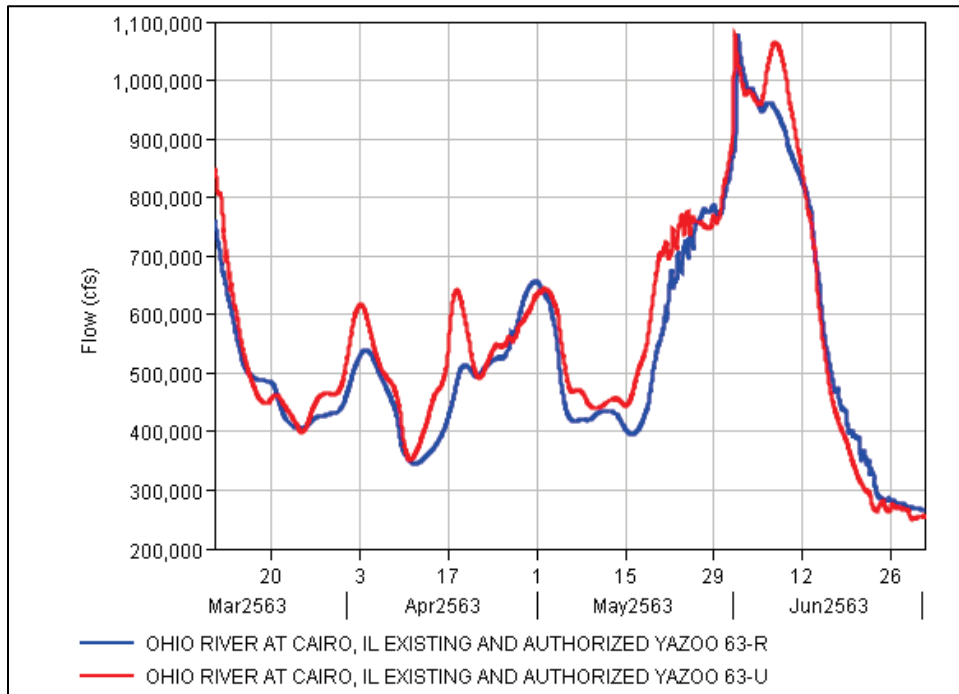


Figure E-39. HYPO 63 HEC-RAS hydrograph: Combined Ohio and Mississippi River flow near Cairo, IL.

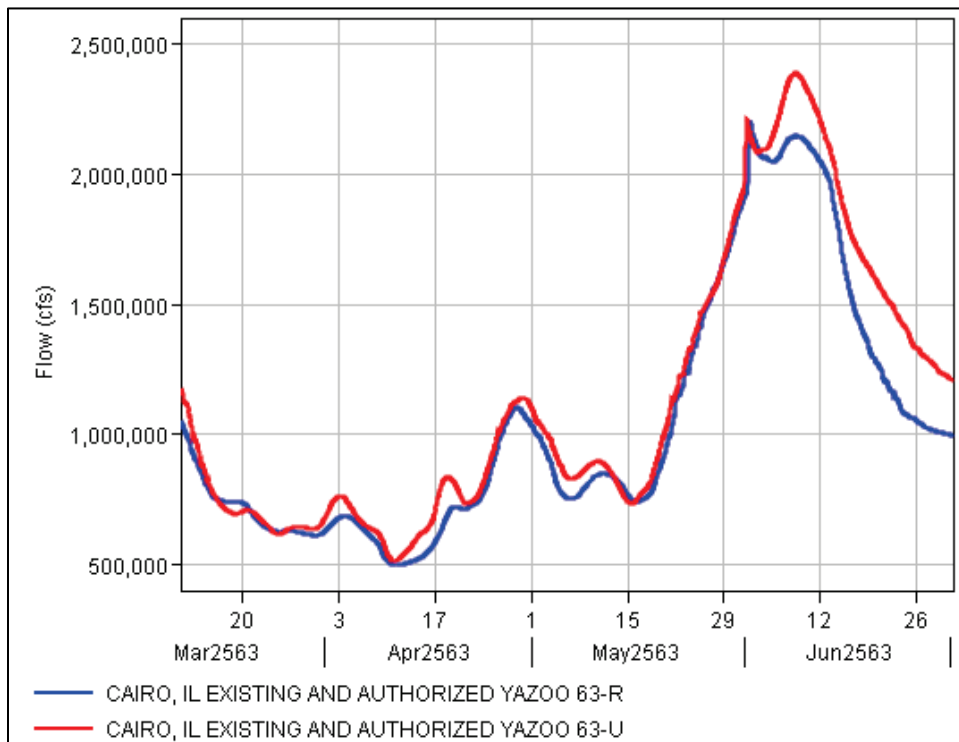


Figure E-40. HYPO 63 HEC-RAS hydrograph: Mississippi River at Hickman, KY.

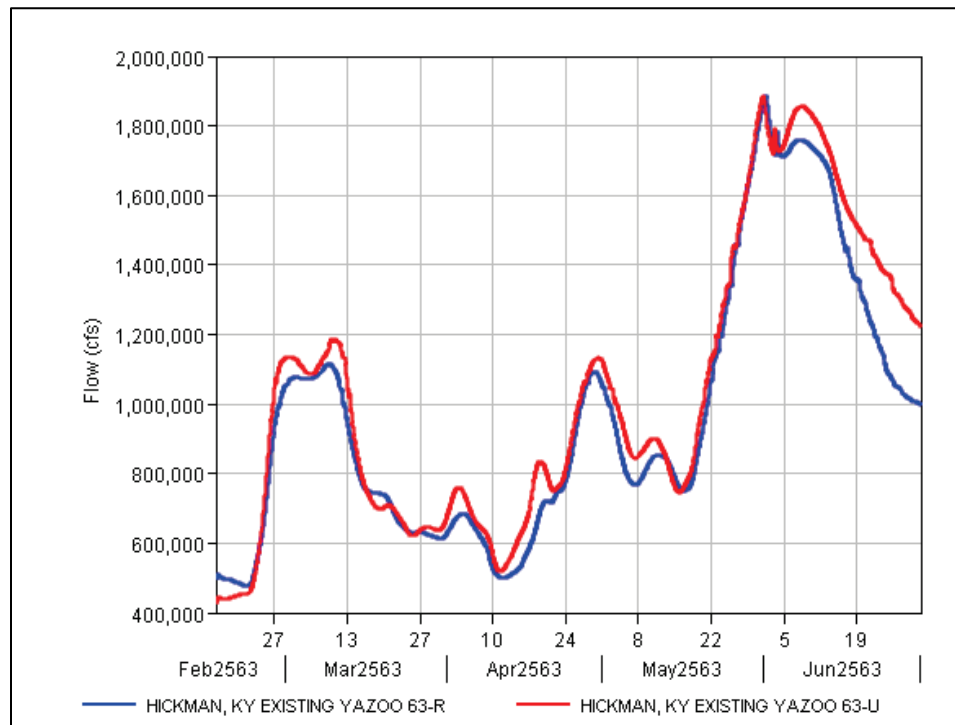


Figure E-41. HYPO 63 HEC-RAS hydrograph: Mississippi River at Memphis, TN.

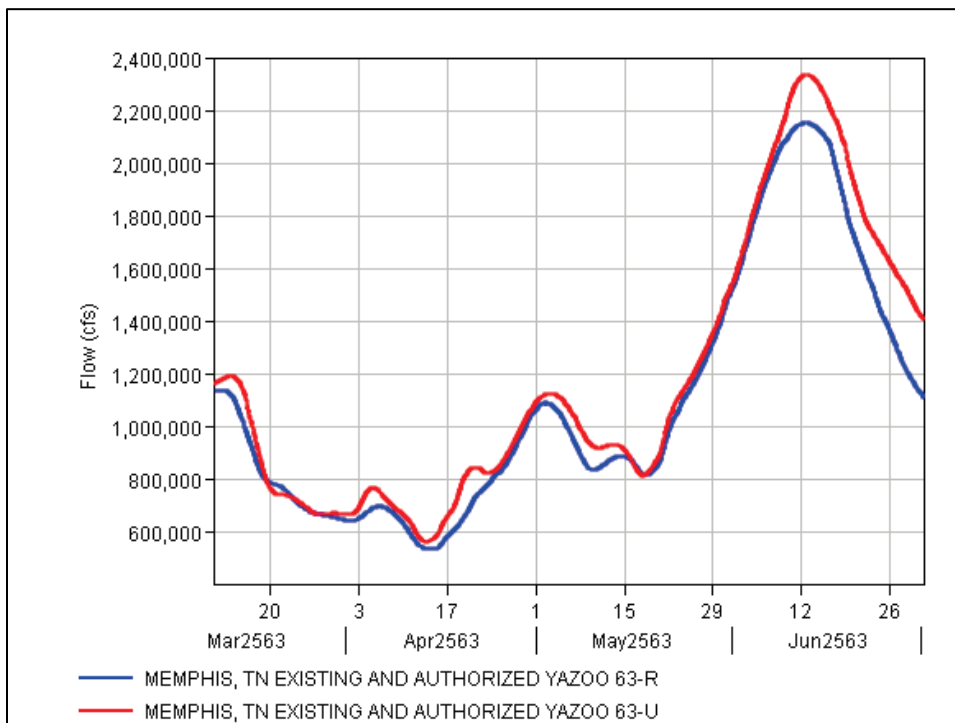


Figure E-42. HYPO 63 HEC-RAS hydrograph: Mississippi River at Helena, AR.

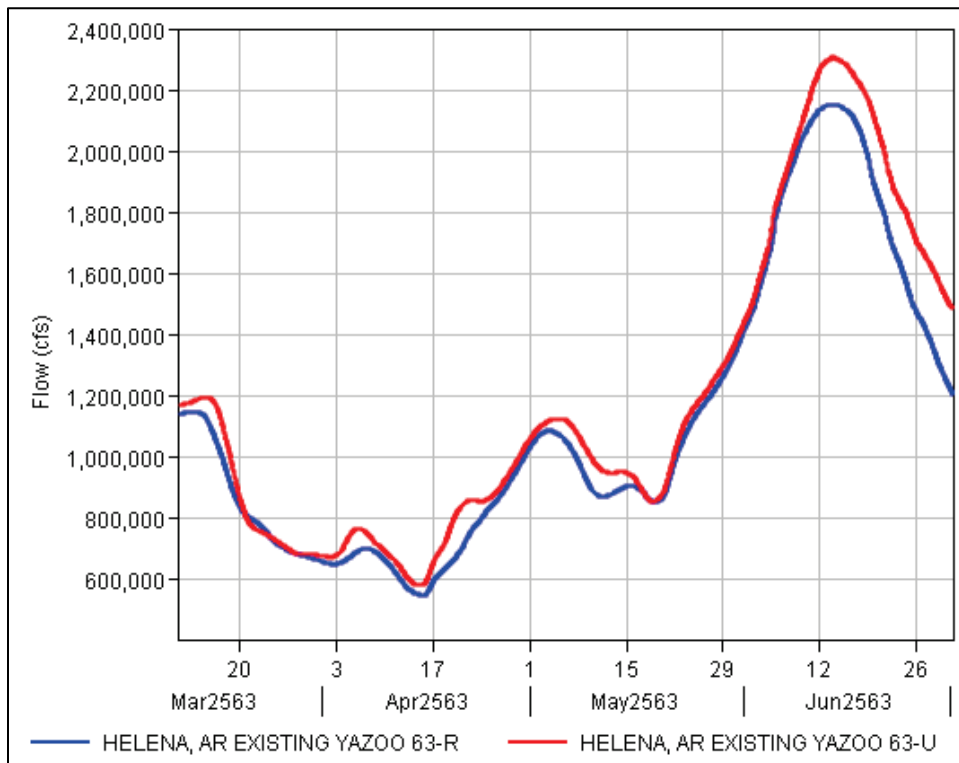


Figure E-43. HYPO 63 HEC-RAS hydrograph: Mississippi River at Arkansas City, AR.

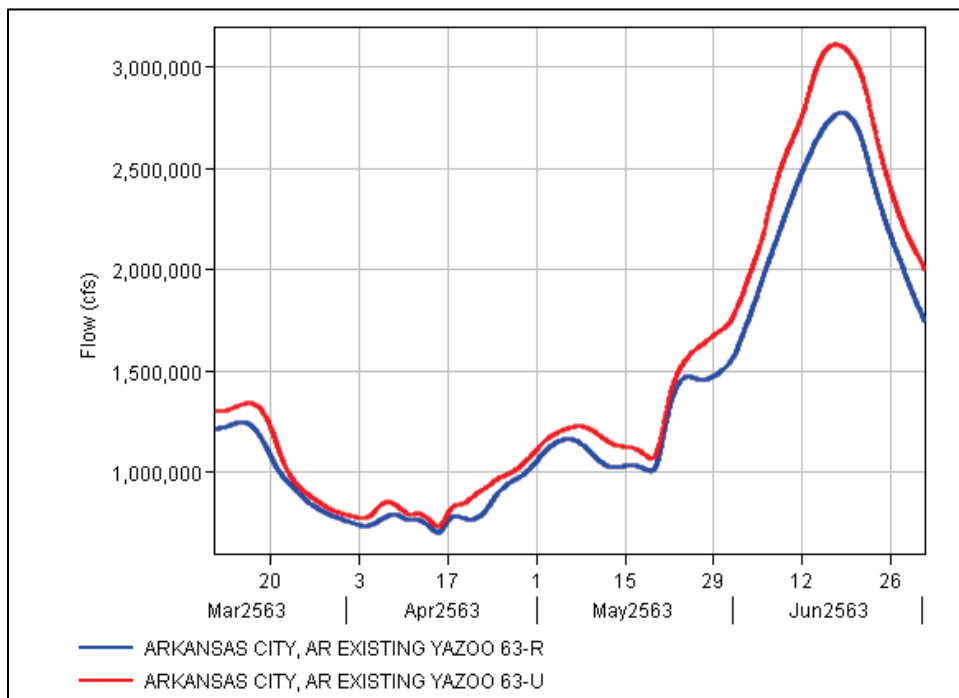


Figure E-44. HYPO 63 HEC-RAS hydrograph: Mississippi River at Greenville, MS.

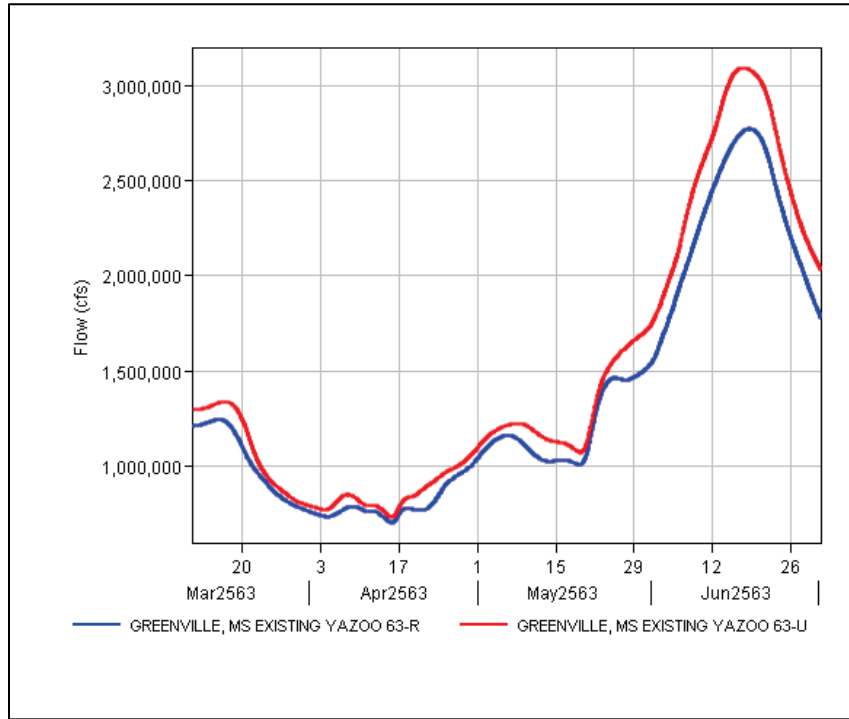


Figure E-45. HYPO 63 HEC-RAS hydrograph: Mississippi River at Lake Providence, LA.

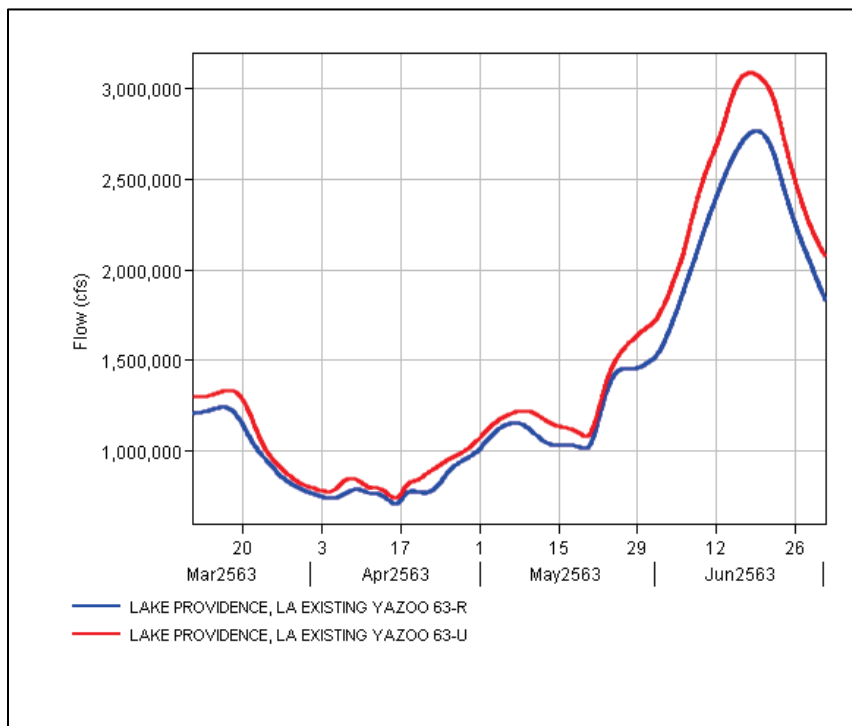


Figure E-46. HYPO 63 HEC-RAS hydrograph: Mississippi River at Vicksburg, MS.

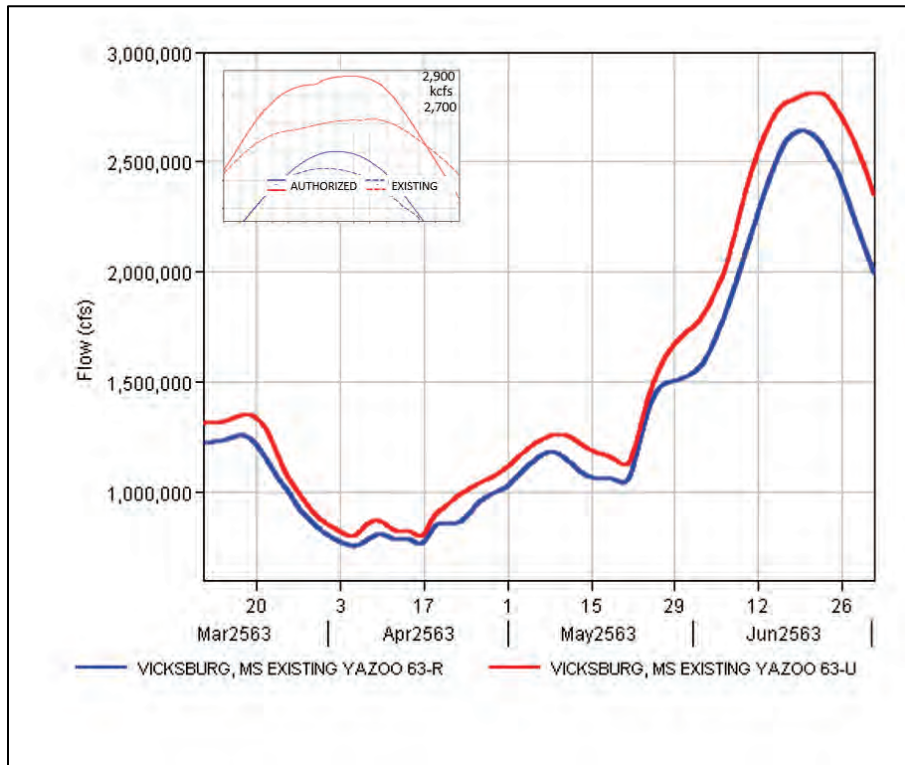


Figure E-47. HYPO 63 HEC-RAS hydrograph: Mississippi River at Natchez, MS.

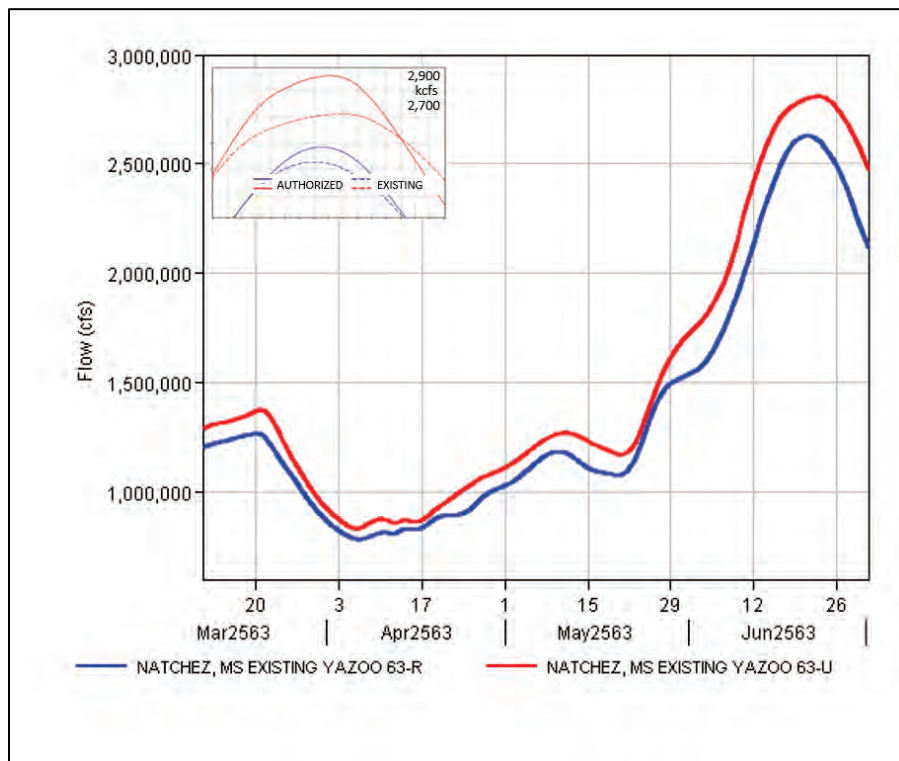


Figure E-48. HYPO 63 HEC-RAS hydrograph: Mississippi River at Red River Landing, LA.

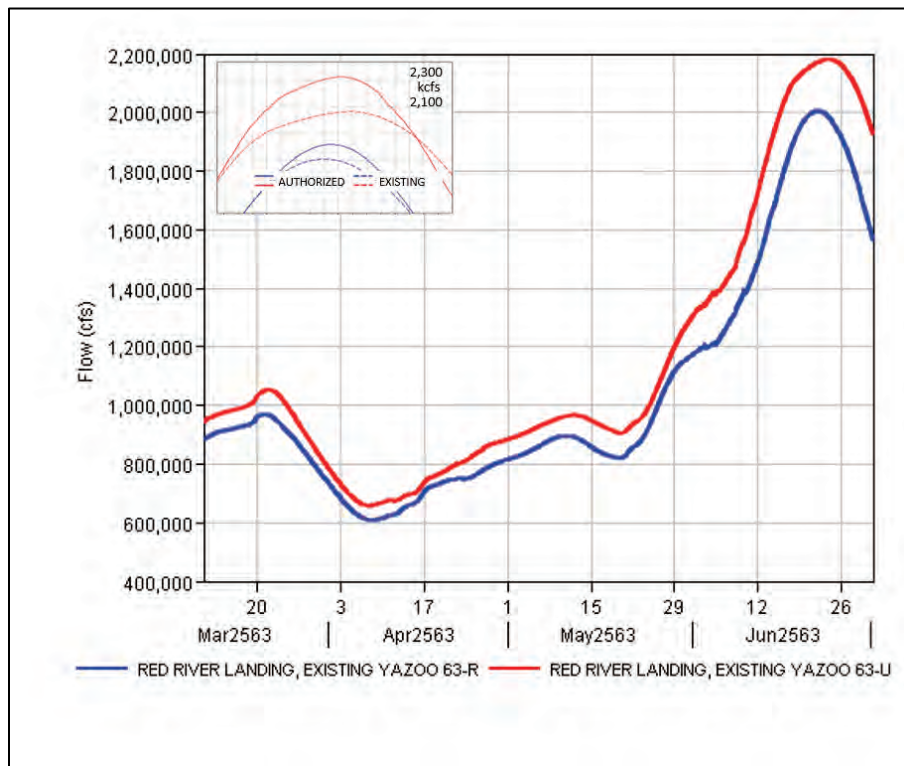


Figure E-49. HYPO 63 HEC-RAS hydrograph: Mississippi River at Baton Rouge, LA.

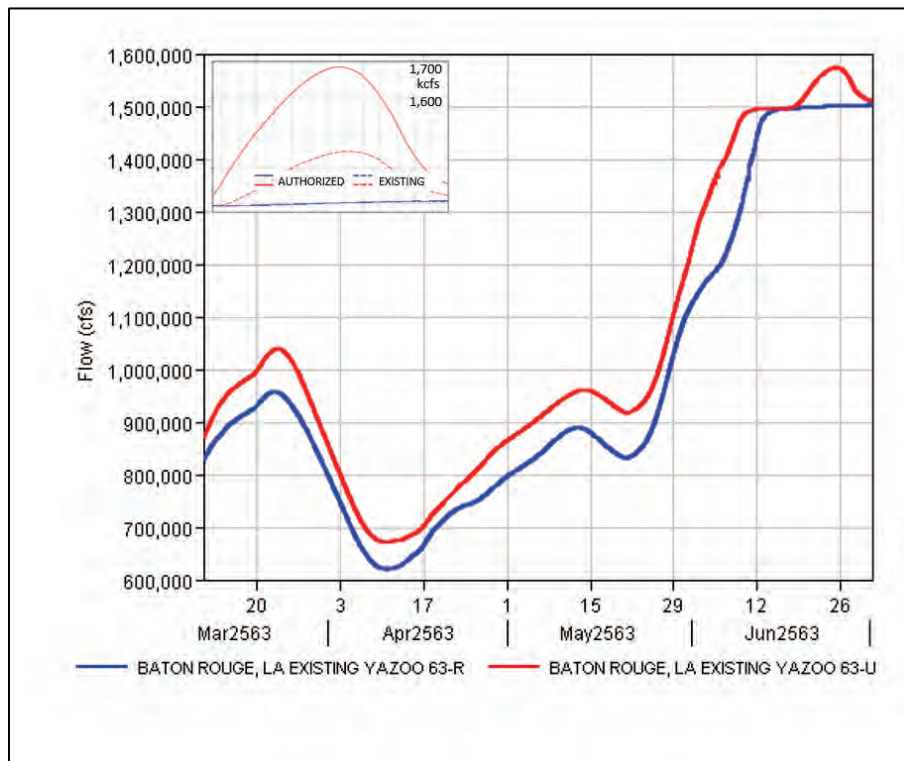


Figure E-50. HYPO 63 HEC-RAS hydrograph: Mississippi River at Donaldsonville, LA.

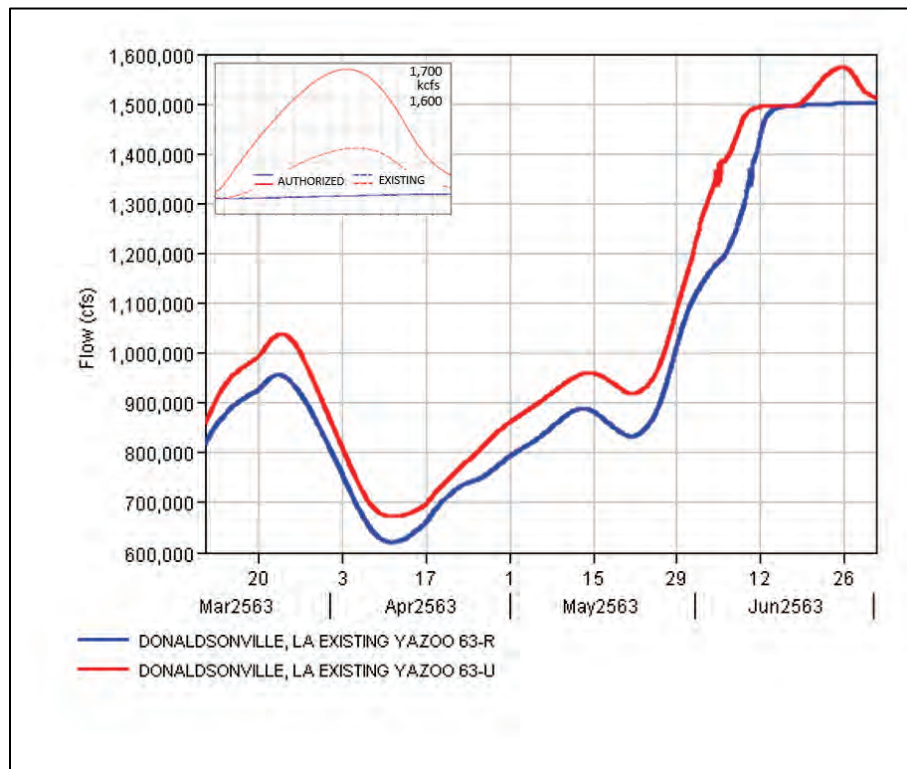


Figure E-51. HYPO 63 HEC-RAS hydrograph: Mississippi River at Carrollton, LA.

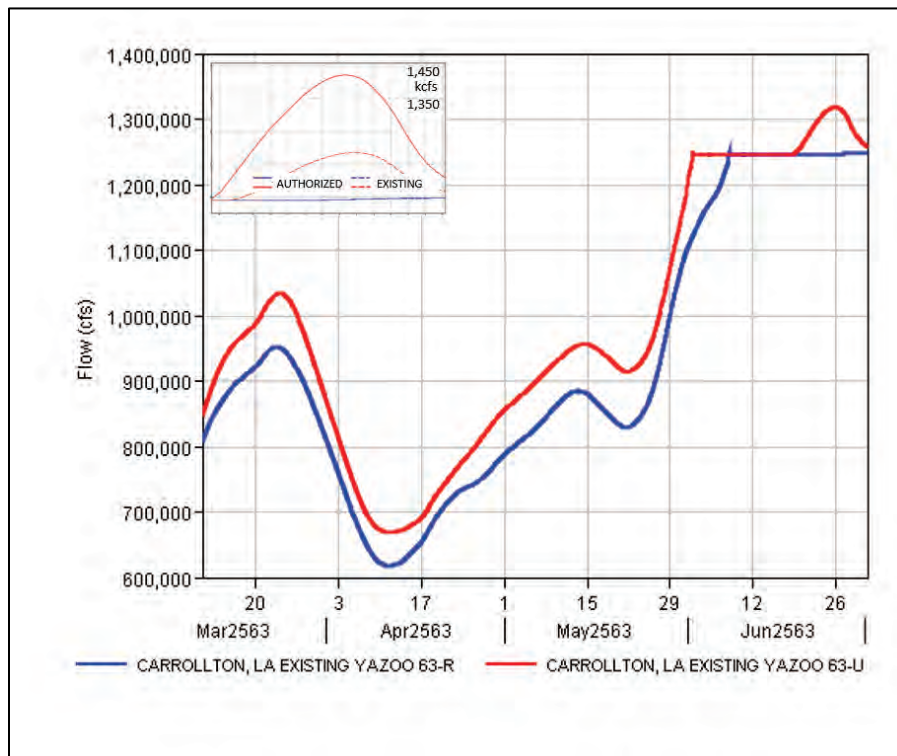


Figure E-52. HYPO 63 HEC-RAS hydrograph: Mississippi River at Empire, LA.

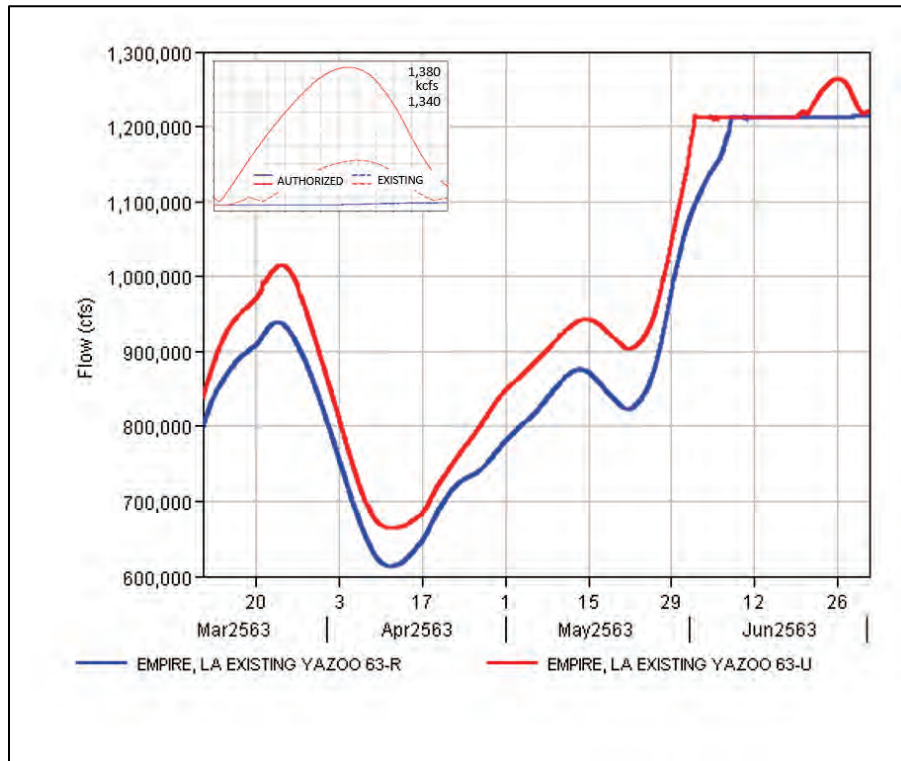
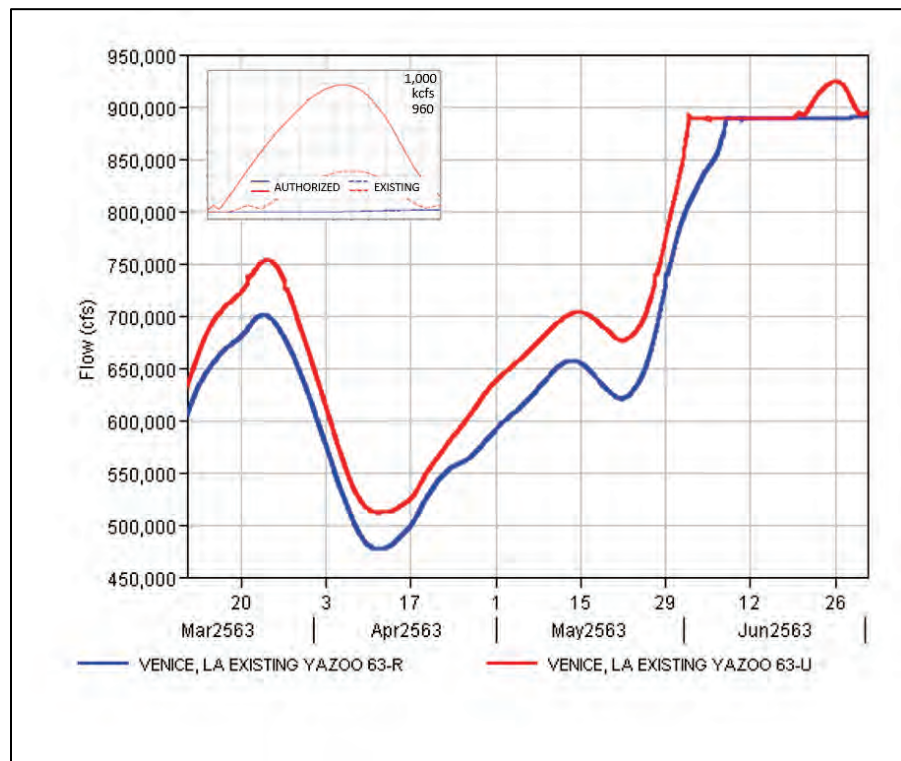


Figure E-53. HYPO 63 HEC-RAS hydrograph: Mississippi River at Venice, LA.



E.4 Reservoir inflow and outflow hydrographs for regulated simulations

Figures shown in this section provide data used to develop regulated flows for each reservoir as computed by the USACE district offices. The resulting reservoir outflows for each project were used by the NWS River Forecast Centers to define reservoir outflows in their CHPS-FEWS model simulations. Some figures shows slight oscillations that were due to model instabilities; these were outside the primary period of analysis and did not impact results obtained for peak flow periods.

E.4.1 LRL reservoir hydrographs

Figure E-54. Barren River Lake HYPO 63 inflow compared to outflow.

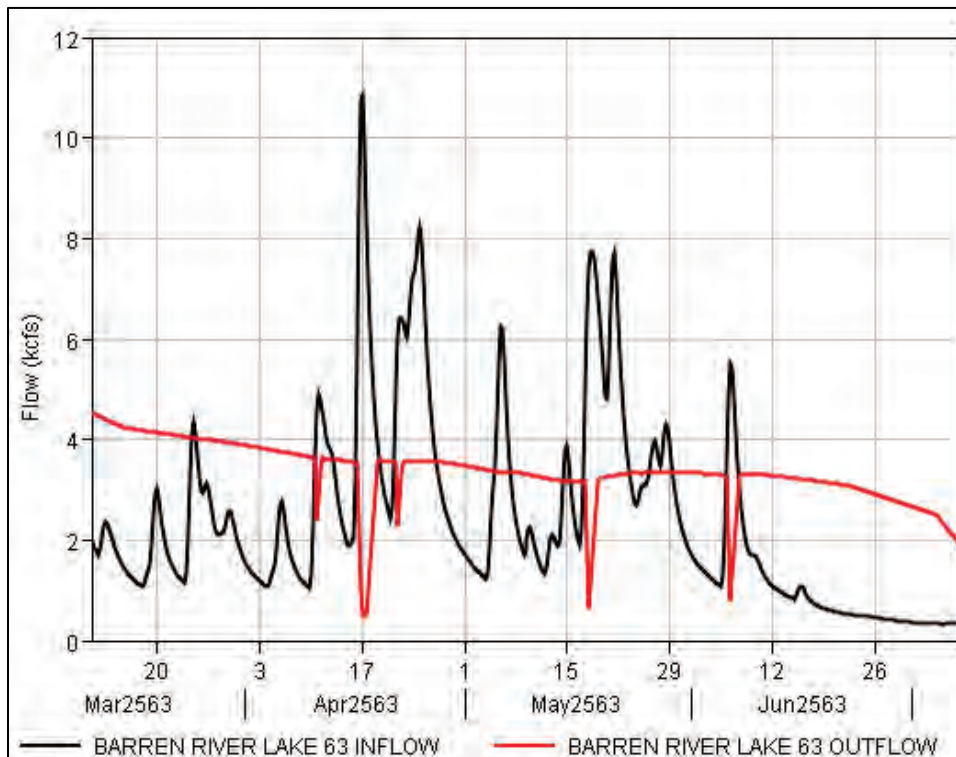


Figure E-55. Cagles Mill Lake HYPO 63 inflow compared to outflow.

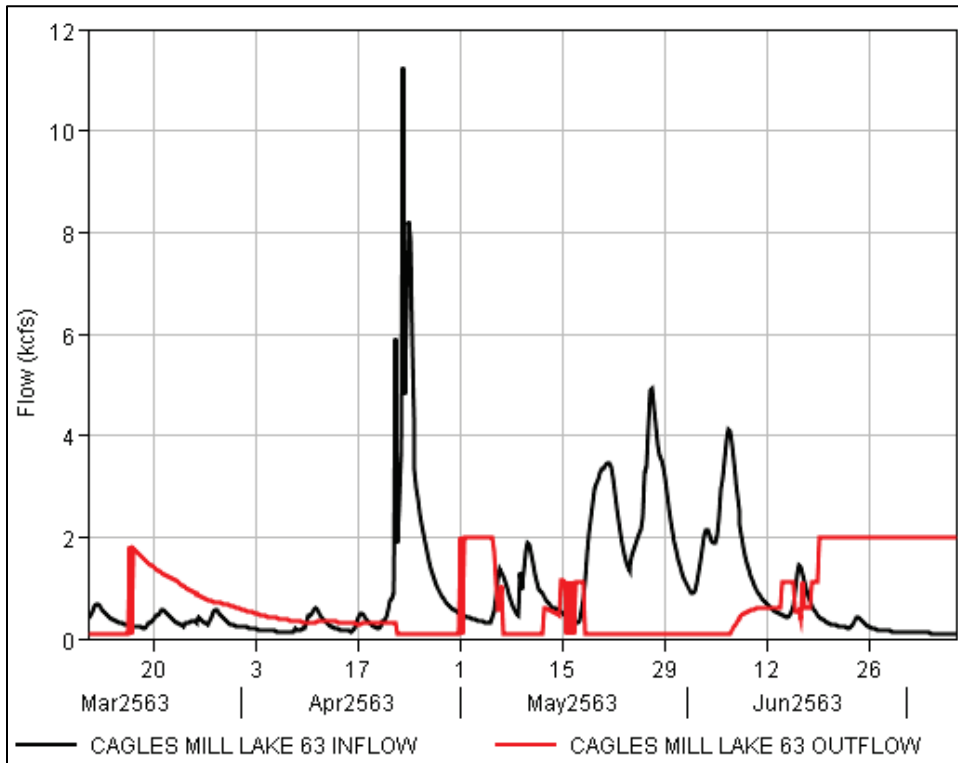


Figure E-56. CM Harden Lake HYPO 63 inflow compared to outflow.

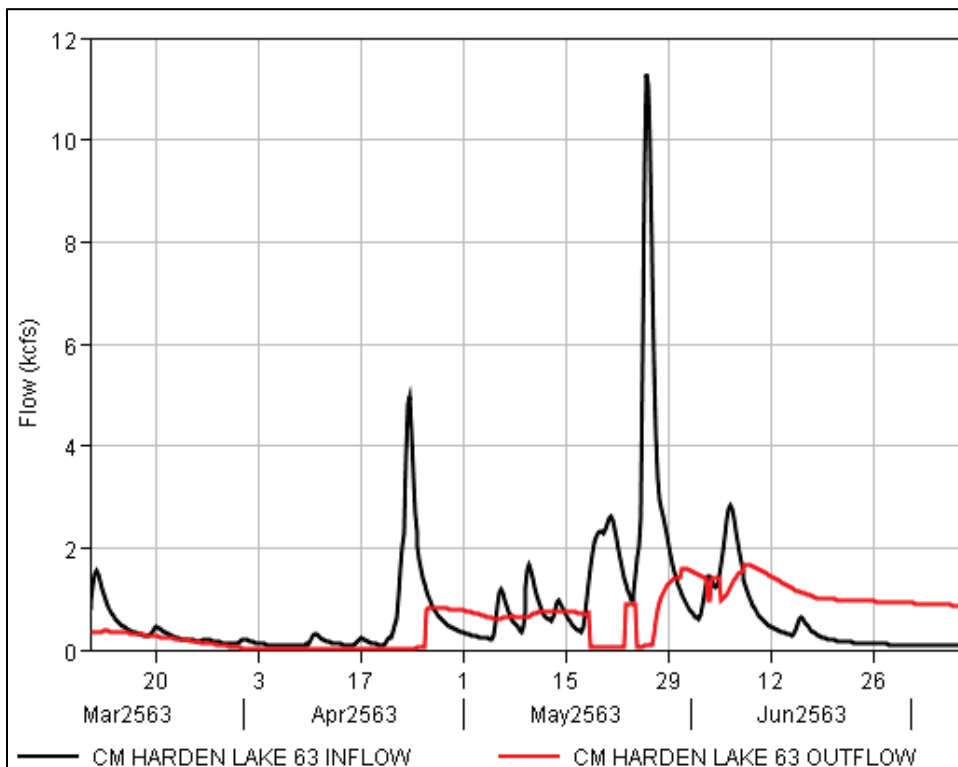


Figure E-57. Green River Lake HYPO 63 inflow compared to outflow.

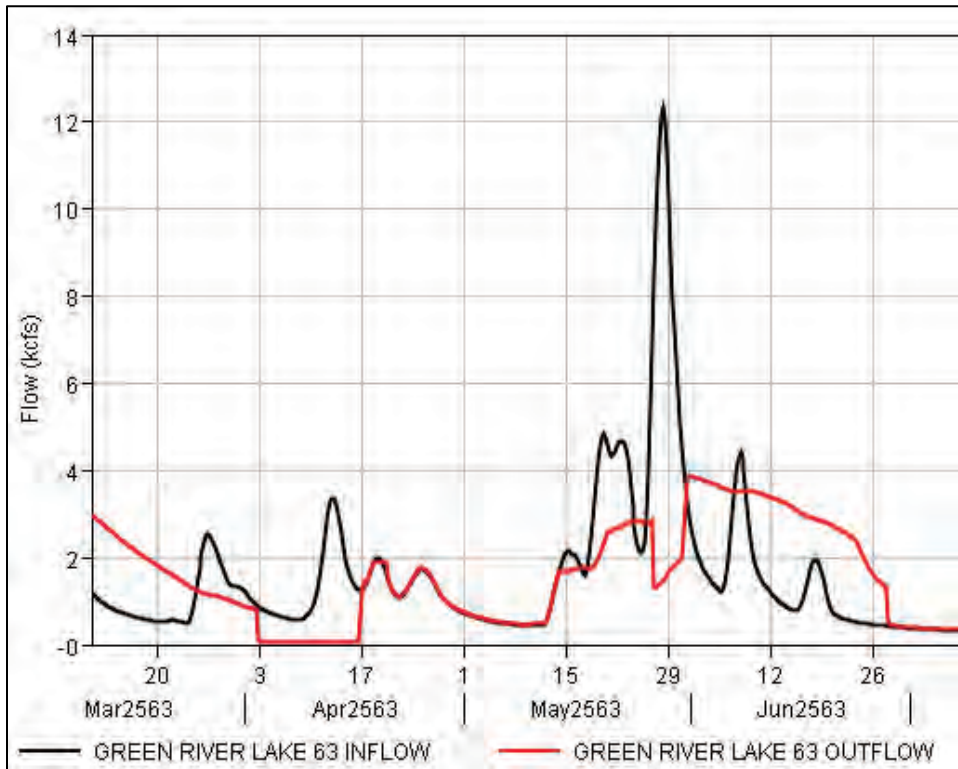


Figure E-58. J. E. Roush Lake HYPO 63 inflow compared to outflow.

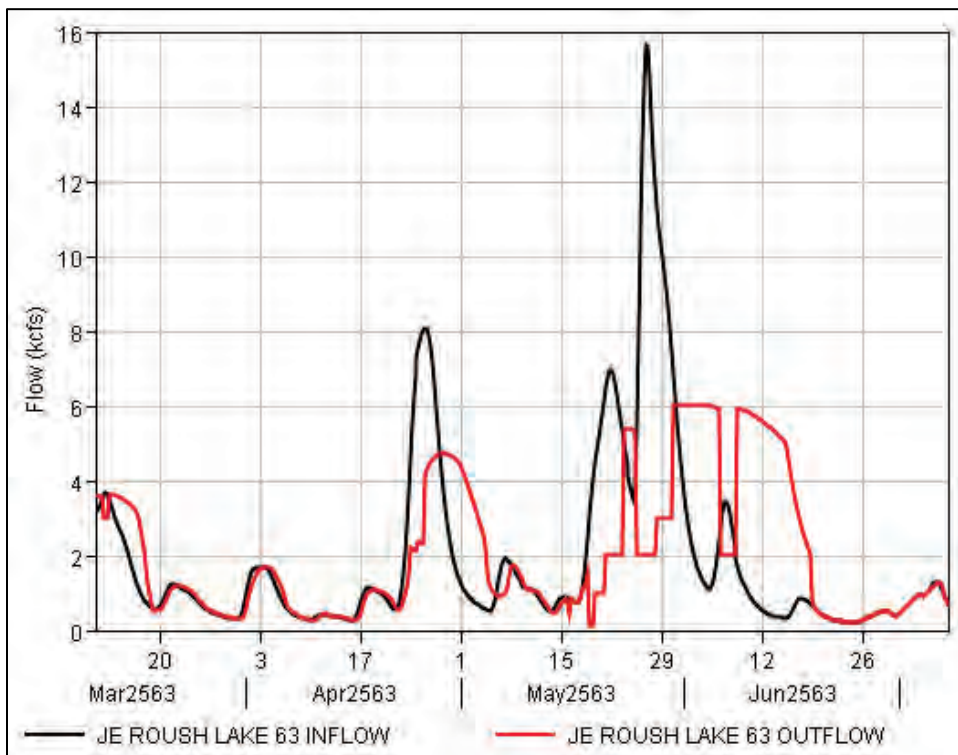


Figure E-59. Mississnewa Lake HYPO 63 inflow compared to outflow.

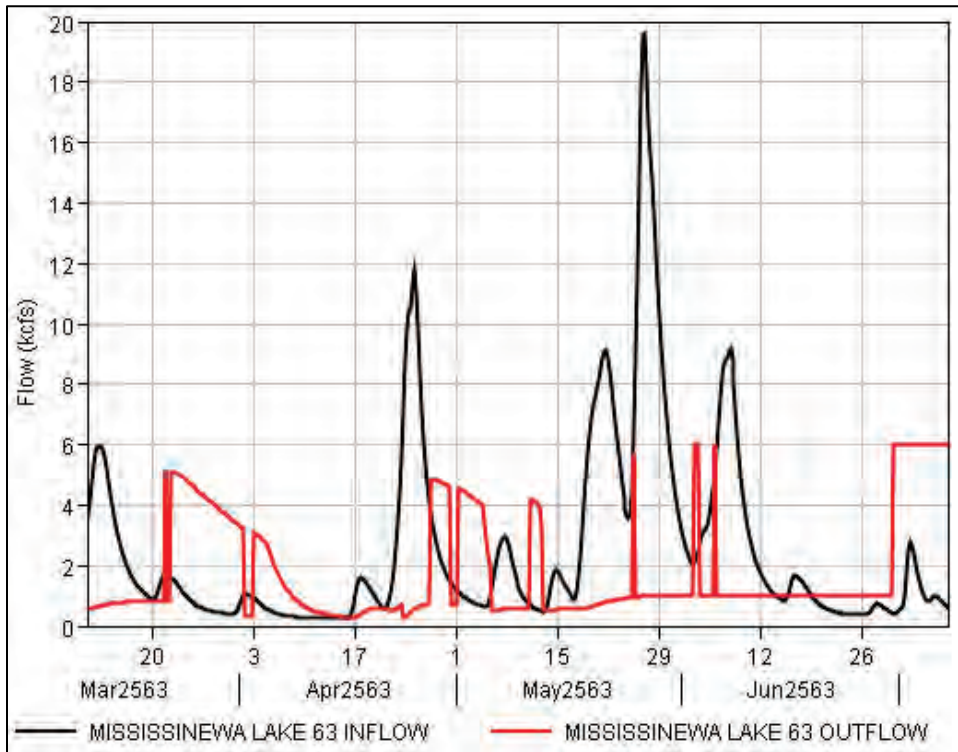


Figure E-60. Monroe Lake HYPO 63 inflow compared to outflow.

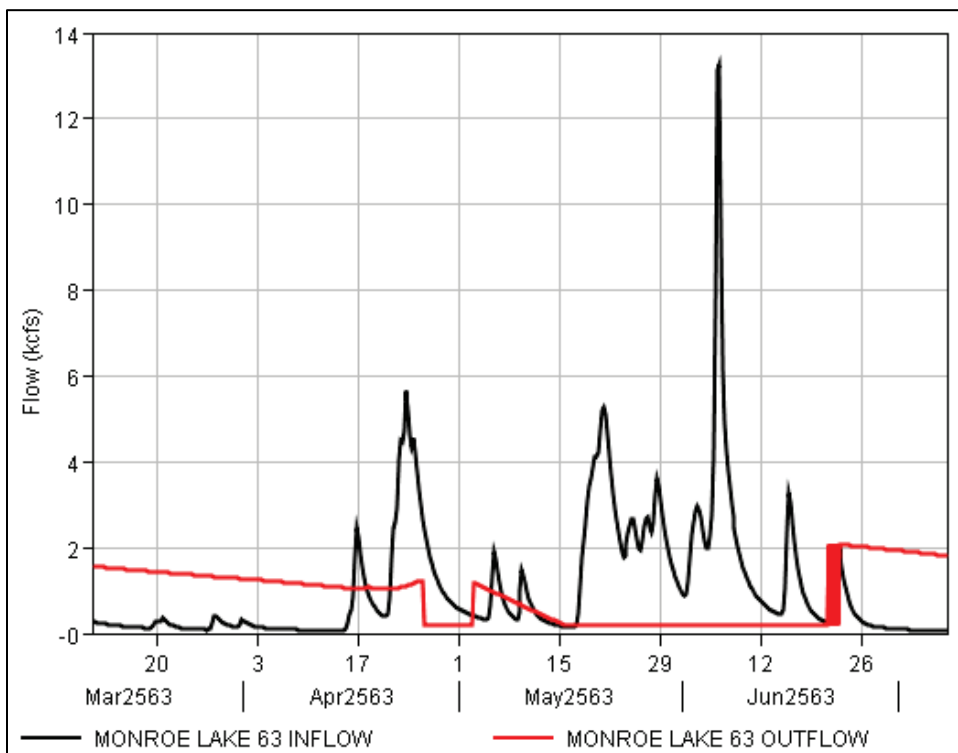


Figure E-61. Nolin River Lake HYPO 63 inflow compared to outflow.

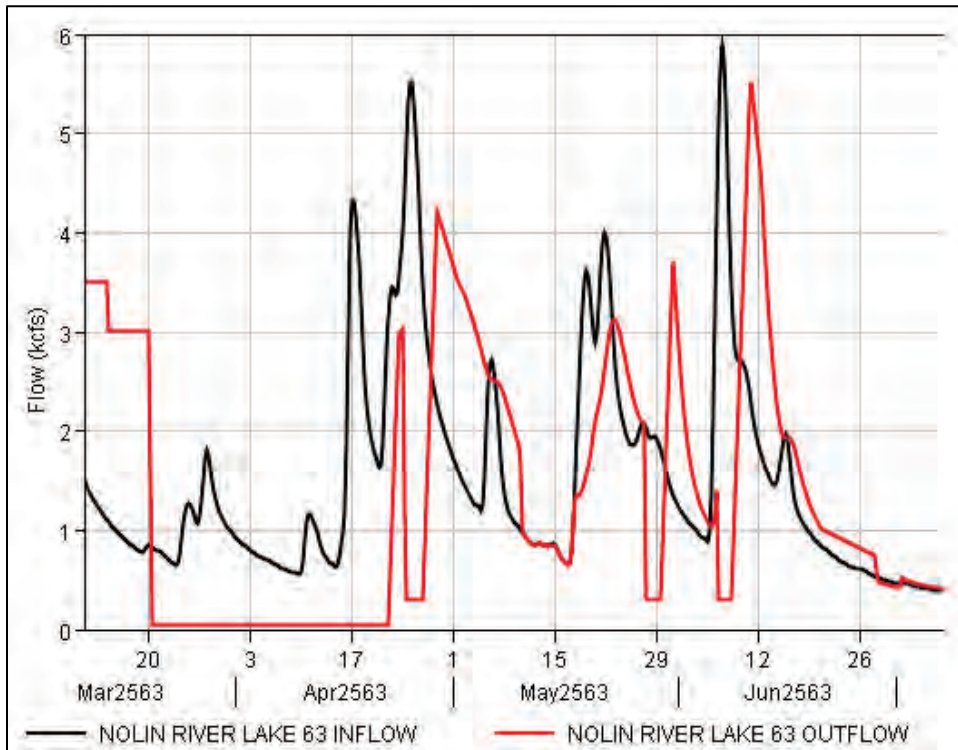


Figure E-62. Patoka Lake HYPO 63 inflow compared to outflow.

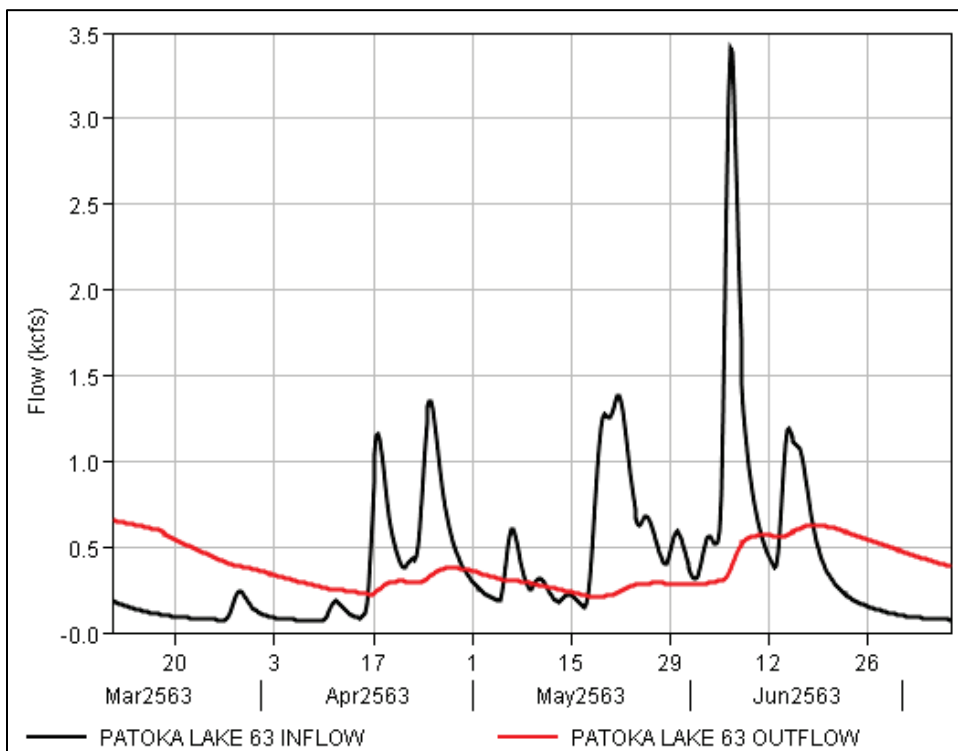


Figure E-63. Rough River Lake HYPO 63 inflow compared to outflow.

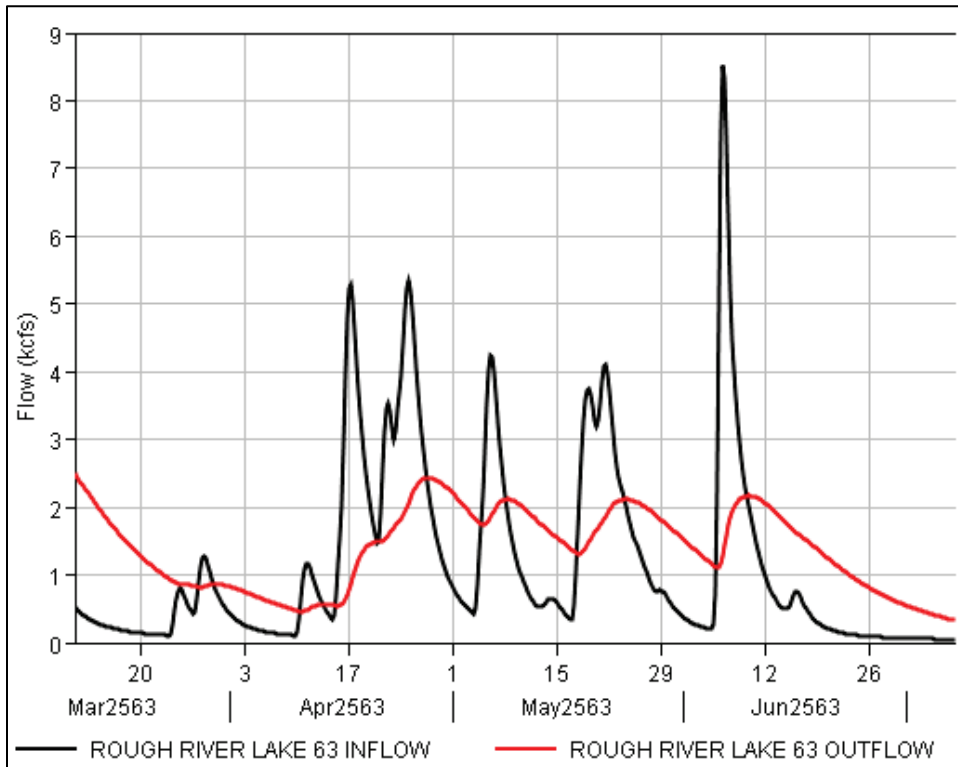
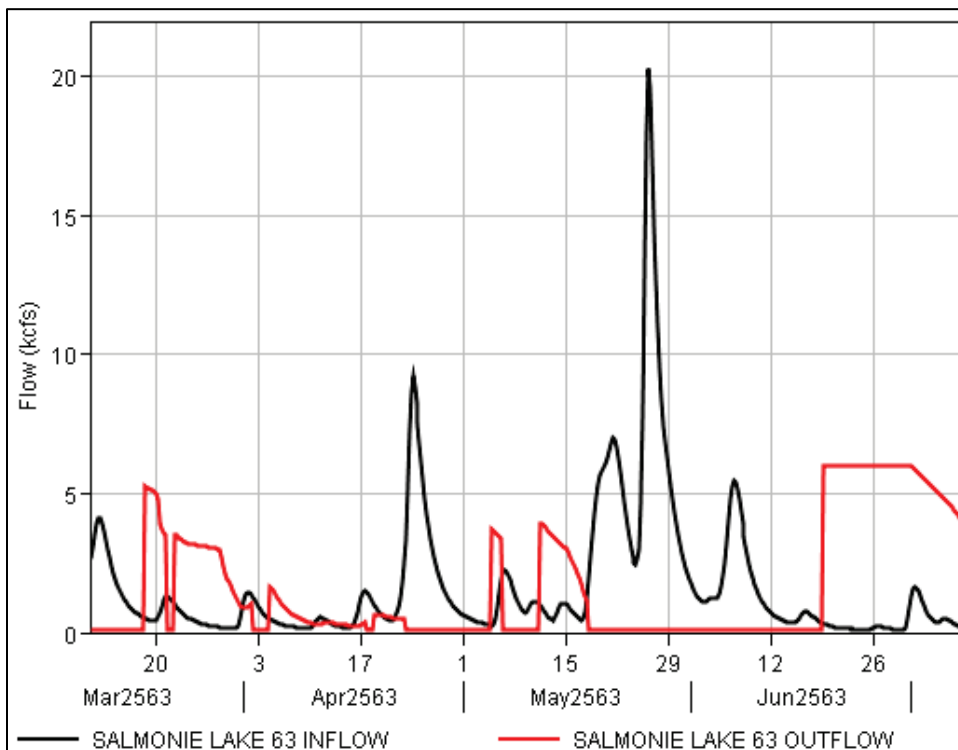


Figure E-64. Salmonie Lake HYPO 63 inflow compared to outflow.



E.4.2 LRN reservoir hydrographs

Figure E-65. Barkley Dam HYPO 63 inflow compared to outflow.

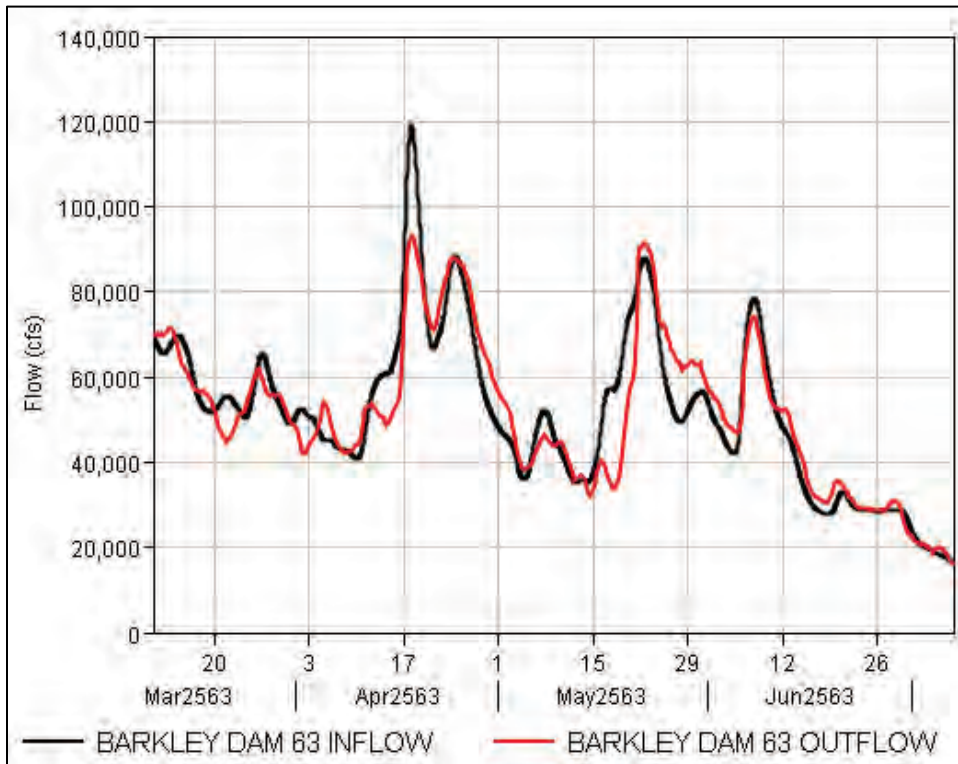


Figure E-66. Center Hill Dam HYPO 63 inflow compared to outflow.

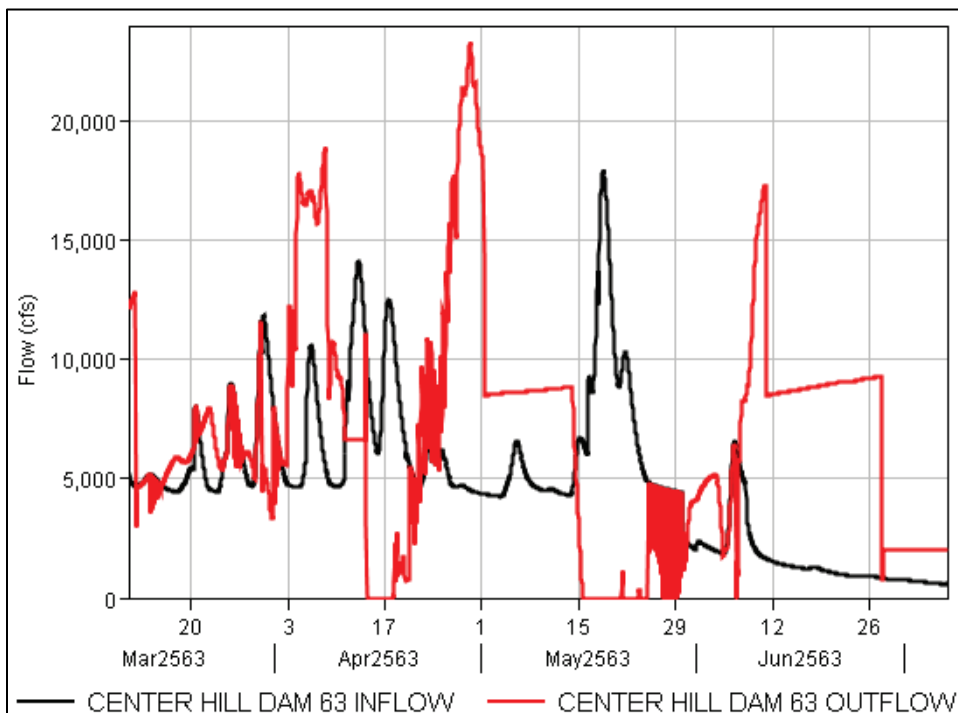


Figure E-67. Cheatham Dam HYPO 63 inflow compared to outflow.

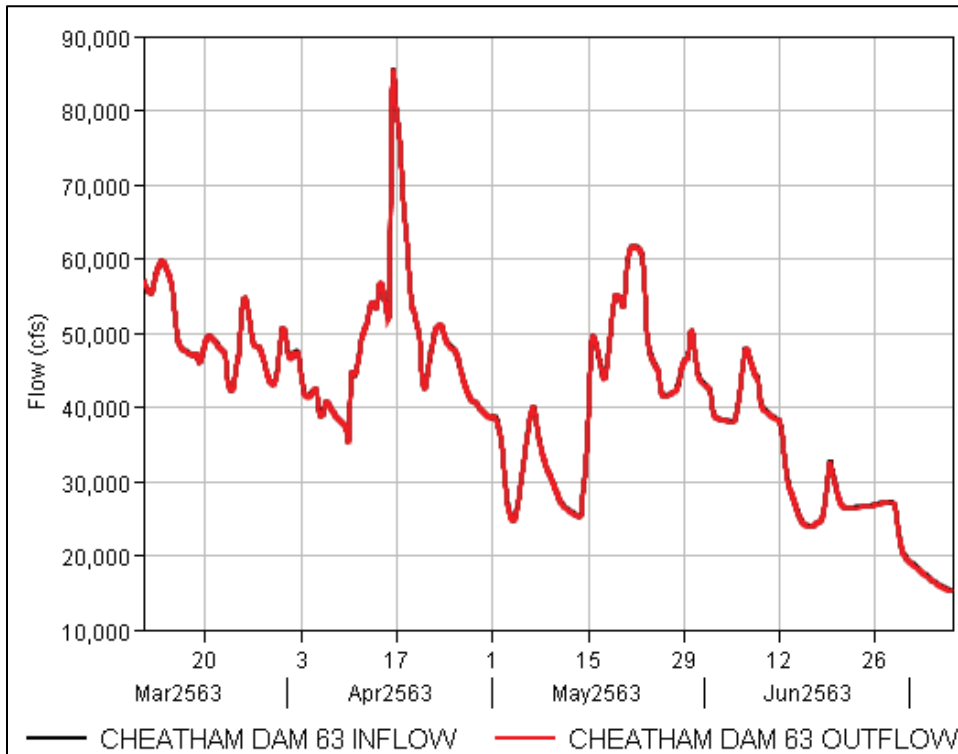


Figure E-68. Cordell Hull Dam HYPO 63 inflow compared to outflow.

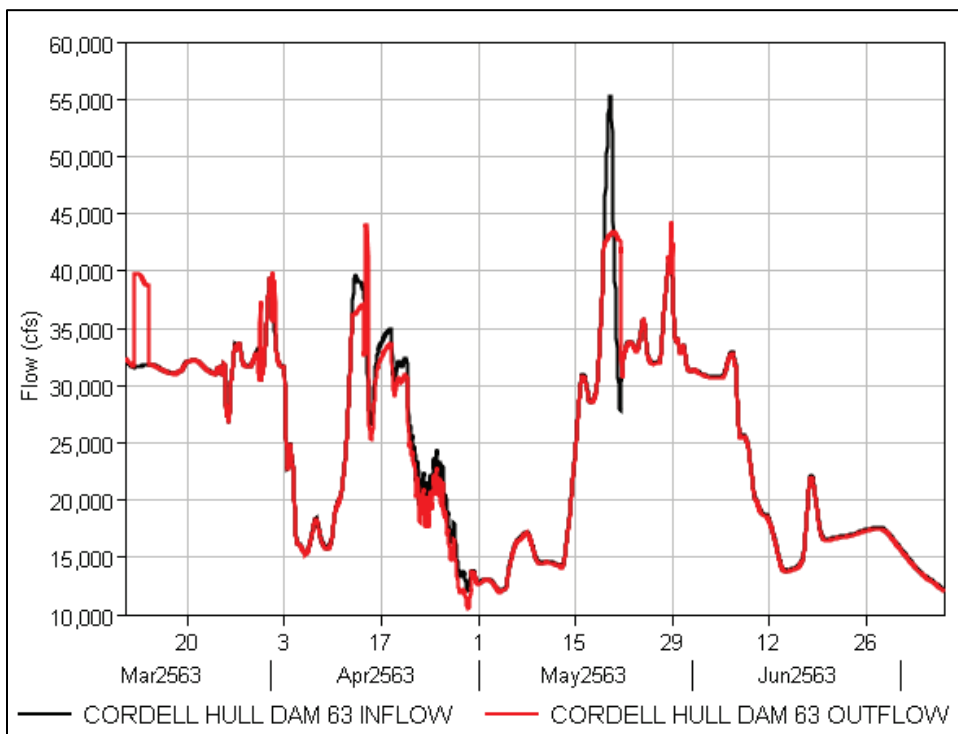


Figure E-69. Dale Hollow Dam HYPO 63 inflow compared to outflow.

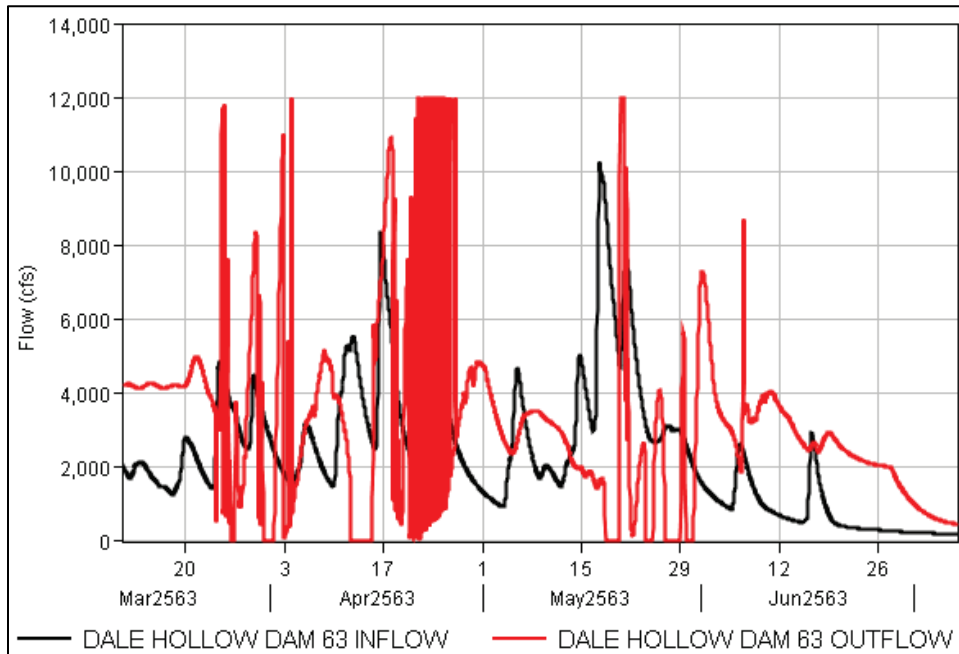


Figure E-70. Great Falls HYPO 63 inflow compared to outflow.

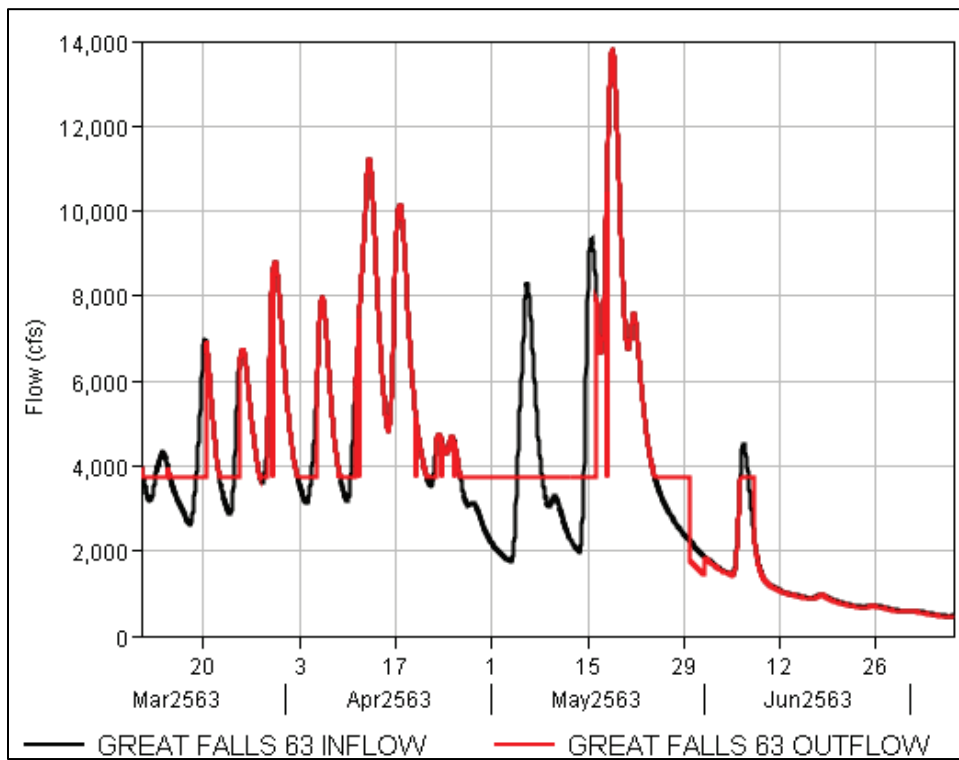


Figure E-71. Barkley Dam HYPO 63 inflow compared to outflow.

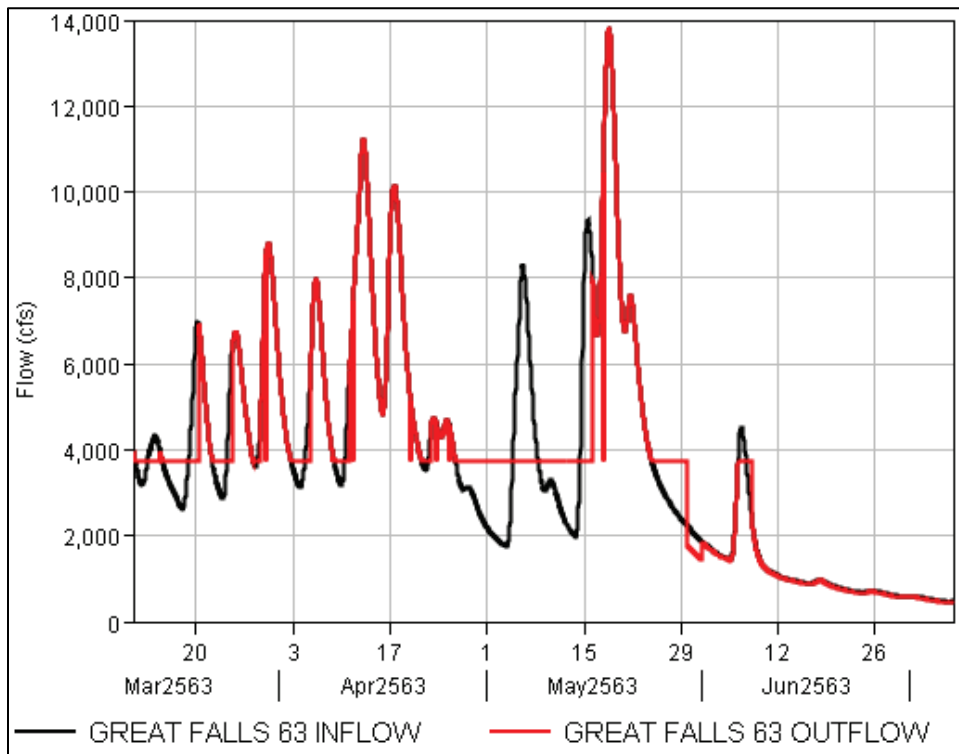


Figure E-72. J. Percy Priest Dam HYPO 63 inflow compared to outflow.

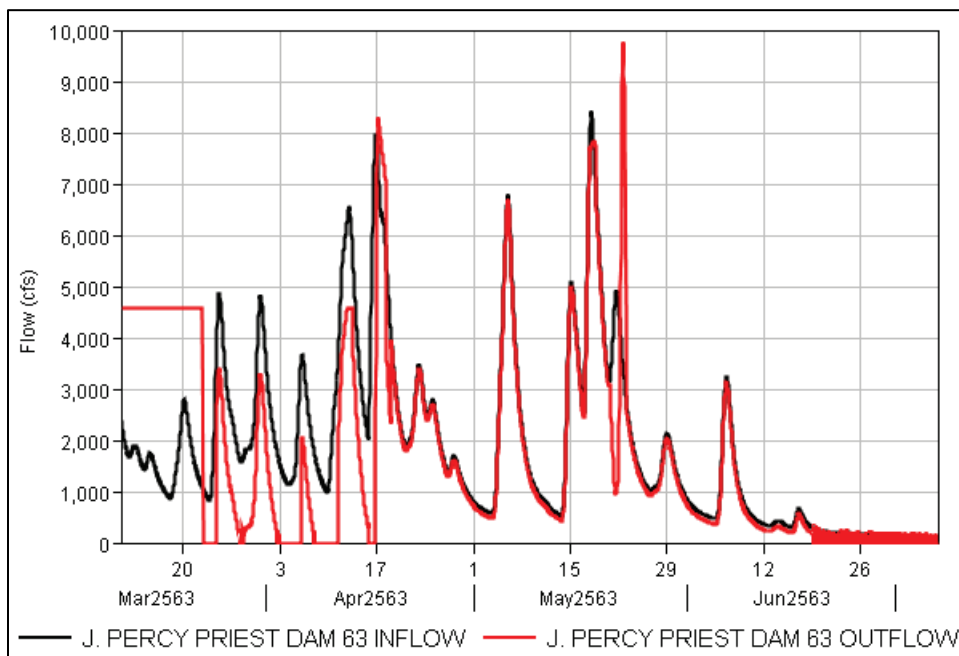


Figure E-73. Kentucky Dam HYPO 63 inflow compared to outflow.

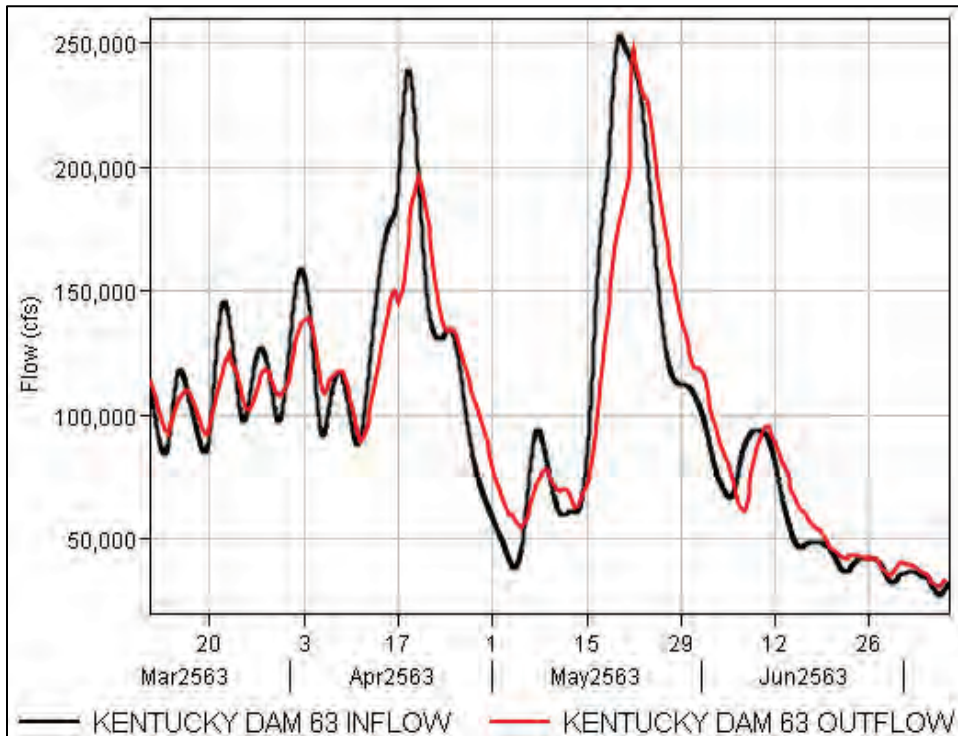


Figure E-74. Old Hickory Dam HYPO 63 inflow compared to outflow.

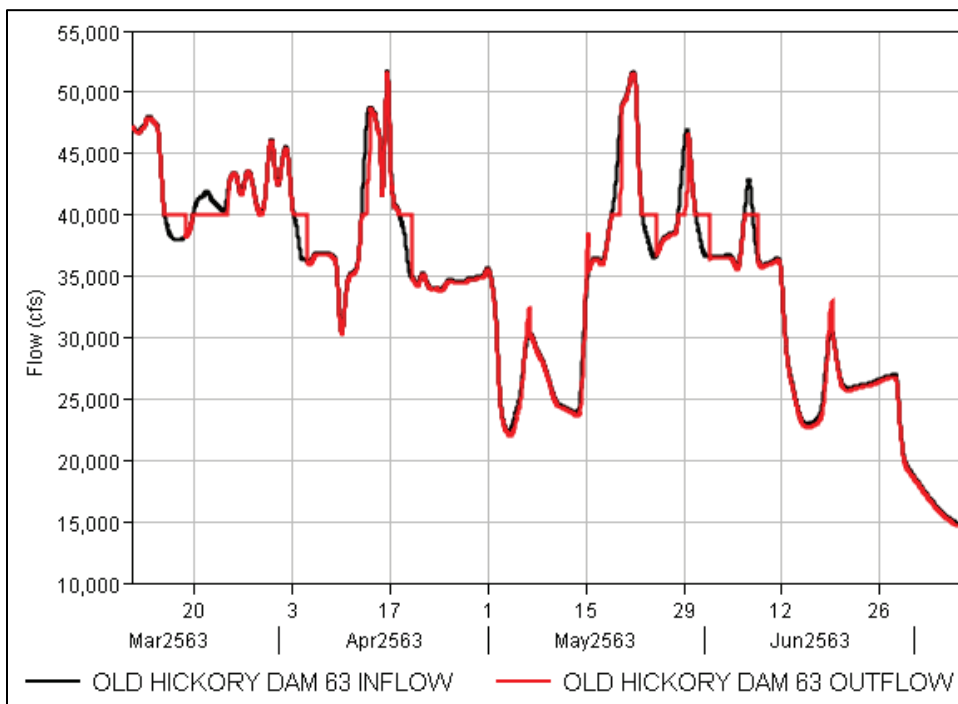
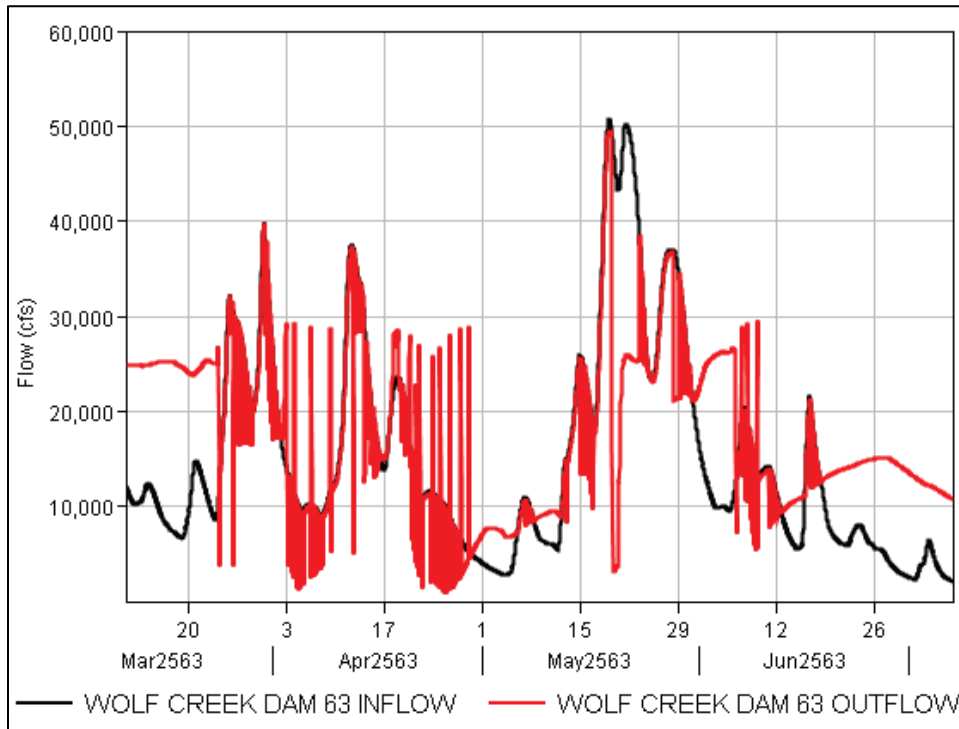


Figure E-75. Wolf Creek Dam HYPO 63 inflow compared to outflow.



E.4.3 MVK reservoir hydrographs

Figure E-76. Arkabutla Dam HYPO 63 inflow compared to outflow.

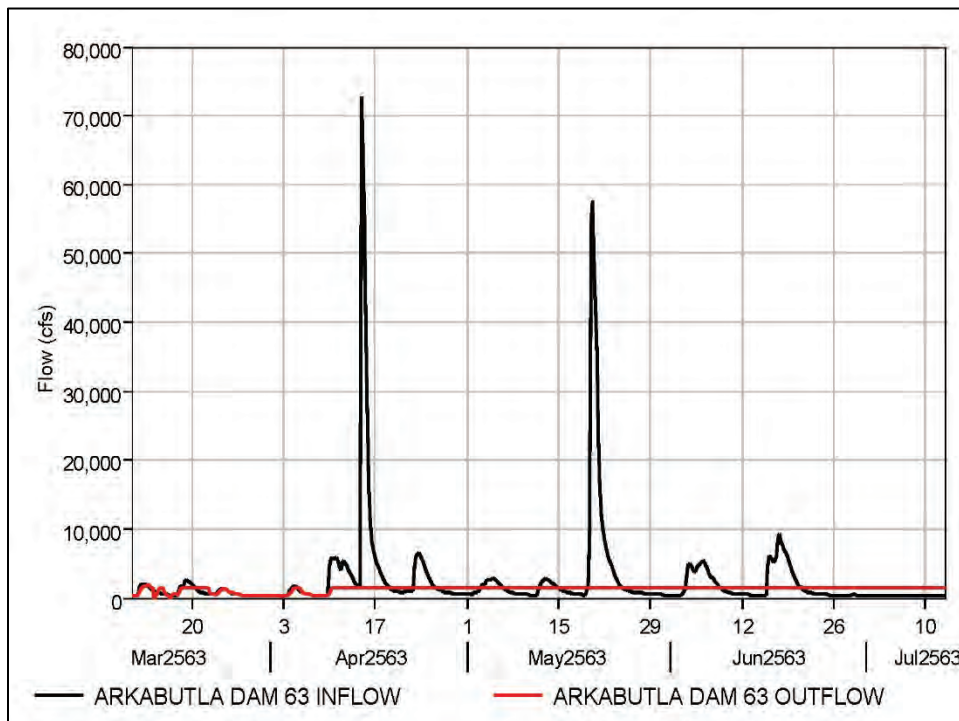


Figure E-77. Bayou Bodcau Dam HYPO 63 inflow compared to outflow.

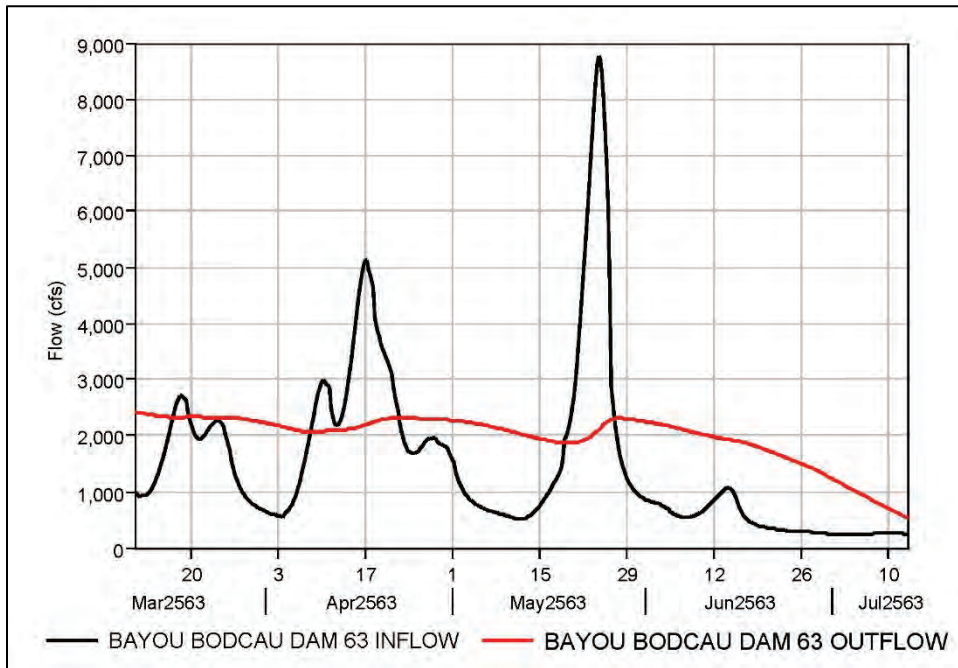


Figure E-78. Blakely Mountain Dam HYPO 63 inflow compared to outflow.

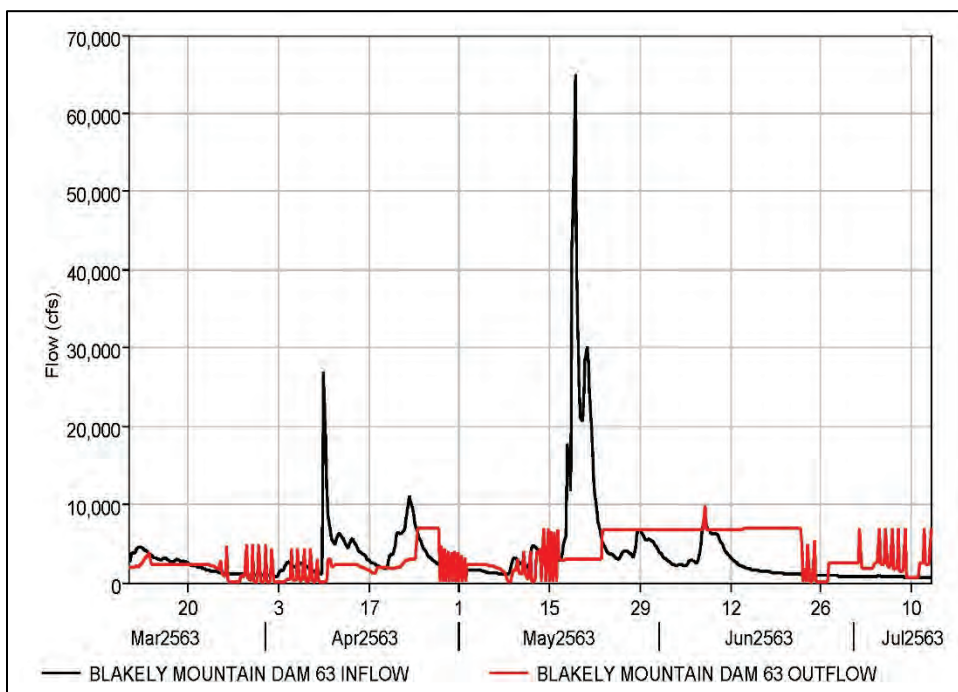


Figure E-79. Caddo Dam HYPO 63 inflow compared to outflow.

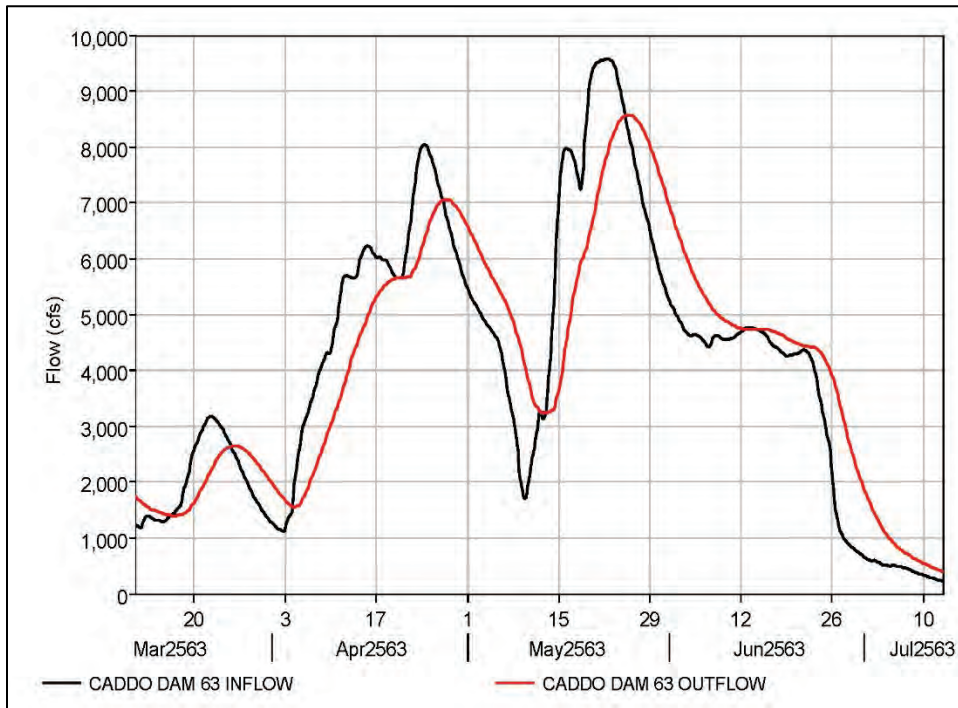


Figure E-80. Degray Dam HYPO 63 inflow compared to outflow.

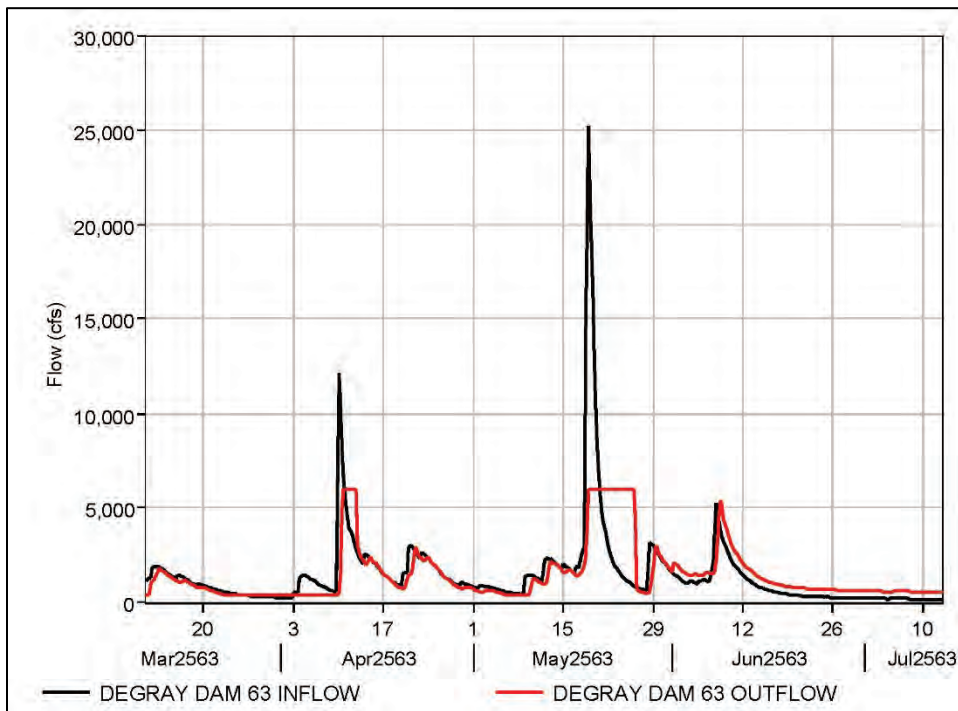


Figure E-81. Enid Dam HYPO 63 inflow compared to outflow.

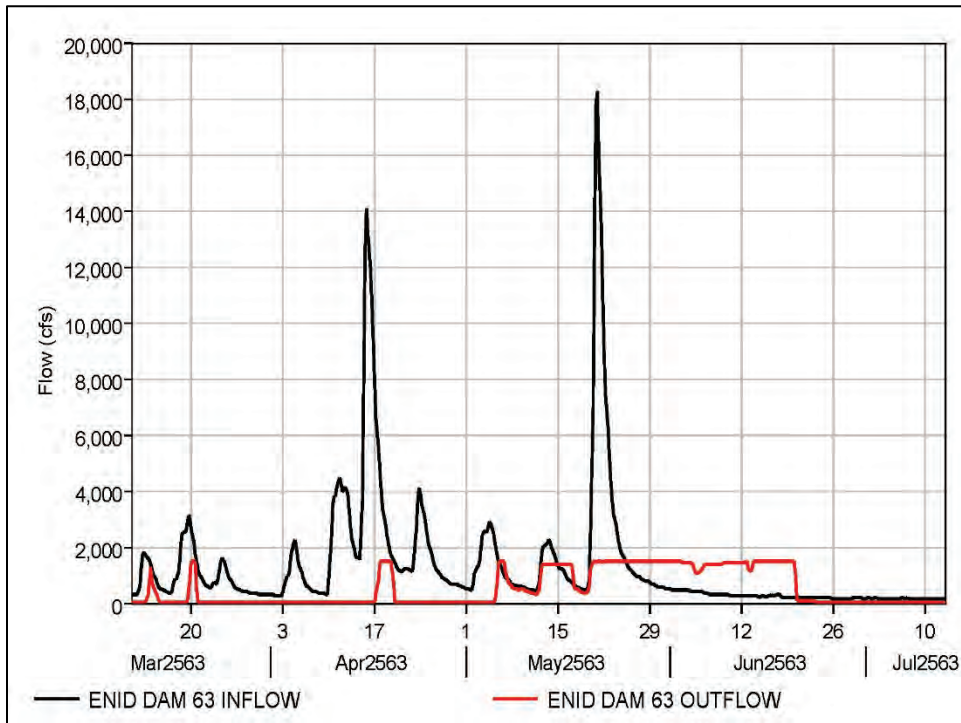


Figure E-82. Grenada Dam HYPO 63 inflow compared to outflow.

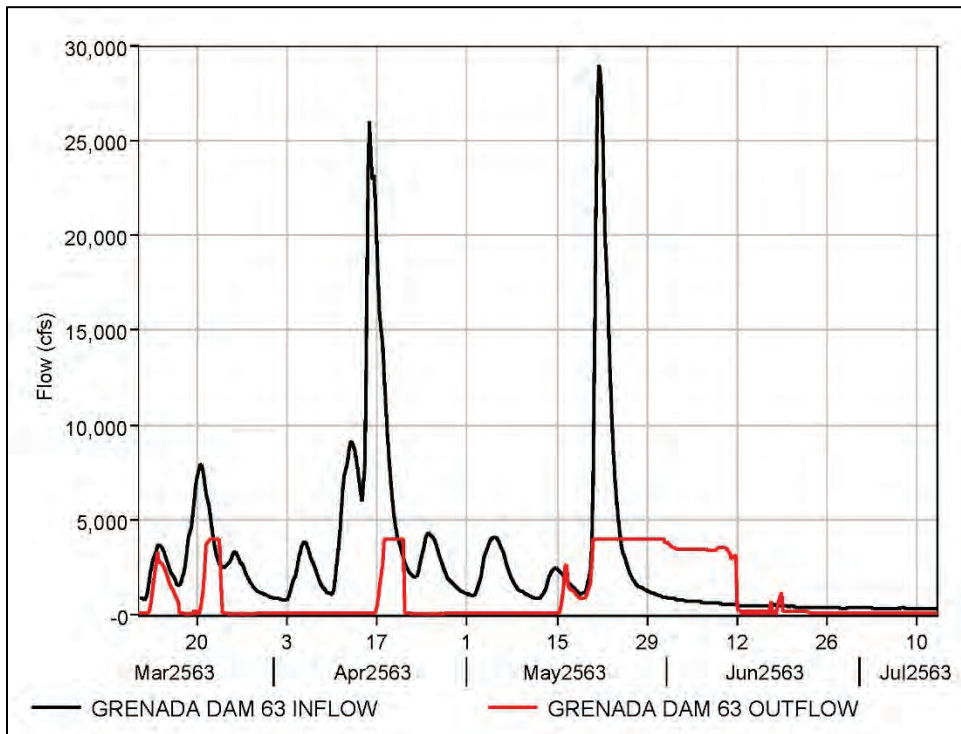


Figure E-83. Narrows Dam HYPO 63 inflow compared to outflow.

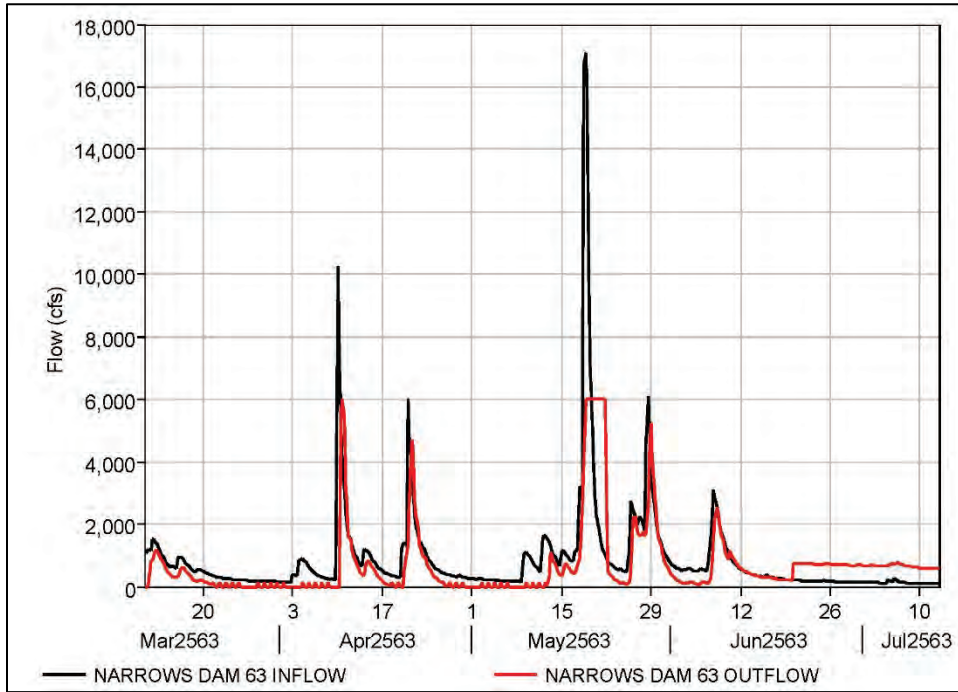


Figure E-84. Sardis Dam HYPO 63 inflow compared to outflow.

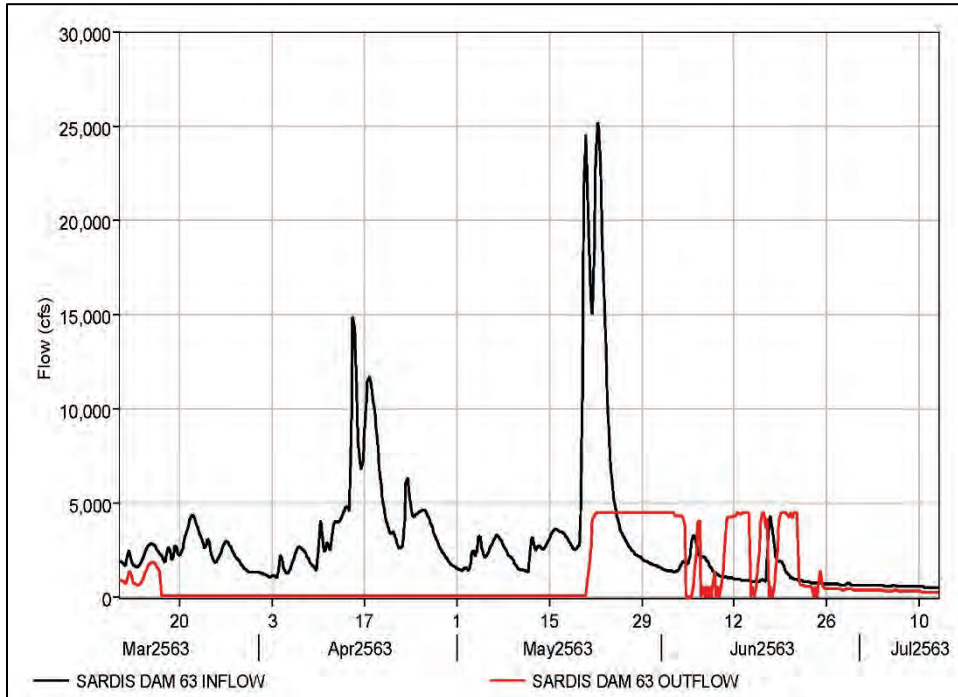
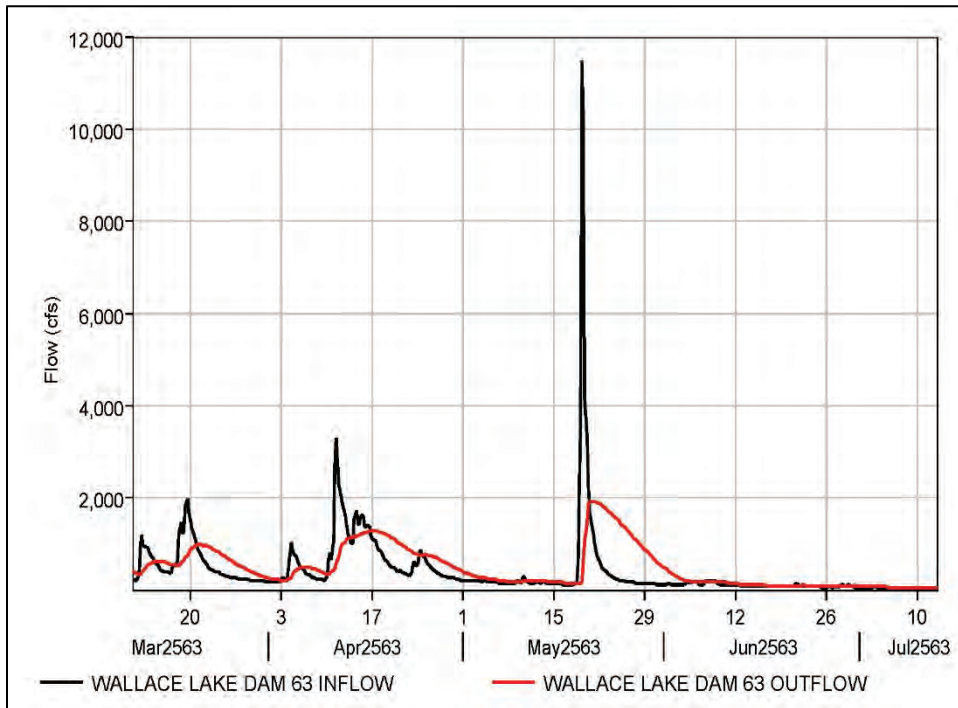


Figure E-85. Wallace Lake Dam HYPO 63 inflow compared to outflow.



E.4.4 MVS reservoir hydrographs

Figure E-86. Carlyle Lake Dam HYPO 63 inflow compared to outflow.

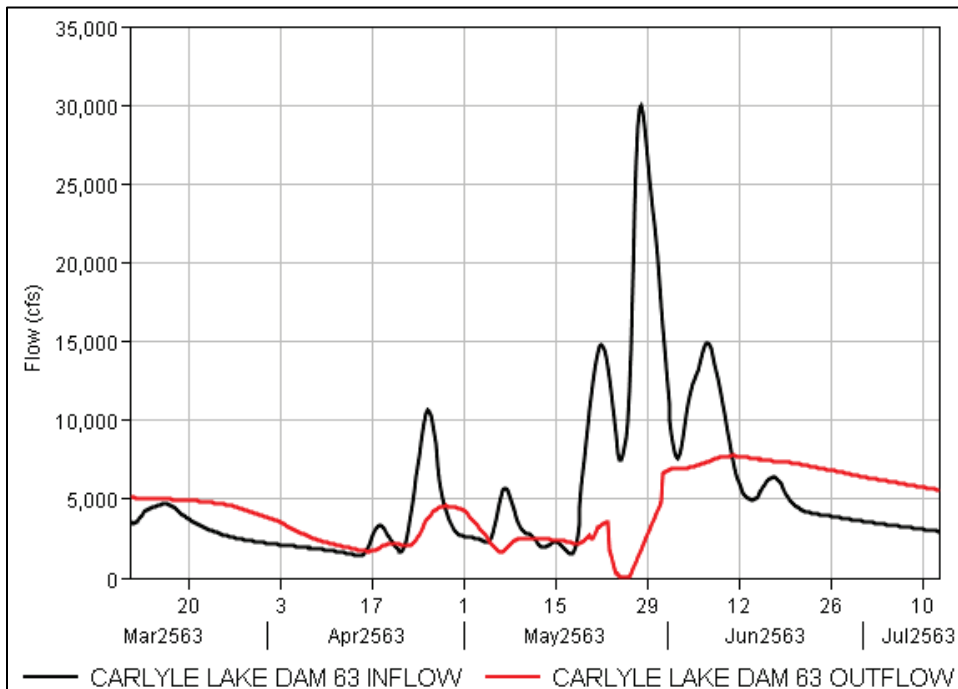


Figure E-87. Lake Shelbyville Dam HYPO 63 inflow compared to outflow.

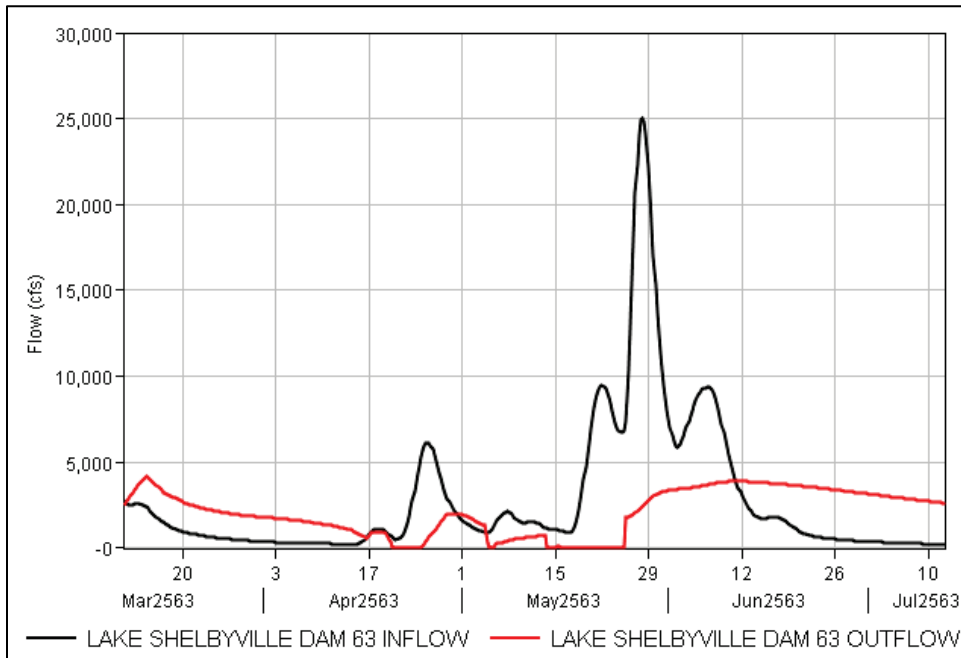


Figure E-88. Mark Twain Lake HYPO 63 inflow compared to outflow.

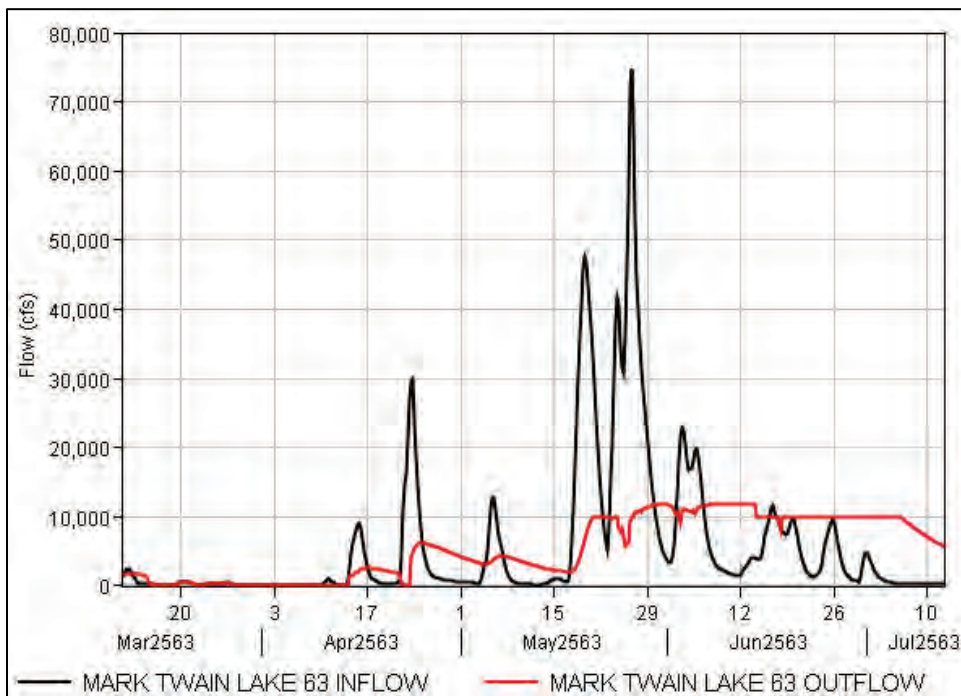
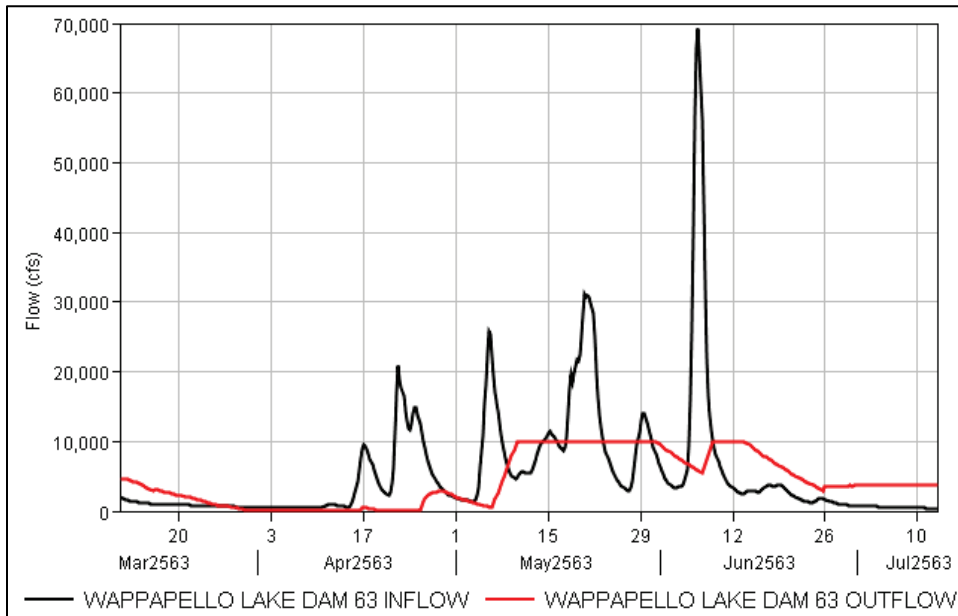


Figure E-89. Wappapello Lake Dam HYPO 63 inflow compared to outflow.



E.4.5 NWD Missouri River reservoir hydrographs

Figure E-90. Big Bend Dam HYPO 63 inflow compared to outflow.

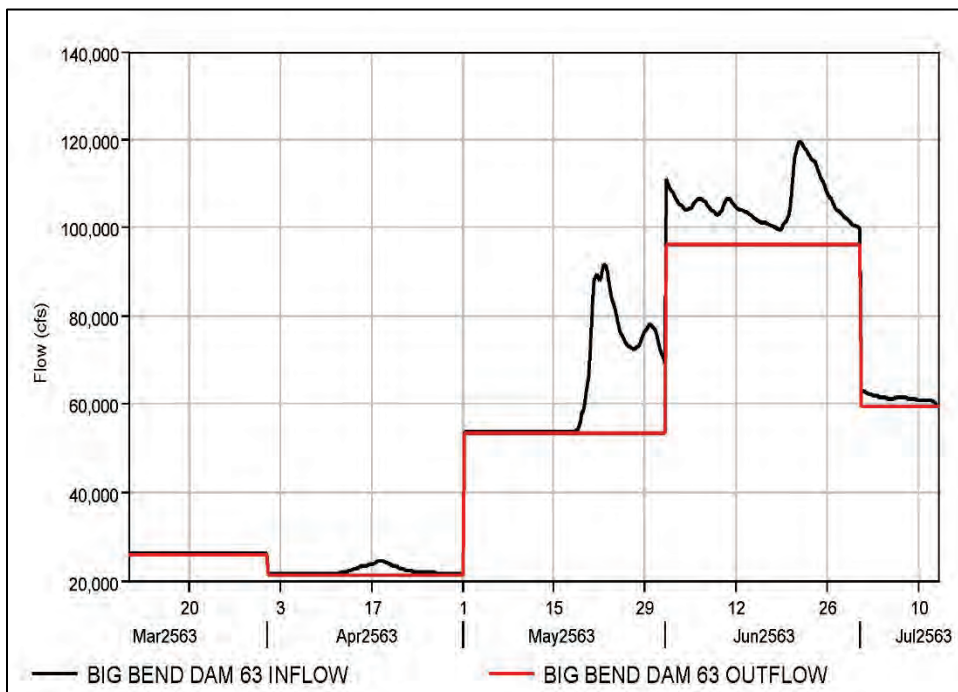


Figure E-91. Fort Peck Dam HYPO 63 inflow compared to outflow.

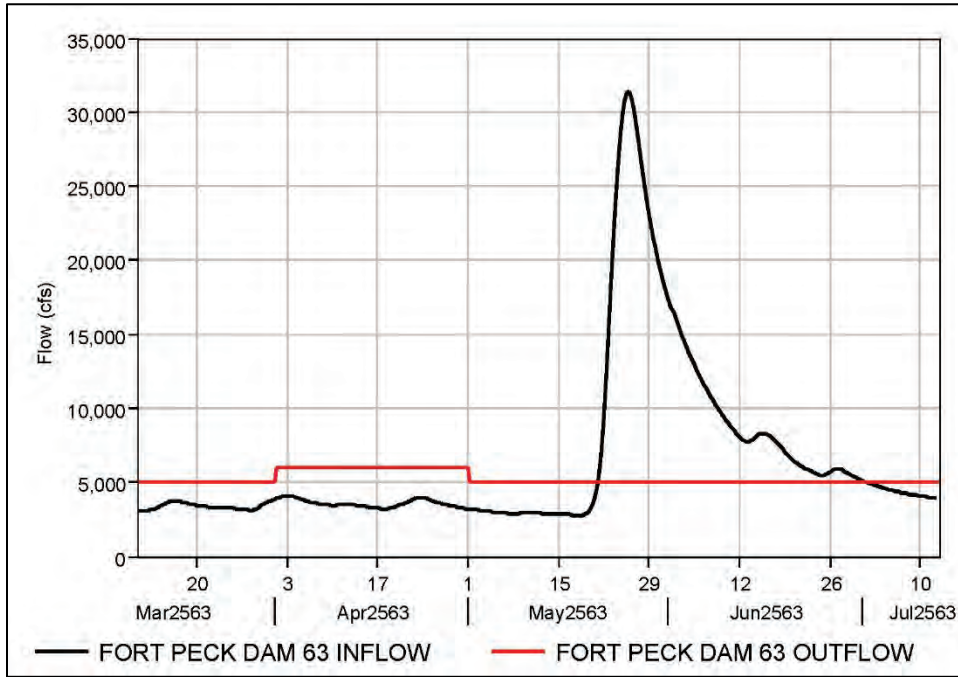


Figure E-92. Fort Randall Dam HYPO 63 inflow compared to outflow.

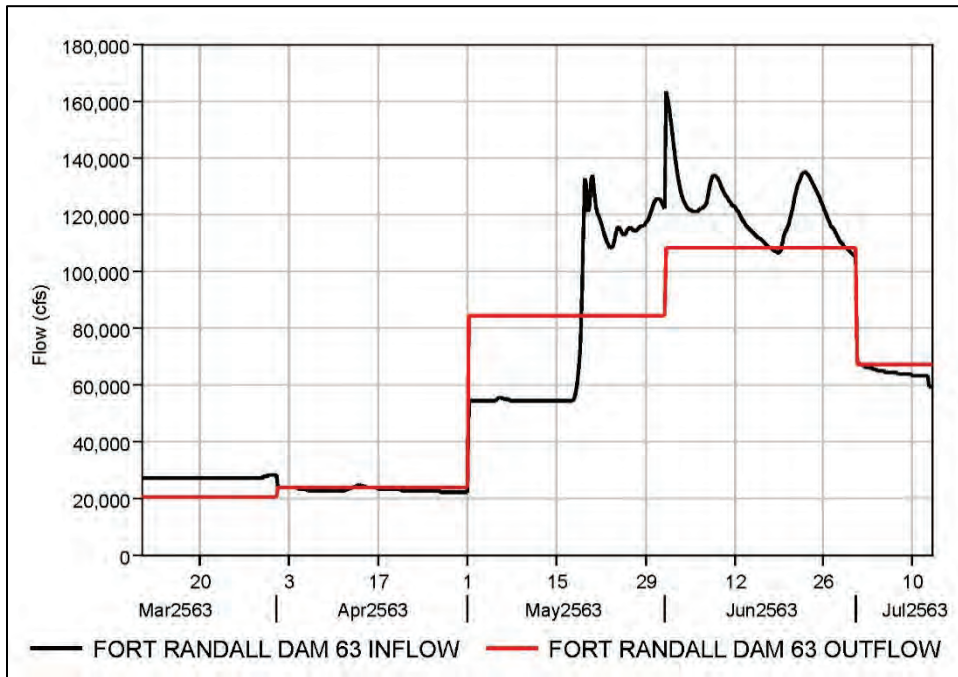


Figure E-93. Garrison Dam HYPO 63 inflow compared to outflow.

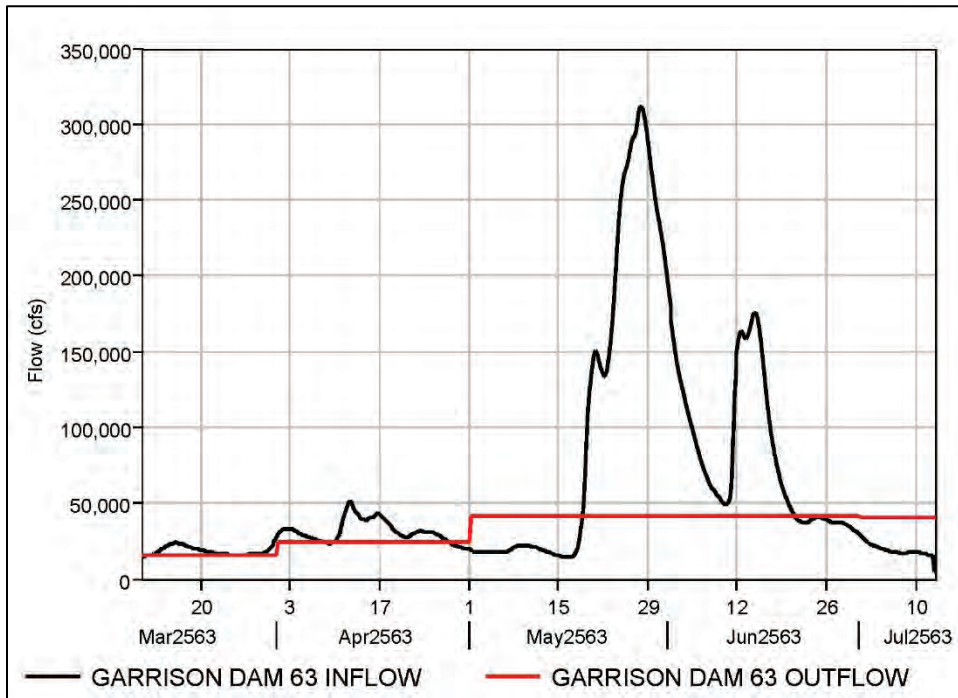


Figure E-94. Gavin's Point Dam HYPO 63 inflow compared to outflow.

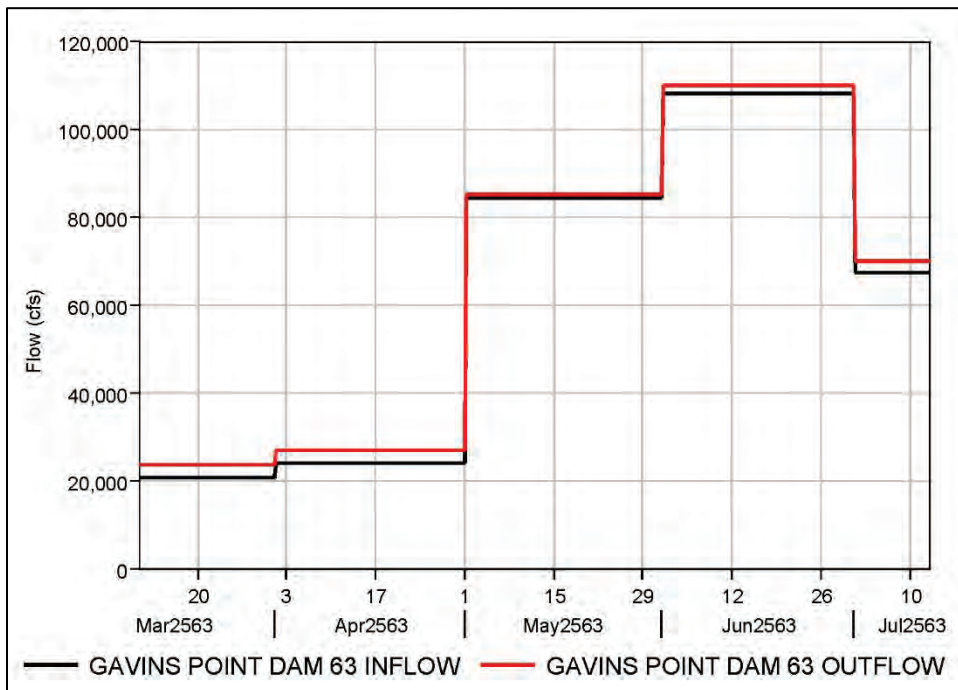
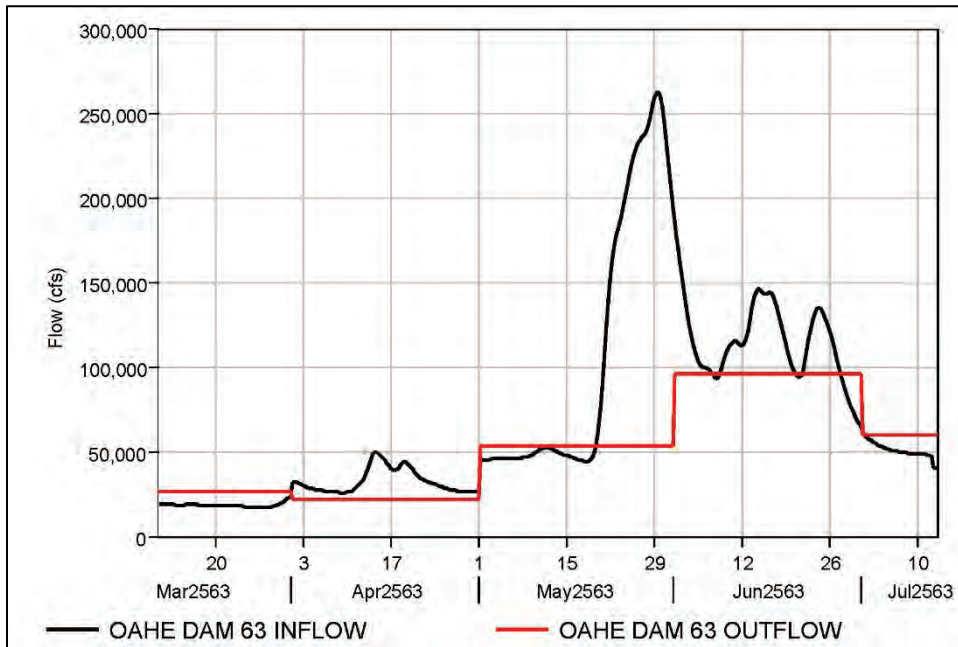


Figure E-95. Oahe Dam HYPO 63 inflow compared to outflow.



E.4.6 NWK reservoir hydrographs

Figure E-96. Clinton Dam HYPO 63 inflow compared to outflow.

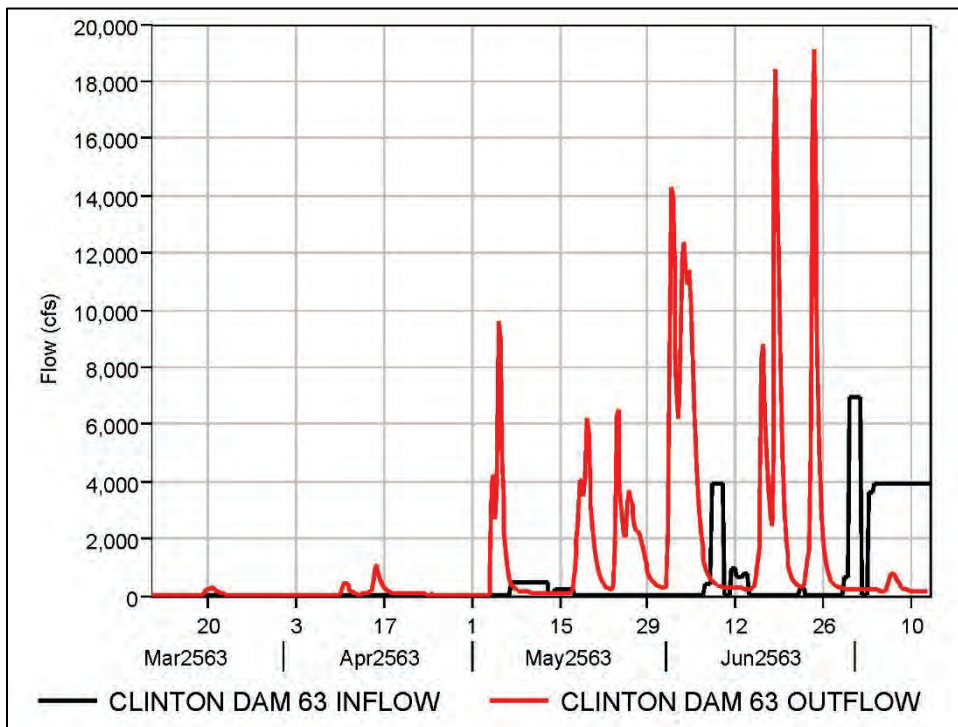


Figure E-97. Glen Elder Dam HYPO 63 inflow compared to outflow.

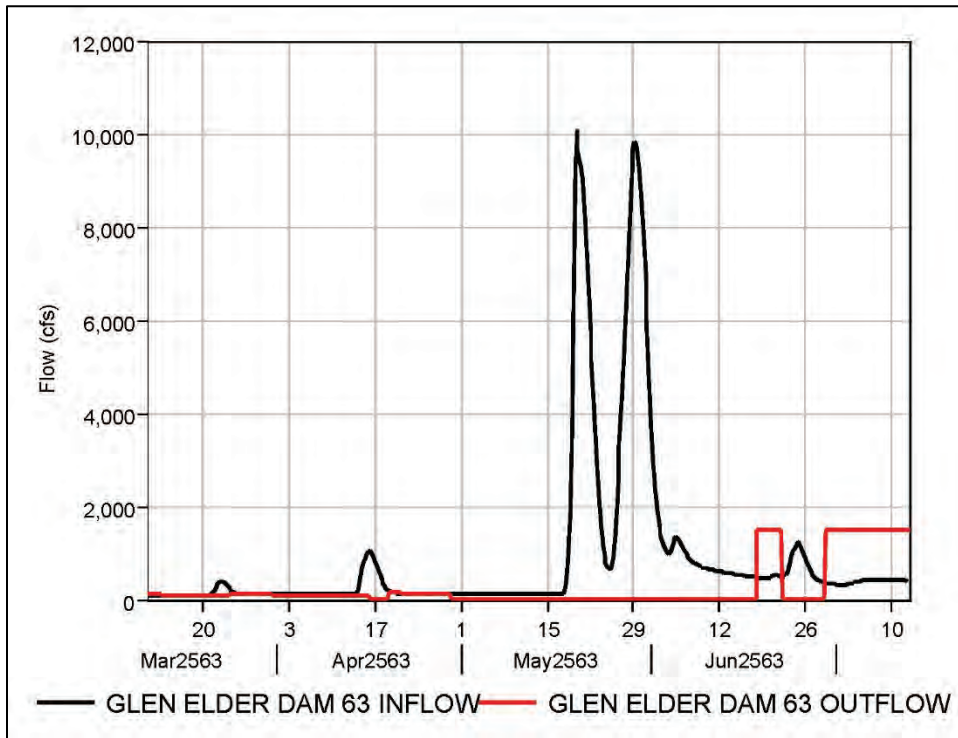


Figure E-98. Hillsdale Dam HYPO 63 inflow compared to outflow.

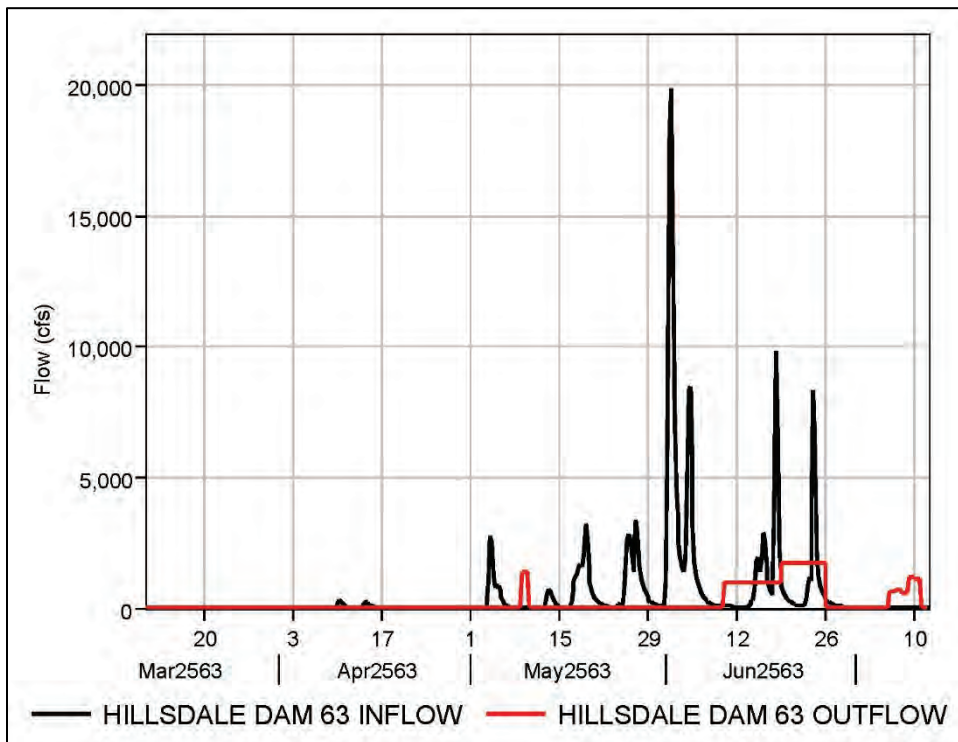


Figure E-99. Kanopolis Dam HYPO 63 inflow compared to outflow.

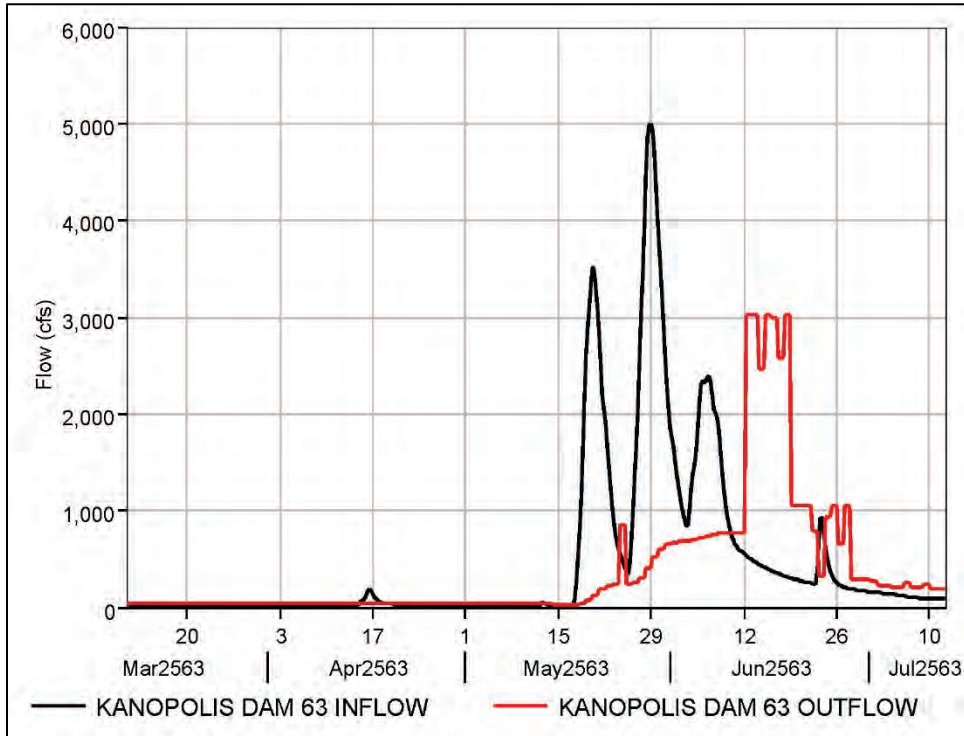


Figure E-100. Melvern Dam HYPO 63 inflow compared to outflow.

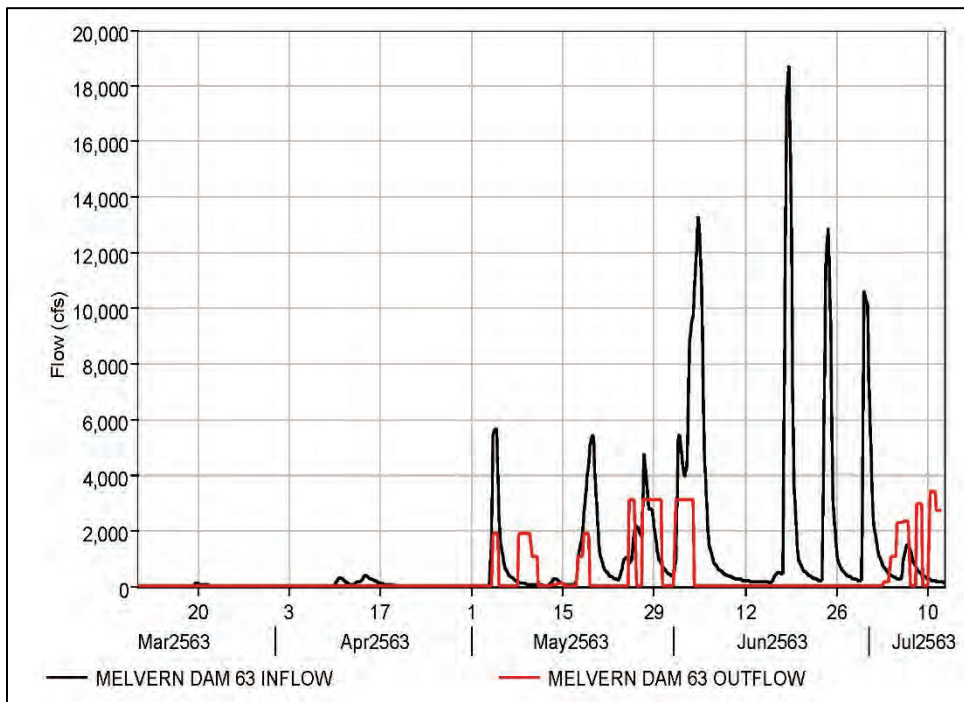


Figure E-101. Milford Dam HYPO 63 inflow compared to outflow.

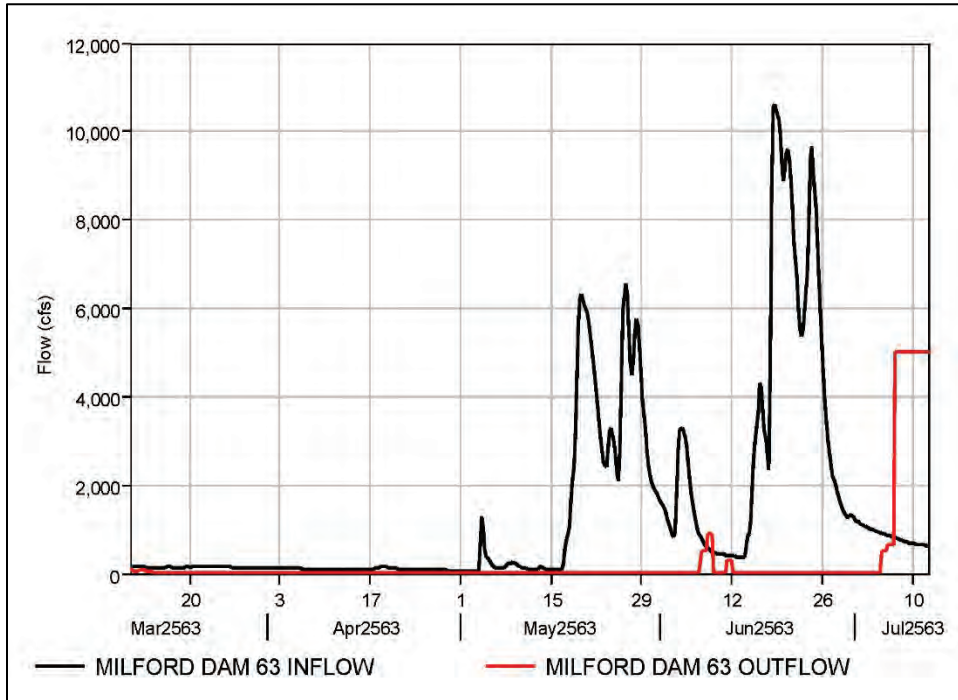


Figure E-102. Perry Dam HYPO 63 inflow compared to outflow.

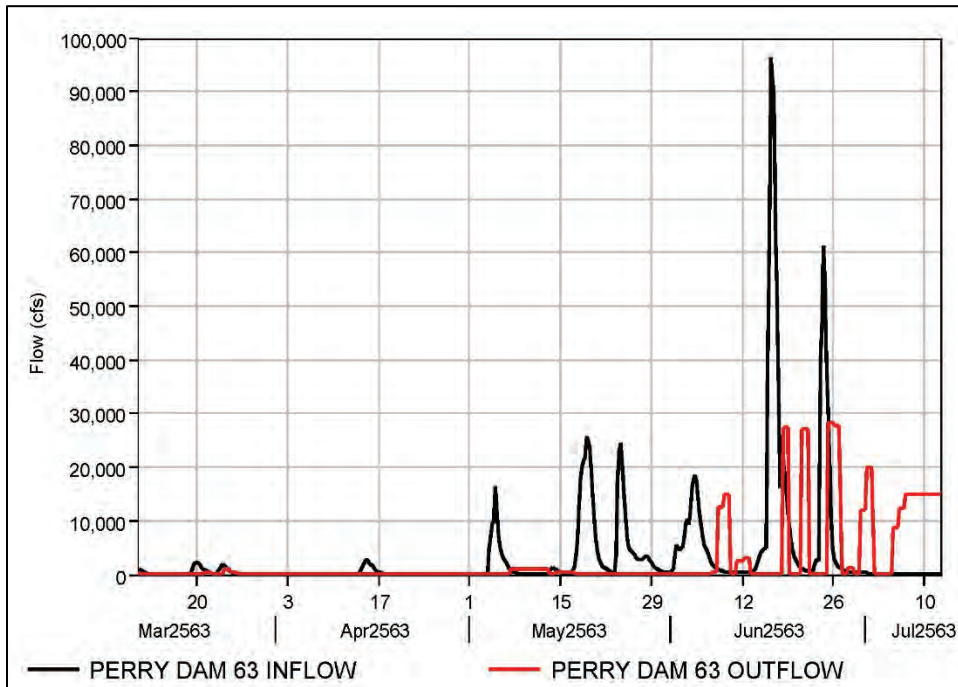


Figure E-103. Pomme De Terre Dam HYPO 63 inflow compared to outflow.

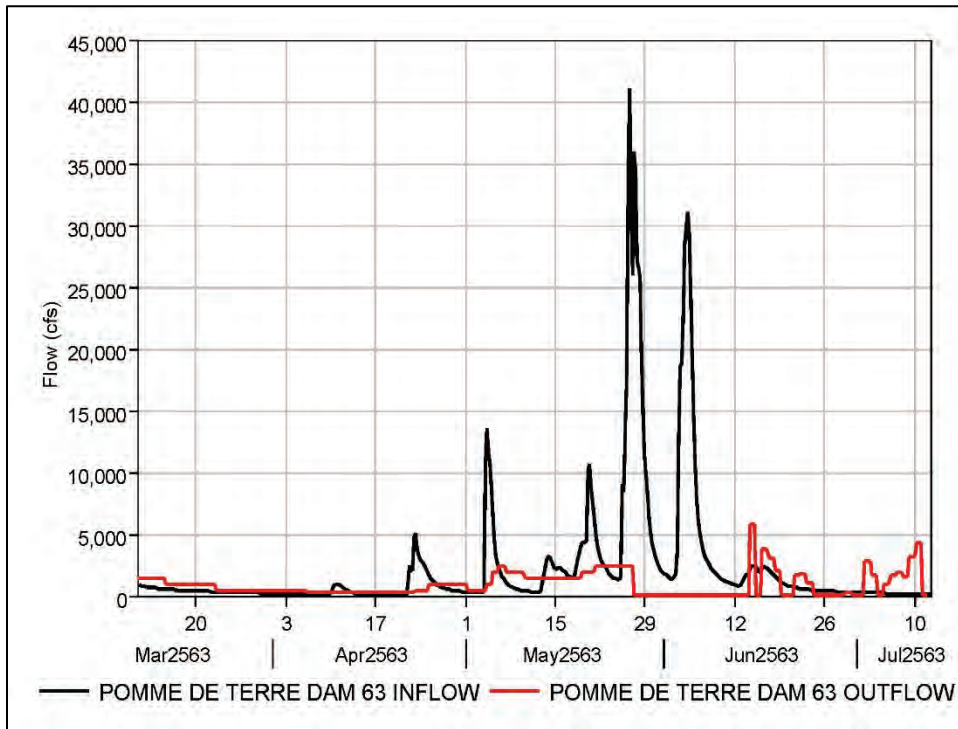


Figure E-104. Pomona Dam HYPO 63 inflow compared to outflow.

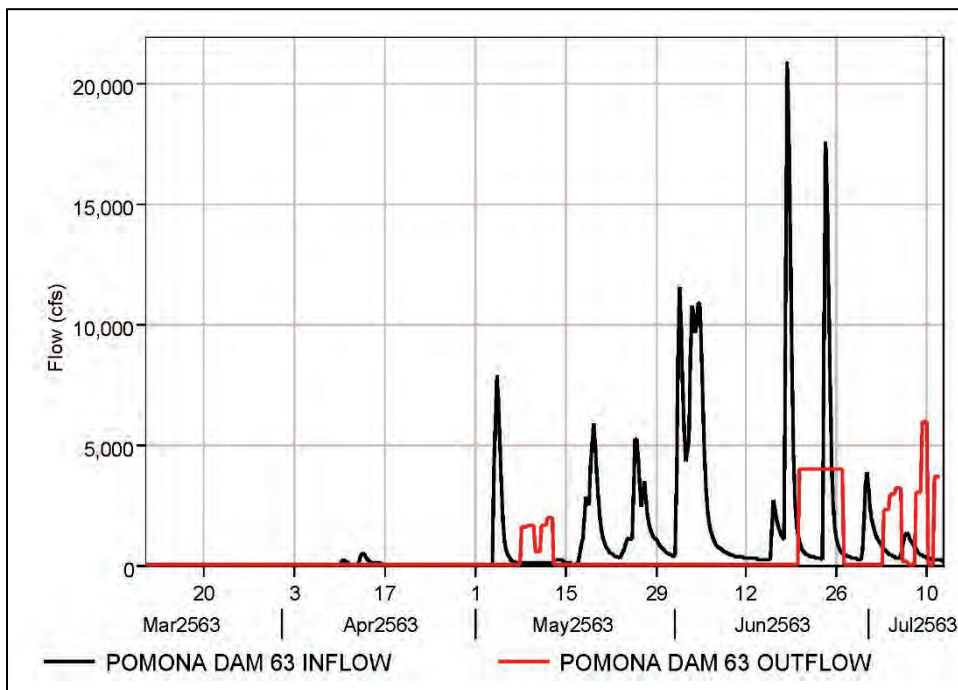


Figure E-105. Rathbun Dam HYPO 63 inflow compared to outflow.

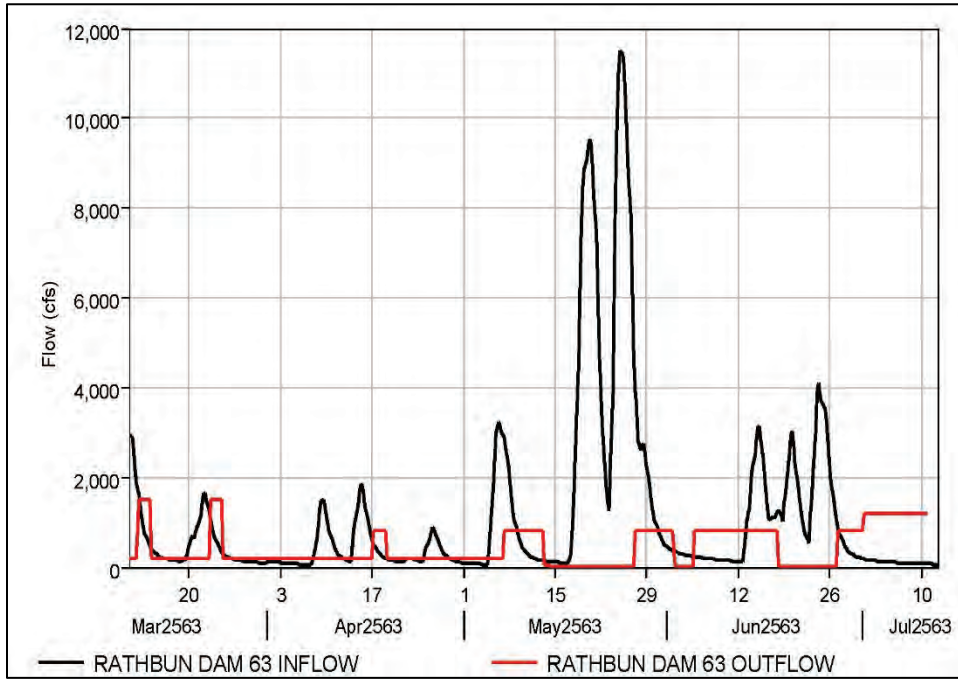


Figure E-106. Smithville Dam HYPO 63 inflow compared to outflow.

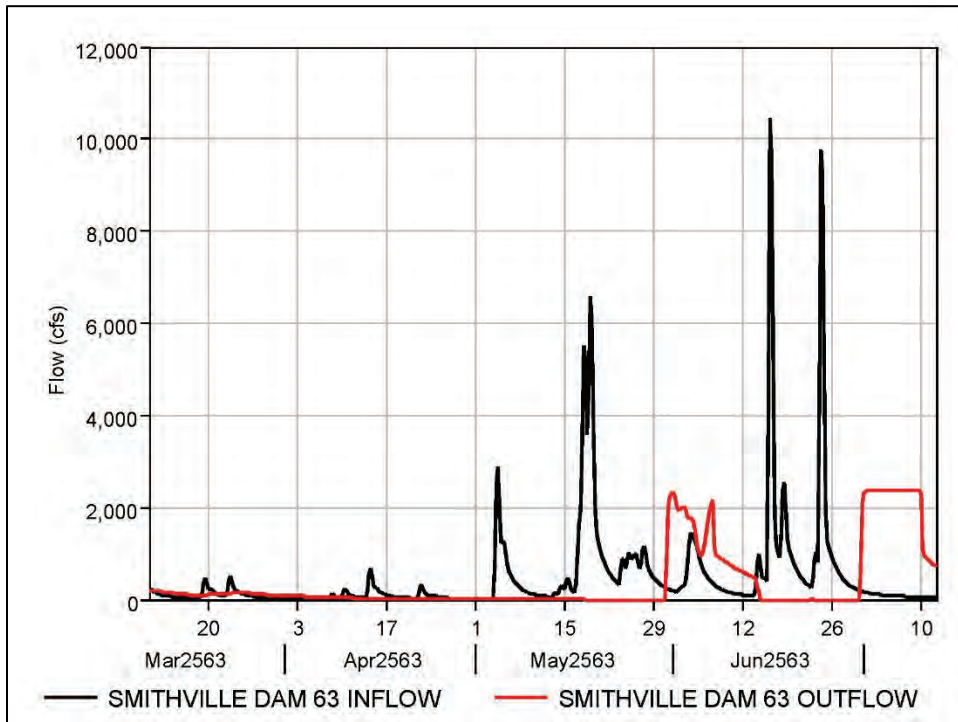


Figure E-107. Stockton Dam HYPO 63 inflow compared to outflow.

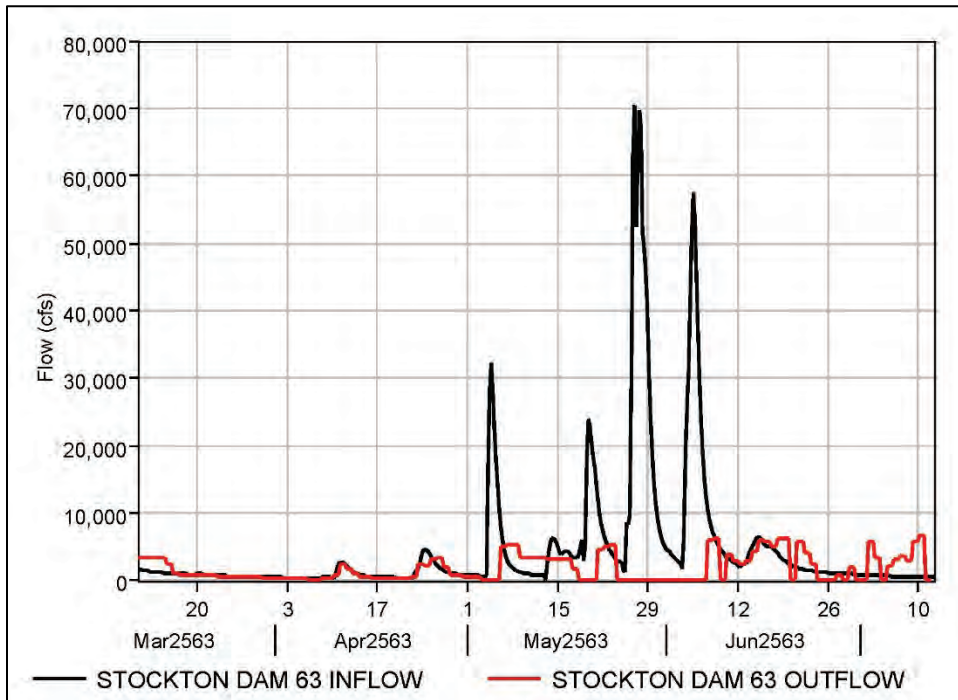


Figure E-108. Truman Dam HYPO 63 inflow compared to outflow.

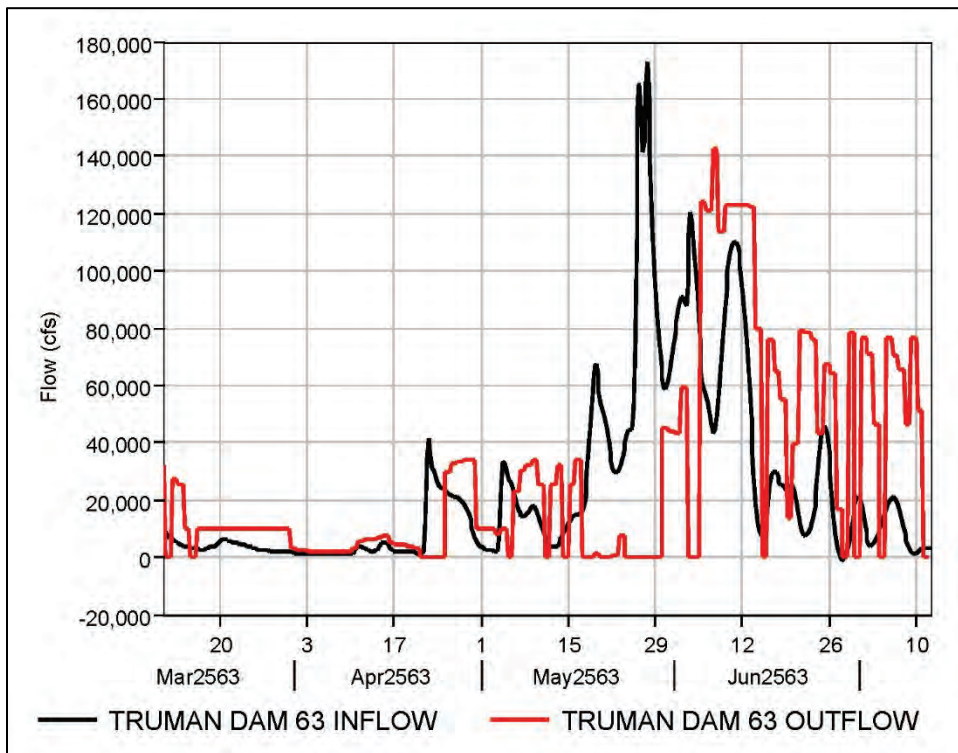


Figure E-109. Tuttle Creek Dam HYPO 63 inflow compared to outflow.

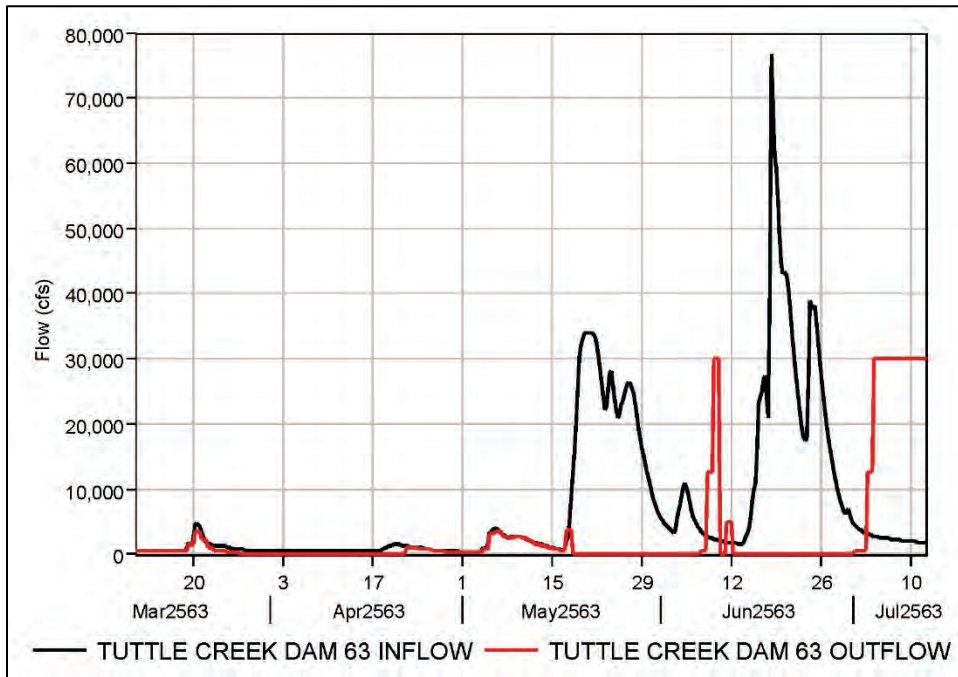
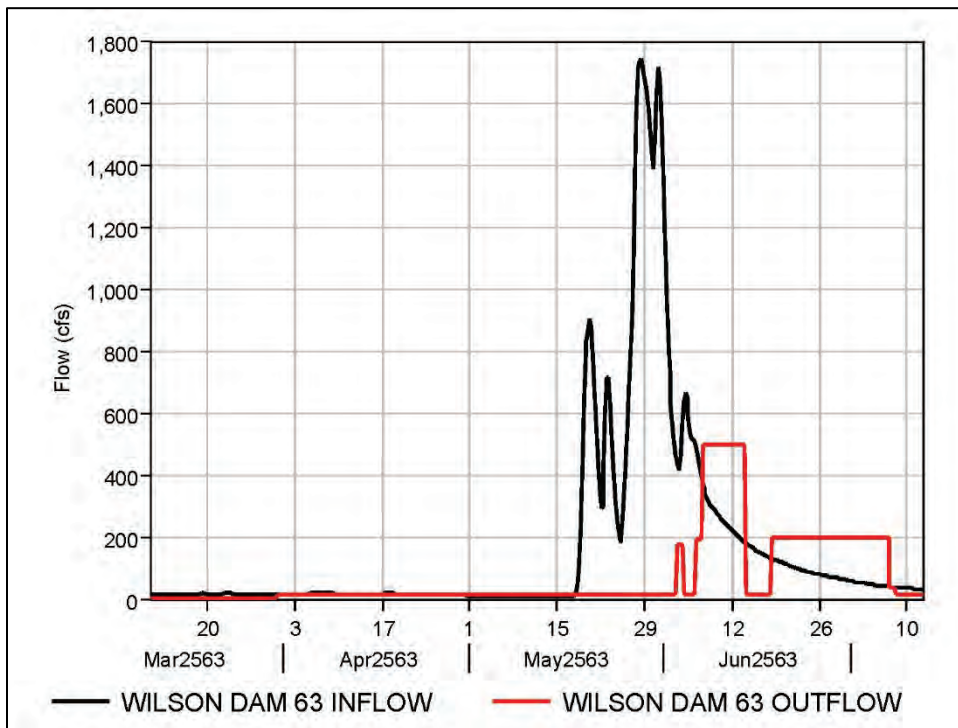


Figure E-110. Wilson Dam HYPO 63 inflow compared to outflow.



E.4.7 SWL reservoir hydrographs

Figure E-111. Bull Shoals Dam HYPO 63 inflow compared to outflow.

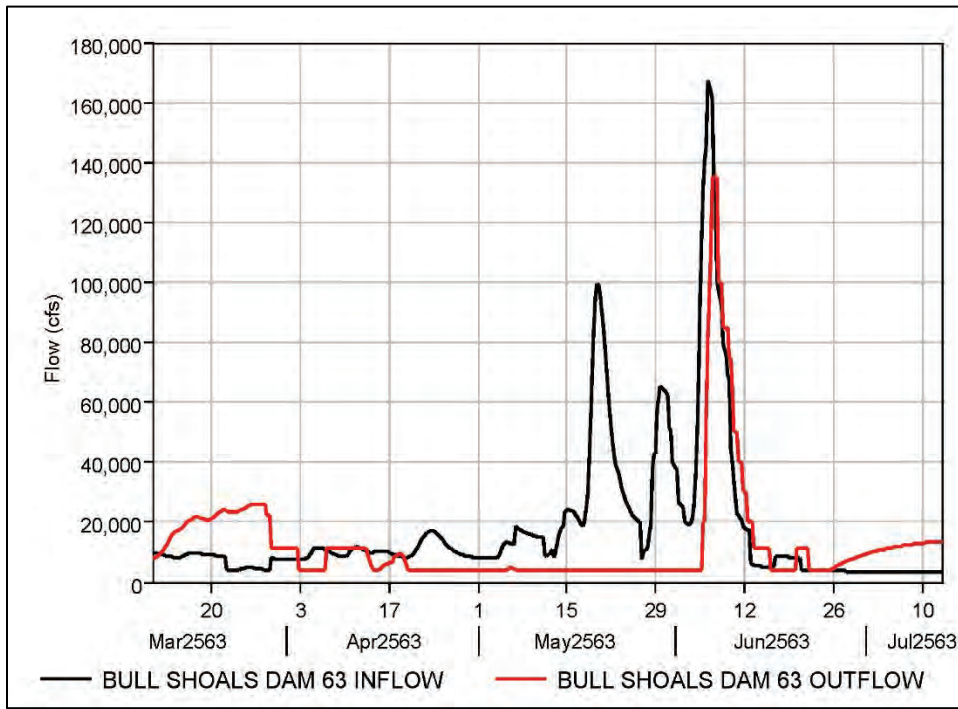


Figure E-112. Greer's Ferry Dam HYPO 63 inflow compared to outflow.

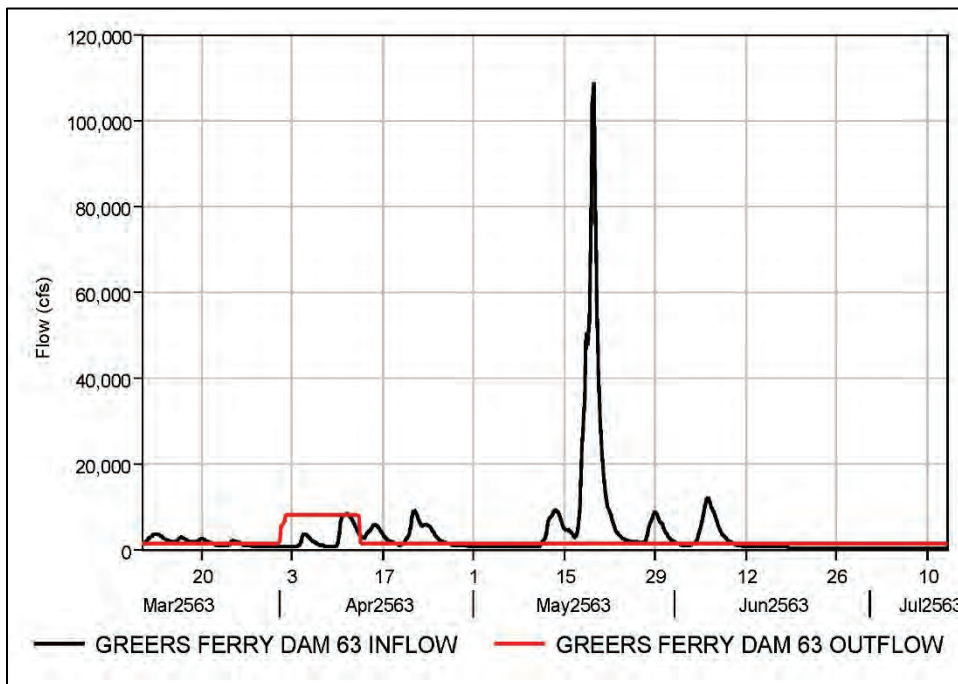
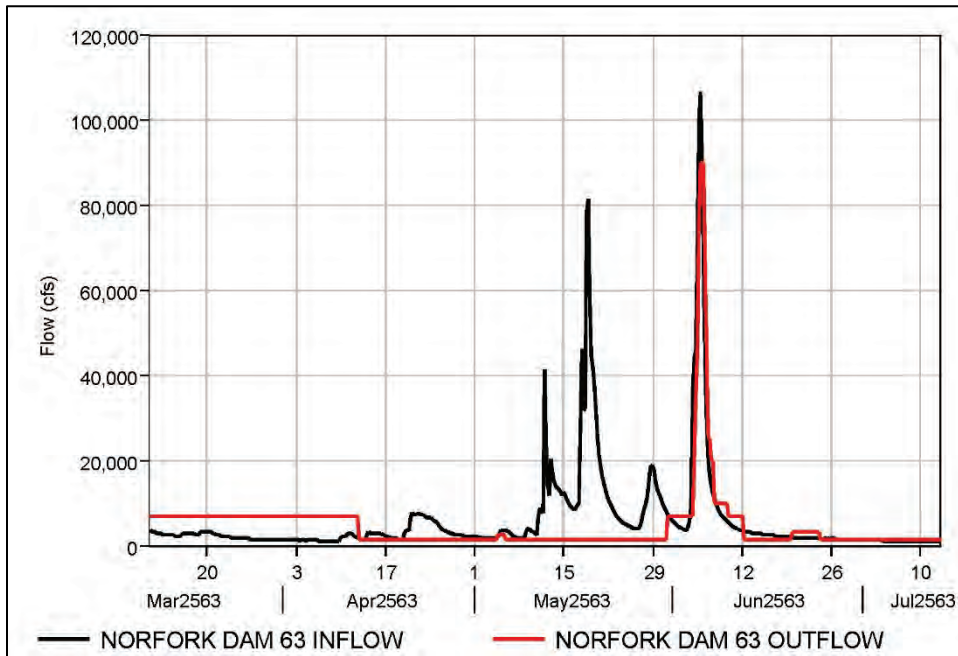


Figure E-113. Norfolk Dam HYPO 63 inflow compared to outflow.



E.4.8 SWT reservoir hydrographs

Figure E-114. Fort Gibson Dam HYPO 63 inflow compared to outflow.

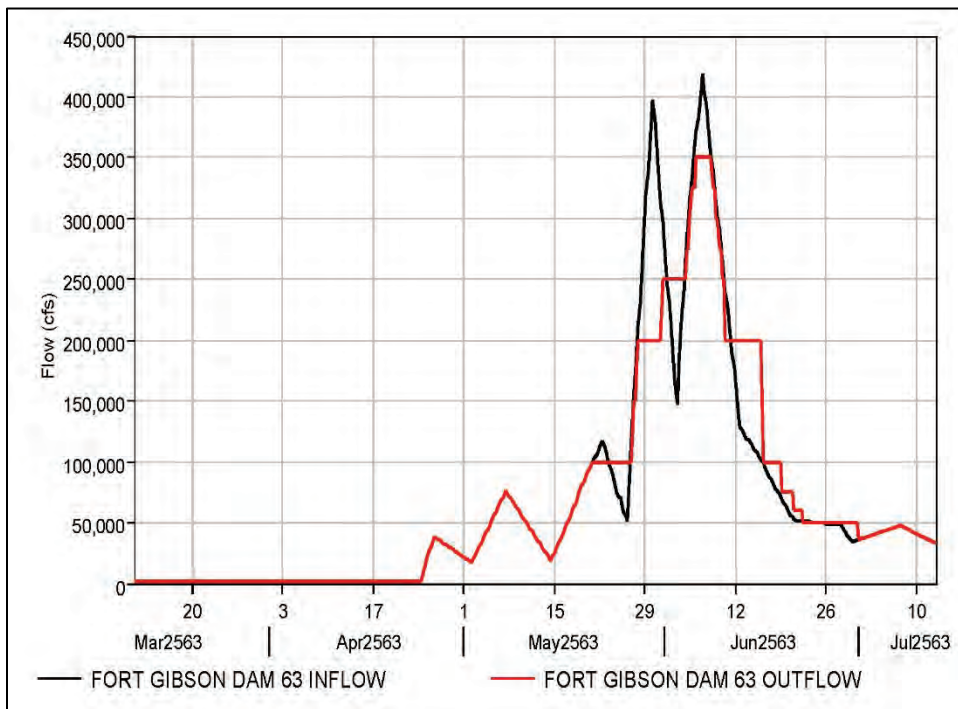


Figure E-115. Hugo Dam HYPO 63 inflow compared to outflow.

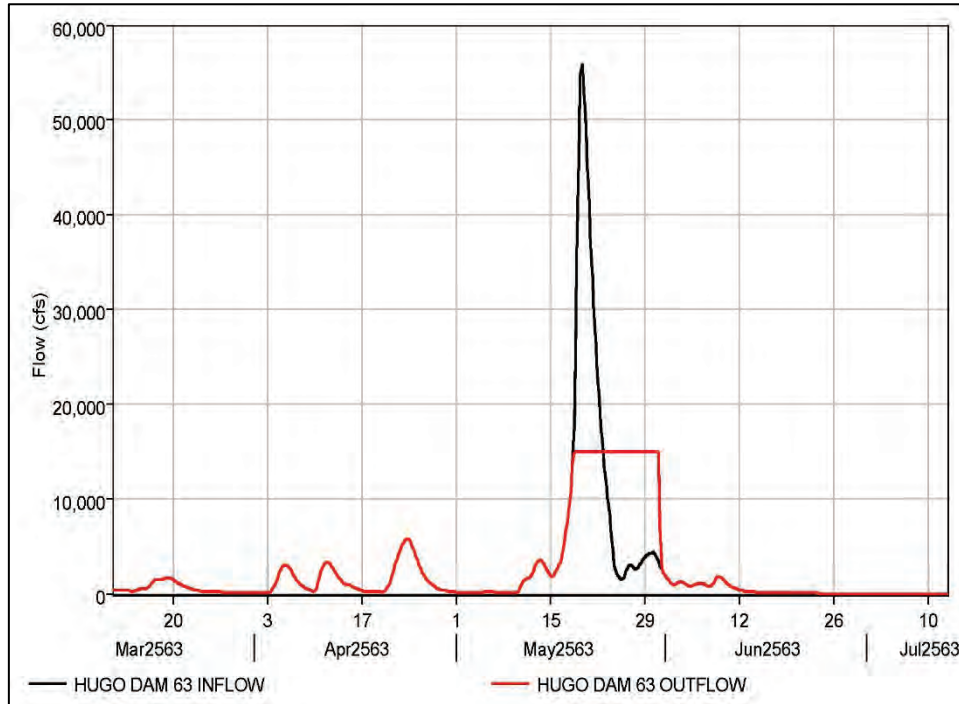


Figure E-116. Keystone Lake HYPO 63 inflow compared to outflow.

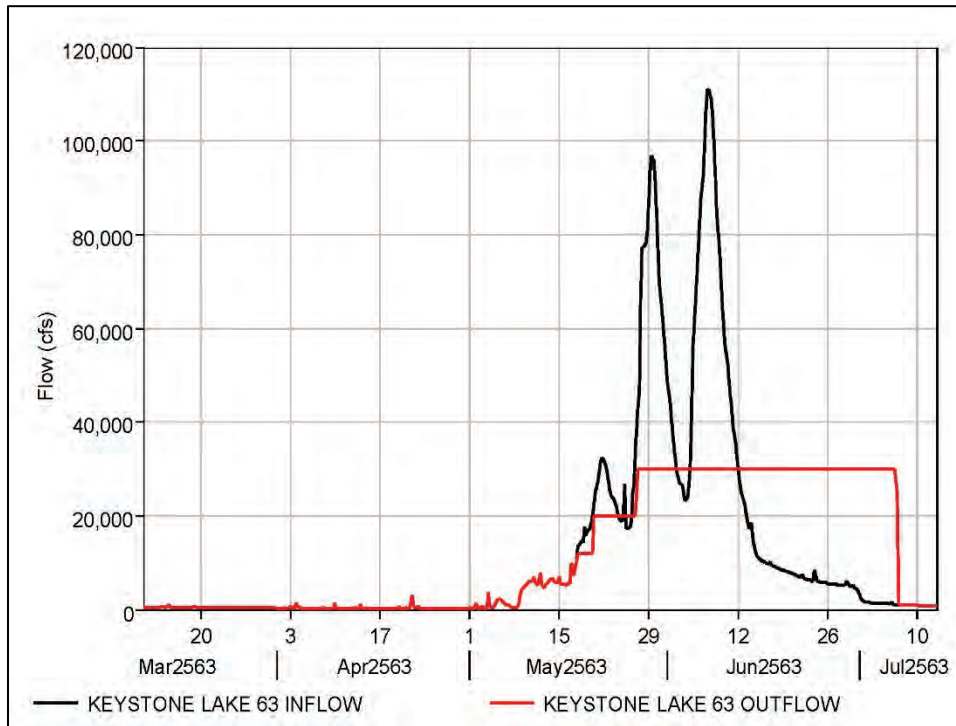


Figure E-117. Lake Texoma HYPO 63 inflow compared to outflow.

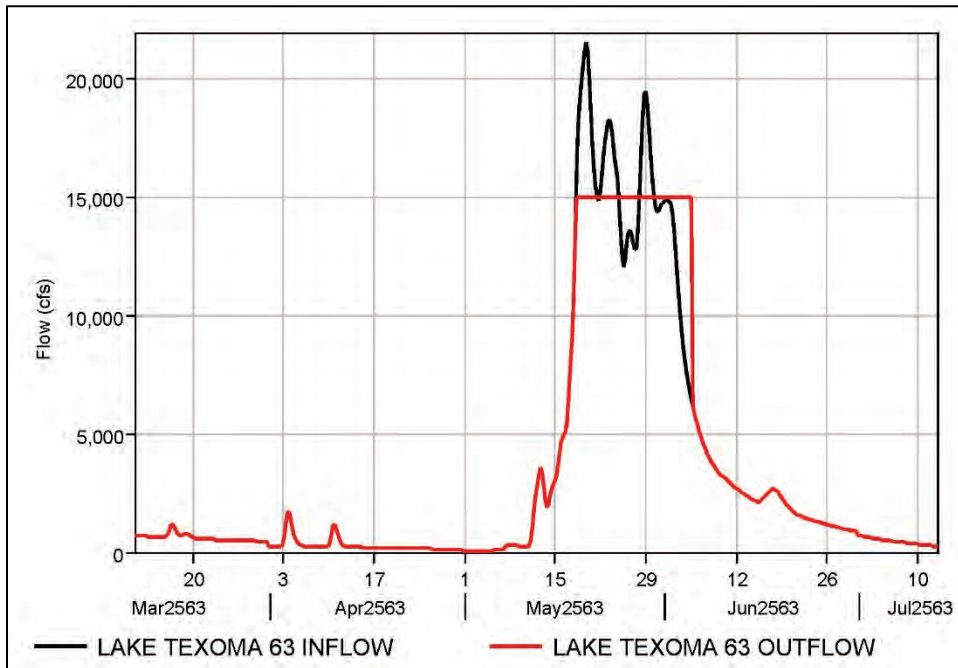


Figure E-118. Oologah Lake HYPO 63 inflow compared to outflow.

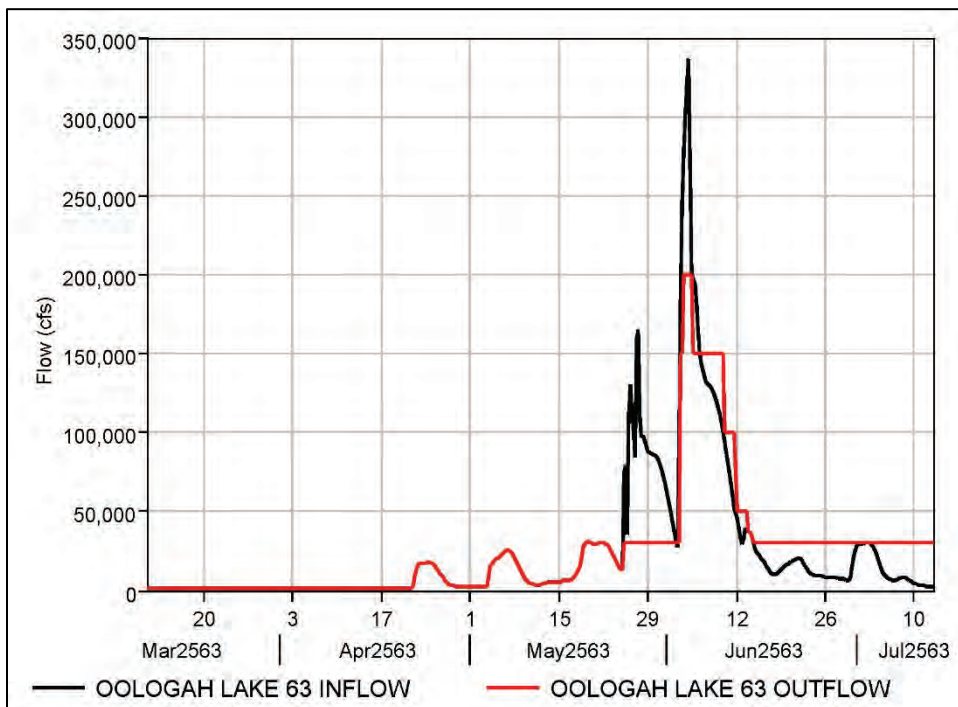


Figure E-119. Skiatook Lake HYPO 63 inflow compared to outflow.

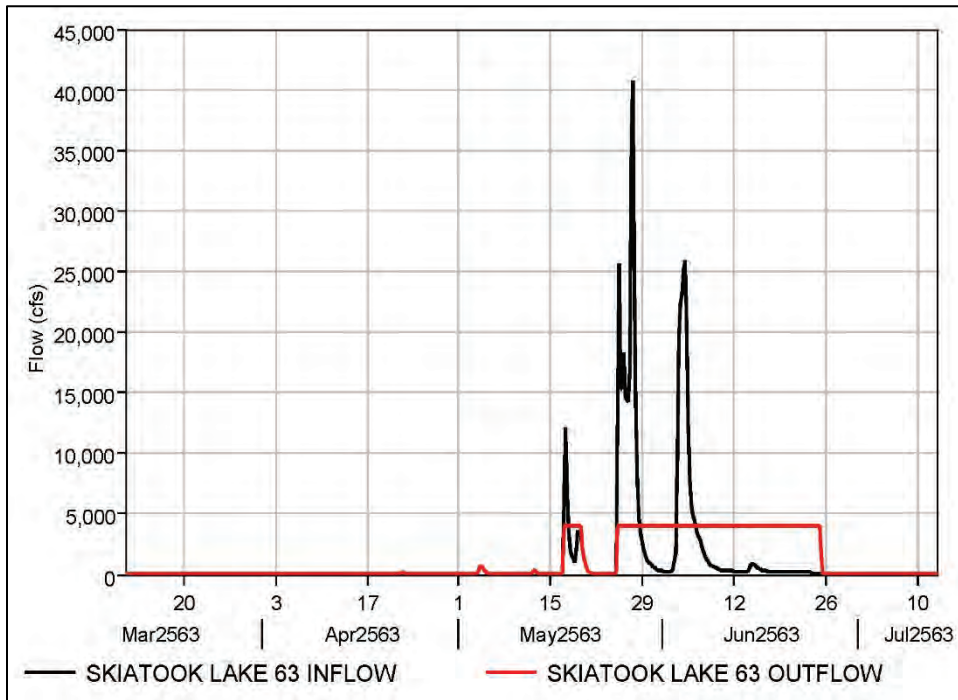


Figure E-120. Tenkiller Lake HYPO 63 inflow compared to outflow.

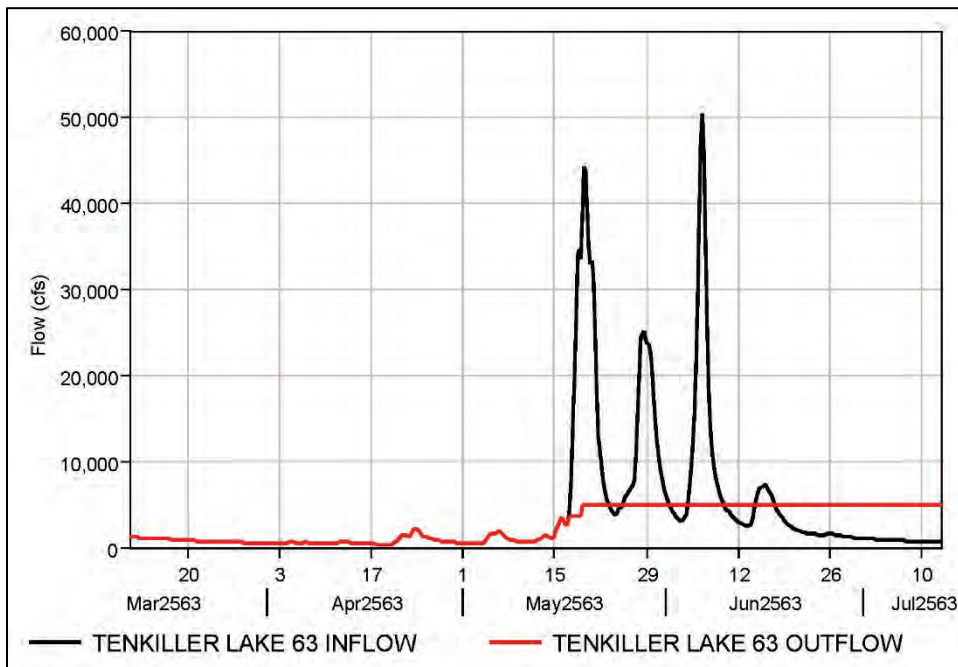
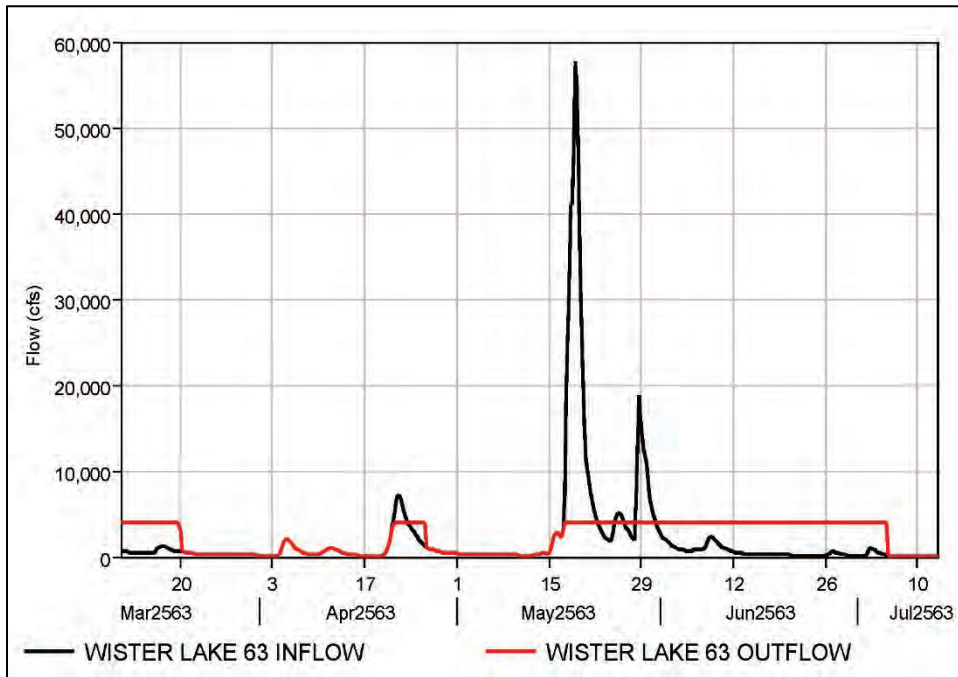


Figure E-121. Wister Lake HYPO 63 inflow compared to outflow.



Appendix F: Decision Documents

This Appendix provides information about the process used for documenting critical decisions regarding the Mississippi River Flowline Assessment.

An Executive Steering Committee (ESC) was formed at the initiation of the assessment. The purpose of the ESC was to (1) guide the overall investigation, (2) provide technical oversight regarding the scope and detail of analysis, (3) resolve questions pertaining to the assessment, and (4) ensure that collaborative, regional efforts across all offices engaged in the modeling effort met the Mississippi River Commission objectives. The ESC consisted of members from the MVD office and from each of the four lower districts: MVN, MVK, MVM, and MVS (see Table F-1).

Table F-1. ESC membership.

ESC Membership Mississippi River Flowline Assessment, 2016		
Member	Office	Position
Joseph Windham	MVD	Chief, Watershed Division
Mike Turner	MVD	
Dennis Norris	MVD	
David Busse	MVS	Chief, Engineering and Construction Division; MVD HHC CoP Champion
Julie LeBlanc	MVN	Chief, Hydraulics and Hydrology Branch
Kent Parrish	MVK	Regional PM and MRL Coordinator
Michael Sorrels	MVK	Chief, Hydraulics and Hydrology Branch
David Berretta	MVM	Chief, Hydraulics and Hydrology Branch
Leonard Hopkins	MVS	Chief, Hydraulics and Hydrology Branch

As the assessment progressed, it was necessary for the Project Delivery Team (PDT) to coordinate with the ESC thereby making sure that the analysis met expectations while keeping on schedule. Early in the analysis, several critical technical areas surfaced due to schedule constraints. Later, it was necessary to achieve consensus on use of climate change and future change parameters and finally on how results would be presented.

The ESC was called upon to approve recommendations based upon Decision Documents prepared by the PDT. Decision Documents included a short description of the relevant issues and gave a recommended course of action in light of those issues. In some cases, they included additional reports that addressed specific components of the analysis. Each Decision Document was provided to the ESC prior to either a face-to-face meeting or a conference call. The individual PDT member responsible for that technical issue presented the pertinent information during the meeting or call following which the ESC made a decision on the best course of action moving forward.

There have been nine issues identified requiring ESC decisions (Table F-2).

Table F-2. Decision Documents for ESC approval.

Number	Topic	Approved
1	Pickwick Regulated Flows	
2	Straight versus Clipped-Merged Sequence (for HYPO storms)	
3	Simulations of Historic 1950s HYPO events	
4 ¹	Plotting Scripts	
5	Flow Diagram Correction for 1955 HYPO 58A-EN	
6 ²	Loop Effect Methodology	
7 ²	Future Downstream Boundary	
8 ²	Subsidence	
9 ²	Future Deterioration from Sedimentation	

¹ Decisions related to presentation of results—implications for Hydrology and HEC-RAS modeling

² Decisions related to HEC-RAS modeling. These Decision Documents are not included in this Appendix.

The Decision Documents pertaining to the hydrologic assessment are provided in the following sections.

F.1 Pickwick Regulated Flows

HYPO 58A-EN Decision Regarding Use of NWS Model Results for Pickwick Regulated Outflows versus Use of TVA Modeled Pickwick Regulated Outflows

SUBJECT: Mississippi River Flowline Assessment: HYPO 58A-EN Decision regarding use of NWS model results for Pickwick regulated outflows versus use of TVA-modeled Pickwick regulated outflows.

BLUF: TVA support to Flowline study projects slippage of 3-6 months to generate Pickwick outflows; alternate method using NWS-LMRFC models is recommended for primary results with TVA method to be completed to resolve any final ATR/IEPR comments.

LRN provided study support to run models of Kentucky and Barkley Dams to develop the required outflows for the HYPO 58A-EN condition. These outflows become inflow boundaries for the Flowline HEC-RAS unsteady model.

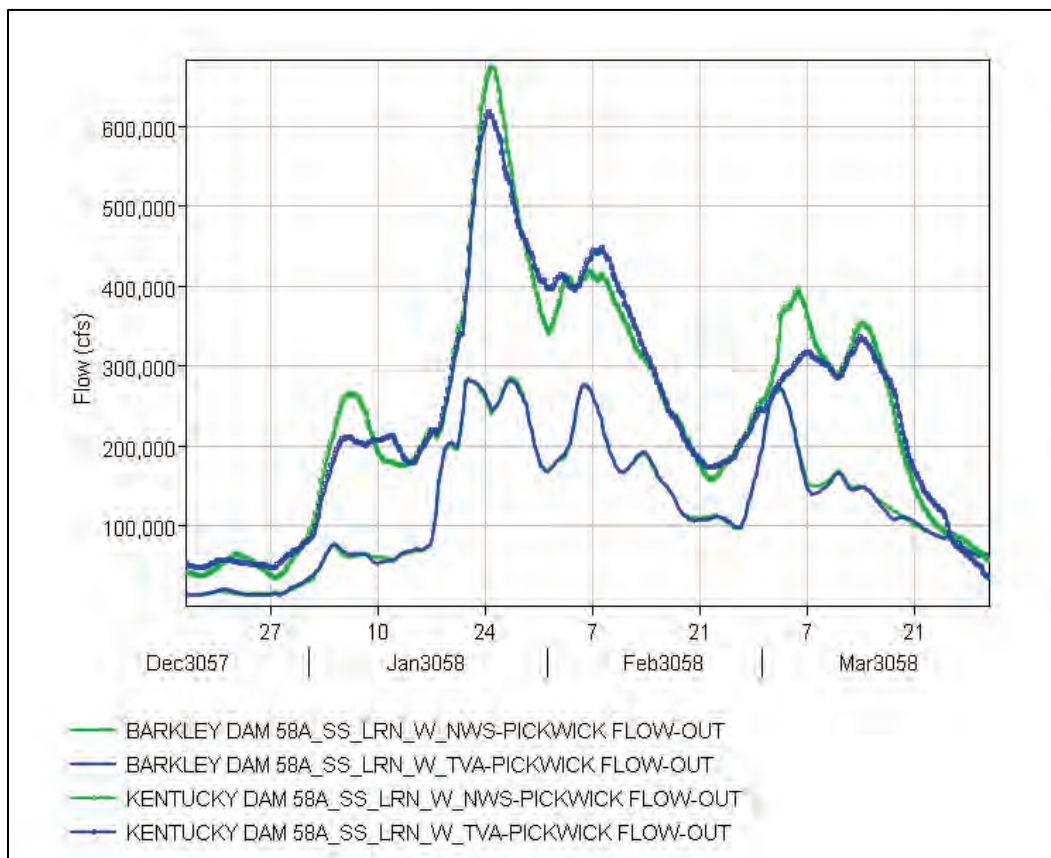
Development of regulated outflows from Kentucky and Barkley Dams for HYPO 58A-EN requires regulated outflows from the upper Cumberland River at Cheatham Dam and from the Tennessee River at Pickwick Dam. LRN also performed system regulation for the Cumberland River. LRN has been very responsive and projects no issues in meeting future requirements in a timely manner. The TVA performed system regulation for the Tennessee River down to Pickwick Dam. TVA reported that it took 40 hours for staff to perform system regulation needed to generate Pickwick outflows. TVA stated that they are not able to dedicate this level of effort in producing similar outflows for the three (3) remaining HYPO storms (52A, 56, and 63). TVA projects that they could accomplish this regulation over the next 3 to 6 months.

NWS LMRFC also models the Tennessee River. The LMRFC model captures basic reservoir operations for the TVA projects but does not capture intricate operational rules or joint operation considerations

which are included in the TVA modeling. However, LMRFC indicates that they can include this additional modeling as part of their other modeling. This additional effort by LMRFC is expected to add minimal time to their efforts.

The LMRFC made runs to generate the Pickwick releases for only the SS HYPO 58A. Their results were then passed to LRN, which made additional runs of the combined Kentucky/Barkley (KY/BK) reservoir model. Resulting KY/BK outflows using the LMRFC model Pickwick flows were approximately 10% higher than when using the TVA generated Pickwick flows. Figure F-1 below illustrates the difference in KY/BK outflows for the two methods.

Figure F-1. Flow difference due to NWS and TVA Pickwick outflow calculations.



From Figure F-1, there is little impact on Barkley Dam releases. There is approximately a 10% increase in the peak outflow from Kentucky Dam.

The two simulations were run in the HEC-RAS unsteady model to see how changes might result along the mainstem Mississippi River. The

10% increase in Kentucky Dam outflow translates into very minor changes at Cairo and below. The changes are given in Table F-3.

Recommend adopting the NWS method for generating Pickwick regulated outflows for HYPO 52A, 56, and 63. Also recommend continuing forward with TVA regulation to have available should final ATR or IEPR comments require that information.

Table F-3. Peak flows from HEC-RAS simulation for different regulation methods for Tennessee River, HYPO 58A.

	MVM 58 Regulated SS A (NWS Pickwick Outflows)	MVM 58 Regulated SS B (TVA Pickwick Outflows)	Percent Change (NWS versus TVA)
Tennessee River_at_Downstream of Kentucky Dam	672,210	617,490	8.86
Cumberland River_at_Downstream of Barkley Dam	286,371	282,235	1.47
Mississippi_at_Chester	501,451	501,448	0.00
Mississippi_at_Cape Girardeau	512,824	513,010	(0.04)
Mississippi_at_Thebes	514,539	514,854	(0.06)
Ohio River_at_Cairo	2,303,676	2,331,371	(1.19)
Mississippi_at_MS_OH Confluence	2,767,225	2,793,557	(0.94)
Mississippi_at_Hickman	2,007,986	1,963,755	2.25
Mississippi_at_New Madrid	2,543,957	2,526,756	0.68
Mississippi_at_Tiptonville	2,771,887	2,790,620	(0.67)
Mississippi_at_Caruthersville	2,330,311	2,332,402	(0.09)
Mississippi_at_Osceola	2,727,595	2,748,706	(0.77)
Mississippi_at_Memphis	2,727,899	2,738,423	(0.38)

Mississippi River Flowline Executive Steering Committee held conference call on 19 January 2016 at 0900 and concurred with recommendation. Participants were Joey Windham, Michael Sorrels, David Berretta, Don Duncan, the MVN Advisory Committee member was not on the call (Andy Gaines, Charlie Mckinnie, Kent Parrish, David Welch, Brantley Thames, and David Bogema were team members from the study who participated).

F.2 SS versus CM Sequence

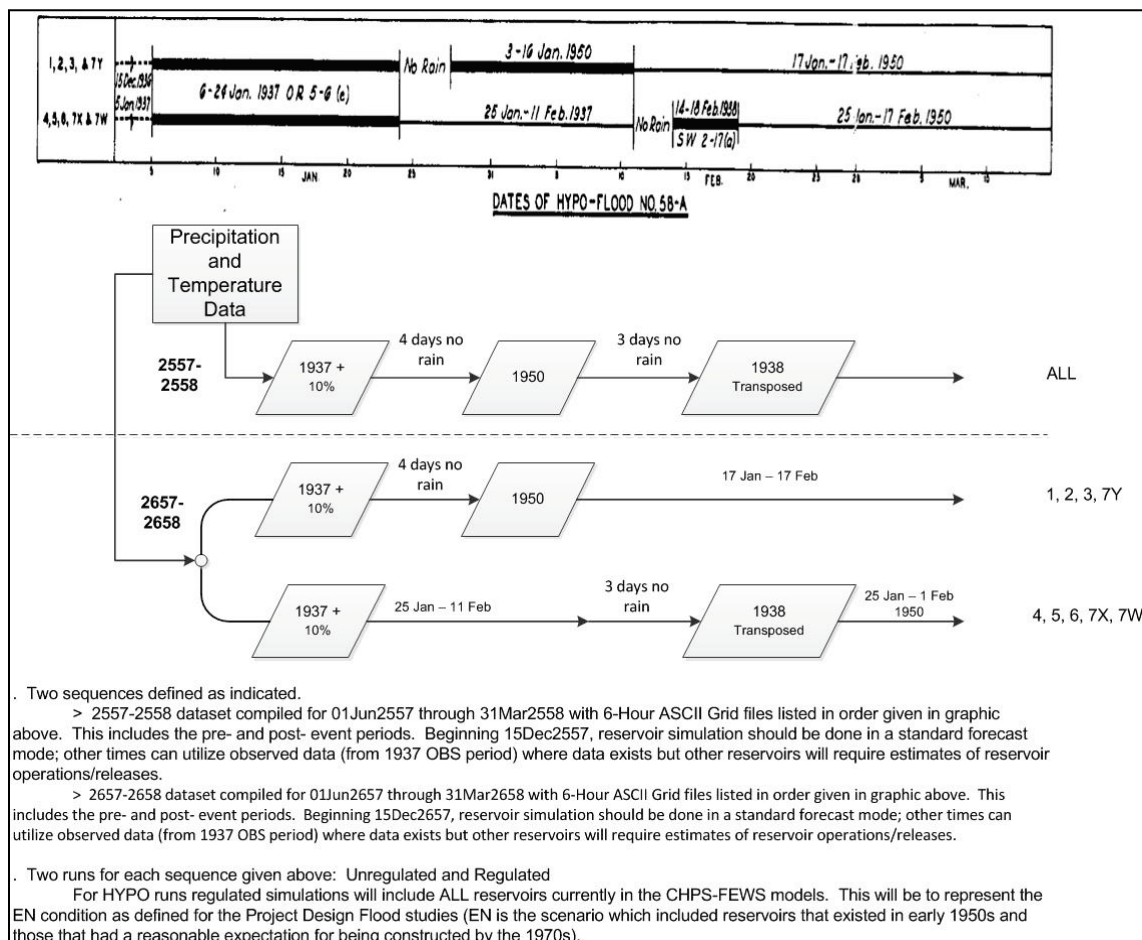
HYPO 58A Decision Regarding Use of Straight Sequence or Clipped-Merged Sequence for Constructing HYPO storms

SUBJECT: Mississippi River Flowline Assessment: HYPO 58A Decision regarding use of straight sequence or clipped-merged sequence for constructing HYPO storms.

BLUF: Recommend using current methodology for modeling precipitation events for revised HYPO storm analysis. Current methodology applies continuous spatial event across all parts of the basin. Previous analysis conducted in early 1950s used different storm distributions across Mississippi River Basin.

Previous 1950s study applied different storm periods over different parts of the Mississippi River watershed to (1) maximize tributary effects and (2) to facilitate the myriad of manual calculations needed to develop peak design discharges. This is illustrated in the following graphic taken from the Memorandum Report No. 1 (MRC 1955) (Figure F-2). The numbers in the left of the bar diagram indicate sub-basins where the storm sequence is applied. The flow charts in Figure F-2 attempt to clarify how this is done. This approach results in discontinuities in rainfall amounts for adjacent sub-basins.

Figure F-2. Diagram of HYPO 58A storm sequences.



Current methodology and modeling utilizes continuous simulation of precipitation as it moves across an entire watershed. Precipitation input for the NWS models is in the form of spatial grids for each time-step (6-hour intervals for this study).

To compare the NWS model outputs with previous published hydrographs and peak flows, a method was developed to attempt capturing the sequence as applied in the 1950s work. This method required clipping portions of rainfall from the different events then combining them into a new spatial grid—referred to as the *clipped-merged sequence*. The clipped portions were based on the sub-basins delineation used in the 1950 analysis—for example, one set of storms was used to build precipitation inputs for sub-basins 1, 2, 3, and 7Y, and another was used to build precipitation inputs for sub-basins 4, 5, 6, 7X, and 7W.

The original plan was to run both SS and CM datasets in the NWS models to facilitate comparisons with the original published values. Because there are no historic hydrographs for the 52A, 56, and 63 HYPO results (only peak values), there is no way to compare those results.

The HYPO 58A simulations provide a way to compare the two sequences. Table F-1 shows a comparison of HEC-RAS generated peak flows. Note that the SS results in higher peak flows than are produced by the CM sequence. Both SS and CM sequence peaks are higher than the historic peaks published for the HYPO 58A-EN (regulated). Values for the HYPO 58A (unregulated) are not too far off published values (Table F-2) for either the SS or CM sequence results although the SS seems to best match the historic values overall.

The entire process for modeling the Regulated (EN) condition involves five river forecast centers and 10 USACE districts, quite an involved and lengthy process which impacts project schedules.

Due to schedule constraints, only one sequence can be modeled at present. Additional simulations may be run at a later time.

It is recommended that the remaining HYPO storms (52A, 56, and 63) only use the current methodology, which utilizes the SS simulations.

Mississippi River Flowline Executive Steering Committee held conference call on 19 January 2016 at 0900 and concurred with recommendation. Participants were Joey Windham, Michael Sorrels, David Berretta, Don Duncan, the MVN Advisory Committee member was not on the call (Andy Gaines, Charlie Mckinnie, Kent Parrish, David Welch, Brantley Thames, and David Bogema were team members from the study who participated).

F.3 Simulations of Historic 1950s HYPO Events

Simulations of Historic 1950s HYPO Events

SUBJECT: Mississippi River Flowline Assessment: Decision regarding performing Unsteady HEC-RAS simulations of historic 1950s HYPO events 52A, 56, 58A, 58A-EN, and 63.

BLUF: There are not sufficient data to run unsteady HEC-RAS for the historic 1950s HYPO events 52A, 56, and 63, and there is no benefit in running the historic 1950s HYPO 58A event.

During a conference call held on 27 January 2016 with the Flowline RAS team, MVD, Charlie Mckinnie, and Andy Gaines, it was discussed whether there was a need to run the Historic HYPO floods 52A, 56, 58A, and 63 using the unsteady HEC-RAS model. It was pointed out that some of the historic floods (i.e., 52A, 56, and 63) would be difficult to run as they did not have daily flow hydrographs like the 58A and 58A-EN floods and would have nothing to check against if the daily flows were now computed; however, there can be a comparison of the hydrology between the historic HYPO events and the new hydrology being jointly developed by the NWS and USACE. The method used for the original study for these events consisted of asking each district (LRD, SWL, etc.) for a percent reduction based on reservoirs. There do not seem to be any *regulated* hydrographs for tributary inputs, and the only data published were the unregulated for the tributaries. The Mississippi River flow was just reduced below that particular point by that percentage. As for the 58A HYPO event, the flood was selected to be used as the basis for the PDF for the 1955 Study, and it does have daily flow hydrographs. Since the approved PDF used the 58A-EN (i.e., 58A event, which is regulated with existing reservoirs and those to be constructed by 1970), it was concluded that only the historic 58A-EN flood should be run with the combined districts HEC-RAS model for comparison of the historic flood routing to the approved 1955 division model. The comparison of the two models will indicate the degree of confidence felt in using the new HEC-RAS model to route the new flood flows for the 52A, 56, 58A, 58A-EN, and 63 that NWS will furnish for the MR&T Levee Design Project. Specific runs to be made during the current study include the following.

Historic

- 1955 HYPO 58A-EN; flow routing with water surface profiles

Updated 2016

- 2016 HYPO 58A-EN; flow routing with water surface profiles
- 2016 HYPO 56-EN; flow routing with water surface profiles
- 2016 HYPO 52A-EN; flow routing with water surface profiles
- 2016 HYPO 63-EN; flow routing with water surface profiles
- 2016 HYPO 58A; flow routing only, no profiles
- 2016 HYPO 56; flow routing only, no profiles
- 2016 HYPO 52A; flow routing only, no profiles
- 2016 HYPO 63; flow routing only, no profiles

It is recommended that only the 1950s historic HYPO 58A-EN be run using the unsteady HEC-RAS model. The other 1950s historic HYPO events (i.e., 52A, 56, 58A, and 63) should only be compared with the new hydrology being jointly developed by NWS and USACE.

F.4 Plotting Scripts

Using MatLab Scripts for Processing HEC-RAS Output Data to Aid in Visualization and Impact Analysis

SUBJECT: Mississippi River Flowline Assessment: Using MatLab scripts for processing HEC-RAS output data to aid in visualization and impact analysis.

BLUF: Recommend using scripts to do hydrograph plots and tables for key locations on the HEC-RAS model results. Recommend using scripts to develop river profile plots from the HEC-RAS model results. Recommend using scripts to develop levee profile plots and/or tables describing potential deficiencies due to existing levee heights or existing water control structure operations. The scripts will be more expedient and consistent for all three lower MVD districts than traditional plotting techniques provided that all the necessary inputs are provided to the MVM within a reasonable time. The examples provided in this document are based on preliminary datasets and are not considered finalized. Additional input from the study team is necessary to refine the scripts to maximize utilization for everyone's needs. A detailed presentation at the ESC meeting on how the scripts work and their capabilities and limitations will be given.

Hydrograph Script

Previous 1950s study had fewer hydrograph locations plotted — especially on the mainstem Mississippi River. The intent of this study is to document in as much detail as possible and prudent. A MatLab script is already available that can read the HEC-RAS results and plot comparison hydrographs for as many cross-section locations as desired within the HEC-RAS model for all the different HYPO simulations. It is understood that various other plots may be necessary to document more specific features of the study and that those can be generated by each district as needed to fully describe the study results.

The MatLab script was developed by the MVM, and it is the recommendation that the MVM run the script to produce plots equivalent in nature (with additional locations) to Figure F-3 below (see Figure F-3 and Figure F-4). Due to the strict timeline of the study and the fact that more complex decisions for the modeling are

necessary by the MVK and MVN, having the MVM run the script for some of the plots at key locations as the simulations are ongoing will help expedite the documentation process due to the large amount of data to be processed.

The team will have input on the scaling, format, and presentation of the plots for the final document. Because the plotting is in a script format, many changes in the presentation can be modified and re-plotted in a much shorter timeframe than other, more manual plotting techniques.

Figure F-3. Historic hydrograph example.

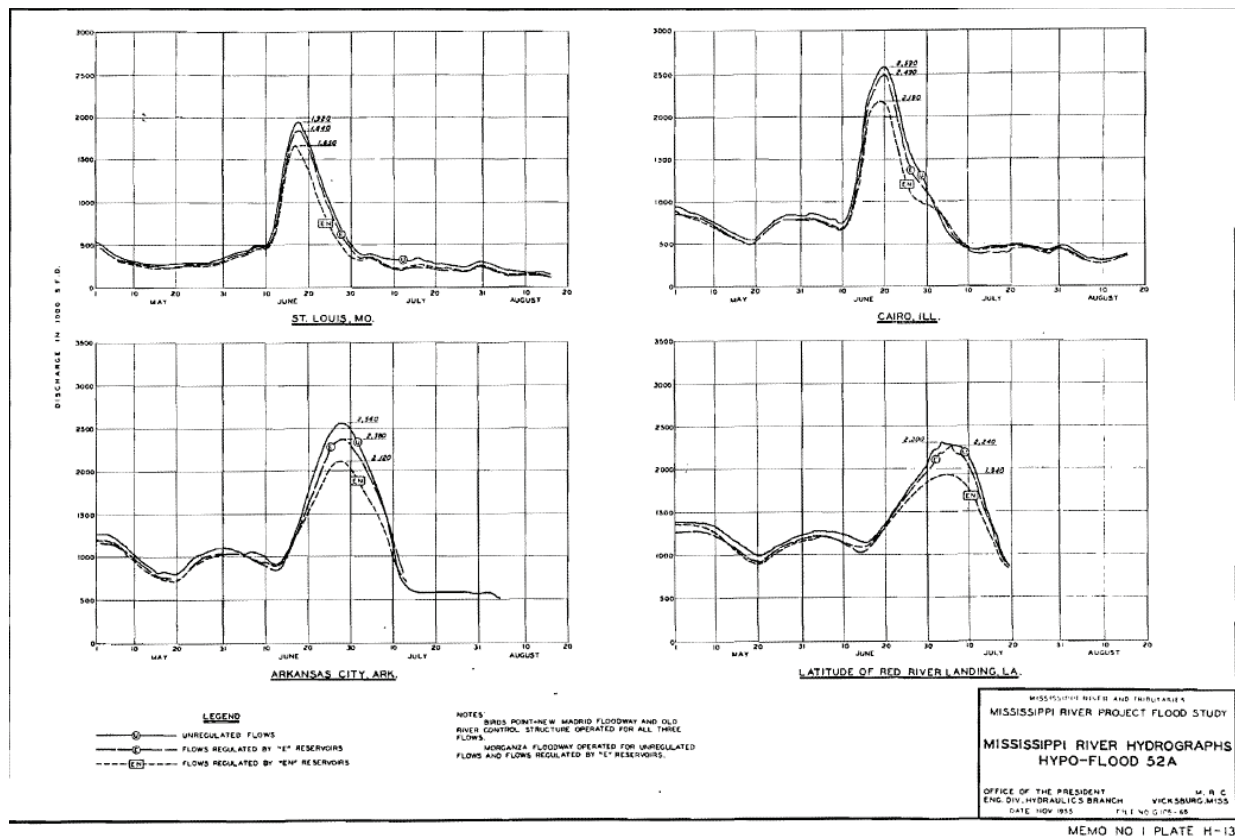


Figure F-4. Script output hydrograph example.

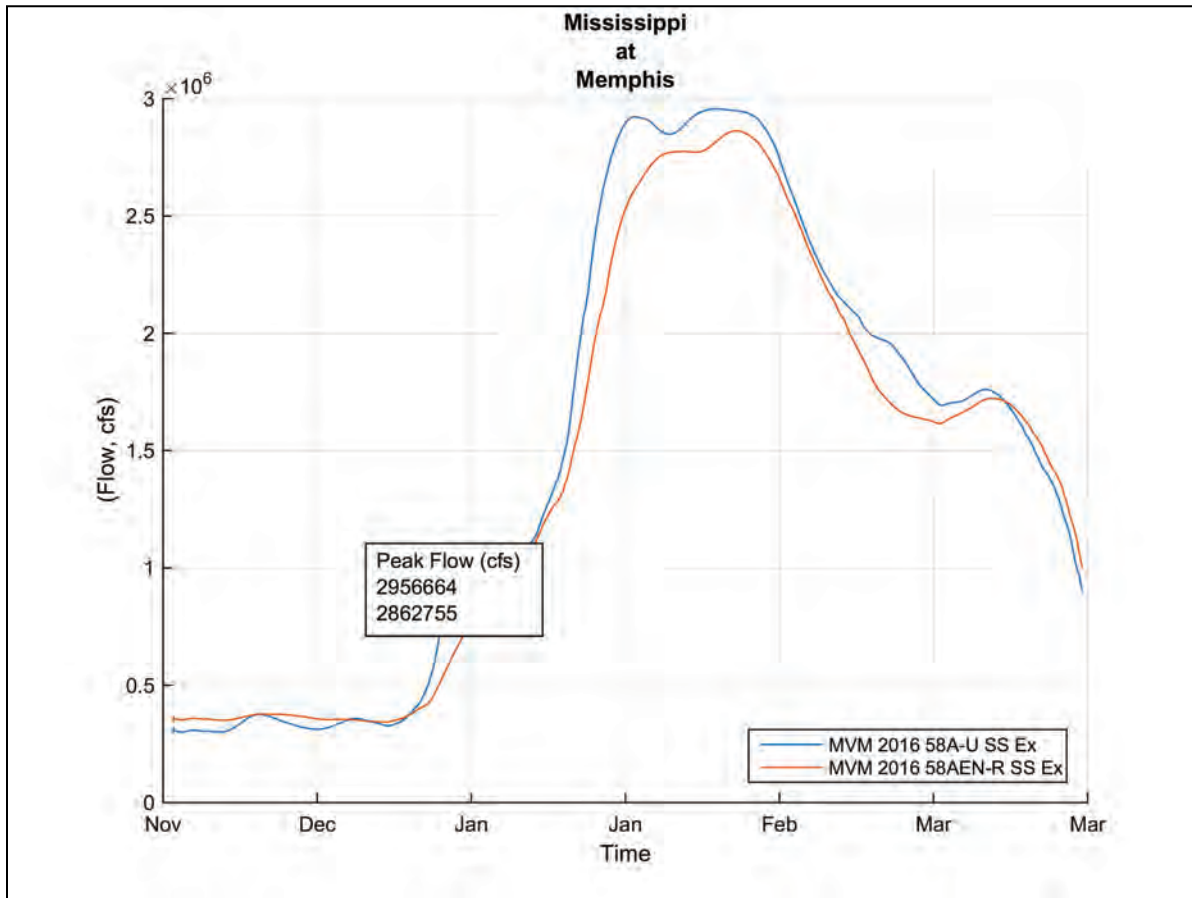


Table F-4. Current key locations identified.

<u>River</u>	<u>Reach</u>	<u>Label</u>
<u>Tennessee River</u>	<u>Tennessee River</u>	<u>Downstream of Kentucky Dam</u>
<u>Cumberland River</u>	<u>Cumberland River</u>	<u>Downstream of Barkley Dam</u>
<u>Mississippi</u>	<u>Upper Miss</u>	<u>Chester</u>
<u>Mississippi</u>	<u>Below Big Muddy</u>	<u>Cape Girardeau</u>
<u>Mississippi</u>	<u>Below Big Muddy</u>	<u>Thebes</u>
<u>Ohio River</u>	<u>OHS</u>	<u>Cairo</u>
<u>Ohio River</u>	<u>OHS</u>	<u>Metropolis</u>
<u>Mississippi</u>	<u>Below Cairo</u>	<u>MS_OH Confluence</u>
<u>Mississippi</u>	<u>Below Cairo</u>	<u>Hickman</u>
<u>Mississippi</u>	<u>Below Cairo</u>	<u>New Madrid</u>
<u>Mississippi</u>	<u>Below Cairo</u>	<u>Tiptonville</u>
<u>Mississippi</u>	<u>Below Cairo</u>	<u>Caruthersville</u>
<u>Mississippi</u>	<u>Below Obion</u>	<u>Osceola</u>
<u>Mississippi</u>	<u>Below Wolf</u>	<u>Memphis</u>
<u>Mississippi</u>	<u>Below Nonconnah</u>	<u>Tunica</u>
<u>Mississippi</u>	<u>Below St. Franc</u>	<u>Helena</u>
<u>Mississippi</u>	<u>Below Arkansas</u>	<u>Arkansas City</u>
<u>Arkansas River</u>	<u>Arkansas River</u>	<u>Dam 02</u>
<u>White River</u>	<u>White River</u>	<u>Newport</u>
<u>White River</u>	<u>White River</u>	<u>Clarendon</u>
<u>White River</u>	<u>White River</u>	<u>Mouth of White River</u>
<u>Black River</u>	<u>R3</u>	<u>Acme</u>
<u>YazooRiver</u>	<u>Reach2</u>	<u>Redwood</u>
<u>Mississippi</u>	<u>Below White</u>	<u>Rosedale</u>
<u>Mississippi</u>	<u>Below Arkansas</u>	<u>Greenville</u>
<u>Mississippi</u>	<u>Below Vicksburg</u>	<u>Lake Providence</u>
<u>Mississippi</u>	<u>Below Vicksburg</u>	<u>Vicksburg</u>
<u>Mississippi</u>	<u>Below Vicksburg</u>	<u>St. Joseph</u>
<u>Mississippi</u>	<u>Below Vicksburg</u>	<u>Natchez</u>
<u>Mississippi</u>	<u>Below Vicksburg</u>	<u>MVN Boundary</u>
<u>Mississippi</u>	<u>Below Vicksburg</u>	<u>Oldr River Complex</u>
<u>Mississippi</u>	<u>Below Vicksburg</u>	<u>Old River Lock</u>
<u>Mississippi</u>	<u>Below Vicksburg</u>	<u>Red River Landing</u>
<u>Mississippi</u>	<u>Below Vicksburg</u>	<u>Morganza</u>
<u>Mississippi</u>	<u>Below Vicksburg</u>	<u>Bayou Sara</u>
<u>Mississippi</u>	<u>Below Vicksburg</u>	<u>Baton Rouge</u>
<u>Mississippi</u>	<u>Below Vicksburg</u>	<u>Donaldsonville</u>
<u>Mississippi</u>	<u>Below Vicksburg</u>	<u>Bonnet Carre</u>
<u>Mississippi</u>	<u>Below Vicksburg</u>	<u>Carrollton</u>
<u>Mississippi</u>	<u>Below Vicksburg</u>	<u>Empire</u>
<u>Mississippi</u>	<u>Below Vicksburg</u>	<u>Venice</u>

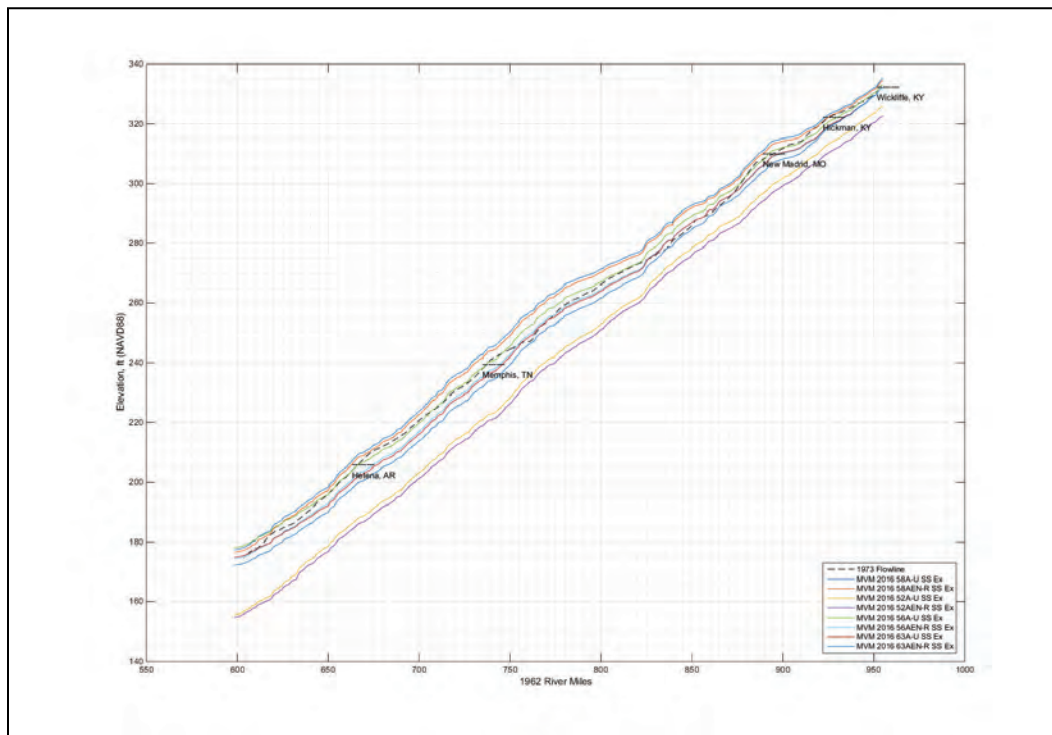
It is recommended that a script be used for plotting many key locations in the HEC-RAS model to help expedite documentation and maintain uniformity in all three districts.

River Profile Script

Besides a tabulated comparison of the historic hydrology 1955 HYPO flood flows to the 2016 HYPO flood flows, a river stage profile comparison is also necessary. The flowline from the 1970s was based on the same historic hydrology 1955 HYPO flood flows; however, the flowline from the 1970s has different datums, river miles, and multiple components that differ from the newest HEC-RAS model. The flowline from the 1970s is in NGVD29, and the 2016 data will be in NAVD88. The flowline from the 1970s uses the 1962 Navigation River Miles and the 2016 data uses a 2011 thalweg alignment to compute river miles. The flowline from the 1970s has a raw computational component as well as an additional variable(s) component. The additional variable(s) was added to the computational flowline to take into account various items not fully, or adequately captured in the steady-state modeling. These items included, but not limited to, general freeboard, loop-effect, wind, and waves. While the river profile script can easily include the additional items, much discussion will still need to take place in determining the magnitude and locations of these various types of additional considerations.

With an adequate shapefile depicting the continuous alignment for the 1962 river miles, a tabulation of river mile and elevation for the 1970s flowline, and the HEC-RAS output files, the script (combined with CorpsCon6) can convert datums and river miles to be consistent by reporting elevations in NAVD88 and miles in 1962 river miles. Figure F-5 is an example output of the script showing how it can plot elevations in NAVD88, 1962 river miles for a tabulated 1970s flowline, and multiple HEC-RAS output plans. The team will have input on the scaling, format, and presentation of the plots for the final document. Because the plotting is in a script format, many changes in the presentation can be modified and re-plotted in a much shorter timeframe than other, more manual plotting techniques.

Figure F-5. River profile example plot.



It is recommended that a script be used for plotting river profile comparisons of the historic flowline to the preliminary 2016 computations for either documentation or informational purposes to help expedite impact analysis and maintain uniformity in all three districts.

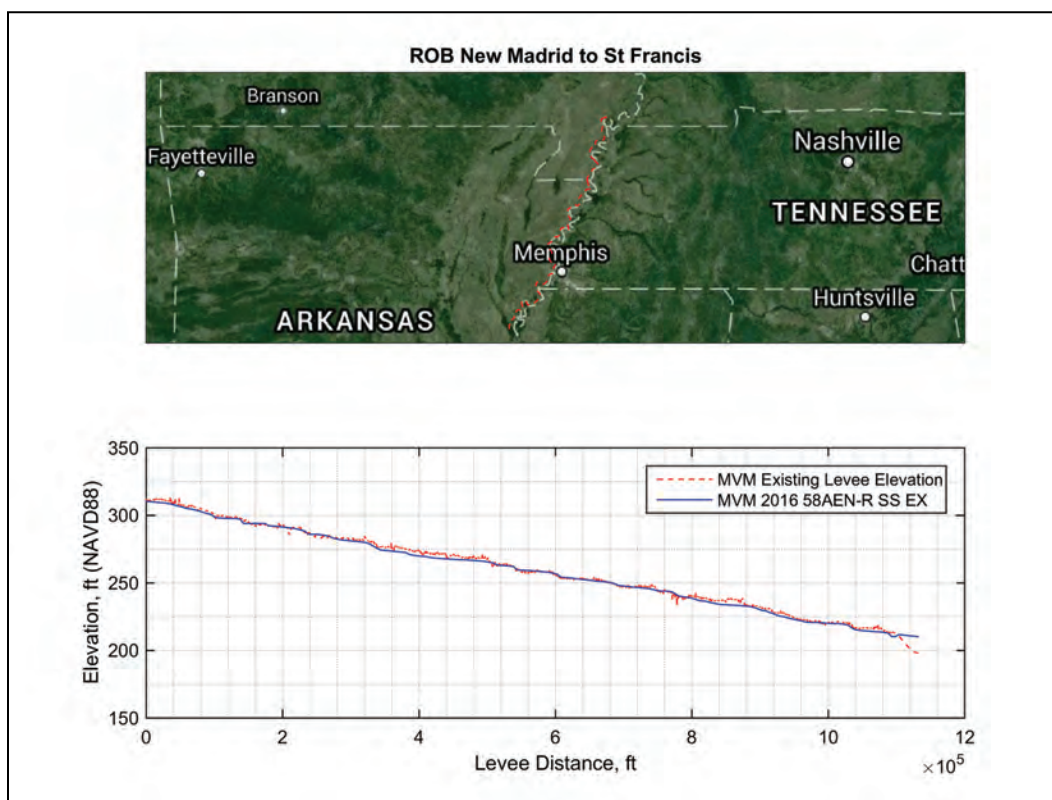
Levee Profile Script

An essential piece to this new flowline study is being able to relate the newest water surface computations to the existing grades of levee. Previous flowline studies did not include such relationships directly or as comprehensively as would be done today — they were determined afterwards as part of the design process and documented by more tedious, time-consuming drafting techniques. Because the first effort of this current study is more of an evaluation of the current design and not a comprehensive redesign, the relationship between water surface elevations and existing levee grades is indubitably essential. This current study is a delicate balance between updating methodology and technology and making a useful comparison to the previous design study. Due to such differences in methodology and technology, it is not prudent to compare the newest, preliminary flowline to the previous

flowline at the levee. It is recommended that the comparison between the newest, preliminary flowline and the previous flowline be made in relation to the river; however, to evaluate deficiencies in the system, a comparison of the newest, preliminary flowline to the existing levee heights must be made.

The levee profile script utilizes two main inputs, an inundation grid for a scenario simulated in HEC-RAS, and a set of three-dimensional polylines representing the alignment and elevations of the existing grades of levees that the flowline study team intends to evaluate. The script uses all this data and determines a water surface profile at the levee based on user-defined intervals and offsets for a given segment's coordinates. The intervals and offsets are used to overcome challenges such as river mile to levee stationing relationships, inundation on both sides of a levee, and discrepancies between the inundation mapping and the levee alignment. Some example plots are shown in Figure F-6 and Figure F-7.

Figure F-6. Example levee profile plot.



The script also uses the elevation information and can color-code specified thresholds of the water surface elevation in relation to the

existing levee grade. It can also compute a summation of the horizontal distances at each one of the specified intervals as shown in Table F-5. Example deficiency table.

Figure F-7. Example levee profile plot.

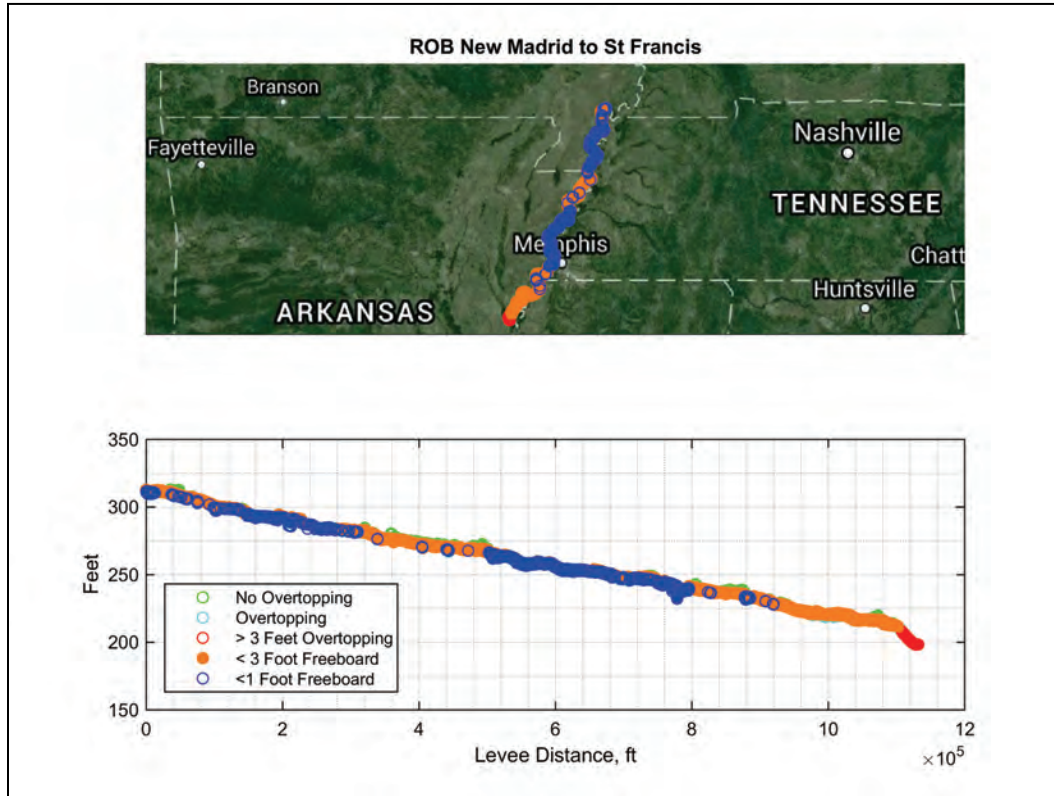


Table F-5. Example deficiency table.*

ROB New Madrid to St Francis					
Total Levee Length	1,131,756.64	Feet	214.35	Miles	
Category	No Overtopping	Overtopping	> 3 Feet Overtopping	< 3 Foot Freeboard	< 1 Foot Freeboard
Horizontal Distance (feet)	854,912.60	276,844.20	28,382.80	756,902.70	233,376.50
Horizontal Distance (miles)	161.92	52.43	5.38	143.35	44.20

*note that < 3 Foot Freeboard includes < 1 Foot Freeboard in computations.

It is recommended that a script be used for determining the preliminary impact analysis of the newest flowline to the existing levee grades to help determine the deficiencies of the current system's design.

F.5 Flow Diagram Correction for 1955 HYPO 58A-EN

SUBJECT: Mississippi River Flowline Assessment: Flow diagram correction for 1955 HYPO 58A-EN

BLUF: New hydrologic model results appear to show significant increase in peak flows for the Middle Mississippi River when compared to the 1955 flow diagram. It is necessary to confirm that correct values are used in this flow diagram. The flow diagram (plumbing diagram) in current use to represent the 1955 HYPO 58A-EN PDF shows a flow of 240,000 cfs originating from the Mississippi River above the Ohio River confluence. This diagram was also used for developing the refined 1973 flowline. The correct value for flow entering from the Mississippi River at this location should be 410,000 cfs. All future correspondence and communication should reference the correct value of 410,000 cfs for flow entering from the Mississippi River immediately upstream of the Ohio River confluence for HYPO 58A-EN.

Background: The 240,000 cfs flow rate from the Mississippi River above the confluence with the Ohio River is the flow rate at St. Louis and can be misinterpreted as the contributing flow from the Mississippi River above the Ohio River confluence (Figure F-8). In the 1955 Project Design Flood study, engineers combined the flow from St. Louis, the local basin flow from sub-basin 7-Y, and the total flow at Metropolis, IL, on the Ohio River to determine the combined flow of 2,360,000 cfs below the confluence. An intermediate computation point was not used in the original study between St. Louis and the confluence with the Ohio River. Although not published, the flow from the hydrograph at St. Louis added to the local basin flow from 7-Y would have been computed as 410,000 cfs for February 11, coincident with the date of the combined flood peak for the Mississippi and Ohio Rivers.

Method: The tabulated hydrographs from the 1955 Study were obtained from the MRC archives. The tabulation shows daily flow at St. Louis, MO, sub-basin 7-Y, which is the contributing area along the Mississippi River between St. Louis, MO, and the Ohio River confluence, and at Metropolis, IL, on the Ohio River. These three

hydrographs were combined to provide the PDF flow hydrograph for the Mississippi River downstream of its confluence with the Ohio River.

Figure F-9 shows the tabulated data plotted for the 1955 Study.

Figure F-10 shows 1955 unregulated and regulated hydrographs for HYPO 58A for the Mississippi and Ohio Rivers combined flow and for the St. Louis hydrograph added to the flow from sub-basin 7-Y. Figure F-2 also shows hydrographs at these locations for the 2016 model results for comparison.

Figure F-8. Flow diagram representing 1955 PDF discharges (also used for Refined 1973 Flowline).

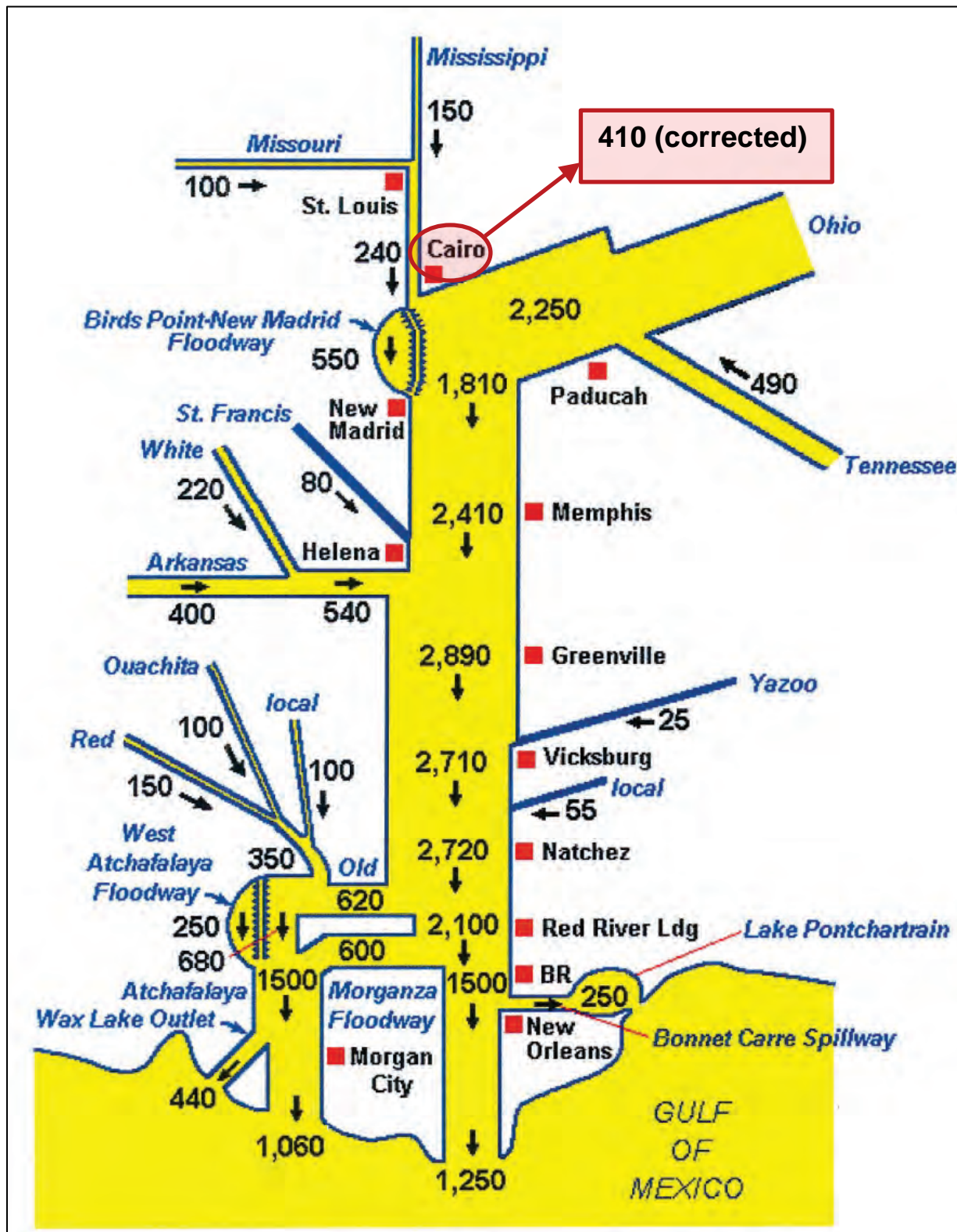


Figure F-9. Plotted discharge hydrographs from MRC archive 1955 tabulations.

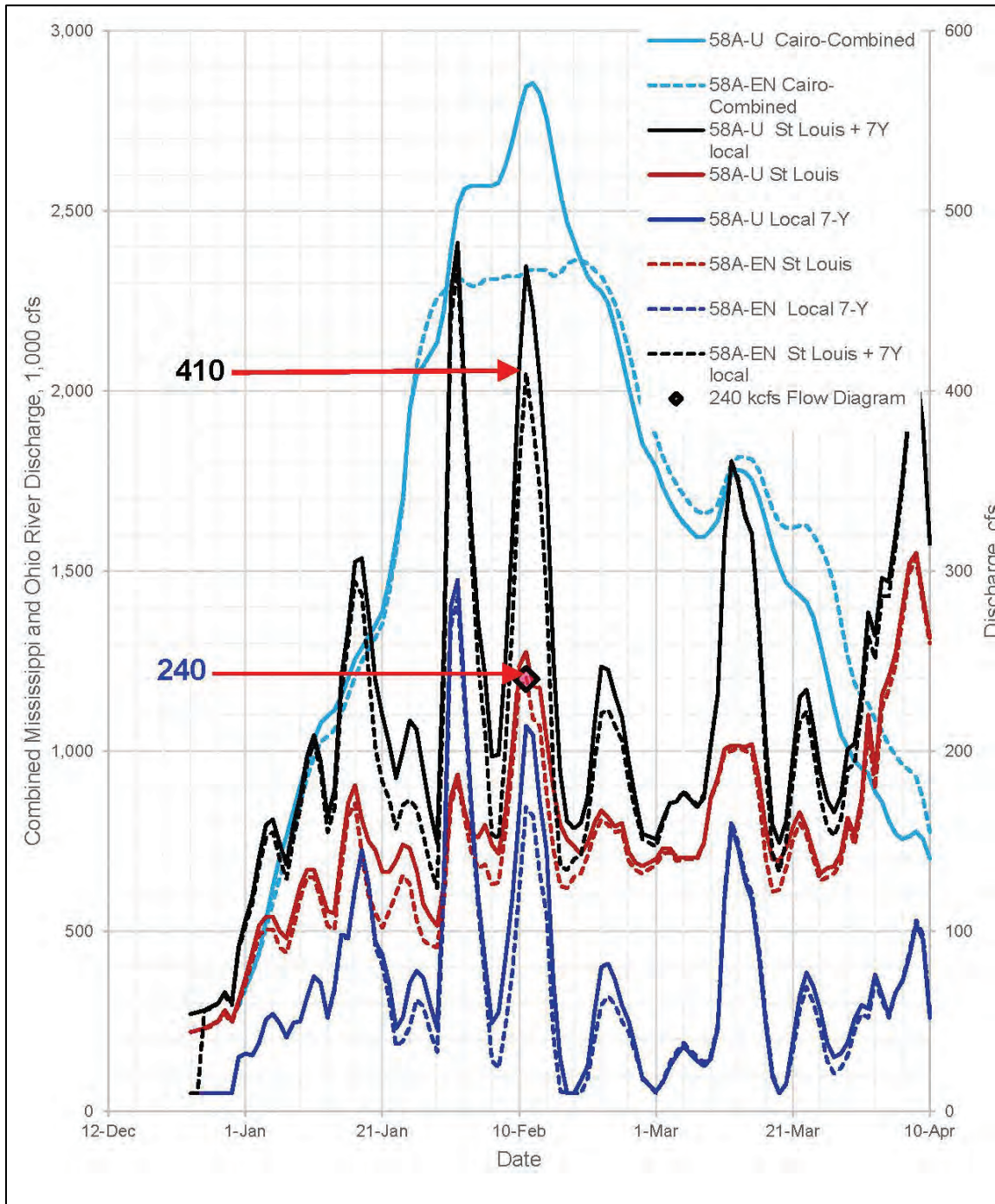
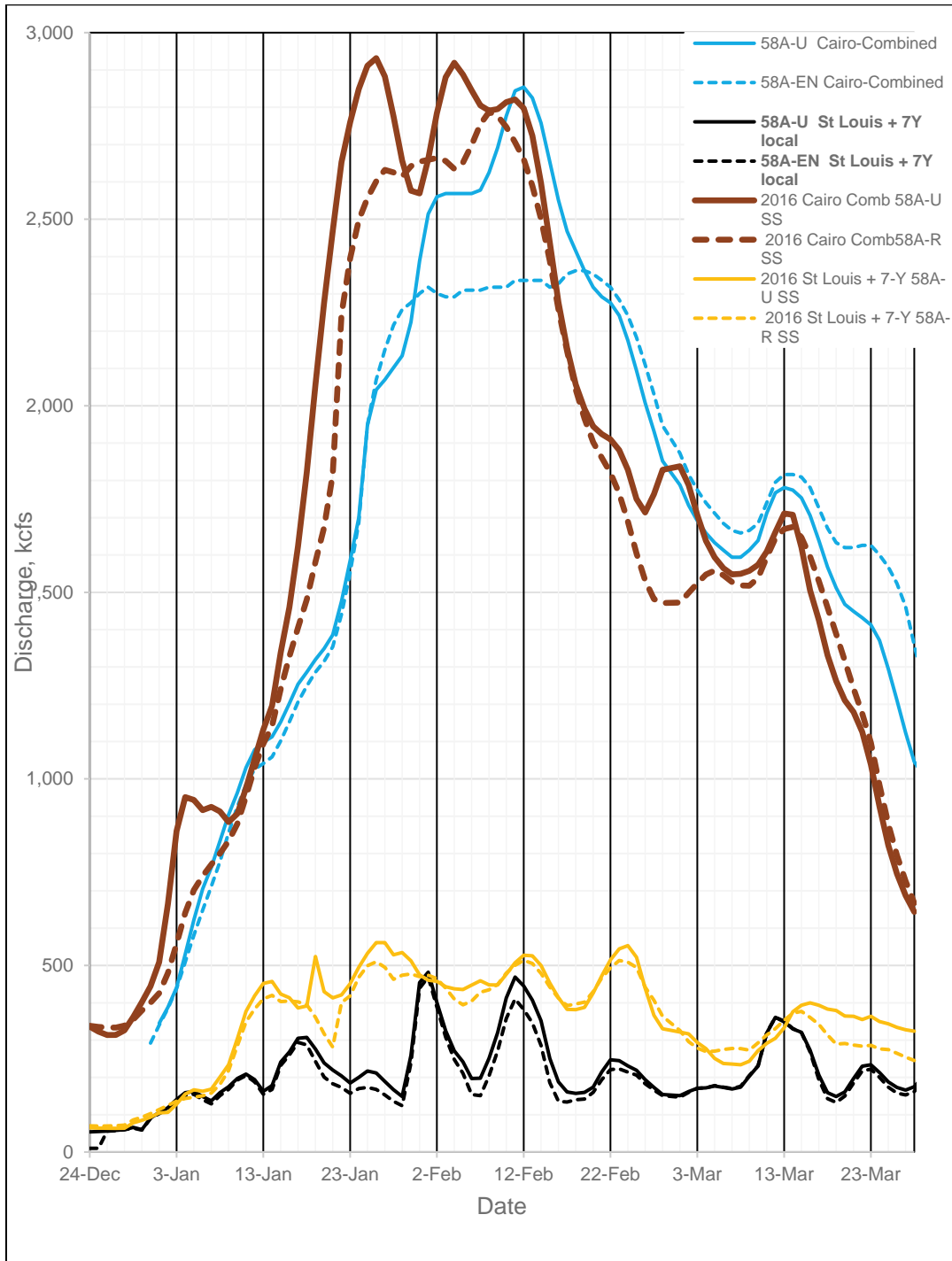


Figure G-10. Comparison of 1955 and 2016 hydrographs for HYPO 58A.



Appendix G: Historic and HYPO Storm Meteorology

G.1 General

The earlier studies concluded that “all great floods on the Lower Mississippi River are the consequences of great rains. Snow melt may make a not negligible contribution, but the major volume of water on every major Lower Mississippi flood fell as rain.” (MRC 1955) The study also stated that—based on observational data recorded until approximately 1950—the greatest potential flood season would occur between January through July.

The following is an excerpt from Memorandum Report No.1:

The important meteorological factors for Lower Mississippi floods, then, are those factors that produce great rainstorms over the middle basin during the months of January through July. The upper reaches of the Mississippi, the Upper Missouri, and the slopes west of about the 100th meridian are comparatively unimportant because of flood-control reservoirs, in operation and proposed, and the relatively low winter and spring precipitation.

Over the western tributaries the marked seasonal change in precipitation, with the spring precipitation potential several times that of winter, more than compensates for faster evaporation, and the greatest flood threat is two to three months later than over the Ohio. (MRC 1955)

Immediately following the 2011 flood on the Lower Mississippi, an assessment of the MR&T PDF compared maximized 2011 precipitation to the PDF storms (Mississippi River 2011 Post Flood Assessment, Task 1—Adequacy of MR&T PDF, March 2013 [Appendix H of this report]). In this assessment, actual storm and climatic conditions during the storm were evaluated to determine if additional available moisture could have occurred (given prevailing climatic conditions) that would have increased the storm’s potential for increased precipitation amounts. The increased storm potential rainfall was referred to as the maximized 2011 precipitation. Table G-1 shows the maximum

precipitation amounts at specific locations for the time period 1930 – 2011. Table G-2 shows the minimum, average and maximum runoff from the Mississippi River Basin for the time period 1930 – 2011.

The present assessment did not revisit meteorological conditions previously evaluated. Further details of the meteorology report are not included in this document.

Table G-1. Maximum precipitation amounts at specific locations (1930–2011).

	Precipitation Depths, inches												
	Jan	Feb	Mar	Apr	May	Jun	Jul	Aug	Sep	Oct	Nov	Dec	Annual
Cincinnati, OH	14.88	6.55	11.49	13.52	10.46	10.48	10.70	9.07	8.68	9.52	8.33	8.04	73.28
Iowa City, IA	4.80	4.82	6.30	9.30	13.31	12.60	13.41	12.33	10.56	8.24	8.07	4.50	62.50
Omaha, NE	3.70	3.10	5.96	8.48	11.30	12.70	17.10	13.10	13.75	6.23	6.30	5.50	64.50
Tulsa, OK	6.74	5.74	11.95	9.84	18.00	14.87	11.41	11.20	18.81	19.21	8.52	8.71	70.90
Batesville, AR	13.86	10.53	12.89	16.41	14.54	12.10	15.20	15.20	10.47	15.30	13.73	13.17	88.90
Paris, TX	10.80	9.80	10.21	13.89	15.15	11.82	14.70	12.84	14.84	14.65	15.13	14.49	76.80
Arkansas City, AR	15.69	13.11	14.50	19.63	14.23	12.10	15.05	14.98	15.93	13.47	12.88	18.06	83.80

Table G-2. Runoff from Mississippi River Basin (1930–2011) (sfd = square feet per day).

Month	Runoff in Inches			Runoff in 1000 sfd		
	Minimum	Average	Maximum	Minimum	Average	Maximum
January	.14	.82	1.61	146	731	1869
February	.18	.88	1.83	209	857	1923
March	.37	1.06	1.69	316	1021	2112
April	.41	.96	1.96	366	1100	2157
May	.40	.80	2.03	331	1034	2304
June	.23	.56	1.66	170	835	2149
July	.17	.40	1.20	150	603	1374
August	.10	.32	1.08	109	411	1186
September	.10	.33	.78	112	331	1042
October	.11	.40	.86	117	352	1176
November	.09	.55	1.19	105	411	1221
December	.12	.66	1.29	128	597	1581

G.2 Historic storm events

There were seven historic storm events used in building the selected HYPO storm sequences.

G.3 HYPO storm combinations

Memorandum Report No. 1 (MRC 1955) gives detailed descriptions of the meteorological events considered for HYPO storm combinations. Appendix J of Memorandum Report No. 1 contains the meteorology report developed by the U.S. Weather Bureau. The original analysis included approximately 35 different storm combinations (USACE 1959). Of these, four were ultimately selected for detailed analysis as the PDF (Table G-3).

Table G-3. HYPO Storms and historic events used to assemble them.

Hypothetical Storm Combinations		
58A	6 – 24 January + 4 days later 3 – 16 January + 3 days later 14-18 February	1937 and +10% 1950 1938 T
52A	7 – 11 May + 3 days later 15 – 20 May + 2 days later 28 – 30 June	1943 T and - 20% 1943 1928
56	23 – 26 March + 3 days later 12 – 16 April	1913 1927
63	12 – 15 April + 2 days later 15 – 20 May + 3 days later 7 – 12 May	1927 1943 1943 T

G.4 Basic methodology

In developing HYPO flood estimates, seven historic storms were combined by arranging recorded precipitation events in a critical sequence. These sequences were developed by adjusting time of occurrence, transposing the event, and scaling the event based upon maximum moisture potentials. Storms were selected on the basis of their flood magnitude and the seasons of the year in which they occurred (storms were only combined within the same season). Table G-4 lists the dates of events used in developing the HYPO storm sequences.

Table G-4. Historic storm events used to build HYPO storm sequences.

Date of Event	Flood from Area	Storm Assignment Number for Intense Portion of Rainfall (MRC 1955)
March 1913	All areas	OR 1-15
March 1913	1, 2, 3, 4, 5, and 7Y	OR 1-15
April 1927	All areas	LMV 4-8
June 1928	1, 2, 3, and 7Y	OR 7-10
January 1937	All areas	OR 5-6
May 1943	All areas	SW 2-21
January 1950	1, 2, 3, and 7Y	-----

Based on storm-rainfall intensities, depths, areal coverage, and season of year, the storms listed in Table G-5 were transposed to locations that would produce critical floods and were used in combination with events listed above.

Table G-5. Storm transpositions used to build HYPO storm sequences.

Date of Event	Storm Assignment Number (MRC 1955)	Storm Transposed over Area Number	Storm Transposition Number
14-19 Feb 1938	SW 2-17	4, 5, 6, 7X, and 7W	4
6-12 May 1943	SW 2-20 ¹	2 and 3	5
6-12 May 1943	SW 2-20 ¹	4, 5, 6, 7X, and 7W	6

¹ Two different transpositions were used for this event.

Storm Transposition Number 4: (Storm of 14–19 February 1938—SW 2-17). This storm was transposed 90 miles north and rotated 20° clockwise about Calvin, OK, as center. No adjustment was made in rainfall depths.

Storm Transposition Number 5: (Storm of 6–12 May 1943—SW 2-20). This storm centered at Warner, OK, and was transposed 430 miles north and rotated 14.5° clockwise about the center. Rainfall depths were reduced 4%.

Storm Transposition Number 6: (Storm of 6–12 May 1943—SW 2-20). This storm was transposed 105 miles north and rotated 21° clockwise about the center at Warner, OK. No adjustment was made in rainfall depths.

G.5 MR&T flowline study: Precipitation

The original intent of the MRPFS performed during the 1950s was “to determine whether changes in the present [1941] design-project flood are deemed advisable in the light of improved techniques and basic data now available and determine the magnitude of flows to be used” (MRC 1955). The steps used to perform this task were the following:

1. Determine the meteorological situations and related rainfall quantities in the Mississippi River Basin that may be reasonably expected to produce critical discharges at key points along the Mississippi River from St. Louis to Latitude of Red River Landing.
2. Develop hypothetical hydrographs of runoff for the key discharge stations near the mouth of each major tributary for the meteorological situations and rainfall quantities determined.
3. Develop HYPO flood hydrographs to be used as the basis for the determination of the official Mississippi River Comprehensive Project Flood and select the hydrographs to recommend for adoption.
4. Provide sufficient information regarding the derivation of the selected HYPO flood hydrographs to enable the division and district offices concerned to develop hydrographs of runoff from various drainage area subdivisions upstream from key points near the mouth of major tributaries of the Mississippi River.
5. Determine approximately the combined effects of upstream reservoirs in reducing the selected HYPO flood hydrographs at key

- points near the mouth of major tributaries and at key points along the Mississippi River for selected groups of reservoirs.
6. Select hydrographs to be recommended based on improved techniques and basic data now available, engineering limitations, broad economic considerations, assumptions regarding timing of reservoir construction, and other related factors.

This section describes the initial step of this process. During the original PDF study performed in the 1950s, 19 heavy precipitation events were analyzed in detail by the U.S Weather Bureau during the MRPFS in the 1950s. These storms were deemed the most appropriate to analyze as prototypes of the precipitation required to produce the design flood. Data for each storm were collected and analyzed to produce incremental isohyetal maps at 6- or 12-hour time periods that show the distribution of the principal rainfall. These maps are contained in the document Hydrometeorological Report No. 34: Meteorology of Flood-Producing Storms in the Mississippi River Basin (USACE, Weather Bureau 1956).

The original study proposed two methods for developing the storms required to produce the hypothetical floods.

- Method 1—Combinations of storms of record in place. The combinations of selected storms in their respective locations were shifted in timing and modified on basis of sound meteorological and hydrological principles to produce a maximum combination of flood flows.
- Method 2—Combinations of storms in place and transposed. Storms in place, determined as described in Method 1, were incorporated in the storm series with another storm transposed critically over a major tributary with regard to timing and locations.

Method 2 was determined most appropriate during the MRPFS with specific transposition rules to be followed. Based on the meteorological conditions accompanying storms of record and on the advice of meteorological experts, the following criteria were adopted in an effort to provide reasonable limits to the amount of movement in time, location, and rotation of the transposed storms:

- Tropical storms over the lower portions of the basin could not be moved in location.
- Storms should be used only in the season of the year in which they occurred. Seasons for MRPFS were determined to be winter (December–February); early spring (March–May); and late spring (May–July).
- Movements of several hundred miles were permissible provided the storms were not moved beyond the major drainage basins adjoining the basin over which the storms occurred.
- Rotation of storms about axis should be limited to a maximum of approximately 20°.

The current MR&T project design was based primarily on the findings from the 1950s study. With the occurrence of the 2011 record flood over the Lower Mississippi Valley, which produced a flow of approximately 85% of the PDF, it became prudent to re-assess the MR&T project Flowline to determine whether the Flowline is still applicable. To perform this task, it was deemed necessary to reproduce the original storm precipitation events and combine the precipitation in conformity with the original HYPO scenarios to attempt to replicate the peak flows and volumes for each HYPO. This was required to assess the hydrologic and hydraulic differences in the watershed that have occurred since the MRPFS was performed.

Several approaches were discussed as to how to generate the original precipitation events. These included the following:

- Maximizing the 2011 precipitation event and comparing the results with the PDF rainfall amounts.
- Digitizing the hard copy maps from HMR 34 and converting them into shapefiles and then ASCII grids that could be used as input to the NWS hydrologic models.
- Compile all available data from the NCDC and other sources to produce the most robust dataset of precipitation observations available.

All of these approaches were investigated. The process, major roadblocks, and results of each of these methods are discussed. The analysis of the actual data was deemed to produce the most realistic

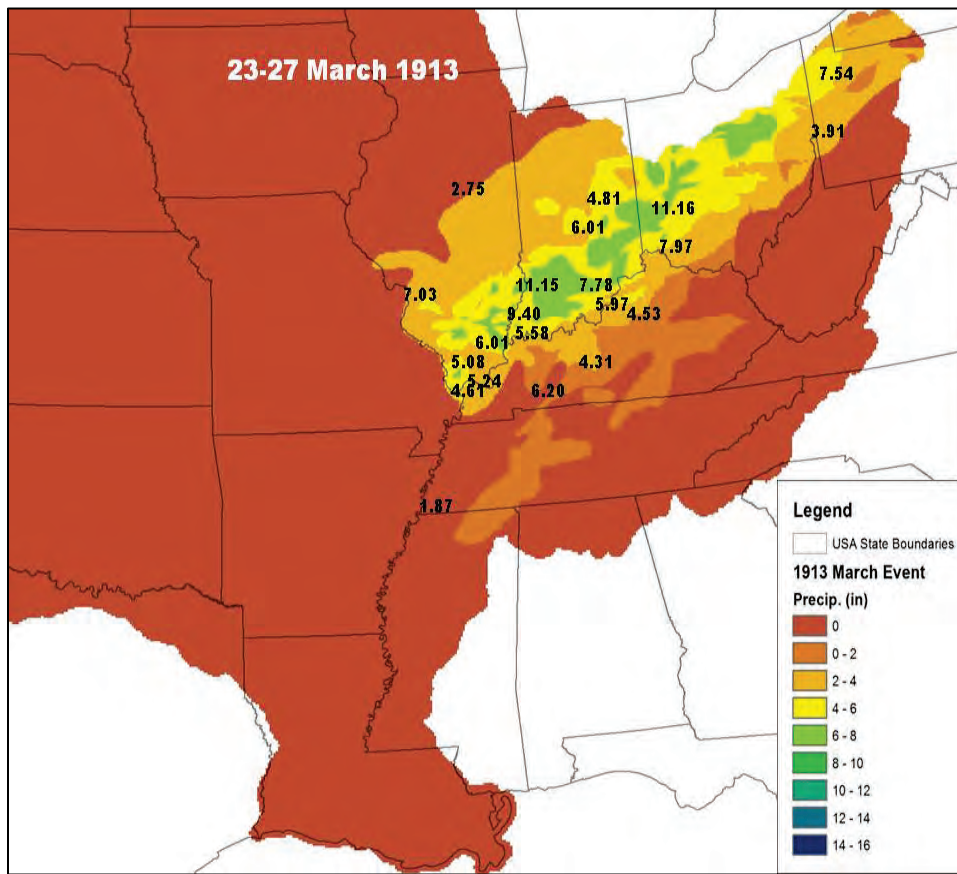
depiction of the actual precipitation events that were studied during the MRPFS.

Additional heavy precipitation events that have produced 13 of the top 20 stages at the confluence of the Mississippi and Ohio Rivers in Cairo, IL, have occurred since the MRPFS was performed. With this in mind, it was also deemed prudent to investigate the precipitation events that produced these floods after MRPFS to determine whether the original storm combinations would still produce the maximum flood over the MR&T with a reasonable chance of occurrence. Development of new HYPO flood scenarios for storm combinations that have occurred since MRPFS were required to follow the same restrictions that were imposed in the original report.

G.5.1 23–27 March 1913

- Heaviest rains for this event occurred over the Ohio Valley.
- Rainfall totals appear to be lighter than normal at most locations with differences up to 4 in. occurring at maximum value locations.
- Issues and concerns
 - Although rain fell during the event from March 23–27, 6- or 12-hour isohyets maps were prepared in HMR 34 only for the main bursts that occurred between the morning of the 24th and the evening of the 25th. Omission of the remainder of the storm in the 12-hour isohyets maps resulted in significant deficiencies in storm total precipitation. Observations at Bellefontaine, OH, show 1.37 in. on the 23rd; 1.52 in. on the 24th; 5.61 in. on the 25th; 2.13 in. on the 26th; and 0.53 in. on the 27th of March. Therefore, 3.42 in. of the storm total 11.16 in. of the event at Bellefontaine is not included in the 12-hour isohyets maps.
 - The 12-hour isohyets maps for 0600 and 1800 CST on March 25 show a large area of over 3 in. of rainfall north of the Ohio River. As a result of Decision 3 in the previous section, all locations were given the value 3.5 in. March 25 daily rainfall totals at Louisville, KY, are recorded by NCDC to be 4.95 in.

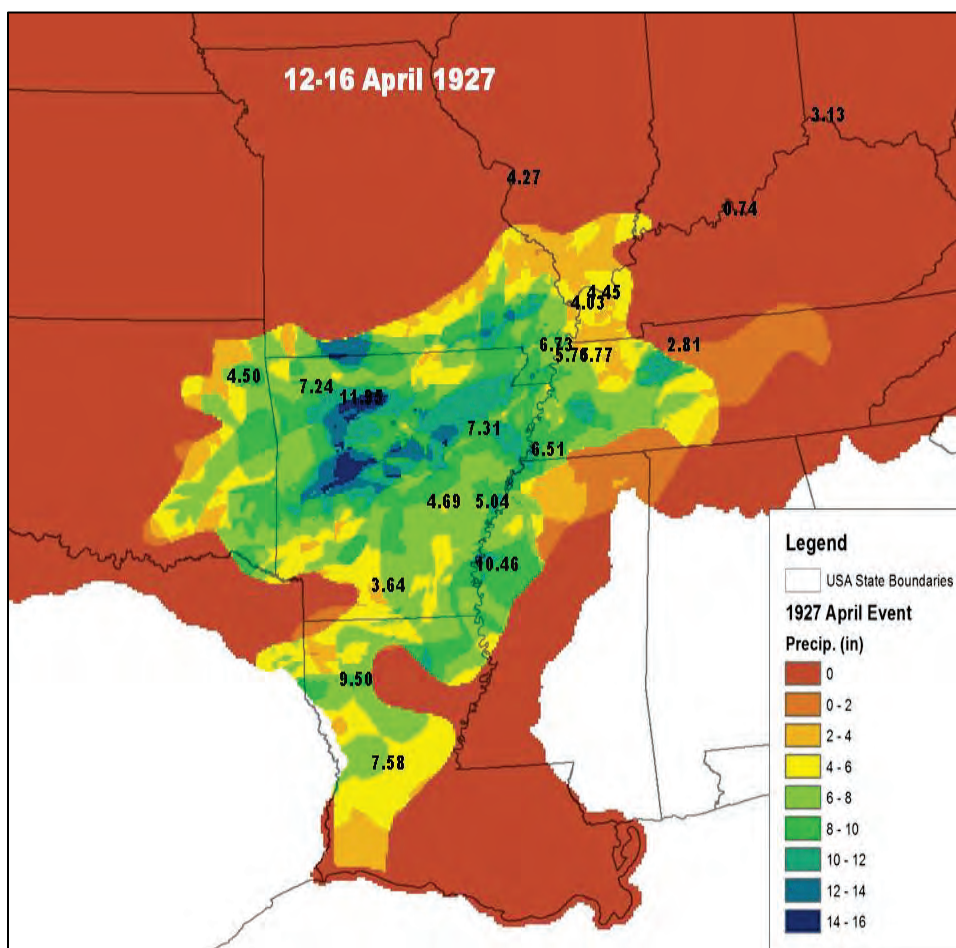
Figure G-1. Comparison of generated storm total precipitation with observational data for the 23–27 March 1913 storm event.



G.5.2 12–16 April 1927

- Rainfall occurred from eastern Texas to southern Illinois and from eastern Oklahoma to northeastern Mississippi.
- Rainfall totals produced from the 12-hour isohyets maps generally matched the storm totals from observational data.
- Issues and concerns
 - No issues or concerns.
 - Entire storm was included in the 12-hour isohyets maps.

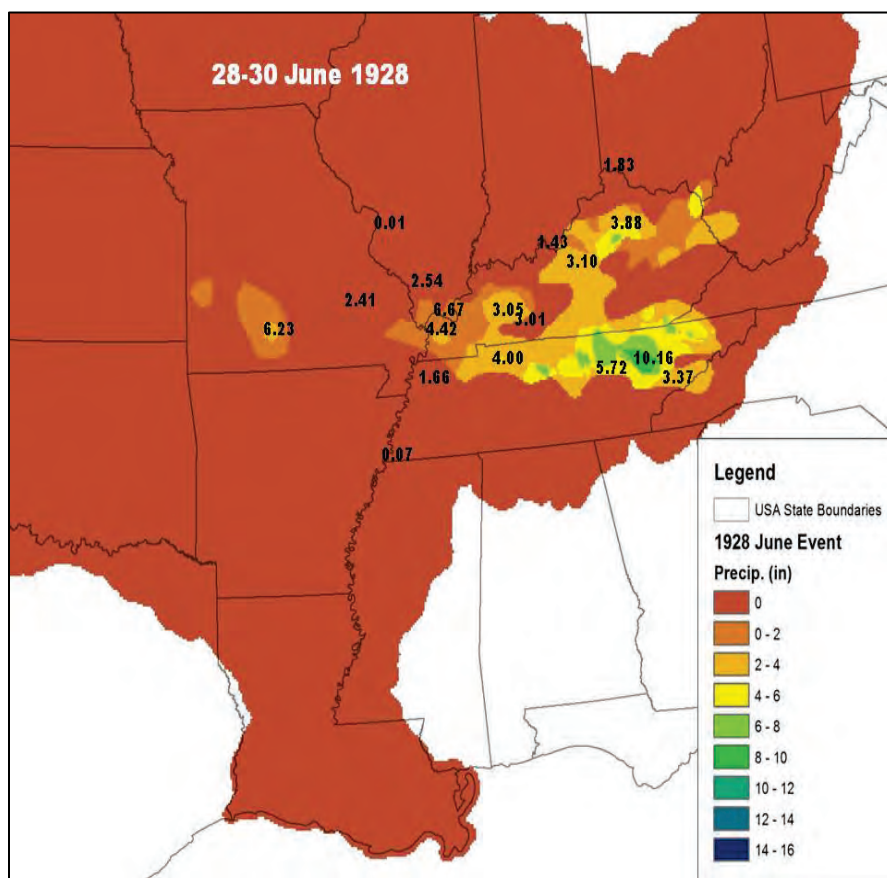
Figure G-2. Comparison of generated storm total precipitation with observational data for the 12–16 April 1927 storm event.



G.5.3 28–30 June 1928

- Rainfall occurred principally in Kentucky, Tennessee, and parts of Missouri as shown in Figure G-3.
- Rainfall totals produced from the 12-hour isohyets maps generally matched the storm totals from observational data. They were slightly deficient in some of the areas where the maximum precipitation occurred such as southern Missouri.
- Issues and concerns
 - No issues or concerns.
 - Entire storm was included in the 12-hour isohyets maps.

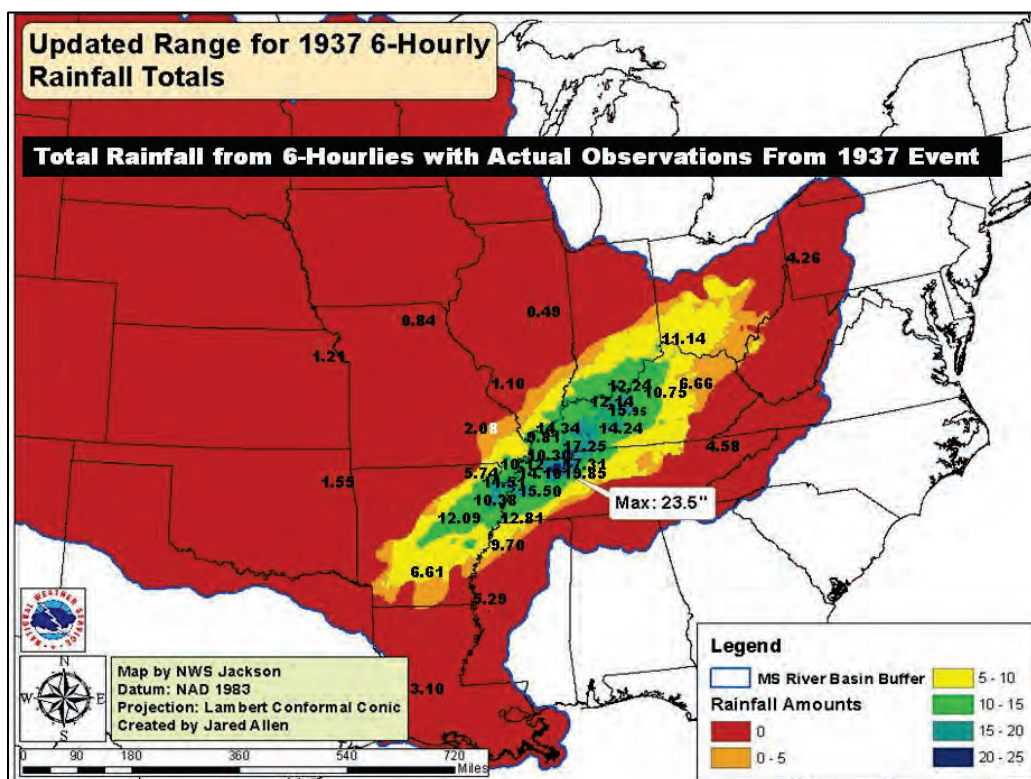
Figure G-3. Comparison of generated storm total precipitation with observational data for the 28–30 June 1928 storm event.



G.5.4 17–25 January 1937

- According to HMR 34 (USACE, Weather Bureau 1956), “January 1937 may represent conditions near the extreme for January under our present climatic regime.”
- Rainfall totals produced from the 6-hour isohyets maps generally matched the storm totals from observational data as shown in Figure G-4. They were slightly higher in some of the areas where the maximum precipitation occurred.
- Issues and concerns
 - Isohyets maps were provided at 6-hour time periods and were included for the entire storm. The 6-hour time increments limited the number of over 3 in. rainfall amounts.
 - The biggest concern is that when this storm was used in producing HYPO 58A, precipitation from 6–25 January 1937 was considered. Data had to be supplemented with daily data to produce the entire event.

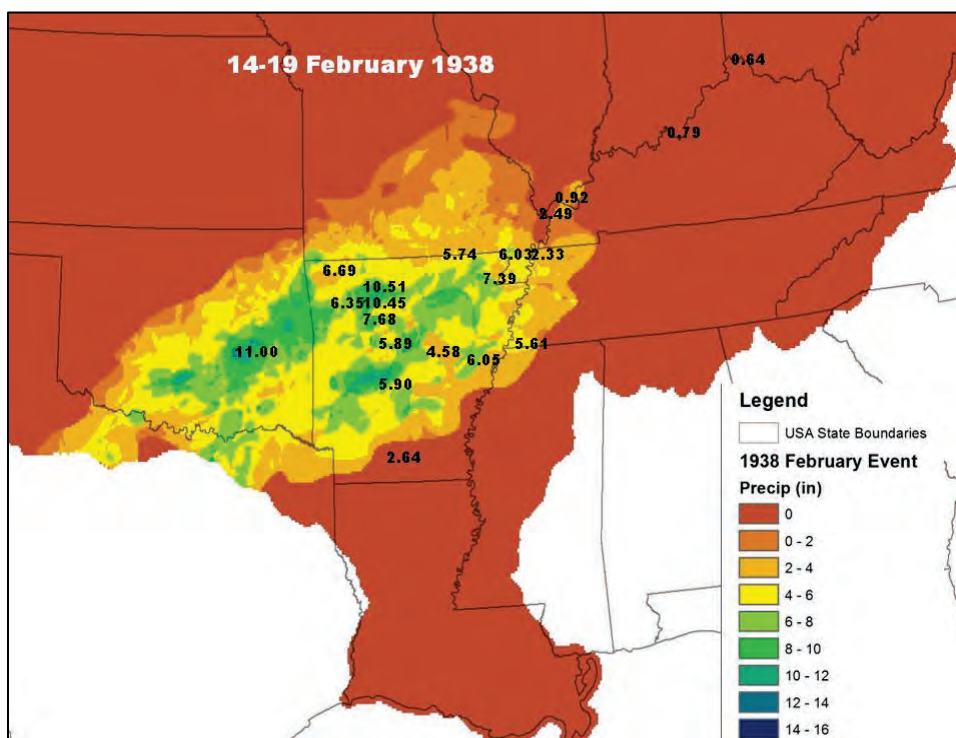
Figure G-4. Comparison of generated storm total precipitation with observational data for the 17–25 January 1937 storm event.



G.5.5 14–19 February 1938

- Heaviest rain primarily fell in Arkansas and Eastern Oklahoma with large amounts also occurring in parts of bordering states as shown in Figure G-5.
- Rainfall totals produced from the 6-hour isohyets maps generally matched the storm totals from observational data. They were slightly lower in some of the areas where the maximum precipitation occurred.
- Issues and concerns
 - No issues or concerns.
 - Isohyets maps were provided at 6-hour time periods and were included for the entire storm. The 6-hour time increments limited the number of over 3 in. rainfall amounts.
 - Transposition of this storm was required for initialization into HYPO 58A.

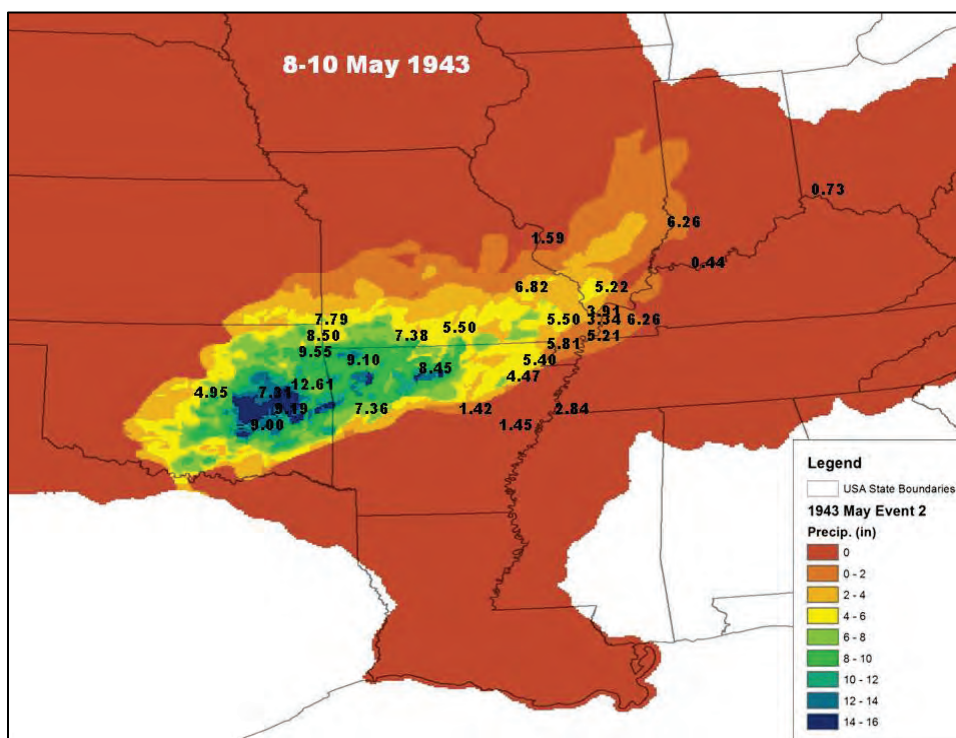
Figure G-5. Comparison of generated storm total precipitation with observational data for the 14–19 February 1938 storm event.



G.5.6 8–10 May 1943

- Termed the Warner, OK, storm since 25 in. fell there in a 48-hour period. Heaviest rainfall was concentrated over Oklahoma, Arkansas, and southern Missouri as shown in Figure G-6.
- Rainfall totals produced from the 6-hour isohyets maps did not match that of the observations. Geo-referencing techniques appear to have placed this storm too far to the southwest.
- Issues and concerns
 - Geo-referencing of this storm has to be redone. It appears to be offset too far to the southwest.
 - Intense rainfall demonstrated in the 6-hour isohyets maps affords a large area of over 3 in. rainfall amounts that produced much deficient amounts in the areas that received the greatest rainfall.

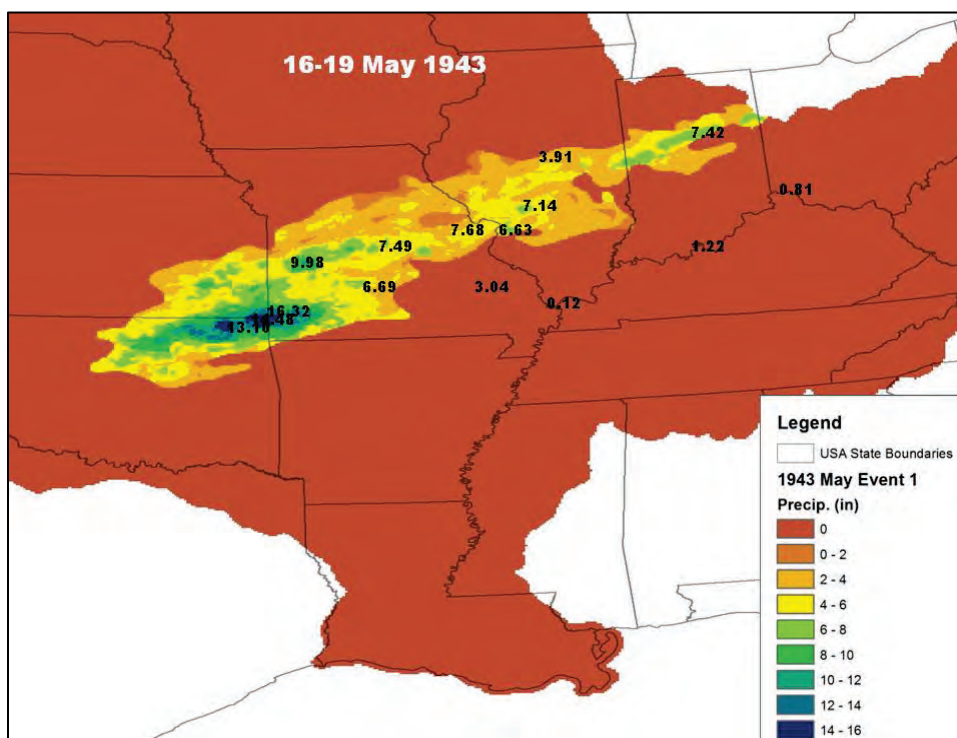
Figure G-6. Comparison of generated storm total precipitation with observational data for the 8–10 May 1943 storm event.



G.5.7 16–19 May 1943

- This storm occurred 1 week after the intense rainfall event of May 8–10 shown above. Heaviest rainfall fell along an axis from north-central Oklahoma to northwestern Ohio as shown in Figure G-7.
- Rainfall totals produced from the 6-hour isohyets maps matched well with the observational data.
- Issues and concerns
 - No issues or concerns.
 - However, when this storm was used for HYPO 52A, precipitation from May 12–20 was included. The 6-hour isohyetal maps were not available and thus had to be supplemented with daily observational data. On days where no 6-hour data existed, the daily total was placed in the first 6-hour time period and zeros used for the remaining three 6-hour periods for that day.

Figure G-7. Comparison of generated storm total precipitation with observational data for the 16–19 May 1943 storm event.



G.5.8 27–30 March 1945

- This set-up storm for the HYPO 56 was not included in the isohyets maps. This storm produced the flood of record at several locations along the Red River.

G.5.9 3–9 June 1947

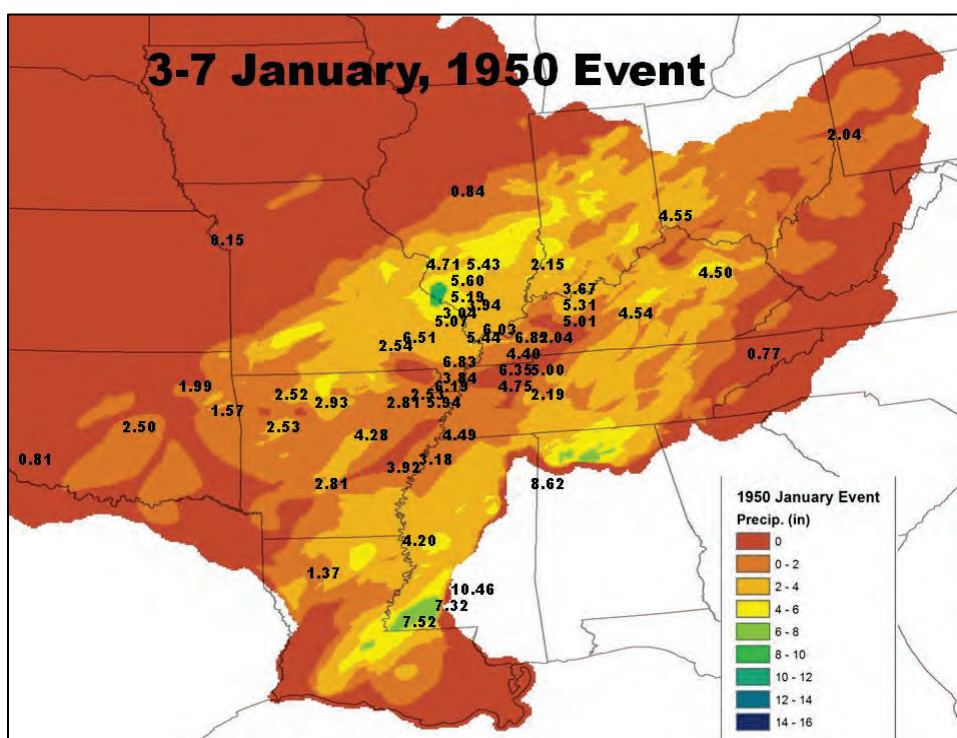
- This set-up storm for the HYPO 52A was not included in the isohyetal maps.

G.5.10 3–7 January 1950

- The area of heavy rainfall was at first oriented northeast-southwest from Lake Erie to northeastern Texas with later displacement southeastward as shown in Figure G-8.
- Rainfall totals produced from the 6-hour isohyets maps matched well with the observational data.
- Issues and concerns
 - No issues or concerns with the January 3–7 portion of the storm.

- HYPO 58A extended the rainfall event to January 16, which generally doubled the rainfall for the event. HMR34 (USACE, Weather Bureau 1956) states, “For the next 3 days following the cessation of rainfall over the area of interest, the large polar High moved very slowly eastward, its center reaching the Atlantic Coast on January 9, blocking the entrance of another depression into the central U.S. and return of rainfall until January 10.” Addition of rainfall from the next event, January 10–16, needed to be supplemented using daily observational data since HMR34 did not contain 6-hour isohyets maps for that time frame.

Figure G-8. Comparison of generated storm total precipitation with observational data for the 3–7 January 1950 storm event.



G.6 Compilation of all available data

The NCDC is the official source of climate data for the United States. NCDC datasets contain global daily precipitation and temperature data dating back to the 1800s. Hourly precipitation datasets across the United States are available beginning in 1948. With the exception of the 1950 storm event, only daily data of total precipitation amounts and maximum/minimum temperatures were available from NCDC for use in the development of the precipitation event for the storms in the

original MRPFS. Hourly and daily data for precipitation and daily maximum/minimum temperatures were available for the 1950 storm.

MVD historian, Charles Camillo, researched the availability of data that were used during MRPFS. He located paper versions of precipitation data at the National Archives (NA) in Kansas City. With the exception of the 6–10 May 1943 and the 3–16 January 1950 events, 6-hourly precipitation amounts were available for the other storms used to produce the four HYPO floods. These data were manually entered into the dataset. Although these data were most useful, the main issue was that it did not contain official latitude/longitude values for the points in the dataset. Latitude and longitude values were determined using georeferencing techniques and are near, but not exactly, where the actual observations were taken.

To ensure proper initialization of the hydrologic models, NWS determined that the data period should be 6 months prior to the actual heavy precipitation events, the precipitation event, followed by 1 month post precipitation event. The dataset ensured that the NWS models would have proper initialization, attempt to produce base flow conditions prior to the occurrence of the event, and produce peak flows and volumes for the each storm in MRPFS. The 6-hourly precipitation and temperature data were developed for this period. It was determined during the analysis that the post-event period should be extended to ensure sufficient time to route the event downstream to the Gulf of Mexico. For this reason, the post-event simulation was extended approximately 1 month by adding zero precipitation grids to the CHPS-FEWS model ingest.

Due to the expanse of the Mississippi River Basin, it was determined that the 6-hour datasets would contain all available data for watersheds of the Missouri, Illinois, Ohio, Tennessee, Arkansas/Red, and Mississippi Rivers. Data include available information from New Mexico, Colorado, Wyoming, Montana, Texas, Oklahoma, Kansas, Nebraska, South Dakota, Nevada, Louisiana, Arkansas, Missouri, Iowa, Minnesota, Mississippi, Tennessee, Kentucky, Illinois, Wisconsin, Michigan, Indiana, Ohio, Pennsylvania, New York, West Virginia, Virginia, North Carolina, South Carolina, Georgia, and Alabama.

Since a robust dataset of hourly precipitation is not available for storms prior to 1948, daily precipitation data were used. With the absence of actual precipitation breakdowns for the 6-hour periods, all of the daily precipitation data were placed into the 00 UTC time period with the other three daily time periods containing 0 in. for the 6-month warm-up period and the 1-month post-storm intervals. During the event and the month of the event, percentages of 6-hour breakdowns were calculated from the NA dataset and multiplied by the daily data points outside of the area available from the NA and combined with the dataset from the NA.

For storms after 1948, hourly precipitation datasets were available but were not as dense as daily precipitation datasets. Daily precipitation data were available for approximately 4 to 10 times more stations than that of the hourly precipitation data. To incorporate both datasets and retain the integrity of the hourly data, percentages for the 00, 06, 12, 18 UTC time frames were calculated from the hourly data for each day by state. The daily precipitation totals were then multiplied by these percentages on a daily basis to develop the final 00, 06, 12, 18 UTC daily datasets.

The storms that were studied during this project are included in Table G-6 along with several storms that have produced major floods since the MRPFS was last performed in the 1950s. Additional storms, 1979, 1983, 1984, 1995, 2005, and the Nashville storm of 1–5 May 2010, were considered but not selected. These storms were not included in the final analysis because storms of greater intensity over the watershed were available.

Table G-6. Selected storms for analysis in producing and verifying HYPO flood scenarios.

Storms	Storm Dates	Season	HYPO Storm	Major Basins Impacted
Phase I Analysis				
1913	23-27 March	Early Spring	56	White, Red
1927	12-16 April	Early Spring	56, 63	White, Red///Upper Mississippi, White, Red
1928	28-30 June	Late Spring	52A	Missouri, Upper Mississippi
1937	6-25 January	Winter	58A	Ohio, Arkansas, Red, Lower Mississippi
1938	14-19 February	Winter	58A	Ohio, Arkansas, Red, Lower Mississippi
1943	6-10 May	Late Spring	52A, 63	Missouri, Upper Mississippi ///Upper Mississippi, White, Red
1943	12-20 May	Late Spring	52A, 63	Missouri, Upper Mississippi ///Upper Mississippi, White, Red

Storms	Storm Dates	Season	HYP0 Storm	Major Basins Impacted
1945	28 March-2 April	Early Spring	56	White, Red
1950	3-16 January	Winter	58A	Ohio, Arkansas, Red, Lower Mississippi
Phase II Analysis (Not currently scoped or funded)				
1973	15-26 April	Early Spring		Arkansas, Red
1975	18-29 March	Early Spring		Ohio, White
1993	28 June-28 July	Late Spring		Missouri, Upper Mississippi
1997	1-9 March	Winter		Ohio, Lower Mississippi
2008	18-21 March	Early Spring		Ohio, White, Lower Mississippi
2011	22 April-3 May	Early Spring		Upper Mississippi, Ohio, Lower Mississippi, White

G.7 Analysis of precipitation events

Hydrometeorological Report No. 34, *Meteorology of Flood-Producing Storms in the Mississippi River Basin* (USACE, Weather Bureau 1956), stated that the purpose of the meteorological study was to enable USACE to “determine flood magnitudes that will be used as a basis for establishing levee grades on the main stem of the Mississippi River and for planning, designing, and determining benefit valuations of a large number of other comprehensive flood control works within the Mississippi River Basin.” To do this, a suite of heavy precipitation storm events were developed that required the U.S. Weather Bureau to perform the following:

1. Examine meteorological conditions that produced past major floods over various portions of the total basin.
2. Investigate historical storms of large intensity that, because of ground conditions or straddling of adjacent basins, may not have caused serious floods.
3. Establish plausible sequences of major storms based on meteorological consideration that under suitable conditions of placement and runoff appear to indicate a great flood potential.
4. Liaise between the hydrologist and the meteorologist.

Thirteen of the top twenty stages at Cairo, IL — the confluence of the Mississippi and Ohio Rivers — have occurred since the completion of the MRPFS over 60 years ago, as shown in Table G-7.

Table G-7. Significant flood crest stages and dates at Cairo, IL.

Stage in Feet	Crest Date	Stage in Feet	Crest Date
61.72	2 May 2011	54.7	18 April 1979
59.5	3 February 1937	54.5	16 May 1961
56.5	3 April 1975	54.2	17 April 1994
56.4	20 April 1927	54.2	8 May 1983
56.2	11 March 1997	54.0	16 May 1984
55.9	15 February 1950	53.9	6 April 1912
55.7	28 May 1995	53.9	11 March 1945
55.6	1 April 1973	53.89	25 March 2008
54.95	19 May 2002	53.6	26 March 1922
54.7	4 April 1913	53.5	18 May 1996

The 2011 April and May flood event produced the record stage at Cairo, IL, and also produced numerous record flows along the Lower Mississippi River downstream from Cairo. It was prudent to evaluate the precipitation events that produced floods after the 1950s to determine if a sequence of precipitation events has occurred that exceed the four HYPO flood storm sequences. To do this, precipitation observations were compiled for the historical storms and recent storms from the NCDC COOP database¹.

Eleven precipitation events were evaluated within the Mississippi River Basin. Daily data were used due to the availability of a greater network of reporting stations. The storm sequences were compiled according to the rules of transposition from the original study:

- Tropical storms over the lower basin could not be moved in location.
- Storms should be used only in the season of the year that they occurred.
- Movements of several hundred miles are permissible provided the storms are not moved beyond the major drainage basins adjoining the basin which they occurred.
- Rotation of storms about axis should be limited to a maximum of 20°.

¹ <http://www.ncdc.noaa.gov/IPS/coop/coop.html>

Heavy precipitation events from four HYPO 52A, 56, 58A, and 63 were studied in conjunction with the more recent storms. Table G-8 lists the precipitation events, the main drainage basins affected, and the HYPO storm(s) used. The max rainfall may not represent the maximum amounts realized in the storms (especially 1937) because of data availability issues.

Table G-8. Storms and summary information.

Dates of Precipitation	Main Drainage Basin Affected	HYPO	Max Rainfall
Phase I Analysis			
23-27 March 1913	Ohio, Middle Mississippi, TN, Cumberland	56	11.60"* Bellefontaine, OH
12-16 April 1927	Lower Mississippi, Arkansas, White, Red	56,63	11.95" Marshall, AR
28-30 June 1928	Middle Mississippi, Ohio, Cumberland	52A	10.16" Clinton, KY
17-24 January 1937	Lower Mississippi, Ohio, TN, Cumberland, White	58A	22.65" McKenzie, TN
14-18 February 1938	Arkansas, White	58A	11.00" Calvin, OK
7-11 May 1943	Middle Mississippi, Ohio, Arkansas, White	52A,63	25.00" Warner, OK
15-20 May 1943	Middle Mississippi, Lower Missouri, Arkansas	52A,63	16.60" Lowell, KS
3-16 January 1950	Lower Mississippi, Ohio, TN, Cumberland, White, Red	58A	12.86" Owensboro, KY
Phase II Analysis (Not currently scoped or funded)			
14-20 March 1973	Lower Mississippi, TN, Arkansas		11.01" Winona, MS
16-26 April 1973	Lower Mississippi, Lower Ohio, Arkansas, White		15.65" Gordon, AR
12-29 March 1975	Lower Mississippi, TN, White		12.58" Newbern, TN
28 June-9 July 1993	Lower Missouri, Middle Mississippi, Upper Mississippi		17.35" Beattie, KS
27 February-9 March 1997	Lower Ohio, TN, Cumberland		14.04" Madisonville, KY
22 April-3 May 2011	Lower Mississippi, Ohio, TN, Cumberland, White		23.16" Poplar Bluff, MO

* " = inches

Storm explanations were compiled from the MRPFS Appendix J (MRC 1955). Daily weather maps are included for each storm to demonstrate the development of the precipitation event. The Daily Weather Maps were compiled by NOAA in the NOAA Central Library Data Imaging Project.

G.7.1 23–27 March 1913

This storm had major rain bursts associated with a series of waves on a quasi-stationary front, the type generally considered to be the most important heavy-rain producer in the central United States. Isohyetal maps were prepared for the main bursts, which occurred between the morning of the 24th and the evening of the 25th, Figure G-11. Figures G-9 and G-10 show weather patterns for the days around the primary event. Table G-9 shows the top 20 recorded rainfall gauge amounts.

Two days before the storm (March 21), light rain left the ground wet enough so that the early period of intense rain saturated it. The resulting surface conditions were conducive to a large runoff.

As in almost all flood-producing storms in the central United States, the pressure was above normal over the Bermuda area. During the 4-day period 23–26 March 1913, the pressure averaged approximately 1034 millibars (mb) at Bermuda in contrast to a normal 1019 mb for this period. The warm air current brought into the southern United States by the Bermuda high was characterized by dew points ranging as high as the upper 60s (°F) within approximately 3 °F of maximum observed dew points for the area and season.

During the same time, a polar high centered in southern Canada on the morning of the 24th poured unseasonably cold air into the Central Plains States. The average temperature at Havre, MT, during the period of the storm, was 34 °F below normal.

From detailed weather charts, two lines of discontinuity were found to lie between the Bermuda high and the arctic high: (1) the major polar front, extended southwestward from a cyclone center near Sault Ste. Marie, MI, at 0700 CST March 24 and (2) the warm sector of the same cyclone (Figure G-13, bottom right). The second discontinuity line, the important one to produce heavy rain, was likely formed originally as an instability line. The formation of instability lines in

the warm sector of winter cyclones is a rather common occurrence in the central United States.

Rarely does the instability line become oriented to lie nearly at right angles to the incoming low-level southerly jet. The temperature contrast component of the differential advection in the instability line case is supplied by the agency of rain cooling. A combination of factors, including cooling due to the melting snow at upper levels and the cold rain resulting at lower levels and local cooling by moist adiabatic descent of air in the rain area, are responsible for the temperature falls behind the instability line. After the cool air mass between the two discontinuities formed, the southern edge acted like a front, having had waves on it over a period of 36 hours. The temperature gradient thus interposed in the strong northward-moving air current formed a band of differential advection that was alternately augmented and diminished as waves moved along the discontinuity. This trigger mechanism, in conjunction with the probable latent instability of the warm air mass, resulted in heavy rains centered between the two lines of discontinuity. Although warm differential advection was noted as having existed behind the northern front, much less rain fell in that area. This is explained by the depletion of moisture by the huge convective system immediately upwind (south of this otherwise-favorable area for heavy rain).

Because of an almost perfect balance between the forces urging the cold air southward and the warm air northward (at the earth's surface), the zone of interaction remained nearly stationary for 48 hours. This balance of forces is a necessary condition for the quasi-stationary frontal-type storm, for once mastery by one or the other of the two air masses is obtained, a new set of rain-producing conditions must be set up to start the process again.

Conditions that followed the March 1913 storm were such that a high moisture charge could not quickly return to the central United States. The cold front swept the tropical air out of the entire Gulf of Mexico region. Under favorable circumstances, the moisture necessary for flood-producing storms would take a minimum of 3 days to reestablish itself after the ending of a storm of the March 1913 type. The 12-hour representative dew point for this storm is 65°F. The

maximum possible dew point is 71°F, which allows an upward moisture adjustment of 35% in place.

**Table G-9. Top 20 recorded rainfall gauges
(inches) for the 23–27 March 1913
precipitation event.**

RICHMOND_WATERWORKS	IN	11.26
BELLEFONTAINE	OH	11.20
RICHMOND	IN	11.20
GREEN	OH	10.70
MARION	OH	10.60
SHOALS_5_S	IN	10.51
BANGORVILLE	OH	10.50
UPPER SANDUSKY	OH	10.40
WOOSTER	OH	10.10
CONNERSVILLE	IN	10.08
COLUMBUS	IN	10.02
CONNERSVILLE	IN	10.00
COLUMBUS	IN	9.90
AKRON	OH	9.80
BUCYRUS	OH	9.80
MAUZY	IN	9.75
HUDSON	OH	9.75
MAUZY 2	IN	9.70
FAIRFIELD	IL	9.60
VINCENNES	IN	9.49

Figure G-9. 21-24 March 1913 Daily Weather Maps.

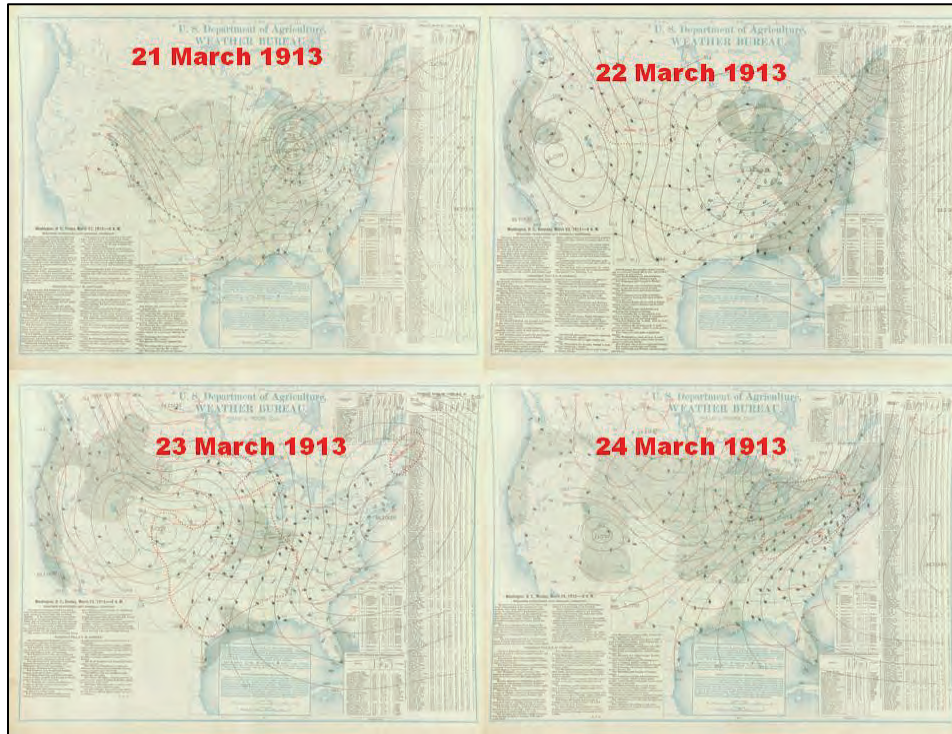


Figure G-10. 25-28 March 1913 Daily Weather Maps.

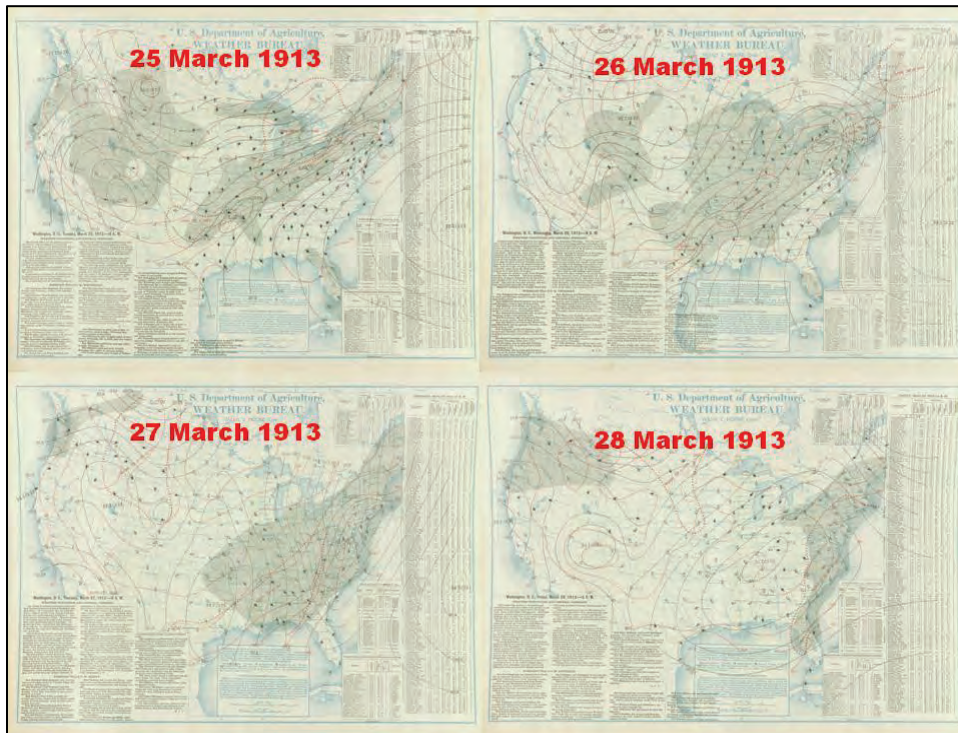
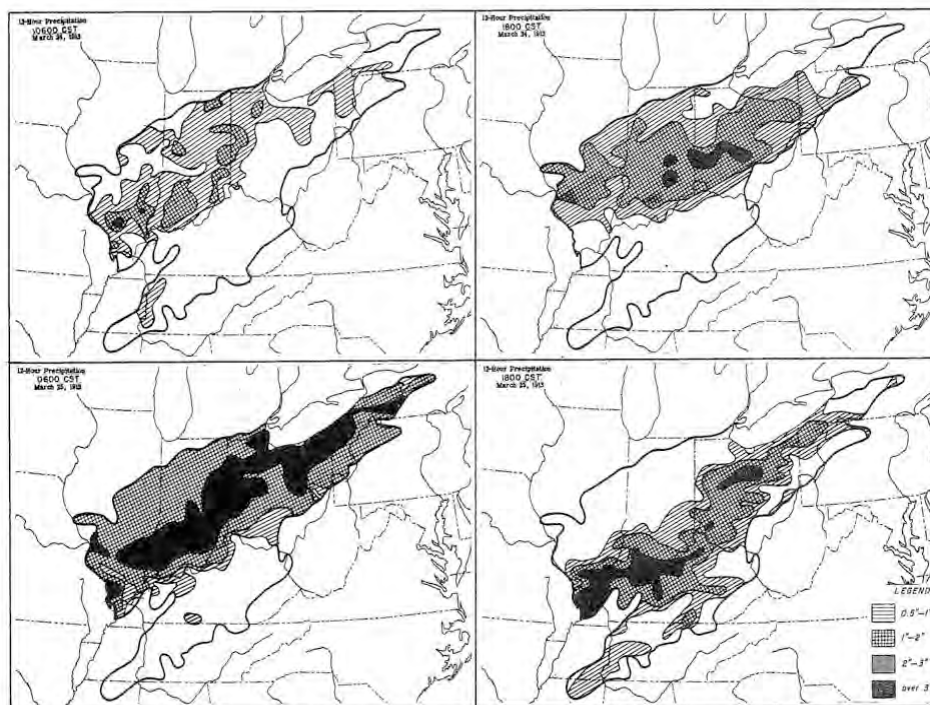


Figure G-11. 12-hour isohyets maps for 24–25 March 1913 storm event.



G.7.2 12–16 April 1927

This storm occurred over the area from east Texas to southern Illinois and from eastern Oklahoma to north-east Mississippi. Amounts of rainfall up to 12 in. occurred in north-central Arkansas and up to 9.6 in. in central Louisiana. Precipitation totals for the top 20 recorded rainfall gauges are shown in Table G-10. Over much of this area, the precipitation during March and the first part of April had been in excess of normal so that ground moisture was high and rivers of the section were flooding during the greater part of the month, and some had the highest stages ever known. Due to the moderate temperature and heavy rains prior to this storm, there was no snow cover at the time.

For several days prior to this rainstorm, a large cyclone moved slowly southeastward across the Rocky Mountains combining with a Low near the Mexican Border on April 9–10. During this time, pressure was high over the eastern part of the country with a frontal trough separating the warm high ridge over the southeast from the polar anticyclone to the north. This same synoptic situation persisted for several days prior to

the beginning of the rainfall with only a slight southeastward drift of the polar anticyclone.

The major synoptic feature associated with this storm was the Low centered over west Texas on April 12. While no upper air data are available, slow moving Lows of this kind are usually associated with a deep upper air trough. Most of the rainfall was a result of thunderstorms, with which occurred a number of hailstorms and tornadoes, in advance of this Low. Figures G-12 and G-13 show weather patterns for days before, during, and after the storm event.

The first isohyetal pattern for the 12 hours ending at 1500 CST April 12 shows some small areas of rainfall due to thunderstorms in eastern Oklahoma and northwest Arkansas and a more intense area of more than 4 in. in southeast Tennessee (Figure G-14, top left). The details associated with this latter area cannot be determined from the available data, but it was in a pressure-fall area and in favorable location for convergence and overrunning of warm moist tropical air from the southwest.

The isohyetal pattern for the 12 hours ending at 0300 CST April 13, shows considerable rainfall from eastern Oklahoma to central Tennessee and northward to southeast Missouri (Figure G-14 top right). The surface data near this time indicate that numerous thunderstorms account for most of this precipitation (Figure G-12, bottom right). The late afternoon and evening increase of precipitation at the time of maximum heating indicates that the increase of instability due to low-level warming was an important factor. The chief cause of the precipitation is still likely to be convergence in the cyclonic flow of maritime tropical air northward in advance of the Low in Texas and with the warm frontal depression that dissipated or merged with the cold front to the north by 0700 CST April 13 (Figure G-12, bottom right).

The isohyetal pattern ending at 1500 CST April 13, shows a continuation of heavy rain mostly in northwest Arkansas and eastern Oklahoma, a favorable location for squall lines in relation to the Low in north Texas and the frontal system to the north (Figure G-14, bottom left).

The isohyetal pattern for the 12 hours ending at 0300 CST April 14, shows the pattern of rainfall still in the warm sector formed by the cold

front approaching from the west and another front to the north (Figure G-14, bottom right). From an examination of the surface maps at approximately this time, the rainfall seemed to be largely a result of thunderstorms, indication instability, and strong convective activity (Figure G-13, top left). Windstorms, hail, and a few tornadoes occurred in eastern Texas as the front passed. The small area of heavy rain in east Texas also seems to be the result of local storms associated with the frontal passage.

The remaining isohyetal patterns of this storm seem to be very closely associated with the frontal passage from the west (Figure G-15). The weather maps show most of the thunderstorm activity along this front, which moved on across the area, bringing heavy bursts of precipitation, the isohyetal patterns progressing eastward with the front (Figure G-13). The rainfall came to an end on April 16 as the front moved out of the area.

The end of the rainfall was brought about by the cessation of convergent flow in the frontal trough over the area of interest and the advection of cooler and drier air. The High following this front was very small, scarcely larger than the rain-cooled area usually following squall lines.

The fact that another rainstorm occurred over Kansas and Missouri from April 7–9 and heavy rain occurred in Tennessee from April 9–12 indicates that a previous storm could have occurred over the area from April 7–12. It would require a slight shift of frontal wave location with the previous heavy rainfall events. This event could have been extended for at least 5 days with no break in the rainfall over the same area in which it occurred.

The 12-hour representative reduced dew point observed in LMV 4-8 storm was 72 °F. The maximum dew point to be expected in the area at that time of year is 76 °F, permitting a 22% moisture adjustment in place.

Table G-10. Top 20 recorded rainfall gauges (inches)
for the 12–16 April 1927 precipitation event.

JEFFERSON-PLAQUIMINE DRAINAGE DISTRICT	LA	20.4
PHAR	LA	18.5
CITRUS PUMPING STATION	LA	15.8
MORGAN CITY	LA	15.6
CLOVELY	LA	14.1
NEWORLEANS 1	LA	14
NEWORLEANS 2	LA	14
CORNING	AR	13.9
PARK	LA	13.3
FACTORY	LA	13.2
MARSHALL	AR	12
DANVILLE	AR	11.7
LAUREL GROVE	LA	11.6
HOLISTER	MO	11.5
ALGIERS	LA	11.1
DELTA FARMS	LA	10.6
LUTHERVILLE	AR	10.6
GRENVILLE	MS	10.5
FRANKLIN	LA	10.4
FREEMAN SPRINGS	AR	10.2

Figure G-12. 10–13 April 1927 Daily Weather Maps.

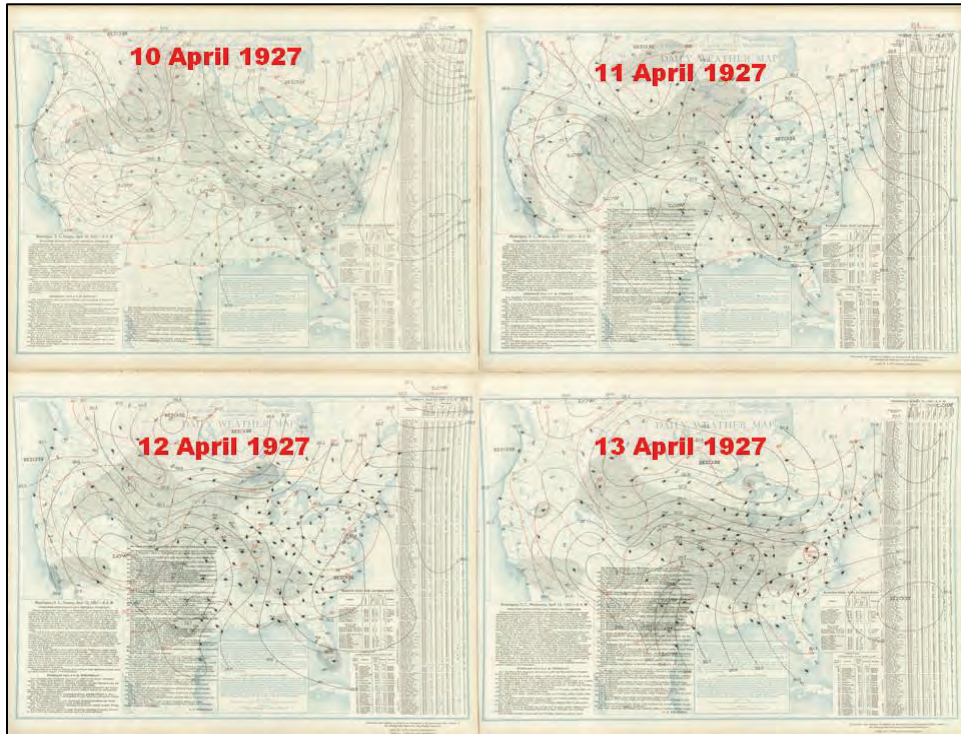


Figure G-13. 14–17 April 1927 Daily Weather Maps.

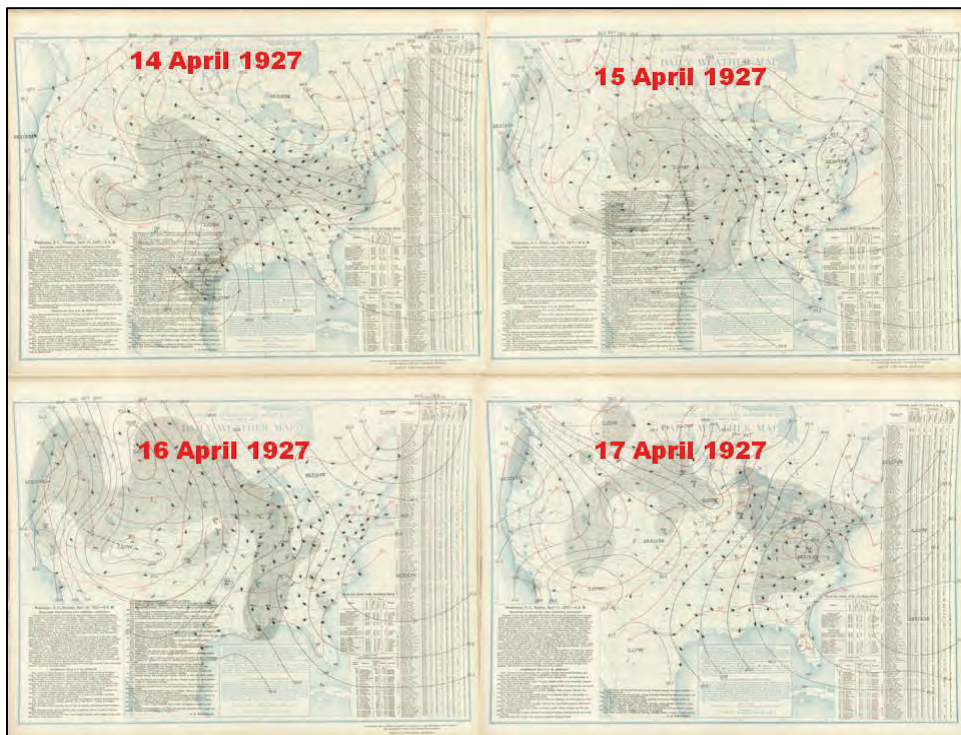


Figure G-14. 12-hour isohyets maps for 12-16 April 1927 storm event (12-14 April).

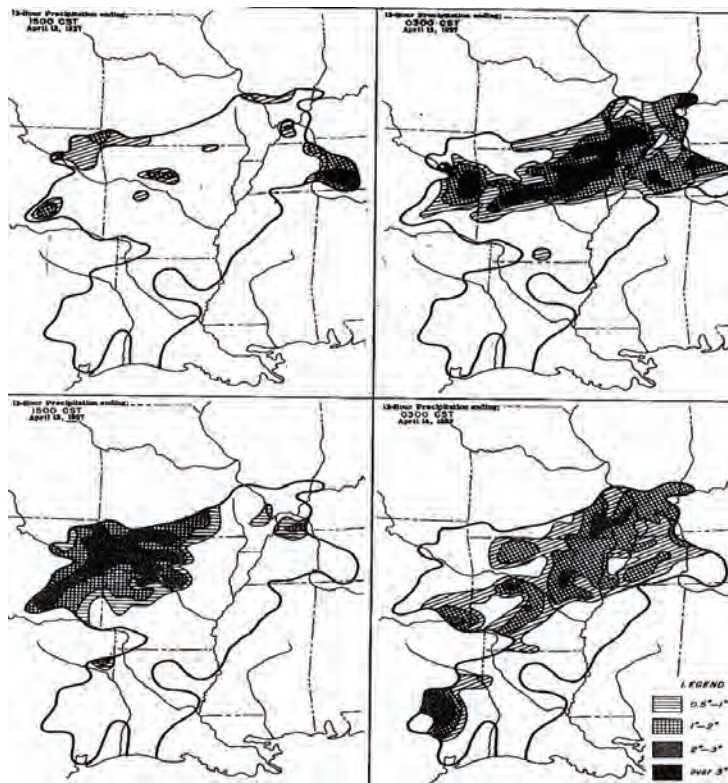
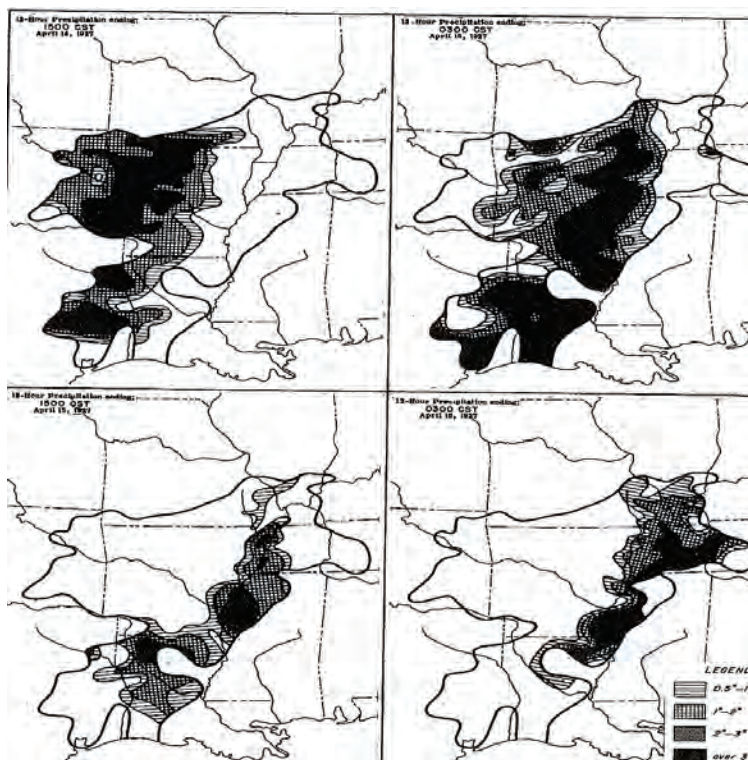


Figure 3.3 12-hour isohyets maps for 12-16 April 1927 storm event (14-16 April).



G.7.3 28 June – 1 July 1928

This storm occurred principally in Kentucky, Tennessee, and parts of Missouri. The largest amount of rainfall recorded was 10.16 in. at Clinton, TN. Precipitation for the top 20 recorded rainfall gauges are shown in Table G-11. Most of the precipitation was the result of severe thunderstorms in moist tropical air that was moving northward and northeastward from the Gulf of Mexico.

June was a remarkably wet month over practically all parts of the country from the Rocky Mountains eastward, and precipitation was rather uniformly distributed during the various portions of the month. This indicates that soil moisture was at least relatively high.

As is frequent for the month of June, the movement of pressure patterns across the United States was rather sluggish. From June 2 to 26, an occluding wave cyclone moved from western Texas into Ontario. Following this cyclone, a weak anticyclone of modified polar air traveled to the Atlantic Coast by June 27. A weak cold front proceeded this anticyclone that on the 27th reached from the western Atlantic through the Gulf States and northwestward into a Low over the southwest (Figure G-16, top left). This weak front interfered very little with the ridge of high pressure that extended from the Atlantic subtropical anticyclone westward over the Gulf States while the High following it partially merged with the Atlantic subtropical anticyclone. This series of events repeated itself early on June 28 as the Low in the southwest started intensifying and moving northeastward accounting for the first heavy burst of rainfall of this storm.

The isohyetal pattern for the 12 hours ending at 1300 CST June 28 shows a heavy burst of more than 4 in. in southwest Missouri and more than 5 in. in western Kentucky (Figure G-17, top left). The detailed surface map for 0700 EST June 28 shows a weak warm front moving northward across the area with thunderstorms occurring on both sides of the front (Figure G-16, top right). The weather pattern indicates that most of the rainfall is due to thunderstorms caused by horizontal convergence of the moist maritime tropical air moving northward over the area. An indication of the instability present in this northward-flowing air was the occurrence of two tornadoes in the afternoon of June 28 in southern Iowa just north of the heavy rainfall area.

The next isohyetal map, which was for the 12 hours ending 0100 CST June 29, shows an increase of rainfall in northeastern Tennessee and eastern Kentucky as the warm front trough advanced across the area as part of an open wave with a Low to the northwest from which a cold front extended southwestward (Figure G-17, top right). The cause of rainfall was still convergence in the warm frontal trough with the addition of orographic lifting over the more mountainous terrain of northeastern Tennessee and eastern Kentucky. Note that surface dew points in the maritime tropical air flowing northward were in the 70s indicating a plentiful supply of moisture. At 0100 CST June 29, two tornadic thunderstorms were reported near Nashville, TN, in this northward flowing current of moist tropical air along with the thunderstorms and heavy rainfall that occurred near this time.

The heaviest 12-hour burst of rainfall of the storm occurred during the period ending at 1300 CST June 29, where 4 in. or 5 in. fell over parts of northeast Tennessee and Kentucky (Figure G-17, middle left). The detailed surface map for 0700 CST June 29 shows that a cold front with a large trough of maritime tropical air in advance of it approaching the area during this time (Figure G-16, bottom left). Convergent flow in the trough in advance of the front and orographic lifting over the mountainous terrain of the moist unstable air mass seems to account for most of the rainfall.

The isohyetal pattern for the 12 hours ending at 0100 CST June 30 shows a smaller amount of precipitation than the previous periods, and the surface maps show that it was more directly associated with the frontal passage over the area (Figure G-17, middle right). The final isohyetal pattern for the 12 hours ending at 1300 CST June 30 shows only a small area of rainfall in southwest Missouri due to thunderstorms in advance of a warm frontal trough moving in from the southwest (Figure G-17, bottom).

Little upper-air data are available for this storm due to the early date of occurrence. Located at approximately 1,500 m, the winds over the eastern United States on June 28 were southerly, gradually shifting to southwesterly above this level. Upper air humidity values for June were above normal upward through the 2,000 m level at Broken Arrow, OK, the nearest recording station to the air current flowing over the area of interest.

A cold front passed through the area of interest on June 25, accompanied by moderate rainfall. This front subsequently moved to the Gulf Coast and returned northward becoming an integral factor in the mechanism of this storm. This rocking motion of a cold front followed by a warm front can occur somewhat more rapidly than in the case of this event. Under most favorable conditions of the synoptic features, a minimum interval of 2 rainless days would be required to include prior rainfall.

The 12-hour representative reduced dew point observed in the OR 7-10 storm was 72 °F. The maximum dew point to be expected in this area the same time of year is 78 °F permitting a 41% moisture adjustment in place.

Table G-11. Top 20 recorded rainfall gauges (inches) for the June 28 – July 1 precipitation event.

MADISON	TN	10.4
CLINTON	TN	10.2
COLUMBIA	MO	7.51
BUFFALO_VALLEY	TN	7.1
WORSHAM	TN	7.09
SPRINGFIELD	MO	7.05
SHARPLES	WV	7.03
RUGBY	TN	6.8
PADUCAH	KY	6.7
NEWRIVER	TN	6.6
EUBANK	KY	6.38
LIBERTY	TN	6.2
PRINCETON	KY	6.2
SEYMOUR	MO	6.2
TYRONE	KY	6.2
COKEVILLE	TN	5.7
KERMIT	WV	5.6
MARION	KY	5.56
LEXINGTON_BLUEGRASS_AIRPORT	KY	5.5
SALVISA	KY	5.4

Figure G-16. 27–30 June 1928 Daily Weather Maps.

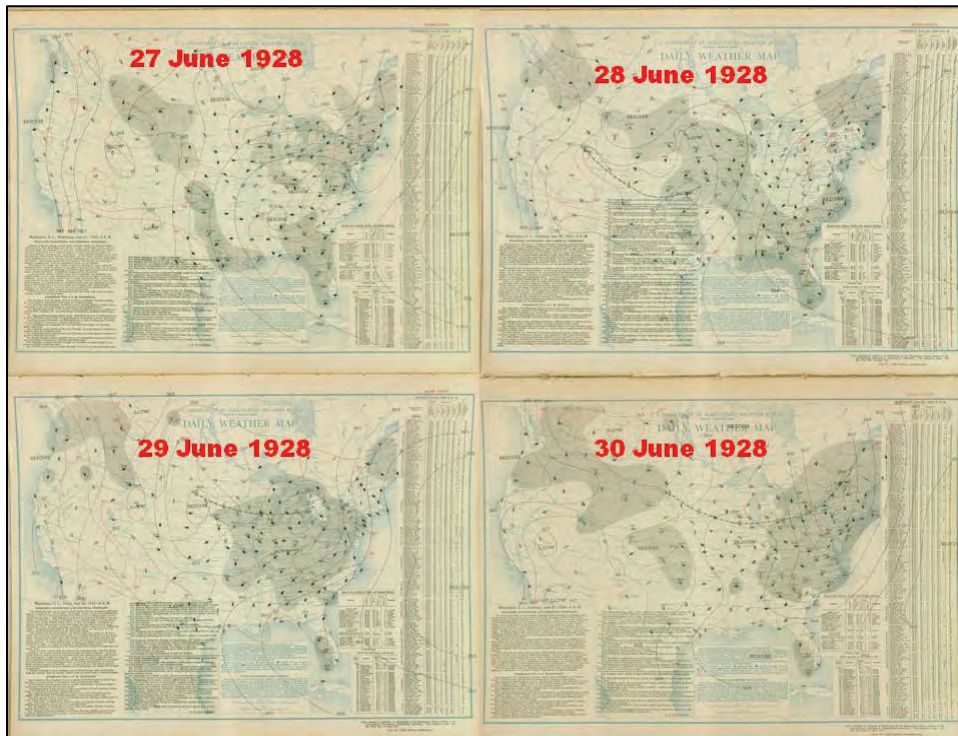
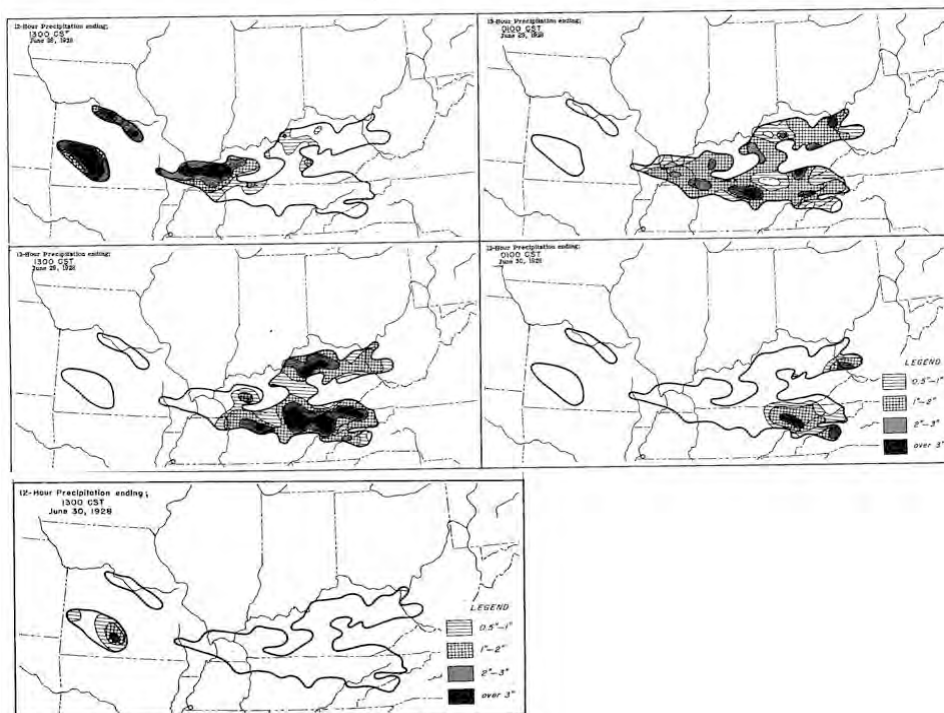


Figure G-17. 12-hour isohyets maps for the June 28–July 1 storm event.



G.7.4 6-25 January 1937

January 1937 represents conditions near the extreme for January under the present climatic regime for the persistence of the warm moist current that sweeps westward through the Antilles. During an average winter month, cold dry air sweeps through the Gulf of Mexico into the northern Caribbean Sea cutting off the flow of tropical air for several days at a time. In January 1937, no cold air was able to pass southern Florida until the 30th of the month and only by a few miles. The southeastern gulf was overlain by unmodified tropical air all month. Simultaneously, temperatures in the western half of the country were below normal, approaching record Lows in some of the Rocky Mountain States. Frontal activity was frequent and intense. In fact, the mean surface position of the polar front for January 1937 was 400–500 miles north of its most frequent January position through central and southern Florida. Storms were frequent all month; particularly intense frontal activity accompanied by almost continuous rain in the eastern United States occurred during the period 17th through the 25th. The detailed surface weather maps (Figures G-18–G-22) and 6-hour incremental isohyetal maps (Figures G-23–G-26) are included.

Pressure was above normal to the east of Florida during this storm period and had been prior to January 1. High pressure is almost always present in the western Atlantic at the time of heavy rainfall in the Mississippi Valley. The cause of persistent high pressures in the subtropical belt is not yet known. The Pacific high cell was also much stronger and at a higher latitude than normal. This situation brings arctic air into the western states accompanied by a semi-permanent trough aloft while at a distance of one-half wave length downwind the ridge aloft is found near the east coast of the United States. This sets up a persistent southwesterly flow aloft over the Mississippi and Ohio Valleys — necessary for heavy rains in this region.

Storm precipitation fell in three main bursts: one on the 17th, the 21st, and the 24th. Precipitation amounts for the top 20 recorded rain gauges are shown in Table G-12. These bursts were associated with frontal cyclones in various stages of their life histories. Although a small quantity of snow was on the ground at the beginning of the period in some localities, the amount did not materially add to the magnitude of the flood.

As the first rain burst commenced over the Ohio Valley, the following rather characteristic synoptic weather picture prevailed. A Low of Pacific origin was situated in the western plains with intensely cold air northwest of it, a cold anticyclone was moving off the New England Coast, and the semi-permanent Atlantic sub-tropical high and anticyclone extended westward into the Gulf of Mexico. The large-scale maps show in detail the surface weather situation in the eastern part of the country during the first burst. The front between the tropical air and the cold air over the northeastern United States exhibits various contortions due in part to the effect of the mountains. Although the Low system seems complex in this case, at upper levels a simple southwesterly flow of moist air is evident over the eastern United States. An atmospheric sounding taken at Murfreesboro, TN, in the warm air current just before the first burst showed saturation of the air above the inversion at 935 mb (Figure G-31, top left). The temperatures in this layer are exceeded by only approximately 10% of the observations in January, and since high temperatures are not always accompanied by high moisture charges, it may be inferred that the water vapor content of the air was even more unusual.

After the rains of the 17th and 18th, an extension of an arctic High moved eastward along the northern border of the United States while at the same time a second Pacific Low with its attendant upper-air trough was located in the mountain states on the 19th. By morning of the 20th, while the front accompanying the Pacific Low lay near the longitude of El Paso, a rapidly deepening secondary wave cyclone had formed over Kansas. By evening of the 20th, this secondary Low was occluded and centered in northern Wisconsin. Moderate warm-front rains occurred over the Ohio valley on the 20th with a heavy burst (the most intense of the January 1937 storm) due to the passage of the occluded front early on the 21st. The Murfreesboro sounding for the morning of the 21st revealed moisture values at this time were even higher than on the 17th in the critical 900 to 700 mb layer. Latent instability was present in this layer, a condition prevailing in most heavy rainstorms.

The cold front that extended from the occluded front became stationary on the 21st through Tennessee and Kentucky. Almost continuous wave action along this front prevailed until the 23rd. A brief break in the rainfall over the Ohio valley occurred during the

morning of the 23rd. This was due to a weak thrust of arctic air that temporarily shunted off the moist upper current to the south and east of the Ohio Valley.

On the 24th, the polar front moved northward at the instigation of another Pacific Low and caused the last major rain-burst over the Ohio Valley. The Murfreesboro sounding for January 24 was taken in the warm inflow air during this last rain burst (Figure G-27, bottom right). Compared with the previous soundings, somewhat drier conditions in the layers above 850 mb were apparent and account, in part, for the lighter rain observed in this last burst, but latent instability was present in some of the layers and moisture below the 850 mb level was still at an extraordinarily high value. The last Pacific Low track was north of the tracks of its predecessors, having entered the United States near Williston, ND. The rain effect was similar to that in the storms with a more southerly track, but the subsequent air mass movements were different, for the dry cold air mass stopped the rain over the Ohio Valley on the morning of the 25th.

The final front that swept cold, dry air over the eastern United States did not penetrate beyond the middle of the Gulf of Mexico. This event may allow a quick resurgence of moisture into the Mississippi Valley if a rather deep trough happens to be approaching the Mississippi Valley from the west. Records indicate that this outcome did not occur in the 1937 storm, but rather a very weak trough passed through the Northern Plains and Great Lakes region on the 27th and 28th. Depending on the depth (intensity) of the trough, heavy rain under favorable circumstances can begin in the Ohio Valley approximately 48 hours after the preceding rainfall. This statement proceeds from many single winter storm observations that regularly traverse this stormy region.

The representative 12-hour surface dew point for the storm is 66 °F while the maximum observed dew point in January at the same location is 68 °F. This allows an increase of 10% in the rainfall values on the basis of surface moisture adjustment only.

Table G-12. Top 20 recorded rainfall gauges (inches) for the 5 January – 25 January 1937 precipitation event.

EARLINGTON	KY	37.28	-87.51	19370125	22.1
JOHNSONVILLE	TN	36.06	-87.95	19370125	21.2
MARTIN	TN	36.34	-88.85	19370125	21

MCKENZIE	TN	36.14	-88.51	19370125	21
SPRINGVILLE	TN	36.25	-88.15	19370125	20.9
DOVER	TN	36.49	-87.84	19370125	20.8
LOCKPORT	KY	38.44	-84.96	19370125	20.8
HOPKINSVILLE	KY	36.87	-87.49	19370125	20.7
ERIN	TN	36.32	-87.69	19370125	20.2
CLARKSVILE	TN	36.53	-87.36	19370125	19.8
MARKED_TRE	AR	35.53	-90.42	19370125	19.7
ANCHORAGE	KY	38.26	-85.54	19370125	19.5
CALHOUN	KY	37.54	-87.26	19370125	19.5
ST_JOHN	KY	37.7	-86	19370125	19.2
HARTFORD	KY	37.45	-86.9	19370125	19
ROME	IN	37.93	-86.53	19370125	18.9
BROWNSVILLE	TN	35.6	-89.26	19370125	18.6
LEAVENWORTH	IN	38.2	-86.34	19370125	18.6
PRINCETON	KY	37.11	-87.88	19370125	18.6

Figure G-18. 6–9 January 1937 Daily Weather Maps.

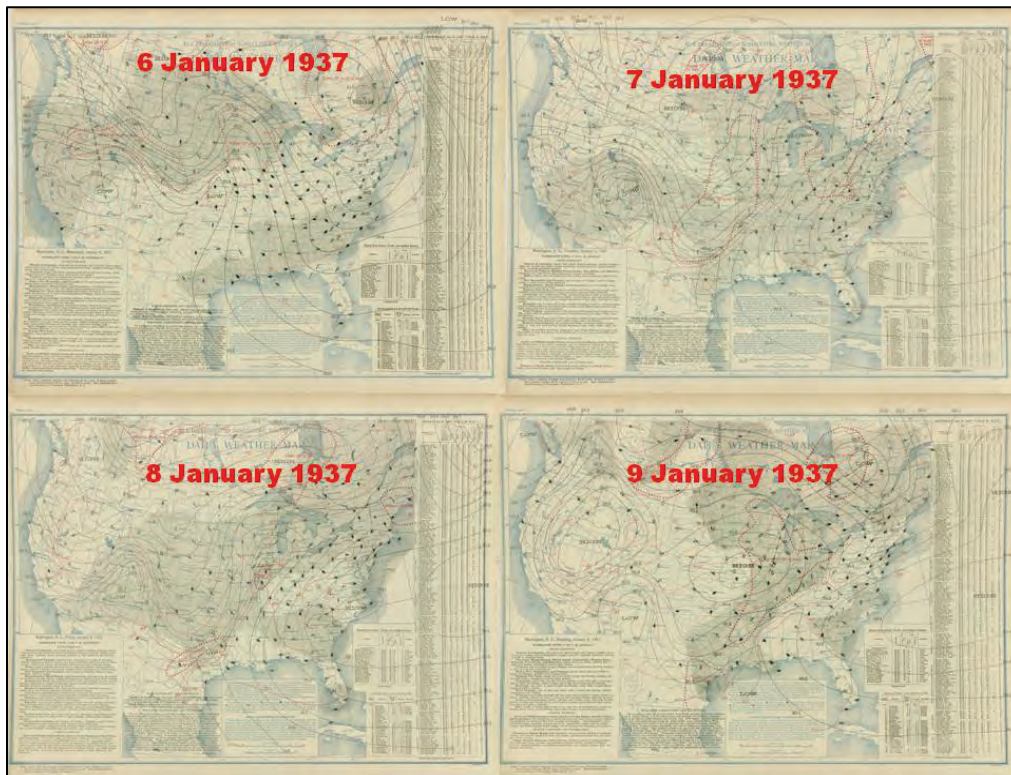


Figure G-19. 10–13 January 1937 Daily Weather Maps.

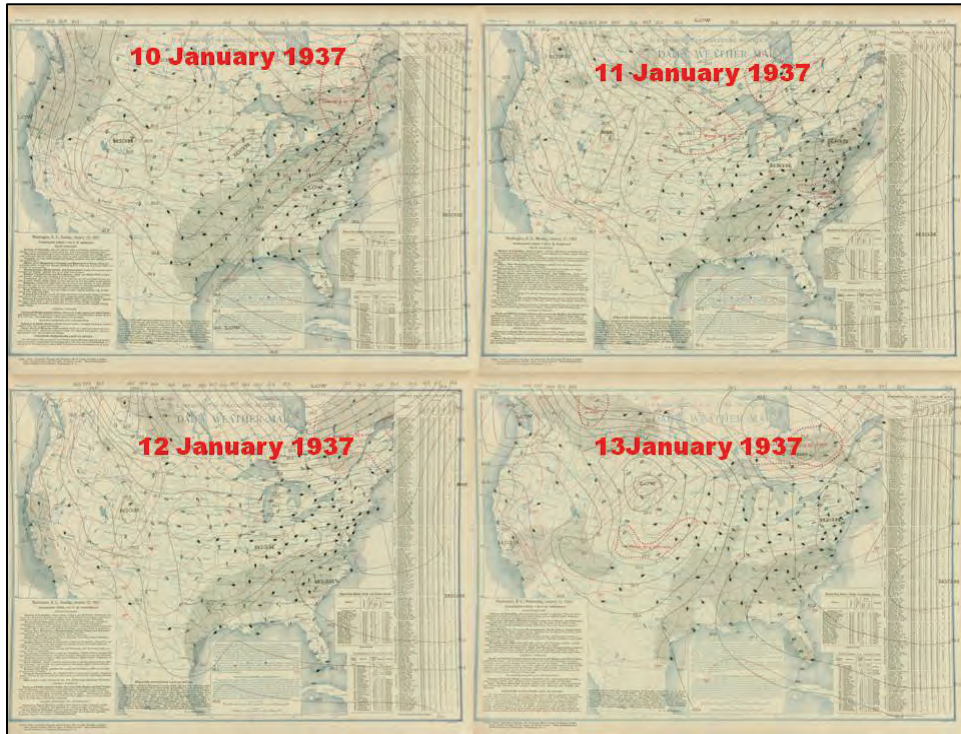


Figure G-20. 14–17 January 1937 Daily Weather Maps.

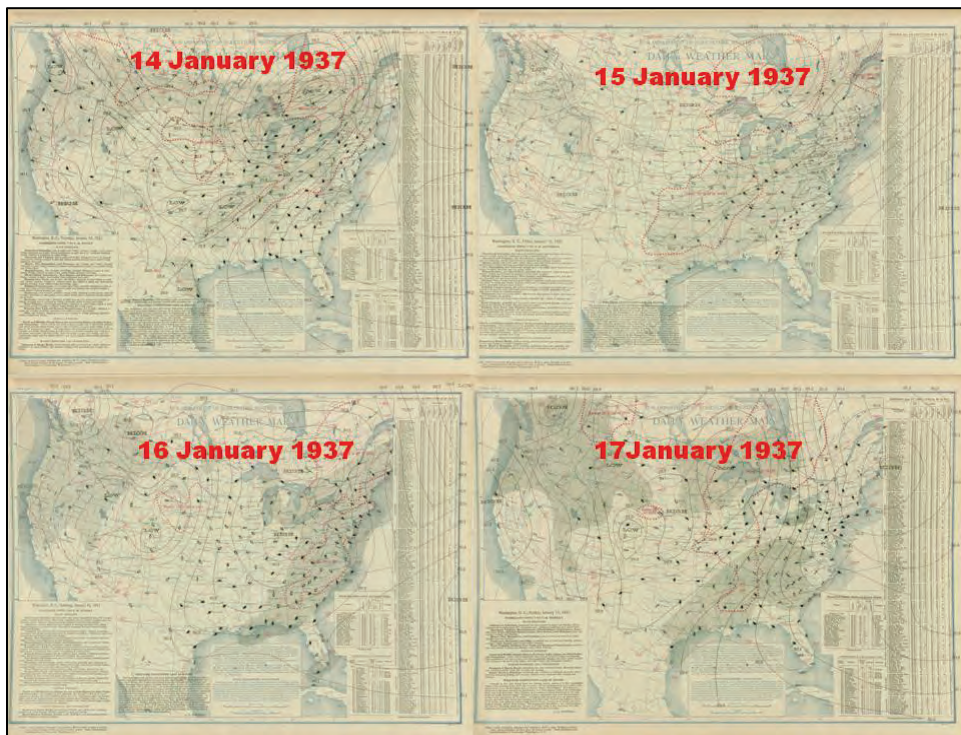


Figure G-21. 18–21 January 1937 Daily Weather Maps.

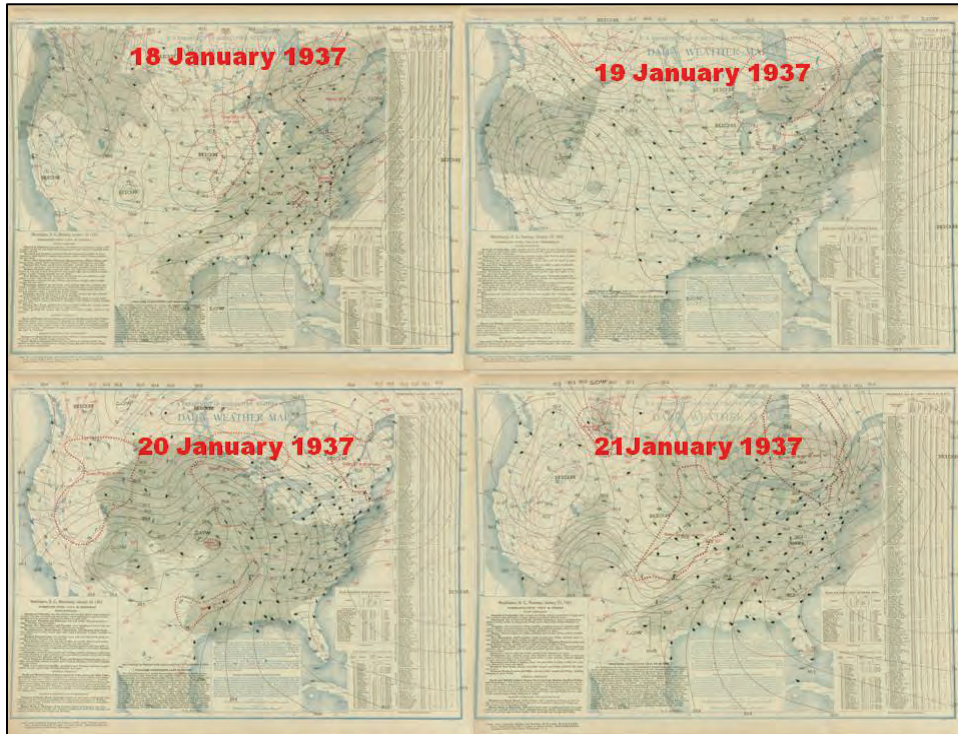


Figure G-22. 22–25 January 1937 Daily Weather Maps.

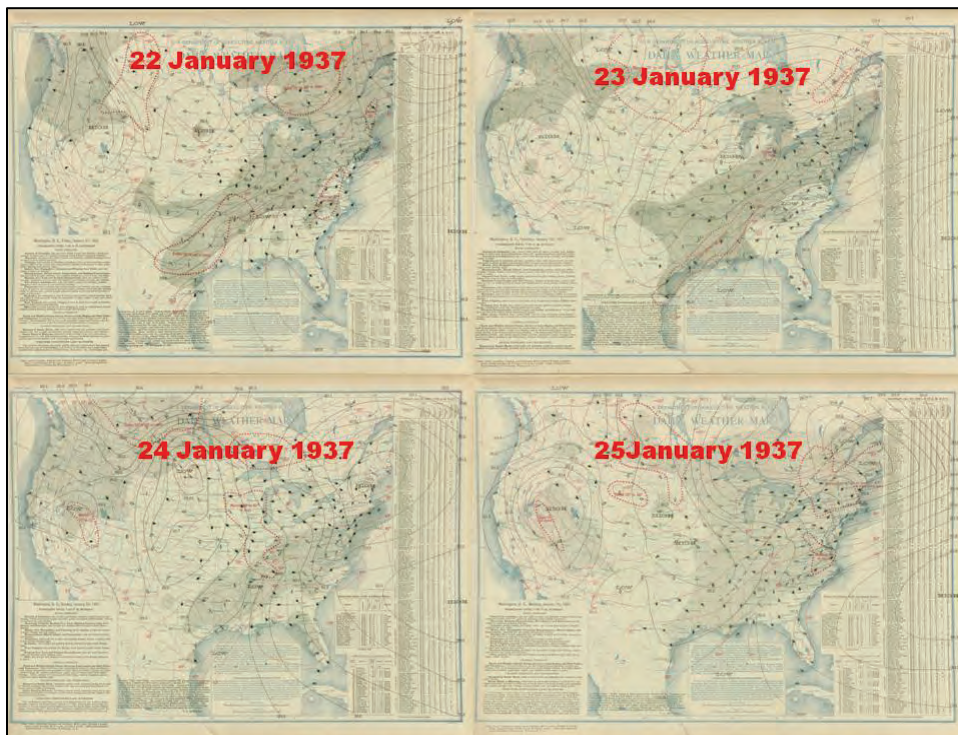


Figure G-23. 6-hour isohyets for the 17-25 January 1937 storm event (17-18 January).

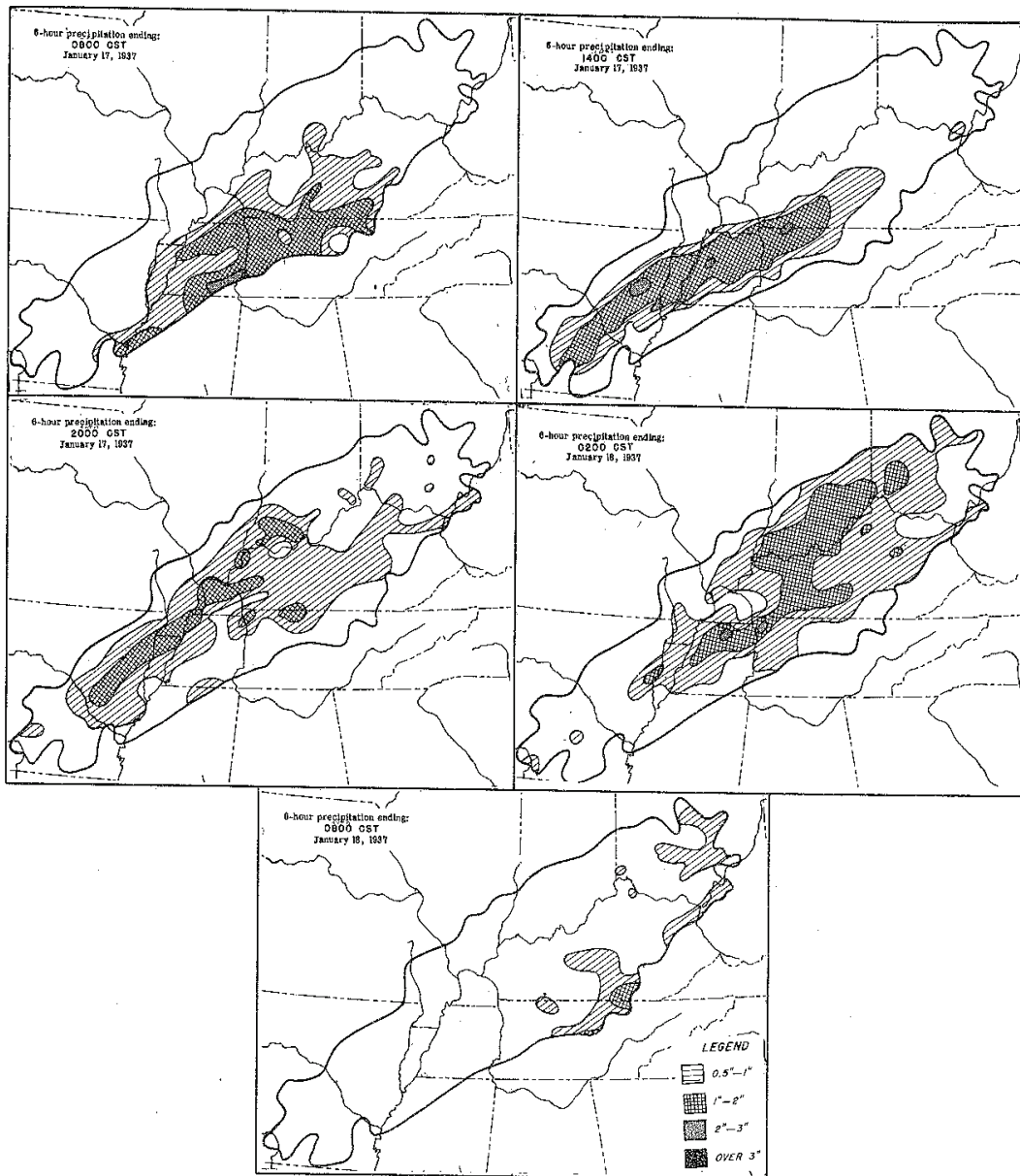


Figure G-24. 6-hour isohyets maps for 17-25 January 1937 storm event (17-20 January).

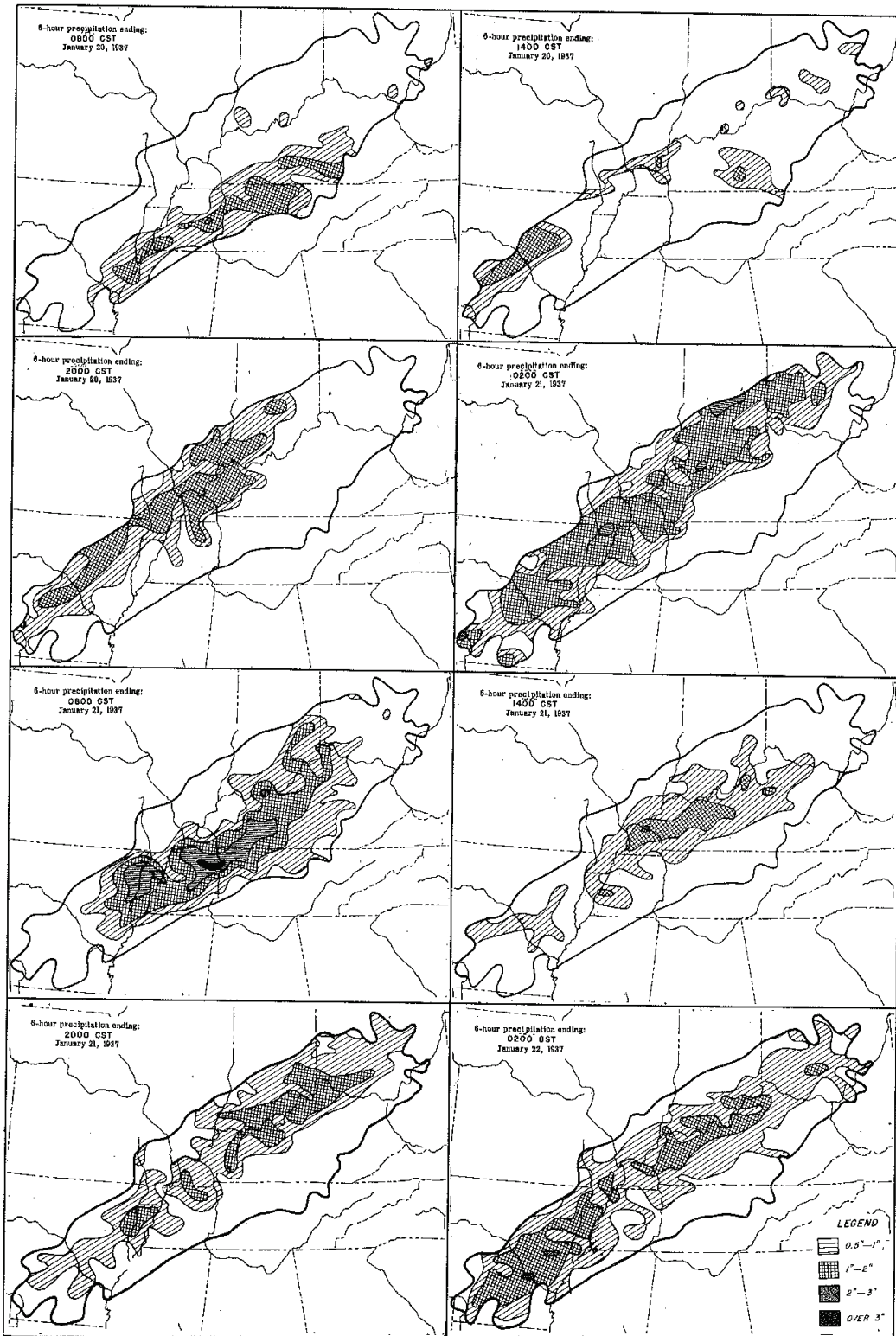


Figure G-25. 6-hour isohyets maps for 17-25 January 1937 storm event (22-24 January).

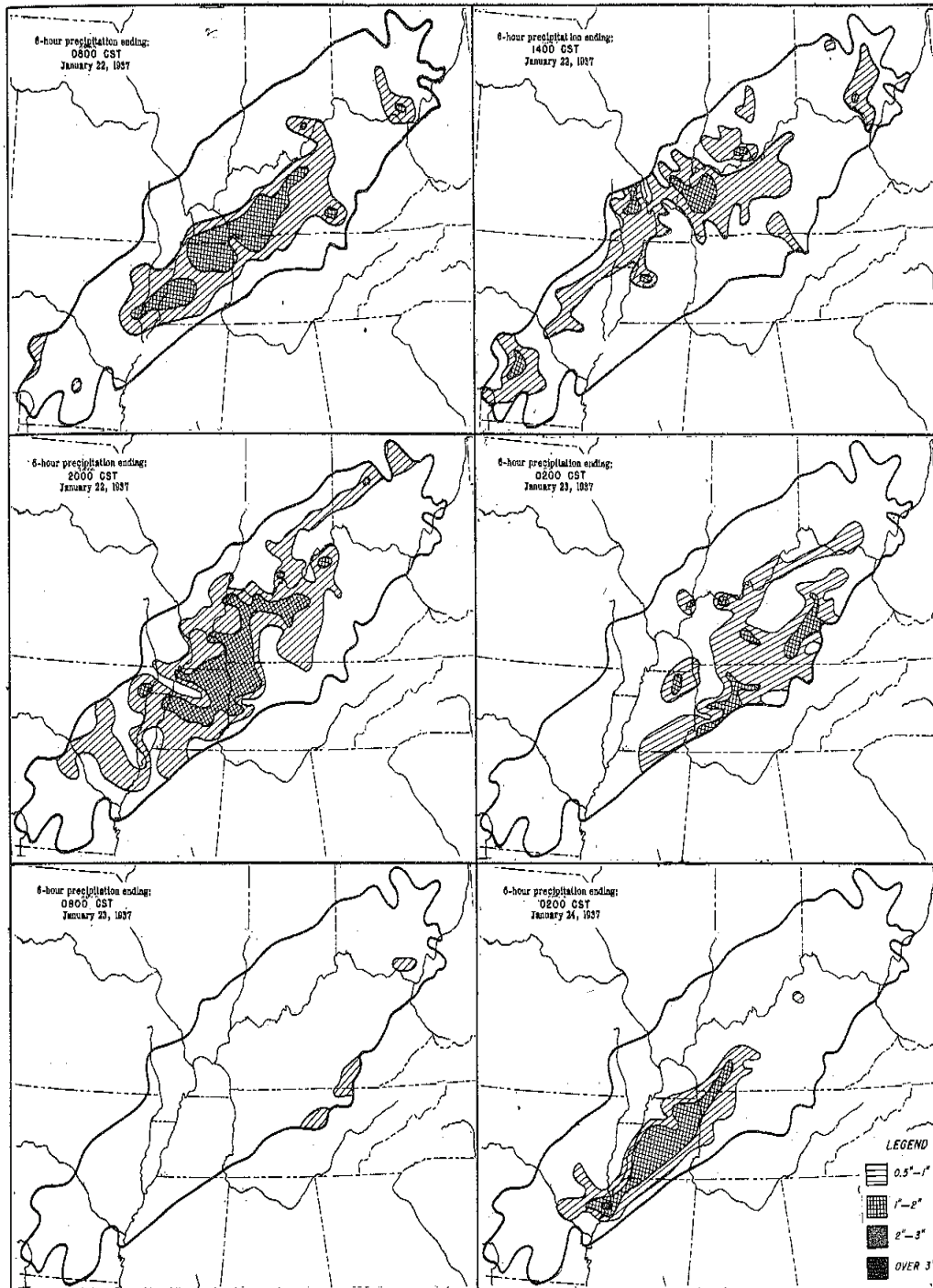


Figure G-26. 6-hour isohyets maps for 17-25 January 1937 storm event (24-25 January).

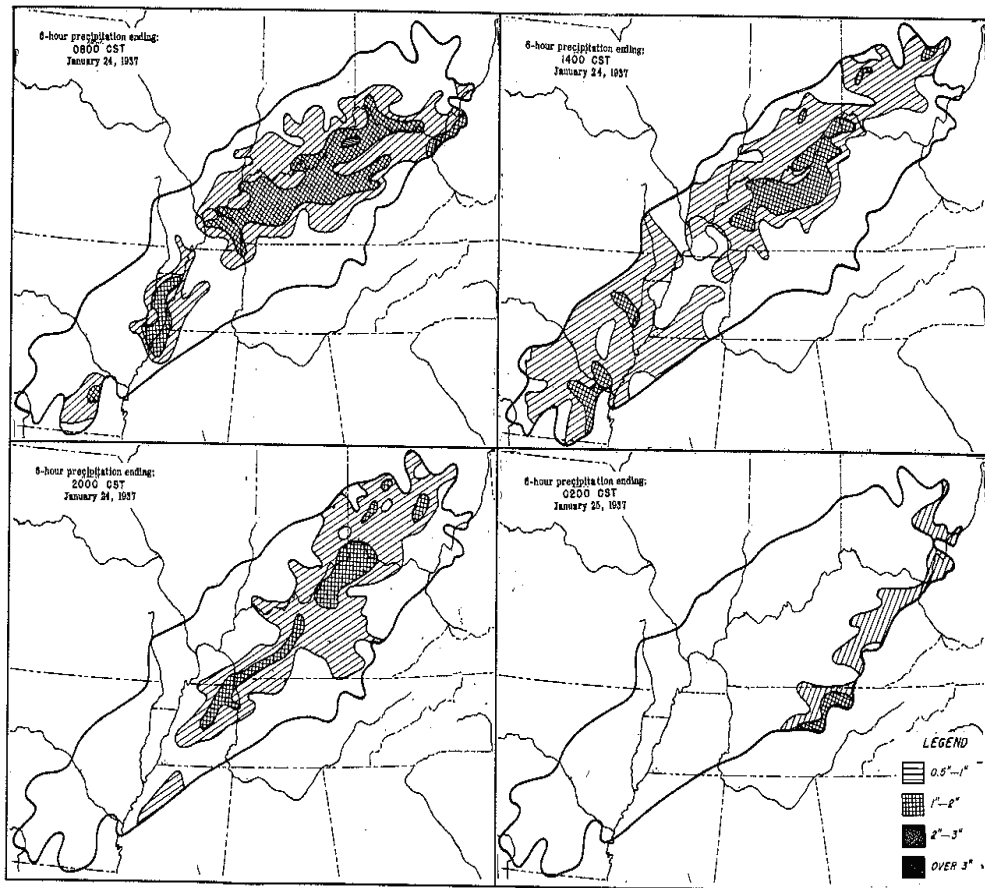
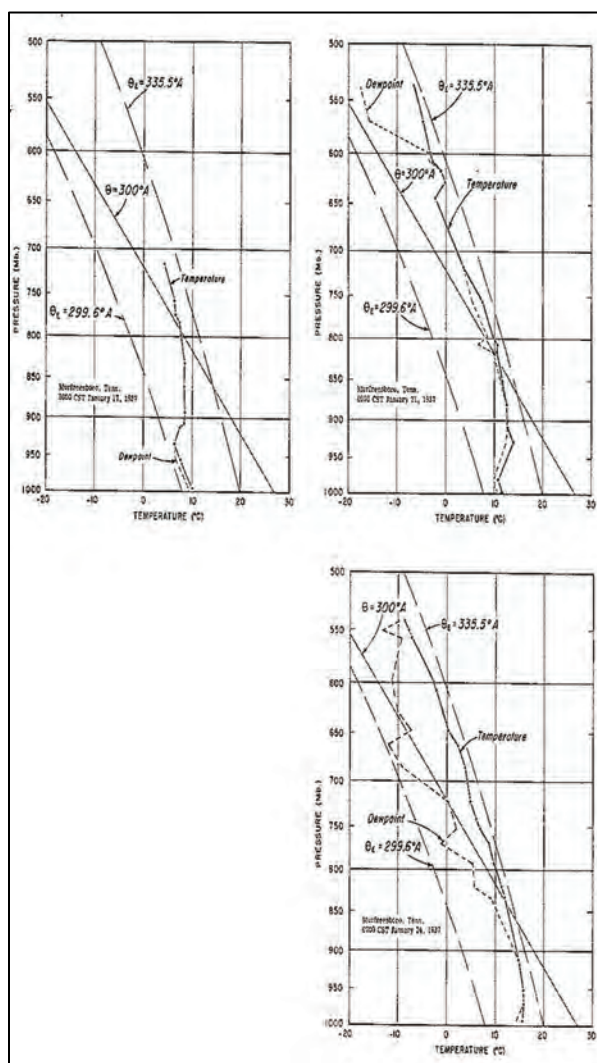


Figure G-27. Atmospheric soundings at Murfreesboro, TN, on 17, 20, and 24 January 1937.



G.7.5 14–19 February 1938

This storm was centered in Arkansas and eastern Oklahoma with large amounts of rainfall also falling in parts of bordering states. Precipitation amounts of the top 20 recorded rainfall gauges are shown in Table G-13. Up to 11 in. of rain fell at the center, and considerable flooding resulted. Daily Weather Maps (Figures G-28–G-29) and 6-hour isohyetal graphics (Figures G-30–G-34) are included.

The meteorological events that led to this storm started early in February. An extension of the Pacific subtropical high-pressure cell over the southwestern states on February 4–5 separated from the Pacific High and started moving eastward. On February 6–7, this

high-pressure cell was reinforced by a polar High from Canada moving down through the Northern Plains States. The combined high-pressure cell covered all of the eastern United States on February 8 and in the southern part extended as a high pressure ridge westward through Texas. While the northern part of this High gave way to passing cyclones and polar Highs during the next week, the southern part, which extended westward through the Gulf States, persisted as an extension of the Atlantic subtropical high pressure-cell throughout the period of this storm. The residuum of this stationary high pressure-cell lay east-west from the western Atlantic through the Gulf States from February 9 through 19. This caused continuous flow of maritime tropical air across the Gulf of Mexico and the southern half of the nation east of the Rockies.

A huge outbreak of polar continental air from Canada pushed as far southward as northern Texas and Arkansas on the 14th and became almost stationary. This high was oriented in a west-northwest to east-southeast direction on the 15th and 16th, which in large measure was responsible for the rain falling as far west as it did. While there were some showers as the cold front separating this air mass from the maritime tropical air pushed southward, the heaviest rainfall did not start until the front became quasi-stationary. It will be shown below how the heaviest bursts of rainfall were associated with waves that occurred in association with this front.

The first heavy burst of rainfall (up to 3 in.) occurred in Oklahoma after the surface cold front had become quasi-stationary in northeast Texas. The surface map on February 14 shows a slight wave on the front in northeast Texas with a trough extending northward through eastern Oklahoma. Wind aloft observations near this time showed southerly winds from approximately 4,000 ft through 10,000 ft over this area. This surface trough appears to be the reflection at the surface of the advection of warm air of less density aloft. Convergence in this trough near the ground and overrunning of warm moist air aloft accounts for this heavy downpour. This condition persisted through the next 12 hours. Then the trough filled, and a new surge of polar air began to push southward just east of the Rocky Mountains, approaching the storm area, and the rainfall amounts diminished.

The high-pressured ridge accompanying this new surge of cold air had pushed southward into north Texas by 0700 CST of the 16th intensifying the trough over Oklahoma between this High and the one remaining to the northeast. This situation produced frontogenesis in the trough and more heavy bursts of precipitation. The rainfall patterns of the 16th were oriented more or less along the frontal trough and progressed slowly south and eastward along with the front. This movement of the colder air southeastward again seemed to cause the frontal trough to decrease in extent and the precipitation to diminish, but still rather heavy amounts continued to occur along the frontal zone.

This front became stationary over Arkansas late on the 17th, and a wave began to form along the front. An increase in precipitation resulted, with isohyetal patterns oriented from southwest to northeast across Arkansas. After this, the wave cyclone occluded rapidly and moved northeastward followed by the large high-pressure cell that brought an end to the precipitation in the storm area. There are enough upper air data available on this storm to indicate the presence of a pronounced trough aloft, which approached the area of rainfall slowly from the west (Figure G-35). The presence of a deep trough at upper levels has been observed in association with many of the heavy rainfall situations. As is usually observed, the rainfall occurred under the eastward half of the mid-tropospheric trough.

The obvious cause of precipitation was the lifting of the warm moist air with a recent trajectory over the Gulf of Mexico by the colder air mass to the north. This lifting or overrunning resulted in the release of latent instability that was present in the maritime tropical air mass. Surface dew points in this air mass were generally in the 60s °F, and also moisture values aloft indicate that there was a sufficient moisture charge for heavy rainfall given the necessary physical processes to release it. Several of the surface charts and isohyetal patterns show considerable rainfall in the warm air ahead of the cold front. This precipitation may partially be caused by the release of latent instability due to flow over the gradually rising terrain north and west of the Gulf Coast.

The frontal positions prior to SW 2-17 must be considered an important factor when estimating the minimum time interval required between a severe Ohio Valley rainstorm followed by a storm similar to

SW 2-17. On February 13, a small Low moved through the Great Lakes region causing 3 in. to 4 in. of rain. The cold front accompanying this Low crossed the Ohio Valley during the afternoon and evening of the 13th attended by light precipitation. Heavier precipitation could have accompanied this frontal passage, but it required a deeper trough aloft. These deep troughs move slowly (approximately 3 days) and usually longer for one to follow another.

The 12-hour representative dew point for SW2-17 was 64 °F. The maximum possible dew point for the area is 70 °F allowing a 35% upward adjustment of moisture.

Table G-13. Top 20 recorded rainfall gauges (inches) for the 14–19 February 1938 precipitation event.

CALVIN	OK	11
JESSIEVILLE	AR	10.5
WEBBERS FALLS	OK	10.3
EUFAULA	OK	10.2
DEVILS KNOB	AR	10.1
SALLISAW	OK	10.1
MCALESTER	OK	9.8
MOUNTAINBURG	AR	9.7
LUTHERVILLE	AR	9.4
SULPHUR	OK	9.3
GRAVETTE	AR	9.1
COALGATE	OK	9
KNOX CITY	TX	8.8
ALUM FORK	AR	8.7
CONWAY	AR	8.7
FORT SMITH	AR	8.7
HOLDENVILLE	OK	8.7
ADA	OK	8.5
DARDANELLE	AR	8.3
TAHLEQUAH	OK	8.3

Figure G-28. 13-16 February 1938 Daily Weather Maps.

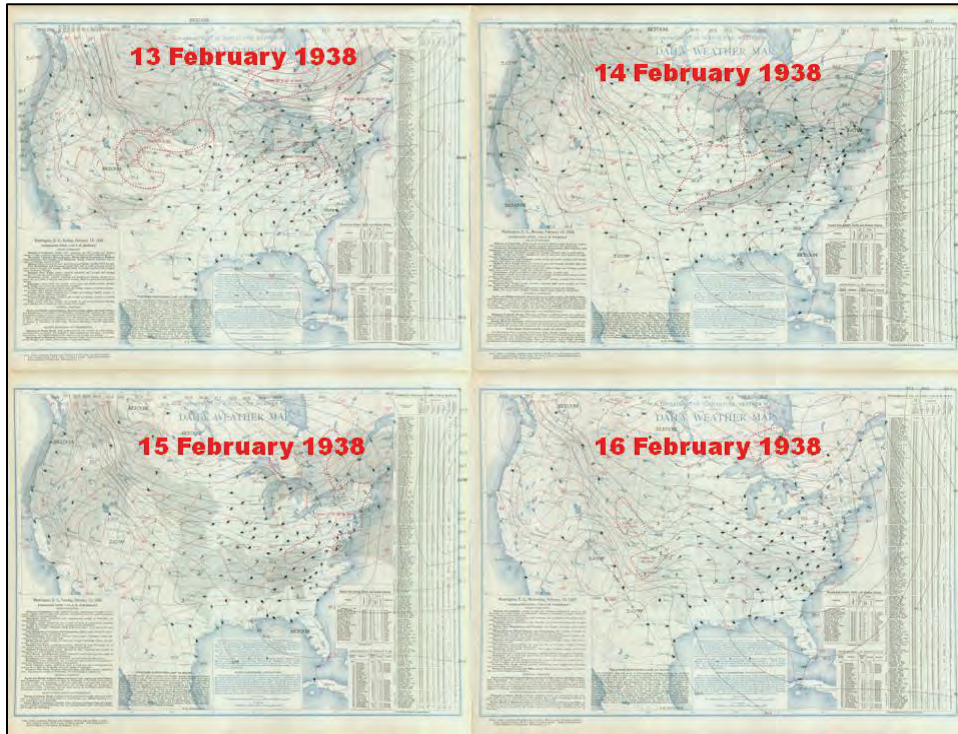


Figure G-29. 17-20 1938 Daily Weather Maps.

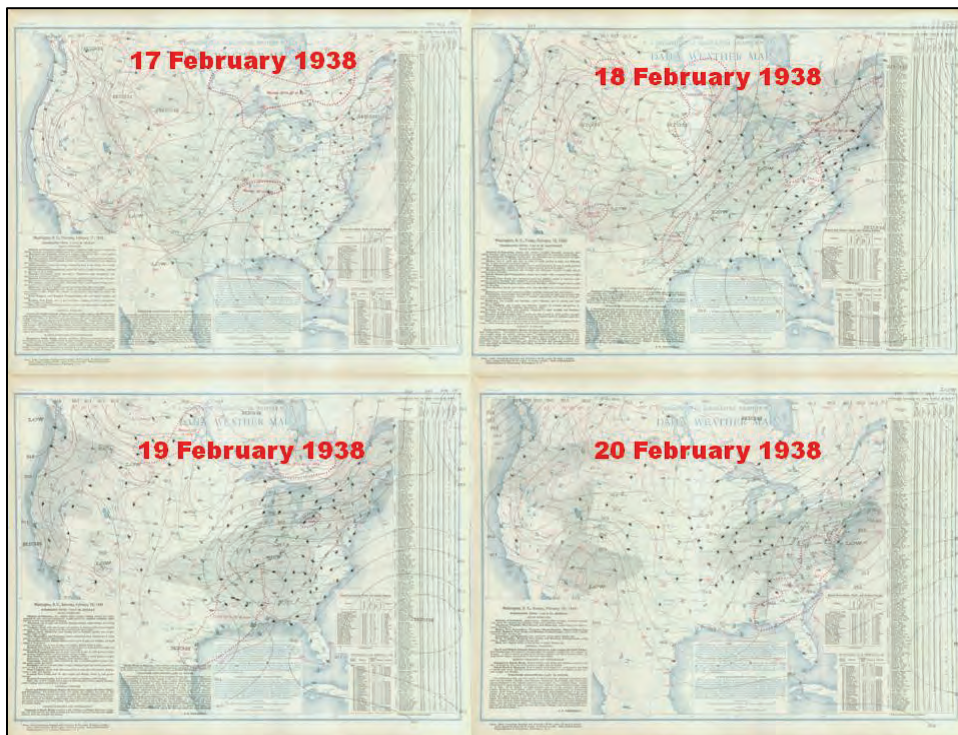


Figure G-30. 6-hour isohyets maps for the 14–19 February 1938 storm event (14-15 February).

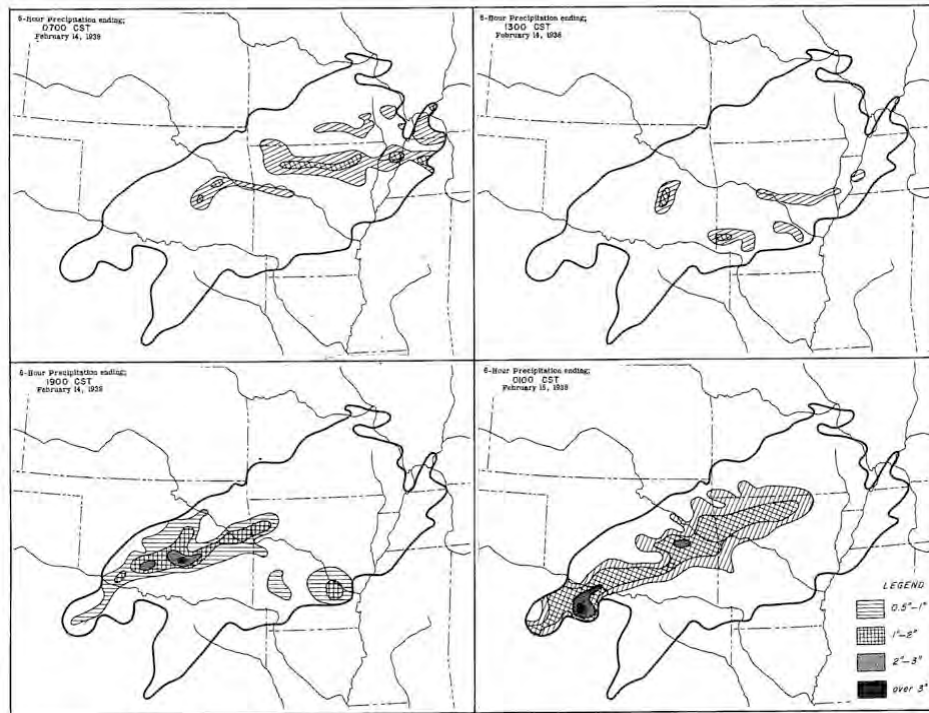


Figure G-31. 6-hour isohyets maps for 14–19 February 1938 storm event (15-16 February).

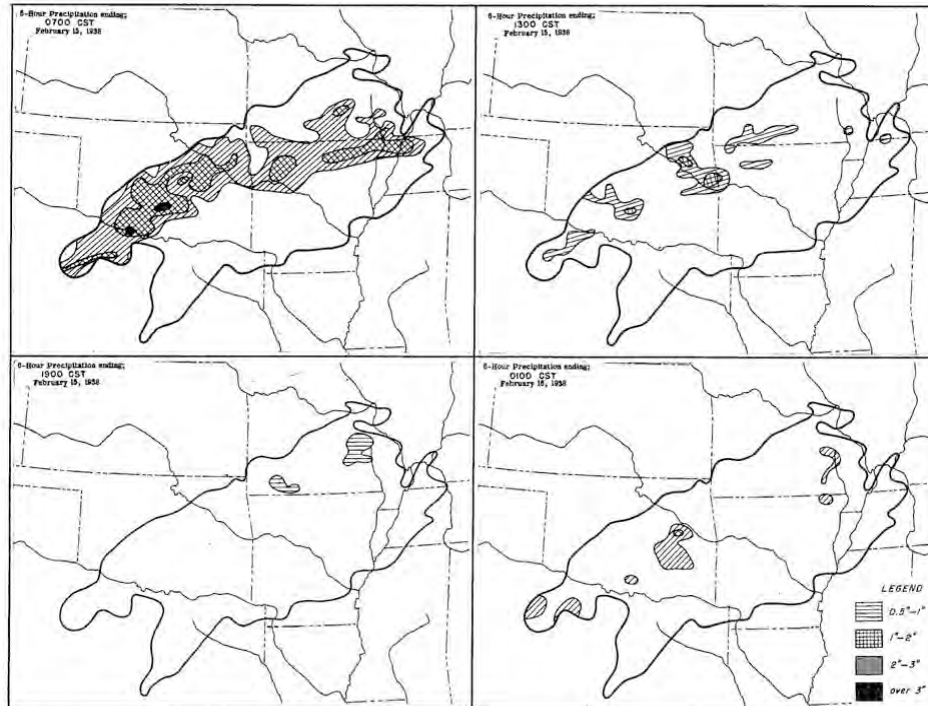


Figure G-32. 6-hour isohyets maps for 14–19 February 1938 storm event (16-17 February).

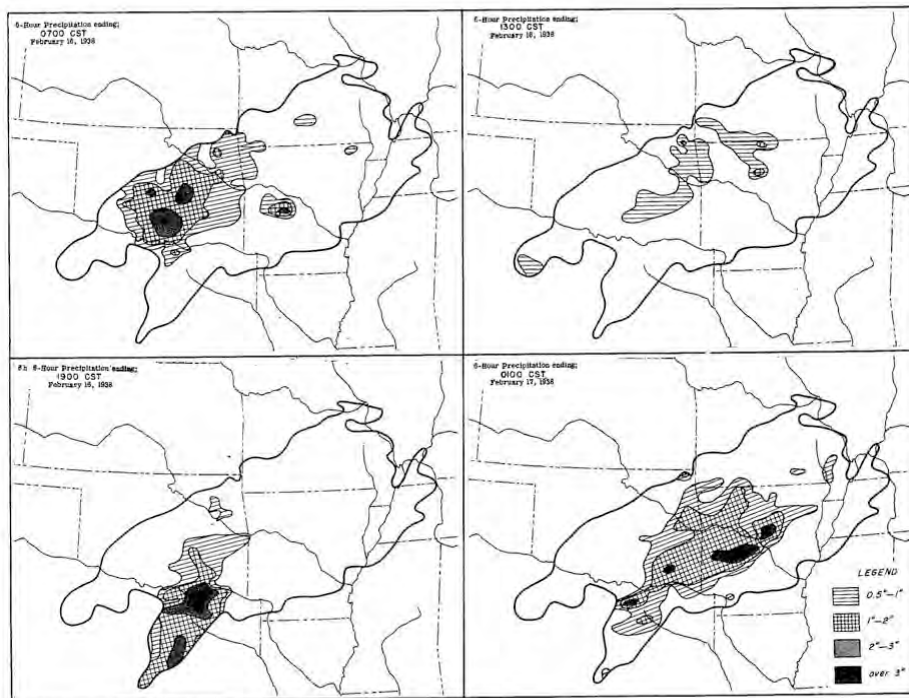


Figure G-33. 6-hour isohyets maps for 14–19 February 1938 storm event (17-18 February).

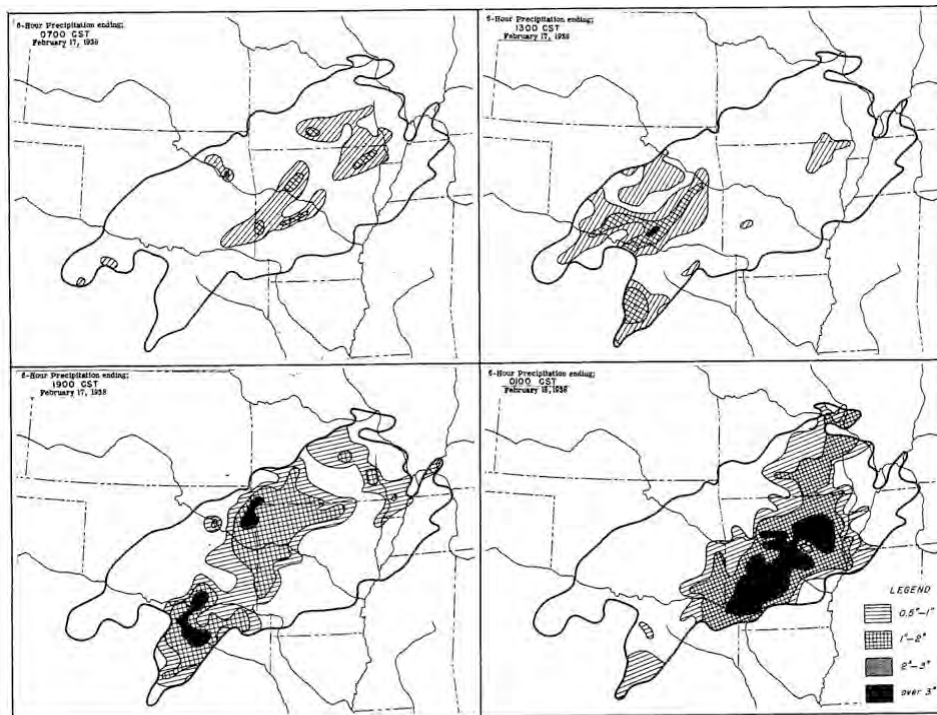


Figure G-34. 6-hour isohyets maps for 14–19 February 1938 storm event (18-19 February).

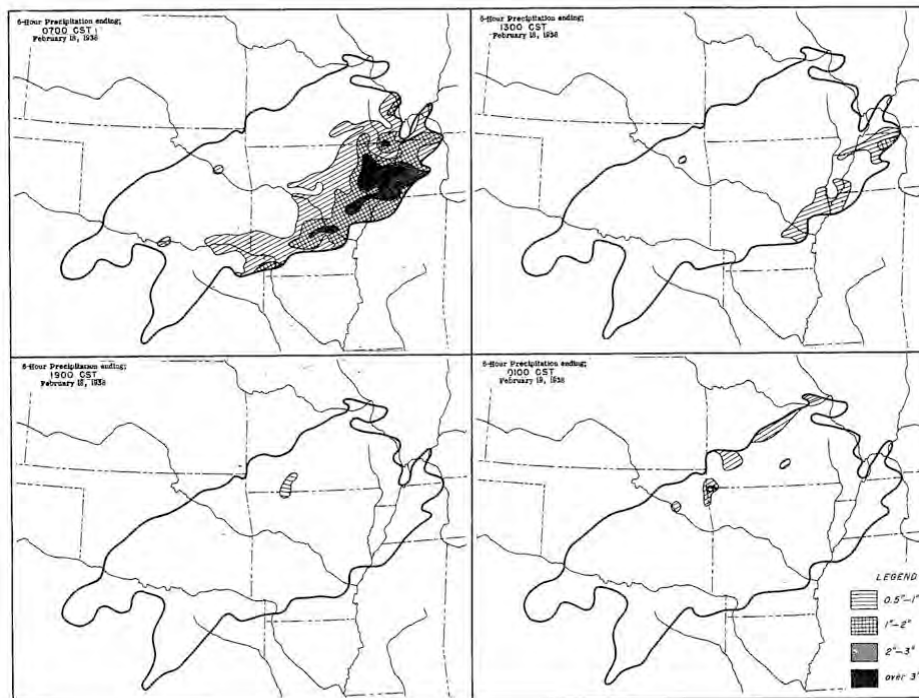
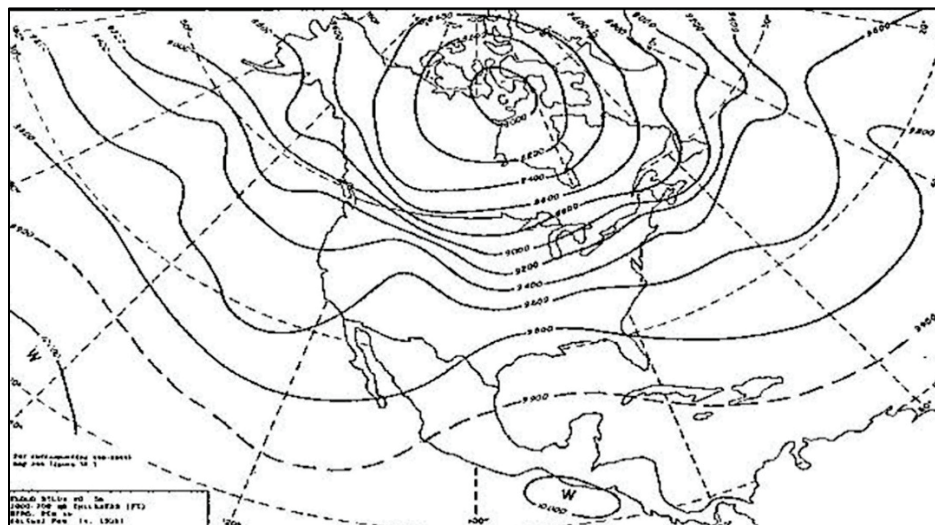


Figure G-35. 100–500 mb thickness chart for 14 February 1938.



G.7.6 8–10 May 1943

The Warner, OK, storm of 8–10 May 1943, in which the title station measured 25 in. of rain in 48 hours, was the first of two exceptionally large storms that occurred within a remarkably short interval of time. The Mounds, OK, storm, the second of the two, formed in conjunction

with the very next front that entered the Mississippi Valley after the front associated with the Warner storm had passed into the Atlantic and Gulf of Mexico.

On May 6, the precursory signs of a favorable pressure and temperature condition for heavy rainfall could be observed. The weather map of that date shows a High off the East Coast with a very strong southerly jet of tropical air developing in the Texas-Louisiana region (Figure G-36, top right). At the same time, a large supply of polar air was entering the country from Canada. During the next 2 days there was a gradual migration of the polar air southward to the Texas-Arkansas area and into the strong southerly jet. The pressure was 5–7 mb above normal in Florida during the period of heavy rain. Above-normal pressure over the Florida Peninsula and to the east seems to be a necessary condition for an extended period of heavy rain in the Mississippi Valley. Weather maps from 5–12 May 1943 are included (Figures G-36–G-37) along with 6-hour isohyetal graphics (Figures G-38–G-40). Broadly speaking, a series of stable waves followed by a deepening unstable wave characterized the weather maps for the Warner rainstorm. The rain at Warner was of the frontal thunderstorm type with the heaviest downpour occurring during the early hours of May 9.

On May 8, the polar front extended from Cape Cod southwestward through the Ohio River Valley into a minor stable frontal wave in northeastern Arkansas, thence to a large nearly stationary frontal wave near Dallas, TX, and on to a low pressure area in New Mexico (Figure G-36, bottom right). This New Mexico Low, with its associated trough aloft, increased the low-level southerly wind jet over the Texas-Oklahoma area. To the north of the frontal zone an elongated, double-centered, high-pressure area stretched from the Great Lakes to the Rocky Mountains with the main center located over northern Minnesota. The edge of this cold air dome supplied the temperature gradient while the southerly jet associated with the eastward moving trough aloft supplied the air motion to set up a field of intense differential advection in the Oklahoma area on the 8th, 9th, and 10th.

The pressure gradient to the west side of the Bermuda High was concentrated along the western Gulf Coast and provided the moisture supply to the trough in which the front lay. During the 12 to 24 hours previous to the heavy rain at Warner, rising surface pressures were

experienced in the Mississippi Valley. The resulting filling of the trough to the east increased the pressure gradient and aided in setting up in the warm air advection in eastern Oklahoma.

During the afternoon of May 8, as the rain was starting, the temperature difference at the ground between the center of heaviest rain and the warm side of the front 100 miles to the southeast was 30 °F. This gradient was abetted oppositely directed surface winds converging at the front. An area of falling surface pressure was located over the storm center and coincided vertically with the center of strongest warm air advection at 10,000 ft.

Differential advection computed for three observations at the 5,000 ft level indicated warm advection over eastern Oklahoma throughout the storm period and a maximum during the period of heaviest rainfall. However, the value over the area of heaviest rain was exceeded in intensity by an area to the northeast and one to the southwest a few hundred miles along the front.

Coupled with the warm differential advection in the lower levels, a maximum cooling aloft at 10,000 ft over the storm area during the early morning hours of May 9 was present when the heaviest rainfall was occurring. During the 12 hours ending 1100 CST May 9, a 4 °C cooling was experienced at 10,000 ft while in the same period a 4–6 °C low-level warming took place in eastern Oklahoma. The resulting instability plus the effects of the frontal surface itself were factors contributing further to the intense downpour during the early morning hours of May 9.

The front that brought cold dry air over the heavy rain area proceeded into the Gulf of Mexico, stalled, and dissipated in the region of the Yucatan Peninsula. This would allow a resurgence of moist air into the central United States in approximately 3 days at a minimum. The observed time interval between the last significant rainfall in the Warner storm and the first significant rain of the Mounds storm was three and one-half days.

The 12-hour representative reduced dew point observed in SW 2-20 was 70 °F, and the maximum possible for the area and time of year is 76 °F. This permits an upward moisture adjustment in place of 34%.

Note that rainfall amounts in Table G-14 do not include the Warner, OK, 25 in. totals because the data downloaded from NCDC did not include this station for the event.

Table G-14. Top 20 recorded rainfall gauges (inches) for the 8–10 May 1943 precipitation event.

FORT_SMITH	AR	20.14
TULSA_INTERNATIONAL_AIRPORT	OK	20.04
INDEPENDENCE	KS	19.17
CHELSEA	OK	18.12
NORTH_GRAND_LAKE	OK	17.76
SUBIACO	AR	16.62
FORT_GIBSON	OK	16.52
JOPLIN	MO	15.31
SEDAN	KS	15.22
PILOT_KNOB	MO	15.21
LEAD_HILL	AR	14.19
ROCKVILLE	IN	13.79
MOUNTAIN_HOME_1_NNW	AR	13.21
GLENCOE	OK	12.27
MOUNT_IDA	AR	12.26
SPRINGFIELD	MO	12.22
COLUMBUS	KS	11.90
ELEVENPOINT	AR	11.72
HANNIBAL_1_N	MO	11.62
BATESVILLE	AR	10.93

Figure G-36. 5-8 May 1943 Daily Weather Maps.

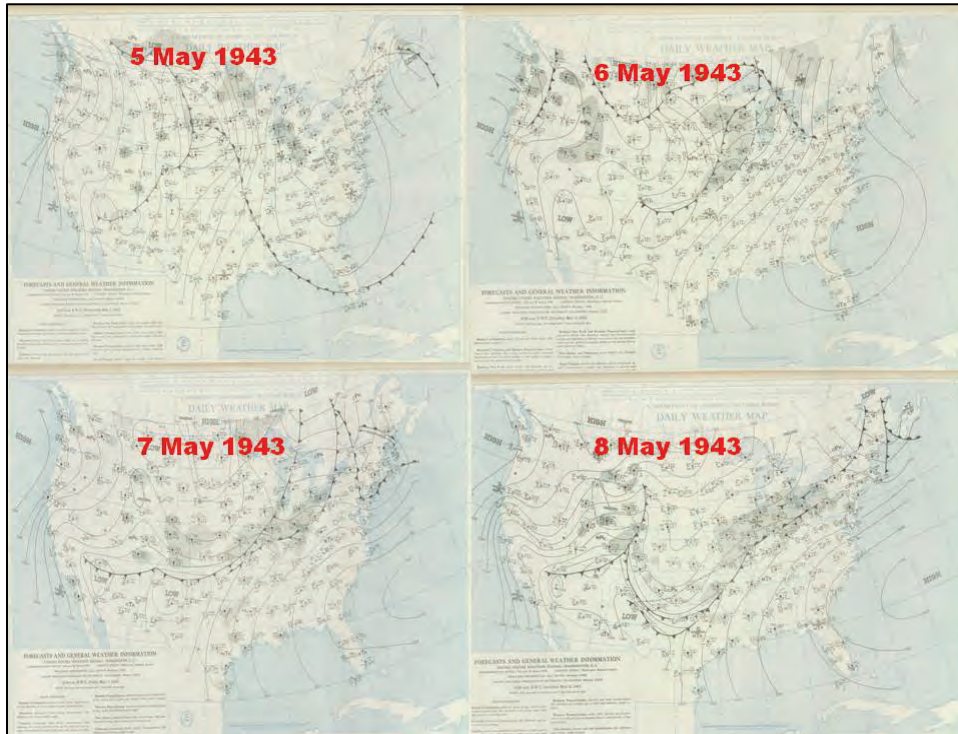


Figure G-37. 9-12 May 1943 Daily Weather Maps.

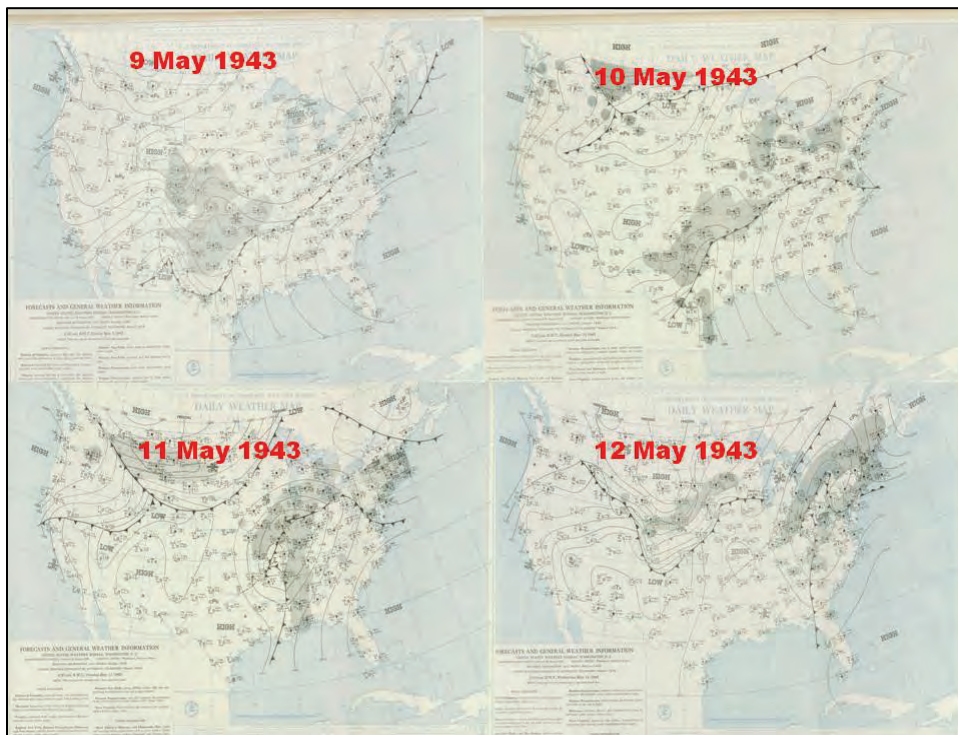


Figure G-38. 6-hour isohyets maps for the 8-10 May 1943 storm event (8-9 May).

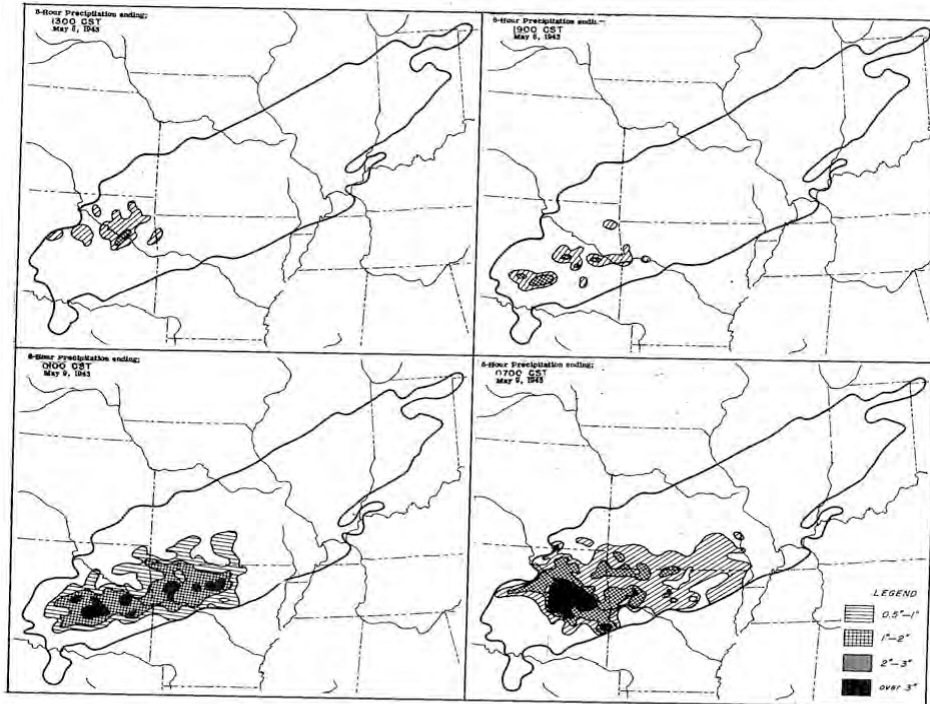


Figure G-39. 6-hour isohyets maps for 8-10 May 1943 storm event (9-10 May).

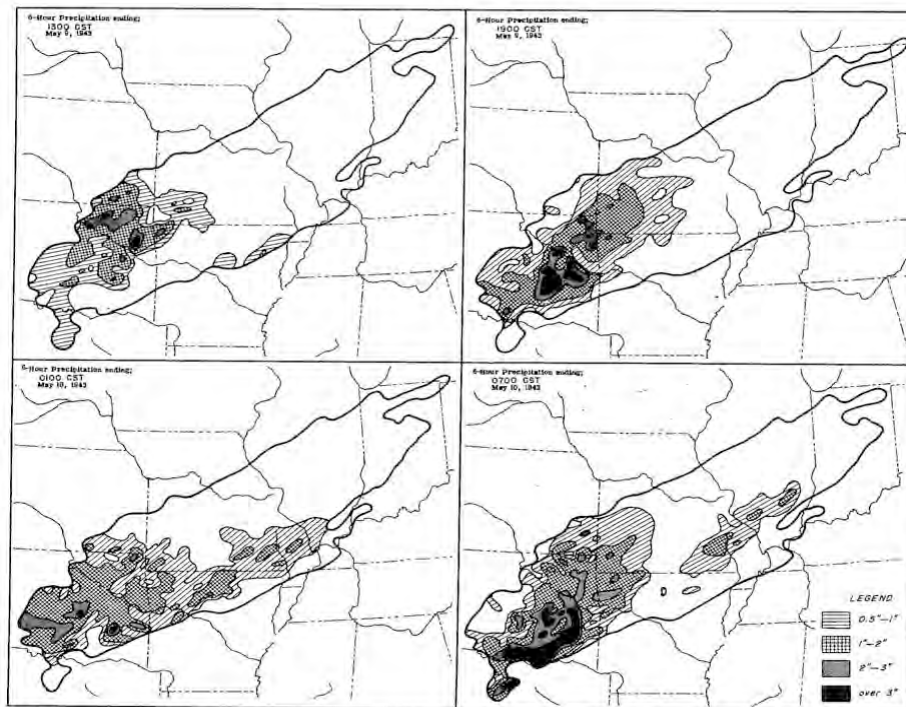
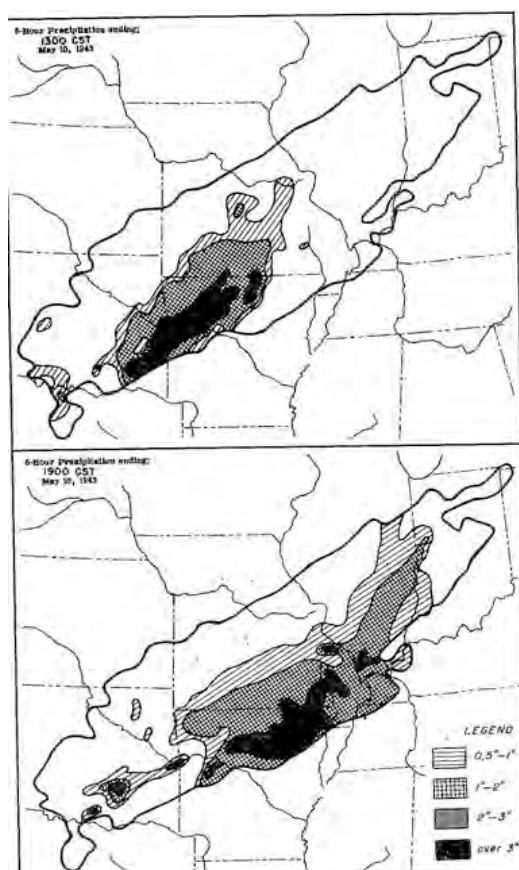


Figure G-40. 6-hour isohyets maps for 8–10 May 1943 storm event (10 May).



G.7.7 16–19 May 1943

This storm, in which up to 17 in. of rainfall occurred, extended from north central Oklahoma northeastward to northwestern Ohio. Precipitation amounts at the top 20 recorded rainfall gauges are shown in Table G-15. The broad scale pressure patterns of this storm are somewhat similar to those of January 1937 and other winter-time storms¹. These patterns consist of a stationary high pressure ridge over the southeastern states and a quasi-stationary front extending northeastward from a low pressure area in western Texas.

The ridge over the southeastern states had existed for several days prior to this storm and persisted throughout the period of rainfall. The presence of this ridge appears to be common to most heavy rainfall storms in the central United States and plays a major role in their

¹ The material in this section is primarily from the MRC (1955) report. Additional insights on the seasonality effect are included here. Winter storms may have stronger dynamics with a more powerful jet stream, but spring-time has higher moisture availability from a climatological perspective. Therefore, this produced an almost worst-case scenario.

occurrence. It not only circulates warm moist air, usually maritime tropical, into the central part of the country, but by remaining stationary it continues this flow and clocks the eastward movement of other systems. In the 16–19 May 1943 storm, the heavy rainfall occurred in the stationary frontal trough just to the northwest of the sub-tropical ridge over the southeast.

Another very important feature of this storm was the deep upper air trough over the western United States. This trough moved very slowly eastward during the storm. These deep, slow-moving upper air troughs are associated with almost all winter-time heavy rainfall situations in the central part of the country.

A cyclone formed on May 15 in the southwest just east of the Rocky Mountains. This cyclone had moved northeastward to Wisconsin on May 16 (Figure G-41, bottom right). The cold air moving southward on the west side of this cyclone formed the stationary front with the maritime tropical air moving northward from the Gulf. This front persisted throughout the period of heavy rainfall. The cyclone over Wisconsin on May 16 moved on into Canada, and a large high-pressure cell of maritime polar air moved across the Rocky Mountains and southward into the southern Plains States.

The isohyetal patterns and detailed surface maps show that the rainfall started as showers and thunderstorms along the front late on May 16 after it became stationary and moved slightly northward (Figures G-41–G-44). The first of this rainfall of importance was for the 6 hours ending at 2300 CST May 16, when more than 4 in. fell over a small area between Oklahoma City and Tulsa, OK (Figure 43, top right). This burst of precipitation was the result of thunderstorms that occurred as the front moved northward over the area.

One of the heaviest bursts of precipitation is shown by the isohyetal pattern for the 6 hours ending at 0500 CST May 17, with the largest amount in northeast Oklahoma (Figure G-43, middle left). While the front remained in this vicinity, the unusually heavy rainfall of more than 6 in. in as many hours seems to require more of an explanation than just frontal lifting. This front is in an inverted V-shaped trough extending from a small cyclone that developed in southeastern Colorado on the 16th and has moved to the Texas Panhandle area. The 5,000 ft chart

showed a large cyclonic curvature of the streamlines in this area, which is just far enough east to allow a continuous inflow of moist tropical air from the Gulf. The occurrence of thunderstorms on both sides of the front indicated convergence in the moist unstable air within this area of cyclonic curvature of streamlines. The flow was also toward higher elevations making a further contribution to the vertical motion, which releases the instability. The more nearly south-to-north flow of air at lower elevations accompanied by advection of higher temperatures insured a supply of moist unstable air into the area. The northern part of this isohyetal pattern, an inspection of the associated surface map reveals, seems to be more nearly the result of frontal lifting.

The next two isohyetal maps for the 6-hour periods ending at 1100 CST and 1700 CST on the 17th, show an increase in rainfall north-eastward along the front simultaneously with the advection of warmer temperatures that occurred at 5,000 ft (Figure G-43, middle right and lower left).

The isohyetal pattern for the 6 hours ending 2300 CST May 17 shows up to 6.6 in. of precipitation near Joplin, MO (Figure G-43, lower right). This extremely heavy burst of rainfall was the result of severe thunderstorms as a surge of cooler air pushed into the area, which can be seen by examination of the detailed surface maps. This push southeastward of the cooler air resulted in a wave on the front in this area that remained almost stationary with only a slight northeastward movement throughout the remainder of the period of the storm.

The isohyetal patterns for 0500 CST and 1100 CST May 18 shows a continuation of the rainfall but with smaller intensities (Figure G-44, top left and top right). These smaller intensities might be due partially to the decrease of convective activity during the night hours. Also, the wave that formed in northeast Oklahoma the day before moved northeastward and decreased in intensity. The fact that only light amounts of rainfall occurred during the 6 hours ending at 1700 CST May 18 was a result of the end of wave activity and only a slight trough along the front (Figure G-44, middle left).

Late on the 18th, another wave formed on the front in north central Texas and moved northeastward, causing the bursts of rainfall shown by the isohyetal patterns for 2300 CST May 18 and 0500 CST on May

19 (Figure G-44, middle right and bottom left). As this wave moved northeastward, the anticyclone that had been almost stationary over the Plains States for the past few days intensified and moved southeastward, bringing an end to the rainfall in the storm area at about noon on May 19 (Figure G-44, bottom right).

The temperature difference between the two air masses involved in this storm was significantly strong. However, it differed from the major mid-winter storms in that the cold air mass was maritime polar air coming in from the Pacific with more moderate temperatures. The maritime tropical air mass to the south was somewhat warmer than that of the mid-winter storms with surface dew points in the 60s and low 70s (°F), furnishing a large supply of moisture.

The representative dew point of this storm is 71 °F. The maximum possible 12-hourly reduced dew point is 76 °F, which permits a moisture adjustment of 28% in place.

For the next few days following the cessation of rainfall, the front gradually moved southeastward to the Gulf Coast, and the anticyclone following it intensified and by May 22, covered most of the country east of the Rocky Mountains. It seems reasonable to conclude that another major rainstorm could have developed as this High reached the eastern seaboard, or 3 days after the end of the heavy rainfall of this storm. The tropical air was in a position to make a rapid re-entry into the Mississippi Valley if a deep trough aloft had entered the Rocky Mountain area. This, however, did not happen following this event, so no major rainfall ensued at that time.

Table G-15. Top 20 recorded rainfall gauges (inches) for the 12–20 May 1943 precipitation event.

LOWELL	KS	16.6
LENAPAH	OK	16.5
JOPLIN	MO	16.4
LENAPAH_2	OK	15.2
OCHELATA	OK	15.2
ALUWE	OK	14.5
QUEPAW	OK	14.5
MIAMI	OK	14.4
DELAWARE_2	OK	14.1
GRAND_FALLS	MO	14.1
JOPLIN_B	MO	14.0
WELCH	OK	13.7
COX_STORE	OK	13.5
PAWHUSKA	OK	13.5
LAKE_CARL_BLACKWELL	OK	13.1
RALSTON	OK	13.1
FAIRFAX	OK	13.0
PAWHUSKA_2	OK	12.8
BATTLESVILLE_B	OK	12.7
OSWEGO	KS	12.6

Figure G-41. 13-16 May 1943 Daily Weather Maps.

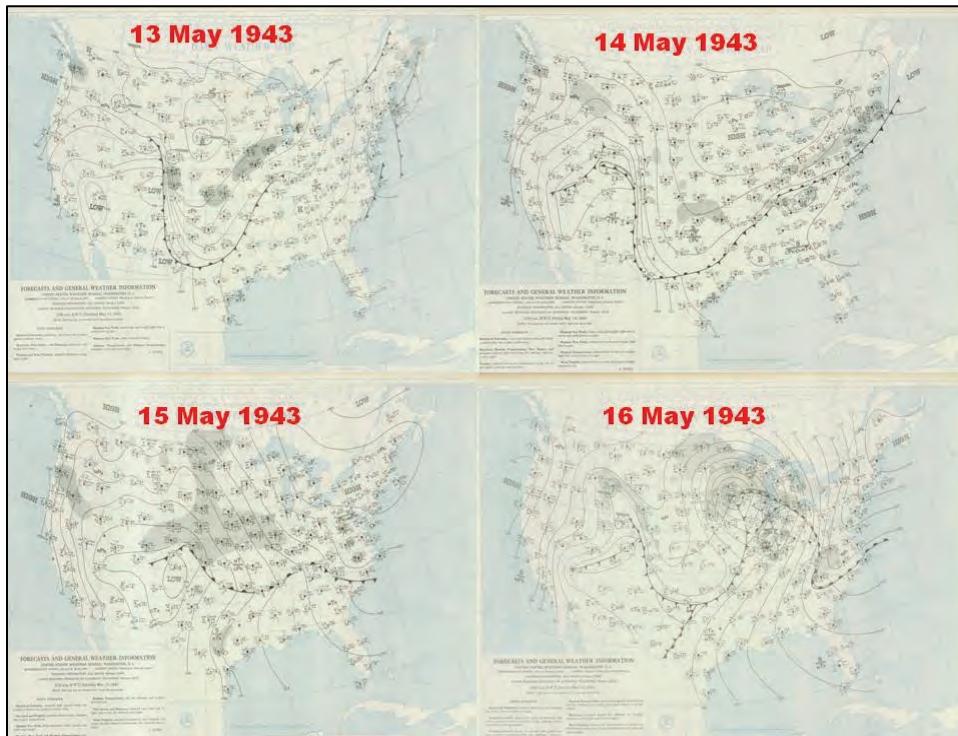


Figure G-42. 17-20 May 1943 Daily Weather Maps.

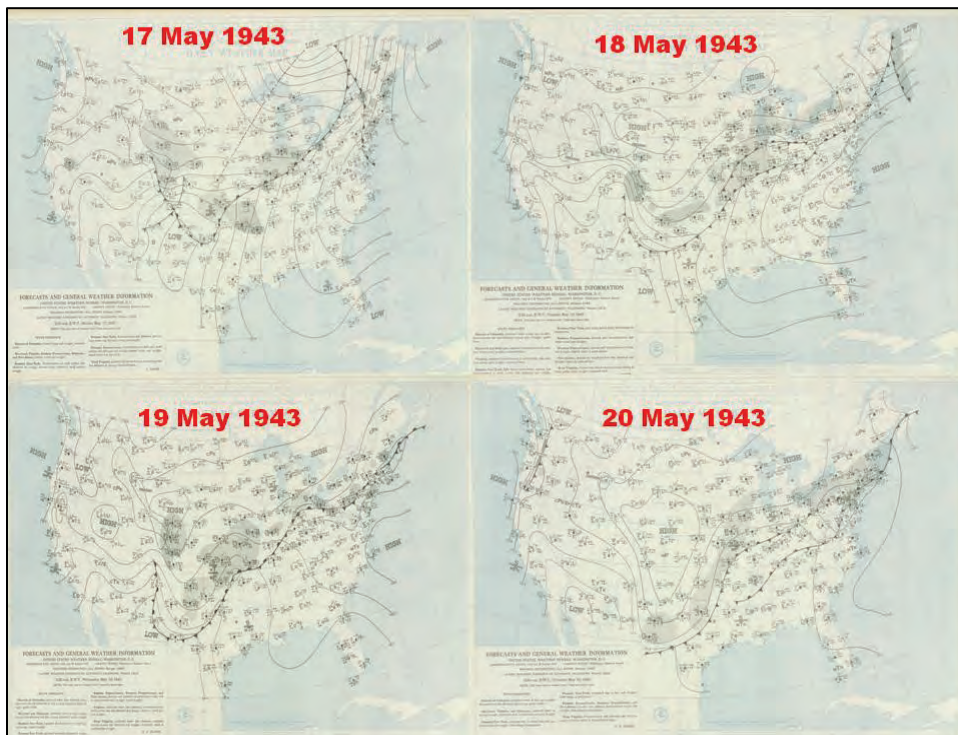


Figure G-43. 6-hour isohyets maps for the 16-19 May 1943 storm event (16-17 May).

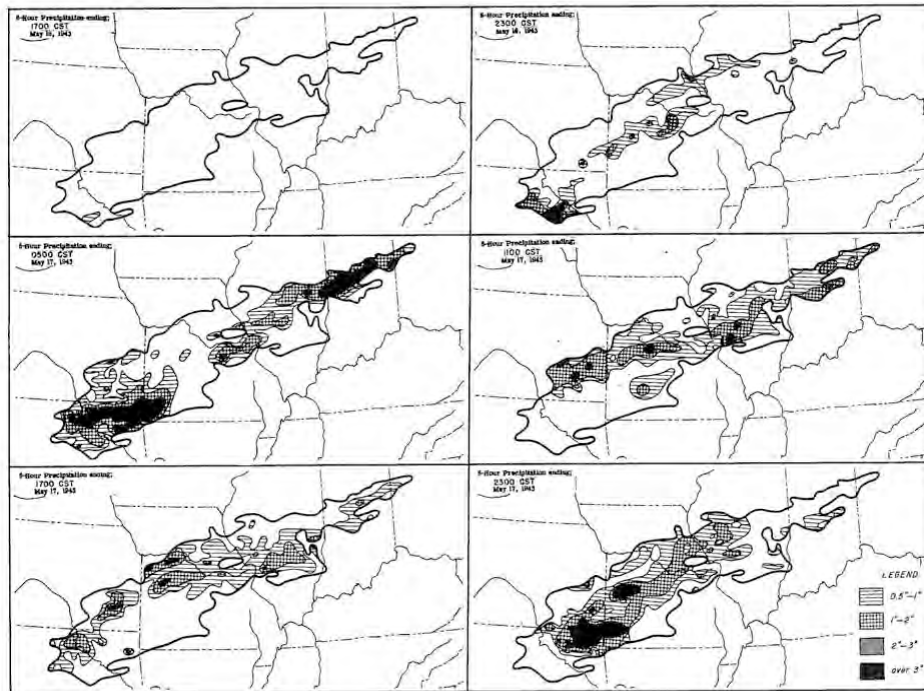


Figure G-44. 6-hour isohyets maps for 16-19 May 1943 storm event (18-19 May).

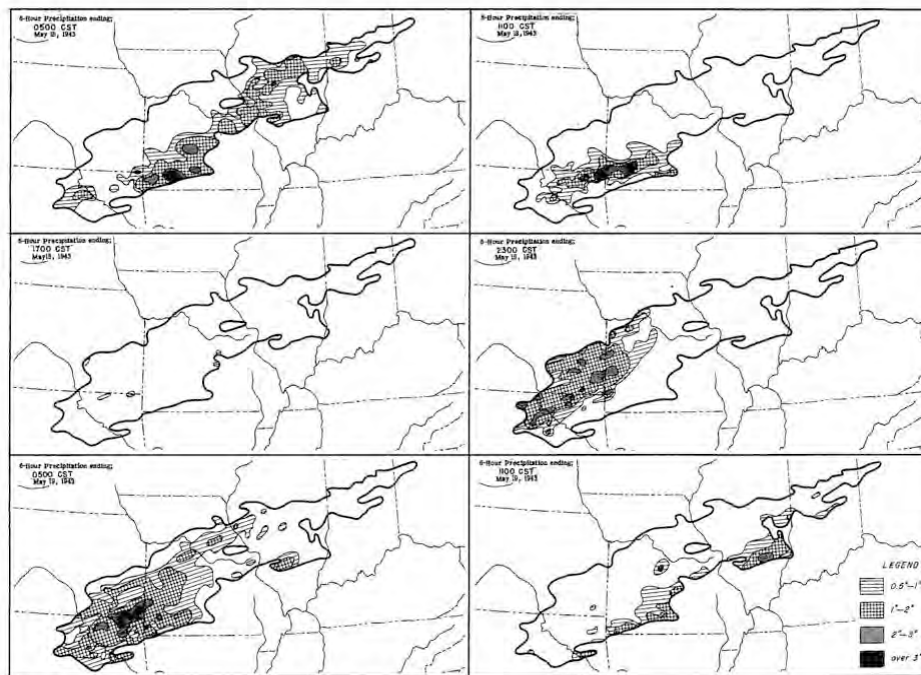


Figure 153. Incremental Isohyetal Patterns

G.7.8 28 March – 2 April 1945

This end-of-March, early-April flood event was preceded by a major flood on the Ohio River from mid-February to 7 March 1945. The following description of the 1945 flood is compiled from discussion in the Daily Weather Maps of 30 March 1945 and 27 April 1945 describing the earlier flood event. The winter of 1944–1945 was noteworthy for the heavy accumulation of snow in Pennsylvania, New York, and New England, which very seriously hindered transportation and essential industrial operations. Average snowfall for the Pennsylvania up to 31 January was 48 in., which was the greatest on record and 27 in. above average. Warm weather during the first 3 weeks of February resulted in some depletion of the snow cover in Pennsylvania. On February 21, a storm developed in the Lower Mississippi Valley that brought rain and the necessary high temperatures to melt much of the remaining snow in Pennsylvania and western New York.

This storm also laid down a new blanket of heavy snow approximately 200 miles wide from southeastern Colorado to northern Wisconsin.

On February 17, a cyclone entered the western United States along the Oregon coast. This storm weakened and move slowly southeastward reaching New Mexico on the 20th. Temperatures and dew points to the south of the warm front that extended eastward across the Gulf States indicated very warm and moist maritime tropical air streaming northward. As a low deepened over Texas and moved northeastward across the Middle Mississippi and Illinois Valleys, heavy rains fell in Arkansas, Missouri, and Tennessee with moderate snow falling across the Missouri and Upper Mississippi Valleys.

This storm was one of a series of storms that from mid-February through 7 March 1945 resulted in intermittent heavy rains over most of the Ohio Basin. The total rainfall during this period exceeded 10 in. over a large area along the Ohio River. These rains, aided by snow melt in the northern sections, produced a major flood on the Ohio River during March. Rapidly rising flood waters resulted in loss of life and heavy damage by flooding of large areas of low farmlands, closing of coal mines and many industrial plants manufacturing essential war materials, and disrupting transportation and flooding of many homes.

The rise of the Ohio River began in mid-February (exceptional drought engulfed the Ohio Valley in 1944) with Cairo, IL, exceeding flood stage on February 23. By March 5, the entire Ohio River was in flood. On March 5–6, the final rain storm of the series occurred. The rainfall amounts in this final storm were exceptionally heavy and occurred immediately along the entire Ohio River, causing the river to rise sharply. Although the resulting flood peaks were several feet below the maximum flood of record, they ranked generally in the top five historically at that time. An example of this was Cincinnati, OH, which reached a peak of 69.2 ft on 7 March 1945, which was exceeded only four times prior (1773, 1884, 1913, and 1937); the flood of 1937, when a height of 80 ft was recorded, tops all floods at Cincinnati.

At the onset of the late March to early April rainfall event, the stage at Cairo, IL, had crested at 53.9 ft on April 22 and had begun to recede to 52.7 ft on the morning of March 28.

A cold front moved out of the Rockies on March 27 and became quasi-stationary over the Ohio and middle Mississippi Valleys and extended southwestward into south/central Texas on March 28 (Figure G-45, top left and top right). Strong high pressure was centered off the southeastern coast of the United States. Warm and moist tropical air was transported northward along the periphery of the high pressure (Figure G-45, bottom left). Very heavy rains fell over Texas, Oklahoma, and Arkansas on March 29–30.

A low formed on the southern extension of the stationary front over Texas late on March 30. The low moved northeastward along the front and across the Ohio Valley on March 31 (Figure G-46, top left). The stationary front moved southeastward and extended from the Tennessee Valley, across Mississippi and Louisiana and into coastal Texas. The final low in the series developed over southeastern Texas early on April 1 and moved northeastward across the Arkansas and Ohio Valleys on April 1–2, dragging the front through the remainder of the Mississippi River Basin (Figure G-50, top right and bottom left). Very heavy rains fell over Mississippi and Louisiana with additional moderate to heavy rains falling over Arkansas and Oklahoma on April 1–2. Precipitation amounts for the top 20 recorded rainfall gauges are shown in Table G-16.

The 6-hourly isohyet maps were not available in the original documentation. Where no 6-hour data existed, the daily total precipitation was placed in the first 6-hour period for the day, and zeros were used in the remaining three 6-hour periods.

Rain during this event caused Cairo to slowly rise to a second crest of 53.7 ft on April 4. The heavy rains over Texas and Louisiana caused the Red River at Alexandria to rise to a peak discharge of 233,000cfs and a record stage of 45.23 ft on April 17. USACE records indicate the peak total latitude flow of Red River Landing was recorded at 2,123,000 cfs on April 30.

Table G-16. Top 20 recorded rainfall gauges (inches) for the 28 March–2 April 1945 precipitation event.

VAN	TX	17.40
QUITMAN	TX	16.70
WINTHROP	AR	16.50
YANTIS	TX	16.30
WINSBORO	TX	15.50
MENA	AR	14.80
L&D 3	AR	14.60
FARMERVILLE	LA	14.30
ALTA LOMA	TX	14.04
BATESVILLE	AR	13.80
FOREMAN	AR	13.60
PRICE	TX	13.30
SULPHUR SPRINGS	TX	13.20
DALBY SPRINGS	TX	13.00
NATCHITOCHEs	LA	12.95
MOUNT VERNON	TX	12.90
LINDALE	TX	12.70
MOUNT PLEASANT	TX	12.60
NAPLES	TX	12.60
MINEOLA	TX	12.50

Figure G-45. 27–30 March 1945 Daily Weather Maps.

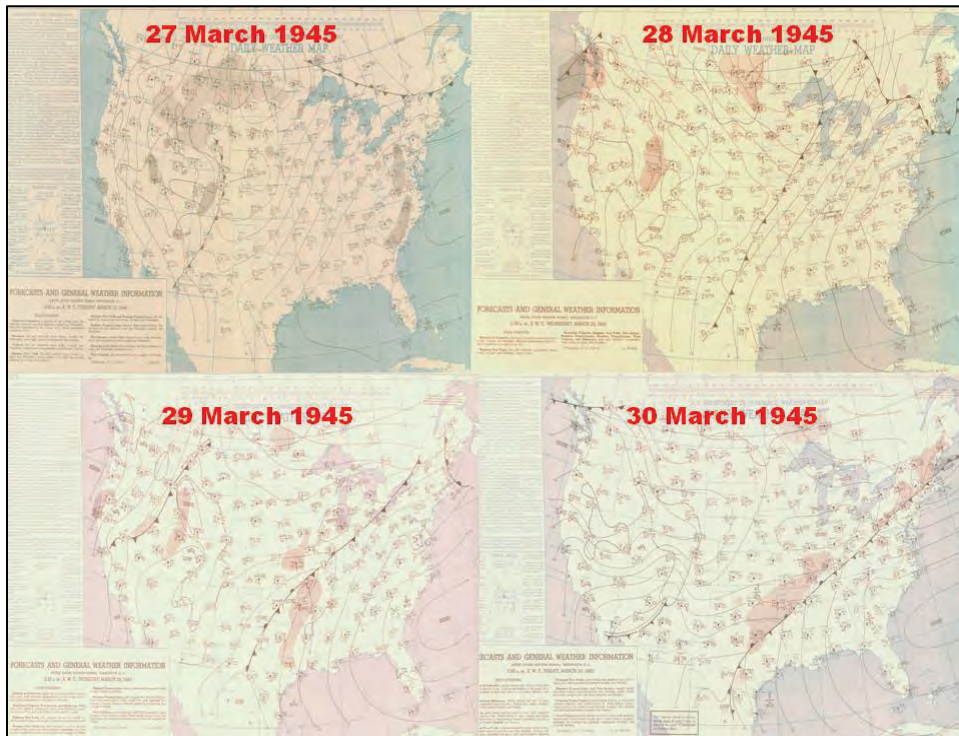
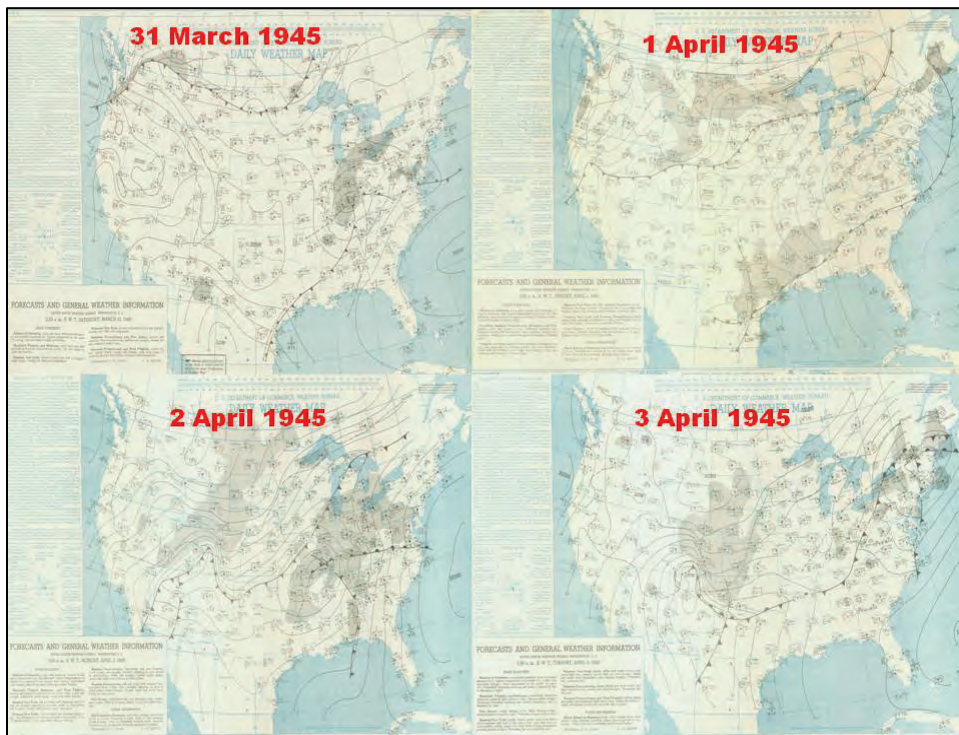


Figure G-46. 31 March–3 April 1945 Daily Weather Maps.



G.7.9 3–16 January 1950

The area of heavy rainfall of this storm was at first oriented northeast-southwest from Lake Erie to northeast Texas with later displacement southeastward. Total precipitation amounts are shown in Figure G-47, and the top 20 recorded rainfall gauges are shown in Table G-17.

During the last few days of 1949, a large polar anticyclone slowly moved southeastward over the United States east of the Rocky Mountains and with considerable warming from below became a somewhat modified continental polar air mass as its center reached the Atlantic coast on January 1. Upon reaching the Atlantic Coast and Gulf of Mexico, the surface temperatures and dew points in the western part of this anticyclone increased rapidly, and by 2 January 1950, the air over the Gulf States had maritime tropical characteristics.

While the high pressure persisted over the eastern states at the surface the first 2 days of January, a Low moved very slowly across the northern Rocky Mountains, and extremely cold air from Canada poured southeastward into the Northern Rockies and Northern Plains States. By 0630 CST on January 3, the Low had moved eastward to the Great Lakes, and a cold front extended from it into Oklahoma and northwestward to the Rocky Mountains. Until this time, only light amounts of rainfall had occurred in the northward flow of maritime tropical air in advance of the front.

The upper-level flow pattern of this storm resembled to a very great extent that of other large rainfall situations in the same general area, consisting of a deep trough over the western United States and a ridge over the eastern states. This represents a reversal of the normal January circulation pattern in the United States. William H. Klein, in the article "Winter Precipitation as Related to the 700-mb Circulation" (Klein 1948), points out that in good agreement with numerous studies, the southerly flow in advance of a deep trough aloft is intimately associated with heavy precipitation and that "these findings can be attributed to the horizontal convergence, upward vertical motion, abundant moisture, and convective instability which characterize southerly flow from the Gulf of Mexico."

Daily weather patterns are shown in Figures G-48 through G-51 and 6-hour isohyetal graphs are shown in Figures G-52 through G-55. The

isohyetal pattern for the 6 hours ending at 1500 CST January 3 shows the first major burst of rainfall of this storm. The rainfall as far northward as Farmington, MO, (approximately 50 miles south of St. Louis), was all in the cold air at this time, indicating no rainfall until the frontal passage. However, in parts of Ohio, Indiana, and Illinois, that rainfall extended ahead of the front due to an instability line in a trough ahead of the front. While there is no one generally accepted theory explaining the mechanism of instability lines, their location is usually in a warm air trough ahead of a cold front or in the warm sector of a cyclone.

The isohyetal pattern for the 6 hours ending at 2100 CST January 3 is very similar to the preceding one and is located slightly southeast of it. The rainfall here seems to be due to the same causes as above. The surface map near the end of this period showed a small wave, which had formed in northern Arkansas. A thunderstorm was in progress at Westplains, MS, just to the north of this Low.

The isohyetal pattern for the 6 hours ending 0300 CST January 4 covers a somewhat broader area than the previous 6-hourly periods with a shifting slightly southward of the largest amounts. The broader area of this rainfall seems to be due to the lag of the trough aloft behind the surface cold front while the displacement southward of the rainfall pattern is probably associated with development of the small Low near northeast Arkansas.

The isohyetal pattern for the 6 hours ending 0900 CST January 4 shows a smaller amount of rainfall due to the fact that the cold front is past the area at the surface and colder drier air is becoming deeper. For the 12 hours following this time, the rainfall is very light due to still more progress of the cold air over the area.

From an examination of the surface maps alone, it is difficult to determine why there was so little rain in the area of this storm for the 12 hours ending at 2100 CST January 4 and its beginning again for the 6-hour period ending at 0300 CST January 5. At 850 mb and 700 mb, however, a trough approached from the west, and a more southerly flow of air with higher dew points moved into the area.

The continuous progress of the trough aloft approaching the rain area and the front at the surface account for the occurrence of the remaining rainfall of this storm. A Low that developed on the front near the Gulf Coast on January 5 and moved northeastward along the front while intensifying was also a contributing factor.

Finally, the movement of the Low to New England and progress of the cold front across the Appalachian Mountains followed by the polar High brought an end to the rainfall over the Mississippi and Ohio Valleys.

For the next 3 days following the cessation of the rainfall over the area of interest, the large polar High moved very slowly eastward, its center reaching the Atlantic Coast on January 9, blocking the entrance of another depression into the central United States and the return of rainfall until January 10.

Light to moderate rains occurred in the northward flowing air over the Ohio and Mississippi Valleys on January 1–2. This rainfall was associated with a weak trough aloft that preceded the major trough that caused the storm of January 3–7. The weak trough aloft was accompanied by a front that stalled over the central United States near Kansas City on January 1. Since this system did not progress southward out of the area of interest and in fact did give moderate rains over the Mississippi Valley up to the time of the beginning of the January 3–7 storm, it is reasonable to suppose that under most favorable circumstances a heavy rainstorm could precede with no appreciable time interval.

The 12-hour representative dew point for this storm was 68 °F. The maximum dew point for this area is 71 °F, allowing an upward adjustment of 16%.

Figure G-47. Total Precipitation for the 3–16 January 1950 storm.

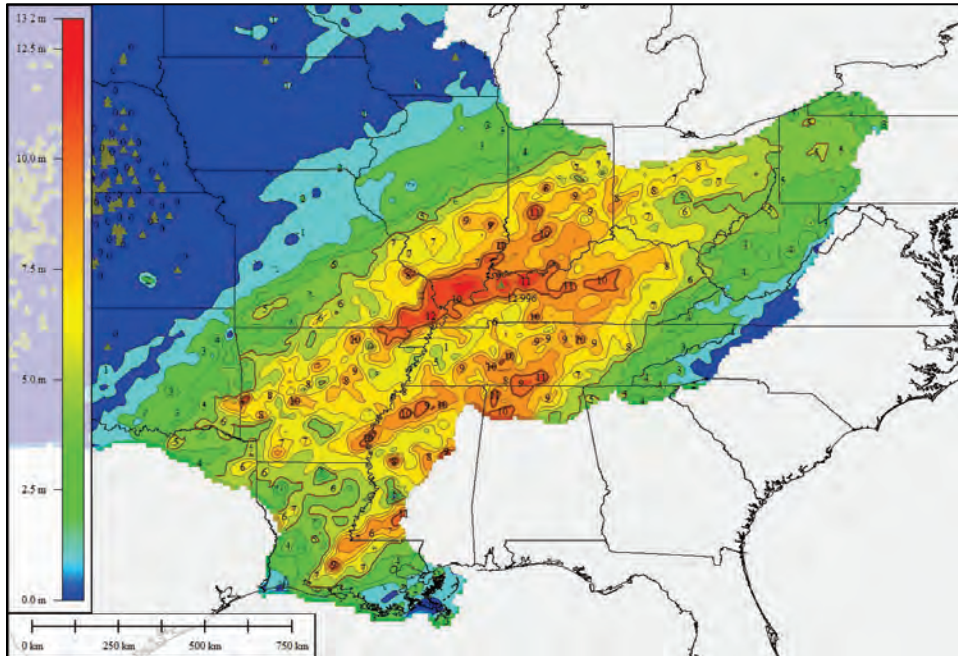


Table G-17. Top 20 recorded rainfall gauges (inches) for the 3–16 January 1950 precipitation event.

HENDERSON_8_SSW	KY	12.95
NEW_BURNSIDE	IL	12.50
HARRISBURG	IL	12.44
CYPRESS_DAM_48	IN	12.42
SIKESTON	MO	12.09
HARRISBURG_DISPOSAL	IL	11.96
MARION_4_NNE	IL	11.87
OWENSBORO_TRTMNT_PLANT	KY	11.84
PETERSBURG	TN	11.77
EAGLE_GAP	AR	11.54
MOREHOUSE	MO	11.52
CP_GIRARDEAU_ST_UNIVERSITY	MO	11.41
FISK	MO	11.39
BELLEVILLE	TN	11.33
DUMAS	AR	11.29
DIXON_SPRINGS_AGR_CE	IL	11.21
ALBION	IL	11.16
TELL_CITY	IN	11.16
CARBONDALE_SEWAGE_PLANT	IL	11.10
WEST_FRANKFORT_8_E	IL	11.10

Figure G-48. 2-5 January 1950 Daily Weather Maps.

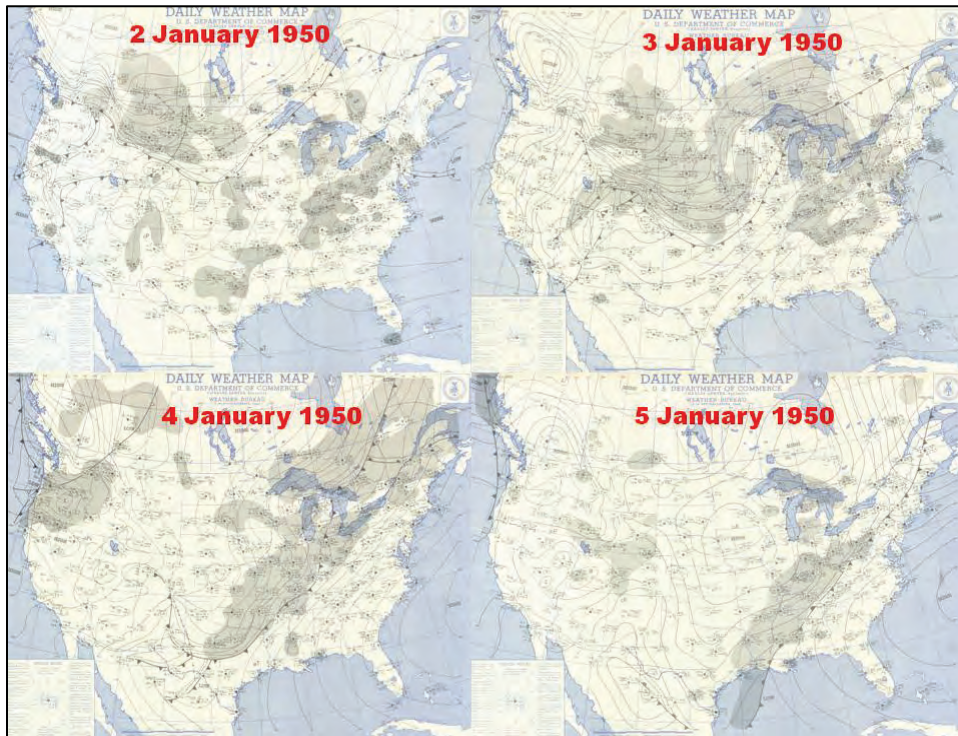


Figure G-49. 6-9 January 1950 Daily Weather Maps.

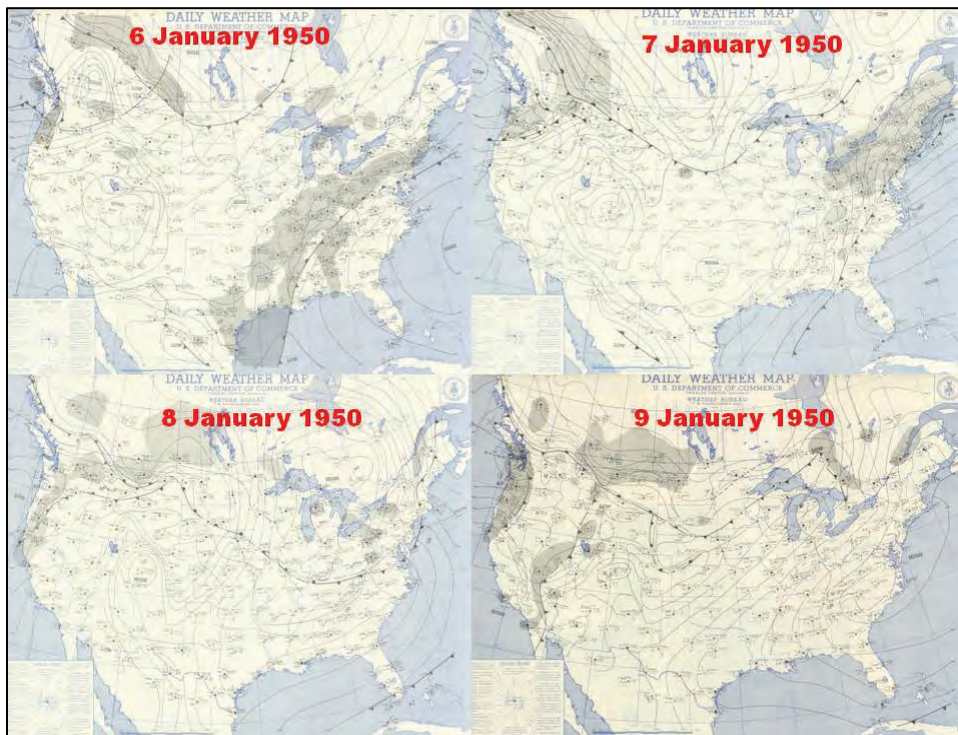


Figure G-50. 10–13 January 1950 Daily Weather Maps.

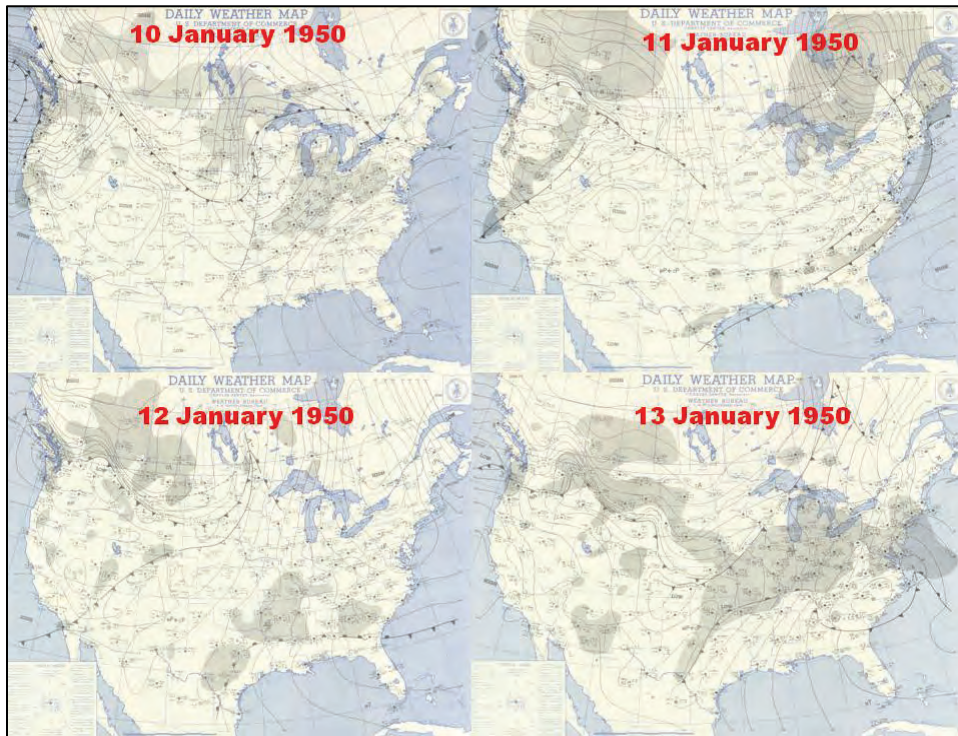


Figure G-51. 14–17 January 1950 Daily Weather Maps.

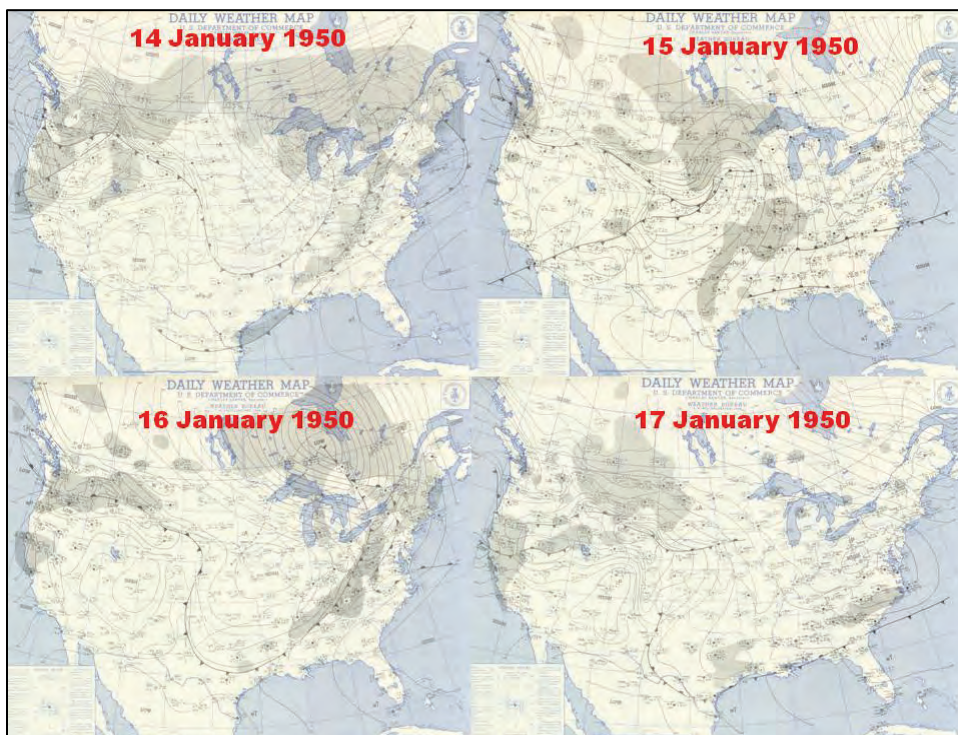


Figure G-52. 6-hour isohyets for the 3-7 January 1950 storm (3 January).

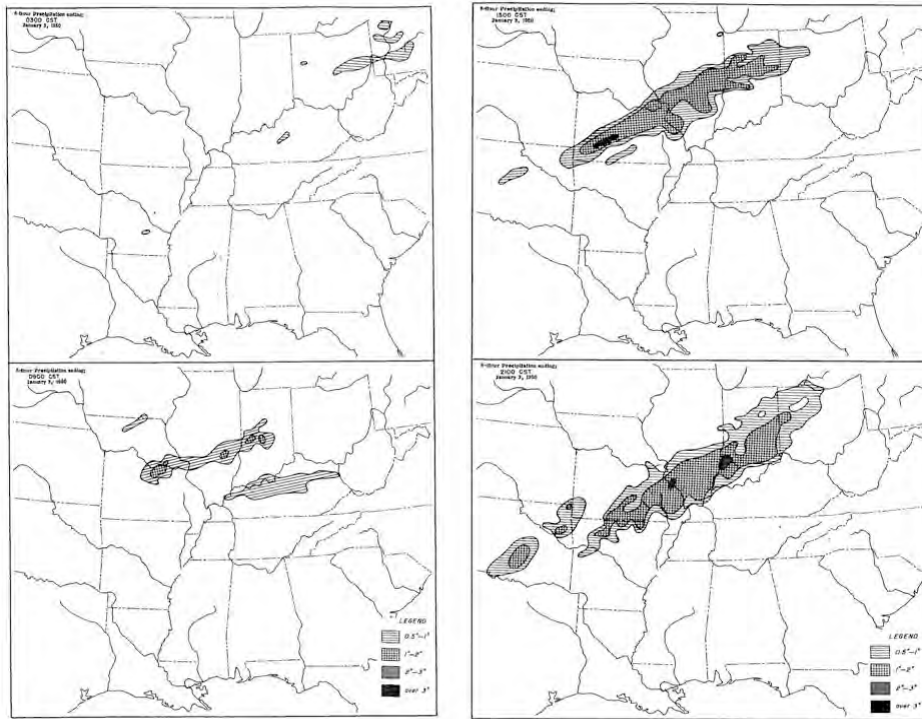


Figure G-53. 6-hour isohyets maps for 3-7 January 1950 storm event (4 January).

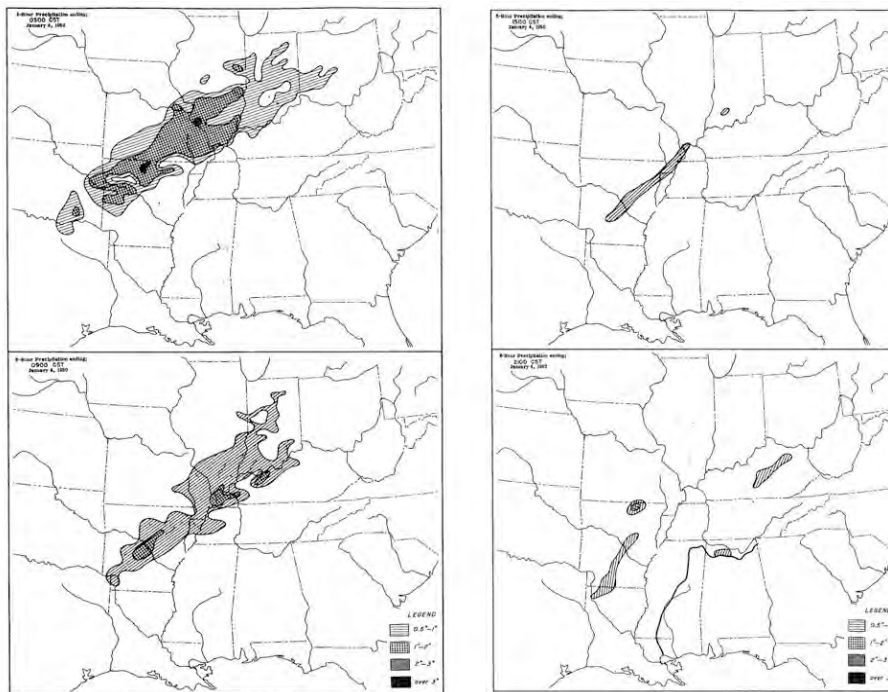


Figure G-54. 6-hour isohyets maps for 3-7 January 1950 storm event (5 January).

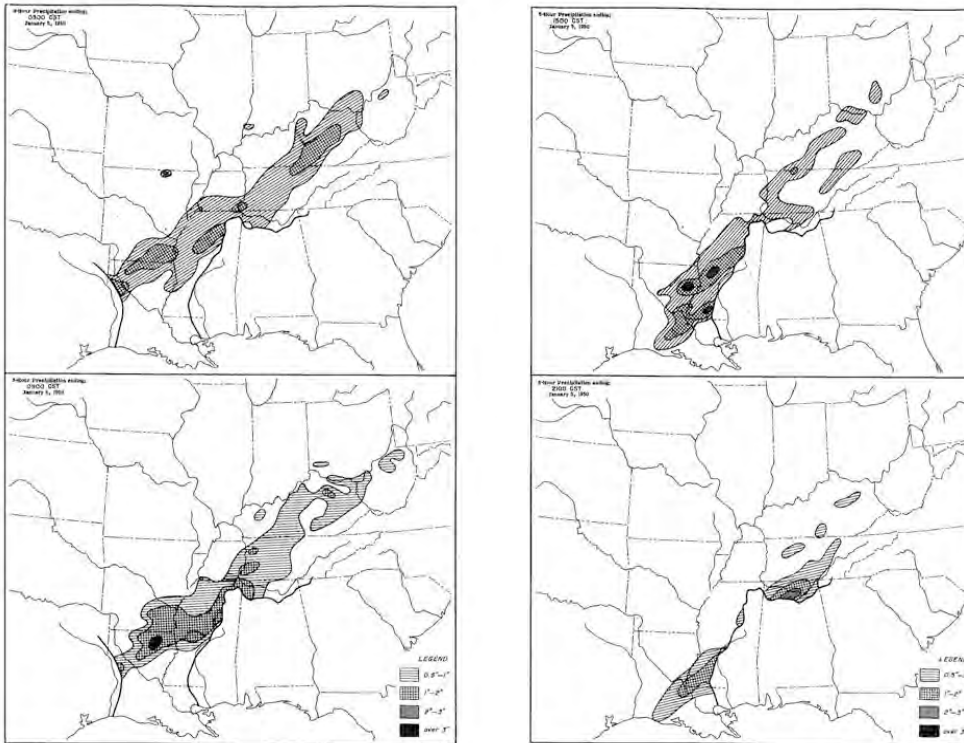
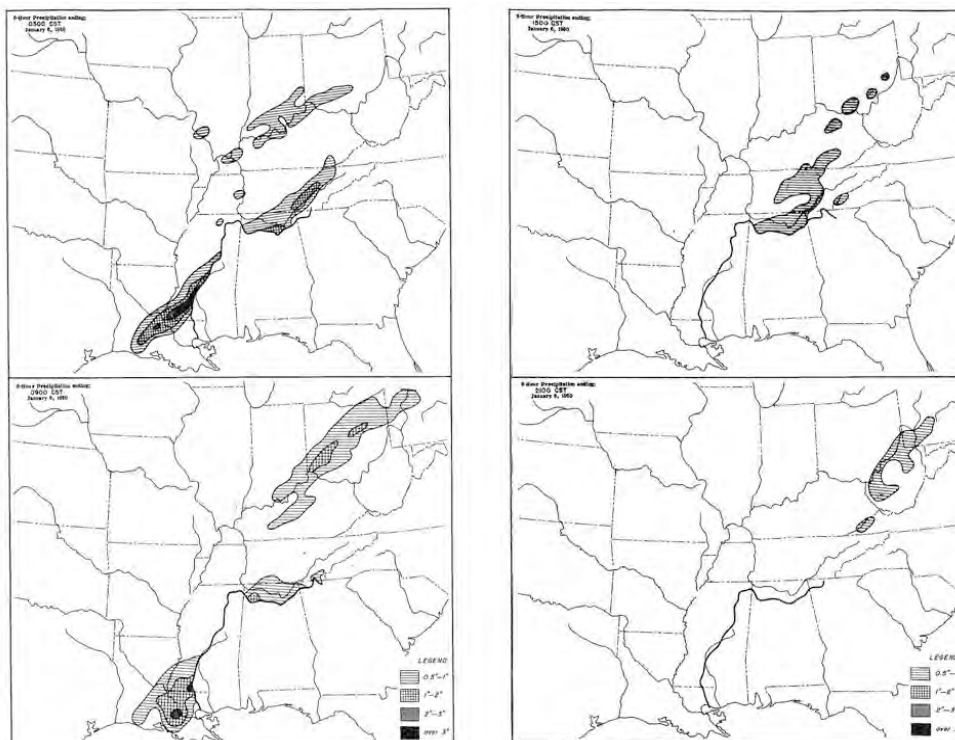


Figure G-55. 6-hour isohyets maps for 3-7 January 1950 storm event (6 January).



G.8 Temperature data

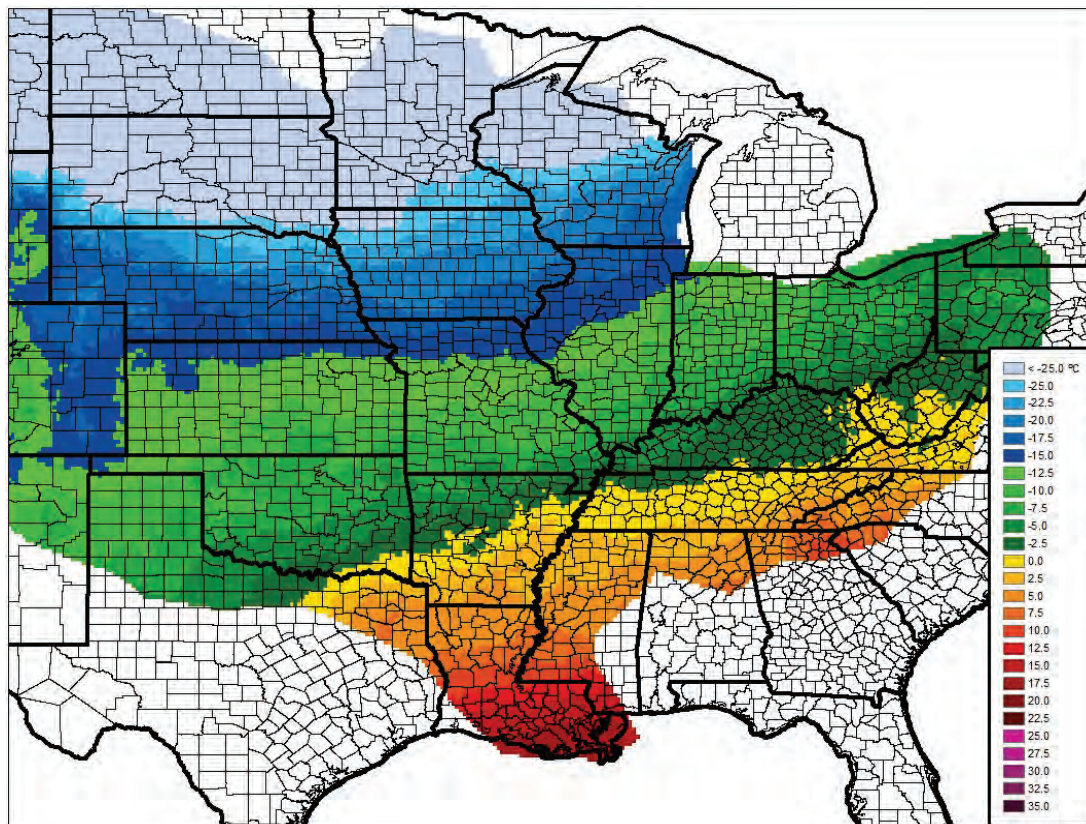
Although the majority of major floods in the Mississippi Valley are caused by heavy rainfall events, snow melt also can play an important role in peak stages and volumes. During the Mississippi River Flood of 2011, snow melt contributed to approximately 3 to 4 ft of stage at the confluence of the Mississippi and Ohio Rivers at Cairo, IL. The additional water from snowmelt, which reached the confluence in conjunction with the runoff from a very heavy rainfall event, was a major contributing factor into the decision to operate the Birds Point/New Madrid Floodway. Since snow melt can contribute to major flooding, datasets for temperature were required for the same time period as the precipitation data. The temperature datasets aided in determining precipitation type, amount of accumulation, and timing of snow melt, which were used by the NCRFC, Missouri River Forecast Center, Ohio River Forecast Center, and Arkansas/Red River Forecast Center during the production of the storm and HYPO flood events.

NCDC datasets for temperature contain the daily maximum and minimum values along with an observation taken at a variable time during the day. To develop the temperature dataset, the maximum and minimum values were used. Temperatures were considered to uniformly rise or fall between the daily maximum and minimum values at a given location. With the unavailability of the exact time of maximum and minimum occurrences in the dataset, it was assumed that the temperature maximum occurred at 21 UTC and the temperature minimum occurred at 12 UTC. The following formulas were used to compute the 6-hourly temperatures. The difference in time between $TMAX_{day\ 1}$ and $TMIN_{day\ 2}$ is 15 hours, and the difference between $TMIN_{day\ 1}$ and $TMAX_{day\ 1}$ is 9 hours.

- $T00 = (TMAX_{day\ 1} - (3 * (TMAX_{day\ 1} - TMIN_{day\ 2})) / 15)$
- $T06 = (TMAX_{day\ 1} - (9 * (TMAX_{day\ 1} - TMIN_{day\ 2})) / 15)$
- $T12 = TMIN_{day\ 1}$
- $T18 = (TMIN_{day\ 1} + (2 * (TMAX_{day\ 1} - TMIN_{day\ 1})) / 3)$

GIS datasets were generated for the exact warm-up period, storm event period, and 1-month post-storm period. These shapefiles were converted to ASCII grids for assimilation into the NWS Hydrologic models. Figure G-60 depicts an example of the shapefiles generated for the 1950 storm event.

Figure G-56. Example temperature (°C) shapefile for 6 January 1950, 12 UTC for the Mississippi River Basin.



G.9 Additional extreme storms: Post MRPFS

The timing and magnitude of the 2011 flood on the Lower Mississippi River surfaced the question of whether there has been a change in seasonality for floods in the basin. The April–May 2011 flood had a significant contribution coming from the Middle Mississippi River, a much larger proportion than indicated by the HYPO 58A-EN hydrographs as defined by the 1955 Study. For this reason, additional storms (Table G-18) were considered for use in assembling new HYPO storm sequences.

Table G-18. Additional historic events for building new HYPO storm sequences.

Event Dates
16-26 April 1973
12-29 March 1975
28 June – 9 July 1993
27 February – 9 March 1997
22 April – 3 May 2011

The precipitation for the additional historic events is described below.

G.9.1 16–26 April 1973 storm

According to the Mississippi River and Tributaries Post Flood Report 1973,

The development of the 1973 flood was very similar to that of the 1927 flood in that above normal rainfall began in the fall, proceeded through the winter, and climaxed in the early spring. (USACE 1973, 12)

Conditions that led to the flooding, in March and April of 1973, in the basin began in September of 1972. ...Storms in September, October, and November were generally concentrated in the lower regions as evidenced by the fact that accumulated rainfall exceeded normal by a total of 9.3 inches or about 200 percent of normal, while the accumulated rainfall for the central and upper regions exceeded normal by a total of 2.1 inches or about 130 percent of normal. Storms in December, January, and February were generally minor with the exception of January for the central and upper regions which experienced 2.5 inches, about 200 percent of normal. Repeated rainfall, beginning about the first of March and extending through April, occurred over much of the Arkansas Basin. The lower region experienced 20.3 inches of rainfall in the two-month period, which was slightly more than 200 percent of normal. The central and upper regions experienced 12.9 inches of rainfall, which was more than 250 percent of normal. Of the 12.9 inches, 8.2 inches fell in the month of March, which for the central and upper regions was more than 400 percent of normal. The total accumulated

rainfall for the lower region, and the central-upper region for the nine-month period, September 1972 to May 1973, was 57.7 and 31.0 inches, respectively. These totals exceeded normal accumulations by almost 150 percent. The most severe general storms during the March and April period, occurred on 9-11 March, 24-26 March, and 16-26 April. (USACE 1973, A2-A3)

A new maximum monthly rainfall record for April was established at Little Rock's Adams Field. The previous April high, spanning 32 years, was 11.34 inches. This was exceeded when 14.20 inches of rainfall fell during April of 1973. This was about a 50-year frequency. The rainfall over the Lower Arkansas Basin during the 16-26 April storm, had a recurrence interval of approximately 5 years. Little Rock's Adams Field recorded 12.02 inches during the 16-26 April period, which is about a 20-year recurrence interval for any 10-day period during the year. (USACE 1973, A3)

[In AR and LA,] March began with a hydrologic bang! Significant rainfall accumulations were recorded on more than half of the days of the months with severe weather occurring on a number of days. The first storm system moved across the Ouachita River Basin on 1 through 3 March, depositing amounts of precipitation ranging from 1-1/2 to 5-1/2 inches. ...A second storm system formed on 11-12 March and moved across the basin leaving rainfall amounts in excess of 2 inches. The third significant storm system of the month swept across the basin 24-25 March, leaving measured amounts of rainfall ranging from 2 to 7 inches. In summary, precipitation over Arkansas was extremely heavy with monthly totals averaging 5 to 8 inches above normal. Louisiana monthly totals were in excess of 10 inches through most of the state. (USACE 1973, G5)

In April, rainfall amounts were slightly below normal in most areas allowing streams to begin receding. During the period 19-24 April, extreme weather conditions were observed over large areas of the basin. Severe thunderstorms with tornadoes pelted areas with high winds, hail, and torrential rainfalls. On four of the six days during this period, daily rainfall amounts were reported in excess of 5 inches. The storm series actually began on 16 April when general rainfalls of 1 to 3 inches were recorded.

Another storm system quickly developed on 18 April, again saturating the northern portion of the basin with 1 to 8 inches being recorded by the 19th. An example of the intense 24-hour rainfall occurred at Gurdon, Arkansas where 8.67 inches fell. ...These intense rainfalls caused severe flash flooding in local areas. Less than a week after this storm system moved across the Upper Ouachita Basin, a third significant system developed and similarly spawned widespread severe thunderstorms and tornadoes with accompanying flood-producing rainfalls. This storm produced intense rainfalls varying from a few tenths of an inch to amounts in excess of 5-1/2 inches. ...Rainfall for April was well above normal, particularly over the Lower Arkansas and White Basins where amounts were more than three times the monthly normal. (USACE 1973, G5–G6)

Precipitation amounts for the top 20 recorded rainfall gauges of the 16-26 April 1973 event are shown in Table G-19. Daily weather patterns are shown in Figures G-57 through G-59.

Table G-19. Top 20 recorded rainfall gauges (inches) for the 16–26 April 1973 precipitation event.

GURDON	AR	15.65
SAINT_CHARLES	AR	15.53
BATESVILLE_LOCK_AND_DAM_1	AR	14.67
WYNNE	AR	14.14
REMMEL_DAM	AR	13.84
DES_ARC	AR	13.63
GALLIANO	LA	13.25
LSU_CITRUS_RES_STATION	LA	12.68
CARPENTER_DAM	AR	12.51
NEW_ORLEANS_ALVIN_CALLENDER_FIELD	LA	12.51
STUTTGART_9_ESE	AR	12.33
ROSEDALE	MS	12.32
STUTTGART	AR	12.24
BONNERDALE_1_ESE	AR	12.21
OWENSVILLE_3_E	AR	12.2
TUNICA_2_N	MS	12.13
GILMER_4_WNW	TX	12.12
HOT_SPRINGS_1_NNE	AR	11.86
PARAGOULD	AR	11.84

Figure G-57. 15–18 April 1973 Daily Weather Maps.

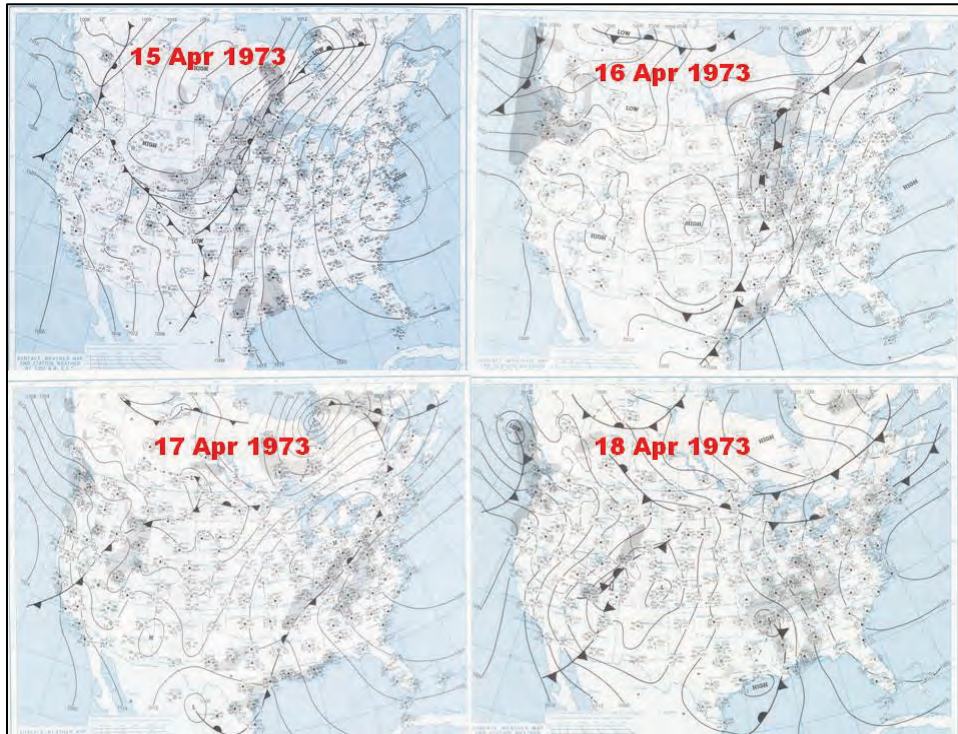


Figure G-58. 19–22 April 1973 Daily Weather Maps.

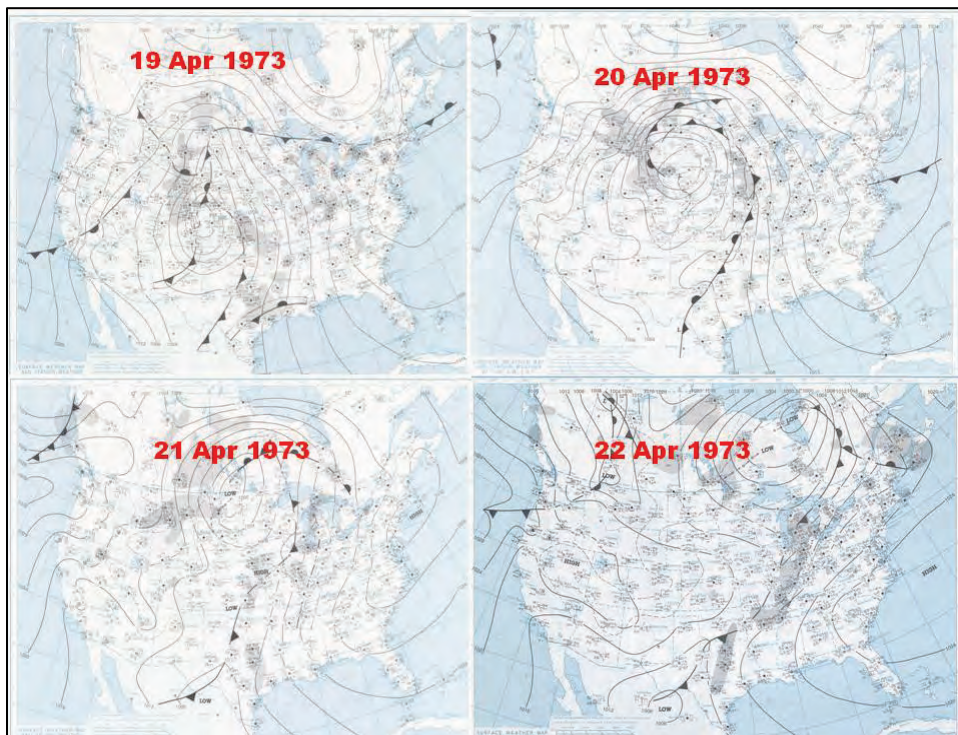
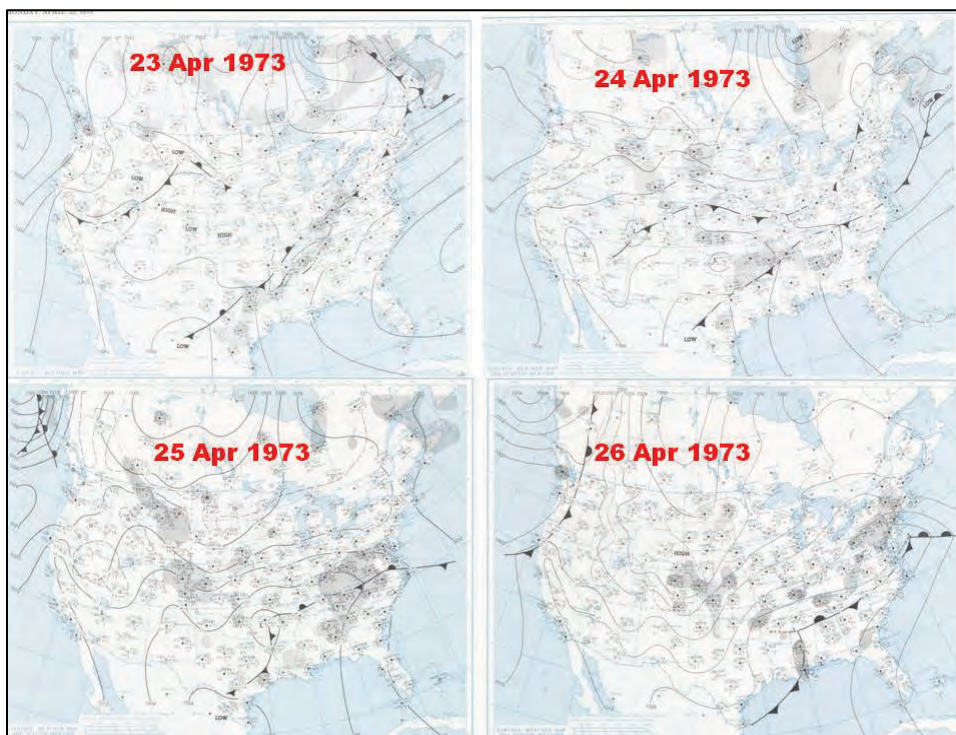


Figure G-59. 23–26 April 1973 Daily Weather Maps.



G.9.2 12–29 March 1975 storm

Like most major floods on the Mississippi River, heavy rains during prior months caused river stages to rise and soils to become saturated in 1975. Precipitation amounts for the top 20 recorded rainfall gauges for the 19-30 March 1975 time period are shown in Table G-20. Daily weather maps are shown in Figures G-60 through G-62.

The flood of 1975 was made up of four events during which the stage at Cairo exceeded flood stage (40 feet). These events were 14-19 January 1975, 2-16 February 1975, 24 February – 17 April 1975, and 28 April – 14 May 1975. The latter three events were major floods with 24 February – 17 April the most significant due to the stage at Cairo. (USACE 1989, 37)

The stage at Cairo, IL rose to 56.4 feet on 4 April, the second highest historical stage at the time behind only 1937.

The heaviest rainfall occurred over KY and TN during the event.

The conditions in the Ohio Basin in January were relatively warm and wet. Most of the observed precipitation occurred during two storms, one on the 4th and another on the 10th of January. These storms caused minor flooding at the confluence of the Ohio and Mississippi Rivers. (USACE 1989, 37)

In February, both the temperature and precipitation were above the long-term normal for the entire Ohio Basin. A storm on the 23rd and 24th brought heavy rains which caused above normal precipitation. This event caused flooding in the Ohio and its tributaries from Cincinnati to the mouth. (USACE 1989, 38)

Precipitation for March was above normal in the Ohio Basin with two distinct storm systems. One occurred on the 12th and 13th and a similar storm occurred during the 27th through the 29th. Precipitation amounts recorded at stations in western Kentucky and Tennessee-North Carolina were 4 inches and 6 inches, respectively. This precipitation produced record breaking floods within the Cumberland and Green River Basins and along the lower Ohio main stem. (USACE 1989, 38)

Stages at Cairo, IL, exceed bankfull stage for a period of 58 days as compared to a period of 97 days in 1973. The volume of flood water to pass Cairo during this period was 27 million acre-feet and was for the most part out of the Ohio River Basin. (USACE 1989, 41)

Table G-20. Top 20 recorded rainfall gauges (inches) for the 19–30 March 1975 precipitation event.

GREENSBURG	KY	12.24
CORNING	AR	10.97
POCAHONTAS_1	AR	10.78
NORTH_WILKESBORO	NC	10.77
MALDEN_MUNICIPAL_AIRPORT	MO	10.04
PARMA	MO	9.93
SAINT_FRANCIS	AR	9.68
DEXTER	MO	9.55
NEWPORT	AR	9.53
QULIN	MO	9.51
GREERS_FERRY_DAM	AR	9.49
BERNIE	MO	9
NANTHALA	NC	8.98
SHIRLEY	AR	8.97
ALICIA_2_NNE	AR	8.67
PUXICO_1_SE	MO	8.57
SEARCY	AR	8.33
BALD_KNOB_5_N	AR	8.23
MOUNTAIN_VIEW	AR	8.19
GILBERTSVILLE_KY_DAM	KY	8.14

Figure G-60. 19–22 March 1975 Daily Weather Maps.

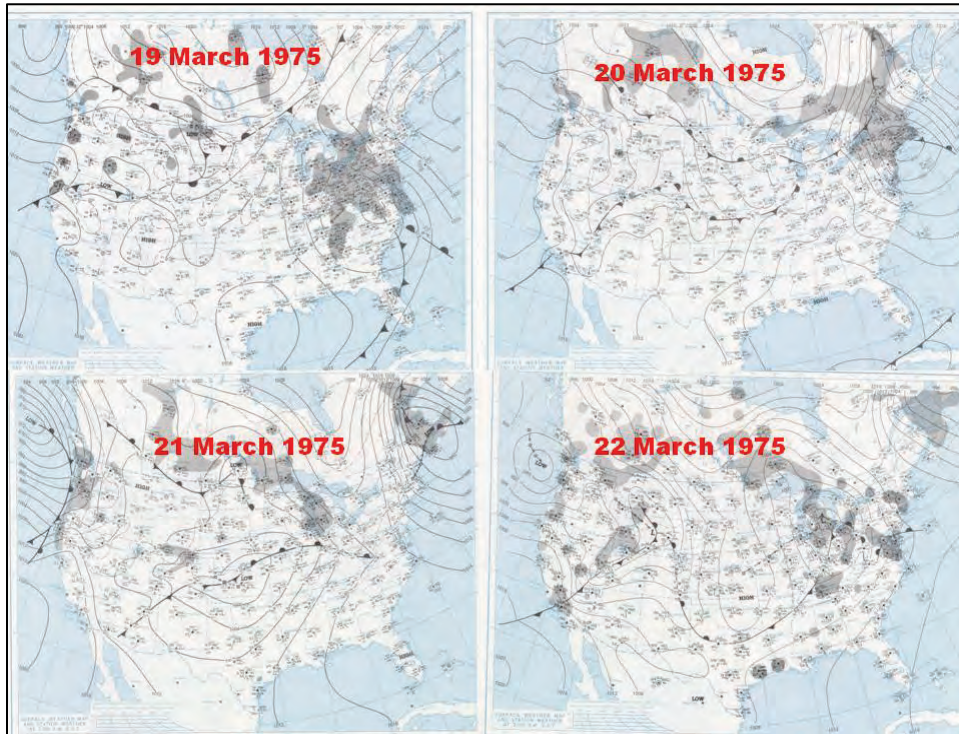


Figure G-61. 23–26 March 1975 Daily Weather Maps.

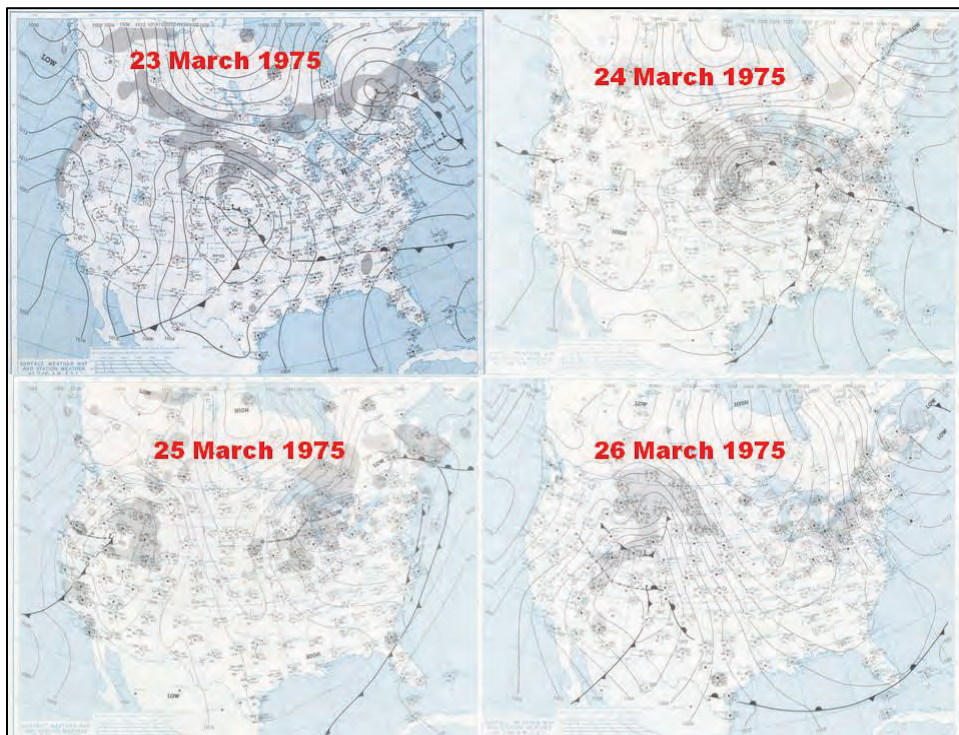
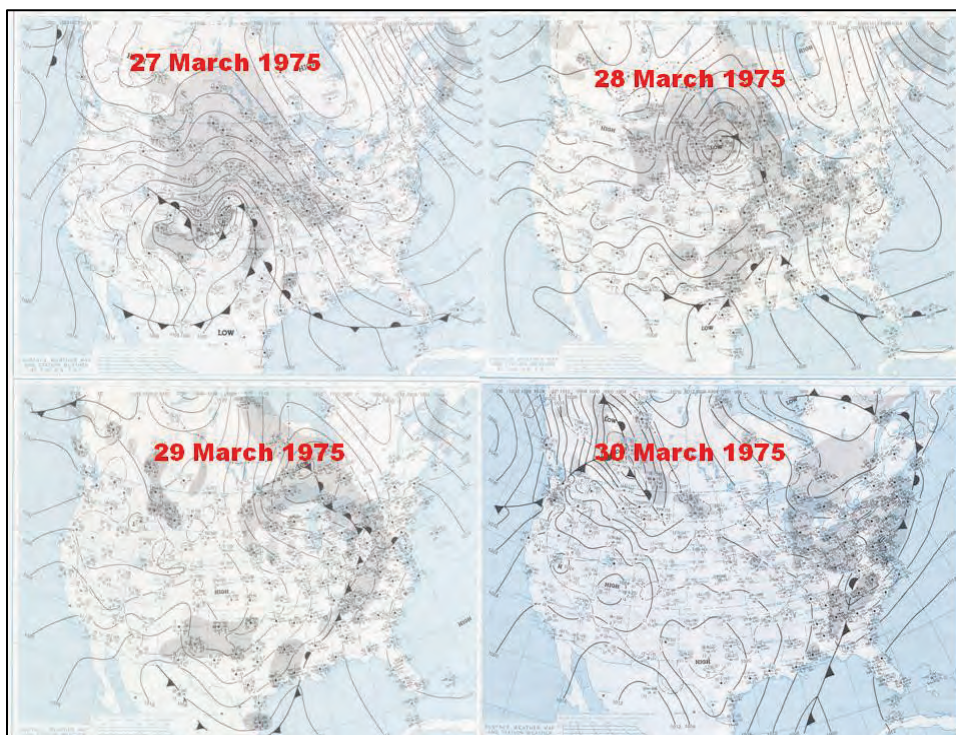


Figure G-62. 27–30 March 1975 Daily Weather Maps.



G.9.3 1993

The NOAA Natural Disaster Survey Report, The Great Flood of 1993 (NOAA 1994) presents the following:

The [1993] flood event was exceptional due to the combination of several factors:

1. The antecedent hydrometeorology: the scene was set for flooding across the flood-impacted area long before major flooding actually developed.
2. The meteorology: the meteorological analysis that caused the excessive rainfall over the region from mid-June in August 1993 was uncommonly persistent.
3. The magnitude of flooding: the areal extent of the flooding was unusually large.
4. The severity of the flooding: major to record flooding occurred along dozens of rivers, including portions of the main stems of both the Mississippi and Missouri Rivers.

5. The season of flooding: major flood events in the Upper Mississippi River basin typically occur in spring while this occurred throughout the summer.
6. The duration of the flooding: most significant floods last on the order of days–to-weeks, while this flood lasted on the order of weeks-to-months.
7. The damage: preliminary estimates establish this as the costliest flood event in U.S. history.

All or parts of nine states were declared Federal disaster areas: North Dakota, South Dakota, Minnesota, Wisconsin, Nebraska, Iowa, Illinois, Kansas, and Missouri. Within these nine states, some 500 counties received some form of federal assistance. (NOAA 1994, 72)

The Great Flood of 1993 was an unprecedented hydro-meteorological event since the U.S. started to provide weather services in the mid-1800s. In terms of precipitation amounts, record river stages, areal extent of flooding, persons displaced, crop and property damage, and flood duration, this event (or sequence of events) surpassed all floods in the U.S. during modern times. (NOAA 1994, 52)

Record and near-record precipitation during the spring of 1993, on soil saturated from previous seasonal precipitation, resulted in flooding along many of the major river systems and their tributaries in the Upper Midwest. Rivers climbed above flood stage at approximately 500 forecast points in the nine-state region. Moreover, record flooding occurred at 95 forecast points in the Upper Midwest during the summer of 1993. Flood records were broken at 44 forecast points on the upper Mississippi River system, at 49 forecast points on the Missouri River system, and at 2 forecast points on the Red River of the North system. Within the Mississippi River system, 1993 floods of record include those set at 15 forecast points on the main stem, at 4 forecast points on the Iowa River, at 5 forecast points on the Des Moines River, and at 2 forecast points on the Raccoon River. (NOAA 1994, 52)

Within the Missouri River system, 1993 floods of record include those set at 14 forecast points on the main stem and at 4 forecast points on each of the Saline, Smoky Hill, and Grand Rivers. During the event, near flood of record stage occurred at an additional 23 forecast points on the Missouri River system alone. Record flood stages surpassed old record stages by more than six feet in some cases. For example, in 1993, flood records set more than 42 years ago on the main stem of the Missouri were broken by more than 4 feet at multiple forecast points. In at least one case, a new flood of record was established early in the event only to be broken by higher water later in the event. The historic flood of record on the Mississippi at St Louis was established on April 28, 1973, at 43.2 feet; reestablished on July 21, 1993, with a flood stage of 46.9 feet; and reestablished again 11 days later on August 1, 1993, with record flood stage of 49.58 feet. (NOAA 1994, 52)

The duration of The Great Flood of 1993 was as overwhelming as the areal extent of flooding and the number of record stages established. Spring flooding began in March as a result of a previous wet fall, normal to above-normal snow accumulation, and rapid spring snowmelt accompanied by heavy spring rainfall. On May 8, record flooding occurred in South Dakota on Split Rock Creek at Corson and in Minnesota on the Rock River at Luverne. On May 22-24, heavy thunderstorms produced 3-7 inches of rain in 3 hours over Sioux Falls resulting in major urban and residential flooding across the city. The Big Sioux and Vermillion Rivers in South Dakota went above flood stage in late May and remained in flood through mid-June. Major flooding continued throughout the summer along the Missouri and Mississippi Rivers. For example, on September 1, 1993, the towns of Hannibal, LA, and Clarksville, MO, had experienced 153 consecutive days of flooding. Flooding at levels above flood stage continued through the middle of September in many regions along the Mississippi River. ...[On the Mississippi River] Every gage, from Quad Cities [IA] to below St Louis [MO] set new, all-time record stages! (NOAA 1994, 53-54, 94)

The flood had its origins in an extended wet period starting 9-10 months prior to the onset of major flooding. This wet period

moistened soils to near saturation and raised many stream levels to bankfull or flood levels. This set the stage for rapid runoff and record flooding that followed excessive June and July rainfall. The precipitation was the direct result of major, global-scale circulation anomalies which can be attributed to significant climate variations. (NOAA 1994, 72)

A highly anomalous and persistent atmospheric pattern of excessive rainfall occurred across much of the upper Mississippi River valley and the northern and central Great Plains during June, July, and the first half of August 1993. ...Climatologically, a low pressure trough is located near the Gulf of Alaska during the summer months. ...An El Nino/Southern Oscillation (ENSO) episode occurred during 1992 and 1993. ...In April 1993, below-normal sea-level pressures were established in the central and western North Pacific Ocean. This pressure anomaly pattern persisted through June. During June and July 1993, the mean position of the Pacific low-pressure trough moved west to the international dateline. Below-normal sea-level pressures also covered the western U.S. and much of the North Atlantic from Newfoundland to Scandinavia. Corresponding shifts occurred in the mean position of the jet stream. (NOAA 1994, 76, 84)

By the summer of 1993, the mean position of the jet stream had become firmly established over the northern portion of the Mississippi River basin with a southwest-northeast orientation. To the northwest lay a deep trough of low pressure, while an unusually strong, clockwise circulation lay over the eastern United States. Hot and dry conditions were characteristic of the surface conditions beneath the ridge. The quasi-stationary jet stream aloft was associated with a stationary surface front that allowed frequent and nearly continuous overrunning of the cooler air to the north by the moisture-laden air from the south... The front also served as a preferred location for unusually strong and frequent cyclones, spawned by the combination of the unseasonably vigorous jet stream overhead... and the relatively strong frontal boundary at the surface. (NOAA 1994, 76)

North-south transport of moisture was enhanced by strong low-level advection brought about by the unusually large contrast between the trough of low pressure over the northwestern section of the Nation and the ridge of high pressure over the Southeast. Much of this low-level moisture originated in the subtropics in the vicinity of the warm Caribbean Sea waters... The increased moisture transport and the presence of the front supported production of widespread areas of prolonged and excessive precipitation throughout large portions of the north-central United States. (NOAA 1994, 80)

Finally, by late July and early August, a change in the upper air circulation pattern brought drier conditions to the Midwest as the trough shifted eastward, simultaneously increasing rainfall and decreasing temperatures in the East while warmer weather returned to the Pacific Northwest... Unfortunately, locally heavy thunderstorms generated some additional flooding problems in parts of the soaked Midwest during mid-August; however, these rains were associated with more typical summertime convection caused by frontal passages that were enhanced by strong advection of southwestern monsoonal moisture. (NOAA 1994, 80)

During the summer (June-August 1993), rainfall totals surpassed 12" across the eastern Dakotas, southern Minnesota, eastern Nebraska, and most of Wisconsin, Kansas, Iowa, Missouri, Illinois, and Indiana. More than 24 inches of rain fell on central and northeastern Kansas, northern and central Missouri, most of Iowa, southern Minnesota, and southeastern Nebraska, with up to 38.4 inches in east-central Iowa... These amounts were approximately 200-350 percent of normal from the northern plains southeastward into the central Corn Belt. Since the start of the growing season (April 1), precipitation amounts through August 31 were even more impressive...: totals approached 48 inches in east-central Iowa, easily surpassing the area's normal annual precipitation of 30-36 inches. (NOAA 1994, 80)

From a seasonal standpoint, above- to much above-average rainfall fell over the entire Upper Midwest from May through

August 1993... The May-August 1993 rainfall amount is unmatched in the historical records of the central United States. In July, there were broad areas in North Dakota, Kansas, and Nebraska, as well as a smaller pocket in Iowa, that experienced more than four times normal precipitation. ...The June-July precipitation amounts are remarkable not only in magnitude but also in their broad regional extent. Record wetness existed over 260,000 square miles. (NOAA 1994, 84)

In summary, the genesis of The Great Flood of 1993 had been set by June 1 with saturated soils and filled streams across the Upper Midwest. The water from the ensuing persistent heavy rains of June, July, and August had no place to go other than into the streams and river courses. Record summer rainfalls with amounts achieving 75- to 300-year frequencies thus produced record flooding on two major rivers, equaling or exceeding flood recurrence intervals of 100 years along major portions of the upper-Mississippi and lower Missouri Rivers. (NOAA 1994, 93).

Precipitation totals for the top 20 recorded rainfall gauges are shown in Table G-21. Daily weather maps for 28 June through 5 July 1993 are shown in Figures G-63 and G-64.

**Table G-21 Top 20 recorded rainfall gauges
(inches) for the 28 June–9 July 1993
precipitation event.**

BEATTIE_2_NNW	KS	17.35
AXTELL	KS	16.98
MARYVILLE_2_E	MO	16.20
BETHANY	MO	16.12
CONCEPTION	MO	15.93
PAWNEE_CITY	NE	15.15
LAMONI	IA	14.82
BARNESTON	NE	14.67
LEON_6_ESE	IA	14.59
BLUE_RAPIDS	KS	14.58
MARYSVILLE	KS	14.25

EDINA	MO	13.37
GRANT_CITY	MO	13.17
FALLS_CITY_BRENNER_FIELD	NE	13.16
KEOKUK_LOCK_DAM_19	IA	13.16
CAWKER_CITY	KS	12.88
BEACONSFIELD	IA	12.77
CALIFORNIA	MO	12.66
BLAINE	KS	12.63
WASHINGTON	KS	12.56

Figure G-63. 28 June–1 July 1993 Daily Weather Maps.

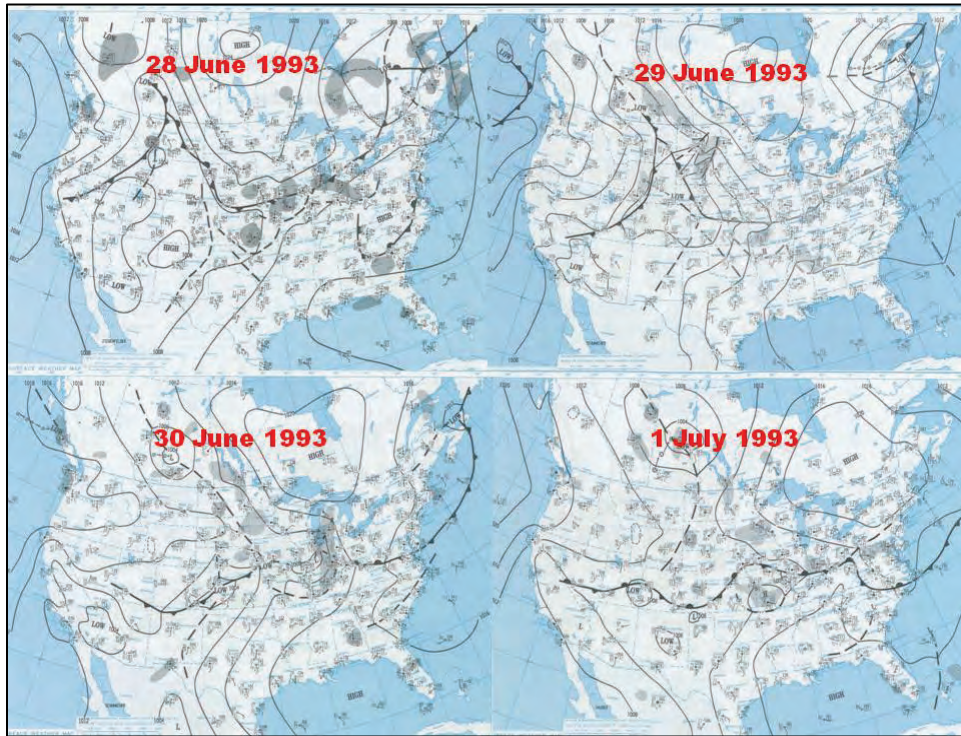
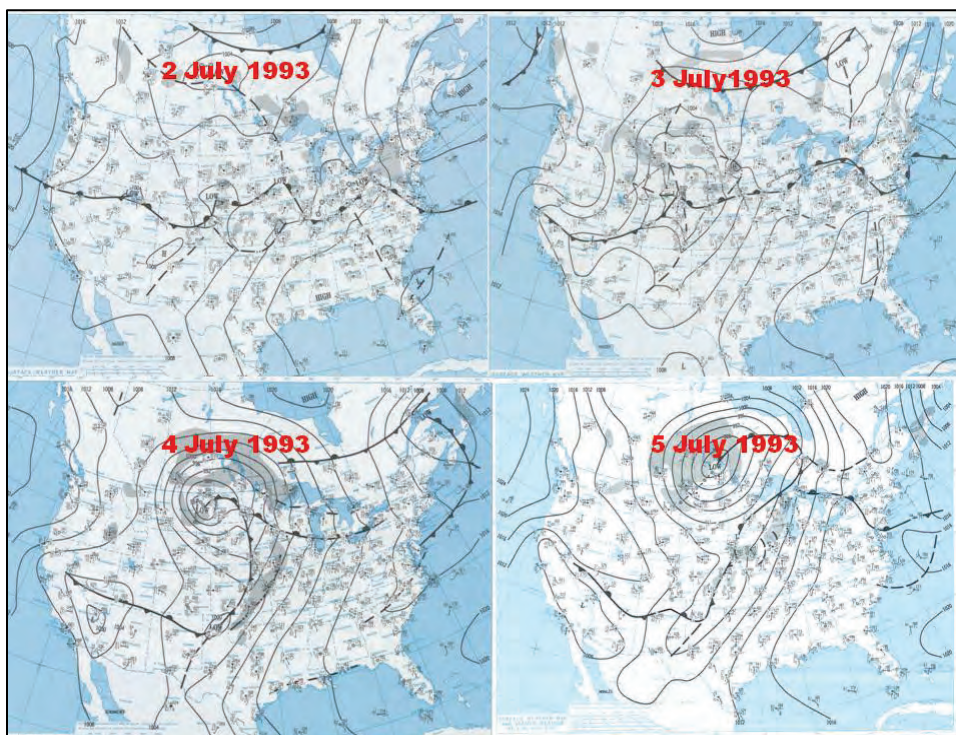


Figure G-64. 2–5 July 1993 Daily Weather Maps.



G.9.5 27 February–9 March 1997

The USACE 1997 Post Flood Report (USACE 1999) presents the following:

...during the period October 1996 through April 1997, the normal rainfall was exceeded in October, January, February, and April. The month of October had the greatest excess with twice the normal average. (USACE 1999, 11)

Rainfall in the NOD [New Orleans District] had little or no effect on stages of the Mississippi River as there is a minimal drainage area between the levees and no tributaries within the NOD contributed significant flows. Headwater flow along the Main Stem of the Mississippi River was the major cause of the 1997 flood. This headwater was caused by several storm systems which developed from unusual upper-air circulation patterns during February and early March 1997 over Texas and the northwestern Gulf of Mexico which then moved slowly northeastward towards the Great Lakes, generating heavy rains over the Mississippi River Valley. This pattern occurred several

times with the storm of March 1-3 being the most devastating with heavy rains of 8 to 11 inches causing massive flooding in portions of Arkansas, Mississippi, Tennessee, Kentucky, and Ohio. (USACE 1999, 11)

Precipitation amounts for the top 20 recorded rainfall gauges are shown in Table G-22. Daily weather maps for 27 February through 10 March are shown in Figures G-65 through G-67. Table G-22. Top 20 recorded rainfall gauges (inches) for the 28 February–12 March 1997 precipitation event.

MADISONVILLE	KY	14.04
MUNFORDVILLE_5_NW	KY	13.92
RIPLEY	TN	13.23
DRESDEN	TN	12.96
HOPKINSVILLE	KY	12.72
CANNELTON	IN	12.53
RIPLEY_EXPERIMENTAL_FARM	OH	12.38
SHEPHERDSVILLE_5_NE	KY	12.21
PARIS_2_SE	TN	12.20
ABERDEEN	KY	12.10
WILLIAMSTOWN	KY	11.85
MURRAY	KY	11.69
KEENE_1_WSW	KY	11.67
ROUGH_RIVER_LAKE	KY	11.65
WOODBURY	KY	11.59
FRANKFORT_ST_POLICE	KY	11.31
BOWLING_GREEN_ST_POL	KY	11.18
DYERSBURG_MUNICIPAL_AIRPORT	TN	11.11
SPRINGFIELD_2_W	KY	11.07
NOLEN_RIVER_LAKE	KY	11.03

Figure G-65. 27 February–2 March 1997 Daily Weather Maps.

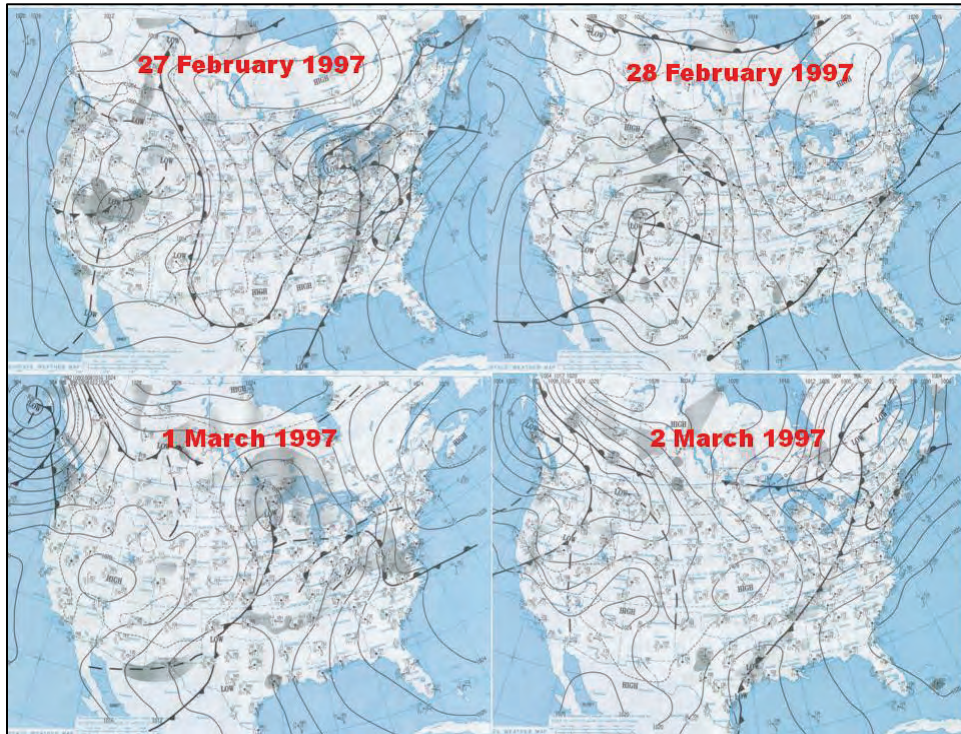


Figure G-66. 3–6 March 1997 Daily Weather Maps.

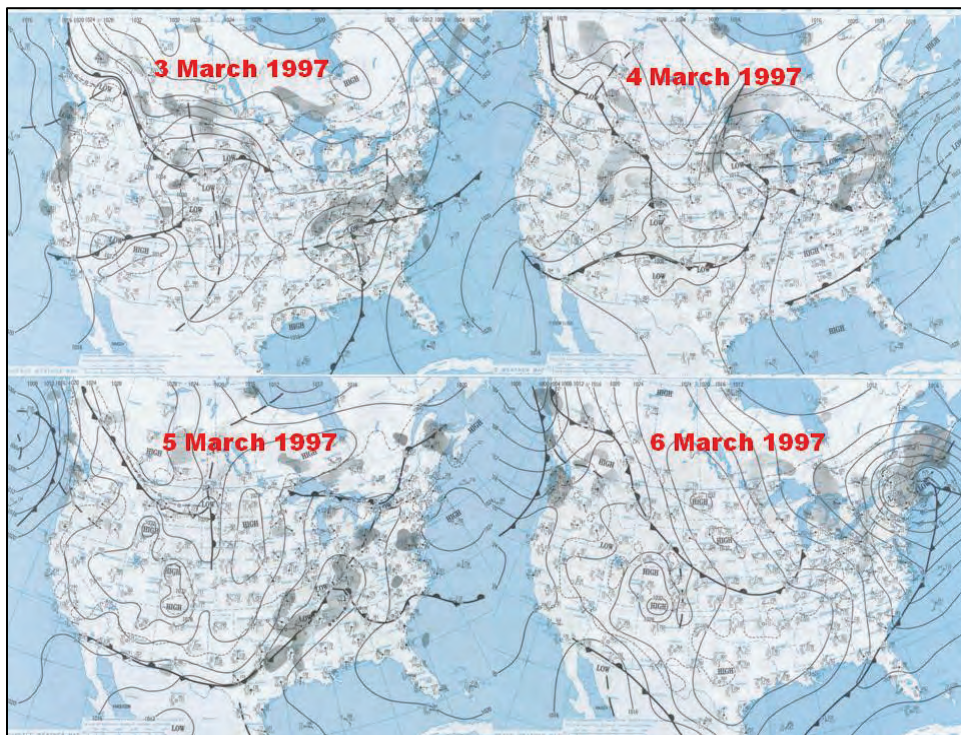
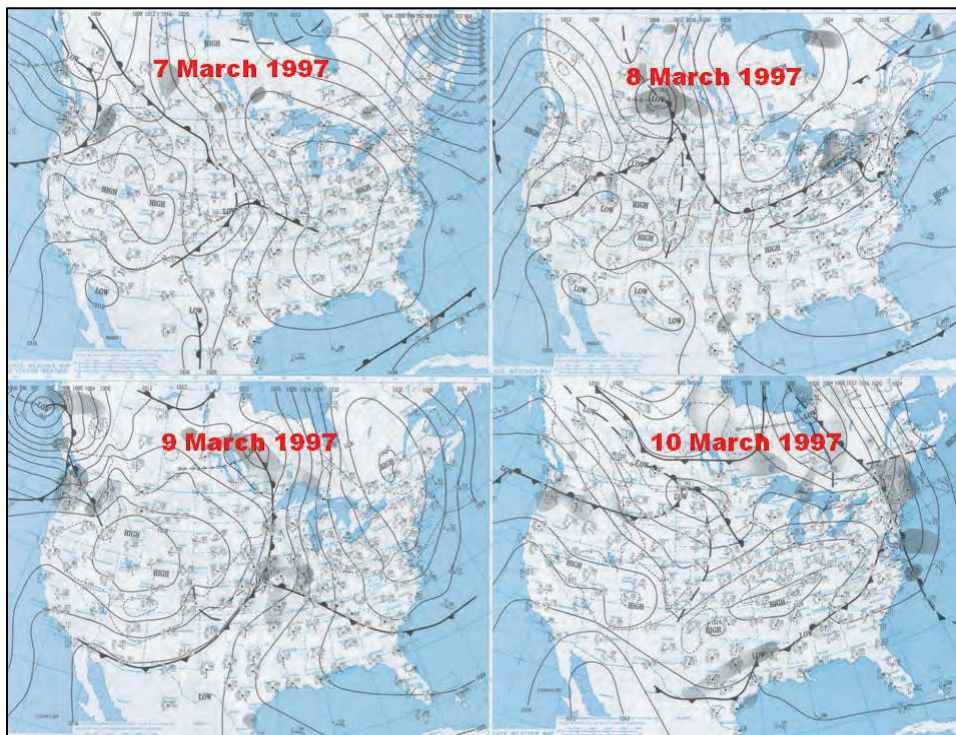


Figure G-67. 7–10 March 1997 Daily Weather Maps.



G.9.6 22 April–3 May 2011 storm

According to USACE Weather Bureau (1937), “The continued threat that at some future date a combination of intense storm action and general thawing of snow and ice on the Missouri, Upper Mississippi, and Ohio watersheds may cause a coincidence of maximum flood discharges from all three of these rivers, resulting in a flood on the Lower Mississippi of a degree as yet unknown, necessitated that a thorough investigation of the relationship of floods to weather be made to determine, if possible, what chance there may exist toward the future occurrence of such a coincidence.” (USACE Weather Bureau 1937, 1)

It goes on to say “When the almost perfect balancing of world-wide atmospheric systems necessary to cause such stagnation of movement in the Bermuda and continental high-pressure systems is considered, we can better realize the unusual nature of the past January storm. When we also consider the fact that when intense storm-rainfall is occurring on the Ohio watershed there will be only a light or moderate discharge from the more north and northwesterly-located Missouri and Upper Mississippi Rivers, and that the opposite will be the case when the

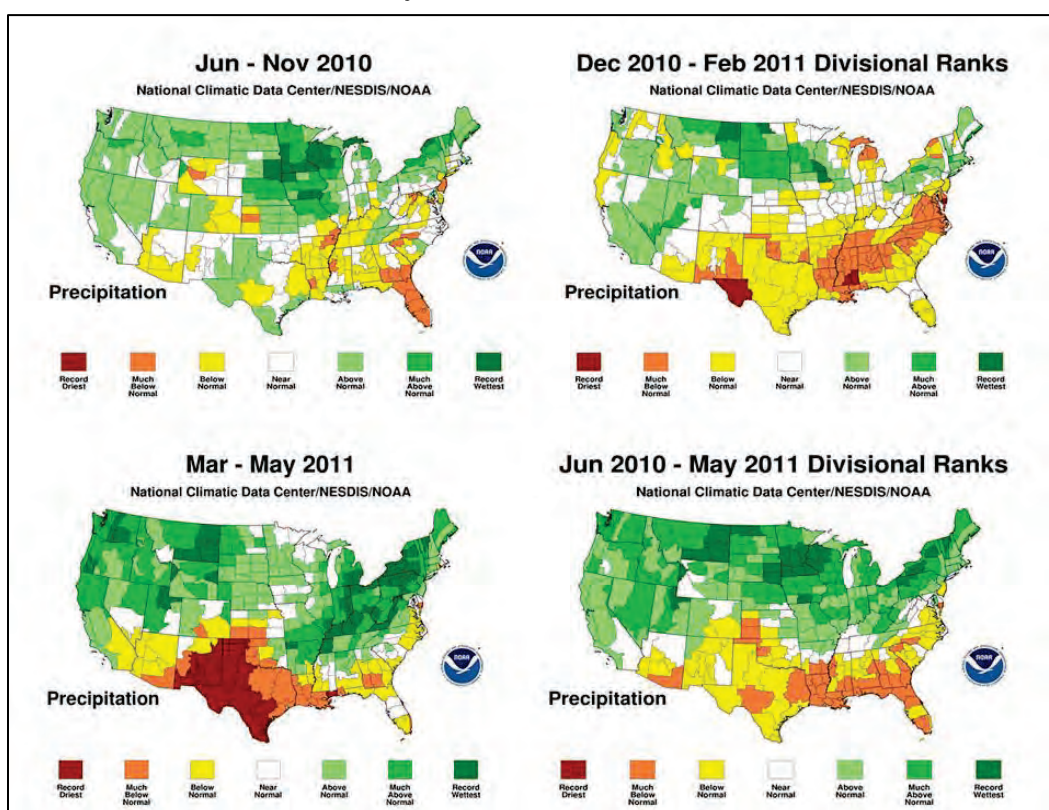
center of air-mass action during the winter and spring months is over the Missouri and upper Mississippi Basins, we may be safe in estimating that the future combined discharges of the Missouri, Ohio, and Upper Mississippi Rivers will not exceed 2,600,000 c.f.s. A discharge of such a magnitude would necessitate that the Ohio River discharge 20% in excess of that during January 1937, and that the Missouri and Upper Mississippi Rivers exceed their January 1937 discharge by more than 100%. Another point strongly in opposition to the possibility of the occurrence of flood coincidence of the Missouri, Ohio, and Upper Mississippi Rivers is the size of their combined drainage areas. Our records have shown that it is entirely possible for intense storm-action to occur over portions of such a combined drainage area. They afford absolutely no indication, however, that storm-action could be so widespread as to cause maximum river discharges, simultaneously, on the Missouri, Upper Mississippi and Ohio Basins, which would coincide at Cairo, Illinois, to overwhelm the Lower Mississippi River.” (USACE Weather Bureau 1937, 12) Such an incident occurred during the Flood of 2011 when runoff from excessive rains over the Ohio and White River Basins reached the confluence of the Mississippi and Ohio Valleys in direct synchronization with the water from rain and snow melt traveling down the Missouri and Upper Mississippi Rivers. Due to reservoir operation, flows at the confluence of the Mississippi and Ohio Rivers at Cairo peaked at 2,100,000 cfs, which was 85% of the PDF flow.

The primary meteorological and hydrologic factors that led to the epic floods of 2011 were much above-normal precipitation over the Upper Mississippi and Missouri River Basins during the summer and fall of 2010, an above-normal plains snowpack over the Upper Mississippi and Missouri River Basins during the winter of 2010–2011, above-normal and late-arriving mountain snowpack in the Upper Missouri River Basin, elevated river levels from heavy rain events in February–April, and very heavy, and in some cases record, rain events at the end of April/beginning of May (Mississippi River and Ohio River Basins) and late May (Missouri River Basin).

Much above-normal precipitation occurred over the Upper Mississippi River Basin and the Missouri River Basin during June–November of 2010 as seen in Figure G-68. Portions of Wisconsin, Minnesota, Iowa, and South Dakota recorded their wettest June–November on record.

This precipitation led to soil moisture rankings in the top 3 years when compared to the past 25 years entering the winter months when the ground historically freezes over the Missouri and Upper Mississippi Valleys. In contrast, the Lower Mississippi/Arkansas/Ohio Valleys received below-normal precipitation during June–November 2010, and soil moistures at the end of November ranked in the bottom 10 for the past 25 years.

Figure G-68. Summer/fall 2010 (top left), winter 2010/2011 (top right), spring 2011 (bottom left), and annual (Jun 2010/May 2011) precipitation rankings by U.S. climate division.



Much above-normal precipitation continued over northern Iowa, Minnesota, South Dakota, North Dakota, and Montana during December 2010–February 2011. In fact, northeastern Iowa, southeastern Minnesota, and northeastern Montana received record precipitation during the December 2010–February 2011 time frame. This precipitation led to SWE of 150%–300% of normal over Minnesota and 200%–400% of normal over the Missouri Basin upstream from the Sioux City, IA. With the exception of a brief snow melt that occurred the second week of February, snow continued to accumulate over the Upper Mississippi and Missouri Valleys through the end of February. A heavy

snow event occurred February 19–21, which quickly caused snow depths and SWE to rebound to even higher levels than before the melt. At the end of February, 2–5 in. of SWE was on the ground over Minnesota and Wisconsin. In the Missouri Basin, 4+ in. of SWE were on the ground upstream from Sioux Falls, SD, with 5–8 in. of SWE on the ground over northeastern South Dakota and Montana.

A strong low-pressure area moved out of the Southern Plains on February 24 and across the Middle Mississippi/Ohio Valleys bringing rainfall amounts of 1–4 in. to the watershed from Helena, AR, to St. Louis, MO, and snowfall amounts to 7 in. (0.5 in. SWE) to the watershed north of St. Louis. Ten tornadoes and 202 damaging winds incidents occurred as the system moved through the watershed. A second heavy rain event (1–4 in.) occurred over the watershed from Greenville, MS, to Rock Island, IL, on February 27–28. These two heavy rain events produced precipitation totals 125%–300% of normal during the month of February over a large area that stretched from eastern Kansas to western New York encompassing the Lower Missouri/Middle Mississippi/Ohio Valleys.

The Missouri watershed, already primed by the wet summer/fall of 2010 and December/January received 200%–400% of normal precipitation during the month of February adding to the 4–8 in. of SWE that were present at the end of the month. At the end of winter, plains snowfall totals from October 2010 to April 2011 were well above normal at many locations in the Upper Missouri River basin. Some notable snowfall departures included 16 in. above the normal 56 in. at Billings, MT; 50.7 in. above the normal 56 in. at Great Falls, MT; 35.6 in. above the normal 50 in. at Bismarck, ND; and 35.5 in. above the normal 30 in. at Pierre, SD.

Heavy precipitation continued during March with 1–4 in. falling March 4–5 across the Mississippi watershed to the south of Dubuque, IA, with snow falling over the watershed north of Dubuque. On March 8–9, another low pressure area moved across the watershed bringing snowfall amounts to 8 in. (0.75 in. SWE) over the watershed north of Dubuque, IA, and rainfall amounts of 1–4 in. over the watershed south of Dubuque. As a result of these rain events, minor to moderate flooding occurred on the main stem Mississippi from Osceola, TN, to Grafton, IL; along the Illinois River downstream from

Starved Rock, IL; along the Ohio River downstream from McAlpine Lock and Dam, over numerous tributaries over the Ohio/Tennessee Valleys; and over Mississippi and Louisiana. The stage on the Ohio River at Cairo, IL, had reached 50.7 ft (flood stage is 40.0 ft) on March 10 with the crest forecasted to reach 52.0 ft on March 12. The last rain event in this series occurred on March 14–15 where 2 in. or less of rain occurred over the watershed to the south of Keokuk, IA, with the heaviest rains occurring locally over the Lower Ohio Valley near Cairo, IL. This caused the river to rise to over 13 ft above stage and the fourteenth highest historical crest on March 18. During mid-March, minor to major flooding was being experienced along the main stem Mississippi River from Memphis, TN, to Cape Girardeau, MO, and along the entire Ohio River. Minor to moderate flooding was occurring along the Illinois River downstream from Peoria, IL, and over numerous tributaries to the south of St Louis, MO.

Beginning on March 14, temperatures rose to above normal across the entire Mississippi and Missouri watersheds which initialized the Plains snow-melting process. Above-normal temperatures continued for another 10 days allowing all of the snow over the Mississippi watershed and over the Missouri watershed in central and southern South Dakota to melt. As a result of the snow melting over the Mississippi watershed, minor to major flooding occurred along the main stem Mississippi River beginning the last week of March. The Mississippi River at St. Paul, MN, exceeded major flood stage and reached its eighth highest historical crest on March 29. Warm temperatures during the first week of April rapidly melted the snow in North Dakota, Montana, and northern South Dakota. Snow in the mountain areas of the Missouri Basin continued to increase through April with Fort Peck, MT, peaking at 141% of normal on May 2.

The Ohio River at Cairo, IL, fell below flood stage on April 3. However, rains began again on April 8–9 and April 11–12 causing the Mississippi/Ohio Rivers to once again rise above flood stage on April 10 with a stage crest of 47.0 ft predicted for April 20 at Cairo, IL. A second round of heavy rains occurred on April 14–15 as a cold front moved through the Middle Mississippi/Ohio Valleys.

In mid-April, the leading edge of a very warm, moist air mass advanced north into the central United States and interacted with a stationary

front that stretched from southern Ohio to eastern Oklahoma. Rainfall amounts of 1–4 in. accompanied by widespread severe thunderstorms (32 tornadoes, 396 damaging winds incidents, and 324 large hail reports on April 19) moved through the watershed from Greenville to Dubuque on April 18–20. The surface weather map for April 25 reflects the meteorological situation over the region from the latter half of April to early May 2011. The 500 mb height map for the same day showed a stable long-wave upper atmospheric pattern. A deep trough was anchored along the eastern flanks of the Rockies, with blocking high pressure ridges off the southeast and southwest coasts. This weather pattern resulted in a persistent warm and moist southwesterly flow aloft over the central and eastern United States. Embedded in this flow was a series of potent, mid-level short wave troughs that interacted with the frontal boundary already in place to produce daily intense convective rainfall. As a result, a broad expanse of the central United States from Tulsa, OK, to Cincinnati, OH, received 10 in. to more than 20 in. of rain.

Two-week rainfall amounts during the end of April and beginning of May totaled 600%–1000% of normal for that time period over a very large area. With the addition of the snowmelt water that reached the confluence of the Mississippi and Ohio Rivers in conjunction with the very heavy rains, and already elevated river levels, river stages exceeded record levels at the confluence of the Mississippi/Ohio Rivers on April 29. According to USGS measurements, water levels at the confluence of the Missouri and Mississippi Rivers reached its initial peak of approximately 240,000cfs also on April 29, 3 days prior to activation of the Birds-Point/New Madrid Floodway. The Mississippi and Ohio Rivers continued to steadily rise entering May, and operation of the Birds Point New Madrid Floodway was required on May 2.

Above-normal precipitation was experienced over the majority of the Mississippi and Missouri watersheds during the spring of 2011. Precipitation amounts for the top 20 recorded rainfall gauges for the time period 22 April through 3 May 2011 are shown in Table G-23. Climate divisions in northwestern Arkansas, western Tennessee, most of Kentucky, and over several in the Ohio Valley experienced the wettest March–May on record. Also, eastern and southern Montana received its wettest March–May on record. Overall, from June 2010 through May 2011, precipitation above normal occurred over the

Mississippi watershed upstream from the confluence with the Ohio River. Minnesota and eastern Wisconsin experienced their wettest June–May on record. The Missouri watershed also experienced much above-normal precipitation during the 12-month period. Records were set in eastern South Dakota, northern North Dakota, and eastern and southern Montana from June 2010 through May 2011. Despite the drier-than-normal last 6 months of 2010, the Ohio Valley rebounded to much above normal and above normal values during the 12-month period. Daily weather patterns for 19 April through 4 May 2011 are shown in Figures G-69 through G-72.

**Table G-23. Top 20 recorded rainfall gauges (inches)
for 22 April-3 May 2011 precipitation event.**

POPLAR_BLUFF	MO	23.16
SPRINGDALE_5.8_ENE	AR	22.99
POPLAR_BLUFF_4.2_NW	MO	21.65
CAPE_GIRARDEAU_2.3_N	MO	21.64
WILLIAMSVILLE	MO	21.56
HARRISON	AR	21.49
POPLAR_BLUFF_MUNICIPAL_AIRPORT	MO	21.33
LAKE_WAPPAPELLO_STATE_PARK	MO	21.3
VAN_BUREN_7.2_SW	MO	21.04
CAPE_GIRARDEAU_MUNICIPAL_AIRPORT	MO	20.82
ZALMA_4_E	MO	20.81
JACKSON_1.0_SW	MO	20.49
WHITEWATER_3.4_W	MO	20.49
ALTON_7.2_E	MO	20.14
HOLLY_SPRINGS_4_N	MS	20.12
LAMBERT_0.8_ESE	MO	19.96
DONIPHAN	MO	19.86
BLOOMFIELD_2.9_S	MO	19.81
ANNA_2_NNE	IL	19.26
CLARENDON	AR	19.24

Figure G-69. 19–22 April 2011 Daily Weather Maps.

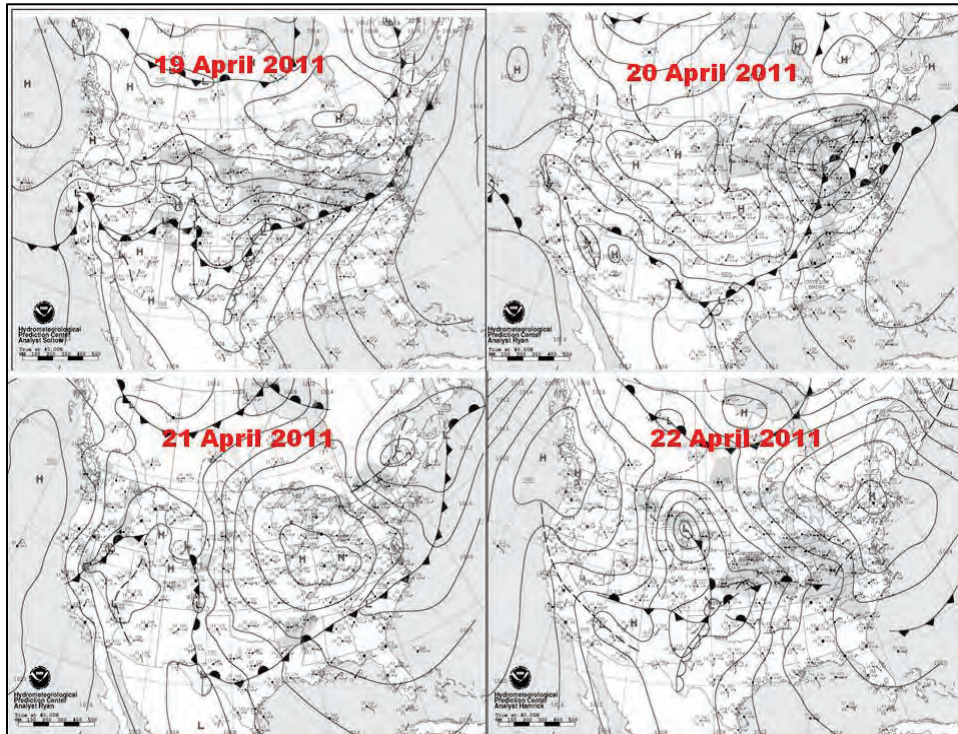


Figure G-70. 23–26 April 2011 Daily Weather Maps.

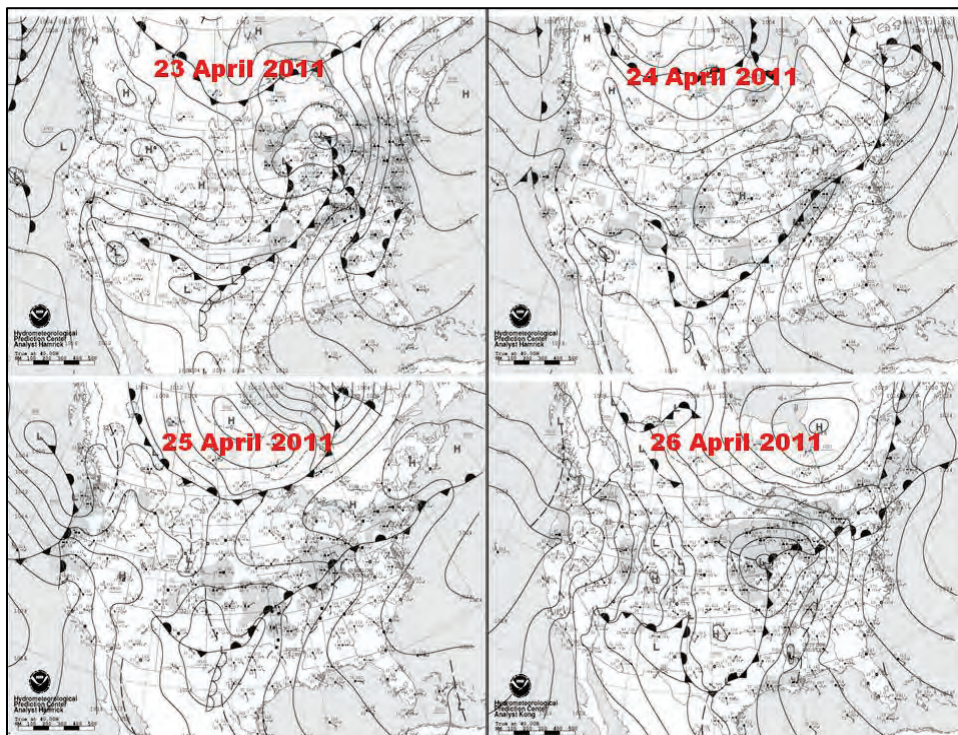


Figure G-71. 27–30 April 2011 Daily Weather Maps.

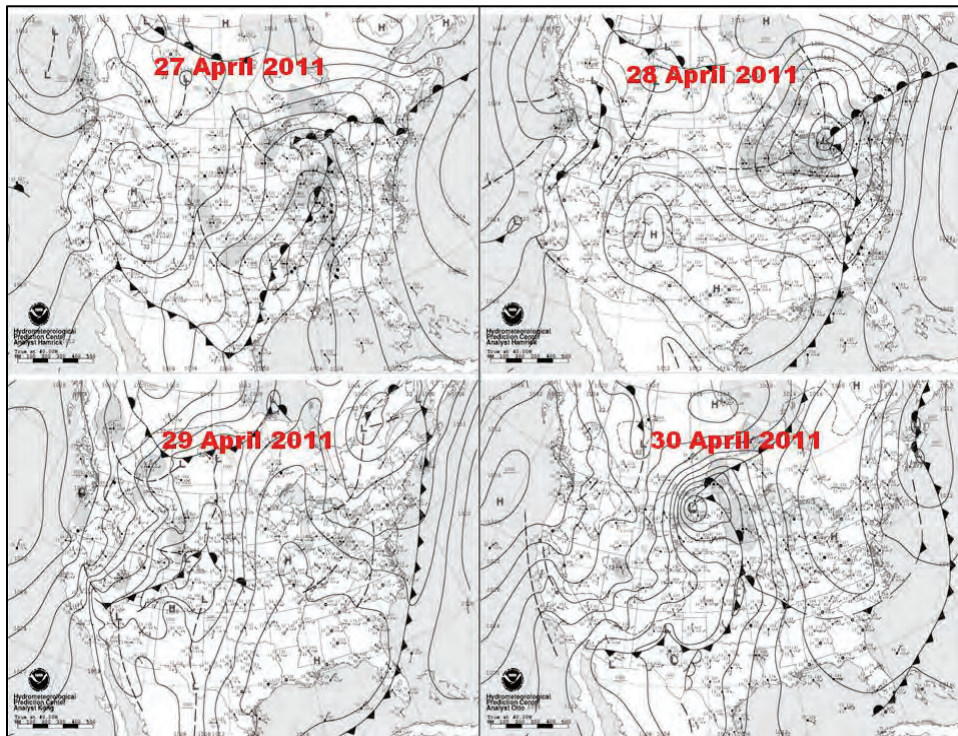
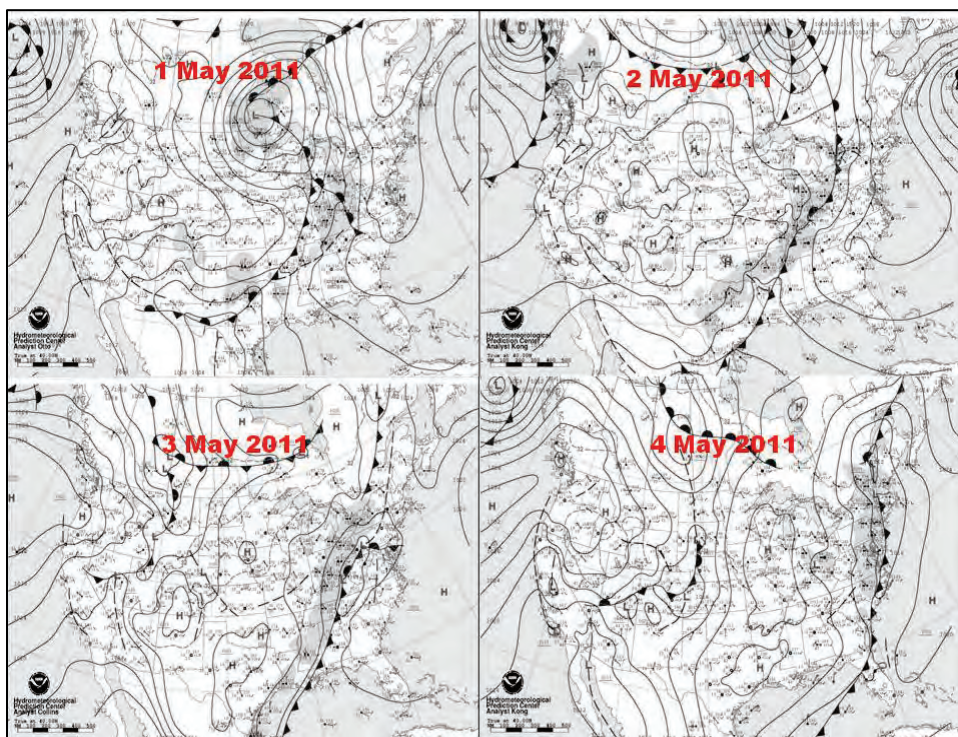


Figure G-72. 1–4 May 2011 Daily Weather Maps.



G.10 Quality control

G.10.1 Precipitation datasets

The original analysis performed for the Memorandum Report No. 1 (MRC 1955) utilized point 6-hour precipitation data over the historic event periods. These data values were processed manually to draw isohyetal contours of precipitation depth. Current hydrologic models used by the NWS require spatial representation of precipitation for its input. Therefore, it was necessary to recompile the point ASCII data for each event, perform rudimentary error checks on the point data, then interpolate the point data to create continuous spatial grid maps. The interpolated grid maps were then subjected to a verification check before they were released to the NWS RFCs.

The USACE archives were used to extract 6-hour precipitation values where available. Other data were obtained from the NCDC databases. The first event to be analyzed was the 1937 storm. This storm was selected as the first because it is one of the events used in creating the HYPO 58A storm. Point data were put into comma-separated format for ingest into ArcGIS software. ArcGIS was then used to perform spatial interpolation using the Kriging method. Kriging was thought to be the most appropriate method for processing stochastic data such as precipitation. Once the 6-hour grid files had been generated, the NWS RFCs ingested the data into their datastore and performed an unregulated simulation. It was thought that in 1937, few reservoirs were in operation, and model results should be comparable to observed discharge data. To contrast model outflow hydrographs with observed discharge data, a historic discharge data set was compiled from USGS and USACE databases. Comparisons were made at relatively few locations because in 1937 there were relatively few discharge gages.

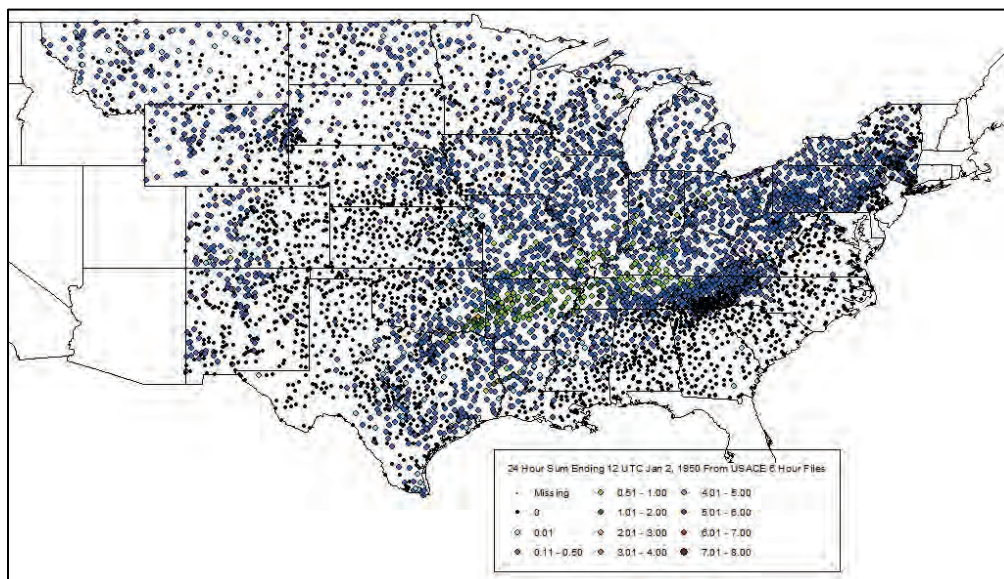
Because there were few locations to use in the interpolation as well as few to compare computed model flows for the earlier storms, the team decided to switch to the 1950 event, which had many more precipitation gages to use in interpolating the grids and a moderate increase in number of discharge gages available for comparisons. In total, the 1950 event had approximately 6,400 precipitation gages that were used to generate the interpolated grids. There were still fewer than 10 locations where stream gage data were found that could be used in assessing modeled versus observed discharges for the 2016 assessment.

After questions surfaced about the initial model results for the unregulated HYPO 58A, the precipitation inputs were put through a series of checks. The process involved these steps:

1. Taking the point data developed by USACE from available archives and NWS database and comparing with NWS observer data.
2. Adjusting USACE point data as required to address inconsistencies.
3. Running the interpolation scripts to generate new ASCII grid files.
4. Cross-checking interpolated results back to five key gage locations that were extracted from the point database.
5. Repeating the process until satisfactory agreement was achieved between the independent locations and the interpolated values for those same locations.

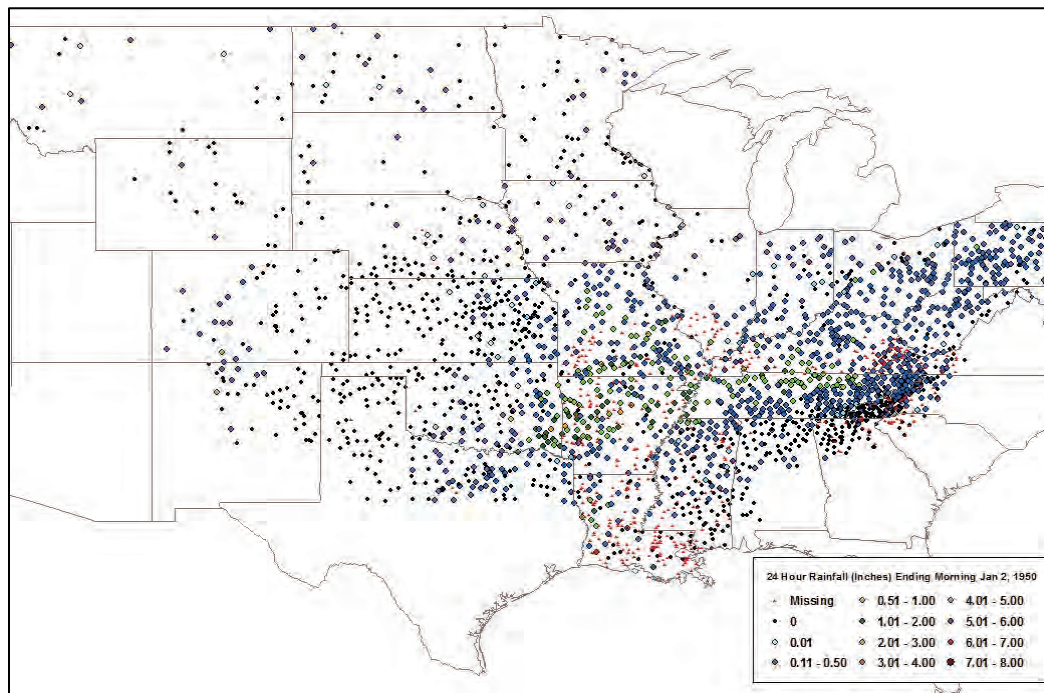
Figure G-73 provides a map showing point locations contained in the 1950 USACE datasets.

Figure G-73. 1950 Precipitation gage locations contained in USACE dataset.



There were fewer NWS observer sites, but there were sufficient locations to validate that the appropriate daily totals were captured for the final interpolations. Figure G-74 shows a map of the NWS observer locations.

Figure G-74. 1950 Precipitation observer locations in NWS dataset.



Only the core storm period was comprehensively validated. No antecedent or recessions periods needed for the CHPS simulation were included in the detailed quality assurance effort. The specific period included in the 1950 QA/QC was 3 January 1950 through 15 January 1950. Figure G-75 provides a snapshot of the Excel file; this file contained 5,865 different point locations. The data shown in this figure show the daily, 24-hour totals and the storm total. Each daily tab contained the 6-hourly values for USACE and NWS observed databases (Figure G-76).

Dr. Suzanne Van Cooten with the LMRFC laboriously entered all of the NWS COOP observer data and performed extensive cross-checks with USACE values and daily totals. A significant complication with using the COOP observer data had to do with the times at which data were reported. It was necessary to interpret which quadrant of the 24-hour period fell within each standard interval used by the CHPS models (0000, 0600, 1200, and 1800 GMT).

The point locations used in the USACE dataset were built using tabulated data from the MRC (1955) report and supplemented by the NWS NCDC database. Available 6-hour precipitation depths were

entered into Excel for further manipulation and validation and for import into ArcGIS to develop the interpolated grids.

Initial calculations and checks indicated that there were some locations in the USACE dataset that had significant differences in precipitation depths when compared to the NWS observer values. Figure G-77 highlights this outcome in red. However, columns O, P, and Q (highlighted in gray, yellow, and blue group) in the sample spreadsheet (FigureG-76) show three different daily totals. The different totals were calculated using three separate combinations of the 6-hour values shown in columns G–M. The differences highlighted in red in this figure are based on using the values in column P (yellow) and the observer data in Column AD. An illustration of how different combinations of the 6-hour values impact the daily totals and thus the comparisons with Observer values is given in Figure G-77.

To facilitate estimating a reliability percentage (i.e., the 99% given), data were separated by state and calculations adjusted for consistency for which 6-hour periods comprised the 24-hour totals. Conditional formatting in Excel was used as a secondary check to confirm the numerical computations—difference cells that fell within agreed tolerances were highlighted as green. Figure G-78 shows a sample from the final spreadsheet showing acceptable differences highlighted in green.

1

Figure G-75. Sample of USACE 1950 precipitation data.

3	LAT	LON	YMMDD	00UTC- Jan-4	USACE 24 HR SUM	USACE 24 Hour Sum	USACE 24 HR SUM	USACE 24 HR SUM	USACE 24 HR SUM	USACE 24 HR SUM	USACE 24 HR SUM	USACE 24 HR SUM	USACE 24 HR SUM	USACE 24 HR SUM	USACE 24 HR SUM	USACE 24 HR SUM	Sum: 04 Jan - 15 Jan
4	44.3	-92.67	19500102	0	0.02	0	0	0	0	0.04	0	0.03	0.32	0.08	0.11	0.6	
5	44.28	-92.42	19500102	0	0	0	0	0	0	0	0	0.01	0.39	0.01	0.18	0.59	
6	40.45	-75.47	19500102	0	0	0	0.12	0.4	0	0	0.72	0	0.19	0	0	1.43	
7	26.88	-99.32	19500102	0	0	0	0	0	0	0	0	0	0	0	0	0	
8	39.93	-82	19500102	0.05	0.16	0.9	1.13	0.63	0	0	0.19	0.13	0	0.17	0.16	3.47	
9	39.95	-81.9	19500102	0	0.6	1.05	1.1	0	0	0	0.44	0	0.29	0.37	0.03	4.17	
10	40.12	-102.73	19500102	0	0	0	0	0	0	0	0	0	0	0	0	0	
11	33.82	-96.2	19500102	0.02	0	0	0	0	0	0	0	0	2.05	1.23	0	3.28	
12	31.7	-106.32	19500102	0.03	0	0	0	0	0	0.4	0	0	0.43	0.07	0	0.9	
13	41.87	-79.33	19500102	0.05	0.29	0.14	0.8	0.11	0	0	0.67	0	0.06	0.3	0.32	1.12	
14	41.25	-80.67	19500102	0.03	0.57	0.12	1.01	0.07	0	0	1.22	0	0.1	0.51	0.05	1.25	
15	34.95	-87.9	19500102	0	0	0.78	1.51	2	0.22	0	0	1.69	0.77	1.65	0.79	9.41	
16	34.93	-83.85	19500102	0	0	0.15	0	0.39	0	0.01	0.04	0.48	0.08	0.15	0.26	0.05	1.61
17	40.57	-86.33	19500102	0	1.21	0	0.37	0.06	0	0.4	0.46	0	0	0.85	0	1.07	4.42
18	41.27	-73.77	19500102	0.02	0.05	0	0.27	0.45	0	0	0	0.58	0.85	0.05	0.19	0	2.44
19	28.98	-97.5	19500102	0	0.11	0	0	0	0	0	0	0.07	0.11	0.23	0	0	0.52
20	33.8	-108.33	19500102	0.08	0	0	0	0	0	0	0	0	0.02	0	0.09	0	0.11
21	40.12	-76.72	19500102	0.04	0.05	0	0	0.3	0	0	0	0.33	0.15	0.04	0	0	0.87
22	39.92	-76.75	19500102	0.02	0.02	0	0.03	0.09	0	0	0.2	0	0.01	0.14	0	0	0.49
23	39.93	-76.73	19500102	0.01	0	0	0.09	0.05	0	0	0.2	0	0.09	0.07	0.04	0	0.54
24	40.87	-97.58	19500102	0.08	0	0	0	0	0	0	0	0	0	0	0	0	0
25	29.3	-97.15	19500102	0	0.09	0	0	0	0	0	0	0.11	0.04	0.05	0.01	0	0.3
26	34.32	-104.73	19500102	0	0	0	0	0	0	0	0	0	0	0	0	0	0
27	34.4	-104.62	19500102	0.05	0	0	0	0	0	0	0	0	0	0	0	0	0
28	36.22	-92.68	19500102	0.1	0	2.62	0	0	0	0	0	0	0	1.41	0	0.49	4.52
29	45.32	-107.92	19500102	0.02	0	0	0	0	0	0	0	0	0	0	0	0.01	0.01
30	44.97	-110.7	19500102	0.03	0	0	0	0	0	0.08	0	0.15	0.04	0.05	0.63	0.1	1.05
31	32.85	-90.42	19500102	0.07	0.02	2.24	3.36	0.14	0	0	0	0.77	0.07	0.19	0.52	0	7.31
32	32.57	-85.9	19500102	0.08	0.06	0.18	0.11	0.54	0	0	0	1.46	0.03	0	0.1	0	2.48
33	37.85	-95.68	19500102	0.03	0	0	0	0	0	0	0	0	0	0.26	0	0	0.26
34	36.05	-103.87	19500102	0.04	0	0	0	0	0	0	0	0	0	0	0	0	0
35	42.92	-97.38	19500102	0	0	0	0	0	0	0	0	0	0.28	0	0	0	0.28
36	36.42	-79.33	19500102	0	0	0	0	0	0	0	0	0.1	0	0.62	0	0	0.72

2

Figure G-76. Sample of daily NWS observer and USACE 1950 precipitation data.

Jan 3 thru 15 Sort Sm to Lg USACE Sum Minus NWS COOP Ob (2015.07.15-AG).xlsx - Microsoft Excel

Home Insert Page Layout Formulas Data Review View Approvalt Acrobat

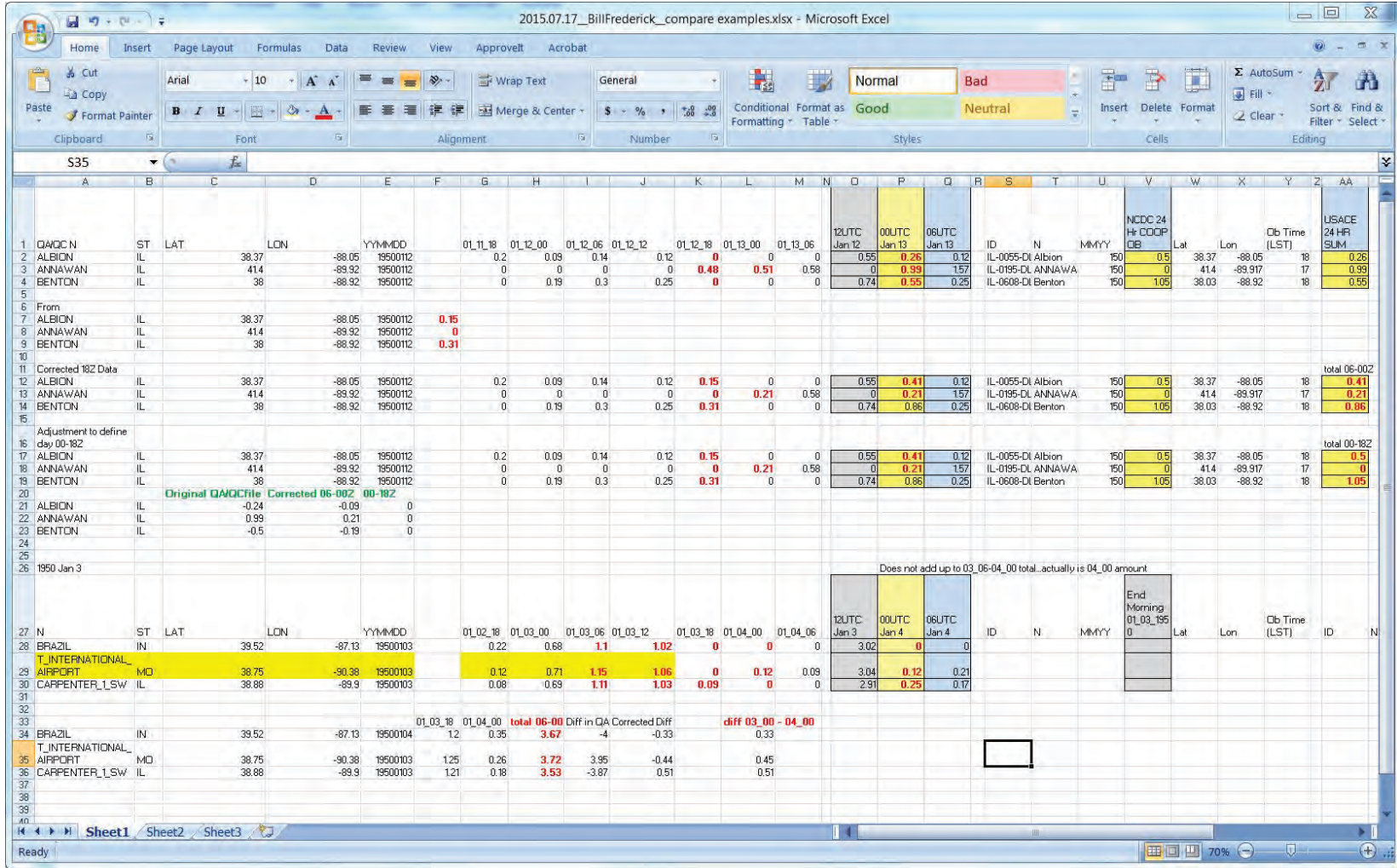
Calibri 11 A Font Wrap Text General Conditional Format as Normal Bad Good Neutral

Clipboard H-K

		USACE 24 HR Sum Ending											NWS		USACE 24 HR Sum		DIFF USACE SUM - NWS COOP		Difference										
N	ST	LAT	LCN	YTMDD	0L14_19	0L15_00	0L15_06	0L15_12	0L15_18	0L16_00	0L16_06	0L16_12	0L16_18	0L16_24	ID	N	MMYY	Lat	Lon	CB Time (LST)	USACE 24 HR SUM	DIFF USACE SUM - NWS COOP	H-K	H-L	Difference				
3	ZUMBROTA	MN	44.3	-92.67	2E-07	0.01	0.02	0.03	0.02	0.04	0.0	0.0	0.0	0.0	0.03	0.03	0.06	44.3	-92.67	18	0.03	-0.02	0.05	0.03	0.07	0.03	0		
4	ZUMBRO_FALLS_L1 SE	MN	44.29	-92.42	2E-07	0	0.003	0.04	0.04	0.07	0	0	0	0	0.11	0.05	0.11	44.28	-92.42	24	0.11	-0.06	0.11	0.05	0.11	0.05	0.01		
5	ZONSVILLE_3 ESE	PA	40.85	-76.47	2E-07	0	0	0	0	0	0	0	0	0	0	0	0												
6	ZAPATA_L1 S	TX	26.68	-95.32	2E-07	0	0	0	0	0	0	0	0	0	0	0	0												
7	ZANESVILLE_VVTP	OH	39.93	-82	2E-07	0.02	0	0	0	0	0.12	0.07	0.02	0.12	0.13	0.13	0.13	39.92	-82	7	0.13	0.02	0.02	0.12	0.13	0.02	0.12	0	
8	ZANESVILLE_MUNICIPAL_AIRPORT	OH	39.95	-81.9	2E-07	0	0.05	0.07	0.06	0.11	0.01	0	0.18	0.25	0.13	0.13	0.13	39.95	-81.9	24	0.13	-0.11	0.11	0.05	0.11	0.05	0.05	0	
9	YUMA	CO	40.12	-92.73	2E-07	0	0	0	0	0	0	0	0	0	0	0	0												
10	YUBA_2 W	OK	33.82	-96.2	2E-07	0	0	0	0	0	0	0.17	0.1	0.17	0.27	0.27	0.27												
11	YULETA	TX	31.7	-96.32	2E-07	0	0	0	0	0	0	0	0	0	0	0	0												
12	YOUNGSVILLE	PA	41.67	-79.33	2E-07	0.04	0.16	0.27	0.34	0.45	0.01	0	0.73	0.95	0.53	0.53	0.53	41.65	-79.32	24	0.85	-0.44	0.73	0.95	0.65	1.12	0.95	0	
13	YOUNGSTOWN_REGIONAL_AIRPORT	OH	41.25	-80.67	2E-07	0.01	0.2	0.3	0.27	0.45	0.01	0	0.73	1.09	0.76	0.76	0.76	41.25	-80.67	24	0.76	-0.48	0.73	1.09	0.76	1.28	1.06	0.01	
14	YOUNGS_STORE	AL	34.95	-87.9	2E-07	0.1	0	0	0	0	0.33	0.2	0.1	0.33	0.53	0.53	0.53	34.95	-87.87	7	0.1	0.1	0.1	0.33	0.53	0.33	0	0	
15	YOUNG_HARRIS	GA	34.93	-83.85	2E-07	0.03	0.01	0.01	0.01	0.02	0.15	0.08	0.06	0.17	0.24	0.24	0.24												
16	YOUNG_AMERICA_3 ESE	IN	40.57	-86.33	2E-07	0	0.17	0.26	0.33	0.41	0	0	0.64	0.3	0.64	0.64	0.64												
17	YORKTOWN_HEIGHTS	NY	41.27	-73.77	2E-07	0.02	0	0	0	0	0.05	0.03	0.02	0.05	0.06	0.06	0.06												
18	YORKTOWN	TX	28.98	-97.5	2E-07	0	0	0	0	0	0	0	0.01	0	0	0	0												
19	YORK_RANCH	NM	35.8	-106.33	2E-07	0.01	0	0	0	0	0	0	0	0	0	0	0												
20	YORK_HAVEN	PA	40.12	-76.72	2E-07	0	0	0	0	0	0	0	0	0	0	0	0												
21	YORK_L1 S FLTR PLANT	PA	39.92	-76.76	2E-07	0	0	0	0	0	0	0.01	0	0	0	0.01	0.01												
22	YORK_L1 S FLTR PLN	PA	39.93	-76.73	2E-07	0.01	0	0	0	0	0	0	0.01	0	0	0	0												
23	YORK	NE	40.87	-97.58	2E-07	0	0	0	0	0	0	0	0	0	0	0	0												
24	YORKAM	TX	29.3	-97.15	2E-07	0	0	0	0	0	0.48	0.3	0	0.43	0.79	0.79	0.79												
25	YESO_OVERTON_BRANCH	NM	34.92	-104.75	2E-07	0	0	0	0	0	0	0	0	0	0	0	0												
26	YESO_2 S	NM	34.4	-104.62	2E-07	0	0	0	0	0	0	0	0	0	0	0	0												
27	YELLVILLE_2 SSE	AR	36.22	-92.66	2E-07	0	0.08	0.12	0.1	0.19	0	0	0.3	0.41	0.23	0.23	0.23												
28	YELLOWTAIL_DAM	MT	45.32	-107.82	2E-07	0	0	0	0	0.01	0	0	0	0.01	0.01	0.01	0.01												
29	YELLOWSTONE_PARK_MAMMOTH	WY	44.97	-110.7	2E-07	0.08	0.02	0.02	0.02	0.04	0.02	0.01	0.14	0.1	0.03	0.03	0.03												
30	YAZDOO_CITY	MS	32.85	-90.42	2E-07	0.07	0	0	0	0	0.01	0.01	0.07	0.01	0.02	0.02	0.02												
31	YATES_HYDRO_PLANT	AL	32.57	-85.9	2E-07	0.01	0	0	0	0	0	0	0.01	0	0	0	0												
32	YATES_CENTER	KS	37.85	-95.68	2E-07	0	0	0	0	0	0	0	0	0	0	0	0												
33	YATES_5 S	NM	36.05	-103.87	2E-07	0	0	0	0	0	0	0	0	0	0	0	0												
34	YAMTOWN	SD	42.52	-97.39	2E-07	0	0	0	0	0	0	0	0	0	0	0	0												
35	YANCEYVILLE_2 NNE	NC	36.42	-78.33	2E-07	0	0	0	0	0	0	0	0	0	0	0	0												
36	YANPA	CO	40.15	-106.9	2E-07	0.01	0.02	0.03	0.03	0.05	0	0	0.03	0.11	0.08	0.08	0.08												
37	YALE	MI	43.13	-82.6	2E-07	0.01	0.08	0.12	0.11	0.19	0	0	0.32	0.42	0.3	0.3	0.3												
38	YADKINVILLE_1 E	NC	36.13	-80.95	2E-07	0	0	0	0	0	0	0.02	0.01	0.02	0.02	0.02	0.02												
39	YATTHEVILLE	VA	36.93	-81.08	2E-07	0	0	0	0	0	0.48	0.3	0	0.43	0.78	0.78	0.78												
40	YVOLA_1 SV	MT	45.13	-107.39	2E-07	0	0	0	0	0	0	0	0	0	0	0	0												
41	YVADRE	NE	40.13	-96.57	2E-07	0	0	0	0	0	0	0	0	0	0	0	0												
42	WRIGHT_PATMAR_DAM_LAKE	TX	35.3	-94.15	2E-07	0	0.01	0.01	0.01	0.02	0	0	0.03	0.04	0.03	0.03	0.03												
43	WRAY	CO	40.07	-92.22	2E-07	0	0	0	0	0	0	0	0	0	0	0	0												
44	WORTHINGTON	MN	43.62	-95.6	2E-07	0	0	0	0	0	0	0	0	0	0	0	0												
45	WORLAND_1 SV	WY	43.95	-108.03	2E-07	0	0	0	0	0	0	0	0	0	0	0	0												
46	WORLAND	WY	44.02	-107.37	2E-07	0	0	0	0	0	0	0	0	0	0	0	0												
47	WOOSTER_EXPERIMENTAL_STATION	OH	40.78	-81.93	2E-07	0	0.16	0.26	0.28	0.44	0	0	0.73	0.57	0.83	0.83	0.83												
48	WOOSTER_2 SE	OH	40.78	-81.93	2E-07	0.03	0.14	0.21	0.19	0.34	0	0	0.97	0.74	0.93	0.93	0.93												
49	WOOSOCKET	SD	44.05	-98.27	2E-07	0	0	0	0	0	0	0	0	0	0	0	0												
50	WOOSTER_RANCH	NM	35.77	-107.3	2E-07	0	0	0	0	0	0	0	0	0	0	0	0												
51	WOODWARD_FIELD_STATION	OK	36.42	-98.4	2E-07	0	0	0	0	0	0	0	0	0	0	0	0												
52	WOODWARD_Z_M	IA	41.95	-93.32	2E-07	0	0	0	0	0	0	0	0	0	0	0	0												
53	WOODWARD	OK	36.45	-98.38	2E-07	0	0	0	0	0	0	0	0	0	0	0	0												
54	WOODVILLE_1 ESE	MS	31.1	-91.3	2E-07	0.03	0.01	0.01	0.01	0.02	0.28	0.17	0.04	0.22	0.41	0.41	0.41												

5

Figure G-77. Illustration of calculating daily values from 6-hourly data and effect on comparison to NWS COOP values.



6

Figure G-78. Sample of final spreadsheet showing precipitation data validation for 1950 event.

Station Name	Station ID	Station Type	Lat	Long	Elev	Obs Precip	Model Precip	Diff (Obs-Mod)	Absolute Diff													
ANDERSON	MD 36.63	-94.45	2E+07	0.06	0.5	0.39	0.29	0.26	0	0	1.24	0.94	0.55	MD-0164 Anderson	150	1.45	36.65	-94.43	7	1.24	Diff 00-182	Absolute difference 002-182
ANDERSON	MD 36.63	-94.45	2E+07	0.26	0	0	0	0	0	0	0.26	0	0	MD-0164 Anderson	150	0	36.65	-94.43	7	0.26		
ANDERSON	MD 36.63	-94.45	2E+07	0	0	0	0	0	0	0	0	0	0	MD-0164 Anderson	150	0	36.65	-94.43	7	0		
ANDERSON	MD 36.63	-94.45	2E+07	0	0	0	0	0	0	0	0	0	0	MD-0164 Anderson	150	0	36.65	-94.43	7	0		
ANDERSON	MD 36.63	-94.45	2E+07	0	0	0	0	0	0	0	0	0	0	MD-0164 Anderson	150	0	36.65	-94.43	7	0		
ANDERSON	MD 36.63	-94.45	2E+07	0	0	0	0	0	0	0	0	0	0	MD-0164 Anderson	150	0	36.65	-94.43	7	0		
ANDERSON	MD 36.63	-94.45	2E+07	0	0	0	0	0	0	0	0	0	0	MD-0164 Anderson	150	0	36.65	-94.43	7	0		
ANDERSON	MD 36.63	-94.45	2E+07	0	0.03	0.04	0.03	0.04	0.02	0.02	0.1	0.09	0.07	MD-0164 Anderson	150	0.14	36.65	-94.43	7	0.1		
ANDERSON	MD 36.63	-94.45	2E+07	0.04	0.39	0.45	0.38	0.24	0	0	1.26	1.07	0.62	MD-0164 Anderson	150	1.46	36.65	-94.43	7	1.26		
ANDERSON	MD 36.63	-94.45	2E+07	0.24	0	0	0	0	0.02	0.03	0.24	0.02	0.05	MD-0164 Anderson	150	0	36.65	-94.43	7	0.24		
ANDERSON	MD 36.63	-94.45	2E+07	0	0.02	0.03	0.03	0.05	0	0	0.08	0.11	0.08	MD-0164 Anderson	150	0.14	36.65	-94.43	7	0.08	-0.01	0.01
APPLETON_CITY	MD 38.2	-94.03	2E+07	0.05	0	0	0	0	0	0	0.05	0	0	MD-0204 APPLETC	150	0	38.18	-94.03	18	0		
APPLETON_CITY	MD 38.2	-94.03	2E+07	0	0	0	0	0	0	0	0	0	0	MD-0204 APPLETC	150	0	38.18	-94.03	18	0		
APPLETON_CITY	MD 38.2	-94.03	2E+07	0	0	0	0	0	0	0	0	0	0	MD-0204 APPLETC	150	0	38.18	-94.03	18	0		
APPLETON_CITY	MD 38.2	-94.03	2E+07	0	0	0	0	0	0	0	0	0	0	MD-0204 APPLETC	150	0	38.18	-94.03	18	0		
APPLETON_CITY	MD 38.2	-94.03	2E+07	0	0	0	0	0	0	0	0	0	0	MD-0204 APPLETC	150	0	38.18	-94.03	18	0		
APPLETON_CITY	MD 38.2	-94.03	2E+07	0	0	0	0	0	0	0	0	0	0	MD-0204 APPLETC	150	0	38.18	-94.03	18	0		
APPLETON_CITY	MD 38.2	-94.03	2E+07	0	0	0	0	0	0	0	0	0	0	MD-0204 APPLETC	150	0	38.18	-94.03	18	0		
APPLETON_CITY	MD 38.2	-94.03	2E+07	0	0.1	0.11	0.1	0.06	0	0	0.31	0.27	0.16	MD-0204 APPLETC	150	0.37	38.18	-94.03	18	0.27		
APPLETON_CITY	MD 38.2	-94.03	2E+07	0.06	0	0	0	0	0.01	0.01	0.06	0.01	0.02	MD-0204 APPLETC	150	0	38.18	-94.03	18	0.01		
APPLETON_CITY	MD 38.2	-94.03	2E+07	0	0.01	0.01	0.01	0.01	0	0	0.03	0.03	0.02	MD-0204 APPLETC	150	0.03	38.18	-94.03	18	0.03	0.01	0.01
ARCADIA	MD 37.58	-90.62	2E+07	0.18	1.13	0.88	0.64	0.59	0.04	0.05	2.83	2.15	1.32	MD-0224 Arcadia	150	3.25	37.6	-90.63	7	2.83	-0.01	0.01
ARCADIA	MD 37.58	-90.62	2E+07	0.59	0.04	0.05	0.04	0.05	0	0	0.72	0.14	0.03	MD-0224 Arcadia	150	0.18	37.6	-90.63	7	0.72		
ARCADIA	MD 37.58	-90.62	2E+07	0.05	0	0	0	0	0	0	0.05	0	0	MD-0224 Arcadia	150	0	37.6	-90.63	7	0.05		
ARCADIA	MD 37.58	-90.62	2E+07	0	0	0	0	0	0	0	0	0	0	MD-0224 Arcadia	150	0	37.6	-90.63	7	0		
ARCADIA	MD 37.58	-90.62	2E+07	0	0	0	0	0	0	0	0	0	0	MD-0224 Arcadia	150	0	37.6	-90.63	7	0		
ARCADIA	MD 37.58	-90.62	2E+07	0	0	0	0	0	0	0	0	0	0	MD-0224 Arcadia	150	0	37.6	-90.63	7	0		
ARCADIA	MD 37.58	-90.62	2E+07	0	0.04	0.06	0.05	0.04	0	0	0.15	0.15	0.09	MD-0224 Arcadia	150	0.18	37.6	-90.63	7	0.15	0.01	0.01
ARCADIA	MD 37.58	-90.62	2E+07	0.04	0	0	0	0	0.31	0.49	0.04	0.31	0.18	MD-0224 Arcadia	150	0	37.6	-90.63	7	0.04		
ARCADIA	MD 37.58	-90.62	2E+07	0	0.31	0.49	0.41	0.5	0.12	0.14	1.21	1.02	0.71	MD-0224 Arcadia	150	1.72	37.6	-90.63	7	1.21	-0.01	0.01
ARCADIA	MD 37.58	-90.62	2E+07	0.5	0.11	0.13	0.11	0.07	0.3	0.13	0.85	0.61	0.61	MD-0224 Arcadia	150	0.42	37.6	-90.63	7	0.85		
ARCADIA	MD 37.58	-90.62	2E+07	0.07	0.3	0.13	0.02	0.07	0.04	0.07	0.52	0.26	0.2	MD-0224 Arcadia	150	0.52	37.6	-90.63	7	0.52		
ARCADIA	MD 37.58	-90.62	2E+07	0.07	0.04	0.07	0.06	0.11	0.21	0.13	0.24	0.45	0.51	MD-0224 Arcadia	150	0.28	37.6	-90.63	7	0.24		
AVA_RANGER_STATION	MD 36.95	-92.67	2E+07	0	0.77	0.6	0.44	0.4	0	0	1.81	1.44	0.84	MD-0365 Ava RS	150	2.21	36.95	-92.67	8	1.81		
AVA_RANGER_STATION	MD 36.95	-92.67	2E+07	0.4	0	0	0	0	0	0	0.4	0	0	MD-0365 Ava RS	150	0	36.95	-92.67	8	0.4		
AVA_RANGER_STATION	MD 36.95	-92.67	2E+07	0	0	0	0	0	0.02	0.02	0	0.02	0.04	MD-0365 Ava RS	150	0	36.95	-92.67	8	0		
AVA_RANGER_STATION	MD 36.95	-92.67	2E+07	0	0.02	0.02	0.04	0.08	0	0	0.08	0.14	0.12	MD-0365 Ava RS	150	0.15	36.95	-92.67	8	0.08	0.01	0.01
AVA_RANGER_STATION	MD 36.95	-92.67	2E+07	0.08	0	0	0	0	0.05	0.08	0.08	0.05	0.13	MD-0365 Ava RS	150	0	36.95	-92.67	8	0.08		
AVA_RANGER_STATION	MD 36.95	-92.67	2E+07	0	0.05	0.08	0.06	0.05	0	0	0.19	0.19	0.11	MD-0365 Ava RS	150	0.24	36.95	-92.67	8	0.19		
AVA_RANGER_STATION	MD 36.95	-92.67	2E+07	0.05	0	0	0	0	0.11	0.29	0.05	0.11	0.29	MD-0365 Ava RS	150	0	36.95	-92.67	8	0.05		
AVA_RANGER_STATION	MD 36.95	-92.67	2E+07	0	0.11	0.18	0.15	0.08	0.25	0.23	0.44	0.66	0.77	MD-0365 Ava RS	150	0.64	36.95	-92.67	8	0.44	-0.12	0.12
AVA_RANGER_STATION	MD 36.95	-92.67	2E+07	0.19	0.42	0.48	0.41	0.25	0	0	1.5	1.14	0.66	MD-0365 Ava RS	150	1.56	36.95	-92.67	8	1.5		
AVA_RANGER_STATION	MD 36.95	-92.67	2E+07	0.25	0	0	0	0	0.06	0.09	0.25	0.06	0.15	MD-0365 Ava RS	150	0	36.95	-92.67	8	0.25		
AVA_RANGER_STATION	MD 36.95	-92.67	2E+07	0	0.06	0.09	0.08	0.15	0	0	0.23	0.32	0.23	MD-0365 Ava RS	150	0.39	36.95	-92.67	8	0.23	-0.01	0.01
BELLEVUE	MD 37.68	-90.73	2E+07	1.18	0	0	0	0	0	0	1.18	0	0	MD-0539 Bellevue	150	0	37.68	-90.78	7	1.18		
BELLEVUE	MD 37.68	-90.73	2E+07	0	0	0	0	0	0.1	0.11	0	0.1	0.21	MD-0539 Bellevue	150	0	37.68	-90.78	7	0		
BELLEVUE	MD 37.68	-90.73	2E+07	0	0.1	0.11	0.1	0.06	0	0	0.31	0.27	0.16	MD-0539 Bellevue	150	0.37	37.68	-90.78	7	0.31		
BELLEVUE	MD 37.68	-90.73	2E+07	0.06	0	0	0	0	0	0	0.06	0	0	MD-0539 Bellevue	150	0	37.68	-90.78	7	0.06		
BELLEVUE	MD 37.68	-90.73	2E+07	0	0	0	0	0	0	0	0	0	0	MD-0539 Bellevue	150	0	37.68	-90.78	7	0		
BELLEVUE	MD 37.68	-90.73	2E+07	0	0	0	0	0	0.05	0.08	0	0.05	0.13	MD-0539 Bellevue	150	0	37.68	-90.78	7	0		
BELLEVUE	MD 37.68	-90.73	2E+07	0.05	0	0	0	0	0.21	0.35	0.05	0.21	0.56	MD-0539 Bellevue	150	0	37.68	-90.78	7	0.05		
BELLEVUE	MD 37.68	-90.73	2E+07	0	0.21	0.35	0.29	0.35	0.08	0.1	0.85	0.72	0.47	MD-0539 Bellevue	150	1.2	37.68	-90.78	7	0.85		
BELLEVUE	MD 37.68	-90.73	2E+07	0.35	0.1	0.12	0.1	0.06	0.28	0.12	0.87	0.56	0.56	MD-0539 Bellevue	150	0.39	37.68	-90.78	7	0.57	-0.01	0.01
BELLEVUE	MD 37.68	-90.73	2E+07	0.06	0.28	0.12	0.02	0.06	0	0	0.48	0.2	0.08	MD-0539 Bellevue	150	0.48	37.68	-90.78	7	0.48		
BELLEVUE	MD 37.68	-90.73	2E+07	0.06	0	0	0	0	0.23	0.14	0.06	0.23	0.37	MD-0539 Bellevue	150	0	37.68	-90.78	7	0.06		
BERNIE	MD 36.67	-89.37	2E+07	0.36	1.06	0.83	0.6	0.56	0.29	0.34	2.85											

Acceptable differences were less than 0.025 in. per day with 0.01 in. being the standard to indicate trace amounts of rain. The larger 0.025 in. was used because of uncertainties in the manually recorded data—both COOP observer and the NCDC database had spot anomalies that could not be fully validated.

This established QC process helped define the procedure by which all other datasets were developed.

G.10.2 Hydrologic modeling

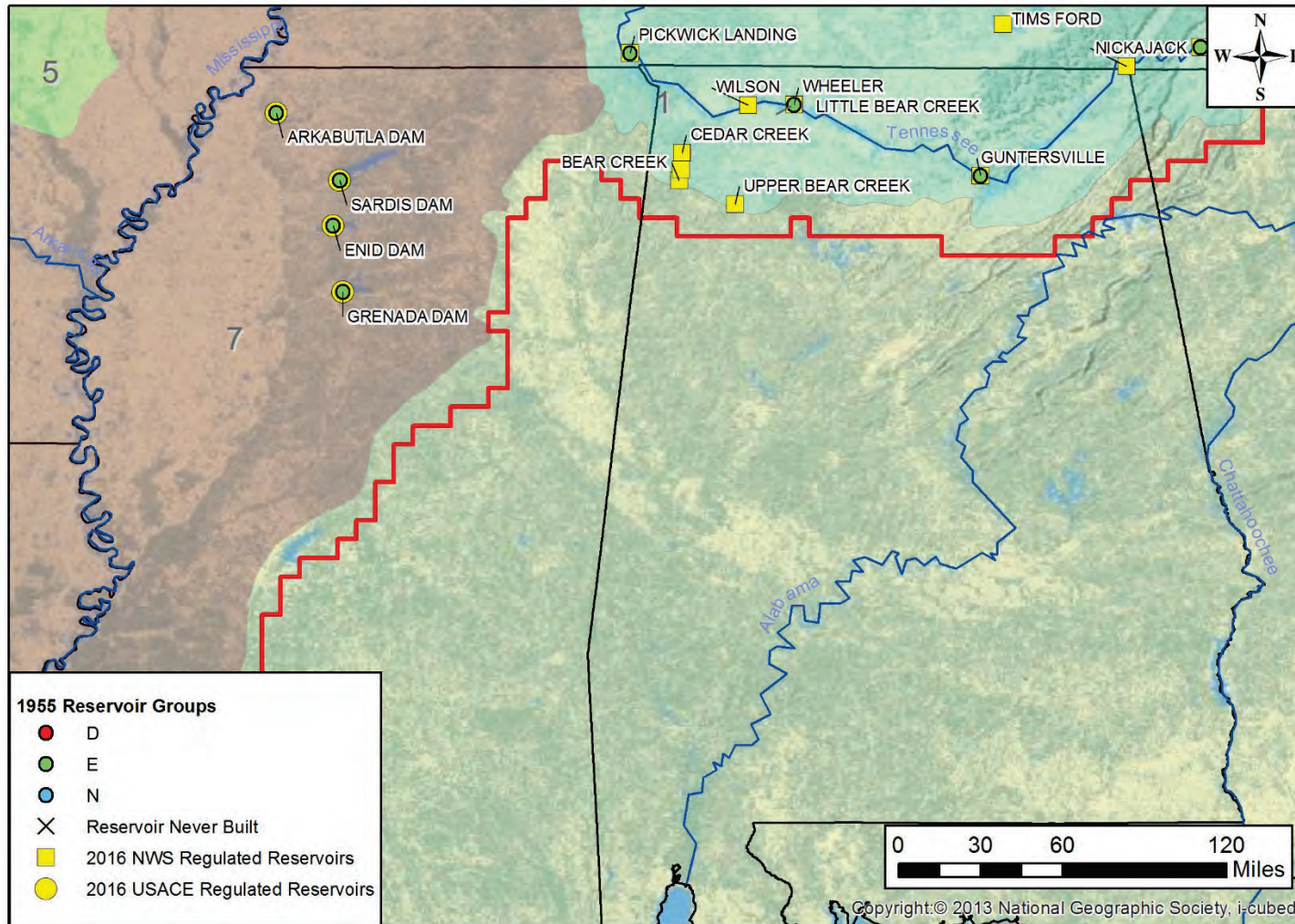
For 1950, there were fewer than 10 locations within the primary study area where comparisons could be made between hydrologic model outputs and observed stream discharges. The hydrograph comparisons were intended to provide insight into how the current methodology differed from that used in the 1955 work. Questions about how changed landuse and different model schematization for soil moisture and infiltration accounting as well as SWE computations would differ from use of 1950s landuse information and initial loss factors and unit hydrograph approaches used in the earlier study. In retrospect, it is not surprising that these questions could not be answered with only a few (eight) model runs. To investigate how the differences would impact model uncertainty would require multiple runs to weigh the effects of model parameters one at a time and jointly. Such repetitive model runs were beyond the scope and allowable time of the 2016 assessment. Such runs could be made in the future if a way could be established to run the multiple RFC models along with the reservoir regulations within a single model environment instead of the 15 or so different ones used.

Appendix H: Mississippi River 2011 Post Flood Assessment: Task 1 – Adequacy of MR&T Project Design Flood

This appendix can be found at <http://dx.doi.org/10.21079/11681/32141>.

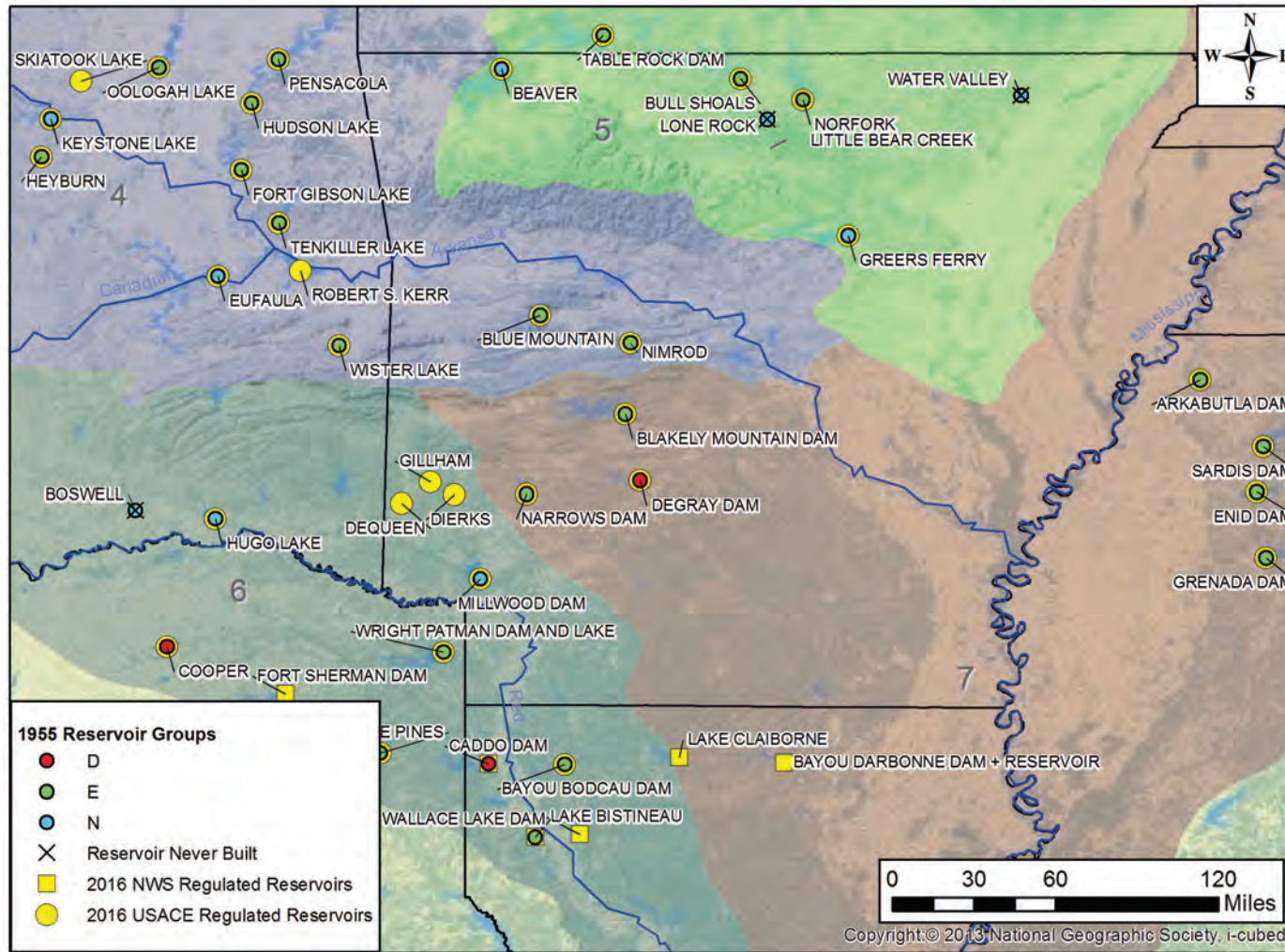
Appendix I: Reservoir Maps

Figure I-1. Reservoir locations, Alabama and Mississippi.



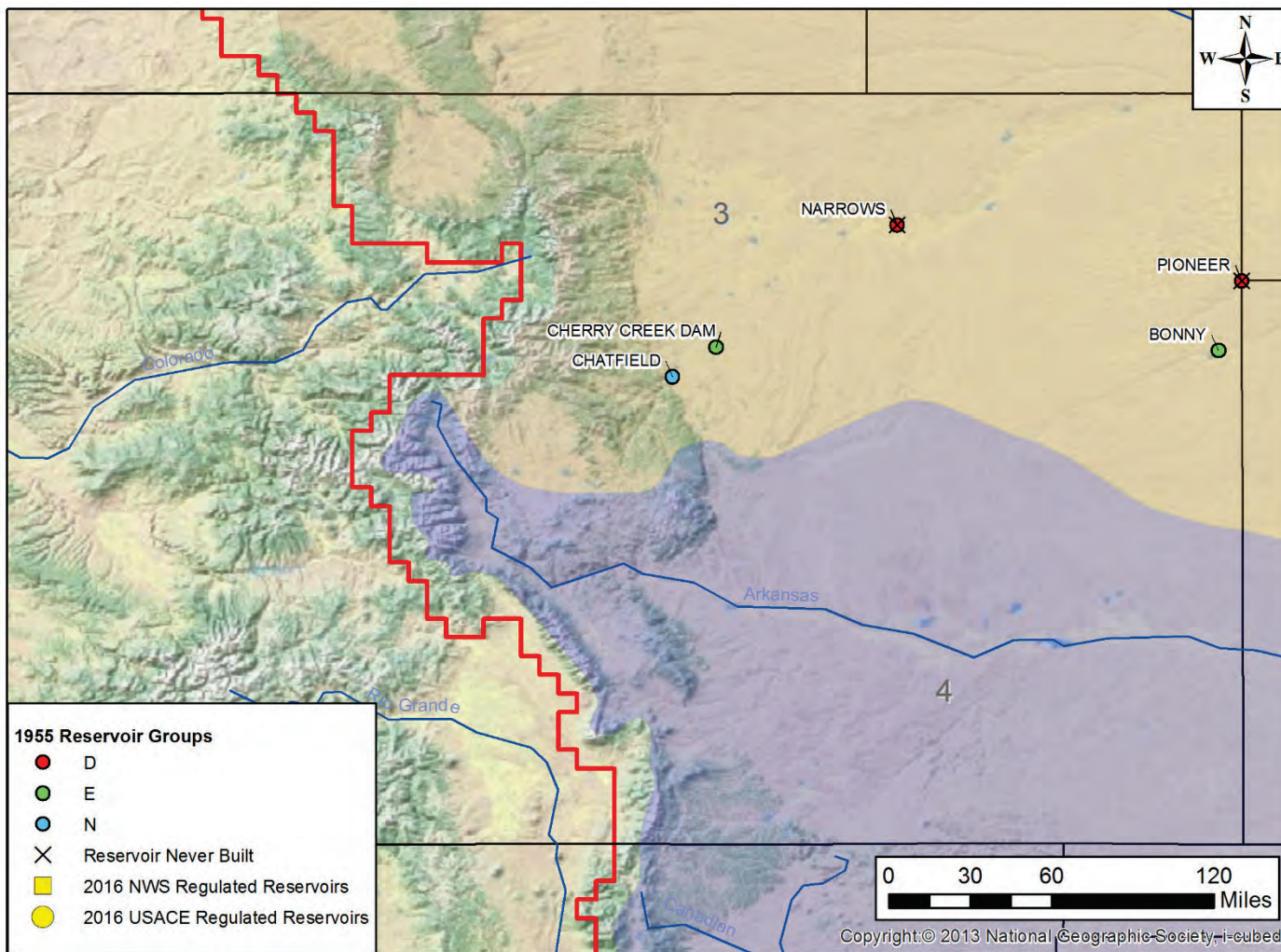
Note: Symbols illustrate which agency's modeling efforts addressed regulation effects of reservoirs; they do not indicate the agency responsible for daily operations of those projects.

Figure I-2. Reservoir locations, Arkansas and Louisiana.



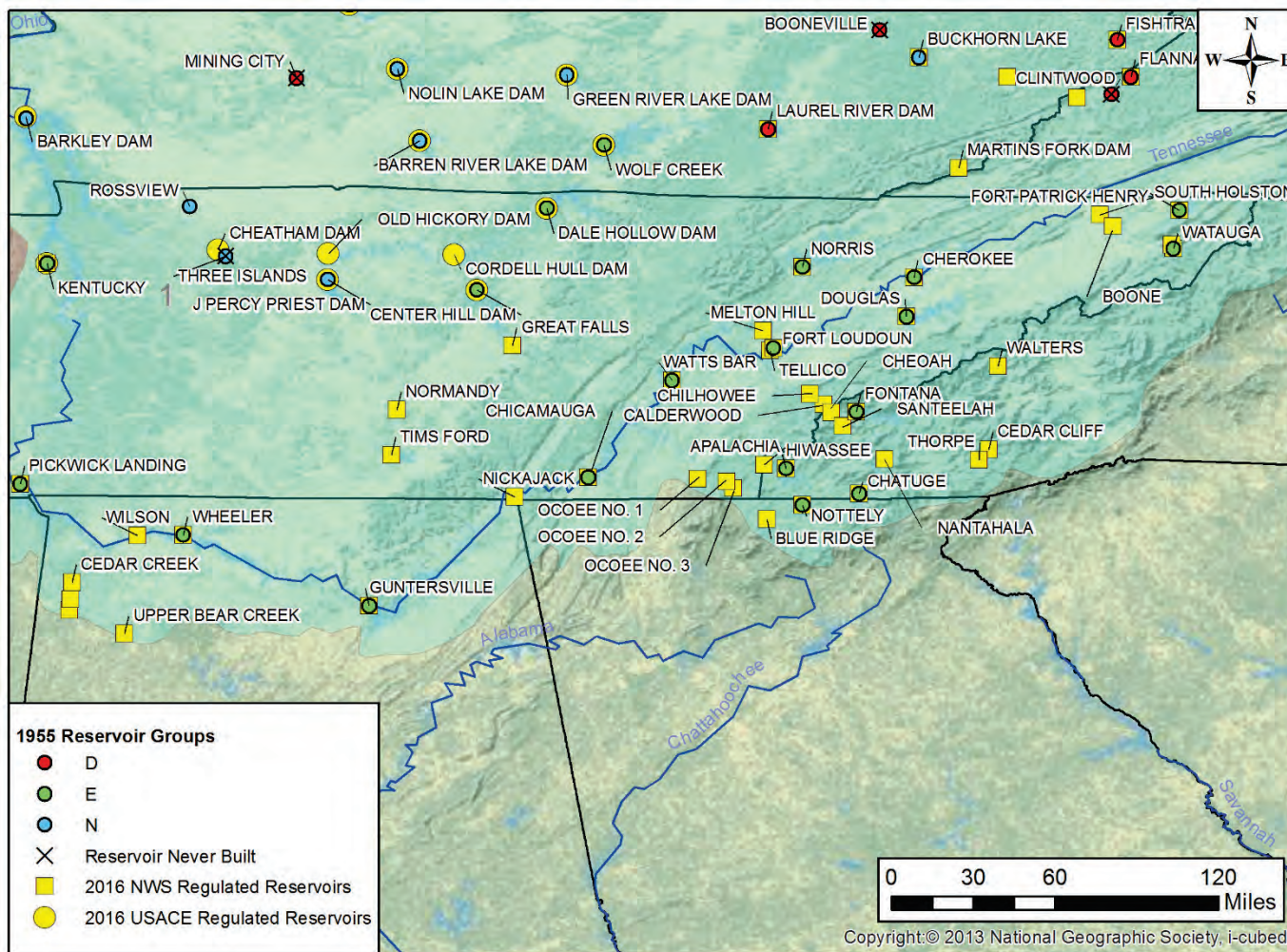
Note: Symbols illustrate which agency's modeling efforts addressed regulation effects of reservoirs; they do not indicate the agency responsible for daily operations of those projects.

Figure I-3. Reservoir Locations, Colorado.



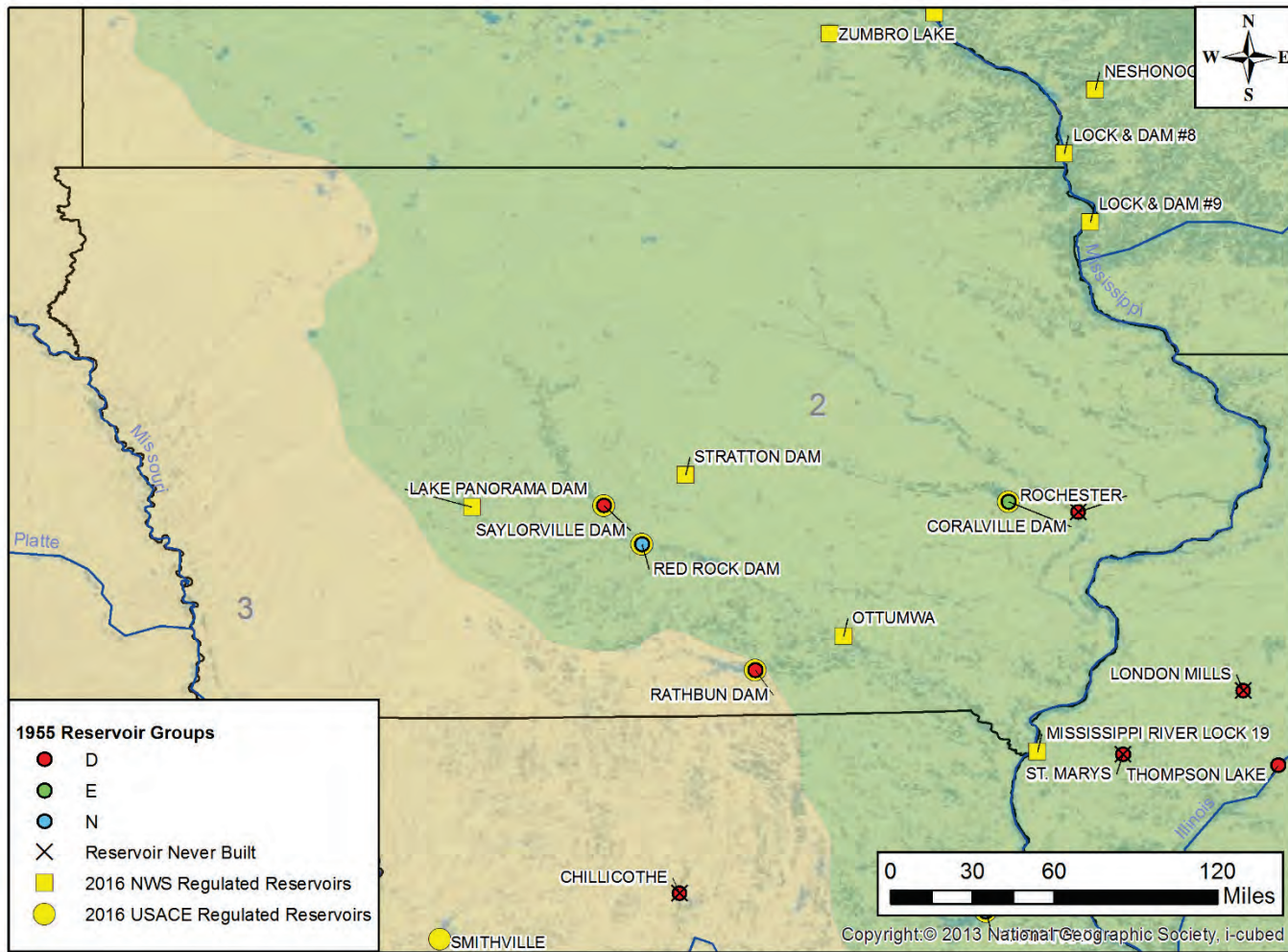
Note: Symbols illustrate which agency's modeling efforts addressed regulation effects of reservoirs; they do not indicate the agency responsible for daily operations of those projects.

Figure I-4. Reservoir locations, Tennessee and Georgia.



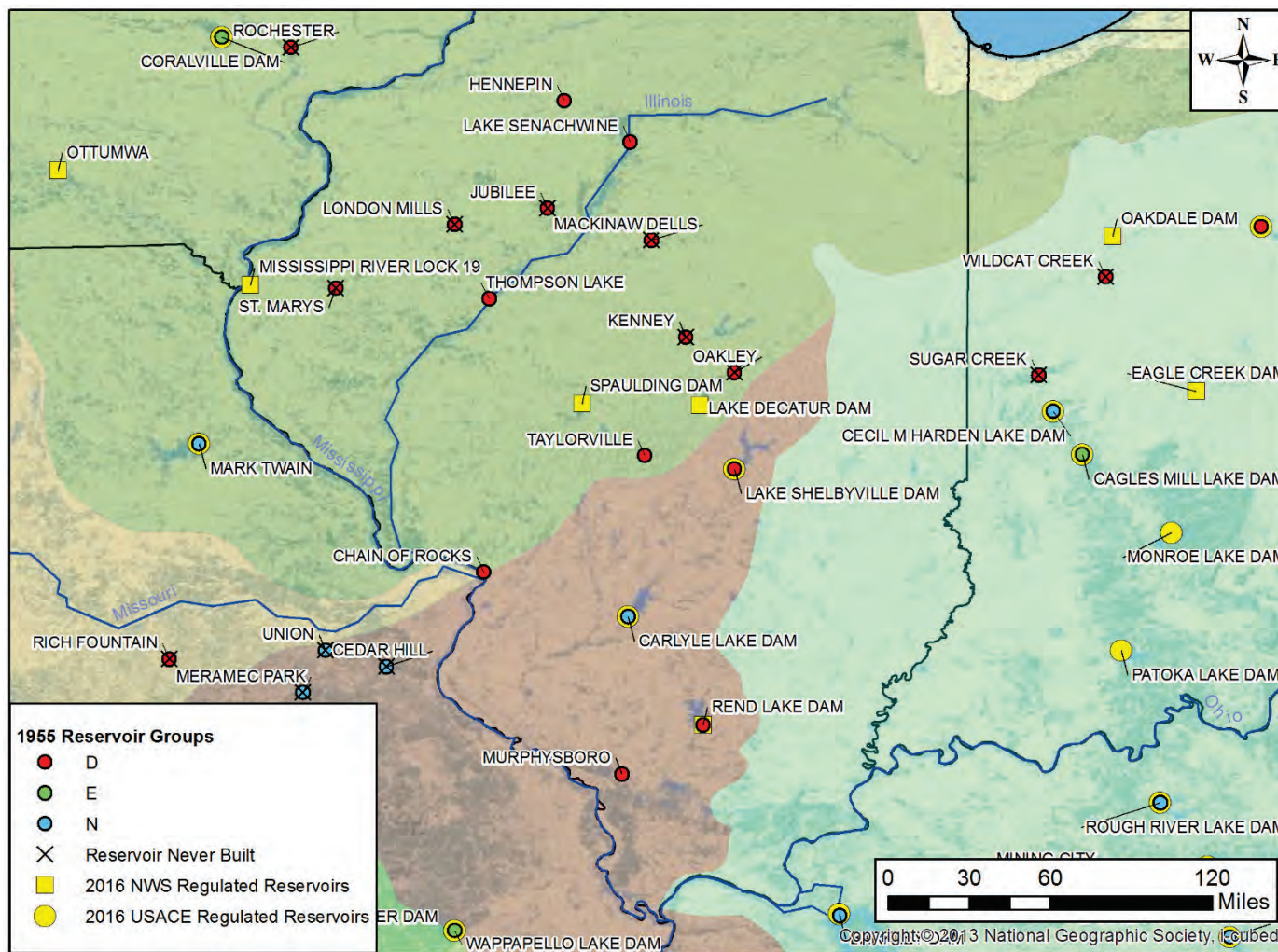
Note: Symbols illustrate which agency's modeling efforts addressed regulation effects of reservoirs; they do not indicate the agency responsible for daily operations of those projects.

Figure I-5. Reservoir locations, Iowa.



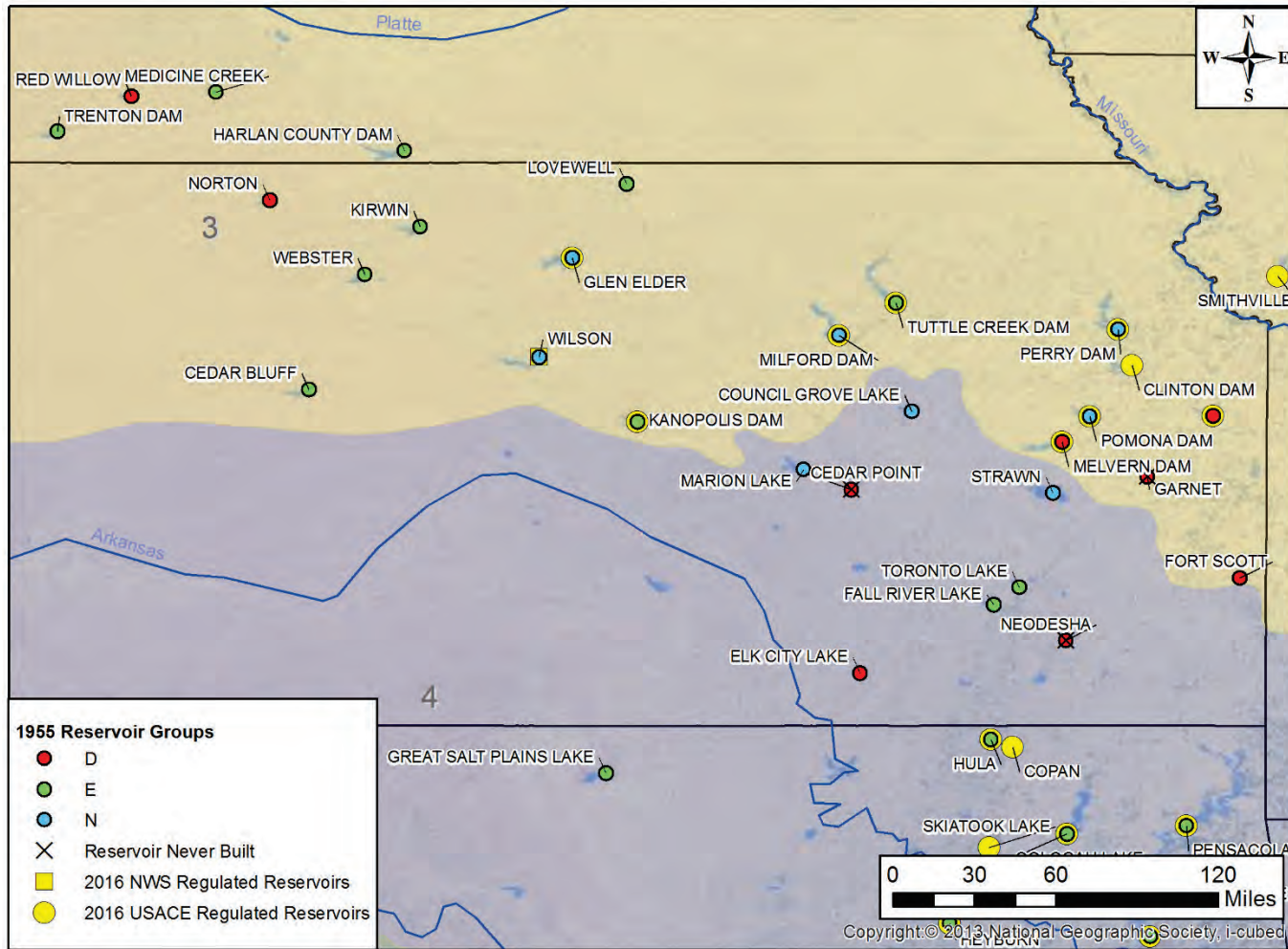
Note: Symbols illustrate which agency's modeling efforts addressed regulation effects of reservoirs; they do not indicate the agency responsible for daily operations of those projects.

Figure I-6. Reservoir locations, Illinois.



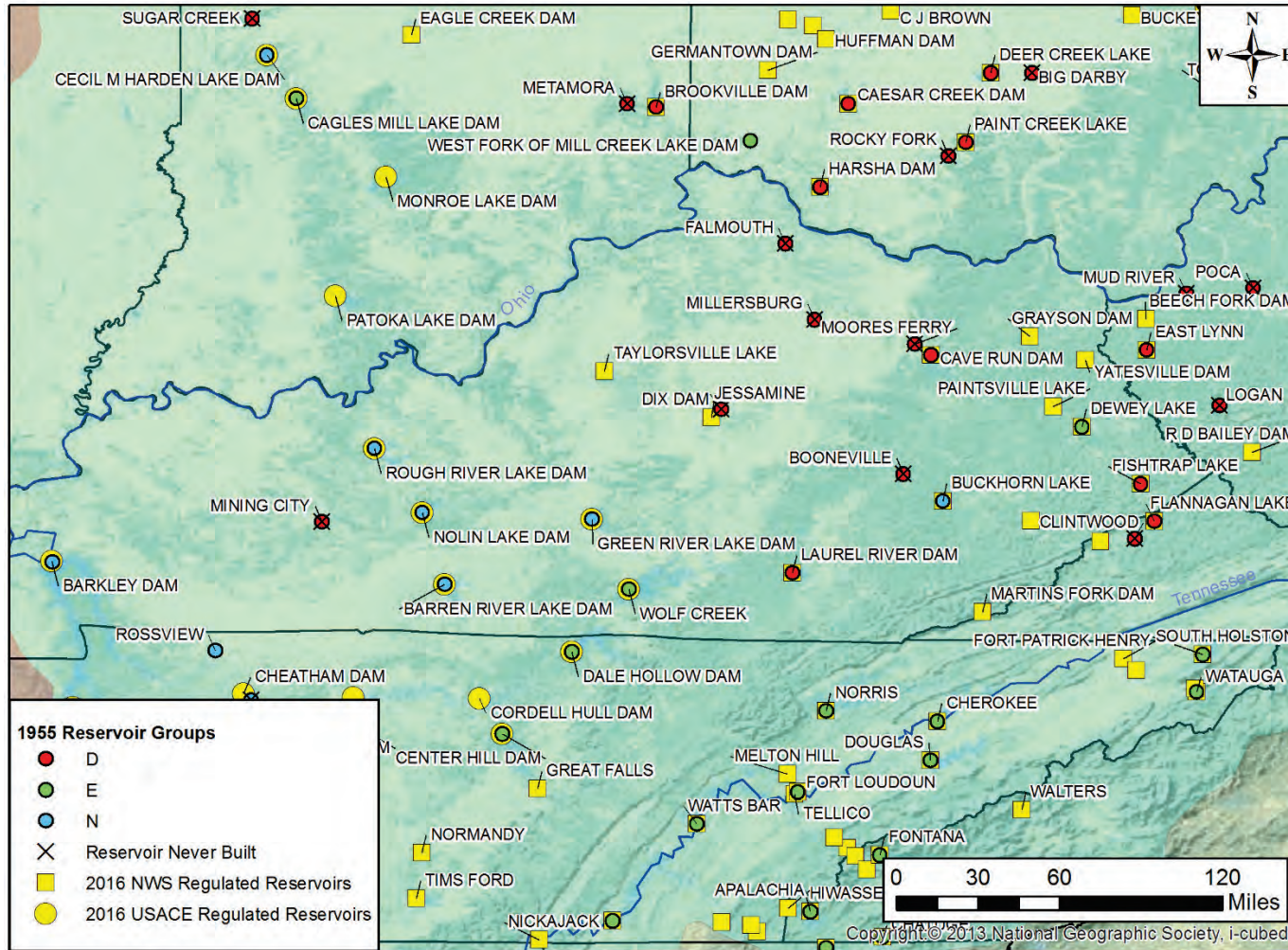
Note: Symbols illustrate which agency's modeling efforts addressed regulation effects of reservoirs; they do not indicate the agency responsible for daily operations of those projects.

Figure I-7. Reservoir locations, Kansas.



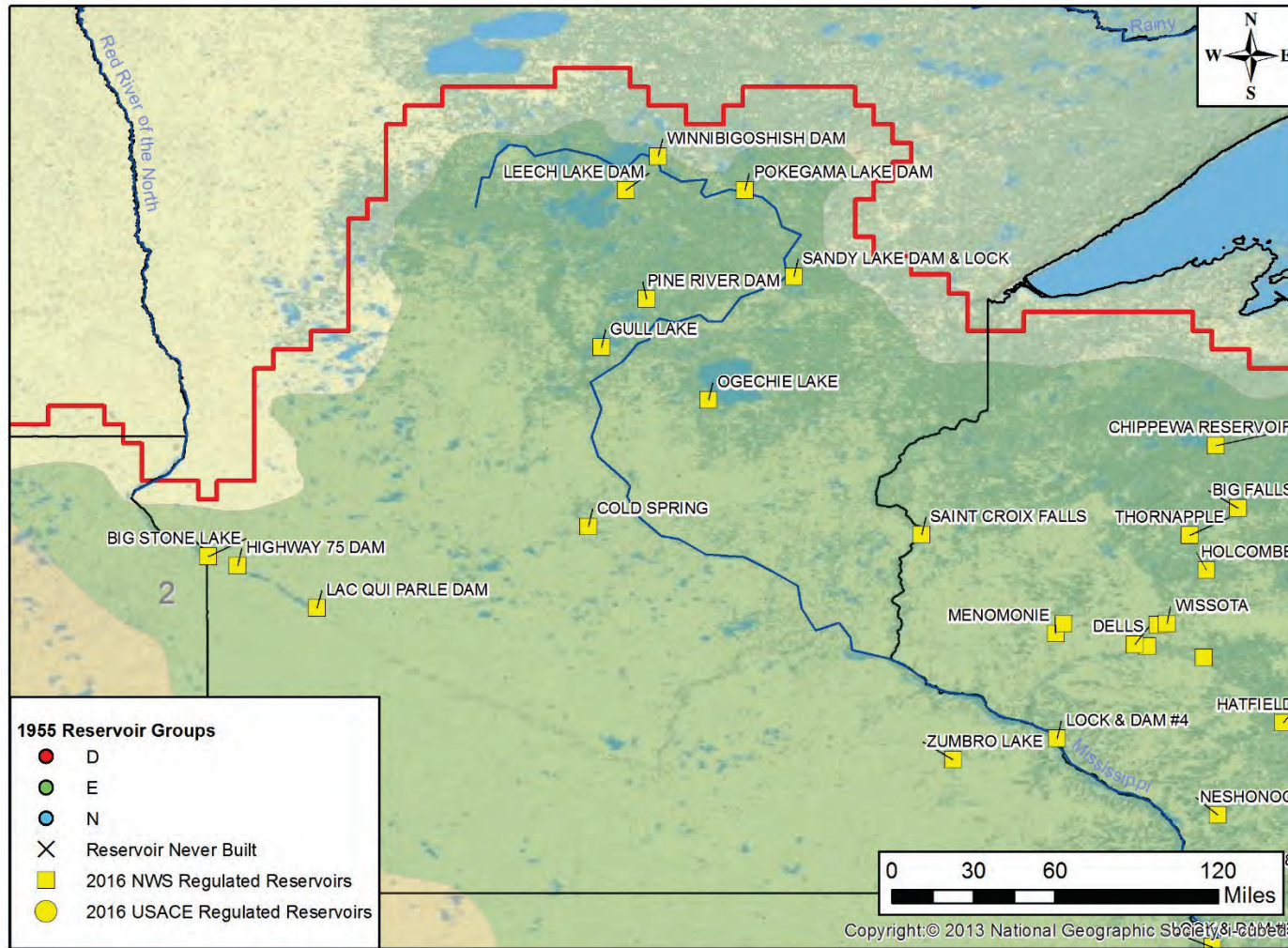
Note: Symbols illustrate which agency's modeling efforts addressed regulation effects of reservoirs; they do not indicate the agency responsible for daily operations of those projects.

Figure I-8. Reservoir locations, Kentucky.



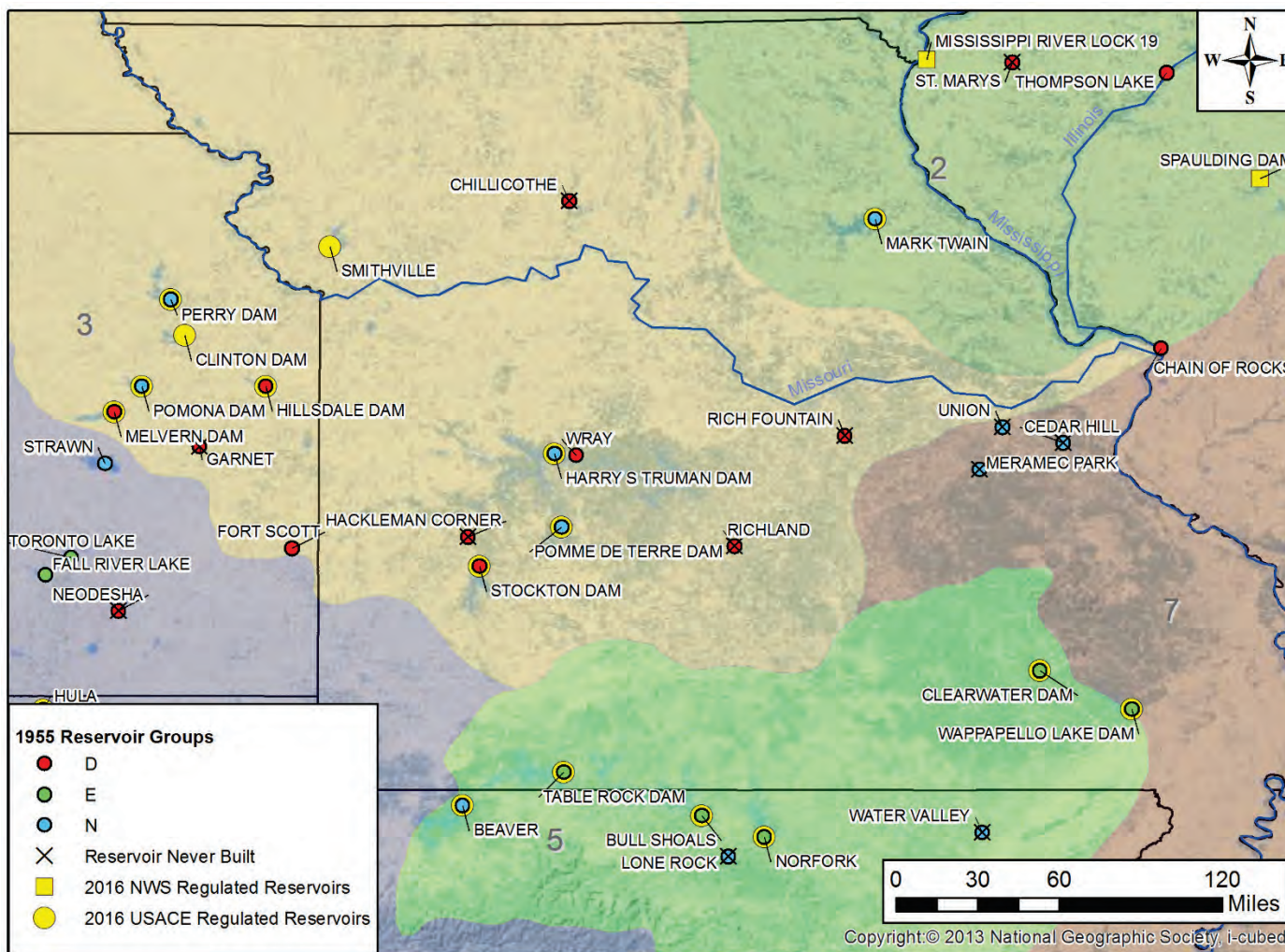
Note: Symbols illustrate which agency's modeling efforts addressed regulation effects of reservoirs; they do not indicate the agency responsible for daily operations of those projects.

Figure I-9. Reservoir locations, Minnesota.



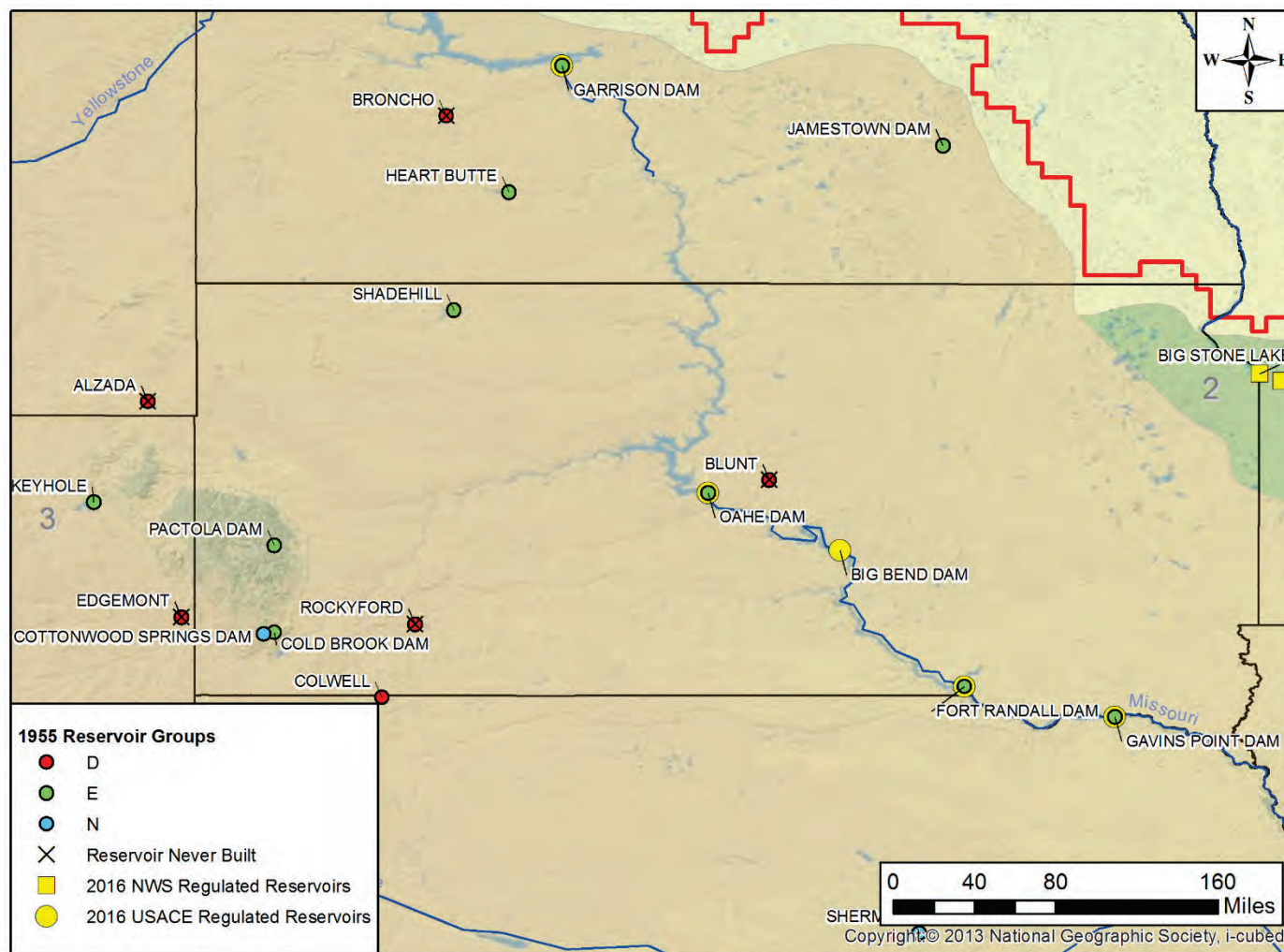
Note: Symbols illustrate which agency's modeling efforts addressed regulation effects of reservoirs; they do not indicate the agency responsible for daily operations of those projects.

Figure I-10. Reservoir locations, Missouri.



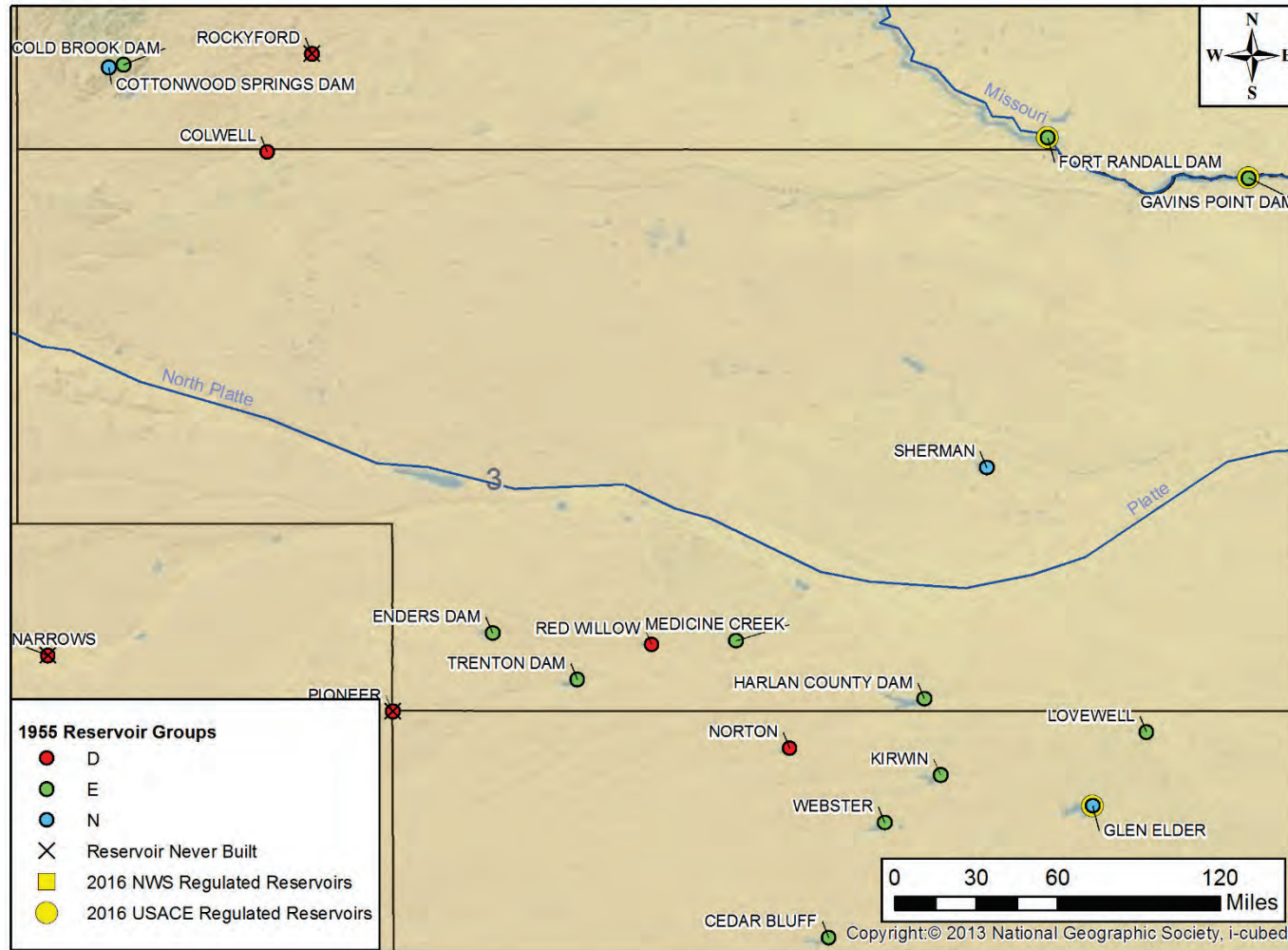
Note: Symbols illustrate which agency's modeling efforts addressed regulation effects of reservoirs; they do not indicate the agency responsible for daily operations of those projects.

Figure I-11. Reservoir locations, North Dakota and South Dakota.



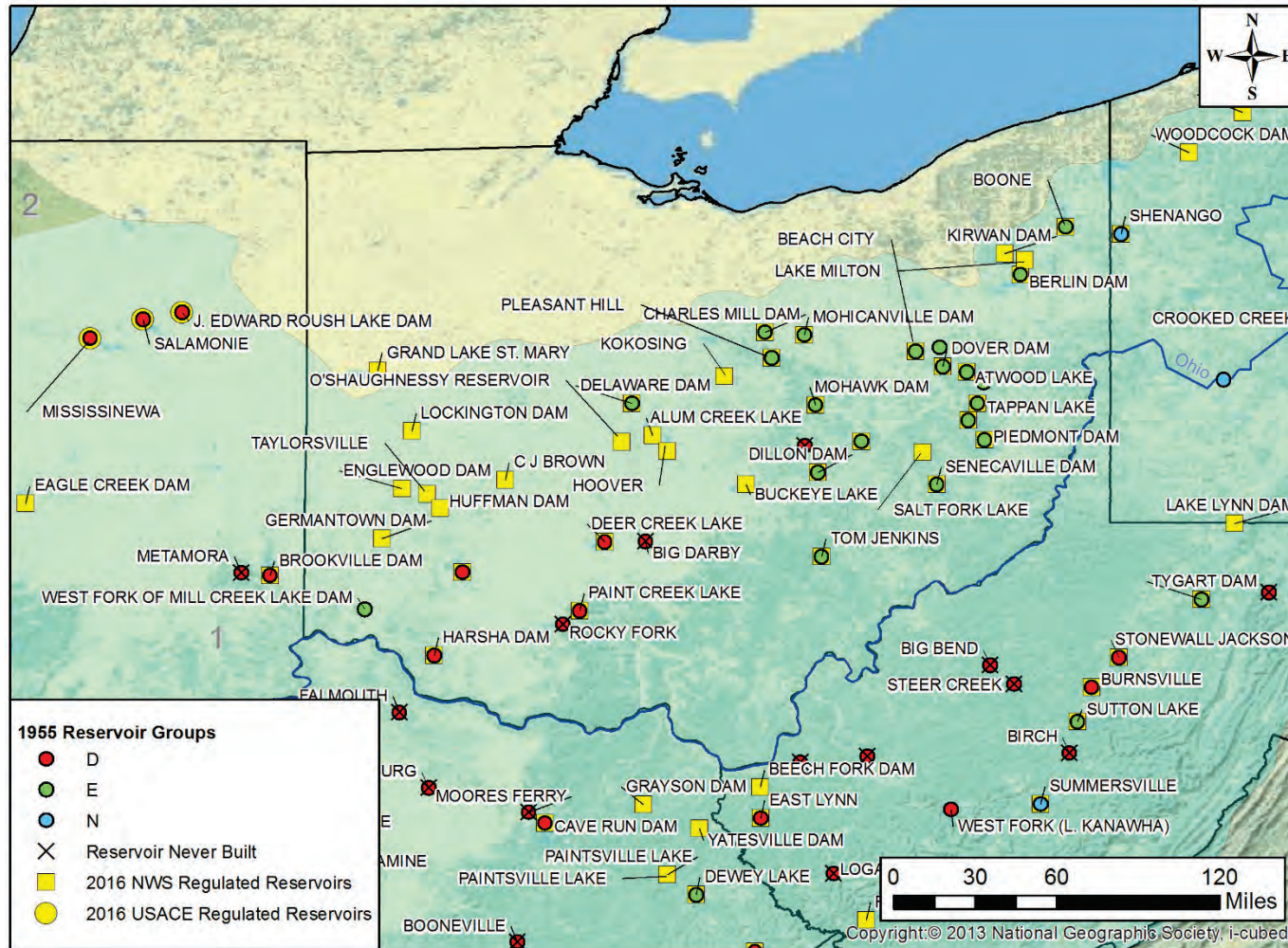
Note: Symbols illustrate which agency's modeling efforts addressed regulation effects of reservoirs; they do not indicate the agency responsible for daily operations of those projects.

Figure I-12. Reservoir locations, Nebraska.



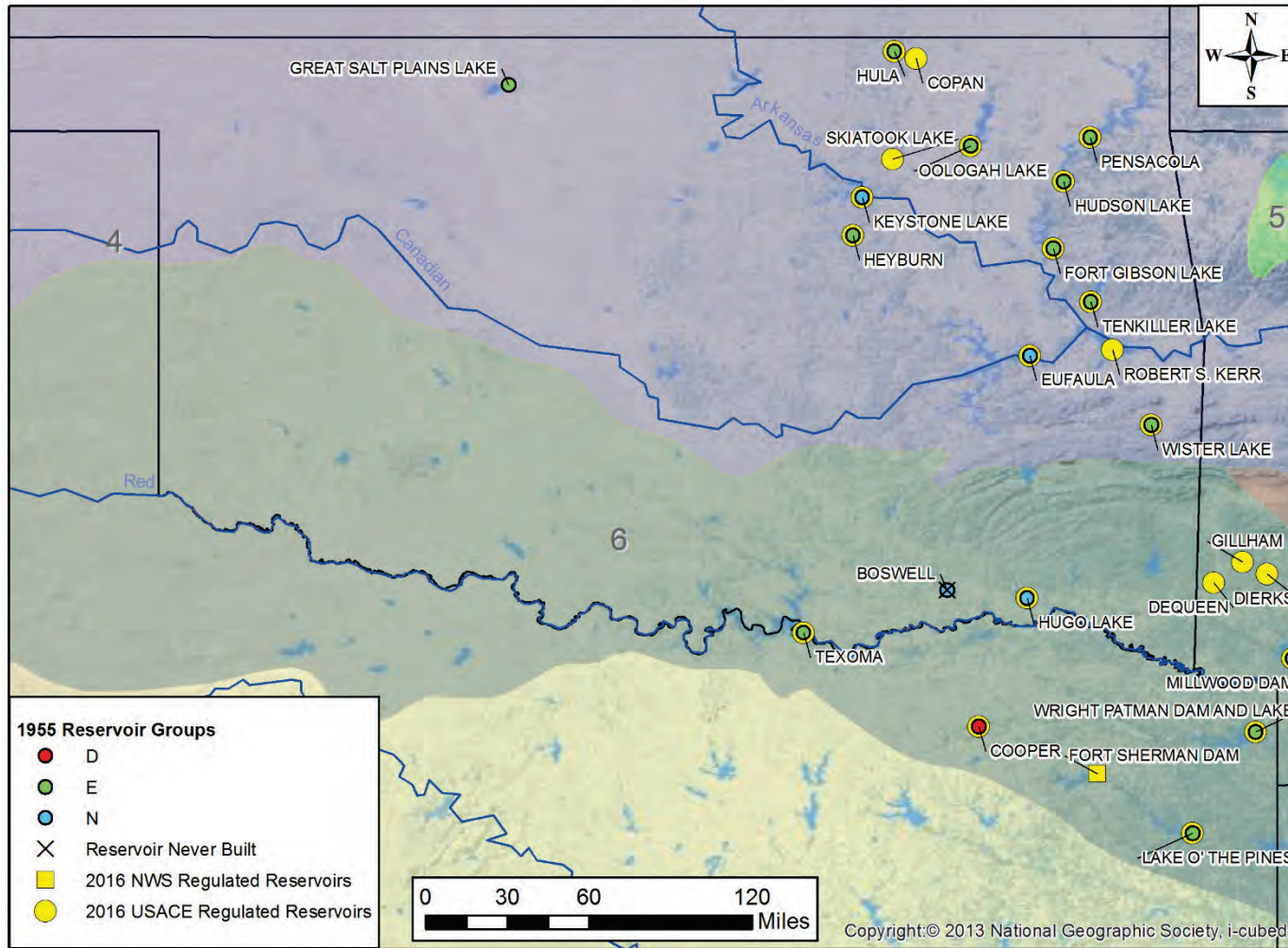
Note: Symbols illustrate which agency's modeling efforts addressed regulation effects of reservoirs; they do not indicate the agency responsible for daily operations of those projects.

Figure I-13. Reservoir locations, Ohio.



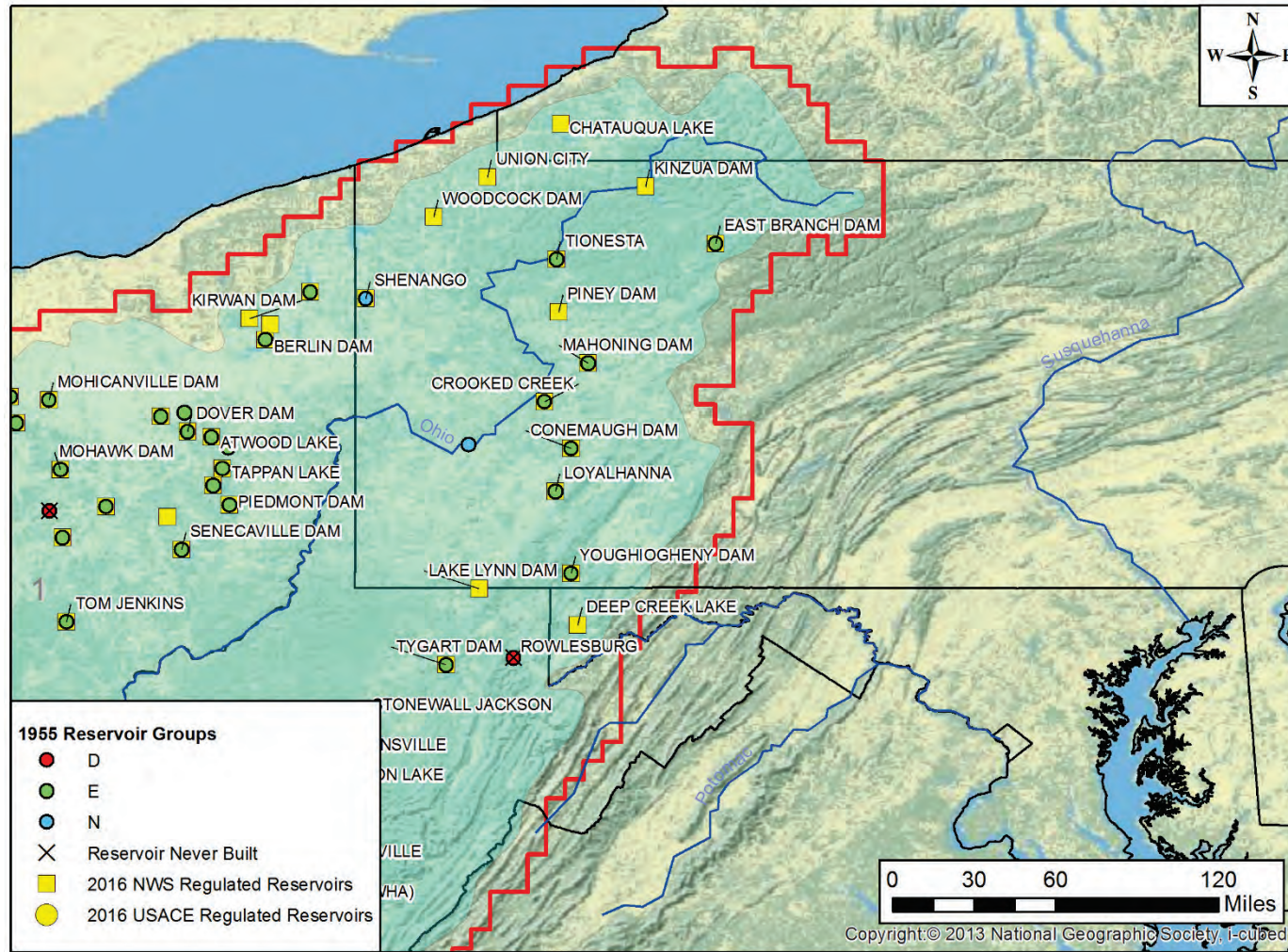
Note: Symbols illustrate which agency's modeling efforts addressed regulation effects of reservoirs; they do not indicate the agency responsible for daily operations of those projects.

Figure I-14. Reservoir locations, Oklahoma and Texas.



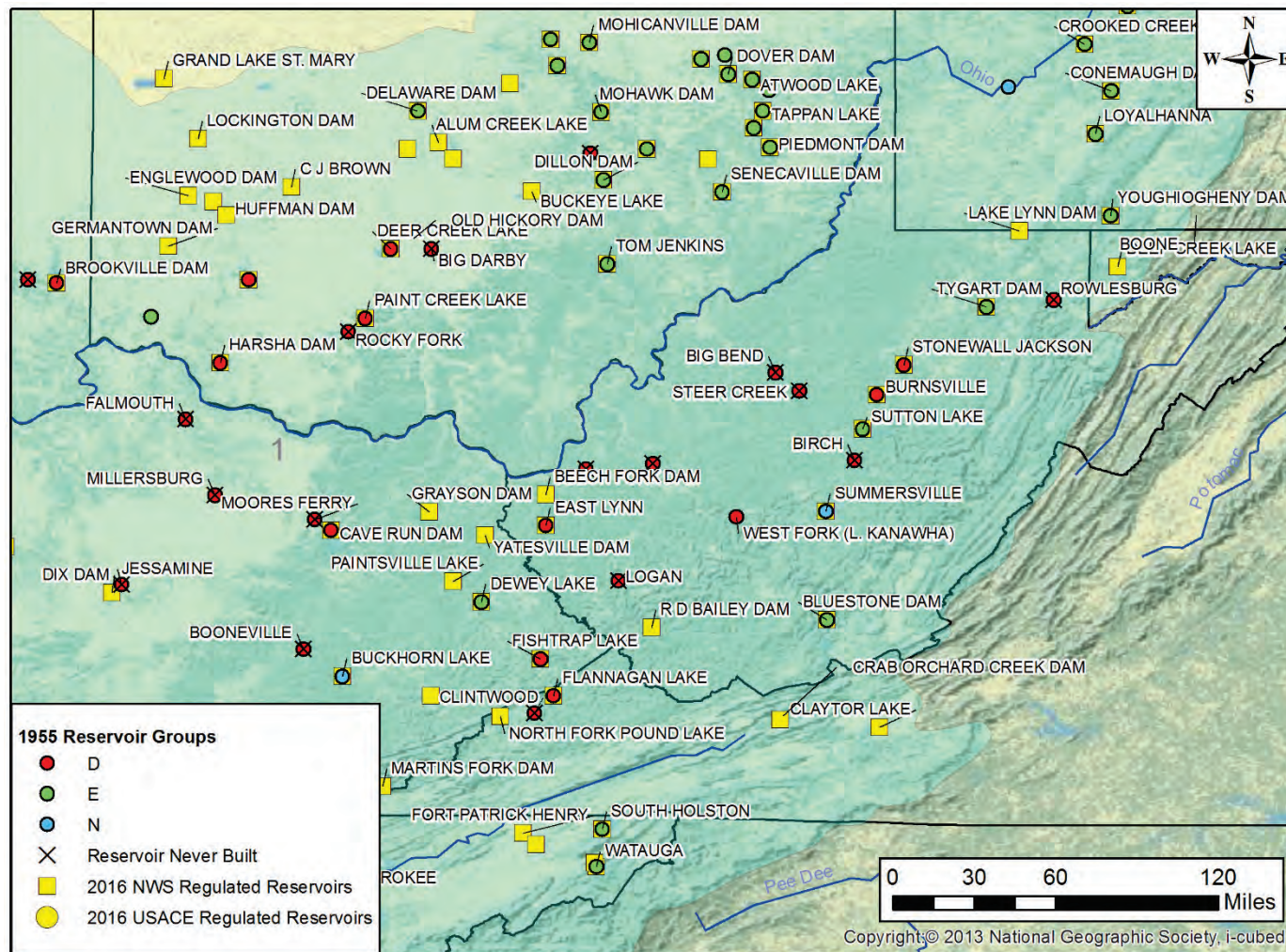
Note: Symbols illustrate which agency's modeling efforts addressed regulation effects of reservoirs; they do not indicate the agency responsible for daily operations of those projects.

Figure I-15. Reservoir locations, Pennsylvania.



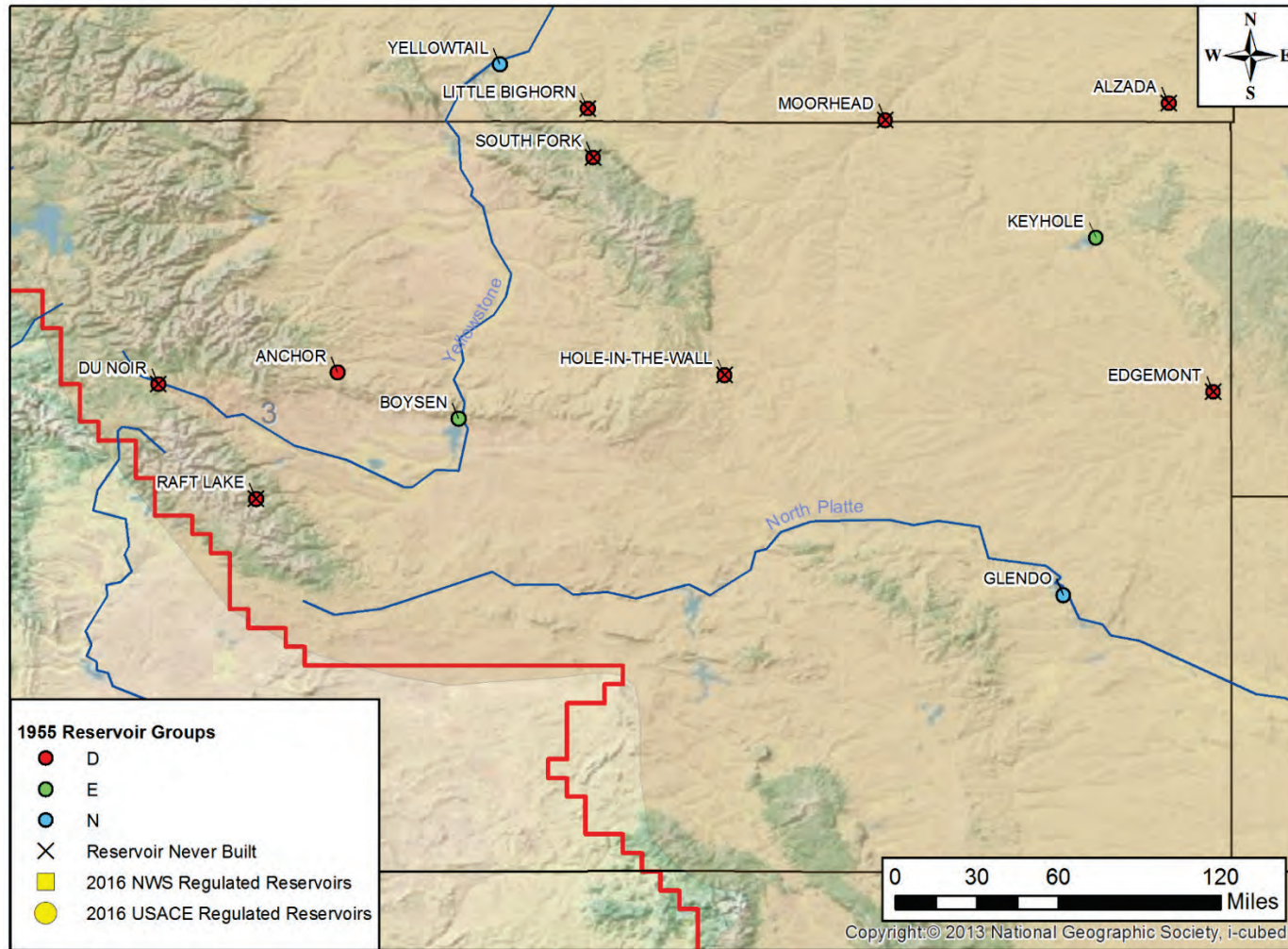
Note: Symbols illustrate which agency's modeling efforts addressed regulation effects of reservoirs; they do not indicate the agency responsible for daily operations of those projects.

Figure I-16. Reservoir locations, West Virginia and Virginia.



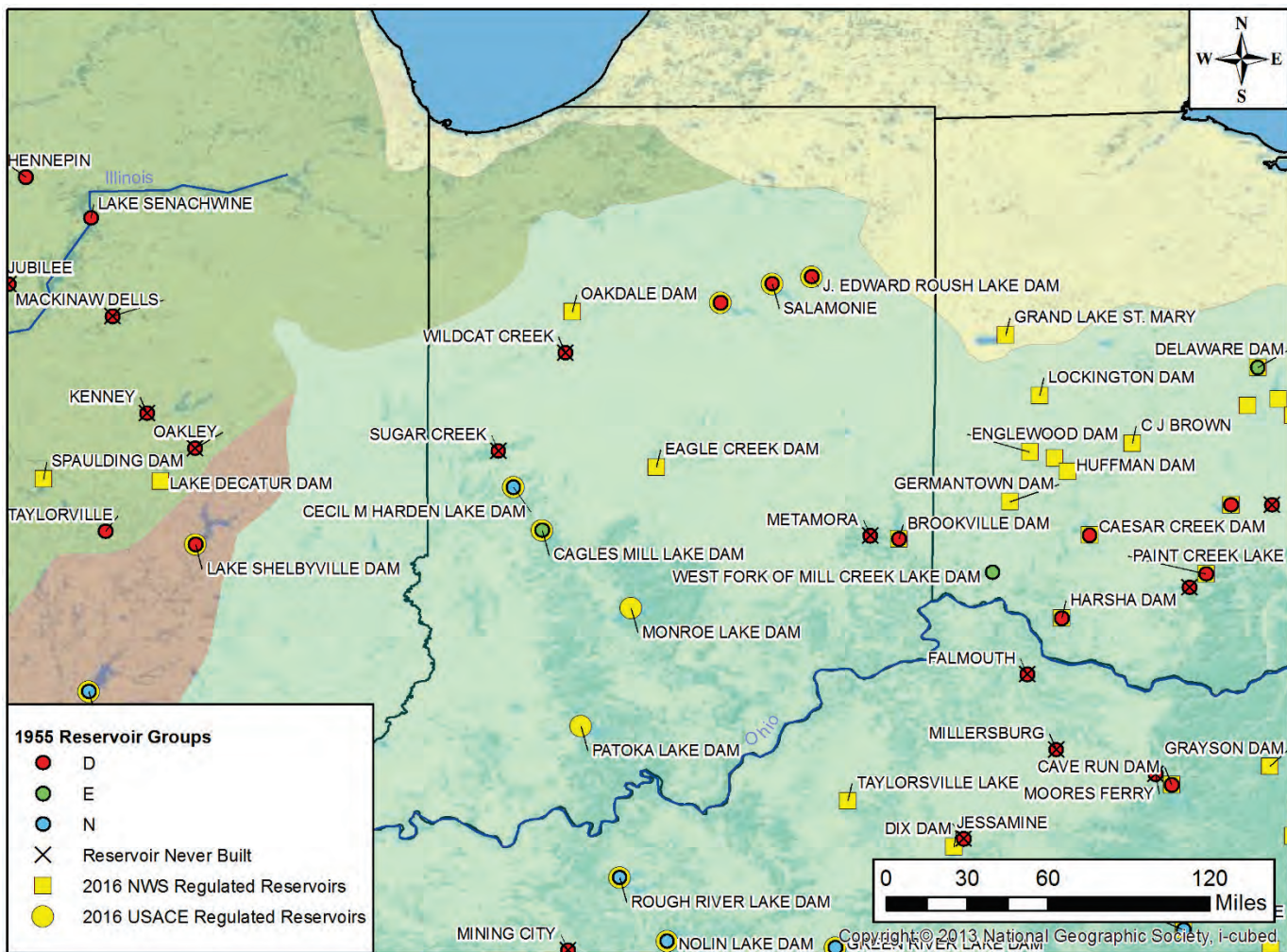
Note: Symbols illustrate which agency's modeling efforts addressed regulation effects of reservoirs; they do not indicate the agency responsible for daily operations of those projects.

Figure I-17. Reservoir locations, Wyoming.



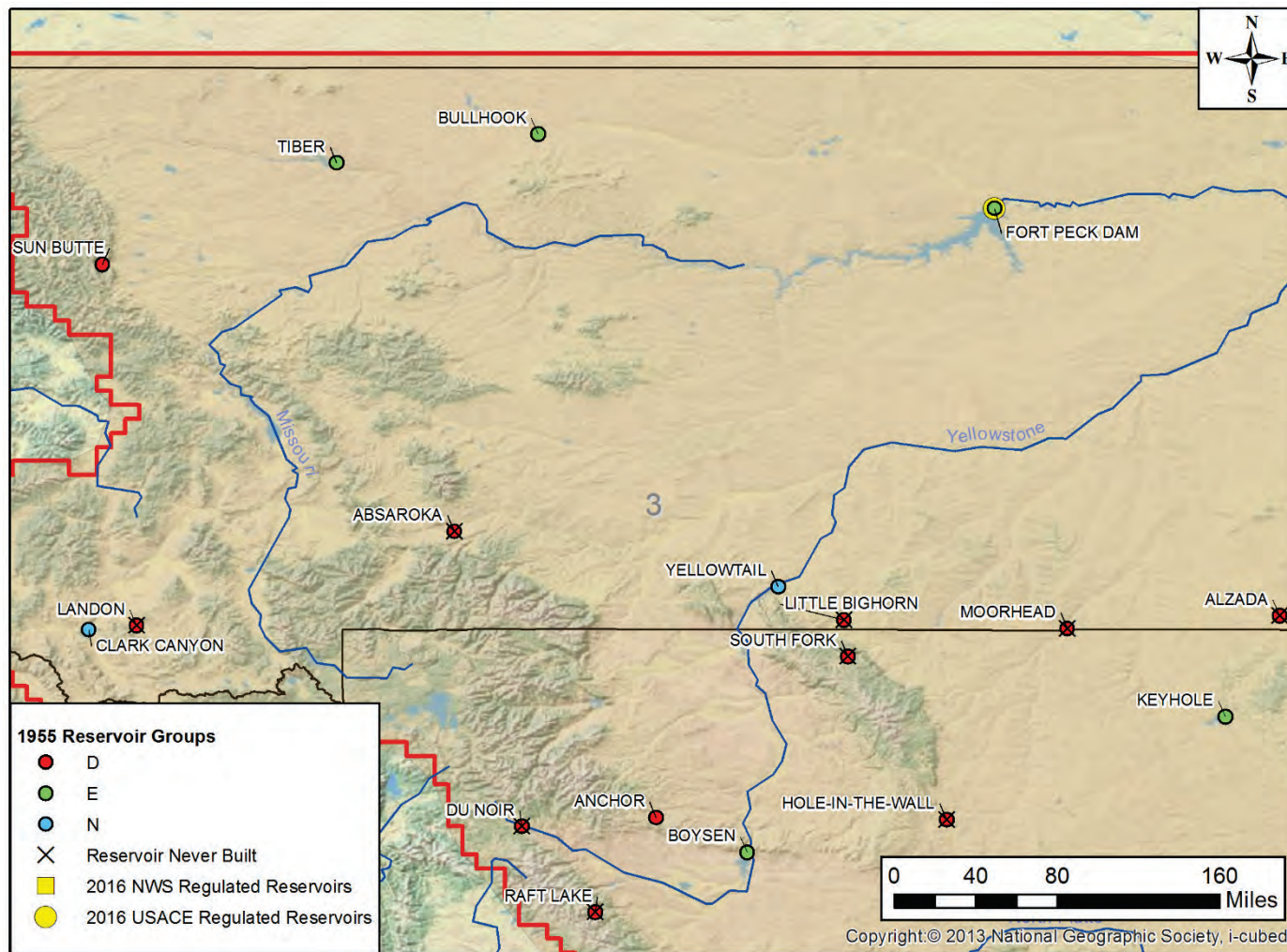
Note: Symbols illustrate which agency's modeling efforts addressed regulation effects of reservoirs; they do not indicate the agency responsible for daily operations of those projects.

Figure I-18. Reservoir locations, Indiana.



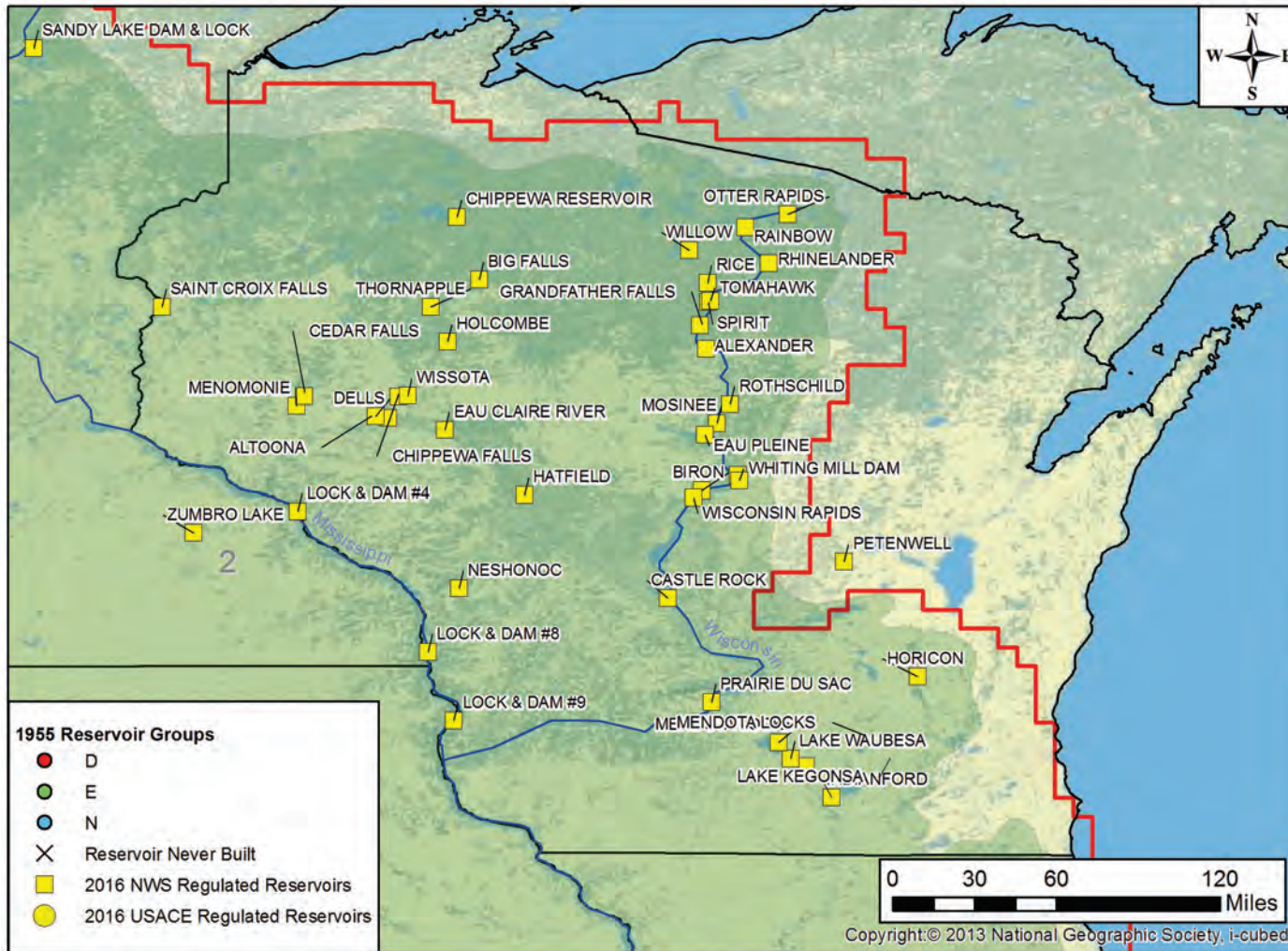
Note: Symbols illustrate which agency's modeling efforts addressed regulation effects of reservoirs; they do not indicate the agency responsible for daily operations of those projects.

Figure I-19. Reservoir locations, Montana.



Note: Symbols illustrate which agency's modeling efforts addressed regulation effects of reservoirs; they do not indicate the agency responsible for daily operations of those projects.

Figure I-20. Reservoir locations, Wisconsin.



Note: Symbols illustrate which agency's modeling efforts addressed regulation effects of reservoirs; they do not indicate the agency responsible for daily operations of those projects.

Appendix J: Hydrograph Tabulations

This appendix can be found at <http://dx.doi.org/10.21079/11681/32141>.

Appendix K: Precipitation Tabulations

This appendix can be found at <http://dx.doi.org/10.21079/11681/32141>.

All values are in units of inches.

REPORT DOCUMENTATION PAGE

Form Approved
OMB No. 0704-0188

The public reporting burden for this collection of information is estimated to average 1 hour per response, including the time for reviewing instructions, searching existing data sources, gathering and maintaining the data needed, and completing and reviewing the collection of information. Send comments regarding this burden estimate or any other aspect of this collection of information, including suggestions for reducing the burden, to Department of Defense, Washington Headquarters Services, Directorate for Information Operations and Reports (0704-0188), 1215 Jefferson Davis Highway, Suite 1204, Arlington, VA 22202-4302. Respondents should be aware that notwithstanding any other provision of law, no person shall be subject to any penalty for failing to comply with a collection of information if it does not display a currently valid OMB control number.
PLEASE DO NOT RETURN YOUR FORM TO THE ABOVE ADDRESS.

1. REPORT DATE December 2018		2. REPORT TYPE Report 2 of a series		3. DATES COVERED (From - To)	
4. TITLE AND SUBTITLE Mississippi River and Tributaries Flowline Assessment Hydrology Report				5a. CONTRACT NUMBER	
				5b. GRANT NUMBER	
				5c. PROGRAM ELEMENT NUMBER	
6. AUTHOR(S) Roger A. Gaines, Sarah E. Girdner, and Bill J. Frederick				5d. PROJECT NUMBER 449963	
				5e. TASK NUMBER	
				5f. WORK UNIT NUMBER	
7. PERFORMING ORGANIZATION NAME(S) AND ADDRESS(ES) (see reverse) U.S. Army Corps of Engineers, Memphis District 167 N. Main St. Room B-202 Memphis, TN 38103		U.S. Army Corps of Engineers, Mississippi Valley Division 1400 Walnut Street Vicksburg, MS 39180		8. PERFORMING ORGANIZATION REPORT NUMBER MRG&P Report No. 24; Volume 2	
9. SPONSORING/MONITORING AGENCY NAME(S) AND ADDRESS(ES) U.S. Army Corps of Engineers, Mississippi Valley Division 1400 Walnut Street Vicksburg, MS 39180				10. SPONSOR/MONITOR'S ACRONYM(S) USACE MVD	
				11. SPONSOR/MONITOR'S REPORT NUMBER(S)	
12. DISTRIBUTION/AVAILABILITY STATEMENT Approved for public release; distribution is unlimited.					
13. SUPPLEMENTARY NOTES					
14. ABSTRACT Periodically, a historical flood of record inundates the Lower Mississippi River and tributaries, which calls into question the adequacy of the Project Design Flood (PDF). The most recent of these, the 2011 flood, was a result of precipitation that was approximately 60% of the PDF rainfall, yet measured discharges were within 78% to 91% of PDF flows. Thus, the 2011 flood was the impetus for the re-evaluation of the 1955 hydrology that derives the PDF. This assessment replicates the 1955 hydrology with current technological advancements, re-generates that hydrology with a new methodology, and assesses extreme flood events that occurred after 1955. Individual storm event precipitation and temperature point data inputs were pieced together from different archives and converted to raster grids to generate a spatially continuous storm event over the entire Mississippi River Basin for Hypothetical (HYPO) 52A, 56, 58A, and 63. HYPO 58A remains the PDF storm for the Mississippi River and Tributaries project.					
15. SUBJECT TERMS Flood control—Mississippi River, Floods—Mississippi River, Hydraulic models, Hydrologic models, Mississippi River Watershed, Water levels					
16. SECURITY CLASSIFICATION OF:			17. LIMITATION OF ABSTRACT	18. NUMBER OF PAGES	19a. NAME OF RESPONSIBLE PERSON James W. Lewis
a. REPORT	b. ABSTRACT	c. THIS PAGE			19b. TELEPHONE NUMBER (Include area code) 601-634-3895
Unclassified	Unclassified	Unclassified	SAR	720	